NUREG-1464

NRC Iterative Performance Assessment Phase 2

Development of Capabilities for Review of a Performance Assessment for a High-Level Waste Repository

U.S. Nuclear Regulatory Commission

Office of Nuclear Material Safety and Safeguards

Office of Nuclear Regulatory Research

Center for Nuclear Waste Regulatory Analyses

DF03

AVAILABILITY NOTICE

Availability of Reference Materials Cited in NRC Publications

Most documents cited in NRC publications will be available from one of the following sources:

1. The NRC Public Document Room, 2120 L Street, NW., Lower Level, Washington, DC 20555–0001
2. The Superintendent of Documents, U.S. Government Printing Office, P. O. Box 37082, Washington, DC 20402–9328
3. The National Technical Information Service, Springfield, VA 22161–0002

Although the listing that follows represents the majority of documents cited in NRC publications, it is not intended to be exhaustive.

Referenced documents available for inspection and copying for a fee from the NRC Public Document Room include NRC correspondence and internal NRC memoranda; NRC bulletins, circulars, information notices, inspection and investigation notices; licensee event reports; vendor reports and correspondence; Commission papers; and applicant and licensee documents and correspondence.

The following documents in the NUREG series are available for purchase from the Government Printing Office: formal NRC staff and contractor reports, NRC-sponsored conference proceedings, international agreement reports, grantee reports, and NRC booklets and brochures. Also available are regulatory guides, NRC regulations in the *Code of Federal Regulations*, and *Nuclear Regulatory Commission Issuances*.

Documents available from the National Technical Information Service include NUREG-series reports and technical reports prepared by other Federal agencies and reports prepared by the Atomic Energy Commission, forerunner agency to the Nuclear Regulatory Commission.

Documents available from public and special technical libraries include all open literature items, such as books, journal articles, and transactions. *Federal Register* notices, Federal and State legislation, and congressional reports can usually be obtained from these libraries.

Documents such as theses, dissertations, foreign reports and translations, and non-NRC conference proceedings are available for purchase from the organization sponsoring the publication cited.

Single copies of NRC draft reports are available free, to the extent of supply, upon written request to the Office of Administration, Distribution and Mail Services Section, U.S. Nuclear Regulatory Commission, Washington, DC 20555–0001.

Copies of industry codes and standards used in a substantive manner in the NRC regulatory process are maintained at the NRC Library, Two White Flint North, 11545 Rockville Pike, Rockville, MD 20852–2738, for use by the public. Codes and standards are usually copyrighted and may be purchased from the originating organization or, if they are American National Standards, from the American National Standards Institute, 1430 Broadway, New York, NY 10018–3308.

NUREG–1464

NRC Iterative Performance Assessment Phase 2

Development of Capabilities for Review of a Performance Assessment for a High–Level Waste Repository

U.S. Nuclear Regulatory Commission

Office of Nuclear Material Safety and Safeguards

Office of Nuclear Regulatory Research

Center for Nuclear Waste Regulatory Analyses

DF03 0/1

AVAILABILITY NOTICE

Availability of Reference Materials Cited in NRC Publications

Most documents cited in NRC publications will be available from one of the following sources:

1. The NRC Public Document Room, 2120 L Street, NW., Lower Level, Washington, DC 20555–0001
2. The Superintendent of Documents, U.S. Government Printing Office, P. O. Box 37082, Washington, DC 20402–9328
3. The National Technical Information Service, Springfield, VA 22161–0002

Although the listing that follows represents the majority of documents cited in NRC publications, it is not intended to be exhaustive.

Referenced documents available for inspection and copying for a fee from the NRC Public Document Room include NRC correspondence and internal NRC memoranda; NRC bulletins, circulars, information notices, inspection and investigation notices; licensee event reports; vendor reports and correspondence; Commission papers; and applicant and licensee documents and correspondence.

The following documents in the NUREG series are available for purchase from the Government Printing Office: formal NRC staff and contractor reports, NRC-sponsored conference proceedings, international agreement reports, grantee reports, and NRC booklets and brochures. Also available are regulatory guides, NRC regulations in the *Code of Federal Regulations*, and *Nuclear Regulatory Commission Issuances*.

Documents available from the National Technical Information Service include NUREG-series reports and technical reports prepared by other Federal agencies and reports prepared by the Atomic Energy Commission, forerunner agency to the Nuclear Regulatory Commission.

Documents available from public and special technical libraries include all open literature items, such as books, journal articles, and transactions. *Federal Register* notices, Federal and State legislation, and congressional reports can usually be obtained from these libraries.

Documents such as theses, dissertations, foreign reports and translations, and non-NRC conference proceedings are available for purchase from the organization sponsoring the publication cited.

Single copies of NRC draft reports are available free, to the extent of supply, upon written request to the Office of Administration, Distribution and Mail Services Section, U.S. Nuclear Regulatory Commission, Washington, DC 20555–0001.

Copies of industry codes and standards used in a substantive manner in the NRC regulatory process are maintained at the NRC Library, Two White Flint North,11545 Rockville Pike, Rockville, MD 20852–2738, for use by the public. Codes and standards are usually copyrighted and may be purchased from the originating organization or, if they are American National Standards, from the American National Standards Institute, 1430 Broadway, New York, NY 10018–3308.

NUREG–1464

NRC Iterative Performance Assessment Phase 2

Development of Capabilities for Review of a Performance Assessment for a High–Level Waste Repository

Manuscript Completed: August 1994
Date Published: October 1995

Editors:
R. G. Wescott, M. P. Lee, N. A. Eisenberg
Office of Nuclear Material Safety and Safeguards

T. J. McCartin
Office of Nuclear Regulatory Research

Nuclear Regulatory Commission
Washington, D.C. 20555–0001

and

R. G. Baca
Center for Nuclear Waste Regulatory Analyses
San Antonio, TX 78228–0510

ABSTRACT

In order to better review a potential license application to construct and operate a geologic repository for spent nuclear fuel and high-level radioactive waste (HLW), the Nuclear Regulatory Commission staff (and its contractor) has expanded and improved its capability to conduct performance assessments. This report documents the demonstration of the second phase of this capability. The demonstration made use of the scenario selection procedure developed by Sandia National Laboratories to provide a set of scenarios, with corresponding probabilities, for use in the consequence analysis of a potential HLW disposal site in unsaturated tuff. Models of release of radionuclides from the waste form and transport in ground water, air and by direct pathways provided preliminary estimates of releases to the accessible environment for a 10,000 year period. The input values of parameters necessary for the consequence models were sampled numerous times using Latin Hypercube Sampling from assumed probability distributions. The results from the consequence models were then used to generate Complementary Cumulative Distribution Functions (CCDFs) for either release to the accessible environment or effective dose equivalents to a target population. CCDFs were calculated for probabilistically significant combinations (scenarios) of four disruptive events; drilling, pluvial climate, seismicity and magmatism. Sensitivity and uncertainty analyses of the calculated releases and effective dose equivalents were also used to determine the importance of the parameters. Because of the preliminary nature of the analysis and the lack of an adequate data base, the results and conclusions presented in this report should be carefully interpreted. They should not be misconstrued to represent the actual performance of the proposed Yucca Mountain repository nor serve as an endorsement of the methods used.

Table of Contents

Table of Contents (continued)

Table of Contents (continued)

[1]Now with the Department of Civil Engineering at the University of Texas, El Paso.

Table of Contents (continued)

Table of Contents (continued)

Table of Contents (continued)

Table of Contents (continued)

Table of Contents (continued)

Table of Contents (continued)

Figures

Figures (continued)

Figures (continued)

Figures (continued)

Figures (continued)

Tables

Tables (continued)

Tables (continued)

Appendicies

EXECUTIVE SUMMARY

1 Introduction and Background

Phase 2 of the Nuclear Regulatory Commission Iterative Performance Assessment (IPA) program is the second major effort undertaken by the NRC staff and its contractor, the Center for Nuclear Waste Regulatory Analyses (CNWRA), to demonstrate the capability to review a performance assessment for a proposed geologic repository for spent nuclear fuel and high-level radioactive waste (HLW) at Yucca Mountain, Nevada. The primary objective of the IPA program is to develop, maintain, and enhance the NRC staff capability to review effectively performance assessments submitted for support of the U.S. Department of Energy's (DOE's) prelicensing activities such as site characterization, and for the license application. Additional and related objectives include:

- Evaluating the ongoing DOE site characterization program (including field studies, laboratory studies, and analyses, and interim performance assessments generated by DOE or its contractors).
- Evaluating the implementability of the 10 CFR Part 60 performance objectives.
- Providing input to the ongoing evolution of the radiation protection standard for the geologic repository, set forth by the U.S. Environmental Protection Agency (EPA) in 40 CFR Part 191, which is incorporated by reference in 10 CFR Part 60.
- Providing input to regulatory guidance and other regulatory products related to performance assessment, especially the staff's License Application Review Plan (LARP).
- Assisting in the definition of the Office of Nuclear Material Safety and Safeguards (NMSS) technical assistance and research programs in the area of HLW.

IPA Phase 1, completed in 1990 and published in 1992, was performed jointly by staff members from NMSS and the Office of Nuclear Regulatory Research. IPA Phase 2 involved considerably more sophistication in model and computer code development than Phase 1, including: (1) the preparation of an executive module to control and operate the computational modules comprising the total-system performance assessment (TPA) computer code; (2) the use of a much more mechanistic and detailed source term model and computer code; (3) more refined modeling of flow and transport in both saturated and unsaturated media, including the addition of gas flow to the transport analysis; (4) the inclusion of seismic and magmatic disruptive scenarios; and (5) the addition of a dose assessment capability. Many of the improvements to the IPA Phase 2 analysis were based, in part, on the preliminary recommendations made as a result of the insights gained from the Phase 1 effort. Planning for IPA Phase 2 began before the publication of the Phase 1 results. The IPA Phase 2 technical work began in 1991, was completed in 1993, and the documentation and review process continued into 1994.

It should be noted that the results presented in the following chapters have had limited formal review, are based on numerous simplifying assumptions, and use only limited site-specific data; thus, the numerical results should not be taken as representative of the performance of the proposed repository at Yucca Mountain, Nevada. The analysis is also replete with uncertainties regarding conceptual models for consequences and scenarios. In the conduct of this limited study, the authors did not encounter any definitive indications that the EPA standard could not be implemented. However, because of the incomplete scenario analysis in this demonstration, not all aspects of the EPA standard were tested (e.g., the difficulties in estimating scenario probabilities). Therefore, taking these tentative results of a preliminary analysis out of context, or separating these tentative results from these caveats, may lead to the inappropriate interpretation and use of the results.

Finally, this report should be considered as an interim demonstration of some of the methods that the NRC staff might use to review a performance assessment submitted by DOE as part of any potential license application. Thus, at the conclusion of some future phase of the IPA

effort, instruction to the NRC staff on which specific compliance determination methods will be used to review a DOE performance assessment will be developed and documented in the LARP. In the future, this work may also aid in developing guidance to DOE.

2 Purpose

As noted above, the primary purpose of IPA Phase 2 was to improve the capability of the NRC staff to conduct and evaluate calculations of key aspects of a total-system performance assessment for a proposed geologic repository. An independent assessment capability is considered to be an important aspect of the licensing review to be conducted by the NRC staff. Specific goals of IPA Phase 2 were to:

- Use the Tuff Performance Assessment Methodology developed by the Sandia National Laboratories (SNL);
- Provide for preliminary dose assessment capability;
- Provide a gas source term and transport capability;
- Provide an executive module to control run parameters;
- Improve the existing IPA source term code;
- Include the saturated zone in the evaluation of the ground-water pathway; and
- Include more disruptive scenarios in the performance assessment.

In addition, IPA Phase 2 achieved some worthwhile secondary goals, including:

- Limited evaluation of existing analytical tools to conduct a performance assessment (both methodologies and computer codes);
- Obtaining insight into the needs for the improvement of existing, or the development of new methodologies;
- Providing insights into the needs of site characterization; and
- Providing a smooth transition of contractor support from SNL to the CNWRA.

3 Scope

The scope of IPA Phase 2 consisted of the same basic steps as were performed for Phase 1 including: system and subsystem definitions; scenario analysis; and consequence analysis, including disruptive scenarios, analyses of results, and documentation. The IPA Phase 2 study included many improvements over Phase 1, which expanded the scope and are discussed in Section 1.2.5 of this report. The auxiliary analyses performed for IPA Phase 2 were performed by both NRC and CNWRA technical staff members and supported modeling in the areas of regional hydrology, site infiltration analysis, model testing, geochemistry, and source term.

The results of IPA Phase 2 included total and conditional complementary cumulative distribution functions (CCDFs) for summed normalized releases to the accessible environment and effective dose equivalents for the exposed population. Maximum concentrations of radionuclides in ground water were not compared with drinking water standards, and maximum doses to individuals were only calculated approximately. Screening analyses were performed, with the results of the calculations, to investigate the relationship between subsystem performance and overall system performance. Recommendations in the areas of additional scientific input (research), modeling improvements, and supporting analyses were formulated from the IPA Phase 2 work. The results of the sensitivity and uncertainty analyses were also factored into the recommendations.

Development of all total-system performance assessment (TPA) computational modules, supporting analyses, and analyses of results are documented in the IPA Phase 2 report. In addition, the values of parameters used, including the statistical distributions, are included in the appendices.

4 Elements of the IPA Phase 2 Total-System Performance Assessment

This report is largely structured along the same lines used to conduct IPA Phase 2, as noted below:

TPA Computer Code Development

The TPA computer code described in Chapter 2 consists of an *executive module* and several computational modules, which are linked together to calculate, in a Monte Carlo probabilistic manner, the total-system performance of a geologic repository. Both cumulative releases to the accessible environment and radiologic population dose are computed. In addition to controlling the execution of the various modules, the executive module computed the total CCDF by combining the results from the consequence modules and the probabilities of various scenario classes, which were determined separately. The TPA *executive module* also controlled data transfer between modules, including: (a) global data common to all modules; (b) sampled data, parameters sampled from a Latin Hypercube Sampling (LHS) module (see Appendix A); and (c) special input files for the various scenarios or particular consequence modules. The modular construction of the systems code is expected to allow for relatively easy modification or replacement of the various consequence modules, without changing the overall structure of the TPA computer code.

Scenario Analysis

Scenario analysis is comprised of scenario identification, scenario screening, and estimates of scenario probabilities. As noted in Chapter 3, four fundamental events were combined to form 16 mutually exclusive scenario classes. These fundamental events are: (1) change to a pluvial climate; (2) human intrusion by exploratory drilling; (3) seismic disruption; and (4) magmatic disruption. Only four scenarios classes were selected for inclusion in the simulations to estimate the radionuclide release CCDF representing repository performance. Of the remaining 11 scenario classes, another 5 were included in the simulations for the purpose of comparing undisturbed repository performance with disruptions caused by single disruptive events.

Flow and Transport Analysis

The flow and transport analysis described in Chapter 4 consisted of constructing models of radionuclide transport from the source term through both liquid and gaseous pathways. For the liquid pathways, the repository was divided into seven distinct regions, to represent the spatial variability. Radionuclide transport in ground water was assumed to be vertical in the unsaturated zone and primarily horizontal along the water table in the saturated zone. Thus, a water transport pathway, for a particular region, consisted of a series of individual one-dimensional segments, each representing a hydrologic unit associated with that region. The matrix-fracture flow characteristics of these one-dimensional flow paths, used for the TPA code simulations, were based on a detailed modeling of unsaturated flow, using a dual-continuum approach, to represent the fracture and matrix system. Gaseous transport was modeled in two dimensions, using the time-varying temperature distribution which resulted from the repository thermal loading to determine a set of time-dependent velocity fields. Time-varying releases of ^{14}C from the source term model were tracked from the repository to the atmosphere, to determine the release over the performance assessment period and to provide input to the dose assessment model. The TPA system code provided sampled hydrologic parameters (described in Appendices A and B) to both the liquid- and the gas-transport models, for each simulation.

Source Term Analysis

The source term module described in Chapter 5 mechanistically modeled the interaction between waste packages and their immediate environment. Failure of waste package containers was modeled as occurring in three categories: (1) due to initial defects; (2) via corrosion of the waste package, followed by buckling; and (3) failures due to disruptive events. The initiation of corrosion was assumed to require the presence of water in the liquid state, which in turn was assumed to depend on whether the temperature computed for a location had dropped below the boiling point. After initiation, corrosion proceeded according to sampled corrosion parameters supplied by the TPA system code. Modeling of spent nuclear fuel

alteration, dissolution, and near-field transport (the last two processes for releases in the liquid pathway only) was employed to determine the time-varying liquid and gaseous releases for use by the transport models.

Disruptive Consequence Analysis

Disruptive consequence modeling described in Chapter 6 estimated the effects of four disruptive events on the performance of the geologic repository. The drilling model assumed a random process to determine the number, location, and time-of-drilling for boreholes, and whether a waste package canister was hit for each simulated borehole. Excavated waste or contaminated rock provided a surface release for transfer to the total release and dose calculations. The seismo-mechanical model determined waste package failure of the corrosion-weakened waste package canisters from a randomly-sampled earthquake acceleration and supplied the information to the source term code, to calculate releases. The magmatic model randomly selected the time of the magmatic event, its size, location, and orientation. Distributions for these parameters were based on geologic evidence. The intersection of these magmatic features, both dikes and cones, with the repository layout, determined the amount of the emplaced inventory contributing to the releases to the accessible environment (either to the groundwater or surface, or, in the case of extrusive magmatic events, airborne release). Climate change was modeled by a shift in the distribution assumed for infiltration, and the depth to the water table under the repository horizon.

Dose Assessment

A dose assessment capability was included as part of the TPA system code activity; this assessment capability is described in Chapter 7. The dose assessment provided estimates of population and individual effective dose equivalent for each simulation. The dose model employed a static biosphere and determined dose to humans from five exposure pathways: (1) inhalation; (2) air submersion; (3) ingestion of vegetable crops; (4) ingestion of animal products; and (5) ground-shine. Dose related parameters were not sampled in the analyses.

Sensitivity and Uncertainty Analysis

With the simulation results from nine scenario classes and 400 realizations from the sampled parameters, sensitivity and uncertainty analyses were performed. These analyses included regression and differential analyses described in Chapter 8 of this report. The regression analyses included stepwise regression analysis to identify the most significant parameters and the construction of linear and transformed regression models, to test the ability of regression modeling to emulate the performance calculation with a limited set of parameters. A number of coefficients were computed from the regression analysis, to represent sensitivity and uncertainty. Differential analysis was performed using additional system code runs with selected input parameters (without sampling). Sensitivity and uncertainty parameters were calculated directly and compared with those determined from the regression analysis.

Analytical Results

Analyses of the results of the TPA system code simulations also included scatter plots of the releases from various disruptive scenarios compared with the base case releases; sensitivity plots showing the sensitivity of the CCDF to various screening criteria; and histograms of calculated parameters such as approximations to waste package failure times and ground-water travel times. These analyses are presented primarily in Chapter 9 of this report.

Fourteen auxiliary analyses were also conducted to support the tasks listed above. Most of the auxiliary analyses support modeling in the areas of regional hydrology, local infiltration, geochemistry, and radionuclide transport. These analyses provided inputs to the performance assessment consequence models such as the transport characteristics of flow paths, elevation of the pluvial case water table, and geochemical parameters for liquid and gas transport. Other analyses supported the source term model by determining volatile radionuclides that could be released during a magmatic event, and providing a basis for using a representative waste package for the source term for each of the seven repository regions modeled. The results of these analyses are summarized in Chapters 4, 5, and 8. Details regarding how 12 of the 14 auxiliary analyses were conducted are described in detail as

Appendices C to M of this report. Also described in the text of the report are other short analyses, as well as analyses that have been published elsewhere.

5 Overall System and Subsystem Performance Assessment Results

The results of the TPA computer code simulations using the parameter distributions provided in Appendix A of this report and the scenario probabilities provided in Chapter 3 are presented in Chapter 9 in Figures 9-7a, 9-7b, 9-8a, and 9-8b. The results as shown in these figures indicate non-compliance with the EPA release standard, where the probability of release exceeding the EPA limit is greater than 0.1. Median population *Effective Dose Equivalents* exceed 10^5 person-rems. The dominant contributor to the EPA *Normalized Release* is ^{14}C, primarily in the gaseous pathway. The primary contributor to population dose is from the liquid pathway and the ingestion of beef raised on a farm 5 kilometers from the repository. Major radionuclides identified as contributing to dose include ^{94}Nb, ^{210}Pb, ^{243}Am, and ^{237}Np.

NRC's subsystem performance requirements (10 CFR 60.113)* are designed to add to the confidence that the overall system requirements will be met. Even though no direct quantitative correlation between subsystem requirements and the overall system requirement is stipulated in the NRC regulation, an effort was made to determine how subsystem performance contributed, to or was related to, overall system performance. For these analyses, only the CCDF of normalized release was used. Four measures of liquid or hydraulic travel times were considered: (1) fastest path; (2) average; (3) most flux; and (4) flux weighted. Evaluation of each of these potential measures showed that long hydraulic travel times were generally correlated with smaller cumulative releases. However, the nature of the travel time distribution for the fastest path and most flux were such that most travel times were 800 and 1200 years. The distribution for average and flux-weighted travel times showed no vectors with travel times less than 10,000 years. For these reasons, the appropriateness of any given criterion was not directly evaluated. The relationship between release and waste package lifetime was found to be strong, with significant sensitivity of the CCDF to waste package lifetimes in the 300 to 1000-year range. Little correlation was found between the EBS release rate criterion and the normalized EPA release. Meeting the EBS release rate criterion alone did not guarantee a normalized EPA release less than 1.0. The correlation of consequences with various potential measures of subsystem performance is discussed in Section 9.5 of this report.

6 Insights and Conclusions From Model Development and the Sensitivity and Uncertainty Analyses

The most significant information gained from the IPA Phase 2 study was determined to be insights and conclusions regarding the evaluation of the IPA Phase 2 methodology and analyses, aspects of the site and repository design that might be important to performance, and the results of the overall system and subsystem performance assessments. These items are discussed in more detail in Chapter 10 of this report.

In regard to the adequacy of the IPA Phase 2 methodology, it was concluded that although the methodology can and must be improved as performance assessments become more detailed and sophisticated, the present methodology is adequate to identify important parameters and processes, gain insights regarding model development and repository performance, and evaluate research and technical assistance needs.

The scientific basis for analysis, that is the published information regarding the site and repository design, was not considered adequate to represent the performance of the repository in regard to compliance. For this reason, the most important information gained from the performance calculations is considered to be the identification of important parameters and processes and the relative effects of events and criteria on the CCDFs.

Significant insights and conclusions from model development and the sensitivity and uncertainty analysis include the following:

- The fractured unsaturated matrix of the site can greatly influence repository performance

*The regulations in 10 CFR 60.113 establish specific performance objectives for the following repository subsystems: (1) the engineered barrier system (EBS); and (2) the geologic setting.

by providing pathways for fast transport of liquids and vapor. The fractured unsaturated matrix is also difficult to model realistically.

- Percolation rate was identified as the most important parameter, from the sensitivity-uncertainty analysis in scenarios where there was a distribution of both matrix and fracture flow (the non-pluvial scenario classes).

- Abstracted flow models used in IPA Phase 2 probably do not include all of the important characteristics of the flow system and should be supported by three-dimensional, non-isothermal, two-phase models.

- Fracture geochemistry appears to be more important than geochemistry for the matrix for gas and liquid transport.

- Corrosion- and dissolution-related parameters were found to be important, in all scenario classes, for dose and release.

- Near-field hydrothermal processes may greatly influence container lifetime in terms of wetting time and corrosion rate.

- Repository heat load is likely to be an important parameter and should be evaluated in terms of performance sensitivity, in future IPA analyses.

- Uncertainty regarding the probability and consequences of the existing model, for magmatism, justifies more sophisticated modeling efforts.

7 Recommendations

Recommendations for additional scientific input generally follow the insights and conclusions determined from model development and the sensitivity and uncertainty analyses. These recommendations described in Section 10.4.1 of this report include:

- Research regarding fracture-matrix hydraulic and geochemical interactions, including those affecting gas transport, should be undertaken or continued.

- Regional hydrogeology will have to be understood sufficiently to determine the effects of disruptive events on site water levels and hydrologic boundary conditions.

- A relationship correlating percolation with precipitation at the site needs to be developed by DOE. This may allow the incorporation of expert judgment or future climate modeling into the estimation of the base case and pluvial climate percolation range and distribution.

- The effects of high humidity and/or water with high ionic strength on waste package corrosion need to be quantitatively understood for incorporation into the waste package failure component of the source term model.

- Realistic source term modeling will require input from near-field hydrothermal research, which may need to consider alternative waste package designs and placement configurations.

- Research in magmatism, including the role of volatiles, multiple dike intrusions, pre-existing geologic structure, and uncertainty in geochronological data, needs to be undertaken.

In Section 10.4.2 of this report, additional recommendations resulting from the IPA Phase 2 work are listed by chapter. The types of recommendations vary, from being very model-oriented, in the modeling chapters (4 to 6), to requiring additional analyses or procedures such as in Chapters 2, 7, and 8. The recommendations for modeling improvements and/or supporting analysis by chapter are:

- Recommendations concerning the TPA computer code (Chapter 2) included better adherence to software quality assurance procedures, the need for greater model abstraction, and need for the TPA computer code be continually upgraded.

- Recommendations in the area of scenario analysis (Chapter 3) consisted of the need to reassess staff judgments and probabilities assumed in the screening of events and

processes, and the need to examine partitioning of scenario classes.

- Flow and transport recommendations (Chapter 4) include model improvements in the area of unsaturated flow, including more complex modeling of fracture-matrix interactions, two-phase fluid movement, and the effects of fracture imbibition on percolation. Also recommended is a closer examination of hydrogeologic features and heterogeneity in the unsaturated zone, to find possible fast pathways or "short circuits." The recommendations also call for improvements in saturated zone modeling, after evaluating more alternative approaches and adding more output (from intermediate calculations) to the computer models, to better interpret results.

- Source term recommendations (Chapter 5) include modeling improvements in the waste package area, such as near-field hydrothermal and heat transfer modeling, more mechanistic corrosion models, and more realistic waste package failure models. Also included in the source term recommendations were improvements in the release modeling, such as accounting for spatial and temporal variability, improved gaseous ^{14}C releases, and improved dissolution modeling.

- Recommendations associated with disruptive consequence modules (Chapter 6) include the need to improve the drilling, seismic, and volcanism models. There is also a recommendation to include recently obtained information from expert judgment in the pluvial climate consequence simulations.

- Dose assessment recommendations (Chapter 7) include improvements to the input and means of presentation of the *DITTY* code results, and the need to perform sensitivity and uncertainty analysis on the dose assessment parameters. It is also recommended that other dose assessment codes be evaluated, as well as methods employed by international organizations.

- Recommendations from the area of sensitivity and uncertainty analysis (Chapter 8) consist of developing techniques specifically for evaluating probabilistic quantities and the need to incorporate correlation between parameters into the regression model.

TABLE SHOWING ENGLISH/METRIC SYSTEM CONVERSION FACTORS

The preferred system of measurement today is the "Système Internationale" or the metric system. However, for some physical quantities, many scientists and engineers prefer the familiar and continue to use the English system (foot-pound units). With few exceptions, all units of measure cited in this report are usually in the metric system.

The following table provides the appropriate conversion factors to allow the user to switch between these two systems of measure. Not all units nor methods of conversion are shown. Unit abbreviations are shown in parentheses. All conversion factors are approximate.

QUANTITY	*TO INCH–POUND UNITS*	*FROM METRIC UNITS*[1]	*CONVERSION FACTOR*[2]
		SPACE AND TIME	
length	statute mile (mi)	kilometer (km)	0.6214
	foot (ft)	meter (m)	3.2808
	inch (in)	centimeter (cm)	0.3937
area	square mile (mi^2)	square kilometer (km^2)	0.3861
	acre	square kilometer	247.1
	square foot (ft^2)	square meter (m^2)	10.7639
	square inch (in^2)	square centimeter (cm^2)	0.1550
volume	cubic yard (yd^3)	cubic meter (m^3)	1.3080
	cubic foot (ft^3)	cubic meter	35.3147
		liter (l)	0.0353
	cubic inch (in^3)	centimeter (cm^3)	0.0610
velocity	feet/second (ft/sec)	meters/second (m/sec)	3.2808
acceleration	feet/square second (ft/sec^2)	meters/square second (m/sec^2)	3.2808
		MECHANICS	
mass (weight)	pounds (lb)	kilogram (kg)	2.2046
	short ton	metric ton (t)	1.1023
density	pounds/cubic foot (lbs/ft^3)	kilograms/cubic meter (kg/m^3)	0.0624
force	pound-force (lbf)	Newton (N)	0.2248
		dyne (dyn)	$.2248 \times 10^5$
pressure	atmosphere (atm)	kilopascal (kPa)	0.0099
	pound-force/square foot (lb/ft^2)	dyne/square centimeter (dyn/cm^2)	0.0021
power	horsepower (hp)	kilowatts (kW)	1.3405
work	footpound-force (ft-lbf)	joule (J)	0.7376
		HEAT	
temperature	degrees Fahrenheit (°F)	degrees Celsius (°C)	°F = 1.8°C + 32
		degrees Kelvin (°K)	°F = 1.8°K - 459.67
		IONIZING RADIATION	
activity (of a radionuclide)	curie (Ci)	megabecquerel (MBq)	2.7027×10^{-5}
absorbed dose	rad	gray (Gy)	100
dose equivalent	rem	sievert (Sv)	100

[1]Not all metric units are shown. Most metric units can be arrived at by multiplying the value by 10^n.

[2]Multiply quantity in metric units by the appropriate conversion factor to obtain inch-pound units. For additional unit conversions, refer to C.J. Pennycuick, *Conversion Factors: SI Units and Many Others*, Chicago, The University of Chicago Press, 1988.

ACKNOWLEDGMENTS

The editors and authors (cited in the "Table of Contents," by Chapter/Section) gratefully acknowledge the many contributions made by other Office of Nuclear Material Safety and Safeguards and the Office of Nuclear Regulatory Research (RES) management and staff, the Office of the General Counsel, and the Center for Nuclear Waste Regulatory Analyses (CNWRA) which have been incorporated into the text of this report. In this regard, L.R. Abramson/RES, L.E. Lancaster/RES, T. Margulies/RES (now with the U.S. Environmental Protection Agency), R.W. Janetzke/CNWRA, and R.D. Manteufel/CNWRA, deserve special recognition. Special thanks are also to the following individuals for their comments and/or reviews of specific chapters of this report: K.R. Hooks/NMSS—Chapter 1; H.K. Manaktala/CNWRA and T.M. Ahn/NMSS—Chapter 5; P.C. Lichtner/CNWRA and R.D. Manteufel/CNWRA—Chapter 6; J.P. Kotra/NMSS—Chapter 7; and B. Mason/Southwest Research Institute and M.G. Bradley/Freddie Mac—Chapter 8. Ellen Kraus provided editorial guidance, M. Linda McKenzie prepared the manuscript for publication, and Lionel J. Watkins supervised the preparation of the illustrations. Overall publication direction was provided by JoAnn Resner.

1 INTRODUCTION

1.1 NRC's Iterative Performance Assessment Program

1.1.1 Background

Work performed under the first demonstration of the staff's capability to execute critical parts of a performance assessment for a geologic repository for high-level radioactive waste (HLW)[1] was intended as an initial step in a sequence of planned iterative performance assessments (IPAs) to be undertaken by the U.S. Nuclear Regulatory Commission staff and its contractor—the Center for Nuclear Waste Regulatory Analyses (CNWRA). This report describes the results of the second phase (designated "IPA Phase 2") of the continuing demonstration of the development of the NRC staff's capability to review a performance assessment for a geologic repository. This capability helps the NRC staff assess whether the U.S. Department of Energy's (DOE's) site characterization activities are adequate, during the pre-licensing phase, and, later, helps the staff review a potential license application to construct a geologic repository for HLW.

As its name indicates, IPA involves repeated iterations directed at improving both the NRC staff's capability for reviewing DOE's demonstration of repository performance and the staff's understanding of combined systems and events and processes that are key to repository performance. Performance assessment of a geologic repository, like other systematic safety-assessment methodologies, benefits substantially by being conducted in an iterative manner, primarily because the lessons learned regarding modeling improvements, data needs, and methodology can be addressed in subsequent iterations.

1.1.2 Objectives

Under Section 114(d)(2) of the Nuclear Waste Policy Act of 1982 (NWPA), as amended (Public Law 97–425), the Commission is required to issue a final decision on the issuance of a construction authorization for a geologic repository for HLW no later than 3 years after DOE's license application is submitted, although the Commission may extend this deadline for 12 months, for good cause, in accordance with the NWPA, as amended. Meeting this schedule depends greatly on the following: (1) early and open pre-licensing consultation between NRC and DOE on the information that would be needed for licensing; (2) adequate DOE site characterization plans and activities; (3) DOE's submission of a complete and high-quality license application; and (4) effective NRC staff preparation for the license application review process, by having its technical assessment capability in place.

The overall objective of NRC's IPA program, therefore, is to maintain and enhance the staff capabilities necessary to support these geologic repository program activities. During the **pre-licensing phase**, the specific objectives of NRC's IPA program thus include:

- Evaluating the ongoing DOE site characterization program (including field studies, laboratory studies, and analyses, and interim performance assessments generated by DOE or its contractors).
- Evaluating ways to implement the 10 CFR Part 60 performance objectives.
- Providing input to the ongoing evolution of the radiation protection standard for the geologic repository, set forth by the U.S. Environmental Protection Agency (EPA) in 40 CFR Part 191 (*Code of Federal Regulations*, Title 40, "Protection of Environment") which is incorporated by reference in 10 CFR Part 60.
- Providing input to regulatory guidance and other regulatory products related to performance assessment, especially the Draft License Application Review Plan (see NRC, 1994).
- Assisting in the definition of the Office of Nuclear Material Safety and Safeguards

[1] As used in this document, HLW includes spent nuclear fuel and transuranic wastes, unless otherwise specifically stated.

(NMSS) technical assistance and research programs in the area of HLW.

Additional specific objectives of NRC's IPA program, during the **licensing phase**, include:

- To provide an independent calculation of key aspects of DOE's total-system performance assessments submitted as part of a license application.
- To probe DOE's assessment for potential weakness, based on a familiarity with the methods, data, and assumptions used in the performance assessments.

1.1.3 Regulatory Basis for IPA

NRC's basic licensing and related regulatory authority are provided by the Atomic Energy Act of 1954 (Public Law 83–703), as amended. This authority applies to certain facilities of DOE (as successor to the Energy Research and Development Administration) under Section 202 of the Energy Reorganization Act of 1974 (Public Law 93–438). Congress further defined NRC's role, as it relates to the disposal of HLW in geologic repositories, in NWPA and the Nuclear Waste Policy Amendments Act of 1987 (Public Law 100–203).

Section 121(a) of NWPA, as amended, called for EPA to promulgate generally applicable environmental standards for the management, storage, and disposal of HLW. In addition, NWPA prescribed (Section 121(b)) that the EPA standards be implemented by NRC as part of the procedural and technical regulations it was to promulgate for the licensing of geologic repositories for the disposal of HLW. The EPA promulgated its standard in the form of 40 CFR Part 191 (EPA, 1985);[2] the NRC standard is in the form of 10 CFR Part 60 (NRC, 1981 and 1983).

40 CFR Part 191 establishes containment requirements that limit releases of radioactive material to the "accessible environment" (10 CFR 60.2), weighted by a factor approximately proportional to radiotoxicity, and integrated over a period of time (10,000 years is the current regulatory requirement) after permanent closure of the geologic repository.[3]

10 CFR Part 60 incorporates 40 CFR Part 191 as the overall performance requirement for a geologic repository. The requirements in 10 CFR 60.112 set an overall system performance objective that amounts to meeting EPA's containment requirements, whereas certain other sections (10 CFR 60.113) set forth subsystem performance objectives. (The use of subsystem performance objectives is consistent with the Commission's multiple barrier, defense-in-depth concept and contributes to developing reasonable assurance that the EPA standards will be met.)

40 CFR Part 191 specifies three broad quantitative performance requirements for the overall geologic repository system:[4]

- Limits on the cumulative release of radioactivity at the boundary of the accessible environment over 10,000 years (40 CFR 191.13—containment requirements).
- Limits on dose to individuals for the first 1000 years (40 CFR 191.15—individual protection requirements).
- Limits on permissible concentrations of radionuclides in special sources of ground water for the first 1000 years (40 CFR 191.16—ground-water protection requirements).

As for the subsystem performance objectives, the regulations in 10 CFR 60.113 establish specific performance objectives for the following repository subsystems: (1) the EBS and (2) the

[2]40 CFR Part 191 was vacated by the U.S. Court of Appeals for the First Circuit and remanded to the EPA for further consideration.

[3]Currently, a revised set of standards specific to the Yucca Mountain site is being developed in accordance with the provisions of the Energy Policy Act of 1992. The Energy Policy Act of 1992 (Public Law 102–486), approved October 24, 1992, directs NRC to promulgate a rule, modifying 10 CFR Part 60 of its regulations, so that these regulations are consistent with EPA's public health and safety standards for protection of the public from releases to the accessible environment from radioactive materials stored or disposed of at Yucca Mountain, Nevada, consistent with the findings and recommendations made by the National Academy of Sciences, to EPA, on issues relating to the environmental standards governing the Yucca Mountain repository. It is assumed that the revised EPA standards for the Yucca Mountain site will not be substantially different from those currently contained in 40 CFR Part 191, particularly as they pertain to the need to conduct a quantitative performance assessment as the means to estimate postclosure performance of the repository system.

[4]As used here, the repository system refers to the combination of: (i) emplaced wastes; (ii) the engineered barrier system (EBS); (iii) the engineered disposal facility; and (iv) the geologic medium surrounding the geologic repository operations area (GROA) facility (i.e., within the controlled area).

geologic setting. These performance objectives require the following:

- Substantially complete containment of waste in the waste packages for a minimum period of 300 to 1000 years after closure (10 CFR 60.113(a)(1)(ii)(A)).
- Controlled fractional release rate from the EBS, based on the inventory at 1000 years after closure (10 CFR 60.113(a)(1)(ii)(B)).
- Pre-waste-emplacement ground-water travel time (GWTT) of at least 1000 years (10 CFR 60.113(a)(2)).

Because the EPA standard is probability-based, the demonstration of compliance must also be probability-based. However, a probabilistic evaluation is useful regardless of the nature of the standard because of large uncertainties. Accordingly, the measure of total system performance for a geologic repository can be expressed by the complementary cumulative distribution function (CCDF) for cumulative normalized radioactive releases to the accessible environment over 10,000 years. The representation of repository performance by a CCDF incorporates:

- Consideration of the various parameters affecting the performance of the geologic repository; and
- Consideration of a range of anticipated and unanticipated processes, conditions, and events that could affect future geologic repository performance.

In conducting a total-system performance assessment, the analysis needs to account for the various uncertainties that are inherent in those processes, conditions, and events considered. The present performance assessment approach undertaken by the staff in its IPA effort incorporates both parameter uncertainty and scenario probability into a single CCDF. Alternative representations show the entire set of single-vector CCDFs or single conditional CCDFs for each scenario. Both of these alternatives are capable of representing parameter uncertainty and scenario probability as separate factors.

1.1.4 Steps in Performing a Total-System Performance Assessment

The general approach to developing and analyzing a total-system performance assessment can be defined by the following steps, outlined below, and shown in Figure 1-1. For both the IPA Phase 1 and Phase 2 efforts, all these steps were performed to various levels of detail.

Step No. 1—System Description

The repository is broken into its component parts for the purposes of modeling. These components include the waste form, the mined geologic repository system (including the engineered barriers such as the waste package), and the portion of the geosphere surrounding the geologic repository through which the radionuclides, in time, may migrate. The system description therefore should include information that supports the development of models describing repository performance, and should identify data and parameters for the models used to support the *Scenario Analysis* (Step No. 2—described below).

Step No. 2—Scenario Analysis

Scenarios representing alternative possible future states of the environment, as they reflect the repository, are identified and screened. For this analysis, scenarios are formulated based on classes of events and processes external to the repository system. (Events and processes internal to the repository system are treated in the *Consequence Analysis* (Step No. 3—described below).) Probabilities were estimated for the selected scenarios.

Step No. 3—Consequence Analysis (release, transport, and dose modeling)

Models are developed to describe the performance of the subsystems of the geologic repository and are linked to describe overall performance. Overall repository performance, in terms of cumulative releases of radionuclides to the accessible environment, over a specified time period (in

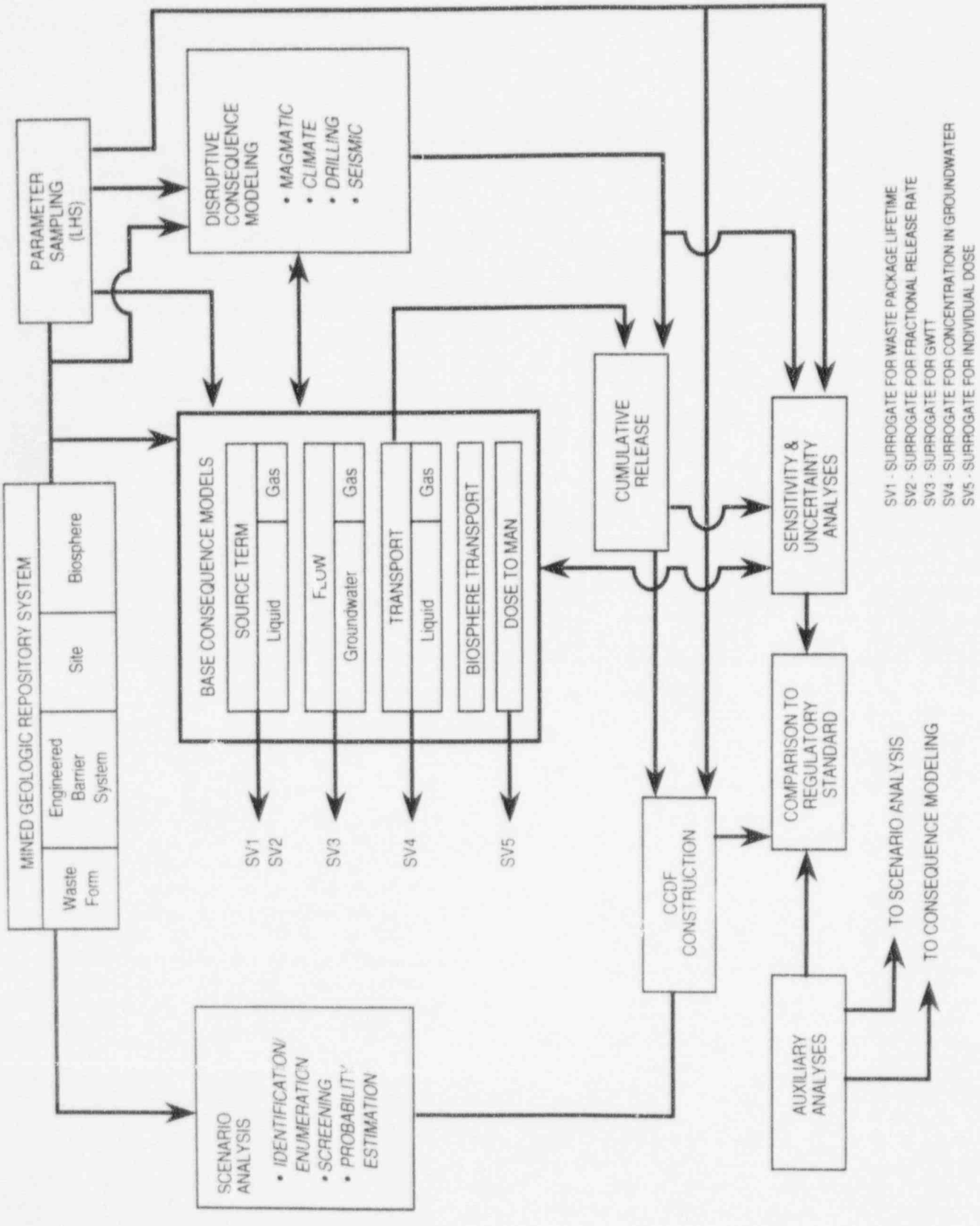

Figure 1–1 Components of a total-system performance assessment

this study, 10,000 years), is calculated for each scenario, using numerous simulations of possible ranges of parameter values. In addition to the CCDF for cumulative releases (Step No. 4), other types of system performance measures, such as maximum doses to individuals, can also be considered.

Step No. 4—Probabilistic Performance Measure Calculation (the CCDF)

For each scenario identified in Step No. 2, the consequences, in terms of normalized cumulative releases of radionuclides to the environment over a specified period of time, are calculated and the results displayed in a plot of total releases versus the probability that such consequences are exceeded (i.e., the CCDF of total releases to the accessible environment for 10,000 years, normalized by the EPA release limit for each radionuclide and summed over all contributing pathways). The total results incorporating scenario probability are compared with release limits established by the EPA standard.

Step No. 5—Sensitivity and Uncertainty Analysis

A sensitivity analysis is conducted to evaluate the fractional change in calculated results caused by incremental changes in the values of input parameters and data. An uncertainty analysis is also conducted to quantify the uncertainty in performance estimates in terms of the major sources of uncertainty, in input parameters. Uncertainty in modeling, however, including conceptual model uncertainty and uncertainty regarding the probability of future states, was not quantified in either IPA Phase 1 or Phase 2.

Step No. 6—Documentation

Documentation is developed to clarify the assumptions used in the analysis, their bases, and the implications of their uses. An important aspect is documentation of auxiliary analyses, which evaluate the adequacy of the consequence modules and the assumptions underlying them, synthesize data into parameters, and provide other insights.

1.2 IPA Phase 2: Overview

1.2.1 Purpose and Scope

As noted earlier, the primary purpose of IPA Phase 2 was to enhance and improve the capability of the NRC staff to conduct and evaluate calculations of key aspects of repository performance by performing a limited total-system performance assessment. It is believed that the NRC staff's capability to perform an independent assessment will be an important aspect of its licensing review. The specific goals of IPA Phase 2 were to:

- Use the Tuff Performance Assessment Methodology developed by Sandia National Laboratories (SNL);
- Provide for a preliminary dose assessment capability;
- Provide a gas source term and transport capability;
- Provide an executive module to control run parameters;
- Improve the existing IPA source term code;
- Include the saturated zone in the evaluation of the ground-water pathway; and
- Include consideration of additional disruptive scenarios.

In addition, IPA Phase 2 achieved some worthwhile secondary goals, including:

- Limited evaluation of existing analytical tools for conducting a performance assessment (both methodologies and computer codes); and
- Insight into the need for the improvement of existing methodologies or the development of new ones.

IPA Phase 2 also provided a smooth transition of contractor support from SNL to the CNWRA.

The scope of IPA Phase 2 consisted of the same basic steps (described in Section 1.1.4) as were performed for IPA Phase 1, including: *system description, scenario analysis, consequence analysis,*

CCDF calculation, and documentation. The IPA Phase 2 study included many improvements, over IPA Phase 1, which expanded the scope and are discussed in Section 1.2.5. The auxiliary analyses undertaken for IPA Phase 2 were performed by both NRC (NMSS and the Office of Nuclear Regulatory Research (RES)) and CNWRA technical staff members, and supported modeling in the areas of regional hydrology, site infiltration analysis, model testing, geochemistry, and source term.

The results computed in the total-system performance assessment included total and conditional CCDFs for summed normalized releases and effective dose equivalents for the exposed population. Maximum concentrations of radionuclides in groundwater were not compared with drinking water standards and maximum doses to individuals were only calculated approximately. Screening analyses were performed, with the results of the calculations, to investigate the relationship between subsystem performance and total system performance. Recommendations in the areas of additional scientific input (research), modeling improvements, and supporting analyses were formulated from the IPA Phase 2 work. The results of the sensitivity and uncertainty analyses were also factored into the recommendations.

Development of all computational modules, supporting analyses, and analyses of results are documented in the IPA Phase 2 report. In addition, the values of parameters used, including the statistical distributions, are included in the appendices.

1.2.2 IPA Organization and Staffing

NRC staff members from both NMSS and RES, and the CNWRA participated in IPA Phase 2. The technical staff involved in IPA Phase 2 came from all three organizations. To coordinate the efforts of the three participating organizations, the organizers designated a technical project manager from NMSS (M. Lee), and three technical coordinators: one respectively from NMSS (R. Wescott succeeding N. Eisenberg); RES (T. McCartin); and the CNWRA (R. Baca succeeding B. Sagar). The assignment of staff to the technical efforts in Phase 2 was done regardless of organizational affiliations and focused on individual technical capabilities.

The project manager and technical coordinators facilitated communication among the various task leaders and technical participants. The technical coordinators also proposed plans for technical activities, schedules, and staffing for IPA Phase 2, for approval by the IPA Management Board. The IPA Management Board was comprised of M. Federline (NMSS) (succeeding R. Ballard); M. Silberberg (RES/Waste Management Branch (WMB)); and B. Sagar, succeeding W. Patrick (CNWRA).

Each of the six major divisions of technical activity was assigned to a working group with a designated task leader. The principal staff (including task leads) assigned to each of these working groups is indicated in the "Table of Contents" of this report: these staff were responsible for conducting the respective analyses and documenting the results. The specific staff responsible for the TPA module development is described in Section 2.1.3 of this report.

However, other NMSS, RES/WMB, and CNWRA staff made substantial contributions during the formative stages of the IPA Phase 2 analysis, as indicated below. Those additional staff members that participated in the initial scoping deliberations for the scenario analysis described in Section 3.3 of this report are listed in Table 1-1. Similarly, in Chapter 5 ("Source Term Module"), important contributions to the analysis were made by: P. Nair, G. Cragnolino, and N. Sridhar of the CNWRA; T. Torng of the Southwest Research Institute (SwRI); and K. Chang and N. Eisenberg of NMSS. Finally, in Chapter 6 ("Disruptive Consequence Analysis"), the Phase 2 analysis benefited from contributions made by those additional staff listed in Table 1-2.

1.2.3 Quality Assurance

The following discussion is intended to briefly outline the quality assurance (QA) measures applied to the software for the IPA Phase 2 computational modules.

As noted earlier, IPA Phase 2 was performed jointly by NMSS, RES, and CNWRA staff. IPA

Table 1–1 Staff Participating in the IPA Phase 2 Scenario Analysis

Individual/Organization	*Discipline(s)*
G. Birchard/RES	geochemistry
J. Bradbury/NMSS	geochemistry
P. Brooks/NMSS	performance assessment
R. Cady/RES	waste package/engineered barrier system
K. Chang/NMSS	waste package/engineered barrier system
D. Chery/NMSS	hydrology, climatology
R. Codell/NMSS	performance assessment
N. Eisenberg/NMSS	performance assessment
B. Gureghian/CNWRA	hydrology, climatology
R. Hofmann/CNWRA	geophysics
A–B Ibrahim/NMSS	geophysics
H. Lefevre/NMSS	economic geology
L. Kovach/RES	geology, volcanism
T. McCartin/RES	hydrology
M. Miklas/CNWRA	geology/climatology
E. O'Donnell/RES	geology
G. Stirewalt/CNWRA	geology
J. Park/NMSS	performance assessment
J. Trapp/NMSS	geology
D. Turner/CNWRA	geology

Table 1–2 Staff Participating in the Analysis of Scenarios used in the IPA Phase 2 Consequence Analysis

Scenario Class	*Analysis Team*/Organization*
Climate	**M. Miklas/CNWRA**
	J. Park/NMSS
	N. Eisenberg/NMSS
	B. Sagar/CNWRA
Drilling	**N. Eisenberg/NMSS**
	J. Firth/NMSS
	A. Drake/CNWRA
	C. Frietas/SwRI
	J. Park/NMSS
	B. Sagar/CNWRA
Seismicity	**N. Eisenberg/NMSS**
	R. Codell/NMSS
	K. Chang/NMSS
	A. Chowdhury/CNWRA
	D. Dancer/NMSS
	C. Frietas/SwRI
	A–B Ibrahim/NMSS
	T. Nair/CNWRA
	B. Sagar/CNWRA
Volcanism	**R. Baca/CNWRA**
	L. Abramson/RES
	L. Lancaster/RES
	R. Codell/NMSS
	R. Drake/SwRI
	N. Eisenberg/NMSS
	L. Kovach/RES
	T. Margulies/RES
	J. Park/NMSS
	B. Sagar/CNWRA
	J. Trapp/NMSS
	C. Lin/SwRI

*Bold type designates principal investigator.

Phase 2 planning and development was performed in accordance with QA guidelines established in the draft IPA Phase 2 Program Plan. The computer programming performed was under the controls of the CNWRA's QA program to avoid the necessity of developing equivalent NMSS/RES procedures for this activity. The CNWRA's implementing procedure in the area of computer codes is Technical Operating Procedure (TOP)-018 (CNWRA, 1991). This procedure imposes methods for configuration management of the scientific and engineering software (e.g., computer codes) acquired, developed, and/or modified and used by NMSS, RES, and CNWRA staff. The procedure is intended to ensure the integrity of such codes by maintaining an auditable and traceable record of any needed changes.

It should be noted that QA requirements contained in TOP-018 conform to the broader QA guidance contained in NUREG-0856 (Silling, 1983). NUREG-0856 recommends guidelines for DOE to use when preparing the documentation for scientific and engineering software used in those analyses submitted in support of any DOE license application for a geologic repository for HLW.

However, it should be noted that Users' Guides for all computational modules are planned and/or under development at this time, to satisfy the requirements of TOP-018.

1.2.4 Approach and Content of the Report

An interdisciplinary, integrated approach was used to conduct the IPA Phase 2 analyses. Working groups or teams of NMSS, RES, and CNWRA staff were organized that roughly correspond to the methodological steps for a performance assessment shown in Figure 1-1. In IPA Phase 2, the areas of investigation included:

- Scenario analysis and selection;
- Simulation of ground-water flow and radionuclide transport;
- Calculation of radionuclide source terms;
- Analysis of disruptive events;
- Modeling of radioactive transport to the biosphere; and
- Analysis of the sensitivity and uncertainty in data, models, and performance estimates.

This report is largely structured along the same lines used to organize the work. Chapters 2 through 8 of this report describe the work performed by the various working groups, as noted below:

Chapter	*Title*
2	"Total-System Performance Assessment Computer Code"
3	"Scenario Analysis"
4	"Flow and Transport Module"
5	"Source Term Module"
6	"Disruptive Consequence Analysis"
7	"Dose Assessment Module"
8	"Sensitivity and Uncertainty Analysis"

A computer code was used to provide the computational algorithms to estimate values of the various performance measures and to performing the calculations leading to an estimate of the CCDF for normalized release and dose.[5] This computer code takes into account a number of the interactions studied among subsystems, components, future states, and processes associated with the geologic repository. Chapter 2 of this report provides a description of this computer code.

One of the IPA Phase 2 activities was a demonstration of the estimation of the total system performance measure (cumulative releases to the accessible environment), as well as some calculation of estimates of those measures related to the performance of natural and engineered barriers. Analytical results from the IPA Phase 2 demonstration and analysis are presented in Chapter 9.

[5]The concepts of normalized release and dose are described in Sections 9.2.1 and 9.2.3, respectively.

Chapter 10 ("Conclusions and Recommendations for Further Work") presents some preliminary thoughts on the adequacy of the staff's current performance assessment capability, as well as some recommendations on the direction of future NRC IPA efforts.

Finally, auxiliary analyses were conducted as part of the investigations described above to examine specific processes and factors that may be important to total system performance. Auxiliary analyses support the performance assessment by using more detailed models to:

- Provide greater insight into cause-and-effect relationships;
- Evaluate conservatism of model assumptions;
- Evaluate alternate modeling approaches; and/or
- Interpret field and laboratory data.

Summary descriptions of these auxiliary analyses are given in Chapters 4, 5, and 8.

1.2.5 Improvements Since Phase 1

The following discussion summarizes the improvements achieved during IPA Phase 2 in the staff capability to execute a performance assessment for a geologic repository for HLW. This summary is structured along the same lines used to organize the work. It should be noted, though, that some of these improvements were based, in part, on the preliminary recommendations made as a result of the insights gained from the IPA Phase 1 effort (see "Preliminary Suggestions for Further Work" in Codell *et al.*, 1992). The suggestions for technical improvements were grouped into three categories:

- Suggestions to improve or extend the modeling capability for reviewing performance assessments;
- Suggestions for refining or adding auxiliary analyses to help better evaluate the performance estimates; and
- Suggestions for refinements or additions to the scientific bases, including the methodologies available and field and laboratory data, for arriving at estimates of repository performance.

Table 1-3 summarizes the IPA Phase 1 recommendations and the extent to which these recommendations were treated in IPA Phase 2. However, some of these recommendations were not implemented, and to the extent that they still apply, they are discussed in Chapter 10 of this report. Refer to Chapters 2 through 8 of this report for a more detailed discussion of these improvements.

Total-System Performance Assessment (TPA) Computer Code (Chapter 2)

In IPA Phase 1, the staff developed a system code to process externally generated information needed to construct the CCDF to represent the performance of the geologic repository for a limited set of scenario classes. In IPA Phase 2, the staff developed a more sophisticated computer code to control the flow of data to and from the computational modules and the sequencing of their execution. This arrangement is believed to offer advantages in eliminating potential data transfer errors and provides an easier means of making changes that affect several modules.

The principal features of the staff's more sophisticated computer code in IPA Phase 2 are:

- The execution of the various scenarios is performed under the control of the TPA executive module, with consistent data (including sampled variables) provided automatically to all the consequence modules; and
- The system executive is responsible for invoking modules automatically and processing release values to construct a CCDF for each run (by nuclide, pathway, zone, module, vector, scenario, and overall, as specified).

In summary, the IPA Phase 1 analysis relied heavily on manual manipulation of files rather than the relatively high degree of automation provided by the system driver for Phase 2.

Scenario Analysis (Chapter 3)

As noted above, only a limited set of scenario classes was considered in IPA Phase 1. These

Table 1–3 IPA Phase 1 Recommendations Implemented during IPA Phase 2

IPA Phase 1 Recommendation	*Implementation in IPA Phase 2*[6]	*Section of IPA Phase 2 Report*
Improvements and Extensions to Modeling:		
General		
Add the capability for modeling additional scenario classes.	Limited	Sections 6.2 and 6.4
Control the CCDF generation with the system code, using the consequence codes as subroutines, instead of generating data sets external to the system code.	Full	Chapter 2
Acquire, test, and evaluate codes that SNL developed for a repository in the unsaturated zone.	Full	Chapter 4, Appendices C, G, and J
Evaluate additional computer codes, which could not be acquired and evaluated during the IPA Phase 1 effort, to determine whether existing codes can meet the NRC modeling needs, or whether additional code development is needed.	Limited	Chapter 4, Appendices C, G, and J
Explore, with the CNWRA, the adaptation of the Fast Probabilistic Performance Assessment methodology to generate the total system CCDF.	Limited	Section 8.8
Perform a sensitivity analysis, using both drilling and groundwater transport parameters.	No longer applicable	——
Flow and Transport		
Refine groundwater modeling (e.g., by considering more dimensions).	Limited	Chapter 4
Incorporate a model of gas-pathway transport in the calculation of the CCDF.	Full	Section 4.3
Include flow and transport through the saturated zone.	Full	Chapter 4
Use a more sophisticated computational model for transport through partially saturated, fractured rock.	Limited	Chapter 4

[6]"Limited" and "full" are relative terms intended to convey the degree of modeling improvement between IPA Phase 1 and Phase 2. The term "limited" suggests only marginal modeling improvement over IPA Phase 1, whereas "full" suggests significant modeling improvement over IPA Phase 1.

Table 1-3 (continued)

IPA Phase 1 Recommendation	*Implementation in IPA Phase 2*	*Section of IPA Phase 2 Report*
Source Term		
Attempt to develop or use a previously developed mechanistic model of waste-package failure.	Limited	Chapter 5
Treat the repository as a source of radionuclides distributed in time and space.	Full	Chapters 4 and 5
Improvements and Extensions to Auxiliary Analyses:		
Perform detailed geochemical analyses to investigate the use of K_ds in estimating radionuclide transport.	Limited	Appendix D
Evaluate the importance of thermally and barometrically driven air flow on repository performance at Yucca Mountain.	Limited	Sections 4.3, 5.4.2, and 5.6.3
Perform detailed hydrologic analyses for Yucca Mountain, to provide a better input to the transport analysis and to examine, in more detail, various alternative hypotheses regarding hydrology at Yucca Mountain.	Limited	Appendices E and I
Recommendations for Additional Scientific Input:		
Develop and demonstrate a mathematically rigorous, scientifically robust method for scenario analysis.	Limited	Chapter 3
Obtain geoscience input for modeling volcanism.	Full[7]	Section 6.4
Obtain geoscience and hydrologic input for modeling faulting, uplift, and subsidence at Yucca Mountain.	Limited	Section 6.2, Appendices F and H
Obtain field and laboratory data on the transport of gaseous radionuclides, especially ^{14}C, at Yucca Mountain.	Limited	Sections 4.3 and 5.6.3, Appendix H

[7]Despite implementation of this IPA Phase 1 recommendation in Phase 2, the staff believes that significant additional work in this area is still needed. See Sections 6.4 and 6.6 for the staff's specific recommendations.

classes were the exploratory drilling (human intrusion) and climate change (pluvial) events leading to four scenario classes. However, for the IPA Phase 2 analysis, the staff applied the SNL scenario selection methodology for use in the consequence analysis of a potential HLW disposal site (see Cranwell *et al.*, 1990). Based on the staff evaluation and modification of the SNL methodology, four scenarios of fundamental events were considered (climate change, seismicity, magmatism, and human intrusion) from which 16 scenario classes resulted.

Flow and Transport Module (Chapter 4)

The IPA Phase 1 effort identified and accounted for a number of important attributes of the Yucca Mountain site (e.g., stratigraphic changes below the repository in the unsaturated zone and differences between matrix and fracture flow). The IPA Phase 2 effort not only has maintained the important attributes identified in the Phase 1 study but has added further modeling complexity such as:

- The number of zones used to represent the repository was increased from four to seven;
- Saturated zone pathways to the accessible environment;
- Calculation of radionuclide concentration for dose assessment; and
- Distribution of mass flux between the fracture and matrix continua.

The additional detailed model complexity is expected to provide further insights into the performance of fractured rock as geologic barrier, data requirements, and the capabilities of the computational methods.

The flow and transport module in IPA Phase 2 built upon the Phase 1 effort. Three transport pathways were considered in IPA Phase 2 (i.e., gaseous, aqueous, and direct) compared with two transport pathways (i.e., both aqueous and direct) in IPA Phase 1. The flow and transport module in IPA Phase 2 provided for treatment of:

- Steady-state liquid phase transport (advection, dispersion, decay, and sorption); and
- Time-varying gas-phase transport (advection, decay, temperature effects, and equilibrium speciation)

Source Term Module (Chapter 5)

Because the modeling of waste-package failure was nonmechanistic and rudimentary in IPA Phase 1, improvement to this aspect of repository performance was sought in Phase 2. The model used by the staff to calculate the source term in IPA Phase 1 was implemented in the *NEFTRAN* (**NE**twork **F**low and **TRAN**sport) computer code developed by SNL (see Longsine *et al.*, 1987). In Phase 1, radionuclide releases were modeled to occur only after failure of the waste package, characterized as a single failure time for the entire repository. The principal features of the staff's source term analysis are discussed below.

In IPA Phase 2, the analysts developed a new computer code to calculate the source term. The *SOTEC* (**So**urce **T**erm **C**ode) module (see Sagar *et al.* (1992)) deals with the calculation of aqueous and gaseous radionuclide time- and space-dependent source terms for the geologic repository. It does so by considering the variations in those physical processes expected to be most important for the release of radionuclides from the EBS. The repository radionuclide inventory was reduced to 20 radionuclides for consideration in the analysis. (The screening process, which selected the more significant radionuclide contributors to the performance measures of interest, is discussed in Section 5.2.4.)

Three primary calculations are done in *SOTEC*: (a) failure of waste packages because of a combination of corrosion processes and mechanical stresses; (b) the leaching of spent nuclear fuel and migration of radionuclides from the EBS; and (c) the release of $^{14}CO_2$ gas from the oxidation of UO_2 and other components in spent nuclear fuel and hardware.

Disruptive Consequence Analysis (Chapter 6)

The ability of the undisturbed repository system to isolate HLW may be modified by a number of disruptive events. These events, individually and

in combination, have the potential to alter the repository performance in several different ways. They may result in direct releases of radionuclides to the accessible environment or modification of the undisturbed release process.

In IPA Phase 1, the staff developed a model and corresponding computer code to treat the disruptive consequences of human intrusion to geologic repository performance by exploratory drilling. In IPA Phase 2, the number of disruptive consequences considered was increased. In addition to the base case (e.g., no disruptive events), the IPA Phase 2 analysis considered four classes of fundamental causative events: pluvial climate change, human intrusion (including exploratory drilling), seismic effects, and magmatic events, for a total of 16 mutually exclusive scenario classes.

Dose Assessment Module (Chapter 7)

A major difference between the IPA Phase 1 and IPA Phase 2 studies was the addition of a dose assessment capability into the TPA computer code in IPA Phase 2. In IPA Phase 2, human exposures were evaluated using a dose assessment software package entitled *DITTY* (**D**ose **I**ntegrated for **T**en **T**housand **Y**ears—see Napier *et al.*, 1988; pp. 3–16—3–18) that was obtained from the Pacific Northwest Laboratories.

Sensitivity and Uncertainty Analysis Module (Chapter 8)

As noted above, performance assessments for a geologic repository will be based on conceptual models that, in part, are based on empirical data embodied as computer programs. Because of the inherent variably of the empirical data and the description of processes included in the models, the predicted performance will be uncertain. An important part of conducting an IPA for a geologic repository therefore is quantifying the sensitivity of the results to the values of the input parameters, and the uncertainty associated with the probabilities of occurrence of credible scenarios.

In IPA Phase 1, the staff performed a statistical analysis of the liquid-pathway calculations using several techniques including Latin Hypercube Sampling (LHS) and regression analysis methods (see Section 9.5 ("Sensitivities and Uncertainties for Liquid-Pathway Analysis") in Codell *et al.*, 1992). In the IPA Phase 2 study, the capability to perform a statistical analysis of the total-system performance assessment results was expanded through the application of statistical techniques, in addition to regression analysis. The LHS scheme was used to sample input parameters for the source term, flow, and transport models, and disruptive consequences affecting the performance of the geologic repository.

Auxiliary Analyses (Chapters 4, 5, and 8)

In IPA Phase 1, four distinct auxiliary analyses were performed:

- The potential for non-vertical flow;
- The sampling requirements for CCDF generation;
- The consequences of $^{14}CO_2$ gaseous releases; and
- The statistical analysis of available hydrologic data for input to flow and transport models

For the IPA Phase 2 analysis, the following 14 additional auxiliary analyses were performed:

In Chapter 4:

- An evaluation of the *DCM3D* computer code for the analysis of three-dimensional ground-water flow;
- An evaluation of the distribution coefficient (K_d) approximation for radionuclide retardation;
- An analysis of a regional ground-water flow model for Yucca Mountain;
- An evaluation of the effects of layering, dipping, angle, and faulting on two-dimensional (2-D), variably saturated flow;
- A *DCM3D* dual-continuum flow modeling demonstration;
- An analysis of $^{14}CO_2$ transport;
- An evaluation of U.S. Geological Survey (USGS) regional flow modeling for the Yucca Mountain region;

- An evaluation of saturated zone flow modeling exercise, using *DCM3D*;
- Considerations in modeling infiltration at Yucca Mountain;
- An analysis of the exchange of major cations at Yucca Mountain; and
- A comparison of *NEFTRAN II* to the *UCBNE41* transport code.

In Chapter 5:

- Ensemble averaging for source term parameters; and
- An analysis of the release and transport of gaseous radionuclides other than ^{14}C.

In Chapter 8:

- An evaluation of several methods of sensitivity and uncertainty analyses.

Many additional, smaller-scope auxiliary analyses were performed as part of developing the computational modules or other aspects of the IPA Phase 2 analysis. These analyses are given limited documentation in this report in the respective chapters in which they occur.

1.3 Description of the Modeled System

As noted in Section 1.1, the first step in a total-system performance assessment is to develop a system description of the geologic repository that includes information to support development of models describing repository performance and to determine assumptions and parameters on which the models depend. In this manner, the geologic repository is broken into its component parts for the purposes of modeling. These components include the waste form, the mined geologic repository system, and the portion of the geosphere surrounding the geologic repository through which the radionuclides, in time, migrate. The following descriptions of the site and the geologic repository (including the waste package) (Sections 1.3.1 and 1.3.2, respectively), are condensed from the 1988 Site Characterization Plan (SCP) (DOE, 1988) and other relevant sources. These descriptions provided the bases for the conceptual models (described in Section 1.3.3) used in the IPA Phase 2 analysis described in subsequent chapters.

1.3.1 Site Description

Although the performance assessment methodology chosen is generic, the transport models, disruptive scenarios, and biological pathways are, to a large part, site-specific. The following is a brief description of the Yucca Mountain site geology, hydrology, mineral resource potential, and climatology—with an indication of where, in the report, each was factored into the IPA Phase 2 analysis. Except as otherwise noted, the following general description of the site geology has been condensed from Chapter 1 ("Geology") of DOE's 1988 SCP.

The Yucca Mountain Site is located in Nye County, which is in southern Nevada, approximately 160 kilometers northwest of Las Vegas. The site (by definition, the location of the controlled area) is entirely located on Federal land managed by DOE and the Bureau of Land Management, whereas the extreme northern portions of the site lie within, or abut, Nellis Air Force Range. Yucca Mountain is located in the southern part of the Great Basin, the northernmost subprovince of the Basin and Range Physiographic Province. Generally this province is characterized by more or less regularly spaced sub-parallel ranges and intervening alluviated basins formed through extensional faulting. The site region is generally arid, with sparse vegetation and low population density.

Yucca mountain itself is an irregularly shaped upland 6- to 10-kilometers wide and about 40-kilometers long. The crest of the mountain ranges between altitudes of 1500 and 1930 meters, about 650 meters higher than the floor of Crater Flat to the west. The physiographic features of the mountain are dominated by a sub-parallel series of *en-echelon*, north-trending ridges and valleys controlled by steeply dipping faults. Fault blocks are tilted eastward so that, in general, the fault-bounded west-facing slopes are generally high and steep, whereas the east-facing slopes are more gentle and deeply dissected by a sub-parallel system of linear valleys. The mountain is bounded by Crater Flat on the west, by Jackass Flat-Fortymile Wash on the east and southeast, the Amargosa Desert to the south, and by the Timber Mountain Caldera complex to the north.

The surface and near surface stratigraphy at Yucca Mountain is comprised of a gently dipping sequence of Miocene ash-flow tuffs, lavas, and volcanic breccias more than 1800 meters thick, and flanked by younger alluvial deposits of late Tertiary and Quaternary age.

The rock unit being considered for a repository is a densely welded ash-flow tuff of the Topopah Spring Member of the Paintbrush Tuff. Although the Paintbrush Tuff regionally is composed of six major ash-flow tuffs and three related lava-flow sequences, at Yucca Mountain only four ash-flow tuffs are recognized. In the general area of the proposed repository, this unit ranges in thickness from approximately 300 meters to almost 600 meters, generally thickest in the north and thinning to the south and east. The Topopah Spring Member is the lowermost member of the Paintbrush Tuff and is the thickest unit in the area of the repository, ranging in thickness from 287 meters (drill hole USW G-2) to 369 meters (drill hole USW H-1). This member is comprised of seven recognizable units, which in ascending order are: the lower nonwelded to moderately welded zone (13 to 42 meters thick); the basal vitrophyre (10 to 25 meters thick); the lower nonlithophysal zone (27 to 56 meters thick); the lower lithophysal zone (43 to 117 meters thick); the middle nonlithophysal zone (20 to 50 meters thick); the upper lithophysal zone (54 to 96 meters thick); and the caprock zone (39 to 62 meters thick). In ascending order, above this unit, are three ash-flow tuffs: the Pah Canyon, Yucca Mountain Member, and the Tiva Canyon Member. The Pah Canyon and Yucca Mountain Members are relatively thin units in the area of the repository reaching a combined thickness of only slightly greater than 100 meters in the area of USW G-2, while normally having a combined thickness of 20 to 30 meters. These units are non-existent in the area of drill hole UE-25p#1. The Tiva Canyon Member is the youngest bedrock unit present over much of the site region, thickening southward from about 90 to nearly 140 meters in the central part of Yucca Mountain and then thinning southward again to about 125 meters. Ten informal map units have been recognized in the Tiva Canyon Member. In ascending order these are: the columnar unit, the hackly unit, the lower lithophysal unit, the red clinkstone, the gray clinkstone, the rounded step, the lower cliff, the upper lithophysal, the upper cliff and, the cap rock unit. The relative proportion of the various units changes from north to south, with the lithophysal units representing about 30 percent of the Tiva Canyon in the northern reaches and only about 10 percent to the south.

Although the Tiva Canyon represents the youngest identified, exposed unit of the Paintbrush Tuff in the Yucca Mountain area, a nonwelded ash-flow and ash-fall tuff has been identified in the subsurface, in the vicinity of the proposed location of the surface facilities. It is possible that this material, which reaches a maximum thickness of 61 meters, is the lateral equivalent of the Pinyon Pass and Chocolate Mountain members of the Paintbrush Tuff.

The Rainier Mesa Member of the Timber Mountain Tuff is locally present above the Tiva Canyon in the lower reaches of Solitario Canyon, in core from boring UE-25p#1, and in Trench 14 on the west side of Exile Hill. This suggests that the Rainier Mesa Member was present as a very thin unit above the Tiva Canyon and has subsequently been eroded, or that this member was only deposited in the lower elevations. The youngest volcanic rocks that have been identified to date, at Yucca Mountain, itself, are basaltic dikes located at the northern reaches of Solitario Canyon, where they are implaced along a fault zone.

The basaltic dikes at the northern reaches of Solitario Canyon have been interpreted by Crowe *et al.* (1983, p. 24) as part of the oldest of three main episodes of basaltic volcanism that has occurred in the Yucca Mountain region after the period of explosive silicic activity responsible for the thick tuff accumulations. This first episode involved bimodal basalt-rhyolite eruptions from approximately 11 to 8 million years before present (mybp). The second phase of basaltic eruptions, the older rift basalts, range in age from 9 to 6.5 million years and include the basalts of Rocket Wash and Pahute Mesa. The third episode of basaltic activity, which has continued into the late Quaternary, occurred after a pause in volcanic activity from about 6.5 to 4.1 mybp and includes the basalts of Buckboard Mesa, Crater Flat, and Lathrop Wells. More detail regarding magmatic activity and how it was factored into the IPA

Phase 2 analysis may be found in Section 3.3.2.2(A) of this report.

Below the Paintbrush Tuffs are the rhyolite lavas and tuffaceous beds of the Calico Hills. In outcrop, this unit comprises a sequence of ash-flow and ash-fall tuffs, volcanoclastic sediments, and rhyolitic lavas. In the northern reaches of Yucca Mountain, this entire unit is zeolitized, but in the southern reaches (near drill holes USW GU-3 and USW G-3) it remains vitric. Underlying the Calico Hills unit are 1000 or more meters of older tuffs and volcanogenic rocks above the pre-volcanic units.

The subsurface extent of pre-volcanic rocks in the Yucca Mountain area is poorly known; however, based on the results from drill hole UE-25p#1, it is known that carbonate rocks of the Silurian-age Lone Mountain Dolomite and Roberts Mountain Formation are present. These rocks comprise part of the lower carbonate aquifer, a regional aquifer used in many parts of Nevada as a primary water-supply source. Based on gravity data, it is suggested that the prevolcanic rocks are approximately 3000 meters thick; however, it is not known if these units are entirely upper Proterozoic and Paleozoic strata, or if younger, post-Silurian units are found beneath the vocanics. It is suggested, based on aeromagnetic data, that the northern portions of Yucca Mountain may be underlain by the Mississippian Eleana Formation (Bath and Jahren, 1984).

Unconsolidated deposits in the region of Yucca Mountain consist primarily of colluvium, alluvium, eolian sand, lacustrian deposits, and playa deposits. In the general site area colluvium, alluvium, and sand deposits are the primary materials found. The thickness of these units is extremely variable, ranging from 0 meters thickness, over much of Yucca Mountain, to in excess of 1000 meters in the center of the surrounding basins.

The main structural grain at Yucca Mountain, as seen from aerial photographs, is a pronounced north-south trending linear fabric defined by parallel, east-tilted fault blocks. In general, the repository block is considered to be a block outlined by faults, with the Solitario Canyon fault to the west, the Drill Hole Wash structure to the northwest, and a zone of imbricate faults to the east and southeast. This relatively simple pattern becomes complex on closer inspection, as all ridge-bounding faults in this area appear to be connected to adjacent faults, most commonly by short, northwest, trending fault splays (O'Neil *et al.*, 1992). The generally north-trending faults primarily display a down-to-the-west sense of fault displacement, but also have a component of left-lateral slip that is displayed by offset stream channels and *en-echelon* fault splays, commonly linked by pull-apart grabens (*op cit.*). Therefore, although the structure can generally be described as a series of high-angle faults believed to merge downward into a detachment system reflective of the extensional mechanism that appears predominant in this region, the actual structural domain is more complex. In general, from north to south, the structural pattern appears younger and displays a clockwise rotation of structure that may be as large as 30 degrees, since the middle Miocene. Although faults are generally displayed as simple lines on maps and cross-sections, detailed field mapping is showing that these fault zones are extremely complex. Ongoing work by Spengler (1993[8]), indicates, for example, that the Ghost Dance Fault, which has 38 meters of displacement along the southeastern margin of the perimeter drift, is a zone of many small faults, with a mapped width of over 200 meters.

Within the Yucca Mountain Region, 32 faults have been mapped that display Quaternary displacement. These include faults such as: the Solitario Canyon Fault, with over 500 meters of mapped displacement; the Paintbrush Canyon Fault, with over 200 meters displacement; and the Bow Ridge Fault, with over 220 meters of displacement. Although the mapped displacement, per event, on the units, is generally on the order of a few centimeters, this normally only includes the vertical component of displacement, so the amount of total displacement for each episode of faulting is poorly constrained. Based on ongoing work by DOE, it appears that the recurrence interval on the various faults is on the order of 50 to 100,000 years for earthquakes of

[8]Spengler, R.W., "Resolution of the Stratigraphic and Structural Settings and Mineral Resource Potential of Yucca Mountain," Unpublished USGS Presentation at DOE/NRC Technical Exchange on Geophysics Integration, Las Vegas, Nevada, June 8, 1993.

approximate magnitude 6.5. (Whitney, 1993[9]). This value would appear to be in the same general range as the "minimum maximum credible earthquake" of dePolo (1993). That the Yucca Mountain area is tectonically active has been demonstrated by the Little Skull Mountain earthquakes or the recent Rock Valley earthquakes. More detail regarding seismic activity and how it was factored into the IPA Phase 2 analysis may be found in Section 3.3.2.2(B) of this report.

A significant aspect of locating a repository at Yucca Mountain is the thickness of the unsaturated zone, allowing the construction of a repository from 180 to 400 meters above the water table. The water table forms the upper boundary of a tuff aquifer that is part of the Alkali Flats-Furnace Creek ground-water subbasin. A major discharge point of the basin is Franklin Lake Playa, at Alkali Flats, in California, through evapotranspiration. Another possible discharge point is at springs in Death Valley near Furnace Creek Ranch. More detailed information regarding the ground-water hydrology of the site and how it was factored into the performance assessment may be found in Section 4.2 and Appendices B, C, E, I, and J of this report.

There are no perennial streams in the vicinity of Yucca Mountain. The springs in Oasis Valley, the Armagosa Desert, and Death Valley are the only reliable sources of surface water in the Alkali Flats Subbasin. Most of the water discharged by the springs travels only a short distance before evaporating or infiltrating into the ground. Floods may occur in the arroyos during heavy rain storms.

The dominant cations in the Yucca Mountain ground water are sodium, calcium, potassium, and magnesium. Sodium is the most abundant cation, accounting for 65 to 95 percent of the cations present. Minerals with high sorption capacity, zeolites, and clays are present along potential ground-water flow paths beneath the repository site. More detailed information regarding the site geochemistry and how it was factored into the IPA Phase 2 analysis can be found in Appendices D, K, and L of this report.

Yucca Mountain is located in a natural, resources-rich geologic region; however, site characterization activities to date have not disclosed any direct evidence of significant mineral or petroleum reserves at Yucca Mountain. Ground water and zeolites are possible resources known to be present at the site; however, they are more economically available elsewhere than in the Yucca Mountain region. More detail regarding the potential for economic mineral resources at Yucca Mountain, and how exploration for such resources was factored into the IPA Phase 2 analysis, may be found in Section 3.3.2.2(D) of this report.

Finally, the present climate at the Yucca Mountain site is classified as a mid-latitude desert climate. Temperatures approach 49°C in the summer time, and the annual precipitation is less than 0.15 meters. The skies are generally clear throughout the year with low relative humidity. During the fall, winter, and early spring, the predominant winds are from the north. During the late spring and summer, the winds shift to a predominantly south to southwesterly direction. More detailed information regarding climate and how it was factored into the performance assessment may be found in Section 3.3.2.2(C) of this report. Information concerning growing season and sources of meteorological data can be found in Sections 7.7 and 7.8 of this report.

1.3.2 Repository Description (Including the Waste Package and Contained Waste Form)

As with the site, knowledge of the design of the geologic repository is also necessary to develop the performance assessment methodology and to construct the proper models. The following is a brief description of the GROA underground facility, the waste package disposal container and contained waste form, and emplacement method, as described in Chapters 6 and 7 ("Conceptual Design of the Repository" and "Waste Package," respectively) of the 1988 SCP, and indicates where these descriptions are factored into the IPA Phase 2 analysis.

The GROA underground facility, where the final emplacement of the nuclear waste would occur, is planned to be constructed at a depth of about 300

[9]Whitney, J. W., "Integration of the Geophysical Studies with Activities in the Tectonics Program," Unpublished USGS Presentation at DOE/NRC Technical Exchange on Geophysics Integration, Las Vegas, Nevada, June 8, 1993.

meters below the eastern flank of Yucca Mountain. The host rock is sufficiently thick over a large enough area to accommodate up to 70,000 metric tons equivalent of waste. Existing information about the site indicates that an area of 848 hectares could be available for waste emplacement; 558 hectares will be used under current plans. The main component of the underground facility is the emplacement panel. Each panel would be about 430 meters wide and about 460 to 980 meters long. The present preliminary layout calls for 18 emplacement panels based on a design areal power density of 57 kilowatts (kW)/acre.[10] Each panel would contain a number of emplacement drifts. The capacity and the layout of the underground facility are factored into the source term analysis described in Chapter 5 of this report. The anticipated thermal loading of the geologic repository is also an input to the source term analysis, as well as the analysis of gas transport examined in Section 4.3 of this report.

The waste package design is expected to consist of the waste form and the disposal container, and is the principal engineered barrier. The principal waste forms will be either spent nuclear fuel from commercial nuclear power reactors or vitrified waste (glass) from both defense and commercial sources, although other waste forms may be disposed of at the proposed site.[11] The reference spent nuclear fuel is 10 years-old with a thermal decay power of about 3.3 kW/waste package (see DOE, 1988; p. 7-29). The gamma dose rate at the surface of the waste package for spent nuclear fuel is about 50,000 rads per hour, and the neutron flux rate is about 10,000 neutrons per square centimeter per second. The vitrified waste will have a thermal power level of about 200 to 470 watts per waste package. The gamma dose at the surface of the waste package is about 5500 rads per hour, and the neutron flux rate will be low. Slightly different assumptions were used for the radionuclide inventory (see Barnard *et al.*; pp. 4-13—4-14 and 6-1—6-16). However, for the purposes of this analysis, only spent nuclear fuel was considered. How the age and composition of the waste forms was factored into the source term analysis is discussed in Chapter 5 of this report.

A key component of the waste package is an overpack container for both the spent nuclear fuel and vitrified waste forms. The reference material for the waste package is stainless steel, with an outside diameter of about 0.66 meters (for stainless steel), and a length of about 3.20 meters for vitrified waste, and 4.7 meters for spent nuclear fuel. The container has a thickness of 0.95 centimeters. After the waste form is loaded into the waste package, the container will be filled with argon gas, and the top will be welded on the container. The loaded waste package would weigh from 2700 to 6300 kilograms, depending on the quantity of waste. The weight, construction, and size of the disposal container are factored into the performance analysis in the seismic scenarios analysis discussed in Section 6.4 of this report.

In the SCP conceptual design, it was assumed that the waste packages would be emplaced in vertical boreholes drilled into the floors of the waste-emplacement drifts. In the vertical emplacement mode, the boreholes, about 7.6 meters deep and about 0.76 meters in diameter, would be drilled vertically into the floor of the emplacement drifts, and a single waste package would be emplaced in each borehole. The container will rest on a support plate inserted into the bottom of the vertical borehole, and the borehole would be lined with a metal casing starting at the top of the hole and extending past the top of the waste package. A metal plug will be inserted on top of the container, to provide shielding from radiation, and crushed tuff would be packed around and on top of this plug and closed with a metal cover. The emplacement hole, its orientation, and geometry are factored into the analysis of the source term discussed in Chapter 5 and the seismic scenarios model discussed in Section 6.4.

Section 60.111(b) requires that the GROA be designed so that the emplaced waste be retrievable at any time up to 50 years after the start of waste emplacement operations. A "caretaker" period of 24 years will begin after the waste emplacement period of 26 years. At the end of the caretaker period, after confirmatory tests of repository performance (10 CFR 60.137), the GROA would be prepared for permanent closure by backfilling the underground facility, and

[10]57 kW/acre is used in this report for easy comparison with the SCP, rather than the metric equivalent of 141 kW/hectare.

[11]Other waste forms that may possibly be disposed of in a geologic repository include low-level, greater-than-Class-C, or transuranic wastes.

permanently sealing the shafts and ramps. Presently proposed concepts for sealing shafts include surface barriers, shaft fill, settlement plugs, and stationary plugs. The backfill would consist of tuff excavated during the construction of the underground facility.

1.3.3 IPA Phase 2 System Model and Methodology

The base case system model used in IPA Phase 2 was comprised of subsystem and process models (or modules). The major subsystems modeled were the waste package and EBS, the local hydrosphere, and a postulated biosphere. Major processes modeled separately were water percolation, gas transport, and ground-water transport. Disruptive events that were considered to act on the system model were pluvial climate change, seismicity, human intrusion, and magmatism.

For the liquid source term and transport (Section 4.2), the site was conceptualized as a layered stratigraphy, and the repository and water pathways were divided into seven distinct columns. These columns helped take into account the variation in stratigraphic sequences and thickness, differences in unsaturated and saturated pathway distances, and temperatures within the repository. Auxiliary analyses conducted with a 2-D dual continuum representation of the repository cross-section (Appendices C and G) were used to determine how percolation from rainfall should be distributed among the seven sub-areas (columns) as well as determine the distribution of flow between rock fractures and matrices in the unsaturated portion of the pathways. The source term module, described in Chapter 5, considers the environment of the waste package and near-field, including the EBS. When disruptive events are not present, the source term module uses repository zone temperature as an indicator of whether each particular zone is wet or dry. After the initial dry-out period in each zone, corrosion is calculated as a function of environmental conditions. When the wall thickness from corrosion is thin enough to result in failure of the waste package canister, water is assumed to enter the canister and the waste dissolution process is assumed to begin. There is also a small quantity of packages assumed to have initial defects which did not require corrosion before dissolution and release could take place. Transport out of the waste package canister by advection and diffusion is calculated as a function of the fracture flow rate into the zone and the results are passed on to the liquid flow and transport module. In the transport model, *in-situ* matrix and fracture velocities and matrix geochemical retardation are used to determine the time-varying amounts of radionuclides reaching the biosphere (e.g., the accessible environment).

In regard to gas source term and transport (Section 4.3), the site was also conceptualized as a layered stratigraphy; however, the site and repository were not subdivided into sub-areas. Yucca Mountain and the repository were modeled as a 2-D cross-section with a time-varying temperature distribution. The temperature distribution was calculated based on conductive heat transfer, taking into account the repository thermal loading and the heat transfer properties of the rock. The gas source term which results from initial defects and corrosion (in the absence of disruptive events), was assumed to be evenly distributed throughout the repository. A model employing many simplified assumptions was developed to determine the velocity vectors throughout the cross-section at various times throughout the performance assessment period. The gas source term releases were tracked through the repository, using these time-varying velocity vectors, and reduced for radioactive decay, in accordance with their travel time (including geochemical retardation) to the surface (e.g., the accessible environment).

To simulate the performance of the repository system under the influence of credible external events, mutually exclusive scenario classes were developed (Chapter 6). For calculation of dose and release within various scenario classes, the base case system model parameters and logic were changed to account for the disruptive event or combination of events being modeled. For scenario classes involving the climate change, the water table was raised and infiltration was sampled from a different distribution than was used for the normal climate. Scenario classes involving drilling allowed damage to emplaced waste packages and also added a pathway (the borehole) as a direct pathway to the accessible environment. Scenario classes involving seismicity required the interaction of a seismic canister failure module with the source term module. The source term module calculates waste package

thicknesses, based on corrosion processes, and combines this information with seismic acceleration probability data from the seismic module to determine when and if a waste package should fail. No changes in the existing pathways or the addition of new pathways is assumed to be caused by seismicity. For classes involving volcanism, the repository is assumed to be in the possible path of intrusive and extrusive volcanic events. The intrusive events are assumed to be underground magma intrusions that damage waste packages but don't provide an additional pathway to the surface. Extrusive events are assumed to entrain a portion of the repository waste and carry it directly to the surface, resulting in an airborne release.

After the transport of radionuclides to the accessible environment (biosphere), as a function of time, is determined, the radionuclides from the various pathways are accumulated, to determine the cumulative release, for comparison with the EPA standard and to calculate the cumulative population dose (Chapter 6). The biosphere used for the dose calculation is assumed to be a 2700-acre farm, with three people maintaining a year-round residence and 177 people off site eating beef cattle, which grazed on the farm, for the waterborne dose; and 22,200 persons in the region for the airborne dose. The dose was calculated in 70-year (lifetime) intervals and accumulated. After completion of the runs and construction of the CCDFs (for both release and dose) sensitivity and uncertainty analyses were performed.

The system code was run 400 times for each modeled scenario class. Over two hundred parameters were sampled for some of the classes. The sampling was performed using the LHS routine. Because of the large uncertainty in both site parameters and process parameters, probability distributions were determined for hydrologic characteristics of the individual geologic strata, corrosion parameters, percolation distribution parameters, and scenario-related parameters, as well as other site- and process-related parameters.

2 TOTAL-SYSTEM PERFORMANCE ASSESSMENT COMPUTER CODE

2.1 Operational Description

2.1.1 Introduction

In IPA Phase 1, the U.S. Nuclear Regulatory Commission staff developed its own system code to process information needed to generate the complementary cumulative distribution function (CCDF) representative of the performance of the geologic repository, for a limited set of scenario classes, using preliminary data and numerous assumptions (see Chapter 4 ("System Code"), in Codell *et al.*, 1992). However, in IPA Phase 2, the staff developed a more sophisticated model and computer code to represent the performance of a geologic repository. The principal features of the staff's improved computer code, designated the total-system performance assessment (TPA) computer code, are discussed below.[1]

The main objectives of the TPA computer code are to develop the computational algorithms for estimating compliance with the performance objectives set forth in 10 CFR Part 60. When fully developed, the TPA computer code will permit estimates of overall system (10 CFR 60.112) and subsystem (10 CFR 60.113) performance, as a function of the specific characteristics of the proposed repository site and design. Such computations take into account the complex interactions among site and design subsystems, components, future states, and processes. Accordingly, the NRC staff expects to use the TPA computer code to review critical aspects of the performance assessment contained in a U.S. Department of Energy (DOE) license application, and as a basis for interactions related to the sufficiency of DOE's site characterization program during the pre-licensing period.

A complete description of the TPA computer code is available in the Center for Nuclear Waste Regulatory Analyses (CNWRA) document 93-017 (Sagar and Janetzke, 1993). The requirements for the code were developed early in the design process (see Appendix C ("Requirements Document for TPA Computer Code") in Sagar and Janetzke (1993)). The TPA computer code was developed using software utilities designed to increase the productivity of the developers and the quality of the final product. One of these was the "preFOR" FORTRAN preprocessor utility, which is described in CNWRA 91-003 (Janetzke and Sagar, 1991a).

2.1.2 Code Organization

The diverse nature of the physical processes present in the natural system being simulated requires that theories from many disciplines be integrated into an overall system model. The TPA program is designed to simulate the behavior of a geologic repository located in a partially saturated medium; both the natural system and the engineered barriers are accounted for in the program design. The evolutionary change in the natural system is described in terms of disruptive scenarios which, in addition to a parametric description of the changed state, also has a probability of occurrence attached to it. Consequently, the TPA computer code is designed as a set of consequence modules largely independent computational units, with their execution controlled by a system manager or executive module. Figure 2-1 shows schematically the data flow and execution dependencies of the subprocesses of the TPA computer code.

Almost all the concepts necessary to model a repository system are included in modules that are controlled by the *executive module* (also referred to as the *system executive* or *executive*). However, the implementation of these modules is kept flexible so that various scenarios may be simulated. In other words, no specific conceptual model is embedded in the *executive module*, except for the fact that the general approach of scenario analysis is adopted. In the scenario approach, the future state of the repository system is defined by a set of parameters whose values are chosen from specified probability distributions. This set of parameters is assumed to be independent of time for a particular scenario, although this is not strictly required for the scenario approach. A different scenario is defined, if parameter values change within the time span of interest (e.g., 10,000 years). In the analyses conducted so far, disruptions defining

[1]The principal features of the staff's advanced model for a geologic repository that forms the basis for this improved computer code are discussed in Chapters 3 through 7.

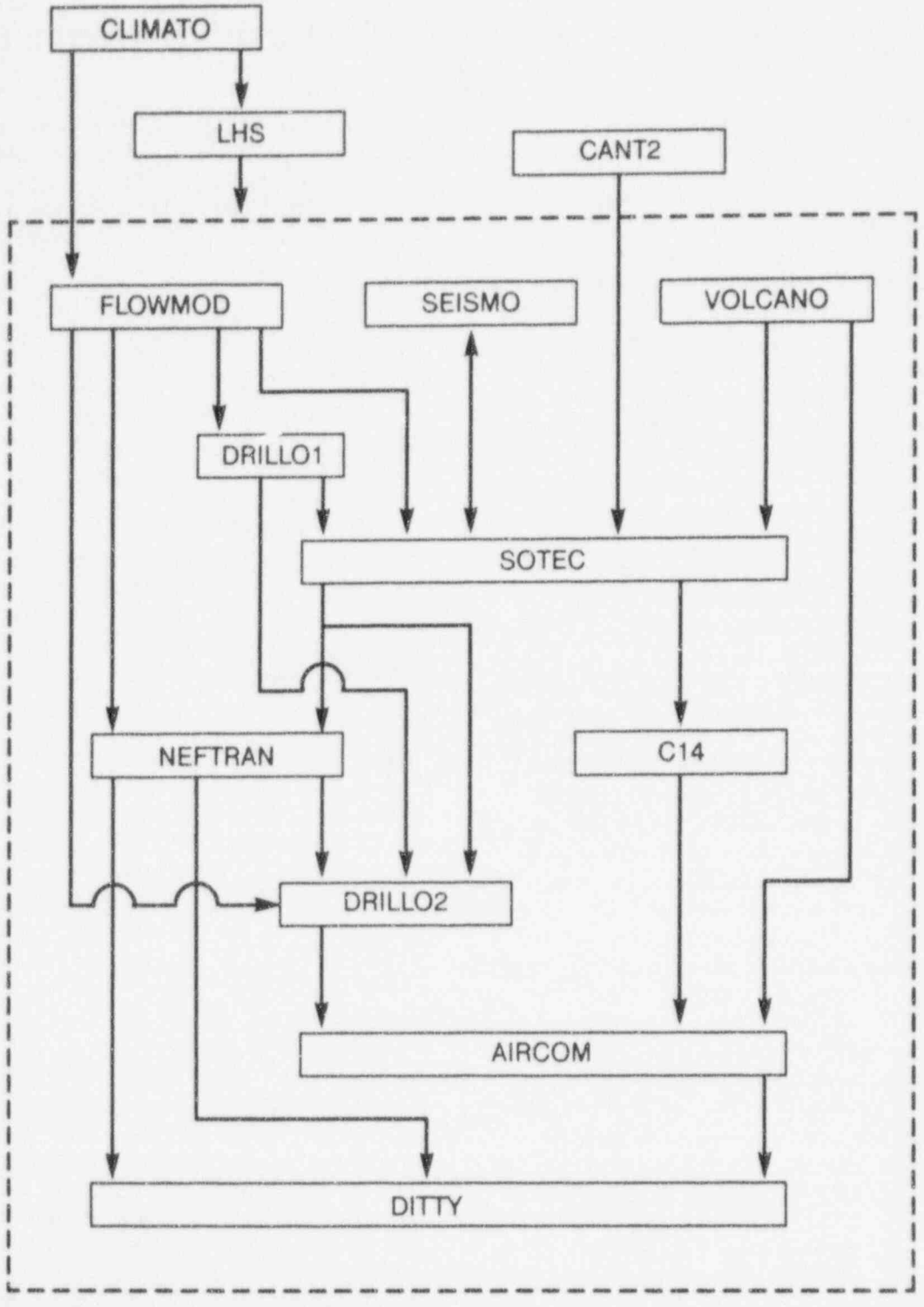

Figure 2–1 Flow diagram showing the elements of the total-system performance assessment computer code (These elements are described in Section 2.1.3. The dashed line shows which elements are controlled by the *executive module*, described in Section 2.1.2.)

scenarios occur at a specified time and the disturbed state then remains constant, which is probably reasonable for every scenario except those involving pluvial climate.

Automated features included in the system facilitate the unattended running of a set of multiple scenarios with associated output.

The TPA computer code consists of four basic parts:

- The system manager or *executive module*;
- Algorithm(s) to sample from statistical distributions;
- Algorithm(s) to model future states or scenarios; and
- Algorithms to model internal repository system processes such as source term, transport, and consequences.

Consequences are quantified in terms of cumulative releases and dose-to-man. In addition, algorithms to compute sensitivities and perform uncertainty analyses are executed separately as an auxiliary process (see Chapter 8).

Although not depicted in the figure, the *executive module* of the TPA computer code acts as the controller for the overall computer code and executes the consequence modules in the desired sequence and ensures that appropriate values of the common parameters are passed to the appropriate consequence modules. The *executive module* controls the sequence of execution of various modules, transfers data to other modules, and controls data transfer from one module to another. Authored principally by R. Janetzke and B. Sagar at the CNWRA, the *executive module* of the TPA computer code currently consists of about 21,000 lines of FORTRAN, whereas the complete system code (including all modules) is about 85,000 lines (see Sagar and Janetzke, 1993). The total execution time for one realization of all consequence modules on the Cray computer was about 100 seconds.

The programs for the consequence modules are also referred to as subprocesses in the sense that together they provide the complete process for describing the behavior of the repository. The consequence modules are designed to be executed either as part of a TPA computer code or independently. The standard documentation prepared for these programs will also apply to their use in the TPA computer code, with minor modifications to input and output procedures, which are explained in CNWRA 91-009 (Sagar and Janetzke, 1991). The TPA computer code uses a dedicated subroutine to handle the setup and initiation of each subprocess. An additional subroutine is required to read any results that may be provided to the *executive* by a particular subprocess. The subprocess is created as the result of a CALL to a utility routine, which is specific to the operating system. This CALL is the mechanism that starts the subprocess. Control is returned to the *executive module* at the end of the execution of the subprocess.

The subprocess for obtaining samples from specified statistical distributions is based on the Latin Hypercube Sampling (LHS) method (see Iman and Shortencarier, 1984). Other programs used as subprocesses include algorithms for computing flow fields, estimation of doses, and calculation of consequences of scenarios such as human intrusion. Modules to calculate sensitivities of the final results (e.g., CCDF) to selected parameters are implemented as external auxiliary processes.

The TPA *executive* code is maintained in the CNWRA configuration management system (TOP-018; CNWRA, 1982), and is fully compliant with it.

2.1.3 TPA Module Descriptions

As noted above and illustrated in the figure, the TPA computer code is organized into a number of modules that perform specific computational functions. A brief description of each of the TPA computer code modules is provided below, in alphabetical order.

AIRCOM—This module is mainly utilitarian in nature and does not perform any calculations relative to the physics of the overall geologic repository system, except for the introduction of fractions of contaminated soil that become airborne and respirable for the drilling and volcanic disruptive events. Its main purpose is to merge the various airborne release data files (*VOLCANO*, *DRILLO*, and *C14*) into one file in

the proper format for use by the dose module—*DITTY* (**D**ose **I**ntegrated for **T**en **T**housand **Y**ears; see Napier *et al.*, 1988), as discussed below, and at greater length in Chapter 7.

In IPA Phase 2, contaminated soil or gaseous $^{14}CO_2$ was assumed to be transported to the ground surface above the repository as a result of disruption of the geologic repository itself, either by human intrusion or by an extrusive volcanic event. In this analysis, only a fraction of this surface radioactivity was assumed to become available for transport by the air pathway to members of the public beyond the controlled area (10 CFR 60.2) of the geologic repository. The fractions of the radioactivity that were assumed to become airborne were stored in the *AIRCOM* module. All the airborne radioactivity was assumed to be respirable (whether in the solid, liquid, or gaseous states). Any radioactivity that did not become airborne was considered to remain undisturbed at the point of release to the above-ground surface.

The *AIRCOM* values were used as inputs to the files used by DITTY, to calculate the exposure of the regional population, or that part of the farm family, to airborne radioactivity released from the geologic repository. First, the *DRILLO*, *VOLCANO*, and *C14* modules were used to calculate the quantities of contaminated soil or gaseous ^{14}C released to the ground surface at various times during the 10,000-year study (as determined by LHS sampling of appropriate model parameters). Next, these quantities were multiplied by the corresponding airborne fractions in *AIRCOM* to generate the input values (curies per year released to air) for use by the *DITTY* module, to calculate dose.

This module was developed by A. O'Campo of the Southwest Research Institute (SwRI).

CLIMATO—This module is a place holder for a future climate-related constituent of a disruptive event. In IPA Phase 2, climate change is treated by specifying climate-dependent infiltration rate and water table position for use in the *FLOWMOD* transport module (see Section 6.2).

CANT2—The time-dependent temperature of the surface of a waste package is calculated in *CANT2*. Developed by R. Codell (NMSS), the *CANT2* module is based upon an analytic solution of the linear heat conduction equation, by the principle of superposition assuming, a finite number of heat sources. In IPA Phase 2, the repository is assumed to consist of seven regions or sub-areas, each repository sub-area comprised of several waste emplacement panels. The main purpose of *CANT2* is to predict the temperature of a representative waste package in each of the seven repository sub-areas needed for the source term module—*SOTEC* (**S**ource **T**erm **C**ode)—to determine the time at which liquid water can come into contact with the waste packages. The output is written to a file, which is read by the *SOTEC* module. *SOTEC* also uses this temperature for the temperature-dependent parts of the source term model (e.g., the *C14* release module).

In IPA Phase 2, none of the parameters used by *CANT2* is considered random; these parameters also did not vary with disruptive scenarios. Consequently, *CANT2* is executed only once, and the resulting temperatures are used by all the vectors of all the scenarios.

C14—In IPA Phase 2, $^{14}CO_2$ is considered to be the only radionuclide that can be transported in the gaseous phase. *C14* calculates the travel time and decay of $^{14}CO_2$ releases from the source term module. Authored by R. Wescott (NMSS) and R. Codell this module uses an independently calculated time-varying far-field temperature field, to determine time-dependent gas velocities. *C14* uses the equations of flow, hydrologic parameters from the LHS sampling module, and the time varying temperature field induced by the spent nuclear fuel, to calculate a time varying gas velocity field from the water table to the atmosphere. Releases from the source term are tracked through this field and reduced by radioactive decay taking into account retardation of $^{14}CO_2$, because of the interaction of the host rock and water. The amount of $^{14}CO_2$ released from the repository, as calculated by the source term module, *SOTEC*, is provided to *C14* as an input. The resulting releases to the atmosphere are then passed to the *AIRCOM* module in terms of curies/year, as points in time from repository closure to the end of the period of regulatory interest, for the purposes of performance assessment.

This module is discussed at greater length in Chapter 4.

DITTY—The transport of radioactivity to the biosphere is modeled in the *DITTY* module. *DITTY* estimates the time integral of collective dose over a 10,000-year duration for releases (or concentrations) of radionuclides to the accessible environment. In IPA Phase 2, the exposure pathways of interest included: the atmosphere, land surfaces, the top 15 centimeters of surface soil, vegetation, animal products (milk, beef), and drinking water. (Aquatic pathways were not considered.) The annual releases to the air or water pathways over the 10,000-year period of interest were provided as input to *DITTY* by other consequence modules, in the form of average annual concentrations. The values for these concentration-time pairs were obtained as outputs directly from *NEFTRAN* or indirectly from *C14*, *DRILL02*, and *VOLCANO*, via the *AIRCOM* module.

Developed originally for the Hanford site, this code was obtained from the Battelle Pacific Northwest Laboratories (PNL) in Richland, Washington. This module considers both air and liquid transport pathways and calculates both the individual and population doses. The *DITTY* module is designed to deal with both acute and chronic releases, and annual, committed, or accumulated doses can be calculated. Several of the Hanford site-specific data coded in *DITTY* were modified. A second generation of dose calculation codes, *GENII*, which includes the original *DITTY* code, is currently available from PNL. For conceptual models included in *DITTY* and its user's manual, see Napier *et al.* (1988).

This module is discussed at greater length in Chapter 7.

DRILLO1—In IPA Phase 2, the human intrusion disruptive event is stipulated to consist of drilling initiated above the geologic repository. The location of boreholes and the timing of drilling are assumed to be random (see Appendix H ("Analysis for Drilling Scenario") in Codell *et al.* (1992)). Although a random spatial distribution may not be physically realizable, it is used here for simplicity. The drill bit can either hit a waste package directly or it may only penetrate contaminated rock. Radioactive material may be brought to the surface, in either case.

Authored by N. Eisenberg (NMSS), J. Firth (NMSS), and C. Freitas (SwRI), the *DRILLO1* module uses sampled data on the seven repository sub-areas and the distribution of waste packages. This information is used, for each borehole, to determine the region where the borehole is located and whether a waste package was struck during the drilling event. These results are then used by *DRILLO2* to determine the consequences. The calculated number of direct hits and their times of occurrence are also supplied to the *SOTEC* module, for inclusion in the calculation of a source term.

DRILLO2—Consequences from the drilling disruptive events identified in *DRILLO1* are calculated in *DRILLO2*. A drill bit hitting a waste package directly or penetrating contaminated rock is assumed to lift a certain portion of the radionuclide inventory to the ground surface. The inventory in a waste package and in the rock surrounding waste packages is as a function of time, and is used by *DRILLO2*, to determine consequences. A small percentage of the radioactive material brought to the surface is assumed to be particulate material that becomes airborne. This information is then provided to the *AIRCOM* module, for calculation of the respirable fraction of the human dose in *DITTY*. The *DRILLO2* module was authored by N. Eisenberg, J. Firth, and C. Freitas.

The detailed features of the *DRILLO* modules are discussed in Frietas *et al.* (1994).

FLOWMOD—The computational module entitled *FLOWMOD* determines the hydrologic flow regime that provides ground-water flux for use in the source term module (*SOTEC*) and transport pathways and properties for use in the transport module—*NEFTRAN* (**NE**twork **F**low and **TRAN**Sport). The primary functions within *FLOWMOD* are the determination of: (a) the spatial distribution of ground-water flux; (b) the quantity of flow in the matrix and the fracture; (c) fluid velocities; and (d) saturation-dependent retardation coefficients. The computational demands of solving partially saturated flow in fractured tuff precluded a direct solution of the flow equation; therefore, a table interpolation scheme was used to determine spatial distribution

of flow and the quantity of matrix versus fracture flow. The tables used for these interpolations were based on the results, using a dual-continuum approach, as set forth in the *DCM3D* computer program (see Updegraff *et al.*, 1991) for simulating Yucca Mountain. The interpolation scheme made use of sampled data for the infiltration rate and the hydraulic properties of the matrix and fractures.

FLOWMOD uses these relationships to determine the mass fluxes and particle travel times for each of the stratigraphic units comprising a certain number of vertical columns corresponding to each of the geologic repository sub-areas (seven in IPA Phase 2). The *DCM3D* computer program is not a part of the TPA computer code. It was executed separately to create the input data for *FLOWMOD*. This module was developed by T. McCartin (RES) and W. Ford (NMSS).

This module is discussed at greater length in Chapter 4.

LHS—The TPA user can specify various parameters pertaining to any number of consequence modules to be sampled where statistical distributions represent uncertainty. The *LHS* module uses the sampling method of Iman and Shortencarier (1984) to create equally likely parameter vectors. Although only uncorrelated parameters were used in IPA Phase 2 calculations, the *LHS* module is designed to sample from correlated parameters also. Two aspects of the *LHS* module to be noted are: (a) all sampled parameters, irrespective of which consequence module they belong to, are sampled at one time; and (b) for the analysis of any one scenario, a single call to the *LHS* module provides all the vectors or realizations.

The computer program for the LHS was obtained from the Sandia National Laboratories (SNL), under contract to NRC. The detailed features of the *LHS* module are discussed in Sagar and Janetzke (1993).

NEFTRAN—The far-field transport of radionuclides is treated in the *NEFTRAN* module. The initial version of the code used during IPA Phase 1 was obtained from SNL (see Longsine *et al.*, 1987) under an NRC research contract. In IPA Phase 2, the staff used an improved version designated *NEFTRAN II* (see Olague *et al.*, 1991).

The *NEFTRAN* module simulates the transport of radionuclides in the aqueous phase away from the geologic repository, and calculates the integrated discharge of radionuclides, over 10,000 years, at the boundary of the accessible environment and the time-varying concentration of radionuclides (used in the calculation of the dose) at the boundary of the accessible environment. In the simulation of radionuclide transport, the following two primary factors are accounted for in the *NEFTRAN* simulations: (a) element-specific retardation of radionuclides, based on the geologic unit and the degree of saturation; and (b) multiple flow paths, to represent the possible dual flow paths caused by fracture and matrix flow. As shown in Figure 2-1, the pore velocities calculated by *FLOWMOD* are provided as input to *NEFTRAN*. In *NEFTRAN*, the transport domain is considered to be made up of one-dimensional (1-D) transport paths, along which the convection-diffusion equation is solved semi-analytically by the distributed velocity method (DVM). Details of the DVM are available in Olague *et al.* (1991).

This module is discussed at greater length in Chapter 4.

SEISMO—The *SEISMO* module calculates the probabilities of failures of waste packages, because of a seismic event. The probability of occurrence of an event of certain magnitude is considered to be time-dependent. To simplify the analysis, a seismic hazard curve representing time-dependence of earthquake magnitudes (peak accelerations) at a certain probability level (e.g., 95 percent) is first obtained. This curve is obtained from a family of postulated plots between the occurrence probability versus earthquake magnitude for a set of fixed time periods. Based on the structural properties of the container material, a fragility curve representing a relation between peak acceleration and the critical container wall thickness is derived. The actual container wall thickness, for waste packages, as affected by corrosion processes, is obtained from *SOTEC* as a function of time, which produces a time history of nominal wall thickness, when considering the undisturbed case. Any time the critical wall thickness obtained from the fragility curve is greater than the actual thickness

produced by the *SOTEC*, failure occurs. The number of such failures is fed back to *SOTEC* for calculation of the source term. This module was authored by N. Eisenberg, R. Codell, and C. Freitas.

This module is discussed at greater length in Chapter 6.

SOTEC—deals with the calculation of aqueous and gaseous radionuclide time- and space-dependent source terms for the geologic repository. It does so by considering the variations in those physical processes expected to be important for the release of radionuclides from the engineered barrier system. As mentioned above, ^{14}C is the only radionuclide that is treated in the gaseous phase in IPA Phase 2. However, all radionuclides, including ^{14}C, are considered in the aqueous phase. As shown in the figure, *SOTEC* provides the aqueous, gaseous, and direct radionuclide releases to the geosphere transport modules—*C14, DRILLO2, NEFTRAN, SEISMO,* and *VOLCANO*.

Three primary calculations are done in *SOTEC*: (a) failure of waste containers because of a combination of corrosion processes and mechanical stresses; (b) the leaching of spent fuel; and (c) the release of $^{14}CO_2$ gas from the oxidation of UO_2 and other components in the spent nuclear fuel and hardware. In Version 1.0 of *SOTEC* (Sagar *et al.*, 1992), general corrosion, pitting, and crevice corrosion are modeled, based on a temperature-dependent corrosion potential. The temperatures obtained in *CANT2* are provided as inputs to *SOTEC*. Leaching rates are considered to be either solubility limited or congruent to UO_2 rates. This module was authored by B. Sagar, R. Codell, J. Walton (CNWRA), and R. Janetzke. More details are available in Sagar *et al.* (1992).

This module is discussed at greater length in Chapter 5.

VOLCANO—Consequences caused by magmatic events are calculated in the *VOLCANO* module. This module was developed by R. Baca (CNWRA), L. Lancaster (RES), R. Drake (CNWRA), and C. Lin (SwRI), and is based on the work of Margulies *et al.* (1992). In the geometric approach followed in *VOLCANO*, Monte Carlo sampling is used to generate a volcanic event randomly in a rectangular region surrounding the repository horizon. Random sampling is used to specify: (a) the location of the sampled volcanic eruption; (b) the nature (intrusive, leading to dike formation and extrusive, leading to dike and/or cone formation) of the volcanic event; (c) the dimensions of the dike or cone; and (d) the orientation of the dike. From the area of the geologic repository intercepted by dikes and cones, the numbers of waste packages failed by the magmatic event are determined assuming all intercepted waste packages have failed. This information is used in *SOTEC*. When the volcanic event is extrusive, the contents of the failed waste packages are assumed to be released to the accessible environment (direct release), and a fraction of this is assumed to be ejected to the atmosphere, which is then used in *AIRCOM* to calculate human dose, and in the *executive module*, to calculate the total release. A more detailed description of the *VOLCANO* module is given in Lin *et al.* (1993).

This module is discussed at greater length in Chapter 6.

Finally, all the consequence modules used for the TPA system code are maintained under the CNWRA configuration management system (TOP-018), and will be fully compliant with it upon the receipt of *User Guides* for *CANT2, FLOWMOD, C14, DRILLO, SEISMO,* and *AIRCOM*.

2.1.4 Data Handling and Control

The input/output (I/O) files for the TPA system code can generally be divided into four different types:

- Input;
- Temporary (used for the duration of the current scenario);
- Reusable (used for more than one scenario); and
- Output.

The input files include the TPA input file, LHS standard input file, and standard input files for each of the consequence modules. The TPA input file is prepared in a free-format style. That is, the

input values are associated with keywords rather than with fixed column positions in the input file. This was implemented using a set of standard FORTRAN routines described in CNWRA 91-005 (Janetzke and Sagar, 1991b).

The temporary files include the files generated by the TPA computer code for the purpose of transmitting control parameters to an external module. These typically contain global parameters (parameters that are common to more than one module) which can override the parameters read from the module's standard input file. The temporary files receive their names from the TPA *executive module* and are overwritten for each new vector processed. In general, only the programmer (and not the end user) needs to access the temporary files.

The reusable files are those on which intermediate results from various consequence modules are written. The data in these files may be processed later by other modules.

The output files include the output file of the TPA computer code itself, standard output files of each one of the consequence modules, error log files, and specially formatted files, for external utilities such as the TECPLOT graphics utility (Amtec Engineering, 1984).

Names of all files except the temporary files can be read as part of the input. The format-free input process of the TPA *executive* is explained in Sagar and Janetzke (1993).

2.1.5 Sampled vs. Global Data

Many of the consequence modules require some of their input parameters to be sampled from a certain statistical distribution over a range with known end points. This feature is adapted in a common manner for all of the computational modules involved. The *LHS* module is used to generate the **sampled data** for all of the parameters, and for all vectors of a given scenario. A standard *LHS* input file is created with distribution specifications for all of the parameters. Appendix A lists the distribution and range specifications for the *LHS*-sampled input parameters used in the IPA Phase 2 analysis. The *LHS* module then produces a single output file, containing a data set for each vector. When a consequence module begins execution, it reads this file sequentially until it finds the correct vector and then reads the entire parameter set for that vector. The consequence module must then select its parameters from this set, as specified in a "map" file, which identifies the location of each parameter.

When the modules are executed in a stand-alone mode, sampled parameters are not used, and all the necessary control input is provided via the standard input file. In the TPA computer code, however, the sampled data must override any values provided in the standard input file. This is done by ensuring that the sampled data are read after the standard input file is read, and before any quantities are derived from them.

One of the primary requirements of the simulation process is that parameters that are common to many subprocesses be specified consistently. Since the design of the TPA software is such that all the subprocesses can run independently, this consistency is maintained through the temporary global data files, which transmit data from the *executive* to the consequence modules. These data files contain parameters in a fixed order, and the corresponding consequence module must follow this order when extracting the parameters from the file. This process is completely automated and does not require manipulation by the user.

2.2 Improvements and Changes Since IPA Phase 1

IPA Phase 1 included releases only via the water pathway and direct drilling pathway. Release and transport of ^{14}C in the gas phase were considered only in an auxiliary analysis, and not in the evaluation of risk. The source term module was a version of the module already existing in *NEFTRAN*, modified somewhat for consideration of unsaturated flow.

The analysis of the liquid phase release and transport to the accessible environment considered the following mechanisms:

- One-dimensional steady-state flow and transport through the unsaturated zone, through four parallel columns consisting of multiple layers of rock under the influence of normal and pluvial rates of water infiltration.

- Waste form dissolution, based on the quantity of water that could enter the waste package container.
- An empirical failure-time distribution for the waste package canisters. All waste packages canisters were considered to fail simultaneously.
- Direct release of a portion of the waste brought to the surface in drill cuttings.

IPA Phase 1 considered four scenarios:

- Normal infiltration, no drilling;
- Normal infiltration with drilling;
- Pluvial infiltration, no drilling; and
- Pluvial infiltration with drilling.

The normal infiltration cases considered 500 vectors each. The pluvial scenarios considered only 98 vectors, because of a problem with long run times. There were a total of 29 radionuclides initially included in the analysis. Results of the scenarios were used to generate the conditional CCDFs for each scenario, and combined with scenario probabilities to produce an overall CCDF. The input and output vectors were also used to generate sensitivity analyses, using multiple linear regression and several other techniques.

The IPA Phase 1 analysis relied heavily on manual manipulation of files, rather than the relatively high degree of automation provided by the system driver for Phase 2. The *LHS*, *NEFTRAN*, and sensitivity/uncertainty analyses were submitted manually and used by the analyst in sequence. By contrast, in IPA Phase 2, the staff developed a more sophisticated model and computer code to represent the performance of a geologic repository. The principal features of the staff's advanced model were:

- The geologic repository is represented by seven repository sub-areas.
- Three transport pathways were considered—gaseous, aqueous, and direct.
- Treatment of mechanistic models of waste package failure (including a specified number of early failures).
- Consideration of four disruptive events—climate change, seismic shaking, human intrusion (including exploratory drilling), and magmatic eruption—for a total of 16 probability combinations.
- Considered only 20 radionuclides, on the basis of screening.

The principal features of the staff's more sophisticated computer code in IPA Phase 2 are:

- The execution of the various scenarios is now performed under the control of the TPA *executive module*, with consistent data provided automatically to all of the consequence modules.
- The *system executive* is responsible for the invocation of the modules and the reading of the release values after each module is run. It is designed to calculate the CCDF for releases by nuclide, pathway, repository sub-area, scenario, and overall.

Although both internal and external modes[2] are available for the TPA *executive module*, the internal mode is preferred. This mode ensures that all the modules receive the same input data automatically. The individual modules obtain much of their control and data information from the *system executive*; therefore the *executive* exercises a degree of precision when invoking the module to execute a particular scenario or vector. The communication mechanism used for this is formatted ASCII files. These files are called global data files, since much of the content is common to the consequence modules.

All the sampled parameters from all of the modules are generated during a single run of the *LHS* module code, and then each module can select its sampled parameters from the file, using identical techniques. A mapping file serves to aid

[2]"Internal" versus "external" refers to the manner of code execution and the time at which the output files from the consequence modules are generated. In the internal mode, consequence modules are run and cumulative radionuclide releases calculated as the system code is executed. In the external mode, the modules are separate from the system code, and as a result, the cumulative releases can be generated and placed in files at any time before iteration of the system code.

the module in extracting the correct parameters from the *LHS* output file, since the *LHS* program does not organize its output with keys for each parameter. The map file contains the exact location of each sampled parameter for a given computational module.

As noted above, in IPA Phase 2, the repository was divided into additional zones (now seven), and the normalized release values were stored separately for each repository sub-area, as well as each of the 20 nuclides. Moreover, as discussed in Section 2.1.3, several new scenario and consequence modules were added to the system code, namely seismicity, volcanism, $^{14}CO_2$ gas flow, and dosimetry.

Finally, the TPA *executive* can produce a CCDF plot in the TECPLOT format for each scenario, as well as a total CCDF for all of the scenarios, from the single internal array that stores the normalized release values from all of the consequence modules.

2.3 Conclusions and Suggestions for Future Work

A number of conclusions and recommendations for further work can be drawn from the design, development, and execution of the TPA computer code (including its modules), during IPA Phase 2. Several of these conclusions and recommendations were first proposed following IPA Phase 1, but not fully implemented during Phase 2. To the extent that these conclusions and recommendations still apply, and should continue to be considered in future IPA work, they are repeated below.

1—The process of abstraction.

Deriving simple, efficient computational modules (and attendant computer codes) from more complete and complex models, to represent the performance of components of the repository system for use in probabilistic simulations, is an issue that requires more focus and analysis. As noted in IPA Phase 1, general approaches for achieving satisfactory computational speed, while maintaining an appropriate degree of physical representativeness, need to be evolved; this still continues to be the case, based on the staff's Phase 2 work.

For example, in IPA Phase 2, the staff discovered that significant modification (simplification) had to be done to the original design concepts during the eventual implementation of the TPA computer code. As noted earlier, the computational requirements of modules became prohibitive, and significant simplifications were required in order to achieve acceptable execution times. Hence, it is recommended that more attention be paid to the appropriateness of abstracting the complicated phenomena, to achieve efficient mathematical models. Moreover, it is recommended that the TPA computer code (and its modules) be considered a dynamic entity, and modifications should readily be pursued, to achieve a more effective TPA computer code.

Finally, considering that the connection between more representative codes and the simpler codes used to demonstrate compliance is likely to be a major issue in licensing, the staff continues to believe that the abstraction process may be a subject suitable for the development of regulatory guidance in the future.

2—Software documentation.

During the development of several computational modules, a number of difficulties were encountered related to software quality assurance (QA), including the lack of: documented module designs, module integration designs, and documented module testing. Hence, it is recommended that more attention in the future be paid to QA procedures.

3—Continue to evaluate additional computer codes, that could not be acquired and evaluated during the IPA Phase 1 or Phase 2 efforts, to determine whether existing codes can meet the NRC modeling needs, or whether additional code development is needed.

As summarized in Section 2.1.3 and noted in subsequent chapters of this report, several computer codes that appeared to be promising in terms of providing missing parts of the analysis, and that offered improved treatment of certain aspects of modeling, were evaluated for use in the IPA Phase 2 demonstration. These codes included *BIGFLOW* (Ababou and Bagtzoglou, 1993), *DITTY, DCM3D* (Updegraff *et al.*, 1991), *MODFE* (Torak, 1992), *NEFTRAN, PHREEQE* (Parkhurst *et al.*, 1980), *PHREEQM* (Nienhuis and Appelo, 1990), and *UCBNE41* (Lung *et al.*, 1987).

However, the staff believes that there are additional computer codes that need to be evaluated that might provide some additional assistance to the staff in its performance assessment efforts. Some of the codes that might be worthwhile investigating in the future are: *TOUGH* (Pruess, 1987), *TOSPAC* (Dudley *et al.*, 1988), *AREST* (Apted *et al.*, 1989), and *EBSPAC* (see Sridar *et al.*, 1993).

3 SCENARIO ANALYSIS MODULE[1]

3.1 Introduction

In IPA Phase 1, a general approach to scenario development was identified, but, because of resource constraints, implemented only to a limited extent (see "Methodology for Scenario Development," in Codell *et al.*, 1992, pp. 31–39). Therefore, to identify scenarios for that effort, a less systematic, more expedient approach was taken. That approach involved selecting two classes of events (climate change/pluvial conditions and human intrusion by exploratory drilling) for the analysis, in part, because the modeling variations needed to accommodate these events in the consequence analysis were not excessive. The probability of occurrence for exploratory drilling was determined by following the guidance provided by the U.S. Environmental Protection Agency (EPA), in Appendix B of 40 CFR Part 191[2] (*Code of Federal Regulations*, Title 40, "Protection of Environment") (see EPA, 1993; 58 *FR* 7936). The probability of climate change/pluvial conditions was determined arbitrarily. A recommendation arising from the IPA Phase 1 effort was to develop and demonstrate a mathematically rigorous, scientifically robust method for scenario analysis (see Codell *et al.*, 1992, p. 91).

In IPA Phase 2, the staff has applied the Sandia National Laboratories (SNL) scenario selection procedure to generate scenarios for use in the IPA Phase 2 consequence analysis. The SNL methodology has been applied by the SNL staff to hypothetical basalt and salt sites, and by international organizations involved in the geologic disposal of high-level radioactive waste (HLW). This section briefly summarizes the SNL procedure and then documents the development of a final set of scenario classes and corresponding probability estimates for use in the IPA Phase 2 effort.

In this analysis, a "scenario" is defined as any postulated future sequence of events and processes (EPs) external to the repository system which is sufficiently credible to warrant consideration of its projected effect on repository performance. These sequences represent some of the potential ways in which the repository system environment might evolve. Such alternate evolutions may result from the occurrence of natural phenomena and/or from human-initiated activity, and could affect the release and transport of radionuclides from the repository to the accessible environment. A "scenario class" is a unique combination of processes and/or events without regard to the order in which they occur.

3.2 Description of the SNL Scenario Selection Procedure

The SNL scenario selection methodology (Cranwell *et al.*, 1990) consists of a five-step process that, when completed, provides a set of scenarios, with corresponding probabilities, for use in the consequence analysis of a potential HLW disposal site. These steps are:

No. 1. Identification of those EPs deemed to be potentially disruptive of long-term isolation of HLW at a disposal site.

No. 2. Classification of these EPs.

No. 3. Screening of these EPs, using well-defined criteria.

No. 4. Formation of scenarios by combining the EPs remaining after screening.

No. 5. Screening of these scenarios, using well-defined criteria.

---

[1]The figures shown in this chapter present the results from a demonstration of staff capability to review a performance assessment. These figures, like the demonstration, are limited by the use of many simplifying assumptions and sparse data.

[2]Currently, a revised set of standards specific to the Yucca Mountain site is being developed in accordance with the provisions of the Energy Policy Act of 1992. The Energy Policy Act of 1992 (Public Law 102–486), approved October 24, 1992, directs NRC to promulgate a rule, modifying 10 CFR Part 60 of its regulations, so that these regulations are consistent with EPA's public health and safety standards for protection of the public from releases to the accessible environment from radioactive materials stored or disposed of at Yucca Mountain, Nevada, consistent with the findings and recommendations made by the National Academy of Sciences, to EPA, on issues relating to the environmental standards governing the Yucca Mountain repository. It is assumed that the revised EPA standards for the Yucca Mountain site will not be substantially different from those currently contained in 40 CFR Part 191, particularly as they pertain to the need to conduct a quantitative performance assessment as the means to estimate postclosure performance of the repository system.

3.2.1 Step No. 1—Identification of Events and Processes

The initial step in the SNL procedure is the identification of EPs that are considered to be potentially disruptive of waste isolation at the particular HLW disposal site in question. These EPs, which should be as comprehensive and complete as possible, are identified by persons knowledgeable in the fields of earth science and waste management and would include both natural and human-induced phenomena. The use of generic lists of EPs (e.g., see International Atomic Energy Agency (IAEA), 1981) can help to ensure that important site-specific phenomena are not overlooked.

3.2.2 Step No. 2—Classification of Events and Processes

The second step in the methodology is the categorization of the EPs. This can be accomplished using any of a number of different classification schemes. Criteria for classification might include:

- The origin and physical characteristics of the EPs (i.e., natural, human-initiated, or waste-/repository-induced);
- The manner of influence the EPs have on the repository system and surrounding geology (e.g., whether they affect near-field or far-field processes or phenomena);
- The time of occurrence (e.g., between 0 to 100, 101 to 1000, or 1001 to 10,000 years); and
- The probability of occurrence (e.g., likely, unlikely but possible, or very unlikely).

The classification of EPs provides an opportunity to ensure that important phenomena are not omitted, and as such, this step is iteratively linked with Step No. 1. In addition, this particular step also imparts an initial organization to the collection of EPs, which is needed to begin developing and analyzing potential scenarios.

3.2.3 Step No. 3—Screening of Events and Processes

Given the potentially large collection of EPs that could be identified and the correspondingly large number of scenarios that could be formed from these EPs, it is essential that the analysis focuses on those EPs that are sufficiently credible to warrant consideration so that the task of scenario identification (and the subsequent consequence analysis) remains tractable. Therefore, using well-defined criteria, it should be possible to eliminate some of the identified and classified EPs from further consideration. Basic screening criteria include:

- The physical reasonableness of occurrence of the EP at the site;

  EPs whose occurrence are impossible because of the characteristics of the waste, facility, or site can be removed from the analysis, based on a lack of physical reasonableness.

- The probability of occurrence of the EP; and

  EPs with very low probabilities of occurrence also can be screened from further consideration. The value used as the criterion for screening should be consistent with the appropriate regulations. For example, EPA guidance in 40 CFR Part 191 is such that categories of EPs estimated to have less than 1 chance in 10,000 of occurring over 10,000 years need not be considered.

- The potential consequences associated with the EP's occurrence.

  EPs may be screened if their occurrence has insignificant potential effects on the natural properties of the site (e.g., the hydraulic head distribution). Such a judgment would require flow and thermomechanical analyses to be made. In addition, EPs with similar consequences may be grouped together as long as their probabilities are appropriately combined.

3.2.4 Step No. 4—Combination of Events and Processes into Scenarios

In the fourth step, the EPs remaining after screening are combined into scenarios. These scenarios are formed using a logic diagram or similar device, to ensure that all possible combinations of the EPs are identified and examined. The number of scenarios developed will depend on the number of EPs available (i.e., if n phenomena remain following initial screening, then 2^n scenarios are possible). For example, in Figure 3–1, five EPs

(designated *R1, R2, T1, T2,* and *T3*) are linked to form 32 (2^5) scenarios, where, under the SNL procedure, each specific path through the tree is called a "scenario."

In Figure 3–1, one of the combinations is labeled "base case." Under the SNL methodology, the base case scenario represents an initial conceptualization of the disposal system, which includes the characteristics of the geologic site, the underground facility, and the emplaced waste (Bonano *et al.*, 1989). In this scenario, all components of the engineered barrier system (EBS), consisting of the underground facility and the waste packages (10 CFR Part 60.2), are assumed to perform as designed, undisturbed by external phenomena (e.g., igneous activity, exploratory drilling). As shown in the figure, other scenarios will be perturbations to these nominal conditions (Cranwell *et al.*, 1990).

3.2.5 Step No. 5 – Screening of Scenarios

The newly-formed scenarios are then screened using criteria similar to those applied in the initial screening of the EPs: physical reasonableness, probability, and potential consequences. Screening based on physical reasonableness, for example, would eliminate incompatible combinations of various EPs.

Provided that the EPs are mutually independent (i.e., the occurrence or non-occurrence of one EP has no influence on the subsequent occurrence or non-occurrence of another EP and vice versa), individual scenario probabilities can be calculated by multiplying the likelihoods of the different EPs comprising the scenario. If the EPs are not mutually independent, then conditional probabilities are used. The probability value used should be consistent with appropriate regulations.

Scenarios can be screened if there are no consequences associated with their occurrence. Consequences, in this case, refer to either radionuclide discharges to the accessible environment or to the health effects resulting from such releases.

3.3 IPA Phase 2 Scenario Development Using the SNL Methodology

The development of scenario classes for IPA Phase 2, using the SNL methodology, was conducted by the IPA staff over a period of several months. Bonano *et al.* (1990) present the process of formalizing the elicitation and use of expert judgment in the performance assessment of HLW repositories in deep geologic formations. However, this *formal* process was not followed in the collection and use of the opinions expressed in the staff discussions. Instead, an *informal* approach was taken in which open discussions of the potentially disruptive EPs, their possible effects on the system, and their relative likelihoods were combined with more detailed individually-submitted written information on the same topics, with documentation of the staff member's reasoning, supported by appropriate references and/or general principles.

3.3.1 Identification and Classification of Events and Processes

Before identifying an initial set of potentially disruptive phenomena for consideration, the boundaries of the repository system first were defined. In an approach similar to that taken in the IPA Phase 1 scenario development effort (Codell *et al.*, 1992; pp. 31–32), these boundaries were chosen to be largely coincident with those of the accessible environment. For this analysis, the repository system was defined as extending 5 kilometers horizontally from the outer perimeter of the proposed repository, and vertically from the land surface to a depth just below the current water table.

Phenomena initiated beyond these boundaries were classified as external perturbations of the system, even if the effects of the phenomena occurred within the repository. Thus, for example, fault displacement in the repository would be classified as an external event, because the tectonic forces responsible for initiating the movement can be considered external to the system. Exploratory drilling would be classified as an external event for similar reasons. Phenomena, such as waste canister corrosion and borehole seal degradation, on the other hand, occur within the system boundaries, and thus would be classified as internal processes. Under this classification, external phenomena were retained for consideration in the scenario analysis, whereas

Figure 3–1 Potential combinations of two releases (R) and three transport (T) phenomena (Adopted from Cranwell *et al.* (1990))

internal events and processes, including features of the site (e.g., faults), were assumed to be incorporated into the models and data bases used to describe the system. This approach differs from that proposed by Cranwell *et al.* since they include internal processes and features (e.g., borehole seal degradation, faults) in their scenario analysis (Cranwell *et al.*, 1990; pp. 26, 44–53).

As discussed previously in Codell *et al.* (1992; pp. 31–32), the approach adopted here differs from those proposed by other analysts. Hodgkinson and Sumerling (1990), for example, describe a scenario development approach in which no distinction is made between "internal" phenomena and those occurring outside the repository. Under this scheme, processes such as waste canister corrosion would be combined into scenarios for analysis, and as a result, their list of "events, features, and processes," incorporating both internal and external phenomena, contains nearly 150 entries. Even after screening of these entries, the number of scenarios that could be constructed would be quite formidable. The approach chosen for the IPA Phase 2 analysis greatly reduces the number of scenarios that can be generated, and thus the complexity of the total-system performance assessment.

For the IPA Phase 2 scenario analysis, an initial set of potentially disruptive EPs (Table 3-1) was compiled from similar lists of those considered:

- In the IPA Phase 1 scenario analysis (Codell *et al.*, 1992);
- In the SNL work of Cranwell *et al.* (1990); and
- From the generic list of EPs assembled by the IAEA (1981).

This list should not be considered complete nor comprehensive; further work may identify additional EPs that warrant at least initial consideration within a scenario analysis for the Yucca Mountain site.

It is important to note that these EPs can be considered as "categories" of events and processes since, implicitly, the entire range of possible manifestation styles, locations, and times (i.e., "subevents" and "subprocesses") is contained under each identified EP. In keeping the detail for the EPs at this broad level, the staff considers that the EPA screening criteria based on probability (i.e., less than 1×10^{-4} over 10,000 years) can be applied more appropriately. Also, because categories of EPs are being considered, classes of scenarios, rather than explicitly-defined individual scenarios, will be produced by this analysis. Consequence modeling of individual scenarios representing the scenario classes generated through this procedure is discussed in the following chapters.

3.3.2 Screening of Events and Processes

All three of the screening criteria (i.e., physical reasonableness, probability of occurrence, and potential consequences) identified in Section 3.2.3 were used to screen the initial set of EPs for this analysis. Flow and thermodynamic calculations, suggested by Cranwell *et al.* (1990), were not used in screening based on potential consequences, primarily because the numerical computer codes necessary for such analyses were not available. Instead, screening on this criteria was based on staff judgment.

After screening, six EPs remained for staff consideration:

- Igneous Activity—Intrusive
- Igneous Activity—Extrusive
- Faulting
- Seismicity
- Climate Change
- Exploratory Drilling

For this scenario development effort, these six EPs were further reduced to four by combining "Intrusive" and "Extrusive Igneous Activity," and "Faulting" and "Seismicity," into single EPs. In addition, with respect to a Faulting/Seismicity EP, consequence analysis modeling for IPA Phase 2 focused solely on the effects of seismicity, and therefore, the final set of EPs to be combined into scenarios for IPA Phase 2 was:

- Igneous Activity
- Seismicity
- Climate Change
- Exploratory Drilling

Table 3-1 Initial Set of Potentially Disruptive Events and Processes

Natural Events and Processes	*Human-initiated Events and Processes*
A. Igneous Activity	A. Climate control (e.g., greenhouse effect)
1. Extrusive	B. War
2. Intrusive	C. Nuclear weapon testing at Nevada Test Site
B. Tectonic Activity	D. Exploratory drilling for natural resources
1. Regional uplift	E. Mining
2. Regional subsidence	1. Surface-based (open pit)
3. Seismicity	2. Underground shafts and drifts
4. Faulting	F. Large-scale alterations to hydrology (e.g., dams)
C. Climatic Conditions	
1. Current climate—extreme phenomena	
2. Climate change	
D. Other	
1. Sea level change	
2. Tsunamis/seiches	
3. Meteorite impact	

3.3.2.1 Rationales Used to Screen Events and Processes

The rationales used to screen particular initial EPs from further consideration in IPA Phase 2 are discussed next. These rationales are necessarily preliminary and will need to be revisited when the appropriate models, codes, and data are available for this purpose.

1. Regional uplift/subsidence

Potential consequences associated with the occurrence of these initial EPs were deemed to be insignificant. The proposed repository will lie approximately 300 meters below the ground surface and about 180 to 400 meters above the regional water table, whereas rates of regional vertical tectonic movement are estimated to be less than 3 centimeters/1000 years (DOE, 1988b; p. 1-28). Therefore, regional uplift/subsidence alone would appear to have negligible direct effects on repository performance over the 10,000-year period of regulatory interest. The potential impacts of erosion, both regional denudation and local incision, associated with current and projected climatic conditions, should be examined, if necessary, in future analyses.

2. Current climate (extreme phenomena)

This initial EP was screened because such phenomena would be included under the current climate conditions, which are part of the base-case scenario class.

3. Sea level changes

This initial EP was screened because of insignificant potential effects on repository performance. Yucca Mountain and vicinity are part of the Death Valley internally-drained groundwater basin system, and therefore, significant sea level changes would not affect the stream baselines or the water-table elevation (Ross, 1987). In addition, changes in the sea level are related to global phenomena and processes, such as climatic variations and plate tectonics. Site performance may be more sensitive to these processes instead.

4. Tsunamis/seiches

These initial EPs were screened because of the low probability of occurrence at the site. Yucca Mountain is located several hundred miles from the Pacific Ocean, in an arid climate, and is not overlain by large bodies of surface-water necessary for seiche formation (DOE, 1988a; p. 29).

5. Meteorite impact

This initial EP was screened because of the low probability of its occurrence at the site. Various studies have calculated the likelihood of a meteorite impact sufficient to disturb a repository at depth to be in the range of 10^{-13}/square kilometer/year (Cranwell *et al.*, 1990).

6. Climate control

This initial EP was subsumed under the initial EP: "Climate Change," because consequences associated with its occurrence would be similar to those associated with natural climatic changes.

7. War

Disruption of a repository at Yucca Mountain would likely require the direct impact of a thermonuclear weapon; however, Yucca Mountain does not appear to be a prime candidate for such a focused attack. In addition, any radioactive release associated with the breaching of the repository would be a minor consideration in a war in which nuclear weapons were employed. For these reasons, this initial EP was screened from further analysis.

8. Nuclear weapon testing at the Nevada Test Site (NTS)

Subsurface testing of nuclear weapons by the U.S. government has been conducted at the NTS to the north and northeast of Yucca Mountain. Currently, however, no weapon tests are being conducted because of the U.S. self-imposed moratorium against such testing, which extends until 1996. Should subsurface nuclear weapon testing be resumed in the future, any effects on site performance in response to the detonation of these weapons would be experienced in terms of seismicity. For this reason, this initial EP was subsumed under the initial EP: "Seismicity."

9. Mining

Mining for mineral resources at Yucca Mountain could involve either surface (e.g., open pit) or subsurface techniques (e.g., shafts and/or drifts). The seismic effects of surface and subsurface mining operations would not appear to have a significant effect on the post-closure performance of a mined geologic repository at Yucca Mountain (Raney, 1990a). The possible impacts of an open pit mine as a potential site of localized infiltration should be examined, if necessary, in future analyses. Subsurface techniques used to exploit a proposed mineral deposit below the repository horizon could result in the repository being intersected. If the repository were intersected, it is assumed that those engaged in such mining activities would recognize the incompatibility of the wastes with their exploration, seal the mined openings, and abandon their activities.

10. Human-initiated large-scale alterations to hydrology

Large-scale alterations to the groundwater hydrology could involve the construction of dams to surface flow or of irrigation systems for farming. The construction of a dam in the Yucca Mountain area would appear to be unlikely, given the arid regional climate and the lack of significant perennial streams in the area (DOE, 1988a; p. 29). The use of ground water for irrigation could have the net effect of lowering the water table, and thus, increasing the thickness of the unsaturated zone beneath the repository. This might be beneficial to site performance. Therefore, this initial EP was screened from further analysis.

3.3.2.2 Rationales Used to Retain Events and Processes for Further Consideration

The events and processes retained for consideration after screening are described in detail next. For each EP, the following is provided: (1) a description of the EP for the Yucca Mountain region; (2) a short summary discussion of potential impacts on repository performance; (3) a discussion of some current issues in estimating probabilities for the particular EP; and (4) the approach (and results) used in IPA Phase 2 for estimating the probability of occurrence for the EP.

1. Igneous activity (Intrusive and Extrusive)

Description: In the Yucca Mountain region, volcanic activity approximately 16 million years

ago (Ma), produced several large caldera complexes located to the north and west of the proposed site (e.g., Timber Mountain Caldera) (Figure 3–2). These calderas are associated chiefly with the explosive eruptions of silicic volcanic rocks. Yucca Mountain is underlain by a sequence of these silicic rocks from about 1,000 to 3,000 meters thick, consisting mainly of welded and non-welded ash-flow and air-fall tuffs (DOE, 1988a; p. 17). Volcanic flows and breccias commonly occur underground in the northern part of Yucca Mountain but are rare in the southern part.

Approximately 6 to 8 Ma, the volcanic activity in the region changed into a more quiescent basaltic-flow type, characterized by low volume eruptions of short duration (DOE, 1988a; p. 18). Within a 30 kilometer radius of the proposed repository site, 29 post-caldera basaltic vents can be identified (Crowe *et al.*, 1992). In addition, within the immediate vicinity of Yucca Mountain, basaltic dikes are exposed in the northern reaches of Solitario Canyon, borings in the vicinity of Yucca Mountain have occasionally intersected basalt, and further away, relatively extensive basaltic intrusions have been mapped in the area of Paiute Mesa. The youngest basalt-type volcanic feature in the area, located at the southern edge of Crater Flat, is the Lathrop Wells cinder cone, which may have originally formed approximately 130,000 years ago, with possible further eruptions up to as recently as 20,000 years ago (DOE, 1988a; p. 18).

At present, there is considerable debate concerning the age of the volcanic features in the Yucca Mountain region. The variance in the opinions stems from differences in both methods of evaluation and interpretations of available data (see Crowe *et al.*, 1995). The difference is greatest for the youngest features, such as the Lathrop Wells cone, and decreases as older and older material is evaluated.

Potential impacts on radionuclide release and transport: Depending on its location and magnitude, igneous activity could directly or indirectly affect the waste isolation capabilities of a proposed repository at Yucca Mountain. Direct impacts could result from the intersection of the repository by intruding igneous bodies. Such intersections could severely disrupt the EBS through:

- Mechanical disruption of the underground facility and redistribution of the local stress regime;
- Contact of the magma with the waste package canisters,[3] which may result in displacement, fracturing, and shearing of the canisters (in addition to thermal and chemical alterations);
- Entrainment of the potentially damaged waste packages in the rising magma body; and
- Potential release of radionuclides at the surface associated with volcanic activity.

Indirect impacts of igneous activity on repository performance could include:

- Formation of a regional hydrothermal circulation system, if the intrusive body were large enough;
- Creation of barrier(s) to ground-water flow, possibly leading to a temporary or permanent change in the water-table elevation;
- Alteration of regional percolation and ground-water flow paths;
- Thermal and geochemical alteration and degassing associated with the magmatic fluids;
- Localization of surface infiltration due to volcanic eruptions; and
- Creation of preferential radionuclide release pathways associated with accompanying fracturing and seismicity.

Probability of occurrence considerations: Estimates of the occurrence of future igneous activity require numerous assumptions concerning the temporal and spatial variability of such activity. To begin addressing such questions of variability, data collected through a program of regional and site surface and subsurface investigations must be available. These data should include the locations, distribution, and physical characteristics of the magmatic features (actual and inferred) in the area, as well as the ages of these various features.

[3]The term "waste package" is used here synonymously with "container" and "canister."

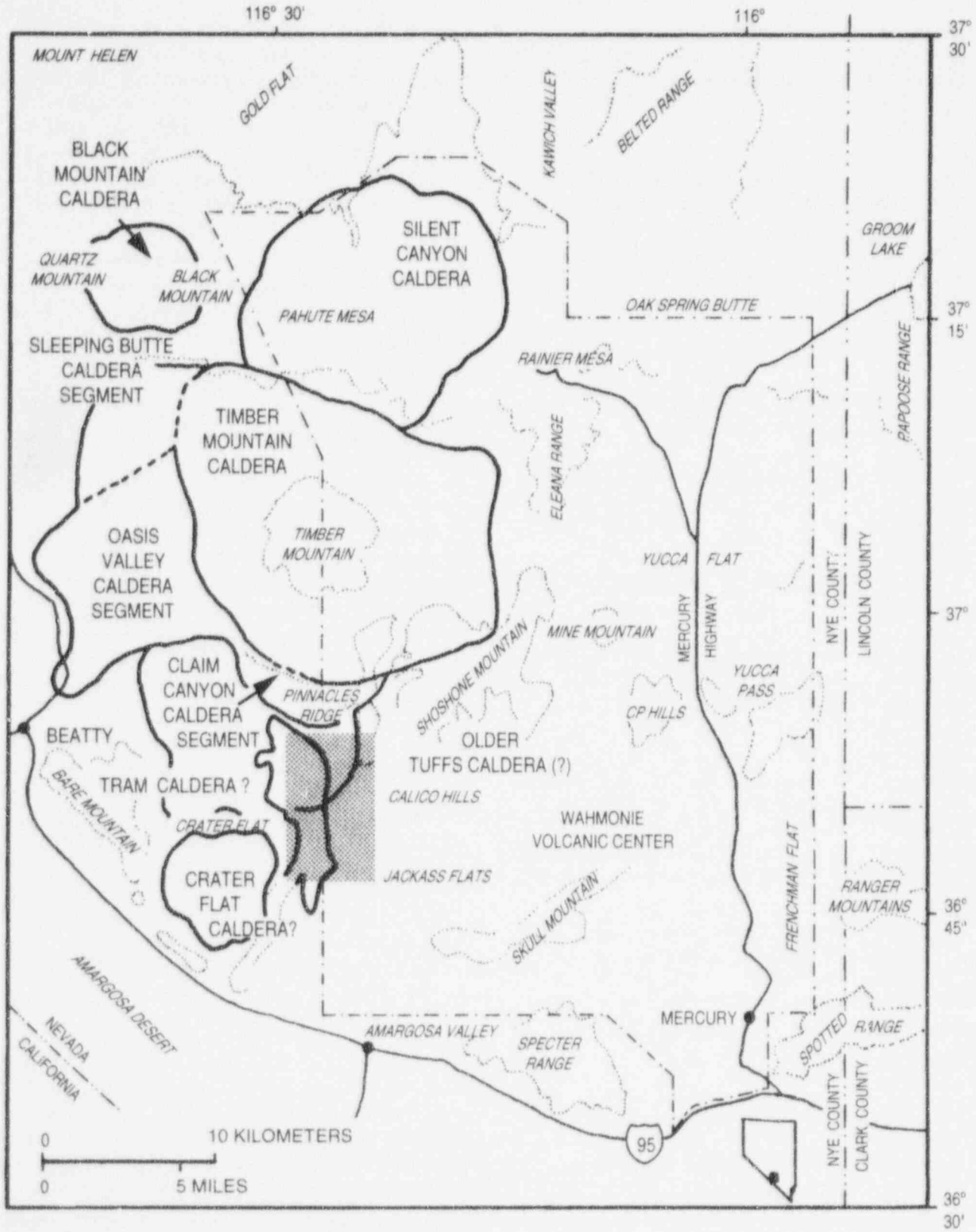

Figure 3–2 Calderas of the Southwest Nevada volcanic field near Yucca Mountain (Modified from Maldonado and Koether (1983))

The program of investigations must also address the extent to which some phenomena may still be present and undetected, taking into account the degree of resolution achieved by the investigations.

The development of a predictive model of future igneous activity for Yucca Mountain requires a description of the igneous "life history" (past, present, and future) for the region, based on interpretations of the collected data and calculated age dates. Various conceptual models based on these interpretations would be necessary, in areas such as:

- The region likely to host potential future igneous activity;
- The mechanics of magmatic emplacement (e.g., mantle-derived magma vs. crustal magma chamber; the rate of magma production in the subsurface; the amount of magma necessary for intrusive or extrusive activity); and
- The cyclic nature of the magmatism in the region (e.g., waxing/waning, monocyclic/polycyclic, relationship of local region to a larger region).

To determine the parameters required for igneous activity probability calculations, it is necessary to define a particular region in which the appropriate data would be gathered. The definition of such regions will need to be based on an understanding of the relationship, both temporal and spatial, between the regional tectonic features (e.g., variously oriented fault zones) and identified and inferred intrusive and volcanic features. Several studies have attempted to do this for the Yucca Mountain region (e.g., Crowe *et al.*, 1982; Crowe and Perry, 1989; and Smith *et al.*, 1990). Crowe and Perry (1989), for example, defined the Crater Flat Volcanic Zone (CFVZ) in their attempt to identify a region potentially more likely to host future volcanic activity (Figure 3–3). The northwest-trend of Quaternary-age volcanic cones (recognized and inferred) and lava flows in the CFVZ is thought to be related to a strike-slip fault beneath Crater Flat and the Amargosa Valley postulated by Schweickert (1989). Smith *et al.* (1990) identified a larger region, the "Area of Most Recent Volcanism" (AMRV), based primarily on the age of the various volcanic centers in the Yucca Mountain region (i.e., including only those younger than 4.5 Ma) (Figure 3–4). Within the AMRV, Smith *et al.* defined narrow north-northeast-trending "high-risk" zones corresponding to cinder-cone alignment orientations that they hypothesize may develop as a result of structural control (Figure 3–5).

Once an appropriate region has been defined, magma production rates may be estimated from the calculated volume of magma extruded at the surface over a particular time period. These production rates have been used to determine the recurrence time for the formation of representative volumes of past magmatic cycles in the Yucca Mountain region (Crowe *et al.*, 1982; and Crowe and Perry, 1989). Based on the available data, Crowe *et al.* (1982) suggest that there has been a decrease in the volume of volcanism (i.e., erupted volumes) through time in the NTS region. Magma production rates based on estimated surface magma volumes may not accurately reflect "true" production rates, because the calculations ignore the subsurface component of the igneous activity. Shaw (1987) has proposed that, in general, only about one-third of the total magma production is reflected at the surface.

To adequately assess the risk to a proposed repository site from future igneous activity, it is also important to determine whether there is a cyclic nature to the activity in the region (i.e., whether activity is waxing or waning, monocyclic or polycyclic, and if so, where in the cycle(s) the region is presently). Ideally, this assessment will be based on a relatively complete understanding of the complex processes involved in magma generation at depth and the controls on the magma's ascent to the surface or near subsurface. Lacking this understanding, other methods of describing the expression of igneous activity have been used. The potential rates of future volcanic activity for the Yucca Mountain region have been estimated using both counts of volcanic centers within a particular age range, and examination of magma production rates (Crowe *et al.*, 1982; Crowe and Perry, 1989; and Margulies *et al.*, 1992).

Crowe *et al.* (1982) used the rates of activity to calculate the range in the probability of volcanic

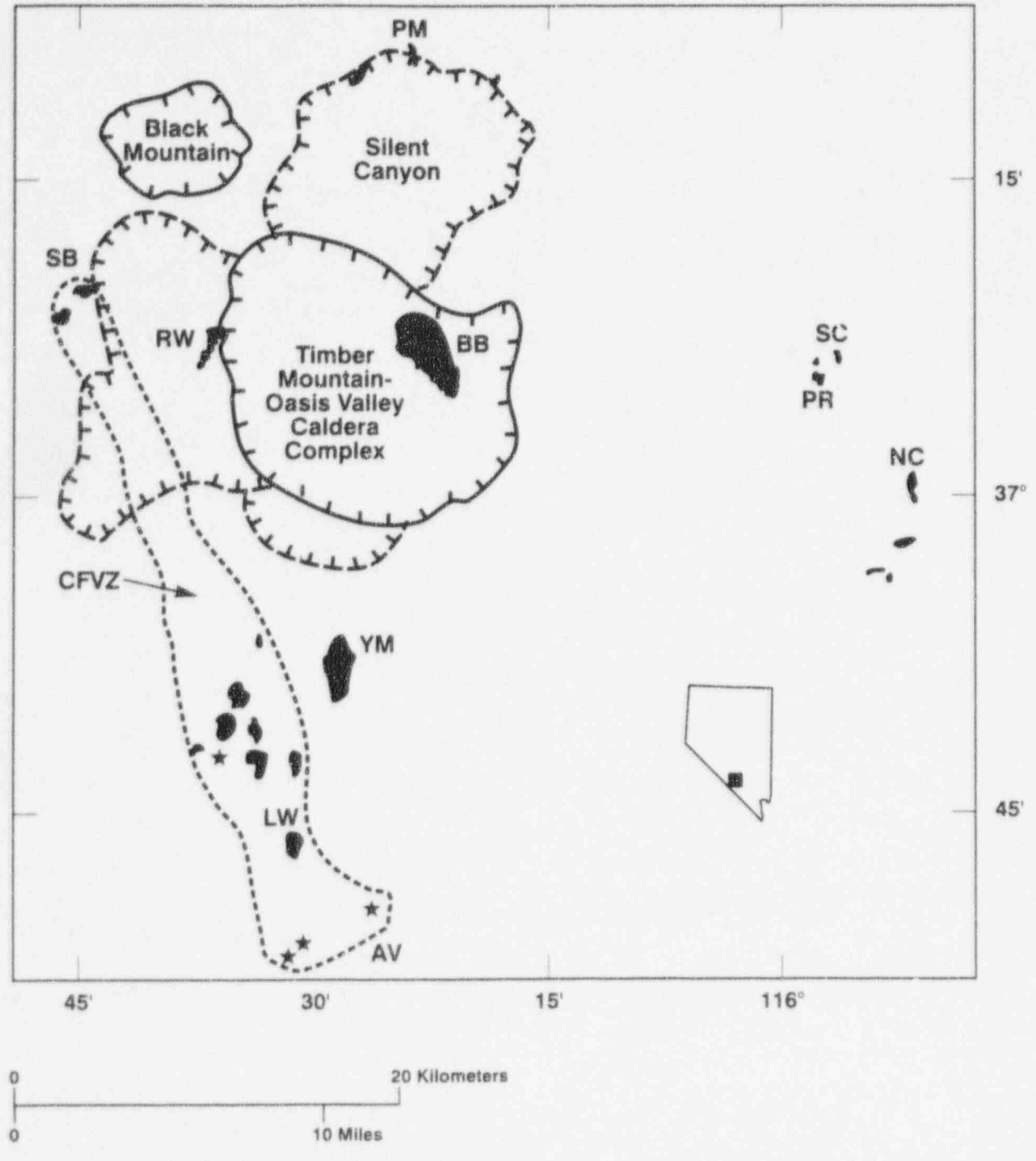

Figure 3–3 **Proposed Crater Flat volcanic zone (CFVZ)** (Generalized geologic map shows the distribution of the youngest episodes of basaltic volcanism in the Yucca Mountain region including outlines of major silicic caldera complexes. **AV:** Aeromagnetic anomalies of Amargosa Valley; **BB:** Buckboard Mesa basalt; **LW:** Lathrop Wells volcanic center; **NC:** Nye Canyon basalt; **PM:** Pahute Mesa basalt; **PR:** Paiute Ridge basalt; **RW:** Rocket Wash basalt; **SB:** Sleeping Butte volcanic centers; **SC:** Scarp Canyon basalt; **YM:** Yucca Mountain; and ***:** Inferred buried basalt centers or intrusive rocks. Modified from Crowe and Perry (1989, p. 328))

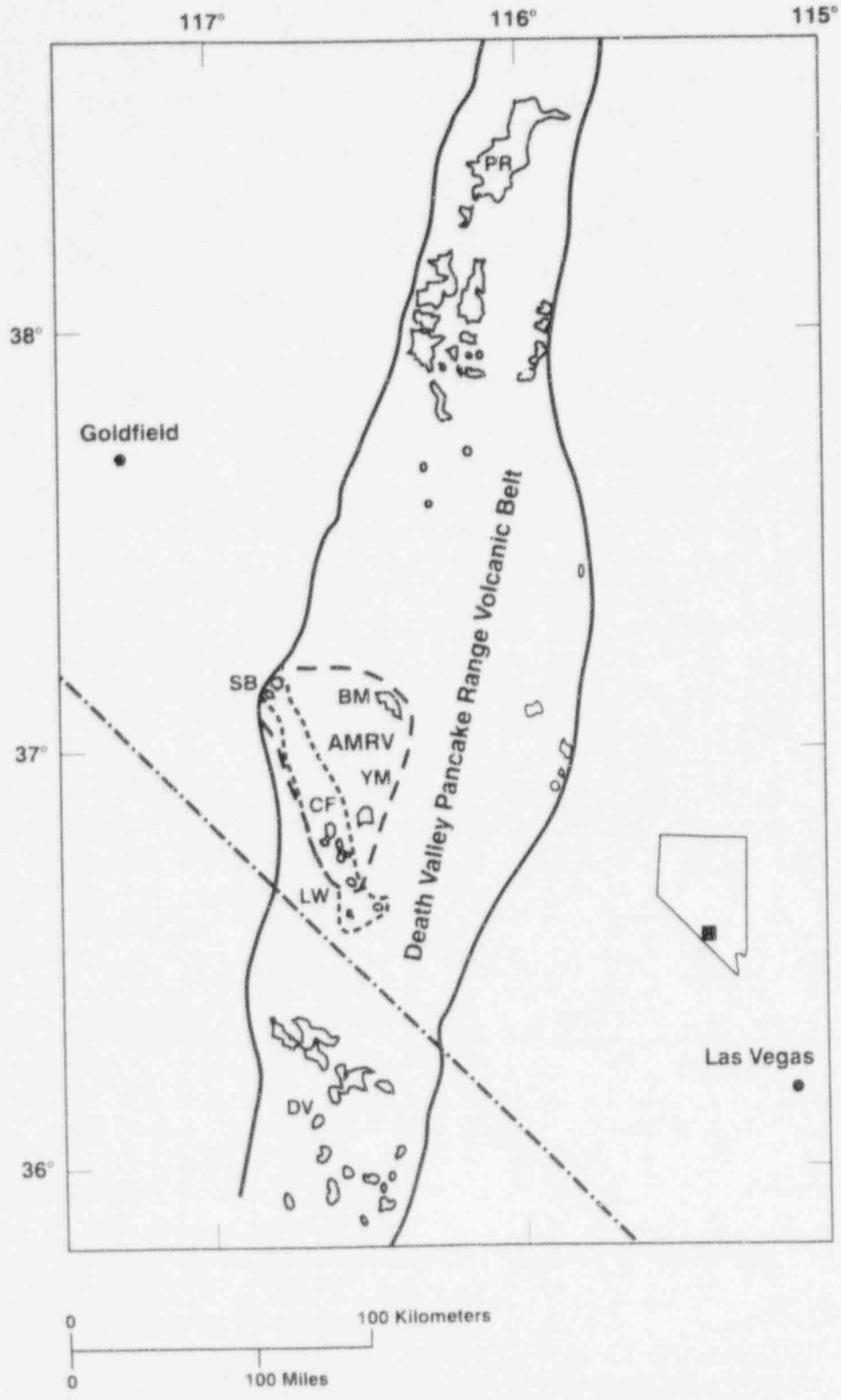

Figure 3–4 **Proposed area of most recent volcanism (AMRV)** (Volcanic areas are as follows: **BM:** Buckboard Mesa; **LW:** Lathrop Wells; **CF:** Crater Flat; **DV:** Death Valley; **PR:** Paiute Ridge; **SB:** Sleeping Butte; and **YM:** Yucca Mountain. Adopted from Smith *et al.* (1990).)

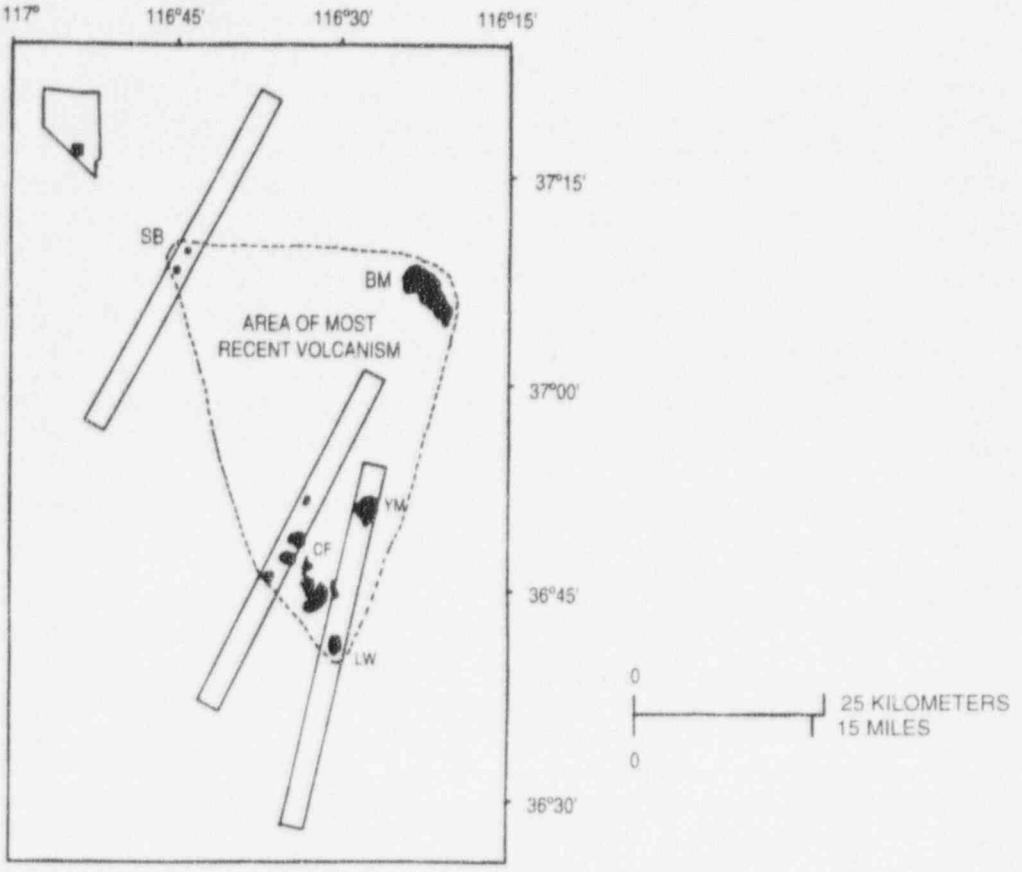

Figure 3–5 Postulated AMRV and "high-risk" zones (designated by rectangles) (Volcanic areas are as follows: **BM:** Buckboard Mesa; **CF:** Crater Flat; **LW:** Lathrop Wells; **SB:** Sleeping Butte; and **YM:** Yucca Mountain. Adopted from Smith *et al.* (1990).)

disruption of the proposed repository site. In determining these probabilities, Crowe *et al.* assumed a simple (homogeneous) Poisson distribution in time and space, such that the rate of magmatic eruption over time is constant and individual eruptive events occur independently. The calculated probabilities ranged from 3.3×10^{-10} to 4.7×10^{-8} per year, depending on:

- Whether the rate was determined from vent counts or magma production rates; and
- The region defined for the calculation.

The basic model proposed by Margulies *et al.* (1992) also assumed a temporally and spatially homogeneous Poisson distribution for volcanic centers. The recurrence rate in the model was estimated by summing the number of volcanos within the AMRV proposed by Smith *et al.* (1990), and dividing this number by the area of the AMRV and the time interval over which the vents have been active. The probability of an igneous event at Yucca Mountain was estimated to be 1.7×10^{-4} over 10,000 years. Margulies *et al.* also examined the effects of:

- A spatially varying recurrence rate, with zones of "enhanced magmatism" within the given region; and
- A change in the rate of occurrence of igneous activity for the region at a given time.

Homogeneous Poisson models, however, may not be appropriate for use in probability calculations for the Yucca Mountain region, because such models do not accurately describe volcano distributions, are unlikely to reflect accurately the probability of future volcanic activity, and may underestimate the probability of volcanic events. Statistical tests, such as the Hopkins F-test and the Clark-Evans test, indicate that, spatially, volcanos in the region do not have a homogeneous Poisson distribution (Connor and Hill, 1993). In addition, several investigators have argued that temporally homogeneous Poisson

models are inappropriate for volcanic fields in general and the probability of future volcanic events in the Yucca Mountain region in particular (Ho *et al.*, 1991; Ho, 1990, 1992; McBirney, 1992; and Sheridan, 1992). Additionally, the scarcity of and the uncertainty in the data for the region may not support the use of a simple Poisson model for predicting future volcanism in the area. For these reasons, employing such models to predict the future occurrence of volcanic activity may underestimate the risk of volcanism for the proposed Yucca Mountain repository site.

Probability for IPA Phase 2. As just discussed, a homogeneous Poisson model does not adequately describe the distribution of existing volcanic cones in the Yucca Mountain region. A model to estimate the probability of volcanic disruption of the proposed site will need to reflect the statistically significant amount of vent clustering in the region. In the IPA Phase 2 analysis, the staff based its probability estimate on the work of Connor and Hill (1993), who used a nonhomogeneous Poisson model calculated by near-neighbor methods to estimate the probability of volcanic disruption within an 8 square-kilometer area, over the next 10,000 years in the Yucca Mountain region. Assuming a late Quaternary recurrence rate of 7 ± 2 volcanos/million years, they estimated a probability of disruption of between 8.0×10^{-5} to 3.4×10^{-4} in 10,000 years, with most estimates between 1×10^{-4} and 3×10^{-4}. For the purposes of this scenario analysis effort, a probability equal to 1.5×10^{-4} over 10,000 years will be used.

Given that the probability of volcanic disruption in the vicinity of the repository is taken to be 1.5×10^{-4}, the probability of such a disruption per unit area (i.e., per square kilometer), p_v, is equal to 1.875×10^{-5}. Next, for the consequence modeling of the effects of igneous activity on repository performance (see Section 6.4), the likelihood of an intrusive dike was assumed to be 10 times that of a volcanic eruption. Therefore, the probability of an igneous event (formation of a volcanic cone or an intrusive dike) per unit area in the next 10,000 years is:

$$\overline{P_m} = 11 p_v \cong 2.1 \times 10^{-4} \quad . \qquad \textbf{(3-1)}$$

In estimating the consequences of igneous activity, a simulation area, A_s, bounding the repository site was assumed to ensure that any potential modeled igneous activity intercepting the repository will be included in the analysis. The size and shape of this area are not related to geologic structure in the region, but were solely based on the distribution of dike sizes assumed for the consequence analysis. The simulation area encompasses a 12- by 12-kilometer area around the repository.

Therefore, for the IPA Phase 2 scenario analysis, the probability of igneous activity within the simulation area over the next 10,000 years is:

$$P_m = \overline{P_m} A_s \cong 0.03 \, . \qquad \textbf{(3-2)}$$

This scenario probability is higher than probabilities estimated previously for the repository area (e.g., Crowe *et al.*, 1982; and Margulies *et al.*, 1992) because of a combination of factors. First, a nonhomogeneous Poisson model, rather than a homogeneous Poisson model, was used. Secondly, the probability of occurrence of an intrusive dike (assumed to be ten times that of a volcanic event) was included in the estimate. Finally, the region for which the probability estimate applies is a simulation area that bounds the repository and which is some 18 times larger than the repository area. It is also important to note, however, that because the simulation area is large enough to include all modeled igneous activity that may intercept the repository, a significant number of igneous events may not do so, and therefore, as modeled in the consequence analysis, such events may have no impact on repository performance. As a result, the probability of igneous activity directly affecting the repository is actually less than the given value.

As a final note, although the use of nonhomogeneous Poisson models can address the tendency of volcanic centers to cluster within a volcanic field through time, estimations of the probability of future volcanic activity (and intrusive activity, as well) will need to take into account additional geological information (e.g., pre-existing tectonic structure, strain rate) before more refined assessments of the probability of such activity can be made with confidence (Connor and Hill, 1993).

2. *Seismicity*

Description: Yucca Mountain is located in the Basin and Range tectonic province that

constitutes the southwestern portion of the North American crustal plate. The Basin and Range is characterized by more or less regularly spaced northerly-oriented subparallel mountain ranges and intervening alluvium basins formed by extensional faulting. The faulting in southern Nevada occurred mainly in response to the tectonic activity that has occurred in the Basin and Range over the last 15 million years (DOE, 1988a; p. 18).

Faults in the Yucca Mountain region can be grouped into three major systems depending upon their orientation: northwest (e.g., the Yucca Wash fault); northeast (e.g., the Rock Valley Fault zone); and north to northeast (e.g., the Solitario Canyon and Ghost Dance faults). Detachment faults have been postulated in many recent models of tectonism for the Yucca Mountain region (e.g., Scott and Rosenbaum, 1986).

Yucca Mountain is composed of a series of north-trending structural blocks that have been tilted eastward along west-dipping, high-angle normal faults. The proposed repository block is bounded by faults: on the west by the Solitario Canyon fault, on the northeast by the Drill Hole Wash structure, and on the east and southeast by the western edge of an imbricate normal fault zone. The Ghost Dance fault transects the proposed location for the underground repository. The faults at Yucca Mountain include both local faults related to the formation of calderas and longer regional faults of the Basin-and-Range type (DOE, 1988a; p. 20).

The site is in a region of diffuse seismicity (earthquake activity). In the past 150 years, eight major earthquakes (with magnitudes of 6.5 or more) have occurred within about 400 kilometers of Yucca Mountain. The nearest was the 1872 Owens Valley earthquake (estimated magnitude of about 8.25) some 145 kilometers west of Yucca Mountain. Although, in some instances, earthquake epicenters in the southern Great Basin appear to be related to mapped faults and regional structures, in the vicinity of Yucca Mountain, generally it has not been possible to correlate earthquakes with specific faults or tectonic structures (*op cit.*, p. 22).

Most of the major faults in the area of Yucca Mountain have experienced displacement during the Quaternary Period. Relatively moderate seismic activity continues today along strike-slip fault zones northwest, southwest, and southeast of Yucca Mountain, and there is evidence that seismic activity with associated surface fault displacements have occurred during this century in the Walker Lane shear zone (Yount *et al.*, 1993) which may extend through the site. Tables 3–2 and 3–3 (modified after DOE, 1988b; p. 1–166) provide a listing of recorded earthquakes of magnitude 4.0 or greater that have occurred in or near the Southern Great Basin since 1857. Meremonte and Rogers (1987) documented all historical Southern Great Basin earthquakes (i.e., from 1868 to 1978).

Studies of tectonic and stress regimes in the Yucca Mountain region are not complete, but they suggest the region is characterized by northwesterly extension, with normal and strike-slip faulting. The chief sources of information on the stress pattern are:

- *In-situ* stress measurements;
- Calculated earthquake focal mechanisms; and
- The orientation and nature (i.e., sense of movement) of the regional and local faults.

Large uncertainties exist in the assessment of the earthquake potential of geologic structures and seismogenic zones in the Southern Great Basin. These are caused, in part, by:

- The sparse historical record (past 150 years) of seismicity in the region;
- An equivocal association of historical earthquakes with mapped tectonic structures;
- Large uncertainties associated with critical fault parameters (e.g., fault segmentation, slip rate);
- Uncertainty associated with estimated recurrence intervals on local faults;
- The potential for earthquake activity to be both temporally and spatially clustered in the Basin and Range Province;

Table 3–2 Significant Earthquakes in or near the Southern Great Basin
(Modified from DOE (1988b, pp. 1-166 - 1-167).)

Date	*Name or Region*	*Magnitude (M) (Richter Scale)*	*Distance from Yucca Mountain (km)*
Earthquakes of $M \geq 6.5$ within 400 km of the Yucca Mountain Site			
9 Jan 1857	Fort Tejon	8 1/4	300
26 Mar 1872	Owens Valley	8 1/4	150
21 Dec 1932	Cedar Mountain	7.3	202
21 Jul 1952	Kern County	7.7	267
6 Jul 1954	Rainbow Mountain	6.8	331
24 Aug 1954	Rainbow Mountain	6.8	331
16 Dec 1954	Fairview Peak	7.2	276
16 Dec 1954	Dixie Valley	6.9	323
28 Jun 1992	Landers, CA	7.5	300

Table 3–3 Significant Earthquakes in or near the Southern Great Basin
(Modified from DOE (1988b, pp. 1-166 - 1-167).)

Date	*Name or Region*	*Magnitude (M) (Richter Scale)*	*Distance from Yucca Mountain (km)*
Selected Earthquakes of $M \geq 4.0$ within 100 km of Yucca Mountain Site			
28 Mar 1934	Gold Flat	4.5	52
13 Jun 1939	Northern Death Valley	5.0	73
14 Jun 1945	Last Chance Range	5.0	96
30 Aug 1948	Amargosa Desert	4.0	42
13 Jan 1950	Dome Mountain	4.1	19
16 Jun 1951	Eleana Range	4.5	72
28 Jan 1959	Skull Mountain	4.0	23
27 Mar 1961	Skull Mountain	4.4	28
6 Jan 1969	Pahute Mesa	4.5	44
10 Jan 1969	Pahute Mesa	4.6	32
5 Aug 1971	Massachusetts Mountain	4.5	42
15 Feb 1973	Ranger Mountains	4.0	49
12 Jun 1973	Pahute Mesa	4.5	43
28 Oct 1975	Timber Mountain	4.0	30
8 Jan 1976	Pahute Mesa	4.6	52
7 Feb 1976	Pahute Mesa	4.8	52
29 Jun 1992	Little Skull Mountain	5.6	30
30 May 1993	Rock Valley	4.0	35

- The potential for earthquake activity outside of the southern Great Basin to initiate earthquakes in or near the site; and
- Large uncertainties associated with conceptual models of faulting at the site, including the potential for coupling of earthquakes with igneous activity.

Potential impacts on radionuclide release and transport: Faulting and seismicity in the Yucca Mountain region could have significant effects on waste isolation. Displacement along the Ghost Dance Fault could potentially shear waste packages, exposing the contents of the packages to transport. In addition to the potential shearing, canisters away from the movement will experience the effects of the accompanying seismic wave, which could include:

- The shaking of the waste packages in their emplacement holes, possibly damaging or even rupturing the canisters; and
- The loss of the air gap because of spalling of material into the emplacement hole.

Host rock material filling an emplacement hole will alter the stress distribution on the waste package and could provide an avenue for water to come into contact with the waste package, thus increasing the probability of corrosion and the potential for failure.

Fault movement and accompanying seismicity could affect the hydrologic system in the Yucca Mountain region, through:

- Creation, destruction, or modification of barriers to ground-water flow;
- Alteration of the fracture network and thereby the flow paths for infiltrating waters; and
- Seismic pumping leading to short-term changes in the water-table elevation (Carrigan *et al.*, 1991).

Repeated seismicity passing through the site could have pronounced effects on waste package lifetimes, especially as the packages age.

Probability of occurrence considerations: A probabilistic seismic hazard analysis provides the frequency distribution of earthquake ground motion (i.e., it develops an estimate (annual probability of occurrence) of earthquakes greater than a given reference earthquake). The annual probability that the peak ground acceleration, A, will exceed a certain acceleration, a, at a given site is defined mathematically by:

$$P(A > a) = \int_m \int_r P(A > a \mid m,r)\, F_{sm}(m) F_{sr}(r) dm\ dr, \quad \textbf{(3-3)}$$

where $P\{A>a|m,r\}$ is the probability that the acceleration A is greater than a, for an earthquake of magnitude m at a distance r, and F_{sm} and F_{sr} are the probability distance functions for magnitude and density, respectively. Figure 3–6 shows the three basic inputs (Step Nos. 1 to 3 in the figure) needed to calculate the probabilistic seismic hazard (Step No. 4).

The development of a probabilistic model for seismic and fault hazards requires data and assumptions concerning such parameters as: fault rupture lengths, fault slip rates, earthquake magnitude distributions, geometry of the seismic source zones, and attenuation of the seismic waves.

Within the last decade, different probabilistic seismic hazard methodologies have been developed. The principal methodologies were those developed to assess the seismic hazard for nuclear power reactors in the eastern U.S. (e.g., Electric Power Research Institute (EPRI), 1986; and Bernreuter *et al.*, 1989); however, the applicability of these methodologies for an HLW repository in the western U.S. has yet to be determined. The seismic hazard model and the basic methodology to estimate seismic hazards at a site have been described in detail by Cornell (1968, 1971), McGuire (1976), and Algermissen *et al.* (1982).

The initial step in conducting a seismic hazard analysis for a site is the definition of a seismic hazard model. To define such a model, it is necessary to:

- Identify the seismic source zones;
- Describe the magnitude recurrence model;

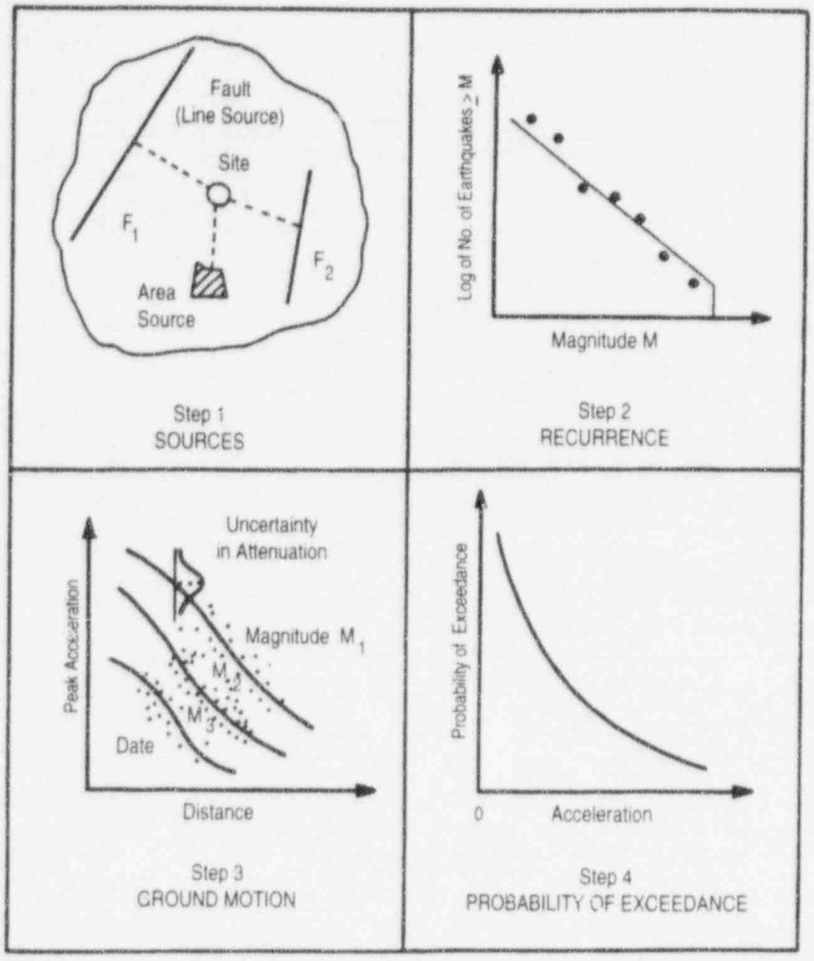

Figure 3–6 Basic steps in a probabilistic seismic hazard analysis (Adopted from the TERA Corporation (1978).)

- Describe the ground attenuation model; and
- Identify the fault slip rate.

After obtaining this information (Step Nos. 1 through 3 of Figure 3–6), the probability of exceeding a certain acceleration or a certain fault displacement value can be calculated (Step No. 4). Software programs developed by EPRI (1986) or Bernreuter *et al.* (1989) can be used to calculate the seismic hazards.

Figures 3–7 to 3–9 present results for seismic hazard and fault displacement analyses conducted for the Yucca Mountain region from the work of URS/John A. Blume & Associates (1987). These results are based on a sparse data set, the Campbell attenuation model for Utah (Campbell *et al.*, 1982) was used, and a specific slip rate was assumed. The results presented here will likely change as site characterization continues and adequate data for use in determining slip rates and the attenuation model become available.

Probability for IPA Phase 2: For the purposes of estimating a probability, seismicity is assumed to affect the repository only through the effects of the seismic acceleration on the waste canisters. Over time, as a waste canister corrodes, the thickness of its walls will decrease, and thus, a progressively reduced level of seismic acceleration will be needed to fail the canister, either by exceeding the yield strength of the canister material or by buckling the canister via impact with the emplacement hole. Therefore, a relationship between the thickness of the canister walls with time and the likelihood of a seismic acceleration necessary to fail the canister was established. As discussed in Section 6.4, canisters were assumed to fail when the seismically-induced stress at the base of the canister exceeded the

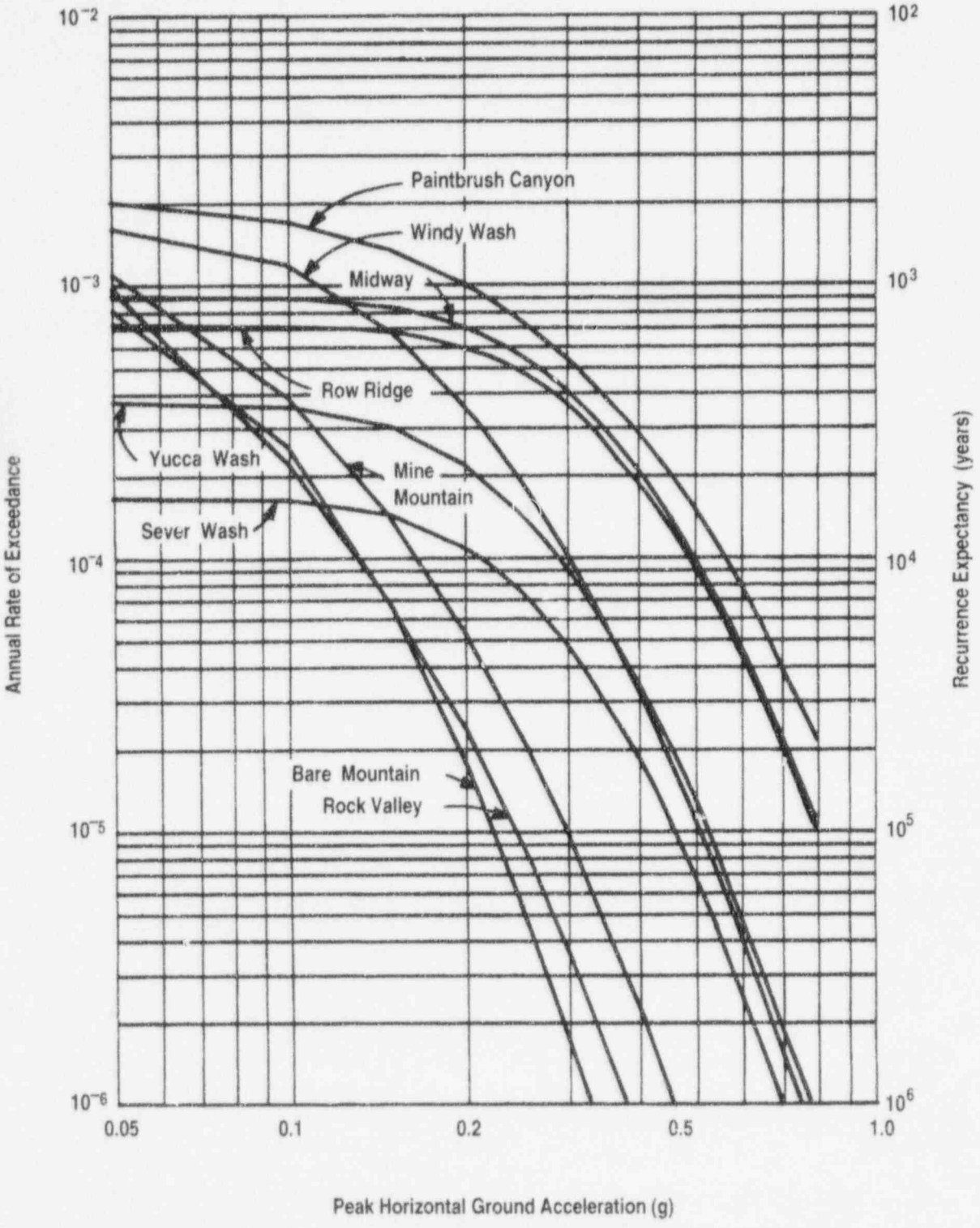

Figure 3–7 Annual probability of exceedance versus peak ground acceleration for several faults near Yucca Mountain (Adopted from URS/John A. Blume & Associates (1987).)

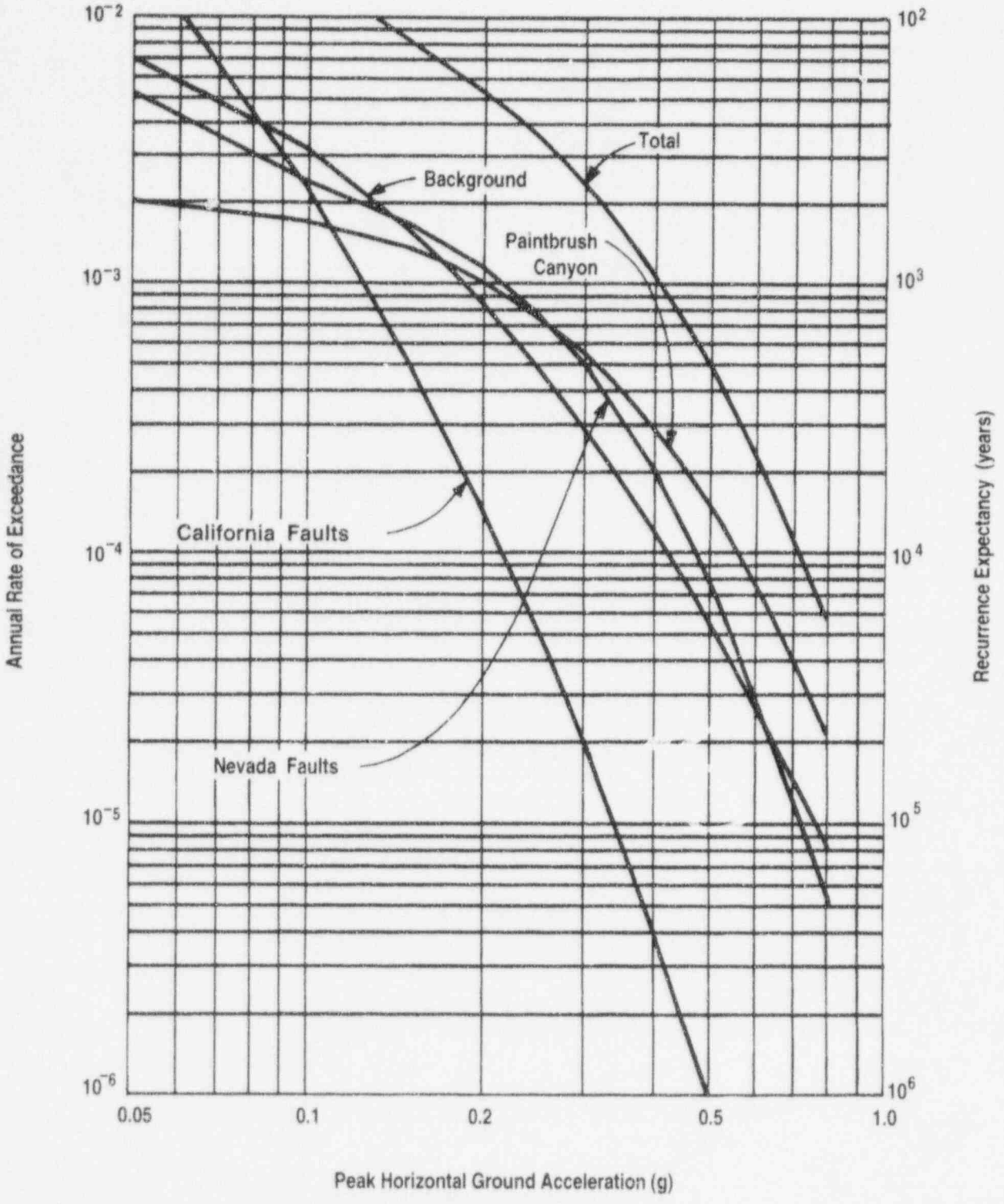

Figure 3–8 Comparison of annual probability of exceedance versus peak ground acceleration by location of faults (Adopted from URS/John A. Blume & Associates (1987).)

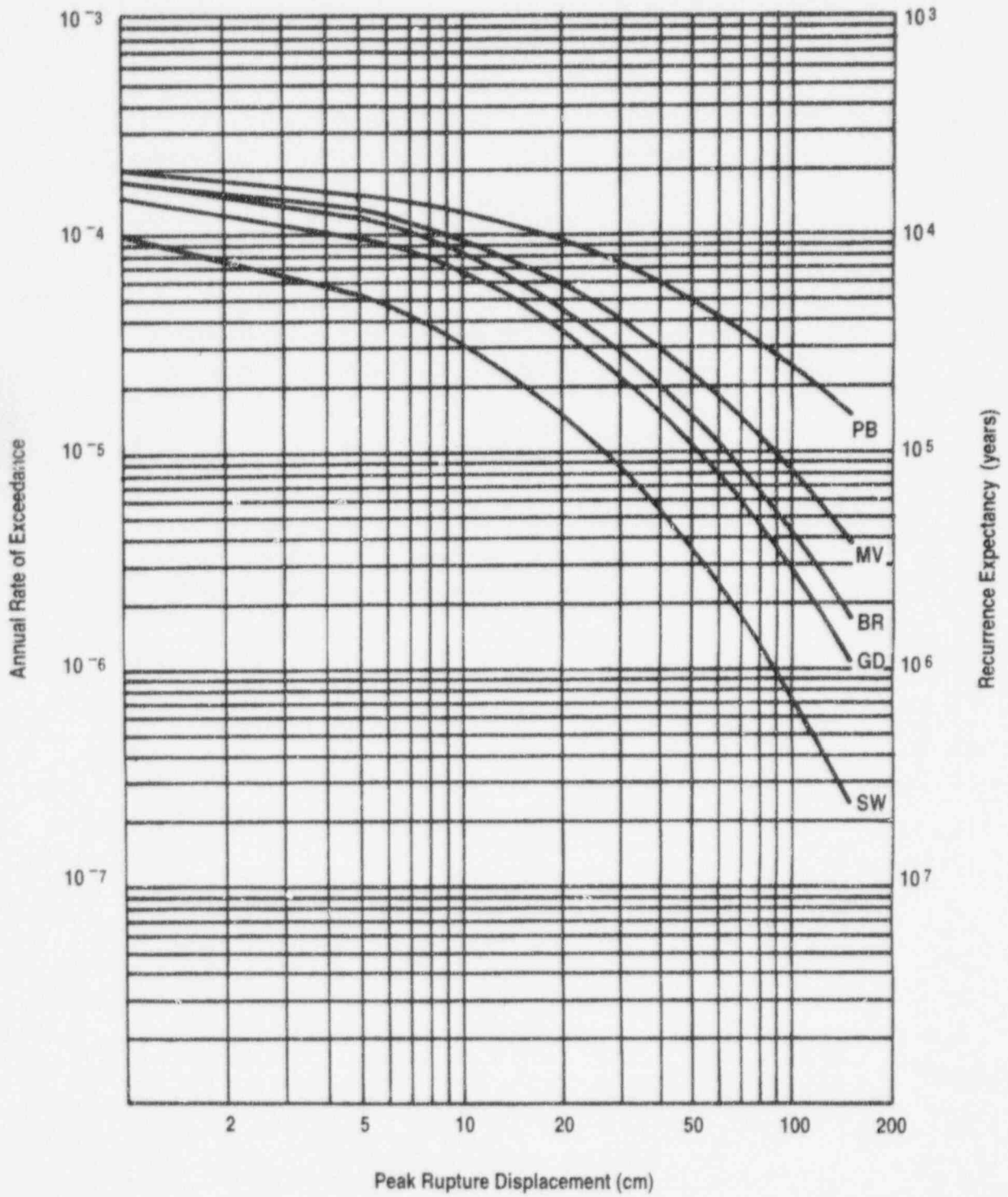

Figure 3–9 **Annual probability of exceedance of peak surface rupture displacement for the Paintbrush Canyon (PB), Midway Valley (MV), Bow Ridge (BR), Ghost Dance (GD), and Sever Wash (SW) faults** (Adapted from URS/John A. Blume & Associates (1987).)

yield strength of the waste canister material. First, a critical canister wall thickness was calculated (9.8×10^{-4} meters); a waste package canister with walls thinner than this would collapse under its own weight. Then, an acceleration necessary to fail a canister with walls of critical thickness was calculated (6.7×10^{-3} g). The recurrence rate for this level of acceleration is approximately equal to 0.02 per year, and therefore, the probability of seismic accelerations equal to or greater than this over the next 10,000 years in the Yucca Mountain region is estimated to be approximately 1.0. This is taken to be the probability of seismicity affecting the repository for this analysis.

3. *Climate Change*

Description: The present climate in which the Yucca Mountain site is located is classified as a midlatitude-desert climate, characterized by temperature extremes and annual precipitation of less than 150 millimeters. The paucity of precipitation in the region is believed to be caused by the rainshadow effect of the Sierra Nevada Mountains to the west of the site and the Transverse Ranges to the south. Rainfall in the area is sporadic, often occurring as showers, sometimes torrential, which can lead to local flooding. DOE currently estimates that perhaps less than 0.508 millimeters of the annual precipitation percolates to the deeper units of the unsaturated zone (DOE, 1988a; p. 27).

Current paleoclimatic data appear to indicate that there has been a general trend toward warmer and drier conditions in the southern Great Basin over the past 18,000 to 20,000 years, interrupted by episodes of cooler and wetter conditions lasting from a few hundred to perhaps 1000 years (Science Applications International Corporation, 1992). In general, the record of climatic conditions previous to this time back to the beginning of the Quaternary (2 Ma) is not well-preserved. However, analysis of calcitic veins at Ash Meadows in the Amargosa Desert and of vein calcite cores from Devils Hole near Ash Meadows indicate that the middle Pleistocene (500 to 750 thousand years ago) water table was tens to hundreds of meters above modern levels (Winograd and Szabo, 1988). Winograd and Szabo inferred the drop in the water table through the Quaternary as resulting from a combination of local erosion and climatic changes associated with the uplift of the Sierra Nevada and Transverse Ranges.

Potential impacts on radionuclide release and transport: Climatic changes over the next 10,000 years could have significant effects on the regional and local hydrologic system and therefore on the long-term performance of a repository at Yucca Mountain. A change to more arid conditions might lead to a further decrease in the frequency and intensity of precipitation in the region, as well as to an increase in evaporation. Such conditions might prove beneficial to repository performance.

A wetter, cooler climate could lead to increased infiltration at the site because of increased precipitation coupled with a reduction in evaporation. Such an increase in surface infiltration could lead potentially to an increase in the amount of ground-water flux through the unsaturated zone. If at sufficient levels, this increased flux could locally saturate formations above the repository horizon, leading to the formation of perched water tables, the transition from matrix flow to fracture flow, and an increased flux through the repository. Additional water could facilitate waste package corrosion, lead to faster dissolution of the UO_2 spent fuel matrix, and enhance the release of the radionuclides from the waste package canisters. Below the repository, transport from the repository to the accessible environment could be accelerated because of:

- Fracture flow, rather than matrix flow, through the unsaturated zone;
- A higher water table; and
- An increased hydraulic gradient in the saturated zone.

If the change to cooler climatic conditions is a presage to a period of glaciation, the annual precipitation rates in the Yucca Mountain region could increase dramatically. In the Pleistocene Ice Age, although the continental glaciers did not advance as far south as Yucca Mountain, increased precipitation associated with the change to a colder climate led to the formation of numerous lakes in the Great Basin province. One of these lakes, Lake Manly, estimated to be about 145 kilometers long and about 10 to 18 kilometers wide, formed in Death Valley (Thornbury, 1967). Presently, few of these lakes still exist, having

evaporated completely over time or shrunk dramatically in size.

The addition of large amounts of carbon dioxide, aerosols, and other trace gases to the atmosphere through man's activities has the potential for significantly altering future climate, especially in the near future (next 1000 years or so). Consideration of these anthropogenic contributions to potential climate change, with respect to the magnitude or probability of the change, were not included in the IPA Phase 2 analysis.

An NRC-sponsored elicitation of expert judgment of climatic conditions in the Yucca Mountain region over the next 10,000 years was conducted in 1993 (DeWispelare *et al.*, 1993). Data from this effort will be considered in future IPA analyses.

Probability of occurrence considerations: Both paleoclimatic data and climate models could be used in making climate predictions for the 10,000-year period of regulatory interest. Paleoclimatic data for the western U.S. may include lake-level records from present and former lakes, lake-bottom sediment cores, macrofossil assemblages from packrat middens, and stratigraphic pollen sequences (SAIC, 1992). When using such data in predictions of future climate, one assumes that the future variations in the climate system will be similar to those of the past. However, study of the past climate can yield only general indications of the future climate; explicit forecasts of the course of future climate are not possible, except as simple extrapolations of past behavior (Hunter and Mann, 1989). Examination of the paleoclimatic record can be used in the verification of modeling past climates and may serve to limit the range of variations expected in the future.

Climate models can be categorized into those that describe the slowly varying components of the climate system (e.g., the deep oceans, ice sheets) and those that model the fast-response components (e.g., the atmosphere, the upper layers of the oceans). Each of these component categories incorporate multiple temporal and spatial hierarchies that contribute additional uncertainties about the causes of past climate variations at a particular location and the likely consequences of future variations in the controls of the climate system (DOE, 1988b; p. 5-94). In attempting to predict future climate for 10,000 years, both types of climate models will be needed, as models of fast-response components provide a "snapshot" view of the climate system under a particular set of boundary conditions and state of slowly varying components (Hunter and Mann, 1989). At present, such integrated models are not available to provide estimates of future climate conditions at the spatial resolution necessary for a proposed repository site.

Given the current knowledge of climatic dynamics and the geological record of past climate changes, major climatic fluctuations may be likely within the next 10,000 years (Spaulding, 1985). Although methods of predicting long-term climatic variations (on the scale of 1000 to 100,000 years) do exist, the specific future variation of climatic parameters may not be entirely predictable (DOE, 1988b; pp. 5-91 - 5-98).

Probability for IPA Phase 2: The determination of a probability of climate change in the Yucca Mountain region over the next 10,000 years for use in IPA Phase 2 is predicated on the assumption that the variation in climatic conditions occurs slowly, such that the period of performance for the repository is short in comparison, and therefore, only a single "climate" will prevail during the period of performance. In making this assumption, "probabilities" can be assigned to a range of specific climatic conditions, which are then modeled in the consequence analysis using a particular data set of precipitation and temperature values. These parametric values are constant then throughout the modeled 10,000-year period of performance.

Given that a change in climate occurs, and that for the purposes of this scenario analysis, climate is represented by ranges in average annual temperature and average annual precipitation, four scenarios are possible under the "Climate Change" scenario class: warmer/drier; warmer/wetter; cooler/drier; and cooler/wetter, all relative to the current conditions.

In the IPA Phase 2 consequence analysis, described in Chapter 6, the "Current Climate" and "Climate Change" scenario classes were represented by distributions of infiltration rates; however, the link between the temperature and precipitation ranges used in this scenario analysis

and the infiltration rates used in the consequence analysis was not made.

For this effort, probabilities were generated for the "Climate Change" and the "No Climate Change" EPs based on paleoclimatic data gathered in a review of available literature, with the majority of the data obtained from studies of plant microfossils contained in the radiocarbon-dated remains found in packrat middens in the NTS vicinity (Spaulding, 1985). These data were used to bound the potential future variation in average annual temperature and precipitation for the Yucca Mountain region, as well as to calculate the scenario probabilities for the two climate EPs.

The data used in this analysis are graphed in Figure 3-10. It should be stated that, as portrayed in the figure, the data reflect only the interpreted general trends in climatic conditions for the past 45,000 years in the Yucca Mountain region and do not show the true variation in these conditions. Data for the entire Quaternary Period were not compiled by the staff. Based on the results from Spaulding's work, it appears that while the average annual temperature in the Yucca Mountain region has ranged from several degrees Celsius (°C) below current levels to several degrees above over the past 45,000 years, the average annual precipitation levels were always higher than those of the present (although the data appear to show indications, particularly in the recent past, that further increases in temperature may actually serve to lessen precipitation at the site). Within the past 45,000 years, the greatest variance from current conditions appears to have occurred approximately 18,000 years ago, at the height of the Pleistocene Ice Age, when average annual temperatures had dropped 5 to 7°C below present levels and the average annual precipitation had increased to roughly 35 percent above current levels. Another interesting point is that there appears to have been a general decline in precipitation, from approximately 20 percent above current levels down to today's precipitation levels in the repository life timeframe of 13,500 years.

Probabilities for this analysis were determined by taking a simple ratio of the timespan encompassed by a particular climate relative to the total time (i.e., 45,000 years). This approach was taken although it was recognized that the timespan in which a particular climate has prevailed in the past is not related to the probability that the same climate (or any other) will occur or not occur in the future. Also, it was assumed arbitrarily that current climatic conditions included variations in the average annual temperature between 2°C below to 2°C above current levels and in the average annual precipitation of up to 15 percent higher or lower than at present. Variations beyond these levels were considered as constituting a change in climate.

Thus, for the 45,000 years before present (ybp) represented on the graph, the average annual precipitation appears to have been less than 15 percent above current levels from 45,000 ybp to 39,000 ybp, and again from 10,000 ybp to the present, while the temperatures were between 2°C below and 2°C above current. For the remainder of the 45,000 years (between 39,000 ybp and 10,000 ybp), the average annual precipitation ranged from 16 percent (with 20 percent as a high estimate) to 35 percent (with 40 percent as a high estimate) greater, while the average annual temperatures were 3 to 6°C cooler than at present. Therefore, the probability of "No Climate Change" was taken to be equal to 16,000 years/45,000 years, or 0.356, and the probability of "Climate Change" was taken to be equal to 1 - (0.356), or 0.644.

With respect to the four potential climate change scenarios identified previously, the data suggest that, given the definitions used in this analysis, only present climatic conditions and cooler/wetter conditions have prevailed in the Yucca Mountain region over the past 45,000 years. Data for the entire Quaternary Period were not compiled by the staff.

4. Exploration Drilling

Description: The Yucca Mountain site is located in a natural resource-rich region that includes current gold production and exploration for hydrocarbons. Gold has been mined within the site vicinity (at Bare Mountain to the west and at Wahmonie to the east) for over a century (Raney, 1990b) and world-class gold deposits are located within 25 kilometers of Yucca Mountain. Gold exploration and exploitation continues as five new mines and prospects have been located within 48

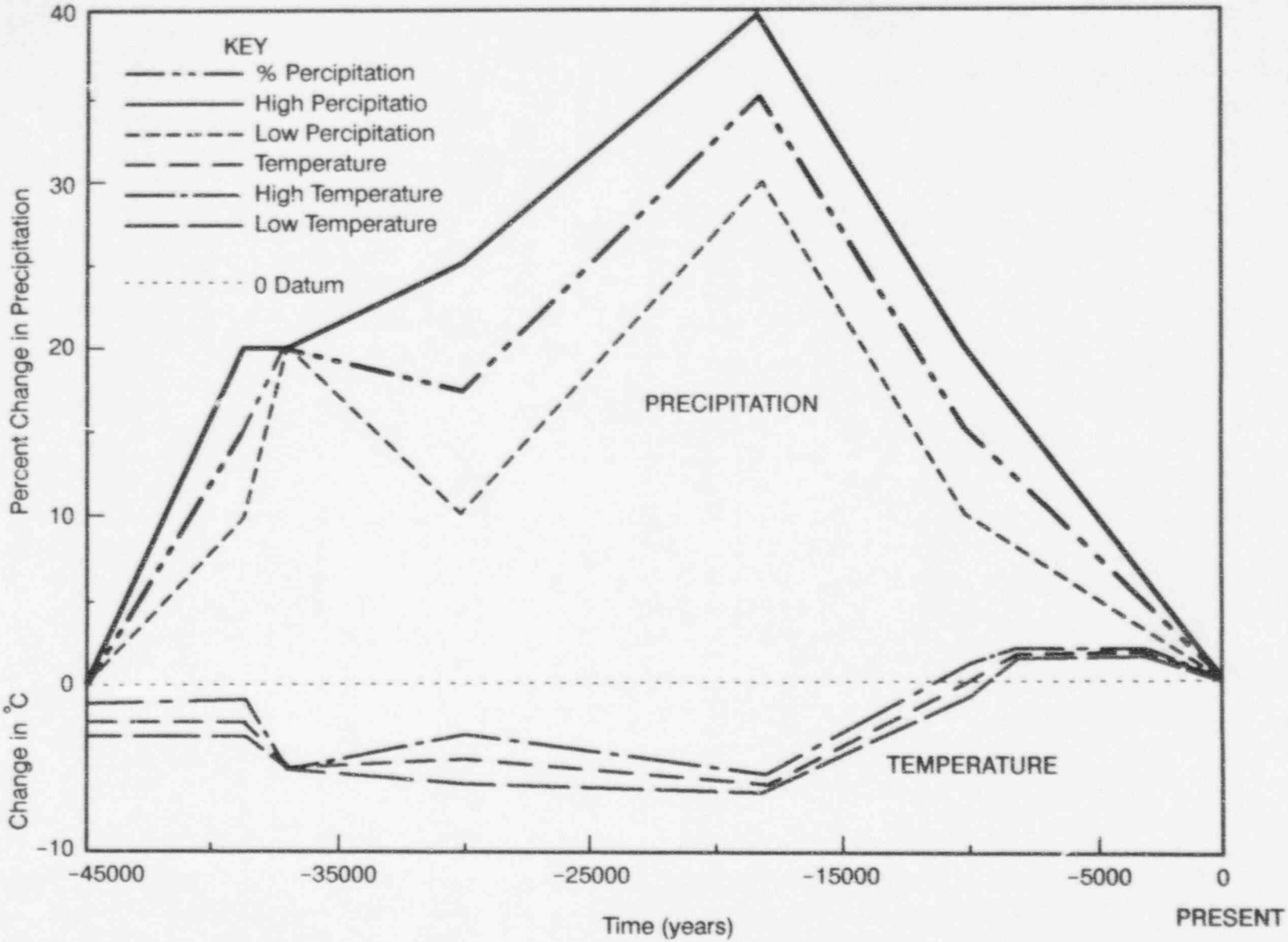

Figure 3–10 Precipitation and temperature variation over the past 45,000 years in the vicinity of the Nevada Test Site (Based on data from Spaulding (1985).)

kilometers of the proposed repository site between January 1988 and July 1990 (Raney, 1990b). The Railroad Valley petroleum deposits are located within 240 kilometers of the site (Garside *et al.*, 1988), and recent exploration for petroleum has occurred within 15 kilometers of Yucca Mountain. However, site characterization activities to date have not revealed any direct evidence of significant mineral or petroleum reserves at Yucca Mountain, although hydrothermal alteration is evident at the site (DOE, 1988b; p. 1-341).

Zeolitic clays are mined in playas south of the site, and significant quantities of zeolites compose part of the Calico Hills formation at the site (Vaniman *et al.*, 1984). However, it seems unlikely that zeolites at Yucca Mountain will become economically attractive because of their depth at the site and the wide availability of zeolites in more accessible locations throughout Nevada and the United States.

Geothermal waters are common in the State of Nevada (Garside and Schilling, 1979) and hot springs are evident within the vicinity of the site. However, in site characterization activities to date, only low-grade geothermal temperatures have been observed in ground water at or near the proposed repository site (DOE, 1988b; pp. 1-305 - 1-313; and Benson and McKinley, 1985).

Ground-water resources are known to be present at Yucca Mountain. DOE water wells presently pump water from the water table for testing and utilization within the DOE program, and this water may have commercial value in mining, agricultural, and residential applications.

Potential impacts on radionuclide release and transport: Future drilling at the site could lead to the inadvertent direct release of radionuclides from the underground repository to the accessible environment (in this case, the ground surface). Waste canisters may be intersected in the course of a exploratory drilling program, and as a result, canisters may be damaged, even punctured, by a drill bit. Under such a situation, spent nuclear fuel, irradiated waste package material, and contaminated host rock may be brought to the surface.

In addition, exploratory drilling for natural resources may have indirect impacts on the repository's ability to isolate waste. Such indirect impacts could include the creation of:

- Preferential pathways from the surface to the repository horizon for infiltrating waters; and
- Short-circuit radionuclide transport pathways through the unsaturated zone below the repository horizon for water-borne radionuclides, and from the repository to the surface for released gaseous radionuclides.

An additional concern is associated with the potential loss of significant amounts of drilling fluids into the geosphere, which may have adverse impacts on hydrologic flow through the repository and the geochemistry of the host rock (e.g., its sorptive capabilities).

The potential magnitude (i.e., severity) of these effects is related to the demand for the particular resource(s) being explored for or exploited, the depth and subsurface extent of the identified or inferred deposit(s), and the economic considerations involved. Such factors will directly impact the location and number of holes needed to exhaustively explore for or exploit the resource(s).

Probability of occurrence considerations: Estimates of the probability of future human intrusion at the Yucca Mountain site will be largely very subjective. For the most part, this is because of two factors:

- The lack of empirical or mechanistic models for determining the probability that a repository will be breached by human activity in the next 10,000 years; and
- The unpredictability of future human behavior, economic factors, and states of technology (Apostolakis *et al.*, 1991).

Despite the inability to predict the likelihood of future inadvertent human intrusion, EPs initiated by human activity, if found to be "sufficiently credible" under 10 CFR Part 60, will be included in assessments of compliance with the containment requirements of 40 CFR Part 191. Under 10 CFR Part 60, human intrusion ". . . may only be found to be sufficiently credible to warrant consideration if it is assumed that: (1) The monuments provided . . . are sufficiently permanent to serve their intended purpose; (2) the value to future generations of potential resources within

the site can be assessed adequately . . . ; (3) an understanding of the nature of radioactivity, and an appreciation of its hazards, have been retained in some functioning institutions; (4) institutions are able to assess risk and to take remedial action at a level of social organization and technological competence equivalent to, or superior to, that which was applied in initiating the processes or events concerned; and (5) relevant records are preserved, and remain accessible, for several hundred years after permanent closure" (10 CFR 60.2).

As the EPA believes that it will be impossible to develop a "correct" estimate of the probability of inadvertent human intrusion, Appendix B of 40 CFR Part 191 provides limits on the rates of inadvertent and intermittent drilling and the severity of the resulting consequences that need be considered (EPA, 1985; 50 *FR* 38089). The rate of drilling ". . . need not be taken to be greater than" 30 boreholes per square kilometer of repository area over 10,000 years for repositories located in or near sedimentary rocks and three boreholes per square kilometer per 10,000 years for repositories located in or near nonsedimentary rocks" (*op cit.*). These rates are believed to be based on average drilling rates determined from oil exploration in the Delaware Basin of the southwestern United States.

Probability for IPA Phase 2: For IPA Phase 2, it was assumed that the occurrence of future exploratory drilling is distributed randomly in space and time (and therefore can be approximated as a Poisson process). The rate of future inadvertent exploratory drilling was based on the guidance provided by EPA in Appendix B to 40 CFR Part 191 (EPA, 1985; 50 *FR* 38066–38089). Although sedimentary rocks underlie the site, the proposed repository horizon is in volcanic tuffs, and therefore, the EPA-recommended rate of three boreholes per square kilometer per 10,000 years was used.

For the purposes of this analysis, the repository area was defined to be 5.13 square kilometers (DOE, 1988b; p. 8.3.5.13–83), and therefore, the "expected" number of boreholes at the site over the next 10,000 years is 15.4. Further, if a Poisson distribution is assumed to describe the drilling, the probability of no boreholes being drilled (i.e., "No Exploratory Drilling") is approximately 2.3×10^{-7}, and therefore, the probability of one or more boreholes at the site (i.e., "Exploratory Drilling") is very nearly 1.0.

There are at least several problems with treating the probability of drilling in this way. First, the use of the EPA-derived drilling rate may not be completely applicable to the Yucca Mountain site or region, because it is believed that the EPA rate was derived from oil exploration drilling rates, whereas the Yucca Mountain region may more likely host exploration for precious metals. Apostolakis *et al.* (1991) calculated an example drilling rate for gold exploration using a common exploration technique for Nevada, which involves drilling a series of boreholes, and assuming a single gold-prospecting event every 100 years over the period of regulatory interest for the repository. This rate was equal to 7534 boreholes per square kilometer per 10,000 years.

Secondly, modeling drilling with a simple Poisson distribution precludes consideration of exploration programs that employ multiple boreholes in specific arrangements to appropriately assess a potential natural resource deposit(s). Finally, assuming that drilling is to be distributed randomly in space does not take into account topographical considerations (i.e., that drilling will likely take place preferentially at lower elevations on more level terrain (e.g., in drilling for water), rather than on the side or top of mountains, like Yucca Mountain).

Given that exploratory drilling occurs, the borehole could either intersect (for the IPA Phase 2 consequence analysis, "intersection" is equivalent to "penetration") a canister or merely excavate some of the surrounding host rock. The method used to calculate the likelihood of a random borehole intersecting a waste package canister in any one of the seven sub-areas of the modeled repository relative to any other is discussed in Section 6.3.

3.3.3 Combination of Events and Processes into Scenario Classes

Following screening, the remaining EPs ("Igneous Activity," "Seismicity," "Climate Change," and "Exploration Drilling") were combined to form scenario classes, as discussed in Section 3.2.4. The so-called "Latin square" is used to display all the possible combinations in Figure 3-11. In the far

left and top squares of the figure, the occurrence and non-occurrence of each initial EP are shown; the non-occurrence of an EP is represented by placing shading over the letter denoting the EP. Since there are four fundamental classes of EPs, 2^4 or 16 different combinations are possible. "Non-occurrence" should be interpreted as "not any occurrence;" e.g., since *D* represents drilling any boreholes within the perimeter of the mined facility projected to the surface, *D* represents no boreholes within that surface region over the 10,000-year performance period.

Figure 3-12 is similar to Figure 3-11 except the literal symbols for the EPs and their combinations are replaced with their assigned probabilities. In the IPA Phase 2 analysis, these initial EPs are assumed to be mutually independent, and therefore, the probability of the various scenario classes formed through these combinations is equal to the product of the constituent initial EPs (i.e., the probability of both event *A* and event *B* occurring is equal to the probability of event *A* occurring multiplied by the probability of event *B* occurring). In addition, in the figure, each row and column is summed.

Figure 3-13 is identical to Figure 3-12, except all combinations of the EPs (i.e. scenario classes) that have probabilities of occurrence less than 1 chance in 10,000 over 10,000 years are shaded. If the screening criteria for individual categories of events and processes in the EPA guidance were applied, these scenario classes would be screened out.

These figures present the information concerning the various combinations in an idealized, general format such that, for a particular scenario class, no conclusions can be drawn regarding:

- The number of times or the time(s) at which a particular EP will occur within the 10,000-year period of regulatory interest; or
- The order or sequence in which two or more EPs in the scenario class will occur within that same time period.

Instead, the calculated probability values refer only to the likelihood that a particular scenario class will occur in the Yucca Mountain region over the next 10,000 years. For example, the scenario class involving "Drilling" and "Seismicity" in the region (with "No Climate Change" and "No Igneous Activity") has the assigned probability of approximately 0.35 in the next 10,000 years. This is the probability of having any occurrence of both drilling and seismicity that will affect the site in the coming 10,000 years, and not the probability of having *x* episodes of drilling followed by *y* earthquakes of a given size, followed by *z* more holes being drilled or any such combination.

A manifestation, therefore, of the approach the staff has taken in its application of the SNL scenario methodology, particularly in defining the repository system boundaries as the staff did, is the issue of selecting the appropriate representative scenario(s) for the individual scenario classes. Addressing this issue will require answering:

- How many times a constituent EP will occur over the time period of regulatory interest;
- How the EP will manifest itself, once it does occur; and
- When during the period of interest the EP will occur(s).

It is likely that each of the various permutations of these three variables will affect the repository system differently, thus leading to a range in estimated radionuclide releases to the accessible environment. The approaches taken to modeling each of the scenario classes and their consequences are discussed in the following chapters of this report. This issue will need to be addressed explicitly in future staff work in this area.

3.3.4 Screening of Scenario Classes

EPA guidance set forth in Appendix B to 40 CFR Part 191 states that ". . . performance assessments need not consider categories of events or processes that are estimated to have less than one chance in 10,000 of occurring over 10,000 years" (EPA, 1985; 50 *FR* 38088). In its proposed conforming amendments to 10 CFR Part 60, NRC reaffirmed the application of the 1×10^{-4} in 10,000-years criterion to categories of events and processes, when it stated, "The term "categories" is used to refer to general classes of processes and events, such as faulting, volcanism, or drilling"

		V		V	
		D	D	D	D
C	S	C S D V	C S D V	C S D V	C S D V
	S	C S D V	C S D V	C S D V	C S D V
C	S	C S D V	C S D V	C S D V	C S D V
	S	C S D V	C S D V	C S D V	C S D V

KEY

C - No climate change
C - Climate change

S - No seismic activity affecting the repository
S - Seismic activity affecting the repository

D - No human intrusion via exploratory drilling
D - Human intrusion via exploratory drilling

V - No magmatic activity affecting the repository
V - Magmatic activity affecting the repository

Figure 3–11 Combinations of events and processes into scenario classes

		P(V) ≈ 0.97		P(V) ≈ 0.03		
		P(D) = 2.3×10^{-7}	P(D) ≈ 1.0	P(D) = 2.3×10^{-7}	P(D) ≈ 1.0	***SUM (approximate)***
P(C) = 0.356	P(S) ≈ 0.0	0.0	0.0	0.0	0.0	0.0
	P(S) ≈ 1.0	7.9×10^{-8}	0.35	2.5×10^{-9}	0.01	0.36
P(C) = 0.644	P(S) ≈ 0.0	0.0	0.0	0.0	0.0	0.0
	P(S) ≈ 1.0	1.4×10^{-7}	0.62	4.4×10^{-9}	0.02	0.64
SUM (approximate)		2.2×10^{-7}	0.97	6.9×10^{-9}	0.03	1.0

KEY

P(C) - Probability of no climate change
P(C) - Probability of climate change

P(S) - Probability of no seismic activity affecting the repository
P(S) - Probability of seismic activity affecting the repository

P(D) - Probability of no human intrusion via exploratory drilling
P(D) - Probability of human intrusion via exploratory drilling

P(V) - Probability of no magmatic activity affecting the repository
P(V) - Probability of magmatic activity affecting the repository

Figure 3–12 Probabilities of scenario classes for IPA Phase 2 generated by combinations of probabilities of occurrence of constituent events and processes

		P(V) ≈ 0.97		P(V) ≈ 0.03		
		P(D) = 2.3×10^{-7}	P(D) ≈ 1.0	P(D) = 2.3×10^{-7}	P(D) ≈ 1.0	***SUM (approximate)***
P(C) = 0.356	P(S) ≈ 0.0	0.0	0.0	0.0	0.0	0.0
	P(S) ≈ 1.0	7.9×10^{-8}	0.35	2.5×10^{-9}	0.01	0.36
P(C) = 0.644	P(S) ≈ 0.0	0.0	0.0	0.0	0.0	0.0
	P(S) ≈ 1.0	1.4×10^{-7}	0.62	4.4×10^{-9}	0.02	0.64
SUM (approximate)		2.2×10^{-7}	0.97	6.9×10^{-9}	0.03	1.0

Note: Scenario classes with probabilities less than 1.0×10^{-4} over 10,000 years are shaded.

KEY

P(C) - Probability of no climate change
P(C) - Probability of climate change

P(S) - Probability of no seismic activity affecting the repository
P(S) - Probability of seismic activity affecting the repository

P(D) - Probability of no human intrusion via exploratory drilling
P(D) - Probability of human intrusion via exploratory drilling

P(V) - Probability of no magmatic activity affecting the repository
P(V) - Probability of magmatic activity affecting the repository

Figure 3–13 Scenario classes with generated probabilities greater than 1×10^{-4} in 10,000 years (Shading indicates scenario classes with probabilities less than 1×10^{-4} in 10,000 years.)

(NRC, 1986; 51 *FR* 22292). Therefore, use of the EPA criterion is not appropriate for scenario classes; however, if it were applied to the scenario classes shown in Figure 3–13, as suggested by Cranwell *et al.* (1990, p. 10), only 4 of the 16 classes would be retained (Table 3–4).

Table 3–4 Scenario Classes Remaining after Screening

Scenario Class	*Probability (over 10,000 yrs)*
Drilling + Seismicity	0.34
Drilling + Seismicity + Igneous Activity	1.0×10^{-2}
Drilling + Seismicity + Climate Change	0.61
Drilling + Seismicity + Igneous Activity + Climate Change	2.0×10^{-2}

Each of the four retained scenario classes would involve the occurrence of both drilling and seismicity at the Yucca Mountain site over the next 10,000 years. This is because, for the present analysis, the occurrence of both of these initial EPs have estimated probabilities approximately equal to 1.0.

It is also interesting to note that the base-case scenario class (i.e., the scenario class in which there would be no drilling, seismicity, igneous activity, or climate change) would be screened if the probability criterion were applied, as its assigned probability is approximately eight orders of magnitude below the EPA value. This result suggests that, given the currently assigned probabilities, conditions at the repository site over the next 10,000 years appear highly unlikely to remain as they are today.

For this scenario effort, no scenario classes were screened from the analysis. However, only a subset of the 16 scenario classes generated was modeled in the consequence analysis. Treatment of these scenario classes in the consequence analysis and the subsequent calculation of CCDFs for cumulative radionuclide releases to the accessible environment and for dose are discussed in the following chapters.

3.4 Discussion of Results

As noted, the staff has applied the SNL scenario selection procedure to generate scenario classes for consideration in the IPA Phase 2 consequence analysis (see Chapter 6). This section of the report summarizes the SNL procedure and documents the development of a final set of scenario classes and corresponding probability estimates used in the IPA Phase 2 analysis. From an initial list of potentially disruptive EPs, four were determined to be reasonably likely and warranting consideration of their possible effects on long-term repository performance: igneous activity (intrusive and extrusive), seismicity, climate change, and exploratory drilling. Estimates of their probability of occurrence over the next 10,000 years were developed, and these EPs are combined into 16 scenario classes with associated probabilities.

In applying the SNL scenario selection procedure, the staff found it to form an adequate basis for the development of scenario classes for the IPA Phase 2 analysis. The staff did consider that modifications were necessary, particularly the definition of explicit boundaries for the repository system, to meet the needs of the analysis and to keep the number of resultant scenario classes tractable. However, this does not detract from the adequacy of the methodology, in that other international programs that have applied the SNL procedure have also found modifications necessary to meet their specific programmatic needs and requirements (Andersson *et al.*, 1989; and Stephens and Goodwin, 1990). Cranwell *et al.* (1990) have, in fact, stated that ". . . the scenario selection methodology provides a general 'road map' for arriving at scenarios; the fact that [variations to] the methodology have been implemented is an indication of the flexibility of the methodology. . ." (*op cit.*, p. 15).

Suggestions for future work are discussed in Chapter 10.

4 FLOW AND TRANSPORT MODULE[1]

4.1 Introduction: Consequence Models for Flow and Radionuclide Transport

The Iterative Performance Assessment (IPA) effort provides, in part, a formal procedure for evaluating existing computer programs used to simulate ground-water flow and radionuclide transport; evaluating new concepts for flow and transport in unsaturated, fractured rock; and identifying performance assessment needs. IPA Phase 1 used some preliminary concepts regarding the Yucca Mountain site. This section will build on the ground-water IPA Phase 1 effort (see "Flow and Transport Models" (Chapter 6) in Codell *et al.*, 1992) using concepts that have been published since the Phase 1 effort concluded. Additionally this section will discuss the model used in estimating gaseous releases for inclusion into the complementary cumulative distribution function (CCDF) of repository performance (gaseous releases were analyzed as an auxiliary analysis in the IPA Phase 1 effort and were not included in the CCDF). The intent is to provide additional information for making modeling decisions and interpreting results. However, it needs to be pointed out that laboratory and field investigation of fluid flow in unsaturated, fractured rock can require significantly more time than improvements to computer programs; therefore, modeling capability in certain areas has progressed faster than parameter estimation and site characterization.

4.2 Flow and Radionuclide Transport Model for Ground-Water Releases

The IPA Phase 1 effort accounted for a number of important attributes of the Yucca Mountain site (e.g., stratigraphic changes below the repository in the unsaturated zone and differences between matrix and fracture flow). The IPA Phase 2 effort not only has maintained the important attributes of the Phase 1 study, but has added further modeling complexity such as:

- Saturated zone pathways to the accessible environment;
- Calculation of radionuclide concentration for dose assessment; and
- Distribution of mass flux between the fracture and matrix continua.

It is anticipated that additional complexity will provide insights into the performance of fractured rock as a geologic barrier, data requirements, and the capabilities of the computational methods used.

4.2.1 Site Concepts

The Yucca Mountain site is located on and immediately adjacent to the southwestern portion of the Nevada Test Site (see Figure 4–1). Yucca Mountain is a prominent group of north-trending, fault-block ridges. The terrain at the site is largely controlled by high-angle normal faults and eastward-tilted volcanic rocks. Slopes are locally steep (dip angle 15° to 30°) on the west-facing side of Yucca Mountain and along some of the valleys that cut into the more gently sloping (dip angle 5° to 10°) east side of the mountain (see Figure 4–2).

Stratigraphy

The hydrogeologic units of interest at Yucca Mountain are primarily comprised of ash-flow and ash-fall tuffs that originated from eruptions during the development of calderas. The amount of welding, fracturing, unit thickness, and chemical alteration varies greatly from one layer to the next; therefore, the hydrologic and transport parameters have the potential to also vary significantly from one layer to the next. Based on surface mapping and drill hole data, information on stratigraphic sequences and thicknesses for Yucca Mountain are presented in Ortiz *et al.* (1985). The Ortiz *et al.* report gives detailed stratigraphic information from the surface to the water table for a number of drill holes near the repository location and provides cross-sections at various locations of the site (see Figure 4–3). One particular cross-section, presented in

[1]The figures shown in this chapter present the results from a demonstration of staff capability to review a performance assessment. These figures, like the demonstration, are limited by the use of many simplifying assumptions and sparse data.

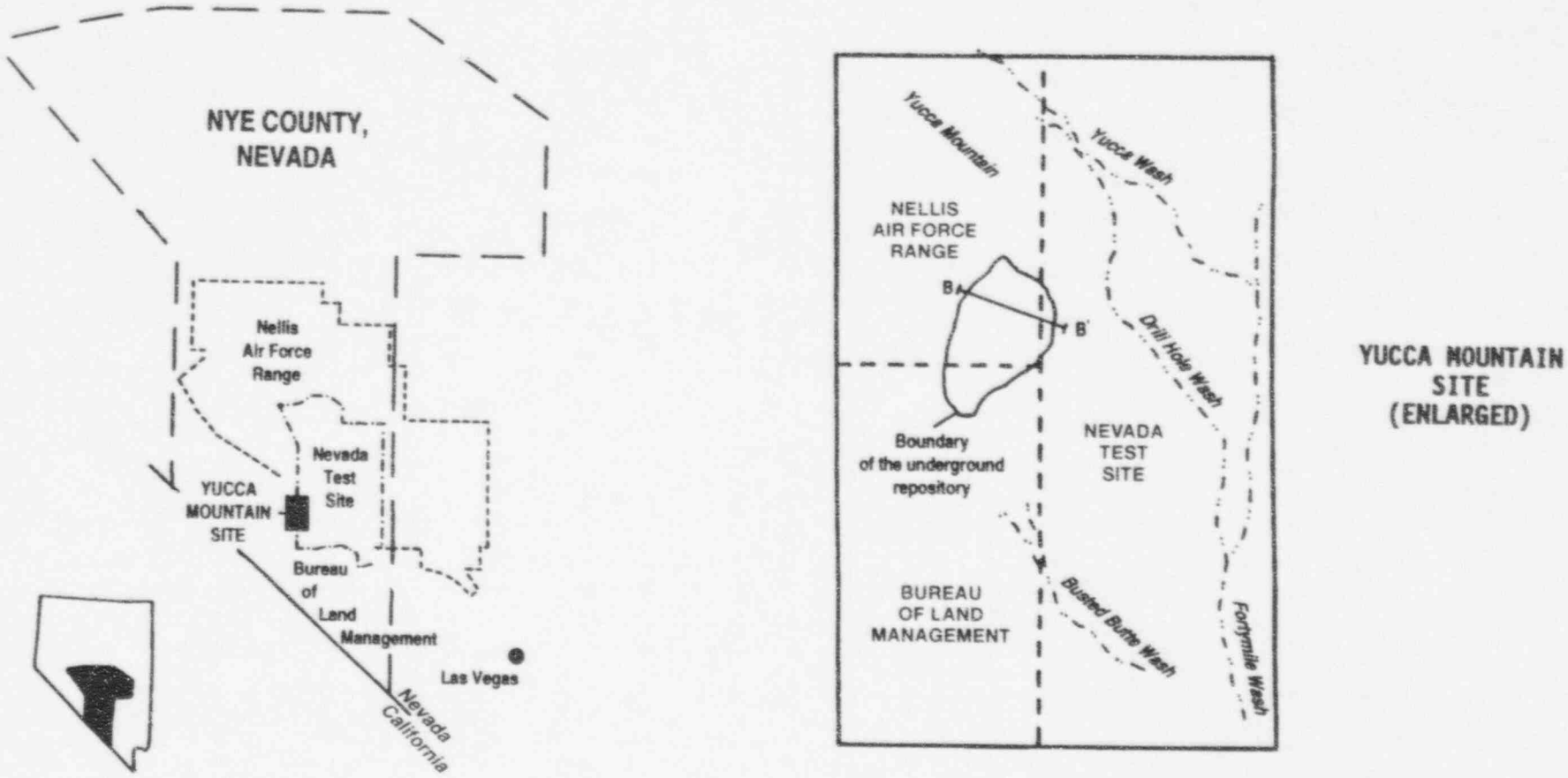

Figure 4–1 Location of the Yucca Mountain site (Adopted from DOE (1988b, p. 13).)

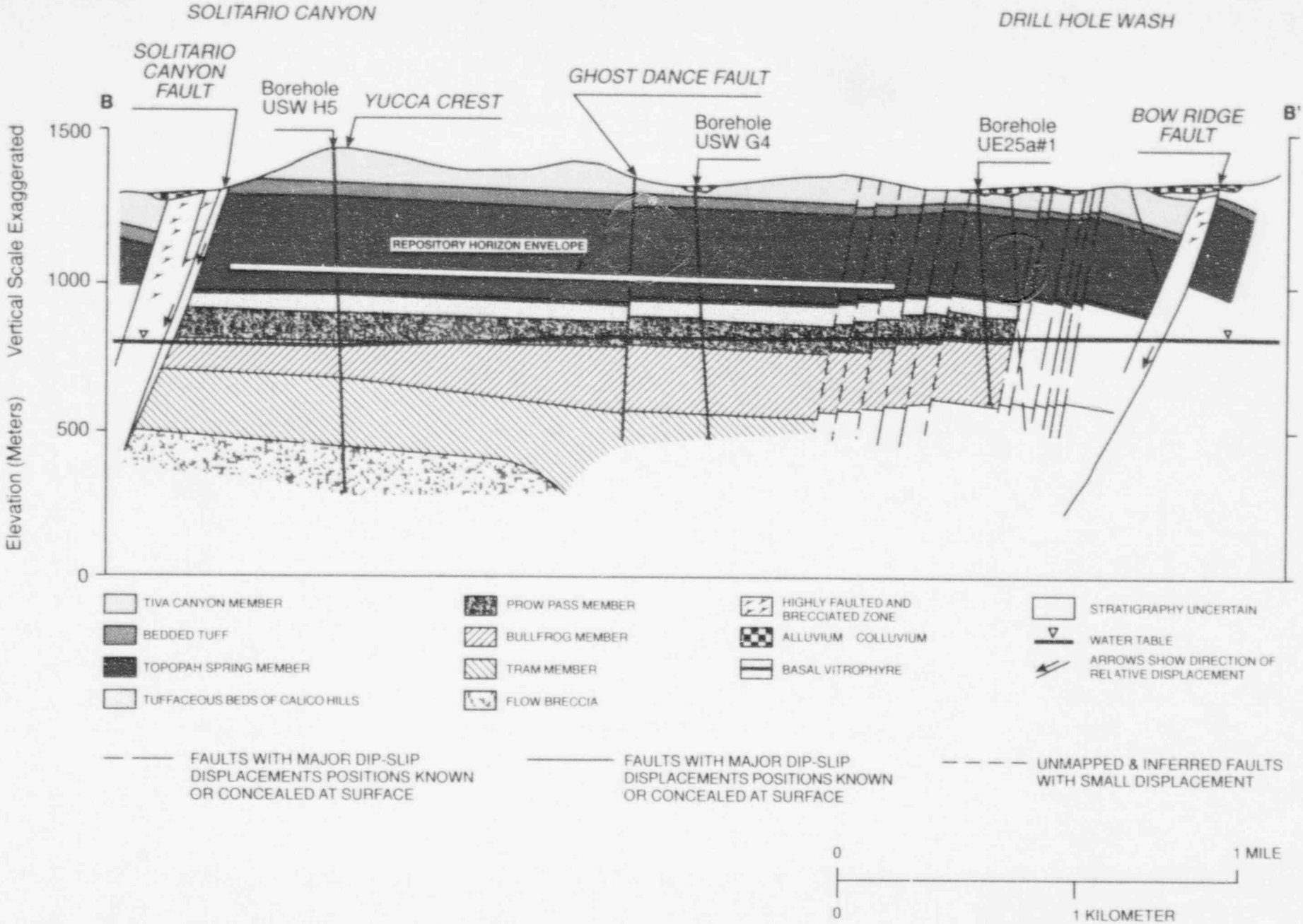

Figure 4–2 East-west geologic cross-section (along B–B′) for the Yucca Mountain site (Adopted from DOE (1988b, p. 19).)

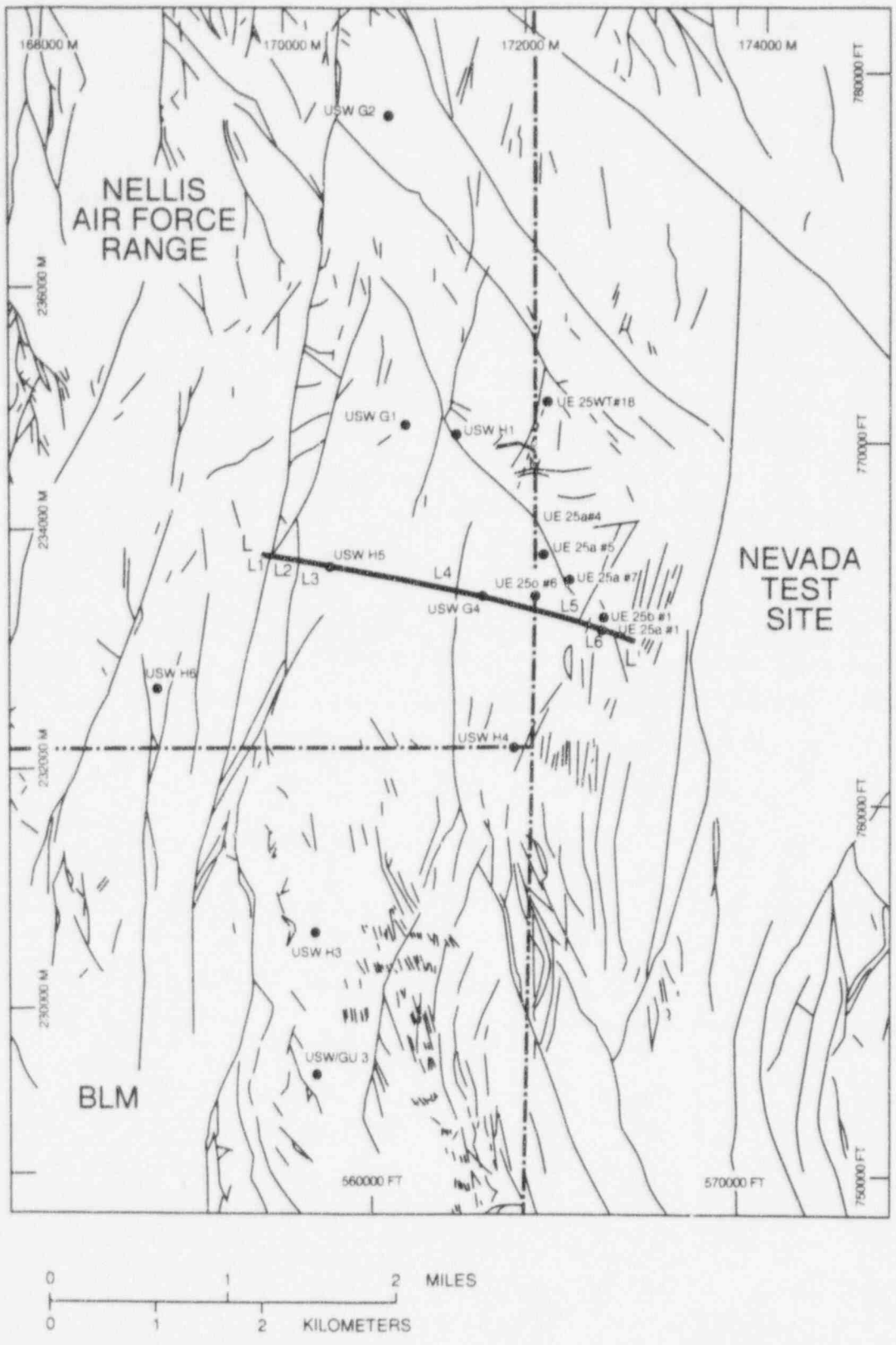

Figure 4–3 Locations of faults, drill holes (solid circles), and generated cross-sections (dotted lines) (Adopted from Ortiz *et al.* (1985, p. 17).)

Figure 4–4, has been the basis of preliminary studies attempting to better understand modeling limitations with respect to flow conditions associated with the unsaturated zone at Yucca Mountain (Barnard *et al.*, 1992; Prindle and Hopkins, 1990; and Dudley *et al.*, 1988). This cross-section possesses some of the primary features, of the Yucca Mountain site, anticipated to be important when calculating system performance. The important features are:

- Dipping strata with large contrasts in permeability between strata;
- Variation in the unit sequences and thicknesses between the water table and the repository horizon; and
- Variation in the distance from the suggested repository horizon to the water table.

Liquid Flow

Hydrologic data are rather limited for the Yucca Mountain site. The Peters report (1984) is a primary source of parametric data for recent modeling studies (Barnard *et al.*, 1992; Nitao and Buscheck, 1991; Prindle and Hopkins, 1990; and Dudley *et al.*, 1988) and for DOE's Site Characterization Plan (SCP) (see DOE, 1988a). Two important aspects of the hydrologic data, as reported in the SCP, are the contrast in matrix conductivity between hydrogeologic units (see Table 4–1) and the significant contrast between laboratory measurements and *in-situ* or field measurements for many of these units (see Table 4–2). This contrast, between laboratory and field measurements, could be indicative of the contribution of fractures to the saturated conductivity, which is more easily controlled in a small-scale laboratory measurement.

Generally, matrix data are very limited and provide little information to define defensible parametric ranges for use in performance assessments. The fracture data, being primarily derived from capillary theory rather than the results of hydrologic measurements, are even more limited than the matrix data. Recent modeling work by Nitao and Buscheck (1991) provides some insights on how matrix permeability affects fracture flow attenuation because of matrix imbibition. Although the Nitao work is based on preliminary field data and hypothetical fluxes, it clearly indicates the need to better understand fracture-matrix interactions and the need for more data to estimate parameters in both the fractures and the matrix.

Possibly the largest contributor to uncertainty in the fracture-matrix interactions is the assignment of the percolation rate. The SCP (DOE, 1988a; pp. 3–201 – 3–214) cites a number of studies that span a range of percolation rates (e.g., 0.015 – 4.5 millimeters/year). Recent analyses (Barnard *et al.*, 1992) using "representative" Yucca Mountain data and adopting a steady-state model wherein the fracture and matrix pressures are in equilibrium tend to support low values (0.01 millimeter/year) for percolation rates. However, the work of Nitao and Buscheck (1991) indicates that the time necessary to reach equilibrium can be significant and Ababou (1991, p. 2–8) has pointed out additional limitations of using mean values of percolation and simplified models for subsurface flow:

- The ground surface at Yucca Mountain is fractured since the "highly fractured" Tiva Canyon unit crops out throughout most of the repository (DOE, 1988a; p. 3–203);
- Rainfall occurs in bursts and the rainfall rate is far from periodic at any time scale accessible to observation;
- The interactions between rainfall intensity, infiltration, ponding, and runoff are not well-understood; and
- The linear theory of damping applied to the non-linear unsaturated flow equation may be overly inaccurate under certain conditions (such as Item Nos. (1) through (3) above).

A better understanding of transient effects, fracture-matrix interactions, and the effects of heterogeneity is necessary if defensible estimates of percolation are to be provided for performance assessments.

Gas Flow

One difference between disposal in the saturated zone as compared to disposal above the water table is the possibility for radionuclide migration via the gas pathway. Fractures, if dry and interconnected, could provide a fast pathway for gas

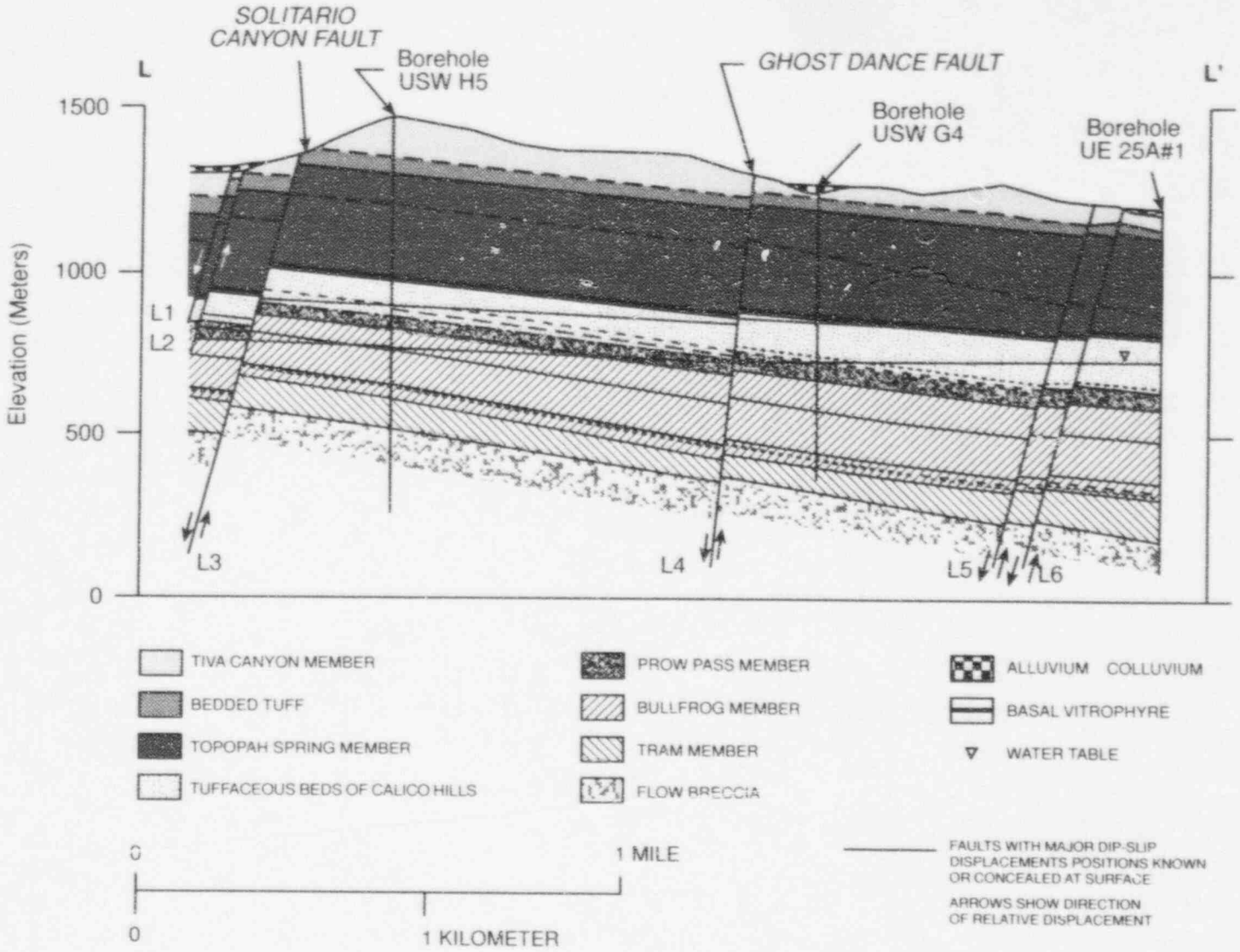

Figure 4–4 Cross-section L–L′. (See Figure 4.3 for location of cross-section in relation to Yucca Mountain. Adopted from Ortiz *et al.* (1985, p. 19).)

Table 4–1 Summary of Hydrogeologic Properties of Hydrogeologic Units within the Unsaturated Zone at Yucca Mountain (From DOE (1988a, p. 3–170).)

Hydrologic Unit	*Source of Data*	*Range of thickness (m)*	*Grain Density (kg/m^3)*	*Fracture Density[a] ($no./m^3$)*	*Matrix Porosity*	*Saturated Matrix Hydraulic Conductivity (m/sec)*
Tiva Canyon (welded)	b	0 – 150	No data	10 – 20	0.12	2.1×10^{-11}
	c	No data	2,490		0.08	9.7×10^{-12}
Paintbrush (non-welded)	b	20 – 100	No data	1	0.46	1.0×10^{-7}
	c	No data	2,350		0.40	3.9×10^{-7}
Topopah Spring (welded)	b	290 – 360	No data	8 – 40	0.14	3.5×10^{-11}
	c	No data	2,580		0.11	1.9×10^{-11}
Calico Hills (non-welded, vitric)	b	100 – 400	No data	2 – 3	0.37	5.0×10^{-8}
	c	No data	2,370		0.46	2.7×10^{-7}
Calico Hills (non-welded, zeolitic)	b	100 – 400	No data	2 – 3	0.31	9.0×10^{-11}
	c	No data	2,230		0.28	2.0×10^{-11}

[a]Scott *et al.* (1983).
[b]Montazer and Wilson (1984).
[c]Peters *et al.* (1984) and Peters *et al.* (1986).

Table 4–2 Summary of Hydrogeologic Characteristics, as Determined through Laboratory and Field Measurements, of Major Stratigraphic Units in the Vicinity of Yucca Mountain (From DOE (1988a, pp. 3–182 — 3–183))

In-Situ (field) Analyses

Stratigraphic Unit	*Typical Character*	*Saturated*	*Transmissivity*[a] *(m^2/day)*	*Average Conductivity*[b] *(m/day)*	*Borehole Tested*
Topopah Spring	Moderately to densely welded tuff	167	120	0.7	J–13
Calico Hills	Zeolitized, nonwelded tuff, vitric tuff	148	(82)	0.5	UE–25b#1
Prow Pass	Nonwelded to moderately welded tuff	116	167	1.44	USW H–1
		135	150	1.1	USW H–1
		174	36 – 142	0.2 – 0.8	USW H–4
		150	(65)	0.4	UE–25b#1
		111	14	0.1	UE–25p#1
Bullfrog	Nonwelded to densely welded tuff	125	0.8	0.006	USW H–1
		119	70 – 276	0.6 – 2.3	USW H–4
		159	(65)	0.4	UE–25b#1
		132	(7)	0.05	UE–25p#1
Tram	Nonwelded to moderately welded ashflow and bedded tuffs	284	0.002	7.0×10^{-6}	USW H–1
		354	0.7	0.002	USW H–3
		352	70 – 276	0.2 – 0.8	USW H–4
		183	(3.3)	0.02	UE–25p#1
Lithic Ridge Tuff	Partially welded ashfall tuffs	594	0.001	2.0×10^{-6}	USW H–1
		110	0.1	0.001	USW H–3
		371	> 10	> 0.03	UE–25p#1

[a]Parentheses ( ) indicate approximate value because reported values reflect more than one stratigraphic unit.

[b]Obtained by dividing transmissivity by saturated thickness.

Table 4–2 (continued)

Laboratory (Core) Analyses

Stratigraphic Unit	Typical Character	Saturated Matrix		Matrix Porosity		Borehole Tested
		Conductivity (m/day)	No. of Samples	Percent	No. of Samples	
Topopah Spring	Moderately to densely welded tuff	3×10^{-7} to 2×10^{-4}	5	4 – 33	5	J–13
		7×10^{-7} to 5×10^{-4}	18	6 – 30	24	UE–25a#1
		8×10^{-7}	1	12	1	UE–25b#1
Calico Hills	Zeolitized, nonwelded tuff, vitric tuff	4×10^{-6} to 3×10^{-4}	6	20 –34	7	UE–25a#1
Prow Pass	Nonwelded to moderately welded tuff	6×10^{-5} to 1×10^{-4}	3	28 – 29	3	USW H–1
		2×10^{-5} to 1×10^{-3}	8	10 – 25	12	UE–25a#1
		6×10^{-7} to 1×10^{-3}	5	17 – 30	18	USW G–4
Bullfrog	Nonwelded to densely welded tuff	3×10^{-5} to 1×10^{-3}	10	19 – 34	9	USW H–1
		2×10^{-4} to 1×10^{-3}	3	17 – 34	3	UE–25a#1
		2×10^{-4} to 5×10^{-4}	2	24 – 27	6	USW G–4
Tram	Nonwelded to moderately welded ashflow and bedded tuffs	4×10^{-6} to 4×10^{-4}	9	18 – 26	9	USW H–1
Lithic Ridge Tuff	Partially welded ashfall tuffs	6×10^{-5} to 3×10^{-4}	2	9 – 17	2	USW H–1

phase radionuclides (e.g., ^{14}C). Air flow has been observed at some boreholes at Yucca Mountain (Weeks, 1987). Weeks has suggested that this phenomenon is caused by topographic and barometric effects combined with outcrops on the side of the mountain of rock units that intercept the boreholes.

Simulation work (Tsang and Pruess, 1987) has examined the effect of the thermal output of the repository on gas flow. Simulated gas pore velocities in fractures varied from 4.5 to 1174 meters/year (*op cit.*, p. 1963). Although these simulations were preliminary, the results indicate that further investigation may be needed to properly characterize boundary conditions and the fracture properties for gas flow.

Transport

The transport of radionuclides will be governed by properties associated with the transporting fluid (i.e., advection, dispersion, and diffusion) and properties associated with geochemistry (i.e., sorption and precipitation). The advective and dispersive components of transport are associated with the fluid flow and were highly dependent on the heterogeneous nature of the formation being studied. The presence of fractures can put increased demands on transport models. Although the presence of near horizontal strata or fractures can increase the horizontal/longitudinal spreading of radionuclides relative to isotropic media, the presence of vertical fractures could lead to contrary effects, depending on ambient moisture and the interplay between porous rock and fracture hydraulic properties (Ababou, 1991; p. 2–13).

Matrix diffusion in and out of fractures has been suggested as a possible mechanism for retarding transport (DOE, 1988b; p. 31). Consideration of this effect will require an understanding of the nature of the fracture surface (i.e., fracture coatings) that will affect the mass transfer at the fracture/matrix interface (Parsons *et al.*, 1991).

Sorption and precipitation of water-borne radionuclides will generally depend on the mineral surfaces present and the chemical composition in the ground water. The sorption properties of Yucca Mountain tuff can be significantly affected by the presence of zeolites. It has been suggested that model development should modify the hydrologic layering with a geochemical stratigraphy (see Figure 4-5) to account for geochemical variation (i.e., mineralization and ground-water chemistry) in the formation (*op cit.*). This type of more detailed geochemical stratigraphy provides a simple way to modify ground-water models with geochemical information.

4.2.2 Recent Modeling Studies

Parsons *et al.* (1991) reviewed a number of modeling studies relevant to Yucca Mountain. It is worthwhile to point out some simplifying assumptions that have been used in fluid flow simulations involving fractured tuff, such as: constant percolation rate; one-dimensional (1-D) vertical flow; steady-state conditions that imply pressure equilibrium between the fracture and matrix; fractures represented as a porous continuum; and transient flow with instantaneous pressure equilibration between the fracture and matrix. Some simplifying assumptions that have been used in transport simulations involving fractured tuff are: retardation calculated from a distribution coefficient (K_d); 1-D transport paths; and transport not occurring simultaneously in the fractures and matrix (*op cit.*). Many of the assumptions are because of computational constraints and limitations in characterization data (e.g., fracture properties and sorption parameters).

The above simplifications suggest that a better understanding is needed at both the fine-scale (phenomena that control fracture/matrix interactions and retardation mechanisms) and large-scale (accounting for multiple dimensions, spatial variability, and structural features such as faults). Recent work (Nitao and Buscheck, 1991; and Dykhuizen, 1990) has been examining different approaches to the fracture/matrix interaction. Nitao and Buscheck's work has examined a single fracture and quantitatively identified three distinct flow periods (predominantly fracture flow, flow primarily from the fracture into the matrix, and matrix flow) for flow in unsaturated, fractured tuff. There is, of course, a question of how best to incorporate modeling improvements of the fine-scale nature into performance assessments that need to address very large scales. Ababou (1991) in his review of modeling approaches to large-scale flow, has suggested that a compromise between direct high-resolution simulation of

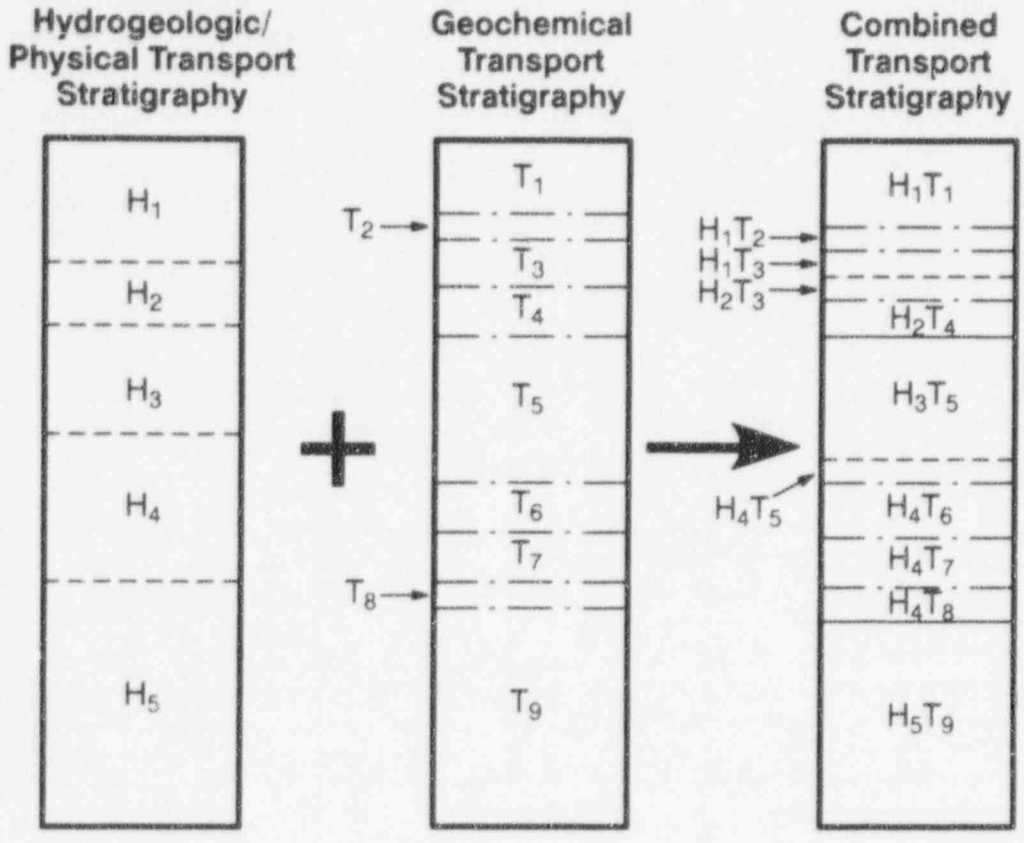

Figure 4–5 Hypothetical example of a "combined" transport stratigraphy that accounts for hydrologic and geochemical stratification (From Parsons *et al.* (1991, p. 76).)

fine-scale details and the indirect simulation approach based on uniform equivalent media models would be less computationally demanding and would capture a broad range of fine-scale to large-scale phenomena.

Additionally, the assignment of parameter values is oftentimes just as important as the underlying theory supporting the equations being solved. Ababou (1991, p. 7–1) has made the following important suggestion with respect to the interaction of modeling and data collection:

> "Realism dictates that the spatial structure of the least accessible material properties, such as the relative conductivity curves, be analyzed indirectly through correlations with more easily measured parameters. Therefore, auxiliary models need to be developed and tested in order to correlate the parameterized conductivity curves with say, void structure, porosity, and saturated conductivity."

It is important to understand the limitations and assumptions inherent with derived parameters (such as percolation) and their associated measurements (such as moisture contents). The rock properties desirable for a repository (i.e., low permeability, low percolation) also impose limitations on the ability to easily measure and quantify those same properties. As Ababou has pointed out above, a variety of models will be needed to assist the collection and interpretation of site information.

4.2.3 Site Conceptual Model

Despite the limitations and uncertainties described above, there are a number of published reports containing site information and parametric determinations to allow the development of site conceptual models and assignment of parametric values. The following section provides the details of the site conceptual model that includes the stratigraphy, boundary conditions, and parametric data.

4.2.3.1 Stratigraphy

The tilting hydrostratigraphy (generally dipping 7°) at the Yucca Mountain site results in significant differences in which hydrostratigraphic units are present at particular locations both in the unsaturated zone (between the repository horizon and the water table) and in the saturated zone (along the water table extending from a location directly below the repository to the accessible environment). The boundaries for the vertical (unsaturated zone) and near horizontal (saturated zone) flow systems are determined by the location of the water table. Therefore, assumptions regarding the location of the water table are important in identifying the hydrogeologic units present for the base case (undisturbed) and pluvial conditions (increased percolation). The assumptions and hydrogeologic units used for liquid flow are discussed below for the unsaturated zone, saturated zone, and pluvial conditions.

4.2.3.1.1 Unsaturated Liquid Flow

Ortiz *et al.* (1985) identified a number of reference stratigraphic units within the Paintbrush Tuff (Tiva Canyon welded unit, Paintbrush non-welded unit, and Topopah Spring unit); Tuffaceous beds of the Calico Hills (Calico Hills non-welded vitric unit, and Calico Hills non-welded zeolitic unit); and the Crater Flat Tuff (Prow Pass non-welded zeolitic unit, Upper Crater Flat non-welded zeolitic unit, Middle Crater Flat non-welded zeolitic unit, Bullfrog welded devitrified unit, and Tram non-welded unit) that can be used to identify where rock properties change within a particular tuff. Borehole stratigraphic data taken from Ortiz *et al.*, were used to identify hydrogeologic units and assign thicknesses below the repository. Tables 4.3 and 4.4 present information taken from Ortiz *et al.*, for selected boreholes at the Yucca Mountain site. For the purpose of defining the hydrogeologic units present in the unsaturated zone below the repository, stratigraphic information from the selected boreholes was used to represent the hydrogeology below seven distinct regions (or sub-areas) of the repository (see Figure 4–6). The seven selected boreholes depicted in Figure 4–6 were each associated with seven repository sub-areas (sub-area sizes were determined based on proximity to individual boreholes). The hydrogeologic units below each of the seven repository sub-areas were then assumed to correspond to its associated borehole stratigraphy, thus producing seven different hydrogeologic sequences over the entire repository (it should be noted that this approach assumed vertical flow in the unsaturated zone and ignored explicit site features such as the Ghost Dance fault).

The information contained in Tables 4.3 and 4.4 was simplified (i.e., rounding off thicknesses and neglecting very thin layers) to provide seven distinct hydrogeologic sequences for the unsaturated zone modeling (see Table 4–5).

4.2.3.1.2 Saturated Liquid Flow

The hydrogeologic units of the saturated zone, for this analysis, were assumed to correspond to the stratigraphy along the surface of the water table directly below the repository out to the accessible environment (5 kilometers). For the saturated zone, it was assumed that contaminant migration occurred only in the fractures and there would be minimal vertical mixing because of the relatively small volumetric flux in the unsaturated zone as compared to the volumetric flux in the saturated zone. This lack of vertical mixing and the low percolation rates result in the stratigraphic sequences along the water table being a reasonable representation for the portion of the saturated zone that affects radionuclide migration.

A map of stratigraphic changes along the surface of the water table (see Figure 4–7) in the area of interest was constructed. The map was built using available stratigraphic data from boreholes, water-table elevations, geologic maps, and stratigraphic cross-sections (see Czarnecki, 1984; Scott, 1984; and DOE, 1988a). Therefore, to account better for structural effects, both hard and soft

Table 4–3 Elevations (Reported as Meters Above Sea Level) and Distances (in Meters) for Boreholes in the Vicinity of Yucca Mountain That Were Used to Define Hydrogeologic Units for the Unsaturated Flow Model (Based on Ortiz *et al.* (1985) and the assumption that the base of the repository is 60 meters above the base of the Topopah Spring unit.)

Information	*UE25a#1 Sub–Area 1*	*USW G4 Sub–Area 2*	*USW H4 Sub–Area 3*	*USE H3 Sub–Area 4*	*USW H6 Sub–Area 5*	*USW H5 Sub–Area 6*	*USW G1 Sub–Area 7*
Elevation of Wellhead	1199	1270	1249	1484	1302	1479	1199
Elevation of Water Table	730	730	730	732	776	775	730
Distance to Water Table	469	540	519	752	526	704	469
Thickness of Topopah Spring	317	336	294	245	297	331	317
Elevation of Base of Topopah Spring	798	860	878	1102	904	974	798
Distance from Base of Topopah Spring to Water Table	68	130	148	370	128	199	68
Distance from Base of Repository to Water Table	128	190	208	430	188	259	128
Distance from Base of Repository to the Surface (Elevation of the Base of the Repository)	341 (858)	350 (920)	311 (938)	321 (1163)	338 (964)	445 (1034)	341 (858)

Table 4–4 Hydrogeologic Unit Thickness (in Meters) and Location of Water Table (Denoted by: Thickness Above the Water Table/Thickness Below the Water Table) for Boreholes in the Vicinity of Yucca Mountain (Based on information provided by Ortiz *et al.* (1985).)

Hydrogeologic Unit	*UE25a#1 Sub–Area 1*	*USW G4 Sub–Area 2*	*USW H4 Sub–Area 3*	*USE H3 Sub–Area 4*	*USW H6 Sub–Area 5*	*USW H5 Sub–Area 6*	*USW G1 Sub–Area 7*
Alluvium	9	9	—	—	9	—	18
Tiva Canyon	50	27	53	107	49	125	—
Paintbrush	25	38	24	30	43	49	67
Topopah Spring	317	336	294	244	297	331	324
Calico Hills (vitric)	—	5	30	138	73	73	16
Calico Hills (zeolitic)	68 / 93	125 / 6	99	—	—	36	145
Prow Pass	51	51	19 / 18	2	53	34	2 / 37
Upper Crater Flat	98	91	162	88	2 / 24	56 / 11	98
Bullfrog	—	129	88	98	105	111	69
Middle Crater Flat	—	45	65	45 / 2	62	42	64
Tram	—	—	126	2	94	91	83

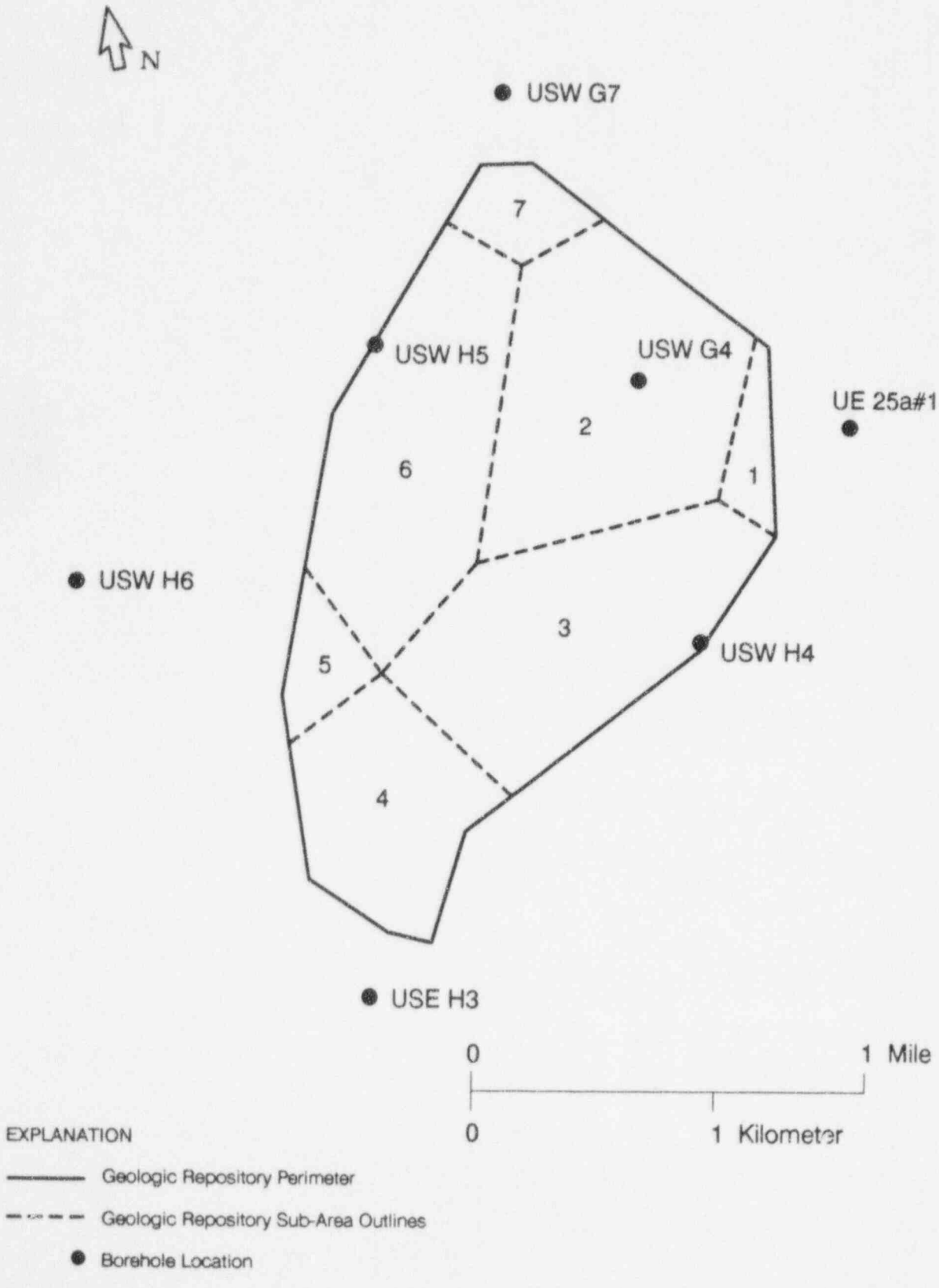

Figure 4–6 Location of seven selected boreholes used to define the hydrogeologic units for seven repository sub-areas

Table 4–5 Hydrogeologic Unit Thickness (in Meters) to be Used in the Unsaturated Flow Model (Base Case Scenario)

Hydrogeologic Unit	*UE25a#1 Sub–Area 1*	*USW G4 Sub–Area 2*	*USW H4 Sub–Area 3*	*USE H3 Sub–Area 4*	*USW H6 Sub–Area 5*	*USW H5 Sub–Area 6*	*USW G1 Sub–Area 7*
Topopah Spring	60	60	60	60	60	60	60
Calico Hills (vitric)	—	—	30	140	70	70	20
Calico Hills (zeolitic)	70	130	100	—	—	40	140
Prow Pass	—	—	20	—	60	30	—
Upper Crater Flat	—	—	—	90	—	60	—
Bullfrog	—	—	—	100	—	—	—
Middle Crater Flat	—	—	—	40	—	—	—
Distance to the Water Table	130	190	210	430	190	260	220

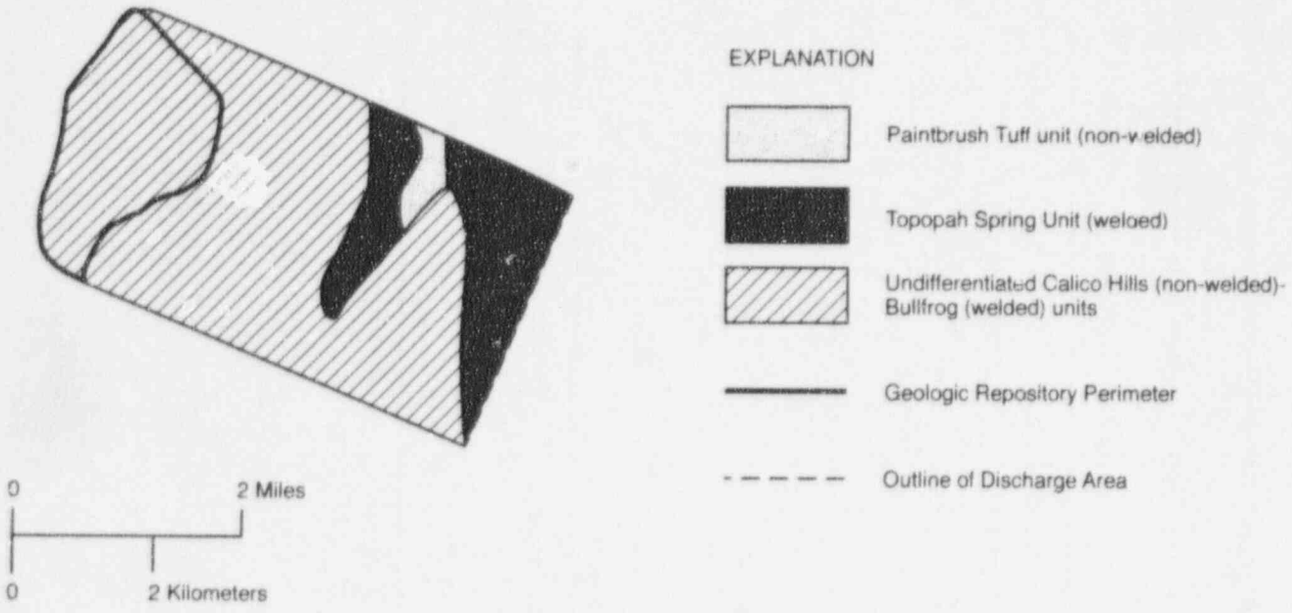

Figure 4–7 Depiction of changes in hydrogeologic units along the surface of the water table from beneath the proposed repository to the accessible environment (used for base case saturated zone model)

(interpretative) data were used to make this map. It is recognized that the interpretation of water-table stratigraphy, in Figure 4–7, is not the only possible interpretation, given the present geologic uncertainties. Future work will need to consider other possible interpretations.

This stratigraphic map was then used to determine unique hydrogeologic units (see Table 4–6 for numeric values) along the assumed saturated ground-water flow path for each of the repository zones identified for the unsaturated flow. The descriptions of the stratigraphic changes along the water table were interpreted for flow paths that assumed ground-water flows in a southeast direction from the repository. Although other interpretations of the direction of ground-water flow are possible, this interpretation agrees with most of the present interpretations found in the literature.

Additionally, as a result of data uncertainties and interpretation complexities, the interpretation of water-table stratigraphy contains no interpretations about stratigraphic units older than the Prow Pass unit. In Figure 4–7, the Prow Pass and older units occur underneath the site. It is recognized that units older than the Prow Pass unit probably occur above the water table, along the western and southern site boundaries. The simplification of using Prow Pass unit fracture properties to represent the fracture properties of the Prow Pass and older units is reasonable. It is anticipated that the rate of ground-water fracture flow over the long saturated flow path (5 kilometers) will be dominated by the fracture

Table 4–6 Length (in Kilometers) of Hydrogeologic Unit Sequences along the Saturated Flow Paths for Each of the Seven Repository Sub-Areas (Base Case Scenario)

Hydrogeologic Unit	*Sub–Area 1*	*Sub–Area 2*	*Sub–Area 3*	*Sub–Area 4*	*Sub–Area 5*	*Sub–Area 6*	*Sub–Area 7*
From the Water Table below the Repository							
Prow Pass	0.40	1.35	0.85	1.50	1.70	1.70	1.10
Calico Hills[a]	2.15	2.12	2.10	4.20	2.05	2.05	2.15
Topopah Spring	0.65	0.65	0.65	—	0.50	0.65	0.70
Paintbrush	0.30	0.25	1.35	—	—	—	0.25
Calico Hills	0.60	0.73	—	—	1.65	1.28	—
Topopah Spring	1.30	1.23	0.95	0.50	0.72	1.00	1.90
To the Accessible Environment							
Total Length	5.40	6.33	5.90	6.20	6.62	6.68	6.10

[a]Fractured properties of Calico Hills vitric and zeolitic tuff are assumed to be the same; therefore, no distinction is made between the two for the saturated paths that only consider fracture flow.

properties in units, outside the site boundary, that occur over the majority of the saturated flow path.

4.2.3.1.3 Pluvial Conditions

A pluvial scenario (increase in percolation resulting from wetter climatic conditions) was incorporated into the current modeling by assuming a higher range for percolation and an associated rise (100 meters) in the water table. These values are consistent with the initial values used in IPA Phase 1 calculations (see Codell *et al.*, 1992; p. 57) which were based in part on Czarnecki (1984). Additionally, an auxiliary analysis was performed that examined the amount of water-table rise for selected percolation rates attributed to various climatic changes. The auxiliary analysis (see Section 4.4.3) showed a variation in water-table rise (a few meters to 100 meters) for the range of climatic conditions considered.

The rise in the water table causes a decrease in the thickness of the unsaturated zone below the repository (see Table 4–7 for hydrogeologic unit thicknesses) and associated changes in the hydrogeologic units constituting the saturated flow path. The depths to the water table in a pluvial climate were assumed to be 100 meters less than the base-case depths. The stratigraphic changes used to determine hydrogeologic units for the saturated zone were based on a pluvial period as modeled by Czarnecki (1984), which projected the water table under Yucca Mountain to rise by 130 meters.

Since pluvial-period modeling effects are based on regional models they supply very little information on changes in hydraulic gradient and flow direction at a site scale. Therefore, it was assumed that the saturated flow direction and gradient would be the same as the base case. However, the hydrogeologic units along the water table for the pluvial case varied from the base case, because of the rise in the water table resulting in rock at higher elevations becoming saturated. Again, a map of stratigraphic changes along the surface of the pluvial water table was constructed. This map was then used to identify hydrogeologic units along the assumed saturated ground-water flow path for each of the repository zones identified for the unsaturated flow. The map was based on available stratigraphic data from boreholes, water-table elevations, geologic maps, and stratigraphic cross-sections (Spengler *et al.*, 1981; Bently *et al.*, 1983; Craig, 1991; Classen *et al.*, 1973; Thordarson, 1983; Lobmeyer *et al.*, 1983; Lahoud *et al.*, 1984; Healey *et al.*, 1984; Whitfield *et al.*, 1985; Thordarson *et al.*, 1985; Rush *et al.*, 1983; Scott and Bonk, 1984; Scott, 1984; Lobymeyer, 1986; Czarnecki, 1984; Czarnecki and Waddell, 1984; and DOE, 1988a). However, many less drill-hole data were available, because stratigraphic data above the water table could not be obtained for any of the U.S. Geological Survey water-table holes (WT holes). Therefore, the interpretation in Figure 4–8 (see Table 4–8 for numeric values) is less certain than the interpretation used in the base case. Again, it is recognized that the interpretation of water-table stratigraphy, in Figure 4–8, is not the only possible interpretation.

It is also recognized that the pluvial period was based on a 100-meter rise in the water table, whereas the saturated zone stratigraphy was based on a 130-meter rise. The saturated-zone stratigraphy (Figure 4–8) described above, which was based on a 130-meter rise, is considered to be a sufficient reflection of a 100-meter rise in the water table; therefore, no further work was done to refine the water-table-rise stratigraphy to 100 meters.

4.2.3.2 Boundary Conditions

The magnitude of ground-water flux leaving or entering the boundaries of a ground-water model is typically controlled through the assignment of pressure or flux boundary conditions. Understanding of these "inlet" and "outlet" boundary conditions is critical in the development of conceptual models and the interpretation of the results of ground-water models.

The upper or surface boundary condition for many ground-water models of the unsaturated zone is the percolation rate. As discussed above (see Section 4.2.1) the percolation rate is not a well-understood parameter; it can have large uncertainties because of spatial variability and transient conditions. The current analysis uses the same steady-state ranges for the percolation rate (0.1 to 5.0 millimeters/year for base case and 5.0 to 10.0 for pluvial conditions) that were used in

Table 4–7 Hydrogeologic Unit Thickness (in Meters) to be Used in the Unsaturated Flow Model (Pluvial Conditions)

Hydrogeologic Unit	*UE25a#1 Sub–Area 1*	*USW G4 Sub–Area 2*	*USW H4 Sub–Area 3*	*USE H3 Sub–Area 4*	*USW H6 Sub–Area 5*	*USW H5 Sub–Area 6*	*USW G1 Sub–Area 7*
Topopah Spring	30	60	60	60	60	60	60
Calico Hills (vitric)	—	—	30	140	30	70	20
Calico Hills (zeolitic)	—	30	20	—	—	30	40
Prow Pass	—	—	—	—	—	—	—
Upper Crater Flat	—	—	—	90	—	—	—
Bullfrog	—	—	—	40	—	—	—
Middle Crater Flat	—	—	—	—	—	—	—
Distance to the Water Table	30	90	110	330	90	160	120

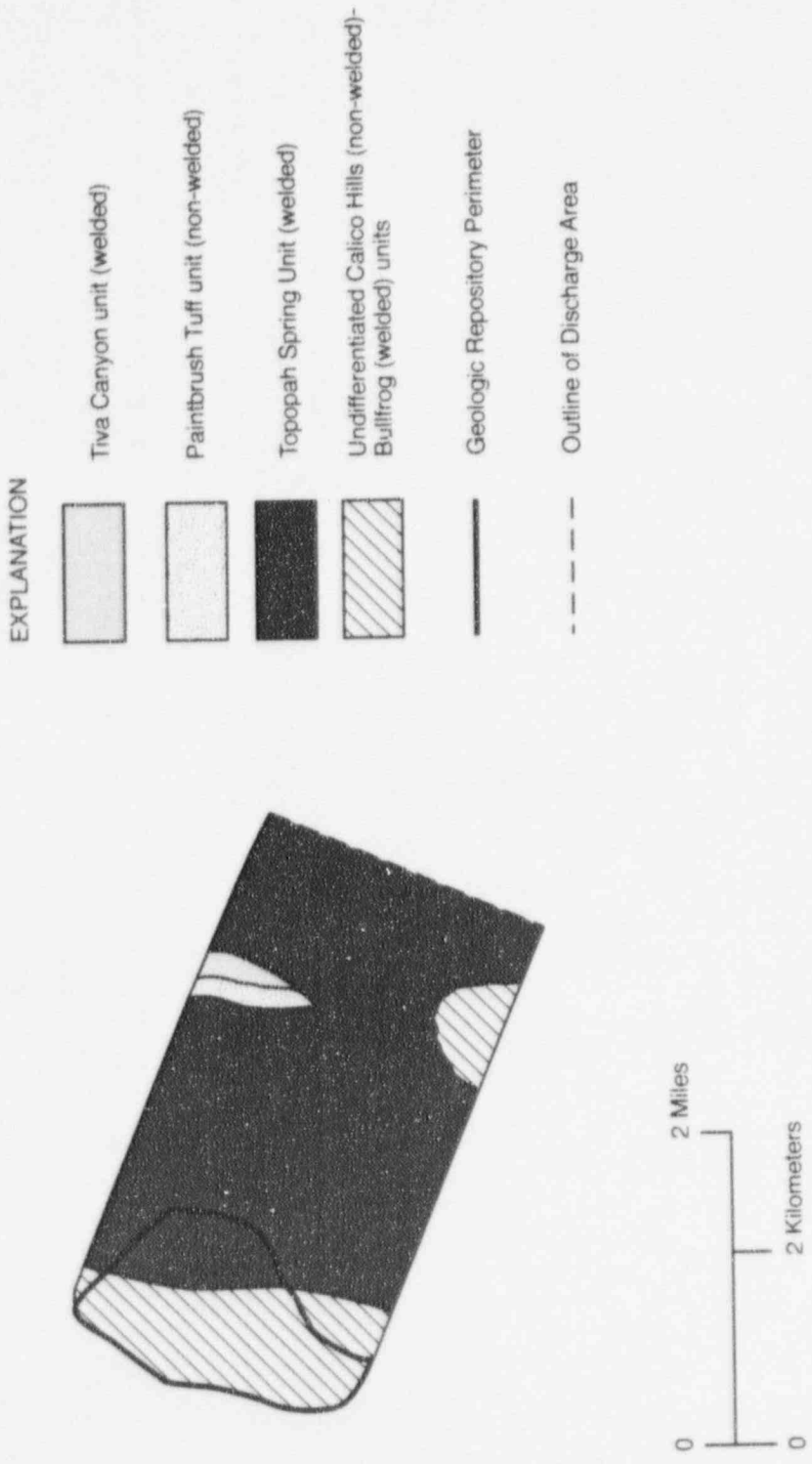

Figure 4–8 Depiction of changes, in hydrogeologic units, along the surface of the water table, under pluvial conditions (water-table rise of 100 meters) that was used for the saturated zone model

Table 4–8 Length (in Kilometers) of Hydrogeologic Unit Sequences along the Saturated Flow Paths for Each of the Seven Repository Sub-Areas (Pluvial Conditions)

Hydrogeologic Unit	*Sub–Area 1*	*Sub–Area 2*	*Sub–Area 3*	*Sub–Area 4*	*Sub–Area 5*	*Sub–Area 6*	*Sub–Area 7*
From the Water Table below the Repository							
Calico Hills[a]	—	0.38	0.28	0.90	1.22	0.90	0.10
Topopah Spring	3.05	3.65	—	3.70	—	—	3.60
Paintbrush	0.15	0.16	—	—	—	—	0.18
Tiva Canyon	0.30	0.22	—	—	—	—	0.30
Calico Hills[a]	—	—	—	0.30	—	—	—
Topopah Spring	1.90	1.92	5.62	1.30	5.40	5.78	1.92
To the Accessible Environment							
Total Length	5.40	6.33	5.90	6.20	6.62	6.68	6.10

[a]Fractured properties of Calico Hills vitric and zeolitic tuff are assumed to be the same; therefore, no distinction is made, between the two, for the saturated paths that only consider fracture flow.

the IPA Phase 1 effort (see Codell *et al.*, 1992; pp. 54 and 57). Future work will need to consider spatial variability, transient flow conditions, and further site characterization information, to provide better estimates on the range of percolation.

The current analysis is evaluating both the integrated discharge of radionuclides and the radionuclide dose. The calculation of dose requires a determination of the concentration of radionuclides in the ground water. Attributes of the "outlet" boundary condition are critical in determining the volume of water crossing the accessible environment boundary for a given time period. This volume of water is determined by multiplying the water velocity times the total pore area at the discharge point or accessible environment. The assumptions used to determine these quantities involved a number of assumptions that are described below.

4.2.3.2.1 Discharge Area

The discharge area refers to the vertical thickness and the lateral extent over which the radionuclide plume arrives at the accessible environment boundary. (In the determination of concentration, it was assumed that the radionuclides were uniformly mixed over the discharge area.) It was assumed there was no transverse dispersion of radionuclides. Therefore, the width of the plume was the lateral width of the repository (Figure 4–9). (Ignoring transverse dispersion over the long times simulated should have the conservative effect of producing higher concentrations of radionuclides at the accessible environment.) The determination of the vertical thickness was based on the assumption all radionuclide transport in the saturated zone occurred in fractures. Therefore, the range for this sampled parameter was determined from estimates of the vertical extent of fracture zones near the surface of the water table.

The vertical extent of fracturing was based on the interpretation of packer pump tests for well J–13 and radiation tracer logs for drill holes G–4, H–1, H–3, H–4, H–5, H–6, UE25b#1, and UE25p#1. In all these interpretations the thickness of the high-production zones was identified. It was assumed that high-production zones resulted from fracturing. This hypothesis was supported by an examination of fracture-hole data. In reaching interpretations of production-zone thickness, when more than one interpretation seemed reasonable, both interpretations were included for input into the simulations. This analysis yielded production-zone-thickness interpretations from 6 meters to 401 meters and averaged 70.2 meters. Table 4–9 contains the results of this analysis (Benson *et al.*, 1983; Bentley *et al.*, 1983; Blankennagel, 1967; Craig, 1991; Craig *et al.*, 1983; Craig and Robison, 1984; Craig and Johnson, 1984; Lahoud *et al.*, 1984; Lobmeyer *et al.*, 1983; Lobmeyer, 1986; Rush, 1984; Rush *et al.*, 1983; Thordarson, 1983; Thordarson *et al.*, 1985; and Whitfield *et al.*, 1984 and 1985). Values from this table were used to define a range for the thickness of the discharge area.

4.2.3.2.2 Discharge Velocity

The discharge velocity was calculated using the fracture permeability and the hydraulic gradient. The fracture permeability (see Section 4.2.3.3) is an input parameter based on laboratory measurements of rock cores, whereas the gradient was determined based on examination of head measurements in the Yucca Mountain area. The gradient was assumed to be constant (.0026). This was considered to be acceptable, since the ground-water gradient has a small dip over much of this area. It was also assumed that the gradient was not affected by variation in percolation rates in the unsaturated zone. This assumption is supported by observations that present day ground-water gradients and water-table elevations under Yucca Mountain are probably caused by percolation in high-elevation recharge areas, rather than from water percolating through the unsaturated zone at Yucca Mountain. Admittedly, a long-term change in local percolation rates at Yucca Mountain should be accompanied by a change in percolation rates in the recharge areas. This in turn should cause a change in water levels and ground-water gradients at Yucca Mountain. However, this type of detailed modeling and data is not presently available and therefore could not be incorporated into the analysis.

4.2.3.2.3 Discharge Radionuclide Concentrations

As discussed above, the product of the discharge area and the discharge velocity yielded the volume of water crossing the discharge point or the

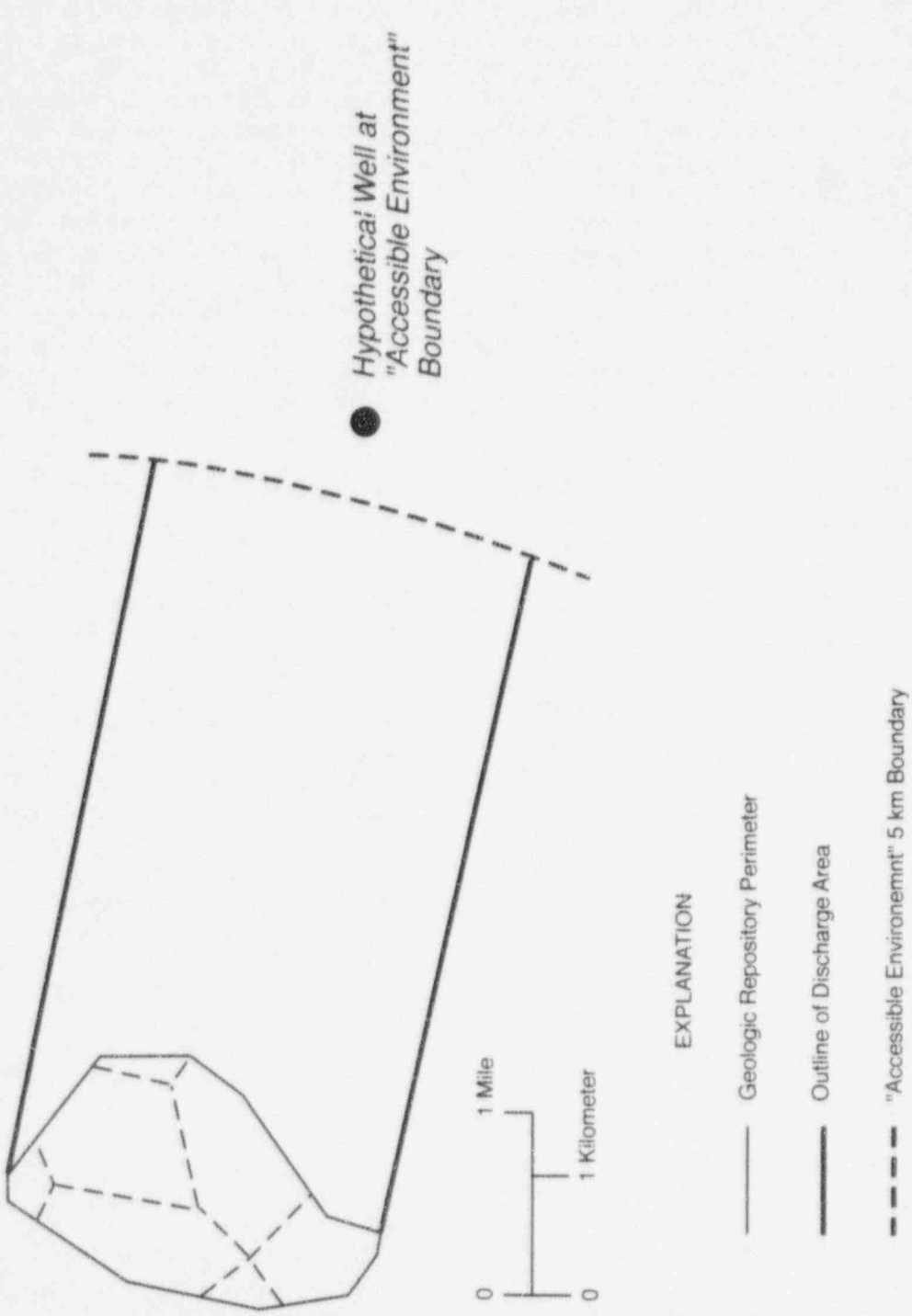

Figure 4–9 Depiction of the assumed radionuclide plume width used for calculating concentrations at a well located at the accessible environment boundary

Table 4-9 Permeability Zones Used to Determine the Range of Radionuclide Plume Depths for Transport in Fractures Within the Saturated Zone

Hole No.	*Hydrogeologic Units*	*Depth (m)*	*Thickness (m)*	*Test Flow Date*
G-4	Tram	890-900	10	1983
H-1	Prow Pass	572-563	81	1980
H-1	Prow Pass, Bullfrog	687-760	73	1980
H-1	Prow Pass	687-694	7	1980
H-1	Bullfrog	736-760	24	1980
H-3	Tram	809-841	32	1982
H-4	Prow Pass, Bullfrog, Tram	519-920	401	1982
H-5	Bullfrog	710-825	115	1982
H-5	Tram, Lava	1010-1090	80	1982
H-6	Bullfrog	616-631	15	1982
H-6	Tram	777-788	11	1982
J-13[a]	Topopah Spring	303.6-422.5	119	1963
UE25b#1	Calico Hills	471-490	19	1981
UE25b#1	Calico Hills, Prow Pass	471-620	149	1981
UE25b#1	Prow Pass	540-620	80	1981
UE25b#1	Bullfrog	799-810	11	1981
UE25b#1	Tram	875-881	6	1981
UE25p#1	Prow Pass	469-501	30	1983

[a]Interpretations of all tests from radioactive tracer logs, with the exception of Well J-13, which was from packer pump tests.

accessible environment. However, a minimum volume of ground water was used to dilute radionuclide concentrations at the discharge point. A minimum dilution volume of 1 million gallons/year was used in calculating radionuclide concentrations when the calculated discharge volume was less than this minimum amount. The 1 million gallons/year was considered consistent with the water usage of the population at the discharge point used to calculate doses. The minimum volumetric discharge amount has no effect on the calculation of integrated discharge for comparison with the U.S. Environmental Protection Agency's radiation protection standard—40 CFR Part 191[2] (*Code of Federal Regulations*, Title 40, "Protection of Environment").

4.2.3.3 Site Parameters

Site information is used to assign parametric values for the hydrologic models and the radionuclide transport models. The hydrologic parameters include permeability, matrix porosity, fracture apertures and density, and the van Genuchten parameters, whereas the transport parameters include dispersion length, K_d, and rock density. A discussion on the use of the site data and an application to the current modeling exercise is presented below, for each of the parametric topics previously listed.

4.2.3.3.1 Hydrologic Parameters

Peters *et al.* (1984) is the basis of hydrologic-parameter assignments in most of the recent modeling studies. The information reported in Peters *et al.* is the result of laboratory experiments, on tuffaceous core (fractured and unfractured), obtained from the Yucca Mountain site, used to measure (i.e., matrix porosity) and derive (i.e., permeability or conductivity, fracture aperture, and van Genuchten parameters) hydrologic parameters. The hydrologic-parametric values used in recent studies and the relevant values from the Peters' *et al.* report for hydrogeologic units present at Yucca Mountain are presented in Appendix B. Additionally, the parametric ranges and distributions used in the sensitivity analysis are reported in Appendix B.

Matrix Porosity: Matrix porosity values reported in Peters *et al.* (1984) were based on laboratory measurements. The parametric range for the sensitivity analysis used the wider range of either the reported results or plus and minus 25 percent of the mean value of the reported results. The assignment of a larger range than the reported results was done to more fully account for spatial variability and parametric uncertainty that may not be accurately reflected in the somewhat limited (two drill-holes) test results.

Matrix Conductivity: Saturated matrix conductivity values reported in Peters *et al.* (1984) were derived based on the laboratory measurement of volumetric flux (using a constant head method) and application of Darcy's Law. The wider range of either the reported results or of plus and minus 50 percent of the mean value reported in Peters *et al.* was used to represent the variability of the parameter in this analysis. As with the matrix porosity, a broader range was used to compensate for the limited data over the Yucca Mountain site.

The range in hydrologic measurements using small drill cores does not account for spatial variability within a hydrogeologic unit. The assignment of a hydraulic conductivity for a specific hydrogeologic unit needs to account for the correlation length of hydraulic conductivity over the thickness of a particular unit. Geostatistical analyses reported in the IPA Phase 1 effort (Codell *et al.*, 1992; p. F-1) indicated that there was no apparent spatial correlation of the core data for saturated hydraulic conductivity beyond the minimum separation distance of 10 meters. A correlation distance of 10 meters was assumed for the current analysis, to determine a range in hydraulic conductivity for each hydrogeologic unit.

A representative conductivity for a hydrogeologic unit was calculated, based on the number of correlated lengths present in a given unit (see

[2]Currently, a revised set of standards specific to the Yucca Mountain site is being developed in accordance with the provisions of the Energy Policy Act of 1992. The Energy Policy Act of 1992 (Public Law 102-486), approved October 24, 1992, directs NRC to promulgate a rule, modifying 10 CFR Part 60 of its regulations, so that these regulations are consistent with EPA's public health and safety standards for protection of the public from releases to the accessible environment from radioactive materials stored or disposed of at Yucca Mountain, Nevada, consistent with the findings and recommendations made by the National Academy of Sciences, to EPA, on issues relating to the environmental standards governing the Yucca Mountain repository. It is assumed that the revised EPA standards for the Yucca Mountain site will not be substantially different from those currently contained in 40 CFR Part 191, particularly as they pertain to the need to conduct a quantitative performance assessment as the means to estimate postclosure performance of the repository system.

Figure 4–10) and the variability in the parameter. To develop a range for the representative conductivity, 100 random samples were generated for each correlated length within an individual unit (for simplicity, the number of correlation lengths in a given unit was based on the smallest unit thickness in Table 4–5; for example, the Topopah Spring unit has 6 correlation lengths over the 60-meter length). The sampling range used for the 100 random samples was based on the parameter variability described above. Table 4–10 presents the resulting matrix representative conductivity ranges and the supporting input values.

Matrix Characteristic Curves: The parameters that describe the behavior of the fluid flow under partially saturated conditions were obtained (Peters *et al.*, 1984) by fitting water-retention data to the following form (Equation 4–1) of the van Genuchten equation:

$$S = (S_s - S_r)\left[\frac{1}{1 + |a\,h|^{\beta}}\right]^{(1-1/\beta)} + S_r \quad , \qquad \textbf{(4–1)}$$

where:

S	=	saturation;
S_s	=	saturation at full saturation;
S_r	=	residual saturation;
h	=	pressure or suction;
α	=	fitting parameter; and
β	=	fitting parameter.

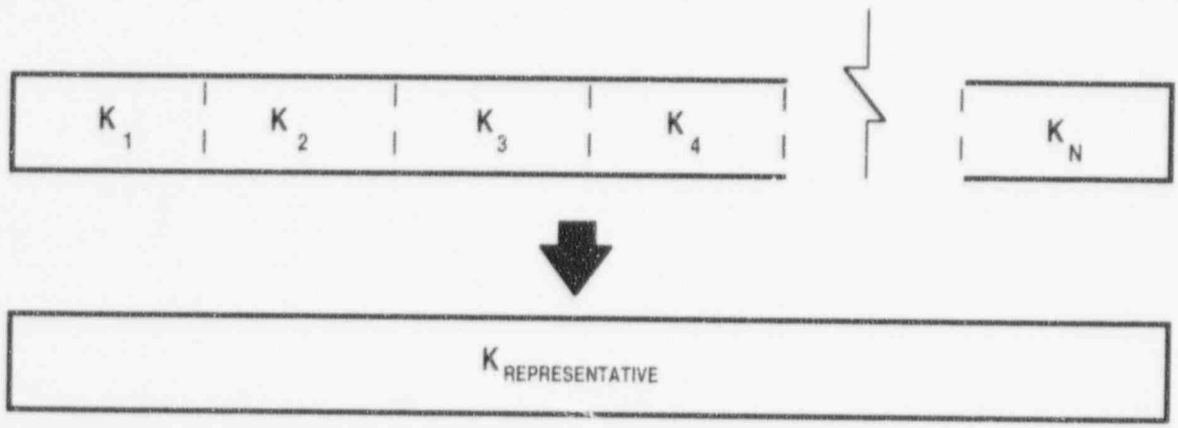

$$\frac{N}{K_{REPRESENTATIVE}} = \sum_{J=1}^{N} \frac{1}{K_J}$$

where:

N is the total number of correlation lengths present in the hydrologic unit

K_J is the conductivity value appropriate over one correlation length

Figure 4–10 Graphical representation of the correlation length of a hydrogeologic unit and its relationship to the calculation of a representative conductivity

Table 4–10 Matrix Representative Conductivities and Permeabilities (Permeabilities Given in Brackets) for the Indicated Hydrogeologic Units and the Values Used to Calculate the Representative Values Based on 100 Data Realizations and the Calculational Approach Presented in Figure 4–10

Hydrogeologic Unit	*Data Range*[a] *(mm/yr)*	*Number of 10 meter Correlation Lengths*	*Representative Range (mm/yr) [m^2]*
Topopah Spring (welded)	.04 to 1.2	6	0.11 to .36 [3.6×10^{-19} to 1.2×10^{-18}]
Calico Hills (vitric, non-welded)	820. to 9,100.	2	1.2×10^{3} to 6.1×10^{3} [3.9×10^{-15} to 2.0×10^{-14}]
Calico Hills (zeolitic, non-welded)	7.6×10^{-4} to 5.0	4	.004 to .21 [1.3×10^{-20} to 6.7×10^{-19}]
Prow Pass (welded)	40. to 440.	2	58.0 to 300. [1.9×10^{-16} to 9.6×10^{-16}]
Upper Crater Flat (non-welded)	0.6 to 14.	6	1.6 to 4.6 [5.1×10^{-18} to 1.5×10^{-17}]
Bullfrog (welded)	72. to 200.	10	110.0 to 140. [3.5×10^{-16} to 4.4×10^{-16}]
Middle Crater Flat (non-welded)	0.6 to 14.	4	1.3 to 4.8 [4.1×10^{-18} to 1.6×10^{-17}]

[a]Based on actual ranges reported in Peters *et al.* (1984).

The two fitting parameters (α and β) control the shape of the characteristic curves (variation of saturation versus pressure, and variation of conductivity versus pressure or saturation) for unsaturated flow. These two parameters can physically be related to the size and distribution of pore space (larger pores will desaturate before smaller pores). A narrow distribution of pore space will result in desaturation occurring over a very small pressure range and thus will exhibit a relatively steep characteristic curve. A second van Genuchten equation (van Genuchten, 1980) based on the method of Mualem (1976) was used to represent the relationship of the conductivity and saturation, assuming the applicability of the desaturation curve (Equation 4–1) fitting parameters to the conductivity curve (Equation 4–2).

$$K_r = \sqrt{S_e}\left[1 - \left(1 - (S_e)^{\frac{1}{\lambda}}\right)^{\lambda}\right]^2 \quad \text{, and} \qquad \textbf{(4–2)}$$

$$S_e = \frac{S - S_r}{S_s - S_r} \quad , \qquad \textbf{(4–3)}$$

where:

S = saturation;
S_s = saturation at full saturation;
S_r = residual saturation;
S_e = effective saturation;
K_r = relative conductivity; and
λ = van Genuchten fitting parameter ($1 - 1/\beta$).

For this analysis, saturations were derived from flux considerations, using Equation 4–2; therefore, only the fitting parameter β was sampled. The parametric ranges for β were based on a 25 percent increase and decrease of values reported in Klavetter and Peters (1986) and supplemented by data ranges reported in Peters *et al.* (1984). Single values for the fitting parameter α were taken from Klavetter and Peters and were supplemented with average values from Peters *et al.*, where necessary. Finally, the residual saturation, S_r, for simplicity was assumed to be zero (this assumption is assumed to have a minimal effect on the analysis).

Fracture Porosity: Fracture apertures reported in Peters *et al.* (1984) were derived based on volumetric flow measurements and assuming the cubic law applied to steady-state laminar flow between parallel plates. These fracture apertures combined with fracture density were used to derive bulk-fracture porosity, as reported in Klavetter and Peters (1986). The bulk-fracture porosities were assumed to be constant in the current analysis.

Fracture Conductivity: Peters *et al.* (1984) reported on laboratory analyses of fractured tuff samples and the derivation of fracture properties based primarily on assuming the cubic law applied to steady-state laminar flow between parallel plates and determined the conductivity of a single fracture. Based on the Peters *et al.* analyses, Klavetter and Peters (1986) reported the fracture conductivities used to represent the initial range of unit properties. Bulk fracture conductivities (conductivity per unit area) were determined by multiplying the single fracture conductivity times the fracture area per unit area for each hydrogeologic unit. The wider range of either the reported results or plus and minus 50 percent of the mean values reported in Klavetter and Peters was used to represent the variability of the parametric range in this analysis. This was done to compensate for the limited data over the Yucca Mountain site and the lack of a range for conductivity, as reported in Klavetter and Peters.

The parametric range for a given hydrogeologic unit was subsequently used to calculate a representative permeability range for a given hydrogeologic unit, using the same procedure to account for spatial variability as was described above for matrix conductivity (see Table 4–11 for resulting representative ranges and supporting input values).

Fracture Characteristic Curves: It was assumed that unsaturated flow within fractures is governed by the same van Genuchten relationships described above for unsaturated matrix flow, in addition to the applicability of the steady-state laminar flow between parallel plates, as well as fracture apertures being sufficiently small so that capillary forces control fluid flow. The range for the fitting parameter β (see discussion under matrix characteristic curves above) was determined by increasing and decreasing by 25 percent the value reported in Klavetter and Peters (1986). Similar to the matrix value, the fitting parameter α was set to a single value corresponding to the value reported in Klavetter and Peters. Unlike the matrix values, which had separate values for each hydrologic unit, the fracture characteristic curves were the same for each unit.

4.2.3.3.2 Transport Parameters

Dispersion Length: The hydrodynamic dispersion process works to disperse contaminants along a flow path through mechanical dispersion and molecular diffusion. The dispersion length is a parameter used in transport equations to capture the spreading of a contaminant. This parameter, not without controversy, is a factor that compensates for a lack of knowledge of the conductivity field and therefore tends to exhibit a strong dependence on the scale over which it is estimated. For the current analysis, a range of 0.3 to 30.0 meters is used.

Retardation Factors: IPA Phase 1 used an element-specific retardation coefficient to represent the chemical reactions affecting radionuclide transport through the geologic medium. The IPA Phase 2 effort also uses a retardation coefficient type of approach (retardation coefficients are calculated from sorption coefficients or K_ds). A departure from the previous analysis is the assignment of K_ds to specific hydrogeologic units, when data were available to make the assignment. K_d values were selected, where appropriate, from Meijer (1990) and Thomas (1987). When information was not appropriate, values consistent with the Codell *et al.* report (1992) were used. The values were specific to the following hydrogeologic units:

Table 4–11 Fracture Representative Conductivities and Permeabilities (Permeabilities Given in Brackets) for the Indicated Hydrogeologic Units and the Values Used to Calculate the Representative Values Based on 100 Data Realizations and the Calculational Approach Presented in Figure 4–10

Hydrogeologic Unit	*Data Range*[a] *(mm/yr)*	*Number of 10 meter Correlation Lengths*	*Representative Range (mm/yr) [m^2]*
Topopah Spring (welded)	20. to 100.	6	33. to 59. [1.1×10^{-16} to 1.9×10^{-16}]
Calico Hills (vitric, non-welded)	145. to 435.	2	170. to 360. [5.6×10^{-16} to 1.2×10^{-15}]
Calico Hills (zeolitic, non-welded)	145. to 435.	4	190. to 310. [6.2×10^{-16} to 9.9×10^{-16}]
Prow Pass (welded)	10. to 30.	2	12. to 25. [3.9×10^{-17} to 8.1×10^{-17}]
Upper Crater Flat[b] (non-welded)	145. to 435.	6	210. to 300. [6.7×10^{-16} to 9.8×10^{-16}]
Bullfrog[c] (welded)	10. to 30.	10	15. to 20. [4.9×10^{-17} to 6.4×10^{-17}]
Middle Crater Flat[b] (non-welded)	145. to 435.	4	190. to 310. [6.2×10^{-16} to 9.9×10^{-16}]

[a]Based on wider range of either the actual range or plus and minus 50 percent of the mean value, as reported in Klavetter and Peters (1986).
[b]Based on Calico Hills.
[c]Based on Prow Pass.

Topopah Spring Member of the Paintbrush Tuff (Tpt); Calico Hills non-welded vitric (CHnv); Calico Hills non-welded zeolitic (CHnz); Prow Pass Member (PP) of the Crater Flat Tuff (Tcp); and Bullfrog Member (BF) of the Crater Flat Tuff (Tcb).

The K_d values for the matrix are presented in Appendix B along with a discussion on how the K_d values for the matrix were derived from the Meijer (1990) and Thomas (1987) reports. A range for sensitivity analysis was developed by assuming a log-uniform distribution and increasing and decreasing the K_d values by one order of magnitude, to develop the ends of the distribution. Sorption was assumed not to occur in fractures, because of the conceptualization that flow will be fast relative to the rates of sorption reactions. Therefore, K_d values in the fractures were all set to zero.

K_d values were used to calculate retardation factors via the following formula:

$$R_f = 1.0 + \frac{\varrho(1-n)}{\Theta} \cdot K_d \quad , \qquad \textbf{(4–4)}$$

where:

R_f = retardation factor;
K_d = distribution coefficient;
Θ = moisture content;
ϱ = grain density; and
n = porosity.

4.2.4 Computational Model Description (Liquid Flow and Transport)

The computational model, for use in the total-system performance assessment (TPA) computer code, used for representing liquid flow and subsequent transport of radionuclides, was developed to gain insights into the following processes and concepts:

- Matrix versus fracture flow;
- Variation in hydrogeologic unit thicknesses between the repository and the water table;
- Transport in the saturated zone; and
- Variation in geochemical retardation between different hydrogeologic units.

The implementation of these processes and concepts into a computational module for the current analysis involved the development of a calculational strategy, selection and development of a computer program(s), and determination of site representation. All of these topics will be discussed in more detail, to provide a better understanding of the representation of liquid flow and radionuclide transport in the current analysis.

4.2.4.1 Computational Strategy

As has been discussed in prior sections (see Section 4.2.3), the flow in the unsaturated zone (between the repository and the water table) is assumed to be primarily in the vertical direction, whereas the flow in the saturated zone, near the water table, has been assumed to be primarily to the south-east. Thus the flow representations, for both the saturated and the unsaturated zones, were assumed to be 1-D, with differing hydrogeologic units for the seven repository sub-areas (see Figure 4-11). The seven repository sub-areas were selected based on a need to represent the variation in hydrogeology below the repository and use stratigraphic information for selected boreholes at the site (Figure 4-6). Therefore, there are seven repository sub-areas, each connected to its own unsaturated and saturated zone hydrogeolgic sequences, similar to the representation presented in Figure 4-6.

The hydrogeologic sequences associated with the seven repository sub-areas define the flowpaths that are to be analyzed. These flowpaths are described as 1-D segments, because in part, of the 1-D nature of the flow and a calculational need for efficient simulation approaches that would be suitable to the numerous simulations that are required for sensitivity and uncertainty analyses. It was anticipated that a simple depiction, which still retained some realism with respect to site description, would be necessary for reasonable simulation times.

Additionally, the horizontal diversion of unsaturated flow, at the interface between hydrogeologic units with contrasting flow properties, and the transfer of liquid water, between fractures and matrix in the unsaturated zone, are two other aspects of unsaturated flow that have the potential to be computationally very demanding. Therefore, special consideration was given to the computational approach used to deal with these two issues. Rather than solve the flow equation explicitly, it was decided to use a "table look-up" (discussed below under computer program development) procedure to account for flow diversion above the repository and the interaction between matrix and fracture flow in the unsaturated zone.

4.2.4.2 Selection and Development of Computational Model(s)

The flow paths are assumed to be 1-D; therefore, the determination of the total amount of fluid flux in a given flow path and the partitioning of flux between the fracture and matrix is crucial. The *NEFTRAN II* (Olague *et al.*, 1991) computer program was selected to simulate liquid flow and radionuclide transport because of its ability to accommodate saturated and unsaturated flow and radionuclide transport, using a minimum amount of computer time. However, to account for the diversion of flow and transfer of fluid between the fractures and the matrix, a pre-processor was developed to determine the total incoming flux for each repository sub-area and the distribution of fracture versus matrix flow for each hydrogeologic unit present.

A detailed description of the pre-processor is required to fully understand the manner in which *NEFTRAN II* is implemented for the current

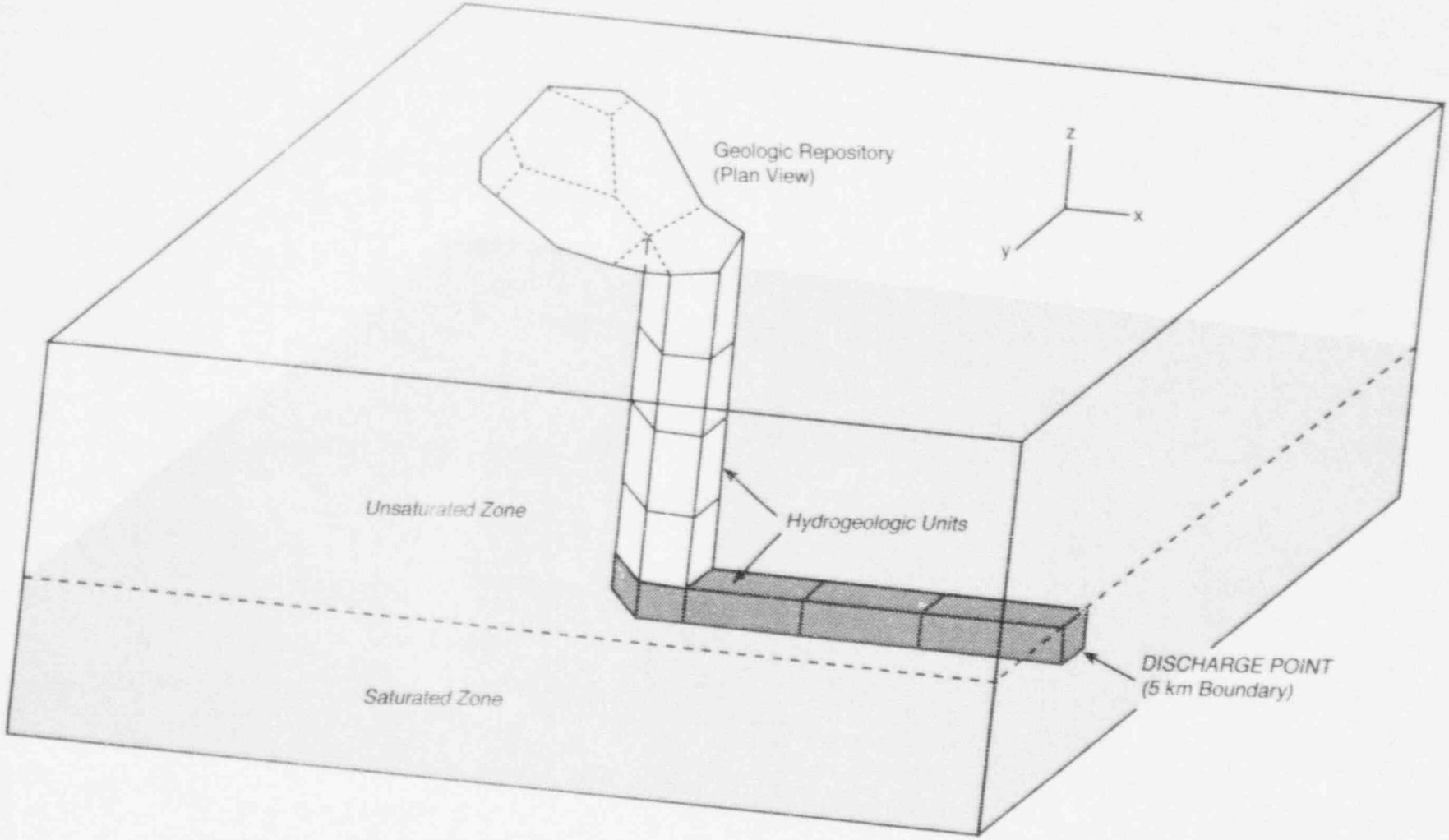

Figure 4–11 Illustration of a representative flow path for a sub-area of the repository, assuming one-dimensional flow in both the saturated and unsaturated zones

analysis. The pre-processor, hereafter referred to as *FLOWMOD*, performs the following primary functions:

- Determination of the areal flux;
- Determination of fracture flow; and
- Determination of retardation factors.

Determination of Areal Flux: The distribution of recharge at the repository depth is anticipated to have a degree of variation because of the tilting of the bedding planes, variation in hydraulic properties, and the amount of recharge. To quantitatively estimate the spatial distribution of percolation, a series of two-dimensional (2-D) simulations were conducted to develop an interpolation table for use within *FLOWMOD*. The 2-D simulations were performed using the *DCM3D* computer program (Updegraff *et al.*, 1991) and made use of the cross-sectional stratigraphy depicted in Figure 4–4 and parametric values (see Table 4–12) found in Klavetter and Peters (1986). *DCM3D* is a dual-continuum unsaturated flow simulator that represents liquid flow in fractures and matrix as separate but connected flow fields. The following flow equations are solved for the matrix and the fracture continuum, respectively:

$$C^m \frac{\partial p^m}{\partial t} = \nabla \cdot \left(\frac{k^m}{\mu} (\nabla p^m + \varrho g \nabla z) \right) - \Gamma + Q^m \ , \quad \textbf{(4–5)}$$

$$C^f \frac{\partial p^f}{\partial t} = \nabla \cdot \left(\frac{k^f}{\mu} (\nabla p^f + \varrho g \nabla z) \right) - \Gamma + Q^f \ , \quad \textbf{(4–6)}$$

where:

p^m = water pressure in the matrix continuum;
p^f = water pressure in the fracture continuum;
C^m = specific storage coefficient of the matrix continuum;
C^f = specific storage coefficient of the fracture continuum;
k^m = permeability of the matrix continuum (dependent on saturation);
k^f = permeability of the fracture continuum (dependent on saturation);
Q^m = volumetric source term for the matrix continuum;
Q^f = volumetric source term for the fracture continuum;
Γ = fracture to matrix transfer term;
ϱ = water density;
μ = viscosity of water;
g = gravitational coefficient;
z = z-direction distance; and
t = time.

A depiction of the hydrogeologic units and the types of boundary conditions applied to the cross-section is presented in Figure 4–12. Unit properties were assumed to be homogenous and isotropic for the all the cross-section simulations. To examine the spatial variation of the percolation, a number of steady-state simulations were performed over a range of percolation rates (.01 to 10.0 millimeters/year). The spatial distribution of recharge at the repository level resulting from these simulations was then used to develop a table (see Table 4–13) which was used to interpolate total flux amounts for each of the seven repository sub-areas (see Figure 4–6). Although this is a simple representation it accounts for a measure of flow diversion that is anticipated to occur for higher flux values. Future work will need to examine this phenomenon with more detailed modeling, which can take into account continuing site characterization activities (e.g., characterization of spatial variability of hydrologic properties, and location of and further understanding of the hydrologic significance of structures like major fracture zones or faults as sources of focused recharge).

Determination of Fracture Flow: The partitioning of fluid flux between the matrix and the fractures is dependent on a number of factors such as the total flux, hydraulic properties of the matrix and fractures, and spatial and temporal heterogeneities. For the present analysis, no attempt was made to account for the effects of spatial and temporal heterogeneities. The current analysis does account for the differences in hydrologic properties, between the fractures and the matrix, and the dependence of these properties on the flux. The sensitivity analysis required an efficient means to calculate fluid flow. Therefore a table interpolation approach was implemented within *FLOWMOD*. The interpolation table used in

Table 4–12 Hydrogeologic Parameters Used for Simulating Two-Dimensional Flow (see Figure 4.12) with *DCM3D*, to Analyze the Spatial Distribution of Percolation at the Repository Depth

Hydrogeologic Unit		*Permeability (m^2) [conductivity, mm/yr]*	*Porosity*	*Characteristic Curve–Fitting Parameters*		*Transfer Factor[a] (m^2) [No. Fractures]*
				α (1/m)	β	
Tiva Canyon (welded)	M[b]	9.7×10^{-19} [0.30]	.08	8.2×10^{-3}	1.6	N/A
	F[c]	5.5×10^{-16} [170.]	1.4×10^{-4}	1.3	4.2	1.6×10^{-15} [20]
Paintbrush (non-welded)	M	3.9×10^{-14} [1.2×10^{4}]	.40	1.5×10^{-2}	6.9	NA
	F	1.6×10^{-15} [490.]	2.7×10^{-5}	1.3	4.2	1.6×10^{-13} [1]
Topopah Spring (welded)	M	1.9×10^{-18} [0.6]	.11	6.0×10^{-3}	1.8	NA
	F	1.9×10^{-16} [59.]	1.1×10^{-4}	1.3	4.2	4.4×10^{-14} [24]
Calico Hills (non-welded, zeolitic)	M	2.0×10^{-18} [.06]	.28	3.0×10^{-3}	1.6	NA
	F	9.4×10^{-16} [290.]	4.6×10^{-5}	1.3	4.2	7.2×10^{-17} [3]

[a]Transfer factor based on assumption of regular planar fractions (equals $4n^2k_m$, where n is the number of fractures and k_m is the matrix permeability).
[b]Matrix.
[c]Fracture.

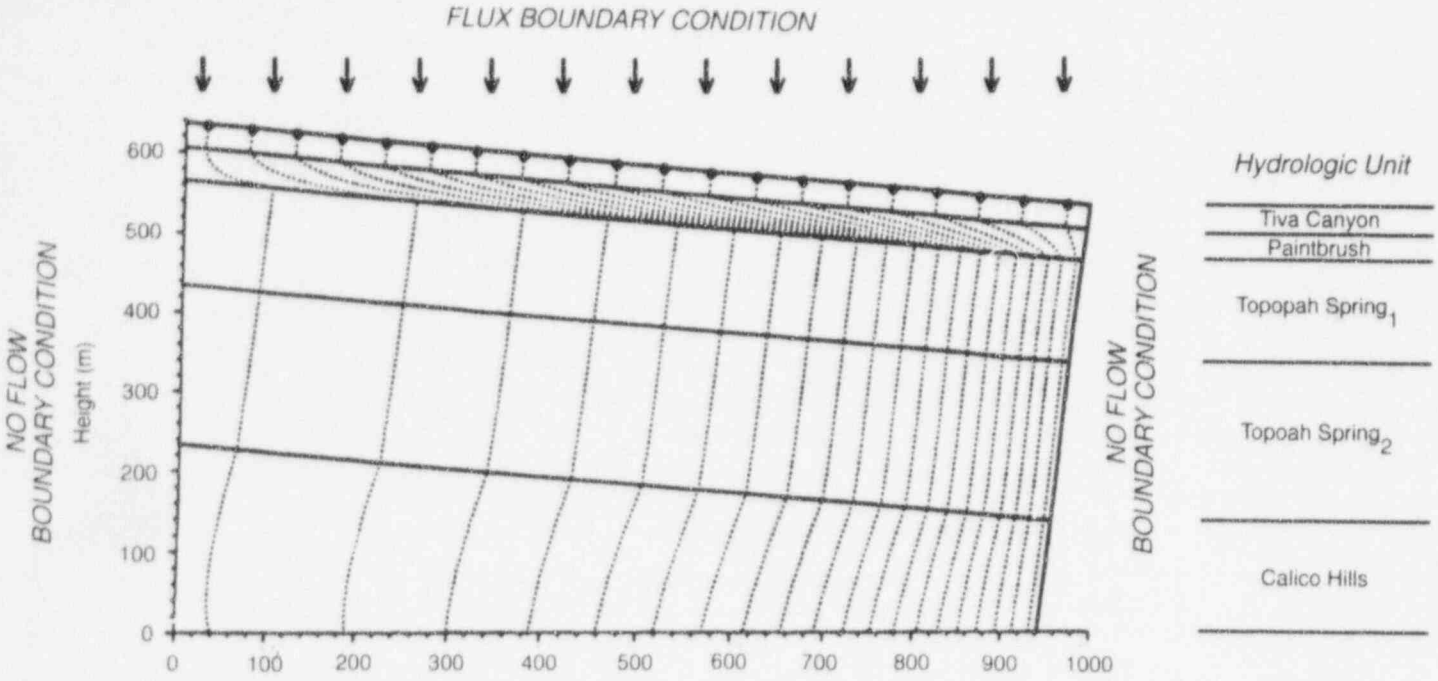

Figure 4–12 Depiction of the hydrologic units and boundary conditions used to evaluate the spatial variation of percolation at the repository depth

Table 4–13 Distribution of Percolation for the Seven Repository Sub-Areas, as Depicted in Figure 4–6

Surface Infiltration (mm/yr)	*Percolation at Repository Depth (mm/yr) for Each Sub–Area*		
	Sub–Areas 1 and 3	*Sub–Area 2*	*Sub–Areas 4, 5, 6, and 7*
0.01	0.01	0.01	0.01
0.05	0.06	0.05	0.04
0.10	0.13	0.09	0.07
0.20	0.26	0.18	0.13
0.30	0.38	0.25	0.18
1.00	1.25	0.80	0.60
2.00	2.25	1.80	1.60
10.0	10.5	9.80	9.50

determining the fraction of fluid flow was based on 1-D flow simulations, using *DCM3D*.

DCM3D was used to simulate 1-D unsaturated zone flow in a dual porosity medium (one fracture continuum and one matrix continuum) for a range of percolation rates. Steady-state flow was modeled for each of the hydrogeologic units, to determine the fraction of the total flow that was in the matrix as a percentage of the saturated conductivity of the matrix. A table, within *FLOWMOD*, was constructed for each unit, to determine the fraction of flow in the matrix. The table expressed the amount of matrix flow and the total flow as a fraction of the saturated conductivity of the matrix (see Table 4-14). The dimensionless aspect of the table allowed the same table to be used throughout the sensitivity analysis, where both the saturated conductivity and the percolation were sampled parameters. The table interpolation procedure determines the fraction of the total flow in the matrix. It was assumed that the remaining flow was in the fractures.

Retardation Factors: The retardation parameter was initially discussed in Section 4.2.3.3, under transport parameters. The retardation parameter is calculated within *FLOWMOD*, based on the K_d value (sampled in the sensitivity analysis); the grain density of the matrix (assumed to be a constant for each unit); porosity of the matrix (sampled in the sensitivity analysis); and the matrix moisture content (as mentioned previously, no retardation was assumed in the fractures, because, primarily, of the limited surface area of the fractures compared with the matrix). Of these values, the moisture content was the only value that required a calculation before determining the retardation factor. The moisture content for a given hydrogeologic unit was derived assuming a unit gradient in the unsaturated zone and using Equation (4-2). Retardation in the matrix above the water table (recall that transport in the saturated zone is assumed to occur entirely in the fractures and is thus unretarded) can vary because of a change of properties in the hydrogeologic units and changes in moisture content, caused primarily by changes in flux.

4.2.4.3 Site Representation

As discussed above, *FLOWMOD* does interpolations to determine the total flux entering each of the seven repository sub-areas and the distribution of flux in the matrix and the fracture continua. This information is then used by *FLOWMOD* to define a series of transport paths from each of the seven repository sub-areas to the accessible environment. The flow in a given hydrogeologic unit could be a combination of fracture and matrix flow; however, for computational simplicity, the fracture flow and the matrix flow are split into separate flowpaths. This approach for simulating the fracture and matrix flow precludes diffusive transport between fractures and matrix (i.e., matrix diffusion). This is likely to be a conservative assumption, because matrix diffusion is a potentially important retardation mechanism for fracture-dominated flow. Parametric uncertainty for the Yucca Mountain cases, and the possible importance of fracture coatings in reducing matrix diffusion, may diminish the importance of this phenomenon at the Yucca Mountain site.

Based on this approach, a flowpath over only one hydrogeologic unit would result in two transport paths (one for the matrix flow and one for the fracture flow). Because of the many hydrogeologic units that comprise the flowpaths from the repository to the accessible environment, there are a series of potential transport paths resulting from all the possible combinations of fracture and matrix flow (see Figure 4-13). *FLOWMOD* defines the transport paths for the flowpaths that have a non-zero flux and provides the input data necessary to simulate the transport of radionuclides with the *NEFTRAN II* computer program. Additionally, *FLOWMOD* distributes the repository releases from the source term according to the fraction of flux in a particular flowpath. For example, a flowpath that has 10 percent of the total flux will receive 10 percent of the source term. While this approach offers limited interaction between the fractures and matrix, it does account for the differing travel times and fluxes caused by fracture and matrix flow.

A common discharge point has been assumed (see Section 4.2.3.2) for all transport paths. Releases to the environment are obtained by summing all the individual releases from all the transport paths for each of the seven repository sub-areas.

Table 4–14 Variation of Matrix Flux Versus the Total Flux for Each of the Hydrogeologic Units Simulated at Yucca Mountain

Total and Matrix Flux (Expressed as Fraction of Saturated Conductivity, K_s) for the Indicated Hydrogeologic Units

	Topopah Spring	*Calico Hills (vitric)*	*Calico Hills (zeolitic)*	*Prow Pass*	*Upper Crater Flat*	*Bullfrog*	*Middle Crater Flat*
K_s (mm/yr)	.60	8,500.	.63	140.	1.0	140.	1.0
Total	.17	1.2×10^{-5}	.16	7.1×10^{-4}	.10	7.1×10^{-4}	.10
Matrix	.17	1.2×10^{-5}	.16	7.1×10^{-4}	.10	7.1×10^{-4}	.10
Total	.50	3.5×10^{-5}	.48	2.1×10^{-3}	.30	2.1×10^{-3}	.30
Matrix	.50	3.5×10^{-5}	.48	2.1×10^{-3}	.30	2.1×10^{-3}	.30
Total	.83	5.9×10^{-5}	.79	3.6×10^{-3}	.50	3.6×10^{-3}	.50
Matrix	.83	5.9×10^{-5}	.79	3.6×10^{-3}	.50	3.6×10^{-3}	.50
Total	1.25	8.8×10^{-5}	1.20	5.4×10^{-3}	.75	5.4×10^{-3}	.75
Matrix	.97	8.8×10^{-5}	.92	5.4×10^{-3}	.75	5.4×10^{-3}	.75
Total	1.67	1.2×10^{-4}	1.60	7.1×10^{-3}	1.00	7.1×10^{-3}	1.00
Matrix	.97	1.2×10^{-4}	.92	7.1×10^{-3}	.98	7.1×10^{-3}	.98
Total	3.33	2.4×10^{-4}	3.20	.01	2.00	.01	2.00
Matrix	.97	2.4×10^{-4}	.94	.01	.99	.01	.99
Total	6.67	4.7×10^{-4}	6.30	.03	4.00	.03	4.00
Matrix	.97	4.7×10^{-4}	.94	.03	.99	.03	.99
Total	11.67	8.2×10^{-4}	11.10	.05	7.00	.05	7.00
Matrix	.97	8.2×10^{-4}	.94	.05	.99	.05	.99
Total	16.70	1.2×10^{-3}	15.90	.07	10.00	.07	10.00
Matrix	.97	1.2×10^{-3}	.94	.07	.99	.07	.99

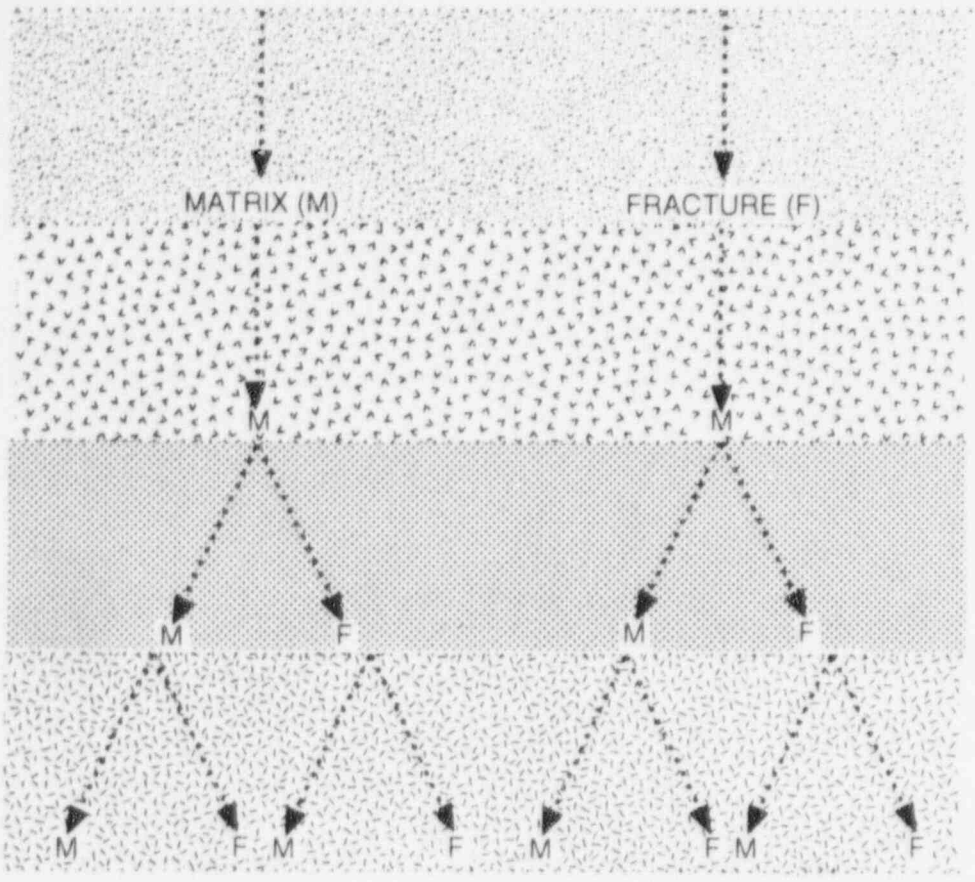

Figure 4-13 Depiction of the multiple transport paths, based on four different hydrogeologic units and the indicated combinations of fracture and matrix flow

4.3 Flow and Radionuclide Transport Module for Gaseous Releases

The elevated topography and unsaturated fractured stratigraphy of Yucca Mountain favor the existence of gas flows driven by thermal gradients. Such flows have been observed in relatively shallow holes (Weeks, 1987). Thermal gradient driven flows are expected to exist in the vicinity of the repository, particularly under the influence of the repository heat load. Such flows have been predicted by various models and researchers.

The conceptual and mathematical gas flow model chosen for IPA Phase 2 was the formulation of the steady-state flow equation as originally presented by Steven Amter and Benjamin Ross (Amter and Ross, 1990) of Disposal Safety Inc. (DSI), a DOE consultant. Because gas flow is expected to have relatively fast transients in comparison to changes in temperature gradients through conductive heat transfer, one can evaluate a series of steady-state flows at snapshots in time, as the temperature field develops, to emulate transient flow conditions. This was a major deviation in NRC's approach from the earlier DSI steady-state calculations. The NRC staff wrote its own computer code to solve the equations of flow, and in the process, made other significant modifications and improvements to the DSI model.

4.3.1 Governing Equations

The DSI model is based on single-phase flow of moist air in Yucca Mountain. The following assumptions are made in the derivation (see Amter and Ross, 1990):

- The gas behaves as an ideal gas.
- The gas is saturated with water vapor.
- Changes in partial pressure of water vapor are accommodated by changes in gas composition, with the total pressure remaining nearly constant.
- Gas viscosity is independent of pressure.

- All gas-filled voids in the matrix may be treated as a single porosity on time scales of years.
- The unsaturated zone stays at constant saturation.

The system is then described by three equations, a volume balance, a constitutive relation, and Darcy's Law. The full equation describing the system is then:

$$\nabla^2 h - m\nabla T \cdot \nabla h + \frac{1}{h_a}(\nabla h)^2 + \left[\frac{1}{T} + g\frac{\Omega_a - \Omega_v}{RT}\frac{dh_v}{dT} + \varrho'\left(\frac{1}{T} + m\right)\right]\frac{dT}{dz} + \left[\frac{1-\varrho'}{h_a} - \frac{g}{RT}\frac{\Omega_a}{RT}\right]\frac{\partial h}{\partial z} - \frac{g\Omega_a}{RT} - \frac{\varrho'}{h_a} + \frac{1}{k}\nabla k \cdot (\nabla h - \varrho'\hat{z}) = 0 \quad , \tag{4-7}$$

where:

$$\varrho' = \frac{g}{RT}(h_v\Omega_v + h_a\Omega_a) - 1 \quad ;$$

$$m = \frac{1}{\mu}\frac{\partial \mu}{\partial T} + \frac{1}{T} + \frac{1}{h_a}\frac{dh_v}{dT} \quad ;$$

$$h_v = \frac{P_v}{g\varrho_0} \quad ; \text{ and}$$

$$h_a = \frac{P_0}{g\varrho_0} + z + h - h_v \quad .$$

The term ϱ' is the buoyant density of the air using the concept of "freshwater head." This concept is used in calculating stratified flows in surface water and ground water when dealing with two fluids that have only a small difference in density (e.g., salt water and fresh water, or hot and cold water). The terms h_v and h_a are the vapor-pressure and air pressure heads respectively, in cm.

Constant terms are defined as:

Ω_a = molar weight of dry air (28.96 g mol^{-1});
Ω_v = molar weight of water vapor (18.02 g mol^{-1});
R = gas constant (8.3144 $\times$ 10^7 g cm^2 s^{-2} mol^{-1} °K^{-1});
g = acceleration of gravity (980 cm sec^{-2});
P_0 = reference pressure (880,521 dyn cm^{-2}); and
ϱ_0 = reference fluid density (.001007 g cm^{-3}).

Other terms are defined as:

T = Temperature (degrees Kelvin (°K) from an externally calculated temperature field);
P = total pressure (dyn cm^{-2});
P_v = vapor pressure (calculated for temperature) (dyn cm–2);
μ = fluid viscosity (g cm^{-1} sec^{-1});
k = intrinsic gas permeability (cm^2); and
z = elevation (cm)

Boundary conditions on Equation (4–7) are no-flow on the sides and the bottom, and atmospheric pressure on the surface. The DSI model rationalized that the sides were modeled as topographic valleys that are air divides, much as the centerline of the mountain is a ground-water divide. No-flow at the bottom boundary was chosen because of either low-permeability rock or the presence of liquid water that wo .ld effectively cut off the air flow.

The DSI model linearized certain terms in Equation (4–7) in order to simplify the solution, and also because DSI did not have the necessary relationships for temperature dependence programmed into their model. The terms dh_v/dT and $d\mu/dT$ were replaced by their linearized equivalents taken at a reference temperature of 300°K. The term m was evaluated only at the reference temperature. They also eliminated some of the terms of Equation (4–7) altogether, namely those containing $(\nabla h)^2$ and $\partial h/\partial z$. The terms containing ∇k were included only where there were permeability contrasts.

The no-flow boundary conditions were simulated by setting flux to zero across boundaries:

$$q \cdot \hat{n} = -\frac{g\varrho_0 k}{\mu}\left[\frac{\partial h}{\partial n} - \varrho' \hat{z} \cdot \hat{n}\right] = 0 \quad , \qquad \textbf{(4–8)}$$

where n is the unit vector normal to the boundary. They chose to satisfy Equation (4–8) by setting the head at adjacent boundary nodes, so that the terms within the brackets were zero.

In a later improvement to the model, DSI (Ross *et al.*, 1992) developed a formulation that included atmospheric lapse rate (linear decrease in temperature with elevation) to determine the free atmospheric heads. Considering the atmospheric lapse rate and assuming a constant mole fraction of water vapor at all elevations resulted in the equation:

$$P = P_{atm}\left[1 + \frac{\lambda z}{T_a}\right]^{\frac{\Gamma}{\lambda}} \quad , \qquad \textbf{(4–9)}$$

where:

P_{atm} = atmospheric pressure at $z = 0$;
λ = the atmospheric lapse rate;
T_a = the air temperature at $z = 0$;

and

$$\Gamma = \frac{g}{R}\left[\Omega_a + \eta \frac{P_v(T_a)}{P_{atm}}(\Omega_v - \Omega_a)\right] \quad , \qquad \textbf{(4–10)}$$

where η is the relative humidity outside the mountain at $z = 0$.

This formulation was also adopted for IPA Phase 2.

DSI originally used a node-centered, explicit finite difference equation with Gauss-Siedel acceleration to solve the head field. Once the head field was solved, the velocity field was calculated from Darcy's Law, and particle tracking was used to calculate travel times from the repository to the earth's surface.

4.3.2 NRC Model

The goal of the IPA Phase 2 gas-flow-model development effort was to attempt to duplicate the DSI results and extend the model, if possible.

The NRC model improved on the original DSI model in several significant ways:

- Equation (4–7) was modeled with all terms except the one containing $(\nabla h)^2$ and $\partial h/\partial z$. Furthermore, several of the terms in Equation (4–7) were recast so that it was in a form more suitable for no-flow boundary conditions, using a block-centered finite difference scheme. The term:

$$\nabla^2 h + \frac{1}{k}\nabla k \cdot (\nabla h - \varrho' \hat{z}) \quad , \qquad \textbf{(4–11)}$$

expressed in two dimensions x and y, in relation to the downward unit vector, becomes:

$$\frac{1}{k}\left[\frac{\partial}{\partial x}\left(k\frac{\partial h}{\partial x}\right) + \frac{\partial}{\partial y}\left(k\frac{\partial h}{\partial y}\right)\right]$$
$$-\frac{\varrho'}{k}\left[\frac{\partial k}{\partial x}\sin\theta + \frac{\partial k}{\partial y}\cos\theta\right] , \qquad \textbf{(4–12)}$$

where θ is the dip angle.

The finite difference model was set up in an orthogonal x–y grid, with the layers parallel to the y axis. The entire grid was tilted by the dip angle.

The advantage of the reformulation set up in Equation (4–12) is that the no-flow boundary condition can be expressed simply as zero permeability in the centered finite difference scheme.

- The NRC model did not linearize most of the terms, but instead included formulas for temperature dependency of h_v and viscosity. The relationship for vapor pressure was taken from the "Steam Tables" in *Thermodynamic Properties of Steam* (Keynan and Keyes, 1936). The relationship for viscosity was a quadratic-curve fit for dry air, with data coming from the *Handbook of Chemistry and Physics* (Weast, 1984). The finite-difference model was solved using an explicit algorithm and Gauss-Seidel iteration, with an acceleration factor.

- After initially testing its model, using the linear temperature profile developed by DSI, NRC decided to use a full 2-D temperature profile calculated from the equation for the time-dependent conduction of heat. Although, this model did not take multiphase processes into account, it did account for the growth of the isotherms as a function of time, and calculated the temperature profiles on the sides of the repository as well as above and below the repository.

Two forms of the temperature model have been used, to date. The first is a solution using Green's functions in a semi-infinite, uniform medium in two dimensions, with a fixed-temperature boundary condition at the earth's surface and an instantaneous heat source from a semi-infinite plane (Codell, 1984). A semi-infinite region was considered to best represent the repository; the isotherms will extend out great distances unaffected by boundaries, except at the surface and at contrasts in conductivity. The Green's function solution was for an instantaneous heat source. This was generalized to a time-dependent heat source, based on 10-year-old spent nuclear fuel using a convolution integral evaluated numerically with Simpson's rule quadrature. The geothermal gradient was added to the temperature calculated from the Green's function model. This model calculated temperatures for all locations needed by the flow model. Temperature gradients were calculated by finite-differencing of the nodal temperature.

Temperature distributions were also calculated using a semi-implicit finite difference model based on the Prickett-Lonnquist (Prickett and Lonnquist, 1971) model for aquifer drawdown. The advantage of this approach is that it lets the irregular surface boundary condition be represented explicitly, whereas the Green's function solution allowed the surface of the earth to be represented as flat, only. Another advantage is that the solution is no longer confined to uniform heat-transfer coefficients and heat capacities. The finite difference model also allows the simulation of the geothermal gradient more explicitly by input of a heat flux at the lower boundary of the model. A disadvantage of the finite difference model is that it is difficult to represent an infinite medium for heat conduction. This problem has been partially overcome by creation of a buffer zone around the computed area, to include a larger quantity of rock.

It must also be recognized that the DSI model has, thus far, been used to determine gas-flow pathways and travel times. The NRC model had to be capable of determining output flux of ^{14}C for dose calculations and the cumulative release for determining compliance with the performance requirements. This was accomplished by adding the following modifications:

- The capability to calculate the velocity fields for up to 10 different points in time after repository closing. This was done by providing a temperature input file with temperature distributions at up to 10 selected times and calculating the steady-state Darcy velocity field for each time. The particle tracing routine interpolated the velocity field tables through space and time. The tables were spaced at a few hundred years, for the first 1000, years and then by a few thousand years thereafter to more accurately reflect conditions during the initial period of rapid temperature change.

- A source of ^{14}C released within the engineered barrier system (EBS) in units of (curies/year) was provided to the model as input. In the particle-tracking routine, a fraction of the appropriate source term is attached to each particle released and the fraction remaining on that particle after radioactive decay is accumulated with other particles, according to the year in which the particle emerges into the atmosphere. This "bookkeeping" was required because particles released at different locations within the repository experience different travel times. The model approximates a continuous release from the repository by an instantaneous release of particles across the width of the repository, at the middle of discrete time intervals (every 50 years, for example).

- A file containing the calculated output flux (curies/year) is transferred as input to the dose-calculation model. The accumulated release over the performance assessment period is used as input to the CCDF, for that particular vector and scenario.

A logic diagram of the ^{14}C module is shown in Figure 4–14.

4.3.3 Application to Yucca Mountain

The gas-flow model was applied to Yucca Mountain using the simplified cross-section developed for the flow and transport-modeling tasks. The section was extended 600 meters on each side, to reach the natural no-flow boundaries needed to contain the entire flow field. This cross-section was further simplified by characterizing the stratigraphy as parallel layers at a 6° angle with the horizontal. The finite difference representation consists of 52 columns and 62 rows of nodes with DX = 50 meters and DY = 10 meters. The repository is 400 meters below the top of the land surface. The unsaturated stratigraphy was represented by five parallel layers, as follows, with their respective symbol and the assumed constant thickness in meters in parentheses: Tiva Canyon welded tuff (TCw, variable), Paintbrush non-welded tuff (PTn, 40 meters), Topopah Spring welded tuff (TSw, 340 meters), Calico Hills non-welded vitric tuff (CHnv, 50 meters), and Calico Hills non-welded zeolitic (CHnz, 60 meters). This representation of the repository cross-section is shown in Figure 4–15.

4.3.4 Parameters and Modeled Results

Ranges of the sampled parameters used to model gas transport at Yucca Mountain are shown in Table 4–15.

The values for bulk-fracture properties were determined through measurements of fracture aperature widths and counts of fractures per unit area (see Klavetter and Peters, 1986). As such, the accuracy is questionable. In addition, since there is no reduction in permeability because of moisture in the fractures, the staff has assumed that the full fracture conductivity is available for vapor flow. Also in the simulations, the two Calico Hills layers were treated as one layer and not separately sampled.

The temperature profiles for the simulation runs were determined from the means of the measured heat-transfer properties presented in the SCP (DOE, 1988a; Table 6–16). Only one temperature field was used for all gas-flow runs in the performance assessment simulations; however, as discussed later in this section, the effects of different thermal loadings on gas transport were also investigated using this model.

During the development of the model, runs were made with preliminary estimates of typical hydrologic parameters to determine the sensitivity of the velocity field to the time varying temperature distribution. The permeabilities used for these calculations (in 10^{-16} square meters) were: 5.2 for Tiva Canyon (TCw); 16.0 for Paint Brush (PTn); 0.97 for Topopah Spring (TSw); and 9.7 for Calico Hills (CHn). The porosities and retardation coefficients were not used for the calculation of flux distribution. The results of the calculations are shown in Figures 4–16 to 4–19.

The vapor-flux distribution shown in Figure 4–16 is for vapor transport induced by the geothermal gradient alone, without the additional gradient created by the repository heat load. Most of the convective movement is contained in the upper layers of the stratigraphy, because of the higher permeability and the relief. Figure 4–17 shows vapor flux distribution at 500 years after permanent closure of the repository. This is near the time of highest thermal gradients in the host rock, and the greatest convective vapor movement is being induced. The vapor movement appears to be symmetric about the repository, implying that the heat load of the repository is the major influence at this time. Figure 4–18 shows vapor-flux distribution at 5000 years after repository closure. The magnitude of flux at the repository for 5000 years is about 20 percent of the flux for 500 years. The flux movement is still primarily influenced by the repository heat load, as shown by the arrows. Figure 4–19 shows fluxes at 10,000 years after permanent closure of the repository. The magnitude of flux at the repository for 10,000 years is about 10 percent of that for 500 years. The circulation pattern, however, is again starting to show the influence of topography and the geothermal gradient.

The gas-flow model also appears to be useful for investigating the effects of thermal loading. The same typical cross-section was used to compare gas travel times for a release at 500 years after closure for thermal loadings at areal power densities of 57 kilowatts (kW)/acre (the present

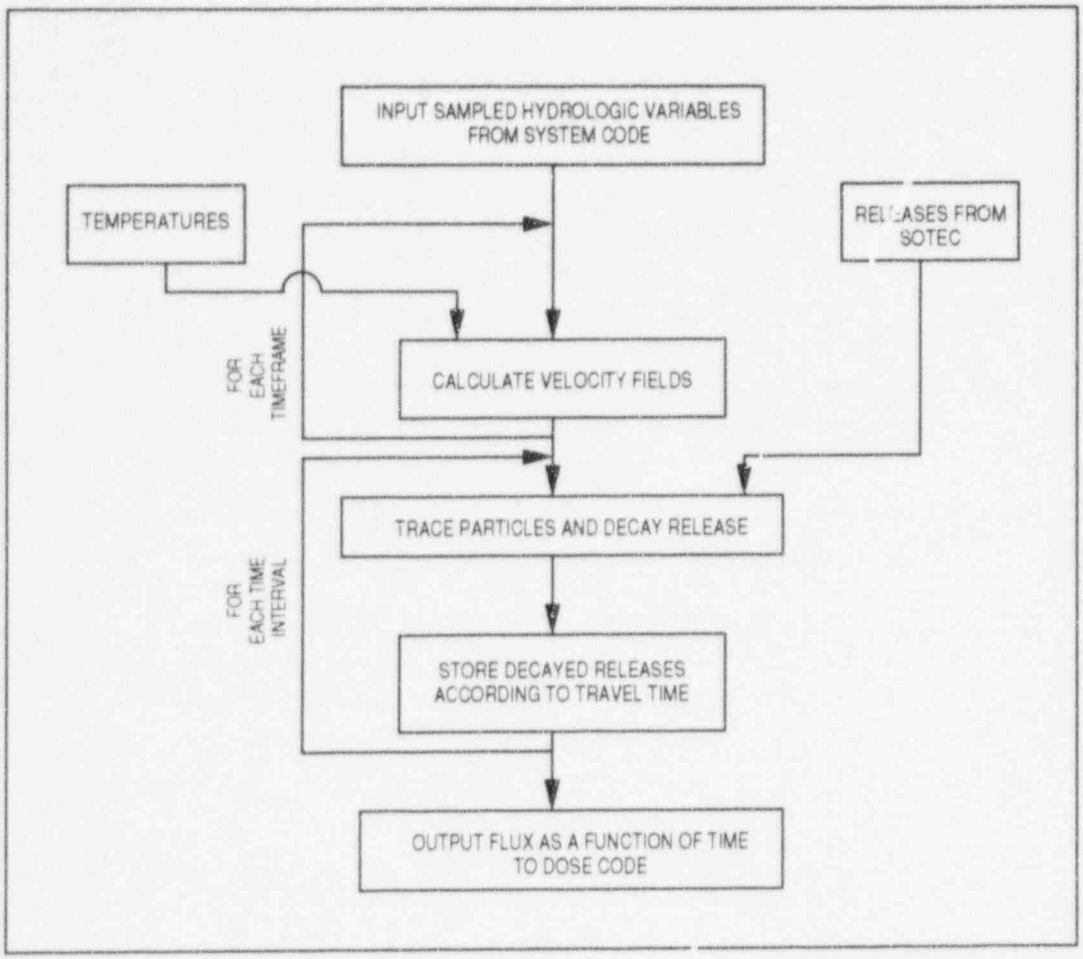

Figure 4–14 ^{14}C module logic diagram

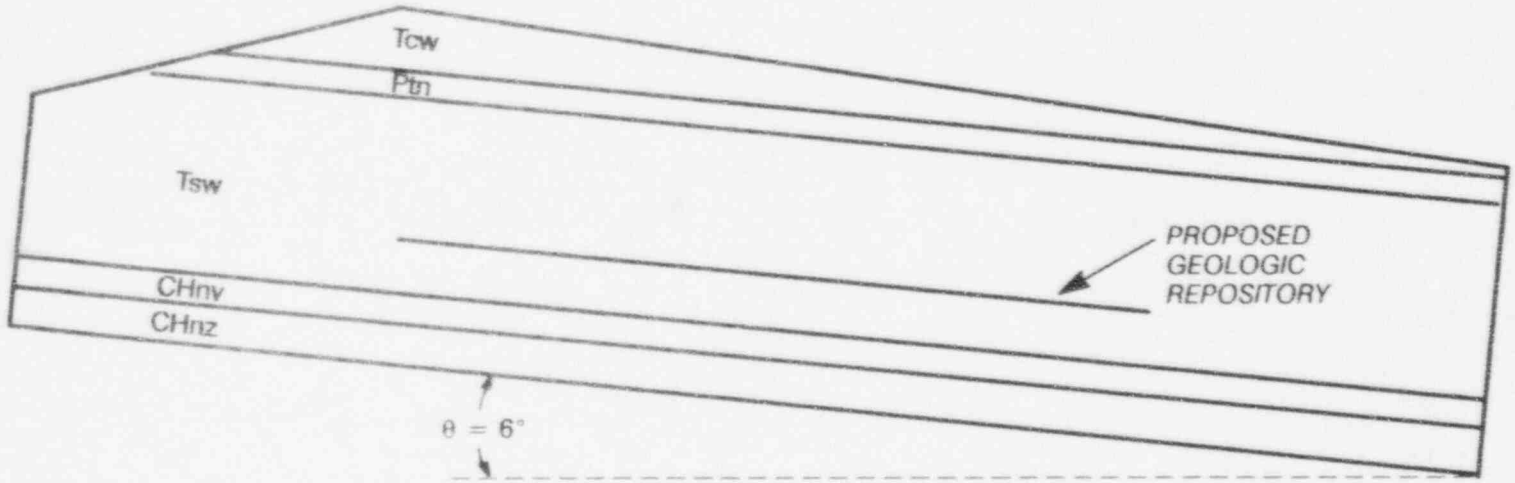

Figure 4–15 Modeled repository section (The hydrogeologic units depicted in Figures 4–15 through 4–22 are as follows: Paintbrush Tuff Members – Tiva Canyon welded unit (Tcw), Paintbrush non-welded unit (Ptn), and Topopah Spring unit (Tsw); and tuffaceous beds of the Calico Hills (non-welded vitric unit (CHnv) and non-welded zeolitic unit (CHnz).)

Table 4–15 Selected Hydrologic Parameters for Yucca Mountain

Stratigraphic Unit	*Permeability Range (m^2)*	*Porosity*	*Retardation Range*
Tiva Canyon (welded)	6.5×10^{-17} 5.5×10^{-15}	.00014	10 - 100
Paintbrush (non-welded)	1.6×10^{-16} 1.6×10^{-14}	.000027	10 - 100
Topopah Spring (welded)	3.2×10^{-17} 3.2×10^{-15}	.000041	10 - 100
Calico Hills (non-welded, vitric)	9.7×10^{-17} 9.7×10^{-15}	.000046	10 - 100
Calico Hills (non-welded, zeolitic)	9.7×10^{-17} 9.7×10^{-15}	.000046	10 - 100

design value[5]), 114 kW/acre and 28.5 kW/acre. The particle paths for these releases under the different loading conditions are the nearly vertical lines from the repository to the surface shown in Figures 4–20 to 4–22. The nearly horizontal lines that cross the particle paths are front lines that show the positions of particles along the different pathways at various times after release. Both porosity and geochemical retardation (assumed to be 10) were accounted for in the particle trackings. The actual average travel time for particles to reach the surface under the design loading condition of 57 kW/acre was 2100 years, resulting in an overall decrease because of radioactive decay of 22 percent of ^{14}C transport. The actual average travel time for a particle to reach the surface under the loading of 114 kW/acre was 980 years, resulting in an overall decrease of 11 percent. The actual average travel time for a particle to reach the surface under the loading of 28.5 kW/acre was 5900 years, resulting in an overall decrease of 55 percent.

A major assumption in the coupling of the source term model with the gas-transport model is that the ^{14}C moves directly from the waste package to the fractures in the host rock outside of the EBS. If the gas were to migrate first to the backfilled repository or even to pass through the repository on the way to the surface, travel times would be greatly increased because of the relatively large porosity of the backfill. Also, the fracture porosity of rock is used in the model, rather than the matrix porosity, which is much larger. The assumption is made that the gas stays in the fractures and does not migrate laterally on the way to the surface. It should be noted that if only 10 percent of the matrix porosity is available in the Topopah Spring unit for lateral migration, travel time through the unit would be increased by over three orders of magnitude. Although we consider our assumptions and our model to be conservative, we also consider that this assumed confinement of gas transport to the fracture, by possible fracture coatings, may be realistic.

[5]Kilowatts per acre is used in this report for easy comparison with the SCP rather than the metric equivalent of kilowatts per hectare.

4.4 Flow and Transport Auxiliary Analyses

Eleven auxiliary analyses conducted for this demonstration were performed to evaluate the appropriateness and limitations of various computational approaches and interpretations of data used in this study. These analyses are summarized below and discussed in detail in the appendices at the end of this document. They included: the evaluation of computer programs (*DCM3D* and *NEFTRAN II*); evaluation of the K_d assumption;

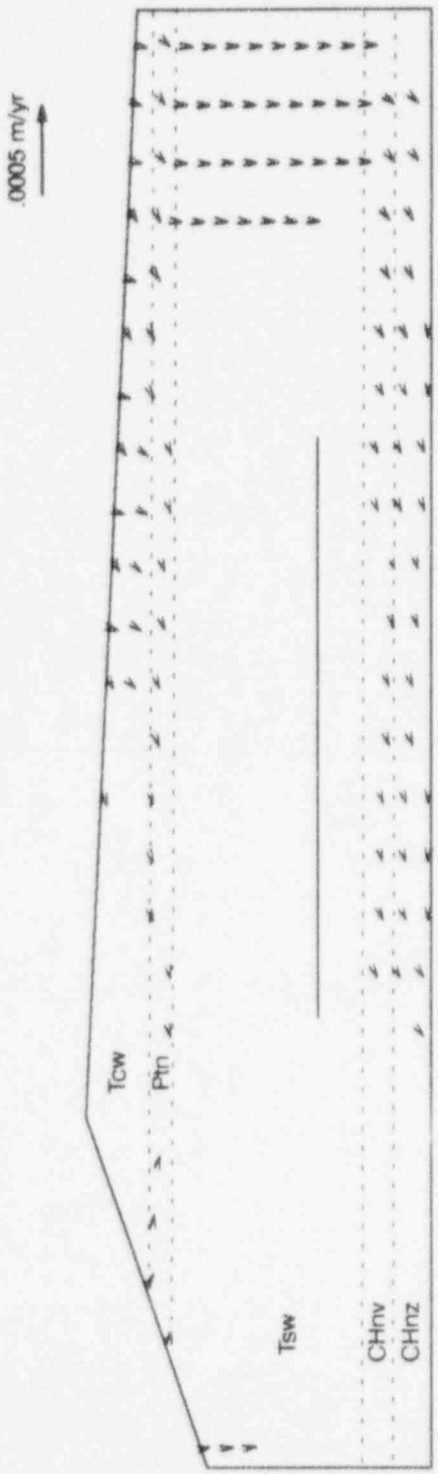

Figure 4–16 Vapor flux at ambient conditions

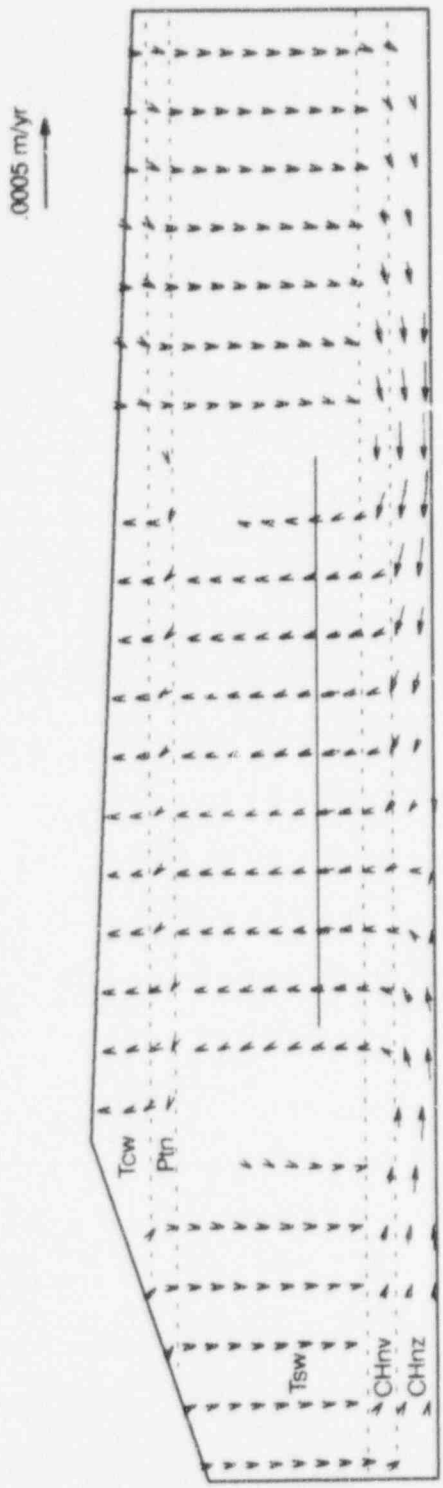

Figure 4–17 Vapor flux at 500 years after permanent closure of the geologic repository

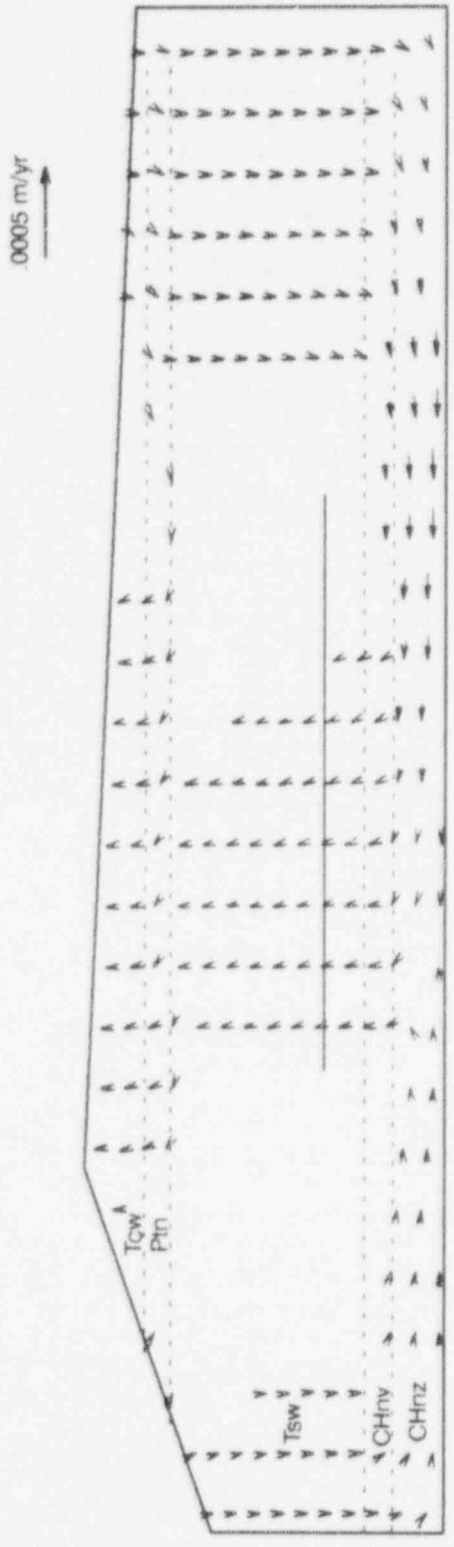

Figure 4–18 Vapor flux at 5,000 years after permanent closure of the geologic repository

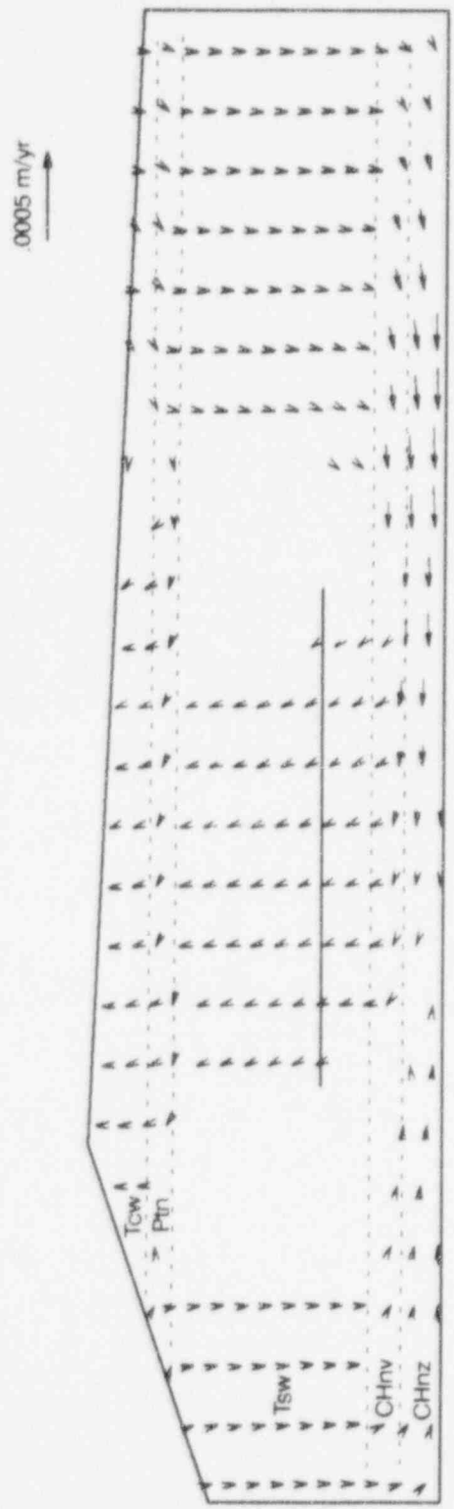

Figure 4–19 Vapor flux at 10,000 years after permanent closure of the geologic repository

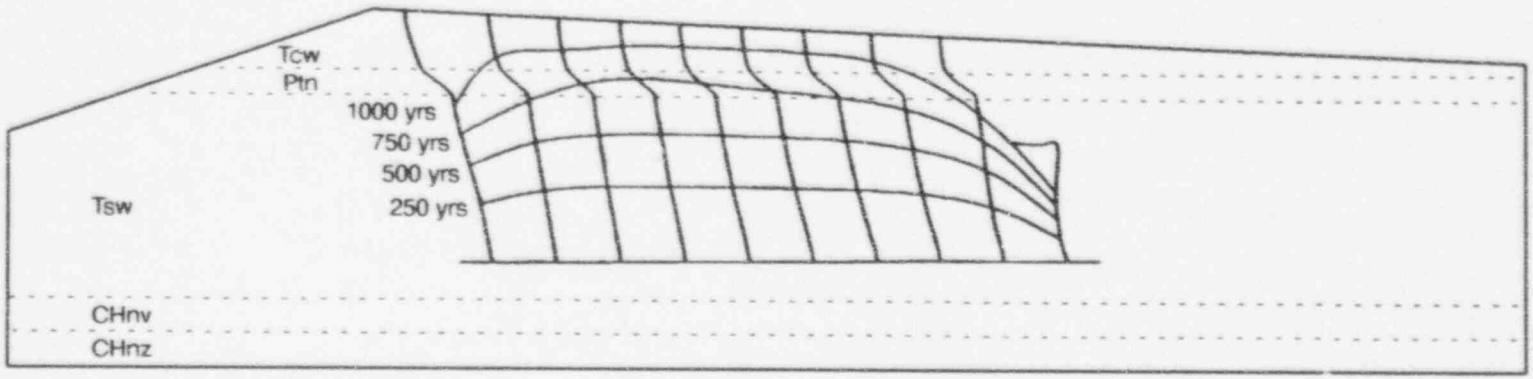

Figure 4–20 Paths and travel times for design thermal loading

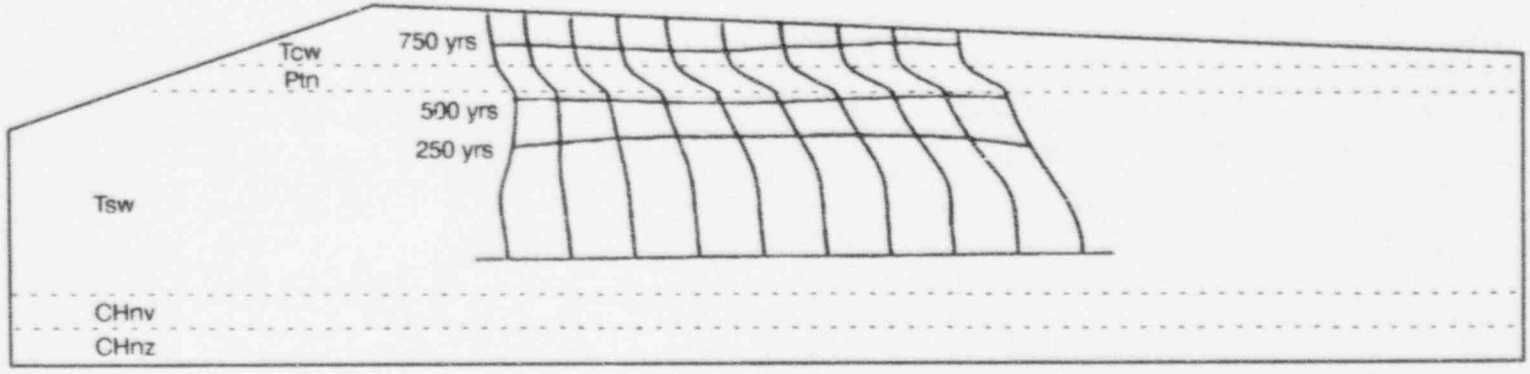

Figure 4–21 Paths and travel times for 2× the design thermal loading

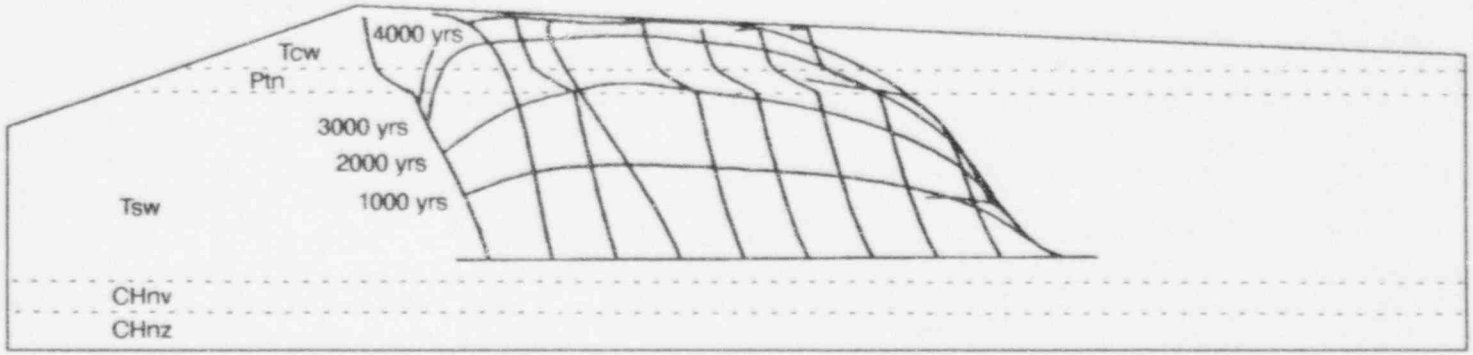

Figure 4–22 Paths and travel times for .5 × the design thermal loading

modeling of the saturated zone at Yucca Mountain, to determine flow paths and evaluate water table changes caused by climatic variation; evaluation of topography and transient conditions on percolation; evaluation of modeling considerations for unsaturated, fractured media; evaluation of the effects of hydrologic structures on 2-D, variably saturated flow; evaluation of ^{14}C transport in the unsaturated zone; and cation exchange.

4.4.1 Evaluation of the SNL Technology: Testing of the *DCM3D* Computer Code

Sandia National Laboratories (SNL), formerly under contract to NRC, developed a computer program for solving three-dimensional (3-D) ground-water flow problems in variably saturated, fractured porous media. To explicitly evaluate a fractured media, the program implements a dual-continuum approach that simulates the fractures and matrix as separate continua connected by a transfer term that depends on the unsaturated permeability of the porous medium (sometimes referred to as a dual-porosity approach). This approach, a departure from the more traditional composite characteristic curve approach, has not been previously used by NRC staff to simulate fluid flow at Yucca Mountain. An auxiliary analysis was conducted that compared *DCM3D* with other computer programs, to allow NRC staff to gain experience with *DCM3D* and better understand the implications of the dual continuum approach in the context of fluid flow in a fractured medium.

Because of the relatively recent interest in modeling fluid flow in partially saturated, fractured media it is difficult to find problems in the literature with which to evaluate the dual porosity concept. Despite this limitation, four test cases were used to provide some initial insights. The four cases involved:

- 1-D flow in a horizontal soil column (analytic solution available);
- 2-D flow in saturated-unsaturated soil (comparison with *PORFLO-3*);
- 2-D flow in a multi-layer unsaturated soil, based on a field experiment (comparison with *PORFLO-3, FLASH*, and *TRACER3D*); and
- 2-D flow through a layered, fractured, unsaturated rock (comparison with *NORIA*).

Overall, the comparison of *DCM3D* results for the four test cases compared well with the other computer programs and the analytic solution, indicating that the basic equations are correctly implemented. However, basic questions regarding the applicability of different approaches for simulating partially saturated flow in fractured rock have not been resolved by the testing provided by the four test cases. Many basic questions remain, such as:

- Anisotropic considerations of a fractured system;
- Representation of pressure equilibration between the matrix and fracture; and
- Transient effects.

Future work needs to examine problems that will provide more insights into differences in fracture-matrix interactions, because of different modeling approaches and assumptions.

This auxiliary analysis is discussed in greater detail in Appendix C.

4.4.2 Evaluation of the K_d Assumption

The system code of the present NRC performance assessment effort uses the K_d approach in estimating retardation of radionuclides. The relationship of K_d to retardation is:

$$R_f = 1 + \varrho \frac{K_d}{\theta} \quad , \qquad \textbf{(4-15)}$$

where ϱ is the bulk density, θ is the moisture content, and R_f is the retardation factor that is defined as the ratio of the velocity of ground water to that of the radionuclide. Freeze and Cherry (1979) state that this relationship is valid only when:

- The sorption reaction is fast and reversible; and
- The sorption isotherm is linear.

A sorption isotherm is the locus of points describing the concentration of radionuclide on

the solid as a function of the concentration of radionuclide in the liquid. Drever (1988) adds that for the relation to hold:

- The concentration of the radionuclide is small, compared with the total concentration of sorbing ions in solution.

In a system as complex as Yucca Mountain, it remains to be demonstrated that simplifications such as the K_d approach in estimating retardation are valid. This auxiliary analysis tests two of the three requirements described above. These requirements are that:

- The sorption isotherm is linear; and
- The radionuclide is in trace amounts relative to the total solute concentration.

The method of testing involves modeling sorption reactions in a 1-D flowing system. This modeling exercise simulates ion exchange involving sodium and potassium. The reaction considered is:

$$K^+ + NaX = KX + Na^+ , \qquad \textbf{(4-16)}$$

where X is the sorbing site on the solid. This system can be viewed as an analog for both the Na-K ion-exchange reactions involving zeolites and radionuclide-tuff reactions at Yucca Mountain. The computer code capable of simulating these processes is *PHREEQM*, an adaptation of *PHREEQE*, for use in mixing cell flowtube simulations. This code can simulate speciation and mass-transfer processes, including precipitation and dissolution; it also can simulate ion-exchange reactions, 1-D flow and transport, diffusion, and dispersion in a porous medium. The reaction written above describes the situation where a solution containing potassium flows through a column initially loaded with sodium. The potassium replaces sodium on the solid and this solute-solid interaction retards the movement of potassium down the column relative to that of water. In this study, the reverse of the reaction above is also simulated, where a solution containing sodium flows through a column initially loaded with potassium. This auxiliary analysis studies the effect of varying relative concentrations of sodium, potassium, and sorption site X, on the validity of the relationship between K_d and R_f. The equilibrium constant for the reaction potassium replacing sorbed sodium is arbitrarily given a value of 5 (i.e., > 1). The reverse reaction thus has an equilibrium constant that is the inverse of 5 (i.e., < 1).

Results

The results of the simulations are presented in the Table 4–16.

Conclusion

The requirement that the sorption isotherm be linear so that the retardation factor can be calculated from K_d is correct. However, the concentration front of the migrating ion can spread if dispersion or diffusion is significant. A linear isotherm results from the condition where the concentration of the migrating ion is trace relative to the competing ion. Linear isotherms do not result from the condition where the migrating ion is trace relative to the sorbing site. When the isotherm is nonlinear and convex up, the K_d value associated with the highest concentration of the migrating ion to be expected can be used to determine the retardation factor. This method does not work when the isotherm is concave up.

While dispersion tends to spread the concentration front of the migrating ion, ion exchange, where the corresponding nonlinear isotherm is convex up, tends to maintain a steep concentration gradient. On the other hand, ion exchange, where the corresponding nonlinear sorption isotherm is concave up, works in concert with dispersion, to spread the front.

This auxiliary analysis can be applied to the modeling of conditions and processes expected at Yucca Mountain. The assumption that all radionuclides will be in trace amounts relative to competing ions has not yet been proven. The waters at Yucca Mountain contain low concentrations of solute. Based on the solubility values from the SCP (DOE, 1988a; p. 4–100), uranium, neptunium, cesium, and technetium could be at concentration levels comparable to those in the uncontaminated waters. Furthermore, what constitutes a competing ion has not been established. Thus, in a solution with multiple species, the competing ion could be a major, minor, or trace constituent. Furthermore, at the low temperatures

Table 4–16 Results of K_d Simulations

Equilibrium Constant	*Concentrations (meq/l)*			*Isotherm*	*K_d (ml/g)*	*Concentration Front Spread*	*Predictability of R_f from K_d*
	Migrating Ion	*Competing Ion*	*Sorbing Site*				
>1	1	1	1	Convex Up	0.6–0.12	Least	Yes
>1	2	1	1	Convex Up	0.6–0.06	Least	Yes
>1	1	1	167	Convex Up	100–20	Least	Yes
>1	0.001	1	1	Linear	0.6	Least	Yes
<1	1	1	1	Concave Up	0.12–0.024	Most	No
<1	1	1	167	Concave Up	3.3–2	Most	No
<1	0.001	1	1	Linear	0.024	Least	Yes

at Yucca Mountain, certain ion-exchange reactions may be kinetically inhibited, thus allowing less thermodynamically favorable reactions to control the system. The questions concerning competing ions will have to be addressed by experimentation.

The simulations done in this auxiliary analysis involved the binary system Na-K. Consequently, changes in one component could affect the other, as shown when the two components were in comparable concentrations. When the one component was trace relative to the other, its addition to the system did not affect the other. This resulted in a linear isotherm, and constant K_d values along the column. However, Reardon (1981) has shown that variations in the concentrations of a major component can affect the partitioning (K_d) of a trace component. Thus, in a system as complex as Yucca Mountain, it is crucial that there be a demonstration that the (competing constituent) chemistry of the far field is relatively constant or predictable over the lifetime of the repository. Otherwise, the application of the K_d approach would be very difficult to defend technically.

This auxiliary analysis is discussed in greater detail in Appendix D.

4.4.3 Regional Flow Analysis

Simulation of flow in the saturated zone in the region containing Yucca Mountain in Nevada was undertaken as an auxiliary analysis for the IPA Phase 2. The primary purpose of the study is to gain experience in modeling large-scale saturated flow and to draw very preliminary inferences regarding the effects of certain selected conditions on the position of the water table. No effort, however, was made to make the analysis comprehensive; only data that were readily available were used. Some parameter values are taken from other published reports without verifying their accuracy. The analysis results should be considered as very preliminary and are likely to change when actual field data are used in simulations.

For this application, *PORFLOW* (Runchal and Sagar, 1989; and Sagar and Runchal, 1990), an integrated finite difference code, was modified to incorporate the free surface (water table) in a ground-water flow model. The model was set up in the *x–y* (horizontal) plane. Provision was made to allow for specification of recharge and discharge areas. A finite-difference grid (13161 computational cells) is imposed on a region approximately 200- by 200-kilometers. At this regional scale, the Yucca Mountain repository area is represented approximately by two grid nodes. In addition, to conduct more detailed saturated flow modeling in the vicinity of Yucca Mountain, a sub-regional model consisting of a finite difference grid (18,225 computational cells) is imposed on a region 50- by 50-kilometers around the proposed repository site. Boundary conditions for this sub-regional model consisted of fixed pressures that were read from the simulation results of the larger regional model. The hydrological data for the simulations are obtained from previously published studies that

themselves depended on numerical model calibration for their parameter values.

Recharge was assumed to occur on outcrops at higher elevations. Recharge areas included the Spring Mountains, Sheep Range, Pahranagat Range, Kawich Range, and Pahute Mesa (see Figure 4–23). Current recharge in these areas average from 25 to 50 millimeters/year. Discharge areas include Alkali Flats and the Furnace Creek Ranch, which were modeled as fixed-head boundaries. The entire modeled region was divided into eight zones, in which the hydraulic conductivity varied from 0.05 to 0.0035 meters/second. The model contains a low permeability zone northwest of Yucca Mountain for simulating the present-day high hydraulic gradient at that location. The actual cause of the steep gradient is not yet fully know.

Considering the present-day conditions, a steady-state solution to the flow system was obtained. The steady-state solution was then used as the starting point or initial state for simulating other conditions. The conditions simulated in the regional model include: (i) climatic change in the future, increasing the recharge at higher elevations by factors of 10, 20, and 30; (ii) increase of recharge in Fortymile Wash by a factor of 10; (iii) rise in water level at Alkali Flats discharge area by 10 meters; (iv) geologic activity (volcanic or tectonic) to the south of Yucca Mountain, creating a flow barrier 20 kilometers long; and (v) geologic activity to the north of Yucca Mountain, breaking the existing flow barrier. Most of the above conditions were simulated in a transient mode, so that the time variation of the water table could be studied.

Using the steady-state solution obtained from the regional model for the present-day conditions, a total of 10 additional simulations of volcanic dike intrusions in the vicinity of Yucca mountain were conducted, using the sub-regional model. These volcanic dikes were situated at various orientations directly below the repository site, as well as approximately 5 kilometers southeast of the site, to determine their impact on the ground-water flow.

Based on the regional analysis, the rise in the water table under Yucca Mountain because of various postulated conditions ranged from only a few meters to 275 meters. When the recharge at higher elevations was increased by a factor of 20, the water table under Yucca Mountain rose by 85 meters in about 700 years. Increase of recharge in Fortymile Wash by a factor of 10 raised the water table by about 100 meters. Backing up of ground water because of creation of a flow barrier south of Yucca Mountain resulted in a water table rise, under Yucca Mountain, of about 200 meters. The largest water-table rise of 275 meters was calculated when the flow barrier to the north of Yucca Mountain is removed. Figure 4–24 shows the results of the modeling of Condition (i), described previously, in which the water table rise at nodal points near Yucca Mountain and Fortymile Wash is plotted as a function of a multiple of the increased recharge rate into the regional model. Figure 4–24 does not include the effect of recharge into Fortymile Wash, which would cause an additional rise in the water table.

Results of the sub-regional model analysis of the intrusive volcanic dikes in the vicinity of Yucca Mountain showed water-table rises ranging from only a few meters to as much as 103 meters. For certain dike locations and orientations, the water table actually dropped several meters in the vicinity of the site. Figure 4–25 shows the simulated results of water-table rise, at the potential repository site, as a function of dike orientation, for the case in which the single intrusive dike extends vertically through the saturated zone directly beneath the repository site. The dike length is assumed to be 4 kilometers. The points on the plot represent the nodal points where the maximum water-table rise occurred, which in all cases was located somewhere along the fault. The maximum water-table rise for a single dike intrusion can be seen from Figure 4–25, to occur, for the dike orientation, approximately 75° counterclockwise from the east direction. The NRC staff has indicated that this particular dike orientation is the most likely to occur, because of the present faulting patterns in the Yucca Mountain area.

A number of assumptions were made in this study, with regard to the numerical model, as well as the data. These assumptions, which are discussed in the body of the report (Ahola and Sagar, 1992), should be kept in mind in interpreting the preliminary results given above. Specifically, with regard to the high water-table rises

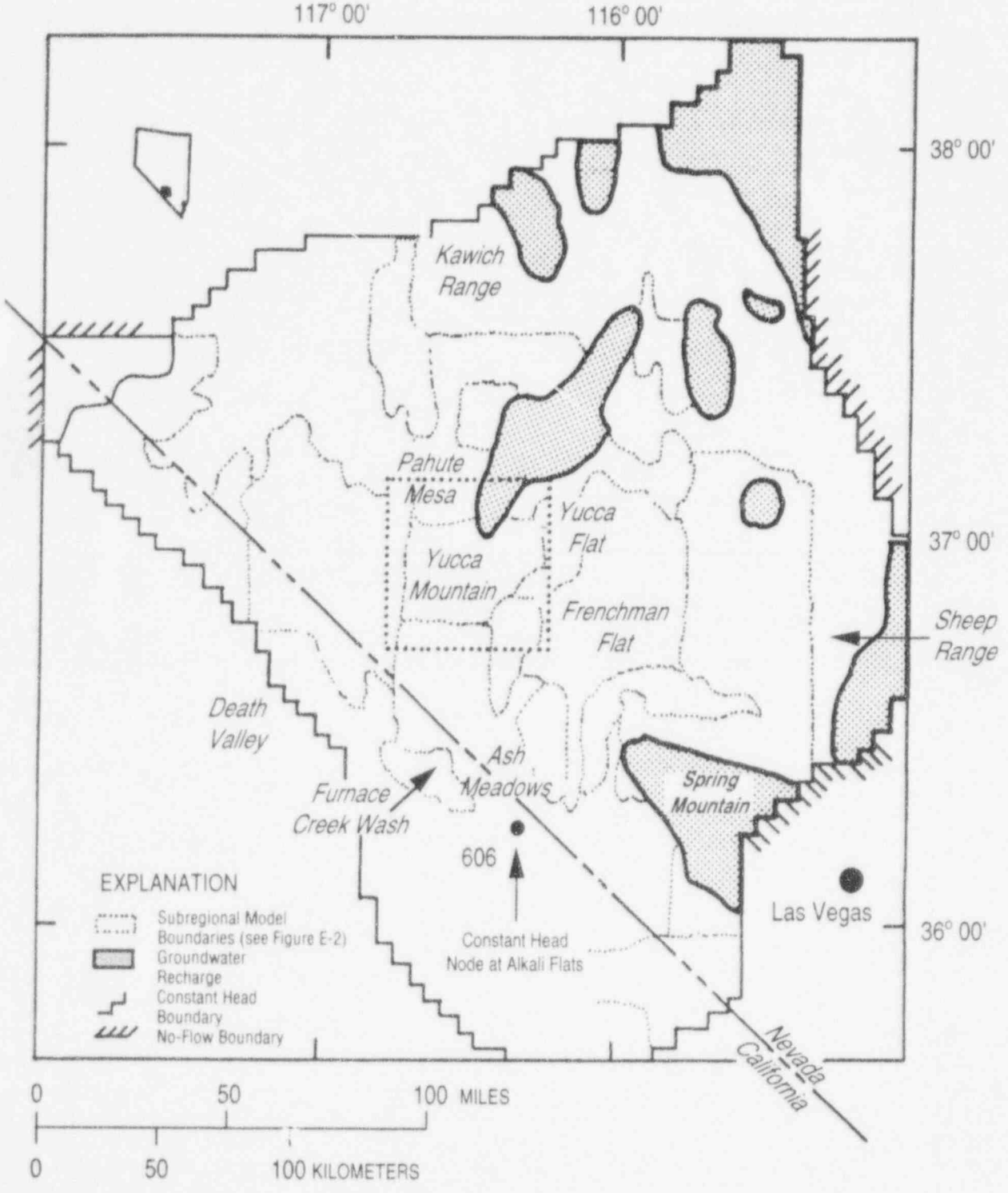

Figure 4–23 Location of recharge and discharge areas for the regional model

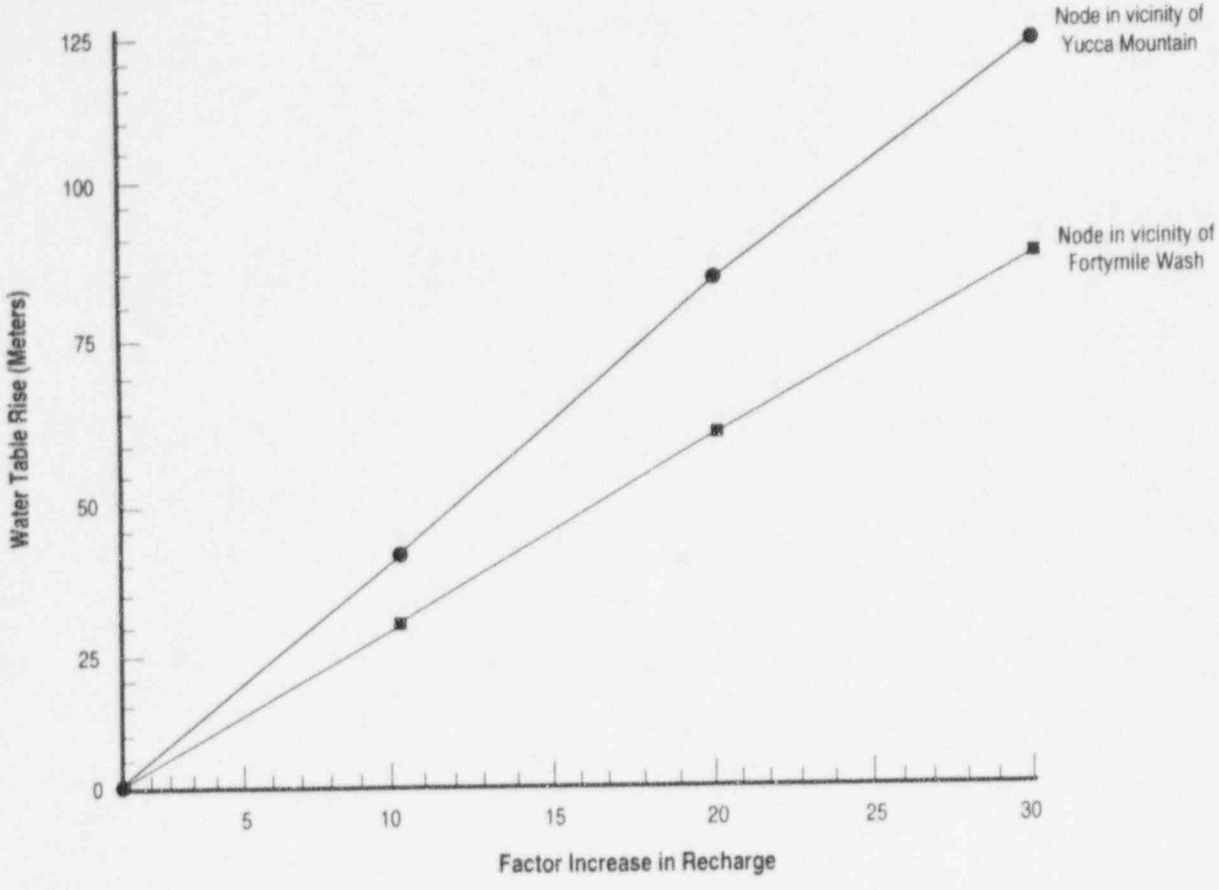

Figure 4–24 Water-table rise at Yucca Mountain as a function of increased recharge rate

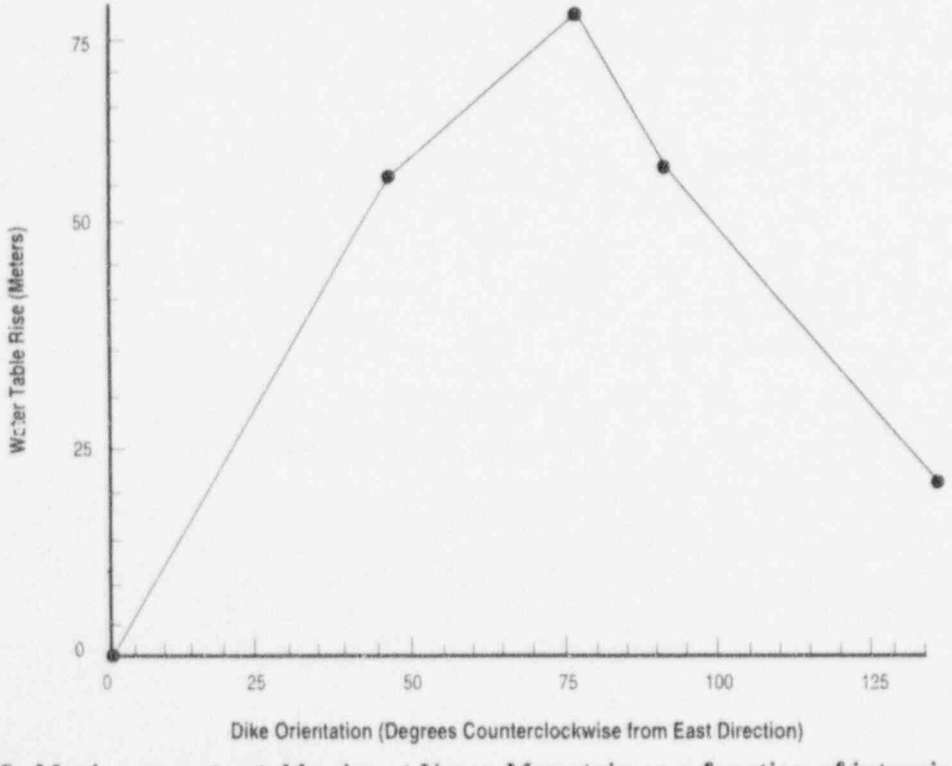

Figure 4–25 Maximum water-table rise at Yucca Mountain as a function of intrusive dike orientation (The volcanic dike is assumed to exist directly below the repository site and extend vertically through the saturated zone.)

predicted, the staff did not consider the formation of new discharge areas that such a rise may cause.

This auxiliary analysis is discussed in greater detail in Appendix E.

4.4.4 Effects of Stratification, Dip of Strata, and Sub-Vertical Faults

A numerical investigation of quasi-2-D unsaturated flow in a vertical cross-section with dipping strata and sub-vertical fault is reported in detail in the Center for Nuclear Waste Regulatory Analyses (CNWRA) report by Bagtzoglou *et al.* (1992) and a technical paper by Bagtzoglou *et al.* (1993). This work was performed as a part of IPA Phase 2 effort. The objectives and results of the work are summarized below.

IPA Phase 2 includes performance assessment of the total system and detailed auxiliary analyses of selected important features of subsystems. The main objectives of the auxiliary analyses in IPA are to provide support to simplifications made in performance assessment of the total system by obtaining better understanding of a subsystem through detailed analysis. Detailed analyses of flow in fully and partially saturated domains containing heterogeneous porous media and discrete fractures were planned as auxiliary analyses in the IPA Phase 2. Analyses of saturated flow in a region containing Yucca Mountain were reported in an earlier report (Ahola and Sagar, 1992), which discussed fluctuations of water table for various cases, including hypothesized changes in recharge/discharge conditions and stratigraphy. In the CNWRA report by Bagtzoglou *et al.* (1992), an analysis of the flow field in variably saturated zone has been developed to understand the effect of stratigraphic layering, presence of a fault zone, and the dipping of strata.

An analysis has been performed for a deep (approximately 530 meters) hard-rock system. Some of the data for the analysis were taken from the Yucca Mountain project reports, but were freely modified to enhance the effects that are being studied. However, at this stage, the report does not aim at analyzing unsaturated flow at the Yucca Mountain site. Hydraulic and stratigraphic parameters only resemble the Yucca Mountain site. For example, the depths to water table, the number of geologic strata, their dip angle, and the existence of a fault zone are characteristics used in the analysis that were based on information on Yucca Mountain. Whereas, the width of the faulting zone, the net percolation rate, and the hydraulic parameters of the matrix and fault media used in the analysis were based only partially on information on Yucca Mountain. Therefore, conclusions regarding suitability of Yucca Mountain for the proposed nuclear waste repository are not directly derivable from this analysis. Rather, the objective of this work is to help develop assumptions for the flow module in the total performance assessment system. Also, the investigation is limited to 2-D or quasi-2-D simulations in a vertical cross-section or 'thin slice,' with dipping strata intersected by a sub-vertical fault zone. The simulations are performed in a transient mode, to study the manner in which the solutions to the flow equation approach steady-state. Many other aspects of multi-dimensional flow in the unsaturated zone are worthy of detailed study. For a comprehensive review of variably saturated flow and field heterogeneity, see Ababou (1991).

In particular, the steady-state flow regime resulting from a 'wet' hydro-climatic scenario, corresponding to a net annual percolation rate of 50 millimeters/year was investigated. A hypothetical test problem was developed, to take into account, at least qualitatively: the effects of bedding (represented by five alternating layers); the presence of the sub-vertical Ghost Dance Fault (represented by a thin layer of very coarse material); and the effect of inclination of the beds (dipping six degrees eastward). A number of auxiliary tests were also conducted using variations on these hypothetical data. The main conclusions and results from this study, obtained with the aid of the *BIGFLOW* simulation code (Ababou and Bagtzoglou, 1993) and data processor, are as follows.

First, it was observed that initial-boundary conditions must be generated in a manner consistent with the hypothetical (and largely unknown) state of the system *in-situ*. More precisely, a method was devised for generating initial-boundary conditions that are consistent with: (i) the assumed input percolation rate; and (ii) the assumed material properties of the modeled cross-section. For instance, artificial boundary conditions are needed for the East-West and for the North-South lateral boundaries. This is because, in part, the cross-section is represented as a rectangular

domain bounded below by the water table, rather than a more complicated domain following the actual 'Yucca Mountain' topography. Artificial boundaries connecting ground surface to water table are also needed, particularly for the East-West faces.

Recognizing that there are no simple, natural, initial-boundary conditions that can be used for the more complex problems, a method of successive approximation was implemented. This method uses solutions of auxiliary flow problems to set up pressure conditions for the more complex problems. Unfortunately, for the 'thin-slice' simulations reported in this study, the results suggest that it is particularly difficult to design 'consistent' initial-boundary conditions in the case where the fault intersects lateral boundaries (in the case at hand, the North-South oriented fault intersected the North-South boundaries). An oscillating flow regime was obtained at large times, that is, after all initial transients died out, and this was done for both a horizontal and dipping stratigraphy. This process appeared to be localized in regions where the fault intersects these boundaries, although this requires further confirmation. This was shown to be an effect of the discrete-time nature of the equations being solved, and was eliminated by using extremely small time steps ($\Delta t \rightarrow 0$). The techniques used to identify these effects relied on detailed plots of global mass balance in terms of instantaneous net discharge rate and instantaneous rate of change of total mass. Large Δt yielded oscillations for both 2-D and 3-D flow systems, but seemed more consequential in 3-D (fault-cutting pressure boundaries).

Based on the parameters used, and simulations performed in this study, the following conclusions can be reached:

- The effects of stratification are important only for low net percolation rates and during the early parts of transient simulations;
- A dip angle of 6° to the East has a minimal effect on the pressure-head distributions (approximately 2 percent of the maximum pressure-head difference); and
- The flow behavior (ground-water fluxes and travel times) of a system consisting of highly contrasted matrix and vertical fault properties is greatly influenced by the ratio of the slopes of the matrix and fault unsaturated hydraulic conductivity curves.

Finally, the staff recognizes the need for introducing in future work, data that are more directly representative of the Yucca Mountain site. The stratigraphy should be refined regarding: the spatial configuration of geologic units; the orientation of the fault; the existence of a fault offset of the beds because of fault slip; the replacement of the exponential conductivity curve with the smoother van Genuchten-Mualem curve; the increase in contrast of some of the fault properties; a more refined mesh, to simulate a thinner fault zone; and generally a more careful selection of the unsaturated parameters of the fault and of the rock matrix in each geologic unit.

This auxiliary analysis is discussed in greater detail in Appendix F.

4.4.5 Exploration of Dual-Continuum Flow Modeling Concepts

To develop the ground-water flow and transport module, several different modeling approaches were attempted. One of the approaches required the staff to learn and experiment with *DCM3D*, a Dual-Continuum, three-dimensional (3D), Ground-Water Flow Code for Unsaturated, Fractured, Porous Media (Updegraff *et al.*, 1991). The *DCM3D* code is based on a dual-continuum model with matrix media comprising one porous equivalent continuum and fractures the other. It is attractive to use continuum codes to model ground-water flow at Yucca Mountain, because explicitly modeling individual fractures at the scale of Yucca Mountain at this time may not be possible or necessary.

At present, two main types of continua approaches are being used to model Yucca Mountain site unsaturated fracture and matrix ground-water flow; single continua and dual continua. Single continua approaches often use the same porosity values for both matrix and fractures, and a single characteristic curve to represent matrix and bulk fracture-matrix hydrologic properties (Klavetter and Peters, 1986). In contrast, dual-continuum models consist of two interconnected continua, with one continuum simulating flow through the rock matrix and the other simulating

flow through large numbers of fractures. The two continua are connected by a fracture-matrix transfer term allowing water to flow between the fracture and matrix continua. This enables a dual-continuum code to model the resistance to water movement between the matrix and fracture continua and may allow the code to simulate situations where a single-continuum approach could experience code-convergence problems.

A dual-continuum code may also be able to simulate conceptual models that single-continuum codes cannot. For example, in a single-continuum model of unsaturated fracture and matrix groundwater flow, when water saturation in the matrix reaches a level where bulk fracture flow occurs, faster velocities are computed, but with no change in direction. Therefore, this approach assumes that bulk fracture flow contains the same anisotropies as the matrix. However, individual fractures tend to be linear features with strong anisotropies. Therefore, for a single fracture it is reasonable to assume that irrespective of the flow direction in the matrix, flow in the fracture will be strongly influenced by the anisotropic properties of the fracture. Furthermore, when there are large numbers of fractures with similar linearities, a general fracture anisotropy may be created that is different from the rock matrix. This may be the case at Yucca Mountain, where faults and fractures are believed to be vertical or steeply dipping (DOE, 1988a; pp. 3–175, 3–179, and 3–185; and Barton *et al.*, 1989). Use of a dual-continuum code in this type of situation may be advantageous, because in a dual-continuum code, different anisotropies can be assigned to both the matrix and fracture continua.

In this auxiliary analysis, simulations using the *DCM3D* code demonstrate that the dual-continuum code *DCM3D* can model flow in two continua with different anisotropies, and that depending on the problem to be modeled, it may produce significantly different answers than a single continuum code.

This auxiliary analysis is discussed in greater detail in Appendix G.

4.4.6 Release and Transport of Potentially Gaseous Radionuclides Other than ^{14}C during Volcanism and Normal Operations

Several potentially volatile compounds of ^{99}Tc, ^{79}Se, and ^{129}I may be present in spent nuclear fuel. Because of the possibility of a gaseous pathway through the unsaturated rock at Yucca Mountain from the buried waste to the atmosphere, this auxiliary analysis investigated, using a series of conservative calculations, the phenomena by which volatile radionuclides could be released, and whether they posed enough of a threat to warrant further study.

Vapor pressure of possible volatile radionuclide compounds were taken from the available literature and estimated thermodynamic information. Given the estimated vapor pressures, a portion of the inventories of the volatile radionuclides could be released at normal repository operating conditions. The bulk of the inventories of these radionuclides would be contained within the structure of the spent nuclear fuel, however, and the vapor pressures of those inventories would be reduced. Barometric pumping caused by changes in atmospheric pressure was considered a possible mechanism for release of volatile radionuclides from breached waste-package containers. For temperatures and atmospheric pressure variations in the SCP design, the staff's conservative calculations estimated that less than 1 percent of the inventory of volatile radionuclides would be released from the waste packages to the geosphere in 10,000 years. The staff further estimated that most of the volatile compounds would become associated with liquid water in the rock rather than remaining in the gas phase.

The staff also estimated the effects of an intrusive basaltic dike causing temporary heating of the rock near waste packages. For a 10-meter-wide dike of 3000 meters length, the staff conservatively assumed that all volatile radionuclides in a 100 meter wide region would be driven off by the increased temperature. This represents an area approximately 6 percent of the total repository area for the SCP design. Even if all of the inventories of ^{99}Tc, ^{79}Se, and ^{129}I in 6 percent of the repository were released to the accessible environment, the total consequences would sum to only about 0.125 of the releases allowed under 40 CFR Part 191. On this basis, the staff concluded that

the releases were not large enough to warrant further study.

This auxiliary analysis is discussed in greater detail in Appendix H.

4.4.7 Evaluation of USGS Ground-Water Modeling for the Region That Includes Yucca Mountain

This section describes the major ground-water modeling work that has been performed by the U.S. Geological Survey (USGS) for the region of southern Nevada. Emphasis will be placed on the evolution of the subregional model originally developed by Czarnecki and Waddell (1984).

In the late 1970's,the USGS began an appraisal of the Nevada Test Site for potential disposal sites for high-level nuclear wastes. This work included regional geologic and hydrologic investigations, and a regional ground-water flow model was developed by Waddell (1982). Waddell produced a 2-D, steady-state, finite-element model that covered an area of about 18,000 square kilometers. This model extended from the Pahranagat Range and Las Vegas Valley on the east to Pahute Mesa and Death Valley on the west. The model included the Yucca Mountain area and almost all of the Nevada Test Site.

Following identification of the proposed Yucca Mountain site, Czarnecki and Waddell (1984) developed a subregional model within the hydrologic subbasin that includes the site. This model was derived using a parameter-estimation procedure developed by Cooley (1977, 1979, 1982). Czarnecki (1985) later revised and improved this model to help develop smaller site-scale models of ground-water flow and transport for the Yucca Mountain site. He initially prepared a steady-state base-case model and revised it to simulate the geohydrologic effects of increased recharge in the region. A transient version of the model was later used to evaluate scenarios related to the large hydraulic gradient located north of Yucca Mountain (Czarnecki 1990a). The work of Czarnecki and Waddell (1984), Czarnecki (1985, 1989, 1990a, 1990b), and Czarnecki and Wilson (1989) illustrates a methodical process for developing and improving numerical models of ground-water flow.

Because of the importance of the USGS regional modeling work, with respect to site characterization of the Yucca Mountain site, the NRC staff have acquired the subregional model of Czarnecki (1985) and the *MODFE* computer code. PC-based versions of the code and model have been prepared to facilitate staff evaluation. This evaluation is provided below, and serves as an example of how the staff can directly obtain and evaluate numerical codes and models developed under DOE's high-level waste program. In this way, the NRC staff can become more knowledgeable about codes and models during site characterization and before receipt of a potential license application.

Finally, the work of Czarnecki (1992) represents an important 10-year forecast of how future ground-water levels will be affected by human activities. After 10 years of site characterization, it will be possible to see how well the regional model has predicted the perturbations caused by pumping at Wells J-13 and J-12. It is expected that one of the many scenarios analyzed by Czarnecki will approximate actual ground-water withdrawals at the well sites, providing a test of how well the regional model represents present-day conditions in the flow system near Yucca Mountain.

This auxiliary analysis is discussed in greater detail in Appendix I.

4.4.8 Modeling Saturated Flow to the Accessible Environment

In the development of the ground-water flow and transport module, several different modeling approaches were attempted. *DCM3D* was used to analyze a dual-continuum approach for modeling a fractured, porous media. Using this code, a 1-D saturated zone flow model was built from the Yucca Mountain site, across that portion of the saturated zone simulated by the performance assessment flow module, to a location near the presently defined "accessible environment boundary" (10 CFR 60.2).

Simulations of ground-water flow and water-table elevation were conducted for a range of material properties. From these simulations, it was observed that:

- The slowest velocities and longest flow times were obtained from runs that used matrix properties. Seepage velocities were 1.3×10^{-6}

and 1.6×10^{-5} meters/year, resulting in extremely long calculated flow times of 3180 million years and 31.7 million years;

- The fastest velocities and shortest flow times were obtained from runs that used hydrologic properties from well tests. The average seepage velocity was 473 meters/year and the calculated flow time was 10.6 years; and

- A simulation of fracture flow that, like matrix property simulations, used low saturated hydraulic conductivities, produced faster flow velocities, and shorter flow times than matrix property runs. This simulation contained smaller porosity values than the matrix property runs and illustrates the importance of determining fracture porosity values, which at this time are hypothetically determined for bulk fracture property flow codes.

This auxiliary analysis is discussed in greater detail in Appendix J.

4.4.9 Geochemical Model for ^{14}C Transport in Unsaturated Rock

Under the unsaturated, oxidizing conditions expected for a geologic repository at the Yucca Mountain site, ^{14}C contained in spent nuclear fuel may be converted to carbon dioxide and be transported with moving gas to the atmosphere. There are several mechanisms that could facilitate the transport of gaseous radionuclides, including ^{14}C, to the atmosphere, and these are discussed in Section 5.6.

Carbon-14, as carbon dioxide, would interact with ions in the ground water and country rock, and would therefore be retarded with respect to the transport of inert gases. Since the temperature, gas flow, and water saturation of the rock will respond to the large amount of heat caused by the decaying nuclear waste, the chemical processes leading to retardation of gaseous ^{14}C will be complicated. The staff investigated the geochemical interactions of ^{14}C for a geologic repository in partially saturated rock. The ^{14}C transport model consists of three parts:

- A geochemical model describing the state of all carbon species in a representative volume of rock;

- A flow and transport model, for movement of total carbon through the system that consists of a number of connected volumes or "cells"; and

- A model of ^{14}C migration as a trace quantity in the general movement of total carbon.

For a simple 1-D example of vertical gas flow from the repository to the atmosphere, the staff reached the following conclusions:

- The results of the analysis show a significant redistribution of autochthonous carbon among solid, liquid, and gas phases, even in areas remote from the repository plane. Carbon remains predominantly in the aqueous solution, in spite of the fact that near-field heating results in a reduction of liquid saturation, abundant calcite precipitation, and increased equilibrium fractionation of CO_2 into the gas phase.

- Transport of ^{14}C released from the repository is generally retarded by a factor of approximately 30 to 40 because of immobilization in the liquid phase. In addition, ^{14}C released early during the period of solid calcite precipitation can be fixed for a long period before repository cooling leads to redissolution of the calcite.

This auxiliary analysis is discussed in greater detail in Appendix K.

4.4.10 The Exchange of Major Cations at Yucca Mountain

Zeolites are crystalline, hydrated aluminosilicates, which are characterized by an ability to readily exchange cations with aqueous solutions. The presence of zeolites is seen as an important barrier to the migration of radionuclides to the accessible environment. This auxiliary analysis was undertaken to address two questions related to the exchange of cations in Yucca Mountain.

The first question concerned the stability of zeolites. Using potassium/argon (K/Ar) dating techniques, WoldeGabriel *et al.* (1992) determined that the zeolites from boreholes in the Yucca Mountain vicinity range in age from 2 million years to 10 million years old. However, ion exchange involving potassium and sodium on zeolites has been shown to reach equilibrium in

about 2 days (Pabalan, 1991). How, then, can a mineral that can alter within a couple of days exist unchanged for at least 2 million years? To answer that question, simulations were performed in which pore water, whose composition approximates that found at Yucca Mountain, percolates through site-specific zeolite layers for a period of approximately 150,000 years. The simulation was intended to represent the chemical reactions that would take place between the cations dissolved in the pore water and the cations sorbed onto zeolites. If, in the simulation, the potassium ions attached to the zeolites become mobile, there would be reason to doubt the zeolites could be accurately dated using a K/Ar technique. If, however, the K is immobile, the K/Ar ratios would not be affected by ion-exchange reactions.

The second question to be answered by this analysis involved the determination of pore-water compositions from the unsaturated zone. Peters *et al.* (1992) describe methods of measuring pore water compositions from rocks of the unsaturated zone, plus the possible causes of changes in the compositions of the pore waters, due to the method of extraction (compression). Given that ion-exchange reactions involving zeolites are fast (Pabalan, 1991), can it be determined what the chemical composition of pore water from the unsaturated zone is if the composition of the zeolite in direct contact with the pore water is known?

The simulations performed to address the first question in this auxiliary analysis concerning the validity of K/Ar dating relied on the geochemical modeling code *PHREEQM* (Nienhuis and Appelo, 1990). This analysis involved simulating the flow of site-specific ground water through site-specific porous rock, at a site-specific rate. The simulation that was performed used mole fractions of Na, Ca + Mg, and K, derived from the zeolite compositions reported by Broxton *et al.* (1986). The flushing solution composition in the simulation approximates that of the site-specific water from Peters *et al.* (1992).

The results of this auxiliary analysis demonstrate that the K in the zeolites is relatively immobile. This is because of the large reservoir of K held in the zeolite, versus the amount of exchangeable cations in the liquid. There simply are not enough cations in the pore water to exchange with the K on the zeolites, and therefore the K remains immobile. Consequently, the K/Ar technique for determining the age of the zeolites should not be affected by ion exchange, given the low concentrations of cations in the ground water and slow flow rate in the vadose zone.

The simulations performed to address the second question in this auxiliary analysis required modeling the three ion-exchange reactions:

$$NaX + K^+ \leftrightarrows KX + Na^+ \quad , \qquad \textbf{(4–17)}$$

$$2Na^+ + CaX_2 \leftrightarrows 2NaX + Ca^{2+} \quad , \qquad \textbf{(4–18)}$$

$$2K^+ + CaX_2 \leftrightarrows 2KX + Ca^{2+} \quad . \qquad \textbf{(4–19)}$$

Equilibrium constants for Equations (4–17) and (4–18) were from Pabalan (1991). Equation (4–19) was derived by multiplying Equation (4–17) by 2 and adding the result to Equation (4–18). The equilibrium constant for Equation (4–19) was derived similarly.

By using the compositions of clinoptilolites from Yucca Mountain (Broxton *et al.*, 1986) and the equilibrium constants from Pabalan (1991) and this study for Equations (4–17) through (4–19), the relative concentrations of the exchangeable cations in the pore were calculated.

The results of the exercise demonstrate the wide variation in the pore-water chemistry which is possible in the vicinity around Yucca Mountain. In addition, this analysis has shown that the chemical composition of the pore waters in contact with the solids in the unsaturated zone may be different from the composition of the water in the saturated zone.

This auxiliary analysis is discussed in greater detail in Appendix L.

4.4.11 Considerations in Modeling Percolation at Yucca Mountain

The infiltration at Yucca Mountain could vary considerably because of topography, spatial variation in hydrologic properties, and the intensity and duration of the rainfall. The effect of these variations on the rate of percolation at the repository depth is uncertain. Detailed spatial and

temporal hydrologic modeling exercises have been proposed to provide insights on the impact of these variations.

The surface boundary condition for many modeling exercises is assumed to be a constant value over large areas. Although this type of assumption may offer a type of "average" behavior of percolation, a more explicit model which takes into account both the change in hydrologic properties and topography (e.g., alluvium in a wash), is needed, to better understand the effect this type of spatial variation has on percolation. Although very detailed topography of Yucca Mountain is readily available, site characterization is still quite limited in providing a detailed description of the hydrologic layering and structures below Yucca Mountain, to determine the effect on percolation (isolated areas of increased recharge may either be of benefit or detriment to performance, depending on whether the recharge intercepts the repository). Despite this characterization limitation, the current exercise was conducted to gain insights into the importance of this effect, examine the viability of modeling on a small spatial scale (meters to tens of meters), and gain experience on the recently developed computer program *DCM3D* (Updegraff *et al.*, 1991). A 2-D simulation based on detailed spatial variation and topography was conducted to analyze the affect on percolation. The simulation revealed an ability to concentrate recharge in the low-lying alluvium and indicated the numerical difficulties in examining this type of localized, focused recharge.

Likewise the duration of rainfall could have a significant impact on the determination of the amount of percolation at Yucca Mountain. Typically, surface boundary conditions assume a small annual, steady-state average infiltration rate. The effect of using an infiltration rate based on averaging rainfall over an entire year, as compared to using a transient infiltration rate, needs to be evaluated, to better understand any correlations with percolation and fracture flow. A 1-D simulation was conducted with transient infiltration rates, to examine the effect on percolation and fracture-flow rates.

The above two simulations experienced similar numerical difficulties simulating the infiltration of a sharp wetting front (either infiltration from a wet, high permeability alluvium in a wash into an underlying dry, low permeability unit or large episodic infiltration into a dry unit). The numerical difficulties were traced back to the manner in which pressures are evaluated at the grid block interface (either a linear interpolation or a Newton-Raphson iteration scheme). Numerical problems arose when very dry-node (meters of suction) and wet-node (near zero suction) pressures are interpolated to arrive at an interface pressure. When this situation occurs the saturated node increases in positive pressure (meters of pressure) before any appreciable water flows between the two nodes. This situation is a result of the interface pressure value remaining a large negative value, until the wet node attains the very large positive pressure to balance the high suction value of the dry node. This effect in the 1-D transient simulation resulted in large oscillations in the pressure, as the recharge front moved down the column. This type of behavior is considered to be an artifact of the numerics, rather than caused by the physical system. Upstream-weighting of the pressure interpolation scheme has been introduced into the *DCM3D* computer program, to correct this effect. This technique has corrected the observed aberrant behavior; however, further testing is needed to examine numerical dispersion effects before performing the above simulations again.

4.4.12 Comparison of *NEFTRAN II* to *UCBNE41*

NEFTRAN II, an SNL transport code (Longsine *et al.*, 1987), was compared to *UCBNE41* (Lung *et al.*, 1987). *UCBNE41* is a saturated 1-D transport code that uses an analytic solution. During the comparison an error in the internal documentation to the *UCBNE41* code was found and corrected.[4] The initial concentrations should be input in moles/cubic meter, not grams/cubic meter.

After making this change, the two computer codes compare well. Figures 4-26 to 4-28 compare the results of *NEFTRAN II* and *UCBNE41*, for a test case based on sample data set No. 3 in the *NEFTRAN II* documentation. Since *UCBNE41* requires a constant velocity, the initial velocity was maintained for all times. Sample data set No.

[4]H.C. Lung and W.W-L Lee were subsequently contacted and agree that the internal documentation for the code was in error. H.C. Lung is the author of *UCBNE41*. W.W-L Lee is NRC's contact at the University of California at Berkeley.

3 prescribes a doubling of the initial velocity at 50,000 years.

Other transport codes such as *UCBNE40*, *UCBNE50*, *UCBNE51*, and *UCBNE52* were not compared to *NEFTRAN II* in this study. However, they are very similar to *UCBNE41*. As transmitted to the NRC staff, all the codes in the *UCBNE40* and *50* series ask for initial concentrations in grams/cubic meter but do not accept the atomic mass as input. *UCBNE40*, *UCBNE50*, *UCBNE51*, and *UCBNE52* have therefore been altered to indicate that the initial concentrations should be input in moles/cubic meter, not grams/cubic meter. *UCBNE40* compiles correctly. *UCBNE50*, *UCBNE51*, and *UCBNE52* contain a non-ANSI (American National Standards Institute)-standard feature. They alter the value of a do loop variable inside the loop. This feature causes problems with some FORTRAN 77 compilers. This problem was documented, but not corrected. Fixing this problem would require reworking the entire looping structure of the program. The codes *UCBNE40*, *UCBNE50*, *UCBNE51*, and *UCBNE52* should be tested further before being used.

4.5 Conclusions and Suggestions for Further Work

A number of conclusions and recommendations resulted from: (1) the development and implementation of computational tools for calculating ground-water flow and radionuclide transport; (2) the analysis of results related to the conceptual models used for ground-water flow and radionuclide transport; and (3) the auxiliary analyses. A description of the more salient conclusions and recommendations relevant to ground-water flow and transport are presented below:

1—Examine modeling issues affecting percolation

Conceptual model assumptions with respect to percolation should have a major effect on water flux through a repository located in the unsaturated zone. One-dimensional approaches, like that used in the IPA Phase 2 analysis, can be very sensitive to assumptions regarding percolation. The modeling assumptions and uncertainties affecting percolation rates need to be analyzed to better understand their effect in relationship to the range assumed for percolation. Uncertainty in the percolation rate, in part, can be attributed to: variations in the infiltration rate; spatial variability of hydrologic properties within a hydrogeologic unit; variability in the thickness of the hydrologic units; and assumptions regarding fracture matrix interactions. The current analysis accounted for some of this uncertainty by use of a correlation length, to develop a representative permeability range for each hydrogeologic unit, use of different hydrogeologic unit sequences, and thicknesses attributed to different sub-areas of the repository, and the use of 2-D flow modeling results to interpolate spatial variation of percolation caused by the slope of the hydrogeologic units. These model abstractions were considered to be very important to the conceptualization of the flow problem and proved to be equally important to obtaining reasonable computer execution times for the TPA computer code. However a number of issues that are considered important to estimating percolation were not evaluated in IPA Phase 2. Issues that need to be examined further include: the relationship between highly transient rainfall and percolation estimates; the effect of topographic lows and fault zones as sources of increased recharge; how spatial variability in hydrologic parameters affect percolation; and the effect of fracture imbibition on percolation (also see *Recommendation 2*).

2—Examine modeling assumptions affecting fracture-matrix interaction

Modeling assumptions regarding the interaction between matrix and fractures are very important, because of differences in fluid velocities and retardation between the two flow systems. These differences are primarily caused by the fracture flow system having a very small bulk porosity (10^{-4} to 10^{-5}) and limited surface area of the fracture walls, compared with the large bulk porosity (.1 to .4) and large surface area associated with the pores of the matrix flow system. The IPA Phase 2 analysis used a dual-continuum approach that represented the fracture and matrix systems as separate but interacting continua.

Steady-state interaction between the two continua were modeled, assuming the fractures were planar, regularly spaced, and without a mineral coating affecting the movement of water across the fracture surface. Further simulation efforts could improve the understanding of conceptual

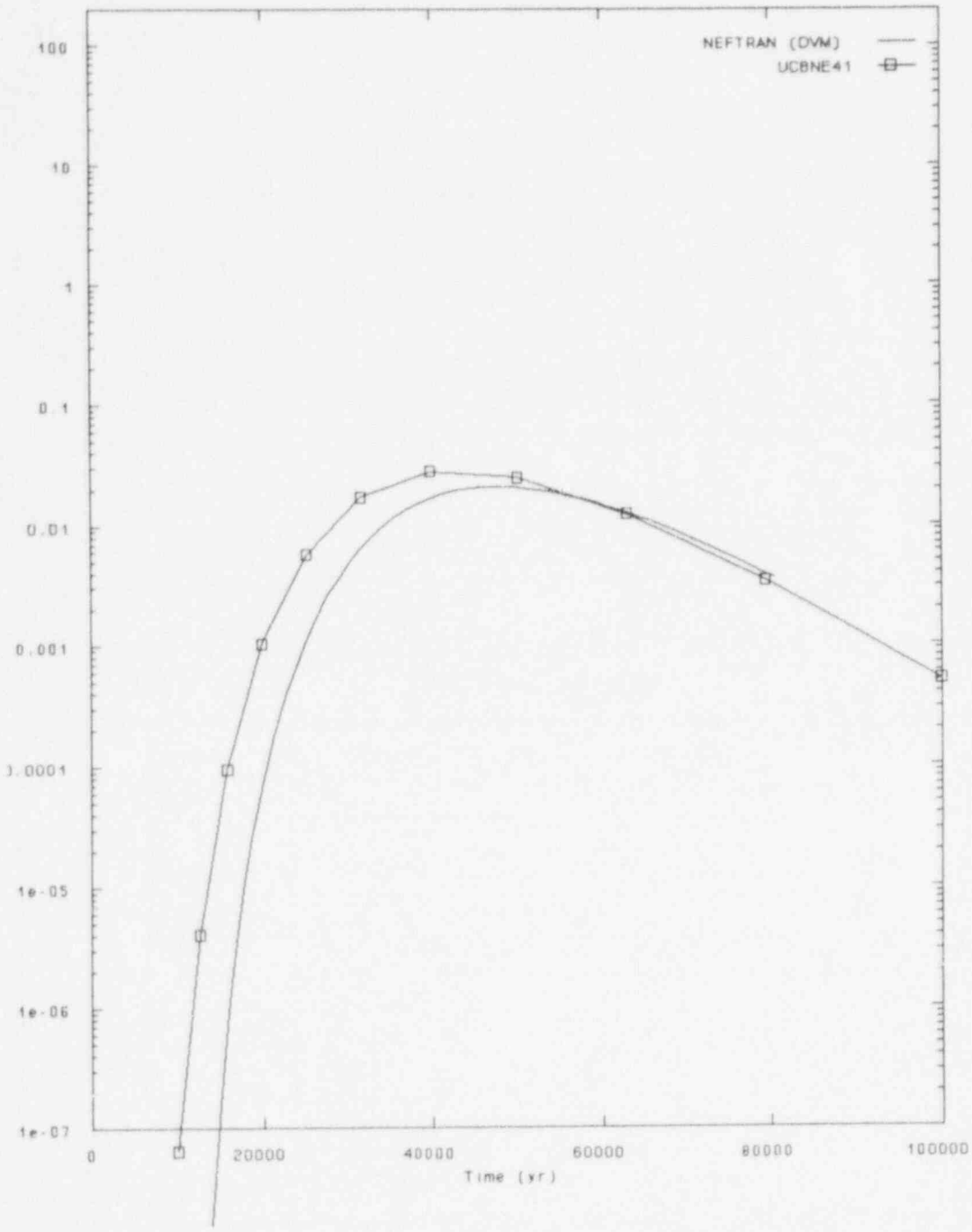

Figure 4–26 Discharge rates for ^{243}Am computed by *NEFTRAN II* and *UCBNE41*, in a benchmarking exercise

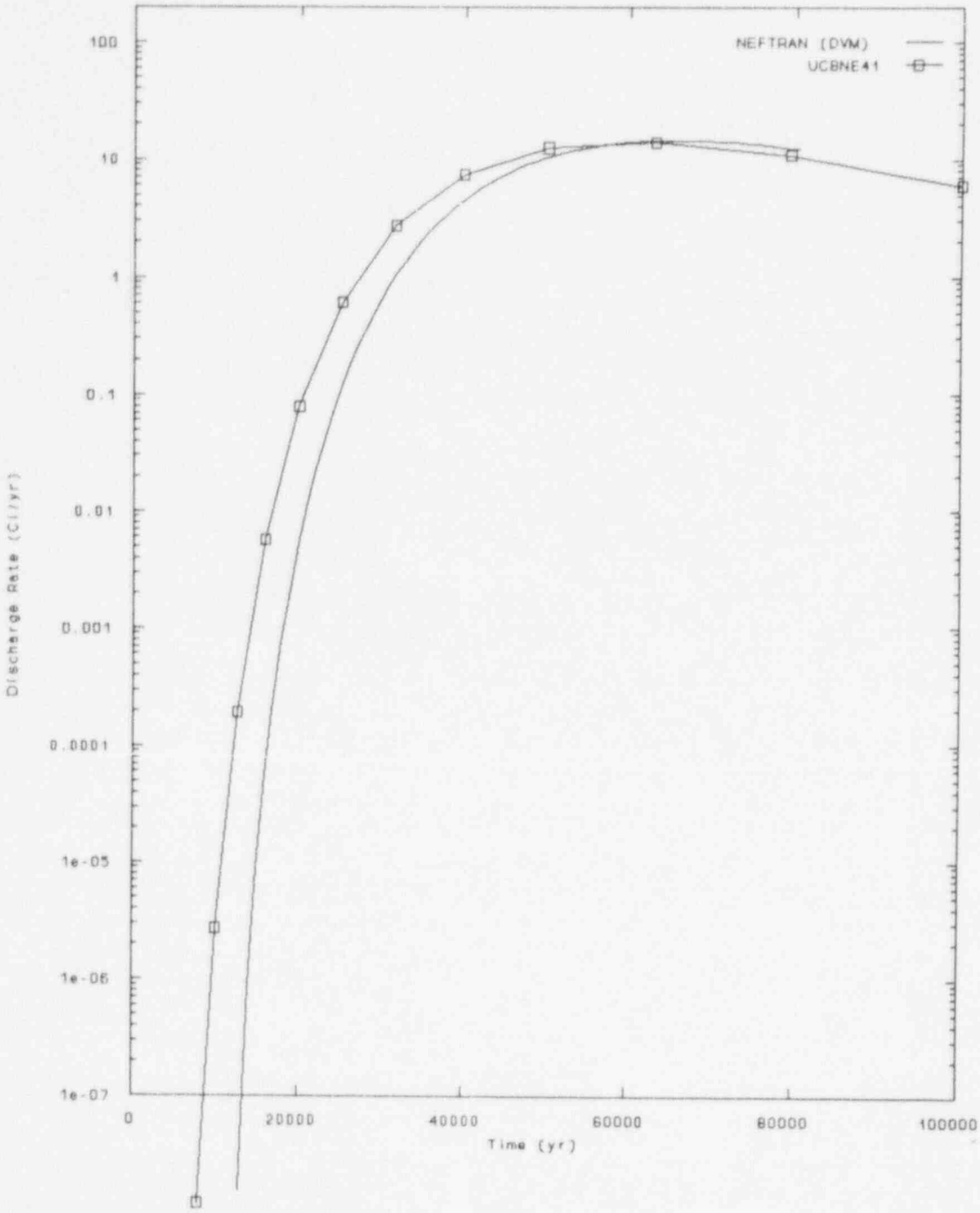

Figure 4–27 Discharge rates for ^{239}Pu computed by *NEFTRAN II* and *UCBNE41*, in a benchmarking exercise

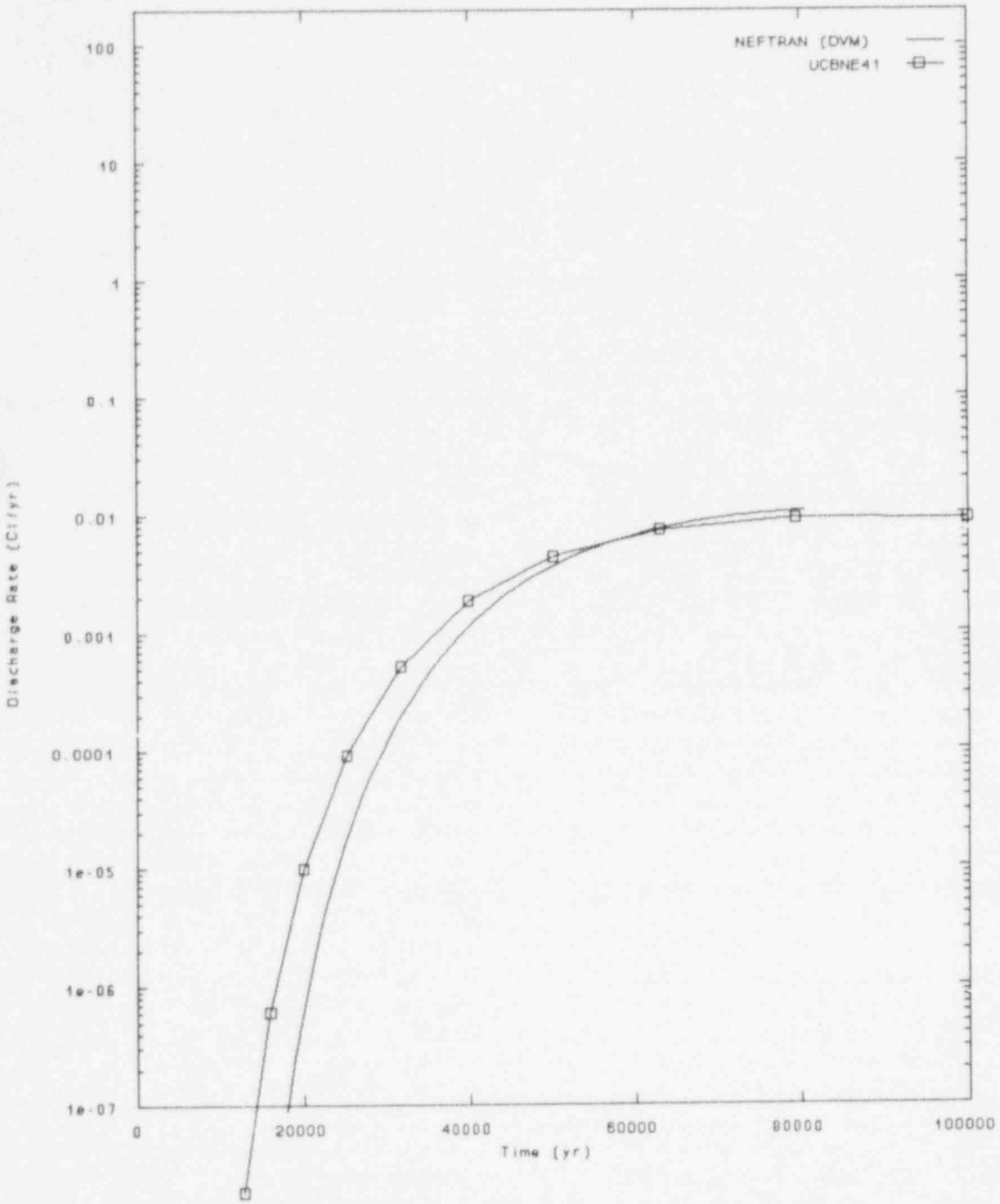

Figure 4–28 Discharge rates for ^{235}U computed by *NEFTRAN II* and *UCBNE41*, in a benchmarking exercise

modeling assumptions regarding small-scale interactions at the fracture-matrix interface (e.g., detailed simulations to examine the equilibration of pressure between the fracture and matrix, considering transient conditions and the effects of mineral coatings on fracture surfaces) and large-scale effects concerning the flow field within a hydrogeologic unit (e.g., examine how the small-scale effects propagate through a geologic unit). These further analyses can be used to modify current IPA models and revise parametric ranges.

3—Examine hydrogeologic features and heterogeneity in the context of providing a "short circuit" through the unsaturated zone

The IPA Phase 2 flow and transport analyses assumed that fluid flow and radionuclide transport could be represented through 1-D stream tubes for each of the hydrogeologic units. This representation does not account for possible "short circuiting" of the low conductivity matrix pathway via hydrogeologic features (i.e., fault zones) or fracture flow initiated by perched water forming in areas of heterogeneity. Two- and three-dimensional analyses could investigate the impact of fault zones and perched water on pathways through the unsaturated zone. If the impact were of sufficient magnitude, then additional pathways could be added to the flow and transport analysis in future IPA phases.

4—Examine the coupling of water in the gaseous and liquid phases

Although a number of characteristics of the flow system have been included in the abstracted models of the TPA computer models, a number of characteristics of the real system have not been included. The real problem is transient, 3-D, partially saturated flow with significant air and water-vapor movement in a fractured, porous medium complicated by potentially significant heat transfer and the associated flows of gas and liquid affecting the redistribution of moisture. How these phenomena can be approximated by simplifying assumptions and still provide an adequate representation for the calculation of system performance is poorly understood at this time and needs further investigation. Abstracted models need to be tested through simulation, comparing the results with those of the "complete" model, which includes the coupling of water movement in the liquid and gaseous phases, under non-isothermal conditions. Simulation efforts could examine the variation in moisture contents and fluid flux, through the repository, caused by vapor movement and condensation (this effect would be especially pronounced during the thermal phase of the repository). These results would provide more realistic fluid flux for the source-term and flow and transport modules.

5—Examine refinements in the saturated modeling to improve concentration estimates for dose calculations

The calculation of dose requires a determination of the radionuclide concentration. The concentration determination required an additional refinement of the transport model, beyond what is required for the calculation of integrated discharge, for comparison with the EPA standard. This determination required not only the integrated discharge of radionuclides, but the quantity of water associated with this discharge. For the current analysis, the contaminant plume was assumed to remain near the water table, and assumptions were made concerning the local population and its water usage. Additional refinements in these assumptions could require significant improvements in the current modeling approach for flow and transport and place greater demands on data requirements. Initial efforts should concentrate on compiling different approaches used for modeling saturated fractured rock and their relationship to field conditions at Yucca Mountain, as a guide for possible improvements to the current analysis.

6—Examine modeling assumptions affecting retardation in fractures

Radionuclide releases, in the liquid pathway, to the accessible environment were affected primarily by the presence of fracture flow. The IPA Phase 2 analysis conservatively assumed that there was no retardation in the fractures and did not consider the process of matrix diffusion in the modeling. Future work needs to evaluate the nature and magnitude of the conservatism of these assumptions and the relationship of fracture coatings in affecting these processes.

7—Access the usefulness of additional intermediate calculations for understanding the flow and transport results

The IPA Phase 2 performance measures were integrated discharge and radionuclide dose. Oftentimes, it is difficult to explain these results in the absence of other information on modeling results for individual modules (e.g., fluid flux or water velocity for the ground-water pathway, and release rates for the source term module). These intermediate results proved extremely valuable in both determining if the modules were performing as expected and in assisting the sensitivity analysis. It would be beneficial to further examine the modeling approaches and identify intermediate calculations that could be performed to provide further insights on model and system performance. For example, the current analysis used a dual-continuum model to represent the fracture-matrix system as separate but interacting continua that enabled a simple procedure to be implemented for performing intermediate calculations concerning fluid flow in the fracture and matrix continua.

Recommendations from the Auxiliary Analyses

The auxiliary analyses contributed to parametric values used in the TPA system code and to understand assumptions and limitations used to represent ground-water flow and radionuclide transport. The assignment of individual parametric values through an auxiliary analysis is not discussed here except in terms of impacting assumptions and limitations of the analysis. A brief description of the more salient conclusions and recommendations related to the auxiliary analyses are presented below (more complete descriptions can be found in the associated appendices):

(1) The representation of a fractured system can be accomplished via a discrete fracture model, a composite approach which attempts to average the matrix and fracture system, or a dual-continuum approach which treats the matrix and fracture as separate but interacting continua. Each of these representations have both benefits and disadvantages. Experimental information with respect to fracture-matrix interactions is extremely scant and is needed to provide insights on the applicability of these approaches.

(2) Ground-water flow modeling is affected by a number of assumptions at a very small scale (millimeters to centimeters) and at a large scale (tens of meters to kilometers). At a very small scale, assumptions with respect to characteristic curves (pore scale) can have dramatic impact on interactions between the matrix and fracture flow fields, in addition to assumptions regarding steady-state versus transient flow. At a large scale, there are a number of assumptions and features (topographic details that lead to spatial variation of recharge and discharge areas, discrete features such as a fault zone, spatial variability in hydrologic properties, and layering of geologic strata) that can have significant impact on the distribution of fluxes throughout the unsaturated zone. Further analysis is needed to better understand the impact of these assumptions on the overall repository performance.

(3) Several potentially volatile compounds of ^{99}Tc, ^{79}Se, and ^{129}I may be present in spent nuclear fuel. Conservative estimates of gaseous releases of these radionuclides during volcanism and normal operations were sufficiently low to not warrant further study.

(4) The transport of gaseous ^{14}C will be affected by variation in saturation, gas flow, and temperature, caused primarily by heat from decaying nuclear waste. Geochemical modeling of ^{14}C transport demonstrated a retardation factor of approximately 30 to 40, because of primarily transfer of carbon between the CO_2 in the gas phase and dissolved carbonate and bicarbonate in the liquid phase. Some ^{14}C might be trapped temporarily, in precipitating calcite during the period when temperatures are rising, and released from the calcite as it redissolves, as temperatures fall.

5 SOURCE TERM MODULE[1]

5.1 Introduction

The model used by the staff to calculate the source term in Iterative Performance Assessment (IPA) Phase 1 was that incorporated in the *NEFTRAN* (**NE**twork **F**low and **TRAN**sport) computer code obtained from the Sandia National Laboratories (SNL) (see Longsine *et al.*, 1987). In this model, radionuclide releases would occur only after failure of the waste package canister,[2] characterized as a single failure time.

In IPA Phase 2, the staff developed its own computer code to calculate the source term. The *SOTEC* (**So**urce **T**erm **C**ode) module (see Sagar *et al.* (1992)) deals with the calculation of aqueous and gaseous radionuclide time- and space-dependent source terms for the geologic repository. It does so by considering the variations in those physical processes expected to be important for the release of radionuclides from the engineered barrier system (EBS).

Three primary calculations are done in *SOTEC*: (a) failure of waste packages because of a combination of corrosion processes and mechanical stresses; (b) the leaching of spent nuclear fuel; and (c) the release of $^{14}CO_2$ gas from the oxidation of UO_2 and other components in spent nuclear fuel and hardware. The principal features of the staff's source term analysis are discussed below.

5.2 Overall Structure of the Source Term Code

5.2.1 Conceptual Model

The proposed geologic repository at Yucca Mountain will consist of a large number of waste packages placed in drifts and perhaps in boreholes. The repository environment will change with time, as a result of radioactive decay, leading to initial heating of the rock, followed by a long cooling period. The heating is anticipated to promote dramatic changes in the chemical and hydrologic environment surrounding the waste packages. Temperature and water flow rates will vary widely in both time and space. The geology of the mountain is of a fractured, porous rock material with high spatial variability. The problems with heterogeneity are increased because the type of water flow of greatest concern is fracture flow. The characteristics of the waste material such as age, burn-up, heavy metal inventory, and spent nuclear fuel versus defense vitrified waste (glass) will vary spatially in the repository. Environmental variables such as water flow rates, water saturation, water chemistry, and temperature will vary in time and in space in the repository.

The problems associated with heterogeneity are addressed in part in the source term module *SOTEC* by dividing the geologic repository into a number of zones, referred to as "repository sub-areas". Within each repository sub-area, all chemical, physical, and waste form properties are assumed to be identical. The release rate for each repository sub-area is then the release rate for an individual waste package in the repository sub-area times the number of waste packages in the repository sub-area. *SOTEC* calculates the performance characteristics for an individual waste package and extrapolates the result to the entire repository area.

Information concerning variability may come either from standard input parameters listed in Appendix A or from output files created by other modules of the total-system performance assessment (TPA) computer code. To limit the amount of input data and code complexity, the assumption is made that (except for temperature) a separation of parameters can be performed between spatial and temporal variations. For each parameter, the input appears as a time-variant repository average (or reference) value and a set of load factors for the individual repository sub-areas. *SOTEC* and the temperature code, *CANT2* (described in Section 2.1.3), consider only seven separate repository sub-areas. The small number of repository sub-areas is inadequate to describe a continuous distribution of failure times for the waste packages and the fractional release rate for the EBS. The concept of ensemble averaging to

[1]The figures shown in this chapter present the results from a demonstration of staff capability to review a performance assessment. These figures, like the demonstration, are limited by the use of many simplifying assumptions and sparse data.

[2]The term "waste package" is used here synonymously with "container" and "canister."

choose parameters that best represent all waste package canisters in discussed briefly in Section 5.3.5 and in greater detail in Appendix L.

5.2.2 Input to and Output from *SOTEC*

The structure and flow of the source term code is illustrated in Figures 5-1 and 5-2. Data are read into *SOTEC* from a series of files. Some of the file names are initially fixed, however the majority of file names are read from the main input files.

As noted in Chapter 2, many of the TPA modules can run in either the "internal" or the "external" mode.[3] In the internal mode, *SOTEC* reads from the file of input parameters produced by the Latin Hypercube Sampling (LHS) procedure. Many of the parameters in *SOTEC* that are read from the stand-alone input files are overwritten. Over-written parameters represent either random parameters or system-wide input parameters. Figure 5-1 presents input and output files for *SOTEC*. Some of the output files for *SOTEC* are only written when operation is in internal mode.

All of the major output files written by *SOTEC* are designed to be read by other codes. The major output of *SOTEC* is the release rate, as a function of time, for each radionuclide for each repository sub-area. Additional outputs are:

- Waste package lifetimes for use in some of the other disruptive consequence models;
- The 1000-year inventory for each radionuclide, assuming radioactive decay only, with no other loss from the waste package;
- The cumulative release from the EBS of each radionuclide in each repository sub-area; and
- The failure times by corrosion necessary for evaluation of the model for seismic failure.

5.2.3 Structure of Calculations

The overall flow of the calculations in *SOTEC* is illustrated in Figure 5-2. Subsequent to reading the input files, *SOTEC* loops over time calculating corrosion penetration for each waste package as a function of time. Waste package failure times for each repository sub-area are recorded for use in the release-rate portion of the code. The corrosion portion of *SOTEC* is not coupled to the liquid release calculations and could be put in a separate code. In the corrosion calculations, the corrosion rate is estimated at the beginning of each time step. At the end of the time step, the total corrosion depth is compared with the critical thickness for buckling. If the remaining waste package thickness is less than the critical thickness, or if the remaining thickness is less than zero, failure is presumed to occur. Depending on input assumptions, the waste package may either fail completely, resulting in a flow-through system, or fail partially, with a specified maximum volume inside the failed waste package.

Calculation of liquid and gaseous releases begins with evaluation of the failure time and types for each repository sub-area. Individual waste packages in each repository sub-area can fail by three different mechanisms. The first type of failure is initial defectives, representing waste packages that were defective at the time of repository closure. Defective waste packages will begin releasing ^{14}C at time = 0 and begin releasing radionuclides in the aqueous phase once the waste package cools below the boiling point and begins filling with water. The second type of failure is by scenario. The scenario option fundamentally allows the TPA computer code, or the analyst, to specify a time of failure for a portion of the waste packages in each repository sub-area. The primary purpose is to facilitate evaluation of alternative scenarios besides corrosion/buckling failure of the waste packages. The scenario option can also be used by the TPA computer code to specify a waste package lifetime distribution independent of the corrosion calculations. The third type of waste package failure is by the corrosion/buckling mechanism discussed in Section 5.4.

After sorting out the type and timing of the failures in each repository sub-area, the liquid and gaseous release calculations begin. The calculations proceed by repository sub-area, with internal time and radionuclide loops in the liquid and gas-release modules. The calculations are set up to handle multiple chains of radionuclides and multiple isotopes of the same element.

[3] "Internal" versus "external" refers to the manner of code execution and the time at which the output files from the consequence modules are generated. In the internal mode, the modules are separate from the system code, and as a result, the cumulative releases can be generated and placed in files at any time before iteration of the system code.

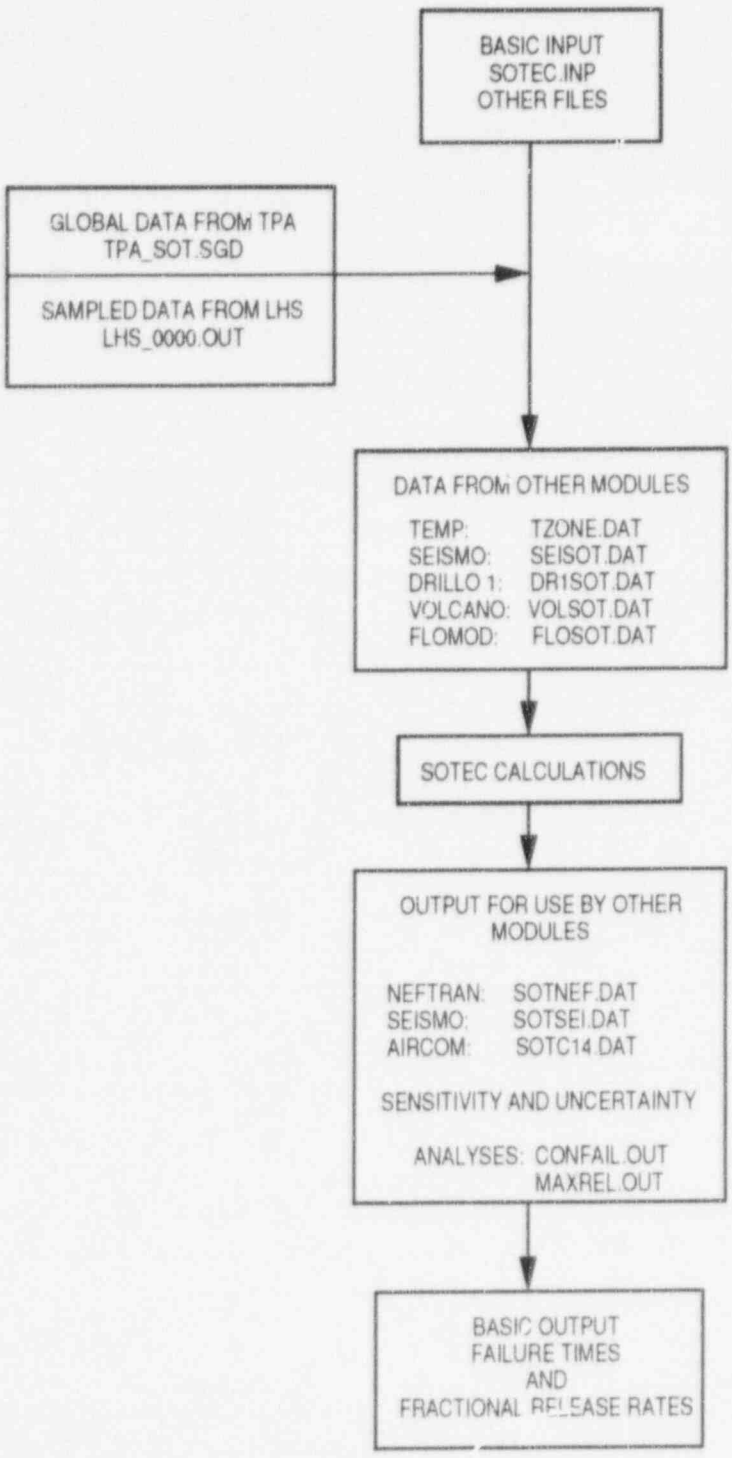

Figure 5-1 *SOTEC*—**Source term code input and output files**

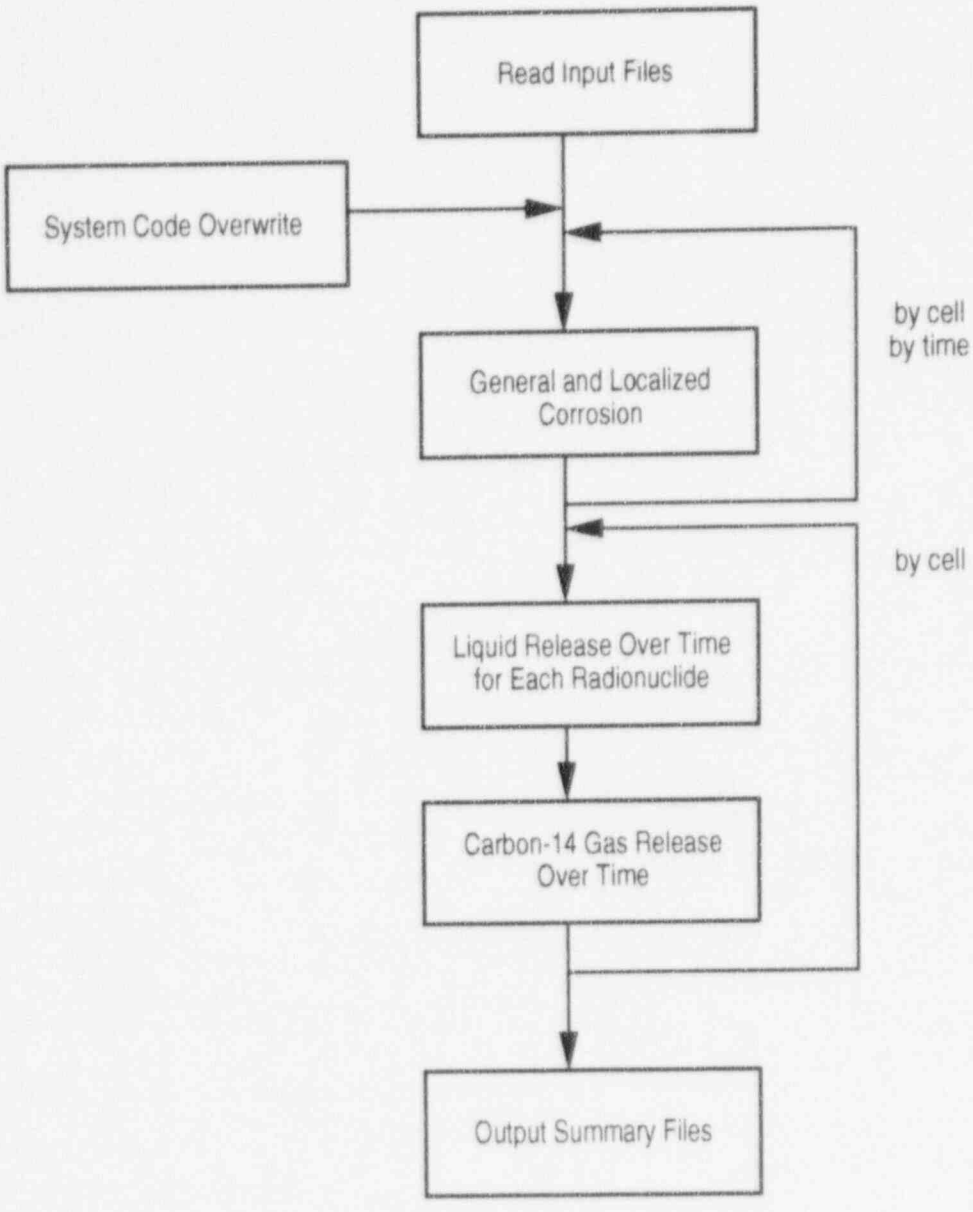

Figure 5–2 ***SOTEC*—Source Term Code**

Subsequent to the release calculations, the release rates are summarized by calculating cumulative release and interpolated to even grids for writing to file.

5.2.4 Radionuclide Inventory

The inventory of radionuclides included in the calculations of IPA Phase 2 were carefully screened from a large list of radionuclides, to include only the major contributors to cumulative release and dose. The primary objective of this screening was to reduce to a minimum the number of calculations in the computer programs, without substantially affecting the results.

Starting with a list of 37 radionuclides, the TPA computer code was run for 50 LHS vectors of the fully disturbed (*csdv*) scenario, and the results tabulated for cumulative release at the accessible environment and on-site dose to the farm family. A radionuclide was retained in the inventory if, in any of the 50 vectors, it contributed more than 1 percent of the U.S. Environmental Protection Agency (EPA) cumulative release limit[4] for that nuclide. The screening analysis also checked the maximum dose to the farm family, to see if any of the radionuclides that might have been screened out on the basis of cumulative release should have been kept on the basis of dose. In all cases, however, the cumulative release criteria were more restrictive than dose.

If a radionuclide screened out of the inventory was a parent to another radionuclide, the inventory of the progeny was adjusted upward to account for the decay of the parent. This was important for the radionuclide ^{238}Pu, which was screened out, and whose decayed inventory was added to that of the progeny ^{234}U. Table 5–1 presents the radionuclide inventory used in the Phase 2 analyses.

Table 5–1 Initial Radionuclide Inventory (in curies per metric ton of heavy metal (Ci/MTHM))

Nuclide	*Ci/MTHM*	*Nuclide*	*Ci/MTHM*
^{246}Cm	0.0258	^{226}Ra	3.67×10^{-7}
^{238}U	0.318	^{210}Pb	4.7×10^{-8}
^{245}Cm	0.126	^{137}Cs	7.66×10^{4}
^{241}Am	1640	^{135}Cs	0.35
^{237}Np	0.288	^{129}I	0.0295
^{243}Am	15.5	^{99}Tc	12.3
^{239}Pu	308	^{59}Ni	3.56
^{240}Pu	508	^{14}C	1.54
^{234}U	1.89	^{79}Se	0.381
^{230}Th	1.29×10^{-4}	^{94}Nb	0.793

5.3 Waste Package Environment

5.3.1 Introduction

The waste emplacement environment at Yucca Mountain is expected to be highly complex. Modeling for the IPA Phase 2 requires a relatively simple conceptual model for the interaction of the waste packages and their immediate environment. The following subsections discuss the thermal, hydrologic, and geochemical environment for the waste package, as conceived in IPA Phase 2.

5.3.2 Thermal Environment

The repository environment will change with time as a result of heat generated in the decaying waste. Heat will be transferred in the host rock primarily by thermal conduction, but heat transfer will be complicated by the evaporation and condensation of water, and the transport of air and water vapor. The movement of water vapor and liquid water will affect the hydrologic environment

[4]Currently, a revised set of standards specific to the Yucca Mountain site is being developed in accordance with the provisions of the Energy Policy Act of 1992. The Energy Policy Act of 1992 (Public Law 102–486), approved October 24, 1992, directs NRC to promulgate a rule, modifying 10 CFR Part 60 of its regulations, so that these regulations are consistent with EPA's public health and safety standards for protection of the public from releases to the accessible environment from radioactive materials stored or disposed of at Yucca Mountain, Nevada, consistent with the findings and recommendations made by the National Academy of Sciences, to EPA, on issues relating to the environmental standards governing the Yucca Mountain repository. It is assumed that the revised EPA standards for the Yucca Mountain site will not be substantially different from those currently contained in 40 CFR Part 191, particularly as they pertain to the need to conduct a quantitative performance assessment as the means to estimate postclosure performance of the repository system.

for periods of time after waste emplacement. The strengths of the thermal effects will be a function of the types of waste and the thermal loading per unit area. The repository temperature model for IPA Phase 2, discussed in Section 5.4.2, considers only heat conduction in a uniform semi-infinite medium, and does not take into account two-phase flow.

IPA Phase 2 considers only simplified aspects of the thermal environment for several of the models:

- *Onset of waste package corrosion*—The waste packages are assumed to remain dry, and no corrosion of the waste packages occurs before the temperature falling below the assumed boiling point, at the repository, of 96 degrees Celsius (°C).

- *Corrosion model parameters*—Several of the corrosion parameters in the model of Section 5.4.1 are temperature-dependent.

- *Carbon-14 source term model*—As described in Section 5.6.3, the release rate of gaseous $^{14}CO_2$ from the spent fuel waste form is temperature dependent. The rate of liquid release predicted by the model does not depend directly on the temperature.

5.3.3 Hydrologic Environment

The assumed disposal concept adopted in the IPA Phase 2 is one of vertically placed waste packages surrounded by an air gap, as discussed in the U.S. Department of Energy's (DOE's) 1988 Site Characterization Plan (SCP) (see DOE, 1988). One of the main intentions of this design is the isolation of the waste packages from liquid water, since there would be little or no direct contact of the waste packages with the surrounding rock. In an unsaturated environment, capillary suction should keep liquid water diverted away from the air gap and confine it to the rock.

If no liquid water could reach the waste packages, there would be little possibility of water-borne radionuclide releases to the geosphere, even if the waste packages failed. Gaseous radionuclides could still be released, however, as could releases in the case of disturbances such as human intrusion and volcanism. The reliance on engineered design to maintain the dryness of the waste packages has not been demonstrated, however, so the authors found it prudent to postulate mechanisms by which liquid water could reach the waste packages, and carry away dissolved radionuclides:

- *Dripping fractures*—Fracture flow in the rock could occur under conditions where infiltration exceeded the hydraulic conductivity of the rock matrix. Several mechanisms could lead to local saturation, such as perching along rock interbeds, fracture flow along continuous pathways from areas of local recharge at the surface, and the return of condensed water that had been evaporated by the waste heat. These phenomena are discussed more thoroughly in Chapter 4.

- *Direct contact of waste package with rock or rubble infilling material*—The air gap surrounding the waste package could be compromised if it were to become filled in with porous material from rock spallation or sedimentation. Another possibility would be the tilting of the waste package so that it leans against the side of the emplacement borehole.

- *Condensation of water onto surface of waste packages*—Minerals contained in the groundwater that might come into contact with the waste package surface could become highly concentrated, leading to a condition of vapor-pressure lowering (Walton, 1993). These highly concentrated mineral solutions might remain liquid at temperatures significantly above the boiling point of water. Furthermore, the solutions would probably be corrosive.

- *Immersion of waste package*—Perched water or a general rise in the regional water table could immerse the waste packages. Another possible mechanism for waste package immersion might be the mineralization of fractures near the waste packages, because of hydrothermal activity induced by repository heat or an external heat source. The plugged fracture might then allow the collection of infiltrating water that would otherwise drain. The possibility of waste package immersion was not considered to be a credible scenario in the IPA Phase 2 analysis.

5.3.4 Interaction of Liquid Water with Waste Form: Direct Contact

The IPA Phase 2 model for release of dissolved radionuclides considers that there might be direct contact of dripping liquid water with some of the waste packages. Based on the infiltration of meteoric water, the carrying capacity of fractures and matrix in the vertical rock columns, and on horizontal diversions by the dipping bedding planes, the hydrologic models discussed in Chapter 4 are used to estimate an areally averaged rate of water carried by fractures. In some cases, all flow will be carried by the matrix, and consequently, there will be no release of dissolved radionuclides by direct contact of liquid water.

For the cases where there is fracture flow, dripping liquid water from fractures is likely to be non-uniformly distributed over the repository. There would be a wide distribution of amounts of dripping water, and many of the waste packages might never receive any. On average however, the total rate of water influx q affecting each waste package is likely to be no greater than the effective cross-sectional area A_e (or "funnel factor") of the emplacement hole times the average fracture infiltration rate I_f; that is:

$$q = A_e I_f \quad . \tag{5-1}$$

The effective cross-sectional area of the emplacement hole A_e is chosen to be a uniformly distributed random area between 0 and 0.4 square meters per waste package, based on a mean area for the borehole of 0.2 square meters. There are several reasons to believe that the flow rate of water affecting the waste packages would actually be far less:

- For partially saturated flow, openings are barriers to flow rather than conduits. Even in fractures and the emplacement borehole, capillary tension would likely restrict water to the fractures and borehole walls; and

- Dripping fractures would occur only occasionally, and drips might not land on the waste package or in places that would lead to corrosion or entry into the waste package.

5.3.5 Ensemble Averaging

For the sake of computational speed, the IPA Phase 2 analysis used a "lumped parameter" approach, in which the entire repository is represented by a relatively small number of waste packages. Since the repository source term, consisting of tens of thousands of waste packages (Johnson and Montan, 1990), is being represented by only seven repository sub-areas, with only one waste package per repository sub-area, there must be careful consideration given to the way in which the repository sub-areas represent the ensemble of waste packages.

Presently, the arithmetic average of external environmental parameter values (e.g., temperature, flow rate) for all waste packages in the repository sub-area is chosen for a representative waste package. Additionally, there is only one set of source term parameter values (e.g., corrosion parameters, solubilities) representing the corrosion, liquid, and gaseous release submodels per repository sub-area.

A demonstration of the conditions under which the lumped parameter approach might be valid is presented as an IPA Phase 2 auxiliary analysis in Appendix L. For solubility limited releases of single, long-lived radionuclides, the ensemble average cumulative release per waste package is represented exactly by the arithmetic averages of the flow rate per waste package $<q>$, the waste package failure time $<t_{fail}>$, and the waste package failure volume $<V_0>$. The waste package failure time, however, is a calculated parameter that is based on temperature and a number of corrosion parameters which might not be represented correctly by their arithmetic means.

The ensemble mean parameters for the congruent release case should be $<1/q>$ (the harmonic mean), $<t_{fail}/q>$, and $<V_0/q>$, which are much more complicated parameters. Use of the arithmetic average values of q, waste package-failure parameters, and V_0 may not necessarily give good results for radionuclides that are not solubility limited.

Numerical experiments with the release rate models themselves confirm that cumulative release of the long-lived solubility limited radionuclides is proportional to flow, which demonstrates that the arithmetic mean flow rate is the correct ensemble average to use for these

radionuclides. Release of congruently released radionuclides is not proportional to the flow rate, but for these radionuclides, the flow rate is relatively unimportant. As expected, numerical experiments with *SOTEC* showed a relatively low sensitivity of radionuclide releases to flow rate q, for congruently released radionuclides. The effects of using the arithmetic mean of V_0 and the parameters for the failure model has not been determined for IPA Phase 2.

5.3.6 Geochemical Environment

The waste package material, the waste itself, and the heat generated by the waste will affect the geochemical environment in a complex way. The IPA Phase 2 source term models do not explicitly consider changes in the geochemical environment, except to the extent these effects have been taken into account in choosing the parameter ranges for the submodels. The effects of heat on the geochemical environment presented in the IPA Phase 2 auxiliary analysis in Appendix K were explored in regard to the transport of ^{14}C in the gas phase. This auxiliary analysis was used to justify a range of retardation coefficients.

5.4 Waste Package Failure Modes

5.4.1 Corrosion Models

SOTEC considers the failure of waste packages from initial defects, corrosion, mechanical processes, and disruptions. For any given metal and set of environmental conditions, the corrosion potential is a major factor influencing the types of active corrosion processes and their rates. The importance of the corrosion potential is reflected in the philosophy and implementation of the corrosion routines in *SOTEC*. *SOTEC* assumes that the corrosion potential is a function of temperature and radiation dose rate:

$$E_{corr} = E_1 + A(T - 298) + \beta e^{-\lambda t} \quad , \qquad \textbf{(5-2)}$$

where:

- A = empirical factor for temperature effect on corrosion potential (millivolts/degrees Kelvin—mV/°K);
- β = empirical factor for radiolysis effect on corrosion potential (mV);
- λ = average decay rate for gamma emitters in waste (year^{-1});
- E_1 = reference corrosion potential (mV);
- T = temperature (°K);
- t = time (years); and
- E_{corr} = corrosion potential (mV).

The equation for the corrosion potential assumes that the influence of radiolysis varies linearly with gamma dose rate, and that temperature affects the corrosion potential in a linear fashion. The impact of radiolysis appears as a maximum corrosion potential effect at time = 0, and declines with time, with radioactive decay of gamma emitters. The dependence of the corrosion potential on temperature and radiolysis is presumed to be obtained from independent theoretical analysis (e.g., Macdonald and Urquidi-Macdonald, 1990) or experimental data and translated into functional forms allowed in *SOTEC*.

Rates of pitting and crevice corrosion depend directly on the corrosion potential. When the potential is elevated above a critical value that is dependent on the type of metal, metal history, and solution composition, localized corrosion begins. The critical potential may be referred to as E_{pit}, E_{crev}, or E_{crit}, depending on the context and the type of corrosion involved. When the potential is lowered sufficiently, the localized corrosion pits generally repassivate. This is sometimes referred to as the repassivation potential or protection potential E_{prot}.

SOTEC currently allows only one critical potential for each of pitting and crevice corrosion and the critical potential is assumed to be a function of temperature, but not of solution composition.

5.4.1.1 General Corrosion

General corrosion is assumed to begin when repository temperatures drop below a specified (input) temperature. In the atmosphere, general corrosion is known to become significant when the relative humidity exceeds 80 percent. At the elevation of Yucca Mountain (approximately 1500 meters above sea level), this corresponds to a temperature of approximately 96°C, assuming conservatively that the air is 100 percent water vapor. Once corrosion begins, the corrosion rate is described by a generic power law equation (for more discussion, see Williford (1991)) of the form:

$$r = ae^{\frac{b}{cT}}\, t^d\, C_1^e\, C_2^f\,, \text{ when } T < T^o\,, \qquad \textbf{(5–3)}$$

where r is the corrosion rate, a, b, c, d, e, and f are empirical constants, T is absolute temperature, and t is time. Instead of concentrations C_1, C_2, etc., of aggressive species, the logarithm (to base 10) of the concentrations can be used. In some interpretations of this equation (e.g., Kubaschewski and Hopkins, 1962), b is the activation energy, and c is the gas law constant.

General corrosion is assumed to represent a passivated metal and as such is independent of the corrosion potential.

5.4.1.2 Crevice Corrosion

Crevice corrosion is affected by a number of coupled processes. These include mass transfer, production of metal ions within the crevice and hydrolysis. In the literature both the steady-state and transient models for crevice corrosion exist (see Watson and Postlethwaite (1990) as an example). However, for inclusion in *SOTEC*, such models are too complex and computationally time consuming. Therefore, a strategy to develop a simple parametric equation for crevice corrosion for use in *SOTEC* has been adopted.

Crevice corrosion has two characteristics: (1) critical potential for initiation and repassivation; and (2) propagation rate. Initiation time depends on the corrosion potential of the metal exceeding the critical potential for crevice-corrosion initiation.

The repassivation potential is taken to be a function of temperature:

$$E_{rc} = E_r + \zeta T\,, \qquad \textbf{(5–4)}$$

where:

E_{rc} = crevice repassivation potential (mV),
E_r = reference potential (mV); and
ζ = temperature-correction factor (mV/°K).

Subsequent to initiation, crevice corrosion is assumed to penetrate the waste package at a constant empirical rate r. The active corrosion rate can be estimated from an equation of the form:

$$r = \frac{i_a w}{\varrho z F}\,, \qquad \textbf{(5–5)}$$

where i_a is the active current density; w is the formula weight of the waste package material; ϱ is the material density; z is the ion valency; and F is the Faraday constant. *SOTEC* assumes a constant active corrosion rate.

5.4.1.3 Pitting Corrosion

Episodic evaporation and condensation of water on the surface of waste packages resulting in high concentration of aggressive ions makes them susceptible to pitting corrosion. Mechanistically, pitting corrosion is similar to crevice corrosion and it is possible to develop detailed models (Farmer *et al.*, 1991) for predicting critical pitting potentials or electrochemical conditions within the pit. Alternatively, heuristic stochastic models may also be developed (Henshall, 1992). For development of the *SOTEC* code, a strategy similar to that for crevice corrosion will be followed. Detailed models for pitting corrosion are still under development, and a constant propagation rate is assumed for pitting, in Version 1.0 of *SOTEC*.

Pitting corrosion is assumed to begin when the critical potential for pitting is reached. Pitting is assumed to begin immediately when the critical potential is exceeded. The critical potential is given by Equation (5–4). The rate of penetration by pitting is assumed to be identical to the rate in crevice corrosion, as described by Equation (5–5).

5.4.2 Temperature Model for Source Term

5.4.2.1 Introduction

Spent nuclear fuel will generate significant quantities of heat, leading to increases in the temperature of the waste package, fuel, and surrounding rock. The increase in temperature, in turn, will lead to changes important to the performance of the repository, such as chemical equilibrium and kinetics of the fuel and rock, mechanical changes to the host rock, waste package corrosion, and movements of gas and liquid. In the IPA Phase 2 analysis, temperature is taken into account explicitly in only three places; the gas velocity for the ^{14}C transport model; the onset of corrosion in

the source term model; and release of ^{14}C from the spent nuclear fuel under dry conditions.

The main purpose for program *CANT2* is to generate temperature for the surface of each waste package, to determine the time at which the temperature falls below the boiling point, assumed to be the onset of corrosion in the source term model. The temperature of the fuel inside the waste packages is calculated from the skin temperature for the ^{14}C source term model, by means of an empirical correlation (see Section 5.6.3.5.5).

5.4.2.2 Heat Transfer in Yucca Mountain

Heat transfer under both natural and repository modified conditions at Yucca Mountain will be complicated because of the unsaturated nature of the geologic media. Air circulates within Yucca Mountain under the influence of forces such as wind, barometric-pressure variations, and natural convection. Heat is transferred through conduction in the rock, and, to some extent, by the moving air, both as sensible and latent heat. Heat-transfer coefficients for conduction are sensitive to the degree of saturation of the rock, which can change both spatially and temporally. Close to the emplaced waste in the proposed repository, latent heat transfer and drying of the rock take on greater importance. Experiments (e.g., Ramirez and Wilder, 1991) and sophisticated mathematical models (e.g., Buscheck and Nitao, 1990) indicate deviations in temperature from model predictions based on conduction only, especially close to the emplaced waste. Furthermore, models of conductive heat transfer cannot predict the drying and re-wetting of the rock close to the waste packages. Models to predict two-phase heat and mass transfer are at the cutting edge of technology. In addition to the long computer run times associated with these models, there are a number of fundamental questions about how to treat two-phase flow through fractured porous media. Although it is possible to simulate two-phase flow at the scale of individual fractures, modeling of the waste package and larger scales must generally rely on the equivalent porous medium approach, to capture the effect of fractures in the matrix. Modeling of individual fractures is not feasible on the larger scale, because of both the large amount of computer resources that would be needed, and the lack of data on the location and characteristics of individual fractures.

5.4.2.3 Thermal Loading of the Repository

Under the design evaluated in IPA Phase 2, each waste panel would contain thousands of waste packages with different waste makeup (i.e., some will be vitrified defense wastes, most will be spent nuclear fuel, but of varying ages, from different types of reactors, and a range of burnups). Therefore, each waste package type will have a different heat output rate as a function of time.

5.4.2.4 NRC Temperature Model

The U.S. Nuclear Regulatory Commission temperature model is similar in some respects to the models of Altenhofen and Eslinger (1992) and also Johnson and Montan (1990). There are a number of significant enhancements that makes the present model more suited to our work in IPA Phase 2. It is very fast and efficient, so it could actually be incorporated into the system model if necessary (although it is not presently implemented this way).

As a first approximation of temperature of the waste packages within the repository, the report authors considered the following simplifying assumptions:

- Heat transfer is by thermal conduction only;
- The medium is homogeneous with constant thermal diffusivity;
- Waste packages are placed on a plane surface in a semi-infinite medium. The semi-infinite medium simulates a constant temperature at the surface of the earth, but extends infinitely in depth and laterally; and
- Heat output of each waste package as a function of time only.

The present model uses linear superposition of the temperature field for all waste packages in a panel, superimposed on the temperature field from all other panels represented as rectangular flat planes, as shown in Figure 5-3. Each waste package is represented as a solid rectangular parallelepiped with an instantaneous release of heat per unit volume. The heat source in each panel can vary from panel to panel. Convolution

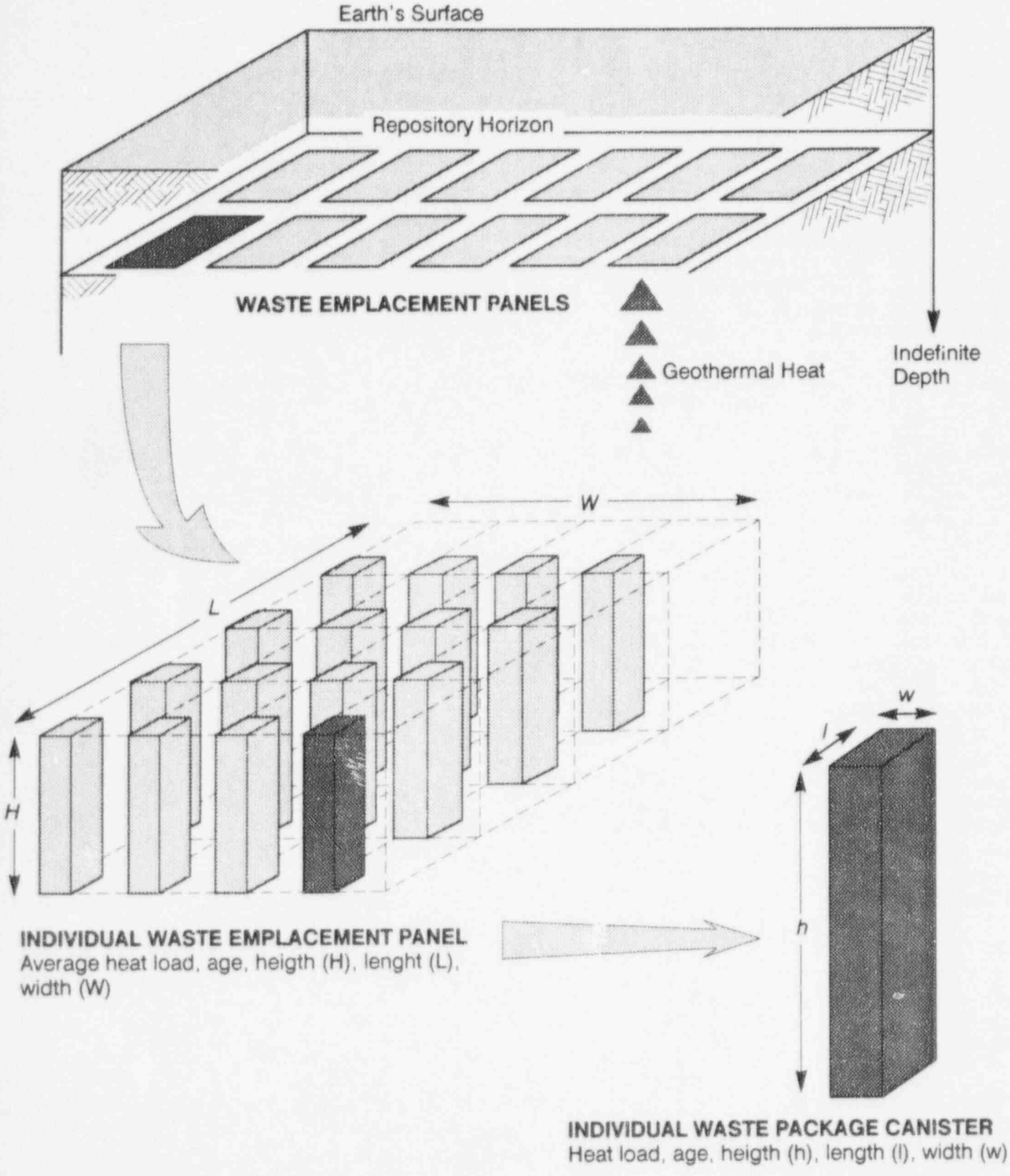

Figure 5–3 Representation of waste package canisters and waste emplacement panels in temperature model

of the instantaneous Green's functions for one waste package is performed numerically, to generalize the temperature to the time-varying heat source term.

Even with high efficiency, it would be very costly to evaluate all of the thousands of waste packages. Instead of calculating the temperature of all waste packages, the program samples a representative number in a Monte Carlo fashion from each panel. For the IPA Phase 2 study, there were a total of 66 waste packages sampled, approximately apportioned to the 17 waste panels according to the spent fuel load per panel. Since the geologic repository is divided into a small number of repository sub-areas (seven in IPA Phase 2), each repository sub-area consists of a whole number of waste panels. The present grouping of the waste packages and panels into individual repository sub-areas is shown in Figure 5–4.

The contribution to the temperature of a sampled waste package from the surrounding waste packages in the panel is simplified greatly by assuming that all waste packages are identical within a panel. The geothermal gradient is assumed to be a constant, so that the temperature of the rock (without the addition of repository heat) would be a function only of depth. In the model, the geothermal temperature addition is constant for each panel, based on the depth below the surface of the earth of the panel center. This temperature is then added to the temperature calculated for the individual waste package.

The temperature model considers only spent nuclear fuel waste. Heat loading, age of waste, and spacing of waste packages may vary between panels, but the model also assumes that all waste is buried instantaneously (i.e., there is no provision for temperature changes during the waste emplacement phase).

Green's Function Model for Individual Waste Package: The parallelepiped representing the waste package has a length equal to the actual cylindrical waste package, but its width and depth are adjusted so that the volume is equivalent to that of the cylindrical waste package. This parallelepiped shape allows the definition of a relatively simple analytical expression for temperature for an instantaneous heat release, whereas the expressions for a cylindrical waste package would be many times more complicated (Carslaw and Jaeger, 1959).

The temperature rise T' at any point x', y', z', and time t', in space relative to the center point of a single parallelepiped, can be calculated by the convolution of a Green's function, for an instantaneous release of heat and a function describing the rate of heat release:

$$T'(x',y',z',t') = \int_0^{t'} G_c(x',y',z',\tau')\, F_c(\tau - t')\, d\tau \ , \quad \textbf{(5–6)}$$

where x', y', z' is the position in the local coordinate system for each parallelepiped, t' is the time relative to the emplacement time for each parallelepiped, G_c is the temperature Green's function for an instantaneous unit release of heat, F_c is the heat-release rate as a function of time evaluated at time $(\tau - t')$, and τ is a dummy parameter of integration. T' is the temperature that would be produced by a single parallelepiped in complete isolation from all others.

For an instantaneous parallelepiped heat source of one Joule in an infinite medium, the Green's function G_c is defined:

$$G_c = \frac{1}{8\varrho C_p}\, G_x \cdot G_y \cdot G_z \ , \quad \textbf{(5–7)}$$

$$G_x = erf\left[\frac{\frac{L}{2} + x}{\sqrt{4kt'}}\right] + erf\left[\frac{\frac{L}{2} - x}{\sqrt{4kt'}}\right] \ ,$$

$$G_y = erf\left[\frac{\frac{W}{2} + y'}{\sqrt{4kt'}}\right] + erf\left[\frac{\frac{W}{2} - y'}{\sqrt{4kt'}}\right] \ ,$$

$$G_z = erf\left[\frac{\frac{H}{2} + z'}{\sqrt{4kt'}}\right] + erf\left[\frac{\frac{H}{2} - z'}{\sqrt{4kt'}}\right] \ .$$

where W, L, and H are the width, length, and height of the parallelepiped, respectively; ϱ = the

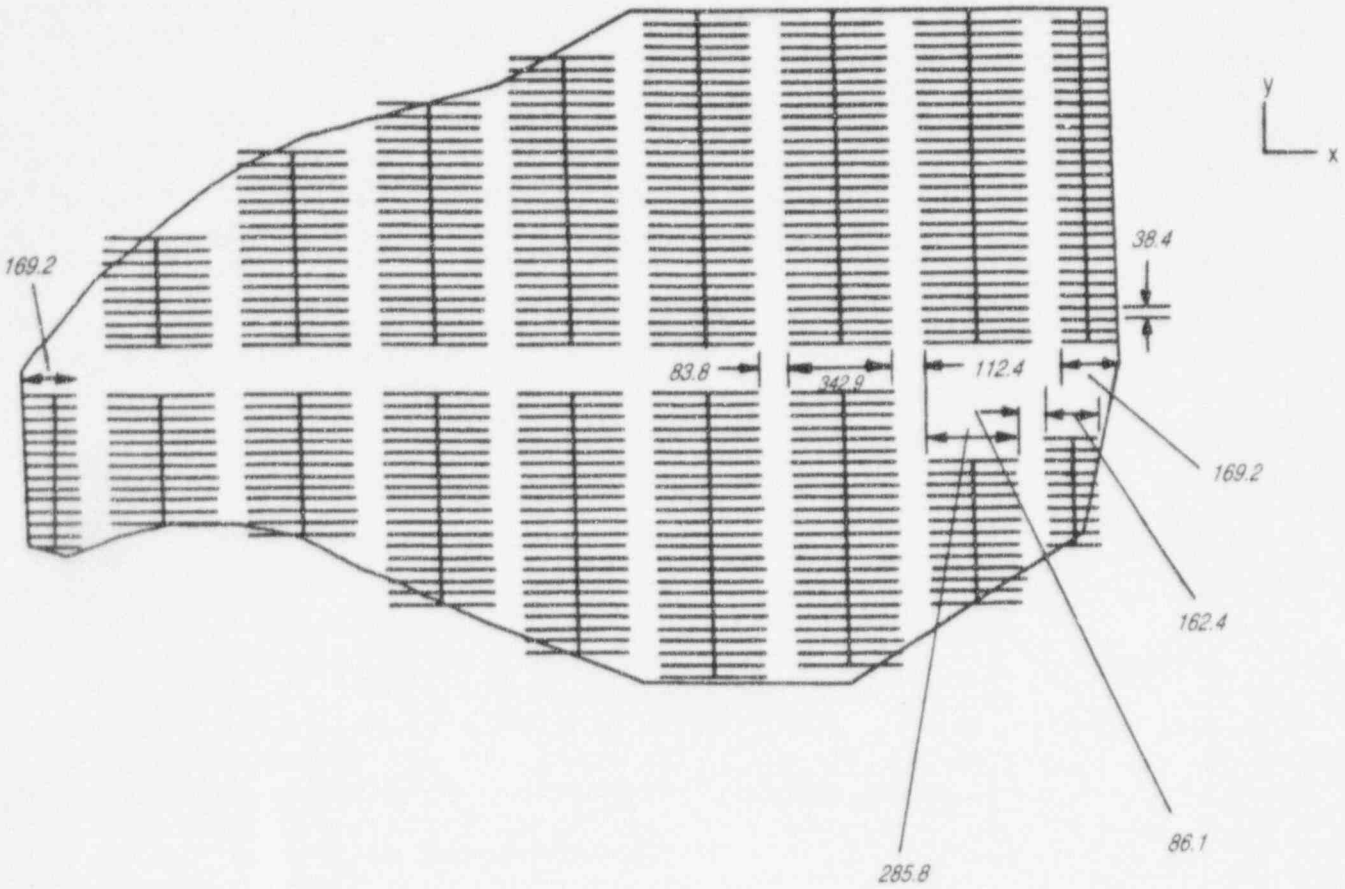

Figure 5–4 Grouping of waste package canisters and waste emplacement panels in temperature model (after Johnson and Montan, 1990)

bulk density of the rock; C_p = the heat capacity of the rock; k = thermal diffusivity of the rock; and *erf* is the error function. The temperature at any point x, y, z in space calculated from the contributions of all the other waste packages in the waste panel, would be:

$$T(x,y,z,t) = \sum_{i=1}^{N_{CL}} T_i'[x_i' - xy_i' - y, z_i' - z, t - t_i'] \quad ; \quad \textbf{(5–8)}$$

where N_{CL} = number of waste packages in panel L; x_i', y_i', z_i' is the location of the center of each parallelepiped; and t_i' is the starting time (i.e., time of emplacement) for each parallelepiped.

All waste packages are assumed to be identical within a waste panel, but may vary from panel to panel. Equation (5–7) is used to define a table of temperature versus time and distance from the waste package. Although Green's function for the parallelepiped is not axially symmetric, the isotherms in the x-y plane around the parallelepiped are approximately circular a short distance from the waste package. These tables are then used to efficiently sum the temperature contributions for a large number of waste packages, using Equation (5–8).

Contribution of Other Waste Panels: The waste package temperature contribution from the other waste panels is calculated in a similar manner to the single panel in a waste package field. The panels are represented as rectangular flat plates. The temperature at the earth's surface is held steady, and is parallel to the repository plane.

The Green's function for temperature at any point x, y, z relative to the panel center (x'', y'', z'') contributed by a panel with an instantaneous heat load of one Joule is:

$$G_p = \frac{1}{4\sqrt{\pi k \varrho C_p}} \, G_{px} \cdot G_{py} \cdot G_{pz} \quad , \qquad \textbf{(5–9)}$$

$$G_{px} = erf\left[\frac{\frac{L_p}{2} + x''}{\sqrt{4kt}}\right] + erf\left[\frac{\frac{L_p}{2} - x''}{\sqrt{4kt}}\right] ,$$

$$G_{py} = erf\left[\frac{\frac{W_p}{2} + y''}{\sqrt{4kt}}\right] + erf\left[\frac{\frac{W_p}{2} - y''}{\sqrt{4kt}}\right] , \text{ and}$$

$$G_{pz} = \exp\left[-\frac{(z'' - z^*)^2}{\sqrt{4kt^2}}\right] - \exp\left[-\frac{(z'' + z^*)^2}{\sqrt{4kt^2}}\right] .$$

W_p and L_p are the width and length of the panel, respectively; ϱ = the bulk density of the rock; C_p = the heat capacity of the rock; k = thermal diffusivity of the rock; and z^* = depth of the repository below the surface of the earth.

The temperature caused by the panel for a general heat release rate can be calculated with the convolution integral:

$$T_p(x'', y'', z'', t'') = \int_0^{t''} G_p(x'', y'', z'', \tau'') \, F_p(\tau - t'') \, d\tau \quad , \qquad \textbf{(5–10)}$$

where t'' is the time relative to the emplacement time for each panel, and F_p is the heat-release rate as a function of time evaluated at time $(\tau - t'')$, and τ is a dummy variable of integration. The temperature T_p is the temperature that would be produced by a single panel in complete isolation from all others.

The temperature at any point (x, y, z) calculated from the contributions of the individual panels would therefore be:

$$T_p(x,y,z,t) =$$

$$\sum_{i=1}^{N_L} T_{pi}[x_{pi} - x,\ y_{pi} - y,\ z_{pi} - z,\ t - t_{pi}] \quad , \qquad (5\text{-}11)$$

where N_L = number of panels; x_{pi}, y_{pi}, z_{pi} is the location of the center of each panel; and t_{pi} is the starting time (i.e., time of emplacement) for each panel. The temperature at the sampled waste package locations is the sum of the contributions of the panel temperatures, the other waste packages, and the geothermal gradient.

5.4.2.5 Use of the Temperature Model

For the source term model, the staff is mainly interested in the waste package surface temperature, because that will determine the minimum time at which the waste package can be wetted by liquid water. The boiling point of water at the Yucca Mountain site is about 96°C, but this might vary slightly because of the tilt of the repository causing an elevation difference from one end to the other. Mineral concentrations in the repository water (especially if concentrated in minerals through evaporation) might also alter the boiling point. This "wetting time" is taken to be the time for the onset of corrosion leading to waste package failure and radionuclide release. The coolest point on the waste package's surface will be at its top, so this temperature is used to determine the minimum time for waste package wetting. Waste packages near the center of the repository stay above the wetting temperature for a longer period than those located at the edge of the repository. The temperature generated by this model is also used for ^{14}C source term modeling. The gas flow model used for the ^{14}C analysis (see Section 4.3) also is temperature-dependent, but uses a numerical solution different than the present model.

A total of 66 randomly selected waste packages were used to determine the temperature for the IPA Phase 2 source term model. The number of waste packages was apportioned between the 17 waste panels approximately proportional to the waste loading per panel. The panels were, in turn, arranged into seven repository sub-areas, as shown in Figure 5-4. Temperature for the onset of corrosion was taken as the arithmetic average of all waste packages within a repository sub-area.

5.4.2.6 Extent of Possible Errors in NRC Temperature Model

Some of these possible errors in the approach are discussed below:

- Heat transfer by conduction-only neglects heat transfer by two-phase flow of gas and liquid (i.e., the heat pipe). Neglecting these effects would underestimate heat transfer, possibly leading to predictions of higher temperature, which, in the present case, would be non-conservative because it could lead to later re-saturation and waste package failure from corrosion;

- Thermal properties of the host rock will be a function of water content, which will vary with time, irrespective of fluid movement. Also, the site consists of multiple layers of materials with differing heat-transfer properties;

- The conduction model does not account for heat transfer by convection or radiation across the air gap between the waste package and the host rock; and

- Averaging the waste package temperatures in a repository sub-area would likely overestimate the cooling time for those waste packages on the edge of the repository sub-area farthest from the center of the repository.

5.5 Structural Failure Models

5.5.1 Introduction

The structural failure considered for IPA Phase 2 is buckling failure of the corroded waste package. External dynamic loads from IPA Phase 2 scenarios may be superimposed onto emplaced waste packages, to predict buckling failure. The analytical expressions (Bazant and Cedolin, 1991; and Roark and Young, 1975) used uniform waste package temperature and uniform waste package thickness.

Consistent with structural engineering analysis practice, the waste package is assumed to be a long slender cylinder subject to both axial and radial symmetric loads. The cylinder is uncon-

strained in the radial direction. The stiffening effect contributed by the waste form inside the cylinder and the end plates is conservatively neglected. The material properties are assumed to be functions of temperature. Only static or quasi-static loads are considered.

In a typical buckling analysis, three types of bucklings are analyzed: elastic buckling, elastic-plastic buckling, and plastic buckling. For the IPA Phase 2 buckling analysis, only elastic buckling is considered, because this form of buckling occurs before elastic-plastic and plastic buckling, and it is conservatively assumed that after elastic buckling, corrosion of the buckled waste package would no longer contain the radionuclides inside the waste package. A safety factor (load factor) of 3 is normally used to account for the uncertainty and inconsistency experienced in the use of the elastic buckling formula.

5.5.2 Buckling Evaluation

For a *uniform radial external load* and for a safety factor of 3, assuming a uniform radial external load P_E, elastic buckling occurs when:

$$\frac{P_E}{3} \geq P_{cr} \geq \frac{E}{4(1-\nu^2)}\left[\frac{t}{R_o}\right]^3 , \qquad \textbf{(5-12)}$$

where:

P_E = external load (Megapascal—MPa);
P_{cr} = buckling load (MPa);
E = elastic modulus (MPa = $182{,}000 \times [1 - 6 \times 10^{-4} \times (T - 20)]$);
t = wall thickness;
T = current temperature (degrees Celsius—°C);
R_o = radius of cylinder; and
ν = Poisson's ratio ($0.25 \times [1 + 4 \times 10^{-4} \times (T - 20)]$).

The critical thickness t_c can be:

$$t_c = \frac{0.32(a)}{1-(a)} , \qquad \textbf{(5-13)}$$

where:

$$a = \frac{4P_E\,(1-\nu^2)^{\frac{1}{3}}}{3E} . \qquad \textbf{(5-14)}$$

For a *uniform axial external load* in the elastic range, with a safety factor of 3, buckling occurs when:

$$\frac{P_E}{3} \geq P_{cr} \geq \frac{1}{\sqrt{3}}\,\frac{E}{\sqrt{1-\nu^2}}\,\frac{t}{R} . \qquad \textbf{(5-15)}$$

The critical thickness is:

$$t_c = \frac{0.32(a)}{1-(a)} , \qquad \textbf{(5-16)}$$

where:

$$a = \frac{P_E\sqrt{(1-\nu^2)}}{\sqrt{3}E} . \qquad \textbf{(5-17)}$$

For a *uniform axial and radial external load*, buckling failure occurs when:

$$\frac{P_E}{3} \geq P_{cr} \geq \frac{0.92\,E}{\left[\frac{L}{R}\right]\left[\frac{R}{t}\right]^{2.5}} , \qquad \textbf{(5-18)}$$

where L = length of the cylinder.

Failure because of buckling is assumed to occur when the calculated critical thickness t_c is greater than the current (corroded) thickness or, equivalently, when the external load exceeds the critical buckling load.

5.6 Waste Dissolution and Radionuclide Releases

5.6.1 Introduction

Figure 5–5 shows a failed waste package, as represented in *SOTEC*. Water is assumed to enter the waste package and exit again, carrying dissolved radionuclides only (colloids are treated as a subcase of dissolved radionuclides and will be discussed further in Section 5.6.2.5). The model also accounts for radionuclides transported away

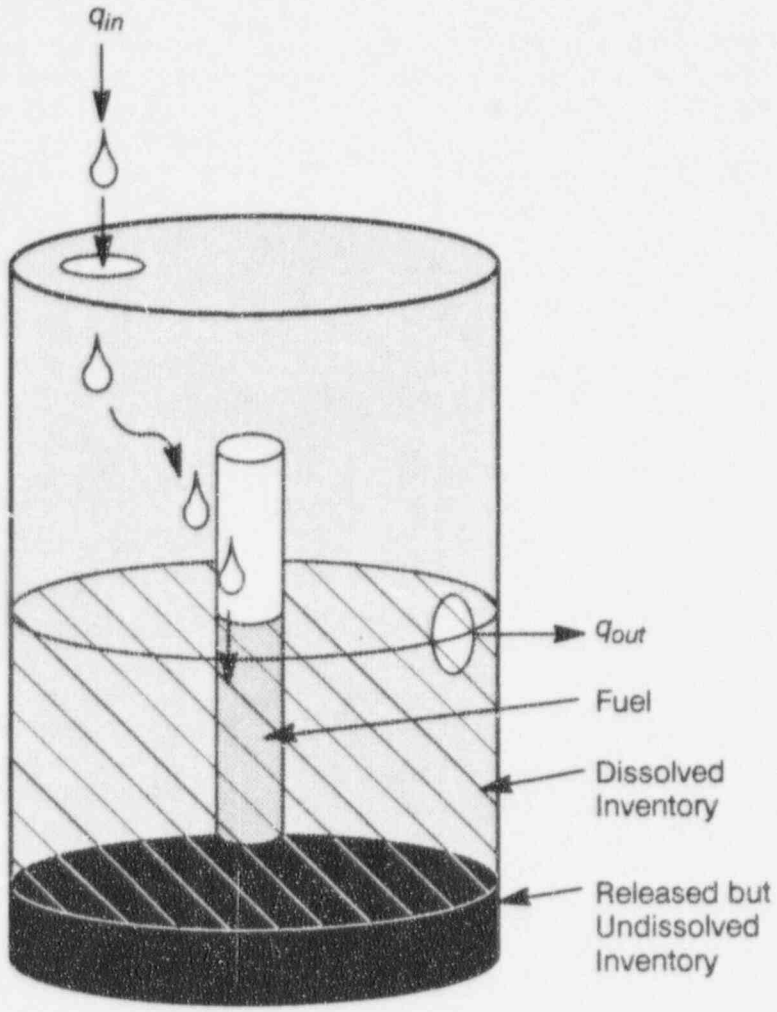

Figure 5-5 Dissolved radionuclide-release model

from the waste package by molecular diffusion through the adjacent rock.

Radionuclides are released from the spent nuclear fuel waste form at a rate determined by the alteration rate of the uranium dioxide fuel, as well as from crud, gap, grain boundary, and cladding. These compartments are shown in Figure 5-6 (see Apted, 1990).

Radionuclides can leave the waste package at a rate no greater than that allowed by the solubility of the element in the water. *SOTEC* allows for radioactive decay of each radionuclide and production from previous elements in the chain. The inventory of the unaltered uranium dioxide is calculated analytically by the Bateman equations (Bateman, 1910). The inventory of released radionuclides inside the waste package is calculated by numerical integration.

Molecular diffusion is accounted for in *SOTEC* by assuming a spherical source with no advection, and then adding the diffusive component to the advective component of transport out of the waste package. In the diffusion model, the inner surface of the sphere is held at the concentration of radionuclides in water inside the waste package. The concentration a fixed distance away from the waste form is held at zero. The diffusion model accounts for molecular diffusion, retardation, and radioactive decay, but does not allow for production from a parent radionuclide.

On waste package failure, water is assumed to begin entering the waste package at a rate q_{in}. There is no outflow until a critical value V_{max} in the waste package is exceeded, at which point the outflow is:

$$q_{out} = q_{in}\, k_q \left(\frac{V}{V_{max}} \right)^2 , \qquad \textbf{(5-19)}$$

where k_q is an arbitrary "weir" coefficient chosen so that the numerical integration of volume occurs smoothly and converges to steady state quickly once the maximum volume is reached; V is the volume of water; and V_{max} is the volume of water at which overflow occurs. For the present model, $k_q = 0.8$.

5.6.2 Waste Dissolution

5.6.2.1 Effective Waste Package Failure Time

No dissolved radionuclides can leave the waste package until it is perforated and water can enter and leave. The waste package fails from damage or corrosion at time t_{fail}. The temperature drops below the boiling point at time t_{cool}. The model assumes that no water can enter or leave the waste package until $t > t_{cool}$ and $t > t_{fail}$. The effective time at which fuel degradation can begin, t_{ftc}, is given by:

$$t_{ftc} = MAX\,(t_{cool},\ t_{fail}) , \qquad \textbf{(5-20)}$$

No dissolved radionuclides can leave the waste package until it is perforated and water can enter and leave.

Upon failure, water flowing into the waste package is assumed to come into intimate contact with the fuel. Radionuclides are released either instantaneously or congruently, with the alteration of the UO_2 fuel. On contact with water, those radionuclides being released congruently are released at a rate tied to the alteration rate of the UO_2 and the inventory of remaining radionuclides in the fuel. The leaching time t_{leach} is defined as:

$$t_{leach} = \frac{1}{(ff \times alt)} , \qquad \textbf{(5-21)}$$

Where *alt* is the fixed alteration rate of the wetted fuel, and *ff* is the fraction of fuel that is wetted at any time, *SOTEC* assumes that all fuel in the waste package will eventually be contacted and consumed, even though only part of it is wetted at any given time.

No alteration of the spent nuclear fuel occurs until t_{ftc}, and release from the spent nuclear fuel continues for t_{leach} years beyond t_{ftc}. The release stop time t_{lt} is defined as:

$$t_{lt} = t_{leach} + t_{ftc} . \qquad \textbf{(5-22)}$$

Subsequent to alteration of all the spent nuclear fuel, at time = t_{lt}, additional release from the waste package may continue from the released, but undissolved inventory (discussed in 5.6.2.2).

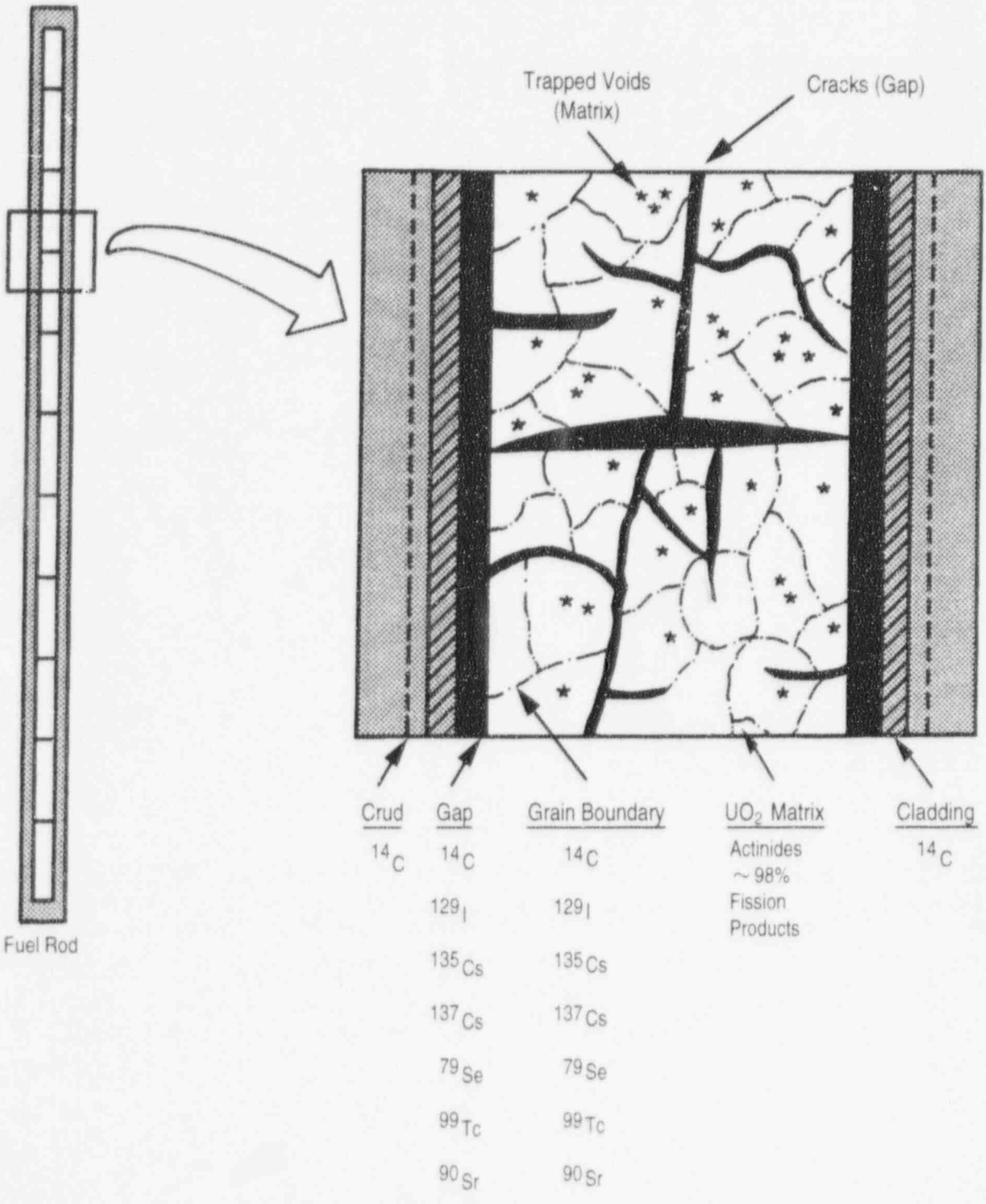

Figure 5-6 Locations of radionuclides in spent nuclear fuel

The model does not consider that oxidation of the fuel in the dry state affects liquid release. Ranges of solubilities used in the source term module are presented in Appendix A.

5.6.2.2 Solubility Limited Release

As the fuel is altered, it releases its radionuclide inventory at the alteration rate into the released but undissolved (RBU) inventory. This assumption is generally called the "congruent-release" mode, and assumes that the radionuclides are contained in the matrix of the UO_2. Radionuclides not contained in the matrix, but collected at the grain boundaries and in the cladding gap, are assumed to be part of the RBU inventory at the moment of failure.

Release of radionuclides from the waste package is possible only in the dissolved state. The inventory of all isotopes of an element are collected, and the model determines if the hypothetical concentration of that element is greater than or less than the solubility limit. If the hypothetical concentration exceeds the solubility, then the actual concentration of the waste package water is held at the solubility limit. Otherwise, the concentration of the waste package water is the RBU inventory divided by the volume of water V in the waste package. There is an assumed minimum volume of water of 1 liter in the waste package, to avoid division by zero. The concentration of the element in the waste package water is reapportioned to the isotopes, when determining the release rates.

The mass of each radionuclide remaining in the waste package water and RBU inventory is calculated by a material balance describing the inputs of:

- Radionuclide released from the fuel;
- Production from radioactive decay of another radionuclide;
- Losses from radioactive decay;
- Advective flow; and
- Diffusion.

5.6.2.3 Advective Mass Transfer

Advective mass transfer from the waste package occurs at the rate at which water leaves; that is,

$$W_{out,i} = C_i q_{out} ,$$

where C_i is the aqueous concentration of radionuclide i. The radionuclide concentration also is the boundary condition for the diffusive mass transfer from the waste package.

5.6.2.4 Diffusive Mass Transfer

The model assumes that mass can be transferred by molecular diffusion, irrespective of convective mass transfer from flowing water into and out of the waste package. Diffusive mass transfer is from an assumed spherical source into a domain unaffected by other waste packages and the flow rate of liquid water through the waste package and the surrounding rock. The boundary conditions are the concentration of water inside the waste package at the inner spherical boundary and zero concentration at the outer radius of the spherical boundary. The differential equation solved is:

$$K \frac{\partial C}{\partial t} = D \frac{1}{r^2} \frac{\partial}{\partial r} \left(r^2 \frac{\partial C}{\partial t} \right) - \lambda KC , \qquad (5\text{–}23)$$

where K is the retardation coefficient, C is the concentration, t is time, D is the coefficient of molecular diffusion, r is radius, and λ is the decay coefficient. The present formulation considers only decay of the radionuclide in question, and does not consider generation of the radionuclide from chain decay of other radionuclides.

The radius of the source sphere for diffusional mass transfer was chosen so that the surface area was equal to that of the cylindrical waste package. The spherical geometry with no advection allows a relatively simple solution either numerically or analytically, since it is one-dimensional. The present formulation for molecular diffusion is an approximation, since the waste package is not a sphere, and advective mass transfer is not considered in its solution. The staff believes that the formulation is conservative for the following reasons:

- The concentration of the inner boundary is held constant at the concentration inside the

waste package, neglecting the substantial barrier of the waste package, itself;

- Neglecting the production of the radionuclide from chain decay of other radionuclides causes the concentration gradient to be steeper than it would be if production from other chains were allowed (for those radionuclides in chains); and

- Setting the concentration at the outer boundary at zero causes the gradient to be steeper than if the effect of buildup from other waste packages were considered.

The numerical solution to Equation (5-23) is obtained in a finite difference grid with varying grid spacing. Diffusion coefficient and effective porosity may vary in each finite difference cell. Each solution requires the solution of N linear algebraic equations, where N is the number of increments in the finite difference grid. The equations are tri-diagonal, and several of the terms do not vary with time. The solution of the equations with the Thomas algorithm is quick and efficient (Lapidus, 1962).

The rate of change of mass m_i of each radionuclide in the waste package is determined by the following equation:

$$\frac{\partial m_i}{\partial t} = m_{i-1}\,\lambda_{i-1} - m_i\,\lambda_i - c_i\,q_{out} + w_i - w_{di} \quad . \qquad \textbf{(5-24)}$$

The rate of release of radionuclide i from the fuel is defined:

$$w_i = m_i \times ff \times alt \quad . \qquad \textbf{(5-25)}$$

The flux of radionuclide i leaving the waste package by molecular diffusion is calculated from the concentration gradient:

$$w_{d_i}(t) = 4\pi r^2 \epsilon D \frac{(C_{0_i} - C_{1_i})}{\Delta R_1} \quad , \qquad \textbf{(5-26)}$$

where C_{0_i} is the waste package concentration, C_{1_i} is the concentration at the first grid point, and ΔR_1 is the grid spacing between the innermost two points. The diffusive flux $w_{d_i}(t)$ is subtracted from the inventory, when evaluating Equation (5-24) by numerical integration.

The parameters of water influx q_{in}, alteration rate *alt*, wetted fraction *ff*, diffusion coefficients, and maximum volume of water in the waste package V_{max} effectively allow the selection of several modes of potential release; e.g., a small V_{max} ensures the so-called "wet drip" case (Pigford *et al.*, 1992), whereas a large V_{max} leads to the "bathtub" case. Very low flow would correspond to the "moist continuous" case where the only mechanism for liquid release would be diffusion.

5.6.2.5 Treatment of Colloids

Colloidal radionuclides are potentially important at the Yucca Mountain site. Radionuclides such as plutonium have large inventories and are long-lived, but have generally low solubilities. Under conditions of a high alteration rate of the fuel matrix, there is evidence that they might form colloids when released from spent nuclear fuel (Wilson, 1990). *SOTEC* does not explicitly handle the release of colloids from spent nuclear fuel. A mechanistic treatment of the phenomena leading to growth of colloids from supersaturated liquids may be incorporated into the next update of *SOTEC*. In IPA Phase 2, colloids are considered to be part of the dissolved inventory, and are treated in the calculations by adjusting the solubility upwards.

5.6.3 Calculations of Gaseous Releases of ^{14}C

5.6.3.1 Introduction

Carbon-14 is a potentially important radionuclide at the partially saturated Yucca Mountain site because, in the gaseous form, it could migrate quickly to the atmosphere. Its abundance in spent nuclear fuel—roughly 10 times the present limit for cumulative releases of radioactive material—and its long half-life of 5720 years, contribute to the importance of the potential issue.

Carbon-14 is generated in nuclear fuel by the neutron activation of ^{14}N, ^{13}C, and ^{17}O contained in the fuel and other materials in the reactor core (Van Konynenburg *et al.*, 1984). The main reservoirs for ^{14}C are the cladding, the cladding/fuel gap and grain boundaries, and the fuel itself. There will be little ^{14}C in vitrified defense waste stored at the site.

Park (1992) estimates the inventories of ^{14}C in both spent nuclear fuels from boiling water reactors (BWRs) and pressurized water reactors (PWRs), as shown in Table 5–2. Currently, Park also estimates that there will be 70,000 MTHM of spent nuclear fuel in the repository, consisting of 22,500 MTHM of BWR fuel and 40,500 MTHM of PWR fuel. The inventory of ^{14}C is estimated to be 78,000 curies.

Van Konynenburg (1991) reports that the chemical forms of the ^{14}C inventories are uncertain, but that they are believed to exist partially as elemental carbon, carbides, and oxycarbides in the fuel, and as dissolved carbon and carbides in the metal. The form in the cladding oxide is unknown, but is at least partially in the reduced state.

Most of the ^{14}C in the fuel, cladding and hardware must first oxidize in order to be released in the gas pathway. Although elemental carbon is generally stable at low temperatures, thermodynamics in air favors the formation of gaseous compounds such as CO_2 and methane. Furthermore, carbon does not form protective oxide layers like corrosion-resistant metals. Van Konynenburg *et al.* (1987) noted that $^{14}CO_2$ was released from cladding in an oxidizing environment with a radiation level of 10,000 rad/hour and a temperature of 275°C. Kopp and Munzel (1990) showed $^{14}CO_2$ releases from ^{14}C-doped zirconium sheets at temperatures as low as 200°C, with virtually no radiation, and in an atmosphere of mostly argon with air and water impurities. In very pure argon, however, there was no measurable release of ^{14}C. The dependence of release on the O_2 content of the gas indicates that carbon was undergoing oxidation in the impure argon. Although kinetic considerations might restrict the formation of gaseous compounds of the ^{14}C in the fuel, the model conservatively assumes that any ^{14}C available to become oxidized is converted to $^{14}CO_2$.

The ^{14}C gas release component of *SOTEC* considers that $^{14}CO_2$ is released from the fuel, cladding, and hardware compartments on failure of the waste package. Several of the release mechanisms depend on the presence of oxygen. Although there may be small quantities of oxygen initially present in the waste package as impurity in the inert gas or as water, most of the oxidation would not occur before waste package failure.

The ^{14}C release model makes the following conservative or simplifying assumptions:

- There can be no release of gas before waste package failure;
- Cladding does not protect the spent nuclear fuel from oxidation;
- Once the waste package fails, it provides no resistance to the inflow of air or the outflow of CO_2;
- On waste package failure, a "prompt release fraction" of approximately 2.5 percent (Van Konynenburg *et al.*, 1991) of the total inventory is released from the waste package instantaneously;
- On waste package failure, cladding and structural metals undergo oxidation, and release ^{14}C at the rate that the metal oxidizes; and
- On waste package failure, oxygen diffuses into the spent nuclear fuel and oxidizes the ^{14}C to $^{14}CO_2$, which then diffuses out to the waste package.

The bases for the assumed release mechanisms are discussed in the following paragraphs.

5.6.3.2 Prompt Release Fraction

On failure of the waste package and cladding (no credit taken for the cladding integrity), a portion of the total ^{14}C inventory estimated at about 2.5 percent (Van Konynenburg *et al.*, 1991) would be released quickly (i.e., within a few hundred years). This inventory represents the ^{14}C held loosely on the cladding and in the cladding/fuel gap and grain boundaries. Experiments on ruptured spent nuclear fuel indicate that on cladding failure, 0.5 percent of the inventory is released from the fuel/cladding gap (Wilson, 1990). The initial layer of oxide and crud on the cladding is the other readily available inventory of loosely held ^{14}C. This layer holds a relatively elevated level of ^{14}C, some produced by activation *in-situ* but, some probably picked up from the circulating water within the reactor. The chemical form of this ^{14}C is uncertain, but experiments in which cladding was heated indicate that the release rate of $^{14}CO_2$ appears to be controlled by a diffusion process from a layer of finite thickness.

Table 5-2 Adjusted ^{14}C Content in Spent Nuclear Fuel (in Ci/MTHM) (after Park, 1992)

Type	*Burnup (MWd/MTHM)*	*UO_2*	*Zircaloy*	*Hardware*	*TOTAL*
BWR	35,000	0.69	0.48	0.13	1.3
PWR	40,000	0.73	0.22	0.26	1.21
Average	----	0.72	0.31	0.21	1.24

Smith and Baldwin (1989) showed that as much as 2 percent of the spent nuclear fuel ^{14}C inventory was released in zircaloy cladding heated to 350°C for 8 hours. The release rate is an Arrhenius relationship consistent with diffusion out of a layer of finite thickness, with an activation energy of between 19 and 25 kilocalories/mole. However, the rate of release depended on the presence of air. In argon with a trace of air (50 parts-per-million oxygen), release rates were lower by a factor of about 10, indicating that the carbon was in a reduced state and had to be oxidized before being released.

If it is considered that the release of ^{14}C from the cladding oxide layer is governed by the diffusion mechanism, it is possible to estimate the upper bound of release rate for the temperature range of interest, approximately 350° to 100°C. One-dimensional molecular diffusion through the film of thickness $2L$ can be expressed by the partial differential equation:

$$\frac{\partial C}{\partial t} = D \frac{\partial^2 C}{\partial x^2} , \qquad \textbf{(5-27)}$$

where D is the diffusion coefficient, C is the concentration of $^{14}CO_2$, and x is the distance measured from the edge of the cladding toward the center. The boundary conditions that apply to Equation (5-27) are:

$$C = C_0 \text{ at } x = 0 ,$$

$$\frac{\partial C}{\partial x} = 0 \text{ at } x = L \text{ (center of film)} .$$

Equation (5-27) has the following solution (Carslaw and Jaeger, 1959):

$$\frac{C}{C_0} = 1 - \frac{4}{\pi} \sum_{n=0}^{\infty} \frac{-1^n}{2n+1} e^{\frac{(2n+1)^2 \pi^2 \tau}{4}} \cos\left(\frac{(2n+1)\pi\zeta}{2}\right) , \qquad \textbf{(5-28)}$$

where $\tau = Dt/L^2$, $\zeta = x/L$, and L is one-half the cladding thickness.

For $Dt/L^2 = 1.5$, C/C_0 is close to unity, meaning nearly all $^{14}CO_2$ would have diffused out of the system. Relying on experimental data of Smith and Baldwin (1989), which indicate virtually complete release of ^{14}C from the oxide layer in 8 hours at 350°C, the fraction removed from the sample at other temperatures is related to the parameter Dt/L^2. Time to reach an equivalent concentration profile is inversely proportional to the diffusion coefficient; that is:

$$\frac{D_1 t_1}{L_1^2} = \frac{D_2 t_2}{L_2^2} , \qquad \textbf{(5-29)}$$

or for constant film thickness,

$$t_2 = t_1 \frac{D_1}{D_2} . \qquad \textbf{(5-30)}$$

The ratio D_1/D_2 can be related by the Arrhenius equation to be:

$$\frac{D_1}{D_2} = e^{-\frac{E}{R}\left(\frac{1}{T_2} - \frac{1}{T_1}\right)} \qquad \textbf{(5-31)}$$

The time for an equivalent release at lower temperatures is illustrated in Table 5-3, assuming $t_1 = 8$ hours, at 350°C, for $E = 19$ and 25 kilocalories/mole. R is the gas law constant, and the subscripts refer to the two different temperatures.

Table 5-3 Diffusion of $^{14}CO_2$ from Surface Oxide

Temperature (°C)	*t_2 (years) E = 19 (Kcal/mole)*	*t_2 (years) E = 25 (Kcal/mole)*
350	0.00091	0.00091
300	0.0035	0.0053
250	0.017	0.043
200	0.12	0.55
150	1.3	13
100	27	690
75	169	7800

Equation (5-30) was used to estimate t_2, for a range of activation energies and temperature.

Results presented in Table 5-3 indicate that for temperatures as low as 75°C, release of the ^{14}C by diffusion out of the oxide film would be nearly complete within 10,000 years, and possibly much less time. Furthermore, there may be sufficient oxygen present in an unfailed waste package as an impurity, or from the radiolysis of water to allow partial escape of $^{14}CO_2$ from the cladding into the waste package before failure. On the other hand, there are few direct data on $^{14}CO_2$ releases from zirconium at low temperature.

The observation that release from the cladding depended on the presence of oxygen indicates that the ^{14}C may be in a reduced state in the oxide film. The oxidation to $^{14}CO_2$ might depend on the combined effects of temperature, oxidizing environment, and ionizing radiation. Considering the uncertainties, the staff must assume a conservative model for release of ^{14}C from the oxide layer. In the present model, the entire quantity of ^{14}C in each waste package contained in the "prompt-release fraction"—2.5 percent of the spent nuclear fuel inventory—is assumed to be released to the geosphere at the time of waste package failure.

5.6.3.3 Cladding Integrity

Protection of the spent nuclear fuel by the cladding has been ignored in the IPA Phase 2 source term models for liquid and gaseous release. The staff believes this to be a conservative assumption, but it is difficult to prove, to the contrary,that the cladding would survive for long periods of time. Factors in favor of cladding integrity are:

- Cladding is usually a highly corrosion-resistant zirconium alloy (but some of the older fuel was clad in stainless steel); and
- Most fuel rods emplaced in the waste packages will be intact, but some will have a small number of undetected pinholes or cracks in the cladding, generally considered to be lower than 1 percent.

Factors in favor of loss of cladding integrity are:

- Under circumstances of sufficiently high temperature in an oxidizing environment to cause oxidation of the fuel to lower-density U_3O_8, fuel rods with cladding defects are known to split further. At temperatures above 250°C, fuel oxidation was high enough to cause propagation of defects, but below 250°C, the defects were not observed to propagate (Einziger and Kohli, 1984). Those defected rods that do split allow oxygen to further oxidize fuel, causing the defect to spread down the length of the fuel rod. The waste package must first fail, to allow oxidation of the fuel and further splitting of the fuel rods;
- While cladding is highly corrosion-resistant, there are factors, such as hydride reorientation, that could lead to failure;
- Cladding could fail by mechanical breakage caused by handling errors, waste package buckling, or earthquakes; and
- The fuel rods will be pressurized up to 50 atmospheres, so the cladding will be under stress.

5.6.3.4 Release of ^{14}C from Oxidation of Cladding

The cladding oxidation layer is about 10 microns thick, initially. The cladding metal itself is on the

order of 0.5 to 1.0 millimeter thick, and contains the bulk of the ^{14}C in the cladding. The zirconium alloy generally used for cladding is highly corrosion-resistant, but in an oxidizing environment with elevated temperatures, could oxidize. Upon oxidation, the ^{14}C contained in the metal as elemental carbon, carbides, and oxycarbides could be released as $^{14}CO_2$.

Studies of zircaloy degradation in air have been performed in connection with dry-cask storage (Einziger and Kohli, 1984). The gain in weight of Zircaloy samples, attributed to oxidation, has been determined to proceed in two modes. The first mode, known as the "pre-transition" phase, shows weight gain proportional to the cube root of time until the oxide thickness reaches a critical value. The "post-transition" phase shows a linear weight gain, for oxide-layer thickness, greater than the critical value. It is most likely that the cladding reaches post-transition within the reactor core.

Post-transition cladding oxidation appears to follow an Arrhenius relationship (Garzarolli *et al.* 1980), that is:

$$\frac{\Delta w}{\Delta t} = AE^{-\frac{E}{RT}} \qquad \textbf{(5-32)}$$

where A is the coefficient, milligrams/square decimeter; E = activation energy, calories/mole; R = gas constant, 1.987 calories/mole/°K; and T = absolute temperature, Garzarolli *et al.* presents several empirical formulas for the post-transitional weight gain because of oxidation. Values of $A = 1.87 \times 10^7$ milligrams/square decimeter, and $E = 22{,}200$ calories/mole, were chosen from the formulas presented by Garzarolli *et al.* because they represented the most pessimistic model. The release model for cladding oxidation makes the following additional assumptions:

- $^{14}CO_2$ is released from the zircaloy at the rate that the metal oxidizes. Zirconium is a strong oxygen getter, so oxygen concentrations available to oxidize carbon would be limited until the zirconium oxidizes; and
- Other irradiated structural metal buried with the waste (other than the waste package itself) is conservatively included with the zircaloy cladding as a source of ^{14}C.

5.6.3.5 Release from UO_2

The largest inventory of ^{14}C is contained in the spent nuclear fuel tied up as solid solutions, elemental carbon, carbides, and oxycarbides. Investigations of the oxidation of grains of spent nuclear fuel indicate that the rate of oxidation is controlled by diffusion through at least two barriers; the grain boundaries, and the film of oxidized fuel surrounding each grain (Einziger and Buchanan, 1988). Irradiated spent nuclear fuel contains numerous cracks which allow gas to easily permeate the mass. The smallest scale of interest is the individual grains, that are on the order of 10 to 20 microns in diameter.

The model for release of ^{14}C from spent nuclear fuel makes the following assumptions:

- UO_2 oxidizes at a rate controlled by the diffusion of oxygen through the grain boundaries and film of higher oxide;
- The oxygen concentration at the oxide/fuel boundary will be zero because all oxygen is being consumed by fuel oxidation;
- ^{14}C can oxidize only after the fuel oxidizes;
- $^{14}CO_2$ will be released from the spent nuclear fuel at the rate that the spent fuel oxidizes;
- $^{14}CO_2$ must diffuse outward through the oxide film and grain boundaries; and
- Concentration profiles for both oxygen and $^{14}CO_2$ are at steady state, although the position of the boundary changes with time.

5.6.3.5.1 Fuel Oxidation Model

The present model assumes that the fuel mass in each waste package can be represented by two concentric spheres, as shown in Figure 5-7. The outer sphere represents the diffusion barrier for the grain boundaries, and has the equivalent spherical diameter of a fuel fragment, about 0.2 centimeter. The inner sphere represents the diffusion barrier through the oxide film on the surface of the fuel grain, with a diameter of about 20 microns. The boundary conditions for the model are zero oxygen concentration at the fuel/oxide

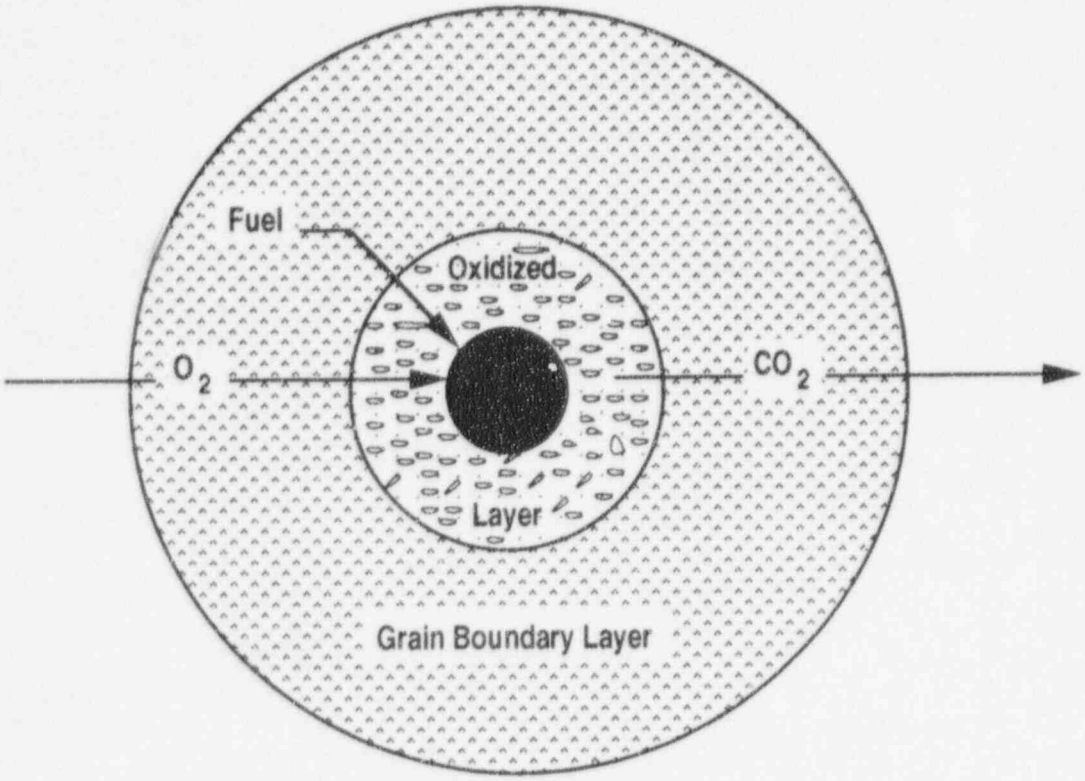

Figure 5–7 ^{14}C gaseous release model

interface and atmospheric oxygen concentration at the outer diameter.

Diffusion of oxygen through the fuel grain will be governed by the following partial differential equation:

$$\frac{\partial C}{\partial t} = \frac{1}{r^2}\frac{\partial}{\partial r}\left(r^2 D \frac{\partial C}{\partial r}\right), \qquad \textbf{(5–33)}$$

where C = oxygen concentration, t = time, r = radius from the center of the sphere, and D = diffusion coefficient.

The diffusion coefficient D is a function of temperature, and differs for the oxide layer and grain boundary layers. The boundary between the spent fuel grain and the oxide layer changes as the oxide layer grows, making this a moving boundary problem. The rate that the boundary recedes is governed by the diffusion rate of oxygen at the interface:

$$\frac{\partial r}{\partial t} = N_{ox}\frac{D}{\varrho_{ox}}\frac{\partial C}{\partial r}\bigg|_{r=r'}, \qquad \textbf{(5–34)}$$

where: r' = radius of fuel/oxide interface; D = diffusion coefficient in the oxide, square centimeters/year; and ϱ_{ox} is the density of the oxide, moles/cubic centimeter. The term N_{ox} is the conversion factor for UO_2, in terms of moles UO_2 oxidized per mole O reaching the boundary. X-ray diffraction analyses of samples of oxidized fuel indicate that for the temperature ranges likely to be encountered in the repository, most of the oxide formed will be U_4O_9, although stoichiometrically, the oxide appears to be U_3O_7, because of excess oxygen loosely held by the lattice (Einziger, 1992). For the purposes of the present analysis, N_{ox} will be taken to be 3 (i.e., 3

moles of UO_2 will be oxidized by 1 mole of O (1/2 mole O_2)).

5.6.3.5.2 Model for Oxygen and $^{14}CO_2$ Diffusion

The model for the release of $^{14}CO_2$ is similar to the UO_2 oxidation model. Diffusion of $^{14}CO_2$ through the fuel grain boundary layer and oxide layer will be governed by the following partial differential equation:

$$\frac{\partial C_c}{\partial t} = \frac{1}{r^2}\frac{\partial}{\partial r}\left(r^2 D \frac{\partial C_c}{\partial r}\right) - \lambda C_c \quad , \qquad \textbf{(5-35)}$$

where C_c = $^{14}CO_2$ concentration, t = time, r = radius from center of fragment, and λ is the decay coefficient for ^{14}C. The outer boundary conditions are:

$$C_c = 0 \text{ at } r = R_1.$$

At the inner boundary, $^{14}CO_2$ enters the oxide layer from the just-oxidized fuel. The gradient of $^{14}CO_2$ concentration is adjusted to account for diffusion:

$$\left.\frac{\partial C_c}{\partial r}\right|_{r'} = \frac{3M}{4\pi r_0^3 D_0}\frac{dr}{dt}\, e^{-\lambda t} \quad , \qquad \textbf{(5-36)}$$

where M is the initial inventory of ^{14}C and D_o = diffusion coefficient in the oxide layer. The ^{14}C diffusion model depends on the UO_2 oxidation model, to provide the position of the moving boundary, and the source flux of $^{14}CO_2$, at the inner boundary, as the oxide layer grows. Release of $^{14}CO_2$ at the outer boundary of the fragment is calculated from the concentration gradient at that boundary:

$$q_{^{14}C} = 4\pi R_1^2 D_1 \left.\frac{\partial C_c}{\partial r}\right|_{R_1} , \qquad \textbf{(5-37)}$$

where q = the rate of release from the fragment, curies/year and D_1 = the diffusion coefficient in the boundary diffusion layer.

5.6.3.5.3 Numerical Solutions

A simple semi-analytical solution to Equation (5-35) was developed, which depends on the assumption that the O and $^{14}CO_2$ gradients are at steady state. At steady state, Equation (5-36) for O concentration reduces to:

$$\frac{\partial}{\partial r}\left(r^2\frac{\partial C}{\partial r}\right) = 0 \quad , \qquad \textbf{(5-38)}$$

which has the general solution:

$$C = \frac{A}{r} + B \quad , \qquad \textbf{(5-39)}$$

where A and B are constants.

The boundary condition for oxygen is atmospheric concentration at the surface of the sphere and zero concentration at the boundary between the U_3O_7 and the fuel:

$$C = C_O, \text{ at } r = R_1, \text{ and}$$
$$C = 0, \text{ at } r = r' .$$

Between r' and R_O, diffusion coefficient D_O applies, and between R_O and R_1, D_1 applies. For a composite hollow sphere between r and R_1, therefore, the mass rate of oxygen transport to the surface of the fuel at steady state is:

$$flux = 4\pi R_1^2 D_1 \left.\frac{\partial C_c}{\partial r}\right|_{R_1}$$
$$= \frac{4\pi(C_o - C_1)}{\left[\frac{1}{D_o}\left(\frac{1}{r'}-\frac{1}{R_o}\right) + \frac{1}{D_1}\left(\frac{1}{R_o}-\frac{1}{R_1}\right)\right]} . \qquad \textbf{(5-40)}$$

The rate of growth of the film is related to the flux of oxygen. In terms of the oxidation rate of the fuel surface, Equation (5-40) becomes:

$$\frac{dr'}{dt} = \frac{(C_o - C_1)\, N_{ox}}{\left[\frac{1}{D_o}\left(\frac{1}{r'}-\frac{1}{R_o}\right) + \frac{1}{D_1}\left(\frac{1}{R_o}-\frac{1}{R_1}\right)\right] r'^2 \varrho_u} , \qquad \textbf{(5-41)}$$

where:

C_0 = the concentration at the surface of the fuel, taken here to be zero; and

C_1 = concentration of oxygen at the surface of the fuel, taken here to be

the volumetric concentration in the atmosphere, 0.2 moles/22,400 cubic centimeters.

The rate of growth depends on R_0 and the diffusion coefficients D_0 and D_1, which are functions of fuel temperature. The temperature of the fuel is estimated from the temperature of the waste package (generated from the *CANT2* program externally) corrected with an empirical formula determined from a calculational exercise on fuel temperature shown in Figure 5-8 (O'Neal *et al.*, 1984). The growth of the oxide layer is calculated by numerically integrating Equation (5-41).

$^{14}CO_2$ generated at the oxide/fuel interface must diffuse out through the oxide and grain boundary layers to leave the fuel fragment. In the steady-state assumption, the gradient of $^{14}CO_2$ in the radial direction is steady, but because the ^{14}C decays radioactively, the gradient will be somewhat different than for a non-decaying substance. Although it is possible to have a separate model for diffusion of $^{14}CO_2$ at steady state, it would be much more complicated (involving series of Bessel functions) than the model necessary for the diffusion of the non-decaying oxygen. Numerical experiments on a somewhat simpler problem however, demonstrated that the error in neglecting the decay of ^{14}C in the diffusing layer was negligible, and therefore the rate of release of $^{14}CO_2$ to the waste package was taken as its rate of production at the oxide boundary.

5.6.3.5.4 Overall ^{14}C Model Conservatism

The ^{14}C release rate model is considered to be conservative for the following reasons:

- The protection of the spent nuclear fuel from oxidation afforded by the cladding is ignored in IPA Phase 2. Zircaloy is a highly corrosion-resistant material, and it is likely that it would protect the fuel, after waste package failure, for a substantial period of time. Protection of the fuel even for a few hundred years would have a substantial impact on the calculated release rate, because the greatest potential for release is the period during which the fuel temperature is highest;

- Most of the ^{14}C in the fuel, cladding, and hardware is likely to be in a reduced state, and must first become oxidized to be released in the gas pathway, although thermodynamics in air favors the formation of gaseous compounds such as CO_2. Although kinetic considerations might restrict the formation of gaseous compounds of the ^{14}C in the fuel, the model conservatively assumes that any ^{14}C available to be oxidized is converted to $^{14}CO_2$;

- The model assumes there is no resistance of $^{14}CO_2$ once it is released from the fuel fragment (i.e., there is no resistance for diffusion through the long length of the failed fuel rod, or through pinhole failures of the waste package). This conservatism is relatively less important for the far-field release calculations because of the long periods involved; that is, diffusion and barometric pumping could allow virtually all $^{14}CO_2$ to escape to the geosphere, even for relatively small failure holes. Resistance to release from the waste package might be more important in evaluating compliance with the EBS subsystem requirements set forth in 10 CFR 60.113, which are more sensitive to short-term rates of release; and

- A portion of the ^{14}C in the spent nuclear fuel may be in a chemical form that is not easily released. Experimental data in which spent nuclear fuel was heated to temperatures of up to 450°C in oxygen indicated that up to half of the ^{14}C remained in the solid, and was not released as $^{14}CO_2$ (Van Konynenburg, 1991).

5.6.3.5.5 Parameter Estimation and Model Verification/Validation

The ^{14}C source term model is based on an abstraction of many complex processes. At the present time, the model can only be compared to data on UO_2 oxidation. It relates UO_2 oxidation to diffusion through two layers of material and outward diffusion of $^{14}CO_2$ through the same two layers. The simplifying assumptions taken in the model are:

- The fuel is represented by concentric spheres, of a single set of dimensions (i.e., the irregular shape of the fragments and grains is not taken into account);

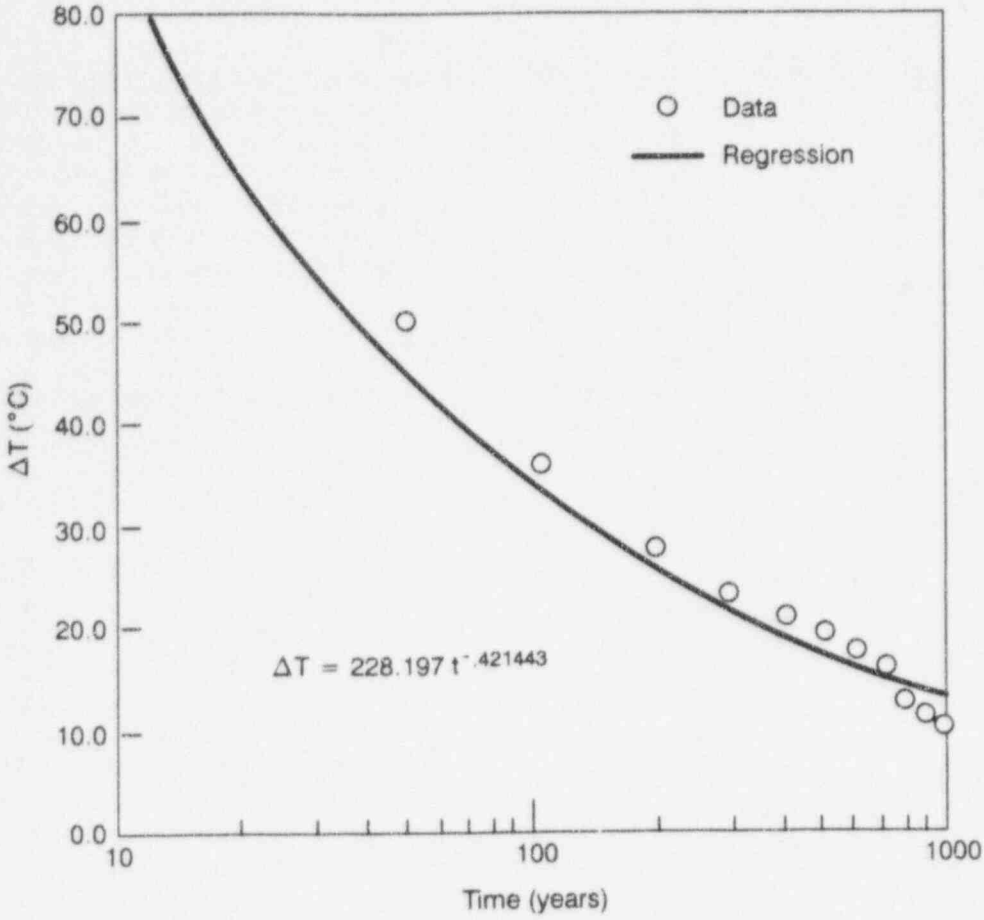

Figure 5-8 Fit of temperature difference between waste package skin and maximum fuel

- The current version of *SOTEC* allows only steady-state diffusion;
- No effects of the waste package or cladding on the diffusional processes are taken into account;
- The increase in surface area caused by oxidation of the grains is not taken into account; and
- Although there are some direct data on release of $^{14}CO_2$ from cladding and the grain/gap inventory, releases from the largest inventory in the fuel itself are lacking. There are data on UO_2 oxidation, but there are apparently no data available for release of $^{14}CO_2$ from fuel grain oxidation.

Nevertheless, the model was considered to be realistic enough that the parameters necessary for its implementation could be obtained from experimental data.

5.6.3.5.6 Data on Spent Nuclear Fuel Oxidation

Several investigators have collected data on the oxidation in air of spent and un-irradiated reactor fuel in connection with intermediate storage (Einziger, 1991, 1992; Einziger and Kohl; 1984; Einziger and Buchanan, 1988; Einziger *et al.*, 1991, 1992; Woodley *et al.*, 1989; and Thomas *et al.*, 1991). The main concern of these investigators was the degradation of the waste form for fuel in contact with oxygen at temperatures of several hundred °C (e.g., dry storage in air). The experimental programs concentrated on the physical changes to the fuel resulting from oxidation in failed rods rather than from the releases of radionuclides.

Quantitative data on fuel oxidation in air were basically of four types:

- Thermal Gravimetric Analysis (TGA);
- Dry-bath analysis;
- Ceramography; and
- X-ray crystallography.

In TGA, samples of spent nuclear fuel were exposed to air at fixed temperatures, and the gain in sample weight because of oxidation was recorded continuously, with an analytical balance. In the dry-bath tests, samples were kept in small crucibles held at fixed temperatures in an aluminum block, and weighed periodically outside the apparatus. The advantage of the dry-bath tests was that they could be performed for very long times, on the order of years, whereas the TGA experiments were limited to shorter periods, up to a few months.

Ceramography is the inspection of thin slices of spent nuclear fuel, to visually observe the growth of oxide films around individual fuel grains. These observations gave valuable, quantitative information about the sizes of fuel grains necessary for the implementation of the mathematical model and the rate of growth of the oxide thickness. In addition, ceramography gave qualitative information about the mechanisms of oxidation (e.g., the fact that the film of oxide appears to be growing at a consistent rate throughout the sample indicated that diffusion of oxygen through grain boundaries and cracks probably was much faster than the diffusion across the oxide layer, itself).

X-ray crystallography gave quantitative information on the chemical species of the oxide formed at different temperatures. Among the more interesting indications of X-ray crystallography was the observation that for temperatures below about 200°C, the oxide formed was primarily U_4O_9, even though it appeared to be U_3O_7 stoichiometrically (Einziger *et al.*, 1992).

5.6.3.5.7 Uses of the Data for Parameter Identification

Aside from identifying the chemical form of the oxide layer, only the quantitative data on grain size, growth of oxide film thickness, and sample weight were used, to determine the model parameters for fuel oxidation. Data on sample weight gain and film thickness at fixed temperatures were put into the form of "conversion fraction" of UO_2 to U_3O_7 versus time. The fuel oxidation model was then exercised to predict the conversion versus time of UO_2 grains to U_3O_7. The only model parameters that could vary were:

- Grain size (i.e., radius of inner sphere);
- Fragment size (i.e., radius of outer sphere);
- Diffusion coefficient through oxide layer at the reference temperature of 200°C;
- Diffusion coefficient through the grain boundary layer at the reference temperature of 200°C; and
- Activation energy for diffusion coefficient (considered to be equal for both layers).

The parameter identification does not at the present time take into account any differences between fragment sizes, grain sizes, or types of fuel.

Data on fuel conversion were collected in eight sets from TGA, Dry Bath, and ceramography, representing experimental periods from 700 to 12,000 hours, with the lower temperatures represented by the longer periods. Although data were available on whole-fuel fragments, as well as crushed fuel, only the whole-fragment data were used for the parameter identification for IPA Phase 2, because these samples were more like the actual spent nuclear fuel that would be in the repository.

The parameter identification was performed by manually varying the parameters and observing the agreement between predicted and observed conversion for the eight data sets. Parameters giving the best comparisons are given in Table 5-4.

Graphical results of the model/data comparison are given in Figures 5-9(a) through 5-9(h). Although there is a degree of scatter in the data, the model prediction is quite reasonable for the parameters chosen. Bear in mind that only one set of parameters was used to represent what are certainly nonhomogeneous samples.

5.6.3.5.8 Discussion

There are several facets of the model for ^{14}C release from the fuel matrix that could lead to errors. These factors are discussed below, and in the recommendations for further work, in Section 5.8:

- The IPA Phase 2 model considers only steady-state concentrations of oxygen and $^{14}CO_2$ in the fuel. Although it was possible to get a consistent fit of the model predictions to measured UO_2 conversion rates, there is some indication, from the transient modeling discussed in Section 5.6.3.5.1, that the coefficient for diffusion of oxygen through the grain boundaries should be relatively bigger than it appears in the steady-state model fit (Grambow, 1989). Thermal gravimetric analysis data on many samples indicate a period of very slow initial weight gain, followed by a substantially higher rate. This result has been interpreted as the transient diffusion of oxygen through the grain boundaries before oxidation of the grains. A transient model would be capable of simulating this phenomenon, but was not successfully completed for IPA Phase 2, because of problems with mass balance. The steady-state model used in IPA Phase 2 is incapable of simulating such a transient. At high temperatures where diffusion coefficients are large, there is relatively little difference between the conversion of large fuel fragments and crushed samples, indicating that the grain-boundary diffusion is fast. At lower temperatures, the difference between whole and crushed samples is much more evident. Although the steady-state model appears to fit the data well, it may, in fact, be portraying the transient diffusion as a much lower rate of conversion, especially at lower temperatures. This could lead to inaccurate predictions of conversion rates at low temperatures, for times much larger than the period of 12,000 hours, for the longest experiment;

- The IPA Phase 2 model assumes that the oxidizing fuel can be characterized by a single set of parameters. Actually, each sample of fuel oxidized in the laboratory consisted of grains of varying sizes, and material properties determined by their position in the fuel rod and distance from the pellet edge. Furthermore, the fuel would be expected to vary from one rod to the next, in the same core, and from one set of spent nuclear fuel to another, depending on such factors as reactor type, burnup, and fuel manufacturer; and

- The present model calculates an ensemble release rate from all waste packages, to feed into the gaseous transport model. Waste packages in different portions of the repository would be expected to have quite different gaseous release rates of $^{14}CO_2$, because of factors such as temperature, thermal loading, and age of the waste. Furthermore, the same factors would lead to gas-flow velocities varying from one portion of the repository to another, and these variations would be correlated to the variations in the $^{14}CO_2$ release rates.

Table 5-4 Model Parameters from Manual Identification

Model Parameter	*Value*
Grain radius (cm)	0.001
Fragment radius (cm)	0.1
Reference film diffusion coefficient (cm^2/yr)	5.256×10^{-4}
Reference grain diffusion coefficient (cm^2/yr)	5.942×10^{-3}
Reference temperature (°C)	200.0
Activation Energy (Kcal/mole)	32.0

5.7 Source Term Auxiliary Analyses

Two auxiliary analyses conducted for this demonstration were performed to evaluate the appropriateness and limitations of various computational approaches and interpretations of data used in this study. These analyses are summarized below.

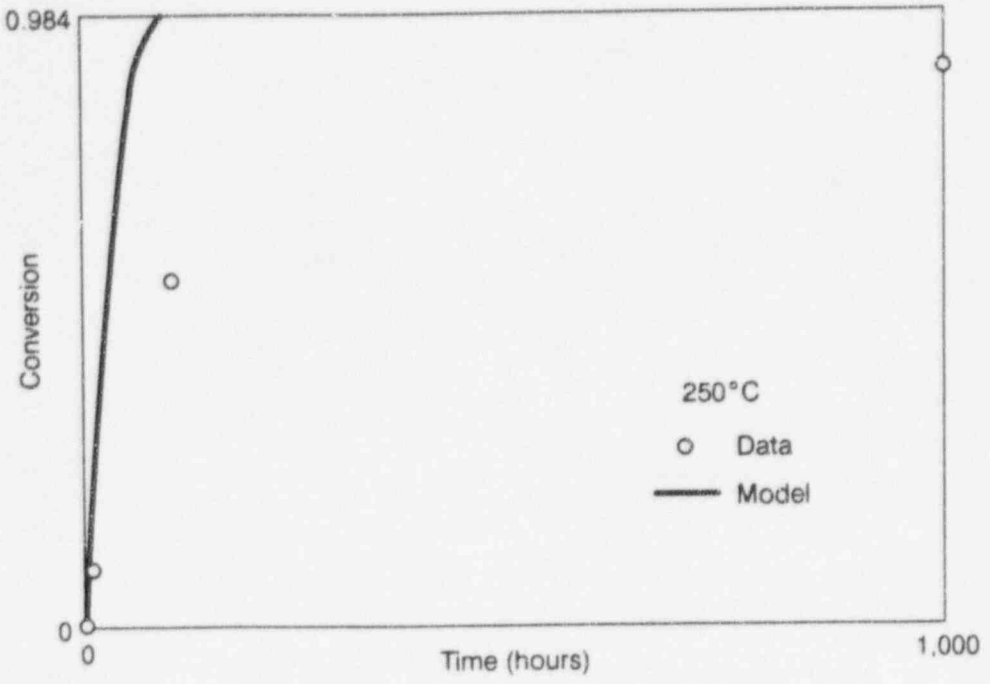

Figure 5–9a Model-prototype comparison, 250°C

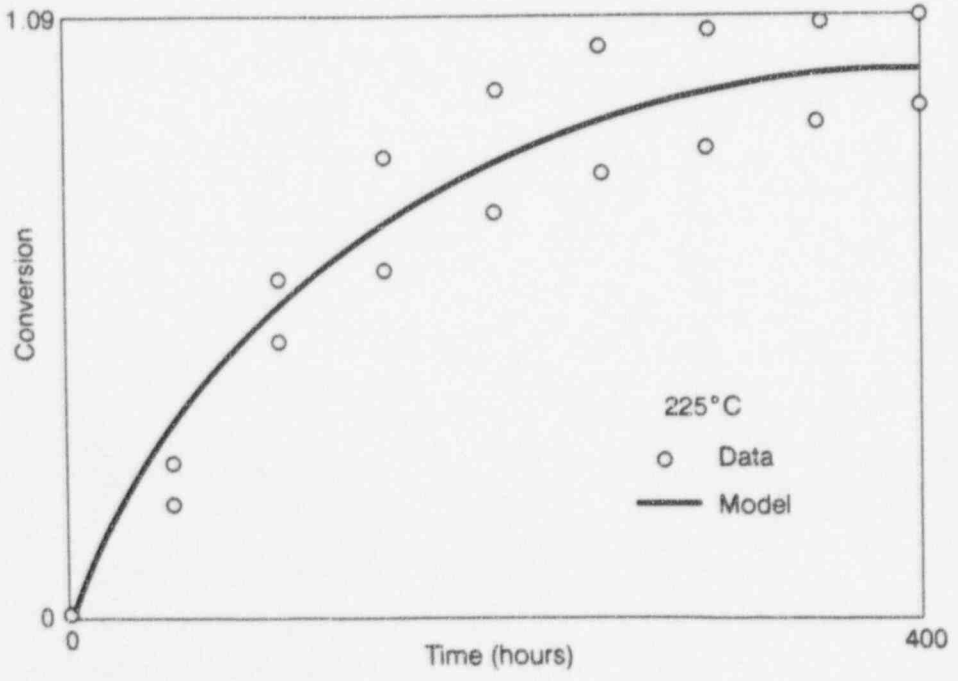

Figure 5–9b Model-prototype comparison, 225°C

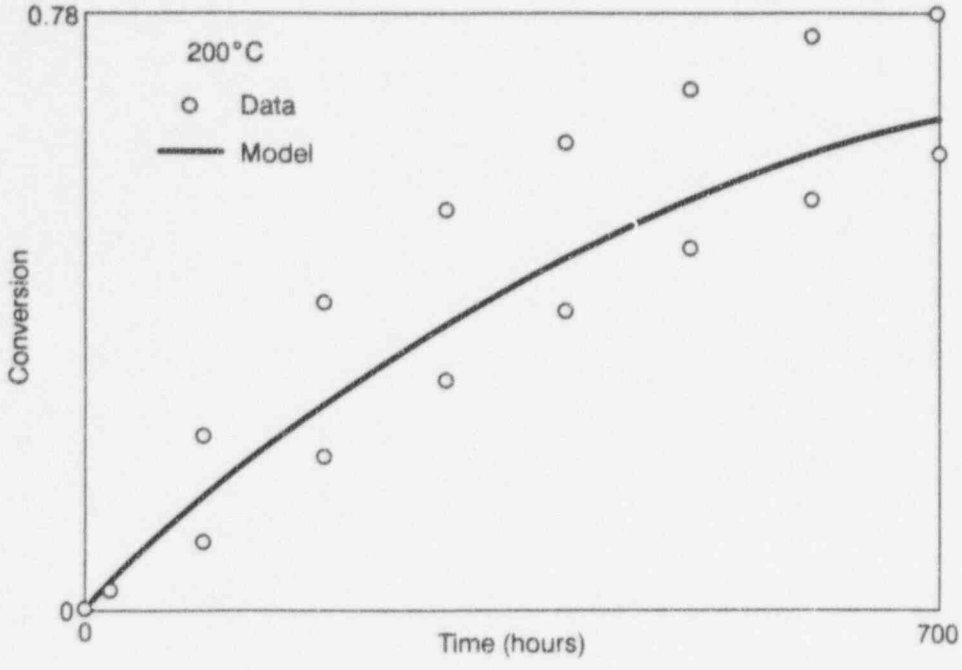

Figure 5–9c Model-prototype comparison, 200°C

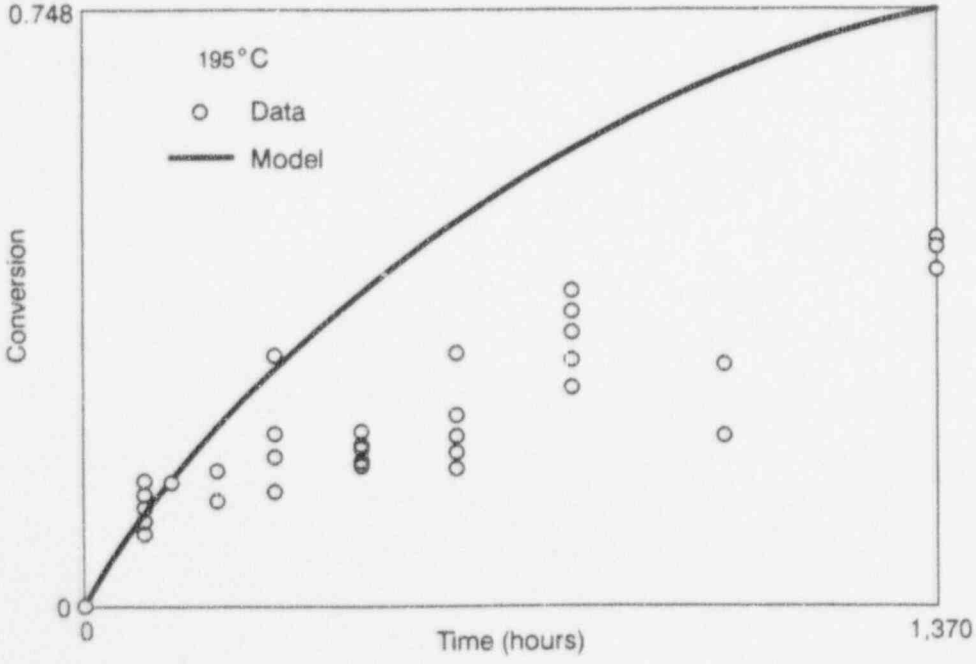

Figure 5–9d Model-prototype comparison, 195°C

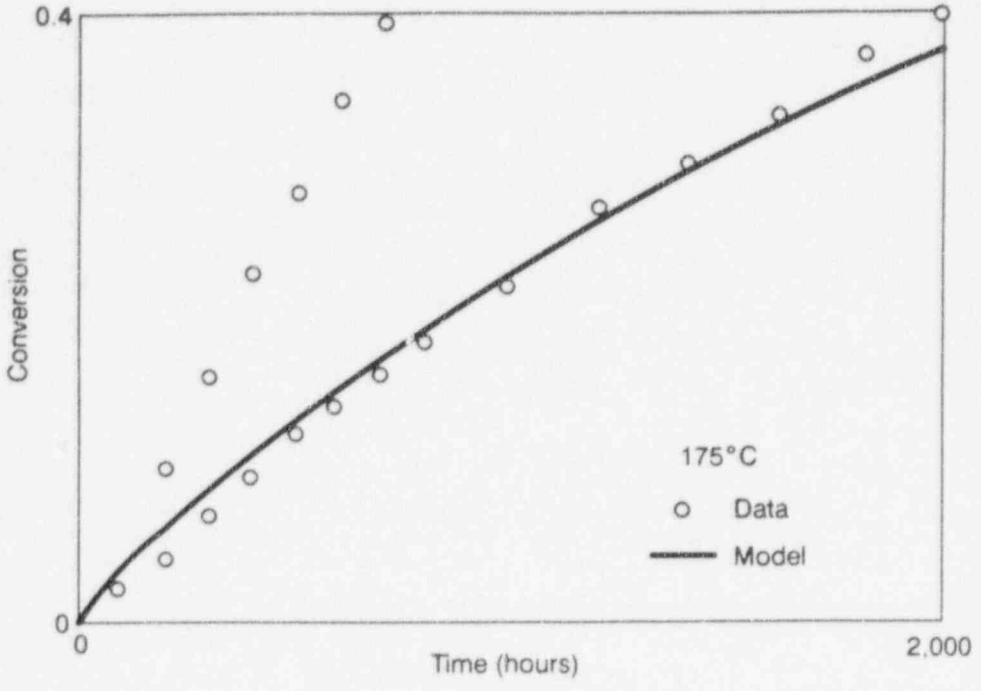

Figure 5–9e Model-prototype comparison, 175°C

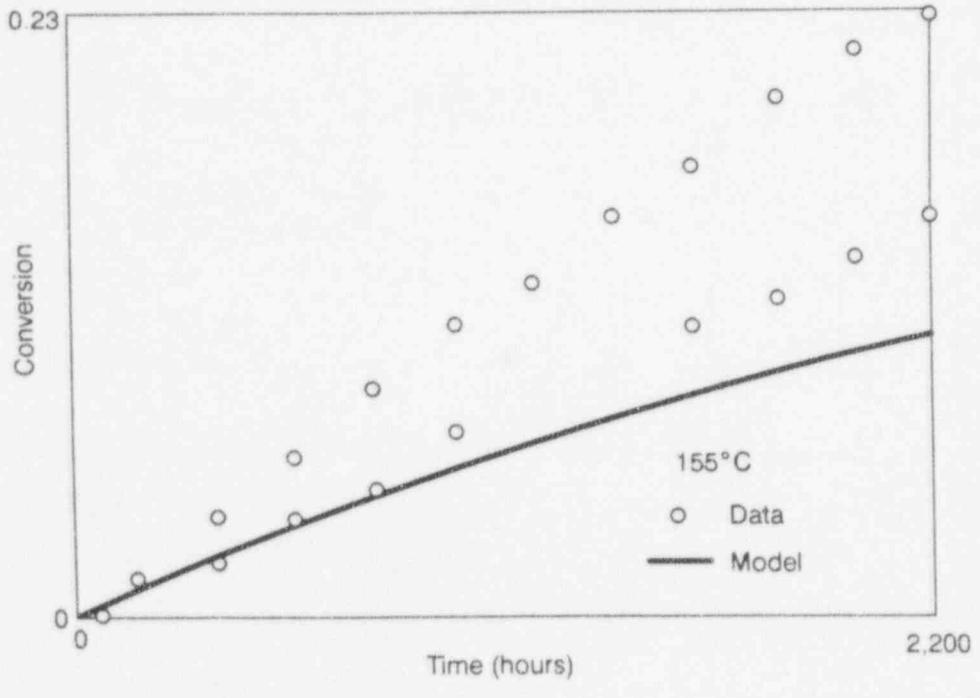

Figure 5–9f Model-prototype comparison, 155°C

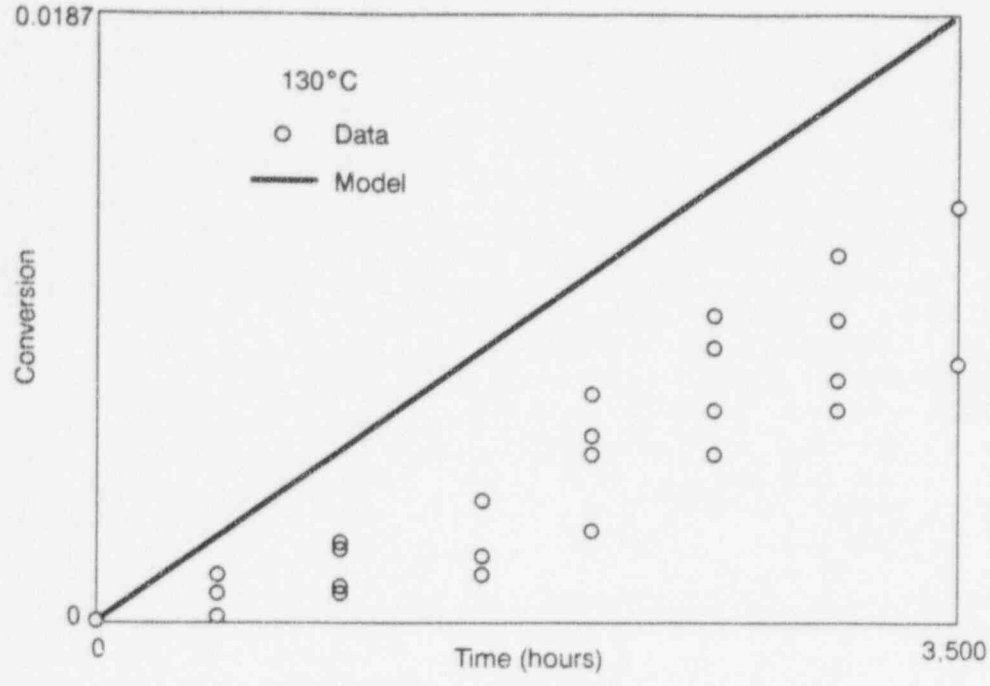

Figure 5–9g Model-prototype comparison, 130°C

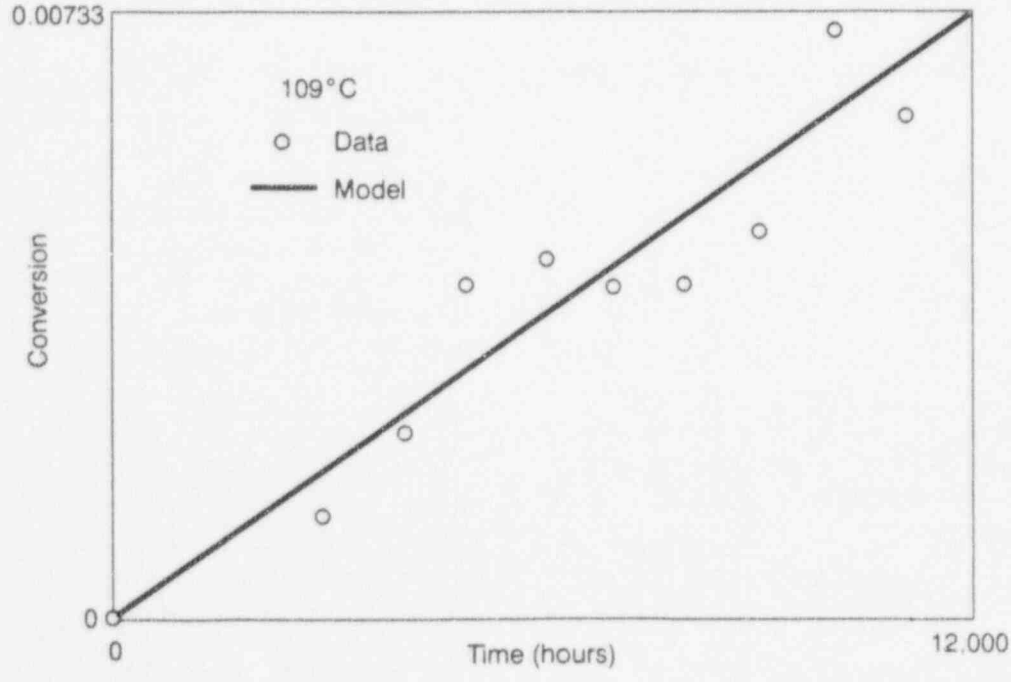

Figure 5–9h Model-prototype comparison, 109°C

5.7.1 Ensemble Averaging for Source Term Parameters

For the sake of computational speed in the systems model, the IPA Phase 2 analysis approximated the large number of individual waste packages by only seven repository sub-areas, with one waste package per repository sub-area. This analysis evaluates the way in which the averaging of a large number of waste packages can be accomplished with the least error. The demonstration of the effects of ensemble averaging of the parameters associated with the source term code was performed for a simplified case of only two radionuclides, one solubility limited and the other limited by congruent dissolution of the UO_2 fuel. Furthermore, both radionuclides were considered to have long half lives and the analysis did not consider decay daughters.

The staff concluded that for solubility limited releases of single, long-lived radionuclides, the ensemble average cumulative release per waste package would be represented by the arithmetic averages of the liquid flow rate q per waste package, waste package failure time, and the volume V_{fail} held by the waste package at the time of failure t_{fail}. The corresponding ensemble parameters for the congruent release case would be the harmonic mean flow rate per waste package, the mean of t_{fail}/q, and the mean of V_{fail}/q. There is presently no apparent way to choose the ensemble means of environmental parameters to use in the system analysis that would apply to all radionuclides.

This auxiliary analysis is discussed in greater detail in Appendix M.

5.7.2 Release and Transport of Potentially Gaseous Radionuclides Other than ^{14}C during Volcanism and Normal Operations

Several potentially volatile compounds of ^{79}Se, ^{99}Tc, and ^{129}I may be present in spent nuclear fuel. Because of the possibility of a gaseous pathway through the unsaturated rock at Yucca Mountain from the buried waste to the atmosphere, this auxiliary analysis investigated, using a series of conservative calculations, the phenomena by which volatile radionuclides could be released, and whether they posed enough of a threat to warrant further study.

Vapor pressure of possible volatile radionuclide compounds were taken from the available literature and also estimated thermodynamic information. Given the estimated vapor pressures, a portion of the inventories of the volatile radionuclides could be released at normal repository operating conditions. The bulk of the inventories of these radionuclides would be contained within the structure of the fuel, however, and the vapor pressures of those inventories would be reduced. Barometric pumping caused by changes in atmospheric pressure was considered a possible mechanism for release of volatile radionuclides from breached waste packages. For temperatures and atmospheric pressure variations in the 1988 SCP design, the staff's conservative calculations estimated that less than 1 percent of the inventory of volatile radionuclides would be released from the waste packages to the geosphere in 10,000 years. The staff further estimated that most of the volatile compounds would become associated with liquid water in the rock, rather than remaining in the gas phase.

The staff also estimated the effects of an intrusive basaltic dike causing temporary heating of the rock near waste packages. For a 10-meter-wide dike of 3000 meters length, the staff conservatively assumed that all volatile radionuclides in a 100-meter-wide region would be driven off by the increased temperature. This represents an area approximately 6 percent of the total repository sub-area for the 1988 SCP design. Even if all of the inventories of ^{99}Tc, ^{79}Se, and ^{129}I in 6 percent of the repository were released to the accessible environment, the total consequences would sum to only about 0.125 of the releases allowed under 40 CFR Part 191. The results of this analysis supported the staff's decision to neglect, for the time being, releases of volatile radionuclides other than ^{14}C in the Phase 2 analyses. This analysis, however, was based on preliminary models and data, and does not intend to foreclose further study of the issue of volatile radionuclides at Yucca Mountain.

5.8 Conclusions and Suggestions for Further Work

The following recommendations to improve the source term model came out of the work presented in Chapter 5:

1—Improve modeling of interaction between the waste and the near-field environment.

IPA Phase 2 analyses simplified treatments for the thermal, hydrological, and geochemical environments, based on the disposal concept of vertically placed waste packages surrounded by an air gap, as presented in DOE's 1988 SCP. Failure of the waste packages, by corrosion and transport of dissolved radionuclides from the waste package, is expected to depend on contact with liquid water. In IPA Phase 2, waste packages were considered to remain dry until their surface temperature dropped below the boiling point, and then assumed to come into contact with liquid water from dripping fractures and wet rock. Future models need: (1) plausible re-wetting mechanisms for dry rock; (2) the possible influx of liquid water such as dripping fractures; (3) condensation of water vapor on waste package surfaces, because of capillary and solution effects; (4) rise in the water table, and (5) water reflux, driven by repository or geothermal heat. Additionally, alterations to the hydrologic environment from climate change or hydrothermal processes, along with man-made changes, need to be factored into models for water influx. Models to determine accurately the contact of waste with liquid water will be highly design-specific to the repository concept finally adopted. Much of this work is expected to stem from confirmatory lab-scale and field-heater tests used to validate mathematical models of two-phase heat and mass transfer (Buscheck *et al.*, 1993). Since the experimental data must be necessarily of short duration and small-scale, relative to those of the repository, reliable mathematical models may be the only way to extrapolate results to greater times and distances. In this regard, the basis for the development of these models will rely on a mechanistic understanding of the processes and events related to waste package interaction with its environment.

2—Revise model for current DOE disposal concept.

IPA Phase 2 was based on the waste package concept described in DOE's 1988 SCP of single-walled packages placed vertically in boreholes, with an air gap between the waste package canister and the surrounding host rock. However, since the issuance of the SCP, DOE has developed a significant interest in more robust waste package concepts for both borehole and drift emplacement, including consideration of overpacked multi-purpose canisters for spent nuclear fuel. As part of its ongoing waste package Advanced Conceptual Design (ACD) (see TRW Environmental Safety Systems, 1993), DOE has identified various concepts for evaluation: (1) metallic multi-barrier containers; (2) metallic shielded containers; (3) small metallic multi-barrier containers; (4) nonmetallic multi-barrier containers; (5) overpacked multi-purpose canisters; (6) universal cask; (7) SCP single containers; and (8) defense HLW containers. Concurrent with the waste package ACD program, DOE is assessing the merits of various repository thermal loading strategies (i.e., cold, intermediate, and hot). Any decision regarding repository thermal loading should be integrated with the waste package concept. The behavior of the waste packages in the environment of the geologic repository will depend markedly on the concept finally adopted, the mode of emplacement (e.g., borehole or drift), and whether backfill or an air gap will be employed in the balance of the EBS design. The current models will have to be modified as DOE progresses in site characterization and makes decisions about its thermal loading strategy, waste package design, waste package materials, and additional engineered barriers.

3—Develop more mechanistic models for waste package corrosion.

Corrosion will be affected by a number of coupled processes that include heat and mass transfer, production of metal ions within the crevices and pits, and hydrolysis. Episodic evaporation and condensation of water on the surface of waste packages may result in high concentration of aggressive ions at temperatures well above the normal boiling point. The present version of *SOTEC* used in IPA Phase 2 considered simplified models for corrosion. General corrosion was assumed to begin when repository temperatures drop below boiling, and was described by a generic power law equation. Models of crevice and pitting corrosion assume an empirically derived temperature and radiation-dependent corrosion, critical and repassivation potentials,

and constant corrosion propagation rate. Needed improvements to *SOTEC* include codes abstracted from complex physics-based models, and inclusion of other localized corrosion modes, taking into account the geochemical environment and mechanical stresses. The models should also investigate the correlation between near-field chemical conditions, and corrosion and leaching.

4—Improve models for the effects of heat.

The present temperature model uses a semi-analytical approach for conduction-only. More realistic models could take heat and mass transfer in two-phase flow into account, to better estimate the temperature in the near field and the transfer of liquid water and water vapor (Buscheck, 1993), inputs needed to predict the onset of corrosion and the interaction of liquid water with the waste.

5—Take spatial and temporal variability into account in source term models.

For the sake of computational speed, IPA Phase 2 used an approach in which the entire repository was represented by only seven zones or sub-areas, within which all waste packages were of the same design and experienced the same environment. Future IPAs should deal with the difficult problem of spatial and temporal variability of material properties and external driving forces. If highly simplified models are required, then the IPAs should be able to demonstrate how spatial and temporal variabilities propagate through the system. IPA Phase 2 began to explore appropriate ensemble averages of the temporally and spatially varying input parameters for the simplified models.

An issue related to spatial and temporal variability is the distributed nature of some parameters. The distinction here is that the models might be able to account explicitly for known variations of parameters in space (e.g., temperature) and time (e.g., water flux). The distributed parameters cannot be completely characterized spatially or temporally, but should nevertheless be taken into account in the models. For example, *SOTEC* assumes that the oxidizing fuel can be characterized by a single set of parameters. The spent nuclear fuel, however, is highly heterogeneous, consisting of grains of varying size and material properties (Stout *et al.*, 1991). Improved source term models should take the variability of the properties of the spent nuclear fuel into account, either explicitly, or by defining effective input parameters that capture the variability without making the models too complex for total-system performance assessments.

6—Improve models for the release of gaseous ^{14}C.

For several reasons, the release of ^{14}C from the waste was one of the most important radionuclides identified in the IPA Phase 2 study: (1) ^{14}C can be released from the waste form as a gas whether or not there is liquid water involved; (2) the estimated inventory of ^{14}C in the spent nuclear fuel probably exceeds that which would be allowed under 40 CFR Part 191; and (3) there may be direct pathways for gaseous flow from the waste to the atmosphere through the unsaturated zone. *SOTEC* considers the release of gaseous $^{14}CO_2$ emanating from the waste form, tied to the oxidation of UO_2 from diffusing oxygen and escape of $^{14}CO_2$ through the oxidized film (Codell, 1993). There is little if any direct evidence of gaseous ^{14}C emanation from spent nuclear fuel, however, and the ^{14}C releases in *SOTEC* were based largely on speculation on the mechanisms for oxidation of the UO_2, and diffusion of $^{14}CO_2$ through the oxidized film and interstitial spaces.

A better model for gaseous ^{14}C emanations must await more definitive experimental data on spent fuel. Among the questions that await experimental results for the ^{14}C model are (Van Konynenburg *et al.*, 1987): (1) the chemical form of ^{14}C in the spent nuclear fuel; (2) the diffusion of the ^{14}C through the spent fuel matrix and the product of its oxidation, and the form of the diffusing substance (e.g., elemental carbon, CO, CO_2); (3) the variation in ^{14}C inventory in the different fuel assemblies, because of type of fuel, type of reactor and burn-up; (4) the rate of oxidation of ^{14}C in elemental or compound form; (5) the preferential locations of unoxidized ^{14}C in the fuel (e.g., along grain boundaries, within fuel grains); and (6) the effect of the state of UO_2 fuel oxidation on release (e.g., powdering of U_3O_8 at high temperature) (Tempest *et al.*, 1988).

Additional points concerning the model for $^{14}CO_2$ release are:

- The IPA Phase 2 model considers the release of gaseous $^{14}CO_2$ emanating from the waste, based on steady-state diffusion of oxygen and $^{14}CO_2$. Although it was possible to get a

consistent fit of the model predictions to measured UO_2 conversion rates, there is evidence that transient diffusion may be important. Failure to include the transient diffusion of oxygen evident from the data could lead to inaccurate predictions of conversion rates at low temperatures. The model could be improved by considering transient diffusion.

- The Phase 2 model assumes that the oxidizing fuel can be characterized by a single set of parameters. The spent fuel, however, is highly heterogeneous, consisting of grains of varying size and material properties. Future IPA models should take the variability of the properties of the fuel into account explicitly.

- The present implementation of the model for the release of gaseous ^{14}C mixes the contribution from the seven repository sub-areas for use in the two-dimensional gas flow model. Since the release rate of ^{14}C is highly dependent on the temperature of the waste packages and the times of failure, this procedure might lead to needless errors in the release rate at the accessible environment. The procedure for calculating transport to the atmosphere should be revised to take into account the variations in release rate from the seven repository sub-areas.

7—Improve structural failure models.

Analytical expressions for buckling are only available for simplified geometries and loading conditions with static loads. A buckling model for a complex geometry and multiple and transient loads would require a complicated and computationally intensive simulation unsuited for IPA. The structural failure considered in IPA Phase 2 was for buckling of a highly simplified waste package weakened by corrosion, with external forces from seismic shaking. Structural failure depends on the engineering design, and the model should be adjusted accordingly, for changes. Once the engineering design has been finalized, the structural failure of the waste packages from dynamic and other forces could be analyzed deterministically by numerical and experimental techniques, and abstracted for IPA. These analyses would include the possible impact of mechanical fatigue of the waste packages from recurrent, low-intensity, seismic activity.

8—Consider modes of waste package failure other than corrosion.

Waste packages might also fail from mechanisms other than corrosion, such as seismic shaking, volcanism, and inadvertent human intrusion. Although IPA Phase 2 considered failure by drilling, volcanism and seismicity, the models were highly simplified. Improved models of seismic failure might take into account the range of frequencies of earth motion, and realistic dynamic modes of the waste packages. Models for failure by volcanism might take into account mechanisms of interaction between magma and the waste packages (e.g., corrosive gases and viscous forces). Improved models for human intrusion might consider the site-specific likelihood for exploratory drilling, shear forces from drilling fluids, and mechanisms that could bring radioactive material to the surface. These disruptive events could also have a significant effect on the other aspects of the repository performance.

9—Improve model for the dissolution of radionuclides from the waste form.

The chemistry within the waste package was treated in a highly simplified manner in IPA Phase 2. On waste package failure, water was assumed to infiltrate the waste package and come into intimate contact with the fuel. Radionuclides were released from the waste form to the inside of the waste package at a rate determined by the alteration rate of UO_2, and instantaneously from crud, gap, grain boundaries, and cladding. Transport out of the waste packages was limited by solubility of the nuclides. The models did not consider colloids explicitly; colloids were considered to be part of the dissolved inventory. The model could be improved by taking into account the formation and subsequent transport of colloids. Reflective of this interest, the NRC staff is presently conducting a literature survey of the role of colloids in the release and transport of radionuclides from vitrified waste forms and spent nuclear fuel. Improvements in the model for waste form dissolution should also consider speciation of the elements released to the water, the contribution of minerals from the groundwater and corrosion products from the waste package, the changing temperature, and other factors such as ionizing radiation. Subsequent iterations should also investigate models of spent

fuel dissolution based on electrochemical theories (Shoesmith and Sunder, 1992).

10—Improve model for transport of radionuclides from the waste package.

Mass transfer out of the waste package by flowing water and diffusion was included in IPA Phase 2, based on the 1988 SCP conceptual waste package. These transport mechanisms are highly specific to both waste package and overall repository design. Plausible mechanisms for transport from failed waste packages will need to take into account the design finally adopted by DOE. Both NRC and DOE total-system performance assessments considered rather simplistic idealizations for transport from the waste packages, such as bathtub or moist continuous cases (see Sagar *et al.*, 1992). However, in future assessments, the NRC staff plans to develop a more mechanistic model, which predicts the mass transport of radionuclides from the waste packages. The transport model, in conjunction with the waste form dissolution model, should consider the rates that water contacts and enters the waste package, interacts with the waste form and transports radionuclides from the waste package by both advection and diffusion. The model should recognize that the suite of waste packages will represent a broad range of varying stages of degradation, with some completely intact and others significantly degraded from both anticipated and unanticipated processes and events. These conditions are progressive over the 10,000-year period of regulatory interest. Although conservatively neglected in *SOTEC*, the model could include recognition that degraded waste packages, including failed fuel (e.g., defective cladding), can still contribute to the isolation or controlled release of radionuclides, as demonstrated in static dissolution tests (Wilson, 1990).

11—Include models for other waste forms.

The NRC staff's first two IPAs focused on evaluating the performance of waste packages for spent fuel, recognizing that by the year 2030, spent fuel will constitute roughly 97 percent of the curie inventory of waste expected to be emplaced in a repository (DOE, 1992). However, this does not mean that the waste form resulting from the planned vitrification of existing defense-related HLW can be neglected as a potential contributor to the overall source term. Accordingly, in future IPAs, the staff should develop a source term model for the expected inventory of glass waste packages, with special consideration to the kinetics of glass dissolution, formation of secondary silicate mineral, colloid formation, and mass transport of radionuclides. Further, waste forms other than light water reactor spent fuel and defense-related glass may ultimately need to be considered if they are determined to be potentially significant sources. These may include any transuranic or greater-than-Class-C wastes.

12—Develop source term model abstractions for IPA.

Even though the analysis of the release of radionuclides to the geosphere from the waste form was highly simplified, the source term models and codes represented a large proportion of the overall complexity of IPA Phase 2. The recommended improvements listed above will further add to the complexity of the models. A substantial effort will be required to develop models that both take into account the complexity of the source term, yet are simplified enough to be practical for IPA.

6 DISRUPTIVE CONSEQUENCE ANALYSIS[1]

6.1 Overall Approaches for Treating Consequences of Disruptive Events

The performance of the undisturbed geologic repository may be modified by a number of disruptive events, as discussed in Chapter 3. Those considered in Iterative Performance Assessment (IPA) Phase 2 were: climate change (pluvial scenario); human intrusion (including exploratory drilling—drilling scenario); seismic shaking (seismic scenario); and magmatic eruption (volcanic scenario). These events, individually and in combination, have the potential to alter repository performance in several different ways. They may result in direct releases of radionuclides to the surface in the form of contaminated drill cuttings, or indirect releases, by way of the liquid or gas pathway, augmented by premature failure of waste packages.[2]

The approach employed in developing the disruptive models was to use the undisturbed system models, or "base case," to the extent practicable, to assume a "reference biosphere"[3] for computing doses, and to use the least aggressive approach feasible. This involved generally altering the input data to the computational modules to simulate a disrupted condition (e.g., earlier failure of the waste package to simulated drilling, seismic or volcanic failures, or increased infiltration to simulate a pluvial climate). However, there were several modules developed specifically to simulate the time and extent of the drilling, seismic, and volcanic failures.

Each scenario class is denoted by a four-tuple (a_1 a_2 a_3 a_4), with $a_{1, 2, 3, 4}$ corresponding to the letter *c, s, d* and *v*, respectively, referring to the four disruptive events, or the letter *o*, to denote that the particular disruptive event is absent. There are a maximum of $2^4 = 16$ distinct scenario classes that are possible. For example, the base case is denoted by *oooo*, and the fully disturbed by *csdv*. In addition to the base case *(o)*, the four categories of fundamental causative events from which scenario classes are formed for Phase 2 are: climate change *(c)*; drilling *(d)*; seismic *(s)*; and volcanic *(v)*.

- Climate change is represented by change in the infiltration rate at the surface of the mountain and in the height of the water table. The infiltration rate is treated as a sampled parameter, where its value is determined using Latin Hypercube Sampling (LHS) (described in Section 2.1.3). The height of the water table is increased by 100 meters, compared with the base case in the climate scenario model. Climate change can only indirectly affect release of radionuclides from the repository.

- Human intrusion into the repository is considered to occur by exploratory drilling. Drilling is considered to cause both a direct and indirect release of radionuclides to the surface. Indirect release is caused by drilling-initiated failure of waste packages, which determines the source term. In computing the direct release of radionuclides from drilling, removal of radionuclides from the engineered barrier system (EBS) and rock column, by liquid and gaseous pathways, up to the time of drilling, are taken into account.

- Seismic events are assumed only to lead to premature failure of waste packages, affecting only indirectly the release of radionuclides from the repository. The model does not allow the alteration of site hydraulic properties, because of fault movement along the linear segment representing the fault. Because there are numerous faults and fractures intersecting the repository perimeter and its surroundings, it is expected that movement along existing faults will change the hydraulic characteristics of the site to a minimal degree.

- Magmatism is modeled as both intrusive and extrusive magmatic events. Intrusive magmatism is modeled as a linear dike in the plane of the repository and results in an indirect release of radionuclides. Extrusive magmatism is modeled as a volcanic eruption of ash

[1]The figures shown in this chapter present the results from a demonstration of staff capability to review a performance assessment. These figures, like the demonstration, are limited by the use of many simplifying assumptions and sparse data.

[2]The term "waste package" is used here synonymously with "container" and "canister."

[3]Defined in Section 7.2.1.

flow extending from the basement. This event is assumed to result in a direct release of radionuclides. Coupling among magmatism and other release mechanisms are not considered. For example, the removal of radionuclides from the EBS and rock column by magmatic events is not taken into account in computing the release of radionuclides by liquid and gaseous pathways, and vice versa.

The models of disruptive events for early failure of the waste packages work in conjunction with *SOTEC* (Source Term Code), described in Chapter 5 (and in Sagar *et al.* (1992)). *SOTEC* considers only one representative waste package per repository sub-area, but is invoked three times to include: (1) initial failures (e.g., manufacturing defects); (2) failures from corrosion; and (3) failures by scenarios (i.e., drilling, seismic, or volcanism). For scenario classes with drilling-only (*oodo*) or drilling combined with pluvial climate (*codo*), a direct hit from drilling will fail only a single waste package within the repository sub-area (unless it has already failed from corrosion). However the version of *SOTEC* used in the Phase 2 analyses cannot distinguish between types of scenario failures, so the analysis incorporates the most conservative assumption about the number of failed waste packages and the time of failures: the number of failures is the sum of the failures from drilling, seismicity, and volcanism, but the failure time is the shortest of the three failure times.

In IPA Phase 2, the consequences from disruptive events are treated by adjusting submodel parameters, introducing LHS parameters, or through additional dependent or independent calculations. A summary of the disruptive events, the names of the parameters, and their respective release modes is presented in Table 6–1. The LHS parameters (including those associated with the base case) are itemized in Appendix A.

The choice of LHS parameters was determined by the individual investigators responsible for the disruptive scenario modules, based where available from data on Yucca Mountain site or similar rocks. Parameter choices are discussed further in individual sections and in Appendix A. A detailed description of methods for computing consequences of disruptive scenarios is provided in the following sections.

6.2 Treatment of Climate

The climate at Yucca Mountain for the past approximately 50,000 years was assumed to characterize future climates at the proposed repository site. Variation in precipitation and temperature in the Yucca Mountain vicinity was no more than a few degrees Celsius (°C) decrease in temperature, accompanied by an up to 40 percent higher than present (ca. 150 millimeters annually) precipitation. To ensure a conservative analysis in IPA Phase 2, pluvial scenarios were incorporated by assuming an increase in infiltration from the possible wetter climatic conditions associated with likely cooler temperatures in the next 10,000 years. The conservative increase in infiltration was modeled by assuming a higher range for infiltration (5.0 to 10.0 millimeters/year in future scenarios, versus 0.01 to 5.0 millimeters/year for the base case (*oooo*)). Associated with the increase in infiltration was a rise of 100 meters in the water table, resulting in a decrease in the thickness of the unsaturated zone. The increased infiltration values and associated rise in the water table were within the values espoused in Czarnecki (1985). Thus, the approach to treating climate change in the development of performance assessment scenarios in IPA Phase 2 was essentially the same as that used in IPA Phase 1 (see Codell *et al.*, 1992; p. 57). Further discussion of the treatment of climate change within the modeling effort can be found in Chapter 4.

6.3 Improved Drilling Model and Code

6.3.1 Introduction

The techniques used in the Phase 2 drilling modules differ from those used in IPA Phase 1. The releases in IPA Phase 2, resulting from drilling, are determined using a series of geometric arguments and radionuclide inventories in the waste packages within each region of the repository and the rock columns encompassing the repository and extending down to the water table. The number of drilling events for each trial was sampled from a normal distribution as an approximation to a Poisson distribution. Each event was assumed to occur independently of any other drilling events and to occur randomly in time and space.

Table 6–1 List of Disruptive Events, Their Corresponding LHS Parameters, and Whether Release of Radionuclides Associated with the Event Occurs Directly or Indirectly

Event	*Type of Treatment*[a]	*LHS Parameter(s)*	*Mechanism of Release to the Accessible Environment*[b]
Climate	V	– Infiltration at surface	Indirect
Drilling	M	– Number of boreholes – Borehole radius, location, time of drilling – Statistical hit indicator	Direct, Indirect
Seismic	M	– Statistical failure indicator	Indirect
Magmatism – Cone – Dike	M	– Location, time of event – Area – Area, length, angle.	Direct, Indirect

[a]V = change input parameters; M = one or more additional models.

[b]Indirect = release by liquid or gas pathway only, enhanced by potentially early failure of waste package;
Direct = release of contaminated rock directly to surface.

6.3.2 Model for Release of Radionuclides from the Rock Column

As noted earlier, the geologic repository was divided into seven different sub-areas, as shown in Figure 4–6, and was modeled using vertically emplaced waste packages, and assuming vertical boreholes only. IPA Phase 2 adopted the repository layout of Johnson and Montan (1990) for the number of waste packages in each of the seven repository sub-areas, as shown in Figure 5.4. The number of waste packages per repository sub-area is given in Table 6–2. The probability of a drilling event directly striking a waste package depends on the number of packages per repository sub-area, the cross-sectional area of the sub-area, and the size of the incident borehole. For IPA Phase 2, the boreholes are assumed to be vertical, extending from the surface to the water table. The vertical boreholes, however, do not establish new pathways for either the transport of gas to the surface, or of liquid to the water table. Furthermore, there is considered to be no physical transport of waste from the repository to the water table by the drilling process itself, although radionuclides are assumed to be transported to the surface in drill cuttings.

The model assumes that radionuclides released from a waste package will migrate vertically through one of seven rock columns underlying the repository, where each rock column corresponds to a repository sub-area, until they reach the water table. Within the water table, transport is assumed to be horizontal along the regional ground water gradient. In the unsaturated zone, the model assumes that all transport is confined to the rock columns, with no horizontal transport by diffusion or dispersion. For the drilling model, all radionuclides are assumed to be confined to either the waste packages, the rock column between the surface of the earth and the water table, or in the water table itself. This inventory is corrected for radioactive decay, but not for losses to the earth's surface.

Each drilling incursion has the potential to release radionuclides that were confined to either the rock column *(RC)* or the waste package. The module keeps track of the radionuclide inventories within the waste packages (for each sub-area) and each of the seven rock columns. Since the drilled hole extends all the way to the water table, $I^{R}_{i,\,k,\,RC_i}(t_b)$, the content of radionuclide i in a borehole in rock column k would be the amount

Table 6–2 The Distribution of Waste Packages by Repository Sub-Area

Repository Sub-Area	*Surface Area (km^2)*	*Number of Waste Packages*
1	0.31	2335
2	1.40	6150
3	1.10	4875
4	0.66	3675
5	0.26	1275
6	1.20	5625
7	0.20	1073
Total	5.13	25,008

present in the rock column at the time of the drilling event, $I_{i,k,RC}(t_b)$, times the ratio of the borehole cross-sectional area A_b to that of the rock column $A_{k,RC}$ and can be written as:

$$I^R_{i,\,k,\,RC_i} = \frac{A_b\ I_{i,k,RC}\,(t_b)}{A_{k,RC}}\ , \qquad \textbf{(6–1)}$$

where $I^R_{i\,,\,k,\,RC}\,(t_b)$ is the total inventory released from the rock column through the drilling event that occurred at time t_b, and N is the number of radionuclides.

For instance, where the borehole intersects a waste package, the inventory released includes radionuclides from the EBS and from the rock column. As a conservatism, any direct hit of a waste package assume that the entire borehole intersects that package. The amount released for each repository sub-area through a drilling event that intersects a waste package can be expressed as:

$$\begin{aligned} I^R_i &= I^R_{i,\,k,WP} + I^R_{i,\,k,RC} \\ &= \frac{A_b\ I_{i,k,WP}\,(t_b)}{A_{WP}} + \frac{A_b\ I_{i,k,RC}\,(t_b)}{A_{k,RC}}, \end{aligned} \qquad \textbf{(6–2)}$$

where I^R_i is the inventory of radionuclide i released, $I^R_{i\,,\,k,\,WP}$ is the amount of radionuclide i released from the waste package, A_{WP} is the cross-sectional area of the top of the waste package, and $I_{i,k,WP}(t_b)$ is the inventory of nuclide i in a waste package, within region k of the repository at time (t_b).

6.3.3 Consequences

The drill hole, itself, does not establish any new pathways either to the atmosphere or the water table; the only effect of drilling on liquid and gaseous releases would be through the premature failure of the waste package. However, the drilling model does consider the direct release of contaminated rock at the surface of the earth, contributing to the cumulative release at the accessible environment. Additionally, the model takes into account the assumption that a fraction of the radionuclides in the drill cuttings is capable of becoming airborne and respirable, which has been conservatively estimated to be about 4 percent of that brought to the surface. These respirable releases are factored into the dose model described in Chapter 7. The drilling events are still modeled somewhat simplistically and, as such, may not be fully conservative.

The probability of drilling incursions into the repository was estimated to be 0.0003 boreholes/square kilometer/year, and was based on the guidelines outlined by the U.S. Environmental Protection Agency (EPA) (see Appendix B in EPA, 1985). This translates into approximately 15.4 events within the repository horizon in 10,000 years (the period of regulatory concern). A

Poisson distribution of drilling events, approximated for convenience by a Gaussian normal distribution with $\sigma = 3.88$ and $m = 15.5$, was used in the analysis and can be expressed as:

$$P(Z) = \frac{e^{\left(-\frac{|Z-m|^2}{2\sigma^2}\right)}}{\sigma\sqrt{2\pi}} \qquad (6\text{–}3)$$

6.3.4 Hit Probability

The consequences also depend on whether the borehole intersects a waste package. The radii of the boreholes were held constant over a given realization and were sampled from a uniform distribution between 0.02 and 0.1 meters. The incident region was determined for each borehole by weighting the probability of penetrating a given region by its relative size. The time of occurrence was uniformly distributed over a range of 100 to 9900 years, for each borehole. The stated range includes the effects of drilling up to 10,000 years, and a nominal period of 100 years for active control over the site. The chance of striking a waste package in region k of the repository, assuming that no waste package is within $2r_b$ from another, can be expressed as:

$$P_k\,(hit) = \frac{n\pi\,[(r_b + r_{WP})]^2}{A_{k,RC}}\ , \qquad (6\text{–}4)$$

where $P_k(hit)$ is the probability of a hit, n is the number of waste packages within the region, and r_b and r_{WP} are the radii of the borehole and the waste package, respectively. The values of n are given in Table 6–2. If a uniformly sampled parameter, $[0,1]$, is within the range of $[0,P_k(hit)]$, then the borehole intersects a waste package.

6.3.5 Radionuclide Inventory Determination

The inventory of radionuclides in the rock in each of the seven repository sub-areas depends on the initial inventory, radioactive decay, and the transport out of the area by water and gas flows. The inventory of radionuclides in the intact waste packages can be determined easily by considering initial inventory and radioactive decay, alone. *SOTEC* also keeps a running inventory of the radionuclides, for failed waste packages, considering transport by diffusion and flow. The inventory of radionuclides in the rock column is more problematic, however, because there is incomplete information on radionuclide releases from *SOTEC* available to the drilling module. One approach to modeling the inventory is to develop a series of differential equations and to allow continuous and arbitrary time functions for the addition and the removal of mass from the rock columns.

The approach that was used in IPA Phase 2 is better suited for use, and simpler to integrate, with the limited information available from *SOTEC*. The differential equation for the inventory I_i in the rock column is:

$$\frac{dI_i}{dt} = -\lambda_i I_i + \lambda_{i-1} I_{i-1} + M_i(t)\ , \qquad (6\text{–}5)$$

where λ_i is the decay constant for nuclide i, and $M_i(t)$ is the rate of mass injection or removal of nuclide i from the rock column.

Given initial concentrations of each nuclide and no injection or removal of nuclides (i.e., $I_i(t = 0) = I_{i0}$ and $M_i(t) = 0$), then this equation simplifies to a series of coupled, linear, ordinary differential equations, generally known as the Bateman equations. Letting B_i designate the solution of the Bateman equation for nuclide i, the inventory I_i can be written as:

$$I_i(t) = B_i(t, \lambda_i, I_{i0})\ . \qquad (6\text{–}6)$$

Knowledge of the initial inventory of a given nuclide, I_{i0}, and its parent nuclides allows the inventory of nuclide I_i to be found at any time t. It is much more difficult to solve Equation (6–5) when mass is added to or withdrawn from the compartment. *SOTEC* calculates and outputs information on the rate of nuclide release from the EBS into the geosphere as a function of time. These values can be used to represent $M_i(t)$ for the EBS and will contribute to the $M_i(t)$ for the *RC*. The $M_i(t)$ for the *RC* is further complicated by the loss of mass to the accessible environment.

Let the rate of release of radionuclide i, from the EBS into the *RC*, be denoted by $f_i(t)$. *SOTEC* will output discrete values of $f_i(t)$ at times t_j, which may not be uniformly spaced. Let F_{ij} be defined

as $f_i(t_j)$, and it will be assumed that $F_{i0} = 0$ for all i.

There are several options to represent the release rate $f_i(t)$ from the point estimates F_{ij}. One option is to determine a curve fit to F_{ij}, which would require assumptions of linearity and continuity of the release rate from the *SOTEC* output. A second option would be to represent the source terms with a series of steps centered about the points $f_i(t)$. However, the method adopted for IPA Phase 2 simplifies the solution of the equations. This formulation adds and removes mass in instantaneous pulses, using the Dirac delta function. This technique avoids the introduction of new recursive relationships:

$$t_{L,j} = \frac{(t_j + t_{j-1})}{2} , \qquad \textbf{(6–7)}$$

$$t_{L,j+1} = \frac{(t_{j+1} + t_j)}{2} . \qquad \textbf{(6–8)}$$

Considering, for the time being, only mass withdrawal, which applies to the inventories in the waste packages, let:

$$\Delta t_{L,j} = t_{L,j+1} - t_{L,j} , \qquad \textbf{(6–9)}$$

$$M_i(t) = -f_i(t) = -\sum_{j=1}^{J} \delta(t - t_j)\Delta t_j F_{ij} , \qquad \textbf{(6–10)}$$

where $\delta\ (t - t_j)$ is the Dirac delta function and J is the total number of time steps.

This representation of the source term by a delta function makes the mass removal term zero for all $t \neq t_j$. The mass removal rate at $t = t_j$ is infinite. The integral of the constant rate, F_{ij}, over the interval Δt_j, is, however, $F_{ij}\Delta t_j$.

Consider a 2-member decay chain, where:

$$M_1(t) = -\sum \delta (t - t_j) F_{1j} , \qquad \textbf{(6–11)}$$

$$M_2(t) = -\sum \delta (t - t_j) F_{2j} . \qquad \textbf{(6–12)}$$

Using Laplace transformations, the solutions for the inventory of each radionuclide at an arbitrary time t, can be found:

$$I_1(t) = I_{10}e^{-\lambda_1 t} - \sum_{j=1}^{J} [H(t - t_j)] F_{ij} [e^{-\lambda_1 (t - t_j)}] , \qquad \textbf{(6–13)}$$

$$I_2(t) = I_{20}e^{-\lambda_2 t} + \frac{I_{10}\lambda_1}{(\lambda_1 - \lambda_2)} [e^{-\lambda_2 t} - e^{-\lambda_1 t}]$$

$$- \sum_{j=1}^{J} [H(t - t_j)]\ F_{2j}\Delta t_j\ (e^{-\lambda_2 (t - t_j)}) \qquad \textbf{(6–14)}$$

$$- \sum_{j=1}^{J} [H(t - t_j)]\ F_{1j}\Delta t_j \left[\frac{\lambda_1 (e^{-\lambda_2 (t - t_j)} - e^{-\lambda_1 (t - t_j)})}{(\lambda_1 - \lambda_2)} \right]$$

where $H(t–t_j)$ is the Heaviside step function at time t_j. It may be noted that for the I_2 solution, in this instance, that the relationships between the second and first terms are congruent to those of the fourth and third terms. Therefore, by superposition, the solution to the chain decay problem is given by:

$$I_i(t) = B_i(t,\ I_{l0},\ \lambda_l) , \qquad \textbf{(6–15)}$$

where $l = 1, ..., i$.

The solution to this problem is given by:

$$I_1 = B_i(t,\ I_{l0},\ \lambda_l)$$

$$- \sum_{j=1}^{J} [H(t - t_j)] B_i([t - t_j], \Delta t_j, F_{lj}, \lambda_l) , \qquad \textbf{(6–16)}$$

where $l = 1, ..., i$.

Modifying the theoretical development now to include mass being added and withdrawn from the compartment, requires modification to Equation (6–15) to:

$$M_i(t) = \sum \delta(t - t_j)[F_{ij} - G_{ij}] \ , \qquad \textbf{(6–16)}$$

where F_{ij} is the amount of mass added to the rock column, equal and opposite to the amount withdrawn from the EBS, and G_{ij} is the amount lost to the accessible environment. The solution for the inventory of nuclide i in the rock column is:

$$I_i = \sum_{j=1}^{J} [H(t - t_j)]B_i([t - t_j],\ \delta t_j[F_{ij} - G_{ij}]\ \lambda_i) \ , \qquad \textbf{(6–17)}$$

where $l = 1,..., i$.

6.3.6 Overview

The present formulation of the drilling consequences offers a limited degree of sophistication. It does not, nor does it intend to, consider the full range of expected consequences of a drilling event. The effect of drilling fluid has, for example, been neglected throughout the analysis, which introduces an element of non-conservatism into the analysis. Furthermore, the model assumes that the process of drilling does not create any additional pathways for liquid or gaseous releases. The conceptual models of the drilling events were selected, in part, to allow effective use of, and integration with, the other IPA Phase 2 models, and to avoid unnecessary complexity. In light of the uncertainties in other parts of the IPA Phase 2 analyses, and the relatively minor contribution of drilling to either cumulative releases or doses, the drilling model appears to have received an appropriate level of attention.

6.4 Improved Seismic Scenarios Model and Code

6.4.1 Introduction

The physical integrity of the waste package is modeled, for the case of no seismicity, as if corrosion will proceed until the thickness of the waste package material reaches a critical value. With seismicity, a presumably lesser degree of corrosion can cause waste package failure. Since all waste packages are considered to be identical in each repository sub-area, all of them would fail at a time earlier than the time of corrosion-induced collapse. The seismic analysis, therefore, calculates the time of failure for all the packages in the repository sub-area, which is less than the failure time of corrosion-induced failure. The critical thickness is calculated from models of pitting, crevice, and uniform corrosion, choosing the greatest corrosion depth from among the three without regard to the obvious differences in the likely effect of these processes on the mechanical strength of the waste packages.

The seismic analysis is embodied in the computer code *SEISMO* (see Freitas *et al.*, 1994). The seismic failure analysis relies on *SOTEC* for the depth of pitting and crevice corrosion. Premature failures of the waste packages are communicated back to the *SOTEC* code, to allow the release of radionuclides to commence sooner.

The *SEISMO* code determines the time step(s) during which waste package failure occurs. The probability that a seismic event of sufficient magnitude to cause waste package failure occurs (failure probability) is compared to an event indicator. If the event indicator, a random number ranging from zero to unity, is less than the failure probability, then it is assumed that seismicity during the time step is sufficient to cause premature waste package failure. The details of the calculation are presented in the succeeding sections. (See Table 6–3 for a description of the parameters used in the *SEISMO* code.)

6.4.2 Response of Waste Package to Seismic Shaking

The waste package is considered to be a hollow, slender, elastic cylinder of length L standing vertically, and attached at the bottom to the ground, as illustrated in Figure 6–1.

The moment of inertia of the cylinder, I, given by:

$$I = \frac{\pi}{4}[R^4 - (R - d)^4] \approx \pi R^3 d \ , \qquad \textbf{(6–18)}$$

where R = outer radius of cylindrical waste package, and d = thickness of cylinder walls.

The spring constant K is given by:

$$K = \frac{3EI}{L^3} \ , \qquad \textbf{(6–19)}$$

Table 6–3 Parameters Used in the *SEISMO* Code

Parameter Name	*Symbol*	*Description*	*Nominal Value and Units*
pacleng	L	package length	4.7625 m
pacrad	R	package radius	0.3302 m
pacthik	d	package thickness	0.01 m
dampfac	ξ	damping factor	0.03
elasmod	E	modulus of elasticity of package material	2.0×10^{11} N/m^2
densss	ϱ_{ss}	density of stainless steel	7.75×10^3 kg/m^3
wmass	M_w	mass of waste per package	6.4×10^3 kg
freqacc	ω_a	seismic wave frequency	5 hertz
widthag	w_{ag}	size of the air gap	0.0381 m

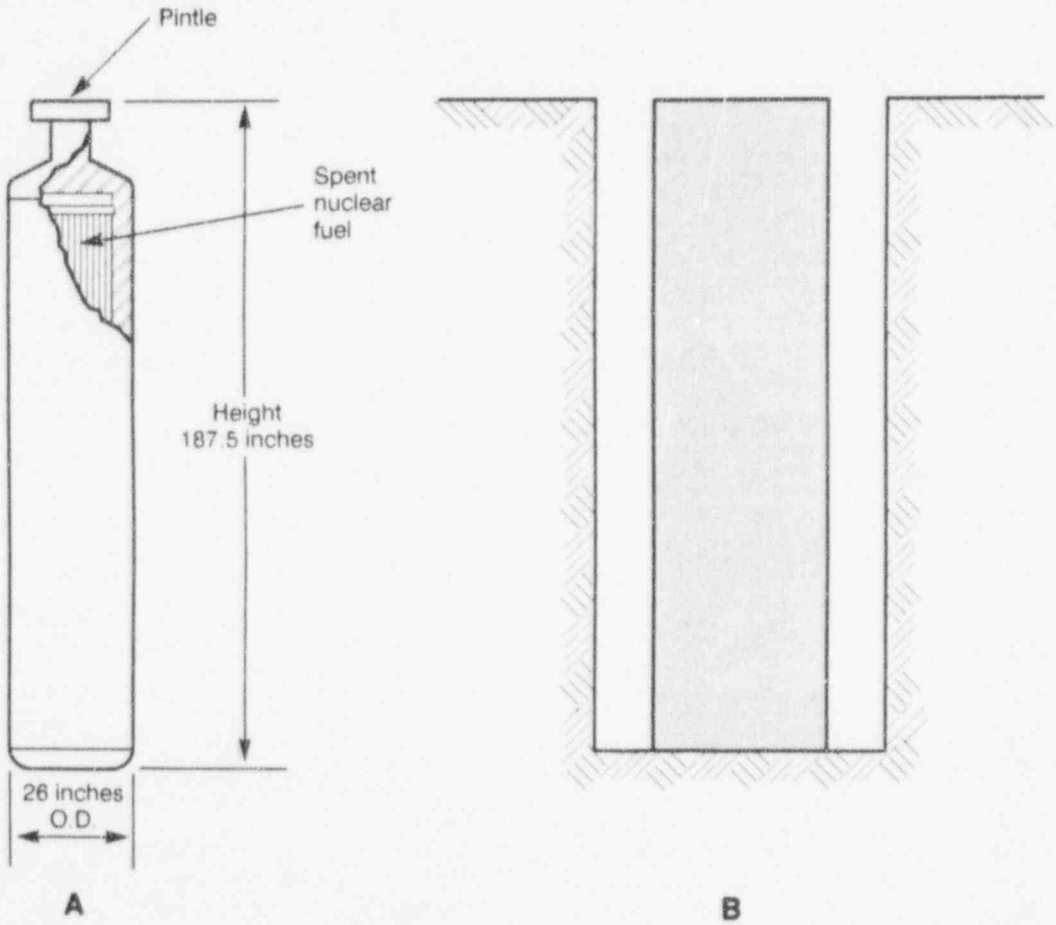

Figure 6–1 Representation of waste package canister for improved seismic scenarios model ((a) SCP disposal container concept for spent fuel (from DOE, 1988; p. 50). (b) IPA Phase 2 waste package representation.)

where E = elastic modulus and L = length of waste package.

Assuming that the cylinder is thin-walled, the volume of metal in the top or bottom ends of the waste package V_e is given by the expression:

$$V_e = \pi R^2 d. \quad \textbf{(6–20)}$$

The volume of the side V_s is given by:

$$V_s = \pi [R^2 - (R - d)^2] L. \quad \textbf{(6–21)}$$

The total volume V_T is given by:

$$V_T = 2 V_e + V_s. \quad \textbf{(6–22)}$$

The mass of the waste package is therefore:

$$M_p = V_T \varrho_{ss}, \quad \textbf{(6–23)}$$

where ϱ_{ss} = density of stainless steel.

The total mass is the sum of the waste package mass and the waste mass,

$$M_T = M_w + M_p. \quad \textbf{(6–24)}$$

The natural frequency of the undamped system is:

$$\omega_n = \left[\frac{K}{M_T/2}\right]^{\frac{1}{2}} . \quad \textbf{(6–25)}$$

Half the total mass is used in this calculation, because a simple lumped-system model of the waste package and its contents would be for half the total mass at the end of the cantilever and half at the bottom. The mass at the bottom is assumed to travel with the ground, so it does not enter into the calculation.

The excitation frequency (i.e., the frequency of the ground motion) is an input parameter chosen for this seismic analysis to be similar to the resonant frequency of the object involved; in this case, the excitation frequency was chosen to be 5 hertz. The amplitude of the ground motion is a function of the excitation frequency, and, for the present analysis, has been taken from regional seismic data in the vicinity of Yucca Mountain (URS/Blume, 1986). The ratio of the excitation frequency to the resonant frequency is defined:

$$\Omega = \omega_a/\omega_n . \quad \textbf{(6–26)}$$

For the nominal waste package parameters, the natural frequency of the waste package will start off much higher than the excitation frequency, but declines as the metal thickness is reduced by corrosion. As an added conservatism in the model, the natural frequency is not permitted to decrease below the excitation frequency (i.e., $\Omega > 1$).

Let the displacement of the center of the mass be denoted by $x(t)$, the motion of the ground by $x_g(t)$, and the relative motion of the mass with respect to the ground (and the emplacement hole) by $x_r(t)$. Then,

$$x_r(t) = x(t) - x_g(t). \quad \textbf{(6–27)}$$

Further, since the analysis was interested in the harmonic motion solution, these functions are written in the form:

$$x_g(t) = A_g \sin(\omega_a t), \quad \textbf{(6–28)}$$

$$x_r(t) = A_r \sin(\omega_a t - \phi), \quad \textbf{(6–29)}$$

where A_g and A_r equal the amplitude of the ground and waste package displacement, respectively, and ϕ is the phase difference between ground and waste package movement.

For a simple spring mass system with damping associated with the velocity term, we find that:

$$\frac{A_r}{A_g} = \frac{\Omega^2}{[(1-\Omega^2)^2 + (2\xi\Omega)^2]^{\frac{1}{2}}} , \quad \textbf{(6–30)}$$

where ξ is the damping factor accounting for frictional forces opposite the direction of motion of the center of mass.

Since we are assuming sinusoidal motion, we obtain, by differentiating Equation (6–28) twice:

$$\ddot{x}_g(t) = -\omega_a^2 x_g(t) = -\omega_a^2 A_g \sin(\omega_a t) . \quad \textbf{(6–31)}$$

Further, we may take the peak ground acceleration a to be equal to the amplitude of the acceleration of the seismic wave, that is:

$$a = \omega_a^2 A_g . \quad \textbf{(6–32)}$$

Then, the maximum displacement A_r is:

$$A_r = \frac{a}{\omega_a^2} \frac{\Omega^2}{[(1-\Omega^2)^2 + (2\xi\Omega)^2]^{\frac{1}{2}}} \quad . \tag{6-33}$$

6.4.3 Waste Package Fragility

The waste package canister is assumed to fail if one of the following conditions occurs:

- The stress at the base exceeds the yield strength of the waste package material (Mode 1 failure), or;
- The motion induced in the end of the waste package is great enough to impinge on the side of the emplacement hole, thereby buckling the waste package (Mode 2 failure).

Failure by Mode 1.

Failure by Mode 1 is induced when the magnitude of the vibration of the waste package becomes so great that the stress at the base (which is assumed to be a cantilever support—hence stress is greatest at the base) exceeds the yield strength of the waste package material. Consider the forces at the base of the spring-mass system used to represent the waste package. The force F_M exerted by the movement of the mass at the free end of the cantilever beam can be derived from the definition of the spring constant:

$$F_M = -K x_r \quad , \tag{6-34}$$

where x_r = deflection.

Then by using the formula for the spring constant, Equation (6–19), the moment M_A at the base is given by:

$$M_A = LF_M = -\frac{3\,EIx_r}{L^2} \quad , \tag{6-35}$$

and the stress at the base is given by:

$$\sigma_A = M_A \frac{L}{I} = -\frac{3\,Ex_r}{L} \quad . \tag{6-36}$$

Since we are interested in the maximum stress, hence the maximum deflection, we can replace x_r with A_r, to obtain:

$$\sigma_A = 3\frac{EA_r}{L} \quad . \tag{6-37}$$

A failure will occur if $\sigma_A \geq \sigma_Y$, that is:

$$A_r \geq \frac{L\sigma_Y}{3E} \quad , \tag{6-38}$$

where σ_Y is the stress at the yield point.

Failure by Mode 2.

Failure by Mode 2 is induced when the motion of the end of the waste package is so great that it impinges on the side of the emplacement hole, thereby buckling the waste package. For failure to occur by this mechanism, two conditions must be met:

(1) The displacement of the end of the waste package must be large enough so that the package hits the side of the emplacement hole; and

(2) The force induced by this impact is great enough to buckle the side of the waste package.

For Condition (1) we can merely compare the amplitude of the displacement, given by Equation (6–33) with the magnitude of the air gap, ω_{ag}, which is read in as data. The 1988 Site Characterization Plan design calls for a 3.81 centimeter-air gap all around the package (see DOE, 1988). Thus,

$$A_r \geq w_{ag} \tag{6-39}$$

implies a failure could take place by this mechanism. For the IPA Phase 2 version of the model, the staff conservatively assumed that any contact of the waste package with the side of the borehole will lead to failure.

6.4.4 Computational Algorithm for Seismic Failure of Waste Packages

At each time step, input on the corroded thickness of the waste package is supplied by *SOTEC*.

The thickness of the waste package metal is chosen from the largest corrosion depth calculated from models for pitting, crevice, or general corrosion. The strength of the remaining material, however, is conservatively calculated, assuming that the entire surface corrodes uniformly to the calculated depth, irrespective of which model (pitting, crevice, or general corrosion) gave the greatest depth of corrosion.

Given the thickness of the metal and the parameters presented in Table 6–3, the critical displacement of the waste package A_{rc} is calculated for Mode 1 or Mode 2 failure mechanisms, Equations (6–33) or (6–39), respectively. The smaller of the two amplitudes is then used to determine at what acceleration the waste package would fail.

The fragility f corresponds to the acceleration in g's needed for the smaller amplitude:

$$f = A_{rc} \frac{\omega_a^2 \left[(1-\Omega^2)^2 + (2\xi\Omega)^2\right]^{\frac{1}{2}}}{9.81\ \Omega^2} \qquad \textbf{(6–40)}$$

The fragility f has a corresponding annual rate of recurrence r_a, derived from a curve fit to a published relationship at Yucca Mountain (URS/Blume, 1986), that includes all events sufficient to cause displacements equal to or greater than the critical displacement. The fragility can be expressed as follows—

for $f < 0.1$ g:

$$r_a = 0.01 \text{ [occurrences/year]}, \qquad \textbf{(6–41a)}$$

for $0.1 < f < 4$:

$$\log_{10}(r_a) = a_0 + a_1 l + a_2 l^2 + a_3 l^3 + a_4 l^4 + a_5 l^5 + a_6 l^6 , \qquad \textbf{(6–41b)}$$

where $l = \log_{10}(f)$:

$a_0 = -4.67174$, $a_1 = -4.16482$, $a_2 = 1.91376$, $a_3 = 3.75132$, $a_4 = -3.06375$, $a_5 = -2.04791$, $a_6 = 1.65667$.

for $f > 4$:

$$r_a = 0 \text{ [occurrences/year]}. \qquad \textbf{(6–41c)}$$

An approximation of the probability that the failure occurs within the time step t to $t + \Delta t$ is approximated from the annual rate of recurrence r_a to be:

$$p\Delta t = 1 - (1 - r_a)^{\Delta t} , \qquad \textbf{(6–42)}$$

where Δt is number of years in the time step.

Whether or not the failure occurs during a particular time step is a matter of chance. In the present model, the failure probability $\{p\Delta t\}$ is compared with a number U between zero and unity, selected randomly from a uniform distribution. If the random number is less than $\{p\Delta t\}$, the waste package is assumed to fail. The random number is sampled once per vector from the main sampling routine, to keep all randomness in the control of the system-level program. Although it would appear that the random number U should be sampled for each time step within the vector, numerical experiments with the model indicate that the results are about the same statistically for either case, given a sufficiently large number of vectors.

6.4.5 Estimating Probability of Seismic Failure Scenario

The task of this section is to define an acceleration and its probability below which there would be no perceptible difference between failure and no-failure by seismic forces.

Since the system code calculations are discretized in time, anything happening in less than one time step is below our ability to discern its cause. The curve of waste package thickness vs. time from the corrosion model is very steep and fairly insensitive to the environmental conditions, once corrosion commences. Figure 6–2 is a typical set of curves describing the decrease in metal thickness, with time, for the seven repository sub-areas. The thickness θ_f for six of the repository sub-areas is 9.8×10^{-4} meters, 50 years before failure.

The natural frequency ω_n at failure, can be calculated from Equations (6–18), (6–19), and (6–25), by

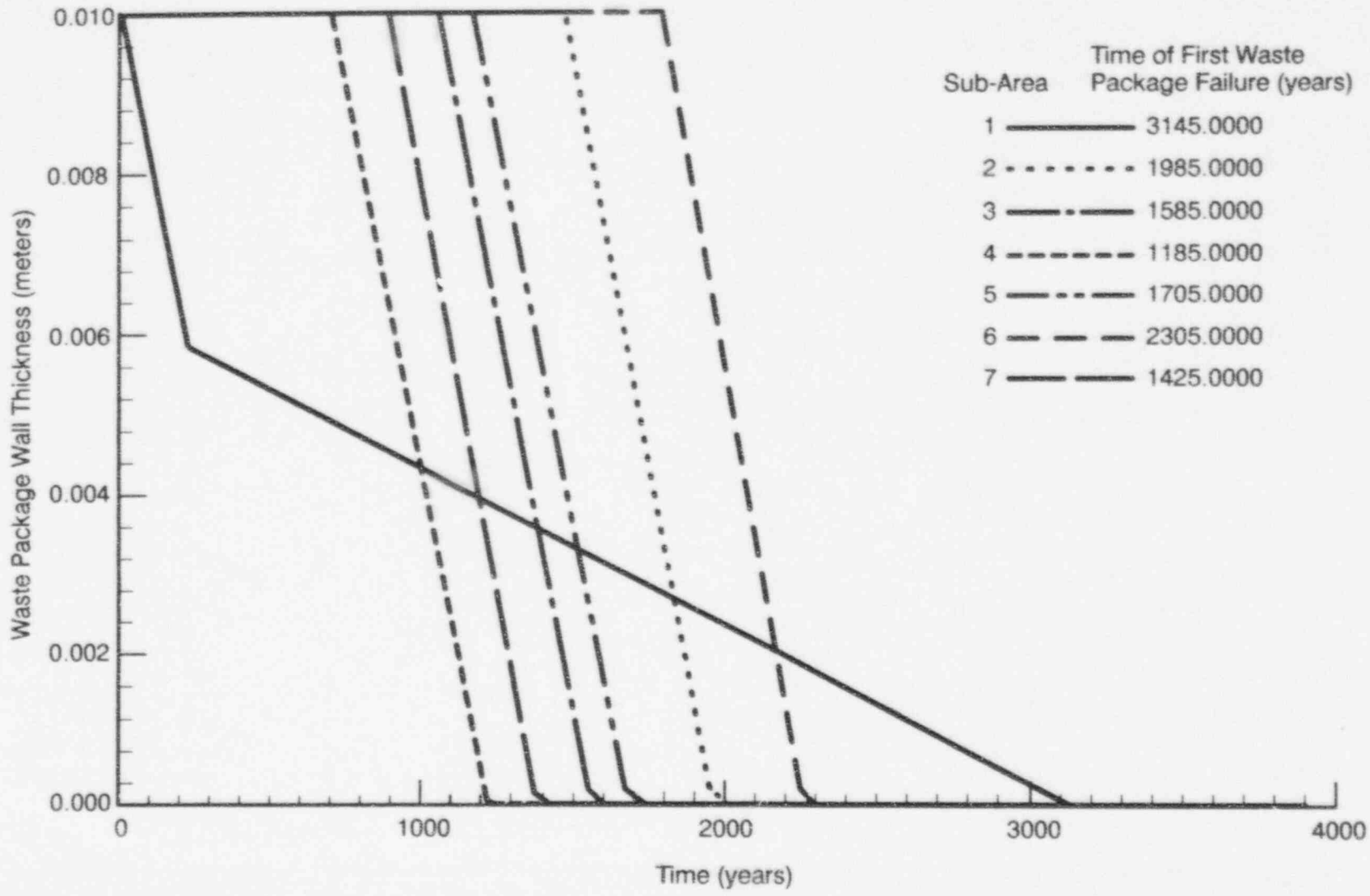

Figure 6–2 Waste package canister thickness versus time for seven repository sub-areas for the base case *(oooo)* scenario

substituting θ_f for d. For the assumed model parameters of R = 0.33 meters; L = 4.7 meters, ω_a = 5 hertz; $E = 2 \times 10^{11}$ Newtons/square meter; $\sigma_a = 2.067 \times 10^8$ Newtons/square meter; the mass of the fuel plus waste package M_i = 2925 kilograms; thickness θ_f (50 years before failure) = 9.8×10^{-4} meters; and the natural frequency from Equation (6–25) = 13.9 hertz, or $\Omega = \omega_a / \omega_n$ = 0.36.

In most cases, the waste package fails first by failure Mode 1, so one can write:

$$A_r = \frac{\sigma_a L}{3E} = \frac{a}{\omega_a^2}\left[\frac{\Omega^2}{[(1-\Omega^2)^2 + (2\xi\Omega)^2]^{1/2}}\right] \quad . \qquad \textbf{(6–43)}$$

The acceleration needed for the waste package to fail is:

$$a_f = \frac{\sigma_a L \omega_a^2}{3E} \; \frac{[(1-\Omega^2)^2 + (2\xi\Omega)^2]^{1/2}}{\Omega^2} \qquad \textbf{(6–44)}$$

Evaluating Equation (6–44) for the resonance ξ and ξ = 0.03 gives an acceleration of only 0.028 g. Earthquakes of this magnitude would be expected to be very frequent. Equation (6–41) gives a default annual recurrence rate of 0.01/year. Conversely, the expectation of no earthquakes of this magnitude in 10,000 years would be vanishingly small:

$$\{p\Delta t\}_{(no\ seismic\ failure)} = (1-0.01)^{10,000}$$

$$= 2 \times 10^{-44} \quad . \qquad \textbf{(6–45)}$$

6.5 Improved Magmatic Scenarios Model and Code

6.5.1 Introduction

This section describes models and codes that have been used to simulate magmatic activity for the IPA Phase 2 consequence analysis. Magmatic scenarios are important for performance assessment because some repository material may be ejected onto the earth's surface if a magmatic event penetrates the repository during a volcanic eruption (Valentine *et al.*, 1992). Even in the absence of actual eruption of waste, subsurface magmatic effects may also affect repository performance. In the case of intrusive events that occur within the repository area, dikes emplaced through and above the repository may damage the waste packages. In addition, dikes or sills below or in the repository horizon could affect the repository by producing hydrothermal processes or altering hydrology. The effects of intrusive dikes on the regional hydrology are presented in Appendix E. For the parameters chosen in the model, the model predicts a potential water table rise of over 100 meters for the case of two perpendicular dikes. The main effect of the intrusions would be to decrease the distance between the repository and the water table, but increase the travel time in the saturated zone. Hydrothermal processes could cause rapid corrosion of waste packages. As a result, radionuclides could be transported to the accessible environment by either ground-water flow or gaseous release. The hydrologic properties of the dike itself may produce important changes in the long-term flow of ground water.

Two areas of current investigation that are critical to consequence models are: (i) the mechanics of cinder cone eruptions, the duration of these eruptions, and the areal distribution of vents at active cinder cones, and; (ii) the secondary effects of volcanism, including the effects of diffuse degassing and thermal loading on waste package performance, geochemical transport, and groundwater movement. Many of these volcanic processes are incompletely characterized. For example, recent studies at historically active cinder cones indicate that these eruptions are, under some circumstances, considerably more energetic than normally inferred. During the 1992 eruption of Cerro Negro, Nicaragua, volcanic ash rose to much higher altitudes and was dispersed over a greater area than is typical for mafic eruptions. Although this volcano is in a magmatic arc, the rheological properties of its magmas are similar to those of Lathrop Wells (Connor and Hill, 1993). These data suggest that cinder cone eruption mechanics and their impact on waste entrainment and dispersal must be investigated more fully. The secondary effects of degassing and cooling of cinder cones are long-term processes, and their impact on repository performance also will need to be more fully integrated into future IPA models, as studies progress.

Two approaches have been used previously to model volcanism consequences related to damage of the repository and release of waste (Crowe *et al.*, 1983; Valentine *et al.*, 1992; Sheridan, 1992; and Margulies *et al.*, 1992). The first method involves development of a geometric model to estimate the amount of waste entrained in an ascending dike during both intrusive and extrusive events (Sheridan, 1992; and Margulies *et al.*, 1992). In this model it is assumed that the amount of waste entrained is directly proportional to the size of the dike. In the second approach, the likely amount of waste entrainment is estimated by considering the abundance of shallow crustal xenoliths identified at volcanoes near the repository site and at other cinder cones in the Great Basin (Crowe *et al.*, 1983). The basic premise in this approach is that the amount of waste entrained should be proportional to the lithic fraction in scoria cones, should a basaltic eruption occur through the repository. For IPA Phase 2, the geometric approach was adapted to develop the magmatic consequence model and code.

In the magmatic consequence model, the number of waste packages damaged is computed from the area of the repository intercepted by the ascending magma. Only one igneous event, either an intrusive (modeled as a dike only) or an extrusive event (modeled as a coincident dike and cone), is assumed to occur during each simulation run. It was assumed that all radioactive waste affected by the dike is released to the surface of the earth through the cinder cone, for extrusive events. For intrusive events, the magma is assumed to compromise the intercepted waste packages, leading to early failure, but not providing additional gas or liquid pathways for radioactive release.

6.5.2 Relevant Literature

The volcanic release probability at Yucca Mountain region during the period of regulatory concern for a potential repository has been studied by Crowe *et al.* (1982; 1983; 1992). The volcanic release probability was examined in these studies as the product of three factors: (i) the probability that a volcanic event will affect the repository site; (ii) the temporal probability of a volcanic event; and (iii) the probable amount of release of radionuclides because of a volcanic event. However, these studies underestimated some parameters in the consequence analysis, such as erosion depth, conduit shape, speed of entrainment, and total lithic fraction.

The effects of volcanism on performance of the potential Yucca Mountain radioactive waste repository were studied by Crowe *et al.* (1983) and Valentine *et al.* (1992). They adapted the implicit assumption of the geometric model that the amount of waste entrained is directly proportional to the size of the dike. Valentine *et al.*, then estimated the amount of waste entrained from the total volume of erupted lithics and the volume of repository intercepted by the dike.

Sheridan (1992) used Monte Carlo simulation to estimate the probability of occurrence of future volcanic dikes in the vicinity of Yucca Mountain. His model incorporates the geometric approach and addresses only the spatial probability of the various volcanic scenarios. In this model, the volcanic field defining the area in which dikes can occur is approximated by an elliptical outline. The centers of the dikes are distributed according to a bivariate Gaussian distribution centered in the middle of the volcanic field. The geometric parameters of dikes are specified by a mean value and a standard deviation. After each dike is located, the length and orientation are chosen from the Gaussian distributions specified by the mean and standard deviation. Because the location of dike centers and the dike geometry are generated independently, it is possible to have a dike field oriented in a different direction away from the orientation of the elongated volcanic field. This study sets upper bounds on the probability of intersection of dikes with the repository. Using this technique, Sheridan estimated that the worst-case probability of a volcanic dike intersection with the repository in the next 10,000 years is between 0.001 and 0.01.

Using a Monte Carlo simulation approach, Margulies *et al.* (1992) estimated the areal extent that a basaltic dike or volcanic cone intercepts the repository, by assuming the occurrence of magmatic activity in the region near the repository. The magmatic events modeled were represented by planar geometrical figures. Cones were represented as disks, and dikes were represented as rectangles. The repository area and borders were represented realistically in the simulations. Based only on geometry, Margulies *et al.* obtained the estimates of radionuclide release by assuming that

any radioactive waste intercepted by the magma would result in release of radionuclides to the accessible environment.

Margulies *et al.* (1992) assume an inhomogeneous Poisson model for the occurrence of a magmatic event. The probability of magmatism was uniform within simulation regions, but could vary between regions in their study. Similarly, the rate of occurrence of magmatic events was allowed to vary discretely in time. The vent distribution in the Yucca Mountain area indicates a clustering of vents (Connor and Hill, 1993). From geologic evidence and theory, the probability of magmatism is not likely to be constant in time in the vicinity of Yucca Mountain (Trapp and Justus, 1992). Important geological information, such as the temporal and spatial variation in the rate of magmatism, therefore, remains to be incorporated into the geometric approach of simulating magmatic events in the repository site.

6.5.3 Description of Modeling Approach

6.5.3.1 Introduction

The geometric approach used is an extension of the work by Margulies *et al.* (1992). In the geometric approach, Monte Carlo sampling was used to estimate the areal extent that a basaltic dike or a volcanic cone intercepts the repository. From a probabilistic point of view, magmatic events are distributed in both space and time. For the purposes of IPA Phase 2, an estimate of the probability of magmatism in the Yucca Mountain repository (over the next 10,000 years) is needed.

6.5.3.2 Simulation Procedure

In the Monte Carlo simulation, the staff considered a rectangular region surrounding the repository horizon. As shown in the simulation configuration of the repository (Figure 6–3), the repository is represented by a total of 17 rectangles. To obtain the simulation configuration of the repository, the outline of the perimeter of the proposed Yucca Mountain repository has been traced from actual drawings. The rectangles are further grouped into seven areas, also shown in Figure 6–3.

The simulation generates a volcanic event randomly in the simulated region. The volcanic event occurrence time is chosen randomly within the specified time period. The simulation chooses an intrusive magma event (with only a dike) with a probability 10 times that of an extrusive event (with a feeder dike and a cone) (Crisp, 1984). Cones are represented as circular disks, whereas dikes are represented as narrow rectangles. The dimensions of cones and dikes are selected by a random sampling procedure. The Monte Carlo simulation procedure for estimating the occurrence and consequences of a magmatic event is described below:

- Locate the centerpoint of a dike event or an extrusive event by random sampling.
- Determine geometry parameters (e.g., length, width, radius) by random sampling.
- Calculate the overlapped area in each repository cell and convert the area to number of waste packages, if a dike or a cone intercepts the repository.
- In the case of cones, calculate and output the radioactive release amount in this trial. For dikes, report number of affected waste packages to *SOTEC*.

In the procedure of determining geometry parameters, parameters are chosen randomly from a range of values, based on the available data. Margulies *et al.* (1992) assumed that the length of the rectangular dike ranges between 1000 and 4000 meters, and the dike width ranges between 1 and 10 meters. Therefore, the area of the rectangular dike varies between 1000 and 40,000 square meters. The area of the rectangular dike is chosen at random, in the code, as given by the following expression (*op cit.*):

$$A = a^{(1-\mu)}\, b^{\mu} \quad , \tag{6–46}$$

where a = 1000 square meters is the minimum area, b = 40,000 square meters is the maximum area, and μ is a random number chosen uniformly between 0 and 1. The probability density function of A for uniformly distributed μ is skewed toward the smaller areas.

After the dike area is chosen, the length is chosen at random between $max\{c, A/f\}$ and $min\{A/e,d\}$, with equal probability. The corresponding width

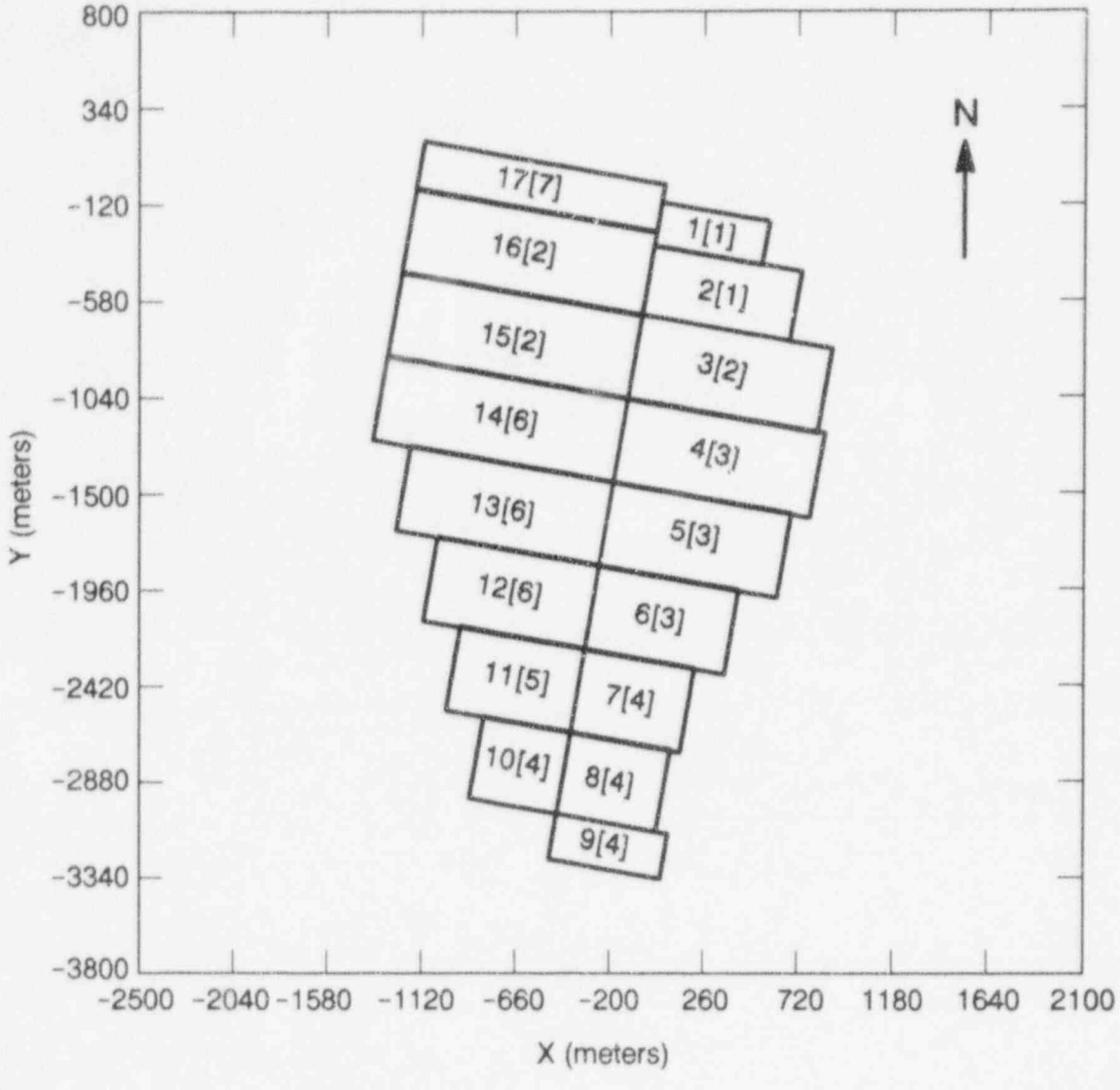

Figure 6–3 Configuration of the geologic repository in the magmatic scenarios simulation (The repository is divided into seven sub-areas with a total of 17 rectangular panels. The number inside the brackets represents the sub-area number, and the number outside the brackets gives the panel number.)

of the rectangular dike W is then determined from the area A and length L, as $W = A/L$. Here the parameters c and d define the minimum and maximum length, respectively, whereas the parameters e and f define the minimum and maximum width, respectively. The values of these parameters in the code are:

c = 1000 meters (minimum length);
d = 4000 meters (maximum length);
e = 1 meter (minimum width); and
f = 10 meters (maximum width).

This randomly generated rectangular dike has an angle of orientation that is chosen at random with equal probability between two angles specified in the input. Typically, the input parameters for the angles are chosen to be 75° and 90° counterclockwise from the horizontal axis, corresponding to the dike orientations ranging from due north/south to north 15 degrees east. However, this distribution of dike orientation is based on a postulate by Smith *et al.* (1990), Ho (1990), and Ho *et al.* (1991), that there is a NE-trending structural control on vent distribution within the "area of most recent volcanism" (AMRV). Crowe and Perry (1989) have delineated a different area, the "crater flat volcanic zone" (CFVZ), that extends north-northwest from the buried Amorgosa Valley vents, located about 35 kilometers south of Yucca Mountain, to those at Sleeping Butte, about 65 kilometers northwest of the site.

To simulate the formation of volcanic cones through extrusion events, circular areas are used to represent cones. Since we are interested in the effect of the volcano on the subsurface repository, these circular areas more properly represent the stem-like conduit of magma feeding the volcanic eruption, which may intersect the repository. The cone radius then corresponds approximately to the radius of the approximately vertical, nearly circular magma conduit. The radius of the volcanic cones is chosen uniformly at random between two input parameters, the minimum and maximum cone radii. Margulies *et al.* (1992) have chosen the minimum and maximum radii to be 25 and 100 meters, respectively. Currently the simulation adapts the parameters chosen by Margulies *et al.* However, the minimum and maximum radii chosen in the simulation appear to be unrealistically small. The smallest cones in the Yucca Mountain area have basal radii varying from 250 meters for Lathrop Wells and Little Black Peak, to 300 meters for Hidden Cone (e.g., Crowe *et al.* 1983). Future simulations should address more realistic values for the cone radii.

The program calculates the area of intersection between the dike and the repository by strictly geometrical computations. For an extrusive event, it also calculates the area of intersection between the cone and the repository. The predicted area of interception from the simulations is used to estimate the number of waste packages damaged, assuming a uniform distribution of waste packages within each repository cell. For extrusive events, upper bound and conservative estimates of radionuclide release into the atmosphere are calculated by assuming that the radioactive material damaged by the dike has been transported to the cone and a fraction of the transported material, 4 percent, released into the air. The amount of radionuclides released into the air is considered to be zero for intrusive events.

The simulation estimates the amount of release Q_k of radionuclide k to the atmosphere, for the extrusive event, by summing over the radioactive inventory at the time of the event,

$$Q_k = \sum_{j=1}^{n} N_j \, I_{jk}(t) \quad , \tag{6-47}$$

$$I_k(t) = I_k(0) \exp(-0.693t/t_k) \quad , \tag{6-48}$$

where N_j is the number of the damaged waste packages in area j, and I_{jk} is the inventory of k^{th} radionuclide in each waste package at time t in area j. This approach neglects the generation of radioactive progeny, which is non-conservative. The amount of radioactivity release for each radionuclide is used as input by the *AIRCOM* program, to calculate dose by the *DITTY* code (**D**ose **I**ntegrated over **T**en **T**housand **Y**ears). In addition, the number of damaged waste packages predicted by the Monte Carlo simulation is used by the *SOTEC* program to determine the release of waste in air and water. (See Section 2.1.3 for a description of these other total-system performance assessment (TPA) computer code modules.)

6.5.3.3 Assumptions and Limitations

Several assumptions are implied, in applying the geometric approach, to estimate the amount of waste entrained in an ascending dike, as discussed in Valentine *et al.* (1992). The Monte Carlo simulation model of basaltic igneous activity assumes: (i) any magma that intrudes into the repository will have a low volatile content; (ii) any igneous event will involve the intrusion of a single igneous dike; (iii) the repository itself will not affect magma flow or eruption dynamics; (iv) magmatic events are of relatively short duration; (v) ground water, possibly derived from a perched water table, will not interact with magma; and (vi) the probability of an intrusive event is 10 times that of an extrusive event. As the code is developed further, these assumptions will be explored in more detail.

The basic assumption that the amount of waste entrained in an ascending dike is determined by the dike size is justified if the magma intruding the repository has a low volatile content. High-volatile content magmas will likely erode wallrock during the eruption and thus entrain a larger volume of waste than what is calculated using a standard dike width.

The simulation results for magmatic activity are normalized according to the magma scenario probability and the area of the simulation region. The magma scenario probability, an input parameter to the TPA computer code, was determined from the work of Connor *et al.* (1993) and Connor and Hill (1993) (see Section 3.3.2.2 (A) for detailed discussion). They used a nonhomogeneous Poisson model calculated by near-neighbor methods to estimate the probability of volcanic disruption of a repository-sized area in the Yucca Mountain area over the next 10,000 years.

The simulation region used in the *VOLCANO* code (Lin *et al.*, 1993) is an assumed area of 12- by 12-square kilometers around the repository. The origin of the simulation region is the upper right corner of Area 7. In the simulation system, the x coordinate ranges from –6000 meters to 6000 meters, and the y coordinate from –7500 meters to 4500 meters. Because the maximum length of a dike is assumed to be 4000 meters, this simulation system is sufficiently large to ensure that it will include any magmatic events intercepting the repository.

The current simulation model has several limitations. At present, effects of faults on magma activity are not considered in the *VOLCANO* code. At least two faults are known to be located in the area: the Ghost Dance fault passing through the repository and the Solitario Canyon fault west of the repository. Faults may localize magma ascent in the shallow crust if fault orientation corresponds to the current orientation of principal crustal stress (Nakamura, 1977). All these faults could localize magmatism and may influence dike occurrence in the repository area. The *VOLCANO* code needs to be improved by including magma events related to these faults. The model also considers only radioactivity release for intrusive and extrusive events. The consequence analysis has not taken into account the interaction between intruding magma and a perched body of water around the repository. However, Appendix E discusses an auxiliary analysis that considers the effect on saturated ground-water flow and water table elevation, at the regional scale resulting from intrusive dikes. Finally, the simulation model has not included the possibility of multiple eruptions. There is evidence of multiple eruptions (polycyclic activity) at some of the Quaternary-age cinder cones in the Yucca Mountain area (e.g., Crowe *et al.*, 1992). The effects of this type of igneous activity remain to be included in the model.

6.5.3.4 Summary

A geometric simulation approach has been used to model the consequence of volcanism in the proposed repository. The model *VOLCANO* obtains the area of intersection between the repository and the area of an intrusive magma event occurring randomly in a region encompassing the repository. The actual geometry of the proposed Yucca Mountain repository is used as input to the model. Using the repository initial inventory as input, the area of interception is converted into the number of waste packages damaged from which the amount of radioactivity released into the atmosphere is calculated. The predictions of the *VOLCANO* model are used as input by the *AIRCOM* and *SOTEC* modules in the TPA computer code. The number of waste packages damaged by magma activity is used in computing the source term in the *SOTEC* module. The

results of the radionuclide release calculations are used in *AIRCOM* (described in Section 2.1.3) to calculate human dose, and in the TPA *executive module* (Sagar and Janetzke, 1993), to calculate the total release. A detailed description of the *VOLCANO* code and its output is given in the *VOLCANO* User Guide (Lin *et al.*, 1993).

6.6 Overall Conclusions and Suggestions for Further Work

A number of conclusions were drawn from the disruptive consequence analyses. These conclusions are summarized here, with specific recommendations for improvement during the next phase of IPA:

1—Improve model for climate change.

The current implementation for climate change is very simplistic, and should be updated. Currently, climate change is modeled as a change in the infiltration rate. The relationship between infiltration and increased precipitation should be investigated. In particular, DeWispelare *et al.* (1993) have compiled an expert elicitation about future climate at Yucca Mountain that may be used to improve the model. It is recommended that the climate change scenario take into account the most recent understanding of climate at Yucca Mountain and how climate relates to infiltration.

2—Drilling model: Consolidate calculations of radionuclide inventory.

The drilling code calculates inventory, using the Bateman equations, and determines the inventory for the time of the earliest drilling event. Greater efficiency may have been attainable by calculating the evolution of the inventory one time only. The calculated inventory could be used by the source term, drilling, seismic, and volcanic models, rather than being repeated in several different modules.

3—Drilling model: Allow multiple waste package failure times.

The effect of drilling is predicted to be small relative to the other releases calculated in IPA Phase 2, in part because drilling affects only a small number of waste packages. However, for cases where there is both drilling combined with volcanism or seismicity, the source term model predicts all failures occur at the earliest time for any event. This simplifying modeling assumption could lead to predictions of earlier and larger total releases when a later disruption (volcanic or seismic event) causes widespread failure of waste packages. The drilling code and source term code should be modified to allow multiple waste package failures at different times within the same run.

4—Drilling model: Reduce number of parameters and tie sampled parameters to the extent of drilling activity.

The drilling model uses a total of 92 sampled parameters, to determine mainly the time of the drilling event, the repository area in which the drilling occurs, and whether or not the drill hole intersected a waste package. The purpose for generating these parameters in the main sampling procedure was to avoid the necessity for generating random variables at the level of a consequence module, and to maintaining tight control over all sampled parameters, for further statistical analysis. Unlike most of the other variables sampled by the LHS procedure, the parameters used in the drilling model have little physical significance. Including these parameters in the statistical correlations did not yield meaningful results, and may have detracted from the correlations between performance and other sampled parameters. Possible alternatives to the present sampling of the drilling parameters might be to have the random sampling built into the drilling module, but relying on a random seed passed to the module as a sampled parameter generated from the system-level LHS routine. Alternatively, some of the analyses in the drilling code presently done in a Monte-Carlo fashion could be reduced to closed-form statistical formulae.

5—Seismic model: Improve waste package failure model for mechanical and seismic input.

The mechanisms for failure of waste packages from seismic shaking and buckling used in IPA Phase 2 were highly simplified, and design-dependent. The model was based on the response of a flexible beam rigidly attached to the ground and oscillating at a single frequency. Failure was caused by either contact of the waste package with the wall, or exceedance of stress at the point of attachment. A more mechanistic model of seismic failure would take into account a number of additional factors, including: (1) a realistic

mechanical model of the waste package and its contact with the ground; (2) a spectrum of frequencies of ground motion; (3) the reduction in strength of the waste package walls predicted by realistic models for pitting, crevice, and general corrosion; (4) the mechanical contact between the waste package, rock, and backfill; (5) repeated mechanical response of the waste package to oscillatory forces; and (6) failure caused by the repeated responsive motion, including the degradation of the metal by fatigue, heat, and radiation. Seismic failure models for future iterations must, of course, take into account the most recent design of the waste package.

6—Improve volcanism model in regard to probability and volcanic processes.

As discussed in Section 6.5.3.3, the volcanism model presented is preliminary. Some assumptions inherent in the *VOLCANO* code can be improved on through additional research. For example, the near-neighbor nonhomogeneous Poisson model used to generate the probability of magmatic activity for IPA Phase 2 is one example of a spatial model that accounts for cinder cone clustering in the region. Other models, such as Neymann-Scott and Poisson cluster models, should be explored, possibly as auxiliary analyses, with an emphasis on how they would be implemented in the future IPAs. Additional geologic information, including the role of volatiles in driving magma ascent, the importance of multiple dike intrusions, and the role of pre-existing structure, also needs to be incorporated. Effects of uncertainty in geochronological data, and related factors, need to be explored. Future models should incorporate these kinds of analyses to provide a robust and defendable estimate of the probability and effects of volcanic disruption.

7—Improve volcanism model in regard to magma interaction with waste.

In the *VOLCANO* module, only direct effects of magma interacting with the radioactive waste are considered. It is recognized that magma may have a number of indirect effects, such as changing the groundwater conditions, and accelerating the corrosion of nearby waste packages. It is recommended that the scope of consequence analyses be expanded to include indirect affects of a nearby volcanic event.

8—Improve tracking of radioactive inventory in the VOLCANO module.

The present version of *VOLCANO* keeps track of the radionuclide inventory by considering only simple decay of radionuclides present in the waste packages, with no generation of radioactive progeny. It does not keep track of radionuclides that have left the repository sub-area by the liquid or gaseous pathway. Although the latter assumption is conservative, ignoring the ingrowth of radioactive progeny of chain decay could underestimate radioactive releases of several radionuclides. *VOLCANO* should be updated to include the ingrowth of radioactive progeny in the source term.

7 DOSE-ASSESSMENT MODULE

7.1 Background

A major difference between the Iterative Performance Assessment (IPA) Phase 1 and IPA Phase 2 studies was the incorporation of a dose-assessment capability into the total-system performance assessment (TPA) computer code in IPA Phase 2. A dose assessment for the proposed repository at Yucca Mountain was not included in IPA Phase 1 for the following reasons. First, the U.S. Environmental Protection Agency (EPA) adopted, as its primary criterion for compliance with the containment regulations in 40 CFR 191.13[1] (*Code of Federal Regulations*, Title 40, "Protection of Environment") a restriction on the quantity of any radionuclide that could be **released** to the accessible environment for 10,000 years after permanent closure, not on the exposures of individuals or populations that might result from these releases. Second, it appeared there was little likelihood of any non-compliance with the individual dose provisions in 40 CFR 191.15, "Individual Protection Requirements" (and therefore little need for a dose assessment capability) because EPA calculations showed that radionuclides released from a geologic repository located in volcanic tuff would not reasonably be expected to expose any human being for at least 1000 years after disposal. Section 191.15 restricts the annual dose to any individual only during the first 1000 years after permanent closure of the geologic repository operations area (GROA). Third, the staff believed that, if needed, existing computer codes for dose assessment could readily be assimilated into the TPA computer code.

In its original form, the criteria to be used for licensing a geologic repository were published in 1985 by EPA as: "Environmental Standards for the Management and Disposal of Spent Nuclear Fuel, High-Level and Transuranic Radioactive Wastes; Final Rule," 40 CFR Part 191 (EPA, 1985; 50 *FR* 38066). On July 17, 1987, the U.S. Court of Appeals for the First Circuit in Boston vacated Subpart B of this 1985 version of 40 CFR Part 191 and remanded the rule to the EPA for further consideration (see EPA, 1993; 58 *FR* 7924).

In response to this action by the court, EPA published a final revision to 40 CFR Part 191 on December 20, 1993 (EPA, 1993; 58 *FR* 66398). The revised dose provisions included an extension of the period that applied to individual dose, from 1000 to 10,000 years after disposal. This proposal would significantly increase the probability for a subsequent exposure of a member of the public to releases of radionuclides from the geologic repository. Under the Waste Isolation Pilot Project Land Withdrawal Act (Public Law 102-579) and the Energy Policy Act of 1992, this revision is not applicable to a potential Yucca Mountain repository. However, since the Energy Policy Act of 1992 directed the EPA to evaluate a health-based standard based on doses to individuals, the staff believed that addition of a dose-assessment capability in the TPA computer code for a potential Yucca Mountain site would be prudent.

7.2 Basis for the Calculation of Human Exposures in IPA Phase 2

7.2.1 Concept of the "Reference Biosphere"

The NRC staff adopted a concept of a stable, or reference biosphere for its studies in IPA Phase 2 (see Federline, 1993[2]). A reference biosphere will provide a basis for quantification of dose. This "reference biosphere" implies that the locations, lifestyles, and physiology of persons who live and work in the vicinity of Yucca Mountain over the future periods of interest (up to 10,000 years and beyond) are difficult to predict. The environmental pathways that could result in human exposure to ionizing radiation will remain unchanged from those that exist in today's biosphere. In IPA Phase

[1]Currently, a revised set of standards specific to the Yucca Mountain site is being developed in accordance with the provisions of the Energy Policy Act of 1992. The Energy Policy Act of 1992 (Public Law 102-486), approved October 24, 1992, directs NRC to promulgate a rule, modifying 10 CFR Part 60 of its regulations, so that these regulations are consistent with EPA's public health and safety standards for protection of the public from releases to the accessible environment from radioactive materials stored or disposed of at Yucca Mountain, Nevada, consistent with the findings and recommendations made by the National Academy of Sciences (NAS), to EPA, on issues relating to the environmental standards governing the Yucca Mountain repository. It is assumed that the revised EPA standards for the Yucca Mountain site will not be substantially different from those currently contained in 40 CFR Part 191, particularly as they pertain to the need to conduct a quantitative performance assessment as the means to estimate postclosure performance of the repository system.

[2]Federline, M.V., "U.S. Nuclear Regulatory Commission Staff Views on Environmental Standards for Disposal of High-Level Wastes," Unpublished Presentation to the NAS Committee on Technical Bases for Yucca Mountain Standards, Washington, D.C., May 27, 1993.

2, scenarios that impacted the geosphere at Yucca Mountain were assumed not to disrupt this reference biosphere.

7.2.2 Similarity to Assumptions in 40 CFR Part 191

The use of a "reference biosphere" in NRC's approach to dose assessment is similar to that taken by EPA during the development of the background information for 40 CFR Part 191 (see EPA, 1985; p. 7-1). EPA's approach to dose assessment for the final rule contained the following caveat: "... it is pointless to try to make precise projections of the actual risks due to radionuclide releases from repositories. Population distributions, food chains, living habits, and technological capabilities will undoubtedly change in major ways over 10,000 years. Unlike geological processes, they can be realistically predicted only for relatively short times ...." (*op cit.*) The conceptual model for the human physiology adopted by EPA included the concept of a present-day "reference man" (see International Commission on Radiological Protection (ICRP), 1975).

EPA also proposed a definition for a "reference population" as another draft revision to 40 CFR Part 191 (see EPA, 1993). The "reference population" was defined as the entity of persons that, for 10,000 years after disposal, has the following features: (a) major population relocations or emergencies have not occurred; (b) the size of the (world) population is 10 billion; and (c) characteristics and behavior affecting estimates of radiation exposure and its effects are assumed to be as today; this includes level of knowledge, technical capability, human physiology, nutritional needs, societal structure, and access to pathways of exposure."

7.2.3 Similarity to the Approach Taken by BIOMOVS

The use of a "reference biosphere" in NRC's approach to dose assessment is also similar to that taken by a working group in BIOMOVS, the **Bio**spheric **M**odel **V**alidation **S**tudy. BIOMOVS is a cooperative effort by the selected members of the international nuclear community to develop and test models that were designed to quantify the transfer and bio-accumulation of radionuclides in the environment (see BIOMOVS, 1992). BIOMOVS recommends that long-term assessments of dose be based on the conceptual model of a "reference biosphere," that is analogous to the "reference-man" concept developed by the ICRP. The participants in BIOMOVS believe that it is impossible to predict all the possible **future** evolutions (future states) of the biosphere. However, they believe it may be possible to identify a comprehensive list of important features, events, and processes that are essential for safe disposal of high-level radioactive waste (HLW) in a geologic repository sited in the **present-day** environments. The range of present- day environments is expected to bound the biospheres expected in the various future states. (Because of the diversity of nature, BIOMOVS recognizes that it may be necessary to define a number of different "reference biospheres".) NRC staff is currently considering this concept.

7.3 Computer Code Selected for Dose Assessment

Human exposures in the IPA Phase 2 study were evaluated by *DITTY* (**D**ose **I**ntegrated for **T**en **T**housand **Y**ears) (see Napier *et al.*, 1988a; pp. 3-16—3-18), a new module added to the version of the TPA computer code. *DITTY* was selected for IPA Phase 2 because: (a) it could be used to calculate the relative variation in doses for the various scenarios used in Phase 2 (it does not predict the absolute doses for comparison with other performance-assessment studies); (b) it was easily interfaced to the outputs of other consequence modules used in the TPA computer code; (c) it could calculate population doses over durations of 10,000 years or more; and (d) it was available and could be executed with little further development.

7.3.1 Overview of DITTY

DITTY estimates the time integral of collective dose over a 10,000-year duration for releases of radionuclides to the accessible environment. *DITTY* can treat both chronic and acute releases of radionuclides. Only a few input parameters to *DITTY* can be entered as input variables at various times during the 10,000-year period. These include:

- Annual releases of radioactivity to air and water;

- The number of persons in the exposed regional population; and
- The dispersion factors in the terrestrial and aquatic environments.

DITTY breaks the 10,000-year duration into 143 periods of 70 years (each period is considered to be the length of a human lifetime), and the total population dose is determined for each of the 143 periods. The radioactivity present during any 70-year period is the sum of the activity in the nuclides released during that period and the residual radioactivity in the environment caused by releases in previous periods.

In IPA Phase 2, the exposure pathways to the accessible environment that were of interest are illustrated in Figure 7-1. These include: the atmosphere, land surfaces, the top 15 centimeters of surface soil, vegetation, animal products (milk, beef), and drinking water. Aquatic pathways were not considered in this study because they are not credible pathways near Yucca Mountain. The quantities of radionuclides released from the repository that move into the environmental media along these pathways are used to calculate concentrations and dose in the reference biosphere. *DITTY* cannot calculate concentrations of radionuclides in the lithosphere or the ground water contained therein.

For IPA Phase 2, the annual releases to the air or water pathways at selected times, during the 10,000-year period of regulatory interest (the source terms), were provided as input to *DITTY* by other TPA computer code modules in the form of average annual concentrations. Up to 450 of these paired values can be entered as an input file (e.g., as curies per year/time or curies per volume/time). The values for these concentration-time pairs were obtained as outputs directly from the *NEFTRAN* module, or indirectly, from the *C14*, *DRILL02*, and *VOLCANO* modules (see Figure 2-1).

DITTY calculates the downwind regional air concentrations as the product of the release rate of radionuclide (from the ground surfaces above the geologic repository into the atmosphere) and a dispersion factor, commonly designated as X/Q. For waterborne releases, in addition to the calculation of collective doses, *DITTY* will identify that 70-year period when the individual lifetime (70-year) dose is highest.

7.3.2 General Approach to Dose Calculations in *DITTY*

A calculation of internal dose to a human-body organ in *DITTY* can be visualized as the product of four parameters, so that for any single radionuclide:

$$D = C \times FTC \times U \times DCF \ ,$$

where D is the dose to a body organ from the radionuclide per year of intake; C is the concentration of radionuclide in a specific media (e.g., curies per kilogram of pasture grass eaten by beef cattle); *FTC*, is identified in *DITTY* as the food-transfer coefficient, is a dimensionless factor that expresses the distribution ratio of a radionuclide between two media at steady-state (e.g., the ratio of the steady-state concentration in the edible tissues of the beef cattle to the steady-state concentration in pasture grass); U is the human- or animal-use factor (e.g., kilograms of beef eaten per year) for the media; and *DCF* (dose conversion factor) is the quantity that will convert radioactivity ingested or inhaled into dose (e.g., rem/curie). The *DCF* values and the *FTC* values used in this study, which are described in Section 7.7, are different from values in the original *DITTY* databases.

7.3.3 Calculation of Total Dose in *DITTY*

The total population dose is expressed in terms of an *Effective Dose Equivalent* (EDE). This dose is the sum (over all organs) of internal and external doses that result from direct radiation or uptakes of radionuclides into the human body along the pathways illustrated in Figure 7-1.

Internal doses to body organs can result from the inhalation of airborne radioactivity or from the ingestion of radionuclides in contaminated food and water. In *DITTY*, these organ doses are multiplied by a risk-based weighting factor to give "effective" organ doses (i.e, committed EDE). The values used for these organ-weighting factors in *DITTY* are the same as those given in ICRP-26 (ICRP, 1977). All internal doses are integrated over the 50-year period that follows an intake of

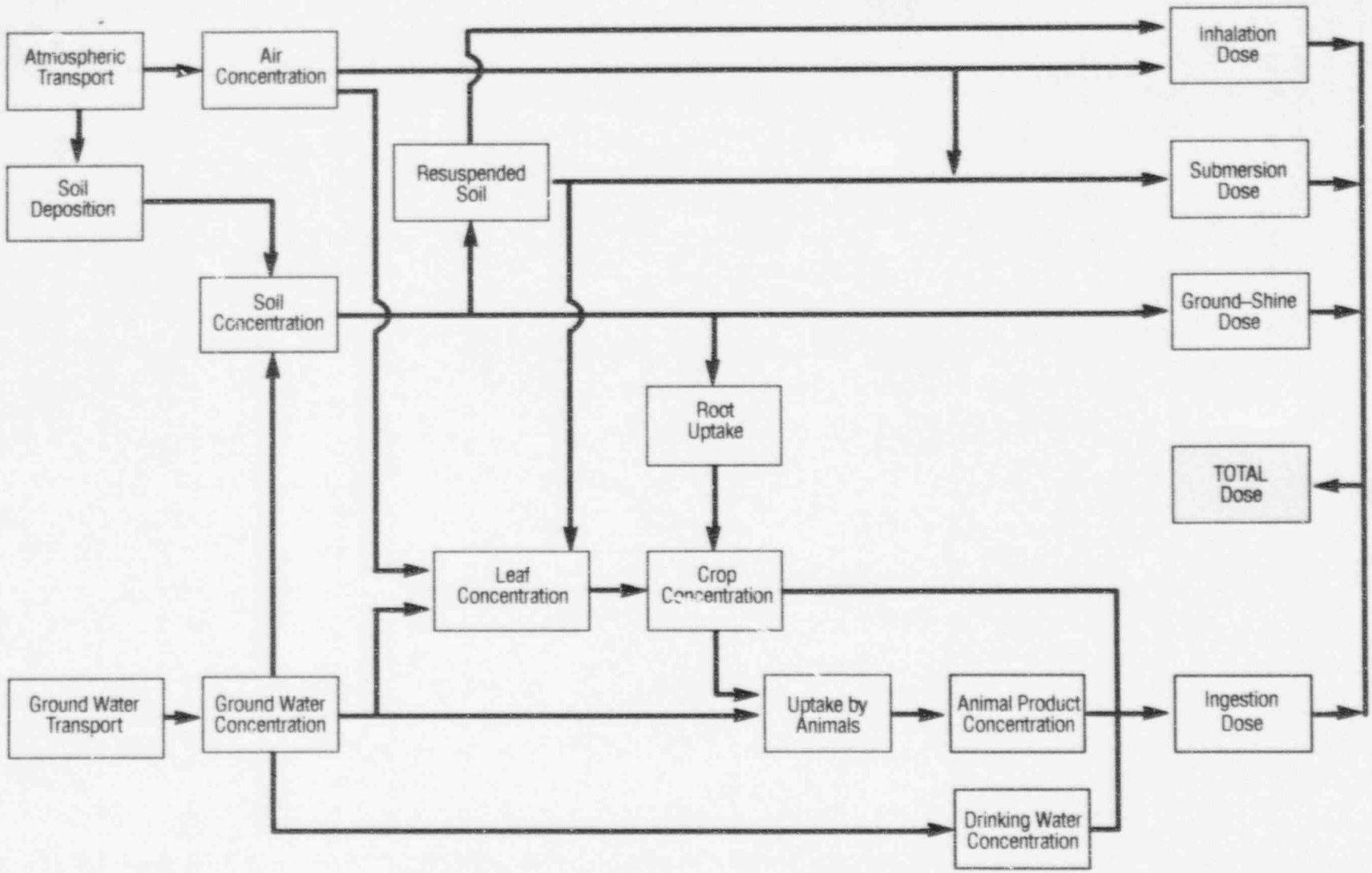

Figure 7–1 Human exposure pathways in the accessible environment, as calculated by the *DITTY* computer code

radionuclides (i.e., for a dose-commitment period of 50 years in the human body). The integrated dose is formed from the sum of the doses to six designated body organs and to the five remaining organs with the highest doses.

External exposures can result either from submersion of the human body in airborne radioactivity or from exposure to direct radiation (ground shine) that emanates from the surface of contaminated soil. In *DITTY*, organ doses caused by external exposures are expressed in terms of the EDE, instead of the more common dose equivalent quantities. A special energy-dependent dose factor (rem/rad) is used in *DITTY* to convert external doses to the body surfaces to deep organ-doses (Kocher, 1981). The use of these conversion factors in *DITTY* has preceded any guidance by the Commission on acceptable methods for calculation of EDE from external photon and particulate radiation.

7.3.4 Selection of *DITTY* Model Parameters

For IPA Phase 2, default values for the model parameters from *DITTY* were used in the dose-assessment models unless indicated otherwise. Probability density functions were not defined, and Latin Hypercube Sampling (LHS—discussed in Chapter 2, "Total-System Performance Assessment Computer Code") was not attempted for any parameter used in the dose-assessment models. This was done intentionally to focus attention on the magnitude of the uncertainties introduced into the resulting doses by the collective uncertainties associated with the source term and geosphere models used in IPA Phase 2. In the future, it will be necessary to estimate site-specific values for the *DITTY* model parameters to make the most meaningful calculations of dose. In many cases, a literature study should be sufficient to select these values. However, for those radionuclides that are major contributors to the dose, laboratory and field studies may also be desirable. Sensitivity studies, similar to those conducted in other IPA Phase 2 modules (see Chapter 9, "Sensitivity and Uncertainty Analysis"), should also be carried out for parameters in the biosphere models. In this way, the parameters that significantly influence the magnitude of the doses and that may require further study in the field may be identified.

7.4 Differences From Internal Dosimetry Models in ICRP-30

The major differences of the biokinetic models in *DITTY* from those in ICRP-30—"Limits for Intakes of Radionuclides by Workers" (ICRP, 1979)—are found in the computer program *GENMOD*. *GENMOD* (Johnson and Carver, 1981), which was adapted directly from ICRP-30, incorporates additional models other than those developed by the ICRP (such as the alkaline earth model, the *MIRD* iron model, and the ^{14}C model). *GENMOD* was used to generate databases that include values for the following metabolic parameters for each radionuclide used in *DITTY*: organ uptake, transfer coefficients from compartment to compartment, and elimination rates from compartments. The metabolic models for carbon assume it is inhaled as carbon dioxide gas, and that ingested carbon is in the form of carbohydrates that are readily absorbed through the gut and rapidly distributed throughout the body.

Although metabolic parameters for various ages, sexes, and ethnic groups were not available when this study was undertaken, they may require further consideration when guidance for members of the public becomes available. A rough estimate of the variation of lifetime dose with the age of initial exposure may be inferred from the Statement of Considerations for the final rule for 10 CFR Part 20 (*Code of Federal Regulations,* Title 10, "Energy") which notes that "... those organs for which age dependency is important, such as the thyroid gland, are of lesser importance because of the lower w_T values [risk-weighting factors] ... used to calculate the effective dose. A factor of 2 is included ... which, in part, accounts for age dependency ...." (NRC, 1991; 56 *FR* 23390). This appears to be a reasonable assumption, given the observation recently made by Charles and Smith (1991, p. 10) that "... the generally higher committed doses per unit intakes for non-adult age groups are in the main cancelled by the lower consumption of foodstuffs ...."

7.5 Selection of DCFs for this Study

7.5.1 DCFs for Ingestion and Inhalation

In IPA Phase 2, the *DCFs'* values were assumed to be without bias and of the highest precision. Since it was assumed that a "reference man" in a "reference biosphere" was exposed over the

10,000-year period when radionuclides were released from the geologic repository, the same *DCFs* were used for calculations of dose during each of the 70-year human lifetimes considered in *DITTY*. The *DCFs* for the radioactive daughters that are produced *in vivo* were generally also described with the same metabolic parameters as those for the parent radionuclide.

The *DCFs* for inhalation and ingestion, used in IPA Phase 2, which were prepared by Dr. Paul Rittman of Westinghouse Hanford Company, from the revised computer code *INTDF* (Version 1.483) (see Napier *et al.*, 1988a; pp. 3–13—3–16), are the "worst-case" values. These parameters, which pertain to each radionuclide used in *DITTY*, maximize either the inhalation dose by an intentional selection of the chemical form with the worst-case solubility in the lung, or the ingestion dose, by selection of the chemical form that results in the largest uptake in the small intestine (f_1 value) for each radionuclide, or both. When normalized to an annual basis, the *DCFs* generated by *INTDF*, a *DITTY* sub-routine, are essentially the same as those reported in EPA's Federal Guidance Report No. 11 (i.e., to within two significant figures, but with a few differences for very short-lived nuclides) (EPA, 1988).

The dose-commitment period for all *DCFs* used in this study is 50 years. This is consistent with 10 CFR Part 20 and also with the recommendations of both national and international committees on radiation protection. A 50-year dose-commitment period was also suggested by EPA for Appendix B of 40 CFR Part 191 (see EPA, 1993; 58 *FR* 7936). Since *DITTY* assumes that an individual will experience an annual intake of radionuclides during each year of his 70-year lifetime, the use of this 50-year dose commitment period will overestimate his lifetime dose for those radionuclides with a long biological half-life (but in no case by more than a factor of 2).

7.5.2 DCFs for External Exposure

The *DCFs* for air submersion and for direct radiation exposure to radionuclides deposited on land surfaces (ground shine) were used in this study are unchanged from those as found in the databases of the *DITTY* code. These values will be reviewed when EPA publishes Federal Guidance No. 12 (in preparation), a tabulation of dose coefficients for external exposure to photons and electrons emitted by radionuclides distributed in environmental media.

7.6 Selection of Parameters for the Ingestion Pathways

The bases for selection of data used in the terrestrial-ingestion pathway models of *DITTY* are discussed below.

7.6.1 Drinking-Water Parameters

The original version of the database *BIOACI.DAT* contained factors to simulate the treatment of drinking water by a municipal water-treatment plant. For IPA Phase 2, drinking water was assumed to be taken from a surface well without any treatments to remove radionuclides (all treatment factors were set to a value of 1). This is equivalent to the assumption that the concentration of a radionuclide in drinking water has the same concentration as it had in the ground water that feeds the well. The IPA Phase 2 analysis did not consider mitigating measures available in present-day technology. These measures may include devices to monitor waterborne radiation or procedures, such as water treatment or condemnation of the well.

7.6.2 Food-Transfer Parameters

The documentation in *DITTY* does not identify the sources of the soil-to-food transfer parameters stored in the *DITTY* file *FTRANS.DAT*. The *User's Manual* for *DITTY* indicates that the "... sources of these parameters are to be published in a separate document" (see Napier *et al.*, 1988b; pp. 2.28–2.29). Since literature citations were not available during IPA Phase 2, *FTRANS.DAT* parameters were replaced by "generic" parameters taken from the well-known study by Baes *et al.* (1984).

The "Baes" parameters used in this study (B_v, B_r, F_f, and F_m) are based on clearly-defined protocols that were used to select them from the multiplicity of experimental values reported in the literature. For example, for the soil-to-crop values, the Baes *et al.* study attempted to select concentration ratios that were based on detailed literature studies in which the soil and plant concentrations were **both** measured at "edible maturity" of the plant. These literature citations show that

large variations (orders of magnitude) of these parameters in various environmental settings are not uncommon, and therefore most studies use site-specific values to increase the reliability of dose estimates.

The *DITTY* parameters for each chemical element that was stored in the file *FTRANS.DAT* were replaced by the following types of Baes parameters (dry-weight to dry-weight basis):

- A B_v value (Baes *et al.*, 1984; Figure 2.1) replaced each soil-to-leafy-vegetable concentration ratio;
- The same B_r value (*op cit.*, Figure 2.2) replaced each of the four soil-to-edible-crop concentration ratios (these crops are vegetable, root, grain, and fruit);
- A F_f value (*op cit.*, Figure 2.25) replaced the feed-to-meat transfer coefficient; and
- A F_m value (*op cit.*, Figure 2.24) replaced the feed-to-milk transfer coefficient. The poultry and egg pathways were not used in the IPA Phase 2 studies, and therefore these food-transfer coefficients were not modified.

These new values, which are stored in a new file *FTRANS.CFB*, were used for all calculations of dose in IPA Phase 2.

The leaching factors for soil in *FTRANS.CFB* are unchanged from the values in *FTRANS.DAT*. The magnitudes of the leaching factors in *DITTY* are directly proportional to the percolation rate of water through the rooting zone and into deeper soil layers (an over-watering term of 15 centimeters/year was assumed in *DITTY*). In IPA Phase 2, small variations in the leaching factors for very mobile radionuclides (e.g. technecium and iodine), were shown to have a significant impact on the cumulative magnitude of dose. For models like *DITTY*, that involve long-term deposition of radionuclides in soil, the leaching factors should be obtained from site-specific investigations, to properly characterize the retention of radionuclides in soil and their biological availability to crops (International Atomic Energy Agency (IAEA), 1982).

7.6.3 Growing-Season Parameters

The site-specific agricultural parameters for Yucca Mountain that were entered as input data to *DITTY* included: the length of the growing season, the irrigation rate for crops during the growing season, and the yields of the various types of crops. The lengths of the growing season depend on the crop type. One of the most important crops in Nevada is alfalfa, which can grow up to 250 days each year and produce up to eight 30-day harvests each year. For most vegetables, the first growing season begins in February and ends in early-March; the second season begins in mid-August and ends in mid-October. Very little appears to grow during the hot, dry summer months between late-May and late-August (Mills, 1993).

The lengths of the growing period selected for this study were: For leafy vegetables, 45 days; for "other" vegetables, 90 days. For alfalfa, and for those pasture grasses that are consumed as by animals as forage, the growing season was taken as 30 days (Kennedy and Strenge, 1992; Table 6.12).

7.6.4 Irrigation Rate for Crops

The State of Nevada issues water-use permits that limit the maximum pumping rate from wells in the vicinity of Yucca Mountain to 127 liters/month/square meter (~152 centimeters/year) of irrigated land (Personal comm., Nevada State Engineer's Office). For areas within 100 kilometers of the geologic repository, the irrigation period was assumed to coincide with the average length of the growing season (i.e. 60 days). Irrigation was assumed to proceed at the maximum pumping rate allowed by the water permit (see "Rate of Irrigation" in Section 7.8.2).

7.6.5 Crop Yields (Human Consumption)

The yields of the irrigated crops (in kilograms per square meter), and the quantities consumed by humans (in kilograms per year, in parenthesis) are taken from Tables 6.14 and 6.15, respectively, in Kennedy and Strenge (1992, Vol. 1). The values used in *DITTY* are: leafy vegetables, 2.0 (11); "other" vegetables, including grains, fruits and root vegetables, 4.0 (172); the pasture grasses and alfalfa that fatten beef cattle and leads to milk production, 1.5 (milk, 100 kilograms/year and beef, 59 kilograms/year). These values are not

inconsistent with those found to grow in Nevada lowlands (Nevada Agricultural Statistics Service, 1988).

Milk cows are assumed to consume vegetation at the rate of 55 kilograms/day and beef cattle at 68 kilograms/day. Milk cows are assumed to drink water at the rate of 60 liters/day and beef cattle at 50 liters/day. These parameters are default values in *DITTY* (found in data statements).

7.7 Selection of Parameters for the Inhalation Pathways

7.7.1 Meteorological Data

The meteorological data selected for *DITTY* was a composite of the annual averaged STAR (**St**ability **Ar**ray) data measured by the National Oceanographic and Atmospheric Administration between 1986 and 1990, at Station Number 03160, Desert Rock, Nevada, which is 935 meters above sea level (U.S. Department of Commerce (USDC), 1992). Data were available for seven stability classes, six wind speeds and for 16 compass directions. Data from this particular location were selected because of their availability. These data was used to calculate the concentrations of airborne radionuclides in the region surrounding the geologic repository.

All releases of radioactivity from the geologic repository were assumed to occur at ground level and to disperse radially out to a distance of 100 kilometers. (The distance between radial segments illustrated in Figure 7–2 is 20 kilometers.) A Gaussian plume model was used to convert releases of radioactivity to long-term, sector-averaged X/Q values (expressed in units of seconds per cubic meter released). In this study, X/Q values were estimated by *DITTY* at the following distances: 2.5, 7.5, 15, 30, 50, 70, and 90 kilometers. These distances are measured radially from the release point in the GROA to the midpoints of the wedge-shaped sectors shown in Figure 7–2 (e.g., a mid-point distance of 30 kilometers (North) is midway between the 20-kilometer (North) and 40-kilometer (North) distance intervals).

7.7.2 Regional Population Distribution at Yucca Mountain

The size of the regional population exposed to airborne releases of radioactivity was assumed to be stable throughout the entire 10,000-year period. Members of this population were located at the mid-points of the wedge-shaped sectors shown in Figure 7–2 (i.e., those distances identified in Item (1), above).

The dispersion studies were extended to 100 kilometers, to include the 5500 persons who were residents of the city of Pahrump in 1988. This regional population distribution in Figure 7–2 was taken from Logan *et al.* (1982) and was updated with information obtained from DOE's 1988 Site Characterization Plan (see DOE, 1988; Table 3–21).

7.8 Application of the Dose-Assessment Methodology to Yucca Mountain: Biosphere Scenarios

7.8.1 Application of the "Critical-Group" Concept

Whenever a radiological assessment is undertaken before the operation of a new nuclear facility, the specific individuals who may receive the highest exposures and greatest risks in future time cannot be identified. In these circumstances, it is appropriate to **define** a hypothetical critical group (i.e., those persons who receive the highest exposures) because this approach avoids the need to forecast future lifestyles, attitudes to risk, and developments in the diagnosis and treatment of disease. In principle, the critical group should be defined by age, sex, and ethnic origins since intakes, metabolism, and dosimetry of radionuclides are all strongly conditioned by these factors (IAEA, 1982). As noted in Section 7.4, a rough estimate of the variation of lifetime dose with the age of initial exposure may be inferred from the Statement of Considerations for the final 10 CFR Part 20 rule.

7.8.2 Hypothetical Biosphere Scenario: Waterborne Release

Section 191.15 of 40 CFR Part 191 requires that "... all potential pathways ... from the disposal system to people shall be considered ... including the assumption that individuals consume 2 liters/day of drinking water from a significant source of

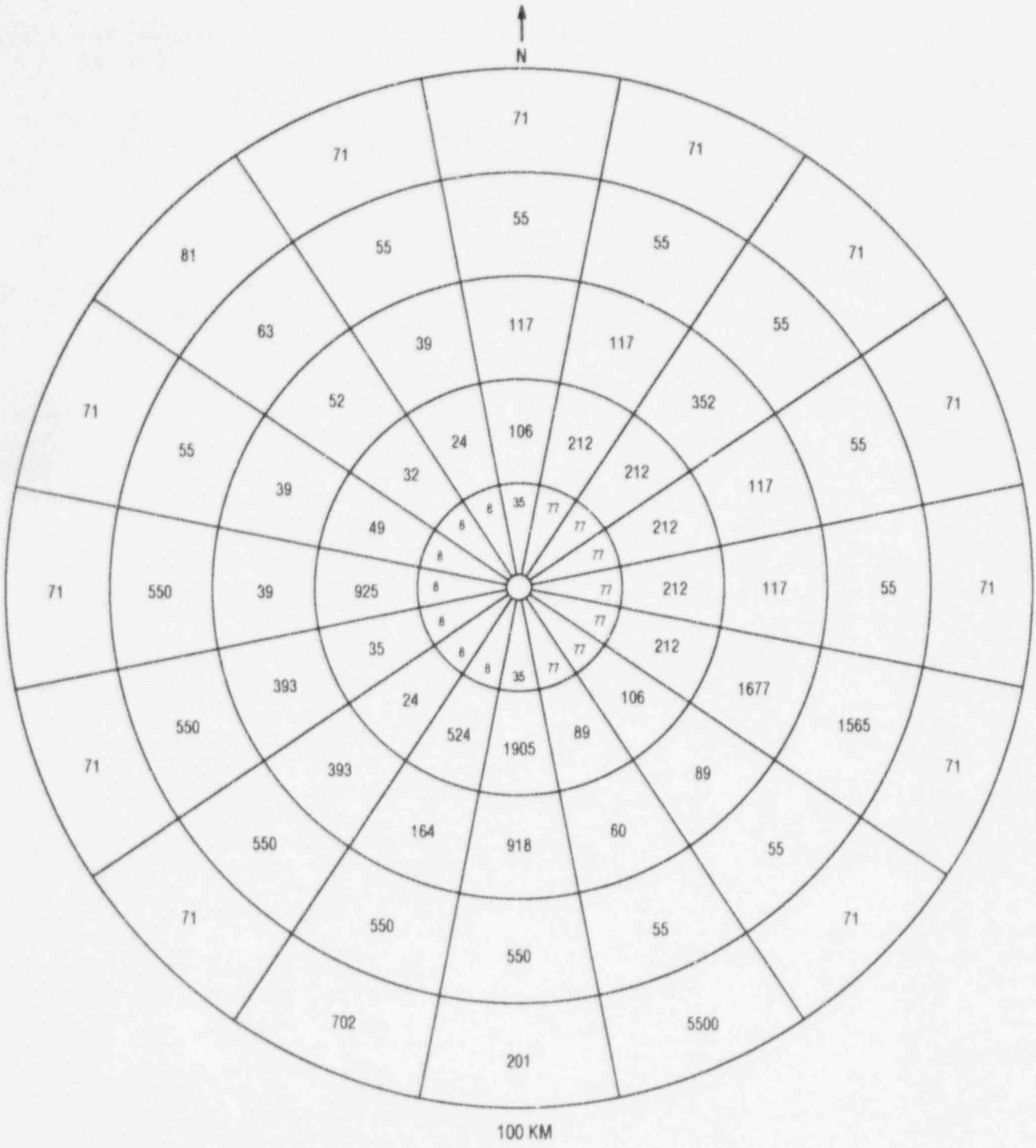

Figure 7–2 **Estimated population distribution in the vicinity of Yucca Mountain, Nevada** (The population distribution, as of December 1988, is 22,200. Adopted from Logal *et al.* (1982) and DOE (1988).)

ground water outside of the controlled area." A contemporary farm family of three persons was selected as the hypothetical critical group, to illustrate the capability for dose assessment that was incorporated into the TPA computer code in IPA Phase 2.

Location: The hypothetical family is assumed to maintain a year-round residence on an average-sized farm (approximately 1093 hectares) located at the boundary of the controlled area (10 CFR 60.2) that surrounds the geologic repository at Yucca Mountain. Contaminated water pumped from a local well irrigates two areas on this farm: a 88-hectare tract, an area which is set aside as irrigated pasture land for calves (yearlings) and other cattle (agricultural statistics for Nevada for the 1987–88 period estimates that approximately 100 farms, with a irrigated land area of 12,146 hectares, are irrigated in Nye County); and a fenced-in tract of 1.2 hectares, which is used to grow a large portion of the family vegetables (leafy and other), fruits and grains for home consumption (the growing periods and yields of crops, and the human consumption of meats and crops were adopted from Kennedy and Strenge (1992, Tables 6.12–6.15)). The remaining 1004 hectares of un-irrigated and un-contaminated land are used to graze mature beef cattle.

Drinking Water: Each member of this contemporary family is assumed to obtain all of his/her drinking water (2 liters/day of drinking water for 365 days/year) from a contaminated well at the boundary of the controlled area. The composition of this well water is assumed to be similar to that found in U.S. Geological Survey Well J-13. Well J-13 is located approximately 13 kilometers southeast from the controlled area boundary of the repository. The current capacity of the pump at Well J-13 is 2385 liters/minute (maximum) which is approximately 4 million liters/day (see Czarnecki, 1992; Table 1).

Rate of Irrigation: Fluxes of radionuclides to the well used by the farm family emanate from the seven subareas in the model of the repository for the Yucca Mountain site, as depicted in Figure 4.6, and are calculated by the TPA computer code that invokes the models for source term releases, flow, and transport. The seven geologic repository sub-areas have different physical and chemical properties that govern the times of release of the radionuclides from the waste form and the travel time through the geosphere. Thus, the concentration of the radionuclides in the well at the point of use by the farm family is a complicated function of time.

To obtain the concentrations of radionuclides in the contaminated well water after a waterborne release, the fluxes of radionuclides in the aquifer (calculated at the location of the well) were diluted to a volume of 4 million liters/day. Approximately 4 millon liters/day would be required to irrigate the garden plot and the pasture area (88 hectares irrigated at a rate of 127 liters/square meter-month). This dilution flow was considered consistent with the water usage by the farm family and for stock watering. These concentrations were calculated at selected times during the 10,000-year period of study and were used as input to *DITTY*.

Consumption of Foods: Reports by the USDC indicate that no farms in Nye County sell dairy products for profit (USDC, 1989; p. 138). The farm family is therefore assumed to own cows only to provide dairy products for their own consumption. Of the 136 farms identified in Nye County in 1987, only eight farms raised poultry, and only nine farms raised hogs and pigs (*op cit.*). The family is assumed to purchase pork, poultry, eggs, and small quantities of fruits, vegetables, and grains at a local supermarket supplied with un-contaminated foodstuffs by a distributor from another geographical area. The family is assumed to consume 100 percent of their beef and milk from farm animals that feed on vegetation irrigated by contaminated well water.

Inside/Outside Activities: Annually, the hypothetical person is assumed to spend 6424 hours (73 percent) inside his home (TV, sleep, etc.), and to spend 2336 hours outside the home (farming, herding cattle, and recreation). If the hours spent inside the home are weighted by a shielding factor of 0.5 (NRC, 1977; p. 43) and added to the hours spent outside, the effective time that this person would be exposed to external ionizing radiation (ground shine and submersion in airborne radioactivity) would be 5548 hours/year.

Exported Beef Cattle: Beef cattle (60 percent mature and 40 percent calves) sold for profit are assumed to obtain 100 percent of their feed from the contaminated vegetation raised on the 88 hectares of irrigated pasture land on the family

farm. Half of the these animals (43 calves and 32 cattle), that are exported off the farm and sold for profit each year, are estimated to produce 10,377 pounds/year of edible beef. This quantity of beef will feed 177 persons/year, if it is assumed that one person consumes 129 pounds (59 kilograms) of beef each year (approximately 1 hamburgers/day every day of the year).

7.8.3 More Realistic Biosphere Scenario: Waterborne Release

A more realistic biosphere scenario would involve exploitation of ground waters near Yucca Mountain, to supplement the municipal water supply for regional populations. Water consumers in the region would then form the critical group whose doses would be limited by an individual protection standard (Federline, 1993). This scenario may be explored further in future IPA analyses.

7.8.4 Hypothetical Biosphere Scenarios: Airborne Releases

Mechanisms of Release to the Atmosphere: In IPA Phase 2, contaminated soil (or gaseous ^{14}C) was assumed to be transported to the ground surface above the repository as a result of disruptions of the geologic repository either by human intrusion (e.g., by exploratory drilling) or by an extrusive volcano (only for cone magma events). As many as 20 radionuclides might contribute to the radioactivity in this contaminated soil. During the 10,000-year period in this study, the times that the releases to the atmosphere from the contaminated ground surface could occur are governed by model parameters. The time of release is therefore a variable, because it depends on the particular vector set used to generate the dose for any given scenario (these times and the vector sets are determined by LHS sampling of appropriate model parameters).

Only a fraction of this released radioactivity was assumed to become available for transport by the air pathway to members of the public beyond the controlled area of the repository. The fractions of the radioactivity that were assumed to become airborne were: 0.04 for the human intrusion scenarios; 0.30 for the magmatic eruption scenarios; and 1.0 for the ^{14}C scenarios. (These values were stored in the *AIRCOM* module of the TPA computer code (see Section 2.1.3).) All the airborne radioactivity was assumed to be respirable (whether in the solid, liquid, or gaseous states). Any radioactivity that did not become airborne was considered to remain undisturbed at the point of release to the above-ground surface.

The NRC staff made preliminary estimates of the fractions of radioactivity, released from the human intrusion and volcano scenarios, that became airborne. For the human intrusion scenario, a company that manufactures drill bits advised the staff that for a large hole, which was drilled into a hard formation such as granite, approximately 25 percent of the drilling would pass through a 200-mesh screen. (This means that 25 percent of the cuttings would be smaller than 62 microns). The staff assumed that the grain sizes of cuttings below 62 microns followed a uniform distribution. From a typical plot of grain size versus cumulative percentage of cuttings retained in the various-sized sieves (e.g., see Freeze and Cherry, 1979; p. 351), the staff estimated that one-sixth of this material would be smaller than 10 microns. It follows that roughly 4 percent of the total mass of the drill cuttings would be smaller than 10 microns (25/6 = 4 percent). For the volcano scenario, the NRC staff obtained the respirable airborne fractions from Fisher and Schmincke (1984). For "explosive" volcanic eruptions, they claim that between 10 to 30 percent of the material that becomes airborne is smaller than 10 microns.

Calculation of Dose for Airborne Releases: The sequence of calculations by the TPA computer code that results in an estimate of the doses to the regional population (or the farm family) after exposure to an airborne release of radioactivity from the geologic repository is as follows. First, the consequence modules *DRILLO2*, *VOLCANO*, and *C14* calculate the quantities of radionuclides in contaminated soil (or gaseous ^{14}C) that are released to the ground surface in any given year. These quantities of surface radioactivity are then multiplied by the corresponding fractions stored in the *AIRCOM* module to generate the quantities of radioactivity that becomes airborne and respirable during that year. These latter values are in a format that is compatible with the *DITTY* module (curies per year released to air at various times).

DITTY calculates the concentrations of radionuclide in the various media (refer to Figure 7-1) that result from an airborne release and converts

these to dose. The semi-infinite plume model was used to calculate doses caused by submersion in contaminated air. For this exercise, wind speeds measured at the Desert Rock Station were not corrected to ground-level.

Airborne Releases of ^{14}C: The models for ^{14}C (gaseous release), human intrusion, and magmatic eruption were used to estimate the releases of gaseous ^{14}C to the atmosphere. Eventually, all of the ^{14}C that escapes from degraded waste package canisters emplaced in the repository is assumed to travel through the geosphere and to be gradually released to the atmosphere as carbon dioxide gas. In *DITTY*, this ^{14}C is further assumed to be incorporated into vegetation by the photosynthesis process, with a resulting specific activity in the plant that is identical to that in the contaminated atmosphere. *DITTY* also assumes that 10 percent of the specific activity in soil is transferred to the edible plant, to augment the photosynthesis process.

In Section 4.3, the releases of ^{14}C were estimated to occur over an area of several square kilometers. But, in this study, all ^{14}C releases to the atmosphere were assumed to emanate from a point source located at the approximate center of the GROA. The exposure values reported in IPA Phase 2 for ^{14}C are therefore expected to overestimate collective dose, since the concentrations of gaseous ^{14}C from the area source would be more diffused, and therefore smaller, than those from a point source.

7.9 Conclusions and Possible Considerations for Future Dose Assessments

7.9.1 Conclusions

Although dose-related parameters were not sampled in this total-system performance assessment, the uncertainty inherent in the dose assessment calculation can be significant, and adds to the uncertainty being propagated in the release model. Much of the uncertainty in dose is associated with inherent uncertainties in the parameters used for the human physiology and environmental pathway models in the *DITTY* computer code. The *DCF* may not always reflect the individual differences (e.g., age, metabolism, sex, etc.) in human response to ionizing radiation. The parameters used in this study for the environmental pathway analyses are not always site-specific, and furthermore, are considered to be invariant in space and time. Nevertheless, the results of the dose assessment provide valuable insights regarding the performance of the geologic repository, and are summarized below:

- A gaseous release of ^{14}C makes a significant contribution to the *Normalized Release*,[3] but its corresponding impact on the cumulative population dose is insignificant.
- The radionuclides that made the largest contributions to the population doses (accumulated over 10,000 years) were: ^{94}Nb, ^{210}Pb, ^{243}Am, and ^{237}Np. (Refer to Section 8.3.2. for additional discussion.)
- The scenario classes most likely to impact dose were those composed of some combination of the following independent events: drilling into a waste package canister, plus a change in climate, plus a seismic event. (Refer to Figure 9-7b in Section 9.3 and the discussion of climate in Section 9.2.3 for additional discussion.)
- The average annual inhalation dose to an individual in the Yucca Mountain region was negligible compared to the average annual dose caused by the ingestion of contaminated drinking water and locally-grown contaminated food (both averaged over a 10,000-year period as discussed in Section 9.6).
- Further data development and site characterization are desirable, if not necessary, to help reduce the uncertainty in many important parameters in the biosphere model (such as the leaching rates in soil).

7.9.2 Considerations for Future Dose Assessments

The following recommendations should be considered for adoption in future dose assessments that might be conducted by the staff as part of its IPA work.

[3]Defined as cumulative total releases of radionuclides at the accessible environment. See Section 8.1.

1—Improve the DITTY dose-assessment model

- Display the results of dose assessments with multi-dimensional plots (cumulative and organ doses should be functions of both the type of radionuclide and the exposure pathway).

- Re-calculate the *DCFs* used in IPA Phase 2, to obtain a more accurate estimate of population doses for long-lived radionuclides (as discussed in Section 7.6).

- Verify that the model parameters currently used in *DITTY* are applicable to the Yucca Mountain site; identify the ranges of these parameters.

2—Evaluate other dose-assessment computer codes

- Evaluate other computer codes that could be used to estimate long-term individual and collective exposures and that should be explored if dose becomes a performance requirement. One code that has these capabilities to be explored is *GENII–S* (see Leigh *et al.*, 1993). Many of the databases in this code are common to the *DITTY* code used in this study.

- Evaluate atmospheric dispersion (or diffusion) models that can calculate atmospheric concentrations caused by releases of radionuclides from area sources. These models could be used to obtain better dose estimates for releases of gaseous ^{14}C.

- Evaluate atmospheric dispersion models that consider aerosols of a variety of particle sizes, shapes, and densities.

- Evaluate demographic models that can project the growth of a population. This feature would be useful for calculation of collective dose.

- Evaluate methods employed by international organizations for calculation of dose into the far future (e.g., BIOMOVS and the Nuclear Energy Agency).

- Incorporate the "1990 Recommendations of the International Commission on Radiological Protection" (ICRP, 1990), into the codes used for dose calculations, when adopted by the Agency.

3—Conduct sensitivity/uncertainty analyses

- Apply the statistical sensitivity and uncertainty methodology developed in IPA Phase 2 for the geosphere models to the dose-assessment models.

8 SENSITIVITY AND UNCERTAINTY ANALYSIS[1]

8.1 Introduction

The purpose of sensitivity and uncertainty analyses is to gain an understanding of the relationships between the repository performance measures and the input parameters used to formulate the models. The overall performance measures for the geologic repository used in the Iterative Performance Assessment (IPA) Phase 2 analysis are cumulative total releases of radionuclides at the accessible environment (*Normalized Release*) and doses to the exposed population (*Effective Dose Equivalent*). Because of the complexity of the systems comprising a geologic repository, it is not usually possible to develop exact analytical expressions for the functional relationship between repository performance and the input parameters used to formulate the models. Empirical relationships may be inferred by inspecting the model performance measures and input parameters in a variety of ways. This section will illustrate a number of techniques used for determining the relationships among parameters and their importance to the model performance.

Performance assessments for the geologic repository are based on conceptual models, embodied as computer programs, and measured field and laboratory data. Because of the inherent variabilities and sparsity of the measured data and the underlying uncertainty concerning the processes included in the models, the results of any performance assessment have significant uncertainty. An important aspect of conducting a performance assessment for a geologic repository is quantifying the sensitivity of the results to, and the uncertainty associated with, the values of the input parameters. An analysis of model sensitivity will provide information concerning which input parameters are most important to the results. A better understanding of those parameters that have the most influence on the results can hopefully lead to improvement in the models. Likewise, from a review standpoint, identification of the most sensitive parameters provides a means of comparing and evaluating different performance assessment models and indicates where reviews of data should be concentrated. This section discusses how variation in model output reflects variation in the input parameters.

[1]The figures shown in this chapter present the results from a demonstration of staff capability to review a performance assessment. These figures, like the demonstration, are limited by the use of many simplifying assumptions and sparse data.

8.2 Overview of Techniques and Methods

8.2.1 Background

A variety of techniques have been used to quantify the uncertainty and sensitivity in complex models for assessing radiological impact on man and the environment. These include: the Monte Carlo method (Helton 1961); fractional factorial design (Cochran, 1963); differential analysis (Baybutt *et al.*, 1981); response surface methodology; Fourier amplitude sensitivity (Helton *et al.*, 1991); and the Limit-State Approach (Wu *et al.*, 1992). No one technique is definitive and several can be used together to evaluate total-system performance assessments. Because comparisons of the methods employed in each approach may be found in several works (Zimmerman *et al.*, 1991; Helton *et al.*, 1991; and Wu *et al.*, 1992), only a limited evaluation is provided here. The Monte Carlo approach was used in the present performance assessment. Regression analysis and differential analysis as means of determining sensitivity to individual parameters are compared in Section 8.4.4.

8.2.2 IPA Phase 1 Sensitivity and Uncertainty Analyses

IPA Phase 1 examined sensitivity and uncertainty for radionuclide releases at the accessible environment for a geologic repository in unsaturated tuff (see Section 9.5, "Sensitivities and Uncertainties for Liquid-Pathway Analysis," in Codell *et al.*, 1992). The consequence models were significantly simpler than those in the present study, and there was a narrower range of scenarios considered.

8.2.2.1 Sensitivity Analyses

Four sensitivity analyses were performed for IPA Phase 1: (a) sensitivity analyses demonstrating the effect of individual parameters on the resultant Complementary Cumulative Distribution Function (CCDF) for cumulative release to the accessible environment (10 CFR 60.112); (b) regression analyses using stepwise linear regression

to estimate the sensitivity to key parameters in the consequence models; (c) determination of relative importance of radionuclides in the waste; and (d) sensitivity of CCDFs to performance of the natural and engineered barriers. The sensitivity analyses considered only liquid releases, not those from drilling. Gas release was not part of the IPA Phase 1 total-system performance assessment results, but was included as an auxiliary analysis (see Appendix D, "Gaseous Release of C14," in Codell *et al.*, 1992).

8.2.2.2 Uncertainty Analyses

The Phase 1 IPA included only two events and processes different from the base-case conditions: pluvial conditions and drilling. These were combined into four scenarios (i.e., base case, base case plus drilling, pluvial conditions without drilling, and pluvial conditions with drilling). Uncertainty analyses were restricted to presentation of CCDF plots of cumulative release at the accessible environment (*Normalized Release*) for each of the scenarios, separately, and a combined CCDF for all scenarios factored by the scenario probability. The CCDFs were the result of the uncertainty in the sampled parameters propagated through the analysis. *Effective Dose Equivalent* was not calculated as a performance measure for the IPA Phase 1 study. Construction of CCDFs is described in Section 9.2 of this report.

8.2.3 Techniques

The techniques used in the evaluation of the performance assessment model include studying the distributions of the input and output variables, evaluating correlations between individual input parameters and the performance measures, and overall model sensitivity to independent variables. The techniques used in this analysis have been described by a number of authors (Draper and Smith, 1966; Mendenhall and Schaeffer, 1973; Bowen and Bennett, 1988; and Sen and Srivastava, 1990) and several have been applied previously to total-system performance assessments (Iman and Conover, 1979; Helton *et al.*, 1991; and McKay, 1992).

The use of regression analysis in this work was an extension of the regression analyses done in IPA Phase 1 (see Codell *et al.*, 1992; p. 62). Previously, the regression analysis was used to determine the most important variables and estimate sensitivities of the total-system performance assessment model output to individual independent variables. In IPA Phase 2, the following techniques for development of a regression equation to emulate the total-system performance assessment model were investigated: transformation of data (Iman and Conover, 1979; and Seitz *et al.*, 1991); test for heteroscedasticity (residual variation—see Draper and Smith, 1966; Bowen and Bennett, 1988; and Sen and Srivastava, 1990); and Mallows' C_p statistic (Sen and Srivastava, 1990). In addition to several techniques used in previous performance assessment work (e.g., the stepwise linear regression), the following techniques were evaluated for determining parameter importance and sensitivity (Kolmogorov-Smirnov and Sign tests (Bowen and Bennett, 1988)); and differential analysis (Helton *et al.*, 1991).

The sensitivity and uncertainty analyses were done with the commercially-available statistical package, *S-plus* (Version 3.1) (Statistical Sciences, Inc., 1991). Programs written in *S-plus* were used in this work to do the compartmental-component analysis, stepwise linear regression analysis, multilinear regression analysis, and statistical tests such as the Kolmogorov-Smirnov test and Mallows' C_p statistic.

8.3 Selection of Most Influential Independent Parameters

8.3.1 Subset Selection by Stepwise Regression Analysis

Stepwise regression analysis has been used in previous total-system performance assessment work (Codell *et al.*, 1992; and Helton *et al.*, 1991) to determine the independent variables that have the most influence on the model output. Stepwise regression analysis selects variables to be in a linear equation based on the correlation coefficient between a single independent variable and the dependent variable (Draper and Smith, 1966; and Iman *et al.*, 1980).

Selection of variables for the linear model by stepwise regression analysis may be based on a variety of criteria, such as the *F*-statistic, the Mean Square Error, the correlation coefficient, or the C_p statistic. As variables are added to the regression equation, the coefficient of determination, R^2, is calculated (Seitz *et al.*, 1991). The coefficient

of determination is the square of the multiple correlation coefficient (Walpole and Myers, 1978) and is proportional to the total variance of the dependent parameter that is explained by the regression model; it increases as more variables are added to the model (Intriligator, 1978). In this analysis, the F-statistic was used for variable selection; the subset giving the largest R^2 was chosen.

In stepwise regression, parameters are ranked in order of importance to the total-system performance assessment model by their effect on the coefficient of determination, R^2 (Seitz *et al.*, 1991). The variable associated with the largest change in R^2 is ranked as the most important.

Subset selection by the stepwise regression technique may be performed at varying levels of significance, α. The level of significance α is the probability that a parameter will be rejected from the regression equation when it should be included. Helton *et al.* (1991) performed stepwise regression analyses at the 0.01 level of significance. In this analysis, the stepwise regression analyses were done for 0.01 and 0.05 level of significance. For the base case (*oooo*) scenario, fifteen parameters were selected by the stepwise regression from a suite of 195 parameters at the 0.01 level of significance, whereas 24 parameters were selected at the 0.05 level of significance. Six parameters were selected at the 0.01 level of significance, from a suite of 29 independent parameters by Helton *et al.*, for the Waste Isolation Pilot Project performance assessment. Helton *et al.* noted that as the number of independent parameters increases, there is more chance for selection of a spurious parameter. An analysis of the relationship between the number of independent parameters used as input to the total-system performance assessment model, the level of significance, and the number of the stepwise-selected parameters was not done in IPA Phase 2. However, such an analysis is needed in order to establish the most appropriate number of variables for the selected subset. A discussion of Mallows' C_p statistic for determining the number of parameters for the "best" fit of a model by a regression equation is given in Section 8.6.2.2.

A small set of parameters that were important in all IPA Phase 2 scenarios were the corrosion potential parameters, *ecorr6*, *ecorr7*, and *ecorr8* that were used in the *SOTEC* module (see Chapter 5 and Appendix A). Infiltration was the most important parameter for the scenarios (see Table 8-1) in which climatic (pluvial) consequences were not considered (*oooo, oodo, osoo, ooov*). The gas retardation coefficient (*betaf*) and fracture permeability (*permf*) for the Topapah Springs member (*C14* gas module) were also included in the list of the most important parameters. The UO_2 alteration rate for sub-area 2 of the repository, *forwar2* (*SOTEC*), was among the important parameters for the scenarios with climatic consequences, *cooo* and *csdv*. Tables 8-2 to 8-5 list the parameters selected by stepwise regression for the base case (*oooo*) and fully disturbed case (*csdv*) for the 0.01 level of significance.

It should be noted that the same subsets were selected for all scenarios without climatic disturbances, *oooo, oodo, osoo, ooov*. Similarly, the scenarios with climatic effects, *cooo* and *csdv*, had the same subsets of important parameters.

Table 8-1 Scenario Classes Modeled in the IPA Phase 2 Analysis

Scenario Class	*Scenario Class Identifier*
Base Case	oooo
Climate Change Only (Pluvial)	cooo
Seismicity Only	osoo
Drilling Only	oodo
Magmatic Activity Only	ooov
Drilling + Seismicity	osdo
Drilling + Seismicity + Magmatic Activity	osdv
Drilling + Seismicity + Climate Change	csdo
Drilling + Seismicity + Magmatic Activity + Climate Change[a]	csdv

[a]Fully disturbed

Table 8–2 Results of Stepwise and Multilinear Regression: *Normalized Release* for Base Case (*oooo*) Scenario[a]

Parameter Name	*Regression Coefficient*	*Confidence Interval*[b]	*Standardized Regression Coefficient*	*Rank Regression Coefficient*	*Elasticity Coefficient*	*Uncertainty Coefficient*
INFIL(UN)	4.86E+02	1.12E+02	0.400	0.417	0.390	0.160
ECORR6	-3.35E-03	1.06E-06	-0.312	-0.348	-2.69	0.0976
ECORR7	-2.68E-03	1.06E-03	-0.248	-0.282	-2.14	0.0619
RETARD3	-1.44E-03	5.57E-03	-0.242	-0.216	-0.510	0.0587
ECORR8	1.28E+03	5.72E+02	0.205	0.243	0.176	0.042
AKR3	9.34E+14	4.03E+14	0.213	0.274	0.255	0.046
Kd39Th	-7.18E-01	4.78E-01	-0.148	-0.092	-0.119	0.019
ECORR5	-2.79E+01	2.25E+01	-0.114	-0.082	-0.213	0.0130
RETARD1	-6.20E-03	5.56E-03	-0.104	-0.110	-0.219	0.0108
KdCm1	1.43E-01	1.27E-01	0.104	0.066	0.089	0.0107
AKR2	9.79E+13	8.24E+13	0.110	0.106	0.132	0.0121
AKR4	1.60E+14	1.34E+14	0.120	0.126	0.131	0.0121
Kd26Am	4.12E-02	4.21E-02	0.090	0.074	0.077	0.008
SOL4Am	2.03E+03	2.00E+03	0.094	—[c]	0.068	0.009
FORWAR2	5.69E+02	5.71E+02	0.092	—[c]	0.068	0.008

[a]See Appendix A for a description of the parameter names. Coefficients are described in Section 8.4.
[b]Values expressed can be added to or subtracted from the *Regression Coefficient*.
[c]Parameter not selected.

Table 8–3 Results of Stepwise and Multilinear Regression: *Effective Dose Equivalent* for Base Case (*oooo*) Scenario[a]

Parameter Name	*Regression Coefficient*	*Confidence Interval[b]*	*Standardized Regression Coefficient*	*Rank Regression Coefficient*	*Elasticity Coefficient*	*Uncertainty Coefficient*
INFIL(UN)	2.91E+07	4.20E+06	0.657	0.870	1.03	0.432
FUNNEL2	8.27E+04	4.63E+04	0.169	0.091	0.469	0.0286
ECORR6	–6.45E+01	3.708E+01	–0.165	–0.138	–2.29	0.0272
FORWAR2	3.57E+07	2.15E+07	0.158	0.101	0.217	0.0249
SOL4AM	1.04E+08	7.46E+07	0.132	0.042	0.154	0.0175
RDIFF13	4.38E+07	3.77E+07	0.110	0.072	0.151	0.0121
KD39Th	–1.87E+04	1.79E+04	–0.099	–0.038	–0.136	0.0098
ECORR5	–8.18E+05	8.43E+05	–0.092	–0.053	–0.278	0.0085
RPOR21	1.51E+05	1.54E+05	0.093	0.043	0.061	0.0087
ECORR7	–3.62E+01	3.71E+01	–0.093	–0.140	–1.28	0.0086

[a]See Appendix A for a definition of the parameter names. Coefficients are described in Section 8.4.
[b]Values expressed can be added to or subtracted from the *Regression Coefficient*.

Table 8–4 Results of Stepwise and Multilinear Regression: *Normalized Release* for Fully Disturbed (*csdv*) Scenario[a]

Parameter Name	*Regression Coefficient*	*Confidence Interval[b]*	*Standardized Regression Coefficient*	*Rank Regression Coefficient*	*Elasticity Coefficient*	*Uncertainty Coefficient*
ECORR6	–6.71E–03	1.37E–03	–0.36	–0.385	–2.22	0.133
ECORR7	–4.55E–03	1.37E–03	–0.25	–0.333	–1.50	0.061
FORWAR2	2.09E+03	8.41E+02	0.20	0.158	0.12	0.038
ECORR8	1.93E+03	8.44E+02	0.18	0.179	0.11	0.033
FORWAR3	1.46E+03	8.45E+02	0.14	0.121	0.08	0.019
KD39TH	–1.25E+00	7.04E–01	–0.14	–0.124	–0.09	0.020
RETARD3	–1.33E–02	8.04E–03	–0.13	–0.148	–0.19	0.017
FUNNEL2	2.87E+00	1.82E+00	0.13	0.120	0.15	0.016
VOLMAX2	–8.64E+01	6.08E–01	0.11	0.032	0.14	0.013
HIT19	1.02E+00	7.29E–01	0.11	0.118	0.13	0.012

[a]See Appendix A for a definition of the parameter names. Coefficients are described in Section 8.4.
[b]Values expressed can be added to or subtracted from the *Regression Coefficient*.

Table 8–5 Results of Stepwise and Multilinear Regression: *Effective Dose Equivalent* for Fully Disturbed *(csdv)* Scenario[a]

Parameter Name	*Regression Coefficient*	*Confidence Interval[b]*	*Standardized Regression Coefficient*	*Rank Regression Coefficient*	*Elasticity Coefficient*	*Uncertainty Coefficient*
FORWAR2	2.13E+08	8.48E+07	0.219	0.378	0.407	0.048
FORWAR3	1.63E+08	1.54E+07	0.167	0.126	0.310	0.028
ECORR6	-2.60E+02	1.47E+02	-0.154	0.346	-2.88	0.024
ECORR8	1.39E+08	8.54E+07	0.143	0.087	0.215	0.020
Kd114Se	3.75E+06	2.84E+06	0.115	—[c]	0.215	0.013
DRILL21	9.85E+00	7.48E+00	0.114	0.099	0.437	0.013
VOLMAX4	-8.07E+04	6.13E+04	-0.115	-0.046	-0.430	0.013
Kd104Ni	1.14E+06	8.51E+05	0.116	—[c]	0.217	0.014
ZONE7	-8.65E+04	7.35E+04	-0.102	—[c]	-0.383	0.010
Kd44Ra	6.65E+03	5.70E+04	0.102	—[c]	0.191	0.010
WAREA4	8.97E+04	7.35E+04	0.106	—[c]	0.398	0.011
FUNNEL2	2.14E+05	1.89E+05	0.101	0.237	0.380	0.010
PERMF1	1.82E+21	1.65E+21	0.096	0.119	2.34	0.009
HIT19	8.37E+04	7.35E+04	0.099	0.086	0.037	0.010
Kd50Pb	1.36E+04	1.26E+04	0.095	—[c]	0.177	0.009
BETAF3	-3.94E+04	3.48E+04	-0.098	—[c]	-1.49	0.010
PORM1	5.08E+05	7.33E+05	0.060	—[c]	0.050	0.004
BETAM	3.54E+04	3.48E+04	-0.088	-0.058	-0.709	0.008
VOLMAX6	-6.04E+04	6.13E+04	-0.086	—[c]	-0.321	0.007

[a]See Appendix A for a definition of the parameter names. Coefficients are described in Section 8.4.
[b]Values expressed can be added to or subtracted from the *Regression Coefficient*.
[c]Parameter not selected.

A means of confirming the selection of the most important parameters for the model is through the use of scatter plots (Helton *et al.*, 1991). By plotting the performance measure (*Normalized Release* or *Effective Dose Equivalent*) against the input variable (e.g., undisturbed infiltration) linear or discontinuous relationships among the parameters may be seen. However, because the performance measures are a function of many independent parameters, distinct relationships may be difficult to detect from scatter plots alone.

8.3.2 Compartmental Component Analysis

Compartmental component analysis was used to illustrate the relative importance of individual radionuclides or release pathways to the *Normalized Release* or *Effective Dose Equivalent*. The compartmental component analysis was done primarily with the use of boxplots. The boxplot (Tukey, 1977; and Helton *et al.*, 1991) is a means of assessing the effect of the full range and distribution of a given component (radionuclide or geosphere pathway) on the output. The boxplot (Figure 8–1) consists of a "box," the ends of which represent the lower and upper quartiles of the distribution (25th percentile ($x_{.25}$) and 75th percentile ($x_{.75}$), respectively). The "*I*" symbol (whisker) represents the values in the distribution that are $x_{.25} - 1.5(x_{.75} - x_{.25})$ and $x_{.75} + 1.5(x_{.75} - x_{.25})$ (Helton *et al.*, 1991). Values outside the whiskers ("outliers") are represented with lines.

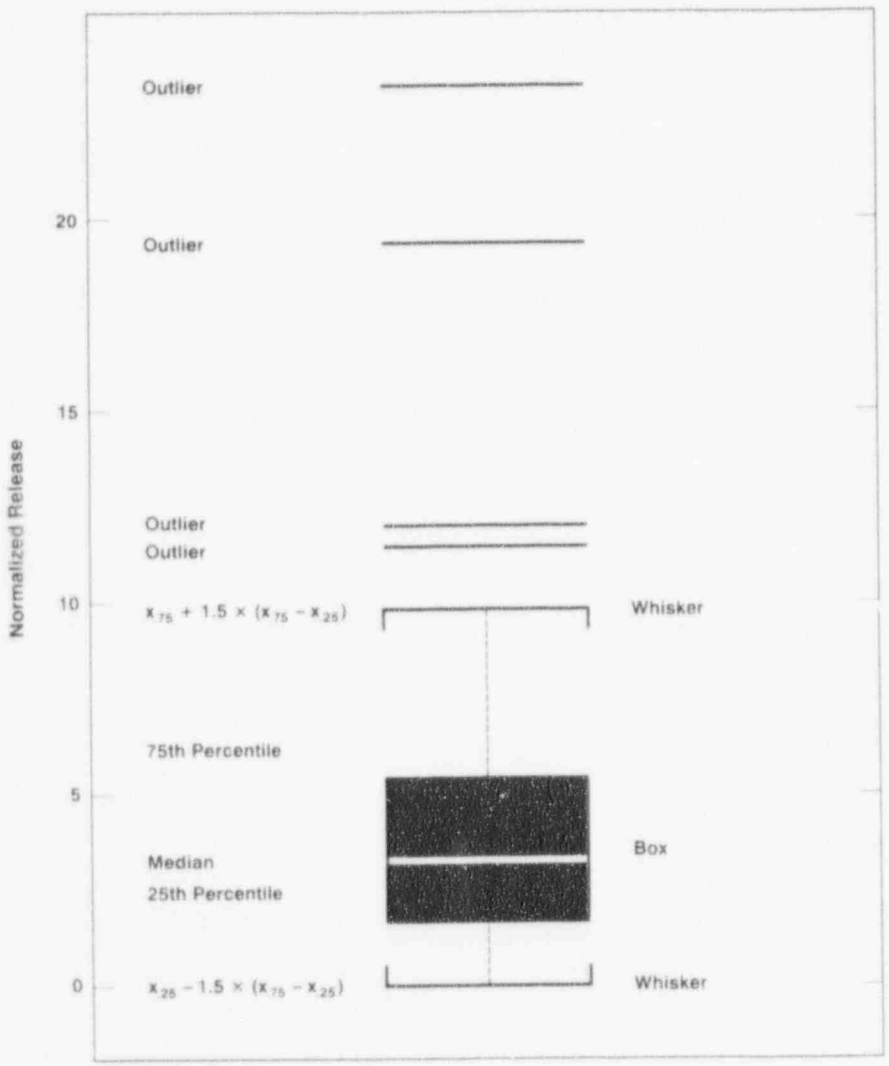

Figure 8–1 Example boxplot showing interquartile region, the whiskers at 1.5 × (interquartile) and outliers in the distribution

8.3.2.1 Contribution of Individual Nuclides to the *Normalized Release* and *Effective Dose Equivalent*

The contribution of individual nuclides to the *Normalized Release* was evaluated in terms of the absolute contribution, the fraction of the total contribution, and the contribution of different transport pathways to the collective release to the accessible environment. The contributions by seven representative radionuclides to the *Normalized Release* and to the *Effective Dose Equivalent* for the base case (*oooo*) are shown in Figures 8–2 and 8–3, respectively. Corresponding results for the fully disturbed case (*csdv*) are illustrated in Figures 8–4 and 8–5.

The dominant radionuclide contributor to the *Normalized Release* is ^{14}C, primarily in the gaseous pathway (Figures 8–2 and 8–4). Fifty percent of the vectors in the base case (*oooo*) have ^{14}C releases greater than 0.8 times the U.S. Environmental Protection Agency (EPA) limit. Although gaseous ^{14}C is important to the *Normalized Release*, it is a very small contributor to the *Effective Dose Equivalent* (Figures 8–3 and 8–5). ^{243}Am is an important contributor to the *Normalized Release* and *Effective Dose Equivalent*, whereas ^{240}Pu and ^{99}Tc are important contributors to the fully disturbed (*csdv*) scenario *Normalized Release*. In some cases, these nuclides exhibit releases greater than the EPA limit.

Federal Regulation 40 CFR Part 191[2] provides that 10 percent of the total releases to the accessible environment may have a *Normalized Release* between 1 and 10. In the IPA Phase 2 total-system performance assessment, more than fifty percent of the vectors gave a *Normalized Release* greater than 1, in large part because of the gaseous ^{14}C release. More than 25 percent of the liquid pathway releases yield a *Normalized Release* greater than 1.

The nuclides making the largest contribution to the *Effective Dose Equivalent* are ^{94}Nb, ^{210}Pb, ^{237}Np, and ^{243}Am. ^{94}Nb, ^{237}Np, and ^{243}Am are important because of their long half-lives, whereas ^{210}Pb continues to build up over time with decay of nuclides in the ^{238}U series, particularly ^{234}U.

8.3.2.2 Releases by Pathway

The relative release by pathway differs between the base (*oooo*) and the fully disturbed (*csdv*) cases. In the base case (*oooo*) scenario, the contribution to the *Normalized Release* is roughly divided between the liquid and the gaseous pathways. The mean contribution to the *Normalized Release* is higher in the liquid pathway for *Normalized Release* less than 1, whereas the mean contribution to the *Normalized Release* is higher in the gaseous pathways for *Normalized Release* between 1 and 10. This is anticipated because much of the exceedence of the EPA limit of 1 is because of gaseous ^{14}C release. The releases for the fully disturbed (*csdv*) scenario are divided much differently among liquid, gaseous, and direct pathways (Figure 8–6). The mean fractional contribution to the *Normalized Release* for the liquid pathway is 0.8, whereas the mean fractional contribution to the *Normalized Release* for the gaseous pathway is 0.2. The direct pathway (via drilling or volcanism), while a much smaller contributor to the *Normalized Release*, exhibits *Normalized Release* values as high as 15.

8.3.3 Significance of Independent Parameters — Kolmogorov-Smirnov Test and Sign Test

The stepwise regression analysis used the change in the coefficient of determination, R^2, to determine which parameters were the most important in the total-system performance assessment model. The Kolmogorov-Smirnov (K-S) test and the Sign test were also used to determine the importance of the input parameters (Bowen and Bennett, 1988). These tests, unlike stepwise regression analysis, test the relationship between the parameters and results, without assuming a specific functional form.

[2]Currently, a revised set of standards specific to the Yucca Mountain site is being developed in accordance with the provisions of the Energy Policy Act of 1992. The Energy Policy Act of 1992 (Public Law 102–486), approved October 24, 1992, directs NRC to promulgate a rule, modifying 10 CFR Part 60 of its regulations, so that these regulations are consistent with EPA's public health and safety standards for protection of the public from releases to the accessible environment from radioactive materials stored or disposed of at Yucca Mountain, Nevada, consistent with the findings and recommendations made by the National Academy of Sciences, to EPA, on issues relating to the environmental standards governing the Yucca Mountain repository. It is assumed that the revised EPA standards for the Yucca Mountain site will not be substantially different from those currently contained in 40 CFR Part 191, particularly as they pertain to the need to conduct a quantitative performance assessment as the means to estimate postclosure performance of the repository system.

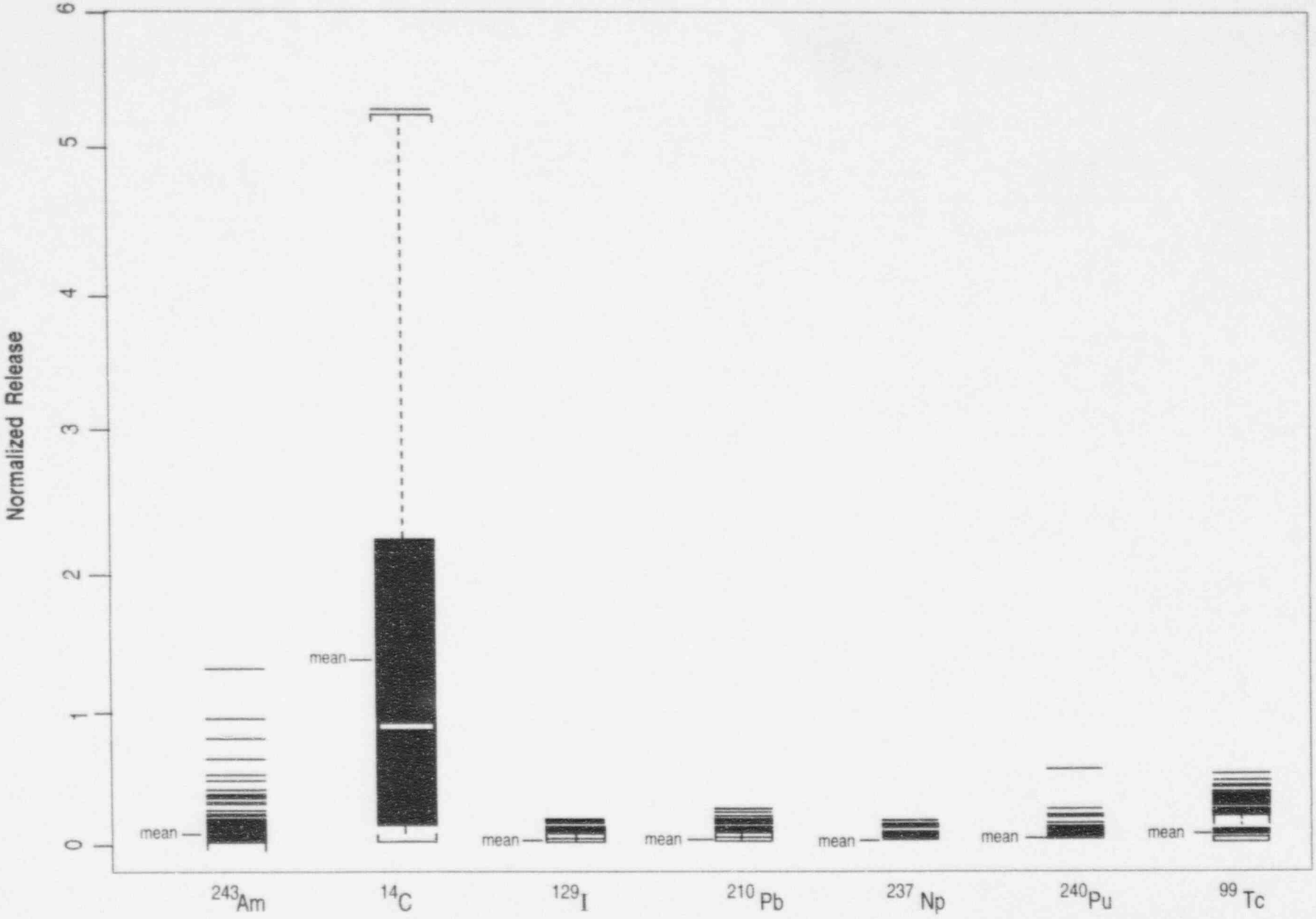

Figure 8-2 Absolute contributions to *Normalized Release* by selected radionuclides, base case *(oooo)* scenario

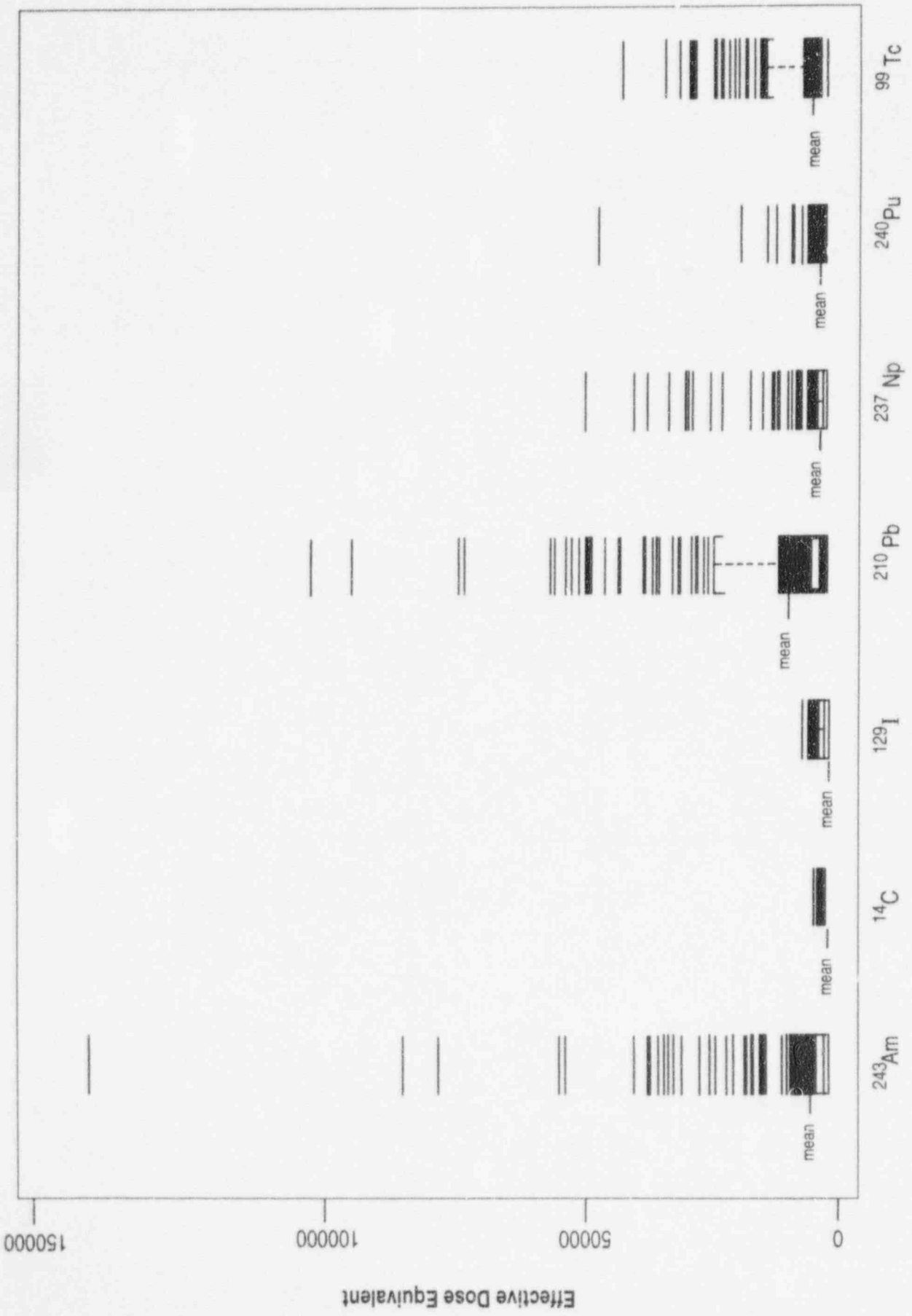

Figure 8–3 Absolute contributions to *Effective Dose Equivalent* by selected radionuclides, base case (*oooo*) scenario

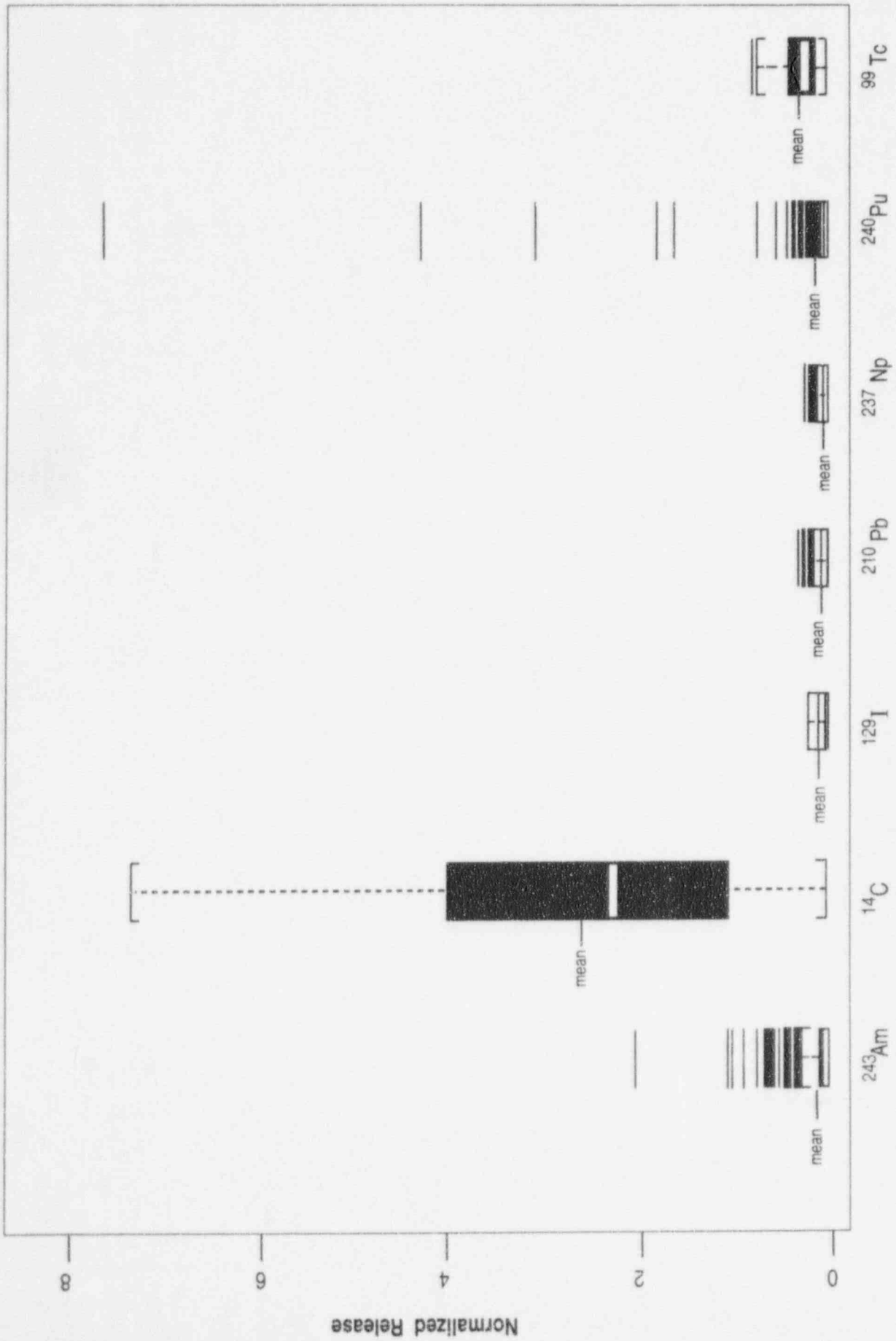

Figure 8–4 Absolute contributions to *Normalized Release* by selected radionuclides, fully disturbed (*csdv*) scenario

Figure 8–5 Absolute contributions to *Effective Dose Equivalent* by selected radionuclides, fully disturbed (*csdv*) scenario

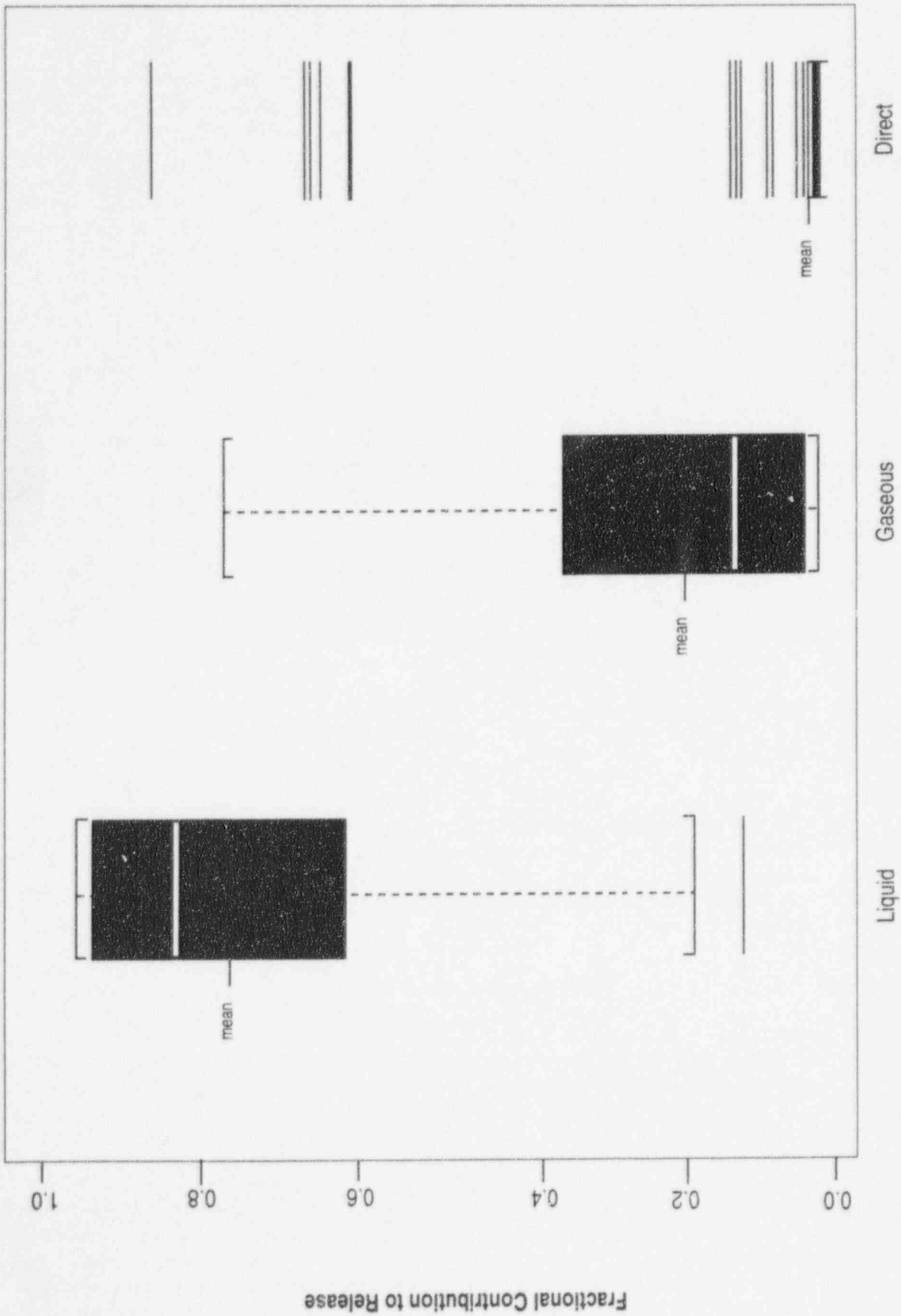

Figure 8–6 Fractional contributions to *Normalized Release* by geosphere pathway

8.3.3.1 The Kolmogorov-Smirnov Test

The K-S test (Bowen and Bennett, 1988) is generally used to test whether two distributions are the same. It was used in the present context as a test of whether a subset of the LHS-determined values for a given input parameter conforms to the distribution defined for the variable. The subsets of input values used in the K–S analysis correspond to the vectors in which the 40 largest values for *Normalized Release* or *Effective Dose Equivalent* were generated in a given scenario. For each input parameter, the defined or theoretical distribution was compared to the distribution of the values in the subsets (Figure 8–7). If the theoretical and subset distributions are similar, the interpretation is that the input parameter will have little or no effect on the results. Conversely, a significant difference between the theoretical distribution and subset distribution would indicate that the parameter is important to the performance measure. Figure 8–7a is a plot of the theoretical distribution (solid line) and the distribution of the sampled values (dots) for the fracture *beta* parameter. The two distributions are very similar, whereas the distributions for undisturbed infiltration (Figure 8–7b) are very different. Fifty percent of the values (cumulative density = 0.5 to 1.0) from the theoretical distribution (solid line) for infiltration rate are greater than 0.00075, whereas 80 percent (cumulative density = 0.2 to 1) of the sampled values (dots) are greater than 0.00075. These large values for the *infiltration rate* are thus significant in affecting the total-system performance assessment (TPA) computer model output as *Normalized Release*.

8.3.3.2 The Sign Test

The Sign test (Bowen and Bennett, 1988) is another test for comparing whether two distributions are the same. Each observation in the subset sample is represented by a plus (+) sign or a minus (–) sign, depending whether it is smaller or larger than the median of the known distribution. The test statistic is the total number of plus (+) signs, and is compared to the number of plus signs expected for a given theoretical distribution and number of samples. If the distributions are significantly different, the independent variable is considered to have an important effect on the total-system performance assessment model output.

Table 8–6 presents the results of applying the K–S and Sign tests to the base case (*oooo*) scenario results for the 0.05 level of significance. The parameters are listed in order of their values for the K–S test. In general, when the K–S test and Sign test were performed on a set of independent parameters one-at-a-time, the resulting subset of important independent parameters agreed with the set of independent parameters selected by the stepwise regression. However, this agreement is conditional on the fact that the samples tested were made up of only the largest values of the *Normalized Release* or *Effective Dose Equivalent*.

The advantage of the K–S and Sign tests over the stepwise regression analysis is that the correlation with the performance measure is strictly related to the distribution of the independent parameter. Different ranges of the performance measure can also be explored to determine the most significant parameters in other parts of the parameter space.

8.4 Sensitivity Analysis

8.4.1 Introduction

The objective of sensitivity analysis is to establish the relative importance of parameters to the conceptual model. One measure of model sensitivity is the amount of variation in model output affected by variation in the model input. The model output, Y, cumulative release of radionuclides at the accessible environment (*Normalized Release* or *Effective Dose Equivalent*) can be expressed in terms of the independent parameters:

$$Y = f(x_1, x_2, \ldots\ldots x_n) \qquad \textbf{(8–1)}$$

Model sensitivity can be defined as the first partial derivative of the model output response Y with respect to the input parameters x_i:

$$s_i = \frac{\partial Y}{\partial x_i} \qquad \textbf{(8–2)}$$

The sensitivity, as defined in the above relationship, has dimensions. To compare sensitivity among parameters in the model, the sensitivities can be normalized and made dimensionless. This may be done in a variety of ways. One method of making the sensitivities dimensionless is to multiply the sensitivity by a ratio of Y and x_i:

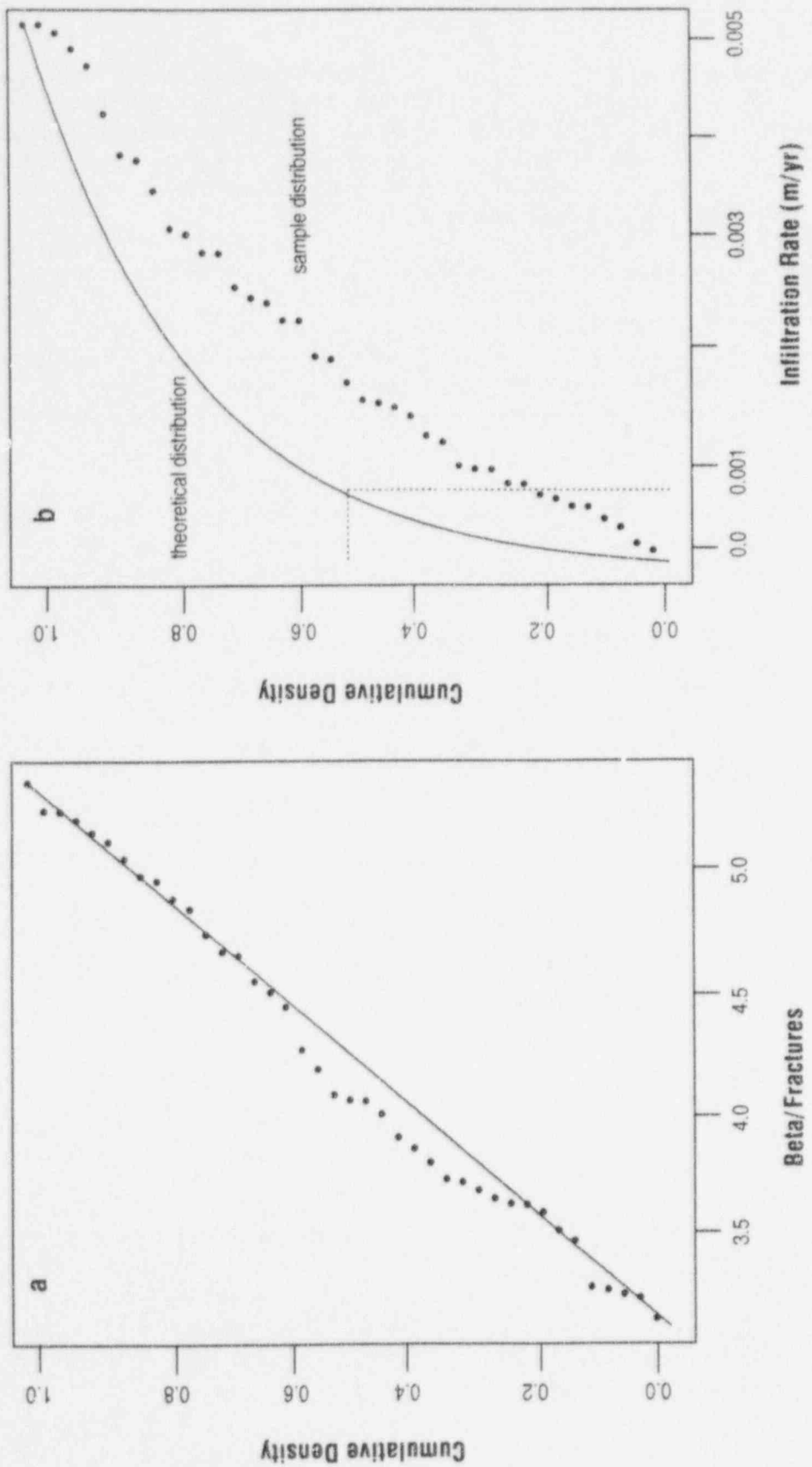

Figure 8–7 **Distributions used in the Kolmogorov–Smirnov test** ((a) Beta coefficient for fractures; (b) Undisturbed infiltration rate.)

$$s' = \frac{\partial Y}{\partial x_i} \cdot \frac{x_i}{Y} \quad . \tag{8-3}$$

If the values for x_i and Y used in the ratio x_i/Y are the estimated means of x_i and Y, the sensitivity is known as the "elasticity" (Intriligator, 1978).

Another way to remove the dimensions and the differences in scale is to standardize each value for the input and response parameters by subtracting the estimated mean $\bar{x}$ and dividing by the standard deviation σ_x (Seitz *et al.*, 1991):

$$x_i^* = \frac{x_i - \bar{x}}{\sigma_x} \quad . \tag{8-4}$$

Table 8–6 Important Parameters Selected by the Kolmogorov-Smirnov and Sign Tests for the Base Case (*oooo*) Scenario at the 0.05 Level of Significance[a]

Normalized Release	*TPA Module*	*Collective Effective Dose Equivalent*	*TPA Module*
INFIL(UN)	FLOWMOD	INFIL(UN)	FLOWMOD
ECORR8	SOTEC	FUNNEL2	SOTEC
AKR3	C14	RPOR(1,2)	SOTEC
RETARD2	C14	ECORR6	SOTEC
SOL4Am	SOTEC	FORWAR2	SOTEC

[a]See Appendix A for a definition of the variable names.

The sensitivities $\partial Y^*/\partial x_i^*$ will have values between 0 and ± 1, which facilitates comparison between disparate parameters.

A number of methods may be used to estimate the sensitivity of the model output to a given independent parameter. Differential analysis (Helton *et al.*, 1991), involves determining the local sensitivity of the response to an individual parameter. Regression analysis may be used to estimate the sensitivity of the model in relation to an individual parameter, or to a group of parameters. Estimations of model performance and overall model sensitivity may be generated with a regression equation.

Generally, a linear regression equation is represented as a linear combination of the independent parameters:

$$Y = \alpha_0 + \sum_{i=1}^{N} \beta_i x_i + \epsilon_i \quad , \tag{8-5}$$

where α_0 is the intercept, β_i are the regression coefficients and ϵ_i is the error (Sen and Srivastava, 1990).

Many submodels in a typical performance assessment behave non-linearly with respect to the values of the input parameters. Regression can include polynomials and cross products of the N independent parameters. For example:

$$Y = \alpha_0 + \sum_{i=1}^{N} \beta_i x_i + \sum_{i=1}^{N} \sum_{j=1}^{N} \beta_{ji}\, x_j\, x_i + \epsilon_i \quad . \tag{8-6}$$

The regression analyses for IPA Phase 2 considered only linear forms and combinations of the

parameters, such as that expressed in Equation (8–5).

8.4.2 Estimation of Sensitivities by Regression Analysis

Multilinear regression was used to estimate the sensitivities of the model with respect to the most important parameters selected by stepwise regression analysis. The estimated regression coefficients for the untransformed data have dimensions. To compare sensitivities for the individual parameters, two different transformations of the data were executed before doing the regression analysis: standardization (Seitz *et al.*, 1991) and rank transformation (Iman and Conover, 1979).

8.4.2.1 Standardization

Data can be standardized to eliminate the dimensions and any scale effects, as illustrated in Equation (8–4) above. The result of this transformation is that all transformed parameter values have a mean of zero and a standard deviation of one. The regression coefficients estimated, using standardized data, are also a measure of the fraction of the standard deviation change in the resonse, Y, as affected by a fraction of the standard deviation σ_x change in the independent parameter (Helton *et al.*, 1991). Thus, the coefficients estimated from regression of the standardized data will be indicative of the importance to the model.

8.4.2.2 Rank Transformation

Rank transformation of the data also eliminates the dimensions and scale associated with the parameters (Iman and Conover, 1979). The rank transformation involves replacing the data used in the model with their corresponding ranks, as determined by ordering the 400 observations from the minimum (1) to maximum (400). The same transformation is done to values of the model output.

The estimated regression coefficients for regressions done with untransformed data, the standardized, and rank-transformed data for the base (*oooo*), and the fully-disturbed (*csdv*) cases are given in Tables 8–2 to 8–5. Because the regression coefficients are estimates, the 95 percent confidence interval was determined for each of the raw regression coefficients. It should be noted that while the regression coefficients are a measure of sensitivity of the model output to the input variables, they are particular to specific models and are not generically applicable.

8.4.3 Estimation of Sensitivities by Differential Analysis

Another method used primarily for sensitivity analyses is differential analysis. This approach consists of approximating the response surface by its Taylor series expansion about a reference point (x^o) such as the mean:

$$Y = Y(x^o) + \sum_{i=1}^{N} \frac{\partial Y(x^o)}{\partial x_i}(x_i - x_i^o) + (\textit{higher order terms}) + \epsilon_i \quad . \tag{8–7}$$

By truncating the Taylor series at the first term, the partial derivative of the response with respect to variable x_i for a small perturbation from the reference point is defined:

$$\frac{\partial Y(x^o)}{\partial x_i} \simeq \frac{Y - Y(x^o)}{x_i - x_i^o} \quad . \tag{8–8}$$

The partial derivatives can be evaluated analytically in some cases, but it is often too difficult to do this directly. A number of techniques, such as the adjoint method and Green's function method, have also been developed (Zimmerman *et al.*, 1990) to increase the efficiency of the evaluation of derivatives analytically within complex computer codes. The partial derivatives can also be evaluated numerically by calculating the performance at the reference point and at points nearby, by perturbing one independent variable at a time.

There are important drawbacks to differential analysis. The Taylor series approximation of the partial derivatives is inherently local, and may not reflect accurately the sensitivity at points far from the evaluation point. Another drawback to differential analysis is that the evaluation of the derivatives is often difficult and expensive. Numerical evaluation of the derivatives, as in Equation (8–8), requires one or more evaluations of the performance assessment model for each derivative, and is often too costly to consider for a large number of input parameters.

Differential analysis provides no information on the possible existence of thresholds or discontinuities in either the independent parameters or the response of the model to the distribution (Helton *et al.*, 1991) (e.g., the change from matrix to fracture flow in unsaturated media). It is possible, however, to evaluate the partial derivatives at any point in the parameter space. Efficient techniques for finding points in the parameter space that are highly significant (e.g., sensitive or high-consequence) have been developed, and demonstrated on a simple representations of a geologic repository (Wu *et al.*, 1992).

8.4.4 Comparison of Sensitivity Coefficients Estimated from Regression and Differential Analyses

Multilinear regression was used to estimate the first derivatives of *Normalized Release (Y)* with respect to the input variables x_i (i.e., $\partial Y/\partial x_i$). These first derivatives are estimates of the coefficients of the multilinear regression equation. In differential analysis, the first derivatives are estimated at a "reference" point; in this analysis, the mean of each input variable. Each input variable is perturbed a small amount from the mean value, one variable at a time, and the first derivatives calculated as described in Equation (8–8).

Differential analysis should not give the same results as regression analysis for the first derivatives (Wu *et al.*, 1992) because multilinear regression analysis uses information from all regions of the parameter space, whereas differential analysis estimates the derivatives at only one point in parameter space.

The analysis for the present comparison was performed for the base case (*oooo*) scenario and the 14 most significant input variables in the following manner:

(1) The mean value of each parameter in the 400-vector Latin Hypercube Sampler (LHS) input file was calculated;

(2) A new input file containing 15 vectors was generated. The first vector contained the average values for each parameter. The next 14 vectors contained the average values for each parameter except for one of the most significant parameters, which differed from its average by a small amount (e.g., 10 percent);

(3) The TPA computer code was run using the new input file for the base case, to generate 15 output vectors of *Normalized Release;* and

(4) The partial derivatives for *Normalized Release* with respect to the 14 independent parameters were estimated using Equation (8–8); the difference between the *Normalized Release* from vector 1 and vectors 2 through 15, divided by the difference in the independent parameter.

The sensitivity coefficients from the differential analysis and multilinear regression for the 14 most significant parameters are compared in Table 8–7. The results agree reasonably well in some cases (e.g., *INFIL(UN), undisturbed infiltration*) and generally have the same sense. The most striking difference is the large number of cases in which differential analysis gave a zero sensitivity. This could be a reflection of the insensitivity to those parameters in the region of the reference point. Additionally, many of the TPA modules switch from one behavior to another rather abruptly, depending on the input parameters. For example, the transition from matrix flow to fracture flow in the module *FLOWMOD* is non-linear over the range of infiltration rates. The insensitivity of the model to several parameters at the reference point indicates the need to apply differential analysis at several points on the response surface.

8.4.5 Model Sensitivity Analysis

8.4.5.1 CCDF Sensitivity

In this work, the CCDF, that is *(1 – CDF (Cumulative Distribution Function))*, which, in a single figure, plots the magnitude and uncertainty of the *Normalized Release* at the accessible environment, is the main vehicle for conveying uncertainty results. However, the CCDF gives no explicit information on the contribution to total uncertainty by each of the input parameters.

Plots illustrating the sensitivity of the CCDF to a single parameter or condition were generated by screening the output vectors according to a criterion, and using only the remaining vectors to produce the CCDFs. The CCDFs of screened

Table 8–7 Comparison of First Derivatives of *Normalized Release* by Regression and Differential Analysis[a]

Parameter Name	$\frac{\partial Y}{\partial x_i}$ *Regression*	$\frac{\partial Y}{\partial x_i}$ *Differential*	*Elasticity Regression*	*Elasticity Differential*
INFIL(UN)	502	377.4	0.403	0.495
ECORR6	–0.0033	0	–2.66	0
ECORR7	–0.0027	0	–2.14	0
RETARD3	–0.015	–0.00194	–0.518	–0.112
ECORR8	1317	0	0.182	0
AKR3	9.6E + 14	3.65E + 13	0.264	0.016
KD39Th	–0.713	0	–0.118	0
ECORR5	–27.3	0	–0.213	0
RETARD1	–0.0062	–0.0021	–0.219	–0.036
KD1Cm	0.014	0	0.049	0
AKR2	9.79E + 13	5.66E + 13	0.132	0.012
AKR4	1.6E + 14	–1.7E + 13	0.131	–0.0022
Kd26Am	0.041	0	0.077	0
SOL4Am	2030	597	0.068	0.0033

[a]See Appendix A for a definition of the parameter names.

data illustrating the sensitivity to performance measures of individual natural and engineered barriers are presented in Section 9.5.

8.4.5.2 Sensitivity of Results to Number of Vectors

The sensitivity of the results to the number of LHS vectors in each scenario is illustrated by comparing spurious correlations among the input parameters and by the sensitivity of the CCDF to the number of vectors.

8.4.5.2.1 Spurious Correlations

Although it is possible to specify correlations among parameters when generating input vectors with the LHS method, this feature was not evoked in IPA Phase 2 (i.e., there was no deliberate attempt to produce correlations among input parameters). Spurious correlations are apparent correlations of the input parameters among themselves, when no correlations were intended. Although computer programs for generating LHS (Iman *et al.*, 1980) generally contain algorithms for minimizing these effects, correlation of the model output variables to the independent parameters is confounded by spurious correlations, if too few vectors are available for the statistical tests.

To demonstrate the problem with spurious correlations, three computations of *Normalized Release* were done with inputs of 100, 200, and 400 vectors generated by the LHS technique. Each vector had

445 parameters, 195 of which were sampled for the base case (*oooo*). The correlation coefficient between each input parameter x_i and the *Normalized Release, Y,* calculated from the performance assessment model was calculated and plotted against the largest correlation between x_i and any other independent parameter. These plots illustrate a limitation of the sensitivity analyses; if the spurious correlations among independent parameters are as large or larger than the correlation between the dependent-independent parameters, then one cannot determine the validity of the latter correlations. Figure 8–8 for 100 vectors clearly shows that the correlations among independent parameters are as large or larger than the correlations between the independent parameters and model output for a significant fraction of the vectors, thereby confounding interpretation of the results for sensitivity. The results are similar for 200 vectors, but are not shown here. Figure 8–9 illustrates that for 400 vectors, the largest correlations between the independent parameters and model output are distinctly larger than the correlations among the independent parameters.

8.4.5.2.2 Sensitivity of the CCDF to Number of Vectors

CCDFs of *Normalized Release* were generated from runs of 50, 100, 150, 200, and 400 vectors, and presented in Figure 8–10. Visually, the CCDFs were quite similar, suggesting a relative lack of sensitivity to the number of vectors.

The conclusions that can be drawn from this analysis are that the usefulness of the sensitivity analysis was limited for fewer than 400 vectors per scenario, as shown by comparing the magnitude of the largest spurious correlations to the model output-independent parameter correlations. However CCDFs were much less sensitive to the number of vectors per scenario.

8.5 Uncertainty Analysis

Different types of uncertainty associated with the modeling of physicochemical processes can be distinguished—in particular:

- The statistical uncertainty because of the inherent random nature of the processes, and
- The state-of-knowledge uncertainty.

The latter uncertainty may be subdivided further into parameter and model uncertainty. Parameter uncertainty is caused by insufficient knowledge about the input information, and can manifest itself in several forms. For example, if a single parameter characterizes a facet of the model (e.g., hydraulic conductivity of a rock unit), then uncertainty about its value would lead to selecting a distribution for the probabilistic sampling of that parameter with wider limits than if the parameter were well characterized. Because it usually is not possible to characterize a spatially varying property of the rock, such as permeability by a single parameter, using a single parameter value over the entire field of calculation to represent a spatially varying parameter also introduces uncertainty.

For IPA Phase 2, the repository was represented by a highly simplified conceptual model, which in many cases, ignored the large spatial variability of the geosphere (e.g., the hydraulic properties of each layer were considered spatially homogeneous for each vector, ignoring the considerable heterogeneity). These parameters could be made to vary in time and space; however, this would make the modeling much more complicated. Models within the system representing the performance assessment do in fact include spatial and temporal variability, but these are only indirectly a result of the values of the input parameters. For example, gas flow is represented in two dimensions and is transient in time. Additionally, some of the parameters such as hydraulic conductivity implicitly take into consideration the spatial scales of correlation to account for the length of flow paths.

Modeling uncertainty is caused by simplifying assumptions and the fact that the models used may not accurately simulate the true physical process. This study, as was the case in the IPA Phase 1 study (Codell *et al.*, 1992), deals primarily with the effects of parameter uncertainty.

Iman and Helton (1985, p. 1–1) give an apt definition of uncertainty, which has been adopted for the present study:

> "Uncertainty analysis is defined here to be the determination of the variation or model imprecision in Y that results from the collective variation in the model variables $x_1 \ldots x_k \ldots$. A convenient tool for providing such information is the estimated cumulative

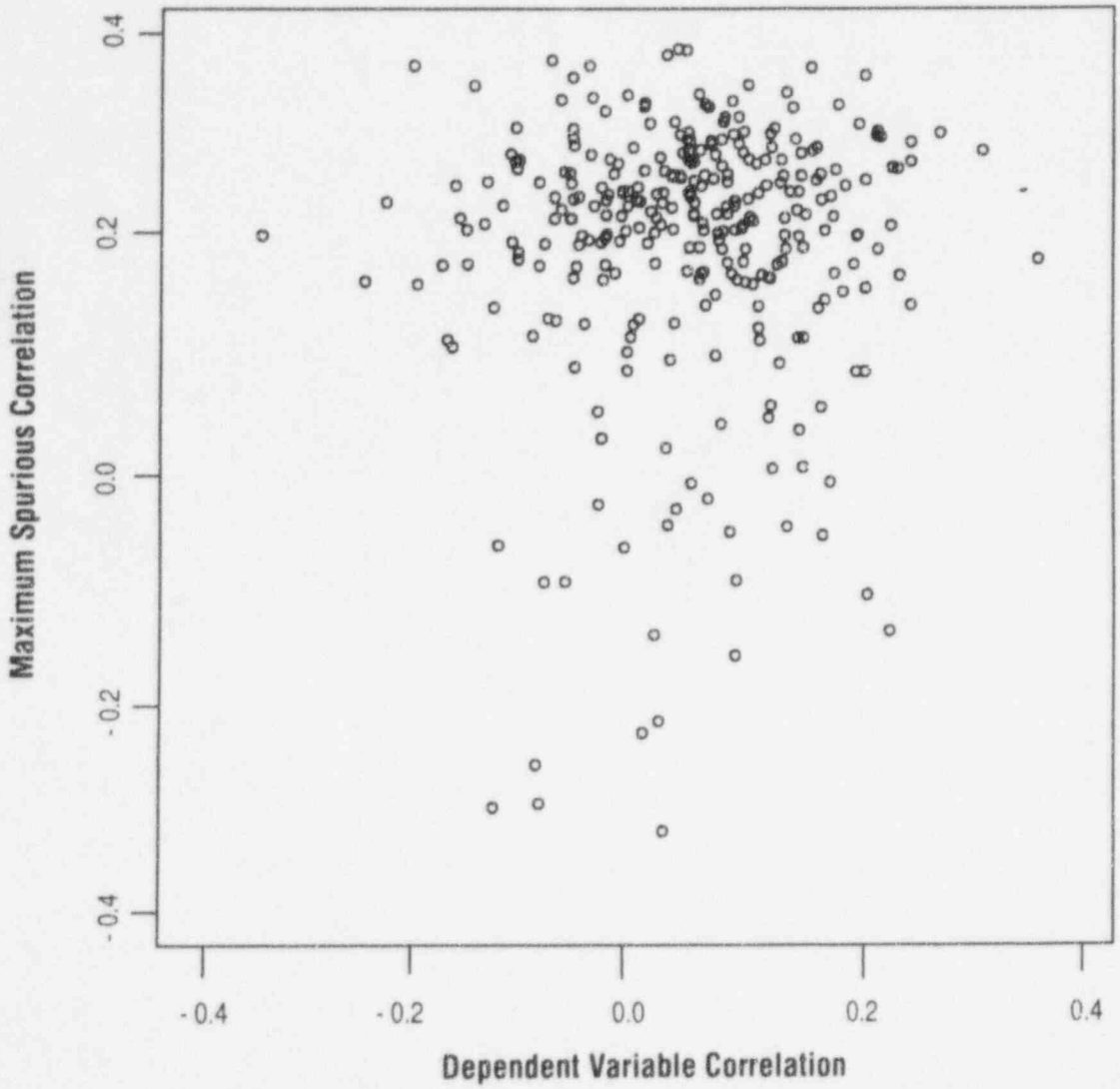

Figure 8–8 Maximum spurious correlations among independent parameters versus correlations between model output and independent parameters for 100 vectors

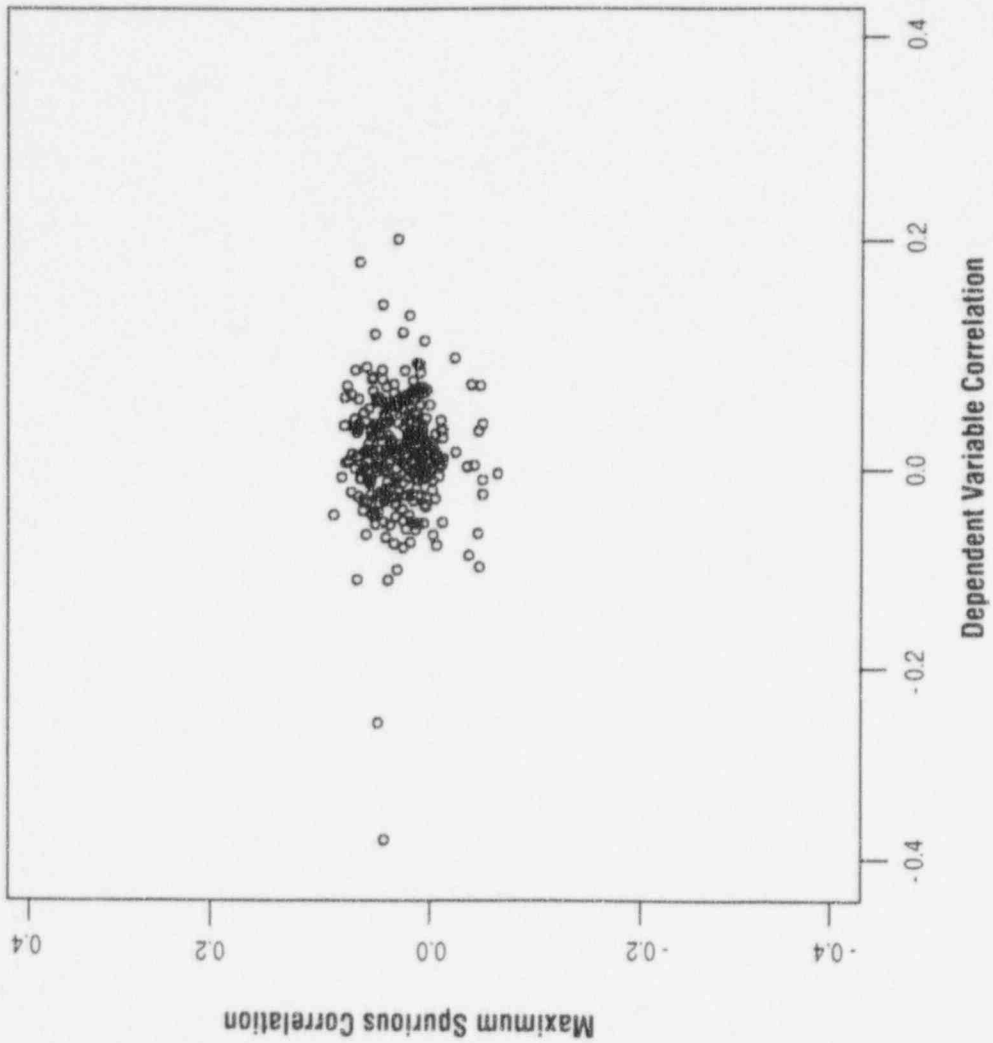

Figure 8–9 Maximum spurious correlations among independent parameters versus correlations between model output and independent parameters for 400 vectors

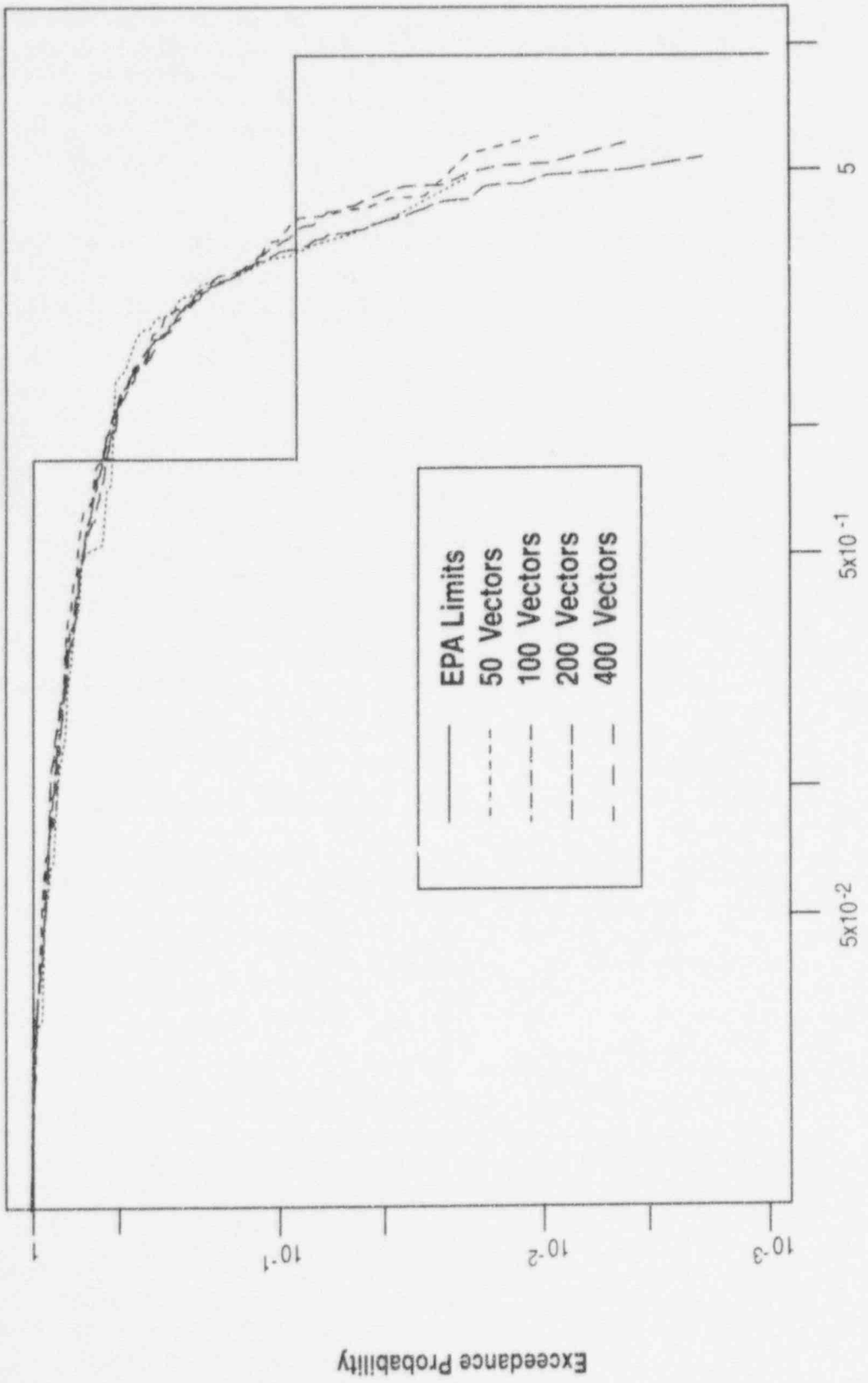

Figure 8–10 Sensitivity of base case (*oooo*) scenario CCDF to the number of vectors

distribution function (CDF) for Y since it summarizes the variability in computer model output which results from the input assumptions."

Although the main presentation of uncertainty in IPA Phase 2 will rest on the CCDF, an additional means of describing uncertainty, the "uncertainty coefficient," has also been developed.

Uncertainty Coefficient

It would be useful to define an "uncertainty coefficient" to represent the contribution of uncertainty from each of the input parameters, but there does not appear to be any standard definition of such a term. Leading toward a definition that can be used in the present work, Zimmerman *et al.* (1990) present an expression for the uncertainty, using the response surface in which the actual model is represented by the multilinear regression of the model results:

$$Var(Y) = E[(Y - \bar{Y})^2] = \sum_i \beta_i^2 Var(x_i) + \sum_i \sum_j \beta_i \beta_j Cov(x_i, x_j) \quad , \qquad \textbf{(8–9)}$$

where Y is the value of the response, β_i is the regression coefficient $\partial Y / \partial x_i$, $E[\ ]$ is the expected value, $\bar{Y}$ is the estimated mean of Y, *Var* is the variance, and *Cov* is the covariance. For the IPA Phase 2 calculations, the independent parameters are not deliberately correlated, so it is assumed that the covariance term is zero. In this analysis, the quantity $Var(Y)$ is estimated by estimating β_i and $Var(x_i)$.

Assuming that there is no covariance among the independent parameters, Equation (8–9) presents a way in which the variance of the response can be tied to variance and sensitivity of each of the independent parameters. Based on this assumption, it is possible to define an "uncertainty" coefficient U_i:

$$U_i = \frac{\beta_i^2 \ Var(x_i)}{Var\ (Y)} \quad . \qquad \textbf{(8–10)}$$

This term is numerically equivalent to the square of the "standardized regression coefficient" described in Section 8.4.2. Ideally, if all the independent parameters were included in the model, the sum of U_i for all independent parameters would be unity. Non-zero covariance of the independent parameters will cause ΣU_i to deviate from unity. The sums of the uncertainty coefficients presented in Tables 8–2 to 8–5 are equal to the coefficient of determination, R^2, for each regression analysis.

8.6 Emulation of the Total-System Performance Assessment Model Using Multilinear Regression

One aspect of doing multilinear regression that has not been explored previously by the NRC staff is the application to emulating the total-system performance assessment model. The regression equation can be used with the suite of values for the input parameter to estimate the response, $\hat{Y}$. The estimated response may then be compared with the full model output (*Normalized Release* or *Effective Dose Equivalent*) to determine how good the regression equation approximation of the model is. The following discussion outlines some of the procedures used to better fit the regression equation to the model and illustrates how the regression equation can be used to estimate model performance.

8.6.1 Estimation of the Response

Values of the response for the simplest form of the multilinear regression equation were calculated using the raw data for the input parameters (x_i) and the estimated regression coefficients, b_i (Tables 8–2 to 8–5).

$$\hat{Y} = a_0 + b_1 x_1 + \ldots + b_n x_n \quad . \qquad \textbf{(8–11)}$$

It should be noted that although the form of the regression described here is linear, several parameters used in IPA Phase 2 do not exhibit a linear relationship with the performance measure.

A non-linear relationship between the response and the independent parameters can often be determined by plotting the residuals for the regression against the values for a given independent parameter (Figure 8–11). If the residuals $e_i = (Y_i - \hat{Y}_i)$ are a function of an independent parameter, there will be a grouping or trend in the residuals as a function of the independent parameter (Figure 8–11a). In Figure 8–11a, there is a

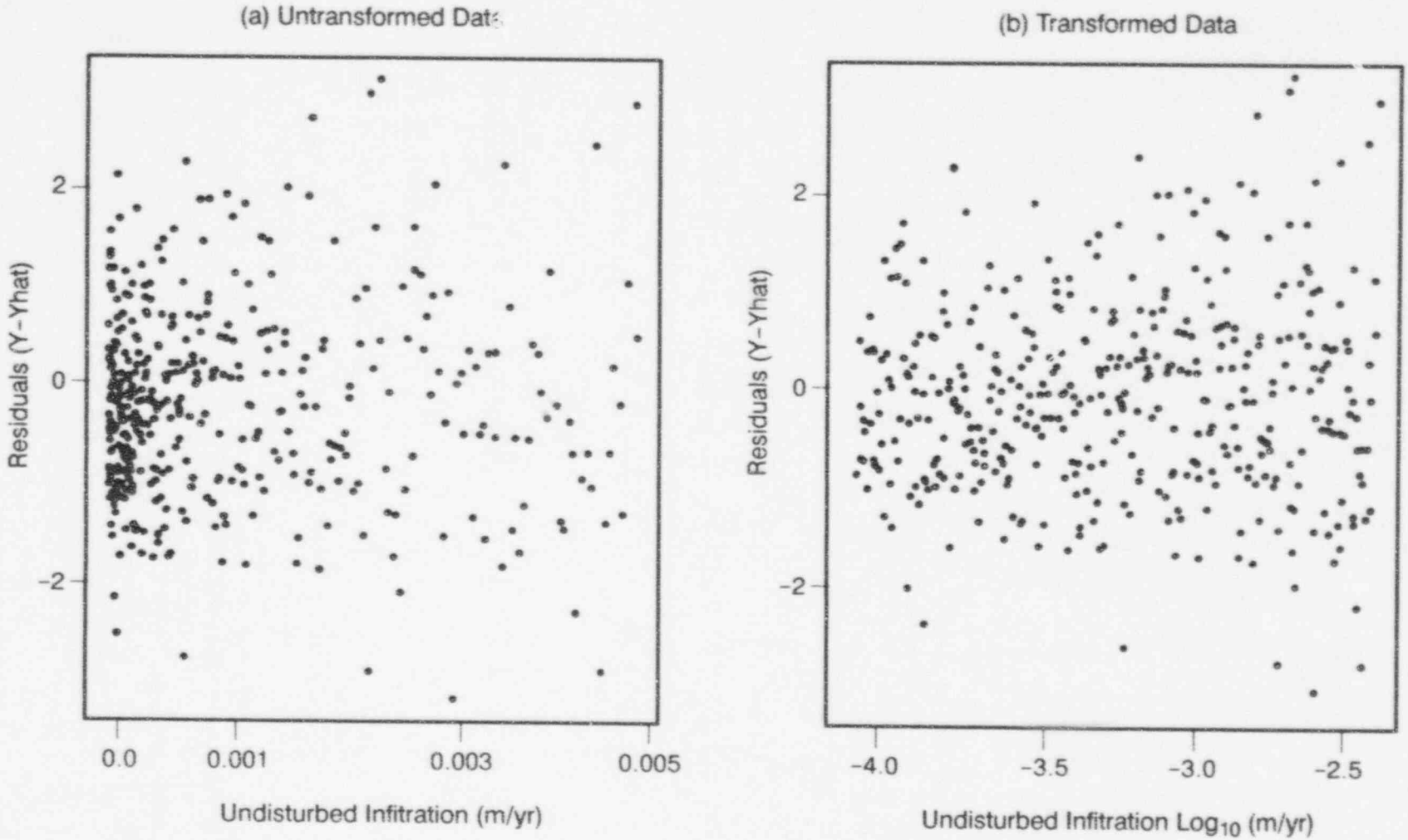

Figure 8–11 Plot of residuals from multilinear regression as a test for heteroscedasticity

skewed distribution of the points toward low infiltration values. Transformation of the independent parameter to a non-linear form (e.g., $1/x$, $log(x)$, x^2) may be appropriate (Sen and Srivastava, 1990). By transforming the independent parameter (e.g., *infiltration* to *log(infiltration)*), the residuals plot (Figure 8–11b) is changed to indicate no functional relationship between the residuals and the independent parameter. This indicates that the new form of the parameter may help provide a better fit of the model.

The process of transforming parameters, doing subset selection and regression analysis, is an iterative process. Several iterations may be required to get the best fit of the model by the regression equation. Non-linear regression techniques are also available, but beyond the scope of the present project.

A regression equation was constructed for the purpose of emulating the total-system performance assessment model. Twenty parameters selected by stepwise regression analysis were used; some parameters were transformed as discussed above.

Figure 8–12 is a plot of the estimated values for *Normalized Release*, $\hat{Y}$, from the regression equation versus the *Normalized Release* for the base case (*oooo*) computed by the TPA computer code. It should be noted that the estimated response parameter $\hat{Y}$ is a function of specific b_i and specific values of x_i. Other regression equations will give different results. The purpose of the plot is to illustrate the degree of fit between the response variable determined by the regression equation and the performance measure computed by the TPA computer code. The correlation coefficient between the estimated response $\hat{Y}$ and the *Normalized Release* is 0.78, which corresponds to a coefficient of determination of 0.61. The 95 percent confidence interval is noted on the plot and indicates the region in which there is high confidence of finding the least-squares fit line. Figure 8–13 illustrates the CCDFs for the estimated responses $\hat{Y}$ and the *Normalized Release* from the total-system performance assessment model.

8.6.2 Evaluation of the Goodness of Fit

8.6.2.1 Correlation Coefficient

The correlation coefficient is often used to estimate the linear relationship between two variables (Walpole and Myers, 1978). The more linear the relationship, the closer the correlation coefficient is to unity. Ideally, the better the regression equation estimates the full total-system performance assessment model, the closer the correlation coefficient is to 1 (or –1). The square of the correlation coefficient, the coefficient of determination (R^2) indicates the percent of the full model that is explained by the regression model. The coefficient of determination for the regression equation with twenty parameters is 0.61. Because the coefficient of determination and the absolute value of the correlation coefficient increase as more parameters are added to the model, they are not necessarily good indicators of the optimal number of parameters to be included in the regression model. Proper selection of the form of the independent parameters is essential to constructing a regression equation that will emulate the total-system performance assessment model well.

8.6.2.2 Mallows' C_p Statistic

Helton *et al.* (1991) stated that as the number of independent parameters increases, there is a greater chance for spurious correlations that result in the inclusion of a variable in the regression model. Mallows' C_p statistic (Mallows, 1973; and Sen and Srivastava, 1990) was used in this analysis, in an attempt to evaluate the optimal number of parameters that should be included in the regression model.

Mallows' C_p statistic compares the error of the restricted model (the regression equation for the subset of parameters) to the error of the full (total-system performance assessment) model (all of the independent parameters):

$$C_p = \frac{\sum_{i=1}^{p} (Y - \hat{Y})^2}{s^2} - (n - 2p) \quad , \qquad \textbf{(8–12)}$$

where Y is the response for the full model with all parameters, $\hat{Y}$ is the response for the restricted model, s^2 is the unbiased estimate of the variance (mean square error) for the full model, n is the number of observations, and p is the number of

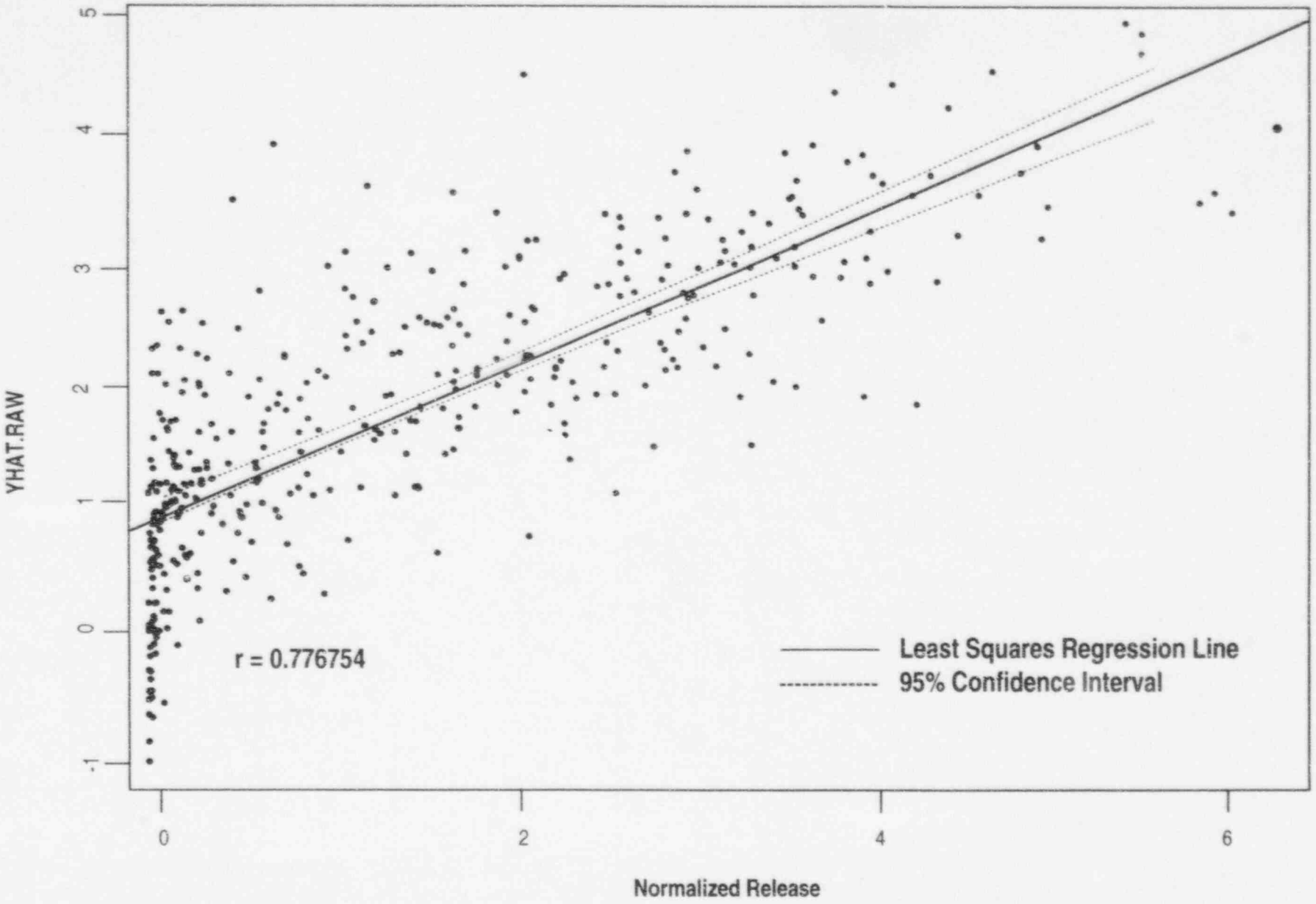

Figure 8–12 Plot of predicted response (YHAT.RAW) from multilinear regression analysis versus *Normalized Release* calculated by the TPA computer code, base case (*oooo*) scenario

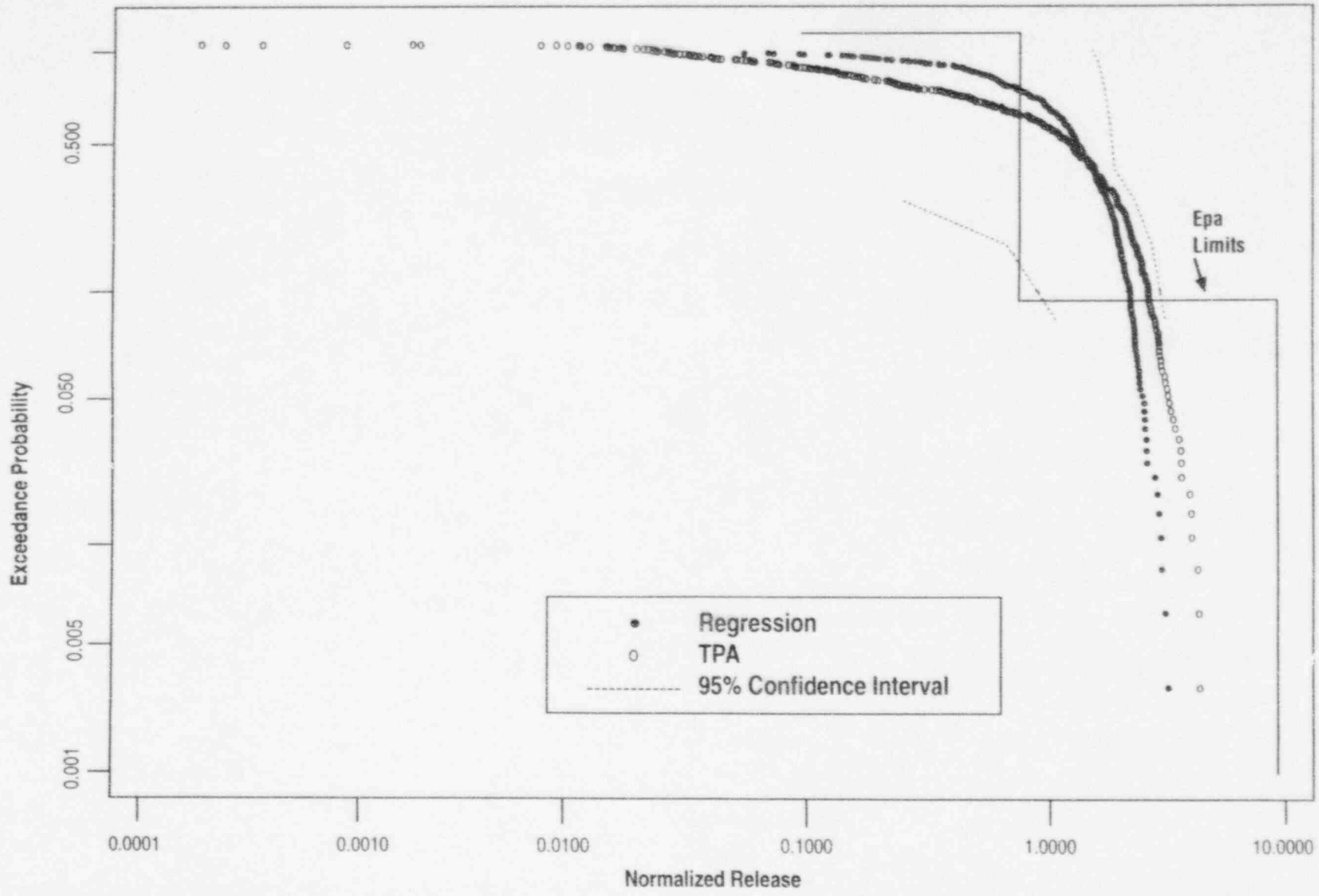

Figure 8–13 Comparison of CCDFs for predicted response (YHAT.RAW) and *Normalized Release* from the TPA computer code, base case (*oooo*) scenario

independent parameters in restricted model, plus one (Walpole and Meyers, 1978).

When $C_p \simeq p$, the optimal number of parameters for the regression equation has been chosen. In this analysis, the use of the C_p statistic for selecting the optimal number of parameters did not give results that were easily interpretable. The C_p statistic is very sensitive to small changes in the fit if $(n - 2p)$ is large (Gunst and Mason, 1980). Attempts were made to reduce the number of independent parameters to consider, by first performing stepwise linear regression, with the F-test criterion using $= 0.1$, and then doing a subsequent subset selection, with $\alpha = 0.05$. The comparison of the $\alpha_{.05}$ model with the $\alpha_{0.1}$ model still did not provide easily interpretable results. More work is needed to establish the optimal number of parameters for subset selection and multilinear regression. One aspect that should be considered is the predictive capability of the individual independent parameters. Another aspect to consider is how effectively this statistic might be applied to highly non-linear models.

8.7 Sensitivity and Uncertainty Auxiliary Analyses

The IPA Phase 2 staff took part in a computational exercise to evaluate several methods of sensitivity and uncertainty analyses. The purpose of these analyses was to demonstrate, on relatively simple flow and transport problems, several methods for sensitivity and uncertainty analysis useful for evaluation of total-system performance assessments.

The work was presented in two reports. The first report (Gureghian *et al.*, 1992) covers the derivation and verification of the closed-form analytical solutions for one-dimensional saturated transport of a radionuclide in a fractured, layered system with diffusion into the rock matrix. The material properties of individual fractures and rock matrix layers were assumed to be homogeneous and isotropic. The sorption phenomenon in fractures and matrix was described by a retardation coefficients. The solutions of the model are based on analytical inversions of the Laplace transforms, verified with inversions performed numerically. The first module of the computer program calculates the space-time dependent concentration of a decaying species migrating in the fractures and the surrounding matrix. The second module predicts the local sensitivities of releases to the independent parameters.

The second report (Wu *et al.*, 1992) evaluates and demonstrates the use of several sensitivity and uncertainty analysis methods using the analytical model developed by Gureghian *et al.* The Limit-State Approach, which was developed initially for structural reliability analyses, was investigated for its usefulness in IPA. This approach is based on partitioning the performance results into two parts, one in which the performance measure is smaller than a chosen value called the Limit-State, and the other in which the performance measure is larger. The optimal expansion point in parameter space, known as the Most Probable Point (MPP), has the property that its location on the Limit-State surface is closest to the origin. Additionally, the projections onto the parameter axes of the vector from the origin to the MPP are the sensitivity coefficients. Once the MPP is determined and the Limit-State surface approximated, the probability of the performance measure being less than the Limit-State can be evaluated. By choosing a succession of Limit-States, the entire cumulative distribution of the performance measure can be determined. Determining the location of the MPP is the crux of the methodology. Methods for determining the MPP and improving the estimate of probability are discussed in the report.

The Limit-State Approach is significantly more complex than the more commonly used Monte Carlo or Latin Hypercube sampling methods. To aid understanding of the Limit-State Approach, all steps of the method were explained by applying it to two simple examples. The first involved calculation of the cumulative probability distribution of the Darcy velocity V, given by $V = -KI$, where K and I are the hydraulic conductivity and hydraulic gradient, respectively. Although simple, this example turned out to be difficult for the application of the Limit-State Approach, because of the possibility of change of sign of I and hence V.

The second example applied the Limit-State Approach to a one-dimensional transport problem developed in Gureghian *et al.*, and compared the results among the more conventional methods such as Monte Carlo, LHS, and differential analysis for computing both the CCDF and the sensitivity coefficients. This problem included 25

independent parameters. The uncertainty analysis used the CCDF for cumulative release as the basis for comparison between the methods. Results indicated that the Limit-State Approach had the potential of being much more efficient in terms of computational resources than Latin Hypercube or Monte Carlo Sampling. In one case, the Limit-State Approach was able to duplicate the CCDF produced by a 5000-vector Monte Carlo run with only about 600 vectors, and in other cases far fewer.

In general, computational efficiency is proportional to the desired accuracy and the choice of an approach will depend on the nature of the problem. However, the reports demonstrate that the Limit-State Approach permits the analyst to concentrate on the critical performance region, with the potential for optimizing the use of the consequence model where it can contribute the most information. By contrast, sampling methods such as Monte Carlo or LHS must cover the entire parameter space, regardless of its importance. In addition, the Limit-State Approach leads to probabilistic sensitivity analyses, with essentially no additional work. In particular, the efficiency of the Limit-State Approach is independent of the probability level. Therefore, it is more suitable for evaluating the tails of the distribution than LHS or Monte Carlo sampling. However, the Limit-State Approach is relatively difficult to implement.

The computational efficiency of the Limit-State Approach in general depends on the number of independent parameters and the efficiency of evaluating local sensitivities. When the number of independent parameters is large, the Limit-State Approach may no longer be efficient unless the sensitivities can be determined efficiently, but at the expense of simplicity. The efficiency of the standard Monte Carlo method depends only on the probability level and desired accuracy. It is not clear that the Limit-State Approach will be the best approach for problems involving large numbers of independent parameters.

8.8 Conclusions and Suggestions for Further Work

The sensitivity and uncertainty analyses in IPA Phase 2 involved evaluation of a number of techniques that have potential use in the evaluation of the performance assessment models in a potential license application. Many of the techniques used have been used in previous performance assessment work: stepwise regression analysis, CCDFs, differential analysis, and boxplots. In addition, the Kolmogorov-Smirnov and Sign tests were used to determine parameters important to the total-system performance assessment model. Techniques for developing regression equation to emulate the total-system performance assessment model were examined for potential use in determining CCDF sensitivity to changes in parameter distribution type, for example.

Selection of the significant parameters by stepwise regression analysis, the *K–S* test, and the Sign test gave similar results. Regression analysis can only be applied over the entire parameter space. The *K–S* test can also be applied to different parts of the parameter space, in order to test for locally important parameters.

The use of standardized data for stepwise regression gave the same results as the untransformed/raw data and had the advantage of giving dimensionless coefficients that could then be compared. The estimated multilinear regression coefficients for the standardized data were used to determine the "uncertainty coefficient" that defined the percentage of the variance of the model response, attributable to variance in the independent parameter.

The results of differential analysis for 14 parameters about the mean for all parameters agreed fairly well with the multilinear regression coefficients. Several parameters exhibited zero sensitivity about the mean, which points to the importance of determining local sensitivities at several points in the parameter space.

The question of how many vectors (observations) will give valid results needs to be explored. The Latin Hypercube sampling strategy reduces the number of vectors needed to do a Monte Carlo simulation. The covariance of the independent variables for 400 vectors was small but non-zero. Difficulties associated with application of the C_p statistic indicates that perhaps more vectors are needed. The sampling of more vectors will have the disadvantage of requiring longer run times. Yet, it should significantly reduce the number of spurious correlations that can result in picking the wrong variables by stepwise regression.

The assumption that covariance was zero was made in the sensitivity and uncertainty analyses. Future work to consider grouping of parameters or covariance among the input parameters is important to developing a better understanding of model sensitivities.

The development of a regression equation for the purpose of verifying important parameter selection by emulating the total-system performance assessment model has potential use in the license application review process. It should be emphasized that regression equations can never replace the total-system performance assessment model, but are a tool by which to study the sensitivities associated with performance assessment models. The linear estimation used in this analysis is the simplest technique; a number of others can be explored in future phases of this work.

In general, the techniques used in the IPA Phase 2 sensitivity and uncertainty analysis were easy to implement. No single technique is valid for the sensitivity and uncertainty analyses. The use of a combination of techniques is essential to bringing out various aspects of the total-system performance assessment model. Future evaluation of other techniques such as the "hat" function (Sen and Srivastava, 1990) or the Limit-State Approach will help to establish which techniques will be most useful to the license application review process.

9 ANALYTICAL RESULTS[1]

9.1 Introduction and Caveats Concerning the Results of IPA Phase 2

This chapter presents the results of the simulation runs of the total-system performance assessment (TPA) computer code using the parameter distributions presented in Appendix A of this report. The results of the simulations are presented as complimentary cumulative distribution functions (CCDFs) of *Normalized Release* and *Effective Dose Equivalent* (defined in Chapter 8), distribution bar graphs, and scatter plots.

The results are presented for demonstration purposes and are not intended to indicate the potential for repository compliance or non-compliance with any of the 10 CFR Part 60 performance requirements.

The following caveats should be taken into consideration when reviewing the results of the Iterative Performance Assessment (IPA) Phase 2 effort:

1. **The models used here are based on limited site data and have had limited review.**
   Preliminary results from some models such as the gas transport and ^{14}C retardation model have been presented at U.S. Nuclear Regulatory Commission/U.S. Department of Energy (DOE) Technical Exchanges and before the U.S. Environmental Protection Agency's (EPA's) Scientific Advisory Board. Although the overall modeling was more sophisticated than that of IPA Phase 1, it was recognized that input data were still very limited. In addition, scientists do not yet agree on how adequately the various models represent repository processes.

2. **The results presented here cannot be confirmed as accurately representing the behavior of the repository.**
   The staff has examined the results of runs for individual vectors to ensure that for these limited cases, the TPA model appears to be performing as designed. However, other than software quality assurance (QA) and the above mentioned checks, there is no comprehensive validation procedure for the TPA model available at present, to ensure that the computed CCDFs are accurate representations of the behavior of the repository system.

3. **There are numerous unverified simplifying assumptions in many of the models.**
   The models for flow and transport considered only a steady rate of infiltration and a constant environment, and did not take into account the significant variations in the driving forces likely to occur over the performance assessment period. Also, the models considered that the geosphere was spatially uniform in the lateral direction, and did not take into account the large variations in material properties that exist at the site. In addition, the behavior of many thousands of waste packages was represented by ensemble averages, using seven representative waste packages.

4. **There are large uncertainties in the input data.**
   Although the TPA model is intended to deal with some data uncertainty through the Latin Hypercube Sampling (LHS) process, many of the most important parameters have variations over several orders of magnitude. For many parameter distributions, the means and distribution shapes are based on only a few measurements. Also, the analysis did not recognize correlations among the independent variables in the Monte Carlo analyses, and treated all variables as independent. These situations are likely to lead to extremes in consequences. However, spatial correlations were considered, somewhat, in choosing hydrogeologic variables.

5. **Coupled effects between processes and events in the scenarios have not been fully modeled nor evaluated.**
   In IPA Phase 2, an attempt was made to couple some events and processes such as corrosion and repository cooling. However, complex coupled interactions such as moisture movement (including infiltration) and gas

[1]The figures shown in this chapter present the results from a demonstration of staff capability to review a performance assessment. These figures, like the demonstration, are limited by the use of many simplifying assumptions and sparse data.

transport have not been modeled in IPA Phase 2.

6. **The dose calculation is for illustrative purposes.**
The dose calculation is based on assumptions regarding a postulated biosphere consisting of a farm irrigated by well water, a family living on the farm, and a distant population consuming cattle raised on the farm. There has been relatively little research, as a part of IPA Phase 2, on the likelihood of these or other assumptions regarding future biospheres. In addition, many of the coefficients in the dose model are generic and not specific to the repository region.

9.2 Conditional CCDFs and Exceedance Probability Curves

9.2.1 Construction of the CCDFs

The CCDFs, which express the uncertainty in the model results for population doses and EPA limits for cumulative release over 10,000 years, are presented in different forms, including:

- Conditional CCDFs for each scenario;
- Conditional CCDFs showing performance of individual and engineered barriers; and
- Total CCDFs combining all scenarios for both release and dose.

Normalized Release, which is the primary measure of consequences displayed by the CCDF is computed by dividing each radionuclide that enters the accessible environment by its limit specified in Appendix A, Table 1 of 40 CFR Part 191 (*Code of Federal Regulations*, Title 40, "Protection of Environment"), and summing the resulting ratios. *Effective Dose Equivalent*, the other measure of consequences displayed by the CCDF, is described in Section 7.3.3.

Both conventional mean CCDFs and "hair" diagrams have been constructed. The following discussion presents salient points of CCDF construction for IPA Phase 2.

9.2.1.1 Conditional CCDFs

A conditional CCDF is a CCDF constructed for a single scenario class with the assumption that the scenario class has a probability of occurrence of 1.0. For each scenario class evaluated under IPA Phase 2, a conditional CCDF was constructed in the following manner:

- A vector represents a single sampling for all of the sampled variables. The total number of vectors to be selected has to be known before sampling so that each selection for each variable is made from equally probable distributions;
- Each vector is assigned an equal probability within the scenario (i.e., for 400 vectors, each vector has a probability $p_i = 1/400$);
- The set of vectors is sorted from lowest to highest consequences R (cumulative release or dose);
- The exceedance probability E of the sorted consequences is calculated by the following formula:

$$E_i = 1 - \sum_{i=1}^{N'} p_i' \quad , \qquad (9\text{–}1)$$

  where p_i' is the probability of the i^{th} vector of the sorted set, and N' is the number of vectors in the set; and
- The CCDF is the graph of E_i versus its sorted consequences R.

9.2.1.2 Screened Conditional CCDFs

This CCDF uses a set of vectors derived from the 400-vector base case scenario by screening for compliance with regulations or ranges of model input parameters. It is constructed identically to the conditional CCDF described above, but for N' = the number of remaining vectors, and still assuming equal probability for each remaining vector, $p_i = 1/N'$. Examples of possible screening criteria are waste package lifetimes greater than 300 years (or 1000 years) and infiltration rates less than 0.3 millimeters/year.

9.2.1.3 Total CCDF

The total CCDF is constructed by combining vectors from all scenarios. The probability of each

vector p_k', however, is taken to be the scenario probability p_j divided by the number of vectors N_j in the scenario:

$$P_k' = \frac{p_j}{N_j} \quad . \tag{9-2}$$

The consequences are then sorted, as before, from lowest to highest. The exceedance probability is then defined:

$$E_k = \sum_{k=1}^{N'} p'_k \quad . \tag{9-3}$$

where N' is the total number of vectors, and p'_k are the probabilities for the sorted consequences.

9.2.1.4 "Hair" Diagrams

Helton *et al.* (1991, Section VI) develops an alternative method of displaying uncertainty about scenarios and parameters for probabilistic models. In this technique, "hair diagrams," there is one CCDF or "hair" per vector, which displays the cumulative probability for each vector (for which there is a new set of sampled parameters) displayed over the range of scenarios. Among the advantage of hair diagrams, Helton *et al.* states the following:

> "... they maintain the distinction between scenarios, probabilities for scenarios, consequences and fixed but imprecisely known quantities.... Further, these representations lead naturally to CCDFs and distributions of CCDFs. The distributions of CCDFs are important because they display the variability that is averaged over to obtain the mean CCDFs that are typically used for comparison with the EPA release limits."

Because one line is plotted for each vector, hair diagrams are complicated and difficult to interpret. To simplify them visually, yet preserve the statistical information they contain, the boundaries of the hair diagram are summarized by finding the density function of the exceedance probability at a range of values of cumulative release, and plotting only the 5th, 50th, and 95th percentiles of this density function; (i.e., for a given value of cumulative release R_i, the exceedance probabilities are interpreted from all hairs, their values sorted, and the 20th, 200th, and 380th values saved to be plotted as the 5th, 50th, and 95th percentile of the hairs.

9.2.2 Conditional CCDFs for Various Scenario Classes

Four-hundred (400) vector runs were made for nine scenario classes. These classes are identified in the following table (Table 9-1) along with their estimated probabilities of occurrence over the next 10,000 years.

Table 9-1 Estimated Probabilities for the Scenario Classes Modeled in the IPA Phase 2 Analysis

Scenario Class	*Scenario Class Identifier*[a]	*Estimated Probability*
Base Case	oooo	≈ 0.0
Climate Change Only (Pluvial)	cooo	≈ 0.0
Seismicity Only	osoo	7.9×10^{-8}
Drilling Only	oodo	≈ 0.0
Magmatic Activity Only	oov	≈ 0.0
Drilling + Seismicity	osdo	0.35
Drilling + Seismicity + Magmatic Activity	osdv	1.0×10^{-2}
Drilling + Seismicity + Climate Change	csdo	0.62
Drilling + Seismicity + Magmatic Activity + Climate Change[b]	csdv	2.0×10^{-2}

[a]See Section 9.2.3 for explanations of the identifiers.
[b]Fully disturbed.

Scenario classes *csdv, csdo, osdv,* and *osdo* were chosen from the 16 possible scenarios (see Chapter 3) to calculate the exceedance probabilities of the releases and doses from their conditional exceedance probability curves (CCDFs). These are the only scenario classes with occurrence probabilities large enough to make a significant contribution to total performance. The other cases were chosen to evaluate the effect on exceedance probabilities by disruptive events acting alone. It is assumed that any significant interaction between disruptive events (within the capabilities of the models to predict) will be picked up in the fully disturbed (*csdv*) case.

9.2.3 Basic Scenarios

The basic scenarios computed for the purpose of comparison are: the base (or undisturbed) (*oooo*) scenario; the fully disturbed (*csdv*) scenario; the base case disturbed by climate-only (*cooo*) scenario; the base case disturbed by drilling-only (*oodo*) scenario; the base case disturbed by seismic-only (*osoo*) scenario; and the base case disturbed by magmatism-only (*ooov*) scenario. The conditional exceedance probabilities (or CCDFs) for the *Normalized Release* for each scenario are presented in Figure 9–1. The dotted lines represent compliance with the EPA release standard.[2] The conditional exceedance probabilities for dose estimates[3] are presented in Figure 9–2.

Scenario plots as defined in this report are scatter plots of the results for one scenario plotted against the results of another scenario. For the IPA Phase 2 analysis, the LHS sets contained 400 vectors for all production runs. Since all scenario runs used the same LHS set and most of the same independent variables, these plots allow the visual inspection of the effects of the scenario on the model outputs. Scenario plots were used to compare the single-event scenarios against the base case; that is, scenario *cooo* (pluvial infiltration and higher water table); *osoo* (seismicity); *oodo* (human intrusion by exploratory drilling); and *ooov* (magmatism); against *oooo* (undisturbed or base case).

The base case (*oooo*) scenario represents the calculated releases and doses from the repository over a 10,000-year performance period, under conditions as they are presently perceived to exist (allowing for parameter uncertainty) and without disturbing events such as drilling, earthquakes, magmatism, or change to a pluvial climate. The thresholds defined for two of these disturbing events, earthquakes and drilling, give them probabilities of occurrence of almost 1.0 during the period of performance. Hence, the probability of occurrence of scenarios not containing these events is almost 0.0. The probability of having a pluvial climate within the performance assessment period is estimated to be 0.64. Therefore, the probability of the base case is very low, and is computed primarily for comparison rather than as a major contributor to the total exceedance probability curve. The fully disturbed (*csdv*) scenario represents the opposite extreme from the base case. In the fully disturbed case, all disruptive events being considered (seismicity, drilling, magmatism, and pluvial) are allowed to act on the repository. This scenario is expected to show the effects of interactions among events, as well as the effects of the events, themselves. An example of an expected interaction is pluvial climate (high water level and increased infiltration) and seismically induced waste package failures.

As can be seen by comparing the climate-only (*cooo*) scenario with the fully disturbed case (*csdv*) in Figure 9–1, almost all the increase in *Normalized Release* in the high probability part of the fully disturbed CCDF over the base case CCDF is due to the influence of the pluvial climate (described in Section 6.2). Figure 9–3 is a scenario plot comparing the releases from the pluvial scenario with the releases from the base case for the same vectors. The influence of climate on the total releases is very significant for most vectors, even

[2]Currently, a revised set of standards specific to the Yucca Mountain site is being developed in accordance with the provisions of the Energy Policy Act of 1992. The Energy Policy Act of 1992 (Public Law 102–486), approved October 24, 1992, directs NRC to promulgate a rule, modifying 10 CFR Part 60 of its regulations, so that these regulations are consistent with EPA's public health and safety standards for protection of the public from releases to the accessible environment from radioactive materials stored or disposed of at Yucca Mountain, Nevada, consistent with the findings and recommendations made by the National Academy of Sciences, to EPA, on issues relating to the environmental standards governing the Yucca Mountain repository. It is assumed that the revised EPA standards for the Yucca Mountain site will not be substantially different from those currently contained in 40 CFR Part 191, particularly as they pertain to the need to conduct a quantitative performance assessment as the means to estimate postclosure performance of the repository system.

[3]Those persons who were assumed to be exposed in the CCDFs for the dose include: the members of the farm family (three persons); and members of the regional population (177 of them are assumed to consume contaminated beef).

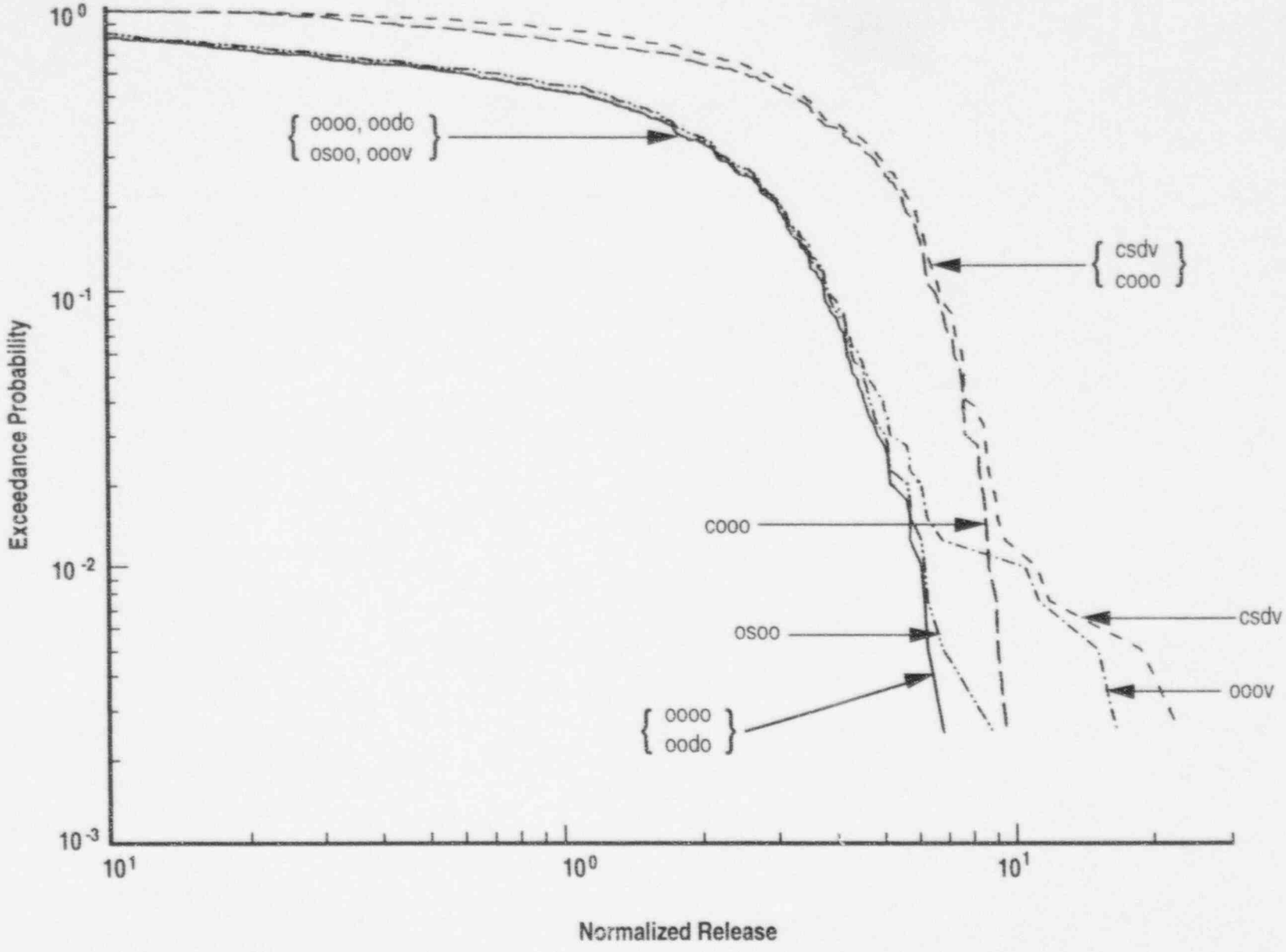

Figure 9–1 Conditional CCDFs for *Normalized Release* for basic scenarios
(Scenario class identifiers are described in Table 9–1.)

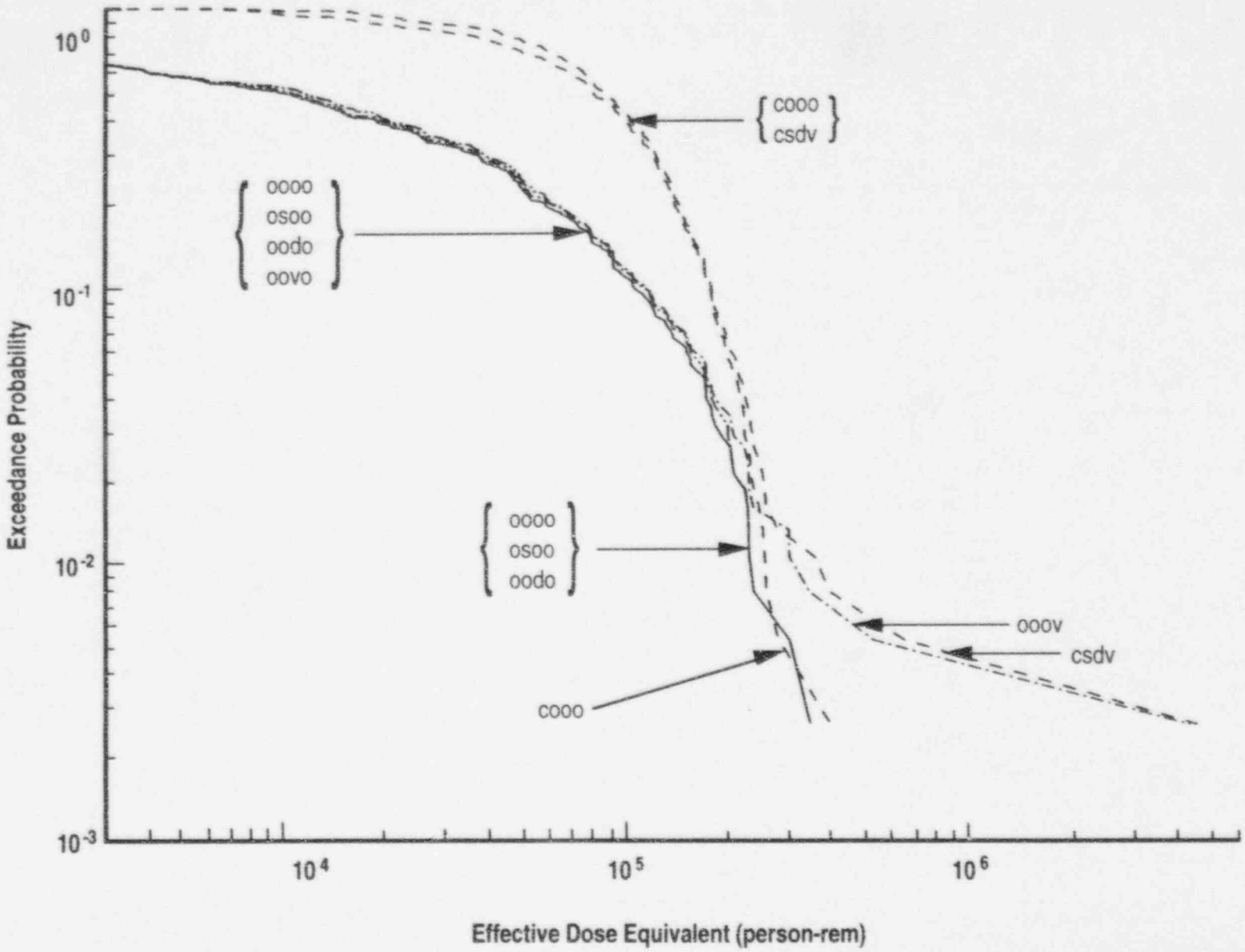

Figure 9–2 Conditional CCDFs for *Effective Dose Equivalent*
(Scenario class identifiers are described in Table 9–1.)

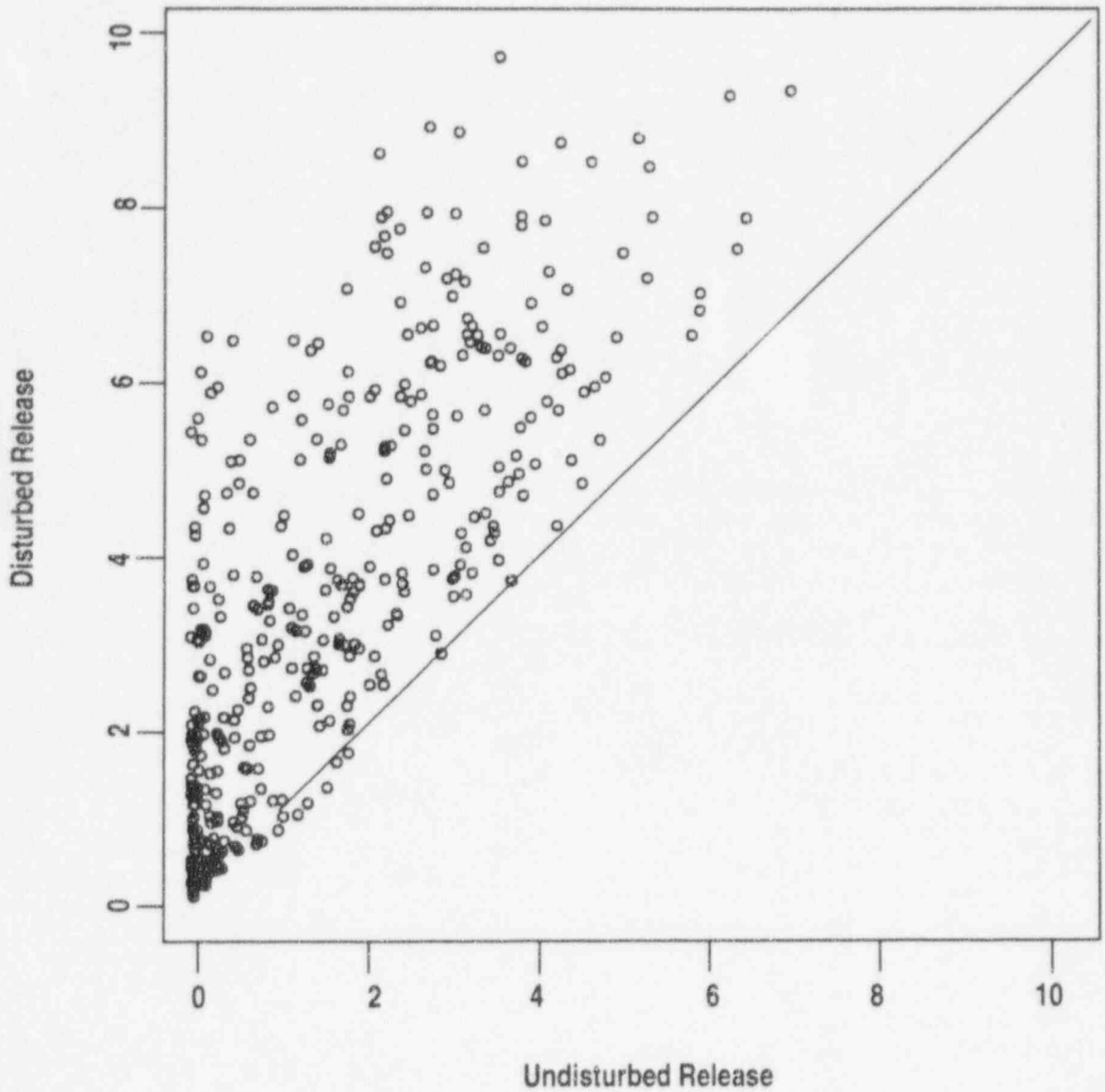

Figure 9–3 Scenario plot of pluvial scenario versus base case scenario

though the gas pathway is insensitive to infiltration (the IPA Phase 2 models did not explicitly consider the effects of infiltrating water on either the release of gaseous radionuclides, nor their transport in the geosphere). Although the effect of the pluvial conditions is large, there are some vectors that are nearly the same or even smaller for the pluvial case. This observation is probably caused by the following conditions:

- Contributions to cumulative release from the gas pathway are relatively large, compared with the liquid pathway; and
- The higher water table during the pluvial scenario causes radionuclides to be released from the vadose zone into a less permeable and slower moving saturated zone than would be the case for the non-pluvial conditions. This results in a smaller release to the accessible environment for the same release to the saturated zone.

Human intrusion, as presented in the base case disturbed by drilling-only scenario (*oodo*) (see Section 6.3), in Figure 9-1, does not appear to have a discernable effect on the exceedance probabilities. There appears to be a low likelihood of a direct hit and relatively minor consequences when a hit is actually made. The scenario plot, Figure 9-4, shows the releases from the liquid, gas, and direct pathways for the drilling-only scenario compared with the base case. There are only minor differences in the releases from drilling, virtually all caused by the direct releases of contaminated rock. Without the releases of contaminated rock, the comparison would plot almost perfectly as a straight line. There are only minor differences in liquid and gas releases caused by a few prematurely failed waste packages, but the results are too small to be visible on a plot. It should be noted that a more in-depth analysis, for example, one accounting for the effects of drilling fluid, could show an increase in consequences and the significance of the scenario.

The seismic-failure mechanism described in Section 6.4 is considered to be very conservative. However seismic failure appears to have only a small effect on the CCDF, as shown by the comparison in Figure 9-1. Seismic loading usually shortens waste package lifetime by a small amount, resulting in little increase in the *Normalized Release*.

The effect of seismicity is more apparent on the scenario plot, Figure 9-5a. This figure shows the total releases for the seismic-only (*osoo*) scenario compared with the base case scenario. There are a significant number of vectors with higher releases. The way in which the seismic model is employed must permit all containers in any zone to fail simultaneously when the seismic criteria are exceeded. The vectors having the largest relative release for the seismic scenario had seismic parameters allowing relatively early seismic failure, which contributed mostly to large gaseous releases from the temperature-dependent ^{14}C source term and transport models. Liquid-only releases, presented in scenario plot, Figure 9-5b, showed a more modest effect of early seismic failures.

Like pluvial climate (*cooo*), magmatism (*ooov*) appears to be the only other event to have a significant, discernable effect on the shape of the exceedance probability plot, as shown in Figure 9-1. Unlike climate, however, magmatism appears to affect only the low probability part of the curve. The likely explanation is that, as with drilling into a waste package canister, the probability of a dike intersection with the repository is very low even under the conditional assumption that the scenario exists. With the magmatism model (see Section 6.5) the probability of an intersection when coupled with the scenario probability and its consequences is high enough and the consequences high enough, that the event of magmatism was able to make a discernable modification to the base case exceedance probabilities at the tail of the distribution function.

The scenario plot in Figure 9-6 shows the total releases from liquid, gas, and direct pathways for the magmatic scenarios. There are a relatively few vectors with large releases. Most of the releases are identical with the base case because there were no magmatic events that happened within the repository area and affected releases. The largest releases were caused by magmatic cones that were assumed to bring radioactive contaminants directly to the surface. In a few cases, magmatic dikes caused premature container failure, but did not bring any contaminant directly to the surface. Subtracting out the direct releases, premature failure caused only minor excess

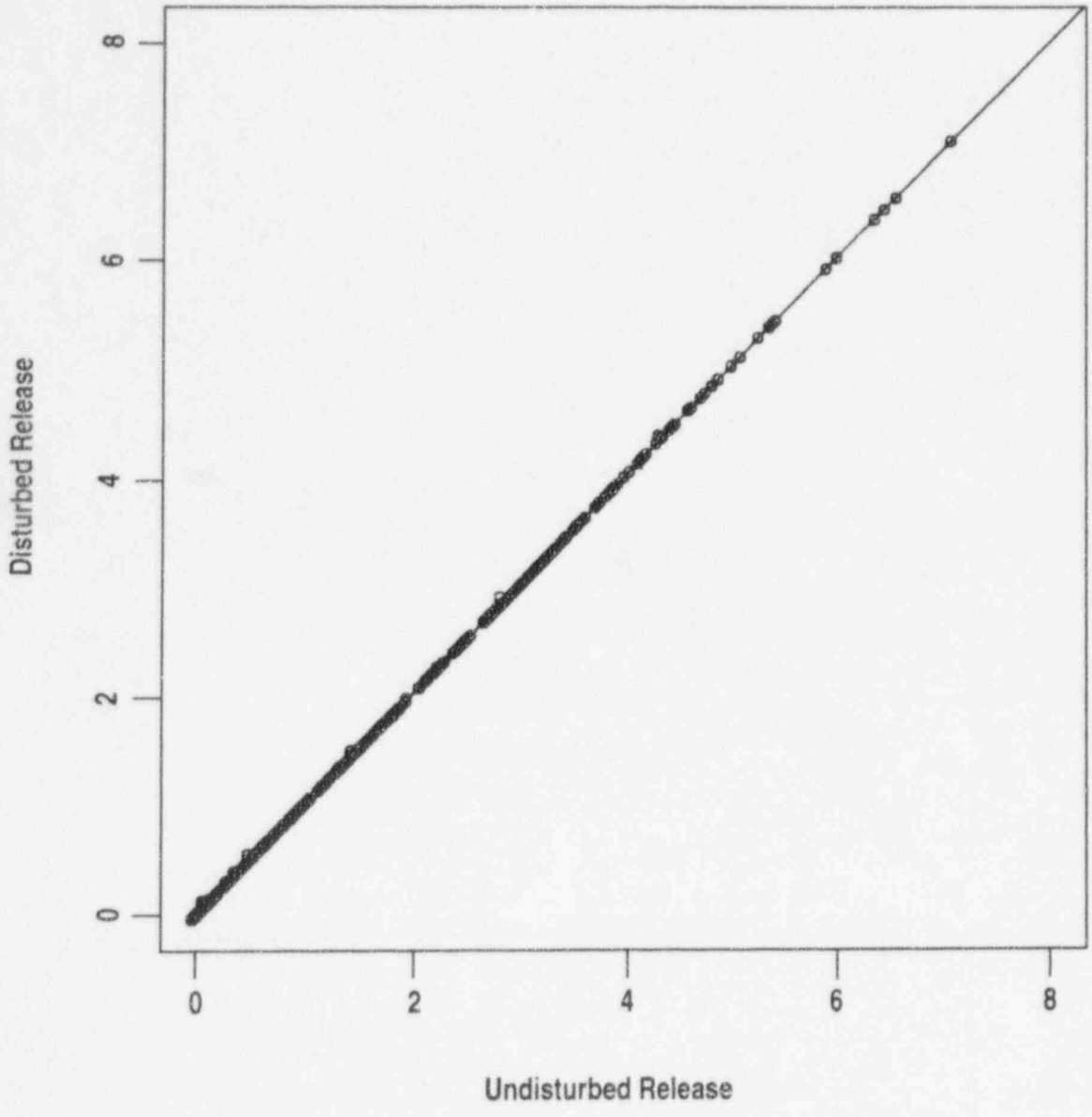

Figure 9–4 Scenario plot of drilling scenario versus base case scenario

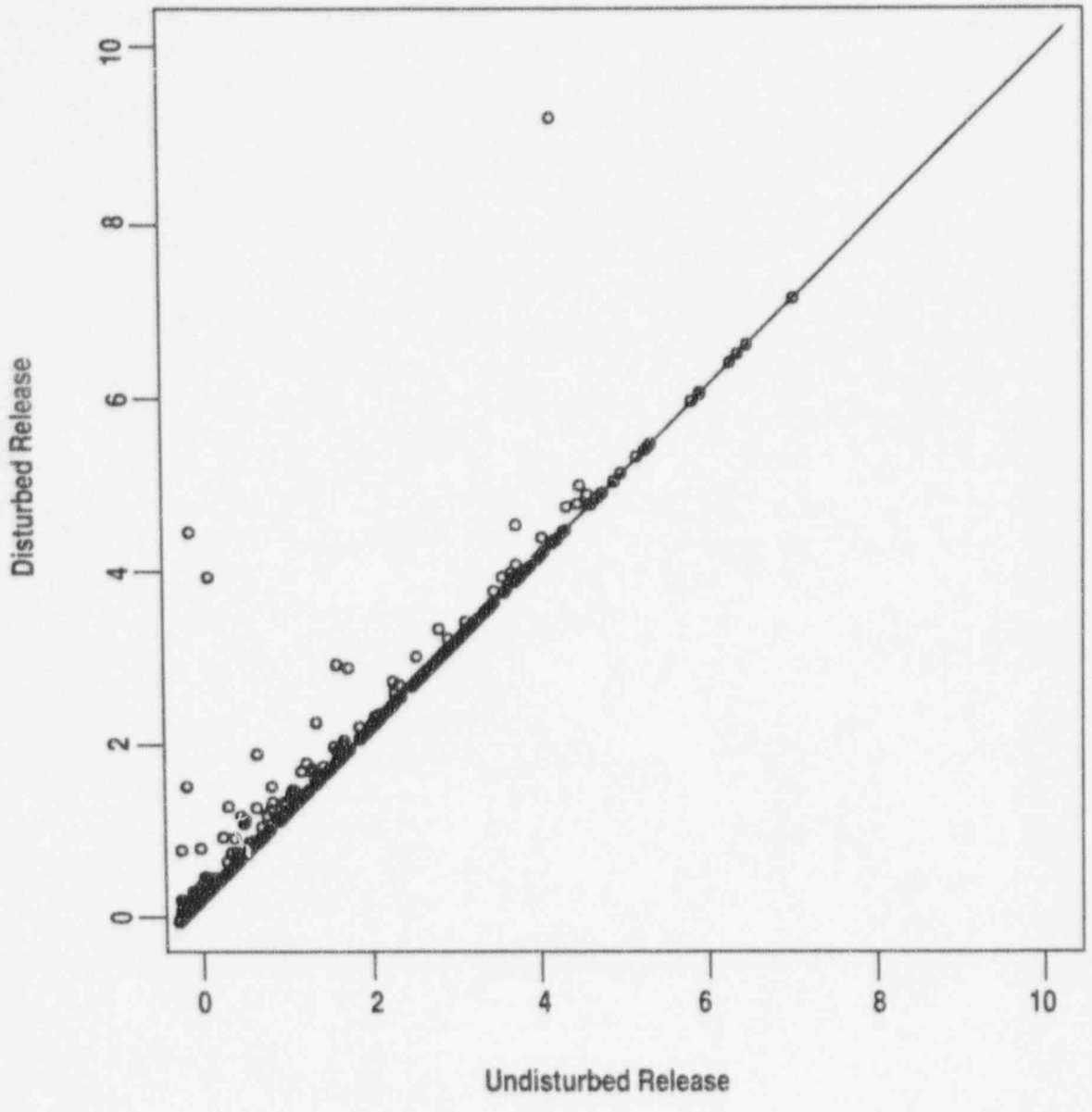

Figure 9–5a Scenario plot of seismic scenario versus base case scenario

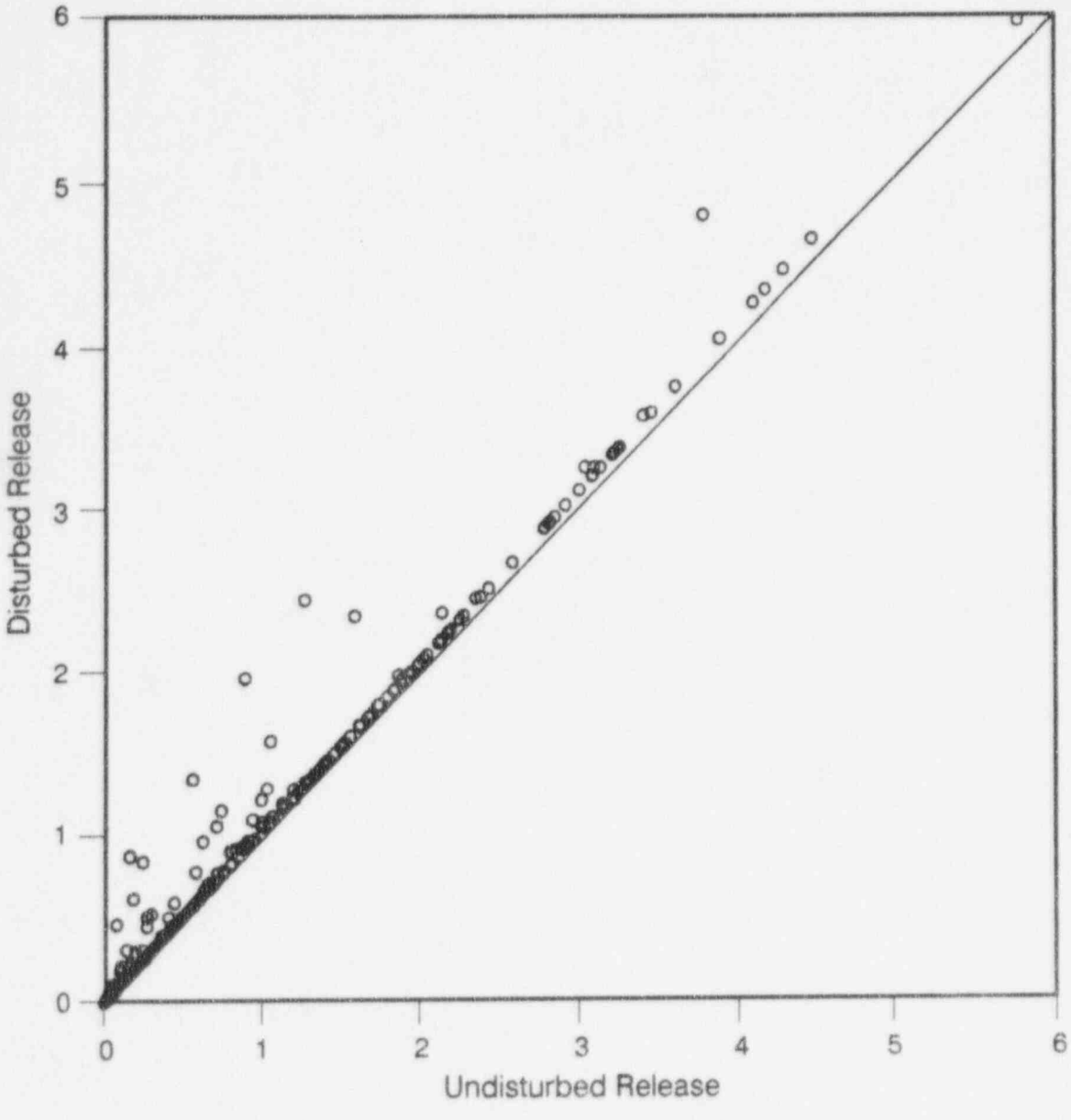

Figure 9–5b Scenario plot of seismic scenario versus base case scenario (liquid releases only)

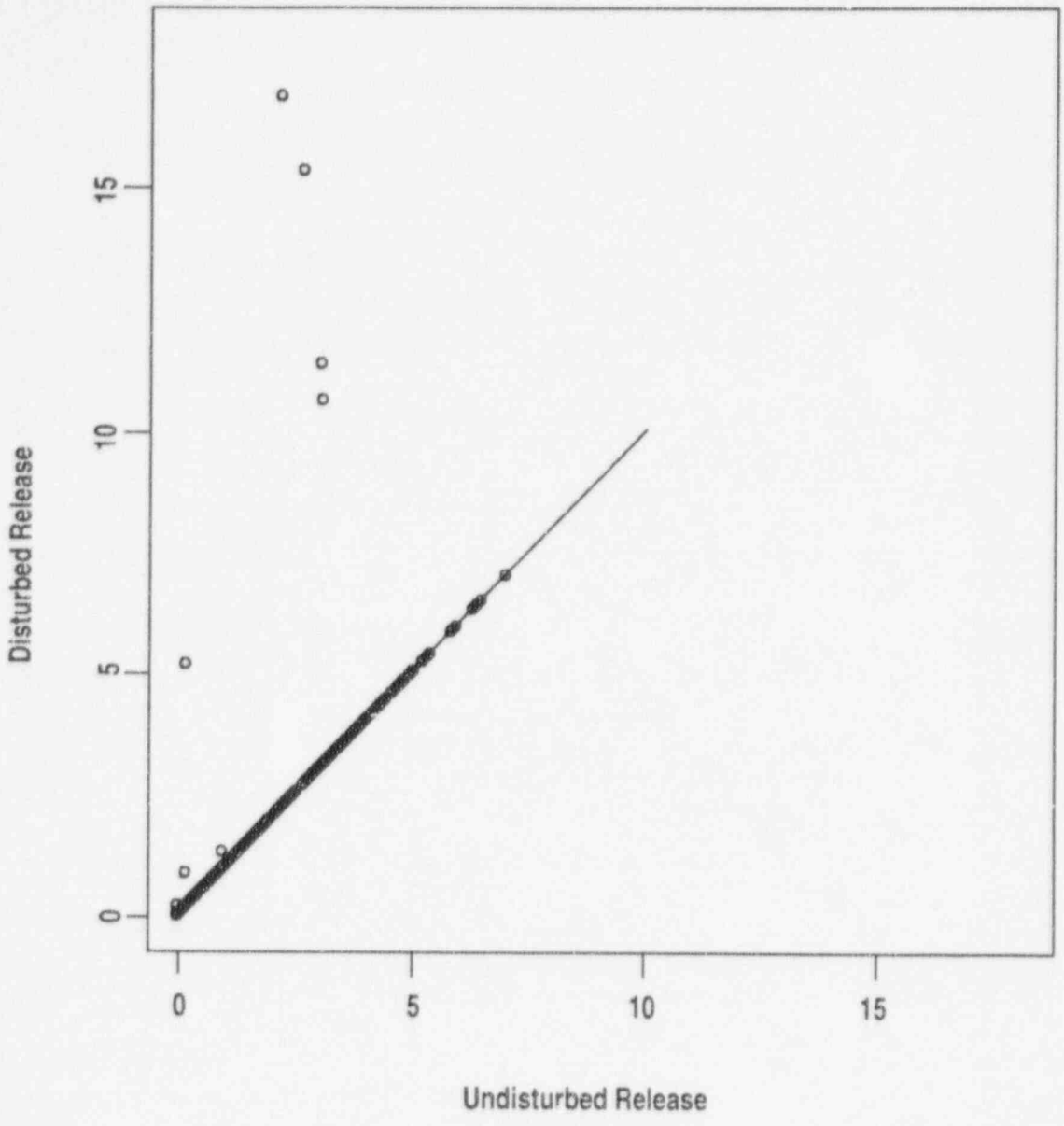

Figure 9–6 Scenario plot of magmatic scenario

releases of liquid and gas, too small to be visible on a plot.

9.3 Total System CCDF

The total CCDF for cumulative release for the significant scenarios, *csdo, osdo, csdv* and *osdv*, was constructed by the procedure described in Section 9.2.1 and is shown in Figure 9–7a. The corresponding CCDF for dose is shown in Figure 9–7b. It should be noted that although the effects of a high-probability event such as pluvial-climate can still be recognized in the total CCDF, the effects of low-probability events such as magmatism are obscured. To better preserve the effects of both low- and high-probability events, Figure 9–8a shows the same information used to construct the total CCDF, but plotted as a "hair" diagram, as described in Section 9.2.1. Figure 9–8b shows the 5^{th}, 50^{th}, and 95^{th} percentiles of the hairs, as boundaries from the hair diagram. The significance of the "hair diagram" is to present the entire range of credible releases from the repository as a function of scenario probability and parameter uncertainty. The curve shown in Figure 9–7a incorporates scenario probability and parameter uncertainty into a single curve, without providing a means of separately evaluating the effects of either.

9.4 Differences Between IPA Phases 1 and 2, and Comparison of Results

A complete discussion of results from this total-system performance assessment and future total-system performance assessments must include an evaluation of why the results differ among various analyses. If a baseline CCDF is established, the effects of changing assumptions and parameter values can be quantitatively examined. At the present time, the only baseline developed by the staff for comparison is the CCDF from the IPA Phase 1 study. IPA Phases 1 and 2 were significantly different in terms of scope and approach, in many areas. A description of the major improvements in IPA Phase 2 over Phase 1 provides an indication of the amount and relative significance of factors that may be influencing the difference.

9.4.1 Improvements in IPA Phase 2 Likely to Affect Results

9.4.1.1 Scenarios

Only a limited set of scenario classes was considered in IPA Phase 1, drilling and pluvial conditions, resulting in four scenarios. However, for the IPA Phase 2 analysis, the staff applied the Sandia National Laboratories (SNL) scenario-selection methodology for use in the consequence analysis of a potential high-level (HLW) waste disposal site (see Cranwell *et al.*, 1990). Based on the staff evaluation and modification of the SNL methodology, four scenario classes were considered (climate change, seismicity, magamatism, and human intrusion) from which 16 scenarios resulted. In IPA Phase 1, the occurrence probability of pluvial climate was assumed to be 0.10. In IPA Phase 2, the occurrence probability of pluvial climate was determined to be 0.64 (Chapter 3). The probability of the drilling scenario class at the site was determined to be approximately equal to 1.0 in both IPA Phase 1 and Phase 2.

9.4.1.2 Pathways

The IPA Phase 1 effort identified and accounted for a number of important attributes of the Yucca Mountain site (e.g., stratigraphic changes below the repository in the unsaturated zone and differences between matrix and fracture flow). As discussed in Chapter 4, the IPA Phase 2 effort not only has maintained the important attributes identified in the Phase 1, study but has added further modeling complexity such as:

- Saturated zone pathways to the accessible environment;
- Calculation of radionuclide concentration for dose assessment; and
- Both fracture and matrix pathways allowed within a vector.

The additional complexity provided additional insights into: the performance of fractured rock as geologic barrier; data requirements; and the capabilities of the utilized computational methods.

Also, three transport pathways were considered in IPA Phase 2 (i.e., gaseous, aqueous, and direct) compared with one transport pathway (i.e., aqueous) in Phase 1. In the gas-phase transport

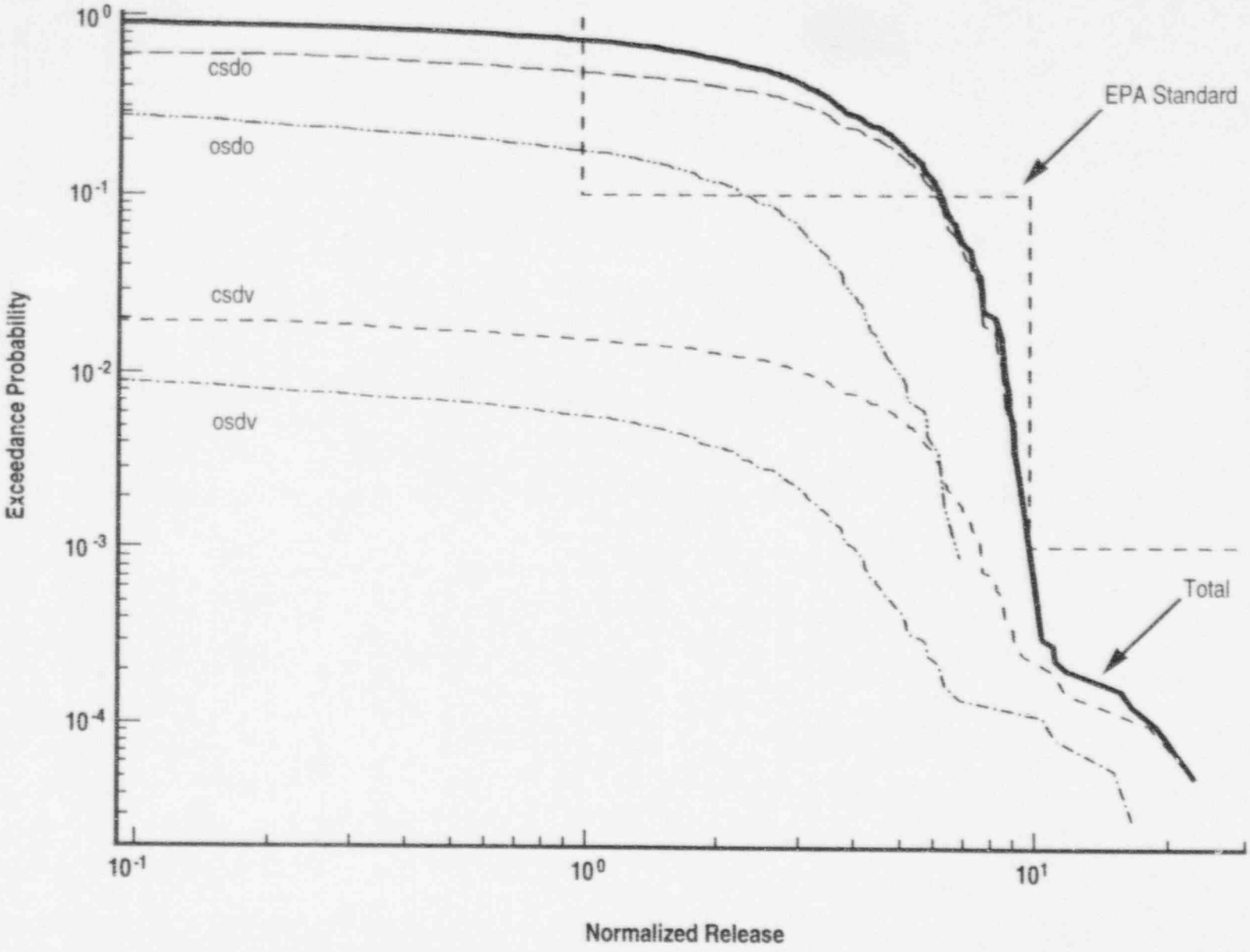

Figure 9–7a Total CCDF for *Normalized Release* from significant scenarios
(Scenario class identifiers are described in Table 9–1.)

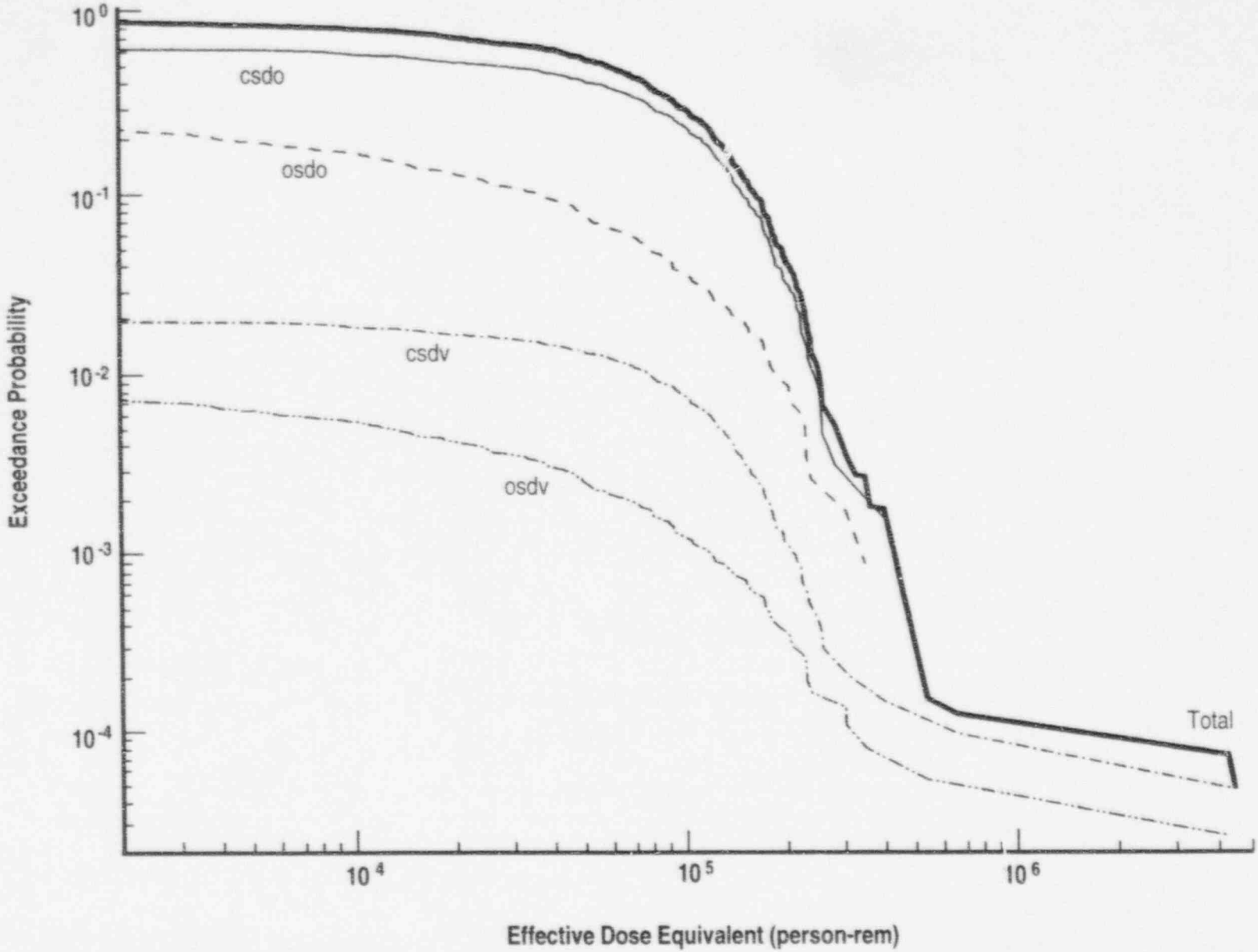

Figure 9–7b Total CCDF for *Effective Dose Equivalent* from significant scenarios
(Scenario class identifiers are described in Table 9–1.)

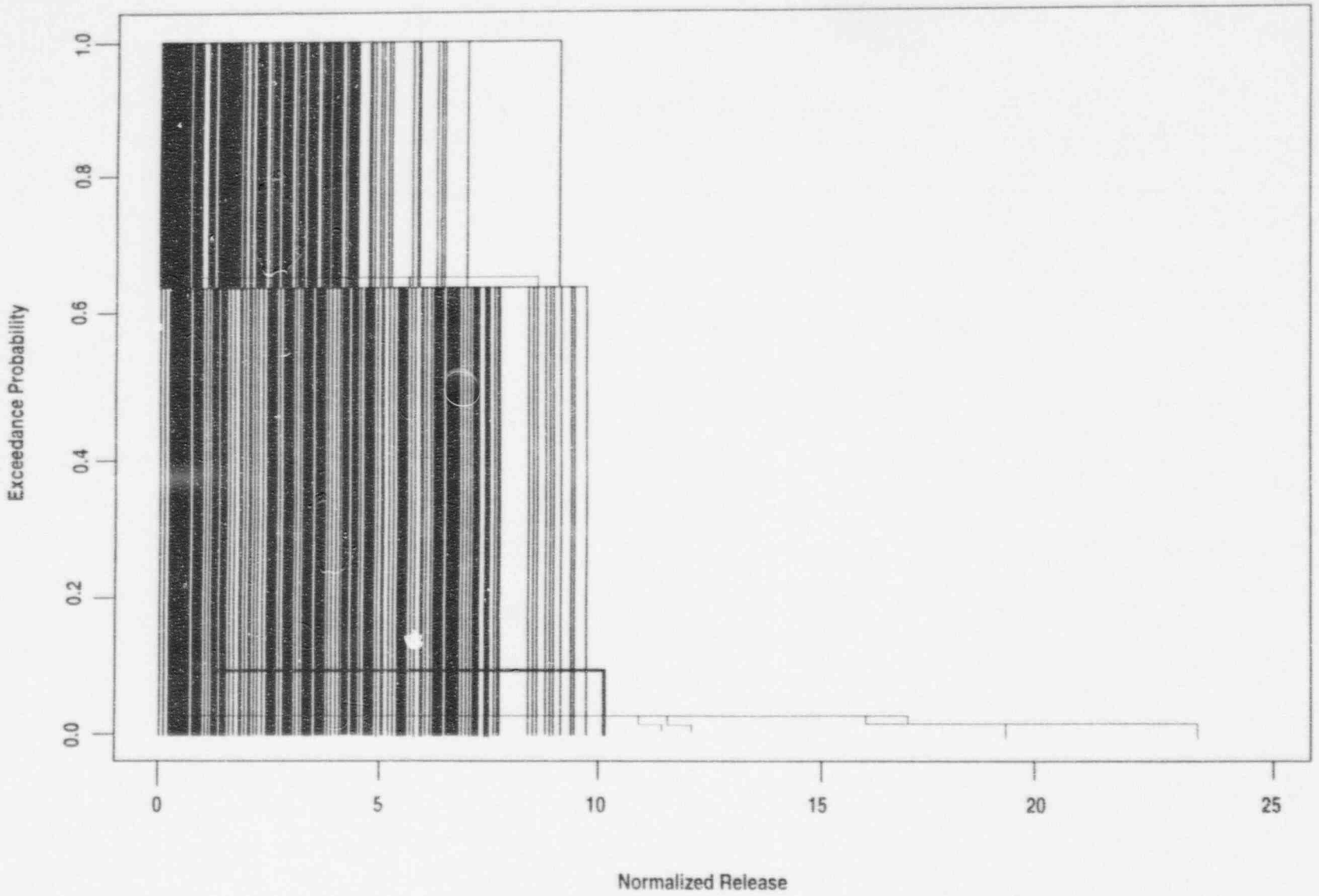

Figure 9–8a "Hair diagram" showing all *Normalized Release* vectors
(for scenarios *osdo, osdv, csdo,* and *csdv*)

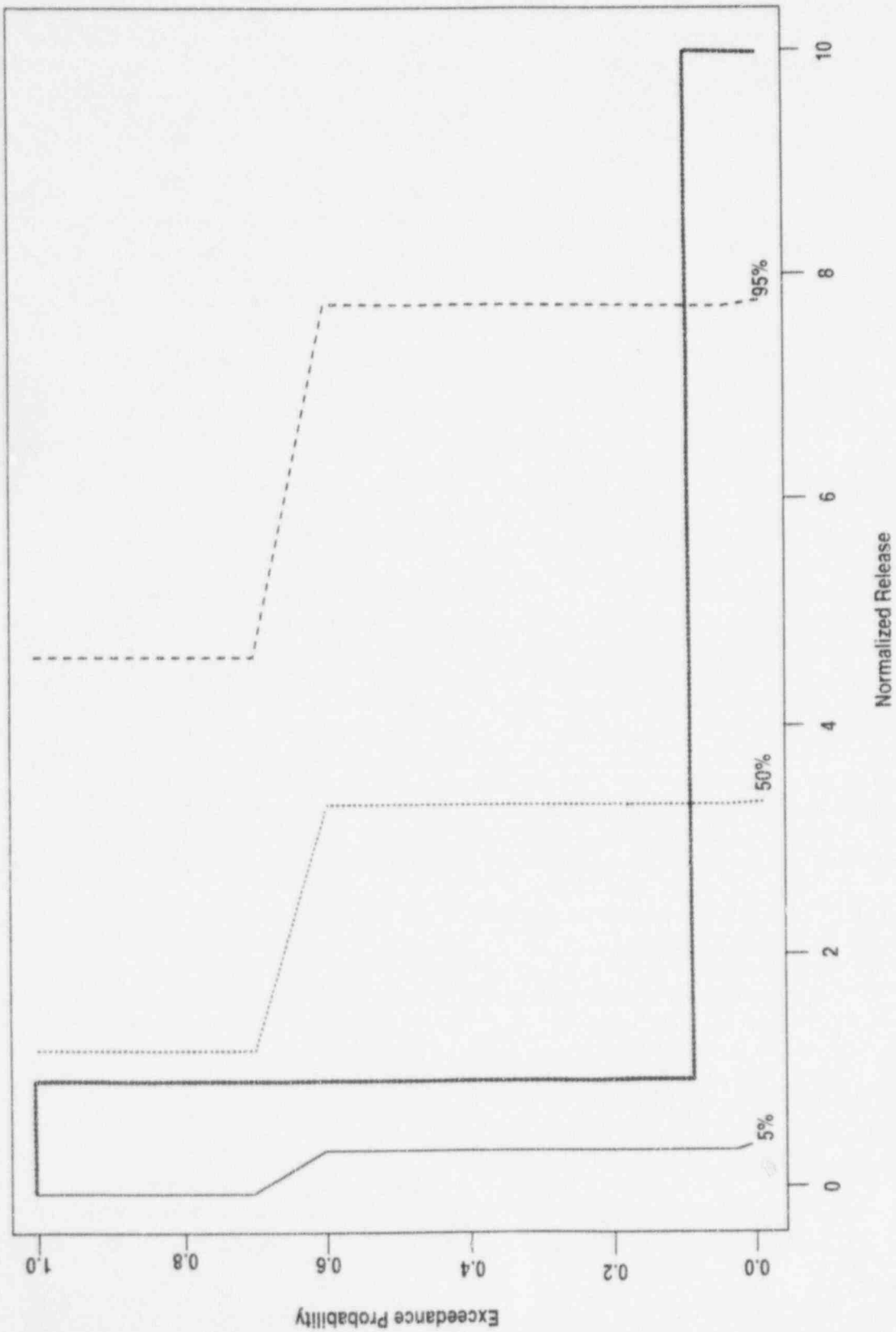

Figure 9–8b Percentile values of release vectors from "hair diagrams"

calculations, advection, radioactive decay, and temperature effects were considered. The retardation coefficients used for the gas-phase calculation also accounted for equilibrium speciation.

9.4.1.3 Source Term

The modeling of waste-package failure was non-mechanistic in IPA Phase 1. The model used by the staff to calculate the source term in IPA Phase 1 was that incorporated in the *NEFTRAN* computer code obtained from SNL (see Longsine *et al.*, 1987). In this model, radionuclide releases would occur only after failure of the waste package, characterized as a single failure time for the entire repository.

As discussed in Chapter 5, the staff developed its own computer code to calculate the source term in IPA Phase 2. The *SOTEC* module (see Sagar *et al.* (1992)) deals with the calculation of aqueous and gaseous radionuclide time- and space-dependent source terms for the geologic repository. It does so by considering the variations in those physical processes expected to be important for the release of radionuclides from the engineered barrier system (EBS).

Three primary calculations are done in *SOTEC*: (a) failure of waste packages because of a combination of corrosion processes and mechanical stresses; (b) the leaching of spent nuclear fuel; and (c) the release of $^{14}CO_2$ gas from the oxidation of UO_2 and other components in spent nuclear fuel and hardware. Other principal features of the IPA Phase 2 source term model include representation of the repository by seven separate regions (or sub-areas) and the consideration of 20 radionuclides, based on a screening analysis. The IPA Phase 1 analysis considered 28 radionuclides. The screening analysis for radionuclides is described in Section 5.2.4 of this report.

9.4.2 Possible Reasons for Differences in Results

Figure 9–9 shows the total system CCDFs for the IPA Phase 1 and Phase 2 analyses. The Phase 1 CCDF has relatively higher releases in the high-risk portion of the curve (i.e., the left side), but lower releases in the low-risk portion. As discussed in Section 9.4.1, the Phase 1 and Phase 2 models were quite different in a number of important aspects, so it is difficult to pinpoint the exact causes of the differences in results. Some of the differences in the total system CCDFs may have been caused by the following specific factors:

1. ***Waste package failure model.*** The IPA Phase 1 study had a non-mechanistic model of waste package canister failure, which assumed a probability distribution of failure times. Furthermore, all canisters in the four modeled repository sub-areas were assumed to fail at the same time. The IPA Phase 2 model employs a mechanistic model of canister failure that calculates the failure time based on assumptions about canister wetting, corrosion, and seismic forces. Furthermore, the failure times of the canisters in the seven modeled sub-areas were independent of each other.

2. ***Release rate from failed canisters.*** The IPA Phase 1 model for source term based release rate of dissolved radionuclides from the waste form on the solubility of either the uranium matrix or the individual radionuclides for a given flow rate through the canister, and carried away only in the advective flow. Carbon-14 gaseous releases were not included explicitly in the IPA Phase 1 model. The IPA Phase 2 model includes several important improvements:

   - Solubility limited by collection of isotopes of each element;
   - A temperature-dependent model for ^{14}C release from several compartments of the fuel; and
   - Diffusive as well as advective transport from the canister.

3. ***Several of the parameters common to both IPA Phases 1 and 2 had different values.*** *Rate of water influx*—This value was an assumed fraction of the infiltration rate in IPA Phase 1, but was calculated explicitly from the fracture-flow modeling in Phase 2. Only fracture flow at the repository horizon contributed to advective transport through the canister.

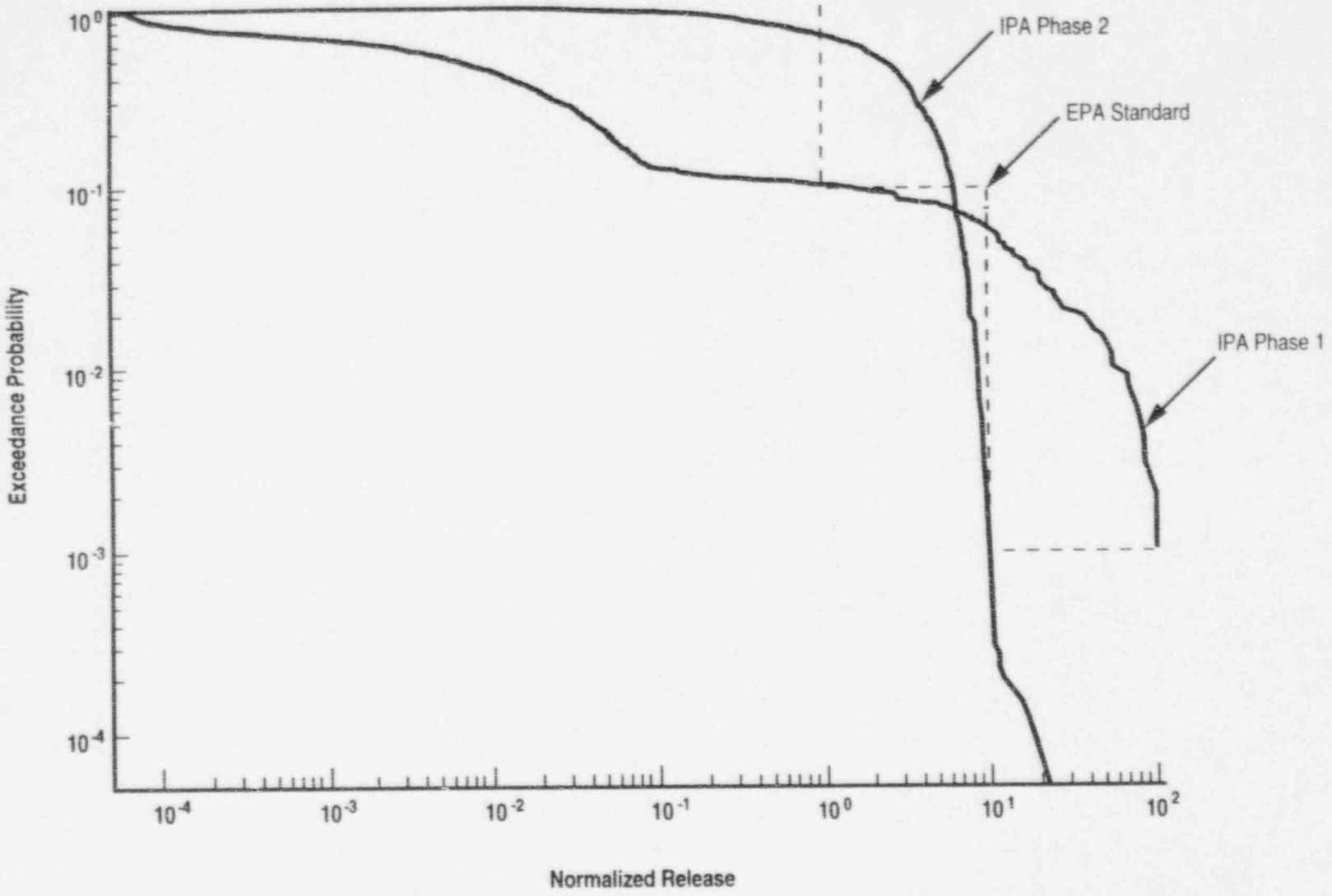

Figure 9–9 Comparison of CCDFs for IPA Phasc 1 and Phase 2 results

Contact fraction with waste—The fraction of infiltrating water contacting the waste was chosen from a uniform distribution in both the IPA Phase 1 and 2 models from a range related to the cross-sectional area of the boreholes. The contact fraction was chosen to be 0.002 to 0.01 in Phase 1. The equivalent range for IPA Phase 2 was about 0 to 0.002, which is considerably lower. Furthermore, only the fracture flow portion of the total infiltration could reach the waste package in Phase 2, whereas both the fracture and matrix flow parts of the flow could be involved in Phase 1.

Infiltration Rate—The range of infiltration rates for the base case (*oooo*) and the pluvial-climate case (*cooo*) was the same in both IPA Phase 1 and Phase 2. The type of distribution chosen was different, however. A uniform distribution was chosen in Phase 1 for both the base case and the pluvial case. For IPA Phase 2, a log-uniform distribution was assumed for both cases.

4. ***Radionuclide contributions.*** The largest contributors to cumulative release at the accessible environment for the IPA Phase 1 study were the isotopes of plutonium, but they were relatively unimportant in Phase 2. The solubility range of plutonium for IPA Phase 1 was 5.0×10^{-5} to 3.0×10^{-3} kilograms/cubic meter sampled from a log-uniform distribution. In IPA Phase 2, thermodynamic calculations and the consideration of both oxidizing and reducing environments resulted in a range of 2.0×10^{-7} to 5.9×10^{-4} kilograms/cubic meter, which is considerably smaller. Furthermore, solubility in Phase 1 was based on single radionuclides, wherever the IPA Phase 2 model considered all isotopes of an element in this determination.

5. ***Carbon-14 gaseous releases.*** The IPA Phase 1 model did not include the releases of ^{14}C gas to the accessible environment. The release of ^{14}C gas was a major contributor to the cumulative release to the accessible environment in the IPA Phase 2 model. Furthermore, the IPA Phase 2 model predicted this release to occur at high conditional probabilities and independent of the release of the dissolved radionuclides.

6. ***Scenario probabilities.*** Except as noted under Item 3, above, the application of the pluvial-climate scenario has been reasonably similar in both IPA Phases 1 and 2. However, the probability of the pluvial climate was arbitrarily assumed to be 0.10 in IPA Phase 1 and determined by analysis of paleo-hydrologic data to be 0.64 in IPA Phase 2. In both IPA phases, pluvial-climate conditions result in a significant increase in releases at high conditional probabilities.

9.4.3 Conclusions

The modeling improvements from IPA Phase 1 to Phase 2 were numerous and in some cases cannot be easily separated, such as in the case of waste canister-failure mechanisms resulting in the release of ^{14}C and other radionuclides and the incorporation of a gas-transport pathway. Hence, the calculation of a quantitative measure of the effect of each individual change or improvement is not considered feasible. A visual inspection of the curves indicates that the difference in occurrence probabilities assigned to the pluvial-climate scenario, and the incorporation of the gas pathway in Phase 2 may be the primary factors. In future IPA phases it will be feasible to analyze the effect on the CCDF for every significant change in the analysis, including modifications to models, parameter distributions, and scenario classes.

9.5 Effects of Modeled Performance of Natural and Engineered Barriers on Total System Performance

This section presents repository performance in terms of factors related to the behavior of the engineered and natural barriers. In IPA Phase 2, the factors investigated were the integrity of the waste packages, the rate of release of radionuclides from the engineered barriers, and the travel time of water through the geosphere. One of the primary goals of the IPA effort is to give insight to the effectiveness and ability to implement NRC's regulation applicable to the geologic repository. The regulatory requirements in 10 CFR 60.113 address "three subsystem performance objectives," namely substantially complete containment (SCC) of waste in the waste packages (10 CFR 60.113(a)(1)(ii)(A)), controlled fractional release rate from the EBS (10 CFR 60.113(a)(1)(ii)(B)), and pre-waste-emplacement ground-water

travel time (GWTT) (10 CFR 60.113(a)(2)). The results presented in this section portray the overall (total) system performance in terms of the staff's understanding of the primary factors contributing to waste containment. The calculations are not for the purpose of directly drawing a comparison between overall system performance in terms of release or dose and the subsystem performance measures. There are primarily two reasons for this distinction: (1) the subsystem performance measures are supposed to be independent requirements ensuring a minimal performance of each of the multiple barriers in a geologic repository, unrelated to the total system performance; and (2) the characterizations of SCC, EBS release rate, and GWTT used in IPA Phase 2 are crude and incomplete, and do not exactly conform to the definitions of those quantities in 10 CFR Part 60. For example, the "liquid" travel time, as used in this report, does not include the 10 CFR Part 60 concept of the "disturbed zone" (10 CFR 60.2) and is for post-emplacement rather than pre-emplacement conditions. Furthermore, the "liquid" travel time calculated in the TPA computer code program (described in Chapter 4) is an abstraction based on the fastest combination of possible fracture and matrix pathways, and does not correspond to a realistic flow path. Nevertheless, the following comparisons shed light on the importance of the engineered and natural barriers to the total system performance.

Screened Conditional CCDFs are used for these comparisons. As explained in Section 9.2.1, these plots are generated by "screening out" vectors according to a criterion, and using only the remaining vectors to produce the CCDFs. The criteria used in the present study were:

- Infiltration less than 1 or 2 millimeters/year (discussed in Section 10.3).
- Travel time of water in geosphere less than 1200, 1100, and 1000 years (discussed in Section 9.5.1).
- Release rates of radionuclides from the EBS less than 10^{-5}/year of the 1000 year inventory (discussed in Section 9.5.2).
- Waste package lifetimes of 300 or 1000 years (discussed in Section 9.5.3).

9.5.1 Effect of Travel Time of Water through the Geosphere

The NRC regulations in 10 CFR 60.113(a)(2) proscribe that the site for a geologic repository possesses the property of pre-waste emplacement GWTT along the fastest pathway from the disturbed zone to the accessible environment of less than 1000 years (or other criteria chosen by the Commission (10 CFR 60.113(b)). Since there is not yet an unambiguous definition of GWTT, four distinct "liquid" travel times have been defined for each vector for the present study:

- *Fastest*—the minimum time for the transport of a non-diffusing particle along the fastest combination of possible matrix and fracture pathways in any of the seven flow columns representing the repository.
- *Most flux*—the travel time through the pathway associated with the greatest flux from the repository to the accessible environment.
- *Flux averaged*—the average travel time for all paths, weighted by the flux in each path.
- *Averaged*—the average travel time for all paths, irrespective of the flux in each path.

For the purpose of IPA Phase 2, only liquid releases were included in this analysis; releases of gaseous ^{14}C were completely insensitive to liquid travel time. Carbon-14 was the major contributor to the normalized releases; therefore the inclusion of gaseous releases would have further masked the sensitivity of *Normalized Release* to travel time. Figure 9-10a shows the scatter plot of liquid travel time versus normalized liquid release for each of the four definitions of travel time listed above. Fastest travel time and most flux travel time are similarly distributed with travel times controlled by fracture flow clustered at the short time end and travel times controlled by matrix flow at the long time end. Also, similarly distributed are average travel time and flux averaged travel time. The fact that the fastest travel times and most flux travel times are clustered around 1000 years for cases controlled by fracture flow is an aspect of the site and the models chosen. Correlation coefficients were also calculated for the relationship between normalized liquid release and travel time for the four definitions. The flux normalized travel time had the highest coefficient

Figure 9–10a Scatter plots of liquid travel times

correlation (-.52), followed by most flux (-.23), fastest (-.17), and average (-.05).

Figure 9-10b shows the sensitivity of the CCDF of liquid release in the base case (*oooo*) scenario to excluding all or portions of cases with some fracture flow. As expected, excluding all cases involving a fast path to the accessible environment reduces liquid releases to very small amounts. Excluding some of the fast path cases by using a criterion of 1000 or 1100 years does not have a significant effect on the CCDF even though a large portion of the fast path cases is being removed.

9.5.2 Effect of Release Rate from the EBS

The NRC regulations set forth in 10 CFR 60.113 (a)(1)(ii)(B) specify that the release rate of any radionuclides from the EBS should be 10^{-5}/year or less of the 1000 year inventory. Figure 9-11 shows that the CCDF for the base case (*oooo*) scenario responds mildly to screening out the vectors that had release rates greater than 10^{-5}/year of the 1000-year inventory and greater than 0.1 percent of the calculated total release rate limit.

9.5.3 Effect of Waste Package Lifetime

Figure 9-12a shows the distribution of waste package failure time for the base case scenario. Figure 9-12b shows the CCDF sensitivity to screening for waste package lifetimes (other than initial failures) that are less than 300 or 1000 years, as specified in 10 CFR 60.113(a)(1)(ii)(A). Long waste package lifetimes substantially decrease the release. Much of this benefit is derived from the suppression of releases of ^{14}C from early failures of waste containers, during the time when the containers are hot and gaseous travel times are shortest. Figure 9-12c shows the CCDF sensitivity plot for the same case, but for gaseous releases only. Figure 9-12d shows a scatterplot for all vectors of gaseous ^{14}C release to the accessible environment as a function of minimum failure time. There is a clear trend of high gaseous releases for short waste package lifetimes.

The effect of waste package failure time on compliance with the NRC release rate criterion was also investigated. Figure 9-12e is a scatter plot of fraction of the 1000-year inventory being released through the EBS, for dissolved radionuclides (including ^{14}C) versus the time of the maximum release for four selected radionuclides. The bimodal nature of the plots for three of the radionuclides is caused by the large differences in cooling time (and therefore time-of-container failure) for different parts of the geologic repository. There does not appear to be any significant relationship between time of release and EBS release rate of dissolved radionuclides. Americium-241 has a relatively short half-life and is not a daughter of any of the other radionuclides in the list, and therefore does not display a bi-modal distribution. Although not plotted, one would expect that short failure times would also be related to higher releases of gaseous ^{14}C because of the dependence of the release model on temperature.

9.5.4 Effects of the Performance of All Natural and Engineered Barriers

Figure 9-13 shows the CCDFs for total liquid and gas cumulative releases in the base case scenario, with the effects of all natural and engineered barriers separately and in unison. Screening the vectors on the basis of barrier performance leads to a CCDF considerably better (in terms of compliance) than the unscreened vectors. Note that only 18 of the 400 vectors "passed" the screening tests, so the CCDF might not be statistically convergent.

9.6 Illustration of Individual Annual Dose Calculation

In IPA Phase 2, two types of average annual individual ingestion doses (rems/year) were derived from the 10,000-year cumulative population doses calculated by *DITTY*: (1) a crude estimate of dose for an individual member of the farm family who obtains his/her only source of drinking water from the contaminated well discussed in Chapter 7; and (2) a crude estimate of dose for the 177 individuals who reside within 100 kilometers of Yucca Mountain and who eat contaminated beef (whose only source of food was vegetation irrigated with the contaminated well water). Estimates of these individual doses are presented as histograms in Figure 9-14.

The doses in Figure 9-14 should not be construed as accurate estimates of individual annual doses

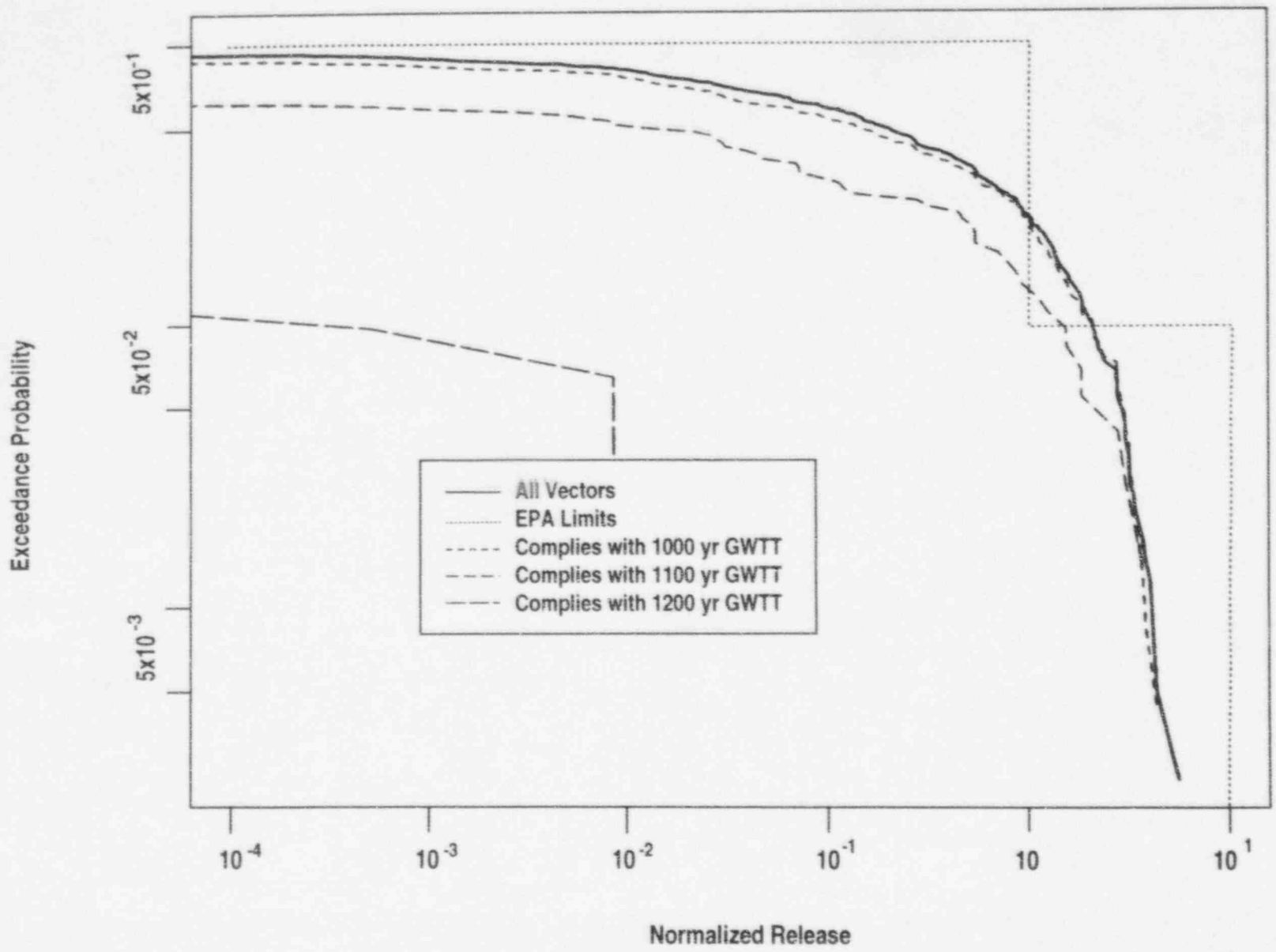

Figure 9–10b CCDF sensitivity plot for "fastest" liquid travel time

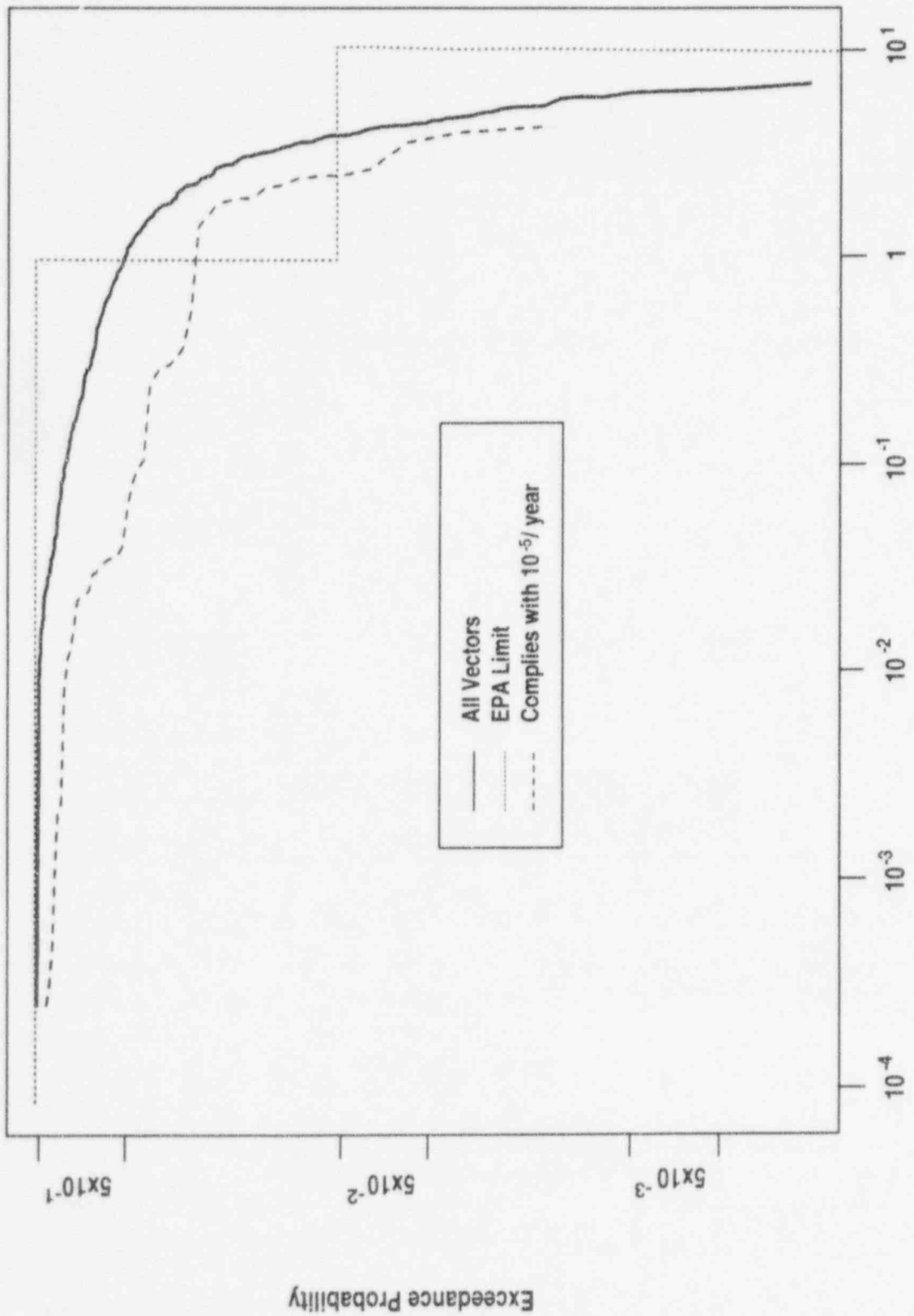

Figure 9–11 CCDF sensitivity plot for release rate from EBS (base case scenario)

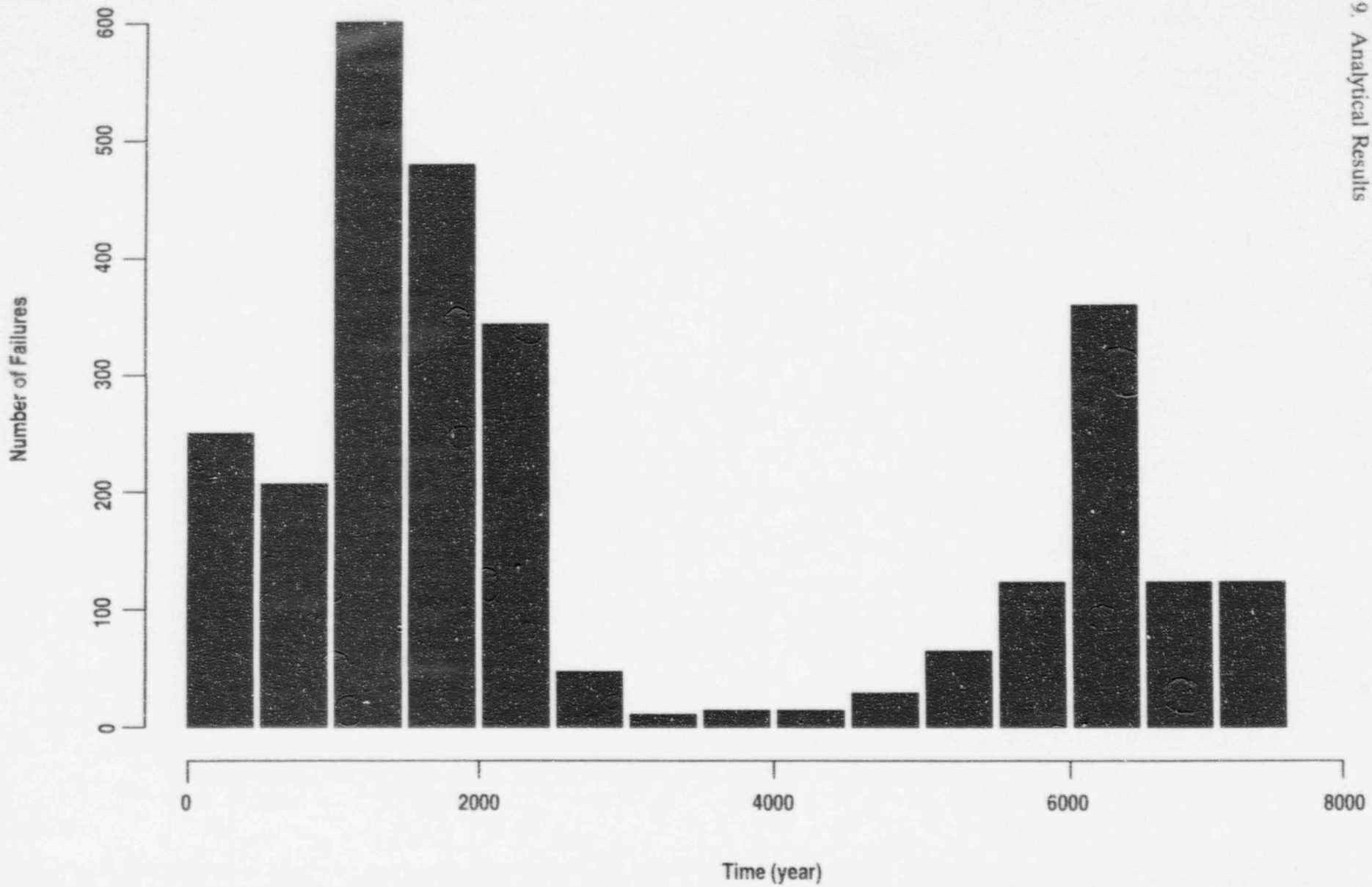

Figure 9–12a Distribution of waste package failure times for base case scenario

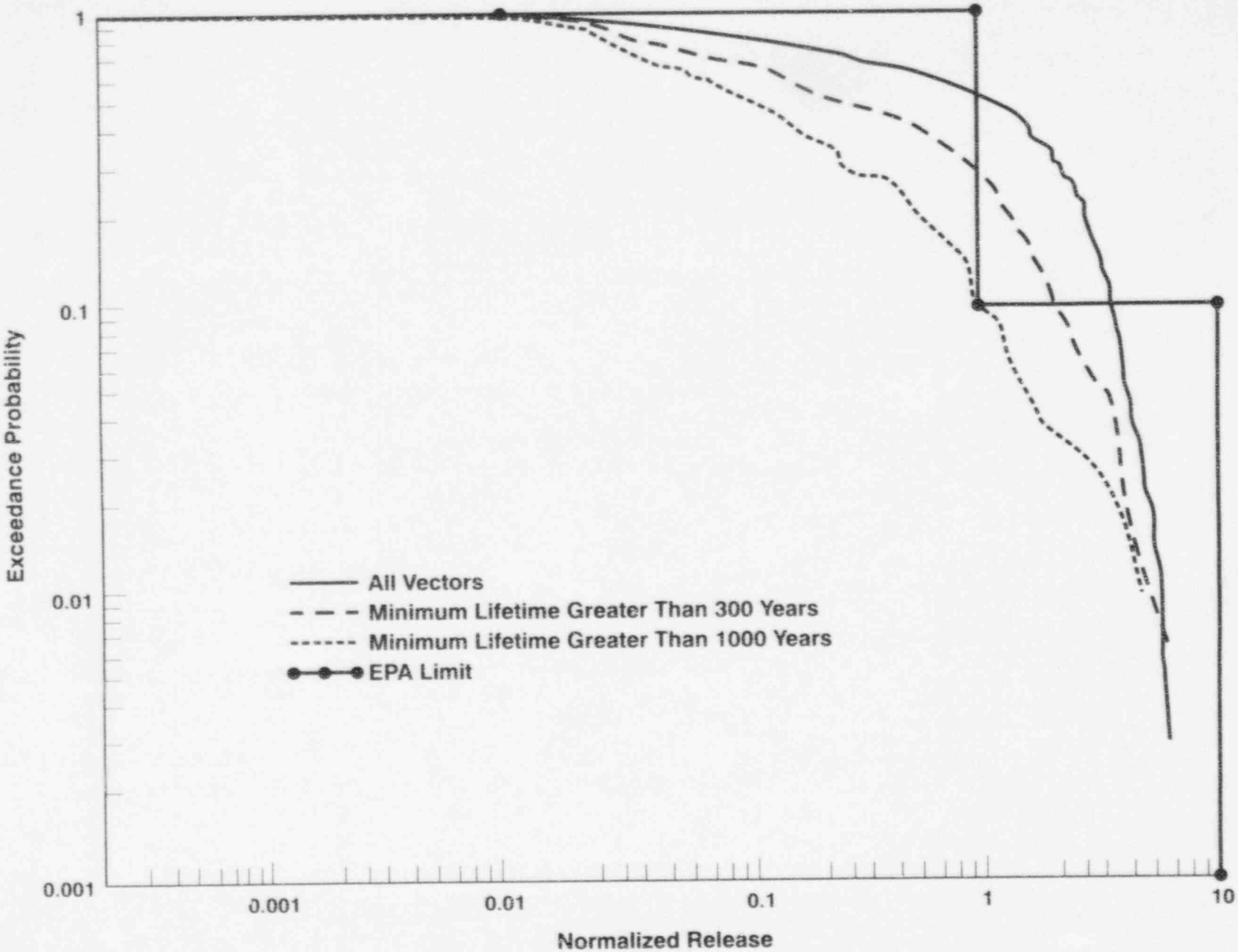

Figure 9–12b CCDF sensitivity plot for waste package failure times for base case scenario

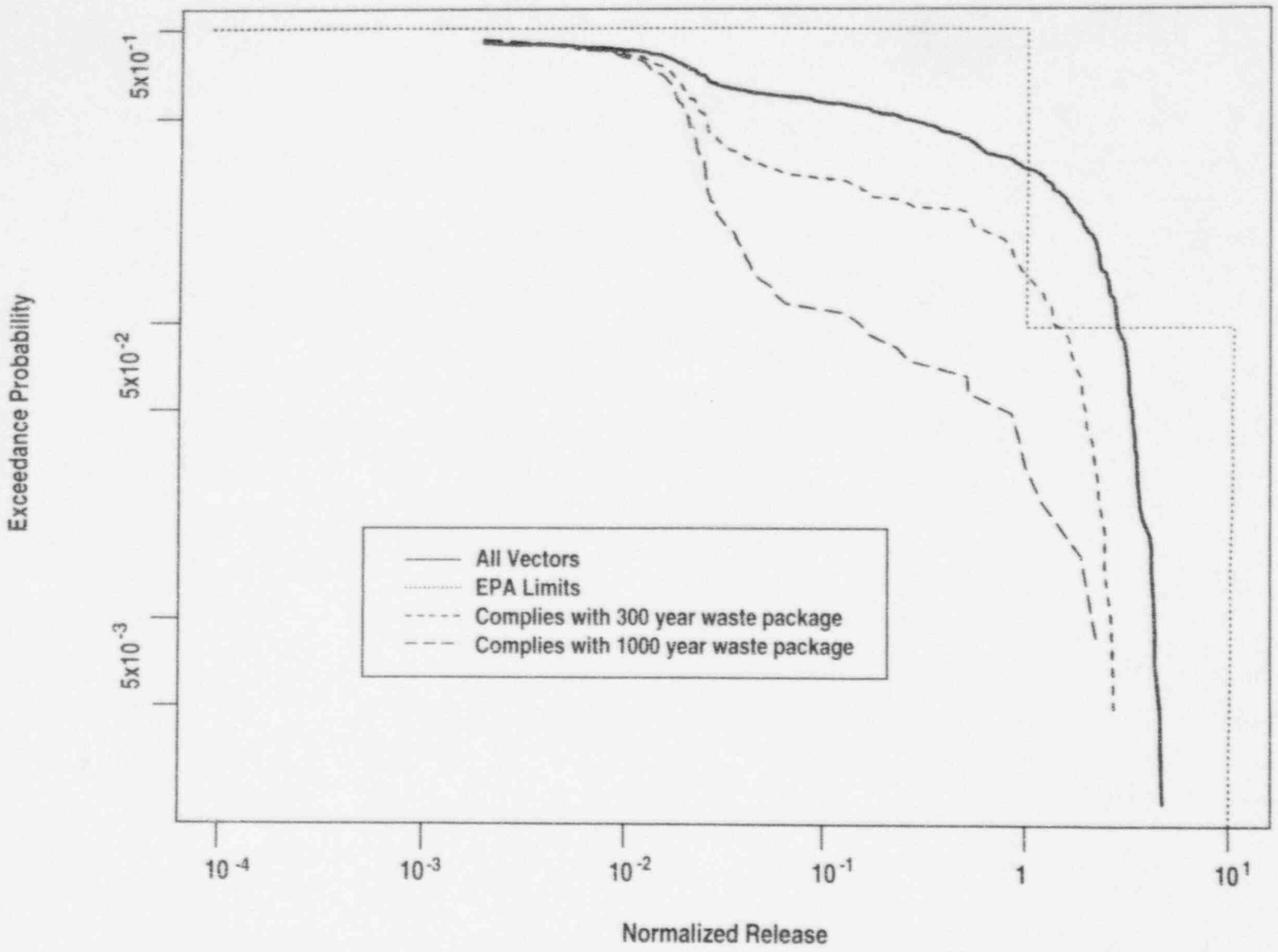

Figure 9–12c CCDF sensitivity plot for waste package failure times for base case scenario (gaseous release only)

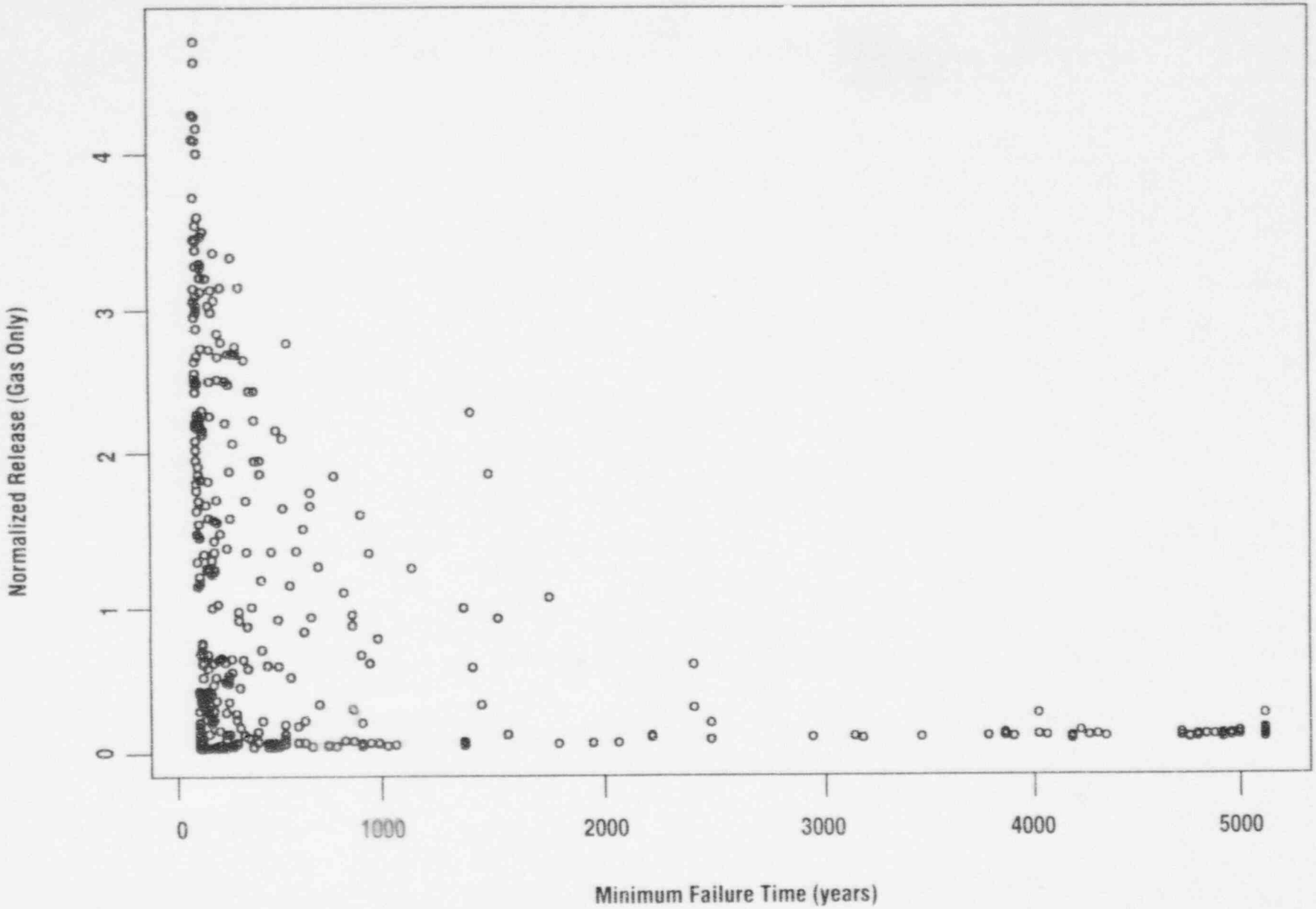

Figure 9–12d Scatter plots of releases to environment versus waste package failure times for base case scenario

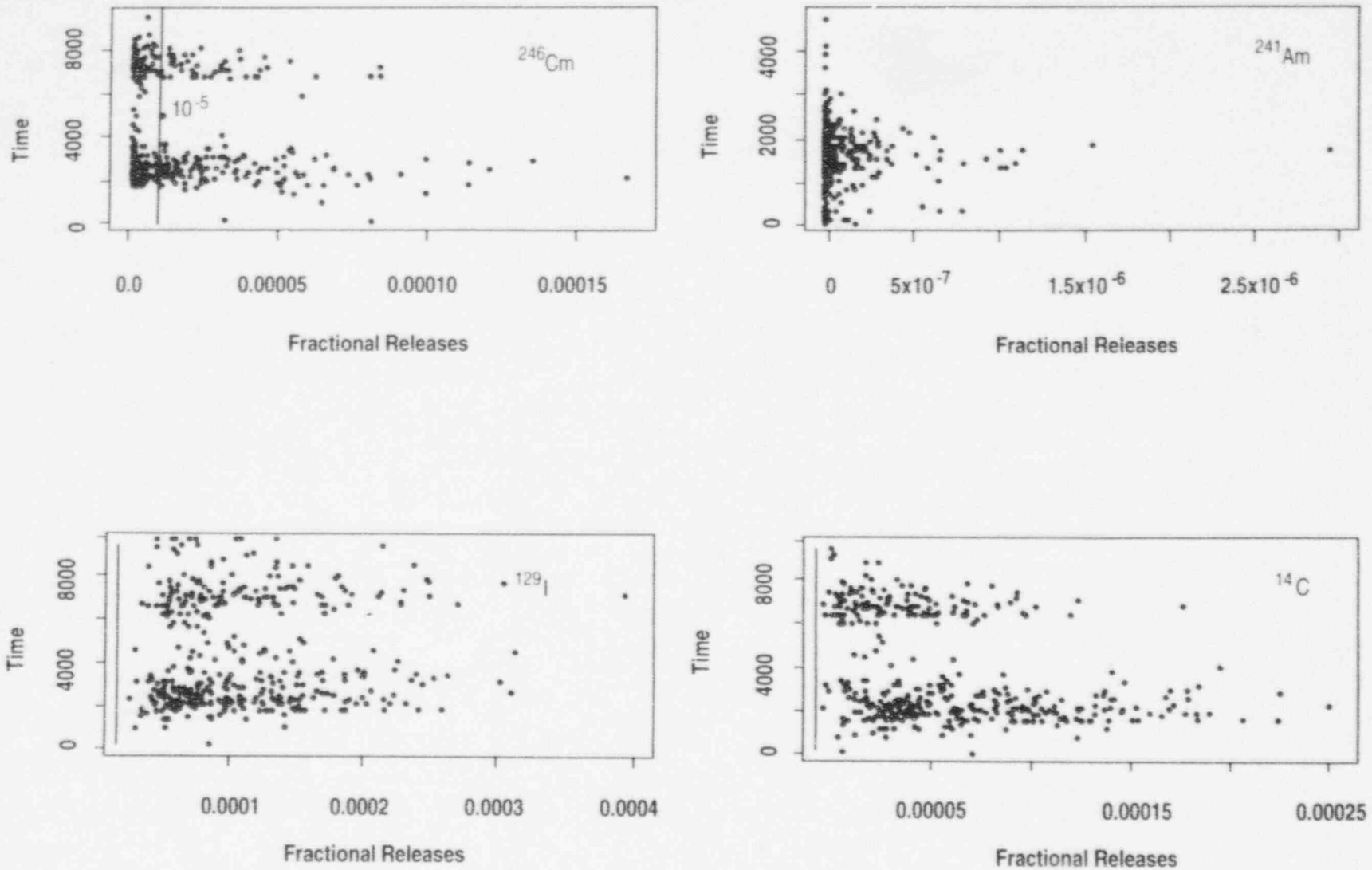

Figure 9–12e Scatter plots of EBS release rates versus time of release for base case scenario

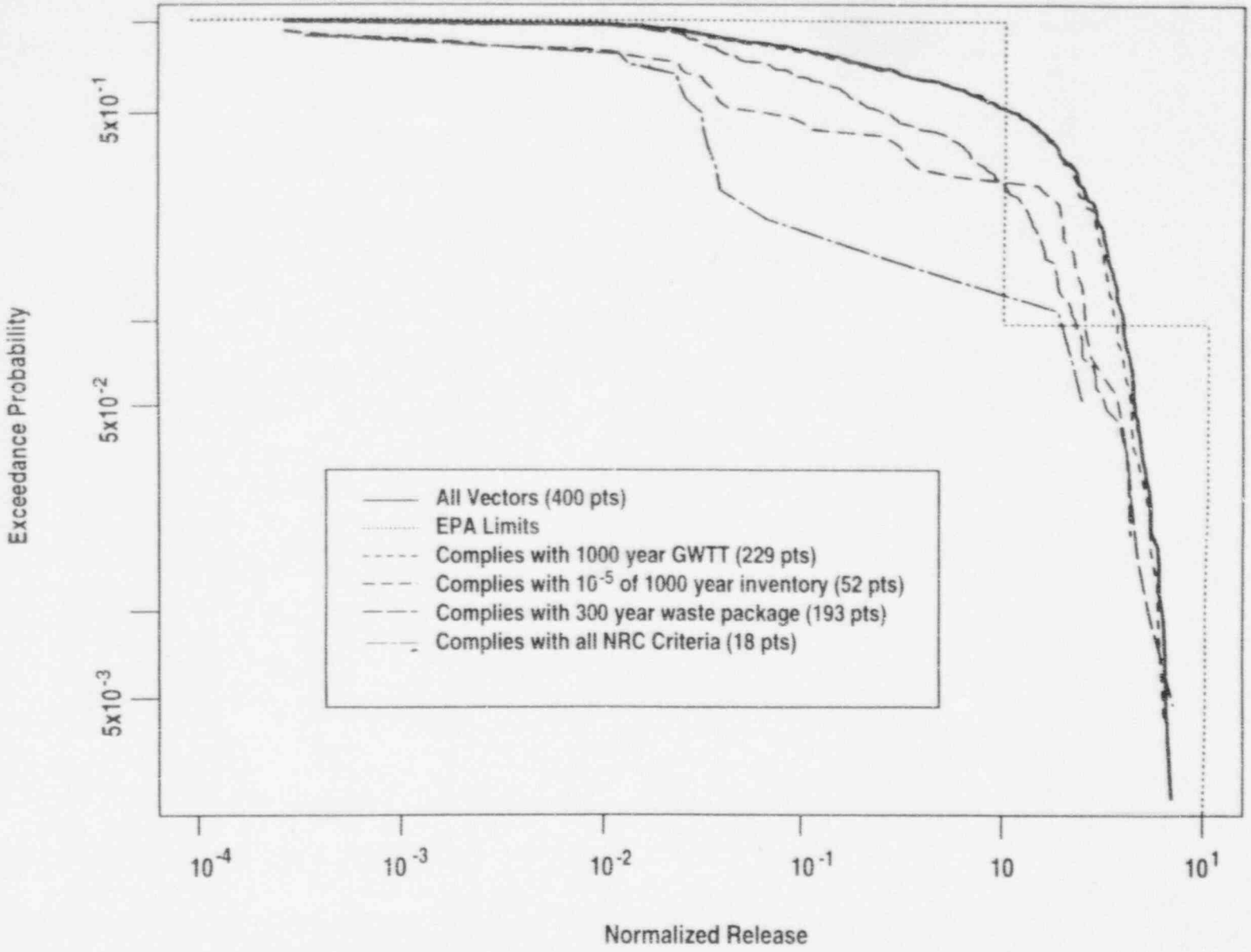

Figure 9–13 CCDF sensitivity plot for all 10 CFR Part 60 subsystem requirements

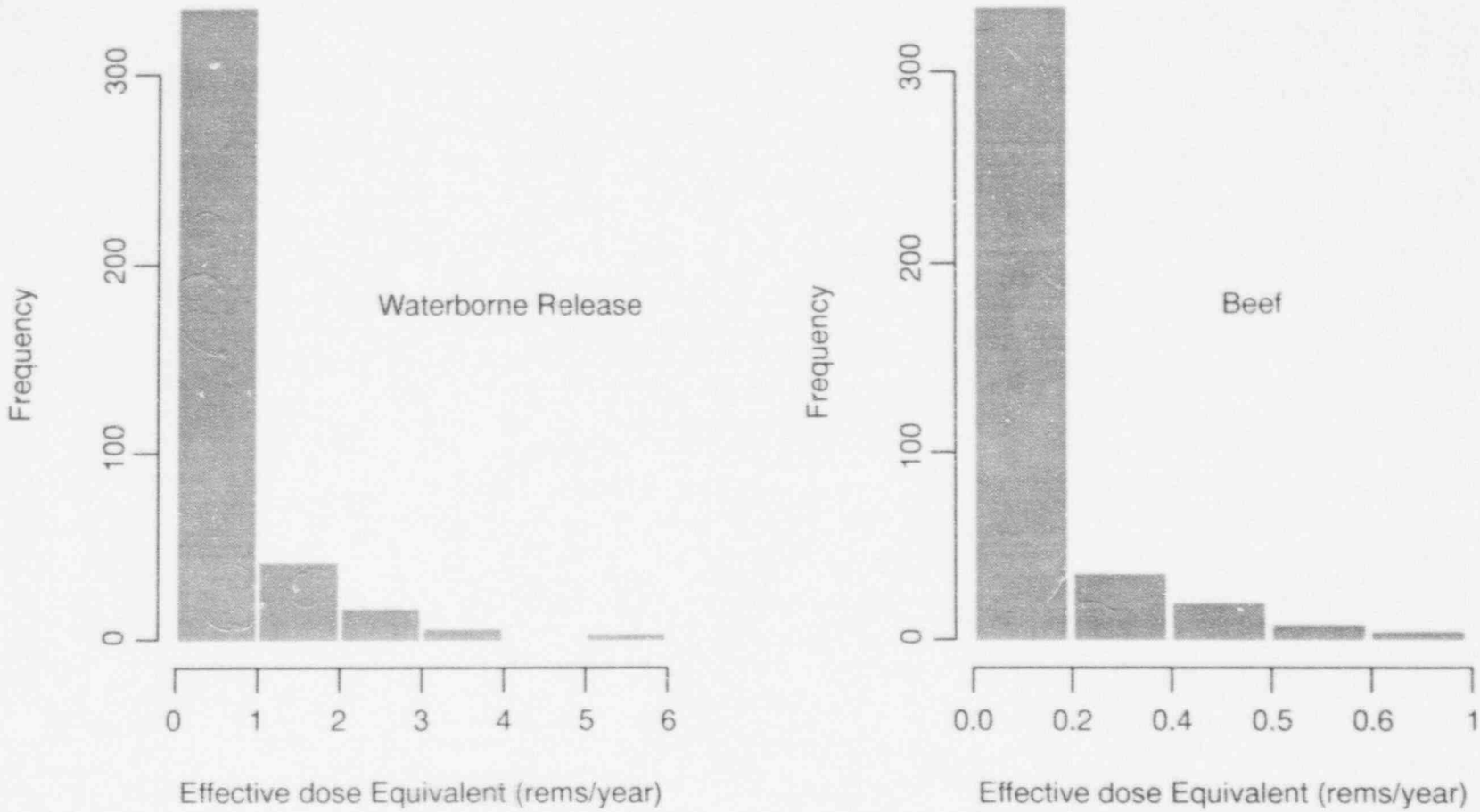

Figure 9–14 Illustration of annual individual dose calculation (base case scenario)

at Yucca Mountain, Nevada. They were included in this report only to illustrate some of the statistical techniques available to the NRC staff for use in future performance assessments. The method used to calculate individual doses in Figure 9–14 is based on the incorrect assumption that the release rate of any single radionuclide into water or beef remains approximately constant throughout the entire 10,000-year period of exposure. Since the times of release of radionuclides from the repository were random (as determined by LHS sampling), and the concentrations in the accessible environment because of these releases are generally pulses or step functions, this assumption is not appropriate. The crude individual dose values in Figure 9–14 therefore underestimate the "peak" individual dose values by an unknown amount.

The doses in Figure 9–14 were derived as follows. For any scenario class, each of the 400 vectors obtained from parameter distributions by LHS sampling was used to generate a corresponding 10,000-year population dose. The 400 dose values plotted in Figure 9–14 correspond to the set of 400 vectors associated with a scenario class in IPA Phase 2. For each vector, the fraction of 10,000-year dose calculated by *DITTY*, which was caused either by ingestion of contaminated beef or contaminated drinking water, was divided by 10,000 years (the exposure period) and either by 3 or 177 (the number of members in the family or the number of beef eaters) to obtain the very crude estimates of the individual doses in rems/year. The doses caused by the inhalation of airborne radioactivity by the 22,200 individuals (those who reside within 100 kilometers of the repository) were of the order of millirems over the 10,000-year exposure period. Since the individual doses caused by inhalation were negligible compared with the individual doses caused by ingestion of water and beef, they were not included in the histograms of Figure 9–14.

In future phases of IPA, more appropriate computer codes (e.g., *GENII* (see Napier *et al.*, 1988)) may be required to obtain significantly better estimates of these individual annual doses. In addition, the transport modules will have to supply time-varying concentration data to the dose modules. In future performance assessments, the NRC staff may also need to devise a strategy to relate distributions of individual doses obtained in a probabilistic performance assessment (such as those illustrated in Figure 9–14) to a deterministic individual dose standard such as that proposed in 40 CFR 191.15 (EPA, 1993; 58 *FR* 7935).

9.7 Summary and Conclusions

In this chapter, the results of the total-system performance assessment analyses were presented in terms of CCDFs, conditional CCDFs, single-vector CCDFs, scatter plots, and screened conditional CCDFs. Although the graphs were presented for demonstration purposes only, many of the representations were found to be especially useful for examining some specific aspects of the analyses. The scenario plots, for example, have proven to be a useful tool for evaluating the effect of disruptive event scenarios on individual vectors. Also, scenario-conditional CCDFs and single-vector CCDF plots ("hair diagrams") proved to be useful for displaying the results of variable uncertainty and scenario probability assumptions.

The difference between CCDFs of releases in the IPA Phase 1 and Phase 2 analyses was primarily caused by the greatly increased probability of the pluvial-climate scenario class in Phase 2, and the addition of the gas pathway for ^{14}C migration in Phase 2.

The relationship between the performance of the natural barrier as measured by liquid travel time and the EPA release criterion depends on what definition of liquid travel time is used. When liquid travel time is defined along the "fastest" pathway or the "most flux pathway," there is a bi-modal distribution because of the sharp distinction between matrix and fracture controlled flow. When travel time is "averaged" or "flux-normalized" this bi-modal distribution does not occur. Correlation analysis showed a significant relationship between flux-normalized travel time and *Normalized Release*. For an averaged liquid travel time there was almost no correlation. Certainly, the type of flow (fracture or matrix) that is strongly influenced by the sampled infiltration rate appears to be the primary factor in reducing waterborne radionuclide movement to the accessible environment.

Little correlation was shown between the fractional release rate performance measure and the *Normalized Release*. Meeting the NRC EBS

release-rate criterion, alone, did not guarantee a *Normalized Release* less than 1. The staff concludes that more work is necessary to evaluate the relationship of the NRC EBS release-rate criterion to total system performance, as well as the feasibility of repository designs to meet the criterion.

Waste package lifetime appeared to have a significant effect on the *Normalized Release* for the liquid and gaseous components. Early waste canister failures were generally found to result in large ^{14}C releases to the accessible environment, primarily because of enhanced transport from large thermal gradients, and increased rates of $^{14}CO_2$ generation at higher temperatures. Significant sensitivity of releases to waste package failure times was observed in the 300- to 1000-year range. The effect of release time (a function of waste package lifetime) on compliance with the NRC EBS release-rate criterion, however, did not appear to be significant.

The effect of compliance with all of the NRC subsystem performance requirements, on meeting the EPA release limit, must be considered inconclusive, because of the small number of realizations that met all three criteria. Future analyses, using selected ranges of sampled values and more realistic (less conservative) models, may provide more definitive insights.

The individual dose calculation, although illustrative for the sake of comparison, is neither conservative nor accurate. Significant improvement in all phases of the performance assessment will be required if individual dose is to be calculated for regulatory purposes.

10 CONCLUSIONS AND RECOMMENDATIONS

10.1 Introduction

As noted in Chapter 1, a major goal of the Iterative Performance Assessment (IPA) effort is to develop the necessary knowledge, tools, and methodologies to provide a basis for the U.S. Nuclear Regulatory Commission staff to evaluate the adequacy of the U.S. Department of Energy's (DOE's) site characterization program (in the context of integrated repository performance) as well as for reviewing the performance assessment submitted as part of a potential license application. Further development of these tools and procedures is planned in future IPA iterations. In reviewing the results of IPA Phase 2, the staff evaluated the adequacy of the methodology and the adequacy of the scientific bases used for these analyses. This evaluation is discussed in Section 10.2.

The staff gained insights from developing and evaluating the system code computational modules, performing the auxiliary analyses, and performing the sensitivity and uncertainty analyses on the results of IPA Phase 2. These insights include the relative importance of various site characteristics, design features, and repository processes to repository performance. Insights gained from performance assessment results (and limited by the accuracy of the models used) include evaluation of the relationships between the performance of natural and engineered barriers and performance of the repository, and evaluation of dose and release estimates and their relationship to scenario class and pathway. Insights and conclusions are discussed in Section 10.3.

Section 10.4 discusses additional research, modeling improvements and supporting analyses that will be needed to improve the methodology and scientific basis of future performance assessments. In Section 10.4.1, necessary research falling under the responsibility of DOE or its contractors has also been included. In some cases it will be necessary for NRC, as well as DOE, to pursue a more thorough understanding of the scientific bases of the subsystem models, as well as improvements to the codes that incorporate the models, so that NRC can evaluate critical DOE assumptions, conceptual descriptions, and mathematical representations of repository performance.

10.2 Evaluation of IPA Phase 2 Methodology and Scientific Bases for Analyses

10.2.1 Adequacy of Methodology

The methodology evaluated, which is described in previous chapters, includes the simulation structure and treatment of uncertainty, scenario analysis, consequence analysis, the calculation of complementary cumulative distribution functions (CCDFs) for the normalized release and dose, and the use of auxiliary analyses to support model assumptions. An objective of IPA Phase 2 was to evaluate particular aspects of the performance assessment methodology, developed and transferred to NRC by the Sandia National Laboratories (SNL), including the models and codes for flow and transport in partially saturated fractured rock (i.e., *DCM3D*—flow; *NEFTRAN II*—radionuclide chain transport) and the scenario analysis methodology. The purpose of this section is to discuss the adequacy of various aspects of the IPA Phase 2 performance assessment methodology, including that developed by SNL.

The Monte Carlo simulation of multiple vectors or realizations, used in IPA Phase 2, is a common approach to uncertainty analysis, and was used in the IPA Phase 1 study (Codell *et al.*, 1992) and other recent studies, such as the SNL performance assessments for the Waste Isolation Pilot Plant (WIPP) (Helton *et al.*, 1991), the SNL performance assessments for Yucca Mountain (Barnard *et al.*, 1992; and Wilson *et al.*, 1994), and the Pacific Northwest Laboratory (PNL) performance assessment for Yucca Mountain (Eslinger *et al.*, 1993). This procedure allows the propagation of parameter uncertainty through a series of linked models. Model uncertainty and uncertainty resulting from the spatial variability of the parameters, however, are not reflected directly in the results (although some of these uncertainties have been represented by input parameter variability).

The SNL scenario selection methodology (Cranwell *et al.*, 1990), whose modification and implementation were described in Chapter 3, provided

an adequate basis for the staff's scenario analysis in IPA Phase 2. Sixteen mutually exclusive scenario classes, with associated estimated probabilities, were generated from an initial list of 17 potentially disruptive events and processes, of which four events and processes remained after screening for combination into scenario classes. These 16 scenario classes were provided for incorporation in the consequence analysis. Definition of repository system boundaries for the analysis kept the number of scenarios requiring evaluation to a tractable number.

The consequence models, described in Chapters 4 to 6, represent a limited attempt to estimate, for the most part using mechanistic models, the performance of the repository under selected scenario classes for each sampled realization. The increasingly mechanistic nature of the consequence models is considered to be a positive improvement over IPA Phase 1, because it has and will allow in future developments, more representative and realistic coupling between processes, and because the use of mechanistic models allows a more direct and transparent identification of needed information and data. The IPA Phase 2 models have not been run for time-varying boundary conditions (e.g., time-varying percolation flux through the repository for source term and dissolved transport models). However, some of the models allow for transient conditions caused by repository heat (e.g., gas flux for ^{14}C transport), which is a function of time. Changing near-field temperatures caused by repository heat also influence the start of waste package corrosion and fuel alteration rates. Changing far-field temperatures influence gas transport. An alternative to this limited dynamic approach may be to employ stochastic time series generation of environmental processes, such as that employed in a performance assessment in the United Kingdom (see HMIP/DOE, 1993). Also, in the IPA Phase 2 consequence models (described in Chapter 6), limitations in site characterization data and excessively long computer code run times required the use of one- (1-D) and two-dimensional (2-D) transport models, where a full three-dimensional (3-D), transient approach may have been more appropriate. Although 3-D models may remain impractical to include directly in the IPA evaluations, they can be used to develop abstracted codes.

The calculation of CCDFs, described in Chapter 9, was based on the assumption of equal probability for each realization determined for a scenario class. There were three presentations of CCDFs in IPA Phase 2: (1) conditional CCDF curves for each scenario class representing the parameter uncertainty; (2) composite or total CCDF curves representing all scenario classes; and (3) "hair diagrams," which are CCDF curves for multiple parameter vectors, each representing all scenario classes. The conditional CCDFs present repository behavior for each scenario class. They are combined to form the composite or total CCDF by weighting each by its scenario probability. The "hair diagram" presents the same information in a different way, keeping separate the scenario and parametric probabilities. For that reason, the extremes of system behavior may be better demonstrated with the hair CCDFs. For example the effects of extreme parametric values can be displayed for both high probability events (climate change) and low probability events (magmatism). The mean of all of the hair CCDFs gives the same composite or total CCDF that would be calculated by combining the scenario CCDFs.

A comparison between the CCDF of cumulative radionuclide release resulting from the IPA Phase 2 analysis and the CCDF computed by the earlier Phase 1 analysis demonstrated several significant differences. Much of the difference could be explained by the incorporation of the gas transport pathway in Phase 2 and the assignment of a higher probability of occurrence for the pluvial (climate) event. Similar comparisons in future climate phases of IPA should be easier and more informative because comparisons are expected to be made after each incremental change rather then only at the completion of major revisions in the total-system performance assessment.

Auxiliary analyses are an important part of NRC's IPA methodology. Auxiliary analyses were used for development of the abstracted models described in Chapters 4 and 5 from more sophisticated models, to synthesize parameter values and distributions from more fundamental data, and to place the results of the analyses in perspective. The auxiliary analyses were used to set some constant parameters such as water level during the pluvial climate event, geochemical parameters for various strata and radionuclides, and to determine the 1-D flow path characteristics for the liquid flow and transport computations. The

auxiliary analyses proved to be an indispensable and integral element of the staff IPA effort.

The use of the *DCM3D* and *NEFTRAN II* computer programs proved to be useful for implementing the conceptual models for liquid flow and transport of radionuclides, respectively. *DCM3D* was not used directly in the total-system performance assessment (TPA) computer code, but was used principally to partition the groundwater flow between the fracture and matrix systems for input to *NEFTRAN II*. The transport of radionuclides was simulated using *NEFTRAN II*, which accounted for element-specific retardation, radioactive decay, and generation of radioactive progeny. This simple representation kept the fracture and matrix flow systems separate. More complex representations may require features of the computer programs not used in the current analysis (e.g., transient flow fields, matrix diffusion, and 3-D models) or computer programs that represent additional processes (e.g., multi-phase flow).

Overall, the methodology provides a structured, analytical approach for estimating performance of a potential geologic repository. Various aspects of the methodology require improvement, such as consequence models, and the estimation of scenario probabilities, as discussed in Section 10.4.

10.2.2 Adequacy of Scientific Basis for the IPA Phase 2 Analyses

For the purposes of this discussion, the scientific basis for analysis was considered to be published information about the site and the proposed repository design, published research conducted by DOE and its contractors, and NRC-sponsored research. Broader scientific and technical literature, including published performance assessments such as that performed for the WIPP project (Helton *et al.*, 1991), was used to supplement this information.

The scientific basis for analysis is improving through site characterization activities and research. However, the existing scientific basis is far from adequate to allow an accurate assessment of compliance with any of the applicable performance objectives with reasonable assurance. The paucity of data about the site is probably the greatest inadequacy. For example, the state of site characterization at the time these analyses were performed did not support a consensus among hydrologists about conceptual models of water movement through Yucca Mountain nor the appropriate paradigm for modeling transport of radionuclides. Far-field geochemistry, especially in its application to transport by fracture flow, is another area where conservative approximations have been used in the IPA Phase 2 analysis to account for uncertainty. In this analysis, there was assumed conservatively to be no retardation in the fractures. Credible models of retardation processes, especially in fractures, would reduce the level of conservatism for this process.

The NRC staff has modeled the 1988 Site Characterization Plan (SCP) repository design (DOE, 1988) to the extent practical, although the staff is aware of proposed design changes. Because of the preliminary nature of the design, many of the calculations have been performed as conservative or bounding analyses. Examples of such analyses are the seismic failure model for the waste packages, the waste package corrosion model, and the waste dissolution model. To the extent practicable, the SCP design has been used as a basis for modeling. Many aspects of the repository design are expected to change and the waste package design is likely to change significantly. Changes in placement configuration, such as from vertical to horizontal, will affect the waste dissolution and release models. Changes to thermal loading will affect the near-field hydrology of the waste packages and the circulation of rock gas.

10.2.3 Conclusions Regarding IPA Phase 2 Methodology and Analyses

The methodology can and must be improved as more data become available and the understanding of the site matures. However, the staff considers the present methodology suitable to gain insight into the significance of many of the germane parameters and processes and to gain insights regarding model development, repository performance, and research and technical assistance needs. However, the data and scientific understanding of the site are not sufficient at the current time to predict potential repository performance with certainty. Furthermore, several areas of modeling need improvement in order to have confidence in the estimates of performance. The computed CCDFs presented in this report

should not be taken to be indicative of actual repository system performance.

10.3 Insights and Conclusions From IPA Phase 2

10.3.1 Significant Insights and Conclusions from Model Development and from the Sensitivity and Uncertainty Analyses

The purpose of this section is to discuss insights identified through model development and the sensitivity and uncertainty analysis that have a significant effect on the results of the performance assessment. Most of these insights at this stage of the IPA process deal with site aspects, repository design, and repository processes.

As noted in Chapter 4, two features of the site that appear to strongly influence the results of the performance assessment are: (1) the rock media are unsaturated and therefore have the potential for advective transport of gas upward to the atmosphere; and (2) the rock media are fractured and have the potential for fast liquid pathways for radionuclide transport to the water table and beyond. The quantitative effects of both these features have been relatively difficult to model in a consistent manner. For example, permeability and porosity for flow through fractures in the dual porosity model for the repository cross-section stratigraphy were estimated from fracture aperture widths and the number of fractures per unit area, where as permeability and porosity for the matrix were based on core analysis. Both of these data types are based on local (small-scale) observations and need to be supplemented by data collected at a larger scale.

From the regression analyses for the base case scenario and other scenario classes not involving pluvial climate, infiltration rate was found to be the most important sampled parameter. There is strong correlation at low to moderate infiltration rates (base case) and weaker correlation at the high infiltration rates (pluvial case). In the former case, there was both matrix flow and fracture flow, but in the latter case, the flow was predominately in fractures. Under conditions of significant fracture flow, radionuclide travel times tended to be low, with relatively little decay. The accompanying figure (Figure 10–1) shows a significant decrease of liquid radionuclide releases for the base case CCDF when vectors with infiltration rates greater than 1 or 2 millimeters/year were eliminated from the CCDF.

Although the flux of liquid water through the repository depends on the parameters infiltration, hydraulic conductivity, and porosity, performance correlates most strongly to infiltration. The saturated hydraulic conductivity and porosity vary from layer to layer for each vector, and are assumed to be uncorrelated. There is only one value of infiltration per vector for all layers, however. Since, in the 1–D representation of unsaturated flow, infiltrating water must pass through all layers, the sensitivity to the value of hydraulic conductivity or porosity of any single layer is reduced.

A number of model simplifications (e.g., 1–D flow paths, permeability ranges, and seven sub-areas for the total repository area) were used to abstract the 3–D problem and allow analysis of the uncertainties with reasonable computer execution times for the Phase 2 analysis. However, the proposed repository is a transient, 3–D, partially saturated system with significant air and water vapor movement in a fractured, porous medium, complicated by potentially significant heat transfer and the associated flows of gas and liquid. How these phenomena can be approximated by simplifying assumptions and still provide an adequate representation for the calculation of system performance is poorly understood at this time and needs further investigation.

The Phase 2 analysis conservatively assumed that there was no retardation in the fractures and did not consider the process of matrix diffusion in the modeling. Future iterations need to evaluate the nature and magnitude of the conservatism of these assumptions and the relationship of fracture coatings to geochemical processes.

The design of the waste package container and its emplacement configuration is expected to have a strong influence on repository performance. As discussed in Section 10.2.2, the design of the waste package will greatly affect waste package failure times and release mechanisms. IPA Phase 2 analyses had varying degrees of ability to treat design details; e.g., *SOTEC* was based on vertically

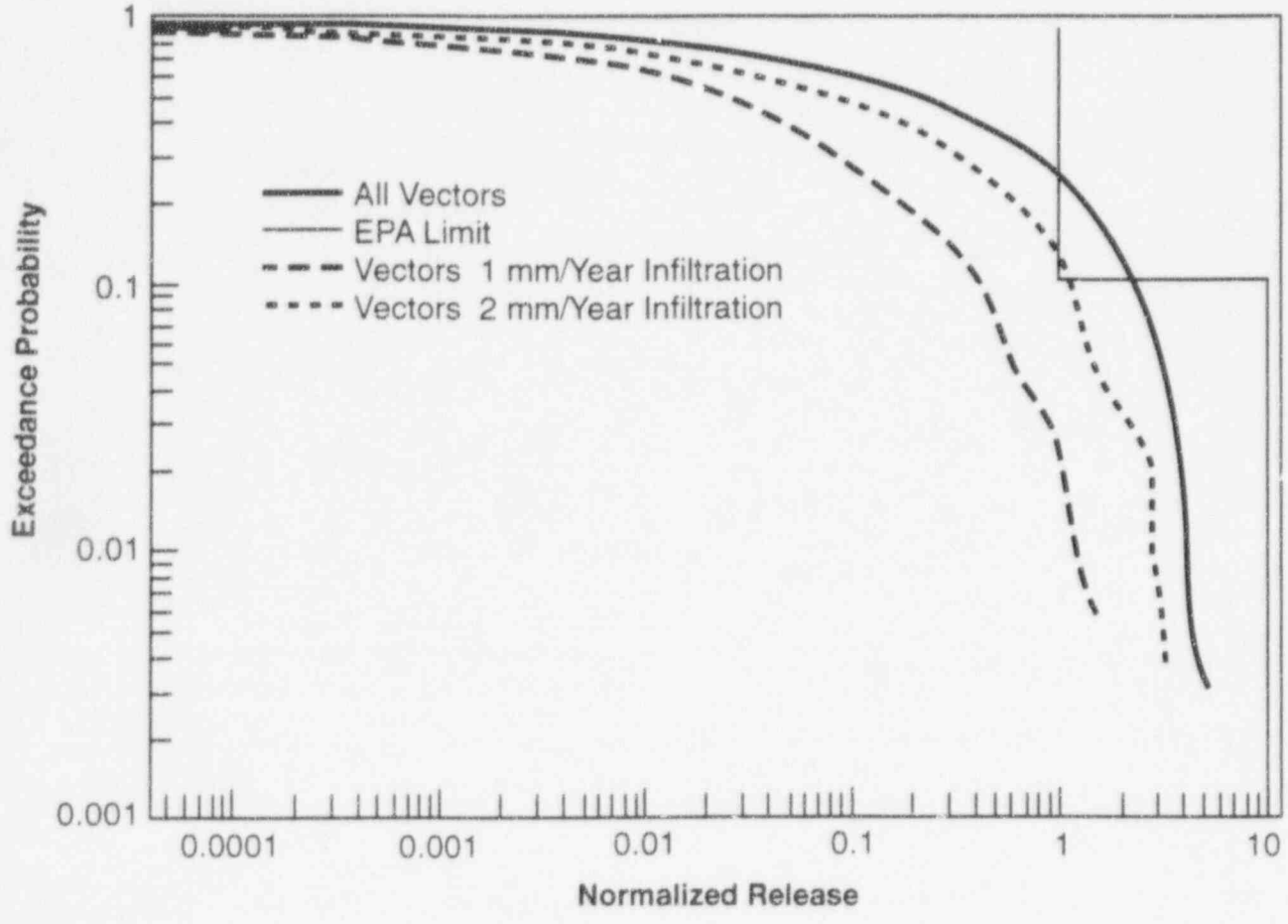

Figure 10–1 **CCDF for dissolved radionuclides, base case scenario** (Vectors screened for less than 1 or 2 mm/yr infiltration.)

emplaced waste packages, with no option for horizontal emplacement. *DRILLO* had the option for horizontal emplacement, but it was not used. Various options for treating the configuration of the waste package will probably need to be incorporated in some of the modules of the system code.

The corrosion-related parameters that showed strong correlation with performance were the (electrochemical) potentials for pitting and crevice corrosion, and the active corrosion rate. Corrosion affects the time of waste package failure under static and seismic conditions. Dissolution-related parameters include the fuel alteration rate and solubilities of radionuclides. Other factors found to be important control the interaction of water with the waste package and influence whether and how water contacts the waste.

Failure of the waste packages by corrosion and transport of dissolved radionuclides from the waste package are expected to depend on contact with liquid water. In IPA Phase 2, waste packages were assumed to remain dry until their surface temperature dropped below the boiling point, and came into contact with liquid water from dripping fractures and wet rock. Future models need the ability to consider plausible rewetting mechanisms for dry rock, the possible influx of liquid water such as dripping fractures, condensation of water vapor on waste package surfaces because of capillary and solution effects, rise in the water table, and water reflux driven by repository or geothermal heat.

Repository heat load is a design parameter that has the potential to significantly affect performance. The present analysis is based on the assumption of a hot repository with a design power loading of 57 kilowatts/acre. This loading results in a strong thermally induced gas flow when typical hydrologic properties are assumed for the rock strata, as shown in Section 4.3. This loading is assumed to cause a period of dryness for the waste packages; that is, there is a period for which the temperature of the rock surrounding any particular waste package will be above the boiling point of water, assumed to protect it from corrosion. Temperature also affects corrosion rates and the rate of oxidation of spent nuclear fuel. Hence, the overall sensitivity of the total-system performance assessment to any particular loading is not clear at this point, because only one loading was assumed for all simulations. A parametric study of repository thermal loading may provide additional insights in future phases.

Gas transport parameters were also identified to be important. Parameters identified are the gas permeability and retardation coefficient for ^{14}C in the Topopah Spring Unit. The gas transport of ^{14}C will be complicated by variations in moisture in the transport medium and gas flow, because of the heat of the decaying nuclear waste as well as chemical processes leading to retardation of carbon. Geochemical modeling of ^{14}C transport demonstrated a retardation factor of approximately 30 to 40, primarily because of the transfer of carbon between the CO_2 in the gas phase and dissolved carbonate and bicarbonate in the liquid phase. Some ^{14}C might be trapped temporarily in precipitating calcite during the period when temperatures are rising, and released from the calcite as it redissolves as temperatures fall. Although not modeled in IPA Phase 2, percolation of moisture and its effect on the upward movement of vapor may tend to reduce ^{14}C releases during pluvial periods, possibly reducing the sensitivity of total normalized release to percolation rate.

Seismicity and volcanism caused large releases compared with the undisturbed (base) case, but did not appear to have a significant effect on the total CCDF. However, more realistic modeling of infiltration, corrosion, seismicity and magmatism could significantly change the importance of disruptive effects relative to one another, as well as their influence on the total CCDF. For example, a more detailed study of magmatism may include changing groundwater chemistry and accelerating the corrosion of nearby waste packages.

Several potentially volatile compounds of ^{99}Tc, ^{79}Se, and ^{129}I will be present in spent nuclear fuel. Conservative estimates of gaseous releases of these radionuclides during volcanism and normal operations demonstrated relatively insignificant impacts, so this potential phenomenon was given a low priority for the IPA Phase 2 study.

10.3.2 Insights and Conclusions Regarding System and Subsystem Performance

This section presents some insights and conclusions regarding system and subsystem performance in terms of factors related to the behavior of the engineered and natural barriers. As noted

earlier, the factors that were investigated in IPA Phase 2 were the integrity of the waste package canisters, the rate of release of radionuclides from engineered barriers, and the travel time of water through the geosphere. The regulatory requirements in 10 CFR 60.113 address "three subsystem performance objectives," namely substantially complete containment (SCC) of waste in the waste packages (10 CFR 60.113(a)(1)(ii)(A)), controlled fractional release rate from the engineered barrier system (EBS) (10 CFR 60.113(a)(1)(ii)(B)), and pre-waste-emplacement ground-water travel time (GWTT) (10 CFR 60.113(a)(2)). The conclusions are not for the purpose of directly drawing a comparison between overall system performance in terms of release or dose and the subsystem performance measures. There are primarily two reasons for this distinction: (1) the subsystem performance measures are supposed to be independent requirements ensuring a minimal performance of each of the multiple barriers in a geologic repository, unrelated to the total system performance; and (2) the characterizations of SCC, EBS release rate, and GWTT used in IPA Phase 2 are crude and incomplete, and do not exactly conform to the definitions of those quantities in 10 CFR Part 60. For example, travel time as used here does not include the concept of the disturbed zone and is for post-emplacement rather than pre-emplacement conditions. Furthermore, travel time calculated in *FLOWMOD* is an abstraction based on the fastest combination of possible fracture and matrix pathways, and does not correspond to a realistic flow path. Nevertheless, the following comparisons shed light on the importance of the engineered and natural barriers to the total system performance.

CCDFs have been drawn by "screening out" vectors that did not meet a given criterion. The screened CCDFs used with the barriers' performance showed waste package lifetime to have a significant effect on the normalized release for liquid and gaseous source term components in the 300-year to 10,000-year range. Early waste package failures were generally found to result in large ^{14}C releases to the accessible environment, primarily because of enhanced transport from large thermal gradients, and increased rates of $^{14}CO_2$ generation at higher temperatures. The relationship between "liquid" travel time and the U.S. Environmental Protection Agency (EPA) release criterion[1] was strong, for flux weighted "liquid" travel time. However, travel times calculated as a result of averaging or flux weighting sub-area travel times were generally in excess of 10,000 years. The relationship between "fastest" travel times from among the seven repository sub-areas and the *Normalized Release* was most significant when used as a factor to determine the presence or absence of fracture controlled flow.

Release of ^{14}C through the gaseous pathway contributed significantly to the *Normalized Release* while not affecting significantly the *Effective Dose Equivalent* estimate. This is probably because the normalized release limit for ^{14}C is related to the world-wide circulation of ^{14}C and the resulting dose, whereas the dose calculation in this study is limited to the assumed population in a circular area of 50-kilometer radius.

The 10,000-year median collective dose for the fully disturbed case was approximately an order of magnitude greater than the corresponding dose for the base case scenario. For the *Normalized Release*, the median (i.e., 50 percent probability) of the fully disturbed case was about 5 times the median of the base case. For both dose and *Normalized Release* at the median probability, the most important disturbing event is pluvial climate and the resulting increase in percolation rate. The contributions by the ingestion pathway dominated the collective doses from both scenarios. The average annual dose to an individual in the region from inhalation was negligible compared with that from ingestion of contaminated drinking water and locally-grown contaminated food. In scenario classes involving magmatism, order of magnitude increases over the base case dose resulted from direct releases to the surface during an extrusive magmatic event. The same type of event increased the *Normalized Release* by about a factor of 4. The radionuclides that made the largest contributions

[1]Currently, a revised set of standards specific to the Yucca Mountain site is being developed in accordance with the provisions of the Energy Policy Act of 1992. The Energy Policy Act of 1992 (Public Law 102–486), approved October 24, 1992, directs NRC to promulgate a rule, modifying 10 CFR Part 60 of its regulations, so that these regulations are consistent with EPA's public health and safety standards for protection of the public from releases to the accessible environment from radioactive materials stored or disposed of at Yucca Mountain, Nevada, consistent with the findings and recommendations made by the National Academy of Sciences, to EPA, on issues relating to the environmental standards governing the Yucca Mountain repository. It is assumed that the revised EPA standards for the Yucca Mountain site will not be substantially different from those currently contained in 40 CFR Part 191, particularly as they pertain to the need to conduct a quantitative performance assessment as the means to estimate postclosure performance of the repository system.

to population dose (cumulated over 10,000 years) were ^{94}Nb, ^{210}Pb, ^{243}Am, and ^{237}Np.

10.4 Recommendations

10.4.1 Recommendations for Additional Scientific Input

Based on the insights and conclusions described above as well as recommendations identified in the Phase 1 report, there is a need for continuing research by both NRC and DOE in the general areas of hydrology and geochemistry, waste form and waste package container materials, repository hydrothermal effects, and probabilities and effects of disruptive events. The ability to identify research needs from the work performed in IPA Phase 2 is limited by the lack of sophistication of the models and paucity of data. When site characterization results are adequate to allow detailed modeling of hydrologic characteristics for different scales, ongoing research in scale effects will prove useful. The same is expected to be true of advanced corrosion and waste dissolution topics, shaft and borehole sealing, natural analogs, and seismic research. Hence, there is a significant amount of research being pursued that will eventually support performance assessment, but cannot be directly justified by insights and conclusions from the present analysis.

Fracture-Matrix Interactions. Considerable research in hydrology will need to be directed at achieving a better understanding of fracture-matrix interactions. Flow in fractured or fractured-porous media can be represented in several ways: (1) *discrete fracture models* that sent flow explicitly in discrete channels and in the porous matrix; (2) *equivalent continuum models* that represent the averaging of the matrix and fracture system into an equivalent porous medium; and (3) *dual-continuum models* that treat the matrix and fracture as separate but interacting continua. Experimental information for fracture-matrix interactions is scarce and is needed to provide insights on the applicability of these approaches. DOE will need to provide detailed characterization of the fracture properties in the repository horizon as a minimum, for examination of near-field hydrothermal effects; and to a degree sufficient to determine percolation, liquid transport, and/or vapor transport properties through the rest of the Yucca Mountain area. Field measurement of gas flow rates and determination of Yucca Mountain pneumatic properties by DOE will need to be continued for adequate modeling of gas transport.

Regional Hydrology. Further research will also be required in the area of regional hydrology to determine maximum water levels and boundary conditions for site hydrologic modeling especially for disruptive consequences. DOE should consider investigating the steep gradient near the site because of the possible influence on future site groundwater elevations.

Percolation. DOE will need to continue the field measurement of deep percolation and its correlation with precipitation. NRC should explore the possible use of such correlations with expert elicitation information in climatology to determine ranges of percolation rates as a function of climatological assumptions. The development of a more sophisticated climate model should also be pursued.

Geochemical Models. NRC and DOE research in geochemistry, including laboratory studies, field studies, and natural analogs must continue to provide adequate verification of present geochemical models or, if required, the bases for alternative models. Research in this area should emphasize flow through fractures because of the importance demonstrated for fracture flow. Further research in gas transport geochemistry should also be undertaken to determine if there are significant barriers to $^{14}CO_2$ release in the geosphere.

Corrosion Models. DOE should continue to collect data on the corrosion of waste container materials. Both NRC and DOE research in corrosion should be directed at obtaining a better understanding of the corrosion mechanism and how corrosion is likely to progress under conditions of high humidity or in contact with water of high ionic strength. In addition, models to determine accurately the contact of the waste form with liquid water will be highly design-specific to the repository concept finally adopted. Much of this work is expected to stem from confirmatory laboratory-scale and field heater tests used to validate mathematical models of two-phase heat and mass transfer. Since the experimental data must be necessarily of short duration and small-scale relative to those of the repository, reliable

mathematical models may be the only way to extrapolate results to greater times and distances. In this regard, the basis for the development of these models will rely on a mechanistic understanding of the processes and events related to the waste package's interaction with its environment. NRC needs to pursue an independent understanding of these processes to evaluate DOE's assumptions. DOE will need to continue characterization of the spent fuel waste form (inventories and dissolution rates) as these control the source term.

Magmatism. Additional geologic information is needed regarding volcanic processes to improve the probability estimates of the magmatic scenario. This information includes determining the role of volatiles in driving magma ascent, the importance of multiple dike intrusions, and the role of pre-existing geologic structure. The effects of uncertainty in geochronological data should also be evaluated. Additional improvements may also have to be made regarding magma interaction with water. NRC should develop an independent understanding in this area.

10.4.2 Recommendations Regarding Modeling Improvements and Supporting Analyses in NRC's IPA Activities

The following recommendations are listed by chapter and include recommendations for modeling improvements and additional analyses based on conclusions in the chapters and include recommendations from the IPA Phase 1 Report (see Chapter 10, "Preliminary Suggestions for Future Work," in Codell *et al.*, 1992) that have not yet been implemented (see Section 1.2.5 of this report). Some of these recommendations parallel those of Section 10.4.1, but emphasize analysis rather than research.

10.4.2.1 TPA Computer Code

1. ***Software Quality Assurance requirements need more prominence in module development.*** There were a number of difficulties encountered during the development of the Phase 2 modules and their integration into the TPA system code. Many of the problems could probably be traced to a lack of documented module designs, lack of module integration designs, and lack of documented module testing. The TPA computer code and its modules need to be developed under a more consistent environment, incorporating aspects of modern code development such as object-oriented design and principles of software quality assurance. The computational platform should be standardized to employ UNIX tools for software development and debugging. Requirements for individual code modules should be specified in advance of integrating them into the system code. There should be careful attention to interfaces among the TPA computer code and its modules.

2. ***Future IPA developments will require more model abstraction and efficient computing techniques.*** The computational requirements of the TPA computational modules can be prohibitive, and significant simplifications were required in order to achieve acceptably low execution costs. It is recommended that more attention be given to abstracting the complicated phenomena to achieve efficient computational modules, and examination of the feasibility of applying high-performance computing procedures including massive parallel computers and advanced computational methods (e.g., adaptive grids, domain decomposition, and efficient matrix solvers).

3. ***The TPA computer code must be easily upgraded.*** It is recommended that the TPA system code be considered a dynamic entity, to be upgraded in future IPA iterations. Possible upgrades include: addition of new modules, changed scope of current modules, centralized use of databases, uniform interfaces between modules, and uniform coding practices among modules.

10.4.2.2 Scenario Analysis Module

1. ***Staff judgments in screening the initial set of events and processes (EPs) should be reassessed using appropriate mathematical models and numerical codes, as recommended by Cranwell et al. (1990).*** This could lead to the assignment of different probabilities to the EPs and result in a different outcome to the screening.

2. ***Future work should investigate methods for generating individual scenarios "representative" of the scenario classes to which they belong.*** The approach taken in the IPA Phase 2 scenario analysis generated scenario classes (i.e.,

unique combinations of events or processes without regard to the order in which they occur). Generating representative events would likely involve the need to "partition" the individual scenario classes into appropriate subevents or subprocesses and then examining various combinations.

3. ***Obtain geoscience input for modeling faulting, uplift, and subsidence at Yucca Mountain.*** In the IPA Phase 2 scenario analysis, the vibratory ground motion from local faulting was combined with regional seismicity. Regional uplift and subsidence were considered to have negligible consequences in the screening analysis, and no attempt was made to model these events. In future IPA iterations, all of these events will be modeled, probably in auxiliary analyses, to make a determination about whether they should be included.

10.4.2.3 Flow and Transport Module

1. ***Examine modeling issues affecting percolation.*** Conceptual model assumptions with respect to percolation should have a major effect on water flux through a repository located in the unsaturated zone. Issues that can be investigated with auxiliary analyses include the relationship between highly transient rainfall and percolation estimates, the effect of topographic lows and fault zones as sources of increased recharge, how spatial variability in hydrologic parameters affect percolation, and the effect of fracture imbibition on percolation.

2. ***Examine modeling assumptions affecting fracture-matrix interaction.*** Modeling assumptions regarding the interaction between matrix and fractures are very important due to differences in fluid velocities and retardation of the two flow systems. Auxiliary analyses could improve the understanding of conceptual modeling assumptions regarding small-scale interactions at the fracture-matrix interface (e.g., detailed simulations to examine the equilibration of pressure between the fracture and matrix considering transient conditions and the effects of mineral coatings on fracture surfaces) and large-scale effects concerning the flow field within a hydrogeologic unit (e.g., examine how the small-scale effects propagate through a geologic unit). These further analyses can be used to modify current IPA models and revise parametric ranges.

3. ***Examine hydrogeologic features and heterogeneity that could allow a "short circuit" through the unsaturated zone.*** The IPA Phase 2 flow and transport analyses assumed that fluid flow and radionuclide transport could be represented as 1-D stream tubes for each of the hydrogeologic units. Two- and 3-D analyses could investigate the impact of fault zones and perched water on pathways through the unsaturated zone. If the impact is of sufficient magnitude, then additional pathways could be added to the flow and transport analysis in future iterations.

4. ***Examine the coupling of water in the gaseous and liquid phases.*** The model of the repository is highly idealized. The prototype is transient, 3-D, partially saturated flow with significant air and water vapor movement in a fractured, porous medium complicated by potentially significant heat transfer and the associated flows of gas and liquid affecting the redistribution of moisture. Abstracted models need to be tested through simulation, comparing the results with those of the more complete model developed in the auxiliary analyses, which includes the coupling of water movement in the liquid and gaseous phases under non-isothermal conditions. Simulation efforts could examine the variation in moisture contents and fluid flux through the repository caused by vapor movement and condensation (this effect would be especially pronounced during the thermal phase of the repository).

5. ***Examine refinements in the saturated zone modeling to improve concentration estimates for dose calculations.*** The calculation of dose requires a determination of the radionuclide concentration. The concentration determination requires consideration of flow and dispersion, in the saturated zone, that is not normally required for the calculation of time-integrated discharge (*Normalized Release*) for comparison with the EPA standard.

6. ***Assess the usefulness of additional intermediate calculations for understanding the flow and transport results.*** The IPA Phase 2 analyses

performance measures were integrated discharge and radionuclide dose. These results are often difficult to explain in the absence of other information on modeling results for individual modules (e.g., fluid flux or water velocity for the groundwater pathway, and release rates for the source term module). It would be beneficial to further examine the modeling approaches and identify intermediate calculations that could be performed to provide further insights on model and system performance.

7. ***Evaluate the importance of thermally- and barometrically-driven air flow on performance.*** In IPA Phase 2, thermal gradient-driven gas transport was incorporated in the calculation of the CCDF. Other pneumatic effects such as barometric pumping should be considered in future iterations of IPA.

10.4.2.4 Source Term Module

1. ***The models in SOTEC will have to be modified in response to the current waste disposal concepts that differ from the SCP design assumed for the IPA Phase 2.*** IPA Phase 2 was based on the waste package concept described in DOE's 1988 SCP of single-walled packages placed vertically in boreholes, with an air gap between the container and the surrounding rock. The current models will have to be modified as DOE progresses in site characterization and makes decisions about its thermal loading strategy, waste package design, waste package materials, and additional engineered barriers.

2. ***Develop more mechanistic models for waste package corrosion.*** The present version of *SOTEC* used in IPA Phase 2 considered simplified models for corrosion. Needed improvements to *SOTEC* include codes abstracted from complex physics-based models, including a mechanistic model for initiation and propagation of localized corrosion, taking into account the geochemical environment and mechanical stresses.

3. ***Improve models for the effects of heat.*** The present temperature model uses a semi-analytical approach for conduction-only. More realistic models could take heat and mass transfer in two-phase flow into account to better estimate the temperature in the near field and the transfer of liquid water and water vapor inputs needed to predict the onset of corrosion and the interaction of liquid water with the waste.

4. ***Take spatial and temporal variability into account in source term models.*** IPA Phase 2 began to explore ensemble averages of the temporally and spatially varying environmental parameters that should be used to represent a large number of waste packages with relatively few calculations. Improved source term models should also take the variability of the properties of the fuel into account either explicitly or by defining effective input parameters that capture the variability without making the models too complex for total-system performance assessments.

5. ***Improve models for the release of gaseous ^{14}C.*** The IPA Phase 2 model considers the release of gaseous $^{14}CO_2$ emanating from the waste, based on steady-state diffusion of oxygen and $^{14}CO_2$. Failure to include the transient diffusion of oxygen evident from the data could lead to inaccurate predictions of conversion rates at low temperatures. The model could be improved by considering transient diffusion. Also, the present implementation of the model for the release of gaseous ^{14}C mixes the contribution from the seven repository sub-areas for use in the 2-D gas flow model. The model should be revised to take into account variations in release rate for each sub-area.

6. ***Consider modes of waste package failure other than corrosion.*** Waste packages might also fail from mechanisms other than corrosion, such as seismic shaking, volcanism, and inadvertent human intrusion. Although IPA Phase 2 considered failure by drilling, volcanism and seismicity, the models were highly simplified. Models for failure by volcanism might take into account mechanisms of interaction between magma and the waste packages (e.g., corrosive gases and viscous forces). Improved models for human intrusion might consider the site-specific likelihood for drilling, shear forces from drilling fluids, or other mechanisms that could bring radioactive material to the surface. These disruptive events could

also have a significant effect on the other aspects of the repository performance. Analytical expressions for buckling are only available for simplified geometries and loading conditions with static loads. A buckling model for a complex geometry and multiple and transient loads would require a complicated and computationally intensive simulation unsuited for IPA. Once the engineering design has been finalized, the structural failure of the waste packages from dynamic and other forces could be analyzed deterministically by numerical and experimental techniques and abstracted for IPA. These analyses would include the possible impact of mechanical fatigue of the waste packages from recurrent, low-intensity seismic activity. Improved models of seismic failure might take into account the range of frequencies of earth motion, and realistic dynamic modes of the waste packages.

7. ***Improve model for the dissolution of radionuclides from the waste form.*** The chemistry within the waste package was treated in a highly simplified manner in IPA Phase 2. The model could be improved by taking into account the formation and subsequent transport of colloids, speciation of the elements released to the water, the contribution of minerals from the ground water and structural materials in the waste package, the changing temperature, and other factors such as ionizing radiation.

8. ***Improve model for transport of radionuclides from the waste package.*** Mass transfer out of the waste package by flowing water and diffusion was included in IPA Phase 2, based on DOE's 1988 SCP conceptual waste package design. The transport model, in conjunction with the waste form dissolution model, should consider the rates that water contacts and enters the waste package canister, interacts with the waste form, and transports radionuclides from the waste package by both advection and diffusion. The model should recognize that the suite of waste packages will represent a broad range of varying stages of degradation, with some completely intact and others significantly degraded from both anticipated and unanticipated processes and events. These conditions are progressive over the 10,000-year period of regulatory interest. Although conservatively neglected in *SOTEC*, the model could include recognition that degraded waste packages, including failed fuel (e.g., defective cladding), can still contribute to the isolation or controlled release of radionuclides.

9. ***Include models for other waste forms.*** The staff's first two IPAs focused on evaluating the performance of waste packages for spent nuclear fuel. In future IPAs, the staff should develop a source term model for the expected inventory of glass waste packages with special consideration to the kinetics of glass dissolution, formation of secondary silicate mineral, colloid formation, and mass transport of radionuclides. Further, waste forms other than light-water reactor spent nuclear fuel and defense-related vitrified wastes (glass) may ultimately need to be considered if they are determined to be potentially significant sources. These may include any transuranic or greater-than-Class-C wastes.

10.4.2.5 Disruptive Consequence Analysis

1. ***Consolidate calculations of radionuclide inventory in the drilling model.*** The drilling code calculates inventory using the Bateman equations and determines the inventory from the time of the earliest drilling event. Greater efficiency may have been attainable by calculating the evolution of the inventory one time only. The inventory could then be moved from one bin to another as needed, rather than having this calculation repeated in several different modules. Having a unified list of inventories would provide more information on the migration of the nuclides through the geosphere and make accounting simpler for radionuclides that migrate through both liquid and gaseous pathways.

2. ***Allow multiple waste package failure times in the drilling model.*** The effects of the number of drilling events are predicted to be small relative to the other releases calculated in Phase 2, in part because drilling affects only a small number of waste packages. However, for cases where there is both drilling combined with volcanism or seismicity, the source term model predicts all failures occur at the earliest time for any event. This simplifying

modeling assumption could lead incorrectly to predictions of large total releases, when a later disruption (volcanic or seismic event) causes widespread failure of waste packages. The drilling code (*DRILLO*—described in Section 6.3) and the source term code (*SOTEC*—described in Chapter 5) should be modified to allow multiple waste package at different times within the same run.

3. ***Reduce the number of variables and tie the sampled parameters to the extent of drilling activity in the drilling model.*** The drilling model required 92 sampled parameters to determine whether, where, and when there was a strike on a waste package. The model should be simplified to require fewer sampled parameters that would be more meaningful in the sensitivity and uncertainty analysis.

4. ***Surface releases should be based on site-specific mechanisms.*** Although IPA Phase 2 considered failure by drilling, volcanism, and seismicity, the models were highly simplified. Future models might consider the site-specific likelihood for drilling, shear forces from drilling fluids, and mechanisms that could bring radioactive material to the surface.

10.4.2.6 Dose Assessment Module

1. ***Improve the DITTY dose assessment model.*** The results of dose assessments should be evaluated as functions of radionuclide type and exposure pathway. In addition, the dose conversion factors used in IPA Phase 2 should be re-calculated to obtain a more accurate estimate of population doses for long-lived radionuclides (as discussed in Section 7.6). Also, the model parameters currently used in *DITTY* must be verified as being applicable to the Yucca Mountain site.

2. ***Evaluate other dose assessment computer codes.*** Codes that should be evaluated include codes for estimating long-term individual and collective exposures, atmospheric dispersion models, and demographic models. Methods employed by international organizations (e.g., the Biospheric Model Validation Study and the Nuclear Energy Agency) for calculation of doses into the far future should be evaluated. The recommendations of the International Commission on Radiological Protection (ICRP, 1990) should be incorporated into the codes, if adopted by NRC.

3. ***Apply the statistical sensitivity and uncertainty methodology developed in IPA Phase 2 for the geosphere models to the dose assessment models.*** Sensitivity and uncertainty analyses can be used to identify the most important dose assessment parameters and the sensitivity of the dose estimate to these parameters.

10.4.2.7 Sensitivity and Uncertainty Analysis

1. ***Sensitivity and uncertainty analysis should explore the use of dimensional analysis to form factors based on combinations of other parameters.*** Dimensional analysis is a useful technique for determining the functional relationships among variables. Principles of dimensional analysis might be applied for the purpose of simplifying the repository system, with its hundreds of independent parameters, into an equivalent system with fewer parameters. These dimensionless factors would make the task of analyzing the system and determining important parameters simpler.

2. ***Importance sampling techniques such as the Limit-State Approach should be evaluated.*** The Limit-State Approach (Wu *et al.*, 1992), discussed in Section 8.4, has the potential for easing the computational burden experienced in the IPA Phase 2 study by reducing the number of vectors needed to construct the CCDFs and perform the sensitivity analyses. This approach should be evaluated further on the full repository system model. However, as presently implemented, the Limit-State Approach cannot deal with hundreds of independent parameters. The number of independent variables analyzed by the Limit-State Approach must be reduced, either by selecting the most important parameters by stepwise regression analysis, or combining parameters into groups.

3. ***A method of directly obtaining CCDF sensitivity to individual parameters should be developed.*** Sensitivity analyses have been developed to determine the effect of changes in the input parameters of the models on scaler measures of repository performance such as cumulative release and effective dose equivalents. Some

effort should be directed at developing a robust method for evaluating system sensitivity for a probabilistic performance measure (e.g., the CCDF).

11 REFERENCES

Chapter 1. Introduction

Barnard, R.W., *et al.*, "TSPA: 1991 An Initial Total-System Performance Assessment for Yucca Mountain", Albuquerque, New Mexico, Sandia National Laboratories, SAND91-2795, September 1992. [Prepared for the U.S. Department of Energy.]

Bath, G.D. and C.E. Jahren, "Interpretations of Magnetic Anomalies at a Potential Repository Site Located in the Yucca Mountain Area, Nevada Test Site," U.S. Geological Survey, Open File Report 84-120, 1984.

Center for Nuclear Waste Regulatory Analyses, "Development and Control of Scientific and Engineering Software," San Antonio, Texas, Technical Operating Procedure [TOP]-018, Revision 1 (Change 0), September 30, 1991.

Codell, R.B., *et al.*, "Initial Demonstration of the NRC's Capability to Conduct a Performance Assessment for a High-Level Waste Repository," U.S. Nuclear Regulatory Commission, NUREG-1327, May 1992.

Cranwell, R.M., *et al.*, "Risk Methodology for Geologic Disposal of Radioactive Waste: Scenario Selection Procedure," U.S. Nuclear Regulatory Commission, NUREG/CR-1667, April 1990. [Prepared by the Sandia National Laboratories.]

Crowe, B.M., *et al.*, "Status of Volcanic Hazard Studies for the Nevada Nuclear Waste Storage Investigations," Los Alamos, New Mexico, Los Alamos National Laboratory, LA-9325-MS, March 1983.

dePolo, C.M., "The Maximum Background Earthquake for the Basin and Range Province, Western North America," Nevada Bureau of Mines and Geology, in press [January 1993 preprint].

Longsine, D.E., E.J. Bonano, and C.P. Harlan, "User's Manual for the NEFTRAN Computer Code," U.S. Nuclear Regulatory Commission, NUREG/CR-4766, September 1987. [Prepared by the Sandia National Laboratories.]

Napier, B.A., *et al.*, "GENII: The Hanford Environmental Radiation Dosimetry Software System," Richland, Washington, Pacific Northwest Laboratory, PNL-6584, 3 vols., December 1988. [Prepared for the U.S. Department of Energy.]

O'Neill, J.M., J.W. Whitney, and M.R. Hudson, "Photogeologic and Kinematic Analysis of Lineaments at Yucca Mountain, Nevada: Implications for Strike-Slip Faulting and Oroclinal Bending," U.S. Geological Survey, Open File Report 91-623, 1992.

Sagar, B., *et al.*, "SOTEC: A Source Term Code for High-Level Geologic Repositories—User's Manual (Version 1.0)," San Antonio, Texas, Center for Nuclear Waste Regulatory Analyses, CNWRA 92-009, July 1992. [Prepared for the U.S. Nuclear Regulatory Commission.]

Silling, S.A., "Final Technical Position on Documentation of Computer Codes for High-Level Waste Management," U.S. Nuclear Regulatory Commission, NUREG-0856, June 1983.

U.S. Department of Energy, "Site Characterization Plan Overview, Yucca Mountain Site, Nevada Research and Development Area, Nevada," Nevada Operations Office/Yucca Mountain Project Office, Nevada, DOE/RW-0198, December 1988.

U.S. Environmental Protection Agency, "Environmental Standards for the Management of Spent Nuclear Fuel, High-Level and Transuranic Wastes [Final Rule]," *Federal Register*, vol. 50, no. 182, September 19, 1985, pp. 38066-38089.

U.S. Nuclear Regulatory Commission, "Disposal of High-Level Radioactive Wastes in Geologic Repositories [Proposed Rule]," *Federal Register*, vol. 46, no. 130, July 8, 1981, pp. 35280-35296.

U.S. Nuclear Regulatory Commission, "Disposal of High-Level Radioactive Wastes in Geologic Repositories [Final Rule]," *Federal Register*, vol. 48, no. 120, June 21, 1983, pp. 28194-28229.

U.S. Nuclear Regulatory Commission, "License Application Review Plan for a License Application for a Geologic Repository for Spent Nuclear

Fuel and High-Level Radioactive Waste, Yucca Mountain Site, Nevada—Draft Review Plan," Office of Nuclear Material Safety and Safeguards/ Division of Waste Management, NUREG-1323, September 1994.

Chapter 2. Total-System Performance Assessment Computer Code

Ababou, R. and A.C. Bagtzoglou, "BIGFLOW: A Numerical Code for Simulating Flow in Variably Saturated, Heterogeneous Geologic Media (Theory and Users' Manual—Version 1.1)," U.S. Nuclear Regulatory Commission, NUREG/CR-6028, June 1993. [Prepared by the Center for Nuclear Waste Regulatory Analyses.]

Amtec Engineering, Inc., *TECPLOT User's Manual: Interactive Plotting for Scientists and Engineers (Version 4.0)*, Bellevue, Washington, 1984.

Apted, M.J., A.M. Liebetrau, and D.W. Engel, "The Analytical Repository Source-Term (AREST) Model: Analysis of Spent Fuel as a Nuclear Waste Form," Richland, Washington, Pacific Northwest Laboratory/Battelle Memorial Institute, PNL-6347, February 1989. [Prepared for the U.S. Department of Energy.]

Center for Nuclear Waste Regulatory Analyses, "Development and Control of Scientific and engineering Software," San Antonio, Texas, Technical Operating Procedure [TOP]-018, Revision 1 (Change 0), September 30, 1991.

Codell, R.B., *et al.*, "Initial Demonstration of the NRC's Capability to Conduct a Performance Assessment for a High-Level Waste Repository," U.S. Nuclear Regulatory Commission, NUREG-1327, May 1992.

Dudley, A.L., *et al.*, "Total System Performance Assessment Code (TOSPAC), Volume 1: Physical and Mathematical Bases," Albuquerque, New Mexico, Sandia National Laboratories, SAND85-0002, December 1988. [Prepared for the U.S. Department of Energy.]

Frietas, C.J., N.A. Eisenberg, and R.G. Baca, "DRILLO Code: A Modules for Simulation of Human Intrusion Scenarios, Model Disruption, and User Guide," San Antonio, Texas, Center for Nuclear Waste Regulatory Analyses, CNWRA 94-005, February 1994. [Prepared for the U.S. Nuclear Regulatory Commission.]

Iman, R.L. and M.J. Shortencarier, "A FORTRAN 77 Program and User's Guide for the Generation of Latin Hypercube and Random Samples for Use in Computer Models," U.S. Nuclear Regulatory Commission, NUREG/CR-3624, March 1984. [Prepared by the Sandia National Laboratories.]

Janetzke, R.W. and B. Sagar, "preFOR: A Pre-Processor for FORTRAN Files: User's Manual," San Antonio, Texas, Center for Nuclear Waste Regulatory Analyses, CNWRA 91-003, April 1991a. [Prepared for the U.S. Nuclear Regulatory Commission.]

Janetzke, R.W. and B. Sagar, "RDFREE: A FORTRAN Utility for Format Free Input: User's Guide," San Antonio, Texas, Center for Nuclear Waste Regulatory Analyses, CNWRA 91-005, June 1991b. [Prepared for the U.S. Nuclear Regulatory Commission.]

Lin, C.S., R.G. Baca, and R. Drake, "VOLCANO Code—A Module for Simulation of Magmatic Scenario Model Description and User Guide," San Antonio, Texas, Center for Nuclear Waste Regulatory Analyses, CNWRA 93-010, October 1993. [Prepared for the U.S. Nuclear Regulatory Commission.]

Longsine, D.E., E.J. Bonano, and C.P. Harlan, "User's Manual for the NEFTRAN Computer Code," U.S. Nuclear Regulatory Commission, NUREG/CR-4766, September 1987. [Prepared by the Sandia National Laboratories.]

Lung, H-C., P.L. Chambré, T.H. Pigford, and W.W-L. Lee, "Transport of Radioactive Decay Chains in Finite and Semi-Finite Porous Media," Lawrence Berkeley Laboratory/University of California, LBL-23987, September 1987. [Prepared for the U.S. Department of Energy.]

Margulies, T., *et al.*, "Probability Analysis of Magma Scenarios for Assessing Geologic Waste Repository Performance," American Society of Mechanical Engineers, New York, Paper 92-WA/SAF-11, 7 p., 1992. [Presented at the ASME Winter Meeting, November 8-13, 1992, Anaheim, California.]

Napier, B.A., *et al.*, "GENII: The Hanford Environmental Radiation Dosimetry Software System," Richland, Washington, Pacific Northwest Laboratory, PNL-6584, 3 vols., December 1988. [Prepared for the U.S. Department of Energy.]

Nienhuis, P. and T. Appelo, "Adaptation of PHREEQE for Use in a Mixing-Cell Flowtube: PHREEQM—User Guide (October 1990)," U.S. Geological Survey, *Training Course on Geochemistry for Groundwater Systems*, Denver, Colorado, April 22 - May 3, 1991.

Olague, N.E., *et al.*, "User's Manual for the NEFTRAN II Computer Code," U.S. Nuclear Regulatory Commission, NUREG/CR-5618, February 1991. [Prepared by the Sandia National Laboratories.]

Parkhurst, D.L., D.C. Thorstenson, and L.N. Plummer, "PHREEQE—A Computer Program for Calculating Mass Transfer for Geochemical Reactions in Gound Water," U.S. Geological Survey, WaterResources Investigations Report, WRI-80-96, 1980. [Revised 1990]

Pruess, K., "TOUGH User's Guide," U.S. Nuclear Regulatory Commission, NUREG/CR-4645, August 1987. [Prepared by the Lawrence Berkeley Laboratory and the Sandia National Laboratories.]

Sagar, B., *et al.*, "SOTEC: A Source Term Code for High-Level Geologic Repositories—User's Manual (Version 1.0)," San Antonio, Texas, Center for Nuclear Waste Regulatory Analyses, CNWRA 92-009, July 1992. [Prepared for the U.S. Nuclear Regulatory Commission.]

Sagar, B. and R.W. Janetzke, "Total-System Performance Assessment Computer Code: Description of Executive Module," San Antonio, Texas, Center for Nuclear Waste Regulatory Analyses, CNWRA 91-009, July 1991. [Prepared for the U.S. Nuclear Regulatory Commission.]

Sagar, B. and R.W. Janetzke, "Total-System Performance Assessment Computer Code: Description of Executive Module (Version 2.0)," San Antonio, Texas, Center for Nuclear Waste Regulatory Analyses, CNWRA 93-107, August 1993. [Prepared for the U.S. Nuclear Regulatory Commission.]

Shidhar, N., *et al.*, "Engineered Barrier System Performance Assessment Codes (EBSPAC) October 1, 1992, through September 25, 1993," San Antonio, Texas, Center for Nuclear Waste Regulatory Analyses, CNWRA 93-021, October 1993. [Prepared for the U.S. Nuclear Regulatory Commission.]

Torak, L.J., "A Modular Finite-Element Model (MODFE) for Areal and Axisymmetric Ground-Water Flow-Problems, Part 1: Model Description and User's Manual," U.S. Geological Survey, Open-File Report 90-194, 1992.

Updegraff, C.D., C.E. Lee, and D.P. Gallegos, "DCM3D: A Dual-Continuum, Three-Dimensional, Ground-Water Flow Code for Unsaturated, Fractured, Porous Media," U.S. Nuclear Regulatory Commission, NUREG/CR-5536, February 1991. [Prepared by the Sandia National Laboratories.]

Chapter 3. Scenario Analyses Module

Algermissen, S.T., *et al.*, "Probabilistic Estimates of Maximum Acceleration and Velocity in Rock in the Contiguous United States," U.S. Geological Survey, Open File Report 82-1033, 1982.

Andersson, J., *et al.*, "The Joint SKI/SKB Scenario Development Project," Stockholm, Sweden, Statens Kärnkraftinspektion (SKI) [Swedish Nuclear Power Inspectorate], SKI Technical Report 89:14, December 1989.

Apostolakis, G., *et al.*, "Techniques for Determining Probabilities of Events and Processes Affecting the Performance of Geologic Repositories: Suggested Approaches," U.S. Nuclear Regulatory Commission, NUREG/CR-3964, vol. 2, June 1991. [Prepared by the Sandia National Laboratories.]

Benson, L.V. and P.W. McKinley, "Chemical Composition of Groundwater in the Yucca Mountain Area, Nevada, 1971-1984," U.S. Geological Survey, Open File Report 85-484, 1985.

Bernreuter, D.L., *et al.*, "Seismic Hazard Characteization of 69 Nuclear Power Plant Sites East of the Rocky Mountains: Methodology, Input Data and Comparison of Previous Results for Ten Sites," U.S. Nuclear Regulatory Commission, NUREG/CR-5250, vols. 1-8, January 1989. [Prepared by the Lawrence Livermore National Laboratory.]

Bonano, E.J., *et al.*, "Demonstration of a Performance Assessment Methodology for High-Level Radioactive Waste Disposal in Basalt Formations," U.S. Nuclear Regulatory Commission, NUREG/CR-4759, June 1989. [Prepared by the Sandia National Laboratories.]

Bonano, E.J., *et al.*, "Elicitation and Use of Expert Judgment in Performance Assessment for High-Level Radioactive Waste Repositories," U.S. Nuclear Regulatory Commission, NUREG/CR-5411, May 1990. [Prepared by the Sandia National Laboratories.]

Campbell, K.W., *et al.*, "A Preliminary Methodology for the Regional Zonation of Peak Ground Acceleration," National Science Foundation, *Proceedings of the Third International Earthquake Microzonation Conference*, June 28–July 1, 1982, Seattle, Washington, 1:365–376 [1982].

Carrigan, C.R., *et al.*, "Potential for Water-Table Excursions Induced by Seismic Events at Yucca Mountain, Nevada," *Geology*, 19:1157–1160 [1991].

Codell, R.B., *et al.*, "Initial Demonstration of the NRC's Capability to Conduct a Performance Assessment for a High-Level Waste Repository," U.S. Nuclear Regulatory Commission, NUREG–1327, May 1992.

Connor, C.B. and B.E. Hill, "Volcanism Research (Chapter 10)" in Sagar, B. (ed.), "NRC High-Level Radioactive Waste Research at CNWRA, January–June, 1993," San Antonio, Texas, Center for Nuclear Waste Regulatory Analyses, CNWRA 93–01S, August 1993.

Cornell, C.A., "Engineering Seismic Risk Analysis," *Bulletin of the Seismological Society of America*, 58:1583–1606 [1968].

Cornell, C.A., "Probabilistic Analysis of Damage to Structure under Seismic Loads," in Howells, D.A., I.P. Haigh, and C. Taylor (eds.), "Dynamic Waves in Civil Engineering," *Society for Earthquake and Civil Engineering Proceedings*, July 7–9, 1970, University College of Swansea, pp. 471–493 [1971]. [Published by Wiley-Interscience, New York.]

Cranwell, R.M., *et al.*, "Risk Methodology for Geologic Disposal of Radioactive Waste: Scenario Selection Procedure," U.S. Nuclear Regulatory Commission, NUREG/CR–1667, April 1990. [Prepared by the Sandia National Laboratories.]

Crowe, B.M., *et al.*, "Calculation of the Probability of Volcanic Disruption of a High-Level Radioactive Waste Repository within Southern Nevada, USA," *Radioactive Waste Management and the Nuclear Fuel Cycle*, 3(2):167–190 [December 1982].

Crowe, B.M. and F.V. Perry, "Volcanic Probability Calculation for the Yucca Mountain Site: Estimation of Volcanic Rates," American Nuclear Society, *Proceedings of the Topical Meeting on Nuclear Waste Isolation in the Unsaturated Zone (FOCUS '89)*, September 17–21, 1989, Las Vegas, Nevada, pp. 326–334 [1989].

Crowe, B.M., *et al.*, "Recurrence Models of Volcanic Events: Applications to Volcanic Risk Assessment," in American Nuclear Society/American Society of Civil Engineers, *High-Level Radioactive Waste Management: Proceedings of the Third International Conference, April 12–16, 1992*, Las Vegas, Nevada, 2:2344–2355 [1992].

Crowe, B., *et al.*, "Status of Volcanism Studies for the Yucca Mountain Site Characterization Projects," Los Alamos, New Mexico, Los Alamos National Laboratory, LA–12908–MS, February 1995 [Updated March 1995]. [Prepared for the U.S. Department of Energy.]

DeWispelare, A.R., *et al.*, "Expert Elicitation of Future Climate in the Yucca Mountain Vicinity: Iterative Performance Assessment Phase 2.5," Center for Nuclear Waste Regulatory Analyses, CNWRA 93–016, August 1993. [Prepared for the U.S. Nuclear Regulatory Commission.]

Electric Power Research Institute, "Seismic Hazard Methodology for the Central and Eastern United States (vols. 1 and 2)," Palo Alto, California, Research Project Number P–101, 1986.

Garside, L.J. and J.H. Schilling, "Thermal Waters of Nevada," Nevada Bureau of Mines, *Geologic Bulletin*, No. 91, 1979.

Garside, L.J., *et al.*, "Oil and Gas Developments in Nevada," Nevada Bureau of Mines, *Geologic Bulletin*, No. 104, 1988.

Ho, C–H., "The Mathematical Model of Volcanism at Yucca Mountain," Carson City,

State of Nevada Agency for Nuclear Projects/ Nuclear Waste Project Office, 1990. [Prepared by the University of Nevada, Las Vegas.]

Ho, C-H., *et al.*, "Eruptive Probability Calculation for the Yucca Mountain Site, USA: Statistical Estimation of Recurrence Rates," *Bulletin of Volcanology*, 54:50–56 [1991].

Ho, C-H., "Risk Assessment for the Yucca Mountain High-Level Nuclear Waste Repository Site: Estimation of Volcanic Disruption," *Mathematical Geology*, 24(4):347–364 [1992].

Hodgkinson, D.P. and T.J. Sumerling, "A Review of Approaches to Scenario Analysis for Repository Safety Assessment," OECD Nuclear Energy Agency/International Atomic Energy Agency/ Commission of the European Communities, *Proceedings of the Symposium on the Safety Assessments for Radioactive Waste Repositories*, October 9–13, 1989, Paris, France, pp. 333–352 [1990].

Hunter, R.L. and Mann, C.J., "Chapter 3: Climatology" in "Techniques for Determining Probabilities of Events and Processes Affecting the Performance of Geologic Repositories: Literature Review," U.S. Nuclear Regulatory Commission, NUREG/CR-3964, vol. 1, June 1989. [Prepared by the Sandia National Laboratories.]

International Atomic Energy Agency, "Safety Assessment for the Underground Disposal of Radioactive Wastes," International Atomic Energy Agency, Vienna, Austria, Safety Series No. 56, 1981.

Margulies, T., *et al.*, "Probability Analysis of Magma Scenarios for Assessing Geologic Waste Repository Performance," American Society of Mechanical Engineers, New York, Paper 92-WA/SAF-11, 7 p., 1992. [Presented at the ASME Winter Meeting, November 8–13, 1992, Anaheim, California.]

Maldonado F., and S.L. Koether, "Stratigraphy, Structure, and Some Petrographic Features of Tertiary Volcanic Rocks at the USW G-2 Drill Hole, Yucca Mountain, Nye County, Nevada," U.S. Geological Survey, Open-File Report 83–732, 1983.

McBirney, A.R., "Volcanology," in Hunter, R.L. and C.J. Mann (eds.), *Techniques for Determining Probabilities of Geologic Events and Processes (Studies in Mathematical Geology No. 4)*, New York, Oxford University Press, pp. 167–184, 1992.

McGuire, R.K., "FORTRAN Computer Program for Seismic Risk Analysis," U.S. Geological Survey, Open File Report 76–67, 1976.

Meremonte, M.E. and A.M. Rogers, "Historical Catalog of Southern Great Basin Earthquakes 1868–1978," U.S. Geological Survey, Open File Report 87–80, 1987.

Raney, R. G., "Possible Effects of Surface and Underground Mining Proximal to a Closed High-Level Radioactive Waste Repository at Yucca Mountain, Nye County, Nevada," U.S. Bureau of Mines, 1990a. [Report to the U.S. Nuclear Regulatory Commission.]

Raney, R.G., "Active Mines and Prospects Within a Thirty-Mile Radius of the Proposed High-Level Repository Site at Yucca Mountain, Nye County, Nevada, Subsequent to January 1988 (As of July 1990)," U.S. Bureau of Mines, 1990b.

Ross, B., "A First Survey of Disruption Scenarios for a High-Level Waste Repository at Yucca Mountain, Nevada," Albuquerque, New Mexico, Sandia National Laboratories, SAND85-7117, December 1987. [Prepared by Disposal Safety, Incorporated (Washington, D.C.) for the U.S. Department of Energy.]

Science Applications International Corporation, "Report of Early Site Suitability Evaluation of the Potential Repository Site at Yucca Mountain, Nevada," SAIC-91/8000, January 1992. [Prepared for the U.S. Department of Energy.]

Schweickert, R.A., "Evidence for a Concealed Dextral Strike-Slip Fault Beneath Crater Flat, Nevada [Abstract]," Geological Society of America, *1989 Annual Meeting: Abstracts with Program*, November 6–9, 1989, St. Louis, Missouri, 21(6):A90 [1989].

Scott, R.B. and J.G. Rosenbaum, "Evidence of Rotation about a Vertical Axis during Extension at Yucca Mountain, Southern Nevada [Abstract]," *EOS Transactions*, American Geophysical Union, 67(16):358 [April 22, 1986].

Shaw, H.R., "Uniqueness of Volcanic Systems," U.S. Geological Survey Professional Paper 1350, 1987.

Sheridan, M.F., "A Monte Carlo Technique to Estimate the Probability of Volcanic Dikes," in High-Level Radioactive Waste Management," American Nuclear Society/American Society of Civil Engineers, *Proceedings of the Third International Conference: High-Level Radioactive Waste Management*, April 12–16, 1992, Las Vegas, Nevada, 2:2033–2038 [1992].

Smith, E.I., *et al.*, "The Area of Most Recent Volcanism Near Yucca Mountain, Nevada: Implications for Volcanic Risk Assessment," American Nuclear Society/American Society of Civil Engineers, *Proceedings of the International Topical Meeting: High-Level Radioactive Waste Management*, April 8–12, 1990, Las Vegas, Nevada, 1:81–90 [1990].

Spaulding, W.G., "Vegetation and Climates of the Last 45,000 years in the Vicinity of the Nevada Test Site, South-Central, Nevada," U.S. Geological Survey Professional Paper 1329, 1985.

Stephens, M.E. and B. Goodwin, "Systematic Scenario Analysis for the Post-Closure Assessment of the Canadian Concept for U.S. Nuclear Waste Disposal," OECD Nuclear Energy Agency/International Atomic Energy Agency/Commission of the European Communities, *Proceedings of the Symposium on the Safety Assessments for Radioactive Waste Repositories*, October 9–13, 1989, Paris, France, pp. 405–416 [1990].

TERA Corporation, *Bayesian Seismic Hazard Analysis: A Methodology*, Berkeley, California, 1978.

Thornbury, W.D., *Regional Geomorphology of the United States*, New York, John Wiley & Sons, 1967.

URS/John A. Blume & Associates, "Technical Basis and Parametric Study of Ground Motion and Surface Rupture Hazard Evaluations at Yucca Mountain, Nevada," Albuquerque, New Mexico, Sandia National Laboratories, SAND86–7013, September 1987. [Prepared for the U.S. Department of Energy.]

U.S. Department of Energy, "Site Characterization Plan Overview, Yucca Mountain Site, Nevada Research and Development Area, Nevada," Nevada Operations Office/Yucca Mountain Project Office, Nevada, DOE/RW–0198, December 1988a.

U.S. Department of Energy, "Site Characterization Plan, Yucca Mountain Site, Nevada Research and Development Area, Nevada," Nevada Operations Office/Yucca Mountain Project Office, Nevada, DOE/RW–0199, 9 vols., December 1988b.

U.S. Environmental Protection Agency, "Environmental Standards for the Management of Spent Nuclear Fuel, High-Level and Transuranic Wastes [Final Rule]," *Federal Register*, vol. 50, no. 182, September 19, 1985, pp. 38066–38089.

U.S. Environmental Protection Agency, "Environmental Radiation Protection Standards for the Management and Disposal of Spent Nuclear Fuel, High-Level and Transuranic Wastes [Proposed Rule]," *Federal Register*, vol. 58, no. 242, December 20, 1993, pp. 66398–66416.

U.S. Nuclear Regulatory Commission, "10 CFR Part 60, Disposal of High-Level Radioactive Wastes in Geologic Repositories: Conforming Amendments," *Federal Register*, vol. 51, no. 118, June 19, 1986, pp. 22288–22301.

Vaniman, D., *et al.*, "Variations in Authigenic Mineralogy and Sorptive Zeolite Abundance at Yucca Mountain, Nevada, Based on Studies of Drili Cores USW GU–3 and G–3," Los Alamos, New Mexico, Los Alamos National Laboratory, LA–9707–MS, June 1984. [Prepared for the U.S. Department of Energy.]

Winograd, I.J. and B.J. Szabo, "Water-Table Decline in the South-Central Great Basin during the Quaternary: Implications for Toxic Waste Disposal," in Carr, M.D. and J.C. Yount (eds.), "Geologic and Hydrologic Investigations of a Potential Nuclear Waste Disposal Site at Yucca Mountain, Southern Nevada," U.S. Geological Survey Bulletin 1790, 1988.

Yount, J.C., *et al.*, "Neotectonics of the Walker Lane, Pyramid Lake to Tonopah, Nevada—Part I," in Lahren, M.M., J.H. Trexler, Jr., and C. Spinosa (eds.), "Crustal Evolution of the Great Basin and Sierra Nevada: Cordilleran/Rocky Mountain Section," Department of Geological Sciences, University of Nevada at Reno, Geological Society of America Guidebook, pp. 383–408, 1993.

Chapter 4. Flow and Transport Module

Ababou R., "Approaches to Large Scale Unsaturated Flow on Heterogeneous, Stratified, and Fractured Geologic Media," U.S. Nuclear Regulatory Commission, NUREG/CR-5743, August 1991. [Prepared by the Center for Nuclear Waste Regulatory Analyses.]

Ababou, R. and A.C. Bagtzoglou, "BIGFLOW: A Numerical Code for Simulating Flow in Variably Saturated, Heterogeneous Geologic Media (Theory and Users' Manual—Version 1.1)," U.S. Nuclear Regulatory Commission, NUREG/CR-6028, June 1993. [Prepared by the Center for Nuclear Waste Regulatory Analyses.]

Ahola, M. and Sagar, B., "Regional Groundwater Modeling of the Saturated Zone in the Vicinity of Yucca Mountain, Nevada," San Antonio, Texas, Center for U.S. Nuclear Waste Regulatory Analyses, CNWRA 92-001, January 1992. [Prepared for the Nuclear Regulatory Commission.]

Amter, S. and B. Ross, "Simulation of Gas Flow Beneath Yucca Mountain, Nevada, with a Model Based on Fresh Water Head," in Post, R.G. (ed.), *Waste Management '90: Proceedings of the Symposium*, February 25–March 1, 1990, Tucson, Arizona, 2:915–925 [1990].

Bagtzoglou, A.C., R. Ababou, and B. Sagar, "Effects of Layering, Dipping Angle, and Faulting on Two-Dimensional Variably Saturated Flow (IPA Phase II)," San Antonio, Texas, Center for Nuclear Waste Regulatory Analyses, CNWRA 92-004, February 1992. [Prepared for the Nuclear Regulatory Commission.]

Bagtzoglou, A.C., *et al.*, "Effect of Some Common Geological Features on Two-Dimensional Variably Saturated Flow," in Interrante, C.G., and R.T. Pabalan (eds.), *Scientific Basis for Nuclear Waste Management XVI: Materials Research Society Symposium Proceedings*, 294:929–936 [1993].

Barnard, R.W., *et al.*, "TSPA: 1991 An Initial Total-System Performance Assessment for Yucca Mountain", Albuquerque, New Mexico, Sandia National Laboratories, SAND91-2795, September 1992. [Prepared for the U.S. Department of Energy.]

Barton, C., W. Page, and T. Morgan, "Fractures in Outcrops in the Vicinity of Drill Hole USW G-4, Yucca Mountain, Nevada-Data Analysis and Compilation," U.S. Geological Survey, Open File Report 89-92, 1989.

Benson, L.V., *et al.*, "Chemical Composition of Ground Water and the Locations of Permeable Zones in the Yucca Mountain Area, Nevada," U.S. Geological Survey, Open File Report 83-854, 1983.

Bentley, C.B., *et al.*, 1983, "Geohydrologic Data for Test Well USW H-5, Yucca Mountain Area, Nye County, Nevada," U.S. Geological Survey, Open File Report 83-853, 1983.

Blankennagel, R.K., "Hydraulic Testing Techniques of Deep Drill Holes at Pahute Mesa Nevada Test Site," U.S. Geological Survey, Open File Report 67-18, 1967.

Bowyer A., "Computing Dirichlet Tessellations," *The Computer Journal*, 24(2):162–166 [1981].

Broxton, D.E., *et al.*, "Chemistry of Diagenetically Altered Tuffs at a Potential Nuclear Waste Repository, Yucca Mountain, Nye County, Nevada," Los Alamos, New Mexico, Los Alamos National Laboratory, LA-10802-MS, October 1986.

Classen, H.C., "Water Quality and Physical Characteristics of Nevada Test Site Water-Supply Wells," U.S. Geological Survey, Open File Report 74-158, 1973.

Codell, R.B., U.S. Nuclear Regulatory Commission/Office of Nuclear Material Safety and Safeguards [NRC/NMSS], Memorandum to M.R. Knapp, NRC/NMSS [Subject: "Analytical Model for Repository Temperature"], May 4, 1984.

Codell, R.B., *et al.*, "Initial Demonstration of the NRC's Capability to Conduct a Performance Assessment for a High-Level Waste Repository," U.S. Nuclear Regulatory Commission, NUREG-1327, May 1992.

Cooley, R.L., "A Method of Estimating Parameters and Assessing Reliability for Models of Steady State Groundwater Flow, 1—Theory and Numerical Properties," *Water Resources Research*, 13:318–324 [1977].

Cooley, R.L., "A Method of Estimating Parameters and Assessing Reliability for Models of Steady State Groundwater Flow, 2—Application of Statistical Analysis," *Water Resources Research*, 15:603–617 [1979].

Cooley, R.L., "Incorporation of Prior Information on Parameters into Nonlinear Regression Groundwater Flow Models, 1—Theory," *Water Resources Research*, 18:965–976 [1982].

Craig, R.W., *et al.*, "Geohydrologic Data for Test Well USW H–6, Yucca Mountain Area, Nye County, Nevada," U.S. Geological Survey, Open File Report 83–856, 1983.

Craig, R.W. and J.H. Robison, "Geohydrology of Rocks Penetrated by Test Well UE–25p#1, Yucca Mountain Area, Nye County, Nevada," U.S. Geological Survey, Water Resources Investigations Report, WRI–34–4248, 1984.

Craig, R.W. and K.A. Johnson, "Geohydrologic Data for Test Well UE–25p#1, Yucca Mountain Area, Nye County, Nevada," U.S. Geological Survey, Water Resources Investigations Report, WRI–84–450, 1984.

Craig, R.W., "Geohydrology of Rocks Penetrated by Test Well USW H–6, Yucca Mountain, Nye County, Nevada," U.S. Geological Survey, Water Resources Investigations Report, WRI–89–4025, 1991.

Czarnecki, J.B., "Simulated Effects of Increased Recharge on the Ground-Water Flow System of Yucca Mountain and Vicinity, Nevada-California," U.S. Geological Survey, Water Resources Investigations Report, WRI–84–4344, 1984.

Czarnecki, J.B., "Simulated Effects of Increased Recharge on the Ground-Water Flow System of Yucca Mountain and Vicinity, Nevada-California," U.S. Geological Survey, Water-Resources Investigations Report, WRI–84–4344, 1985.

Czarnecki, J.B., "Characterization of the Subregional Ground-Water Flow system at Yucca Mountain and Vicinity, Nevada-California," *Radioactive Waste Management and the Nuclear Fuel Cycle*, 13:51–61 [1989].

Czarnecki, J.B., "Preliminary Simulations Related to a Large Horizontal Hydraulic Gradient at the North End of Yucca Mountain, Nevada [Abstract]," American Institute of Hydrology, *1990 Spring Meeting: Abstracts with Program [Topic: Minimizing Risk to the Hydrologic Environment]*, March 12–16, 1990, Las Vegas, Nevada, p. 18, 1990a.

Czarnecki, J.B., "Geohydrology and Evapotranspiration at Franklin Lake Playa, Inyo County, California," U.S. Geological Survey, Open-File Report 90–356, 1990b.

Czarnecki, J.B., "Simulated Water-Level Declines Caused by Withdrawals from Wells J–13 and J–12 Near Yucca Mountain, Nevada," U.S. Geological Survey, Open-File Report 91–478, 1992.

Carnecki, J.B. and R.K. Waddell, "Finite-Element Simulation of Ground-Water Flow in the Vicinity of Yucca Mountain, Nevada-California," U.S. Geological Survey, Water-Resources Investigations Report, WRI–84–4349, 1984.

Czarnecki, J.B. and W.E. Wilson, "Site Characterization and Conceptual Models of the Regional GroundWater Flow System, Yucca Mountain and Vicinity, Nevada-California [Abstract]," in Post, R.G. (ed.), *Waste Management '89: Proceedings of the Symposium on Waste Management*, February 26–March 2, 1989, Tucson, Arizona, 1:473 [1989].

Drever, J.I., *The Geochemistry of Natural Waters*, Englewood Cliffs, New Jersey, Prentice Hall, Inc., 1988.

Dudley, A.L., *et al.*, "Total-System Performance Assessment Code (TOSPAC), Volume 1: Physical and Mathematical Bases," Albuquerque, New Mexico, Sandia National Laboratories, SAND85–0002, December 1988.

Dykhuizen, R.C., "A New Coupling Term for Dual-Porosity Models," *Water Resources Research*, 26:351–356 [1990].

Freeze, R. A. and J.A. Cherry, *Groundwater*, Englewood Cliffs, New Jersey, Prentice Hall, Inc., 1979.

Healey, D.L., F.G. Clutson, and D.A. Glover, "Borehole Gravity Meter Surveys in Drill Holes USW G–3, UE–25p#1, and UE–25c#1, Yucca

Mountain Area, Nevada," U.S. Geological Survey, Open File Report 84-672, 1984.

Keynan, J.H. and F.G. Keyes, *Thermodynamic Properties of Steam Including Data for the Liquid and Solid Phases*, New York, John Wiley and Sons, 1936.

Klaveter, E.A. and R.R. Peters, "Fluid Flow in a Fractured Rock Mass," Albuquerque, New Mexico, Sandia National Laboratories, SAND85-0855, March 1986.

Lahoud, R.G., *et al.*, "Geohydrology of Volcanic Tuff Penetrated by Test Well UE-25b#1, Yucca Mountain, Nye County, Nevada," U.S. Geological Survey, Water Resources Investigations Report, WRI-84-4253, 1984.

Lobmeyer, D.H., *et al.*, "Geohydrologic Data for Test Well UE-25b#1, Nevada Test Site, Nye County, Nevada," U.S. Geological Survey, Open File Report 83-855, 1983.

Lobmeyer, D.H., "Geohydrology of Rocks Penetrated by Test Well USW G-4, Yucca Mountain, Nye County, Nevada," U.S. Geological Survey, Water Resources Investigations Report, WRI-86-4015, 1986.

Longsine, D.E., E.J. Bonano, and C.P. Harlan, "User's Manual for the NEFTRAN Computer Code," U.S. Nuclear Regulatory Commission, NUREG/CR-4766, September 1987. [Prepared by the Sandia National Laboratories.]

Lung, H-C., P.L. Chambré, T.H. Pigford, and W.W-L. Lee, "Transport of Radioactive Decay Chains in Finite and Semi-Finite Porous Media," Lawrence Berkeley Laboratory/University of California, LBL-23987, September 1987. [Prepared for the U.S. Department of Energy.]

Mualem, Y., "A Catalogue of the Hydraulic Properties of Unsaturated Soils," Haifa, Israel, Hydrodynamics and Hydraulic Laboratory, Technion Institute of Technology, Research Project No. 442, 1976.

Meijer, A., "Yucca Mountain Project Far-Field Sorption Studies and Data Needs," Los Alamos, New Mexico, Los Alamos National Laboratory, LA-11671-MS, September 1990.

Montazer, P. and W.E. Wilson, "Conceptual Hydrologic Model of Flow in the Unsaturated Zone, Yucca Mountain, Nevada," U.S. Geological Survey, Water-Resources Investigations Report, WRI-84-4345, 1984.

Nienhuis, P. and T. Appelo, "Adaptation of PHREEQE for Use in a Mixing-Cell Flowtube: *PHREEQM*—User Guide (October 1990), U.S. Geological Survey, *Training Course on Geochemistry for Groundwater Systems*, Denver, Colorado, April 22-May 3, 1991.

Nitao, J.J. and T.A. Buscheck, "Infiltration of a Liquid Front in an Unsaturated, Fractured Porous Media [sic][Medium]," *Water Resources Research*, 27:2099-2112 [1991].

Olague, N.E., *et al.*, "User's Manual for the NEFTRAN II Computer Code," U.S. Nuclear Regulatory Commission, NUREG/CR-5618, February 1991. [Prepared by the Sandia National Laboratories.]

Ortiz, T.S., *et al.*, "A Three-Dimensional Model of Reference Thermal/Mechanical and Hydrological Stratigraphy at Yucca Mountain, Southern Nevada, Albuquerque, New Mexico, Sandia National Laboratories, SAND84-1076, October 1985. [Prepared for the U.S. Department of Energy.]

Pabalan, R.T., "Nonideality Effects on the Ion Exchange Behavior of the Zeolite Mineral Clinoptilolite," in Abrajano, T., Jr. and L.H. Johnson (eds.), *Scientific Basis for Nuclear Waste Management XIV: Materials Research Society Symposium Proceedings*, 212:559-567 [1991].

Parsons, A.M., N.E. Olague, and D.P. Gallegos, "Conceptualization of a Hypothetical High-Level Nuclear Waste Repository Site in Unsaturated, Fractured Tuff," U.S. Nuclear Regulatory Commission, NUREG/CR-5495, January 1991. [Prepared by the Sandia National Laboratories.]

Peters, R.R., *et al.*, "Fracture and Matrix Hydrologic Characteristics of Tuffaceous Materials from Yucca Mountain, Nye County, Nevada," Albuquerque, New Mexico, Sandia National Laboratories, SAND84-1471, December 1984.

Peters, R.R., J.H. Gauthier, and A.L. Dudley, "The Effect of Percolation Rate on Water-Travel

Time in Deep, Partially Saturated Zones," Albuquerque, New Mexico, Sandia National Laboratories, SAND85-0854, February 1986.

Peters, C.A., *et al.*, "A Preliminary Study of the Chemistry of Pore Water Extracted from Tuff by One-Dimensional Compression," in Kharaka Y.K., and A.S. Maest (eds.), *International Water-Rock Interaction Symposium Proceedings*, July 13-23, 1992, Park City, Utah, pp. 741-745 [1992]. [Published by A.A. Balkema, Rotterdam, Holland.]

Prickett, T.A. and C.C. Lonnquist, "Selected Digital Computer Techniques for Groundwater Resource Evaluation," Illinois State Water Survey Bulletin No. 55, 1971.

Prindle, R.W. and P.L. Hopkins, "On Conditions and Parameters Important to Model Sensitivity for Unsaturated Flow Through Layered, Fractured Tuff: Results of Analyses for HYDROCOIN Level 3 Case 2," Albuquerque, New Mexico, Sandia National Laboratories, SAND89-0652, October 1990.

Reardon, E.J., "K_d's—Can They Be Used to Describe Reversible Ion Sorption Reactions in Contaminant Migration?," *Groundwater*, 19:279-286 [1981].

Ross, B., S. Amter, and N. Lu, "Numerical Studies of Rock Gas Flow in Yucca Mountain," Albuquerque, New Mexico, Sandia National Laboratories, SAND91-7034, February 1992.

Runchal, A.K. and B. Sagar, "PORFLOW: A Mathematical Model for Fluid Flow, Heat, and Mass Transport in Variably Saturated Geologic Media—Users Manual (Version 1.0), Richland, Washington, Westinghouse Hanford Company, WHC-EP-0041, July 1989.

Rush, F.E., *et al.*, "Geohydrologic and Drill-Hole Data for Test Well USW H-1, Adjacent to Nevada Test Site, Nye County, Nevada," U.S. Geological Survey, Open File Report 83-141, 1983.

Rush, F.E., "Geohydrology of Test Well USW H-1, Yucca Mountain, Nye County, Nevada," U.S. Geological Survey, Water-Resources Investigations Report, WRI-83-4032, 1984.

Sagar, B. and A.K. Runchal, "PORFLOW: A Mathematical Model for Fluid Flow, Heat, and Mass Transport in Variably Saturated Geologic Media—Theory and Numerical Methods (Version 1.0)," Richland, Washington, Westinghouse Hanford Company, WHC-EP-0042, March 1990.

Scott, R.B., *et al.*, "Geologic Character of Tuffs in the Unsaturated Zone at Yucca Mountain, Southern Nevada,"in Mercer, J.W., P.S.C. Rao, and I.W. Marine (eds.), "Role of the Unsaturated Zone in Radioactive and Hazardous Waste Disposal," Ann Arbor, Michigan, Ann Arbor Science Publishers, pp. 289-335, 1983.

Scott, R.B., "Stratigraphic and Structural Relations of Volcanic Rocks in Drill Holes USW GU-3 and USW G-3, Yucca Mountain, Nye County, Nevada," U.S. Geological Survey, Open File Report 84-491, 1984.

Scott, R.B. and J. Bonk, "Preliminary Geologic Map of Yucca Mountain, Nye County, Nevada, with Geologic Sections," U.S. Geological Survey, Open File Report 84-494, 1984.

Spengler, R.W., *et al.*, "Stratigraphy and Structure of Volcanic Rocks in Drill Hole USW-G1, Yucca Mountain, Nye County, Nevada," U.S. Geological Survey, Open File Report 81-1349, 1981.

Thomas, K., "Summary of Sorption Measurements Performed with Yucca Mountain, Nevada, Tuff Samples and Water from Well J-13," Los Alamos, New Mexico, Los Alamos National Laboratory, LA-10960-MS, 1987.

Thordarson, W., "Geohydrologic Data and Test Results from Well J-13, Nevada Test Site, Nye County, Nevada," U.S. Geological Survey, Water-Resources Investigations Report, WRI-83-4171, 1983.

Thordarson, W., *et al.*, "Geohydrology of Test Well USW H-3, Yucca Mountain, Nye County, Nevada," U.S. Geological Survey, Water-Resources Investigations Report, WRI-84-4272, 1985.

Tsang, Y.W. and K. Pruess, "A Study of Thermally Induced Convection Near a High-Level Nuclear Waste Repository in Partially Saturated Fractured Tuff," *Water Resources Research*, 23:1958-1966 [1987].

Updegraff, C.D., C.E. Lee, and D.P. Gallegos, "DCM3D: A Dual-Continuum, Three-Dimensional, Ground-Water Flow Code for Unsaturated, Fractured, Porous Media," U.S. Nuclear Regulatory Commission, NUREG/CR-5536, February 1991.

U.S. Department of Energy, "Site Characterization Plan, Yucca Mountain Site, Nevada Research and Development Area, Nevada," Nevada Operations Office/Yucca Mountain Project Office, Nevada, DOE/RW-0199, 9 vols., December 1988a.

U.S. Department of Energy, "Site Characterization Plan Overview, Yucca Mountain Site, Nevada Research and Development Area, Nevada," Nevada Operations Office/Yucca Mountain Project Office, Nevada, DOE/RW-0198, December 1988b.

van Genuchten, M.T., "A Closed-Form Equation for Predicting the Hydraulic Conductivity of Unsaturated Soils," *Soil Science Society of America Journal*, 44:892–898 [1980].

Waddell, R.K., "Two-Dimensional, Steady-State Model of Ground-Water Flow, Nevada Test Site and Vicinity, Nevada-California," U.S. Geological Survey, Water Resources Investigations Report, WRI-82-4085, 1982.

Weast, R.C. (ed.), *CRC Handbook of Chemistry and Physics (65th Edition)*, Boca Raton, Florida, CRC Press, Inc., 1984.

Weeks, E.P., "Effect of Topography on Gas Flow in Unsaturated Fractured Rock: Concepts and Observations," in Evans, D.D. and T.J. Nicholson (eds.), "Flow and Transport Through Unsaturated Fractured Rock," American Geophysical Union, Geophysical Monograph 42, pp. 165–170, 1987.

Whitfield, M.S., *et al.*, "Geohydrologic and Drill-Hole Data for Test Well USW H-4, Yucca Mountain, Nye County, Nevada," U.S. Geological Survey, Open File Report 84-449, 1984.

Whitfield, M.S., *et al.*, "Geohydrology of Rocks Penetrated by Test Well USW H-4, Yucca Mountain, Nye County, Nevada," U.S. Geological Survey, Water-Resources Investigations Report, WRI-85-4030, 1985.

WoldeGabriel, G., *et al.*, "Preliminary Assessment of Clinoptilolite K/Ar Results from Yucca Mountain, Nevada, USA: A Potential High-Level Radioactive Waste Repository Site," in Kharaka, Y.K. and A.S. Maest (eds.), *International Water-Rock Interaction Symposium Proceedings*, July 13–23, 1992, Park City, Utah, pp. 457–461 [1992]. [Published by A.A. Balkema, Rotterdam, Holland.]

Chapter 5. Source Term Module

Altenhofen, M.K. and P.W. Eslinger, "Evaluation of Near-Field Thermal Environmental Conditions for a Spent Fuel Repository in Tuff," American Nuclear Society/American Society of Civil Engineers, *Proceedings of the Third International Conference: High-Level Radioactive Waste Management*, April 12–16, 1992, Las Vegas, Nevada, 1:402–409 [1992].

Apted, M.J., "Engineered Barrier System of the Near Field: The 'Little Brother' of Performance Assessment," OECD Nuclear Energy Agency/International Atomic Energy Agency/Commission of the European Communities, *Proceedings of the Symposium on the Safety Assessments for Radioactive Waste Repositories*, October 9–13, 1989, Paris, France, pp. 471–480 [1990].

Bateman, H., "The Solution of a System of Differential Equations Occurring in the Theory of Radioactive Transformation," *Proceedings of the Cambridge Philosophical Society*, 15:473 [1910].

Bazant, Z.P. and L. Cedolin, *Stability of Structures*, New York, Oxford University Press, 1991.

Buscheck, T.A. and J.J. Nitao, "The Analysis of Repository-Heat-Driven Hydrothermal Flow at Yucca Mountain," American Nuclear Society/American Society of Civil Engineers, *Proceedings of the Fourth International Conference: High-Level Radioactive Waste Management*, April 26–30, 1993, Las Vegas, Nevada, 1:847–867 [1993].

Buscheck, T.A., D.G. Wilder, and J.J. Nitao, "Large Scale In-Situ Heater Tests for Hydrothermal Characterization at Yucca Mountain," American Nuclear Society/American Society of Civil Engineers, *Proceedings of the Fourth International Conference: High-Level Radioactive Waste Management*, April 26–30, 1993, Las Vegas, Nevada, 2:1854–1872 [1993].

Carslaw, H.S. and J.C. Jaeger, *Conduction of Heat in Solids*, Oxford, England, Clarendon Press, 1959.

Codell, R.B., "Model for Release of Gaseous ^{14}C from Spent Fuel," American Nuclear Society/American Society of Civil Engineers, *Proceedings of the Forth International Conference: High-Level Radioactive Waste Management*, April 26–30, 1993, Las Vegas, Nevada, 1:22–29 [1993].

Einziger, R.E. and R. Kohli, "Low-Temperature Rupture Behavior of Zircaloy-Clad Pressurized Water Reactor Spent Fuel Rods under Dry Storage Conditions," *Nuclear Technology*, 67:107–123 [1984].

Einziger, R.E. and H.C. Buchanan, "Long-Term, Low-Temperature Oxidation of PWR Spent Fuel," Richland, Washington, Westinghouse Hanford Co, WHC–EP–0070, April 1988.

Einziger, R.E. "Evaluation of the Potential for Spent Fuel Oxidation under Tuff Repository Conditions," Richland, Washington, Westinghouse Hanford Company/Engineering Development Laboratory, HEDL–7452, 1991.

Einziger, R.E., "Effects of an Oxidizing Atmosphere in a Spent Fuel Packaging Facility," American Nuclear Society, *Proceedings of the Topical Meeting on Nuclear Waste Packaging (FOCUS '91)*, September 29–October 2, 1991, Las Vegas, Nevada, pp. 88–99 [1992].

Einziger, R.E., S.C. Marschman, and H.C. Buchanan, 'Spent-Fuel Dry-Bath Oxidation Testing," *Nuclear Technology*, 94:383–393 [1991].

Einziger, R.E., *et al.*, "Oxidation of Spent Fuel in Air at 75° and 195°C," American Nuclear Society/American Society of Civil Engineers, *Proceedings of the Third International Conference: High-Level Radioactive Waste Management*, April 12–16, 1992, Las Vegas, Nevada, 2:1449–1457 [1992].

Farmer, J.C., *et al.*, "Corrosion Models for Performance Assessment of High-Level Radioactive-Waste Containers," *Nuclear Engineering Design*, 129:57–88 [1991].

Garzarolli, F., *et al.*, "Review of PWR Fuel Rod Waterside Corrosion Behavior," Palo Alto, California, Electric Power Research Institute, EPRI–NP–1472, August 1980. [Prepared by Kraftwerk Union A.G. and Combustion Engineering, Inc.]

Grambow, B., "Spent Fuel Dissolution and Oxidation: An Evaluation of Literature Data," Stockholm, Sweden, Statens Kärnkraftinspektion (SKI) [Swedish Nuclear Power Inspectorate], SKI Technical Report 89:13, March 1989.

Henshall, G.A. "Stochastic Models for Predicting Pitting Corrosion Damage of HLRW Containers," American Nuclear Society, *Proceedings of the Topical Meeting on Nuclear Waste Packaging (FOCUS '91)*, September 29–October 2, 1991, Las Vegas, Nevada, pp. 225–232 [1992].

Kubaschewski, O. and B.E. Hopkins, *Oxidation of Metals and Alloys*, London, England: Butterworth Publishers, 36, 1962.

Kopp, D. and H. Munzel, "Release of Volatile Carbon-14 Containing Products from Zircaloy," *Journal of Nuclear Materials*, 173:1–6 [1990].

Johnson, G.L. and D.L. Montan, "Thermal Calculations Pertaining to a Proposed Yucca Mountain Nuclear Waste Repository," Livermore, California, Lawrence Livermore National Laboratory, UCRL–ID–103534, February 1990.

Lapidus, L., *Digital Computation for Chemical Engineers*, New York, McGraw-Hill, Inc., 1962.

Longsine, D.E., E.J. Bonano, and C.P. Harlan, "User's Manual for the NEFTRAN Computer Code," U.S. Nuclear Regulatory Commission, NUREG/CR–4766, September 1987. [Prepared by the Sandia National Laboratories.]

Macdonald, D.D. and M. Urquidi-Macdonald, "Thin-Layer Mixed-Potential Model for the Corrosion of High-Level Nuclear Waste Canisters," *Corrosion*, 46(5):380–390 [1990].

O'Neal, W.C., *et al.*, "Preclosure Analysis of Conceptual Waste Package Designs for a Nuclear Waste Repository in Tuff," Livermore, California, Lawrence Livermore National Laboratory, UCRL 53595, November 1984. [Prepared for the U.S. Department of Energy.]

Park, U.S., "Regulatory Overview and Recommendations on a Repository's Release of Carbon-14,"

San Diego, California, Science Applications International Corporation, January 1992. [Prepared for the U.S. Department of Energy.]

Pigford, Th.H., P.L. Chambré, and W. Lee, "A Review of Near-Field Mass Transfer in Geologic Disposal Systems," *Radioactive Waste Management and the Nuclear Fuel Cycle* 16(3/4):175–276 [1992].

Ramirez, A.L. and D.G. Wilder, "Prototype Engineered Barrier System Field Tests," Livermore, California, Lawrence Livermore National Laboratory, UCID–21640, February 1991.

Roark, R.J. and W.C. Young, *Formulas for Stress and Strain (Fifth Edition)*, New York, McGraw-Hill Book Company, 1975.

Sagar, B., *et al.*, "SOTEC: A Source Term Code for High-Level Geologic Repositories—User's Manual (Version 1.0)," San Antonio, Texas, Center for Nuclear Waste Regulatory Analyses, CNWRA 92–009, July 1992. [Prepared for the U.S. Nuclear Regulatory Commission.]

Shoesmith, D.W. and S. Sunder, "The Prediction of Nuclear Fuel (UO_2) Dissolution Rates under Waste Disposal Conditions," *Journal of Nuclear Materials*, 190:20–35 [1992].

Smith, H.D. and D.L. Baldwin, "An Investigation of Thermal Release of ^{14}C from PWR Spent Fuel Cladding," American Nuclear Society, *Proceedings of the Topical Meeting on Nuclear Waste Isolation in the Unsaturated Zone (FOCUS '89)*, September 17–21, 1989, Las Vegas, Nevada, pp. 46–49 [1989].

Stout, R.B., *et al.*, "Spent Fuel Waste Form Characteristics: Grain and Fragment Size Statistical Dependence for Oxidation Response," American Nuclear Society/American Society of Civil Engineers, *Proceedings of the Second International Conference: High-Level Radioactive Waste Management*, April 28–May 3, 1991, 1:103–111 [1991].

Tempest, P.A., P.M. Tucker, and J.W. Tyler, "Oxidation of UO_2 Fuel Pellets in Air at 503° and 543°K Studied, Using X-ray Photoelectron Spectroscopy and X-ray Diffraction," *Journal of Nuclear Materials*, 151(3):251–268 [1988].

Thomas, L.E., O.D. Slagle, and R.E. Einziger, "Nonuniform Oxidation of LWR Spent Fuel in Air," *Journal of Nuclear Materials*, 184:117–126 [1991].

TRW Environmental Safety Systems Inc., "Initial Summary Report for Repository/Waste Package Advanced Conceptual Design," Las Vegas, Nevada, Document No. B00000000–01717–5705–00015 (Rev. 00), 2 vols., August 29, 1994. [Prepared for the U.S. Department of Energy.]

U.S. Department of Energy, "Site Characterization Plan, Yucca Mountain Site, Nevada Research and Development Area, Nevada," Nevada Operations Office/Yucca Mountain Project Office, Nevada, DOE/RW–0199, 9 vols., December 1988.

U.S. Department of Energy, "Integrated Data Base for 1992: U.S. Spent Fuel and Radioactive Waste Inventories, Projections and Characteristics, Office of Civilian Radioactive Waste Management, RW–0006 (Revision 8), October 1992.

Van Konynenburg, R.A., *et al.*, "Behavior of Carbon-14 in Waste Packages for Spent Fuel in a Repository in Tuff," Livermore, California, Lawrence Livermore National Laboratory, UCRL–90855, November 1984.

Van Konynenburg, R.A., *et al.*, "Carbon-14 in Waste Packages for Spent Fuel in a Tuff Repository," in Bates, J.K. and W.B. Seefeldt (eds.), *Scientific Basis for Nuclear Waste Management X: Materials Research Society Symposium Proceedings*, 84:185–196 [1987].

Van Konynenburg, R.A., "Gaseous Release of Carbon-14: Why the High-Level Waste Regulations Should be Changed," American Nuclear Society/American Society of Civil Engineers, *Proceedings of the Second International Conference: High-Level Radioactive Waste Management*, April 28–May 3, 1991, 1:313–319 [1991].

Walton, J.C., "Effects of Evaporation in Solute Concentration on Presence and Composition of Water in and around the Waste Package at Yucca Mountain," *Waste Management*, 13:293–301 [1993].

Watson, M. and J. Postlethwaite, "Numerical Simulation of Crevice Corrosion of Stainless Steel

and Nickel Alloys in Chloride Solutions," *Corrosion*, 46(7):522–530 [1990].

Williford, R.E., "Uncertainties in Container Failure Time Predictions," in Abrajano, T., Jr. and L.H. Johnson (eds.), *Scientific Basis for Nuclear Waste Management XIV: Materials Research Society Symposium Proceedings*, 212:335–342 [1991].

Wilson, C.N., "Results from NNWSI Series 3 Spent Fuel Dissolution Tests," Richland, Washington, Battelle Pacific Northwest Laboratories, PNL–7170, June 1990.

Woodley, R.E., R.E. Einziger, and H.C. Buchanan, "Measurement of the Oxidation of Spent Fuel Between 140° and 225°C," *Nuclear Technology*, 85:74–88 [1989].

Chapter 6. Disruptive Consequence Analysis

Codell, R.B., *et al.*, "Initial Demonstration of the NRC's Capability to Conduct a Performance Assessment for a High-Level Waste Repository," U.S. Nuclear Regulatory Commission, NUREG–1327, May 1992.

Connor, C.B, and B.E. Hill, "Volcanism Research (Chapter 10)" in Sagar, B. (ed.), "NRC High-Level Radioactive Waste Research at CNWRA, January–June 1993," San Antonio, Texas, Center for Nuclear Waste Regulatory Analyses, CNWRA 93–01S, August 1993. [Prepared for the U.S. Nuclear Regulatory Commission.]

Crisp, J.A., "Rates of Magma Emplacement and Volcanic Output," *Journal of Volcanology and Geothermal Research*, 20:177–211 [1984].

Crowe, B.M. and F.V. Perry, "Volcanic Probability Calculation for the Yucca Mountain Site: Estimation of Volcanic Rates," American Nuclear Society, *Proceedings of the Topical Meeting on Nuclear Waste Isolation in the Unsaturated Zone (FOCUS '89)*, September 17–21, 1989, Las Vegas, Nevada, pp. 326–334 [1989].

Crowe, B.M., *et al.*, "Aspects of Potential Magmatic Disruptions of a High-Level Radioactive Waste Repository in Southern Nevada," *Journal of Geology*, 91:259–276 [1983].

Crowe, B.M., *et al.*, "Recurrence Models of Volcanic Events: Applications to Volcanic Risk Assessment," American Nuclear Society/ American Society of Civil Engineers, *High-Level Radioactive Waste Management: Proceedings of Third International Conference*, April 12–16, 1992, Las Vegas, Nevada, 2:2344–2355 [1992].

Czarnecki, J.B., "Simulated Effects of Increased Recharge on the Ground-Water Flow System of Yucca Mountain and Vicinity, Nevada–California," U.S. Geological Survey, Water-Resources Investigations Report, WRI–84–4344, 1985.

DeWispelare, A.R., *et al.*, "Expert Elicitation of Future Climate in the Yucca Mountain Vicinity—Iterative Performance Assessment Phase 2.5," San Antonio, Texas, Center for Nuclear Waste Regulatory Analyses, CNWRA 93–016, August 1993. [Prepared for the U.S. Nuclear Regulatory Commission.]

Freitas, C.J., R.B. Codell, and N.A. Eisenberg, "SEISMO Version 1.0—A Module for Simulation of Seismo-Mechanical Scenarios, Model Description, and User Guide," San Antonio, Texas, Center for Nuclear Waste Regulatory Analyses, CNWRA 94–008, June 1994. [Prepared for the U.S. Nuclear Regulatory Commission.]

Ho, C–H., "The Mathematical Model of Volcanism at Yucca Mountain," State of Nevada Agency for Nuclear Projects/Nuclear Waste Project Office, 1990. [Prepared by the University of Nevada, Las Vegas.]

Ho, C–H., *et al.*, "Eruptive Probability Calculation for the Yucca Mountain Site, USA: Statistical Estimation of Recurrence Rates," *Bulletin of Volcanology*, 54:50–56 [1991].

Johnson, G.L., and D.L. Montan, "Thermal Calculations Pertaining to a Proposed Yucca Mountain Nuclear Waste Repository," Livermore, California, Lawrence Livermore National Laboratory, UCRL–ID–103534, February 1990.

Lin, C.S., R.G. Baca, and R. Drake, "VOLCANO Code—A Module for Simulation of Magmatic Scenario Model Description and User Guide," San Antonio, Texas, Center for Nuclear Waste Regulatory Analyses, CNWRA 93–010. October 1993. [Prepared for the U.S. Nuclear Regulatory Commission.]

Margulies, T., *et al.*, "Probability Analysis of Magma Scenarios for Assessing Geologic Waste

Repository Performance," American Society of Mechanical Engineers, New York, Paper 92-WA/SAF-11, 7 p., 1992. [Presented at the ASME Winter Meeting, November 8-13, 1992, Anaheim, California.]

Nakamura, K., "Volcanoes as Possible Indicators of Tectonic Stress Orientation: Principle and Proposal," *Journal of Volcanology and Geothermal Research*, 2:1-16 [1977].

Sagar, B. and R.W. Janetzke, "Total-System Performance Assessment Computer Code: Description of Executive Module (Version 2.0)," San Antonio, Texas, Center for Nuclear Waste Regulatory Analyses, CNWRA 93-107, August 1993. [Prepared for the U.S. Nuclear Regulatory Commission.]

Sheridan, M.F., "A Monte Carlo Technique to Estimate the Probability of Volcanic Dikes," American Nuclear Society/American Society of Civil Engineers, *High-Level Radioactive Waste Management, Proceedings of Third International Conference*, April 12-16, 1992, Las Vegas, Nevada, 2:2033-2338 [1992].

Smith, E.I., T.R. Feuerbach, and J.E. Faulds, "The Area of Most Recent Volcanism Near Yucca Mountain, Nevada: Implications for Volcanic Risk Assessment," American Society of Civil Engineers/American Nuclear Society, *High-Level Radioactive Waste Management: Proceedings of the International Topical Meeting*, April 8-12, 1990, Las Vegas, Nevada, 1:81-90 [1990].

Trapp, J.S. and P.S. Justus, "Regulatory Requirements to Address Issues Related to Volcanism and Magmatism: Code of Federal Regulations, Title 10, Part 60, Disposal of High-Level Radioactive Wastes in Geological Repositories," American Nuclear Society/American Society of Civil Engineers, *High-Level Radioactive Waste Management, Proceedings of Third International Conference*, April 12-16, 1992, Las Vegas, Nevada, 2:2039-2046 [1992].

URS/John A. Blume & Associates, "Ground Motion Evaluations at Yucca Mountain, Nevada with Applications to Repository Conceptual Design and Siting" Albuquerque, New Mexico, Sandia National Laboratories, SAND85-7104, February 1986. [Prepared for the U.S. Department of Energy.]

U.S. Department of Energy, "Site Characterization Plan Overview, Yucca Mountain Site, Nevada Research and Development Area, Nevada," Nevada Operations Office/Yucca Mountain Project Office, Nevada, DOE/RW-0198, December 1988.

U.S. Department of Energy, "Site Characterization Plan, Yucca Mountain Site, Nevada Research and Development Area, Nevada," Nevada Operations Office/Yucca Mountain Project Office, Nevada, DOE/RW-0199, 9 vols., December 1988b.

U.S. Environmental Protection Agency, "Environmental Standards for the Management of Spent Nuclear Fuel, High-Level and Transuranic Wastes [Final Rule]," *Federal Register*, vol. 50, no. 182, September 19, 1985, pp. 38066 - 38089.

Valentine, G.A., B.M. Crowe, and F.V. Perry, "Physical Processes and Effects of Magmatism in the Yucca Mountain Region," American Nuclear Society/American Society of Civil Engineers, *High-Level Radioactive Waste Management, Proceedings of Third International Conference*, April 12-16, 1992, Las Vegas, Nevada, 2:2014-2024 [1992].

Chapter 7. Dose Assessment Module

Baes, C.F. III, *et al.*, "A Review and Analysis of Parameters for Assessing Transport of Environmentally Released Radionuclides through Agriculture," Oak Ridge, Tennessee, Oak Ridge National Laboratory," ORNL-5786, September 1984.

Biospheric Model Validation Study, "BIOMOVS II: Progress Report No. 2," Oxon, United Kingdom, INTERA, BIOMOVS II PR2 (Report IE2859-2), May 1992.

Charles, D. and G.M. Smith, "Conversion of Releases from the Geosphere to Estimates of Individual Doses to Man (Version 2)," Oxon, United Kingdom, INTERA, Report IM1802-10, July 1991.

Czarnecki, J.B., "Simulated Water-Level Declines Caused by Withdrawals from Wells J-13 and J-12 Near Yucca Mountain, Nevada," U.S. Geological Survey, Open-File Report 91-478, 1992.

Fisher, R.V. and H.V. Schminke, *Pyroclastic Rock*, New York, Springer-Verlag, Inc., 1984.

Freeze, R.A. and J.A. Cherry, *Groundwater*, Englewood Cliffs, New Jersey, Prentice Hall, Inc., 1979.

International Atomic Energy Agency, "Generic Models and Parameters for Assessing the Environmental Transfer of Radionuclides from Routine Releases, Exposures of Critical Groups: Procedures and Data," Vienna, Safety Series No. 57, 1982.

International Commission on Radiological Protection, "Reference Man: Anatomical, Physiological, and Metabolic Characteristics (Report of the Task Group on Reference Man)," Pergamon Press, Oxford, ICRP Publication 23, 1975.

International Commission on Radiological Protection, "Recommendations of the ICRP," *Annals of the ICRP*, vol. 1, no. 3 [1977]. [ICRP Publication 26]

International Commission on Radiological Protection, "Limits for Intakes of Radionuclides by Workers (Part 1)," *Annals of the ICRP*, vol. 2, nos. 3/4 [1979]. [ICRP Publication 30]

International Commission on Radiological Protection, "Radiation Protection: 1990 Recommendations of the International Commission on Radiological Protection," *Annals of the ICRP*, vol. 21, nos. 1-3, 1990. [ICRP Publication 60]

Johnson J.R. and M.B. Carver, "A **G**eneral **Mod**el [GENMOD] for Use in Internal Dosimetry," *Health Physics*, 41:341-348 [1981].

Kennedy, W.E., Jr., and D.L. Strenge, "Residual Radioactive Contamination from Decommissioning, Technical Basis for Translating Contamination Levels to Annual Total Effective Dose Equivalent, Final Report," U.S. Nuclear Regulatory Commission, NUREG/CR-5512, 2 vols., October 1992. [Prepared by the Pacific Northwest Laboratory.]

Kocher, D.C., "Dose-Rate Conversion Factors for External Exposure to Photons and Electrons," U.S. Nuclear Regulatory Commission, NUREG/CR-1918, August 1981. [Prepared by Oak Ridge National Laboratory.]

Leigh, C.D., *et al.*, "User's Guide for GENII-S: A Code for Statistical and Deterministic Simulation of Radiation Doses to Humans from Radionuclides in the Environment," Albuquerque, New Mexico, Sandia National Laboratories, SAND91-0561, April 1993.

Logan, S.E., *et al.*, "Parametric Studies of Radiological Consequences of Basaltic Volcanism," Albuquerque, Sandia National Laboratories, SAND81-2375, April 1982. [Prepared for the U.S. Department of Energy.]

Mills, L., "Beginning Desert Gardening," University of Nevada Cooperative Extension, 1993.

Napier, B.A., *et al.*, "GENII: The Hanford Environmental Radiation Dosimetry Software System, Volume 1: Conceptual Representation," Richland, Washington, Pacific Northwest Laboratory, PNL-6584, December 1988a. [Prepared for the U.S. Department of Energy.]

Napier, B.A., *et al.*, "GENII: The Hanford Environmental Radiation Dosimetry Software System, Volume 2: Users' Manual," Richland, Washington, Pacific Northwest Laboratory, PNL-6584, December 1988b. [Prepared for the U.S. Department of Energy.]

Nevada Agricultural Statistics Service, "Nevada Agricultural Statistics: 1987-1988," Reno, Nevada, 1988.

U.S. Code of Federal Regulations, "Environmental Standards for the Management and Disposal of Spent Nuclear Fuel, High-Level and Transuranic Radioactive Wastes," Part 191, Chapter I, Title 40, "Protection of the Environment."

U.S. Code of Federal Regulations, "Standards for Protection Against Radiation," Part 20, Chapter I, Title 10, "Energy."

U.S. Department of Commerce/Bureau of the Census, "1987 Census of Agriculture, Volume 1: Geographic Area Series, Part 28: Nevada State and County Data," Washington, D.C., AC87-A-28, June 1989.

U.S. Department of Commerce/National Oceanographic and Atmospheric Administration, "STAR Data for Desert Rock Station, Nevada (1986-1990)," Nashville, North Carolina, National Climatic Data Center, 1992.

U.S. Department of Energy, "Chapter 3, Hydrology," in "Site Characterization Plan, Yucca Mountain Site, Nevada Research and Development Area, Nevada," Office of Civilian Radioactive Waste Management, Nevada Operations Office/ Yucca Mountain Project Office, Nevada, DOE/RW-0199, Vol. II, Part A, December 1988.

U.S. Environmental Protection Agency, "Environmental Standards for the Management of Spent Nuclear Fuel, High-Level and Transuranic Wastes [Final Rule]," *Federal Register*, vol. 50, no. 182, September 19, 1985, pp. 38066–38089.

U.S. Environmental Protection Agency, "High-Level and Transuranic Radioactive Wastes: Background Information Document for Final Rule," Washington, D.C., Report 520/1-85-023, August 1985.

U.S. Environmental Protection Agency, "Limiting Values of Radionuclide Intake and Air Concentration and Dose Conversion Factors for Inhalation, Submersion and Ingestion," Washington, D.C., EPA-520/1-88-020, September 1988.

U.S. Environmental Protection Agency, "Environmental Radiation Protection Standards for the Management and Disposal of Spent Nuclear Fuel, High-Level and Transuranic Radioactive Wastes [Proposed Rule]," *Federal Register*, vol. 58, no. 26, February 10, 1993, pp. 7924–7936.

U.S. Nuclear Regulatory Commission, "Calculation of Annual Doses to Man from Routine Releases of Reactor Effluents for the Purpose of Evaluating Compliance with 10 CFR Part 50, Appendix I," Office of Standards Devlopment, Regulatory Guide 1.109, Revision 1, October 1977.

U.S. Nuclear Regulatory Commission, "Standards for Protection against Radiation [Final Rule]," *Federal Register*, vol. 56, no. 98, May 21, 1991, pp. 23360–23474.

Chapter 8. Sensitivity and Uncertainty Analysis

Baybutt, P., D.C. Cox, and R.E. Kurth, "Methodology for Uncertainty Analysis of Light Water Reactor Meltdown Accident Consequences," Battelle Columbus Laboratories, Letter Report, May 31, 1981. [Prepared for the U.S. Nuclear Regulatory Commission.]

Bowen, W.M. and C.A. Bennett (eds.), "Statistical Methods for Nuclear Material Management," U.S. Nuclear Regulatory Commission, NUREG/CR-4604, March 1988. [Prepared by Pacific Northwest Laboratories, Richland, Washington.]

Cochran, W.G., *Sampling Techniques*, New York, John Wiley and Sons, Inc., 1963.

Codell, R.B., *et al.*, "Initial Demonstration of the NRC's Capability to Conduct a Performance Assessment for a High-Level Waste Repository," U.S. Nuclear Regulatory Commission, NUREG-1327, May 1992.

Draper, N.R. and H. Smith, *Applied Regression Analysis*, New York, John Wiley and Sons, Inc., 1966.

Gunst, R.F. and R.L. Mason, *Regression Analysis and Its Application*, New York, Marcel Dekker, Inc., 1980.

Gureghian, A.B., *et al.*, "Sensitivity and Uncertainty Analyses Applied to One-Dimensional Radionuclide Transport in a Layered Fractured Rock," U.S. Nuclear Regulatory Commission, NUREG/CR-5917, December 1992. [Prepared by the Center for Nuclear Waste Regulatory Analyses.]

Helton, J.C., "A Retrospective and Prospective Survey of the Monte Carlo Method," *SIAM Review*, 12[1]:1–60 [1970].

Helton, J.C., *et al.*, "Sensitivity Analysis Techniques and Results for Performance Assessment at the Waste Isolation Pilot Plant," Albuquerque, New Mexico, Sandia National Laboratories, SAND90-7103, March 1991.

Iman, R.L. and W.J. Conover, "The Use of Rank Transform in Regression," *Technometrics*, 21:499–509 [1979].

Iman, R.L., J. Davenport, and D. Zeigler, "Latin Hypercube Sampling (Program Users' Guide)," Albuquerque, New Mexico, Sandia National Laboratories, SAND79-1473, January 1980. [Also see Iman and Shortencarier (1984) referenced in Chapter 2.]

Iman, R.L., and J.C. Helton, "A Comparison of Uncertainty and Sensitivity Analysis Techniques

for Computer Models," U.S. Nuclear Regulatory Commission, NUREG/CR-3904, March 1985.

Intriligator, M.D., *Econometric Models, Techniques, and Applications*, Englewood Cliffs, New Jersey, Prentice-Hall, Inc., 1978.

McKay, M.D., "Interim Report on the Status of Research on Uncertainty Analysis of Computer Models," Los Alamos, New Mexico, Los Alamos National Laboratory, LAUR 92-4299, December 1992. [Prepared for U.S. Nuclear Regulatory Commission.]

Mallows, C.L., "Some Comments on C_p," *Technometrics*, 15:661-675 [1973].

Mendenhall, W. and R.L. Schaeffer, *Mathematical Statistics with Applications*, North Scituate, Massachusetts, Duxbury Press, 1973.

Seitz, R.R., *et al.*, "Sample Application of Sensitivity/Uncertainty Analysis Techniques to a Groundwater Transport Problem," Idaho Falls, Idaho, Idaho National Engineering Laboratory, DOE/ID/LW-108, June 1991. [Prepared by EG&G Idaho, Inc., for the U.S. Department of Energy.]

Sen, A. and M. Srivastava, *Regression Analysis—Theory, Methods, and Applications*, New York, Springer-Verlag, Inc., 1990.

Statistical Sciences, Inc., *S-PLUS: Guide to Statistical and Mathematical Analysis*, Seattle, Washington, MathSoft, Inc., Version 3.1, September 1991. [Computer program.]

Tukey, J.W., *Exploratory Data Analysis*, Reading, Massachusetts, Addison Wesley, 1977.

Walpole, R.E., and R.H. Myers, *Probability and Statistics for Engineers and Scientists*, New York, Macmillan Publishing Co., Inc., 1978.

Wu, Y.T., A.B. Gureghian, and R.B. Codell, "Sensitivity and Uncertainty Analysis Applied to One-Dimensional Transport in a Layered Fractured Rock," San Antonio, Texas, Center for Nuclear Waste Regulatory Analysis, CNWRA92-002, March 1992.

Zimmerman, D.A., *et al.*, "A Review of Techniques for Propagating Data and Parameter Uncertainties in High-Level Radioactive Waste Performance Assessment Models," U.S. Nuclear Regulatory Commission, NUREG/CR-5393, March 1990.

Zimmerman, D.A., R.T. Hanson, and P.A. Davis, "A Comparison of Parameter Estimation and Sensitivity Analysis Techniques and Their Impact on the Uncertainty in Ground Water Flow Model Predictions," U.S. Nuclear Regulatory Commission, NUREG/CR-5522, May 1991. [Prepared by the Sandia National Laboratories, Gram, Inc., and the U.S. Geological Survey.]

Chapter 9. Analytical Results

Cranwell, R.M., *et al.*, "Risk Methodology for Geologic Disposal of Radioactive Waste: Scenario Selection Procedure," U.S. Nuclear Regulatory Commission, NUREG/CR-1667, April 1990. [Prepared by the Sandia National Laboratories.]

Helton, J.C., *et al.*, "Sensitivity Analysis Techniques and Results for Performance Assessment at the Waste Isolation Pilot Plant," Albuquerque, New Mexico, Sandia National Laboratories, SAND90-7103, March 1991. [Prepared for the U.S. Department of Energy.]

Longsine, D.E., E.J. Bonano, and C.P. Harlan, "User's Manual for the NEFTRAN Computer Code," U.S. Nuclear Regulatory Commission, NUREG/CR-4766, September 1987. [Prepared by the Sandia National Laboratories.]

Napier, B.A., *et al.*, "GENII: The Hanford Environmental Radiation Dosimetry Software System," Richland, Washington, Pacific Northwest Laboratory, PNL-6584, 3 vols., December 1988. [Prepared for the U.S. Department of Energy.]

Sagar, B., *et al.*, "SOTEC: A Source Term Code for High-Level Geologic Repositories—User's Manual (Version 1.0)," San Antonio, Texas, Center for Nuclear Waste Regulatory Analyses, CNWRA 92-009, July 1992. [Prepared for the U.S. Nuclear Regulatory Commission.]

U.S. Environmental Protection Agency, "Environmental Radiation Protection Standards for the Management and Disposal of Spent Nuclear Fuel, High-Level and Transuranic Radioactive Wastes [Proposed Rule]," *Federal Register*, vol. 58, no. 26, February 10, 1993, pp. 7924-7936.

Chapter 10. Conclusions and Recommendations

Barnard, R.W., *et al.*, "TSPA: 1991 An Initial Total-System Performance Assessment for Yucca

Mountain", Albuquerque, New Mexico, Sandia National Laboratories, SAND91-2795, September 1992. [Prepared for the U.S. Department of Energy.]

Codell, R.B., *et al.*, "Initial Demonstration of the NRC's Capability to Conduct a Performance Assessment for a High-Level Waste Repository," U.S. Nuclear Regulatory Commission, NUREG-1327, May 1992.

Cranwell, R.M., *et al.*, "Risk Methodology for Geologic Disposal of Radioactive Waste: Scenario Selection Procedure," U.S. Nuclear Regulatory Commission, NUREG/CR-1667, April 1990. [Prepared by the Sandia National Laboratories.]

Eslinger, P.W., *et al.*, "Preliminary Total System Analysis of a Potential High-Level Nuclear Waste Repository at Yucca Mountain," Richland, Washington, Pacific Northwest Laboratory, PNL-8444, January 1993. [Prepared for the U.S. Department of Energy.]

Helton, J.C., *et al.*, "Sensitivity Analysis Techniques and Results for Performance Assessment at the Waste Isolation Pilot Plant," Albuquerque, New Mexico, Sandia National Laboratories, SAND90-7103, March 1991. [Prepared for the U.S. Department of Energy.]

Her Majesty's Inspectorate of Pollution/ Department of Environment [HMIP/DOE], "A Trial Assessment of Underground Disposal of Radioactive Wastes Based on Probabilistic Risk Analysis", DOE Report No. DOE/HMIP/RR/92.042, January 1993.

International Commission on Radiological Protection, "Radiation Protection: 1990 Recommendations of the International Commission on Radiological Protection," *Annals of the ICRP*, vol. 21, nos. 1-3, 1990. [ICRP Publication 60]

U.S. Department of Energy, "Site Characterization Plan, Yucca Mountain Site, Nevada Research and Development Area, Nevada," Nevada Operations Office/Yucca Mountain Project Office, Nevada, DOE/RW-0199, 9 vols., December 1988.

U.S. Environmental Protection Agency, "Environmental Radiation Protection Standards for the Management and Disposal of Spent Nuclear Fuel, High-Level and Transuranic Wastes [Proposed Rule]," *Federal Register*, vol. 58, no. 242, December 20, 1993, pp. 66398-66416.

Wu, Y.T., *et al.*, "Sensitivity and Uncertainty Analyses Applied to One-Dimensional Radionuclide Transport in a Layered Fractured Rock, Volume 2: Evaluation of the Limit State Approach," U.S. Nuclear Regulatory Commission, NUREG/CR-5917, December 1992. [Prepared by the Center for Nuclear Waste Regulatory Analyses.]

APPENDIX A
LHS-SAMPLED INPUT PARAMETERS

The following is a list of parameters used by the total-system performance assessment computer code (including its modules) in the Iterative Performance Assessment Phase 2 demonstration. It includes constants that were considered as "global parameters" (see Section 2.1.5). The list does not include parameters or constants internal to a particular computational module. All dimensions are in meters-kilograms-years; open brackets ([ ]) are dimensionless parameters.

The parameters sampled for the base case include those parameters listed for the *C14*, *SOTEC*, and *FLOWMOD* modules (described in Section 2.1.3). The parameters sampled for the fully disturbed case are those parameters listed for the *C14*, *FLOWMOD*, *SOTEC*, *VOLCANO*, and *DRILLO* modules. The infiltration rate used for the fully disturbed case was the disturbed infiltration.

Type of Distibution Value (or Range in Value)		*Parameter Name*	*Module*	*Parameter Desciption*	*Basis for Parameter Assignment*
CONSTANT 0.0		alpha	C14	gas dispersivity [m^2/yr]	Assumed
LOGNORMAL 6.5E-17	5.5E-15	AKR(1)	C14	fracture permeability of layer [m^2] (Tiva Canyon)	Klavetter and Peters (1986) (+ /- one order of magnitude of the reported value)
LOGNORMAL 1.6E-16	1.6E-14	AKR(2)	C14	fracture permeability of layer [m^2] (Paintbrush)	Klavetter and Peters (1986) (+ /- one order of magnitude of the reported value)
LOGNORMAL 3.24E-17	3.24E-15	AKR(3)	C14	fracture permeability of layer [m^2] (Topopah Spring)	Klavetter and Peters (1986) (+ /- one order of magnitude of the highest reported value)
LOGNORMAL 9.7E-17	9.7E-15	AKR(4)	C14	fracture permeability of layer [m^2] (Calico Hills, vitric)	Klavetter and Peters (1986) (+ /- one order of magnitude of the reported value)
LOGNORMAL 9.7E-17	9.7E-15	AKR(5)	C14	fracture permeability of layer [m^2] (Calico Hills, zeolitic)	Klavetter and Peters (1986) (+ /- one order of magnitude of the reported value)
CONSTANT 0.00014		pork(1)	C14	fracture porosity of layer [ ] (Tiva Canyon)	Klavetter and Peters (1986) (reported value)
CONSTANT 0.000027		pork(2)	C14	fracture porosity of layer [ ] (Paintbush)	Klavetter and Peters (1986) (reported value)

Type of Distibution Value (or Range in Value)		*Parameter Name*	*Module*	*Parameter Desciption*	*Basis for Parameter Assignment*
CONSTANT 0.000041		pork(3)	C14	fracture porosity of layer [ ] (Topopah Spring)	Klavetter and Peters (1986) (reported value)
CONSTANT 0.000046		pork(4)	C14	fracture porosity of layer [ ] (Calico Hills, vitric)	Klavetter and Peters (1986) (reported value)
CONSTANT 0.000046		pork(5)	C14	fracture porosity of layer [ ] (Calico Hills, zeolitic)	Klavetter and Peters (1986) (reported value)
UNIFORM 10.0	100.	retardk(1)	C14	retardation factor [ ] (Tiva Canyon)	Based on geochemical model presented in Appendix K
UNIFORM 10.0	100.	retardk(2)	C14	retardation factor [ ] (Paintbrush)	Based on geochemical model presented in Appendix K
UNIFORM 10.0	100.	retardk(3)	C14	retardation factor [ ] (Topopah Spring)	Based on geochemical model presented in Appendix K
UNIFORM 10.0	100.	retardk(4)	C14	retardation factor [ ] (Calico Hills, vitric)	Based on geochemical model presented in Appendix K
UNIFORM 10.0	100.	retardk(5)	C14	retardation factor [ ] (Calico Hills, zeolitic)	Based on geochemical model presented in Appendix K
LOGNORMAL 3.6E-19	1.2E-18	permm (1)	FLOWMOD	matrix permeability [m^2] (Topopah Spring)	Peters et al. (1984) (reported range and correlation length considerations)
LOGNORMAL 3.9E-15	2.0E-14	permm (2)	FLOWMOD	matrix permeability [m^2] (Calico Hills, vitric)	Peters *et al.* (1984) (reported range and correlation length considerations)
LOGNORMAL 1.3E-20	6.7E-19	permm (3)	FLOWMOD	matrix permeability [m^2] (Calico Hills, zeolitic)	Peters *et al.* (1984) (reported range and correlation length considerations)
LOGNORMAL 1.9E-16	9.6E-16	permm (4)	FLOWMOD	matrix permeability [m^2] (Prow Pass)	Peters *et al.* (1984) (reported range and correlation length considerations)
LOGNORMAL 5.1E-18	1.5E-17	permm (5)	FLOWMOD	matrix permeability [m^2] (Upper Crater Flat)	Peters *et al.* (1984) (reported range and correlation length considerations)

Type of Distibution Value (or Range in Value)		*Parameter Name*	*Module*	*Parameter Desciption*	*Basis for Parameter Assignment*
LOGNORMAL 3.5E-16	4.4E-16	permm (6)	FLOWMOD	matrix permeability [m2] (Bullfrog)	Peters *et al.* (1984) (reported range and correlation length considerations)
LOGNORMAL 4.1E-18	1.6E-17	permm (7)	FLOWMOD	matrix permeability [m^2] (Middle Crater Flat)	Assumed same as Upper Crater Flat
LOGNORMAL 1.1E-16	1.9E-16	permf (1)	FLOWMOD	fracture permeability [m^2] (Topopah Spring)	Klavetter and Peters (1986) (reported range and correlation length considerations)
LOGNORMAL 5.6E-16	1.2E-15	permf (2)	FLOWMOD	fracture permeability [m^2] (Calico Hills, vitric)	Klavetter and Peters (1986) (+/- 50 percent of reported value and correlation length considerations)
LOGNORMAL 6.2E-16	9.9E-16	permf (3)	FLOWMOD	fracture permeability [m^2] (Calico Hills, zeolitic)	Klavetter and Peters (1986) (+/- 50 percent of reported value and correlation length considerations)
LOGNORMAL 3.9E-17	8.1E-17	permf (4)	FLOWMOD	fracture permeability [m^2] (Prow Pass)	Klavetter and Peters (1986) (+/- 50 percent of reportedvalue and correlation length considerations)
LOGNORMAL 6.7E-16	9.8E-16	permf (5)	FLOWMOD	fracture permeability [m^2] (Upper Crater Flat)	Assumed same as Calico Hills
LOGNORMAL 4.9E-17	6.4E-17	permf (6)	FLOWMOD	fracture permeability [m^2] (Bullfrog)	Assumed same as Prow Pass
LOGNORMAL 6.2E-16	9.9E-16	permf (7)	FLOWMOD	fracture permeability [m^2] (Middle Crater Flat)	Assumed same as Calico Hills
UNIFORM 0.06	0.16	porm (1)	FLOWMOD	matrix porosity [ ] (Topopah Spring)	Peters *et al.* (1984) (reported range)
UNIFORM 0.33	0.56	porm (2)	FLOWMOD	matrix porosity [ ] (Calico Hills, vitric)	Peters *et al.* (1984) (+/- 25 percent of mean)
UNIFORM 0.20	0.33	porm (3)	FLOWMOD	matrix porosity [ ] (Calico Hills, zeolitic)	Peters *et al.* (1984) (+/- 25 percent of mean)

Type of Distibution Value (or Range in Value)		*Parameter Name*	*Module*	*Parameter Desciption*	*Basis for Parameter Assignment*
UNIFORM 0.24	0.40	porm (4)	FLOWMOD	matrix porosity [ ] (Prow Pass)	Peters *et al.* (1984) (+ /– 25 percent of mean)
UNIFORM 0.18	0.30	porm (5)	FLOWMOD	matrix porosity [ ] (Upper Crater Flat)	Peters *et al.* (1984) (+ /– 25 percent of mean)
UNIFORM 0.19	0.32	porm (6)	FLOWMOD	matrix porosity [ ] (Bullfrog)	Peters *et al.* (1984) (+ /– 25 percent of mean)
UNIFORM 0.18	0.30	porm (7)	FLOWMOD	matrix porosity [ ] (Middle Crater Flat)	Assumed same as Upper Crater Flat
CONSTANT 4.1E-5		porf (1)	FLOWMOD	fracture porosity [ ] (Topopah Spring)	Klavetter and Peters (1986)
CONSTANT 4.6E-5		porf (2)	FLOWMOD	fracture porosity [ ] (Calico Hills, vitric)	Klavetter and Peters (1986)
CONSTANT 4.6E-5		porf (3)	FLOWMOD	fracture porosity [ ] (Calico Hills, zeolitic)	Klavetter and Peters (1986)
CONSTANT 1.3E-5		porf (4)	FLOWMOD	fracture porosity [ ] (Prow Pass)	Klavetter and Peters (1986)
CONSTANT 4.6E-5		porf (5)	FLOWMOD	fracture porosity [ ] (Upper Crater Flat)	Assumed same as Calico Hills
CONSTANT 1.3E-5		porf (6)	FLOWMOD	fracture porosity [ ] (Bullfrog)	Assumed same as Prow Pass
CONSTANT 4.6E-5		porf (7)	FLOWMOD	fracture porosity [ ] (Middle Crater Flat)	Assumed same as Calico Hills
UNIFORM 1.4	2.2	betam (1)	FLOWMOD	van Genuchten power term [ ] (Topopah Spring – matrix)	Klavetter and Peters (1986) (+ /– 25 percent reported value)
UNIFORM 1.5	4.9	betam (2)	FLOWMOD	van Genuchten power term [ ] (Calico Hills, vitric – matrix)	Klavetter and Peters (1986) (+ /– 25 percent of reported value—lower bound replaced with reported low value in Peters *et al.* (1984))

Type of Distibution Value (or Range in Value)		*Parameter Name*	*Module*	*Parameter Desciption*	*Basis for Parameter Assignment*
UNIFORM 1.2	3.3	betam (3)	FLOWMOD	van Genuchten power term [ ] (Calico Hills, zeolitic - matrix)	Klavetter and Peters (1986) (+/- 25 percent of reported value—upper bound replaced with reported high value in Peters *et al.* (1984))
UNIFORM 2.0	3.4	betam (4)	FLOWMOD	van Genuchten power term [ ] (Prow Pass - matrix)	Klavetter and Peters (1986) (+/- 25 percent of reported value—upper bound replaced with reported high value in Peters *et al.* (1984))
UNIFORM 1.5	2.4	betam (5)	FLOWMOD	van Genuchten power term [ ] (Upper Crater Flat - matrix)	Peters *et al.* (1984) (+/- 25 percent of mean)
UNIFORM 2.3	4.2	betam (6)	FLOWMOD	van Genuchten power term [ ] (Bullfrog - matrix)	Peters *et al.* (1984) (reported range)
UNIFORM 1.5	2.4	betam (7)	FLOWMOD	van Genuchten power term [ ] (Middle Crater Flat - matrix)	Assumed same as Upper Crater Flat
UNIFORM 3.2	5.3	betaf (1)	FLOWMOD	van Genuchten power term [ ] (Topopah Spring - fracture)	Klavetter and Peters (1986) (+/- 25 percent of reported value)
UNIFORM 3.2	5.3	betaf (2)	FLOWMOD	van Genuchten power term [ ] (Calico Hills, vitric - fracture)	Klavetter and Peters (1986) (+/- 25 percent of reported value)
UNIFORM 3.2	5.3	betaf (3)	FLOWMOD	van Genuchten power term [ ] (Calico Hills, zeolitic - frac.)	Klavetter and Peters (1986) (+/- 25 percent of reported value)
UNIFORM 3.2	5.3	betaf (4)	FLOWMOD	van Genuchten power term [ ] (Prow Pass - fracture)	Klavetter and Peters (1986) (+/- 25 percent of reported value)
UNIFORM 3.2	5.3	betaf (5)	FLOWMOD	van Genuchten power term [ ] (Upper Crater Flat - fracture)	Assumed same as Calico Hills
UNIFORM 3.2	5.3	betaf (6)	FLOWMOD	van Genuchten power term [ ] (Bullfrog - fracture)	Assumed same as Prow Pass
UNIFORM 3.2	5.3	betaf (7)	FLOWMOD	van Genuchten power term [ ] (Middle Crater Flat - fracture)	Assumed same as Calico Hills

Type of Distibution Value (or Range in Value)		*Parameter Name*	*Module*	*Parameter Desciption*	*Basis for Parameter Assignment*
CONSTANT 0.0026		grad (1)	FLOWMOD	gradient in saturated zone [ ] (Topopah Spring)	Based on elevation of water table at the Yucca Mountain site
CONSTANT 0.0026		grad (2)	FLOWMOD	gradient in saturated zone [ ] (Calico Hills, vitric)	Based on elevation of water table at the Yucca Mountain site
CONSTANT 0.0026		grad (3)	FLOWMOD	gradient in saturated zone [ ] (Calico Hills, zeolitic)	Based on elevation of water table at the Yucca Mountain site
CONSTANT 0.0026		grad (4)	FLOWMOD	gradient in saturated zone [ ] (Prow Pass)	Based on elevation of water table at the Yucca Mountain site
CONSTANT 0.0026		grad (5)	FLOWMOD	gradient in saturated zone [ ] (Upper Crater Flat)	Based on elevation of water table at the Yucca Mountain site
CONSTANT 0.0026		grad (6)	FLOWMOD	gradient in saturated zone [ ] (Bullfrog)	Based on elevation of water table at the Yucca Mountain site
CONSTANT 0.0026		grad (7)	FLOWMOD	gradient in saturated zone [ ] (Middle Crater Flat)	Based on elevation of water table at the Yucca Mountain site
NORMAL 0.3	30.0	dispersion	FLOWMOD	dispersion length [m]	Assumed
LOGUNIFORM 1.0E-4	5.0E-3	infiltration	FLOWMOD	infiltration rate (undisturbed) [m/yr]	Assumed (similar to IPA Phase 1; see Codell *et al.* (1992))
LOGUNIFORM 5.0E-3	1.0E-2	infiltration (pluvial)	FLOWMOD	infiltration rate [m/yr] (pluvial conditions)	Assumed (similar to IPA Phase 1; see Codell *et al.* (1992))
LOGUNIFORM 0.045	4.5	kdm (1)	FLOWMOD	Cm K_d [m^3/kg] (Topopah Spring)	Codell *et al.* (1992) (+/– one order of magnitude of the mean of log of retradation factors from IPA Phase 1)
LOGUNIFORM 0.328	32.8	kdm (2)	FLOWMOD	Cm K_d [m^3/kg] (Calico Hills, vitric)	Codell *et al.* (1992) (+/– one order of magnitude of the mean of log of retardation factors from IPA Phase 1)

Type of Distibution Value (or Range in Value)		*Parameter Name*	*Module*	*Parameter Desciption*	*Basis for Parameter Assignment*
LOGUNIFORM 0.166	16.6	kdm (3)	FLOWMOD	Cm K_d [m^3/kg] (Calico Hills, zeolitic)	Codell *et al.* (1992) (+/- one order of magnitude of the mean of log of retardation factors from IPA Phase 1)
LOGUNIFORM 0.116	11.6	kdm (4)	FLOWMOD	Cm K_d [m^3/kg] (Prow Pass)	Codell *et al.* (1992) (+/- one order of magnitude of the mean of log of retardation factors from IPA Phase 1)
LOGUNIFORM 0.132	13.2	kdm (5)	FLOWMOD	Cm K_d [m^3/kg] (Upper Crater Flat)	Codell *et al.* (1992) (+/- one order of magnitude of the mean of log of retardation factors from IPA Phase 1)
LOGUNIFORM 0.12	12.0	kdm (6)	FLOWMOD	Cm K_d [m^3/kg] (Bullfrog)	Codell *et al.* (1992) (+/- one order of magnitude of the mean of log of retardation factors from IPA Phase 1)
LOGUNIFORM 0.132	13.2	kdm (7)	FLOWMOD	Cm K_d [m^3/kg] (Middle Crater Flat)	Codell *et al.* (1992) (+/- one order of magnitude of the mean of log of retardation factors from IPA Phase 1)
LOGUNIFORM 2.0E-5	2.0E-3	kdm (15)	FLOWMOD	U K_d [m^3/kg] (Topopah Spring)	Meijer (1990) (+/- one order of magnitude of log mean of reported values—Wells UE25a1, G3, and J13)
LOGUNIFORM 0.002	0.2	kdm (16)	FLOWMOD	U K_d [m^3/kg] (Calico Hills, vitric)	Meijer (1990) (+/- one order of magnitude of the reported value—Well G3)
LOGUNIFORM 0.0001	0.01	kdm (17)	FLOWMOD	U K_d [m^3/kg] (Calico Hills, zeolitic)	Meijer (1990) (+/- one order of magnitude of log mean of reported values—Wells G1 and G2)
CONSTANT 0.0		kdm (18)	FLOWMOD	U K_d [m^3/kg] (Prow Pass)	Assumed to be zero
LOGUNIFORM 8.0E-5	8.0E-3	kdm (19)	FLOWMOD	U K_d [m^3/kg] (Upper Crater Flat)	Same retardation factor as Calico Hills zeolitic (allowances made for density and porosity)

Type of Distibution Value (or Range in Value)		*Parameter Name*	*Module*	*Parameter Desciption*	*Basis for Parameter Assignment*
LOGUNIFORM 0.0002	0.02	kdm (20)	FLOWMOD	U K_d [m^3/kg] (Bullfrog)	Meijer (1990) (+ /- one order of magnitude of log mean of reported values—Wells G1, J13, and UE25a1)
LOGUNIFORM 8.0E-5	8.0E-3	kdm (21)	FLOWMOD	U K_d [m^3/kg] (Middle Crater Flat)	Same retardation factor as Calico Hills zeolitic (allowances made for density and porosity)
LOGUNIFORM 0.081	8.1	kdm (22)	FLOWMOD	Am K_d [m^3/kg] (Topopah Spring)	Meijer (1990) (+ /- one order of magnitude of log mean of reported values—Wells J13, G3, and UE25a1)
LOGUNIFORM 0.081	8.1	kdm (23)	FLOWMOD	Am K_d [m^3/kg] (Calico Hills, vitric)	Assumed same K_d as Topopah Spring
LOGUNIFORM 0.17	17.0	kdm (24)	FLOWMOD	Am K_d [m^3/kg] (Calico Hills, zeolitic)	Meijer (1990) (+ /- one order of magnitude of the reported value—Well G2)
LOGUNIFORM 0.45	45.0	kdm (25)	FLOWMOD	Am K_d [m^3/kg] (Prow Pass)	Meijer (1990) (+ /- one order of magnitude of log mean of reported values—Wells G1 and UE25a1)
LOGUNIFORM 0.136	13.6	kdm (26)	FLOWMOD	Am K_d [m^3/kg] (Upper Crater Flat)	Same retardation factor as Calico Hills zeolitic (allowances made for density and porosity)
LOGUNIFORM 0.014	1.4	kdm (27)	FLOWMOD	Am K_d [m^3/kg] (Bullfrog)	Meijer (1990) (+ /- one order of magnitude of log mean of reported values—Wells J13 and UE25a1)
LOGUNIFORM 0.136	13.6	kdm (28)	FLOWMOD	Am K_d [m^3/kg] (Middle Crater Flat)	Same retardation factor as Calico Hills zeolitic (allowances made for density and porosity)
LOGUNIFORM 0.00045	0.045	kdm (29)	FLOWMOD	Np K_d [m^3/kg] (Topopah Spring)	Meijer (1990) (+ /- one order of magnitude of log mean of reported values—Wells G3 and UE25a1)

Type of Distibution Value (or Range in Value)		*Parameter Name*	*Module*	*Parameter Desciption*	*Basis for Parameter Assignment*
LOGUNIFORM 0.00045	0.045	kdm (30)	FLOWMOD	Np K_d [m^3/kg] (Calico Hills, vitric)	Assumed same K_d as Topopah Spring
LOGUNIFORM 0.00027	0.027	kdm (31)	FLOWMOD	Np K_d [m^3/kg] (Calico Hills, zeolitic)	Meijer (1990) (+/- one order of magnitude of the reported value—Well G2)
LOGUNIFORM 0.00051	0.051	kdm (32)	FLOWMOD	Np K_d [m3/kg] (Prow Pass)	Meijer (1990) (+/- one order of magnitude of log mean of reported values—Wells G1 and UE25a1)
LOGUNIFORM 0.00022	0.022	kdm (33)	FLOWMOD	Np K_d [m^3/kg] (Upper Crater Flat)	Same retardation factor as Calico Hills zeolitic (allowances made for density and porosity)
LOGUNIFORM 0.00051	0.051	kdm (34)	FLOWMOD	Np K_d [m^3/kg] (Bullfrog)	Assumed same K_d as Prow Pass
LOGUNIFORM 0.00022	0.022	kdm (35)	FLOWMOD	Np K_d [m^3/kg] (Middle Crater Flat)	Same retardation factor as Calico Hills zeolitic (allowances made for density and porosity)
LOGUNIFORM 0.017	1.7	kdm (8)	FLOWMOD	Pu K_d [m^3/kg] (Topopah Spring)	Meijer (1990) (+/- one order of magnitude of log mean of reported values—Wells G3, J13, and UE25a1)
LOGUNIFORM 0.017	1.7	kdm (9)	FLOWMOD	Pu K_d [m^3/kg] (Calico Hills, vitric)	Assumed same K_d as Topopah Spring
LOGUNIFORM 0.0066	0.66	kdm (10)	FLOWMOD	Pu K_d [m^3/kg] (Calico Hills, zeolitic)	Meijer (1990) (+/- one order of magnitude of the reported value—Well G2)
LOGUNIFORM 0.013	1.3	kdm (11)	FLOWMOD	Pu K_d [m^3/kg] (Prow Pass)	Meijer (1990) (+/- one order of magnitude of log mean of reported values—Wells G1 and UE25a1)
LOGUNIFORM 0.0053	0.53	kdm (12)	FLOWMOD	Pu K_d [m^3/kg] (Upper Crater Flat)	Same retardation factor as Calico Hills zeolitic (allowances made for density and porosity)

Type of Distibution Value (or Range in Value)		*Parameter Name*	*Module*	*Parameter Desciption*	*Basis for Parameter Assignment*
LOGUNIFORM 0.0094	0.94	kdm (13)	FLOWMOD	Pu K_d [m^3/kg] (Bullfrog)	Meijer (1990) (+ /- one order of magnitude of log mean of reported values—Wells J13 and UE25a1)
LOGUNIFORM 0.0053	0.53	kdm (14)	FLOWMOD	Pu K_d [m^3/kg] (Middle Crater Flat)	same retardation factor as Calico Hills zeolitic (allowances made for density and porosity)
LOGUNIFORM 0.0048	0.48	kdm (36)	FLOWMOD	Th K_d [m^3/kg] (Topopah Spring)	Codell *et al.* (1992) (+ /- one order of magnitude of mean of log of retardation factors from IPA Phase 1)
LOGUNIFORM 0.034	3.4	kdm (37)	FLOWMOD	Th K_d [m^3/kg] (Calico Hills, vitric)	Codell *et al.* (1992) (+ /- one order of magnitude of the mean of log of retardation factors from IPA Phase 1)
LOGUNIFORM 0.017	1.7	kdm (38)	FLOWMOD	Th K_d [m^3/kg] (Calico Hills, zeolitic)	Codell *et al.* (1992) (+ /- one order of magnitude of the mean of log of retardation factors from IPA Phase 1)
LOGUNIFORM 0.012	1.2	kdm (39)	FLOWMOD	Th K_d [m^3/kg] (Prow Pass)	Codell *et al.* (1992) (+ /- one order of magnitude of the mean of log of retardation factors from IPA Phase 1)
LOGUNIFORM 0.014	1.4	kdm (40)	FLOWMOD	Th K_d [m^3/kg] (Upper Crater Flat)	Codell *et al.* (1992) (+ /- one order of magnitude of the mean of log of retardation factors from IPA Phase 1)
LOGUNIFORM 0.013	1.3	kdm(41)	FLOWMOD	Th K_d [m^3/kg] (Bullfrog)	Codell *et al.* (1992) (+ /- one order of magnitude of the mean of log of retardation factors from IPA Phase 1)
LOGUNIFORM 0.014	1.4	kdm(42)	FLOWMOD	Th K_d [m^3/kg] (Middle Crater Flat)	Codell *et al.* (1992) (+ /- one order of magnitude of the mean of log of retardation factors from IPA Phase 1)
LOGUNIFORM 0.15	15.0	kdm (43)	FLOWMOD	Ra K_d [m^3/kg] (Topopah Spring)	Meijer (1990) (+ /- one order of magnitude of the reported value—Well G1)

Type of Distibution Value (or Range in Value)		*Parameter Name*	*Module*	*Parameter Desciption*	*Basis for Parameter Assignment*
LOGUNIFORM 0.15	15.0	kdm (44)	FLOWMOD	Ra K_d [m^3/kg] (Calico Hills, vitric)	Assumed same K_d as Topopah Spring
LOGUNIFORM 0.15	15.0	kdm (45)	FLOWMOD	Ra K_d [m^3/kg] (Calico Hills, zeolitic)	Assumed same K_d as Topopah Spring
LOGUNIFORM 0.15	15.0	kdm(46)	FLOWMOD	Ra K_d [m^3/kg] (Prow Pass)	Assumed same K_d as Topopah Spring
LOGUNIFORM 0.12	12.0	kdm (47)	FLOWMOD	Ra K_d [m^3/kg] (Upper Crater Flat)	Same retardation factor as Calico Hills zeolitic (allowances made for density and porosity)
LOGUNIFORM 0.5	50.0	kdm (48)	FLOWMOD	Ra K_d [m^3/kg] (Bullfrog)	Meijer (1990) (+ /– one order of magnitude of log mean of reported values—Well G1)
LOGUNIFORM 0.12	12.0	kdm (49)	FLOWMOD	Ra K_d [m^3/kg] (Middle Crater Flat)	Same retardation factor as Calico Hills zeolitic (allowances made for density and porosity)
LOGUNIFORM 0.00068	0.068	kdm (50)	FLOWMOD	Pb K_d [m^3/kg] (Topopah Spring)	Codell *et al.* (1992) (+ /– one order of magnitude of the mean of log of retardation factors from IPA Phase 1)
LOGUNIFORM 0.0049	0.49	kdm (51)	FLOWMOD	Pb K_d [m^3/kg] (Calico Hills, vitric)	Codell *et al.* (1992) (+ /– one order of magnitude of the mean of log of retardation factors from IPA Phase 1)
LOGUNIFORM 0.0025	0.25	kdm (52)	FLOWMOD	Pb K_d [m^3/kg] (Calico Hills, zeolitic)	Codell *et al.* (1992) (+ /– one order of magnitude of the mean of log of retardation factors from IPA Phase 1)
LOGUNIFORM 0.0017	0.17	kdm (53)	FLOWMOD	Pb K_d [m^3/kg] (Prow Pass)	Codell *et al.* (1992) (+ /– one order of magnitude of the mean of log of retardation factors from IPA Phase 1)
LOGUNIFORM 0.0020	0.20	kdm (54)	FLOWMOD	Pb K_d [m^3/kg] (Upper Crater Flat)	Codell *et al.* (1992) (+ /– one order of magnitude of the mean of log of retardation factors from IPA Phase 1)

Type of Distibution Value (or Range in Value)		*Parameter Name*	*Module*	*Parameter Desciption*	*Basis for Parameter Assignment*
LOGUNIFORM 0.0018	0.18	kdm (55)	FLOWMOD	Pb K_d [m^3/kg] (Bullfrog)	Codell *et al.* (1992) (+/- one order of magnitude of the mean of log of retardation factors from IPA Phase 1)
LOGUNIFORM 0.0020	0.20	kdm (56)	FLOWMOD	Pb K_d [m^3/kg] (Middle Crater Flat)	Codell *et al.* (1992) (+/- one order of magnitude of the mean of log of retardation factors from IPA Phase 1)
LOGUNIFORM 0.036	3.6	kdm (57)	FLOWMOD	Cs K_d [m^3/kg] (Topopah Spring)	Meijer (1990) (+/- one order of magnitude of log mean of reported values—Wells G1, G3, and UE25a1)
LOGUNIFORM 0.024	2.4	kdm (58)	FLOWMOD	Cs K_d [m^3/kg] (Calico Hills, vitric)	Meijer (1990) (+/- one order of magnitude of log mean of reported values in Topopah Spring unit—Well G3)
LOGUNIFORM 2.2	220.	kdm (59)	FLOWMOD	Cs K_d [m^3/kg] (Calico Hills, zeolitic)	Meijer (1990) (+/- one order of magnitude of log mean of reported values—Wells G1 and G2)
LOGUNIFORM 0.22	22.0	kdm (60)	FLOWMOD	Cs K_d [m^3/kg] (Prow Pass)	Meijer (1990) (+/- one order of magnitude of log mean of reported values—Wells G1, J13, and UE25a1)
LOGUNIFORM 1.76	176.0	kdm (61)	FLOWMOD	Cs K_d [m^3/kg] (Upper Crater Flat)	Same retardation factor as Calico Hills zeolitic (allowances made for density and porosity)
LOGUNIFORM 0.32	32.0	kdm (62)	FLOWMOD	Cs K_d [m^3/kg] (Bullfrog)	Meijer (1990) (+/- one order of magnitude of log mean of reported values—Wells G1, J13, and UE25a1)
LOGUNIFORM 1.76	176.0	kdm (63)	FLOWMOD	Cs K_d [m^3/kg] (Middle Crater Flat)	Same retardation factor as Calico Hills zeolitic (allowances made for density and porosity)
CONSTANT 0.0		kdm (64)	FLOWMOD	I K_d [m^3/kg] (Topopah Spring)	Assumed to be zero

Type of Distibution Value (or Range in Value)		*Parameter Name*	*Module*	*Parameter Desciption*	*Basis for Parameter Assignment*
CONSTANT 0.0		kdm (65)	FLOWMOD	I K_d [m^3/kg] (Calico Hills, vitric)	Assumed to be zero
CONSTANT 0.0		kdm (66)	FLOWMOD	I K_d [m^3/kg] (Calico Hills, zeolitic)	Assumed to be zero
CONSTANT 0.0		kdm(67)	FLOWMOD	I K_d [m^3/kg] (Prow Pass)	Assumed to be zero
CONSTANT 0.0		kdm(68)	FLOWMOD	I K_d [m^3/kg] (Upper Crater Flat)	Assumed to be zero
CONSTANT 0.0		kdm (69)	FLOWMOD	I K_d [m^3/kg] (Bullfrog)	Assumed to be zero
CONSTANT 0.0		kdm (70)	FLOWMOD	I K_d [m^3/kg] (Middle Crater Flat)	Assumed to be zero
LOGUNIFORM 1.0E-6	1.0E-4	kdm (78)	FLOWMOD	Tc K_d [m^3/kg] (Topopah Spring)	Meijer (1990) (+/- one order of magnitude of log mean of reported values—Wells G3 and UE25a1)
CONSTANT 0.0		kdm (79)	FLOWMOD	Tc K_d [m^3/kg] (Calico Hills, vitric)	Assumed to be zero
CONSTANT 0.0		kdm (80)	FLOWMOD	Tc K_d [m^3/kg] (Calico Hills, zeolitic)	Assumed to be zero
LOGUNIFORM 1.7E-5	1.7E-3	kdm (81)	FLOWMOD	Tc K_d [m^3/kg] (Prow Pass)	Meijer (1990) (+/- one order of magnitude of log mean of reported values—Well J13)
CONSTANT 0.0		kdm (82)	FLOWMOD	Tc K_d [m^3/kg] (Upper Crater Flat)	Same retardation factor as Calico Hills zeolitic
LOGUNIFORM 0.00042	0.042	kdm (83)	FLOWMOD	Tc K_d [m^3/kg] (Bullfrog)	Meijer (1990) (+/- one order of magnitude of the reported value—Well UE25a1)
CONSTANT 0.0		kdm (84)	FLOWMOD	Tc K_d [m^3/kg] (Middle Crater Flat)	Same retardation factor as Calico Hills zeolitic

Type of Distibution Value (or Range in Value)		*Parameter Name*	*Module*	*Parameter Desciption*	*Basis for Parameter Assignment*
LOGUNIFORM 0.00037	0.037	kdm (99)	FLOWMOD	Ni K_d [m^3/kg] (Topopah Spring)	Codell *et al.* (1992) (+/- one order of magnitude of the mean of log of retardation factors from IPA Phase 1)
LOGUNIFORM 0.0027	0.27	kdm (100)	FLOWMOD	Ni K_d [m^3/kg] (Calico Hills, vitric)	Codell *et al.* (1992) (+/- one order of magnitude of the mean of log of retardation factors from IPA Phase 1)
LOGUNIFORM 0.0014	0.14	kdm (101)	FLOWMOD	Ni K_d [m^3/kg] (Calico Hills, zeolitic)	Codell *et al.* (1992) (+/- one order of magnitude of the mean of log of retardation factors from IPA Phase 1)
LOGUNIFORM 0.0009	0.09	kdm (102)	FLOWMOD	Ni K_d [m^3/kg] (Prow Pass)	Codell *et al.* (1992) (+/- one order of magnitude of the mean of log of retardation factors from IPA Phase 1)
LOGUNIFORM 0.0011	0.11	kdm (103)	FLOWMOD	Ni K_d [m^3/kg] (Upper Crater Flat)	Codell *et al.* (1992) (+/- one order of magnitude of the mean of log of retardation factors from IPA Phase 1)
LOGUNIFORM 0.001	0.1	kdm (104)	FLOWMOD	Ni K_d [m^3/kg] (Bullfrog)	Codell *et al.* (1992) (+/- one order of magnitude of the mean of log of retardation factors from IPA Phase 1)
LOGUNIFORM 0.0011	0.11	kdm (105)	FLOWMOD	Ni K_d [m^3/kg] (Middle Crater Flat)	Codell *et al.* (1992) (+/- one order of magnitude of the mean of log of retardation factors from IPA Phase 1)
CONSTANT 0.0		kdm (106)	FLOWMOD	C K_d [m^3/kg] (Topopah Spring)	Assumed to be zero
CONSTANT 0.0		kdm (107)	FLOWMOD	C K_d [m^3/kg] (Calico Hills, vitric)	Assumed to be zero
CONSTANT 0.0		kdm (108)	FLOWMOD	C K_d [m^3/kg] (Calico Hills, zeolitic)	Assumed to be zero
CONSTANT 0.0		kdm (109)	FLOWMOD	C K_d [m^3/kg] (Prow Pass)	Assumed to be zero

Type of Distibution Value (or Range in Value)		*Parameter Name*	*Module*	*Parameter Desciption*	*Basis for Parameter Assignment*
CONSTANT 0.0		kdm (110)	FLOWMOD	C K_d [m^3/kg] (Upper Crater Flat)	Assumed to be zero
CONSTANT 0.0		kdm (111)	FLOWMOD	C K_d [m^3/kg] (Bullfrog)	Assumed to be zero
CONSTANT 0.0		kdm (112)	FLOWMOD	C K_d [m^3/kg] (Middle Crater Flat)	Assumed to be zero
LOGUNIFORM 0.00026	0.026	kdm (113)	FLOWMOD	Se K_d [m^3/kg] (Topopah Spring)	Meijer (1990) (+ /- one order of magnitude of log mean of reported values—Well G3)
LOGUNIFORM 0.0003	0.03	kdm (114)	FLOWMOD	Se K_d [m^3/kg] (Calico Hills, vitric)	Meijer (1990) (+ /- one order of magnitude of the reported value—Well G3)
LOGUNIFORM 0.00045	0.045	kdm (115)	FLOWMOD	Se K_d [m^3/kg] (Calico Hills, zeolitic)	Meijer (1990) (+ /- one order of magnitude of log mean of reported values—Wells G1 and G2)
LOGUNIFORM 0.00025	0.025	kdm (116)	FLOWMOD	Se K_d [m^3/kg] (Prow Pass)	Meijer (1990) (+ /- one order of magnitude of the reported value—Well G1)
LOGUNIFORM 0.00036	0.036	kdm (117)	FLOWMOD	Se K_d [m^3/kg] (Upper Crater Flat)	Same retardation factor as Calico Hills zeolitic (allowances made for density and porosity)
LOGUNIFORM 0.0013	0.13	kdm (118)	FLOWMOD	Se K_d [m^3/kg] (Bullfrog)	Meijer (1990) (+ /- one order of magnitude of log mean of reported values—Well G1)
LOGUNIFORM 0.00036	0.036	kdm (119)	FLOWMOD	Se K_d [m^3/kg] (Middle Crater Flat)	Same retardation factor as Calico Hills zeolitic (allowances made for density and porosity)
CONSTANT 0.0		kdm (120)	FLOWMOD	Nb K_d [m^3/kg] (Topopah Spring)	Assumed to be zero
CONSTANT 0.0		kdm (121)	FLOWMOD	Nb K_d [m^3/kg] (Calico Hills, vitric)	Assumed to be zero

Type of Distibution Value (or Range in Value)		*Parameter Name*	*Module*	*Parameter Desciption*	*Basis for Parameter Assignment*
CONSTANT 0.0		kdm (122)	FLOWMOD	Nb K_d [m^3/kg] (Calico Hills, zeolitic)	Assumed to be zero
CONSTANT 0.0		kdm (123)	FLOWMOD	Nb K_d [m^3/kg] (Prow Pass)	Assumed to be zero
CONSTANT 0.0		kdm (124)	FLOWMOD	Nb K_d [m^3/kg] (Upper Crater Flat)	Assumed to be zero
CONSTANT 0.0		kdm (125)	FLOWMOD	Nb K_d [m^3/kg] (Bullfrog)	Assumed to be zero
CONSTANT 0.0		kdm (126)	FLOWMOD	Nb K_d [m^3/kg] (Middle Crater Flat)	Assumed to be zero
LOGUNIFORM 0.0134	1.34	kdm (71)	FLOWMOD	Sn K_d [m^3/kg] (Topopah Spring)	Codell *et al.* (1992) (+ /- one order of magnitude of the mean of log of retardation factors from IPA Phase 1)
LOGUNIFORM 0.097	9.7	kdm (72)	FLOWMOD	Sn K_d [m^3/kg] (Calico Hills, vitric)	Codell *et al.* (1992) (+ /- one order of magnitude of the mean of log of retardation factors from IPA Phase 1)
LOGUNIFORM 0.049	4.9	kdm (73)	FLOWMOD	Sn K_d [m^3/kg] (Calico Hills, zeolitic)	Codell *et al.* (1992) (+ /- one order of magnitude of the mean of log of retardation factors from IPA Phase 1)
LOGUNIFORM 0.034	3.4	kdm (74)	FLOWMOD	Sn K_d [m^3/kg] (Prow Pass)	Codell *et al.* (1992) (+ /- one order of magnitude of the mean of log of retardation factors from IPA Phase 1)
LOGUNIFORM 0.039	3.9	kdm (75)	FLOWMOD	Sn K_d [m^3/kg] (Upper Crater Flat)	Codell *et al.* (1992) (+ /- one order of magnitude of the mean of log of retardation factors from IPA Phase 1)
LOGUNIFORM 0.035	3.5	kdm (76)	FLOWMOD	Sn K_d [m^3/kg] (Bullfrog)	Codell *et al.* (1992) (+ /- one order of magnitude of the mean of log of retardation factors from IPA Phase 1)

Type of Distibution Value (or Range in Value)		*Parameter Name*	*Module*	*Parameter Desciption*	*Basis for Parameter Assignment*
LOGUNIFORM 0.039	3.9	kdm (77)	FLOWMOD	Sn K_d [m^3/kg] (Middle Crater Flat)	Codell *et al.* (1992) (+/- one order of magnitude of the mean of log of retardation factors from IPA Phase 1)
LOGUNIFORM 0.00048	0.048	kdm (85)	FLOWMOD	Zr K_d [m^3/kg] (Topopah Spring)	Codell *et al.* (1992) (+/- one order of magnitude of the mean of log of retardation factors from IPA Phase 1)
LOGUNIFORM 0.0034	0.34	kdm (86)	FLOWMOD	Zr K_d [m^3/kg] (Calico Hills, vitric)	Codell *et al.* (1992) (+/- one order of magnitude of the mean of log of retardation factors from IPA Phase 1)
LOGUNIFORM 0.0017	0.17	kdm (87)	FLOWMOD	Zr K_d [m^3/kg] (Calico Hills, zeolitic)	Codell *et al.* (1992) (+/- one order of magnitude of the mean of log of retardation factors from IPA Phase 1)
LOGUNIFORM 0.0012	0.12	kdm (88)	FLOWMOD	Zr K_d [m^3/kg] (Prow Pass)	Codell *et al.* (1992) (+/- one order of magnitude of the mean of log of retardation factors from IPA Phase 1)
LOGUNIFORM 0.0014	0.14	kdm (89)	FLOWMOD	Zr K_d [m^3/kg] (Upper Crater Flat)	Codell *et al.* (1992) (+/- one order of magnitude of the mean of log of retardation factors from IPA Phase 1)
LOGUNIFORM 0.0013	0.13	kdm (90)	FLOWMOD	Zr K_d [m^3/kg] (Bullfrog)	Codell *et al.* (1992) (+/- one order of magnitude of the mean of log of retardation factors from IPA Phase 1)
LOGUNIFORM 0.0014	0.14	kdm (91)	FLOWMOD	Zr K_d [m^3/kg] (Middle Crater Flat)	Codell *et al.* (1992) (+/- one order of magnitude of the mean of log of retardation factors from IPA Phase 1)
LOGUNIFORM 0.008	0.8	kdm (92)	FLOWMOD	Sr K_d [m^3/kg] (Topopah Spring)	Meijer (1990) (+/- one order of magnitude of log mean of reported values—Wells G1, G3, and UE25a1)
LOGUNIFORM 0.0034	0.34	kdm (93)	FLOWMOD	Sr K_d [m^3/kg] (Calico Hills, vitric)	Meijer (1990) (+/- one order of magnitude of log mean of reported values in Topopah Spring unit—Well G3)

Type of Distibution Value (or Range in Value)		*Parameter Name*	*Module*	*Parameter Desciption*	*Basis for Parameter Assignment*
LOGUNIFORM 0.89	89.0	kdm (94)	FLOWMOD	Sr K_d [m^3/kg] (Calico Hills, zeolitic)	Meijer (1990) (+/- one order of magnitude of log mean of reported values—Wells G1 and G2)
LOGUNIFORM 0.045	4.5	kdm (95)	FLOWMOD	Sr K_d [m^3/kg] (Prow Pass)	Meijer (1990) (+/- one order of magnitude of log mean of reported values—Wells G1, J13, and UE25a1)
LOGUNIFORM 0.71	71.0	kdm (96)	FLOWMOD	Sr K_d [m^3/kg] (Upper Crater Flat)	Same retardation factor as Calico Hills zeolitic (allowances made for density and porosity)
LOGUNIFORM 0.028	2.8	kdm (97)	FLOWMOD	Sr K_d [m^3/kg] (Bullfrog)	Meijer (1990) (+/- one order of magnitude of log mean of reported values—Wells G1, J13, and UE25a1)
LOGUNIFORM 0.71	71.0	kdm (98)	FLOWMOD	Sr K_d [m^3/kg] (Middle Crater Flat)	Same retardation factor as Calico Hills zeolitic (allowances made for density and porosity)
UNIFORM 3.75E4	3.75E5	areao	FLOWMOD	area of discharge [m^2]	Production zone thicknesses from field determinations (see Table 4-9)
UNIFORM 100.	150.	ecorr(1)	SOTEC	baseline corrosion potential [m/V]	Estimate based on Macdonald and Urquidi-Macdonald (1990)
UNIFORM -2.	-0.5	ecorr(2)	SOTEC	factor for temperature effect [ ]	Estimate based on Macdonald and Urquidi-Macdonald (1990)
UNIFORM -3.40	-3.	ecorr(3)	SOTEC	factor for temperature effect on ambient potential [ ]	Estimate based on Macdonald Urquidi-Macdonald (1990)
UNIFORM 100.	300.	ecorr(4)	SOTEC	factor for radiolysis effect [ ]	Estimate based on Macdonald Urquidi-Macdonald (1990)
UNIFORM 0.001	0.023	ecorr(5)	SOTEC	decay rate for gamma emitters [yr^{-1}]	Upper limit based on ^{137}Cs

Type of Distibution Value (or Range in Value)	*Parameter Name*	*Module*	*Parameter Desciption*	*Basis for Parameter Assignment*
UNIFORM 1000. 1500.	ecorr(6)	SOTEC	crevice corrossion potential [mV]	Estimate based on Watson and Postlethwaite (1990)
UNIFORM 1000. 1500.	ecorr(7)	SOTEC	pitting corrossion potential [mV]	Estimate based on Henshall (1991)
LOGUNIFORM 1.E-5 0.001	ecorr(8)	SOTEC	rate for localized corrosion [m/yr]	Assumed
CONSTANT 1.E-7	carbon(1)	SOTEC	thickness of zirconium oxide [m]	Estimate based on Smith and Baldwin (1989)
CONSTANT 1.E-5	carbon(2)	SOTEC	initial radius of UO_2 grain [m]	Estimate based on Einziger and Buchanan (1988)
CONSTANT 1.786E-2	carbon(3)	SOTEC	O_2 concentration outside of particle [kg-mole/m^3]	Atmospheric concentration value
CONSTANT 37.	carbon(4)	SOTEC	density of UO_2 [Kg-mole/m^3]	Assumed
CONSTANT 5.256E-8	carbon(5)	SOTEC	reference diffusion, inner layer [m^2/yr]	Fitted value from empirical model presented in Section 5.6.3
CONSTANT 3.942E-7	carbon(6)	SOTEC	reference diffusion, outer layer [m^2/yr]	Fitted value from empirical model presented in Section 5.6.3
CONSTANT 32.	carbon(7)	SOTEC	activation energy [Kcal/g-mole]	Fitted value from empirical model presented in Section 5.6.3
CONSTANT 473.	carbon(8)	SOTEC	reference temperature [°K]	Assumed
CONSTANT 3.	carbon(9)	SOTEC	moles of UO_2 per mole of O_2 [ ]	Based on stoichiometry assuming U_3O_8 product
CONSTANT 0.001	carbon(10)	SOTEC	radius of UO_2 fragment [m]	See Einziger and Buchanan (1988)

Type of Distibution Value (or Range in Value)		*Parameter Name*	*Module*	*Parameter Desciption*	*Basis for Parameter Assignment*
CONSTANT 6.1E-4		carbon(11)	SOTEC	thickness of cladding [m]	See Smith and Baldwin (1989)
CONSTANT 7.2E-4		carbon(12)	SOTEC	curies ^{14}C/kg in UO_2 [Ci/kg]	See Park (1992)
CONSTANT 4.89E-4		carbon(13)	SOTEC	curies ^{14}C/kg in cladding [Ci/kg]	See Park (1992)
CONSTANT 2.48E-5		carbon(14)	SOTEC	curies ^{14}C/kg in ZrO_2 [Ci/kg]	See Park (1992)
CONSTANT 6.2E-6		carbon(15)	SOTEC	curies ^{14}C/kg in grain and gap [Ci/kg]	See Park (1992)
LOGUNIFORM 1.0E-5	1.0E-3	forwar(1)	SOTEC	UO_2 alteration rate [1/yr] (repository sub-area No. 1)	Estimate based on Grambow (1989)
LOGUNIFORM 1.0E-5	1.0E-3	forwar(2)	SOTEC	UO_2 alteration rate [1/yr] (repository sub-area No. 2)	Estimate based on Grambow (1989)
LOGUNIFORM 1.0E-5	1.0E-3	forwar(3)	SOTEC	UO_2 alteration rate [1/yr] (repository sub-area No. 3)	Estimate based on Grambow (1989)
LOGUNIFORM 1.0E-5	1.0E-3	forwar(4)	SOTEC	UO_2 alteration rate [1/yr] (repository sub-area No. 4)	Estimate based on Grambow (1989)
LOGUNIFORM 1.0E-5	1.0E-3	forwar(5)	SOTEC	UO_2 alteration rate [1/yr] (repository sub-area No. 5)	Estimate based on Grambow (1989)
LOGUNIFORM 1.0E-5	1.0E-3	forwar(6)	SOTEC	UO_2 alteration rate [1/yr] (repository sub-area No. 6)	Estimate based on Grambow (1989)
LOGUNIFORM 1.0E-5	1.0E-3	forwar(7)	SOTEC	UO_2 alteration rate [1/yr] (repository sub-area No. 7)	Estimate based on Grambow (1989)
UNIFORM 0.0	1.0	warea(1)	SOTEC	fraction of waste packages contacted [ ] (repository sub-area No. 1)	Assumed

Type of Distibution Value (or Range in Value)	*Parameter Name*	*Module*	*Parameter Desciption*	*Basis for Parameter Assignment*
UNIFORM 0.0 1.0	warea(2)	SOTEC	fraction of waste packages contacted [ ] (repository sub-area No. 2)	Assumed
UNIFORM 0.0 1.0	warea(3)	SOTEC	fraction of waste packages contacted [ ] (repository sub-area No. 3)	Assumed
UNIFORM 0.0 1.0	warea(4)	SOTEC	fraction of waste packages contacted [ ] (repository sub-area No. 4)	Assumed
UNIFORM 0.0 1.0	warea(5)	SOTEC	fraction of waste packages contacted [ ] (repository sub-area No. 5)	Assumed
UNIFORM 0.0 1.0	warea(6)	SOTEC	fraction of waste packages contacted [ ] (repository sub-area No. 6)	Assumed
UNIFORM 0.0 1.0	warea(7)	SOTEC	fraction of waste packages contacted [ ] (repository sub-area No. 7)	Assumed
UNIFORM 0.08 0.2	rpor(1,1)	SOTEC	porosity in near field [ ] (repository sub-area No. 1)	Assumed (based on crushed tuff)
UNIFORM 0.08 0.2	rpor(2,1)	SOTEC	porosity in near field [ ] (repository sub-area No. 2)	Assumed (based on crushed tuff)
UNIFORM 0.08 0.2	rpor(3,1)	SOTEC	porosity in near field [ ] (repository sub-area No. 3)	Assumed (based on crushed tuff)
UNIFORM 0.08 0.2	rpor(4,1)	SOTEC	porosity in near field [ ] (repository sub-area No. 4)	Assumed (based on crushed tuff)
UNIFORM 0.08 0.2	rpor(5,1)	SOTEC	porosity in near field [ ] (repository sub-area No. 5)	Assumed (based on crushed tuff)
UNIFORM 0.08 0.2	rpor(6,1)	SOTEC	porosity in near field [ ] (repository sub-area No. 6)	Assumed (based on crushed tuff)
UNIFORM 0.08 0.2	rpor(7,1)	SOTEC	porosity in near field [ ] (repository sub-area No. 7)	Assumed (based on crushed tuff)

Type of Distibution Value (or Range in Value)		*Parameter Name*	*Module*	*Parameter Desciption*	*Basis for Parameter Assignment*
LOGUNIFORM 5.7E-6	5.7E-3	rdiff(1,1)	SOTEC	diffusion coefficient in near field [m^2/yr] (layer No. 1)	Assumed
LOGUNIFORM 5.7E-6	5.7E-3	rdiff(1,2)	SOTEC	diffusion coefficient in near field [m^2/yr] (layer No. 2)	Assumed
LOGUNIFORM 5.7E-6	5.7E-4	rdiff(1,3)	SOTEC	diffusion coefficient in near field [m^2/yr] (layer No. 3)	Assumed
LOGUNIFORM 5.7E-6	5.7E-4	rdiff(1,4)	SOTEC	diffusion coefficient in near field [m^2/yr] (layer No. 4)	Assumed
UNIFORM 0.0	1.2	volmax(1)	SOTEC	max. vol. of water in waste package [m^3] (repository sub-area No. 1)	Upper limit based on volume of Site Characterization Plan (SCP) containers and fuel (see DOE, 1988a)
UNIFORM 0.0	1.2	volmax(2)	SOTEC	max. vol. of water in waste package [m^3] (repository sub-area No. 2)	Upper limit based on volume of SCP containers and fuel (see DOE, 1988a)
UNIFORM 0.0	1.2	volmax(3)	SOTEC	max. vol. of water in waste package [m^3] (repository sub-area No. 3)	Upper limit based on volume of SCP containers and fuel (see DOE, 1988a)
UNIFORM 0.0	1.2	volmax(4)	SOTEC	max. vol. of water in waste package [m^3] (repository sub-area No. 4)	Upper limit based on volume of SCP containers and fuel (see DOE, 1988a)
UNIFORM 0.0	1.2	volmax(5)	SOTEC	max. vol. of water in waste package [m^3] (repository sub-area No. 5)	Upper limit based on volume of SCP containers and fuel (see DOE, 1988a)
UNIFORM 0.0	1.2	volmax(6)	SOTEC	max. vol. of water in waste package [m^3] (repository sub-area No. 6)	Upper limit based on volume of SCP containers and fuel (see DOE, 1988a)
UNIFORM 0.0	1.2	volmax(7)	SOTEC	max. vol. of water in waste package [m^3] (repository sub-area No. 7)	Upper limit based on volume of SCP containers and fuel (see DOE, 1988a)
LOGNORMAL 2.3	131.2	rde(1)	SOTEC	Cm retardation coefficient [ ]	Assumed (based on crushed tuff)
LOGNORMAL 1.003	1.325	rde(3)	SOTEC	U retardation coefficient [ ]	Assumed (based on crushed tuff)

2

IMAGE EVALUATION TEST TARGET (MT-3)

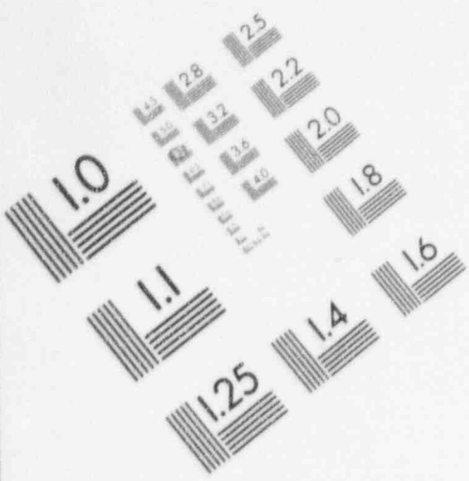

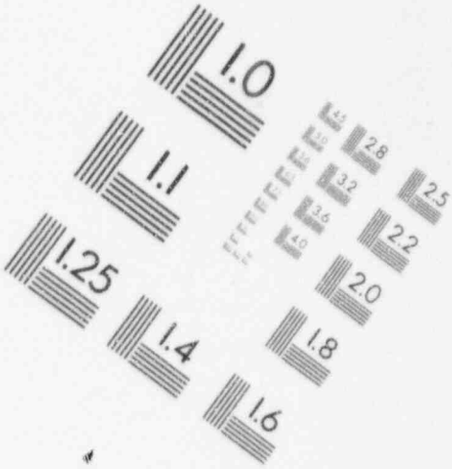

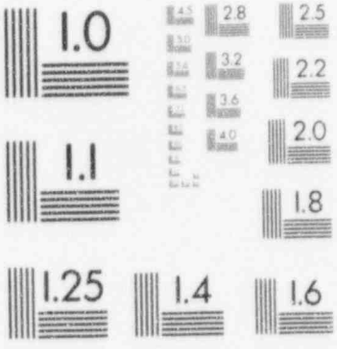

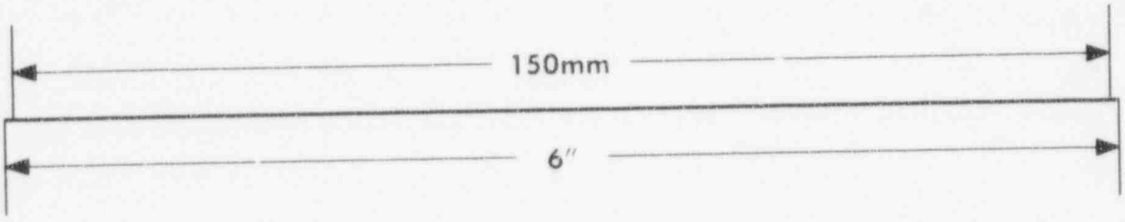

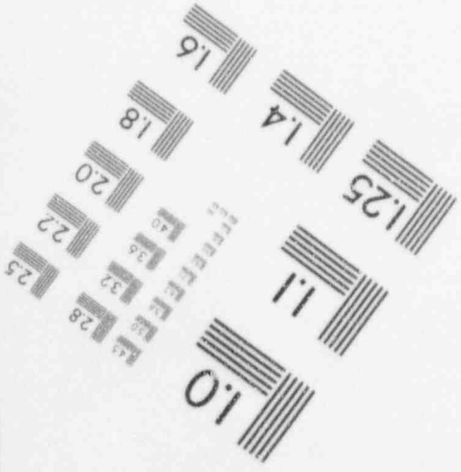

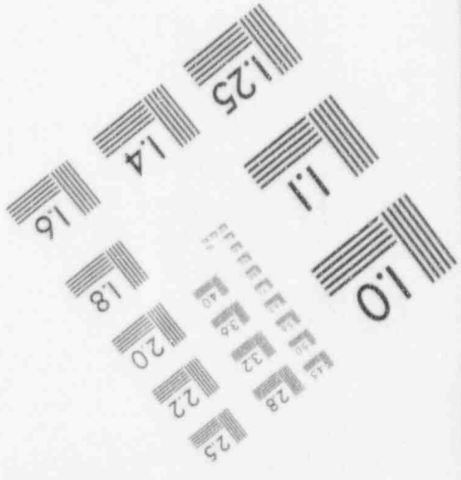

PHOTOGRAPHIC SCIENCES CORPORATION
770 BASKET ROAD
P.O. BOX 338
WEBSTER, NEW YORK 14580
(716) 265-1600

2

IMAGE EVALUATION TEST TARGET (MT-3)

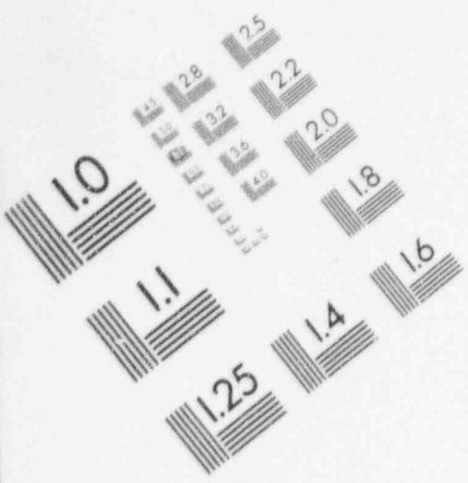

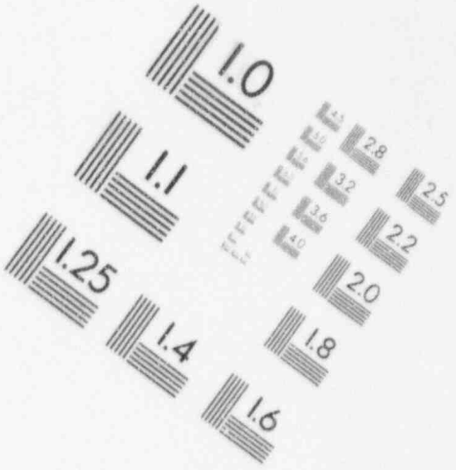

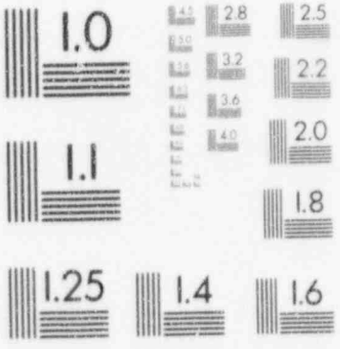

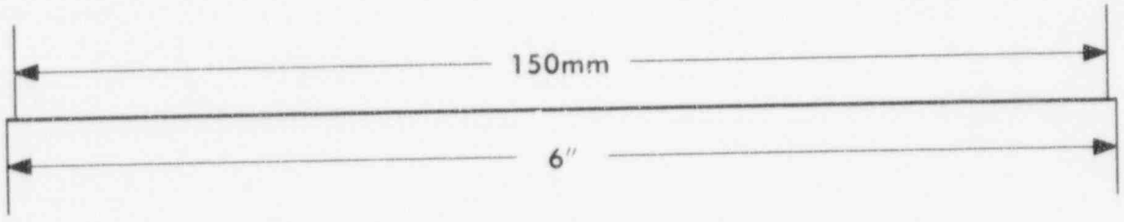

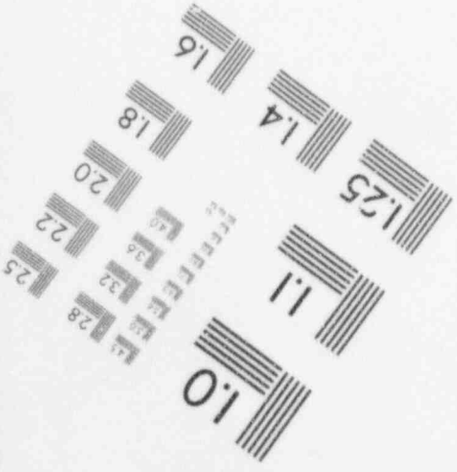

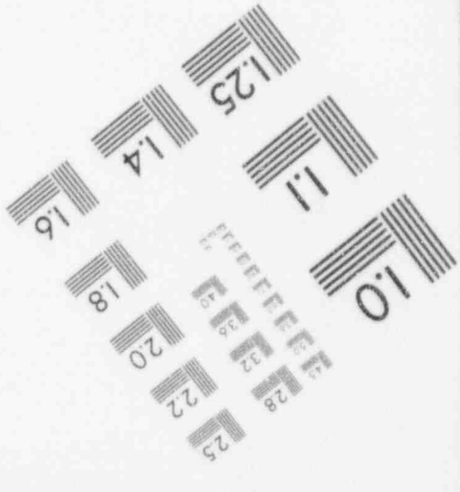

PHOTOGRAPHIC SCIENCES CORPORATION
770 BASKET ROAD
P.O. BOX 338
WEBSTER, NEW YORK 14580
(716) 265-1600

2

IMAGE EVALUATION TEST TARGET (MT-3)

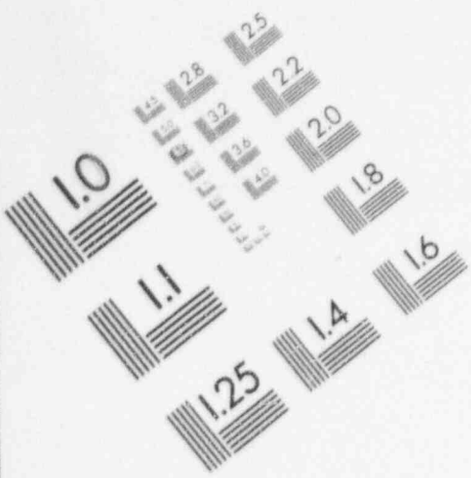

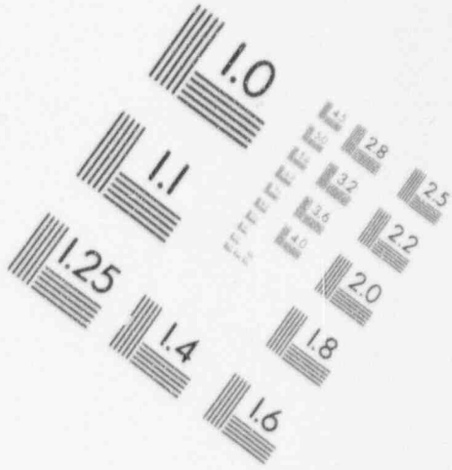

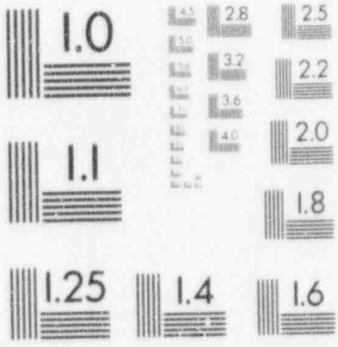

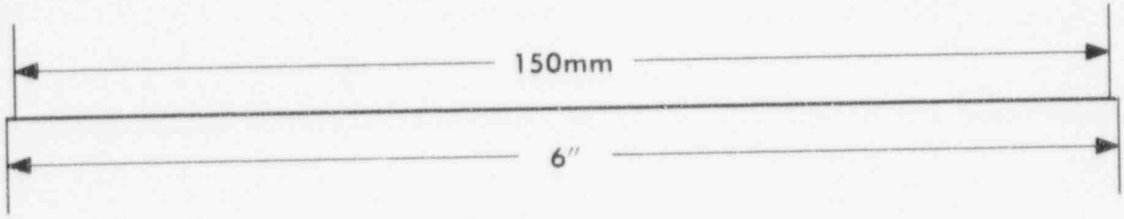

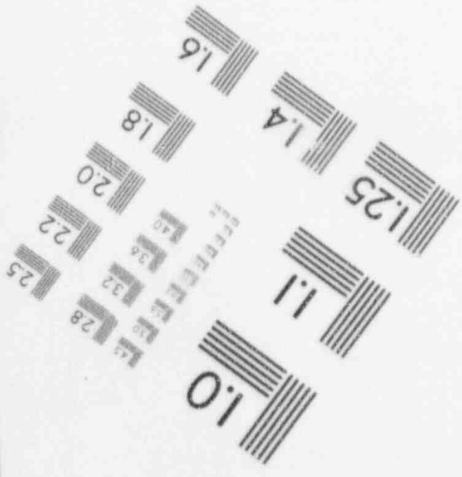

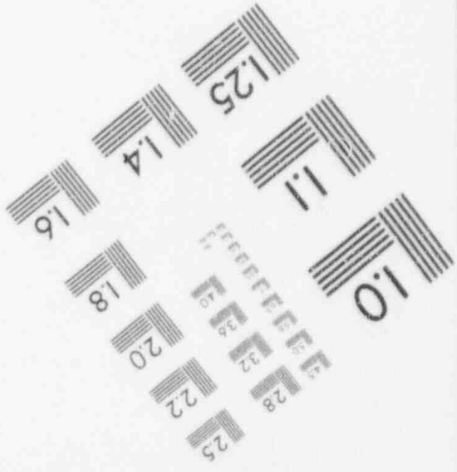

PHOTOGRAPHIC SCIENCES CORPORATION
770 BASKET ROAD
P.O. BOX 338
WEBSTER, NEW YORK 14580
(716) 265-1600

Type of Distibution Value (or Range in Value)		*Parameter Name*	*Module*	*Parameter Desciption*	*Basis for Parameter Assignment*
LOGNORMAL 2.79	165.4	rde(4)	SOTEC	Am retardation coefficient [ ]	Assumed (based on crushed tuff)
LOGNORMAL 1.008	1.81	rde(5)	SOTEC	Np retardation coefficient [ ]	Assumed (based on crushed tuff)
LOGNORMAL 1.3	33.6	rde(2)	SOTEC	Pu retardation coefficient [ ]	Assumed (based on crushed tuff)
LOGNORMAL 1.76	77.5	rde(6)	SOTEC	Th retardation coefficient [ ]	Assumed (based on crushed tuff)
LOGNORMAL 3.44	245.2	rde(7)	SOTEC	Ra retardation coefficient [ ]	Assumed (based on crushed tuff)
LOGNORMAL 1.39	40.07	rde(8)	SOTEC	Pb retardation coefficient [ ]	Assumed (based on crushed tuff)
LOGNORMAL 1.68	69.4	rde(9)	SOTEC	Cs retardation coefficient [ ]	Assumed (based on crushed tuff)
CONSTANT 1.0		rde(10)	SOTEC	I retardation coefficient [ ]	Assumed (based on crushed tuff)
LOGNORMAL 1.0002	1.016	rde(12)	SOTEC	Tc retardation coefficient [ ]	Assumed (based on crushed tuff)
LOGNORMAL 1.08	8.81	rde(15)	SOTEC	Ni retardation coefficient [ ]	Assumed (based on crushed tuff)
CONSTANT 1.0		rde(16)	SOTEC	C retardation coefficient [ ]	Assumed (based on crushed tuff)
LOGNORMAL 1.007	1.65	rde(17)	SOTEC	Se retardation coefficient [ ]	Assumed (based on crushed tuff)
CONSTANT 1.0		rde(18)	SOTEC	Nb retardation coefficient [ ]	Assumed (based on crushed tuff)

Type of Distibution Value (or Range in Value)		*Parameter Name*	*Module*	*Parameter Desciption*	*Basis for Parameter Assignment*
CONSTANT 1.23		rde(11)	SOTEC	Sn retardation coefficient [ ]	Assumed (based on crushed tuff)
CONSTANT 1.39		rde(13)	SOTEC	Zr retardation coefficient [ ]	Assumed (based on crushed tuff)
CONSTANT 1.19		rde(14)	SOTEC	Sr retardation coefficient [ ]	Assumed (based on crushed tuff)
LOGUNIFORM 2.56E-7	5.E-4	sol(1)	SOTEC	Cm solubility [kg/m^3]	Assumed
LOGUNIFORM 4.E-8	3.E-5	sol(3)	SOTEC	U solubility [kg/m^3]	Assumed
LOGUNIFORM 1.E-6	3.E-4	sol(4)	SOTEC	Am solubility [kg/m^3]	Assumed
LOGUNIFORM 1.4E-4	0.0237	sol(5)	SOTEC	Np solubility [kg/m^3]	Assumed
LOGUNIFORM 2.E-7	5.E-4	sol(2)	SOTEC	Pu solubility [kg/m^3]	Assumed
LOGUNIFORM 2.E-12	1.E-4	sol(6)	SOTEC	Th solubility [kg/m^3]	Assumed
LOGUNIFORM 9.E-6	9.E-5	sol(7)	SOTEC	Ra solubility [kg/m^3]	Assumed
LOGUNIFORM 2.1E-6	6.3E-4	sol(8)	SOTEC	Pb solubility [kg/m^3]	Assumed
CONSTANT 1.0		sol(9)	SOTEC	Cs solubility [kg/m^3]	Assumed
CONSTANT 1.0		sol(10)	SOTEC	I solubility [kg/m^3]	Assumed

Type of Distibution Value (or Range in Value)		*Parameter Name*	*Module*	*Parameter Desciption*	*Basis for Parameter Assignment*
CONSTANT 1.0		sol(12)	SOTEC	Tc solubility [kg/m^3]	Assumed
LOGUNIFORM 2.8E-7	1.7E-3	sol(15)	SOTEC	Ni solubility [kg/m^3]	Assumed
CONSTANT 1.0		sol(16)	SOTEC	C solubility [kg/m^3]	Assumed
CONSTANT 1.0		sol(17)	SOTEC	Se solubility [kg/m^3]	Assumed
CONSTANT 1.0		sol(18)	SOTEC	Nb solubility [kg/m^3]	Assumed
CONSTANT 5.E-9		sol(11)	SOTEC	Sn solubility [kg/m^3]	Assumed
CONSTANT 4.E-9		sol(13)	SOTEC	Zr solubility [kg/m^3]	Assumed
CONSTANT 8.E-2		sol(14)	SOTEC	Sr solubility [kg/m^3]	Assumed
UNIFORM 0.0	0.4	funnel(1)	SOTEC	fluid capture area of canister [m^2] (repository sub-area No. 1)	Upper limit based on twice the cross-sectional area of SCP emplacement hole (see DOE, 1988b)
UNIFORM 0.0	0.4	funnel(2)	SOTEC	fluid capture area of canister [m^2] (repository sub-area No. 2)	Upper limit based on twice the cross-sectional area of SCP emplacement hole (see DOE, 1988b)
UNIFORM 0.0	0.4	funnel(3)	SOTEC	fluid capture area of canister [m^2] (repository sub-area No. 3)	Upper limit based on twice the cross-sectional area of SCP emplacement hole (see DOE, 1988b)
UNIFORM 0.0	0.4	funnel(4)	SOTEC	fluid capture area of canister [m^2] (repository sub-area No. 4)	Upper limit based on twice the cross-sectional area of SCP emplacement hole (see DOE, 1988b)

Type of Distibution Value (or Range in Value)		*Parameter Name*	*Module*	*Parameter Desciption*	*Basis for Parameter Assignment*
UNIFORM 0.0	0.4	funnel(5)	SOTEC	fluid capture area of canister [m^2] (repository sub-area No. 5)	Upper limit based on twice the cross-sectional area of SCP emplacement hole (see DOE, 1988b)
UNIFORM 0.0	0.4	funnel(6)	SOTEC	fluid capture area of canister [m^2] (repository sub-area No. 6)	Upper limit based on twice the cross-sectional area of SCP emplacement hole (see DOE, 1988b)
UNIFORM 0.0	0.4	funnel(7)	SOTEC	fluid capture area of canister [m^2] (repository sub-area No. 7)	Upper limit based on twice the cross-sectional area of SCP emplacement hole (see DOE, 1988b)
UNIFORM 0.0	10000.	time	VOLCANO	time of occurrence of volcanic event [yr]	Assumed random over performance period (assumed constant probability)
UNIFORM 0.0	1.0	u1	VOLCANO	probabilities of intrusive magmatism (dike: 0.0–0.9) and extrusive magmatism (cone: 0.9–1.0) [ ]	Assumed
UNIFORM 0.0	1.0	u2	VOLCANO	location scaling factor (dike X_0/cone X_{center}) [ ]	Assumed random over the simulation area
UNIFORM 0.0	1.0	u3	VOLCANO	location scaling factor (dike Y_0/cone Y_{center}) [ ]	Assumed random over the simulation area
UNIFORM 0.0	1.0	u4	VOLCANO	dike area scaling factor [ ]	Assumed (see Section 6.5.3.2)
UNIFORM 0.0	1.0	u5	VOLCANO	scaling factor for dike length [ ]	Assumed (see Section 6.5.3.2)
UNIFORM 0.0	1.0	u6	VOLCANO	scaling factor for dike angle [ ]	Assumed (see Section 6.5.3.2)
UNIFORM 0.0	1.0	u7	VOLCANO	scaling factor for radius of magma conduit of cone [ ] (minimum of 25 meters and maximum of 100 meters)	Assumed (see Section 6.5.3.2)

Type of Distibution Value (or Range in Value)		*Parameter Name*	*Module*	*Parameter Desciption*	*Basis for Parameter Assignment*
NORMAL 4	27	nbore	DRILLO	total number of boreholes drilled [ ]	Poisson distribution centered around the number of drilling events calculated from U.S. Environmental Protection Agency Appendix B guidance (see EPA, 1993; 58 *FR* 7936)
UNIFORM 0.02	0.1	radius	DRILLO	radius of borehole [m]	Assumed based on current exploratory drilling practice
UNIFORM 0.0	1.0	hit(1 through 27)	DRILLO	indicator for borehole No. 1 through No. 27 interception of a waste package [ ] (A minimum of 4 and a maximum of 27 hit indicators are used. A hit indicator is sampled separately for each borehole. The number of boreholes is determined by the sampled parameter *nbore* which ranges from 4 to 27.)	See Section 6.3.4
UNIFORM 100.0	9900.0	Td(1 through 27)	DRILLO	time at which drilling occurs for boreholes No. 1 through No. 27 [yr] (A minimum of 4 and a maximum of 27 hit indicators are used. A hit indicator is sampled separately for each borehole. The number of boreholes is determined by the sampled parameter *nbore* which ranges from 4 to 27.)	Time of drilling randomly occurs after institutional control (100 years) and before end of performance period (9900 years used as an upper limit to allow at least one time step over the 10,000 year performance period)

UNIFORM
0.0
	1.0	Regn(1 through 27)	DRILLO	repository region locator for boreholes No. 1 through No. 27 [ ] (A minimum of 4 and a maximum of 27 region locators are used. A region locator is sampled separately for each borehole. The number of boreholes is determined by the sampled parameter *nbore* which ranges from 4 to 27.)	Sampled value is compared to fraction of total area of each region to locate the borehole in one of the 7 repository sub-areas:
					sub-area 1 = 0.00 to 0.06;
					sub-area 2 = 0.06 to 0.33;
					sub-area 3 = 0.33 to 0.55;
					sub-area 4 = 0.55 to 0.68;
					sub-area 5 = 0.68 to 0.73;
					sub-area 6 = 0.73 to 0.96; and
					sub-area 7 = 0.96 to 1.00.

Type of Distibution Value (or Range in Value)	*Parameter Name*	*Module*	*Parameter Desciption*	*Basis for Parameter Assignment*
UNIFORM 0.0 1.0	U	SEISMO	comparitive number to determine whether a representative (they all fail or none fail) waste package is failed or not [ ] (if "U" is less than the failure probability, the representative waste package is assumed to be failed,and thus all the packages are failed)	See Section 6.4.4

References

Codell, R.B., *et al.*, "Initial Demonstration of the NRC's Capability to Conduct a Performance Assessment for a High-Level Waste Repository," U.S. Nuclear Regulatory Commission, NUREG–1327, May 1992.

Einziger, R.E. and H.C. Buchanan, "Long-Term, Low-Temperature Oxidation of PWR Spent Fuel," Richland, Washington, Westinghouse Hanford Co, WHC–EP–0070, April 1988.

Grambow, B., "Spent Fuel Dissolution and Oxidation: An Evaluation of Literature Data," Stockholm, Sweden, Statens Kärnkraftinspektion (SKI) [Swedish Nuclear Power Inspectorate], SKI Technical Report 89:13, March 1989.

Henshall, G.A., "Stochastic Models for Predicting Pitting Corrosion Damage of HLRW Containers," American Nuclear Society, *Proceedings of the Topical Meeting on Nuclear Waste Packaging (FOCUS '91)*, September 29–October 2, 1991, Las Vegas, Nevada, pp. 225–232 [1992].

Klavetter, E.A. and R.R. Peters, "Fluid Flow in a Fractured Rock Mass," Albuquerque, New Mexico, Sandia National Laboratories, SAND85–0855, March 1986.

Macdonald, D.D. and M. Urquidi–Macdonald, "Thin-Layer Mixed-Potential Model for the Corrosion of High-Level Nuclear Waste Canisters," *Corrosion*, 46(5):380–390 [1990].

Meijer, A., "Yucca Mountain Project Far-Field Sorption Studies and Data Needs," Los Alamos, New Mexico, Los Alamos National Laboratory, LA–11671–MS, September 1990.

Park, U.S., "Regulatory Overview and Recommendations on a Repository's Release of Carbon-14," San Diego, California, Science Applications International Corporation, January 1992. [Prepared for the U.S. Department of Energy.]

Peters, R.R., *et al.*, "Fracture and Matrix Hydrologic Characteristics of Tuffaceous Materials from Yucca Mountain, Nye County, Nevada," Albuquerque, New Mexico, Sandia National Laboratories, SAND84–1471, December 1984.

Smith, H.D. and D.L. Baldwin, "An Investigation of Thermal Release of ^{14}C from PWR Spent Fuel Cladding," American Nuclear Society, *Proceedings of the Topical Meeting on Nuclear Waste Isolation in the Unsaturated Zone (FOCUS '89)*, September 17–21, 1989, Las Vegas, Nevada, pp. 46–49 [1989].

U.S. Department of Energy, "Chapter 7, Waste Package," in "Site Characterization Plan, Yucca Mountain Site, Nevada Research and Development Area, Nevada," Nevada Operations Office/Yucca Mountain Project Office, Nevada, DOE/RW–0199, Vol. III, Part A, December 1988a.

U.S. Department of Energy, "Chapter 6, Conceptual Design of a Repository," in "Site Characterization Plan, Yucca Mountain Site, Nevada Research and Development Area, Nevada," Nevada Operations Office/Yucca Mountain Project Office, Nevada, DOE/RW–0199, Vol. III, Part A, December 1988b.

U.S. Environmental Protection Agency, "Environmental Radiation Protection Standards for the Management and Disposal of Spent Nuclear Fuel, High-Level and Transuranic Radioactive Wastes [Proposed Rule]," *Federal Register*, vol. 58, no. 26, February 10, 1993, pp. 7924–7936.

Watson, M. and J. Postlethwaite, "Numerical Simulation of Crevice Corrosion of Stainless Steel and Nickel Alloys in Chloride Solutions," *Corrosion*, 46(7):522–530 [1990].

APPENDIX B
HYDROLOGIC AND RADIONUCLIDE TRANSPORT DATA FOR THE GROUND-WATER PATHWAY

B-1 Introduction

Parametric values for use in hydrologic flow and radionuclide transport models were based, when possible, on information published for the Yucca Mountain site. Hydrologic information was based primarily on Peters *et al.* (1984) and Klavetter and Peters (1986), whereas retardation information was based on Meijer (1990) and Thomas (1987). The following tables present the information used from these sources and the resulting ranges and distributions used in the current analysis:

Table	*Information*
B-1	Hydrologic information reported from experimental and modeling studies.
B-2—B-5	Sorption information from batch experiments on crushed tuff.
B-6	Parametric values and ranges used to represent the ground-water pathway.
B-7	Values for sorption coefficients (K_ds).

B-2 Table Information

Table B-1 presents the hydrologic information from Peters *et al.* (1984) and Klavetter and Peters (1986), as well as parametric values used in modeling studies since the publication of the Peters report and information from the U.S. Department of Energy (DOE) Site Characterization Plan (SCP) (DOE, 1988). To assist the correlation to the Yucca Mountain site, the borehole at the site associated with the information taken from Peters *et al.* is identified. Although the values reported from the various studies should only be interpreted based on the purpose for which the modeling was conducted, the values are presented to provide additional insights on differing interpretations of hydrologic properties of unsaturated tuff being examined. One obvious conclusion is that more information is available on, and more studies have concentrated on, the repository unit (Topopah Spring), than on other units present at Yucca Mountain.

Tables B-2 through B-5 present the information from Meijer (1990) used to develop the K_d values for individual hydrogeologic units present at Yucca Mountain (abbreviations used in Tables B-2 and B-3 and throughout the remainder of this appendix are as follows: the prefix *JA* indicates drill hole J-13; the prefix *YM* indicates drill hole UE25a-1; and the other abbreviations in the table are unambiguously labeled). A number of assumptions were used to derive the K_d values; therefore, a more detailed discussion of the interpretation and of the use of the data is given here. (The applicability of the K_d approach is not discussed here. See Section 4.4.2 for more information on the applicability of the K_d approach.)

As discussed in Section 4.2.4, the retardation coefficients for each hydrogeologic unit are calculated using the following equation:

$$R_f = 1.0 + \frac{\rho(1-n)}{\theta} \times K_d \ , \qquad \textbf{(B-1)}$$

where:

R_f = retardation factor;
K_d = distribution coefficient;
θ = moisture content;
ρ = grain density; and
n = porosity.

The values for these parameters are specific to the five hydrogeologic units: Topopah Spring Member of the Paintbrush Tuff (Tpt); Calico Hills nonwelded vitric (CHnv); Calico Hills nonwelded zeolitic (CHnz); Prow Pass Member of the Crater Flat Tuff (Tcp); and Bullfrog Member of the Crater Flat Tuff (Tcb). Experimental values (see Tables B-2 through B-5) were used to determine mean K_d values for a specific hydrogeologic unit, while, for certain elements and hydrogeologic units without data, K_d values were assigned,

Table B–1 Hydrologic Properties for Hydrogeologic Units at the Yucca Mountain Site Reported in Modeling Studies and Experimental Studies (Where appropriate, borehole identification labels are provided after the reference.)

TIVA CANYON (Welded, Devitrified)

Matrix Properties:

Reference	*Grain Density (kg/m^3)*	*Porosity*	*Residual Saturation*	*Saturated Conductivity (m/yr)*	*Alpha (1/m)*	*Beta*
Peters *et al.* (1984) [USW G4]	2490	0.08	0.002	3.1E–4	8.2E–3	1.56
Peters *et al.* (1984) [USW GU3]	2480 – 2490	0.09 – 0.15	0.014 – 0.160	2.2E–5 – 8.5E–5	3.9E–3 – 2.3E–2	1.51 – 2.13
Klavetter and Peters (1986)	2490	0.08	0.002	3.1E–4	8.2E–3	1.56
Dudley *et al.* (1988)	2490	0.08	0.002	3.1E–4	8.2E–3	1.56

Fracture Properties:

Reference	*Fracture Aperture (microns)*	*Fracture Density ($1/m^3$)*	*Porosity*	*Residual Saturation*	*Fracture Conductivity (m/yr)*	*Bulk Conductivity (m/yr)*	*Alpha (1/m)*	*Beta*
Klavetter and Peters (1986)	6.7	20	1.4E–4	0.04	1.2E3	0.17	1.28	4.23
Dudley *et al.* (1988)	6.7	20	1.4E–4	0.04	1.2E3	0.17	1.28	4.23

Table B–1 (continued)

PAINTBRUSH (Non-welded, Vitric)

Matrix Properties:

Reference	*Grain Density* (kg/m^3)	*Porosity*	*Residual Saturation*	*Saturated Conductivity* (*m/yr*)	*Alpha* (*1/m*)	*Beta*
Peters *et al.* (1984) [USW G4]	2450	0.65	0.105	75.6	1.6E–2	10.6
Peters *et al.* (1984) [USW GU3]	[illegible]	0.40 – 0.59	0.084 – 0.114	11.0 – 50.4	1.1E–2 – 1.5E–2	2.53 – 8.88
Klavetter and Peters (1986)	2350	0.40	0.100	12.3	1.5E–2	6.87
Dudley *et al.* (1988)	2350	0.40	0.100	12.3	1.5E–2	6.87

PAINTBRUSH (Non-welded, Vitric)

Fracture Properties:

Reference	*Fracture Aperture* (*microns*)	*Fracture Density* ($1/m^3$)	*Porosity*	*Residual Saturation*	*Fracture Conductivity* (*m/yr*)	*Bulk Conductivity* (*m/yr*)	*Alpha* (*1/m*)	*Beta*
Klavetter and Peters (1986)	27.0	1	2.7E–5	0.04	1.9E4	0.50	1.28	4.23)
Dudley *et al.* (1988)	27.0	1	2.7E–5	0.04	1.9E4	0.50	1.28	4.23

Table B-1 (continued)

TOPOPAH SPRING (Welded, Devitrified)

Matrix Properties:

Reference	*Grain Density (kg/m^3)*	*Porosity*	*Residual Saturation*	*Saturated Conductivity (m/yr)*	*Alpha (1/m)*	*Beta*
Peters *et al.* (1984) [USW G4]	2470 – 2580	0.06 – 0.16	0.058 – 0.120	4.1E-5 – 1.2E-3	2.6E-3 – 1.2E-2	1.56 – 2.12
Peters *et al.* (1984) [USW GU3]	2540	0.08	0.008	4.7E-5	1.2E-2	1.49
Klavetter and Peters (1986)	2580	0.11	0.080	6.0E-4	5.7E-3	1.80
Tsang and Pruess (1987)	2580	0.11	0.080	6.0E-4	5.7E-3	1.80
Dudley *et al.* (1988)	2580	0.11	0.080	6.0E-4	5.7E-3	1.80
Pruess *et al.* (1990)	2550	0.10	9.6E-4	1.0E-2	7.0E-3	1.80
Nitao and Buscheck (1991)	—	0.20	0.080	6.0E-4	—	—
Barnard and Dockery (1991)	2500 – 2570	0.06 – 0.12	0.0 – 0.15	1.6E-4 – 6.3E-4	4.0E-3 – 0.01	1.49 – 2.00
DOE (1988; Table 3-27)						
Lab data	—	0.04 – 0.33	—	1.1E-4 – 0.2	—	—
Field data	—	—	—	260.	—	—

Table B-1 (continued)

TOPOPAH SPRING (Welded, Devitrified)

Fracture Properties:

Reference	*Fracture Aperture (microns)*	*Fracture Density ($1/m^3$)*	*Porosity*	*Residual Saturation*	*Fracture Conductivity (m/yr)*	*Bulk Conductivity (m/yr)*	*Alpha (1/m)*	*Beta*
Peters *et al.* (1984) [USW G4]	6. - 67.	—	—	—	1.1E3 - 1.2E5			
Klavetter and Peters (1986)	4.3 - 5.1	8 - 40	4.1E-5 - 1.8E-4	0.04	5.0E2 - 6.9E2	0.02 - 0.10	1.28	4.23
Tsang and Pruess (1987)	—	—	1.8E-3	0.04	—	5.5	—	4.23
Dudley *et al.* (1988)	4.3 - 5.1	8 - 40	4.1E-5 - 1.8E-4	0.04	5.0E2 - 6.9E2	0.02 - 0.10	1.28	4.23
Pruess *et al.* (1990)	64.15	4.5	2.9E-4	—	1.1E5	30.9	—	—
Nitao and Buscheck (1991)	90.	22	—	0.04	2.6E5	—	—	—
Barnard and Dockery (1991)	6. - 20.	5 - 10	3.0E-5	0.04	1.3E3 - 1.3E4	3.8E-2 - 2.5	1.28	4.23

Table B–1 (continued)

CALICO HILLS (Non-Welded, Vitric)

Matrix Properties:

Reference	*Grain Density (kg/m^3)*	*Porosity*	*Residual Saturation*	*Saturated Conductivity (m/yr)*	*Alpha (1/m)*	*Beta*
Peters *et al.* (1984) [USW GU3]	2350 – 2370	0.43 – 0.46	0.020 – 0.048	.82 – 9.1	1.0E–2 – 4.4E2	1.50 – 4.20
Klavetter and Peters (1986)	2370	0.46	0.041	8.5	1.6E–2	3.87
Dudley *et al.* (1988)	2370	0.46	0.041	85	1.6E–2	3.87

CALICO HILLS (Non-Welded, Vitric)

Fracture Properties:

Reference	*Fracture Aperture (microns)*	*Fracture Density ($1/m^3$)*	*Porosity*	*Residual Saturation*	*Fracture Conductivity (m/yr)*	*Bulk Conductivity (m/yr)*	*Alpha (1/m)*	*Beta*
Peters *et al.* (1984) [USW G4]	22	—	—	—	1.4E4	—	—	—
Klavetter and Peters (1986)	15.5	3	4.6E–5	0.04	6.3E3	0.29	1.28	4.23
Dudley *et al.* (1988)	15.5	3	4.6E–5	0.04	6.3E3	0.29	1.28	4.23

Table B–1 (continued)

CALICO HILLS (Non-Welded, Zeolitic)

Matrix Properties:

Reference	*Grain Density (kg/m^3)*	*Porosity*	*Residual Saturation*	*Saturated Conductivity (m/yr)*	*Alpha (1/m)*	*Beta*
Peters *et al.* (1984) [USW G4]	2230 – 2380	0.22 – 0.30	0.037 – 0.215	7.6E–7 – 5.0E–3	6.0E–4 – 6.0E3	1.46 – 3.32
Klavetter and Peters (1986)	2230	0.28	0.110	6.3E–4	3.1E–3	1.60
Dudley *et al.* (1988)	2230	0.28	0.110	6.3E–4	3.1E–3	1.60
Barnard (1991)	2280 – 2320	0.23 – 0.36	0.0 – 0.15	2.2E–4 – 6.3E–4	2.0E–3 – 5.0E–3	1.37 – 1.65
DOE (1988; Table 3–27)						
Lab data	—	0.20 – 0.34	—	1.5E–3 – 0.11	—	—
Field data	—	—	—	180.	—	—

CALICO HILLS (Non-Welded, Zeolitic)

Fracture Properties:

Reference	*Fracture Aperture (microns)*	*Fracture Density ($1/m^3$)*	*Porosity*	*Residual Saturation*	*Fracture Conductivity (m/yr)*	*Bulk Conductivity (m/yr)*	*Alpha (1/m)*	*Beta*
Peters *et al.* (1984) [USW G4]	6 – 31	—	—	—	9.8E2 – 2.5E4			
Klavetter and Peters (1986)	15.5	3	4.6E–5	0.04	6.3E3	0.29	1.28	4.23
Dudley *et al.* (1988)	15.5	3	4.6E–5	0.04	6.3E3	0.29	1.28	4.23
Barnard and Dockery (1991)	6.0	3	1.8E–5	0.04	9.4E2	0.02	1.28	4.23

Table B–1 (continued)

PROW PASS (Welded, Devitrified)

Matrix Properties:

Reference	*Grain Density (kg/m^3)*	*Porosity*	*Residual Saturation*	*Saturated Conductivity (m/yr)*	*Alpha (1/m)*	*Beta*
Peters *et al.* (1984) [USW G4]	2590	0.24	0.066	5.0E–2 – 4.4E–1	1.4E–2	2.64
Peters *et al.* (1984) [USW GU3]	2570 – 2580	0.32 – 0.39	0.018 – 0.066	4.1E–2 – 2.2E–1	1.4E–2 – 3.1E–2	2.96 – 3.44
Klavetter and Peters (1986)	2590	0.24	0.066	0.14	1.4E–2	2.64
Dudley *et al.* (1988)	2590	0.24	0.066	0.14	1.4E–2	2.64
Barnard and Dockery (1991)	2590	0.25	0.05	0.06 – 1.6	1.0E–2	2.7
DOE (1988; Table 3–27)						
Lab data	—	0.10 – 0.30	—	2.2E–4 – 0.36	—	—
Field data	—	—	—	36.0 – 5.3E2	—	—

Fracture Properties:

Reference	*Fracture Aperture (microns)*	*Fracture Density ($1/m^3$)*	*Porosity*	*Residual Saturation*	*Fracture Conductivity (m/yr)*	*Bulk Conductivity (m/yr)*	*Alpha (1/m)*	*Beta*
Klavetter and Peters (1986)	4.16	3	1.3E–5	0.04	4.4E2	0.02	1.28	4.23
Dudley *et al.* (1988)	4.16	3	1.3E–5	0.04	4.4E2	5.7E–3	1.28	4.23
Barnard and Dockery (1991)	20.	3	6.0E–5	0.04	1.3E4	0.8	1.28	4.23

Table B–1 (continued)

Matrix Properties:

Reference	*Grain Density (kg/m^3)*	*Porosity*	*Residual Saturation*	*Saturated Conductivity (m/yr)*	*Alpha (1/m)*	*Beta*
UPPER CRATER FLAT (Non–Welded, Zeolitic)						
Peters *et al.* (1984) [USW G4]	2240 – 2290	0.19 – 0.29	0.135 – 0.322	6.3E–4 – 1.4E–2	3.2E–3 – 4.5E–3	1.87 – 2.02
BULLFROG (Welded, Devitrified)						
Peters (1984) [USW G4]	2620 –2630	0.24 – 0.27	0.056 –0.061	7.2E–2 – 2.0E–1	1.1E–2 – 2.9E–2	2.26 – 4.15
DOE (1988; Table 3–27)						
Lab data	—	0.17 – 0.34	—	1.1E–2 – 0.36	—	—
Field data	—	—	—	2.2 – 8.4E2	—	—
TRAM (Non-Welded)						
DOE (1988; Table 3–27)						
Lab data	—	0.18 – 0.26	—	1.5E–3 – 0.15	—	—
Field data	—	—	—	2.5E–3 – 2.9E2	—	—

Table B–3 Average Sorption Ratios (Distribution Coefficients) from Batch Sorption Experiments on Crushed Tuff for Strontium, Cesium, Barium, Radium, Cerium, and Europium (after Meijer, 1990) (The sorption ratio in parentheses represents the standard deviation of the mean.)

			Sorption Ratios (ml/g)					
Unit	*Sample*	*Depth (ft)*	*Sr*	*Cs*	*Ba*	*Ra*	*Ce*	*Eu*
Tiva Canyon (Tpc)	JA–8	606	270 (5)	2700 (400)	435 (15)			2100 (300)
	YM–5	251	280 (80)	5800 (800)	1100 (200)		450,000 (240,000)	2,300,000 (40,000)
Pah Canyon (Tpp)	G2–547	547	265 (10)	13,300 (1500)	3490 (30)			340 (30)
	G2–723	723	290 (40)	4100 (600)	3500 (400)			> 10,000
	GU3–433	433	45 (9)	630 (20)	810 (100)			100 (14)
Topopah Spring (Tpt)	YM–22	848	53 (4)	290 (30)	900 (30)		1270 (40)	1390 (110)
	GU3–1203	1203	42 (1)	350 (30)	640 (40)			190 (2)
	G1–1292	1292	200 (6)	430 (28)	2100 (300)	1500 (100)	66 (8)	140 (14)
	GU3–1301	1301	28 (4)	160 (40)	570 (60)			45 (12)
	YM–30	1264	260 (80)	855 (5)	3400 (1500)		230,000 (100,000)	160,000 (50,000)
	JA–18	1420	17,000 (3000)	16,000 (1000)	38,000 (18,000)		2800 (1400)	1400 (200)
Calico Hills, tuffaceous beds (Tht)	G1–1436	1436	36,000 (3000)	7800 (500)	150,000 (24,000)		59,000 (7000)	30,000 (2000)
	G2–1952	1952	2200 (400)	63,300 (1100)	25,000 (4000)			89 (14)
Prow Pass (Tcp)	G1–1854	1854	60,000 (14,000)	13,000 (2000)	45,000 (7000)		15,000	
	YM–45	1930	195 (14)	520 (90)	1200 (100)		730 (100)	1600 (200)
	G1–1883	1883	22 (0.2)	187 (3)	183 (12)		1420 (20)	
	YM–46	2002	190 (60)	840 (6)	14,000 (6000)		310,000 (110,000)	307,000 (110,000)
	G1–1982	1982	55 (4)	1120 (110)	700 (50)		560 (40)	970 (150)
	YM–48	2114	2100 (400)	9000 (4000)	18,000 (6000)		1400 (500)	2200 (500)
	YM–49	2221	3200 (300)	36,000 (3000)	42,000 (8000)		550 (100)	1200 (100)
	JA–26	1995	95 (35)	1500 (600)	800 (300)			

Table B–3 (continued)

Unit	Sample	Depth (ft)	Sorption Ratios (ml/g)					
			Sr	*Cs*	*Ba*	*Ra*	*Ce*	*Eu*
bedded tuff (bt)	YM–38	1504	17,000 (2000)	13,000 (2000)	100,000 (10,000)		760 (140)	1600 (200)
	YM–42	1824	3900 (600)	17,000 (1000)	94,000 (14,000)		49,900 (7000)	52,000 (4000)
Bullfrog (Tcb)	JA–28	2001	94 (20)	1640 (210)	820 (50)			2100(1000)
	G1–2233	2233	48,000 (3000)	13,500 (800)	250,000 (30,000)		1400 (300)	900 (200)
	G1–2289	2289	7300 (500)	37,000 (13,000)	66,000 (9000)	46,000 (20,000)		797 (10)
	YM–54	2491	62 (12)	180 (40)	400 (150)		150 (40)	470 (40)
	G1–2333	2333	180 (20)	1400 (130)	1500 (200)			2300 (400)
	G1–2363	2363	64 (3)	470 (40)	235 (9)	540 (60)		730 (50)
	G1–2410	2410	169 (1)	1250 (50)	1780			440 (80)
	JA–32	2533	57 (3)	123 (4)	380 (30)		82 (14)	90 (20)
	G1–2476	2476	41 (1)	700 (40)	385 (11)			3200 (100)
Tram (Tct)	G1–2698	2698	42,000 (3000)	7700 (400)	63,000 (5000)		240 (30)	200 (30)
	G1–2840	2840	860 (1)	2200 (200)	2070 (70)			4900 (400)
	G1–2854	2854	94 (1)	1080 (120)	1000 (50)			1300 (200)
	G1–2901	2901	68 (1)	1290 (110)	1600 (200)		42,000 (3600)	160,000 (50,000)
	G1–3116	3116	2400 (17)	6600 (500)	12,000 (4000)		100 (10)	760 (60)
	JA–37	3497	287 (14)	610 (40)	760 (150)			6000 (800)
older tuffs (Tl)	G1–3658	3658	13,000 (0)	4950 (50)	13,500 (500)		1000 (200)	530 (40)
bedded tuff (Tba)	G2–3933	3923	240 (60)	2500 (1000)	1700 (500)			1500 (700)

Table B–3 (continued)

Unit	Sample	Depth (ft)	Sorption Ratios (ml/g)					
			Sr	*Cs*	*Ba*	*Ra*	*Ce*	*Eu*
bedded tuff (bt)	YM–38	1504	17,000 (2000)	13,000 (2000)	100,000 (10,000)		760 (140)	1600 (200)
	YM–42	1824	3900 (600)	17,000 (1000)	94,000 (14,000)		49,900 (7000)	52,000 (4000)
Bullfrog (Tcb)	JA–28	2001	94 (20)	1640 (210)	820 (50)			2100(1000)
	G1–2233	2233	48,000 (3000)	13,500 (800)	250,000 (30,000)		1400 (300)	900 (200)
	G1–2289	2289	7300 (500)	37,000 (13,000)	66,000 (9000)	46,000 (20,000)		797 (10)
	YM–54	2491	62 (12)	180 (40)	400 (150)		150 (40)	470 (40)
	G1–2333	2333	180 (20)	1400 (130)	1500 (200)			2300 (400)
	G1–2363	2363	64 (3)	470 (40)	235 (9)	540 (60)		730 (50)
	G1–2410	2410	169 (1)	1250 (50)	1780			440 (80)
	JA–32	2533	57 (3)	123 (4)	380 (30)		82 (14)	90 (20)
	G1–2476	2476	41 (1)	700 (40)	385 (11)			3200 (100)
Tram (Tct)	G1–2698	2698	42,000 (3000)	7700 (400)	63,000 (5000)		240 (30)	200 (30)
	G1–2840	2840	860 (1)	2200 (200)	2070 (70)			4900 (400)
	G1–2854	2854	94 (1)	1080 (120)	1000 (50)			1300 (200)
	G1–2901	2901	68 (1)	1290 (110)	1600 (200)		42,000 (3000)	160,000 (50,000)
	G1–3116	3116	2400 (17)	6600 (500)	12,000 (4000)		100 (10)	760 (60)
	JA–37	3497	287 (14)	610 (40)	760 (150)			6000 (800)
older tuffs (Tl)	G1–3658	3658	13,000 (0)	4950 (50)	13,500 (500)		1000 (200)	530 (40)
bedded tuff (Tba)	G2–3933	3923	240 (60)	2500 (1000)	1700 (500)			1500 (700)

Table B–4 Average (De)Sorption Ratios (Distribution Coefficients) from Batch Sorption Experiments on Crushed Tuff for Strontium, Cesium, Barium, Radium, Cerium, and Europium (after Meijer, 1990) (The sorption ratio in parentheses represents the standard deviation of the mean.)

Unit	*Sample*	*Depth (ft)*	*(De)Sorption Ratios (ml/g)*				
			Sr	*Cs*	*Ba*	*Ce*	*Eu*
Tiva Canyon	JA–8	606	311 (3)	4600 (400)	480 (50)		10,000 (3000)
(Tpc)	YM–5	251	320 (30)	8900 (600)	1200 (120)	31,000 (30,000)	36,000 (14,000)
Pah Canyon	G2–547	547	210 (10)	8700 (550)	2900 (200)		1700 (600)
(Tpp)	G2–723	723	330 (4)	4300 (4)	4200 (10)		> 10,000
	GU3–433	433	40 (10)	520 (20)	460 (20)		140 (10)
Topopah Spring	YM–22	848	59 (2)	365 (7)	830 (100)	6500 (800)	3500 (200)
(Tpt)	GU3–1203	1203	47 (1)	340 (10)	720 (30)		650 (50)
	G1–1292	1292	120 (5)	510 (20)	1500 (100)	600 (200)	600 (70)
	GU3–1301	1301	80 (20)	185 (20)	675 (60)		100 (20)
	YM–30	1264	210 (30)	1500 (100)	3100 (600)	170,000 (15,000)	11,000 (700)
	JA–18	1420	15,000 (2000)	17,500 (700)	280,000 (50,000)	1600 (500)	2400 (300)
Calico Hills,	G1–1436	1436	87,000 (12,000)	24,000 (2000)	340,000 (90,000)	6700 (600)	5300 (600)
tuffaceous beds	G2–1952	1952	4200 (200)	46,000 (1400)	40,000 (1000)		1600 (200)
(Tht)	YM–38	1540	22,000	13,000	260,000	2600	7300
	YM–42	1842	4100 (1000)	21,000 (2000)	90,000	44,000 (5000)	64,000 (3000)
older tuffs (Tl)	G1–3658	3658	12,000 (3000)	12,000 (2000)	10,000 (4000)	9000 (4000)	9000 (3000)
Prow Pass	G1–1854	1854	72,000 (13,000)	14,000 (2000)	150,000 (40,000)		4800 (700)
(Tcp)	YM–45	1930	210 (20)	620 (110)	1310 (60)	5800 (600)	7300 (900)
	G1–1883	1883	59 (1)	430 (4)	440 (10)	2200 (100)	1350 (50)
	YM–46	2002	260 (20)	1800 (300)	210,000 (3000)	300,000 (50,000)	31,000 (2000)
	G1–1982	1982	322 (8)	2300 (200)	2780 (120)	7000 (800)	6370 (130)
	YM–48	2114	2700 (200)	27,000 (4000)	34,000 (7000)	128,000 (300)	8100 (1200)
	YM–49	2221	4400 (100)	39,000 (1000)	65,000 (7000)	1040 (40)	2100 (500)
	JA–26	1995	39 (3)	1580 (90)	450 (13)		2900 (200)

Table B–4 (continued)

Unit	Sample	Depth (ft)	(De)Sorption Ratios (ml/g)				
			Sr	*Cs*	*Ba*	*Ce*	*Eu*
Bullfrog (Tcb)	JA–28	2001	114 (3)	2400 (100)	1160 (20)		12,300 (500)
	G1–2233	2233	90,000 (40,000)	23,000 (6000)	240,000 (80,000)	20,000 (13,300)	5000 (2000)
	YM–54	2491	97 (9)	310 (20)	660 (20)	1000 (200)	1840 (110)
	G1–2333	2333	140 (13)	1230 (100)	1460 (130)		9900 (1200)
	G1–2363	2363	150 (6)	1200 (30)	820 (20)	130,000 (6000)	6100 (200)
	G1–2410	2410	140 (14)	1120 (100)	1760 (150)		6000 (3000)
	JA–32	2533	53 (3)	175 (11)	490 (40)	530 (120)	850 (130)
	G1–2476	2476	200 (40)	1520 (0)			
Tram (Tc[illegible])	G1–2698	2698	210,000 (50,000)	17,000 (1100)	190,000 (80,000)	2000 (400)	
	G1–2840	2840	1540 (4)	2300 (130)	2500 (200)		9000 (1100)
	G1–2854	2854	96 (1)	1160 (20)	1330 (0)		5000 (200)
	G1–2901	2901	67 (1)	1380 (30)	1980 (30)	39,000 (1000)	210,000 (50,000)
	G1–3116	3116	24,000 (13,000)	11,000 (3000)	160,000 (80,000)	3000 (1000)	8000 (3000)
	JA–37	3497	312 (9)	850 (50)	920 (40)		11,000 (2000)
bedded tuff (Tba)	G2–3933	3933	140 (20)	1400 (350)	1100 (200)		3000 (1100)

Table B–5 Average (De)Sorption Ratios (Distribution Coefficients) from Batch Sorption Experiments on Crushed Tuff for Americium, Plutonium, Uranium, Technetium, and Neptunium (after Meijer, 1990) (The sorption ratio in parentheses represents the standard deviation of the mean.)

Unit	*Sample*	*Depth (ft)*	*(De)Sorption Ratios (ml/g)*				
			Am	*Pu*	*U*	*Tc*	*Np*
Pah Canyon	G2–547	547	17,000 (1400)	1200 (170)			
(Tpp)	G2–723	723	2.8×10^6 (26,000)	>4700			
	GU3–433	433	9300 (1780)	920 (40)			
Topopah Spring	YM–22	848	2500 (400)	1330 (140)	5 (2)	1.2 (0.3)	33 (5)
(Tpt)	GU3–1203	1203	1300 (200)	920 (15)			
	G1–1292	1292				0	
	GU3–1301	1301	2500 (600)	1300 (460)			
	JA–18	1420	1100 (300)	350 (140)	9.4 (1.4)		
Calico Hills,	G2–1952	1952	5800 (1100)	350 (45)			15 (2)
tuffaceous beds	YM–38	1540	7100 (1200)	1600 (300)	4.8 (1.0)		24 (2)
(Tht)							
Prow Pass	G1–1883	1883	7200 (900)	890 (60)			36 (10)
(Tcp)	G1–1982	1982			4.1		
	YM–48	2114				1.6 (0.2)	
	YM–49	2221	3400 (400)	720 (90)		2.0 (0.3)	12 (4)
Bullfrog	G1–2233	2233			8 (2)		
(Tcb)	YM–54	2491	550 (80)	720 (40)	12 (8)		
	JA–32	2533	2200 (600)		8 (2)		
	G1–2476	2476			1.5 (0.2)		
Tram	G1–3116	3116			1.7 (0.3)		
(Tct)	JA–37	3497	32,000 (10,000)	1400 (300)	9.9 (0.4)		170 (50)
bedded tuff	G2–3933	3933	12,000 (410)	530 (130)		0	
(Tba)							

based on chemical similarity to other measurements. When K_d values could still not be assigned, K_d values were taken from the Iterative Performance Assessment (IPA) Phase 1 report (see Codell *et al.*, 1992; p. 56). In the sensitivity analysis (described in Chapter 8), the IPA Phase 2 effort assumed that the distribution of K_d values was log-uniform. For such a distribution, the sampling procedure used required setting the upper and lower bounds of the parameter range. The upper and lower bounds of the distribution were crudely estimated to be plus or minus one order of magnitude about the mean (the support for this assignment was derived from DOE's 1988 SCP, where the range of K_d values for Sr and Cs varies over two orders of magnitude for different locations in drill hole G1). A mean K_d value was derived from the Meijer (1990) and Thomas (1987) data by averaging the logs of the reported experimental values. The mean K_d values, thus calculated, are as follows for the following hydrogeologic units:

	K_d (m^3/kg)				
Element	***Tpt***	***CHnv***	***CHnz***	***Tcp***	***Tcb***
Am	.810	.810	1.7	4.5	.140
Pu	.170	.170	.066	.130	.094
U	.0002	.020	.001	0.0	.002
Se	.0026	.003	.0045	.0025	.013
Tc	.000013	0.0	0.0	.00017	.0042
Np	.0045	.0045	.0027	.0051	.0051
Sr	.08	.034	8.9	.450	.280
Cs	.36	.24	22.0	2.2	3.2
Ba	1.2	.6	61.0	3.9	1.1
Ra	1.5	1.5	1.5	1.5	5.0
Th	.470				.340
Sn				.230	.660

The experimental K_d values taken from Meijer (1990) and Thomas (1987) were determined using crushed tuff from various drill holes and water, from Well J-13, which was "spiked" with a particular radionuclide. A brief description of the procedure and information used to derive the mean K_d values is presented below:

Am The K_d in the Topopah Spring unit (Tpt) is a log average of the values from experiments using crushed tuff recovered from drill holes J-13, G-3, and UE25a-1. The K_d in the Calico Hills nonwelded vitric unit (CHnv) is estimated to be the same as the Topopah Spring. Glassy units should have low sorption capability. The single value reported from the experiment using crushed tuff from drill hole G-2 is assumed to represent the mean value of the K_d in the Calico Hills nonwelded zeolitic unit (CHnz). For the Prow Pass unit (Tcp), the K_d is again the log average of the values from wells G1 and UE25a-1. The K_d in the Bullfrog unit (Tcb) is the log average of the values from experiments using crushed tuff recovered from drill holes J-13 and UE25a-1.

Pu The K_d in the Topopah Spring unit is the log average of the values from experiments using crushed tuff recovered from drill holes UE25a-1, G-3, and J-13. The K_d in the Calico Hills nonwelded vitric is estimated to be the same as the Topopah Spring unit. The single value reported from the experiment using crushed tuff from drill hole G-2 is assumed to represent the mean value of the K_d for the Calico Hills nonwelded zeolitic unit. The Prow Pass unit K_d is the log average of the values from experiments using crushed tuff recovered from drill holes G-1 and UE25a-1. The Bullfrog unit K_d is the log average of the values from experiments using crushed tuff recovered from drill holes J-13 and UE25a-1.

U The K_d in the Topopah Spring unit is the log average of the values from experiments using crushed tuff recovered from drill holes UE25a-1, G-3, and J-13. The single value reported from the experiment used crushed tuff recovered from drill hole G-3 is assumed to represent the K_d in the Calico Hills nonwelded vitric unit. Figures B-1 through B-4 from the SCP (see DOE, 1988), illustrate where the zeolitic beds are located. The K_d value in the Calico Hills nonwelded

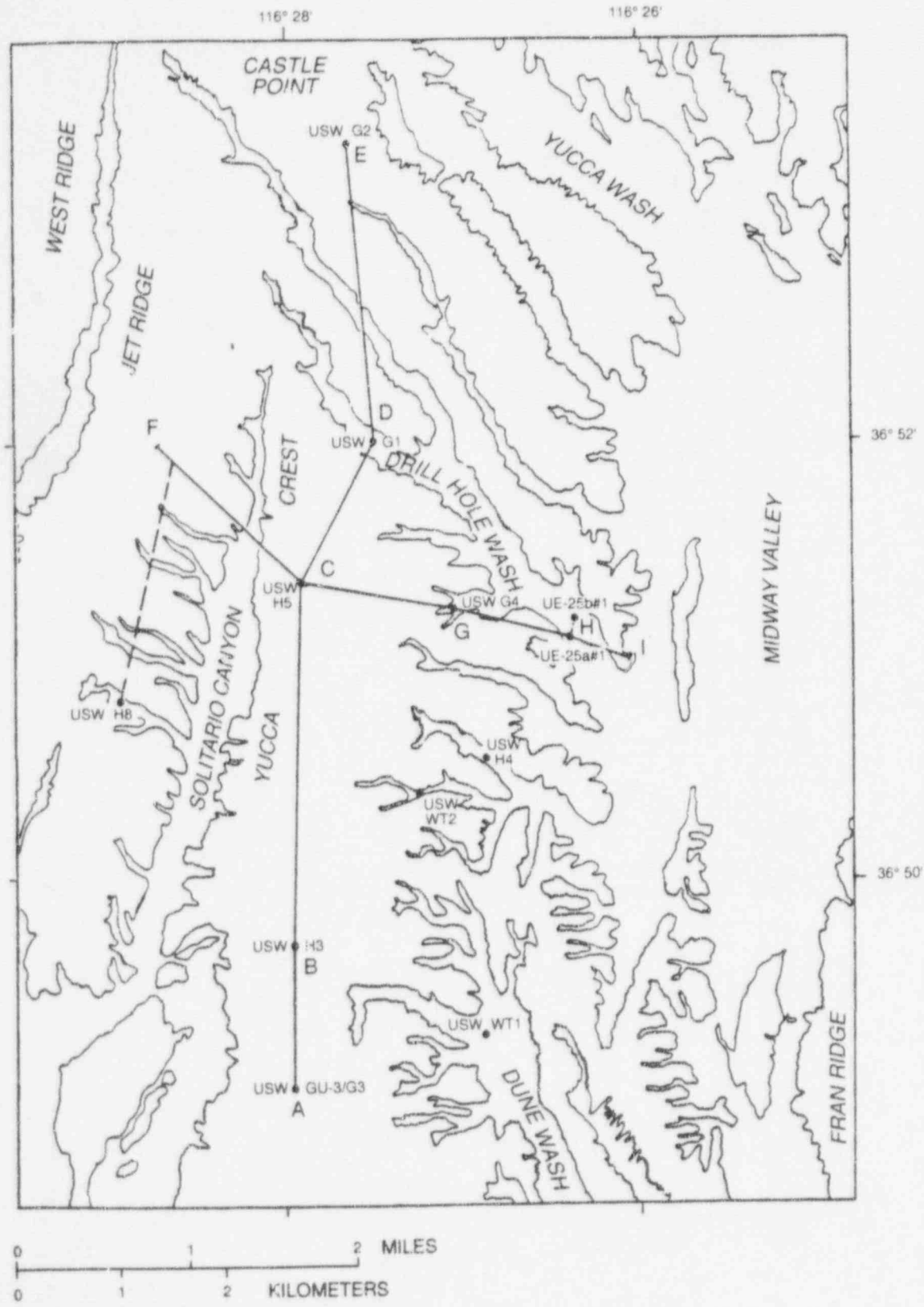

Figure B–1 Location map for the zeolitic cross-sections in Figures B–2, B–3, and B–4 (This figure and the stratigraphy shown in Figures B–2 and B–4 are based on Scott and Bonk (1984). Taken from DOE (1988, p. 4–22).)

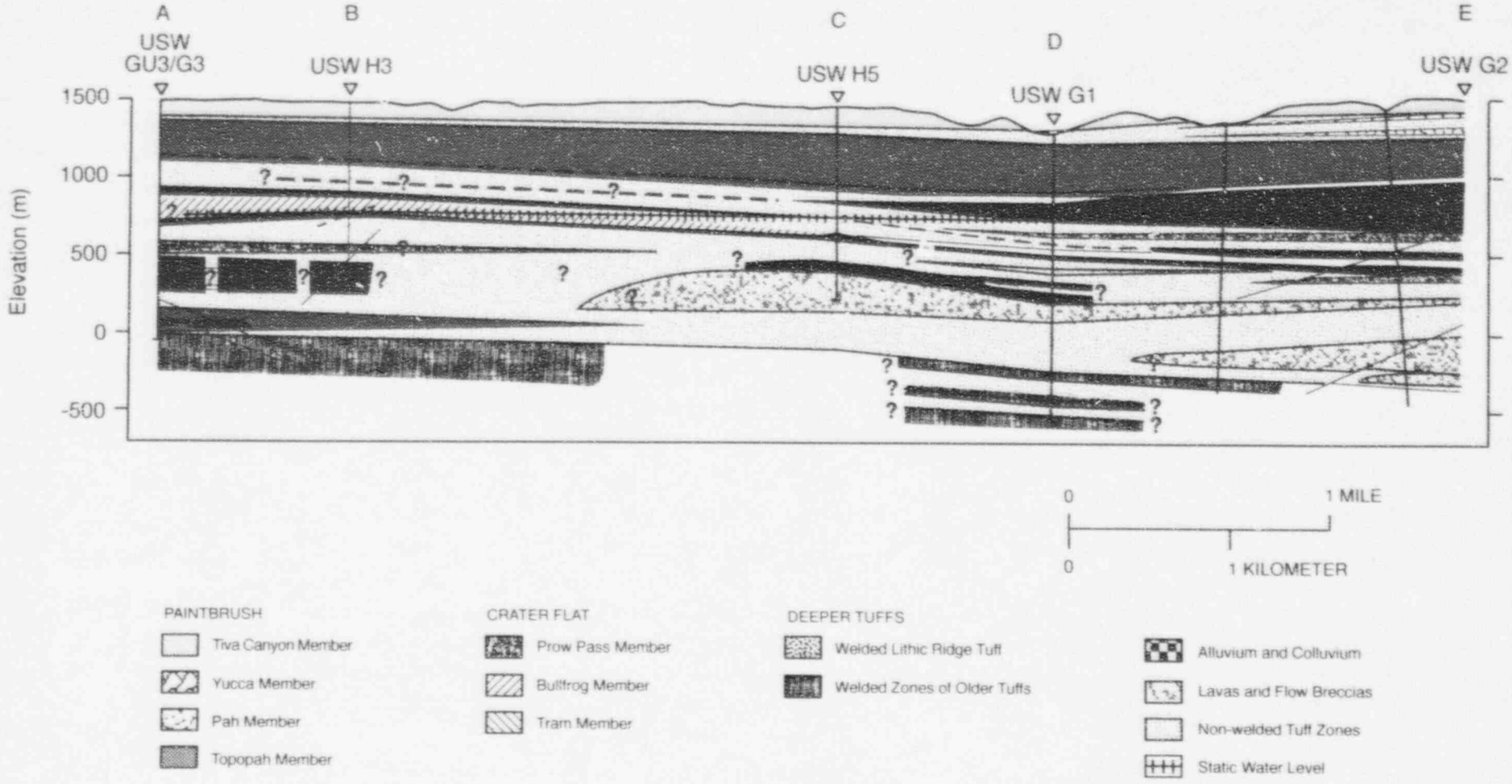

Figure B–2 Major zeolitic distributions (Bish and Vaniman, 1985), north-south cross-section, shown as a dark pattern overlying the stratigraphic cross-section of Scott and Bonk (1984) (Location of cross-section is shown on Figure B–1. The subhorizontal barred line indicates the water table as inferred from static water levels in the drill holes. Taken from DOE (1988, p. 4–24).)

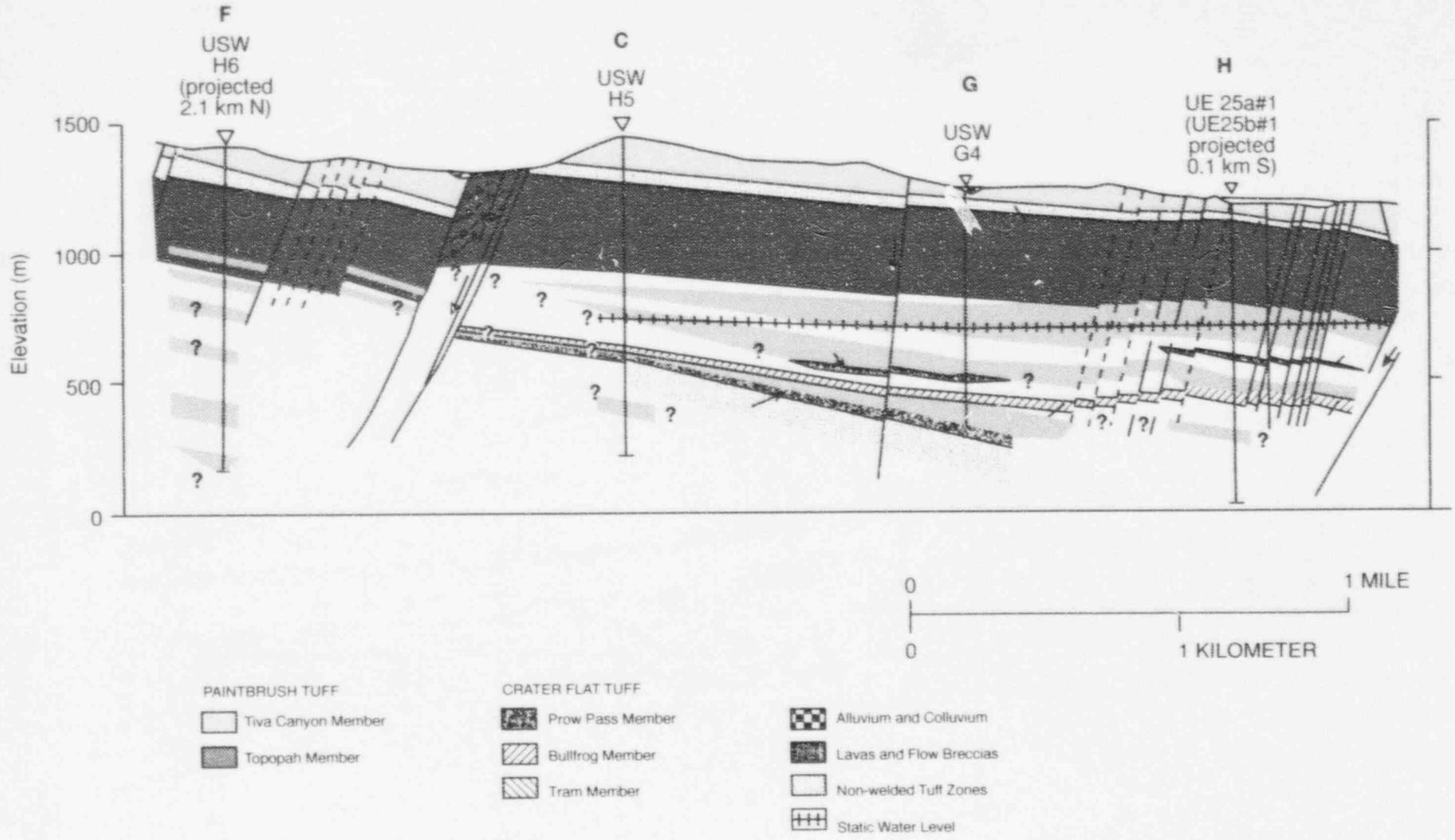

Figure B–3 Major clinoptilolite-mordenite distributions (Bish and Vaniman, 1985), northwest-southeast cross-section (Location of cross-section is shown on Figure B–1. Information on drill hole USW H–5 below 760 meters is from Bentley *et al.* (1983) and information on the central part of the drill hole USW H–6 is from Craig *et al.* (1983). Taken from DOE (1988, p. 4–25).)

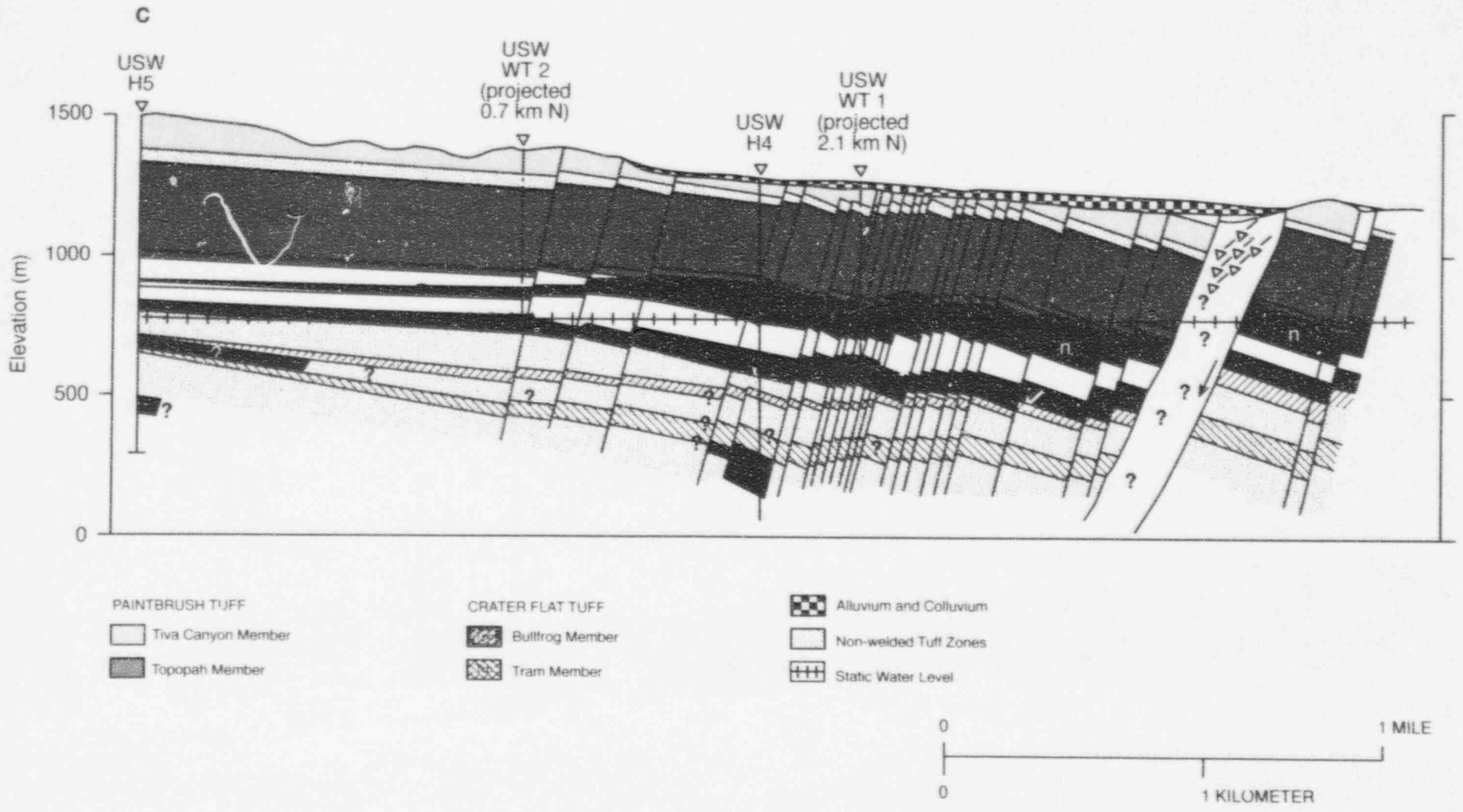

Figure B–4 Major zeolite distributions (Bish and Vaniman, 1985), center to southeast cross-section as depicted in Figure B–1 (Taken from DOE (1988, p. 4–26).)

zeolitic unit is a log average of the values from experiments using crushed tuff recovered from drill holes G-1 and G-2. The K_d in the Prow Pass unit is assumed to be zero, even though no data are available. The K_d in the Bullfrog unit is the log average of the values from experiments using crushed tuff recovered from drill holes G-1, J-13, and UE25a-1.

Se The K_d in the Topopah Spring unit is the log average of the values from experiments using crushed tuff recovered from drill hole G-3. The single value reported from the experiment used crushed tuff recovered from drill hole G-3 is assumed to represent the mean value of the K_d in the Calico Hills nonwelded vitric unit. The K_d value in the Calico Hills nonwelded zeolitic unit is the average of the values from experiments using crushed tuff recovered from drill holes G-1 and G-2. The single value reported from the experiment used crushed tuff recovered from drill hole G-1 is assumed to represent the K_d in the Prow Pass unit. The K_d in the Bullfrog unit is the log average of the values from experiments using crushed tuff recovered from drill hole G-1.

Tc The K_d in the Topopah Spring unit is the log average of the values from experiments using crushed tuff recovered from drill holes UE25a-1 and G-3. In the absence of information, the K_ds in the Calico Hills units are assumed to be zero. The K_d in the Prow Pass unit is the log average of the values from experiments using crushed tuff recovered from drill hole J-13. The single value from the experiment used crushed tuff recovered from drill hole UE25a-1 is assumed to represent the mean of the K_d in the Bullfrog unit.

Np The K_d in the Topopah Spring unit is a log average of the values from experiments using crushed tuff recovered from drill holes G-3 and UE25a-1. The K_d in the Calico Hills nonwelded vitric unit is estimated to be the same as the Topopah Spring unit. The single value reported from the experiment using crushed tuff from drill hole G-2 is assumed to represent the mean value of the K_d in the Calico Hills nonwelded zeolitic unit is assumed to represent the mean. For the Prow Pass unit, the K_d is the log average of the values from experiments using crushed tuff recovered from drill holes G1 and UE25a-1. The K_d in the Bullfrog unit is assumed to the same as the value in the Prow Pass unit.

Sr The K_d in the Topopah Spring unit is a log average of the values from experiments using crushed tuff recovered from drill holes G-3, G-1, and UE25a-1. The K_d in the Calico Hills nonwelded vitric unit is based on the log average of the values from well G-3 for the Topopah Spring unit. The K_d value in the Calico Hills nonwelded zeolitic unit is the log average of the values from experiments using crushed tuff recovered from drill holes G-1 and G-2. For the Prow Pass unit, the K_d is the log average of the values from experiments using crushed tuff recovered from drill holes G1, J-13, and UE25a-1. For the Bullfrog unit, the K_d is the log average of the values from experiments using crushed tuff recovered from drill holes G1, J-13, and UE25a-1.

Cs The K_d in the Topopah Spring unit is a log average of the values from experiments using crushed tuff recovered from drill holes G-3, G-1, and UE25a-1. The K_d in the Calico Hills nonwelded vitric unit is based on the log average of the values from experiments using crushed tuff recovered from drill hole G-3 for the Topopah Spring unit. The K_d value in the Calico Hills nonwelded zeolitic unit is the log average of the values from experiments using crushed tuff recovered from drill holes G-1 and G-2. For the Prow Pass unit, the K_d is the log average of the values from experiments using crushed tuff recovered from drill holes G1, J-13, and UE25a-1. For the Bullfrog unit, the K_d is the log average of the values from experiments using crushed tuff recovered from drill holes G1, J-13, and UE25a-1.

Ba The K_d in the Topopah Spring unit is a log average of the values from experiments using crushed tuff recovered from drill holes G-3, G-1, and UE25a-1. The K_d in the Calico Hills nonwelded vitric unit is based on the log average of the values from

experiments using crushed tuff recovered from drill hole G-3, for the Topopah Spring unit. The K_d value in the Calico Hills nonwelded zeolitic unit is the log average of the values from experiments using crushed tuff recovered from drill holes G-1 and G-2. For the Prow Pass unit, the K_d is the log average of the values from experiments using crushed tuff recovered from drill holes G1, J-13, and UE25a-1. For the Bullfrog unit, the K_d is the log average of the values from experiments using crushed tuff recovered from drill holes G1, J-13, and UE25a-1.

Ra The single value from the experiment used crushed tuff recovered from drill hole G-1 is assumed to represent the mean of the K_d for the Topopah Spring unit. The K_ds for the Calico Hills and Prow Pass units are assumed to be the same as the value used for the Topopah Spring unit. The K_d for the Bullfrog unit is the log average of the values from experiments using crushed tuff recovered from drill hole G-1.

Th The K_d values are taken from Thomas (1987) from experiments using crushed tuff recovered from drill hole G-1.

Sn The K_d values are taken from Thomas (1987) from experiments using crushed tuff recovered from drill hole G-1.

The K_d in the fractures is assumed to be zero, because of the conceptualization that flow will be fast relative to the rates of the sorption reactions. This is the same approach as proposed in DOE's 1988 SCP.

Table B-6 presents the distributions and the ranges used for representing the hydrologic parameters of the ground-water pathway. Table B-7 presents the K_d values used for each of the elements and hydrogeologic units used in the analysis. Section 4.2.3 and Appendix A provide additional information on the approaches and sources of information used to derive the various hydrologic and transport parameters used in the IPA Phase 2 analysis.

B-3 References

Barnard, R.W. and H.A. Dockery (eds.), "Technical Summary of the Performance Assessment Calculational Exercises for 1990 (PACE-90)—Volume 1: 'Nominal Configuration' Hydrogeologic Parameters and Calculational Results," Sandia National Laboratories, SAND90-2726, June 1992. [Prepared for the U.S. Department of Energy.]

Bentley, C.B., J.H. Robison, and R.W. Spengler, "Geohydrologic Data for Test Well USW H-5, Yucca Mountain Area, Nye County, Nevada," U.S. Geological Survey, Open File Report 83-853, 1983.

Bish, D.L., and D.T. Vaniman, "Mineralogic Summary of Yucca Mountain, Nevada," Los Alamos, New Mexico, Los Alamos National Laboratory, LA-10543-MS, October 1985.

Codell, R.B., *et al.*, "Initial Demonstration of the NRC's Capability to Conduct a Performance Assessment for a High-Level Waste Repository," U.S. Nuclear Regulatory Commission, NUREG-1327, May 1992.

Craig, R.W., *et al.*, "Geohydrologic Data for Test Well USW H-6, Yucca Mountain Area, Nye County, Nevada," U.S. Geological Survey, Open File Report 83-856, 1983.

Dudley, A.L., *et al.* "Total System Performance Assessment Code (TOSPAC), Volume 1: Physical and Mathematical Bases," Albuquerque, New Mexico, Sandia National Laboratories, SAND85-0002, December 1988.

Klavetter, E.A. and R.R. Peters, "Fluid Flow in a Fractured Rock Mass," Albuquerque, New Mexico, Sandia National Laboratories, SAND85-0855, March 1986.

Meijer, A., "Yucca Mountain Project Far-Field Sorption Studies and Data Needs," Los Alamos, New Mexico, Los Alamos National Laboratory, LA-11671-MS, March 1990. [Prepared for the U.S Department of Energy.]

Nitao, J.J. and T.A. Buscheck, "Infiltration of a Liquid Front in an Unsaturated, Fractured Porous Media," *Water Resources Research*, 27(8):2099-2112 [1991].

Peters, R.R., *et al.*, "Fracture and Matrix Hydrologic Characteristics of Tuffaceous Materials from

Yucca Mountain, Nye County, Nevada," Albuquerque, New Mexico, Sandia National Laboratories, SAND84-1471, December 1984.

Pruess, K., J.S.Y. Wang, and Y.W. Tsang, "On Thermohydrologic Conditions Near High-Level Nuclear Wastes Emplaced in Partially Saturated Fractured Tuff 1. Simulation Studies With Explicit Consideration of Fracture Effects," *Water Resources Research*, 26(6):1235-1248 [1990].

Scott, R.B. and J. Bonk, "Preliminary Geologic Map of Yucca Mountain, Nye County, Nevada, with Geologic Sections," U.S. Geological Survey, Open File Report 84-494, 1984.

Thomas, K., "Summary of Sorption Measurements Performed with Yucca Mountain, Nevada, Tuff Samples and Water from Well J-13," Los Alamos, New Mexico, Los Alamos National Laboratory, LA-10960-MS, March 1987.

Tsang, Y.W. and K. Pruess, "A Study of Thermally Induced Convection Near a High-Level Nuclear Waste Repository in Partially Saturated Fractured Tuff," *Water Resources Research*, 23(10):1958-1966 [1987].

U.S. Department of Energy, "Site Characterization Plan Overview, Yucca Mountain Site, Nevada Research and Development Area, Nevada," Office of Civilian Radioactive Waste Management, DOE/RW-0198, December 1988.

Table B–6 Hydrogeologic parameteric values and ranges used for the ground-water pathway

Distribution	*Range*		*Description*
Porosity of Matrix			
uniform	.06 – .16		Topopah Spring, welded
uniform	.33 – .56		Calico Hills, non-welded vitric
uniform	.20 – .33		Calico Hills, non-welded zeolitic
uniform	.24 – .40		Prow Pass, welded
uniform	.18 – .30		Upper and Middle Crater Flat, non-welded
uniform	.19 – .32		Bullfrog, welded
Saturated Conductivity (mm/yr) and Permeability [m^2] of Matrix			
lognormal	0.11 – 36.	[3.6E–19 – 1.2E–18]	Topopah Spring, welded
lognormal	1.2E2 – 6.1E3	[3.9E–15 – 2.0E–14]	Calico Hills, non-welded vitric
lognormal	0.004 – .20	[1.3E–20 – 6.7E–19]	Calico Hills, non-welded zeolitic
lognormal	58. – 300.	[1.9E–16 – 9.6E–16]	Prow Pass, welded
lognormal	1.6 – 4.6	[5.1E–18 – 1.5E–17]	Upper Crater Flat, non-welded
lognormal	110. – 140.	[3.5E–16 – 4.4E–16]	Bullfrog, welded
lognormal	1.3 – 4.8	[4.1E–18 – 1.6E–17]	Middle Crater Flat, non-welded
van Genuchten Alpha Parameter, for Matrix (1/m)			
constant	.006		Topopah Spring, welded
constant	.016		Calico Hills, non-welded vitric
constant	.003		Calico Hills, non-welded zeolitic
constant	.014		Prow Pass, welded
constant	.004		Upper and Middle Crater Flat, non-welded
constant	.02		Bullfrog, welded
van Genuchten Beta Parameter, for Matrix			
uniform	1.4 – 2.2		Topopah Spring, welded
uniform	1.5 – 4.9		Calico Hills, non-welded vitric
uniform	1.2 – 3.3		Calico Hills, non-welded zeolitic
uniform	2.0 – 3.4		Prow Pass, welded
uniform	1.5 – 2.4		Upper and Middle Crater Flat, non-welded
uniform	2.3 – 4.2		Bullfrog, welded
Grain Density for Matrix (kg/m^3)			
constant	2580		Topopah Spring, welded
constant	2370		Calico Hills, non-welded vitric
constant	2230		Calico Hills, non-welded zeolitic
constant	2590		Prow Pass, welded
constant	2270		Upper and Middle Crater Flat, non-welded
constant	2630		Bullfrog, welded

Table B–6 (continued)

Distribution	*Range*		*Description*
Porosity of Fracture			
constant	4.1E–5		Topopah Spring, welded
constant	4.6E–5		Calico Hills, non-welded vitric
constant	4.6E–5		Calico Hills, non-welded zeolitic
constant	1.3E–5		Prow Pass, welded
constant	4.6E–5		Upper and Middle Crater Flat, non-welded
constant	1.3E–5		Bullfrog, welded
Saturated Conductivity (mm/yr) and Permeability [m^2] of Fractures			
lognormal	34. – 59.	[1.1E–16 – 1.9E–16]	Topopah Spring, welded
lognormal	170. – 370.	[5.6E–16 – 1.2E–15]	Calico Hills, non-welded vitric
lognormal	190. – 310.	[6.2E–16 – 9.9E–16]	Calico Hills, non-welded zeolitic
lognormal	12. – 25.	[3.9E–17 – 8.1E–17]	Prow Pass, welded
lognormal	210. – 300.	[6.7E–16 – 9.8E–16]	Upper and Middle Crater Flat, non-welded[1]
lognormal	15. – 20.	[4.9E–17 – 6.4E–17]	Bullfrog, welded[2]
van Genuchten Alpha Parameter, for Fracture (1/m)			
constant	1.3		Topopah Spring, welded
constant	1.3		Calico Hills, non-welded vitric
constant	1.3		Calico Hills, non-welded zeolitic
constant	1.3		Prow Pass, welded
constant	1.3		Upper and Middle Crater Flat, non-welded
constant	1.3		Bullfrog, welded
van Genuchten Beta Parameter, for Fracture			
uniform	3.2 – 5.3		Topopah Spring, welded
uniform	3.2 – 5.3		Calico Hills, non-welded vitric
uniform	3.2 – 5.3		Calico Hills, non-welded zeolitic
uniform	3.2 – 5.3		Prow Pass, welded
uniform	3.2 – 5.3		Upper and Middle Crater Flat, non-welded
uniform	3.2 – 5.3		Bullfrog, welded
Infiltration Rate (mm/yr)			
loguniform	0.1 – 5.0		base case
loguniform	5.0 – 10.		pluvial case
Dispersivity (m)			
normal	.3 – 30.		dispersivity for all units
Discharge Area (m^2)			
uniform	3.75E4 – 3.75E5		discharge area for all regions

[1]Values are representative of Calico Hills.
[2]Values are representative of Prow Pass.

Table B–7 **Matrix K_d Values (in cubic meters per kilogram) for Selected Radionuclides for the Hydrogeologic Units of Interest** (Suggested ranges are assumed to +/– one order of magnitude, a loguniform distribution is assumed for all. Where no values are present, a K_d of zero is assumed. Values in parentheses are derived from Codell *et al.*, 1992.)

	Hydrogeologic Unit					
		Calico Hills				
Element	*Topopah Spring*	*vitiric*	*zeolitic*	*Prow Pass*	*Upper and Middle Crater Flat*[1]	*Bullfrog*
Cm	(0.45)	(3.28)	(1.66)	(1.16)	(1.32)	(1.20)
Pu	0.17	0.17	0.066	0.13	0.053	0.094
U	0.0002	0.02	0.001	—	0.0008	0.002
Am	0.81	0.81	1.7	4.5	1.36	0.14
Np	0.0045	0.0045	0.0027	0.0051	0.0022	0.0051
Th	(0.048)	(0.34)	(0.17)	(0.12)	(0.14)	(0.13)
Ra	1.5	1.5	1.5	1.5	1.2	5.0
Pb	(0.0068)	(0.049)	(0.025)	(0.017)	(0.020)	(0.018)
Cs	0.36	0.24	22.0	2.2	17.6	3.2
I	—	—	—	—	—	—
Sn	(0.134)	(0.97)	(0.49)	(0.34)	(0.39)	(0.35)
Tc	0.00001	—	—	0.00017	—	0.0042
Zr	(0.0048)	(0.034)	(0.017)	(0.012)	(0.014)	(0.013)
Sr	0.08	0.034	8.9	0.45	7.1	0.28
Ni	(0.0037)	(0.027)	(0.014)	(0.009)	(0.011)	(0.010)
C	—	—	—	—	—	—
Se	0.0026	0.003	0.0045	0.0025	0.0036	0.013
Nb	—	—	—	—	—	—

[1]Values determined are based on Calico Hills zeolitic values, and allowances are made for differences in porosity and density.

APPENDIX C
EVALUATION OF SNL TECHNOLOGY: TESTING OF THE *DCM3D* COMPUTER CODE

C-1 TASK OBJECTIVE

The objective of this auxiliary analysis is to evaluate the performance assessment technology developed by Sandia National Laboratories (SNL) for the U.S. Nuclear Regulatory Commission (NRC). SNL was the prime NRC contractor for performance assessment from the mid-seventies to 1990, when this technology was transferred to the Center for Nuclear Waste Regulatory Analyses (CNWRA). The SNL-developed computer code *DCM3D*, a three-dimensional (3-D) dual-porosity saturated-unsaturated flow code, is of special interest for potential application to an unsaturated site like Yucca Mountain. This code was evaluated at CNWRA and at NRC, to determine how well it would perform as a flow simulator for use in assessing the performance of the total system.

C-2 INTRODUCTION

The *DCM3D* code evaluation work began with a review of literature on modeling of partially saturated flow (reported in the CNWRA's *First Annual Research Report* (see Gureghian and Sagar, 1991)). A more comprehensive review on unsaturated flow has also been performed by Ababou (1991). In Gureghian and Sagar (1991), preliminary tests consisting primarily of those problems provided by the author of the *DCM3D* computer code were reported. In this second and concluding part of the evaluation, problems not included in the code's *User's Manual* (see Updegraff *et al.*, 1991) have been solved. The document by Updegraff *et al.* also discusses the dual-porosity formulation implemented in *DCM3D* in sufficient detail; therefore, code theory is not discussed any further here.

All four test problems described below were extracted from the literature. Because modeling of flow through partially saturated fractured rock is of recent origin, most of the literature considers flow in unfractured soils. In addition, the concept of dual porosity in modeling flow through fractured rock has rarely been applied to unsaturated regimes; it is even more difficult to find problems in the literature related to this concept. As outlined in Gureghian and Sagar (1991), the major difficulty in applying the dual-porosity concept is the estimation of the fluid transfer term that couples the equations describing flow in the two media (matrix and fracture). This difficulty is also encountered in other approaches. For example, when fractures are treated as networks, the practical determination of hydraulic properties of such networks is a major unsolved problem. Nevertheless, the differences between the predicted flow fields need to be determined, using the dual-porosity concept and other approaches. The last problem, taken from the International Code Intercomparison study (known as HYDROCOIN) is an effort to evaluate such differences. Data for the first three test problems have been taken from Magnuson *et al.* (1990).

C-3 TEST PROBLEM NO. 1: COMPARISON WITH THE STAFF'S OWN ANALYTICAL SOLUTION

Comparison with an analytic solution for one-dimensional unsaturated flow in a horizontal soil column has been discussed by Updegraff *et al.* (1991), in the *User's Manual* of *DCM3D*. Here the staff has added a comparison with a quasi-analytic solution representing flow in a vertical column, so that the effects of gravity on flow can be simulated. For a single-porosity homogeneous medium, the quasi-analytic solution was obtained by Philip (1957). This solution is available as a FORTRAN code—*INFIL* (see El-Kadi, 1987). The object of solving this problem was to assess the accuracy of *DCM3D* in determining the position of the wetting front in a soil undergoing vertical moisture infiltration.

C-3.1 Problem Description

In the test problem, the vertical soil column had a height of 15 centimeters. The finite difference grid was uniform, with a grid spacing of 0.075 centimeters; thus the domain had 200 grid points. The soil was Yolo light clay, with hydraulic properties given by Haverkamp *et al.* (1977)—Equation (C-1) and Equation (C-2), below. The curve-fitting parameters in Equation (C-1) were

a = 739.0 and β = 4.0, and those in Equation (C–2) were A = 124.6 and B = 1.77. The saturated hydraulic conductivity was taken to have a constant value of 0.04428 centimeters/hour. The saturated volumetric moisture content (or porosity) was 0.495, and the residual moisture content was 0.124. The relationship of moisture-content relationship to pressure-head is given by:

$$\theta(\psi) = \frac{a(\theta_s - \theta_r)}{a + [\ln|\Psi|]^\beta} + \theta_r \quad , \qquad \text{(C–1)}$$

and the relationship of hydraulic conductivity to pressure-head is given by:

$$K(\Psi) = K_s \frac{A}{A + |\Psi|^B} \quad , \qquad \text{(C–2)}$$

where:

θ	=	volumetric moisture content;
θ_s	=	saturated volumetric moisture content (porosity);
θ_r	=	residual moisture content;
K	=	unsaturated hydraulic conductivity (centimeters/hour);
K_s	=	saturated hydraulic conductivity (centimeters/hour);
Ψ	=	pressure head (centimeters); and
a, β, A, B	=	curve fitting parameters.

The characteristic curves described in Equation (C–1) and Equation (C–2) are not part of the *DCM3D* code. These were coded for this test.

Initially the domain had a uniform pressure-head distribution of - 601.8 centimeters, which corresponded to a moisture content of 0.238. The pressure-head boundary condition at the bottom surface corresponded to the value of the initial condition. The pressure-head boundary condition at the top surface was set to -1 centimeters which corresponded to essentially full saturation.

C–3.2 Comparison of Results

DCM3D results were compared with the quasi-analytic solution of Philip (1957) generated by the *INFIL* code in Figure C–1. The comparison showed reasonable agreement between the two solutions. Regarding the minor discrepancies, the *INFIL* code had some numerical approximations (e.g., summation of series) of its own. Overall, the *DCM3D* was able to simulate the problem of one-dimensional vertical infiltration reasonably well.

To solve this problem, *DCM3D* used 1.24 CPU minutes on a VAX 8700 computer.

C–4 TEST PROBLEM NO. 2 (BENCHMARK): TWO-DIMENSIONAL (2–D) FLOW ON A SATURATED-UNSATURATED REGION

This problem deals with 2–D movement of moisture in a vertical cross-section of an unconfined aquifer, where the zone above the water table is under unsaturated-state conditions. Both the storativity and the hydraulic conductivity may be discontinuous (have a finite jump) at the water table. For example, the storage in the unsaturated zone is caused by change in moisture content caused by proximity to the water table and drainage (or filling) of pores; in the saturated zone, storage is primarily caused by compressibilities of the water and the medium. The objective of this test problem was to investigate the capability of *DCM3D* to deal with such changes in properties. The problem was solved in a transient mode for a long time to approximate steady-state conditions.

C–4.1 Problem Description

The physical domain was modeled as a 150-meters-wide by 35-meters-deep, vertical cross-section, as shown in Figure C–2. For the numerical solution, 30 evenly spaced nodes were placed in the x-direction. In the y-direction, a node spacing of 2 meters was used, from y = 0 to y = 18 meters. The y-direction model spacing was reduced to 1 meter after that. This led to 26 nodes in the y-direction for a total of 780 nodes. Initially, the water-table gradient was assumed to be constant and equal to 2/150. This slope was represented in the simulation by imposing hydrostatic fixed-head boundary conditions in the saturated parts of the two vertical boundaries. The water table itself was not an external boundary in this problem; that is, the water table was obtained as a part of the solution, except at the two external boundaries where it was fixed.

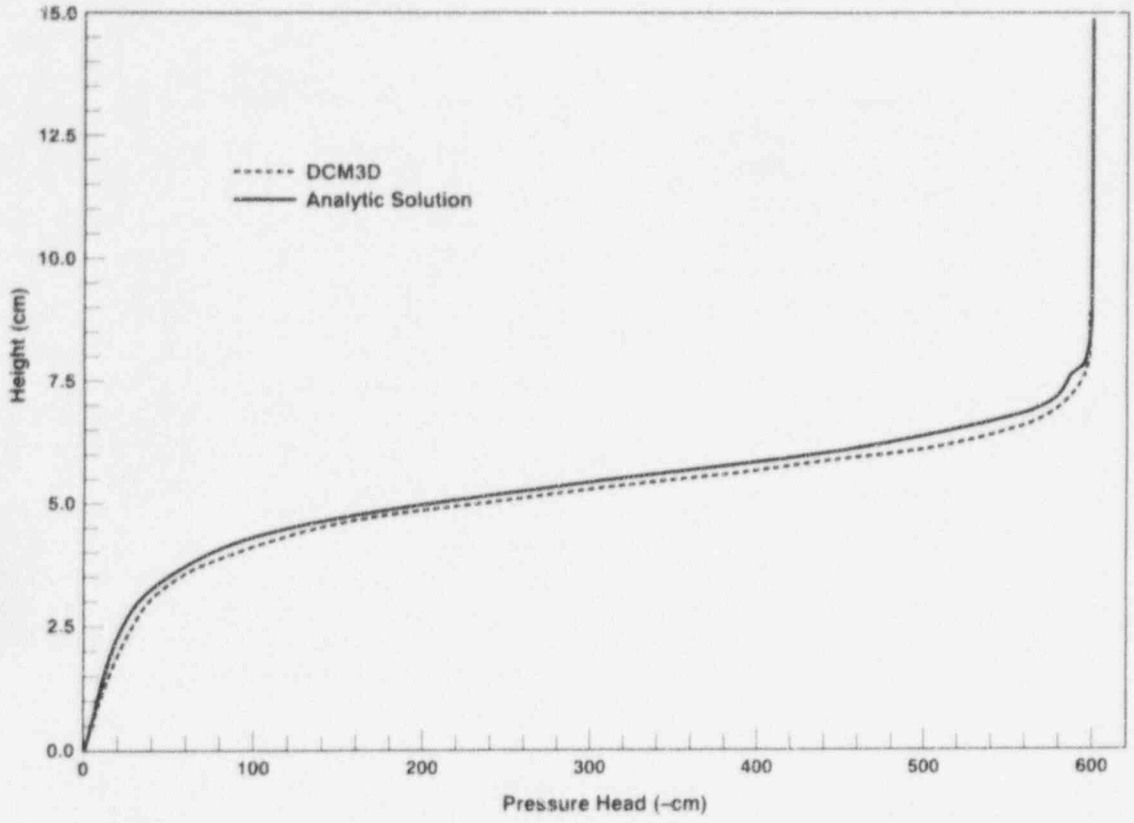

Figure C–1 Comparison of *DCM3D* results with a quasi-analytic solution of a vertical infiltration problem at $t = 2$ hours

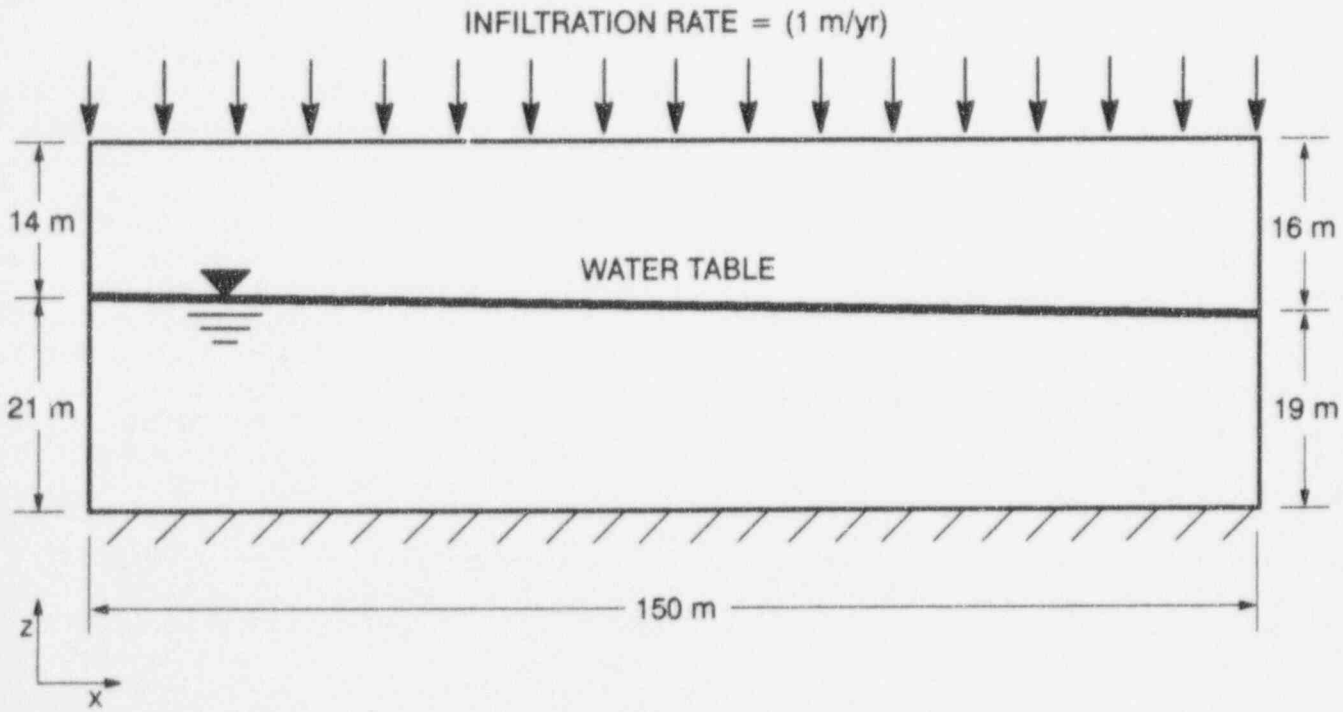

Figure C–2 Definition sketch for Test Problem 2

The hydraulic properties of the soil were those given by Huyakorn *et al.* (1989). The saturated porosity was 0.25 and the saturated hydraulic conductivity was 750 meters/year.

The relationship of saturation to pressure-head is given by:

$$S = 0.25 + \frac{0.75}{1 + (0.2\Psi)^2} \quad , \qquad \text{(C-3)}$$

and the relationship of relative hydraulic-conductivity to pressure-head is given by:

$$K_r = [1 + (0.2\Psi)^2]^{-4} \quad , \qquad \text{(C-4)}$$

where:

S = degree of saturation;
K_r = relative hydraulic-conductivity; and
Ψ = pressure head.

At the top boundary, infiltration was assumed to occur at a constant rate of 1 meter/year. The bottom boundary was assigned a no-flow boundary condition, as were the lateral boundaries of the model above the water table. Pressure heads were prescribed on both upstream and downstream parts of the saturated portion of the aquifer. When using *DCM3D*, either the thermodynamic pressure or the pressure head can be used (but not the total hydraulic head) as the dependent variable. This means that the lateral boundaries in the saturated region have to be assigned pressure heads that vary with elevation.

The initial conditions prescribed were inconsistent with the boundary conditions. The initial conditions were assigned as though there were a water table at a height of 18 meters. Pressure heads were assigned below 18 meters, according to the depth; and above 18 meters, a pressure head of −10 meters was assumed. However, because the problem had to be solved to a steady-state, the initial conditions were not so important.

This problem was solved by *DCM3D* and *PORFLO–3*, Version 1.0 (Runchal and Sagar, 1989; and Sagar and Runchal, 1990), and results are compared below.

C–4.2 Comparison of Results

The *PORFLO–3* results for this problem were taken from the report by Magnuson *et al.* (1990) where these results were compared with those from *FEMWATER* (Yeh and Ward, 1979). In Figure C–3, steady-state pressure-head contours from *DCM3D* are plotted. *PORFLO–3* contours are not shown, as these are exactly the same as those for *DCM3D*, as shown in Figure C–3. Moisture-content profiles at a section 27.5 meters from the left boundary for *DCM3D*, and 30 meters for *PORFLO–3*, are compared in Figure C–4. The difference in locations of these sections is because of the two grid types used in the codes. *DCM3D* places the grid nodes in the middle of a cell, whereas *PORFLO–3* places the cell boundary in the middle of the grid nodes. Despite this difference, the moisture contents compare favorably.

To solve this problem, *DCM3D* used 3.1 CPU minutes on a VAX 8700 computer.

C–5 TEST PROBLEM NO. 3 (BENCHMARK): SIMULATION OF JORNADA TRENCH EXPERIMENT

The Jornada trench experiment is located northeast of Las Cruces, New Mexico, on the New Mexico State University College Ranch. Funded by NRC, this experiment is expressly designed for collected data that can be used in model validation. In the following example, simulation results are not compared with the measured data, but, rather with simulations by another code. Hence, even though the experimental conditions are used as the input data, this test is termed a benchmark (rather than a validation) exercise. A more detailed description of this experiment was provided in the CNWRA's *Quarterly Research Report* (see Sagar and Wittmeyer, 1991).

The Jornada test problem is conceptualized as a vertical 2-D, multi-zone, unsaturated flow problem. Soil-hydraulic properties used in this test are based on those measured at the experimental site. This particular problem involves transient infiltration of water into an extremely dry, heterogeneous soil. Because of the initial dry conditions, the problem is highly nonlinear, and therefore is a good test for *DCM3D*.

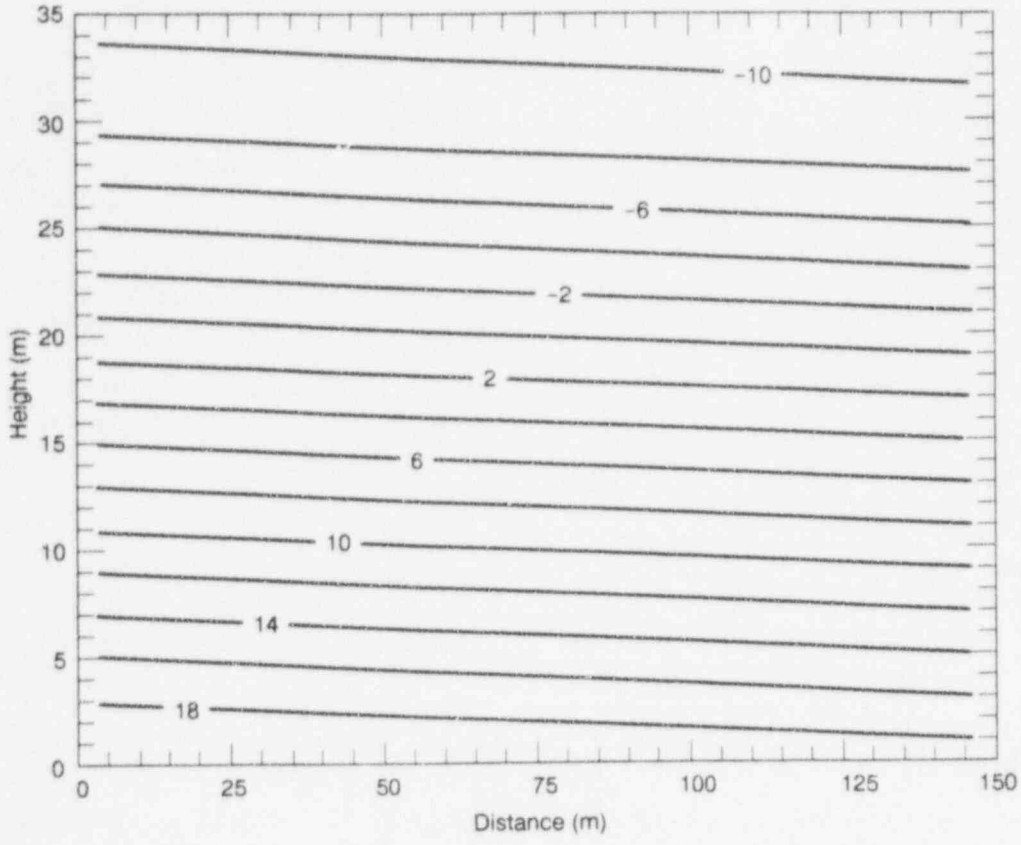

Figure C–3 ***DCM3D*** **pressure-head contour for a 2–D, saturated-unsaturated problem**

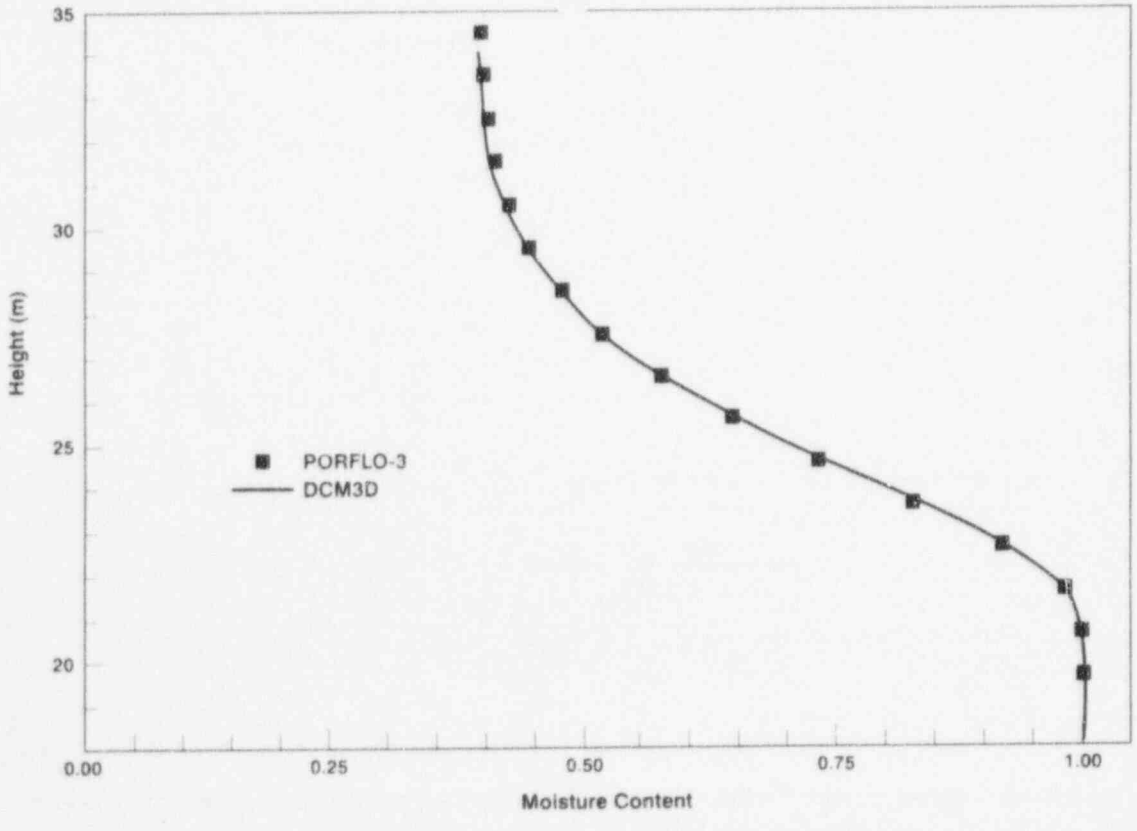

Figure C–4 Comparison of moisture contents from ***DCM3D*** **and** ***PORFLO3,*** **for Test Problem No. 2**

C-5.1 Problem Description

The computational domain of this problem was divided into four zones, as shown in Figure C-5. A portion of the uppermost zone with a 225-centimeter width, measured from the top left hand corner of the domain of interest, was subjected to a water-infiltration rate of 2 centimeters/day (Figure C-5). The rest of the top surface was assumed to be impervious and was modeled as a no-flow boundary. In the experiment, the lateral boundary conditions were difficult to define, because the moisture content along the vertical boundaries would probably vary with time. For this test, the lateral boundaries were assumed to have zero flux crossing them. Such an assumption may cause errors (compared with the actually measured field conditions) unless the lateral boundaries are located at a great distance from the domain of interest. This problem with the lateral boundaries was not investigated further, because the interest here was to compare *DCM3D* results to results from another code. The bottom boundary was arbitrarily assumed to have zero flux. Again, it would probably be more accurate to either extend the domain to the water table, where a zero pressure-boundary condition can be assumed, or to impose a unit gradient (condition of gravity drainage). Using the first option would increase the domain size and consequently the computation time, whereas the second option is not available in *DCM3D*. Initially, the pressure head was assumed to be uniform throughout the entire domain at -734 centimeters.

The physical domain modeled was 800 centimeters by 650 centimeters. There were 56 nodes in the x-direction, and 47 nodes in the y-direction (total of 2632 nodes). From $x = 0$ centimeters to $x = 350$ centimeters, and $y = 350$ centimeters to $y = 650$ centimeters, grid spacing was 10 centimeters. From $x = 350$ centimeters to $x = 800$ centimeters, and from $y = 0$ centimeters to $y = 350$ centimeters, grid spacing was 25 centimeters.

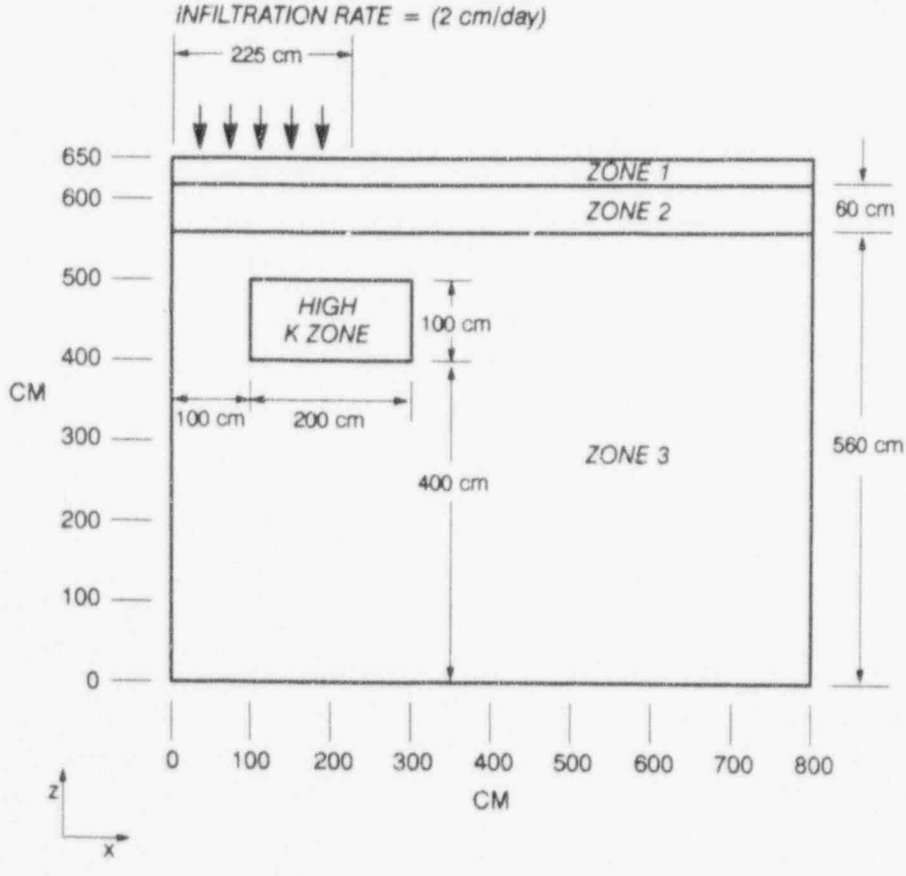

Figure C-5 Definition sketch for the Jornada Trench experiment (Test Problem No. 3)

The relationship of moisture content to pressure-head and the relationship of relative-permeability to moisture content are described by the van Genuchten (1980) equations as follows:

$$\theta = (\theta_s - \theta_r)\left(\frac{1}{1 + (a\Psi)^n}\right)^m + \theta_r \quad , \qquad \text{(C-5)}$$

and

$$K_r = \sqrt{\theta_e}\left\{1 - \left[1 - (\theta_e)^{\frac{1}{m}}\right]^m\right\}^2 \quad . \qquad \text{(C-6)}$$

The variables are defined as follows:

θ = volumetric moisture content;
θ_r = residual moisture content;
θ_s = saturated moisture content;
Ψ = pressure head;
n = van Genuchten parameter;
m = van Genuchten parameter
= $(1 - 1/n)$;
a = parameter; and
K_r = relative hydraulic-conductivity.

The values of the input parameters for the four layers are given in Table C-1. The solver used was the *LSODES*, contained in *ODEPACK* (Hindmarsh, 1983). A relative convergence criterion of 1.0×10^{-5} and an absolute convergence criterion of 1.0×10^{-2} were imposed.

C-5.2 Comparison of Results

Again, *DCM3D* results were compared to *PORFLO-3* results taken from the report by Magnuson *et al.* (1990) in which *PORFLO-3* results were compared with the results from *FLASH* (Baca and Magnuson, 1992). Earlier, Smyth *et al.* (1989) used the same data for a test of *TRACER3D*, a code developed at Los Alamos Laboratories by Travis (1984).

The simulations were run in 30-day durations. The saturations at 30 days after the start of the moisture infiltration are shown in Figure C-6. The previous comparison of *PORFLO-3*, *FLASH*, and *TRACER3D* results are shown in Figure C-7. All four codes showed a pronounced effect of the high permeability zone on moisture distribution. For this complex problem, results of all the codes differed somewhat from each other. Figure C-7 indicates large differences between results (e.g. in advance of the wetting front) from *TRACER3D* and the other codes. The *DCM3D* results were reasonably close to those from *PORFLO-3* and *FLASH*.

DCM3D used 237 minutes of CPU time on a VAX 8700, while *PORFLO-3* used 5.95 minutes of INEL Cray CPU time. For the same problem, the CPU times for *TRACR3D* and *FLASH* were reported to be 5.79 Hanford CRAY minutes and 16.8 INEL CRAY minutes, respectively. Unfortunately, because of different computing environments, these execution times were not directly comparable.

Table C-1 Van Genuchten Soil Parameters

Zone	θ_s	θ_r	a (cm^{-1})	n	K_s
1	0.368	0.1020	0.0334	1.982	790.9
2	0.351	0.0985	0.0363	1.632	469.9
3	0.325	0.0859	0.0345	1.573	415.0
4	0.325	0.0859	0.0345	1.573	4150.0

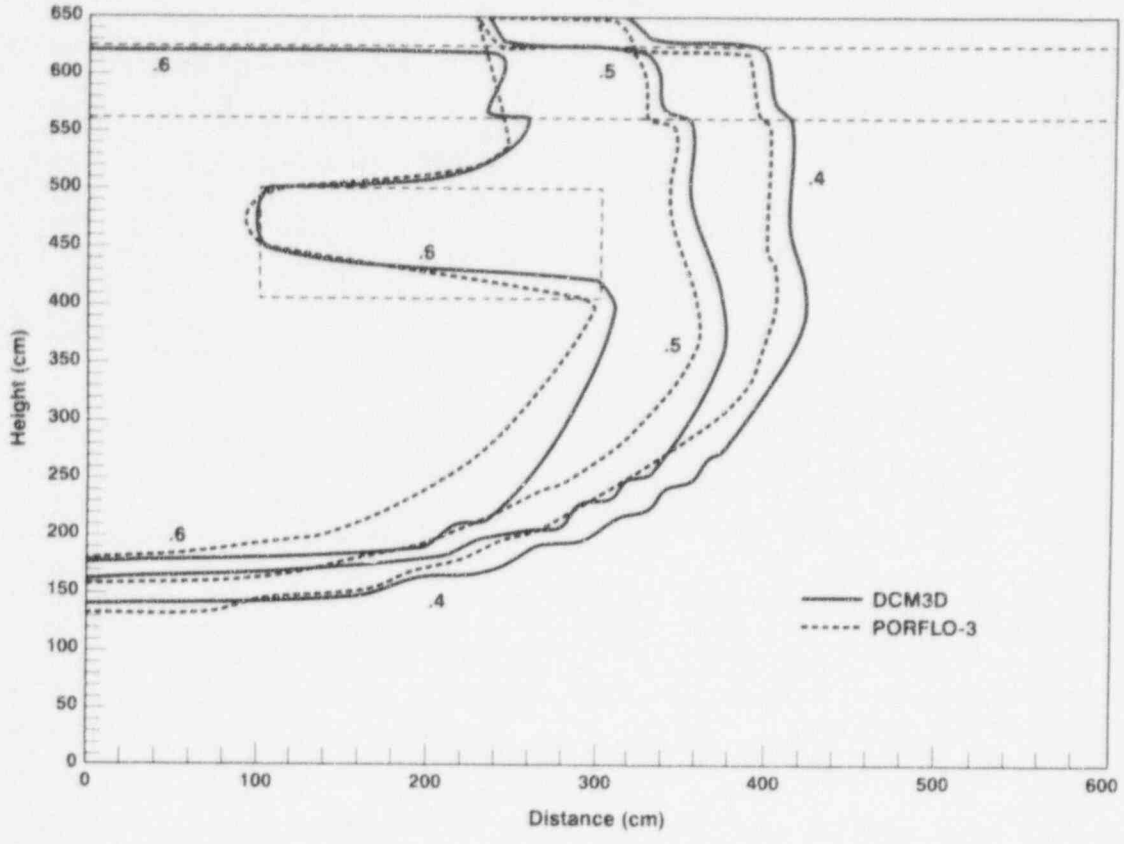

Figure C–6 Comparison of *DCM3D* and *PORFLO–3* results (moisture contents) for the Jornada Trench experiment (Test Problem No. 3)

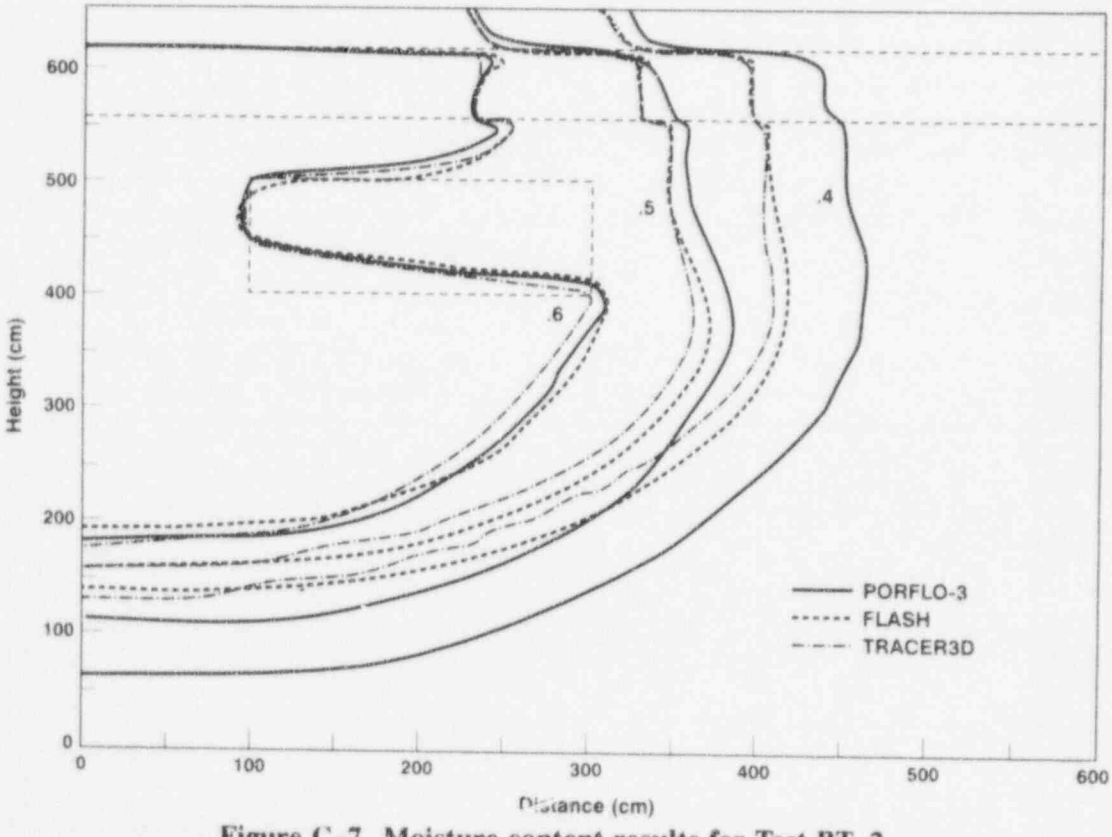

Figure C–7 Moisture content results for Test BT–2

Table C–2 Coordinates of the Numbered Points in Figure C–7 (from Prindle and Hopkins, 1990)

	Coordinates (m)			*Coordinates (m)*	
Point	*x*	*z*	*Point*	*x*	*y*
1	0.0	635.5	13	1000.0	224.0
2	0.0	608.7	14	1000.0	219.5
3	0.0	570.6	15	1000.0	130.3
4	0.0	440.5	16	1000.0	0.0
5	0.0	329.1	17	1000.5	530.4
6	0.0	324.6	18	1000.5	503.6
7	0.0	235.4	19	1000.5	465.5
8	0.0	0.0	20	1000.5	335.4
9	1000.0	530.4	21	1000.5	224.0
10	1000.0	503.6	22	1000.5	219.5
11	1000.0	465.5	23	1000.5	130.3
12	1000.0	465.5	24	1000.5	0.0

C–6 TEST PROBLEM NO. 4: 2–D FLOW THROUGH FRACTURED ROCK

The distinguishing feature of the *DCM3D* computer code is that it employs a dual-porosity conceptualization of the fractured porous medium, instead of an equivalent porous (single-porosity) medium or a fracture-network conceptualization. In the more common equivalent porous-medium approach, the characteristic curves for the rock matrix and the fractures are combined to form a composite characteristic curve. The composite curve assumes a rapid (with respect to the time scale of the flow being simulated) equilibration between the pressures of the fracture and matrix continua; and thus, the equilibration of pressure between the two continua is affected.

An important question is how different are the predicted flow fields for these two different conceptualizations. A convenient test case to explore this question was taken from the HYDROCOIN study. The test case was based on a flow field associated with unsaturated-fractured tuff (Prindle and Hopkins, 1990). The HYDROCOIN test case was used here to examine the differences in the two conceptualizations, as well as to compare the *DCM3D* results with the HYDROCOIN results, to provide a measure of verification for *DCM3D*.

C–6.1 Problem Description

A complete description of the test case is provided in Prindle and Hopkins (1990). Only the information pertinent to the current simulations is provided here. The 2–D cross-section was comprised of five layers, with a uniform dip of 6 degrees at unit interfaces (Figure C–8). Additionally, a repository location and a fault zone were defined for the test case Material properties for the various layers were reproduced from the Prindle and Hopkins report, in Table C–3.

The current simulations used modification 1, from the Prindle and Hopkins (1990) study. Modification 1 changed the original model description by not explicitly considering the fault zone and by modifying the rock properties, according to Table C–4. This modification was selected primarily because the beta parameter used for the van

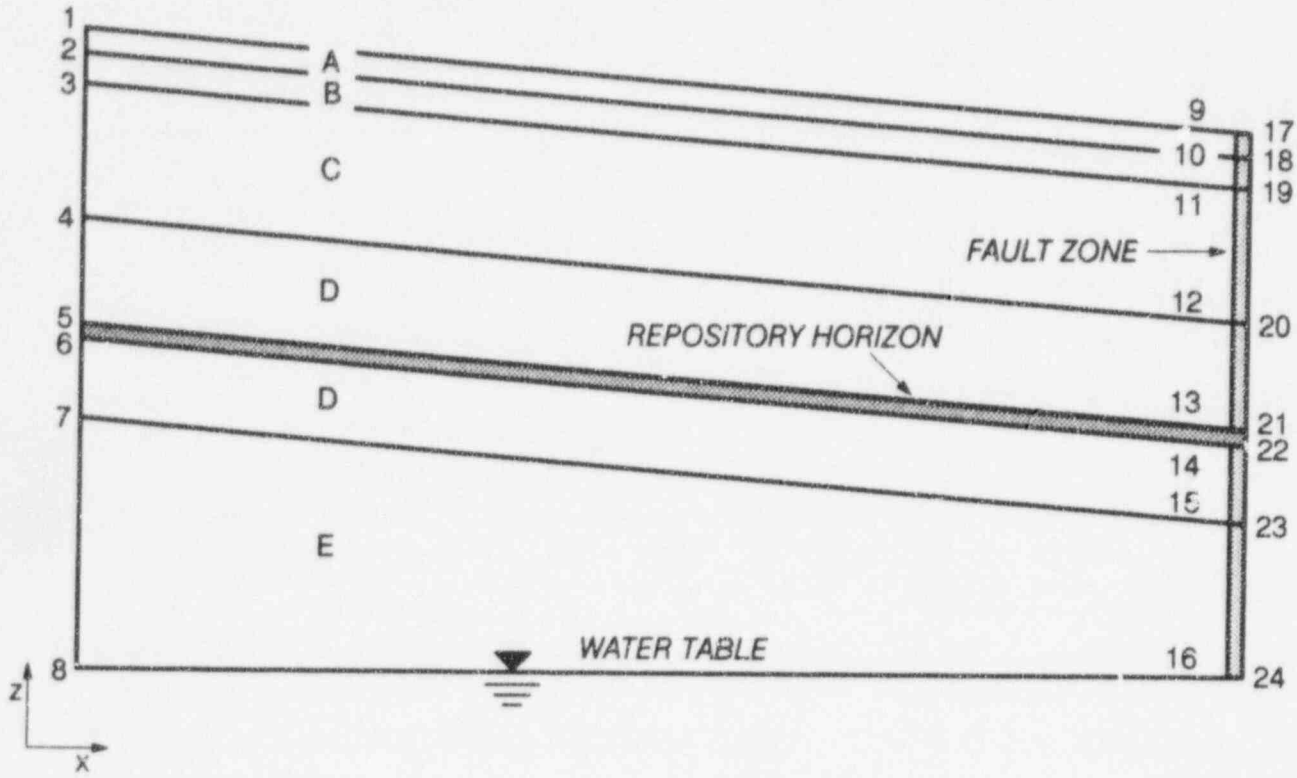

Figure C–8 Two-dimensional base-case stratigraphy (from Prindle and Hopkins, 1990)
(See Table C–2 for coordinates of the numbered locations.)

Table C–3 Base Case Material Properties Used for the Hydrologic Units, as Depicted by Letters in Figure C–7 (from Prindle and Hopkins, 1990)

Matrix Properties

Unit	*Porosity*	*Hydraulic Conductivity (m/sec)*	*Residual Saturation*	*van Genuchten Parameters*	
				Alpha (1/m)	*Beta*
A	0.08 (.05 to .15)	9.7×10^{-12} (1×10^{-13} to 5×10^{-10})	0.002 (0. to .18)	.00821 (.003 to .024)	1.558 (1.3 to 2.4)
B	0.40 (.20 to .70)	3.9×10^{-7} (1×10^{-9} to 5×10^{-6})	0.100 (0. to .15)	.0015 (.001 to .031)	6.872 (1.2 to 15.)
C	0.11 (.05 to .20)	1.9×10^{-11} (1×10^{-13} to 5×10^{-10})	0.080 (0. to .23)	.00567 (.001 to .020)	1.798 (1.2 to 2.5)
D	0.11 (.05 to .20)	1.9×10^{-11} (1×10^{-13} to 5×10^{-9})	0.080 (0. to .32)	.00567 (.001 to .020)	1.798 (1.2 to 2.5)
Ev	0.46 (.30 to .55)	2.7×10^{-7} (1×10^{-13} to 5×10^{-6})	0.041 (0. to .25)	.0016 (.005 to .06)	3.872 (1.3 to 7.0)
Ez	0.26 (.20 to .45)	2.0×10^{-11} (1×10^{-14} to 5×10^{-10})	0.110 (0. to .30)	.00308 (.001 to .03)	1.602 (1.2 to 3.5)

Individual Fracture Properties

Unit	*Aperture (Microns)*	*Hydraulic Conductivity (m/sec)*	*Density (No./m³)*	*Porosity*
A	6.74	3.8×10^{-5} (5×10^{-7} to 5×10^{-3})	20	1.4×10^{-4} (1×10^{-5} to .001)
B	27.0	6.1×10^{-4} (5×10^{-6} to 5×10^{-2})	1	2.7×10^{-5} (2×10^{-6} to 2×10^{-4})
C	5.13	2.2×10^{-5} (5×10^{-7} to 1×10^{-3})	8	4.1×10^{-5} (2×10^{-6} to 1×10^{-3})
D	4.55	1.7×10^{-5} (1×10^{-7} to 1×10^{-3})	40	1.8×10^{-4} (1×10^{-5} to 5×10^{-3})
Ev	15.5	2.0×10^{-4} (2×10^{-6} to 2×10^{-2})	3	4.6×10^{-5} (5×10^{-6} to 5×10^{-4})
Ez	15.5	2.0×10^{-4} (2×10^{-6} to 2×10^{-2})	3	4.6×10^{-5} (5×10^{-6} to 5×10^{-4})

Table C–3 (continued)

Unit	Bulk Porosity	Hydraulic Conductivity (m/sec)	Residual Saturation	van Genuchten Parameters Alpha(1/m)	Beta
	Bulk Fracture Properties				
A	1.4×10^{-4} (1×10^{-5} to .001)	5.3×10^{-9} (5×10^{-12} to 5×10^{-6})	0.0395 (0. to .15)	1.285 (.2 to 6.0)	4.23 (1.2 to 7.0)
B	2.7×10^{-5} (2×10^{-6} to 2×10^{-4})	1.6×10^{-8} (1×10^{-11} to 1×10^{-5})	0.0395 (0. to .15)	1.285 (.2 to 6.0)	4.23 (1.2 to 7.0)
C	4.1×10^{-5} (2×10^{-6} to 1×10^{-3})	9.0×10^{-10} (1×10^{-12} to 1×10^{-6})	0.0395 (0. to .15)	1.285 (.2 to 6.0)	4.23 (1.2 to 7.0)
D	1.8×10^{-4} (1×10^{-5} to 5×10^{-3})	3.1×10^{-9} (1×10^{-12} to 1×10^{-6})	0.0395 (0. to .15)	1.285 (.2 to 6.0)	4.23 (1.2 to 7.0)
Ev	4.6×10^{-5} (5×10^{-6} to 5×10^{-4})	9.2×10^{-9} (1×10^{-11} to 1×10^{-5})	0.0395 (0. to .15)	1.285 (.2 to 6.0)	4.23 (1.2 to 7.0)
Ez	4.6×10^{-5} (5×10^{-6} to 5×10^{-4})	9.2×10^{-9} (1×10^{-11} to 1×10^{-5})	0.0395 (0. to .15)	1.285 (.2 to 6.0)	4.23 (1.2 to 7.0)

Table C–4 Material Properties Used in Modification (from Prindle and Hopkins, 1990)

Property	Unit B	Unit C	Unit D
$K_{m,b}$	1.0×10^{-7}	8.0×10^{-11}	8.0×10^{-11}
a_m	0.010	0.015	0.015
β_m	2.2	1.6	1.6
$K_{f,b}$	3.6×10^{-6}	2.0×10^{-9}	3.1×10^{-9}
n_f	9.0×10^{-6}	9.0×10^{-5}	1.8×10^{-4}

Genuchten equation was significantly lower (2.2 compared with 6.8) than the original value and was anticipated to lead to much shorter simulation times.

The finite difference grid for *DCM3D* was set up to provide the finest discretization in the vertical direction for the upper units (Table C-5) and a constant spacing in the horizontal direction. Rather than "stair-stepping" grid blocks at unit interfaces, the cross-sectional tilt was obtained by tilting gravity and increasing the depth to the water table by 100 meters (the depth to the water table was increased to decrease the affect of tilting the water-table boundary condition on the computational area of interest).

The tilting of gravity was considered to represent the problem description reasonably well, with the exception being near the side and bottom boundaries. Near the side boundaries, rather than a vertical boundary, the tilting of gravity causes the boundary to also appear slightly tilted. Near the bottom boundary, a significant flow is induced because of the tilting of gravity, which results in a gradient of 0.1. Despite these inaccuracies, the conceptualization was considered reasonable for examining flow diversion in the upper units (top 50 meters) and the spatial distribution of flow at the repository level (400 meters below the surface).

One additional parameter (the transfer term between matrix and fracture) was needed to perform the *DCM3D* simulations. The transfer term or factor, together with the gradient between the fracture and matrix controls the rate at which the fracture and matrix continua equilibrate. In the *DCM3D User's Manual* (Updegraff *et al.*, 1991), this parameter is defined by the following equation:

$$A = A_s \frac{k_s^m}{l} \quad , \qquad \text{(C-7)}$$

where:

A = transfer factor;
k_s^m = matrix saturated permeability;
A_s = fracture specific surface area per unit volume; and
l = length parameter for gradient between fracture and matrix.

An attempt to determine the transfer factor in Equation (C-7), based on measurable quantities related to the fractures and matrix, was done by assuming that fractures were regularly spaced and planar and adopting a fracture-coating term. The fracture-coating term is used to represent a decrease (values less than 1) in transfer of water, resulting from a coating on the surface of the fracture, or an increase in transfer of water because of micro-fractures.

This conceptualization is represented by the following equation:

$$A_r = 4\ C\ n^2\ (k_s^m) \quad , \qquad \text{(C-8)}$$

where:

A_r = transfer factor, assuming regular-spaced planar fractures;
C = fracture-coating term;
n = number fractures per unit area; and
k_s^m = saturated permeability of the matrix.

Equation C-8, the parametric values presented in Table C-3, and a coating factor of 0.5 were used to determine the transfer terms (see Table C-6).

One objective of this analysis was to compare the results, assuming a composite curve, with those obtained by assuming a dual-continuum approach. It was considered advantageous to implement a composite curve approach within *DCM3D*, so as to use one input file for both conceptualizations. Modifications to *DCM3D* were made such that it would accept the composite characteristic curve as input.

C-6.2 Comparison of Results

Performance measures used for this analysis were: (1) particle paths starting along the upper boundary; and (2) the spatial distribution of water flux at the repository level. The HYDROCOIN results are taken from Prindle and Hopkins (1990) and are presented in Figures C-9 and C-10. These simulation results were obtained with the computer program called *NORIA* (Bixler, 1985).

Table C–5 ***DCM3D*** **Vertical Discretization Information**
(Horizontal discretization is a constant spacing of 50 meters for 1000 meters.)

Finite Difference Row Indices	*Block Thickness (m)*	*Depth (m)*	*Unit*
1 - 35	10.0	705 - 400	Ez
36 - 55	10.0	400 - 200	D
56 - 60	10.0	200 - 150	C
61 - 63	8.0	150 - 126	C
64 - 65	6.0	126 - 114	C
66 - 67	4.0	114 - 106	C
68 - 70	2.0	106 - 100	C
71 - 100	1.0	100 - 70	C
101 - 140	1.0	70 - 30	B
141 - 170	1.0	30 - 0	A

Table C–6 Transfer Factors Used for the Units Identified in Figure C–7 and Using Equation (C–8)

Unit	*Transfer Factor*
A	7.92×10^{-16}
B	2.04×10^{-14}
C	1.04×10^{-15}
D	2.61×10^{-14}
Ez	3.67×10^{-17}

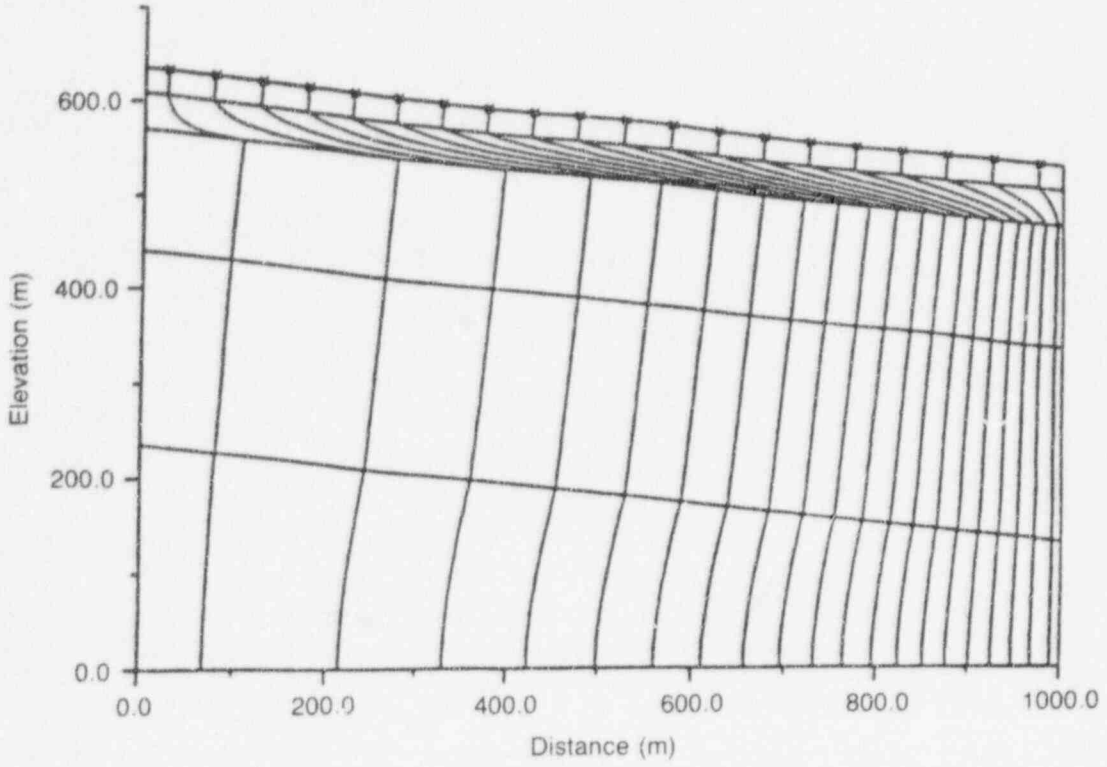

Figure C-9 Particle paths based on the *NORIA* simulation (flux = 0.1 mm/yr) (from Prindle and Hopkins, 1990)

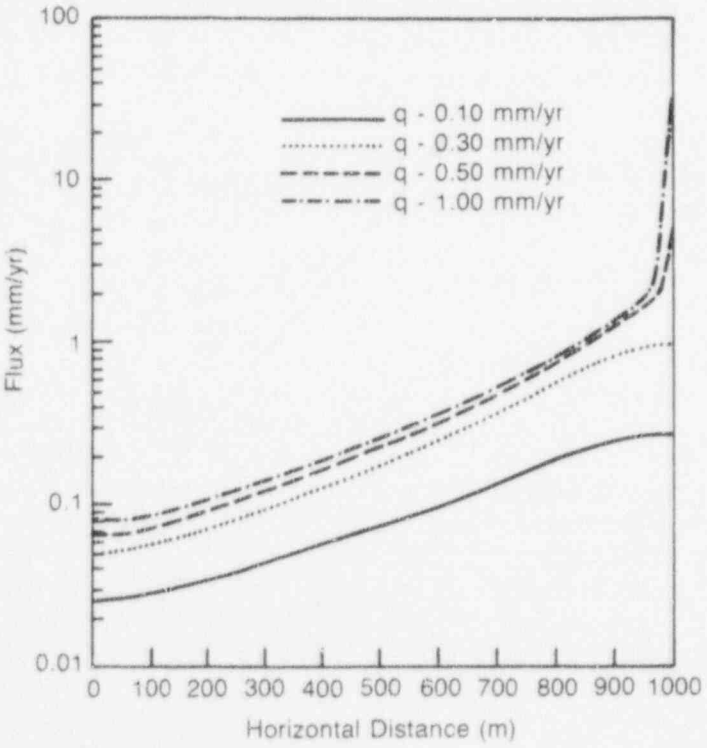

Figure C-10 Spatial distribution of flux at the repository, based on the *NORIA* simulation flux boundary condition values, as indicated by *q* (in the figure) (from Prindle and Hopkins, 1990)

Although CPU times for individual runs were not provided, Prindle and Hopkins reported that the 94 simulations required a combined 1300 hours of CPU time on a Cray X/MP 416.

The *DCM3D* results using the composite curve for representing the fracture/matrix continua are presented in Figures C–11 and C–12. Ignoring some minor discrepancies due to boundary-condition differences, the results compare quite well with the *NORIA* results. This is not surprising because both programs utilize a composite curve conceptualization.

This simulation required approximately 50 minutes of CPU time on an IBM 3090 (for comparative purposes, the IBM is estimated to be 5 to 10 times slower than the Cray computer).

The *DCM3D* results using the dual-continuum approach are presented in Figures C–13, C–14, and C–15. As with the composite-curve results, the dual-continuum results compare reasonably well with the *NORIA* results. Although a somewhat significant discrepancy does exist near the bottom boundary, it can be attributed to the tilted bottom boundary and the fact that the simulation had not reached a steady state. *DCM3D* does not have a steady-state option, and the user is required to select a time sufficient to reach this point. For this simulation, a point in the middle of the domain rather than at the bottom boundary was used to determine steady-state conditions.

The fracture particle paths did not vary significantly from the matrix paths in the dual-continuum approach because of the isotropic conditions assumed for both matrix and fractures, the assumed connectivity of the fracture network, and the application of steady-state boundary conditions. Future work will consider anisotropic fracture conditions, high flux rates, and transient boundary conditions that could result in larger fracture flow (the current flux of 0.1 millimeters/year resulted in fracture flow at the repository level approximately 10 orders of magnitude lower than the matrix flow).

This simulation required approximately 8 hours of CPU time on the IBM 3090.

DCM3D results were generally in good agreement with the *NORIA* results. However, the dual-continuum versus the composite-curve approach needs to be examined further, to provide better insights into the differences in the models. Increased infiltration, anisotropic fracture properties, transient boundary conditions, and ranges of fracture-transfer terms should be used in future work. The current simulations, however, do provide a reasonable starting point for a departure into these more difficult simulations.

C–7 SUMMARY AND CONCLUSIONS

Four test problems of increasing complexity were solved, using the *DCM3D* computer code. In general, the code produced reasonable results for all of the four problems, indicating that the basic equations are correctly implemented in the computer code.

However, basic questions regarding the applicability of the dual-porosity approach for simulating partially saturated flow in fractured rock are not resolved by the testing discussed in this report. The main advantage of the dual-porosity approach is in its simplicity, obtained by lumping the fractures as a continuum superimposed over a matrix continuum. Thus, the geometric details of the fracture network need not be considered. Presumably, such an approach is capable of considering non-equilibrium pressure distribution between the fracture and rock continua. Conceptually, such a pressure non-equilibrium could occur when the flow field changes, for example during transient flow conditions, or at the interface between units with different fracture and matrix properties. This conceptual simplicity, however, introduces a parameter that represents, in a lumped fashion, the fluid interchange between the fracture and rock continua. The technical basis for this parameter (the transfer factor) and its relationship to measurable media properties need to be examined further. It should also be clear that the dual-porosity approach does not provide information on pressure distribution at the scale, for instance, of the fracture width. Again, this is because the fracture continuum has no definite location, but is continuously superimposed over the rock continua.

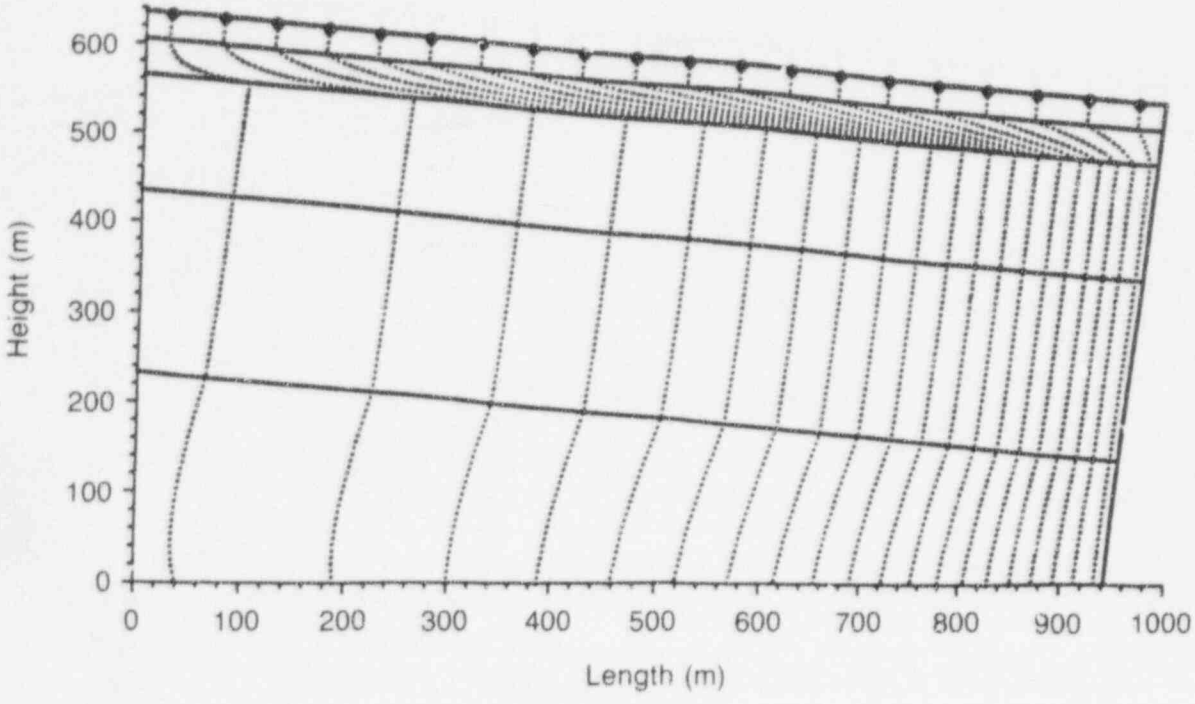

Figure C-11 Particle paths, based on the *DCM3D* simulation, using a composite curve (flux = 0.1 mm/yr)

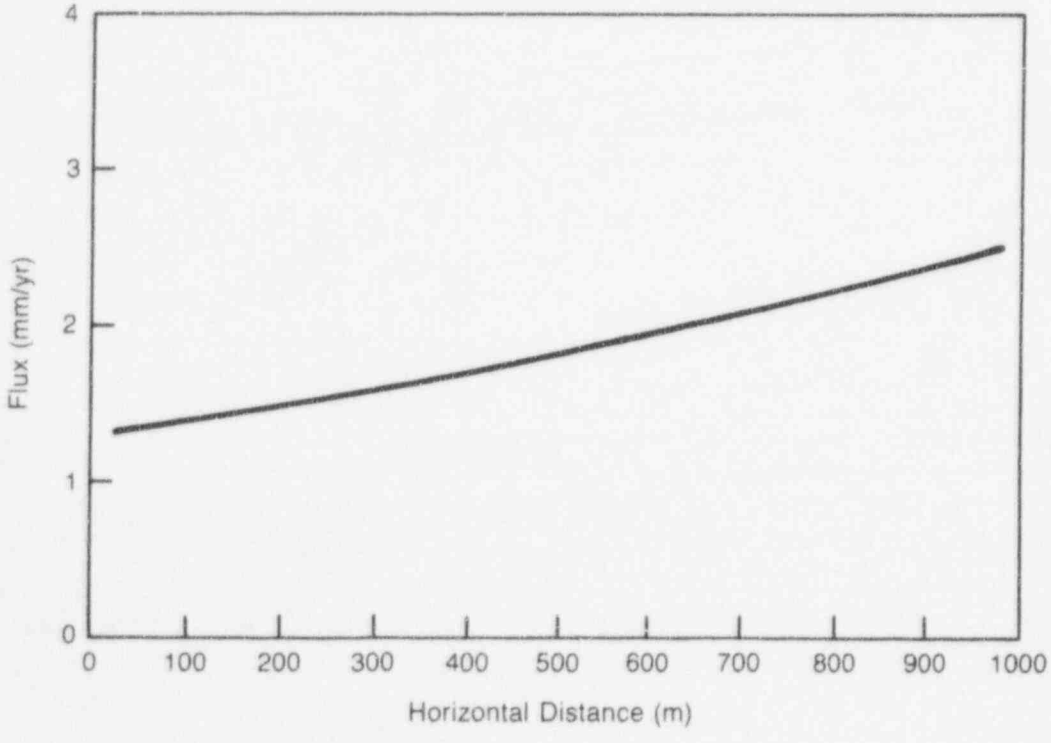

Figure C-12 Spatial distribution of flux, based on the *DCM3D* simulation, using the composite curves (flux = 0.1 mm/yr)

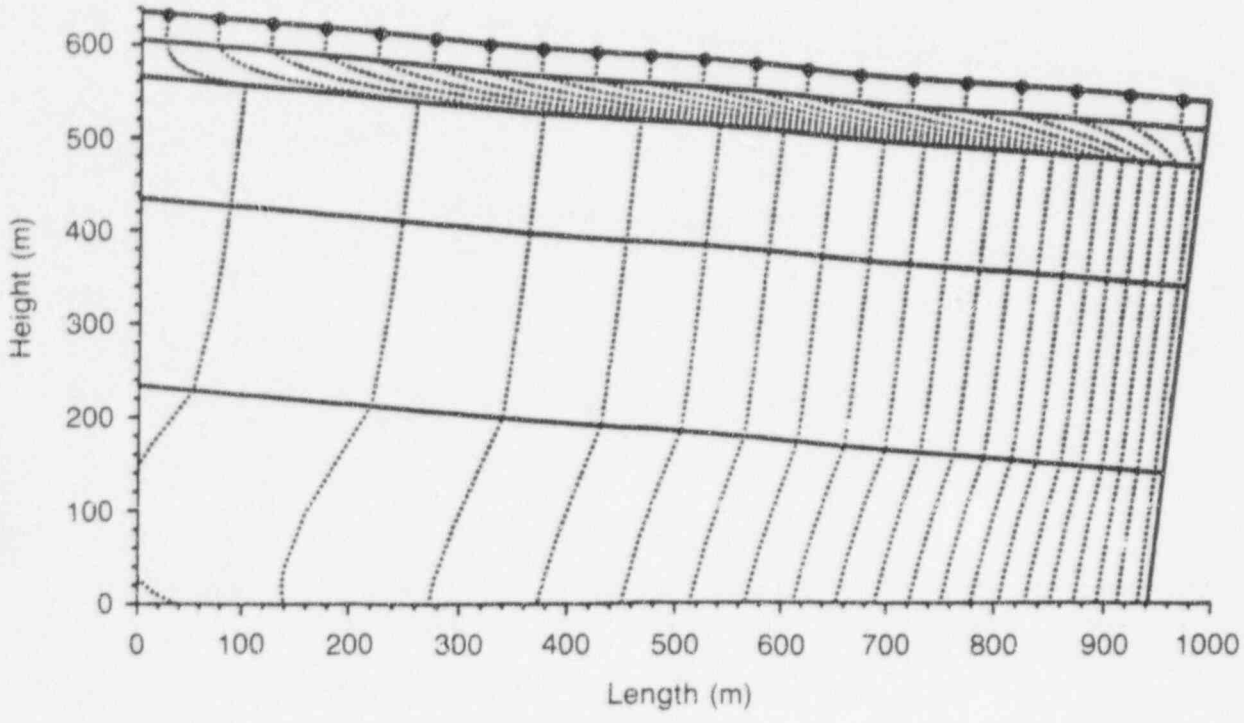

Figure C–13 Particle paths in the matrix, based on the *DCM3D* simulations, using the dual-porosity model (flux = 0.1 mm/yr)

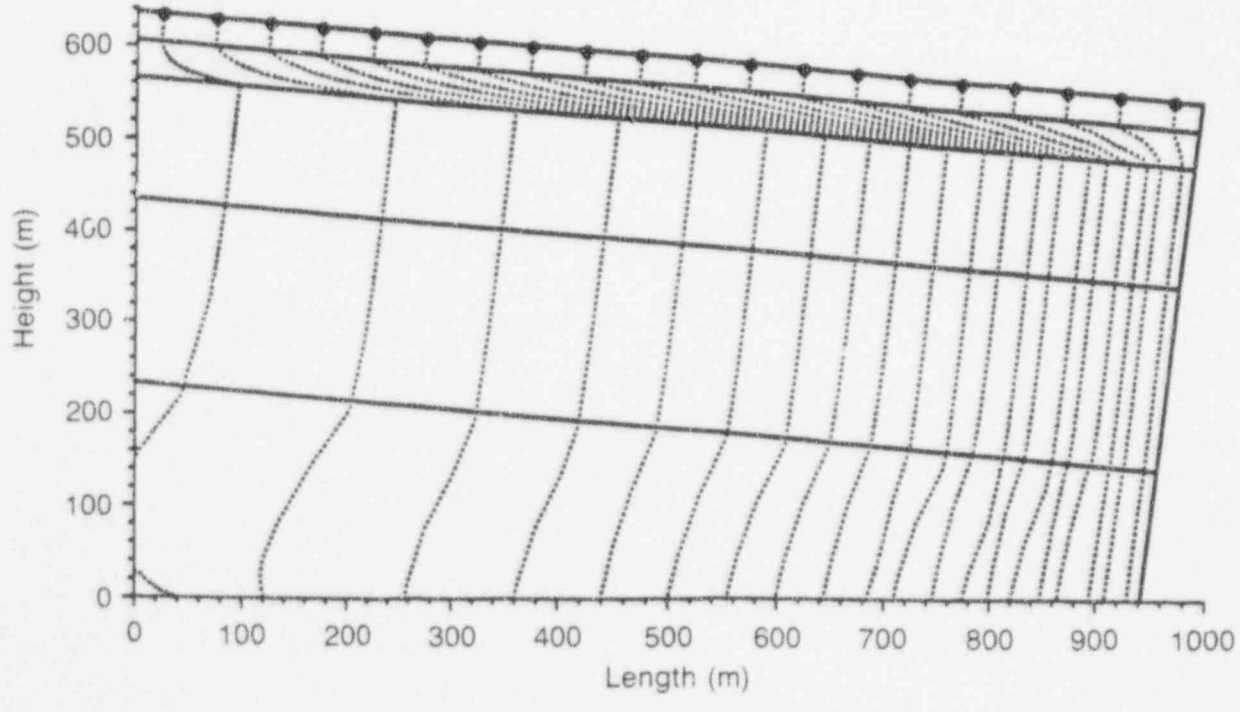

Figure C–14 Particle paths in the fracture, based on *DCM3D* simulations, using the dual-porosity model (flux = 0.1 mm/yr)

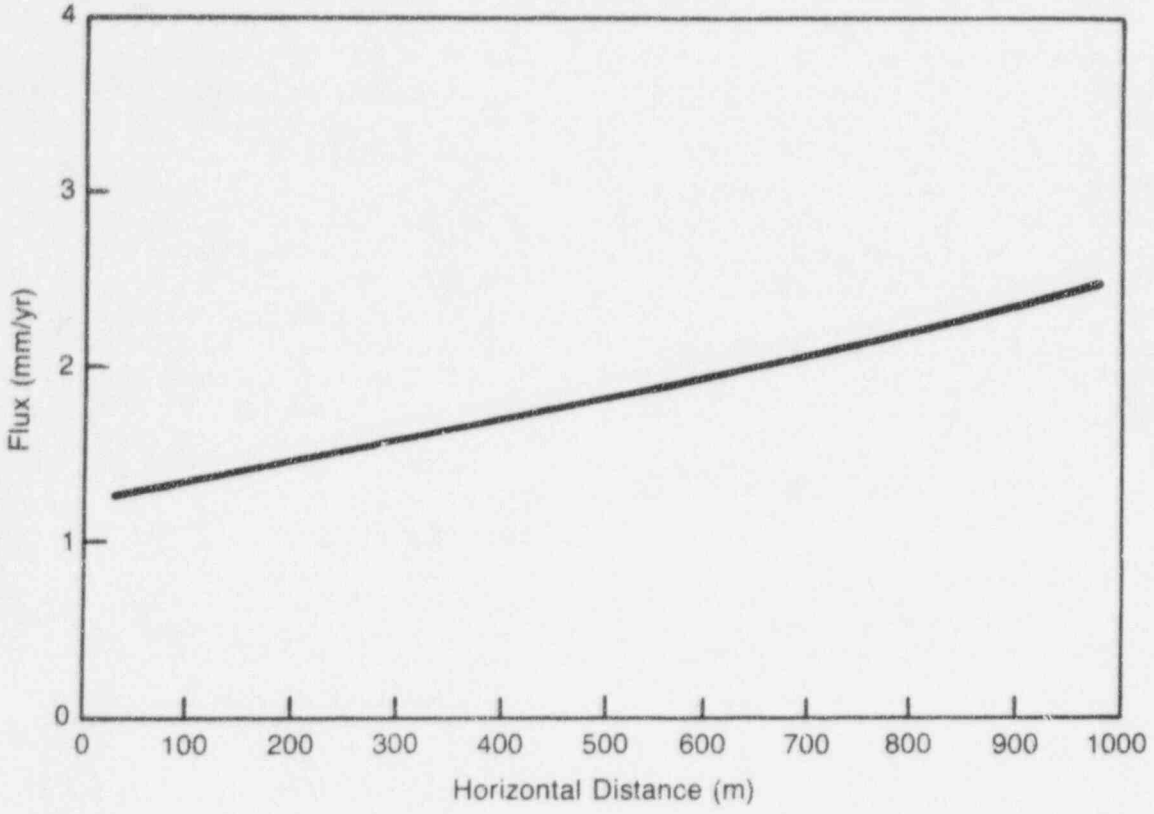

Figure C–15 Spatial distribution of flux in the matrix, based on the *DCM3D* simulation, using the dual-porosity model (flux = 0.1 mm/yr)

Similar problems are also attendant to other approaches to modeling partially saturated flow in fractured porous media. Use of a composite characteristic curve has the same disadvantage as the dual-porosity approach, in not distinguishing the distinct location and geometry of the fractures. In addition, this approach requires the assumption that locally (within a computational cell) the pressures in the fracture and the rock are instantaneously in equilibrium. However, computationally, the composite-curve approach is simpler and less time-consuming than the dual-porosity approach, because only a single governing equation needs to be solved. The fracture-network type of modeling requires not only detailed definition of the fracture topology, but also definition of its characteristic curves. Therefore, not only are the data needs multiplied, but the computation times become large. It may be that a mixed approach is appropriate, where the large faults that could control the flow system to a significant spatial scale (of the order of hundreds of meters) are represented as separate entities in the model, whereas the small fractures are dealt with as dual-porosity or composite curves.

As new users[1] of the *DCM3D* code, the IPA Phase 2 staff had difficulty in setting up the test problems. Some of the problems and recommendations are as follows:

- There is a need for experimental investigations of fracture-matrix interaction, to provide insight into applicability of the dual-porosity concept and the composite-curve approach.
- The idea of using an approach that combines features of the dual-porosity and fracture-network approaches should be investigated.
- The input structure, in general, is cumbersome; no comments are allowed, and the analyst has to input a great deal of

[1]The authors of this report often ran into trouble while setting up the test problems previously discussed. When called upon, Mr. C. David Updegraff, developer of the *DCM3D* computer code, was gracious in providing advice. His help is gratefully acknowledged.

inconsequential quantities. The input can certainly be improved to compress the input files and make these more readable.

- The options for the medium characteristic curves are too limited; at least one option allowing the input of a characteristic curve in a table format should be added.

- Only rectangular coordinates are allowed; it should be a relatively minor matter to add the cylindrical coordinates.

- Steady-state option is not available, and this problem cannot be easily fixed.

- It would be worthwhile to examine what modifications are required to implement a steady-state option and to make the input more user-friendly.

- The manner in which the gravity is introduced in the model is confusing.

- The switch from thermodynamic pressure to pressure head is not straightforward; it essentially requires fooling the code, and total hydraulic head can not be used as a dependent variable, at all.

C-8 REFERENCES

Ababou, R., "Approaches to Large Scale Unsaturated Flow in Heterogeneous, Stratified, and Fractured Geologic Media," U.S. Nuclear Regulatory Commission, NUREG/CR-5743, August 1991. [Prepared by the Center for Nuclear Waste Regulatory Analyses.]

Baca, R.G. and S.O. Magnuson, "FLASH—A Finite Element Computer Code for Variably Saturated Flow," Idaho Falls, Idaho, Idaho National Engineering Laboratory, EGG-GEO-10274, August 1992. [Prepared by EG&G, Inc., for the U.S. Department of Energy.]

Bixler, N.E, "NORIA—A Finite Element Computer Program for Analyzing Water, Vapor, and Energy Transport in Porous Media," Albuquerque, New Mexico, Sandia National Laboratory, SAND84-2057, August 1985. [Prepared for the U.S. Department of Energy.]

El-Kadi, A.I, *INFIL*, Indianapolis, Indiana, Holcomb Research Institute/International Groundwater Modeling Center, June 1987. [Computer program]

Gureghian, A.B. and B. Sagar, "Evaluation of DCM3D—A Dual Continuum, 3-D Groundwater Flow Code for Unsaturated, Fractured, Porous Media," in Patrick, W.C. (ed.), "Report on Research Activities for Calendar Year 1990," U.S. Nuclear Regulatory Commission, NUREG/CR-5817 (vol. 1), December 1991. [Prepared by the Center for Nuclear Waste Regulatory Analyses.]

Haverkamp, R., M. Vanclin, J. Touma, P. J. Wierenga, and G. Vachaud. "A Comparison of Numerical Simulation Models for One-Dimensional Infiltration," *Soil Science Society of America Journal*, 41:285-294 [1977].

Hindmarsh, A.C., "ODEPAK: A Systematized Collection of ODE Solvers," in Stepleman, R.S., *et al.* (eds.), *Scientific Computing*, Amsterdam, North-Holland Publishing Co., pp. 55-64, 1983.

Huyakorn, P.S., J.B. Kool, and J.B. Robertson, "VAM2D—Variably Saturated Analysis Model in Two Dimensions," U.S. Nuclear Regulatory Commission, NUREG/CR-5352, May 1989. [Prepared by Hydro Geologic, Inc.]

Magnuson, S.O., R.G. Baca, and A. Jeff Sondrup, "Independent Verification and Benchmark Testing of the PORFLO-3 Computer Code (Version 1.0)," Idaho Falls, Idaho, Idaho National Engineering Laboratory, EGG-BG-9175, August 1990. [Prepared by EG&G, Inc., for the U.S. Department of Energy.]

Philip, J.R, "Numerical Solution of Equations of the Diffusion Type with Diffusivity Concentration-Dependent II," *Australian Journal of Physics*, 10:29-42 [1957].

Prindle, R.W. and P. Hopkins, "On Conditions and Parameters Important to Model Sensitivity for Unsaturated Flow Through Layered Fractured Tough; Results of Analyses for HYDROCOIN Level 3, Case 2," Sandia National Laboratories, SAND89-0652, July 1990.

Runchal, A.K. and B. Sagar, "PORFLO-3: A Mathematical Model for Fluid Flow, Heat and Mass Transport in Variably Saturated Geologic

Media—User's Manual (Version 1.0)," Richland, Washington, Westinghouse Hanford Company, WHC-EP-0041, July 1989.

Sagar, B. and A.K. Runchal, "PORFLO-3: A Mathematical Model for Fluid Flow, Heat and Mass Transport in Variably Saturated Geologic Media—Theory and Numerical Methods (Version 1.0)," Richland, Washington, Westinghouse Hanford Company, WHC-EP-0042, March 1990.

Sagar, B. and G. Wittmeyer, "Phase 2 Interval Project: Las Cruces Trench Solute Transport Modeling study, Plot 2, Experiment A," in Patrick, W.C. (ed.), *Report on the Research Activities for the Quarter January 1 Through March 31, 1991*, San Antonio, Texas, Center for Nuclear Waste Regulatory Analyses, CNWRA 91-01Q, November 1991.

Smyth, J.D., S.B. Yabusaki, and G.W. Gee, "Infiltration Evaluation Methodology—Letter Report 3: Selected Tests of Infiltration Using Two-Dimensional Numerical Models," Richland, Washington, Pacific Northwest Laboratory, July 1989.

Travis, B.J., "TRACER3D: A Model of Flow and Transport in Porous-Fractured Media," Los Alamos, New Mexico, Los Alamos National Laboratories, LA-9667-MS, May 1984. [Prepared for the U.S. Department of Energy.]

Updegraff, C.D., C.E. Lee, and D.P. Gallegos, "DCM3D: A Dual-Continuum, Three-Dimensional, Ground-Water Flow Code for Unsaturated, Fractured, Porous Media," U.S. Nuclear Regulatory Commission, NUREG/CR-5536, February 1991.

Van Genuchten, M.T., "A Closed-Form Equation for Predicting the Hydraulic Conductivity of Unsaturated Soils," *Soil Science*, 44:892-898 [1980].

Yeh, G.T., and D.S. Ward, "FEMWATER: A Finite-Element Model of Water Flow through SaturatedUnsaturated Porous Media," Oak Ridge, Tennessee, Oak Ridge National Laboratory, ORNL-5567, August 1979.

APPENDIX D
K_d APPROXIMATION TESTING

D–1 INTRODUCTION

The most widely accepted conceptualization for the release of radionuclides from a geologic repository for high-level radioactive waste (HLW) to the accessible environment involves ground water that flows through the repository, interacts with the radioactive waste, and carries the resulting dissolved and/or suspended contaminants to the accessible environment (10 CFR 60.2). In traveling along the path from the repository to the accessible environment, these radionuclides can interact with solids. These interactions can include precipitation/dissolution and sorption/desorption. This auxiliary analysis will focus on sorption/desorption reactions. When associated with the solid as results from sorption reactions, the radionuclide is immobile. The length of time the radionuclide is associated with the immobile solid phase versus the time the radionuclide spends in the flowing ground water affects the rate of radionuclide migration. The more time spent on the solid, the more retarded is the movement of the radionuclide relative to the ground-water flow rate. The retardation of radionuclides by interactions with the geologic medium can limit the amount of radionuclides reaching the accessible environment in 10,000 years, as required by the Nuclear Regulatory Commission's regulation.[1]

Retardation is a process ascribed to dynamic systems. Chromatographic theory, however, states that, given certain assumptions, parameters measured in static systems can be used to calculate retardation in dynamic systems. Traditionally, static, batch experiments are performed in which ground water containing a radionuclide is brought into contact with solids expected to occur along the flowpath to the accessible environment. The radionuclide partitions itself between solid and liquid phases. After the experiment, the concentrations of radionuclide on the solid and in the liquid are measured. When sorption/desorption are the processes controlling radionuclide/solid interactions, the ratio of radionuclide concentration on the solid to that in the liquid is called the sorption coefficient, or K_d, and normally has units of milliliters per gram. The relationship of K_d to retardation is:

$$R_f = 1 + \varrho \frac{K_d}{\Theta} \qquad \textbf{(D–1)}$$

where ϱ is the bulk density, θ is the porosity, and R_f is the retardation factor, which is defined as the ratio of the velocity of the groundwater to that of the radionuclide. Freeze and Cherry (1979, p. 404) state that Equation (D–1) is valid when:

- The sorption reaction is fast and reversible; and
- The sorption isotherm is linear.

A sorption isotherm is the locus of points describing the concentration of radionuclide on the solid as a function of its concentration in the liquid. When the isotherm is linear, K_d is constant (i.e., independent of radionuclide concentration in the liquid.)

D–2 BACKGROUND/DEFINITION OF ISSUES

The total-system performance assessment (TPA) computer code of the present NRC performance assessment effort uses the K_d approach in estimating retardation of radionuclides. The sources of the values of K_d used in the TPA computer code are Meijer (1990) and Thomas (1987). These K_ds are based on batch sorption tests, supported in some cases by corresponding flow-through column experiments performed by investigators from the Los Alamos National Laboratory. The batch sorption tests use site-specific ground water

[1]Currently, a revised set of standards specific to the Yucca Mountain site is being developed in accordance with the provisions of the Energy Policy Act of 1992. The Energy Policy Act of 1992 (Public Law 102–486), approved October 24, 1992, directs NRC to promulgate a rule, modifying 10 CFR Part 60 of its regulations, so that these regulations are consistent with EPA's public health and safety standards for protection of the public from releases to the accessible environment from radioactive materials stored or disposed of at Yucca Mountain, Nevada, consistent with the findings and recommendations made by the National Academy of Sciences, to EPA, on issues relating to the environmental standards governing the Yucca Mountain repository. It is assumed that the revised EPA standards for the Yucca Mountain site will not be substantially different from those currently contained in 40 CFR Part 191, particularly as they pertain to the need to conduct a quantitative performance assessment as the means to estimate postclosure performance of the repository system.

to which radionuclides have been added, and crushed solids expected to occur along the flowpath from the repository to the accessible environment.

In a system as complex as Yucca Mountain, it remains to be demonstrated that simplifications such as the K_d approach in estimating retardation are valid. This auxiliary analysis tests the requirement that the sorption isotherm needs to be linear to make Equation (D–1) valid. The method involves modeling sorption reactions in a one–dimensional flowing system. Two specific sorption reactions are ion exchange and surface complexation. This modeling exercise simulates ion exchange involving sodium and potassium. The reaction considered is:

$$K^+ + NaX = KX + Na^+ \quad , \qquad \textbf{(D–2)}$$

where X is the sorbing site on the solid. This simple system was chosen as a first attempt to investigate the effects of ion exchange on solute migration. Lacking thermodynamic data on site-specific components, this simple system can be viewed as an analog for the radionuclide-tuff reactions at Yucca Mountain. The computer code capable of simulating these processes is *PHREEQM*, for use in mixing cell flowtube simulations described by Appelo and Willemsen (1987). This code, an adaptation of *PHREEQE* (Parkhurst *et al.*, 1990) can simulate speciation and mass-transfer processes, including precipitation, and dissolution, plus it can simulate ion exchange reactions, one-dimensional flow and transport, diffusion, and dispersion in a porous media. The reaction written above describes the situation where a solution containing potassium flows through a porous medium initially loaded with sodium. The potassium dissolved in the aqueous phase displaces sodium on the solid and this solute-solid interaction retards the movement of potassium down the column relative to that of water. One could also imagine that the potassium represents a radionuclide and X represents sorbing site on the tuff.

Investigators involved in the Yucca Mountain geochemical program perform batch sorption tests to determine an isotherm. If the isotherm is linear, a retardation factor is calculated. Sometimes, additional characterization may be performed to establish the actual mechanism responsible for the sorption. In this auxiliary analysis, however, the sorption mechanism is already known. Simulation of a flow-through experiment produces elution curves that are retarded relative to the flow of water. Thus, retardation factors can be determined. Finally, K_d values and sorption isotherms can be generated by characterizing the partitioning of the sorbing species for all points along the column at all times.

The mass-action equation corresponding to Equation (D–2) is:

$$K = \frac{[KX][Na^+]}{[K^+][NaX]} \quad , \qquad \textbf{(D–3)}$$

where K is the equilibrium constant for the reaction and brackets represent activities. For this reaction, K is 5 (an arbitrary value in the database used by *PHREEQM*). For this study, accurate values for thermodynamic constants for specific reactions are not required, as only general relationships among parameters and their effects on solute migration are investigated. In comparison, the exchange constant for the $K^+ - Na^+$ ion-exchange reaction involving clinoptilolite is 17.2 (Pabalan, 1991). If the reverse of Equation (D–2) is considered,

$$Na^+ + KX \leftrightarrows K^+ + NaX \quad , \qquad \textbf{(D–4)}$$

where the equilibrium constant is 1/5.

Vermeulen *et al.* (1987) subdivide sorption reactions into various types, depending on the shape of the isotherm. Isotherms that are convex up are termed favorable (e.g., Figure D–1a) and those that are concave up are termed unfavorable (e.g., Figure D–1b). The terms favorable and unfavorable refer to the ability of a chromatographic process to separate species that are variably sorbed. A favorable sorption reaction would result in elution curves with constant-shaped fronts. These are also termed self-sharpening fronts. An unfavorable sorption reaction would result in elution curves with changing or spreading fronts. For an ion-exchange process, if the equilibrium constant is greater than 1, sorption processes favorable for chromatographic separation are present. If the equilibrium constant is less than 1, unfavorable conditions are present.

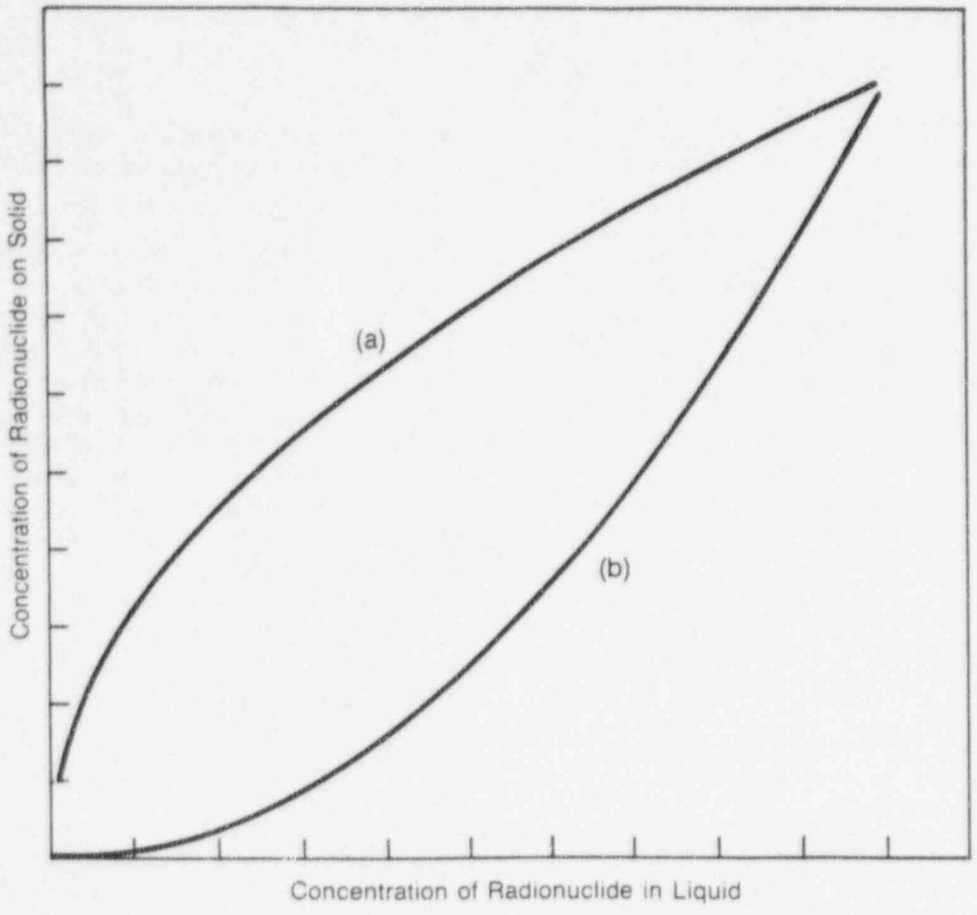

Figure D–1 Nonlinear isotherms ((1a) Favorable isotherm; (1b) Unfavorable isotherm.)

Some of the sorption isotherms using site-specific materials from Yucca Mountain are nonlinear (DOE, 1988; pp. 4–81—4–82). These isotherms have been fitted using a Freundlich formulation:

$$C_s = K C_l^n \quad , \qquad \textbf{(D–5)}$$

where C_s and C_l are concentrations on the solid and in the liquid, respectively, and K and n are empirical constants. When n is greater than 1, the isotherm is concave up, and when it is less than 1, it is convex up. For plutonium, n is 0.84 to 0.88, when YM–22 (welded tuff) is the solid substrate and 0.96 to 1.0, when YM–49 (partially zeolitized and vitric sample) is the solid. For strontium, cesium, barium, and europium, n ranges from 0.71 to 0.92, when the solid substrate is YM–22 (DOE, 1988; p. 4–82). The isotherm for these elements is linear when the solid is zeolitized.

By simulating flow-through experiments involving ion exchange represented by Equations (D–2) and (D–4), both favorable and unfavorable elutions are modeled. The significance of these types of elutions to performance assessment can then be better appreciated.

Simulations

Conceptually, the column is divided into cells. Initially, the chemical constituents in each cell are reacted to equilibrium. The possible reactions include precipitation, dissolution, speciation, and ion exchange. Mixing is then simulated between adjacent cells. The mixing can be caused by both dispersion and diffusion. However, in the present study, it was decided arbitrarily that only dispersion be included in the simulation. Following mixing, the solutions in each cell are moved to the next cell downstream and re-equilibrated. The solution added to the column is called the flushing solution. Its composition remains constant throughout the simulation. Before adding the flushing solution, the compositions of both liquid and solid in the column are defined. The parameters that are varied in this study are the relative

concentrations of competing species, and concentration of the sorbing site or complex, X^-.

The capability of a solid to sorb is commonly described in terms of cation-exchange capacity. The code, however, uses the concentration of the sorbing site, X^- (in milliequivalents per liter—meq/L), which is related to the cation exchange capacity by the relation:

$$X^-(meq/L) = \frac{CEC \times 1000}{100 \times \frac{\theta}{\varrho}} , \qquad \textbf{(D–6)}$$

where *CEC* is the cation exchange capacity in meq per 100 grams soil, θ is the porosity, and ϱ is the bulk density of the soil in kilograms per liter.

Porosity is an input in the simulation and must remain constant along the length of the column, to maintain the constancy of masses of solution moving from cell to cell. The simulations involve only saturated hydrologic conditions. Porosity in these simulations has been set at 0.3, which lies within the range of porosities found at Yucca Mountain (see DOE, 1988; p. 3–192).

In the *PHREEQM* code, mixing between adjacent cells is calculated using the relation:

$$f = \frac{DISP(i) + DISP(i+1)}{L(i) + L(i+1)} + 4 \times DM \times \frac{DELTAT}{(L(i) + L(i+1))^2} , \qquad \textbf{(D–7)}$$

where f is the mixing factor, *DISP* is the dispersivity in meters, L is the length of the cell in meters, i represents the cell number, *DM* is the diffusivity in square meters/second, *DELTAT* is the time for diffusion in seconds. The mixing factor is the percentage of a cell's dissolved contents that is transferred to an adjacent cell. Both upstream and downstream adjacent cells are involved in the mixing process. The code restricts $f < 0.33$ so that at least one-third of the original contents of a cell remain after a mixing simulation. All the factors on the right side of Equation (D–7) are inputs to the code. For this study, no diffusion is simulated, so the second term on the right side of Equation (D–7) is zero, and only the dispersion component of spreading is considered. All the simulations in this study have the same dispersivity.

The first simulation involves the elution of potassium through a column initially saturated with sodium. The initial concentrations are 1 meq/L of X^- and 1 meq/L of Na^+ on the solid, and 1 meq/L of Na^+ in the liquid in the column. A nonsorbing anion, NO_3^-, balances the charge in the liquid initially filling the column. The flushing solution contains 1 meq/L K^+ charge balanced by a nonsorbing anion. The column contains 20 cells. Figure D–2 illustrates the concentration of K^+ in the liquid phase along the column, for different amounts of flushing solution added. The flushing solution is added to the column at cell 1 and leaves the column after cell 20. The numbers associated with each concentration curve refer to the cell volumes of flushing solution added to the column, labelled "shifts" in the figure. Note that the flushing solution concentration curve or front corresponding to various shifts is of constant shape. The rounding of the front is due to dispersion modeled in this simulation. Each cell is 1-centimeter long and has an associated dispersivity of 2 millimeters (thus, $f = 0.2$). Apparently, this amount of dispersion does not affect the shape of the front as it migrates down the 20-centimeter column (i.e., the front does not spread with distance traveled). By defining only the porosity of the cells, only relative volumes of liquid to solid are fixed. Thus, actual amounts of flushing solution are not determined.

Figure D–2 can be used to determine the retardation factor for this simulation. One method for determining the retardation factor is to integrate under the concentration-cell number curve for a given number of shifts. The integration produces the total mass of K^+ in the aqueous phase. By dividing the total mass of K^+ added to the column for a given number of shifts by the total mass of K^+ in the aqueous phase, the retardation factor is obtained. This operation is comparable to converting the spreading front of the elution curve into a square front. For symmetrical fronts, another method for determining the retardation factor is to measure the distance K^+ travels down the column at the half height of its initial concentration. This point represents the center of mass of the migrating front. Note that at 20 shifts, the half height of the K^+ concentration (0.5 meq/L) is

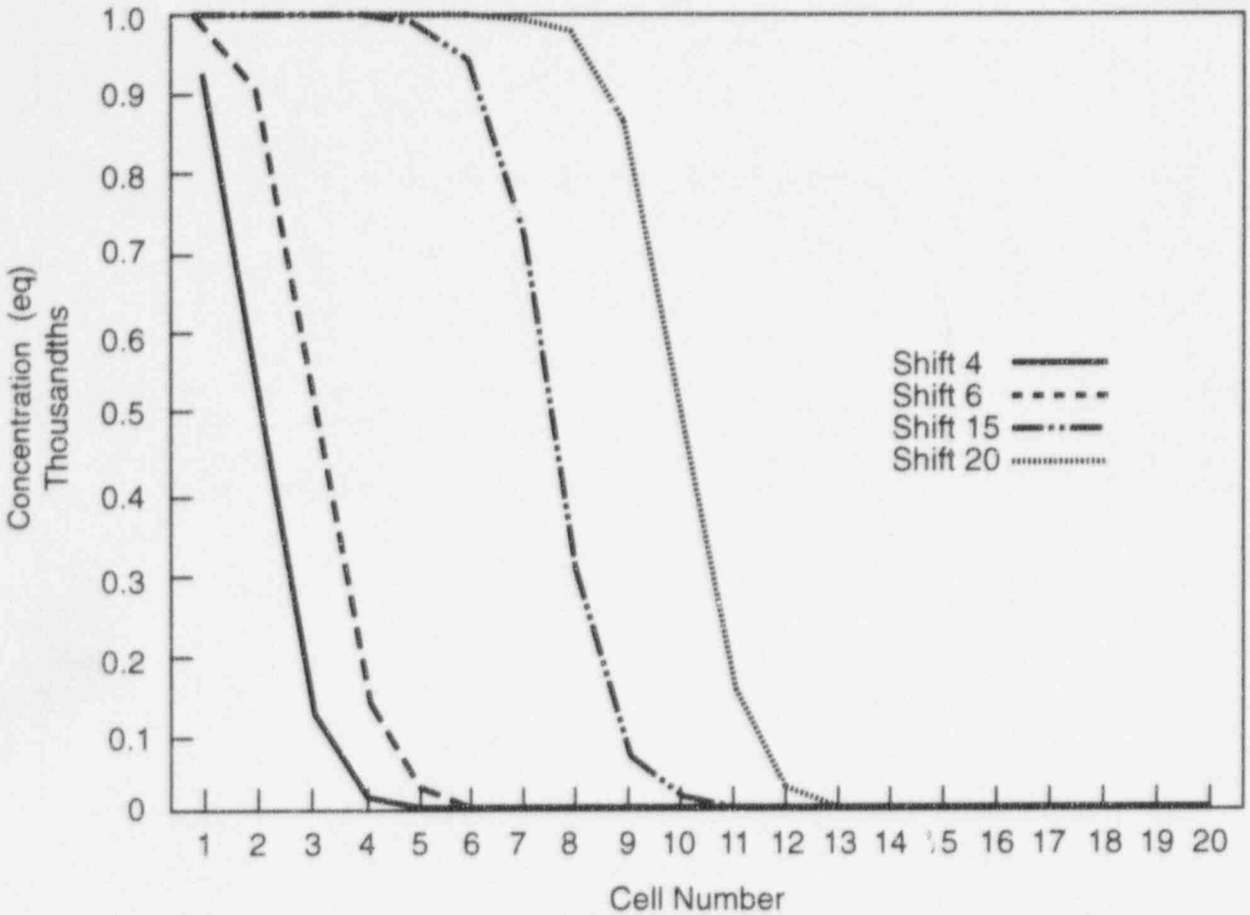

Figure D–2 Flushing solution concentration versus cell number, flushing solution solute preferentially sorbed, equal starting concentrations of flushing solution solute, competing cation and sorbing site

in cell 10. Thus, at this point the water has traveled all the way through the column, but K^+ has traveled only half the distance. Consequently, the retardation factor, R_f, is 2. From Equation (D–1), if ϱ is assumed to be 2.5, the K_d is 0.12.

Each cell can be considered as a separate batch sorption test. The code calculates the partitioning of the ions between solid and liquid. Thus, it is possible to determine a K_d for K^+ for each cell and each shift. Figure D–3 is a plot of K_d versus cell number for various shifts. The K_d values range from 0.6 to 0.12 and are not constant for a particular cell (space), but change with the number of shifts (time). For example, cell 6 has a K_d of 0.6 at 4 shifts and 0.12 at 15 shifts. It should be noted that K^+ has reached cell 6 after only four shifts because of the dispersion where 20 percent of the dissolved contents of each cell is moved downstream per shift. Combined with information from Figure D–2, it is apparent that higher concentrations of K^+ in a particular cell correspond to the lower K_d value and vice versa. This observation provides an explanation for constant shape of the elution curve. Low concentrations lead high concentrations down the column. However, low concentrations correspond to high K_d values and so are slowed more than the high concentrations. The result is a front that maintains its steep concentration gradient.

The fact that this simulation produced a range of K_d values for particular cells raises an important issue, namely, what K_d value should be assigned to each cell? It is clear in this simulation that the appropriate K_d for use in Equation (D–1) to determine retardation corresponds to the one measured at the highest flushing solution concentration. But, what if, as in the case of many of the radionuclides studied in the Yucca Mountain Project, only K_d values as a function of radionuclide concentration are determined for rock-water systems representing various locations in the repository block? Must not the radionuclide

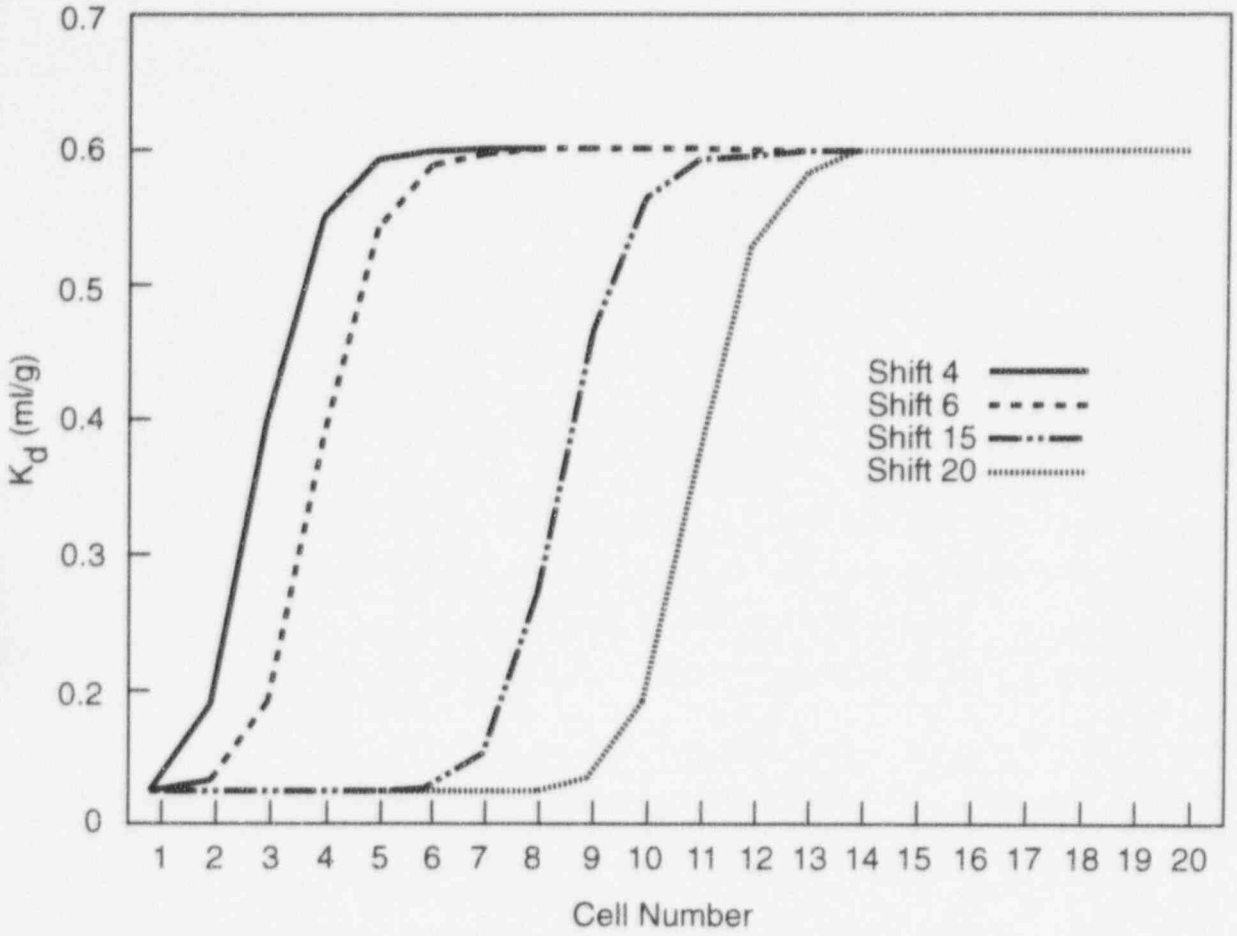

Figure D–3 K_d versus cell number for flow-through ion exchange simulation illustrated in Figure D–2

concentration at each location also be known in order to assign the appropriate K_d value? The approach to modelling radionuclide migration in the Yucca Mountain Project is to assume that K_d values are a function only of space and not time (Meijer, 1992). With this approach, a K_d value is chosen that is conservative relative to all K_d values, no matter what radionuclide concentration is present. However, it must be noted that Equation (D–5), describing the relation of radionuclide concentration on the solid to that in the liquid, has no formulation to limit the radionuclide concentration in the liquid. This limit must be supplied by additional information, such as solubilities.

From Figure D–2, it is evident that the concentrations of K^+ in a particular cell can vary from 0 to 1 meq/L depending on the number of shifts and the position of the cell. By plotting the concentration of K^+ on the solid in milliequivalents per gram versus the concentration in the liquid for all cells and all shifts, the sorption isotherm can be generated. Figure D–4 is such a plot. This isotherm is convex up, and thus produces a front of constant shape, which is consistent with the description of Vermuelen *et al.* (1987). The points on Figure D–4 could be fitted to a curve such as the Freundlich formulation (Equation (D–5)), but it is not necessary for this study.

Figure D–5 illustrates the effect of doubling the concentration of K^+ in the flushing solution while keeping all other parameters the same as in the first simulation. Here, for 20 shifts, or cell volumes added, the front measured at half concentration, falls between cell 12 and 13. This is comparable to a K_d of 0.07. Figure D–6 shows K_d values versus cell number for this simulated elution. Unlike in Figure D–2, where the K_d values monotonically change from one extreme to the other for a given shift, these curves develop a bulge with more shifts. The bulge can be explained by rearranging Equation (D–3) to express K_d as:

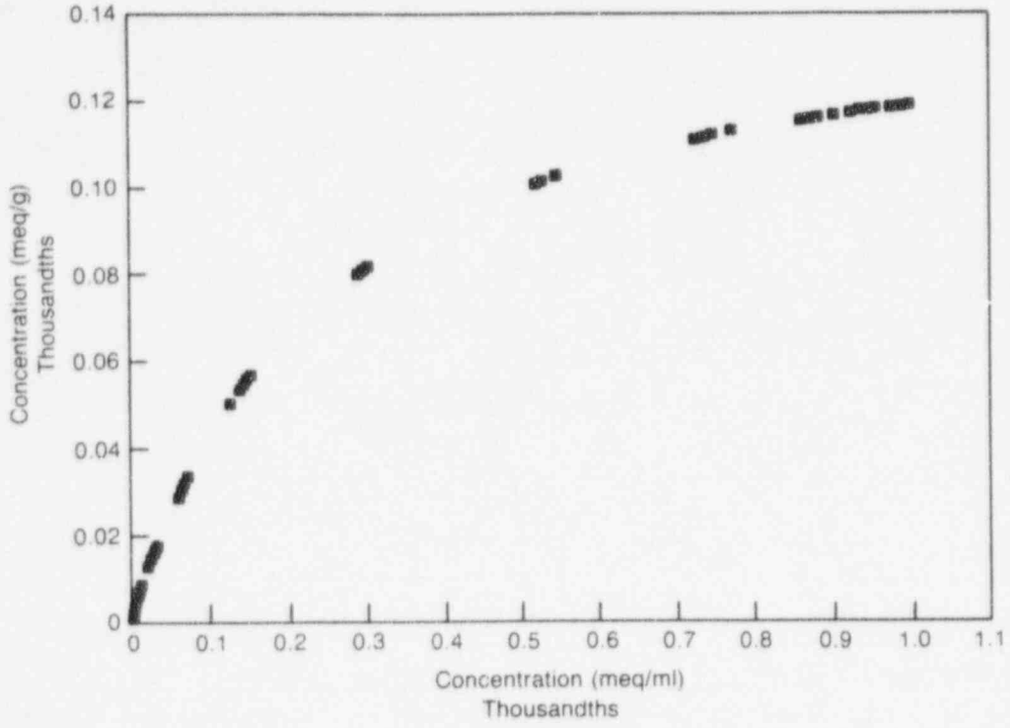

Figure D–4 Sorption isotherm calculated from flow-through ion exchange simulation illustrated in Figure D–3 showing favorable characteristics

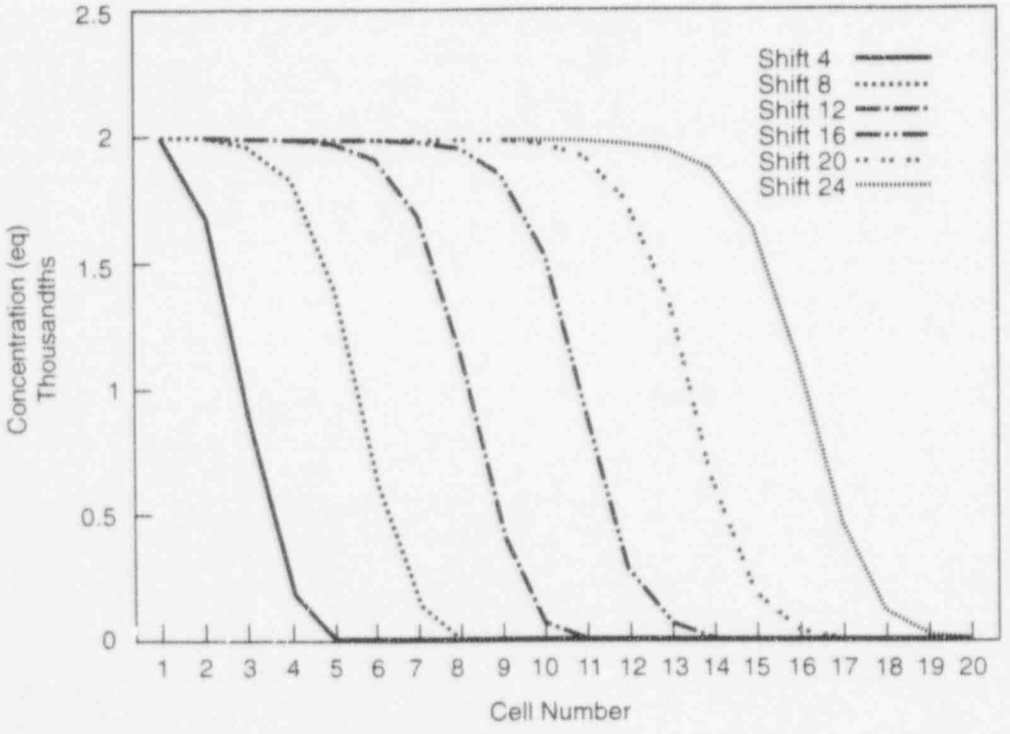

Figure D–5 Flushing solution concentration versus cell number, flushing solution solute perferentially sorbed, effect of doubling starting concentration of flushing solution solute relative to competing cation and sorbing site concentrations

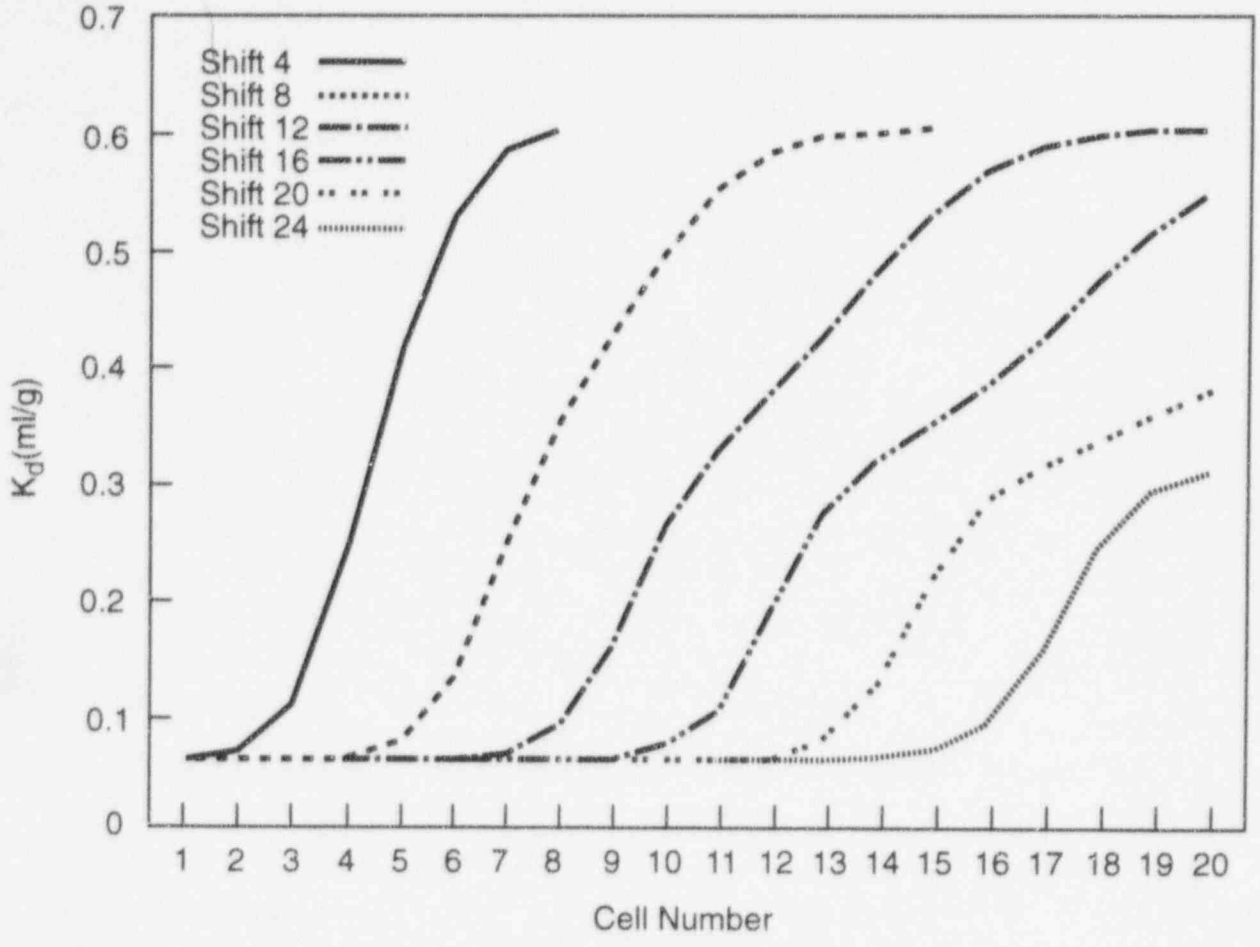

Figure D–6 K_d versus cell number for flow-through ion exchange simulation illustrated in Figure D–5

$$\frac{[KX]}{[K^+]} = K_d = K \times \frac{[NaX]}{[Na^+]} \quad , \qquad \textbf{(D–8)}$$

where activities approximate concentrations. Since the equilibrium constant is fixed, the variation in K_d is caused by a variation in the concentrations of the sodium species. Figure D–7 shows the displacement of sodium on the solid by potassium in the flushing solution. As a result of the higher K^+ concentration, more Na^+ is displaced to the liquid in each cell downstream than was originally present (1 meq/L in liquid and 1 meq/L on solid). A wave of Na^+ develops with its crest increasing with the number of cell volumes added to the column. Thus, although the [NaX] varies smoothly from 0 to 1 meq/L down the column, the $[Na^+]$ goes through a maximum. This variation causes the bulge in the K_d values.

The ion-exchange reaction represented by Equation (D–4) involves the migration of sodium through a column initially saturated with potassium. With an equilibrium constant of 1/5, this simulation should result in the unfavorable condition of non-constant-shaped fronts. Figure D–8 illustrates the elution of 1 meq/L of Na^+ in the flushing solution through a column having 1 meq/L for both KX on the solid and K^+ in solution. The curves representing various shifts definitely are not of constant shape. The retardation factor calculated for shift 16 is approximately 1.6. Unlike the favorable condition (Figure D–2) where, with a retardation factor of 2, no flushing solution solute was exiting the column even after 24 shifts, here significant flushing solution solute passes through the column at 20 shifts. Dispersivity for both favorable and unfavorable simulations is the same (2 millimeters). This simulation demonstrates that, in addition to the retardation factor, the shape of the curve is also important. Thus, with regard to Yucca Mountain, for a given retardation factor, the amount of radionuclide reaching the accessible environment depends on whether the ion exchange is favorable or not.

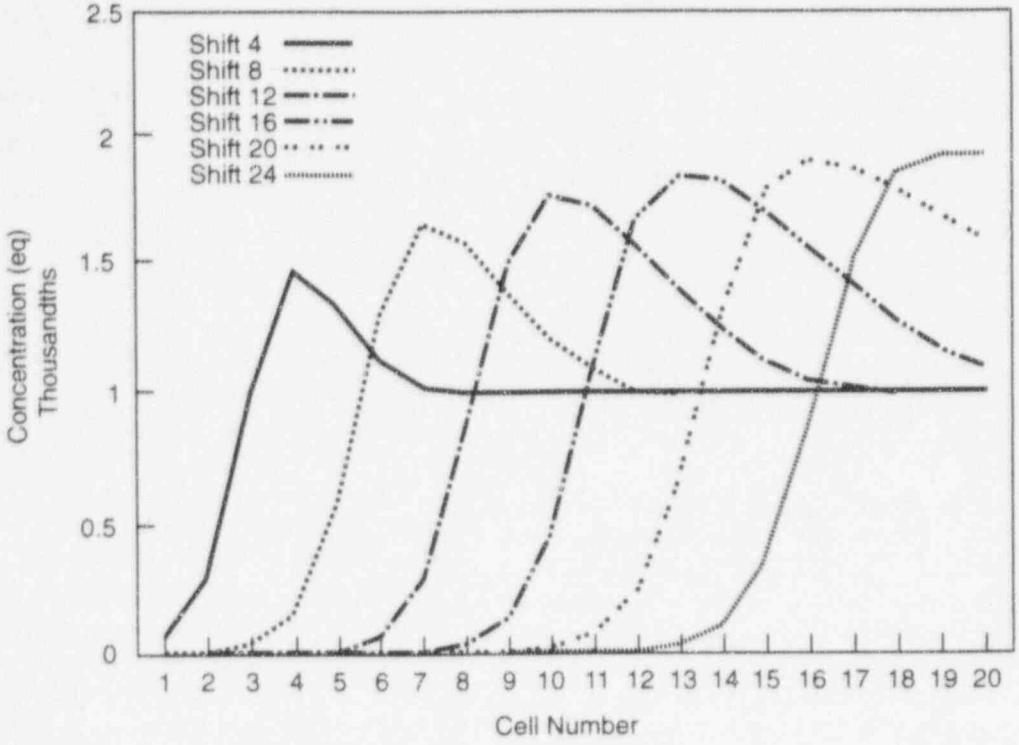

Figure D–7 Concentration of competing cation versus cell number for flow-through ion exchange simulation illustrated in Figure D–5

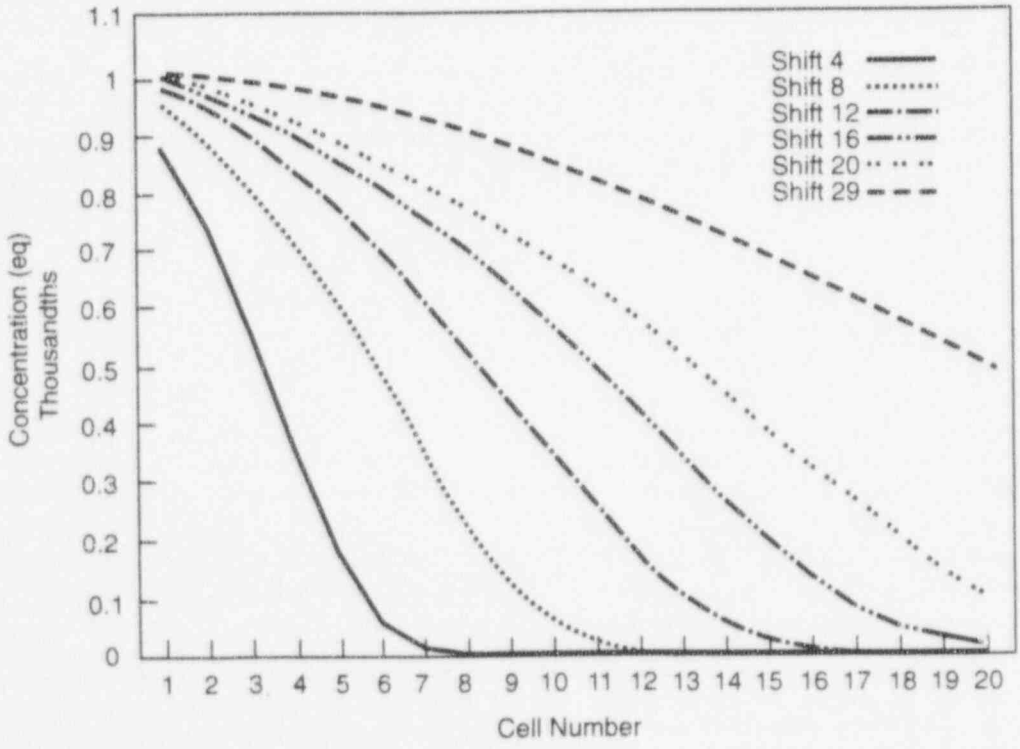

Figure D–8 Flushing solution concentration versus cell number, flushing solution solute perferentially desorbed, equal starting concentrations of flushing solution solute, competing cation and sorbing site

Figure D–9 shows K_d versus cell number for this simulation. Again the K_d values are not constant for a given cell. This graph does not have the same shape as Figure D–3, where the K_d values ranged between two extremes, with a retardation factor appropriately calculated from one of the K_d extremes. Here, the retardation factor corresponds to an intermediate K_d value. Figure D–10 is the sodium isotherm for this simulation. The curve is concave up, consistent with the unfavorable condition as described by Vermuelen *et al.* (1987).

The previous simulations involved 1 meq/L X^-. This amount of sorbing site is relatively small. For comparison, YM–22, a tuff sample from Yucca Mountain that has been used in many sorption experiments has a exchange capacity equivalent to 167 meq/L X^-. Elution simulations similar to the previous ones were performed with this higher sorbing site concentration. Figure D–11 shows the elution of 1 meq/L of K^+ through a column initially loaded with 167 meg/L NaX on the solid in contact with liquid containing 1 meq/L Na^+. As before, the flushing solution front maintains a steep concentration gradient. However, the migration of K^+ is greatly retarded. Note that it takes 800 shifts to move the half-height of the flushing solution to cell 5. The retardation factor is calculated to be approximately 133 corresponding to a K_d of 16. Figure D–12 is the K_d versus cell number plot showing the variation in K_d for each cell at different shifts. The corresponding isotherm in Figure D–13 is nonlinear and convex up.

Although, in Figure D–11 the front maintains a steep concentration gradient, it is evident that the front is not constant in shape. Apparently, the dispersion, which tends to spread the front, is competing against the favorable sorption (nonlinear convex up isotherm) which tends to sharpen the front. Since each shift involves the transfer of 20 percent of the constituents of the aqueous phase of one cell with an adjacent cell downstream, as calculated from Equation (D–7), with 800 shifts, dispersion becomes important in mobilizing the flushing solution solute.

Next, the elution of Na^+ through a column packed with YM–22 is simulated where 1 meq/L of Na^+ is added to a column initially loaded with 167 meg/L KX on the solid in contact with liquid containing 1 meq/L K^+. The spreading of the flushing solution front is evident in Figure D–14. Each cell has a range of K_d values, depending on the number of shifts or cell volumes that have been added to the column (Figure D–15). The sodium isotherm is nonlinear and concave up (Figure D–16).

For the simulations involving YM–22, the concentrations of sorbing ions are in trace amounts relative to the sorbing site concentration. However, the concentrations of the competing ions are initially equivalent. The simulation of elution of potassium in trace concentrations relative to the concentration of the competing ion is depicted in Figure D–17. Again, the shape of the flushing solution front maintains a steep concentration gradient, but is not of constant shape. Dispersion has spread the front slightly, as it moves down the column. A retardation factor of 5.88 is determined (100 shifts/17 cells), from which a K_d of 0.59 is calculated. Figure D–18 illustrates that a single K_d value is associated with every cell. The corresponding isotherm is linear (Figure D–19).

It should be noted that the spreading of the front in Figure D–17, with only 100 shifts, is greater than the spreading of the front in Figure D–11, with 800 shifts. This is demonstrated by comparing the number of cells that correspond to the minimum and maximum flushing solution concentration. In Figure D–17, for 60 shifts, the spread is 18 cells (cell 20 contains the minimum concentration of K^+ and cell 2 contains the maximum); in Figure D–11, for 800 shifts, the spread is 7 cells (cell 10 contains the minimum concentration of K^+ and cell 3 contains the maximum). The difference in the degree of spreading between these two simulations must be caused by the differences in the shapes of the corresponding isotherms. Whereas the convex-up isotherm leads to greater retardation of the solute at lower concentrations, and thus a sharpening of the front and a tendency to compensate for dispersion, the linear isotherm lacks this characteristic.

The elution of sodium, which previously yielded a front that spread significantly, now is tested at trace amounts relative to the competing K^+ concentration. Figure D–20 shows the migration of Na^+ through a column initially loaded with K^+. Note that the spreading of the front is much

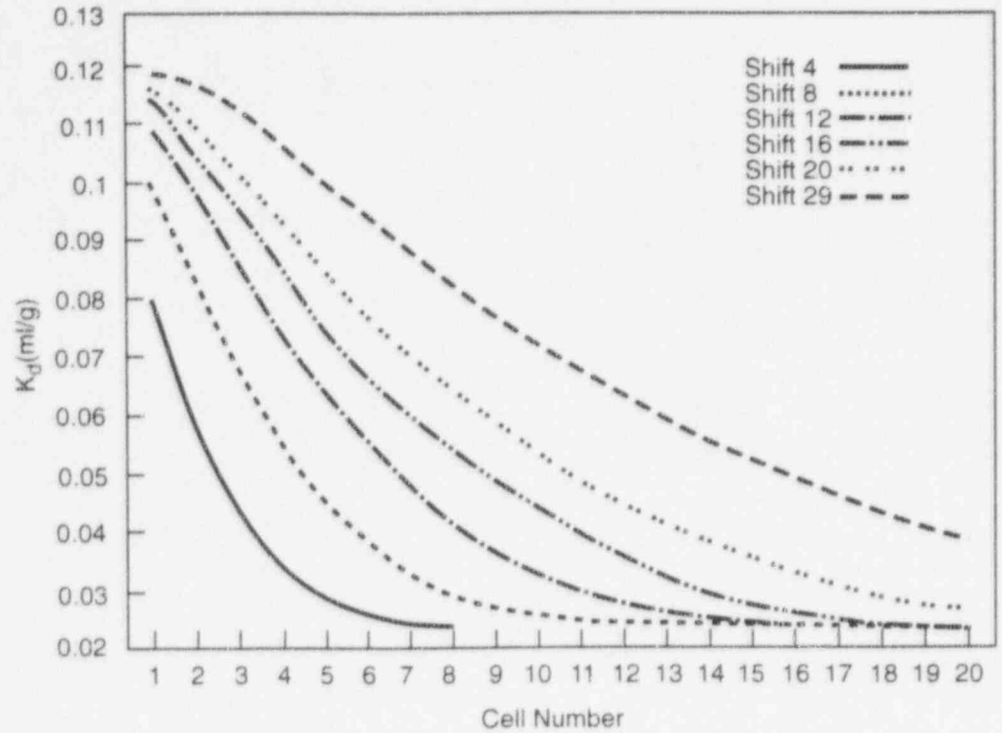

Figure D–9 K_d versus cell number for flow-through ion exchange simulation illustrated in Figure D–8

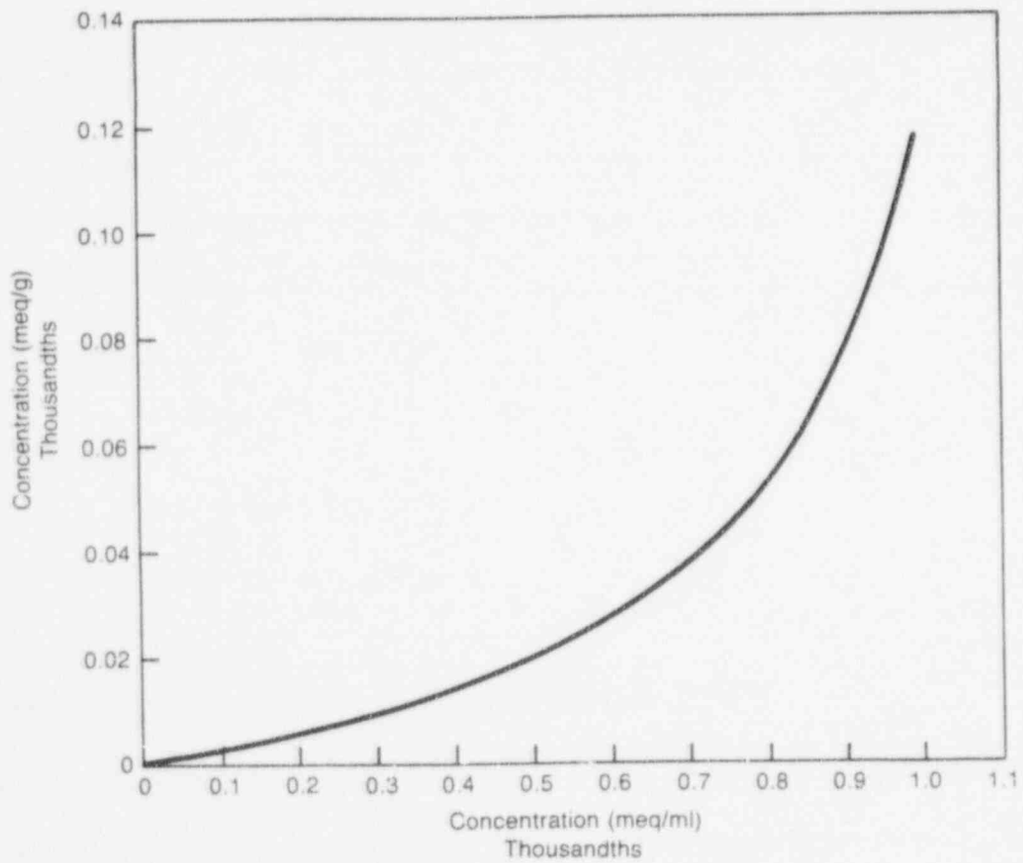

Figure D–10 Sorption isotherm calculated from flow-through ion exchange simulation illustrated in Figure D–8 showing unfavorable characteristics

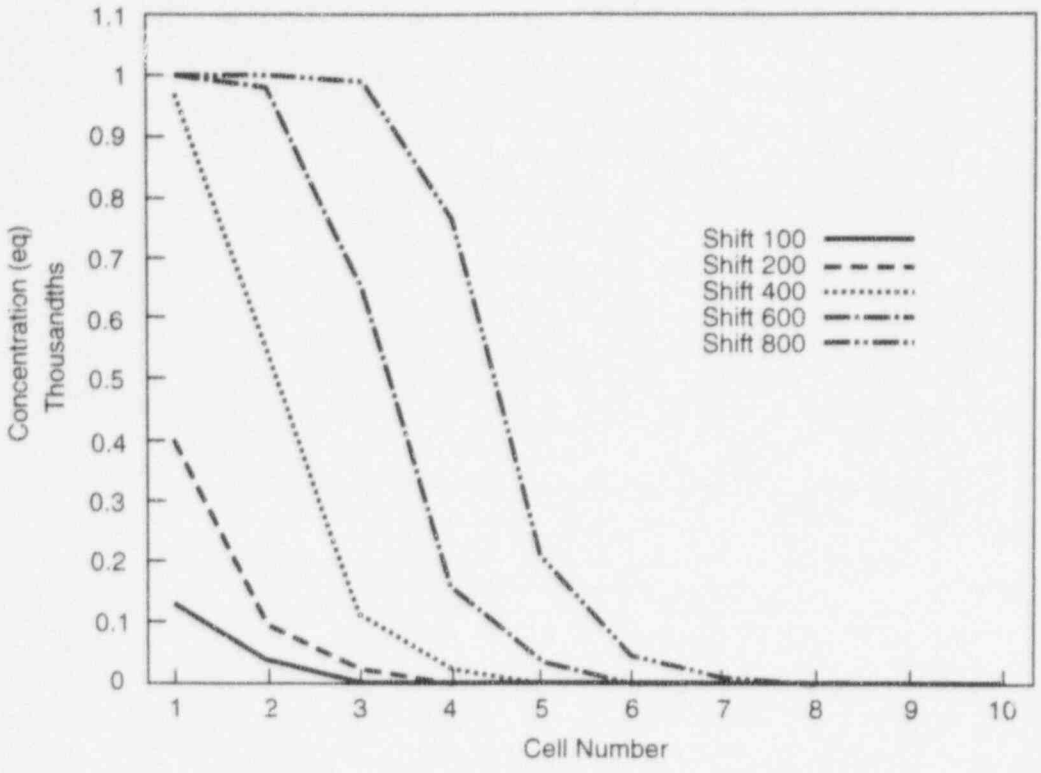

Figure D–11 Flushing solution concentration versus cell number, flushing solution solute preferentially sorbed, effect of increasing sorbing site concentration relative to starting concentrations of flushing solution solute and competing cation

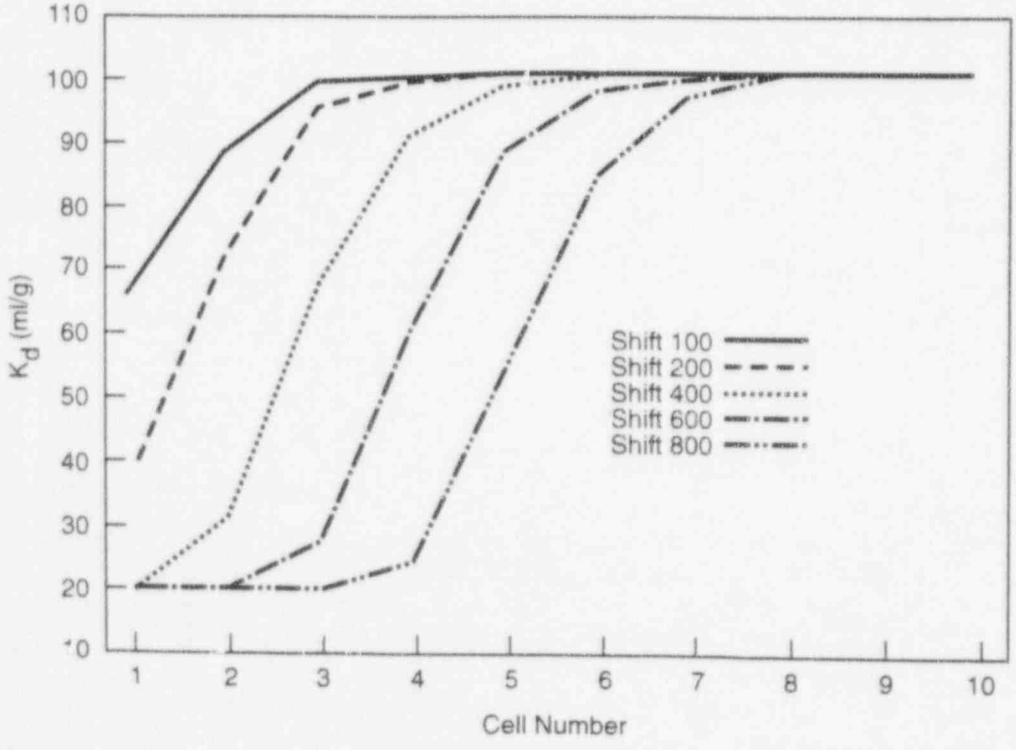

Figure D–12 K_d versus cell number for flow-through ion exchange simulation illustrated in Figure D–11

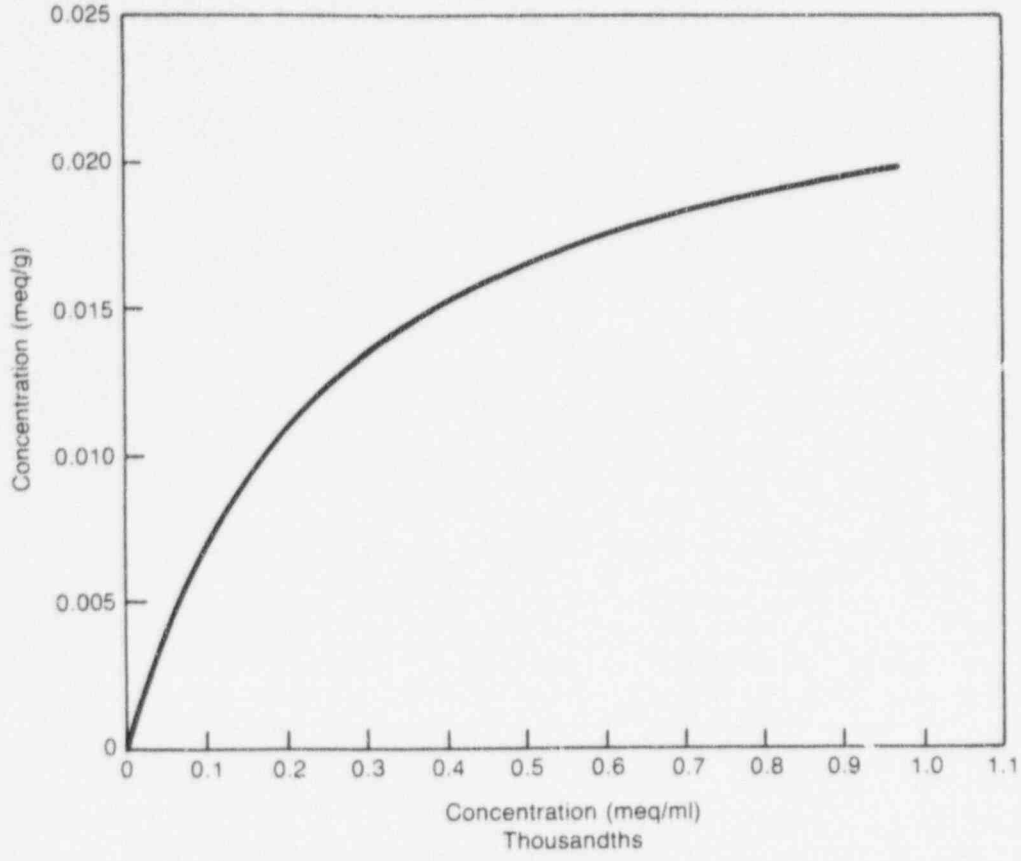

Figure D–13 Sorption isotherm calculated from flow-through ion exchange simulation illustrated in Figure D–11 showing favorable characteristics

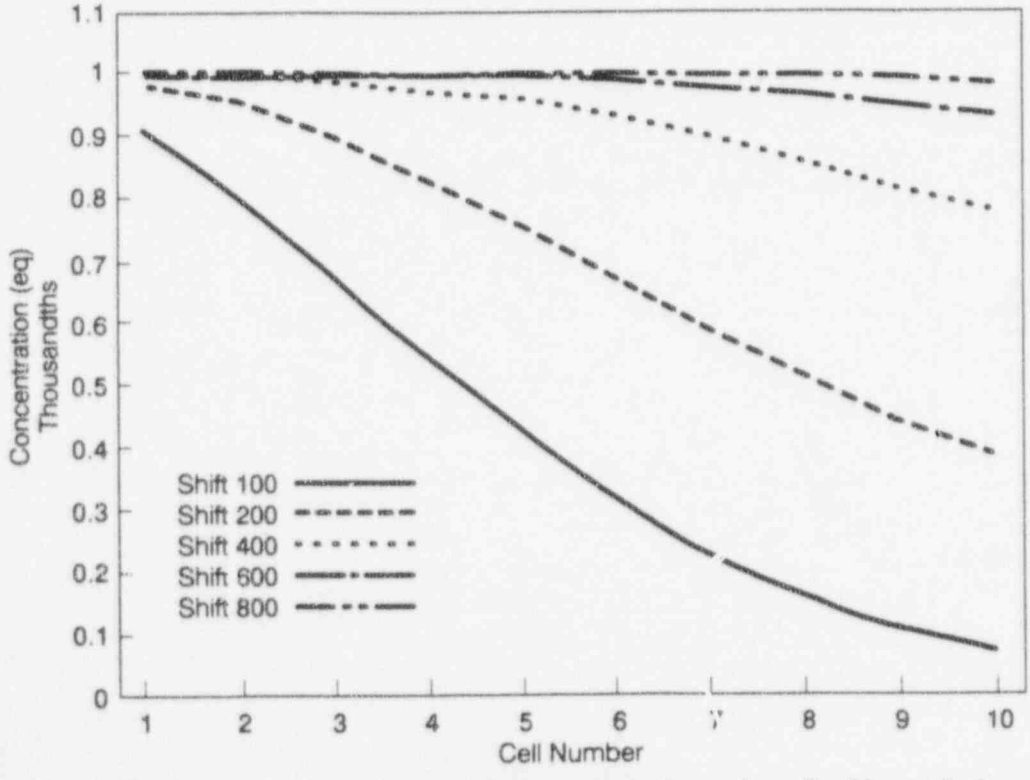

Figure D–14 Flushing solution concentration versus cell number, flushing solution solute preferentially desorbed, effect of increasing sorbing site concentration relative to starting concentrations of flushing solution solute and competing cation

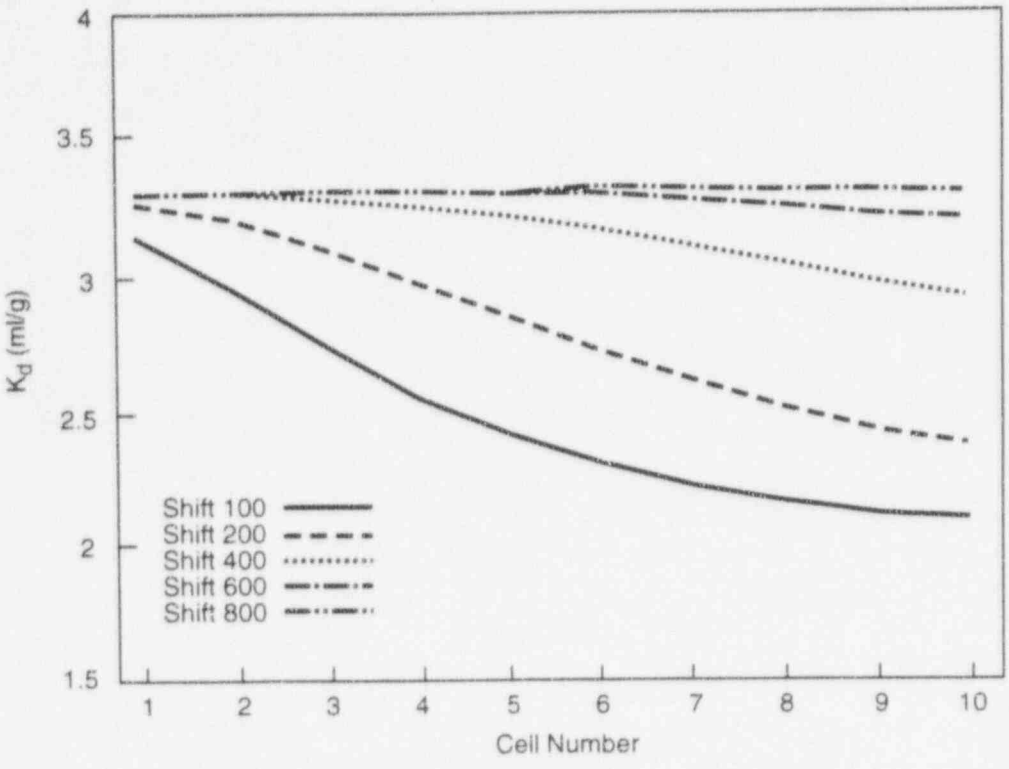

Figure D–15 K_d versus cell number for flow-through ion exchange simulation illustrated in Figure D–14

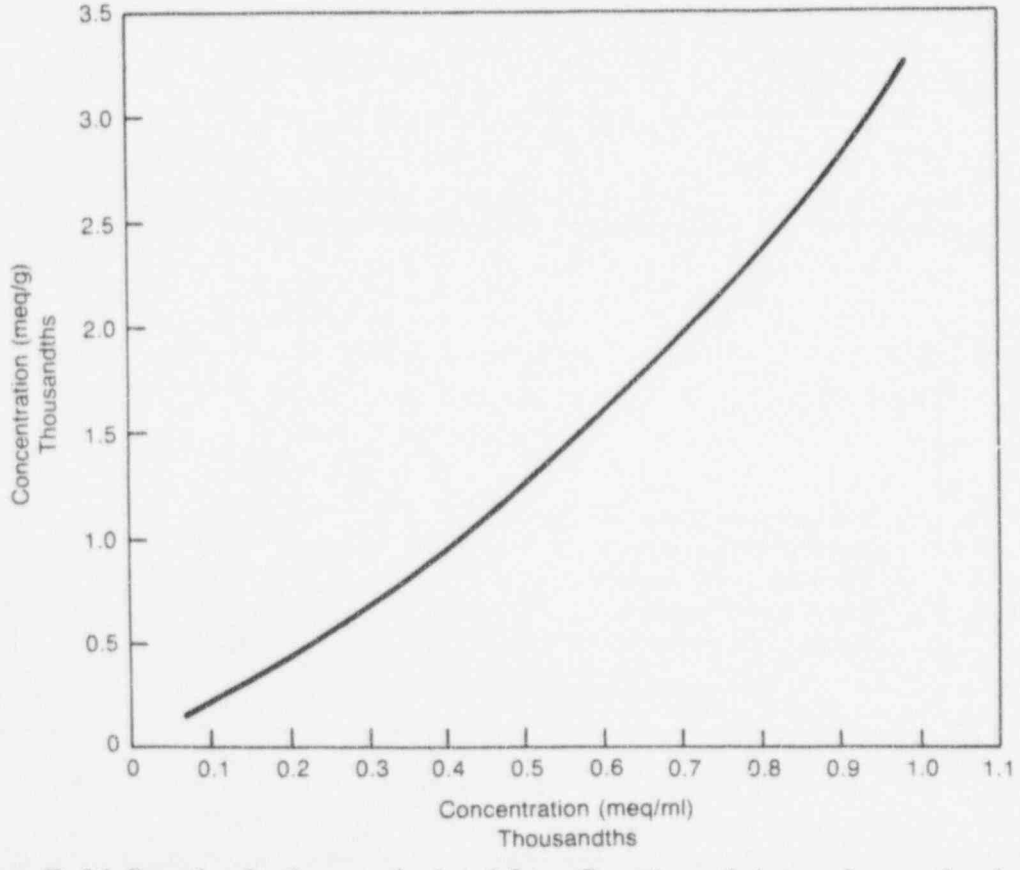

Figure D–16 Sorption isotherm calculated from flow-through ion exchange simulation illustrated in Figure D–14 showing unfavorable characteristics

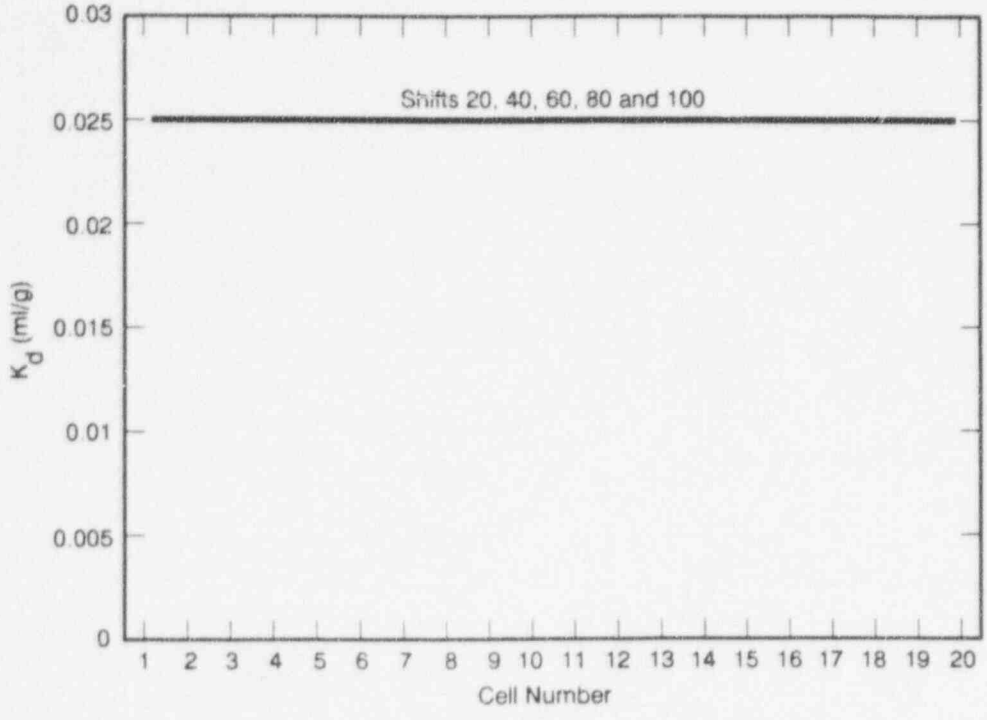

Figure D–17 Flushing solution concentration versus cell number, flushing solution solute preferentially sorbed, trace starting concentration of flushing solution solute, relative to competing cation and sorbing site concentrations

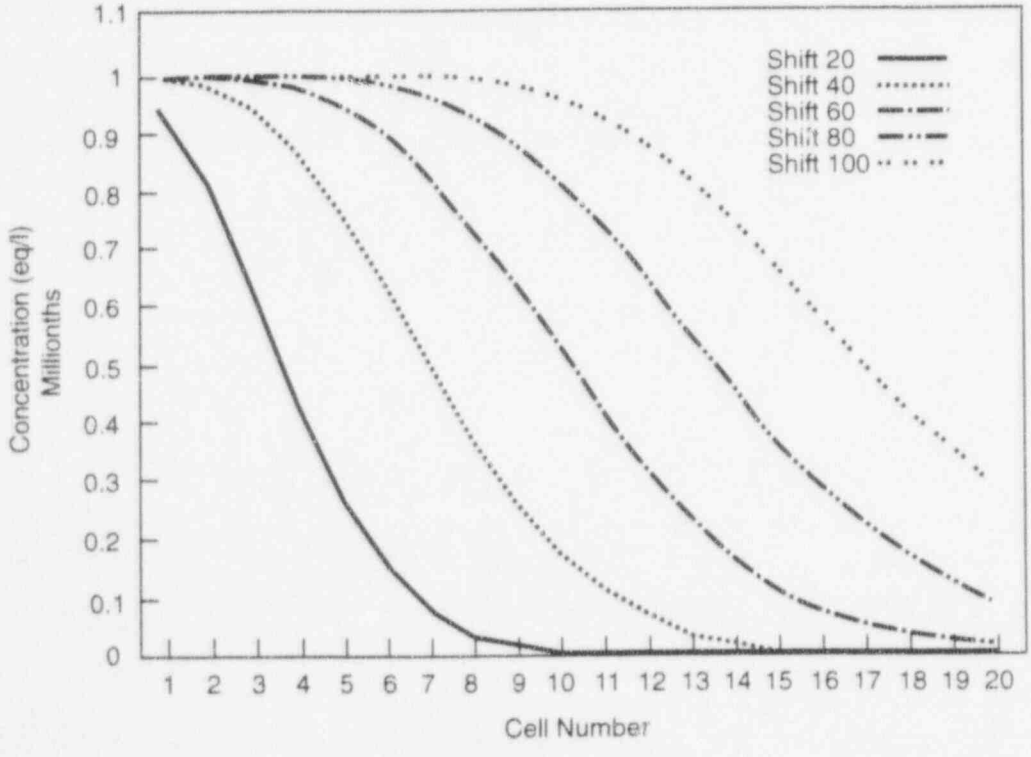

Figure D–18 K_d versus cell number for flow-through ion exchange simulation illustrated in Figure D–17

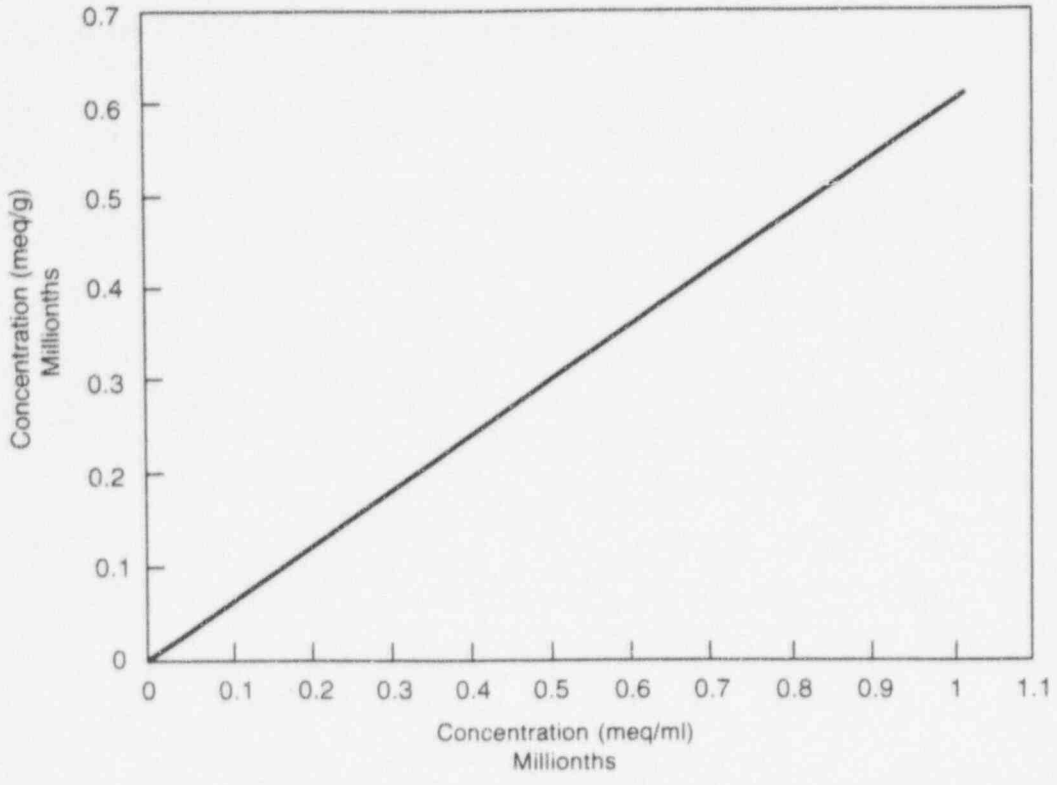

Figure D–19 Sorption isotherm calculated from flow-through ion exchange simulation illustrated in Figure D–17 showing linear behavior

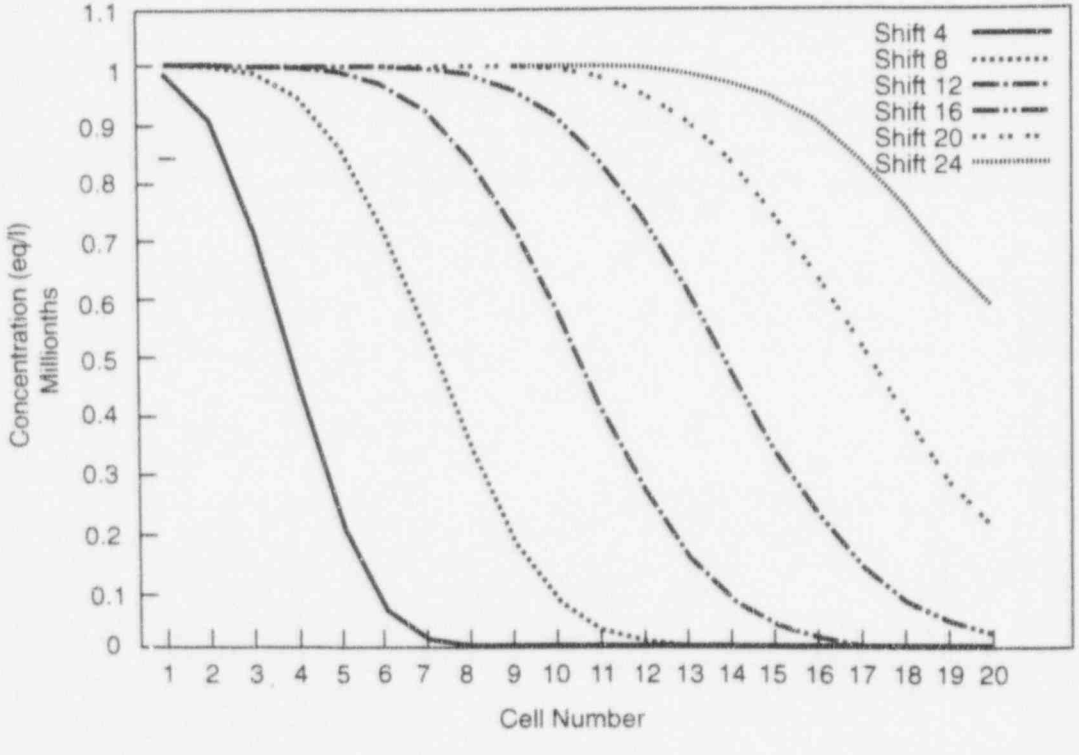

Figure D–20 Flushing solution concentration versus cell number, flushing solution solute preferentially desorbed, trace starting concentration of flushing solution solute, relative to competing cation and sorbing site concentrations

reduced (compare with Figure D–14). The retardation factor is 1.18 (20 shifts/17 cells). The comparable K_d is 0.021. Figure D–21 illustrates that each cell has a constant K_d value. Finally, the isotherm is linear, as shown in Figure D–22. The spreading is caused by dispersion.

D–3 CONCLUSIONS AND RECOMMENDATIONS

The requirement that the sorption isotherm be linear so that Equation (D–1) is valid results in constant K_d values for each cell. However, the flushing-solution solute front is spread if dispersion occurs and thus is not of constant shape. A linear isotherm results from the condition in which the flushing solution solute is in trace amounts relative to the competing ions. Linear isotherms do not result from the condition where the flushing-solution solute concentration is in trace amounts, relative to the sorbing site but comparable to the concentration of the competing ion(s). When the isotherm is nonlinear and convex up, representing a favorable condition, the K_d value associated with the highest expected concentration of the flushing-solution solute can be used to determine the retardation factor from Equation (D–1). This method is not possible when the isotherm is concave up.

Although dispersion tends to spread the flushing solution front, ion exchange, where the corresponding nonlinear sorption isotherm is convex up, tends to maintain a steep concentration gradient. On the other hand, ion exchange, where the corresponding nonlinear sorption isotherm is concave up, works in concert with dispersion to spread the front.

The information from this auxiliary analysis can be applied to the modeling of conditions and processes expected at Yucca Mountain. The assumption that all radionuclides will be in trace amounts relative to competing ions has not yet been proven. The waters at Yucca Mountain contain low concentrations of solute. Based on the solubility values from DOE's 1988 Site Characterization Plan (see DOE, 1988; p. 4–100), uranium, neptunium, cesium, and technetium could be at concentration levels comparable to those in the uncontaminated waters. Furthermore, what constitutes a competing ion has not been established. Thus, in a solution with multiple species, the competing ion could be a major, minor, or trace constituent. Furthermore, at the low temperatures at Yucca Mountain, certain ion exchange reactions may be kinetically inhibited, thus allowing less thermodynamically favorable reactions to control the system. The questions concerning competing ions will have to be addressed by experimentation.

The simulations done in this auxiliary analysis involved the binary system Na–K. Consequently, changes in one component could affect the other, as shown when the two components were in comparable concentrations. When the one component was in trace amounts relative to the other, its addition to the system did not affect the other. This resulted in a linear isotherm, and constant K_d values along the column. However, Reardon (1981) has shown that variations in the concentrations of a major component can affect the partitioning (K_d) of a trace component. Thus, in a system as complex as Yucca Mountain, it is crucial that DOE demonstrate that the (competing constituent) chemistry of the farfield is relatively constant over the lifetime of the repository. Otherwise, the application of the K_d approach would not be technically defensible.

There are a number of aspects to modeling radionuclide transport that can be tested using *PHREEQM*. In future phases of the IPA effort, the modeling should concern the effect of charge of the competing ions on migration, changes in water saturation, and solid substrate heterogeneity. It is recommended that the database, *PHREEDA*, used by this code, be expanded to include radionuclide information.

D–4 REFERENCES

Appelo, C.A.T. and A. Willemsen, "Geochemical Calculations and Observations on Salt Water Intrusions, I., A Combined Geochemical/Mixing Cell Model," *Journal of Hydrology*, 94:313–330 [1987].

Freeze, R.A. and J.A. Cherry, *Groundwater*, Englewoood Cliffs, New Jersey, Prentice Hall, Inc., 1979.

Meijer, A., "Yucca Mountain Project Far-Field Sorption Studies and Data Needs," Los Alamos, New Mexico, Los Alamos National Laboratory, LA–11671–MS, September 1990.

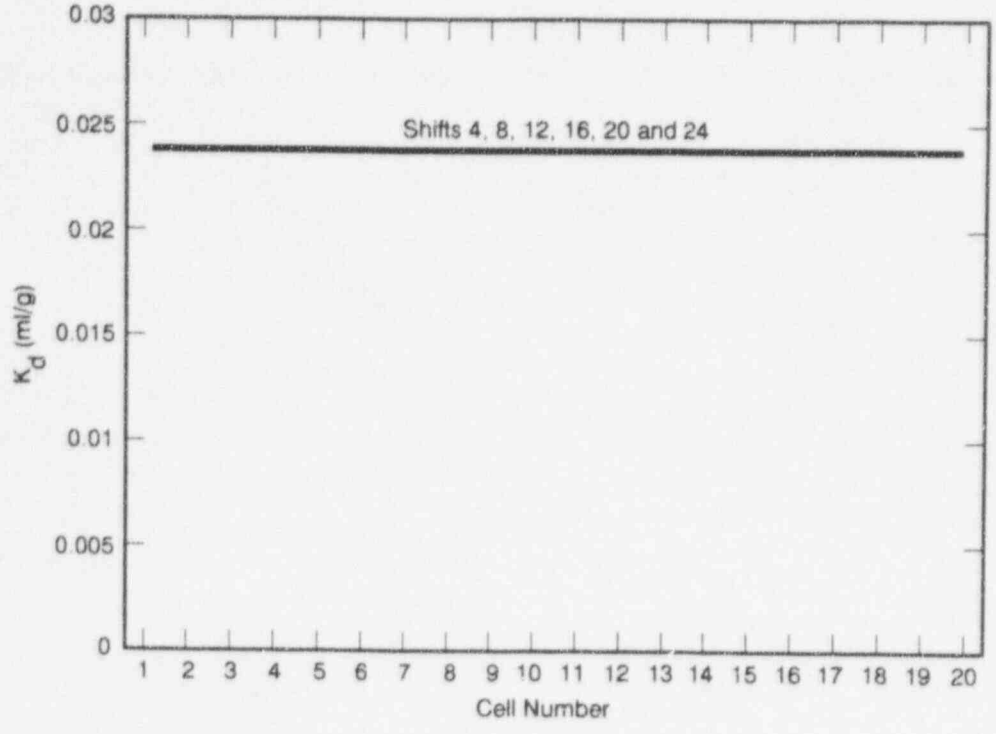

Figure D–21 K_d versus cell number for flow-through ion exchange simulation illustrated in Figure D–20

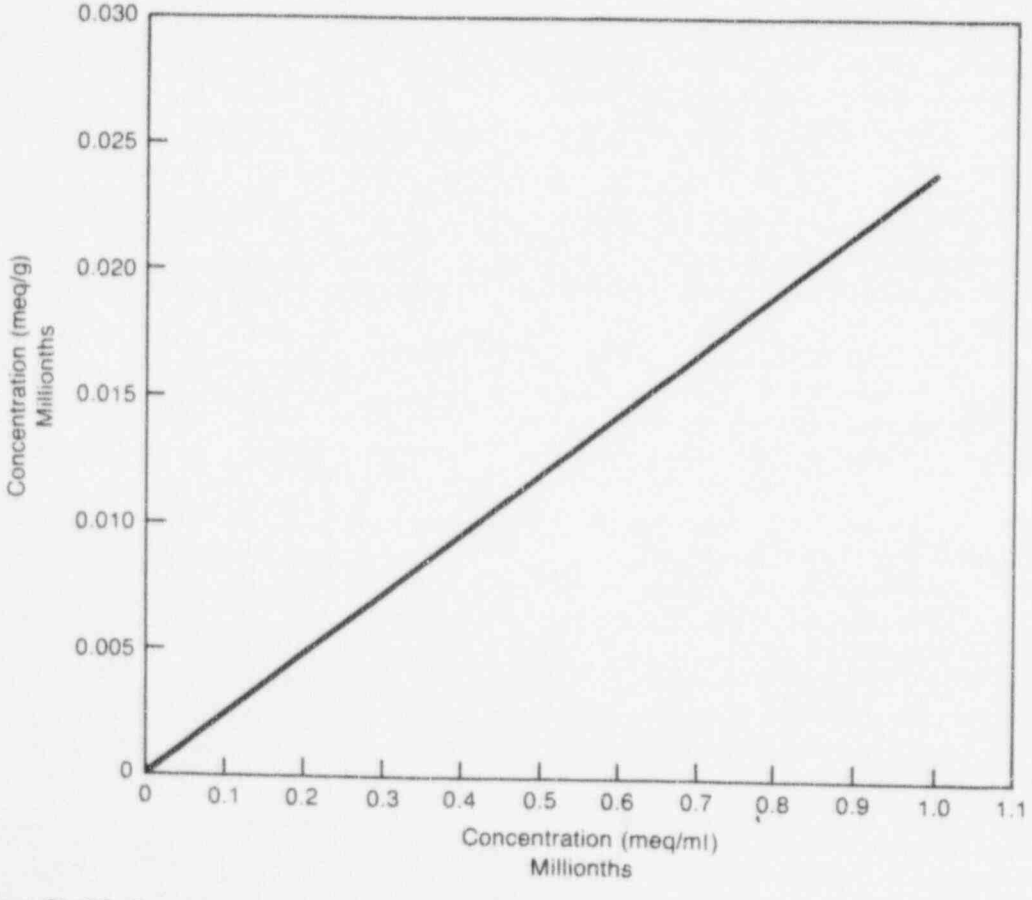

Figure D–22 Sorption isotherm calculated from flow-through ion exchange simulation illustrated in Figure D–20 showing linear behavior

Meijer, A., "A Strategy for the Derivation and Use of Sorption Coefficients in Performance Assessment Calculations for the Yucca Mountain Site," *Proceedings of the DOE/Yucca Mountain Site Characterization Project Radionuclide Adsorption Workshop, September 11–12, 1990*, Los Alamos, New Mexico, Los Alamos National Laboratory, LA–12325–C, August 1992.

Pabalan, R.T., "Nonideality Effects on the Ion Exchange Behavior of the Zeolite Mineral Clinoptilolite," in Abrajano, T., Jr. and L.H. Johnson (eds.), *Scientific Basis for Nuclear Waste Management XIV: Materials Research Society Symposium Proceedings*, 212:559–567 [1991].

Parkhurst, D.L., D.C. Thorstenson, and L.N. Plummer, "PHREEQE: A Computer Program for Geochemical Calculations," U.S. Geological Survey, Water Research Investigations Report, WRI–80–96, August 1990.

Plummer, L.N., *et al.*, "Dissolution of Aragonite-Strontionite Solid Solutions in Nonstoichiometric $Sr(HCO_3)_2$–$Ca(HCO_3)_2$–CO_2–H_20 Solutions," *Geochimica et Cosmochimica Acta*, 56:3045–3072 [1992].

Reardon, E.J., "K_d's—Can They Be Used to Describe Reversible Ion Sorption Reactions in Contaminant Migration?," *Groundwater*, 19:279–286 [1981].

Thomas, K., "Summary of Sorption Measurements Performed with Yucca Mountain, Nevada, Tuff Samples and Water from Well J–13," Los Alamos, New Mexico, Los Alamos National Laboratory, LA–10960–MS, December 1987.

U.S. Department of Energy, "Site Characterization Plan, Yucca Mountain Site, Nevada Research and Development Area, Nevada," Nevada Operations Office/Yucca Mountain Project Office, Nevada, DOE/RW–0199, 9 vols., December 1988.

U.S. Nuclear Regulatory Commission, "Site Characterization Analysis of the Department of Energy's Site Characterization Plan, Yucca Mountain Site, Nevada," Office of Nuclear Material Safety and Safeguards, NUREG–1347, October 1989.

Vermeulen, T., *et al.*, "Adsorption and Ion Exchange (Section 16)" in Perry, R.H., D.W. Green, and J.O. Maloney (eds.), *Perry's Handbook of Chemical Engineering (Sixth Edition)*, New York, McGraw-Hill, 1987.

APPENDIX E
REGIONAL FLOW ANALYSIS

E–1 INTRODUCTION

Assessing the overall long-term performance of the proposed high-level radioactive waste (HLW) geologic repository at Yucca Mountain requires predictions of the impact of postulated disruptive events occurring over the 10,000-year period of regulatory interest. Such predictions will usually be made through the use of computer modeling techniques. One area that has received much recent attention is the likelihood, in the future, of significant rises in the water table beneath Yucca Mountain, because of possible events such as seismic activity, increased precipitation over the region, volcanic intrusions, or changes to existing hydrogeologic barriers. Such events could lead to, for instance, a significant change in the ground-water travel time through the unsaturated zone beneath the repository horizon, because of alterations in the unsaturated pathway.

As one of the auxiliary analyses in Iterative Performance Assessment (IPA) Phase 2, it was decided to simulate the flow field in the saturated unconfined region that contains Yucca Mountain. The specific objective of this analysis is to study the fluctuations in the water table in response to postulated changes in recharge rates and other modifications in geohydrologic structures. The simulations were conducted both on a regional scale as well as a smaller scale, (i.e., the scale of Yucca Mountain). The regional-scale analysis provided the boundary conditions for the simulations of the saturated zone in the subregional model. A full discussion of this analysis and results is given in a recent report by Ahola and Sagar (1992).

Because of the limited objective of the analysis presented in this report, no attempt was made to estimate the probability of occurrence of such events mentioned above. Only data that were readily available from other published reports were used. Also, some parameter values were taken from other published reports (e.g., Rice, 1984; Waddell, 1982; and Czarnecki, 1985) without verifying their accuracy. Consequently, the analysis results should be considered as very preliminary and likely to change when more accurate field data are used in the simulations. Final analyses should also verify the accuracy of existing data taken from other published sources. In addition, evapotranspiration and modifications in surface runoff were not considered in this modeling effort.

The simulation results pertain to a two-dimensional (2–D) regional (about 250- by 250-kilometers) and subregional (50- by 50-kilometers) areas, and saturated ground-water flow analysis beneath Yucca Mountain and the surrounding area. For this application, *PORFLOW* (Runchal and Sagar, 1989; and Sagar and Runchal, 1990), an integrated finite difference code, was modified (Version 1.11) to incorporate the free surface (water table) in a ground-water flow model. The model was set up in the x-y (horizontal) plane, and allowed for specification of recharge and discharge areas. An approximate model of the regional ground-water flow system around Yucca Mountain was first developed for the *PORFLOW* code. Once this was completed, various conditions were postulated, such as increasing the recharge to simulate future climatic changes that might take place in the geohydrologic basin containing Yucca Mountain.

E–2 RELEVANT LITERATURE

A brief summary of relevant literature pertinent to saturated zone modeling that was reviewed for this study follows. For this study, a comprehensive literature review of all hydrologic studies in the Yucca Mountain area was not conducted. A more detailed discussion of previous studies of the saturated-zone hydrology is given by Ahola and Sagar (1992), and can also be found in the U.S. Department of Energy's Site Characterization Plan (SCP) (see "Hydrology" (Chapter 3) in DOE, 1988). The purpose of this review was mainly to determine what other modeling studies were conducted to simulate the regional saturated hydrology, and to use the results and data (i.e., hydraulic conductivities and boundary conditions) from such studies for the *PORFLOW* analysis. These previous studies were more comprehensive in that their models were calibrated on measured heads. For this study, no model calibration was done;

rather, parameter values from previous studies were adopted.

Waddell (1982) conducted flow modeling on a regional basis for the Nevada Test Site and vicinity. The main goals of his investigation were:

- To estimate fluxes for use in predictions of transport of radionuclides; and
- To study the effects of uncertainty in model parameters on these estimates.

Waddell (1982) used a horizontal 2-D finite-element model consisting of 685 nodes. The model encompassed an area measuring approximately 175- by 175-kilometers, the boundaries of which were taken mainly along topographic highs to the north and east, and topographic lows to the southwest. For model calibration, a numerical parameter-estimation technique was used in which parameters such as transmissivities, ground-water sources, and sinks were derived throughout the modeled area such that the weighted sum of the squared residuals (observed head minus simulated head) was minimized. An iteration scheme was used to minimize the weighted sum of squared residuals by successive approximation to model parameters. It was generally found that absolute values of residuals were less than 30 meters.

Czarnecki and Waddell (1984) developed a smaller subregional horizontal finite-element model of the ground-water flow system in the vicinity of Yucca Mountain also using parameter estimation techniques. This model was formulated as a portion of the regional model conducted by Waddell (1982). Some of the boundaries for this subregional model were taken along ground-water barriers from the larger regional model. The remaining boundaries had either specified pressure heads or fluxes, which were calculated from the regional model. The purpose of this subregional model study was to gain a better understanding of the ground-water flow system beneath the Yucca Mountain area. Czarnecki (1985) used this same 2-D finite-element subregional model to assess the potential effects of changes in future climatic conditions on the ground-water system in the vicinity of Yucca Mountain. He found that the simulated position of the water table rose as much as 130 meters near the primary repository area at Yucca Mountain for a simulation involving a 100 percent increase in precipitation compared with current conditions. The average increase in recharge for the case of this 100 percent increase in annual precipitation was set at 15 times the modern-day recharge rate in all areas of his model. This water table rise was caused primarily by the increase in recharge, applied to Fortymile Wash to the east of Yucca Mountain, by a factor of 15 times the baseline rate of 0.41 meters/year. For a factor of 10 increase in flux into the model, Czarnecki shows an increase in hydraulic head near Yucca Mountain of approximately 100 meters. Flooding on the primary repository area would require a water table rise of at least 300 meters.

Rice (1984) also developed a 2-D regional hydrologic model for the saturated flow system surrounding Yucca Mountain. A finite-difference grid consisting of 5600 nodes in the *x-y* plane was used for the simulations. The flow system was modeled under confined conditions, and only horizontal flow was allowed. Model calibration was accomplished by adjusting the transmissivities, within reasonable limits, to minimize the difference between the hydraulic heads simulated by the model and hydraulic heads measured at well locations. Results of simulated heads compared well with U.S. Geological Survey-interpreted head distribution, based on well observations.

E-3 DESCRIPTION OF ANALYSES: CONCEPTUAL MODELS AND DATA

The conceptual models for these analyses consisted of both a regional model (approximately 250- by 250-kilometers), and a subregional model (50- by 50-kilometers), set up in the *x-y* (horizontal) plane, as shown in Figure E-1. Provision was made to allow for specification of recharge and discharge areas in the model. The primary recharge was assumed to occur on outcrops at higher elevations, as shown in Figure E-1. Current estimates of recharge in these areas range from approximately 7 to 200 millimeters/year, depending primarily on the land surface elevation, as given by Rice (1984). Although Figure E-1 shows only the general areas where recharge was applied, the specific values of recharge increased with elevation, with the highest values occurring in regions of snow accumulation.

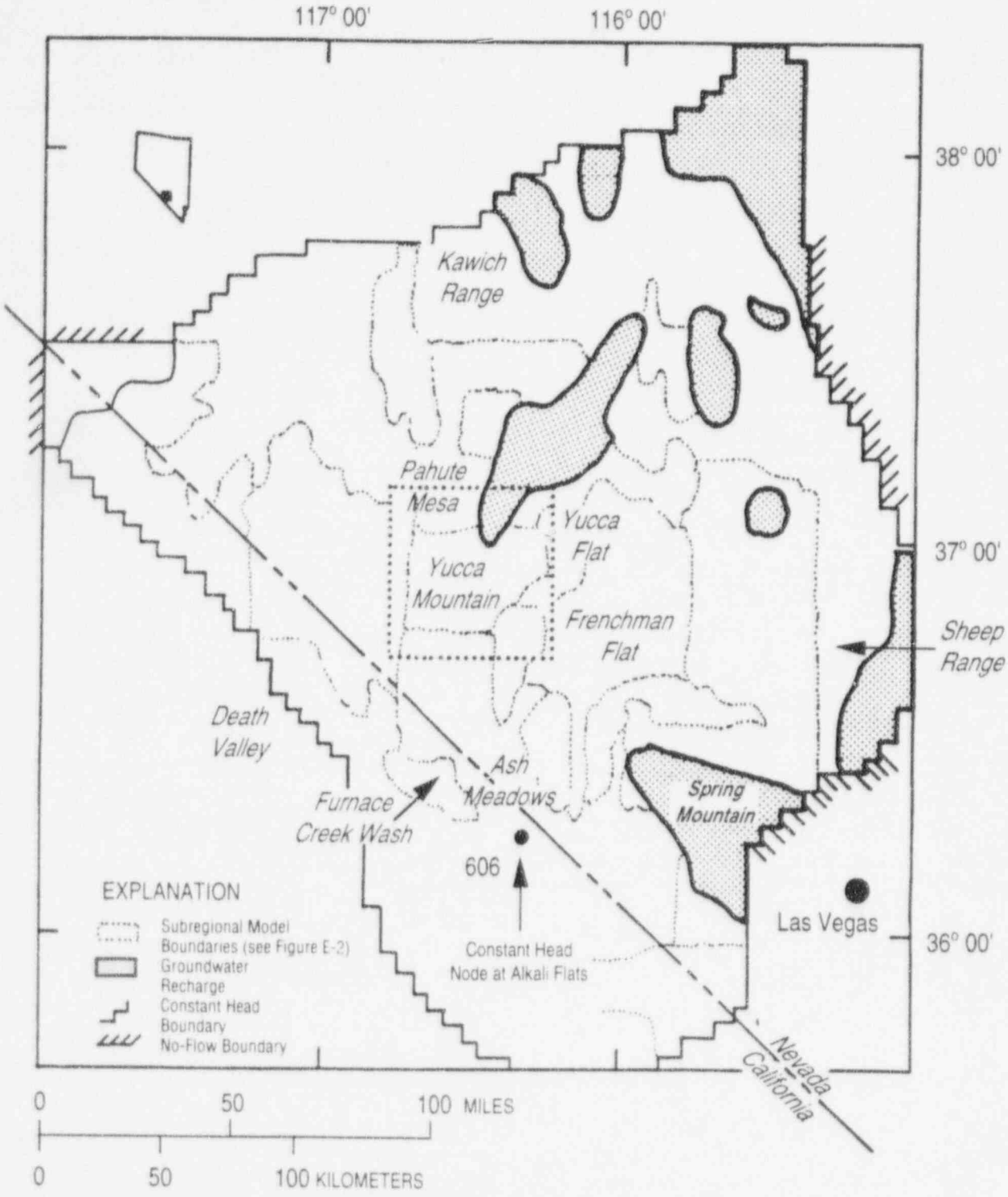

Figure E–1 Regional and subregional models, for *PORFLOW*, depicting location of recharge and constant head discharge areas (modified from Rice, 1984)

Discharge areas included Alkali Flats and the Furnace Creek Ranch, which were modeled as fixed head boundaries. Mathematical boundary conditions for the regional model consisted of both fixed pressures and no-flow boundaries; these boundary conditions were chosen to be consistent with the physical boundaries (Figure E–1). The regional and subregional models consisted of 13,161 and 18,225 finite difference computational cells, respectively. Each grid cell in the regional model was 2.5 kilometers on a side, encompassing an area of 6.25 square kilometers. The grid cells for the subregional model ranged from 100 meters on a side near the center to 2.5 kilometers on a side near the outer edges. The boundary conditions for this model consisted only of fixed pressures that were obtained from the simulation results of the larger regional model. The hydrological data for the simulations were obtained from the review of previously published studies (Rice, 1984; Waddell, 1982; Waddell *et al.*, 1984; Czarnecki and Waddell, 1984; and Czarnecki, 1985).

The entire modeled region was divided into zones having one of eight possible values for the hydraulic conductivity as shown in Figure E–2 and listed in Table E–1. These hydraulic conductivities varied over several orders of magnitude, and were estimated from transmissivity data published by Rice (1984). The model contains a low permeability zone north and northeast of Yucca Mountain indicated in Figure E–2 by Zones 1 and 2 (i.e., hatched regions in the area of Yucca Mountain and Yucca Flats) for simulating the present-day high hydraulic gradient at that location. The actual cause of the steep gradient is not yet fully known.

To conduct the study, *PORFLOW* was modified (Version 1.11) to incorporate the free surface (water table) in a ground-water flow model. The free-surface boundary condition and approximations (e.g., Dupuit) used in the modifications to *PORFLOW* are described in Bear (1988). Ahola and Sagar (1992) provide a detailed discussion of the specific modifications to *PORFLOW*. In essence, the model allowed 2-D flow in the horizontal plane, with the height of the water table adjusted such that the water pressure along this boundary is just equal to zero.

Table E–1 Hydraulic Conductivities for the Model

Zone Number	*Hydraulic Conductivity (m/sec)*
1	5.80E–08
2	6.34E–07
3	3.49E–06
4	8.69E–06
5	3.47E–05
6	1.00E–04
7	6.00E–04
8	3.50E–03

E–4 ANALYSES RESULTS

E–4.1 Regional Model Results

For the regional analysis, a steady-state solution to the flow system was first obtained to represent the present-day conditions under normal precipitation and ground-water recharge. Figure E–3 shows a portion of the simulated regional water table in the area of interest under assumed modern-day recharge. Yucca Mountain is indicated by the small rectangular box in this figure and represents approximately two grid nodes in the regional model (250- by 250-kilometers) because of the 2.5 kilometer grid node spacing. Thus, on the Yucca Mountain scale, the regional model is quite coarse. Based on the simulation, one can see the steep hydraulic gradient to the north and northeast of Yucca Mountain, which is comparable to results obtained in previous studies. It should be noted, however, that no calibration of this model was conducted for this study. The results are based on the use of data published from previously calibrated models. Since the results appeared consistent with previous studies and our objective was to focus more on relative changes in the water table rather than on the absolute water table elevation itself, they were deemed acceptable for use as a base case or initial state for analyzing the effects of various postulated disruptive conditions.

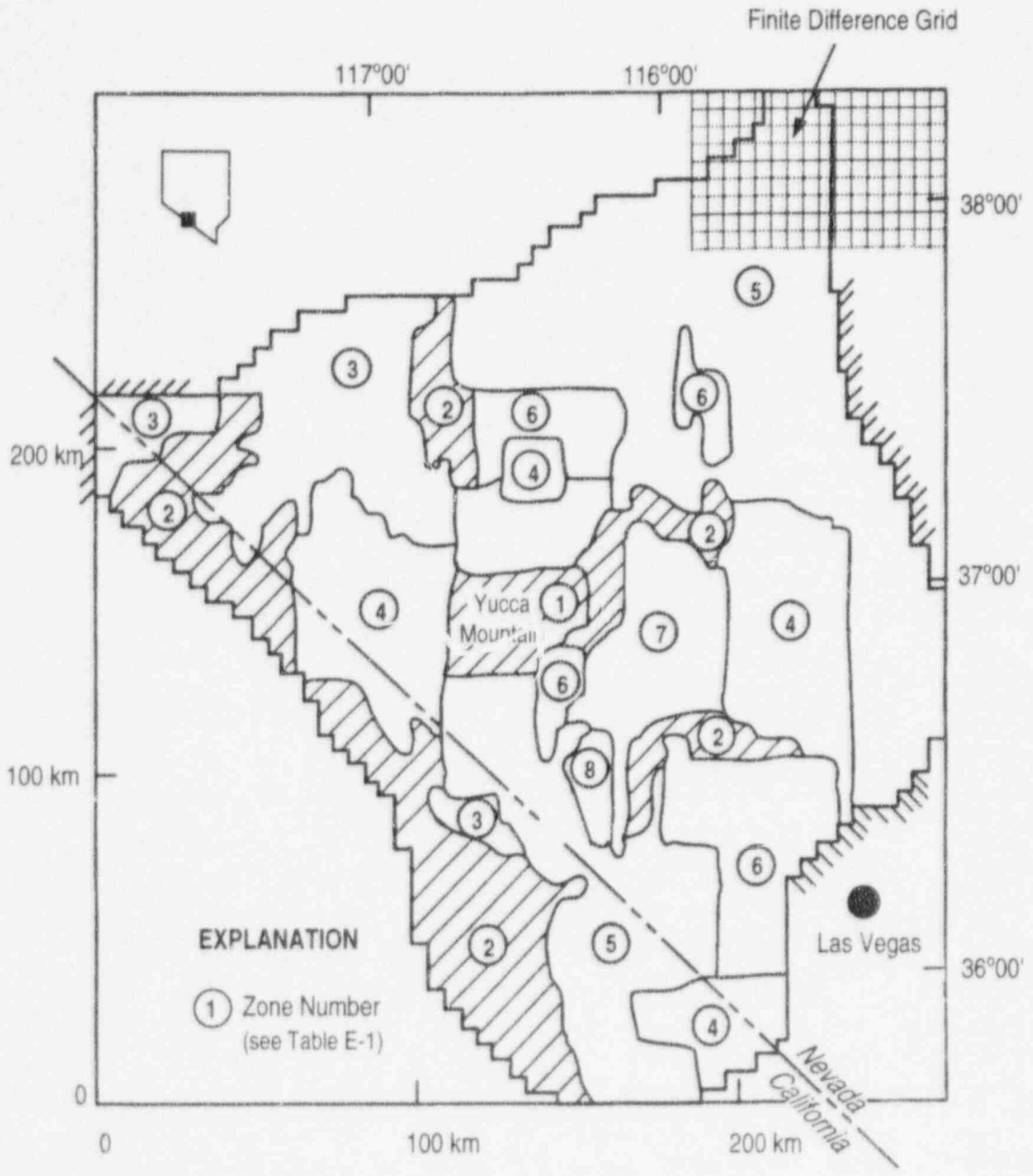

Figure E–2 Regional model for *PORFLOW* depicting boundary conditions and various hydraulic conductivity zones (modified from Rice, 1984) (Hatched areas indicate low permeability.)

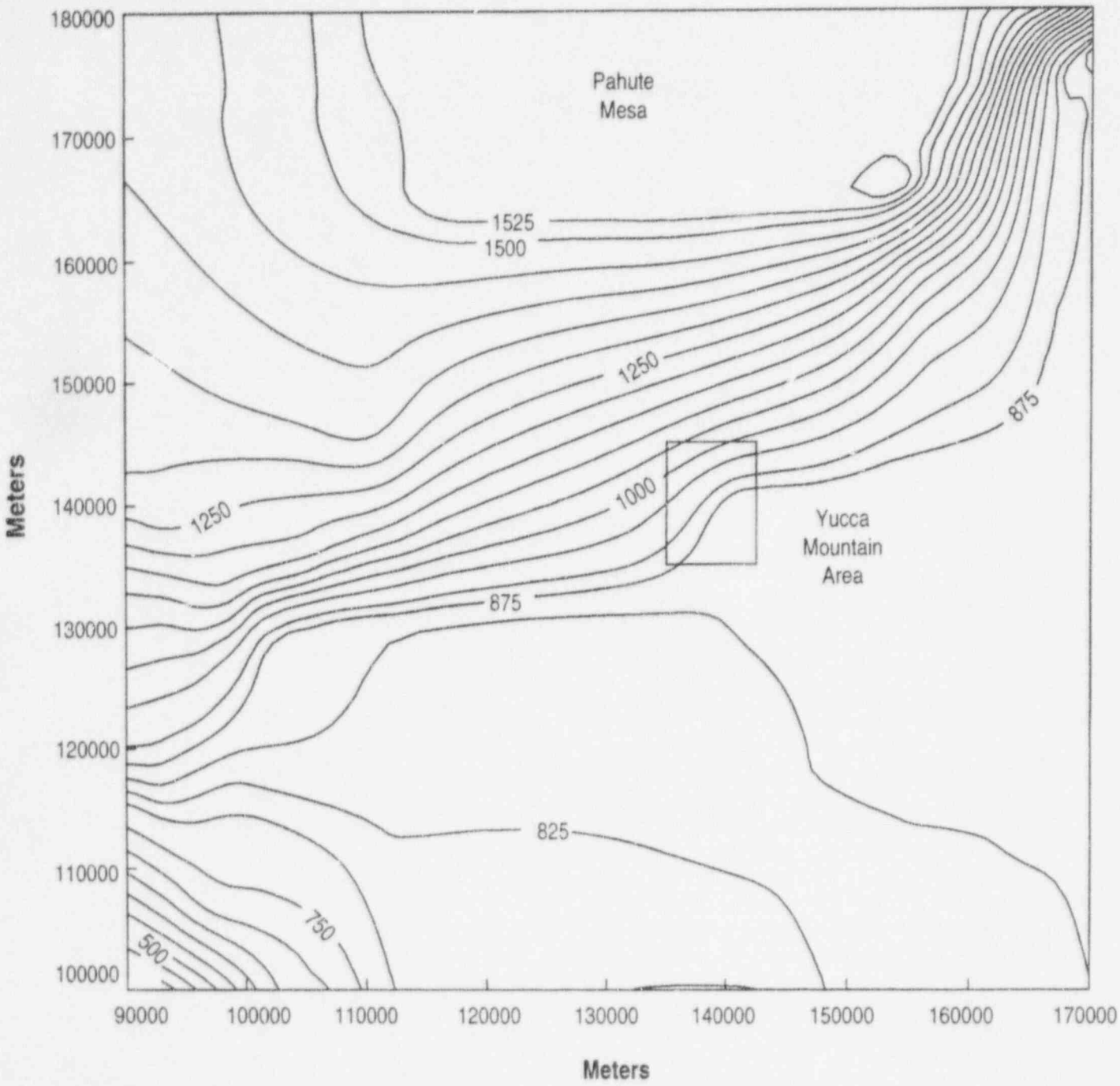

Figure E–3 Simulated hydraulic head distribution in the vicinity of Yucca Mountain, under assumed present-day conditions

One possible condition that could occur over the 10,000-year isolation period for a repository at Yucca Mountain would be increased precipitation and ground-water recharge throughout the region. Such ground-water recharge is thought to be greatest in the higher elevations where there is more precipitation and outcropping of the basement rock. Figure E–4 shows a relationship between increased recharge and water table rise at nodal points in the vicinity of Yucca Mountain and 5 kilometers to the east, at Fortymile Wash. The numbers representing increase in recharge, as shown on the *x*-axis, are multipliers of the baseline (present-day) flux. The recharge is applied over those shaded regions indicated in Figure E–1. The results show a more or less linear relationship between the two parameters. In general, from the transient analysis, a larger increase in recharge resulted in a longer period of time in which the ground-water flow field reached steady state. For instance, the simulated water table configuration took approximately 400 years to equilibrate, when the recharge was increased 10 times, and 700 years to equilibrate when the recharge was increased 20 times. Czarnecki (1985) states that a 100 percent increase in annual precipitation over the region would correspond to an increase in ground-water recharge of approximately 15 times the present-day recharge rate. From Figure E–4, this would correspond to a water table rise at Yucca Mountain of approximately 65 meters. It is likely that a 100 percent increase in annual precipitation would be a conservative upper bound, based on geologic evidence at the site of past climatic conditions. Czarnecki found that, in addition, increasing the recharge into Fortymile Wash above a small annual baseline recharge had a significant effect on the water table rise near Yucca Mountain, primarily because of its close proximity. It is conceivable that increased precipitation in the higher elevations would cause greater runoff into Fortymile Wash, for example, and consequently greater recharge. The results shown in Figure E–4, however, assume no recharge into Fortymile Wash.

As another potentially disruptive condition, it was postulated that future tectonic activity throughout the Basin and Range region could result in slip or opening of fractures through the areas north and northeast of Yucca Mountain, where large hydraulic gradients exist, and increase the flow toward Yucca Mountain. Although the exact cause is not well understood, it is thought that these large gradients may be because a low-permeability geologic unit has been juxtapositioned against a high-permeability unit, or perhaps that large lateral tectonic stresses within this region have closed existing north-south trending fractures. This condition was simulated in the regional model by increasing, to various degrees, the permeabilities through the previous low permeability regions just to the north (Zone 1) and northeast (Zone 2) of Yucca Mountain, as shown in Figure E–2. The relationship between the increase in permeability through these two zones and the subsequent rise in the water table at nodal points near Yucca Mountain and Fortymile Wash is shown in Figure E–5. The numbers along the *x*-axis represent multipliers of the assumed present-day permeabilities in the two zones directly north and northeast of the Yucca Mountain repository site. Figure E–5 shows that a fairly substantial rise in the water table can be expected for even a factor of 10 increase in the permeability of these two zones. If the permeability of these two zones is increased to a value representative of the hydraulic conductivity of Zone Number 7 (Table E–1), which is approximately 1000 times greater, the modeling results show a water table rise in the area of Fortymile Wash of approximately 200 meters. In this case, the steep gradient north and northeast of Yucca Mountain no longer exists.

E–4.2 Subregional Model Results

To study the impact of volcanic dike intrusions occurring directly beneath Yucca Mountain in more detail, an analysis was conducted using a smaller-scale subregional model. These dikes were assumed to be approximately 4 kilometers in length and to extend vertically through the saturated zone. For these simulations, the regional model was too coarse. The location of the subregional model is depicted by the dashed rectangular region in Figure E–1. The finite-difference grid encompassed an area of 50- by 50-kilometers. The grid cells were 100 meters on a side near the center of the mesh, where the volcanic dikes were assumed to be located. At the outer boundaries of the model, the largest grid cells were 2.5 kilometers on a side, which corresponded to the size of the grid cells for the

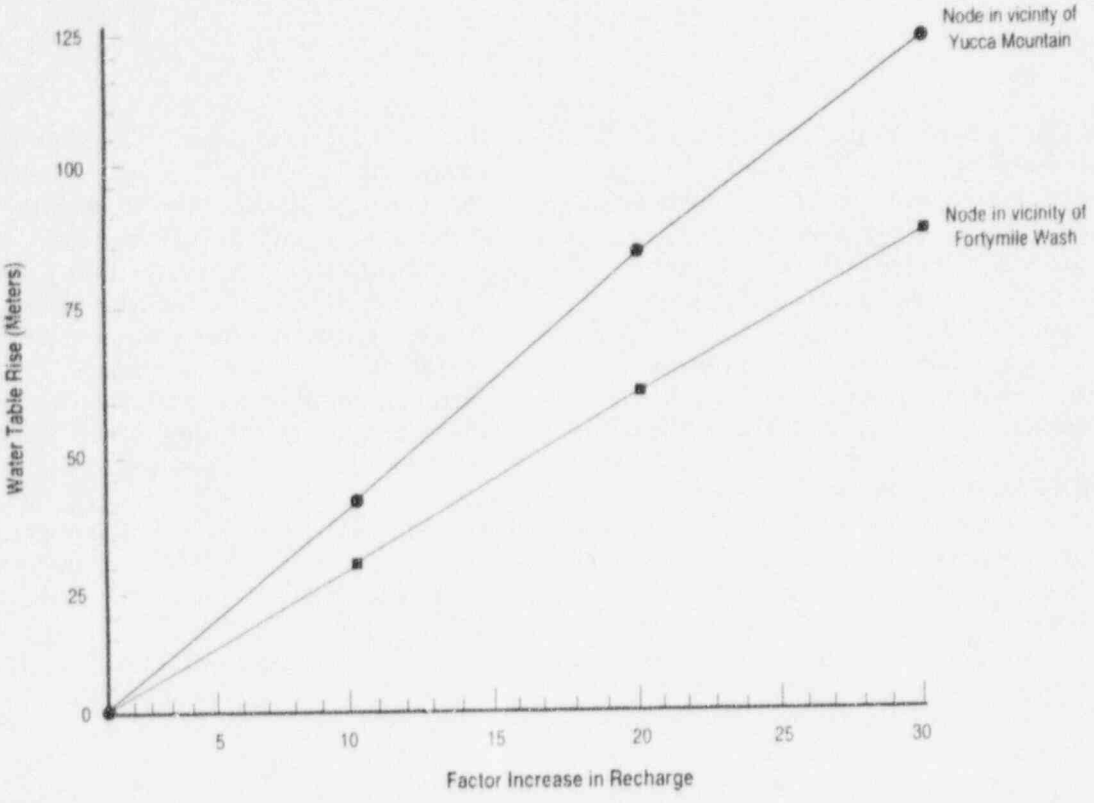

Figure E–4 Water table rise at Yucca Mountain and Fortymile Wash as a function of recharge rate

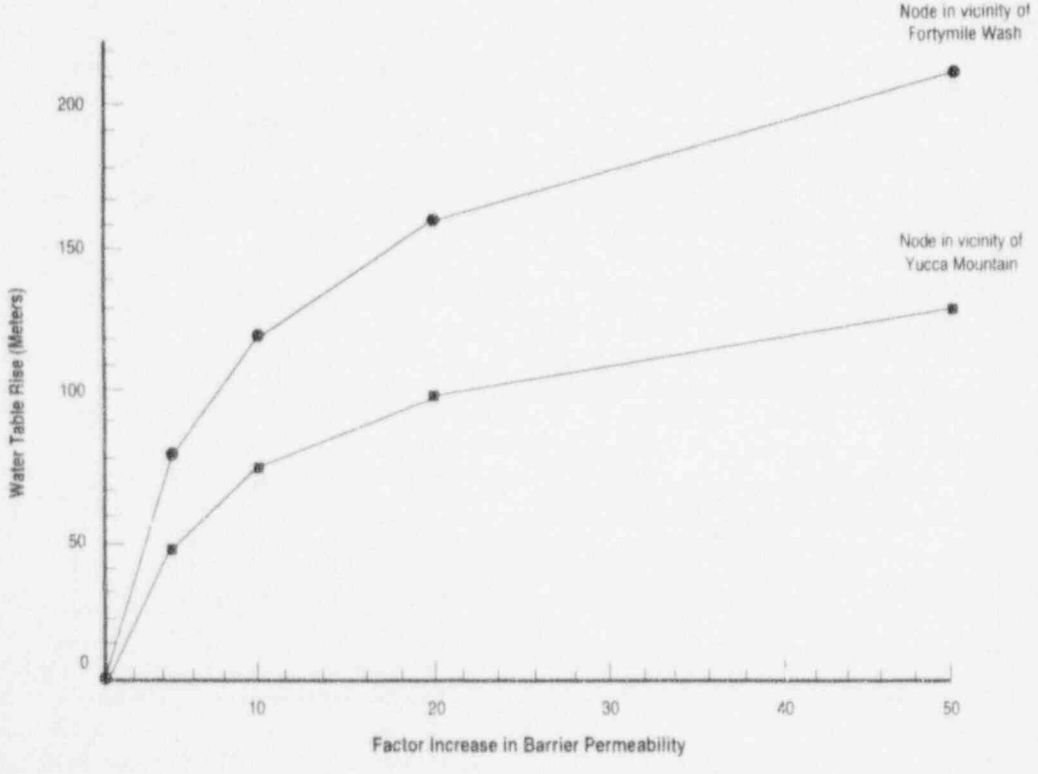

Figure E–5 Water table rise at Yucca Mountain and Fortymile Wash as a result of increasing the permeability through the barriers north and northeast of the site

regional model. The boundary conditions along all four sides of this model consisted of fixed pressures obtained from corresponding nodes in the regional model. Linear interpolation was done to assign values of pressure to those additional nodes along the boundary of the subregional model as a result of refining the mesh. These fixed boundary pressures corresponded to the baseline (or current) water table configuration from the regional model.

No attempt was made to take into account the effect the temperature of the intruding dike might have on the saturated zone. The narrow dikes essentially acted as dams within the flow field, and were assumed to extend through the water table and well above any potential water table rise. They were created by specifying a very low permeability along lines one gridpoint in thickness and 4 kilometers in length. Figure E–6 shows the velocity vectors and several streamlines (dark solid lines) depicting the ground-water flow field directly beneath Yucca Mountain, for the case of a single dike oriented N15°E, where the north direction is to the top of the plot. Based on the existing fracture and faulting pattern at Yucca Mountain, it is believed that this could be a likely orientation for a possible dike intrusion. Figure E–6 shows that to the left of the dike, the flow field can be seen to be directed toward the south. Around the lower tip of the dike, some of the flow is directed back to the north. Without the presence of the dike, the flow through this area is primarily east and southeast. The small circle in this figure indicates the location where the maximum water table rise occurred, which in this case was 79 meters. Even though the groundwater travel time through the unsaturated zone would be somewhat decreased, the travel time in the saturated zone could be substantially increased, especially for the portion of the radionuclide inventory that entered the saturated zone on the left side of the dike. Figure E–7 shows the numerical simulation results for the water table rise at the repository site for various dike orientations. The figure suggests that a dike oriented roughly north to northeast would produce the maximum water table rise for a single dike intrusion.

Figure E–8 shows the intrusion of a second dike, which is perpendicular to the one shown in Figure E–6. This case was simulated because it is believed to be not uncommon for volcanic dikes to occur in pairs at more or less perpendicular orientations. Interestingly, Figure E–8 shows the dikes create stagnant pools of water which again may increase the length of the flow path in the saturated zone to the accessible environment. The maximum water table rise for this case of two perpendicular dikes was 103.4 meters.

E–5 CONCLUSIONS

A summary of the results from both a regional and subregional ground-water flow analysis of the saturated zone surrounding Yucca Mountain, using the *PORFLOW* finite difference code, is presented. These results show the effects of various disruptive conditions on the water table elevations and resulting ground-water flow directions near the proposed HLW repository. The results give an indication of what conditions would have a minimal impact on the saturated zone hydrology near the site, and those that would have a major impact. A rise in water table in the area of Fortymile Wash was calculated to be greater than 200 meters, based on certain disruptive conditions simulated using the regional model. Because evapotranspiration and surface runoff were neglected, the actual rise would be less than calculated. In addition, the subregional model analysis showed a rise in the water table near the repository ranging from a few meters to as much as 103 meters, depending on the orientation of the simulated volcanic dikes.

The results presented here are meant to be preliminary and likely to change as site characterization studies at Yucca Mountain provide more accurate hydrological parameters and better information on which disruptive conditions would be more likely to occur in the future. Also, some of the assumptions in this analysis could be improved in future studies. For instance, with respect to the high water table rises predicted, the formation of new discharge areas that such rises may cause was completely neglected.

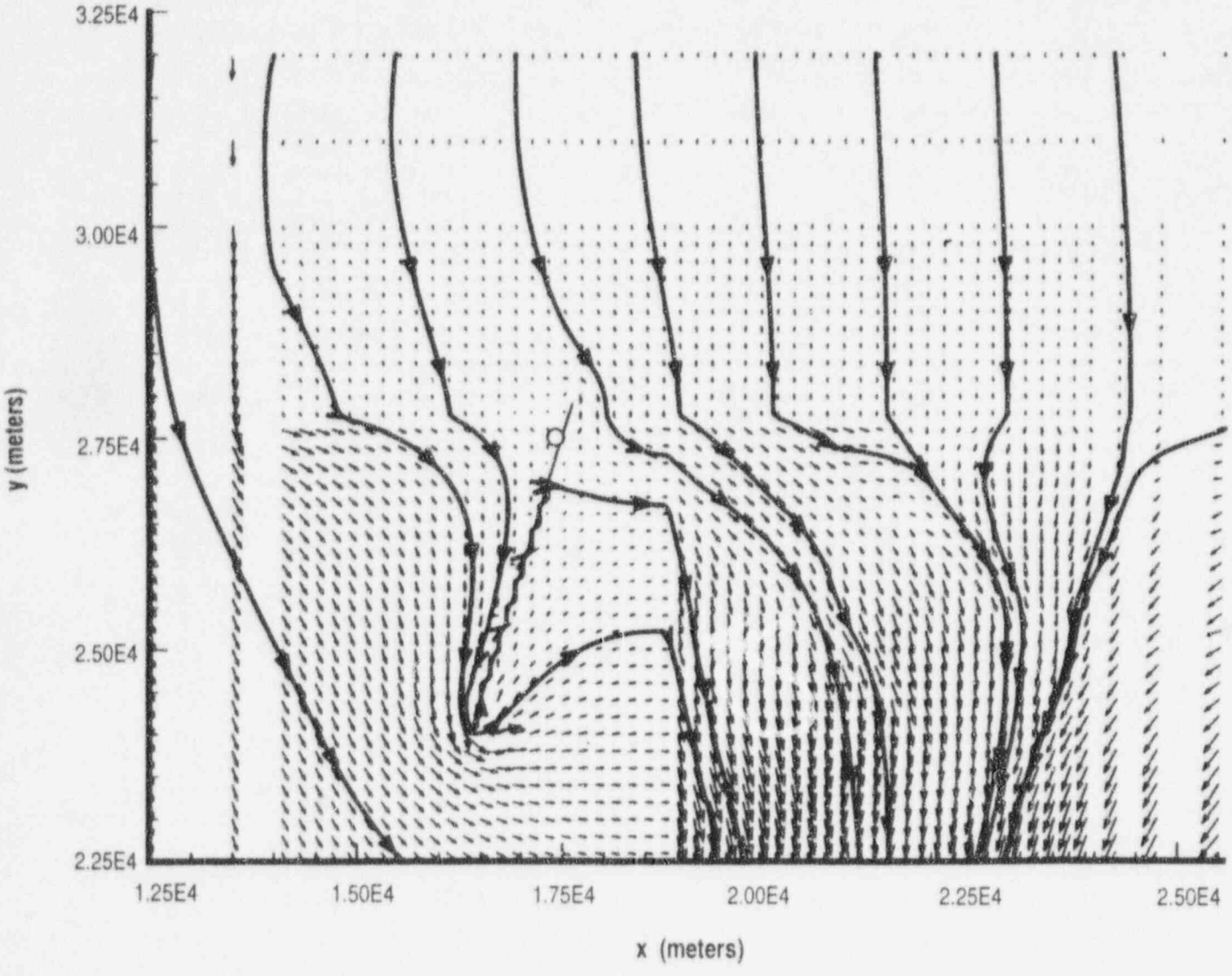

Figure E–6 Impact of the intrusion of a single volcanic dike oriented N15°E on the groundwater flow field directly below the repository (The straight line indicates the location of the dike. The ○ designates the location of the maximum water table rise (79.3 meters).)

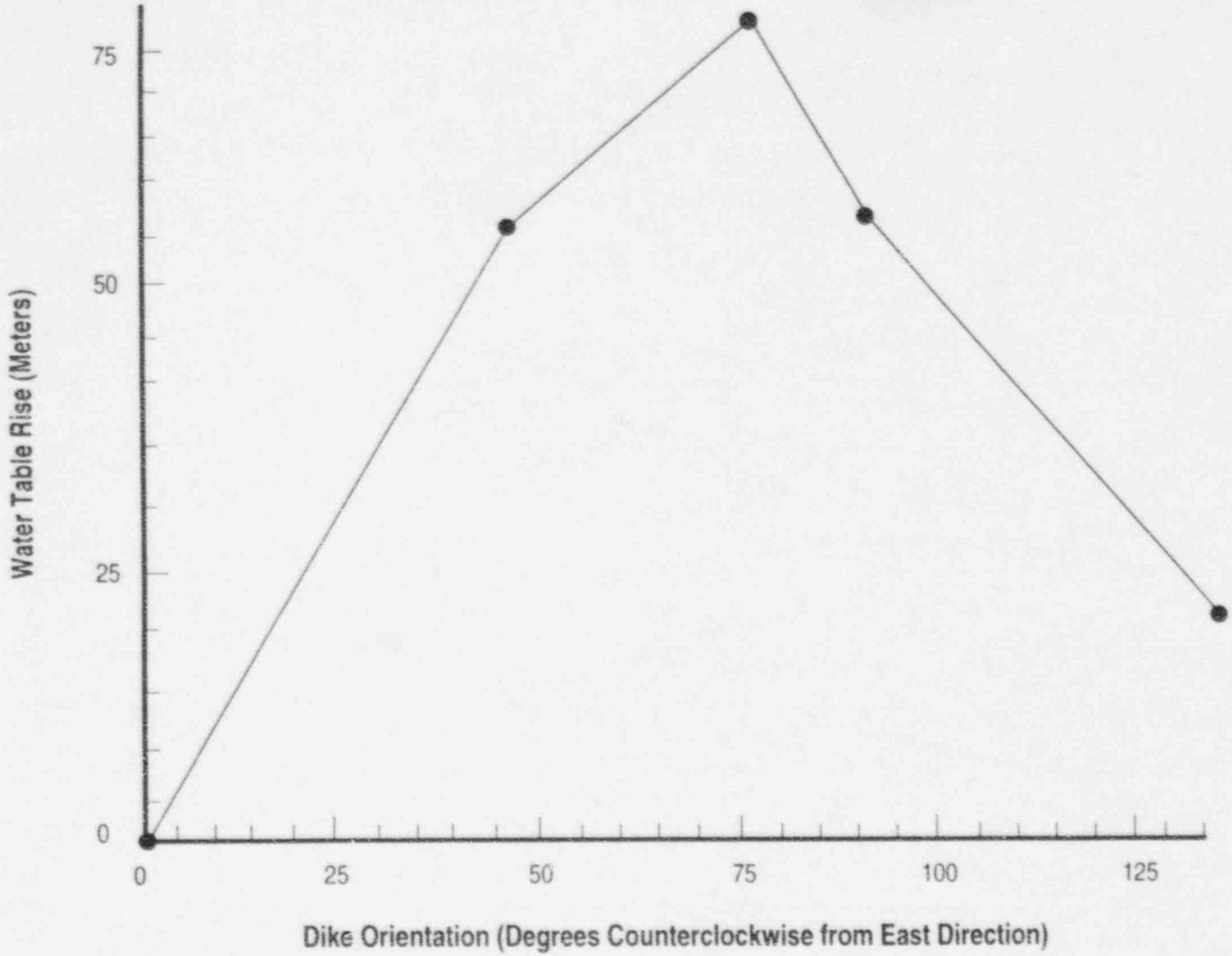

Figure E–7 Maximum water table rise at potential repository site as a function of dike orientation

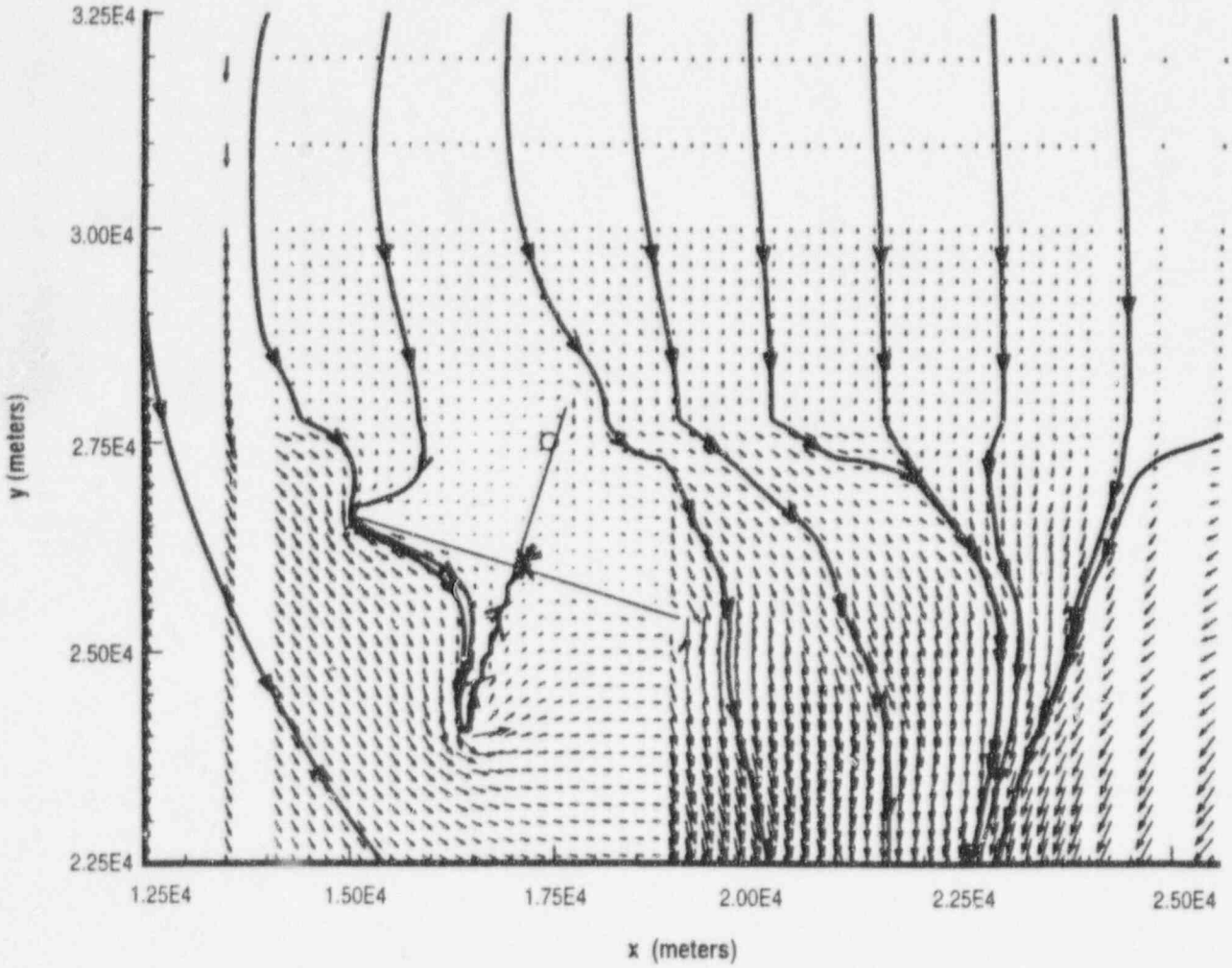

Figure E–8 Impact of the intrusion of multiple volcanic dikes on the ground-water flow field directly below the repository. (The straight lines indicate the location of the dikes. The ○ designates the location of the maximum water table rise (103.4 meters).)

E-6 REFERENCES

Ahola, M.P. and B. Sagar, "Regional Groundwater Modeling of the Saturated Zone in the Vicinity of Yucca Mountain, Nevada," U.S. Nuclear Regulatory Commission, NUREG/CR-5890, October 1992. [Prepared by the Center for Nuclear Waste Regulatory Analyses.]

Bear, J., *Dynamics of Fluids in Porous Media*, New York, Dover Publications, Inc., 1988.

Czarnecki, J.B. and R.J. Waddell, "Finite-Element Simulation of Groundwater Flow in the Vicinity of Yucca Mountain, Nevada-California, "U.S. Geological Survey, Water Resources Investigations Report, WRI-84-4349, 1984.

Czarnecki, J.B., "Simulated Effects of Increased Recharge on the Groundwater Flow System of Yucca Mountain and Vicinity, Nevada-California," U.S. Geological Survey, Water-Resources Investigations Report, WRI-84-4344, 1985.

Rice, W.A., "Preliminary Two-Dimensional Regional Hydrologic Model of Nevada Test Site and Vicinity," Sandia National Laboratories, SAND83-7466, August 1984. [Prepared for the U.S. Department of Energy.]

Runchal, A.K. and B. Sagar, "PORFLOW: A Mathematical Model for Fluid Flow, Heat, and Mass Transport in Variably Saturated Geologic Media—Users Manual (Version 1.0), Richland, Washington, Westinghouse Hanford Company, WHC-EP-0041, July 1989.

Sagar, B. and A.K. Runchal, "PORFLOW: A Mathematical Model for Fluid Flow, Heat, and Mass Transport in Variably Saturated Geologic Media—Theory and Numerical Methods (Version 1.0)," Richland, Washington, Westinghouse Hanford Company, WHC-EP-0042, March 1990.

U.S. Department of Energy, "Site Characterization Plan, Yucca Mountain Site, Nevada Research and Development Area, Nevada," Nevada Operations Office/Yucca Mountain Project Office, Nevada, DOE/RW-0199, 9 vols., December 1988.

Waddell, R.K., "Two-Dimensional, Steady-State Model of Ground Water Flow, Nevada Test Site and Vicinity, Nevada-California," U.S. Geological Survey Water-Resources Investigations Report, WRI-82-4085, 1982.

Waddell, R.K., J.H. Robison, and R.K. Blankennagel, "Hydrology of Yucca Mountain and Vicinity, Nevada-California: Investigative Results Through Mid1983," U.S. Geological Survey Water Resources Investigation Report, WRI-84-4267, 1984.

APPENDIX F
EFFECTS OF STRATIFICATION, DIP OF STRATA, AND SUB-VERTICAL FAULTS

F-1 INTRODUCTION

This section presents results of unsaturated flow simulations undertaken as an auxiliary analysis for the Iterative Performance Assessment (IPA) Phase 2 project, one of the approaches adopted by the U.S. Nuclear Regulatory Commission (NRC) staff to develop its license application review capabilities. The effects of common geological features on flow in a two-dimensional (2-D) domain, such as inclined stratification and vertical or near-vertical fault zones intersecting the strata, are of importance. In this work, numerical analysis is performed for a deep (approximately 530 meters) hard rock system. The *BIGFLOW* numerical code (Bagtzoglou *et al.*, 1992) is used in these simulations. Some of the data (i.e., the depth to water table, the number of primary geologic strata, their dip angle, and the existence of a fault zone) for the analysis were taken from the Yucca Mountain project reports (Scott and Bonk, 1984), but were adjusted to enhance the effects under study. In particular, extreme net infiltration rates (up to 50 millimeters/year) and hydraulic properties similar to the Calico Hills nonwelded, vitric (Chnv) unit were considered. Therefore, conclusions regarding the suitability of Yucca Mountain for the proposed geologic repository for high-level radioactive waste are not directly derivable from this analysis. Recognizing that there are no simple, natural initial-boundary conditions that can be used for the more complex problems, a method of successive approximation is implemented. This method uses solutions of auxiliary flow problems to set up pressure boundary conditions for the more complex problems. This is necessary because, in practice, no natural boundaries exist (or are adequately defined), especially in the lateral directions. The investigation is limited to three-dimensional (3-D) simulations in a vertical, thin slice, cross-section, with dipping strata intersected by a subvertical fault zone. The simulations are performed in a transient mode to study the manner in which the solutions of the flow equation approach steady state. A "wet," in terms of perceived net infiltration rates, hydroclimatic condition corresponding to a net annual infiltration rate of 50 millimeters/year is modeled. A hypothetical test problem is developed to study the effects of bedding, presence of a subvertical fault, and inclination of the beds.

The *BIGFLOW* simulation code accommodates 3-D transient or steady flow in saturated, or partially saturated, porous media with heterogeneous or spatially random hydrodynamic coefficients. For partially saturated flow, a mixed variable formulation of Richards' equation is used. That is:

$$\frac{\partial \theta\ (h,x)}{\partial t} = \nabla\ [K(h,x)\ (\nabla h + g)] \qquad \text{(F-1)}$$

where h is pressure head (meters), θ is volumetric water content (cubic meters/cubic meters), K is hydraulic conductivity (meters/second), and g is the body force unit vector aligned with, and opposed to, the acceleration of gravity. The differential equations are discretized by an implicit finite difference scheme, two-point backward Euler in time, and seven-point centered in space. The spatial mesh is a regular rectangular lattice. The time step is generally variable and self-adjusted. The computational domain is a 3-D parallelepiped, whose coordinate system may be inclined at arbitrary angles with respect to the natural, horizontal-vertical coordinate system.

F-2 DESCRIPTION OF ANALYSES

The hydrogeologic properties in the unsaturated zone of Yucca Mountain, Nevada, were considered in order to represent, to some degree, the general features of the site in the simulations. Yucca Mountain consists of a series of North-trending fault-block ridges composed of strata of volcanic ash tuffs that generally have a regional dip of 5° to 7° to the East (Scott and Bonk, 1984). The proposed repository area is also bounded by steeply dipping faults or by fault zones, and is transected by a few normal faults. Therefore, it is important to study the effects of stratification,

regional dipping, and fault zones on unsaturated water flow.

In the simulations presented herein, the computational domain is assumed to consist of five strata with approximately equal thicknesses spanning a total depth of 530 meters at which depth the water table is assumed to be located. The computational domain used in these simulations is based on a 3-D Cartesian grid system. The axes of this system are aligned with East-West (x-axis), North-South (y-axis), and vertical (z-axis). The dimensions of the computational domain are 1230 meters, 80 meters, and 530 meters in the x-, y-, and z-directions, respectively. The domain is discretized into 29 by 5 by 54 nodes, comprising a total of 7830 nodes (Figure F–1).

The functional forms of pressure-dependent hydraulic conductivity and water content used herein are the exponential Gardner model for $K(h)$ and the van Genuchten model for $\theta(h)$. The exponential conductivity model is:

$$K(h) = K_s \exp\left[\alpha(h - h_b)\right], \quad \text{if } h \leq h_b$$
$$K(h) = K_s, \quad \text{if } h > h_b \qquad \textbf{(F–2)}$$

where K_s is the saturated hydraulic conductivity, α is a characteristic inverse length scale or capillary diffusivity (Ababou, 1991), h is the pressure, and h_b is the air-entry pressure. The van Genuchten model for the retention curve is:

$$\theta(h) = \theta_r + (\theta_s - \theta_r)\left[1 + (-\beta h)^n\right]^{-m} \qquad \textbf{(F–3)}$$

where θ_s and θ_r are the saturated and residual moisture contents, respectively, β is a characteristic inverse length (similar to α in Equation

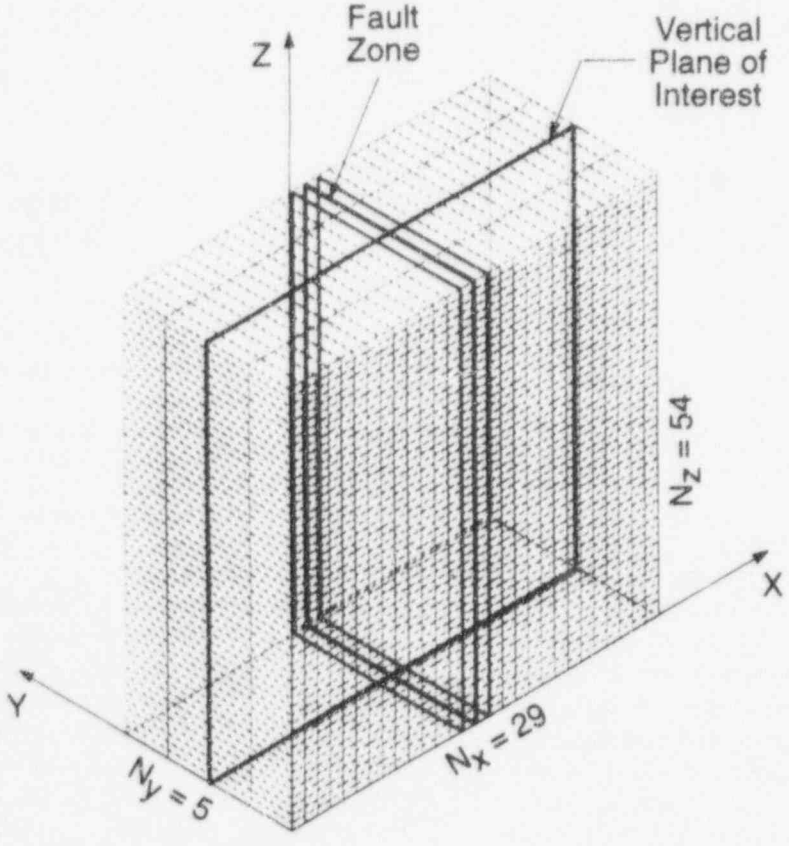

Figure F–1 Computational grid

(F-2)), and n and m are real exponents (dependent upon distribution of pore sizes) related by the Mualem constraint (Mualem, 1976).

All of the parameters in Equations (F-2) and (F-3) are, generally, spatially varying functions in all three dimensions. In the present work, however, they are assumed to be constant within a layer. Furthermore, the layer properties (K_s, α, h_b, and β) are assumed to be interchanging log-deviations around the geometric mean of each respective parameter [$\omega_G \exp(\pm \sigma_{ln\omega})$], taken herein as representative of the Chnv unit. Thus, adjacent layers have a contrast in their hydraulic parameters equal to $\exp(2\sigma_{ln\omega})$. The remaining matrix parameters are assumed to be constant in all strata, and are assigned typical values of the Chnv unit. Thus, θ_s = 44.11 percent, θ_r = 1.89 percent, n = 3.872, and m = 0.7417. The fault was arbitrarily modeled as a three-cell-wide, yz-planar zone located in the middle of the domain. The following table summarizes the hydraulic properties discussed above for the matrix layers and fault zone.

Table F-1 Values of Spatially Variable Hydraulic Parameters

Parameters	K_S *(m/d)*	$\alpha(m^{-1})$	h_b *(m)*	$\beta(m^{-1})$
Geometric Mean (ω_G)	2.33×10^{-2}	2.2×10^{-2}	20	5×10^{-2}
Standard Deviation ($\sigma_{ln\omega}$)	1.0	0.2	0.2	0.2
Fault Zone	9.32×10^{-1}	1.0×10^{-1}	10.417	9.6×10^{-2}

The values of these parameters, when substituted in Equation (F-2), yield different types of pressure-dependent curves $K(h)$. It is worthwhile noticing that the fault hydraulic conductivity is much greater than the matrix hydraulic conductivity near saturation, and remains higher for values of suction head up to about 50 meters. On the other hand, the fault becomes less conductive than the matrix for values of suction head significantly higher than 50 meters. The existence of a crossing point, where the fault becomes less permeable than the matrix, is of particular interest and, as will be shown later in this work, affects directly the overall behavior of the flow system. When parameter α_f is reduced threefold, a crossing point at a higher value of suction, $\psi \approx 260$ meters is attained. Note that, in terms of conductivities, this corresponds to a fault that is more like the porous matrix. Even though parameter β is varied from matrix to fault region, the remaining moisture retention curve properties are kept constant, causing the fault to desaturate at smaller suctions than the porous matrix.

The regional dip (6° to the East) results in an approximately 10 percent fraction of the body (gravity) force being parallel to the x-axis attached to the dipped domain. Finally, the net infiltration rate q_o is taken to vary from 0 to 50 millimeters/year. In particular, the low value q_o = 0 is used as a minimal base case, whereas the high value q_o = 50 millimeters/year accounts for potential occurrence of extreme infiltration conditions.

F-3 ANALYSES RESULTS AND DISCUSSION

Figure F-2 depicts the temporal variation of the vertical pressure head profile, at the central transect y = 40 meters, x = 615 meters, under a net infiltration rate of q_o = 1 millimeter/year. It can be seen that steady state is obtained only after 250 years of simulation. It is also apparent that the steady state solution is much drier than the assumed (linear, but not hydrostatic) initial condition, deduced and modified from saturation values given by Montazer and Wilson (1984), emphasizing the need for consistent initial and boundary conditions discussed before. It can be observed, further, that the effect of stratification in hydraulic properties is felt only during the early times of simulation. However, because of the continuous influx of water from the top boundary, a nonhydrostatic pressure head profile is attained. The infiltration affects only the pressure profile in the coarse top layer. Finally, for the extremely wet case (q_o = 50 millimeters/year), the behavior of

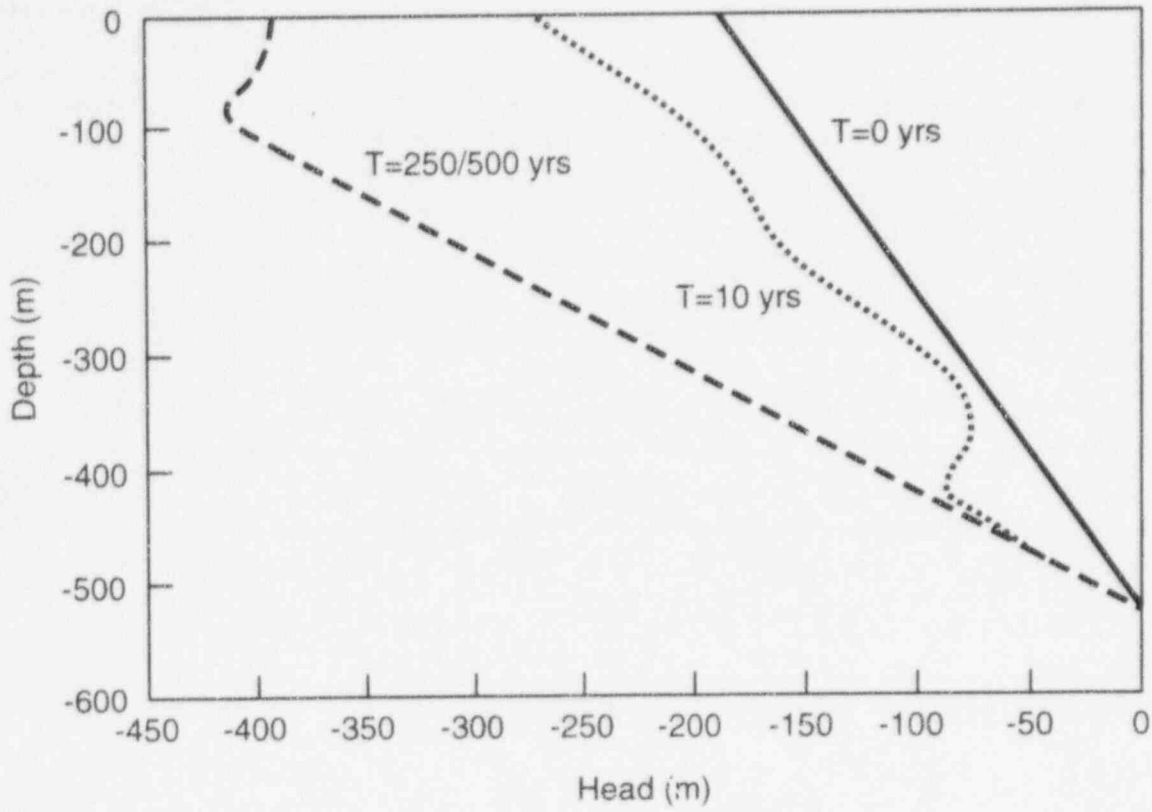

Figure F-2 Pressure profiles for q_o = 1 mm/yr

the flow system changes drastically. Steady state flow conditions are attained faster, that is, after only 100 years of simulation. Figure F-3 presents the temporal variation of the pressure head profile at the vertical transect (y = 40 meters, x = 615 meters). For this simulation, the initial condition is assumed to be hydrostatic. It is also worthwhile noticing that the effect of layering on pressure distribution appears to be almost insignificant for this flow rate, although the influence of the coarse top layer is still perceptible. Following a successive approximation methodology, the initial and boundary conditions for the simulations presented here are taken from the steady state results of less complex flow systems. Figure F-4 depicts results of a simulation with q_o = 50 millimeters/year, and a dip angle of 6° to the East, at time t = 120 years, at vertical transects at three different locations within the flow domain. The effects of infiltration are felt by a region having the same lateral extent as in the previous simulations (about 100 meters on either side of the fault). The infiltration "signal," however, is affecting a greater depth, down to almost 400 meters. It is also shown that the effects of dipping are minor (less than 5 meters of pressure head difference) for the conditions assumed in this analysis.

The high contrast in hydraulic properties between the matrix and fault zones renders the simulations extremely sensitive to the time step used. Choosing a Δt_{max} = 365 days, for example, resulted in a nonbinding constraint for the time step. Even though the actual time step had an upper envelope of $\Delta t \approx 20$ days, mass balance errors as high as 20 percent were observed. This resulted in solutions that were not able to reach steady state following an oscillatory pattern. When the lateral boundaries are set to no-flow (i.e., a 2-D system), the mass balance error causes slight fluctuations of the total discharge rate on the order of 2 percent. This is in contrast with the more pronounced fluctuations obtained for a system with

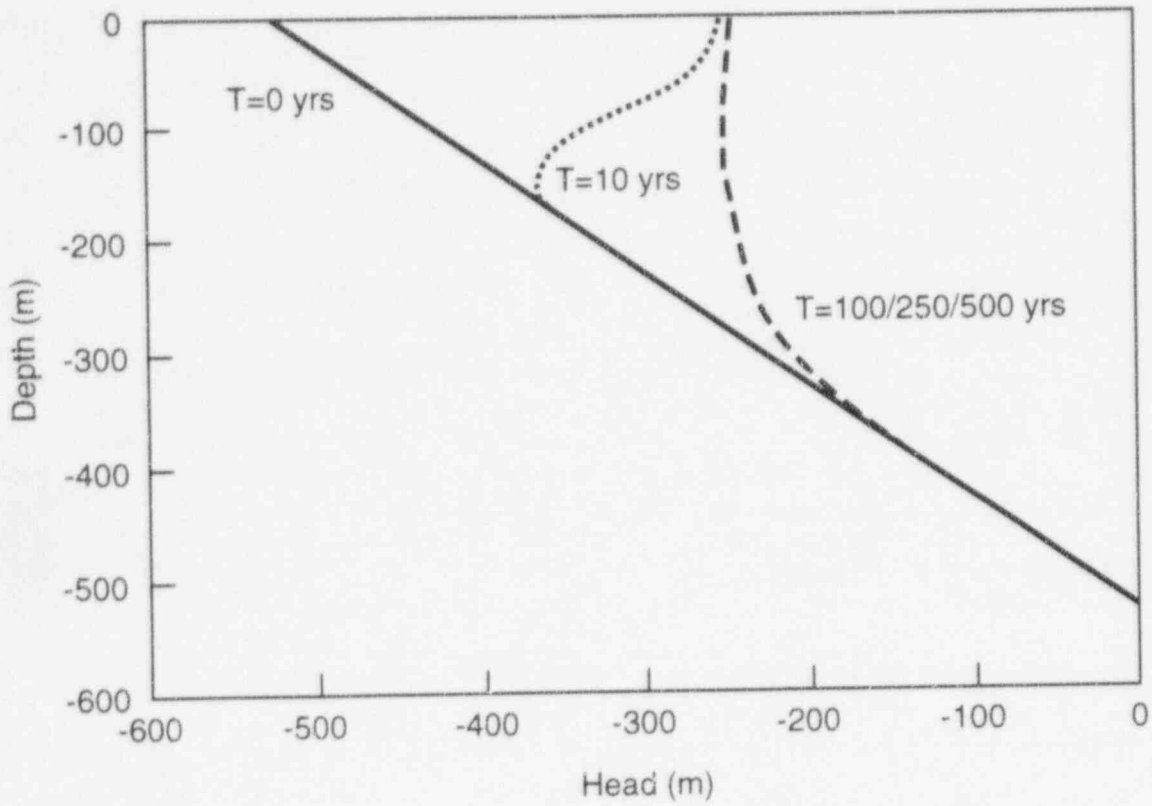

Figure F–3 Pressure profiles for q_o = 50 mm/yr

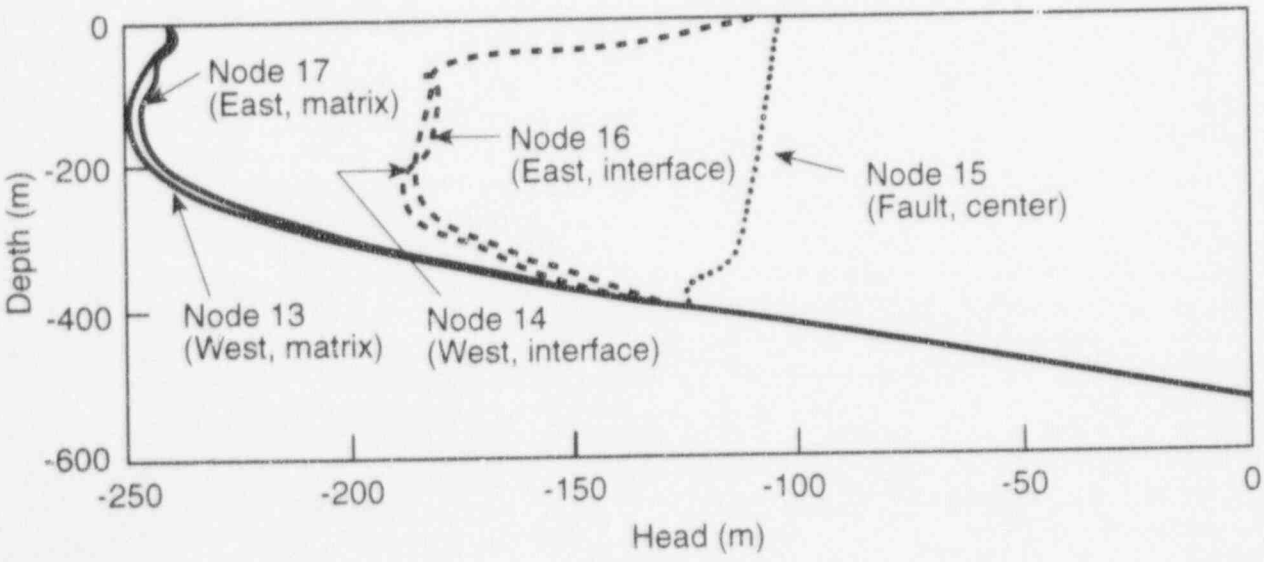

Figure F–4 Pressure profiles for q_o = 50 mm/yr and a dip angle of 6°

the fault cutting Dirichlet boundaries. It was found that in order to obtain a well-behaved numerical solution, with clearly stable convergence to steady state, the time step had to be drastically reduced. When the maximum time step was decreased to Δt_{max} = 10 days, the mass balance plots indicated a complete elimination of large mass balance errors (except for early transients). The conclusion in this case is that, although the discrete-time system was unstable, the continuous time system corresponding to a vanishingly small time step ($\Delta t \rightarrow 0$) is, in fact, stable and leads to a unique steady state solution as $t \rightarrow \infty$. While this phenomenon results from the discreetness (in time) of the numerical flow problem, it indicates a peculiar phenomenon related with the 3-D configuration of the faulted domain and with the direct connection between fault and permeable boundaries.

The steady state flow pattern in each case is best represented by 2-D vector plots of the unsaturated water velocity (or flux), and particle tracks depicting the locations of particles released in the steady flow system at selected points. These 2-D vector and particle tracks are shown in Figures F-5a and F-5b for the higher and milder property contrast case, respectively. Inspection of these figures clearly shows a significant effect of the contrast between slopes of the matrix/fault unsaturated conductivities. When the fault's conductivity slope is comparatively much larger than that of the matrix (a_m = 0.022 meters^{-1}, a_f = 0.10 meters^{-1}), higher fluxes were observed in the matrix. This results in a front that lags within the fault zone. Figure F-5(a) shows this effect for two lines of particles released at elevations 500 meters and 300 meters, respectively, and tracked for 1000 years. In this case, the maximum distance traveled in 1,000 years is approximately 67 meters. When the contrast is milder (a_m = 0.022 meters^{-1}, a_f = 0.035 meters^{-1}), the opposite behavior is observed. The fluxes within the fault zone are greater, but they point towards the matrix (Figure F-5(b)). This creates a frontal shape that continuously expands outward from the fault zone. In this case, the maximum distance traveled in 1000 years is 165 meters and more than 200 meters, for the two release planes, respectively. This important difference in behavior is because of the different values of the crossing- point suction in the two cases. Recall that the contrast between matrix and fault moisture retention curves was not changed. As a consequence, the steady state moisture patterns above the water table are almost identical for the two contrast cases studied. What is important to keep in mind is that the travel time of particles is sensitive to the unsaturated conductivity slope, even when the moisture retention curve is held constant.

F-4 CONCLUSIONS

A hypothetical test problem was developed in order to study the effect of bedding on flow, the presence of a subvertical fault zone, and the effect of inclination of the beds. A number of auxiliary tests were also conducted, using variations on these hypothetical data. There are some similarities between this hypothetical problem and the Yucca Mountain stratigraphy, but since all site properties are not used, these simulations are not representative of the Yucca Mountain flow conditions.

Recognizing that there may not be natural initial-boundary conditions that can be used for the more complex problems, a method of successive approximation was implemented. This method uses solutions of auxiliary flow problems to set up pressure conditions for more complex problems. An oscillatory flow regime was observed at large times, that is, after initial transients died out. This was shown to be an effect of the discrete-time nature of the equations being solved, and was eliminated by using extremely small time steps ($\Delta t \rightarrow 0$). The techniques used to identify these effects relied on detailed plots of global mass balance in terms of instantaneous net discharge rate and instantaneous rate of change of total mass. Large Δt yielded oscillations for both 2-D and 3-D flow systems, but seemed more consequential in 3-D (fault-cutting pressure boundaries).

Based on the parameters used, and the simulations performed in this study, the following conclusions can be reached:

- The effects of stratification are important only for low net infiltration rates and during the early parts of transient simulations.
- A dip angle of 6° to the East has a minimal effect on the pressure head distributions (approximately 2 percent of the maximum pressure head difference).

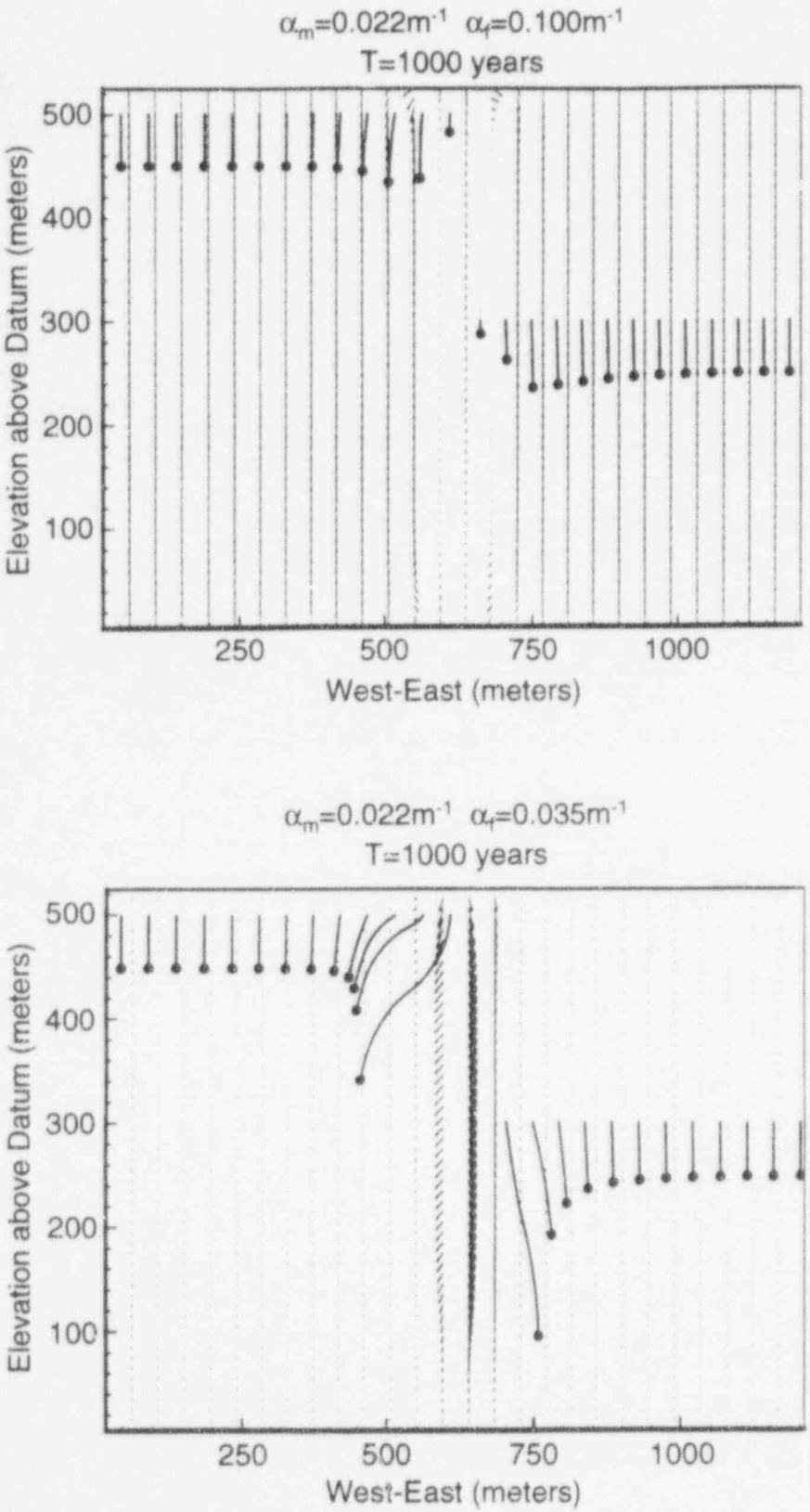

Figure F–5 *XZ* plane flux vector and particle plot (T = 1000 years). (F–5a: α_m = 0.022 m^{-1}, α_f = 0.1 m^{-1}. F–5b: α_m = 0.022 m^{-1}, α_f = 0.035 m^{-1}.)

- The flow behavior (ground-water fluxes and travel times) of a system consisting of highly contrasted matrix and vertical fault properties is greatly influenced by the ratio of the slopes of the matrix and fault unsaturated hydraulic conductivity curves.

F-5 REFERENCES

Ababou R., "Approaches to Large Scale Unsaturated Flow on Heterogeneous, Stratified, and Fractured Geologic Media," U.S. Nuclear Regulatory Commission, NUREG/CR-5743, August 1991. [Prepared by the Center for Nuclear Waste Regulatory Analyses.]

Bagtzoglou, A.C., R. Ababou, and A. Nedungadi, "BIGFLOW: A Multi-Dimensional Code for Flow in Heterogeneous and Variably Saturated Geologic Media (Theory and User's Manual—Version 1.0)," Center for Nuclear Waste Regulatory Analyses, CNWRA92-026, December 1992. [Prepared for the U.S. Nuclear Regulatory Commission.]

Montazer, P. and W.E. Wilson, "Conceptual Hydrologic Model of Flow in the Unsaturated Zone, Yucca Mountain, Nevada," U.S. Geological Survey, Water Resources Investigation Report, WRI-84-4345, 1984.

Mualem, Y., "A Catalogue of the Hydraulic Properties of Unsaturated Soils," Haifa, Israel, Technion Institute of Technology, Hydrodynamics and Hydraulic Laboratory, Research Project No. 442, 1976.

Scott, R.B. and J. Bonk, "Preliminary Geologic Map of Yucca Mountain with Geologic Sections, Nye County, Nevada," U.S. Geological Survey, Open-File Report 84-494, 1984.

APPENDIX G
EXPLORATION OF DUAL-CONTINUUM FLOW MODELING CONCEPTS

G-1 INTRODUCTION

In the development of the ground-water flow and transport module, several different modeling approaches were attempted. One of the approaches required the staff to learn and experiment with *DCM3D*, a **D**ual-Continuum, Three[**3**]-**D**imensional, ground-water flow code, described in Updegraff *et al.* (1991). *DCM3D* is a recently developed computer code by Sandia National Laboratories for solving three-dimensional, ground-water flow problems in variably saturated, fractured porous media (*op cit.*). The code is based on a dual-continuum model with matrix media comprising one porous equivalent continuum and fractures the other. The continua are connected by a transfer term that is a function of the unsaturated permeability of the porous media.

G-2 CONTINUUM APPROACHES

It is attractive to use continuum codes to model ground-water flow at Yucca Mountain, because explicitly modeling individual fractures at the scale of Yucca Mountain at this time may not be possible. For example, in the Yucca Mountain Site Characterization Plan (DOE, 1988; p. 3-173), it is stated that ". . . no way is known to generate a complete set of fracture location and geometry data. Secondly, if the Topopah Spring welded unit has a mean fracture density of 20 fractures/meters^3 and has a mean thickness of 300 meters over the approximately 7×10^6 meters^2 area of the central Yucca Mountain block, then one would have to consider flow in approximately 4×10^{10} discrete fractures. . . ." This amount of detail would be too large to model at this time. Rather than explicitly modeling each fracture, continuum codes represent matrix and fractures as constituting either separate but overlapping continuum systems ("Dual Continua Approaches") or as a single composite continuum system ("Single Continua Approaches"). It should be noted that these approaches assume matrix and fracture properties can be represented as spatial averages over rock mass volumes whose linear dimensions are very much smaller than the thickness of the hydrogeologic unit, but sufficiently large to include a representative, statistical sample of hydraulically connected fractures.

In modeling unsaturated flow conditions in soil, hydrologic properties are represented by characteristic curves, that describe moisture content and conductivity as a function of pressure head. In continuum approaches, rather than using a single characteristic curve to represent the unsaturated hydrologic properties of a single fracture, a single curve represents the hydrologic properties of large numbers of fractures. At present, two main types of continua approaches are being used to model Yucca Mountain site unsaturated fracture and matrix ground-water flow; single continua and dual continua. Single continua approaches often use the same porosity values for both matrix and fractures and a single characteristic curve to represent matrix and bulk fracture-matrix hydrologic properties (Klavetter and Peters, 1986). In contrast, dual continuum models consist of two interconnected continua, with one continuum simulating flow through the rock matrix and the other simulating flow through large numbers of fractures. The two continua are connected by a fracture-matrix transfer term allowing water to flow between the fracture and matrix continua. This enables a dual continuum code to model the resistance to water movement between the matrix and fracture continua and may allow the code to simulate situations where a single continuum approach could experience code-convergence problems.

It may also be possible to simulate conceptual models with dual continuum codes that are not possible with single continuum codes. For example, in a single continuum model of unsaturated fracture and matrix ground-water flow, when water saturation in the matrix reaches a level where bulk fracture flow occurs, faster velocities are computed, but with no change in direction. Therefore, this approach assumes bulk fracture flow contains the same anisotropies as the matrix. However, individual fractures tend to be linear features with strong anisotropies. Therefore, for a single fracture it is reasonable to assume that irrespective of the flow direction in the matrix, flow in the fracture will be strongly

influenced by the anisotropic properties of the fracture. Furthermore, when there are large numbers of fractures with similar linearities, a general fracture anisotropy may be created that is different from the rock matrix. This may be the case at Yucca Mountain, where faults and fractures are believed to be vertical or steeply dipping (DOE, 1988; pp. 3–175, 3–179, and 3–185; and Barton, 1989). Use of a dual continuum code in this type of situation may be advantageous, because in a dual continuum code, different anisotropies can be assigned to both the matrix and fracture continua.

G–3 ZERO TRANSFER SIMULATION

The *DCM3D* computer model simulated a hypothetical two dimensional vertically placed block of tuff (20 meters by 48 meters). Initial simulations assigned Topopah Spring welded properties, obtained from Peters *et al.* (1984), to the matrix and bulk fracture continua. Initial conditions of –2 meters matric potential were assigned to each grid node in both continua and no-flow boundary conditions were assigned to the two vertical sides of the block. A –2 meters of matric potential were assigned to the bottom boundary, and zero matric potential to the left one-quarter of the block top. This meant the code would simulate a wetting front moving down from the upper left side. Hydraulic conductivities for the matrix properties were isotropic and for the fracture continuum strongly anisotropic. In fact, fracture hydraulic conductivities were set to zero in the lateral direction, so that flow in the fracture continuum could only occur in the vertical direction. For the first run, the transfer coefficient was set to zero. This meant that no water could move between the two continua. The objective of this exercise was to see if the code could successfully simulate a situation where the same boundary conditions would cause different flow directions in the two media, as a result of differences in their hydraulic conductivity anisotropies.

After 2 simulated weeks, two areas had formed in the block (Figure G–1): an area of wetting under the upper left one-quarter of the block and an area of dewatering (because of gravity) under the right side of the block. This result can be best understood in light of the characteristic curves used in the simulation (Figure G–2). The initial matric potential conditions of –2 meters meant that initial fracture continuum hydraulic conductivities were much lower than the matrix continuum. Therefore, the matrix dewatered faster than the fracture continuum. However, the zero matric potential upper boundary meant that under wetting conditions, the fracture continuum had a much higher hydraulic conductivity than the matrix. This caused the wetting front in the fracture continuum to move much faster than the matrix wetting front.

In the matrix continua, it can be seen that the wetting plume spreads both vertically and laterally. In the fracture continuum, which has no lateral hydraulic conductivity, water could only move vertically, forming a sharp wetting front down the left-hand side. Therefore, this run illustrates how the *DCM3D* code can be used to simulate separate flow directions in two different media.

G–4 HIGH TRANSFER SIMULATION

To see what would happen to flow directions if water were allowed to pass between the two media, the previous run was duplicated with a high-transfer coefficient. After two simulated weeks (Figure G–3) the matric potentials of both media were the same, because the high transfer coefficient allowed water to move rapidly between the two continua. This resulted in water moving from the wetter continuum to the dryer continuum until the matric potentials in both continua were equal. In other words, as a grid block in one continuum wets or drys, the corresponding grid block in the other continuum wets or drys.

In this simulation, the faster dewatering rate of the matrix continuum caused water to flow from the fracture continuum into the matrix continuum, resulting in much deeper dewatering of the fracture continuum, on the right half of the block. Additionally, the faster wetting of the fracture continuum caused water to flow from the fracture continuum into the matrix continuum, resulting in the formation of a much larger wetting front in the matrix continuum. It can also be observed that the wetting front in the fracture continuum moved laterally. However, when velocity outputs were inspected, the fracture continuum had a lateral flow velocity of zero. This was to be expected, since the lateral hydraulic conductivity of the fracture continuum had been set to zero. Consequently, for the water to move laterally in

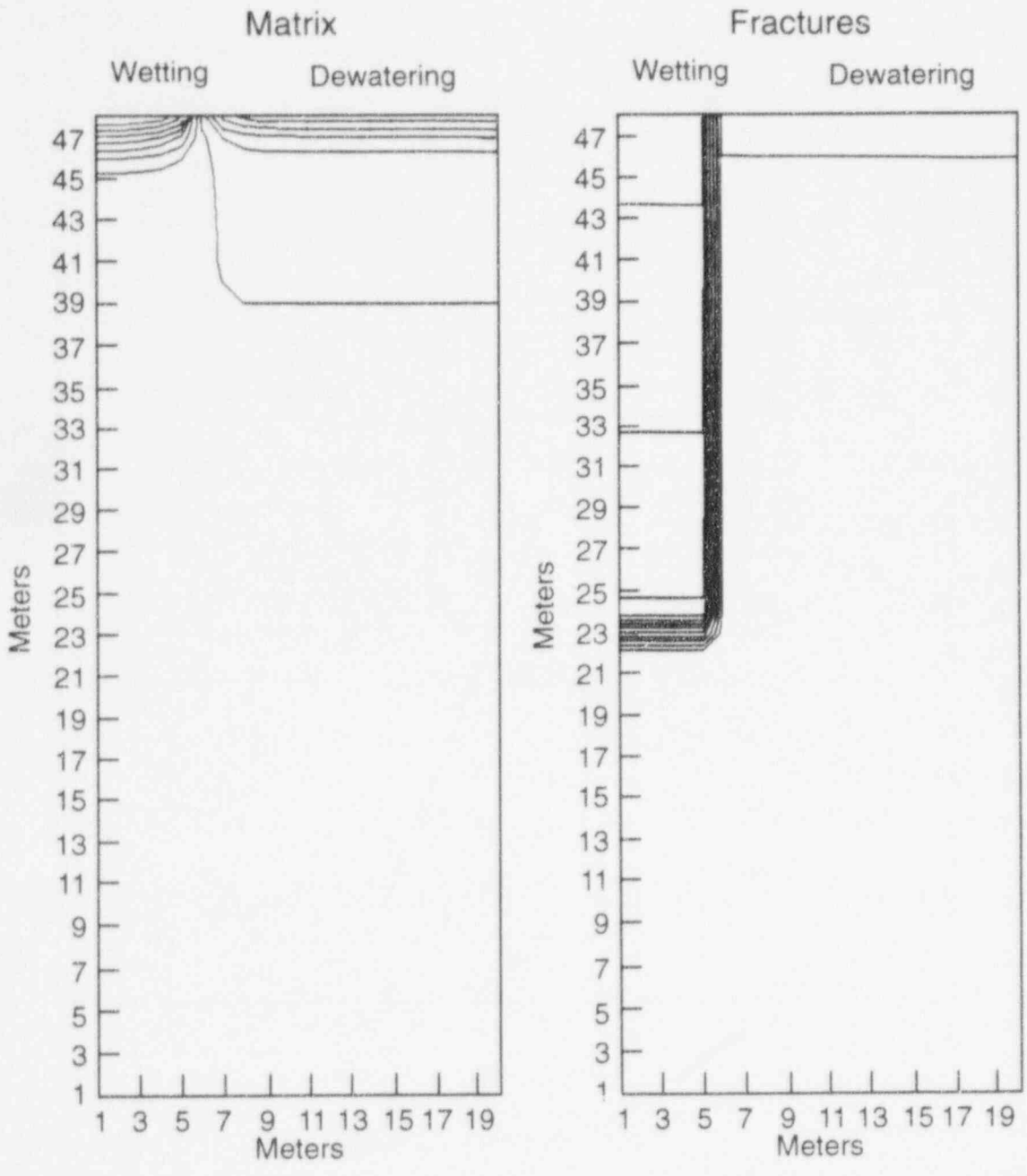

Figure G-1 Contour plot of matric potentials for hypothetical block of Topopah Spring tuff matrix and fracture continua after simulating two weeks of flow (There is no flow between the two continua.)

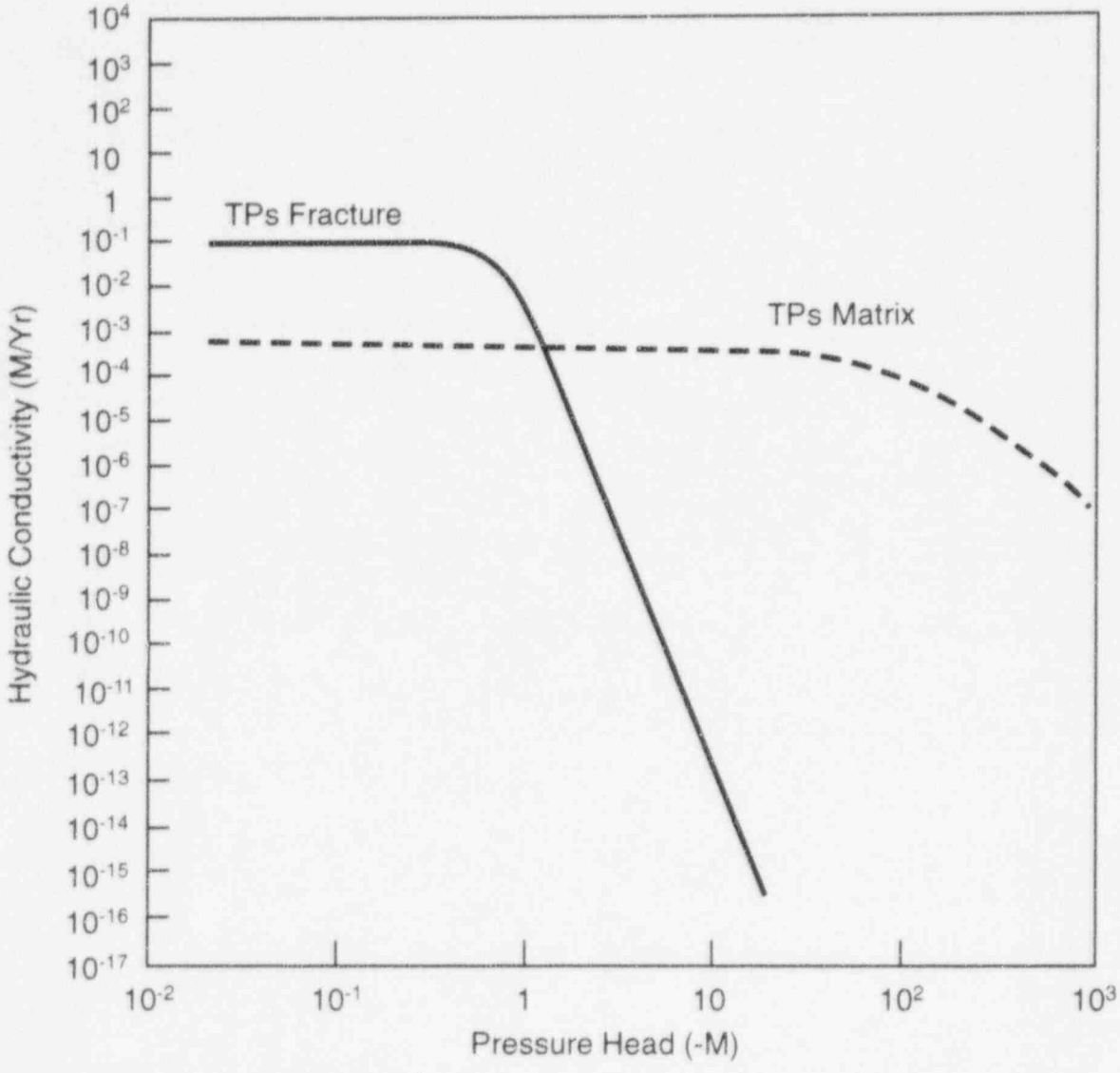

Figure G–2 Topopah Spring welded unit fracture and matrix properties

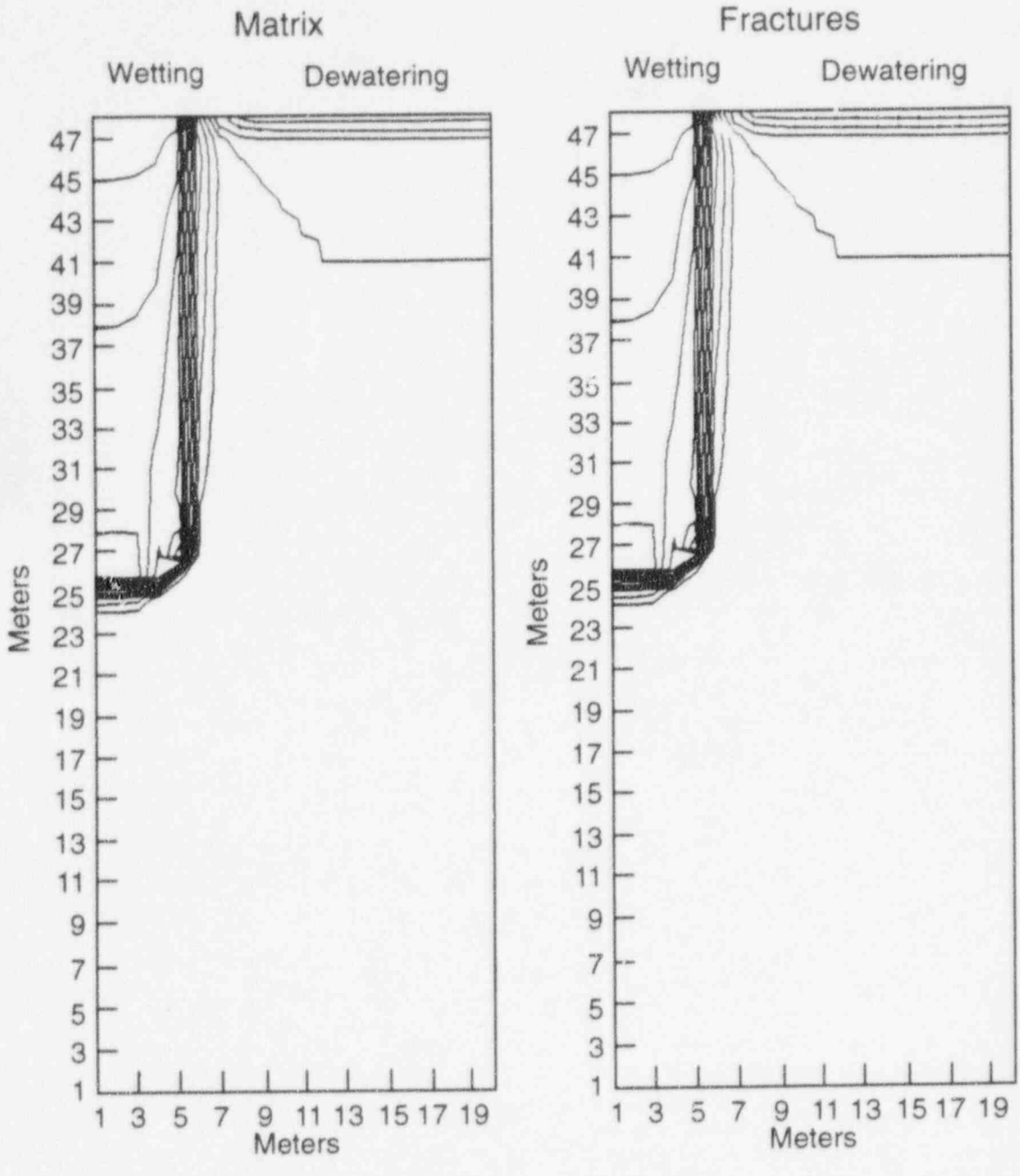

Figure G-3 Contour plot of matric potentials for hypothetical block of Topopah Spring tuff matrix and fracture continua after simulating two weeks of flow (Water can flow between the two continua.)

the fracture continuum, it first had to move into the matrix continuum, move laterally in the matrix continuum, and then move back into the fracture continuum. In nature, this would be analogous to flowing fractures wetting up the matrix, which, in turn, causes other fractures to flow. Therefore, an interpretation of model matric potentials, water contents, and velocities, which ignores water movement between the two continua, may be misleading about the rate and direction of fluid flow.

G–5 SIMULATION COMPARING SINGLE AND DUAL CONTINUUM APPROACHES

To further compare the single and dual continuum approaches, the *DCM3D* input was modified to make it simulate a single continuum approach. In a single continuum code, the combined matrix and fracture flow properties are assumed to have the same porosities and the same hydraulic conductivity anisotropies.

It was decided to make *DCM3D* mimic a single continuum code by assigning isotropic hydraulic conductivities to the fracture continuum, and to repeat the high transfer coefficient run. It was a little less clear what porosity values should be input. If a single porosity value were used for both the matrix and fracture continua, the simulation would contain a much higher total pore space than a single continuum approach would use. It was therefore decided to leave the porosity values the same as the previous high-transfer coefficient run. This meant that the matrix continuum had a porosity of 0.11 and that the fracture continuum, had a porosity of 1.8×10^{-4}. This was believed to be a reasonable compromise, since, in a single continuum approach, fracture flow is simulated when the pore space is nearly filled. The output from the previous dual continuum high-transfer run and the simulated single continuum run is compared in Figure G–4. This comparison shows that the lack of lateral fracture conductivity in the dual continuum simulation caused the wetting front to travel deeper, with less lateral spreading than the single continuum simulation.

G–5 CONCLUSIONS

These simulations demonstrate that the dual continuum code *DCM3D* can model flow in two continua with different anisotropies and that, depending on the problem to be modeled, it may produce significantly different answers than a single continuum code.

G–6 REFERENCES

Barton, C., W. Page, and T. Morgan, "Fractures in Outcrops in the Vicinity of Drill Hole USW G–4, Yucca Mountain, Nevada, Data Analysis and Compilation," U.S. Geological Survey, Open File Report 89–92, 1989.

Klavetter, E.A. and R.P. Peters, "Fluid Flow in a Fractured Rock Mass," Albuquerque, New Mexico, Sandia National Laboratories, SAND85–0855, March 1986.

Peters, R. R., *et al.*, "Fracture and Matrix Hydrologic Characteristics of Tuffaceous Materials from Yucca Mountain, Nye County, Nevada," Albuquerque, New Mexico, Sandia National Laboratories, SAND84–1471, December 1984.

Updegraff, C.D., C.E. Lee, and D.P. Gallegos, "DCM3D: A Dual-Continuum, Three-Dimensional, Ground-Water Flow Code for Unsaturated, Fractured, Porous Media," U.S. Nuclear Regulatory Commission, NUREG/CR–5536, February 1991. [Prepared by the Sandia National Laboratories.]

U.S. Department of Energy, "Site Characterization Plan Overview, Yucca Mountain Site, Nevada Research and Development Area, Nevada," Office of Civilian Radioactive Waste Management, DOE/RW–0198, 9 vols., December 1988.

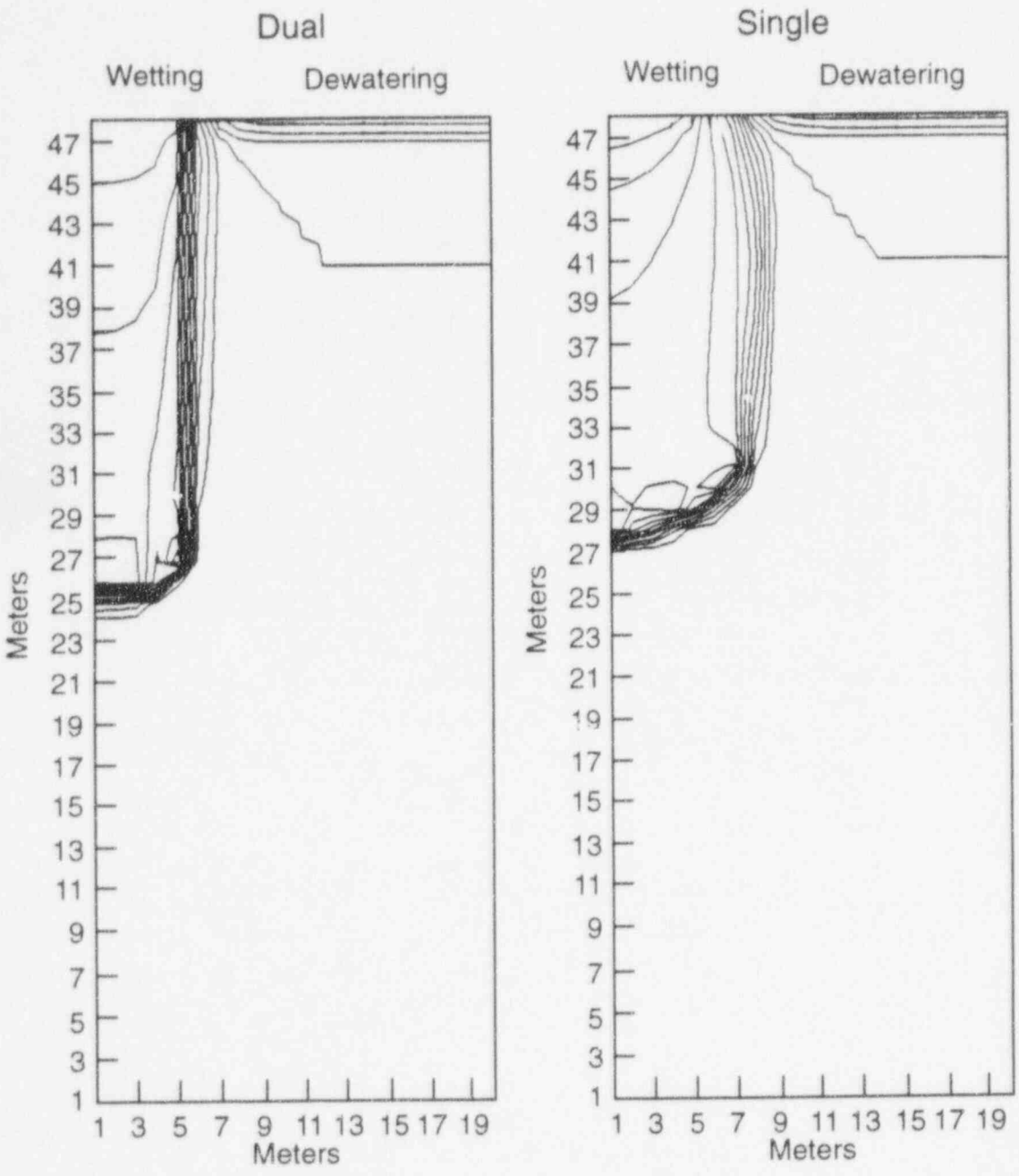

Figure G–4 Contour plot of matric potentials for hypothetical block of Topopah Spring tuff matrix and fracture continua after simulating two weeks of flow

APPENDIX H
RELEASE AND TRANSPORT OF POTENTIALLY GASEOUS RADIONUCLIDES OTHER THAN ^{14}C DURING VOLCANISM AND NORMAL OPERATIONS

H-1 INTRODUCTION

The Yucca Mountain site is unique among other proposed sites for the disposal of high-level radioactive waste because it would be constructed above the water table. One of the considerations at this site is radionuclide release from the waste package in the gas phase and possible transport as a gas to the atmosphere. Even if the gaseous release cannot escape to the atmosphere, it may serve as a source of contamination for the liquid pathway.

Several potentially volatile radionuclide compounds of ^{79}Se, ^{99}Tc, and ^{129}I have been identified in spent nuclear fuel (Lehrman, 1989; and Park, 1991[1]). The question of whether there is sufficient cause to consider the gaseous release and transport of these volatile radionuclides further has been addressed through a series of conservative calculations in the following sections. The direct release of the radioactive inventory by extrusive volcanism (i.e., the direct entrainment of the waste in magma brought to the surface of the earth) has been dealt with in Section 6.5. The present analysis is restricted to conditions of normal repository operation and intrusive volcanism that could potentially release volatile radionuclides from the waste package, but do not necessarily provide a mechanism for transport to the surface.

H-2 VOLATILE RELEASES RESULTING FROM THE INTRUSION OF A DIKE

To demonstrate the potential, caused by magmatic intrusion, for release of volatile radionuclides other than ^{14}C from the engineered barrier system, consider an example of a large dike through the middle of the Yucca Mountain site. The example considers only a single dike that intrudes into the repository and does not continue to flow. The dike is represented as an instantaneous vertical plane heat source with a heat content Q per unit area (but representing a dike of finite thickness). The staff calculated the maximum effect of the temperature increase at distances greater than half the assumed width of the dike, and compared the potential release of volatile radionuclides with present release limits, without specifying, at this point, a mechanistic model for the release of these components from the waste package. Although unlikely, the staff does not consider this example to be necessarily a "worst-case" situation. The example does not include the following phenomena that could lead to predictions of higher temperatures or releases:

- The formation of sills filling horizontal weakness in the rock or the repository drifts;
- Multiple dikes and sills;
- Long-term continuing eruptions;
- Heat transfer by convecting gas and water vapor; and
- Effect of corrosive volcanic gases on the waste form.

Assume for the purpose of this demonstration that a dike 10 meters in width and 3000 meters long intrudes through the middle of the repository, and that the waste packages are randomly spaced throughout the assumed site area of 5 square kilometers. Assuming that the dike intrusion is instantaneous and does not continue to the surface, the maximum range of significant heating can be determined by assuming the dissipation of heat from an infinite plane source (Turcotte and Schubert, 1982):

$$T - T_0 = \frac{Q}{2\,\varrho C\sqrt{\pi \kappa t}} e^{-\frac{y^2}{4\kappa t}} \quad , \qquad \text{(H-1)}$$

where:

ϱ = density of the country rock;
C = heat capacity of country rock;
Q = instantaneous sensible and latent heat content of dike per unit area;
κ = thermal diffusivity;
y = distance from dike centerline;

[1]Park, U.S., "Gaseous and Semi-Volatile Radionuclides," Unpublished Science Applications International Corporation Presentation to the U.S. Nuclear Waste Technical Review board, Denver, Colorado, June 25–27, 1991.

t = time; and
T_0 = ambient temperature.

The maximum temperature at any distance y from the dike centerline is (Turcotte and Schubert, 1982):

$$T_{max} = T_0 + \frac{Q}{\varrho C y}\sqrt{\left(\frac{1}{2\pi e}\right)} \quad . \qquad \text{(H-2)}$$

The time at which the maximum temperature occurs would be (Turcotte and Schubert, 1982):

$$t_{max} = \frac{y^2}{2\kappa} \quad . \qquad \text{(H-3)}$$

For the present example:

Q = 5.44 × 10[9] Joules/square meter;
ϱ = 2640 kilograms/cubic meter;
C = 687 Joules/kilogram – degrees Kelvin (°K); and
κ = 1.1×10^{-6} square meters/second

With the above set of parameters, a maximum temperature increase of 10°K would extend only 78 meters from the dike centerline and would occur only about 0.13 years after dike penetration. The 100°K isotherm would extend a maximum of 7.8 meters from the centerline.

From the above analysis, the staff choose what were believed to be a very conservative maximum extent of thermal influence of the dike as 50 meters from the centerline and a 3000-meter linear extent covering an area of 300,000 square meters. The total repository area is approximately 5×10^6 square meters, so the dike would affect approximately 6 percent of the waste packages. If it were conservatively assume that all of the volatile radionuclides other than ^{14}C were driven off by the excess heat (^{99}Tc, ^{79}Se, and ^{129}I) in the affected area, then the amounts in terms of the 40 CFR Part 191 (EPA, 1986) cumulative release limits would be only 0.125 as summarized in Table H-1.

Table H-1 Cumulative Releases for Selected Radionuclides

Nuclide	*Inventory Curies*	*.06 × Inventory*	*EPA Limit[a] for Repository*	*EPA Ratio R*
^{129}I	2200	132	7000	0.019
^{79}Se	28,300	1698	70,000	0.024
^{99}Tc	915,000	54,900	700,000	0.078
Total	—	—	—	0.125

[a]Currently, a revised set of standards specific to the Yucca Mountain site is being developed in accordance with the provisions of the Energy Policy Act of 1992. The Energy Policy Act of 1992 (Public Law 102–486), approved October 24, 1992, directs NRC to promulgate a rule, modifying 10 CFR Part 60 of its regulations, so that these regulations are consistent with EPA's public health and safety standards for protection of the public from releases to the accessible environment from radioactive materials stored or disposed of at Yucca Mountain, Nevada, consistent with the findings and recommendations made by the National Academy of Sciences, to EPA, on issues relating to the environmental standards governing the Yucca Mountain repository. It is assumed that the revised EPA standards for the Yucca Mountain site will not be substantially different from those currently contained in 40 CFR Part 191, particularly as they pertain to the need to conduct a quantitative performance assessment as the means to estimate postclosure performance of the repository system.

H-3 RELEASES UNDER NORMAL CONDITIONS

Volatility of Radionuclides: Several sources of information for iodine, selenium, and technetium gave widely differing estimates of the vapor pressure. Figure H-1 shows the vapor pressure of several solid and aqueous phases of radionuclides that would occur in spent nuclear fuel, but the source of this information is unknown. Park (1991) reports values that are considerably lower. These values are shown in Table H-2.

The vapor pressure of Tc_2O_7 was also estimated from thermodynamic information:

$$Tc_2O_7(solid) \leftrightarrows Tc_2O_7(gas) \qquad \text{(H-4)}$$

$$\ln P = -\frac{\Delta G_R^{\circ}}{RT} \quad .$$

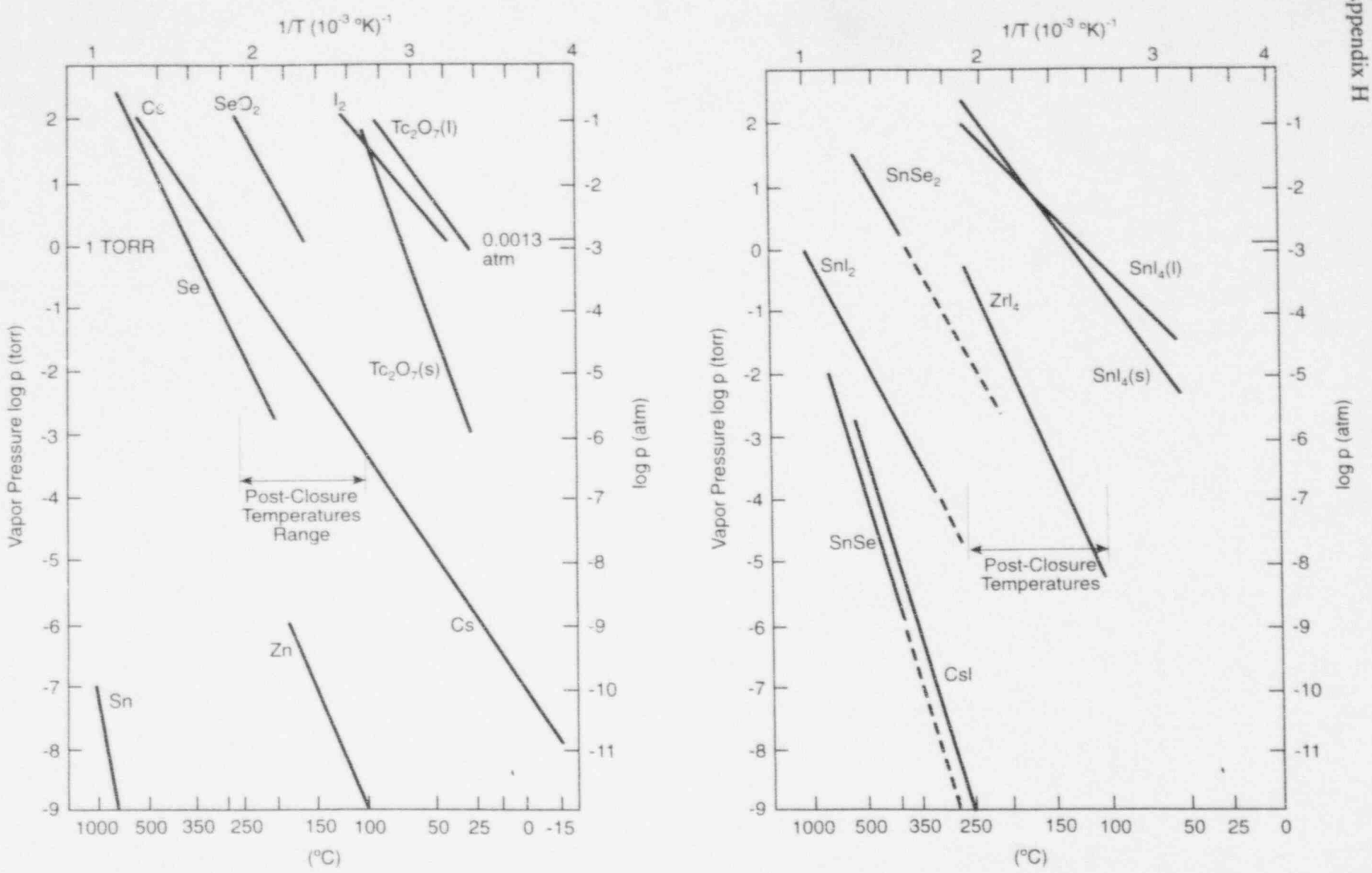

Figure H–1 Vapor pressure of several radioactive compounds (from Lehrman, 1992)

Table H–2
Vapor Pressure Estimates (from Park (1991) and Lehrman (1992))

Species	*P – atmospheres at 100°C*			*P – atmospheres at 200°C*		
	Park	*Lehrman*	*Equation (H–4)*	*Park*	*Lehrman*	*Equation (H–4)*
CO_2	>2000	---	---	12,000	---	---
I_2	0.06	0.01	---	3.7	16	---
SeO_2	0.00091	3E–5	---	0.054	0.02	---
Tc_2O_7	0.00012	0.3	2.6E–7	0.037	---	6.3E–6

The Gibbs free energy of reaction, $\Delta G^0_R = 47.1$ kilojoules/mole for the crystalline phase gives a vapor pressure for $Tc_2O_7 = 2.6 \times 10^{-7}$ atmospheres at 100 degrees Celsius (°C) and 6.3×10^{-6} atmospheres at 200°C (Phillips *et al.*, 1988). Amorphous and hydroxide phases, however, could lead to considerably higher vapor pressures.

The vapor pressures shown would be for pure phases only, and may be affected by the following phenomena:

- Most of the radionuclides would be tied up in the fuel matrix, although some might migrate to the surface of cracks and interstitial boundaries of the fuel;
- Some technetium is associated with highly resistant alloy particles in the fuel (Pearcy and Manaktala, 1992); and
- Much of the ^{129}I would probably be tied up with metallic fission products in the spent fuel, such as cesium and zinc (Park, 1991).

Rapid Release Fraction: Leaching experiments with spent nuclear fuel shows a rapid release fraction for technetium of about 1 percent of the total inventory, but much more modest releases, somewhat less than congruent, with respect to other radionuclides at later times (Wilson, 1990). There is a similar, but smaller, rapid release of ^{129}I from the same experiments of between 0.1 and 0.4 percent of the inventory. This result might indicate that some of the technetium migrated to the surfaces of cracks and grain boundaries, whereas the rest was tied up in the solid fuel. Releases of ^{79}Se were too small to measure.

Given the vapor pressures of technetium and iodine compounds, the rapid release fraction might be volatilized easily at normal operating temperatures in the repository. The effective vapor pressure of technetium, iodine, and selenium, within the matrix of the fuel, or tied up in metallic particles, would be lower than the pure phase vapor pressure. If the volatile components were ideal solid solutions, then Raoult's Law would indicate that the vapor pressure P_j is proportional to the mole fraction of the component N_j and its individual vapor pressure P_j^* (Garrels and Christ, 1978):

$$P_j = P_j^* N_j \quad . \qquad \textbf{(H–5)}$$

The mole fractions for ^{99}Tc, ^{79}Se, and ^{129}I, assuming the rest of the fuel is UO_2 are approximately 0.003, 0.0005, and 0.00003, respectively. If the volatile elements are solid solutions and if Raoult's Law applies, actual vapor pressures would be substantially lower than those for the pure phases. Additionally, the vapor pressures of volatile components might be limited by their slow diffusion from the interior of the solid to the surface.

H–4 MECHANISMS FOR THE RELEASE OF VOLATILE RADIONUCLIDES FROM FAILED WASTE PACKAGES

Within reasonable limits, the gases in the waste package can be considered to behave as an ideal gas and be governed by the relationship:

$$pV = nRT \,, \qquad \textbf{(H-6)}$$

where:

P = pressure;
V = void volume of waste package;
R = universal gas constant;
n = number of moles of gas; and
T = absolute temperature.

According to Equation (H-6), the number of moles of gas n in a container of volume V opened to the atmosphere would be directly proportional to P and inversely proportional to T. Volatile radionuclides can be released from a failed waste package by several processes, including venting of waste package pressure, molecular diffusion, and barometric pumping. Pressure within an intact waste package would depend on the initial pressure of the inert gas, release of pressurized gas within the fuel rods, partial pressure of the volatile components, and expansion of gas, because of the rise in temperature of the waste package. Upon waste package failure, the pressure would be vented, carrying with it any of the volatile radionuclides in the gas phase at that time. The fraction of the gas released $\Delta n/n_0$, assuming constant external pressure, would be:

$$\Delta\frac{n}{n_0} = \frac{\Delta\left(\frac{PV}{RT}\right)}{\left(\frac{PV}{RT_0}\right)} = 1 - \frac{T_0}{T'} \,, \qquad \textbf{(H-7)}$$

where T_0 = the initial temperature at which the waste package was sealed and T' = the temperature at which it fails. Assuming that the void space in a waste package V is 300 liters, and that the inert cover gas was initially charged to the waste package at 25°C (298°K) at one atmosphere, failure of the waste package at 100°C (373°K) would release only 1 - 298/373 = 0.25 of the waste package volume or 75 liters, according to Equation (H-7).

Although molecular diffusion might be a significant effect, barometric pumping is likely to be the most important mechanism for release of volatile radionuclides, in the long term. In this case, the change in the moles of gas in the waste package is proportional to the changes in the pressure. When atmospheric pressure drops, gas leaves the waste package, carrying with it the volatile components. In one complete cycle of pressure change ΔP, the fraction of gas exchanges is:

$$\frac{\Delta n}{n_0} = \frac{\Delta P}{P_0} \,. \qquad \textbf{(H-8)}$$

Atmospheric pressure changes at the surface of the earth vary on several time scales. Small, rapid pressure changes occur because of local meteorological conditions. Larger and slower changes occur because of passing weather systems. Pressure fluctuations are smaller at depth because of the resistance to gas flow through the rock and the volume of gas held in the rock. Pressure fluctuations in the unsaturated zone at Yucca Mountain are shown in Figure H-2, indicating the damping of pressure with depth (Montazer *et al.*, 1988). Although measurements of pressure fluctuations at the repository level are not available at Yucca Mountain, assume for the sake of this example that a 1 percent fully cyclic pressure change takes place 4 times per year at the repository level. This would lead to an exchange of air within the open waste package, according to the ideal gas law, of 0.04, or 12 liters of gas per year. Over 10,000 years, this gas flow would be 1.2×10^5 liters, far exceeding the initial pulse from pressure relief of the waste package.

H-5 TRANSPORT OF VOLATILE RADIONUCLIDES IN THE GEOSPHERE

The most significant volatile radionuclides other than ^{14}C, namely Tc_2O_7, SeO_2, and I_2, are highly reactive chemically and probably will strongly favor the water contained in the unsaturated rock rather than exist as gases in the geosphere (EPA, 1993). Experience with reactor emergency spray systems shows very high removal of iodine gas in slightly alkaline water. Yucca Mountain groundwater is alkaline, leading to the tentative conclusion that most of the iodine released as a gas would transfer to the liquid phase. Escape to the atmosphere, while likely for ^{14}C, is unlikely for the other volatile radionuclides.

Example: To demonstrate the likely maximum consequences of volatile releases of the potential gaseous radionuclides other than ^{14}C, consider

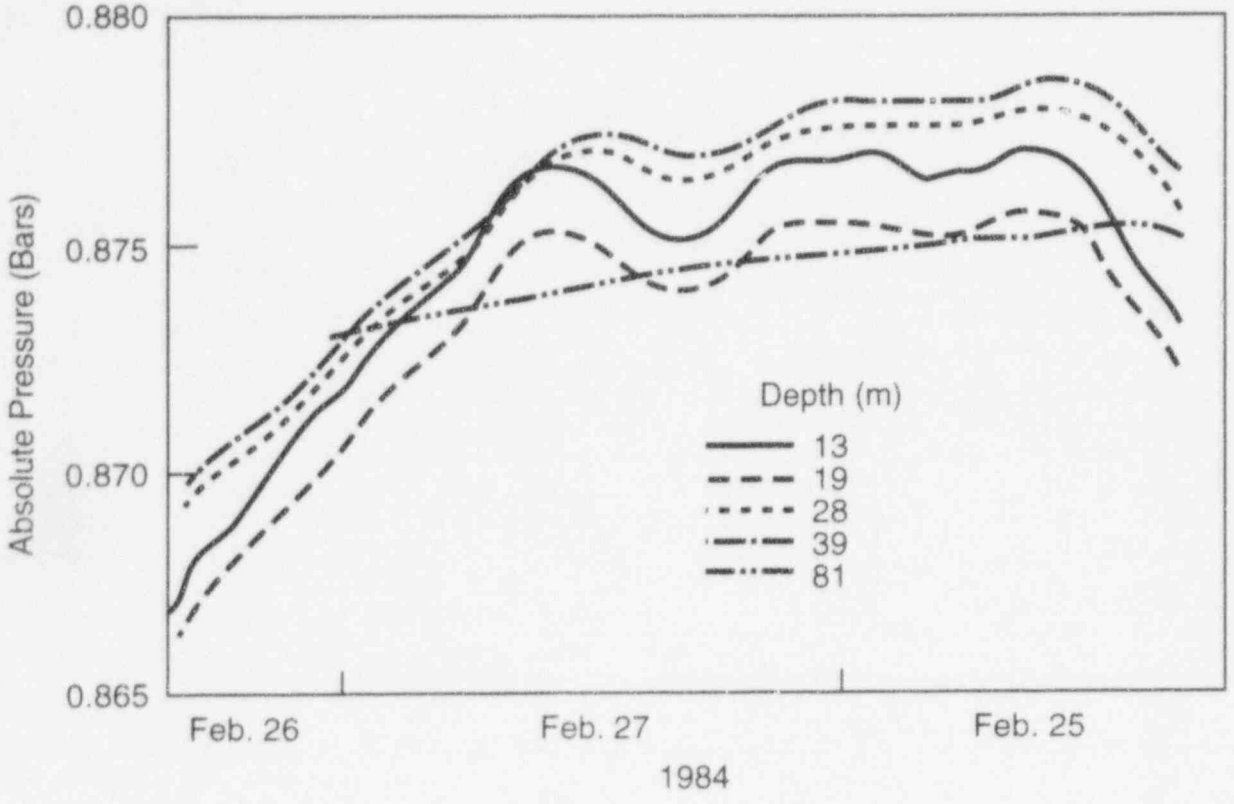

Figure H-2 Down-hole pressure variations at bore hole USW UZ-1 (from Montazer *et al.*, 1988)

the following bounding calculation. The main cause of waste package failure in the Iterative Performance assessment (IPA) Phase 2 assessment (Chapter 5) assumes that most of the waste packages will remain intact until their temperature has fallen below approximately 100°C. For the purpose of this conservative demonstration assume release of volatile radionuclides from a failed waste package under the following assumptions:

- Steady 100°C for a period of 10,000 years;
- The quick-release fractions of readily-volatilized radionuclides will be taken as 1 percent of the inventory for ^{99}Tc, 0.4 percent of the inventory for ^{129}I, and zero for ^{79}Se (Wilson, 1990);
- Vapor pressures for the pure substances at 100°C taken to be the largest values reported in Table H-2, of 0.06 atmospheres for ^{129}I, 0.00091 atmospheres for ^{79}Se, and 0.3 atmospheres for ^{99}Tc;
- The vapor pressures of the quick-release fractions are those of the pure phases;
- The remaining inventories have reduced vapor pressures according to Raoult's Law and their mole fractions in the fuel (i.e., 0.003, 0.0005 and 0.00003 for ^{99}Tc, ^{79}Se, and ^{129}I, respectively); and
- The gas exchange during the period is 12 liters/year per waste package.

Assuming no significant radioactive decay, the rate of loss from the quick-release fraction and the solid-solution fraction depends only on the partial pressure of each component and the flow rate of the gas. For the quick release fraction, the

rate of release at one atmosphere total pressure would be:

$$R_q = \frac{P}{P_T} \times \frac{Q}{22.4} \times \frac{298}{T} \quad , \qquad \text{(H-9)}$$

where:

T = absolute temperature in °K;
P = vapor pressure, atmospheres;
P_t = total pressure, atmospheres;
Q = flow rate out of waste package by barometric pumping, in liters per year;
22.4 = the conversion for liters to gram/moles at standard temperature and pressure; and
298°K = the standard temperature.

A similar expression is used for the rate of release of the volatile radionuclides contained in the matrix, except the vapor pressure is reduced by the mole fraction of the radionuclide in the solid solution. Calculations are summarized in Table H-3. The results of these calculation show that only the quick-release fraction of ^{99}Tc and ^{129}I would be volatilized within 10,000 years, and that overall release would be very small.

H-6 CONCLUSIONS

A series of conservative analyses demonstrate that the release of the potentially volatile radionuclides ^{79}Se, ^{99}Tc, and ^{129}I will not significantly add to the risk of the repository in terms of the EPA cumulative release limits. The first analysis demonstrated that even for a large volcanic intrusion, the effect of the additional heat would be of short duration and range, and would not affect a sufficient number of waste packages to release more than 12.5 percent of the combined EPA limits for those radionuclides. Even total release of the three radionuclides in question would have led to exceeding the EPA limit by a factor of about 2.

The second conservative analysis demonstrated that at temperatures likely to be encountered in the repository as a result of repository heat loads, only a small fraction of the volatile radionuclides could be vaporized and carried outside the waste packages. Furthermore, there is compelling evidence that, once released from the waste packages, the volatile radionuclides would strongly favor the water phase, and not be carried to the atmosphere as gases.

Table H-3 Calculation of Volatile Releases at 100°C

Radionuclide	*Inventory (g/moles per waste package)*	*Quick-release Fraction*[2]	*Vapor Pressure at 100°C (atm.*[3]*)*	*Mole Fraction in Solid*	*Reduced Vapor Pressure (atm.*[4]*)*	*Fractional Release (quick)*[5]	*Fractional Release (solid)*[6]	*Fractional Release (total)*[7]
^{79}Se	7130	0	9.1E-4	5E-4	4.5E-7	0	2.7E-7	2.7E-7
^{99}Tc	7.6E5	0.01	0.3	0.003	9E-4	0.34	1.E-5	0.0034
^{129}I	1.34E5	0.004	0.06	3E-5	1.8E-6	0.98	1.2E-7	0.0039

[2]Based on Wilson (1990).
[3]Maximum values from Table F-1 in Appendix F.
[4]Assuming solid solution and Raoult's Law (Garrels and Christ, 1978).
[5]Fraction of quick-release radionuclide leaving the waste package in 10,000 years.
[6]Fraction of inventory in solid solution of UO_2 matrix leaving in 10,000 years.
[7]Fraction of total original inventory leaving waste form in 10,000 years.

H-7 REFERENCES

Garrels, R.M. and C.L. Christ, *Solutions, Minerals and Equilibria*, San Francisco, California, W.H. Freeman, Cooper and Co., 1978.

Lehrman, A. "Volatile Radionuclides: Limiting Concentrations and Transport Rates in an Unsaturated Rock Pore Space," Lawrence Livermore National Laboratory, *Chemistry and Migration Behavior of Actinides and Fission Products in the Geosphere: Abstracts of the Second International Conference on Radionculide Migration (Migration '89)*, November 6–10, 1989, Monterey, California, Abstract No. 2A3, p. 117.

Montazer, P., E.P. Weeks, F. Thamir, D. Hammermeister, S.N. Yard, and P.B. Hofrichter, "Monitoring the Vadose Zone in Fractured Tuff, Yucca Mountain, Nevada," *Groundwater Monitoring Review*, 8(2):72–85 [Spring 1988].

Pearcy, E.W. and H.K. Manaktala, "Occurrence of Metallic Phases in Spent Nuclear Fuel: Significance for Source Term Predictions for High-Level Waste Disposal," American Nuclear Society/ American Society of Civil Engineers, *Proceedings of the Third International Conference: High-Level Radioactive Waste Management*, April 12–16, 1992, Las Vegas, Nevada, 1:131–136 [1992].

Phillips, S.L., F.V. Hale, L.F. Silvester, and M.D. Siegal, "Thermodynamic Tables for Nuclear Waste Isolation," U.S. Nuclear Regulatory Commission, NUREG/CR-4864, June 1988.

Turcotte, D.L. and G. Schubert, Geodynamics: *Application of Continuum Physics to Geological Problems*, New York, J. Wiley and Sons, 1982.

U.S. Environmental Protection Agency, "Environmental Standards for the Management of Spent Nuclear Fuel, High-Level and Transuranic Wastes [Final Rule]," *Federal Register*, vol. 50, no. 182, September 19, 1985, pp. 38066 – 38089.

U.S. Environmental Protection Agency/Science Advisory Board, "An SAB Report: Review of Gaseous Release of Carbon-14," Washington D.C., EPA-SAB-RAC-93-010, April 1993.

Wilson, C.N., "Results from NNWSI Series 3 Spent Fuel Dissolution Tests", Richland, Washington, Pacific Northwest Laboratories, PNL-7170, June 1990. [Prepared by the Battelle Memorial Institute.]

APPENDIX I
EVALUATION OF USGS GROUND-WATER MODELING FOR THE REGION THAT INCLUDES YUCCA MOUNTAIN

I-1 INTRODUCTION

This report describes the major ground-water modeling work that has been performed by the U.S. Geological Survey (USGS) for the region of southern Nevada. Emphasis will be placed on the evolution of the subregional model originally developed by Czarnecki and Waddell (1984). This report is an auxiliary analysis under the staff's Iterative Performance Assessment effort (IPA Phase 2). Through this program, the staff is developing tools needed to review a license application for a potential high-level radioactive waste (HLW) repository.

In the late 1970's, the USGS began an appraisal of the Nevada Test Site as a potential disposal site for HLW. This work included regional geologic and hydrologic investigations, and a regional ground-water flow model was developed by Waddell (1982). Waddell produced a two-dimensional (2-D), steady-state, finite element model that covered an area of about 18,000 square kilometers. This model extended from the Pahranagat Range and Las Vegas Valley on the east to Pahute Mesa and Death Valley on the west (see Figure I-1). The model included the Yucca Mountain area and almost all of the Nevada Test Site.

Rice (1984) developed a preliminary finite difference model covering an even larger area, extending farther west and south than Waddell's (1982) model. One of the simplifying assumptions used was to simulate the flow system under confined conditions. Initial estimates of transmissivity were based on those obtained from the regional model of Waddell (1982). One of Rice's conclusions was that the model could be improved by calibrating it under unconfined conditions.

Following identification of the proposed Yucca Mountain site, Czarnecki and Waddell (1984) developed a subregional model within the hydrologic subbasin that includes the site. This model was derived using a parameter estimation procedure developed by Cooley (1977, 1979, 1982). Czarnecki (1985) later revised and improved this model to help develop smaller site-scale models of ground-water flow and transport for the Yucca Mountain site. Czarnecki initially prepared a steady-state baseline model and revised it to simulate the geohydrologic effects of increased recharge in the region. A transient version of the model was later used to evaluate scenarios related to the large hydraulic gradient located north of Yucca Mountain (Czarnecki, 1990a). Czarnecki (1992) simulated future water level declines in response to various rates of ground-water withdrawals from Wells J-13 and J-12.

Because of the importance of the USGS regional modeling work with respect to site characterization of the Yucca Mountain site, the NRC staff has acquired the subregional model of Czarnecki (1985) and the *MODFE* computer code. PC-based versions of the code and model have been prepared to facilitate evaluation by the staff.

This evaluation is provided below, and serves as an example of how the staff can directly obtain and evaluate numerical codes and models developed under the U.S. Department of Energy's (DOE's) HLW program. In this way the NRC staff can become more knowledgeable about codes and models during site characterization and prior to receipt of a potential license application.

I-2 REGIONAL SETTING GEOHYDROLOGY

All aspects of the geohydrologic setting must be considered when developing conceptual and numerical flow models for a site or region. The validity of a numerical model depends entirely on the validity of the conceptual model on which it is based. The conceptual flow model must reasonably represent climatic conditions, surface hydrology, hydrostratigraphy, aquifer coefficients, and recharge and discharge conditions. Chapter 3 ("Hydrology") of the Site Characterization Plan (SCP) (DOE, 1988) reports at length on past hydrogeologic work in southern Nevada. The data and interpretations contained in the 1988 SCP provide a basis for previous regional

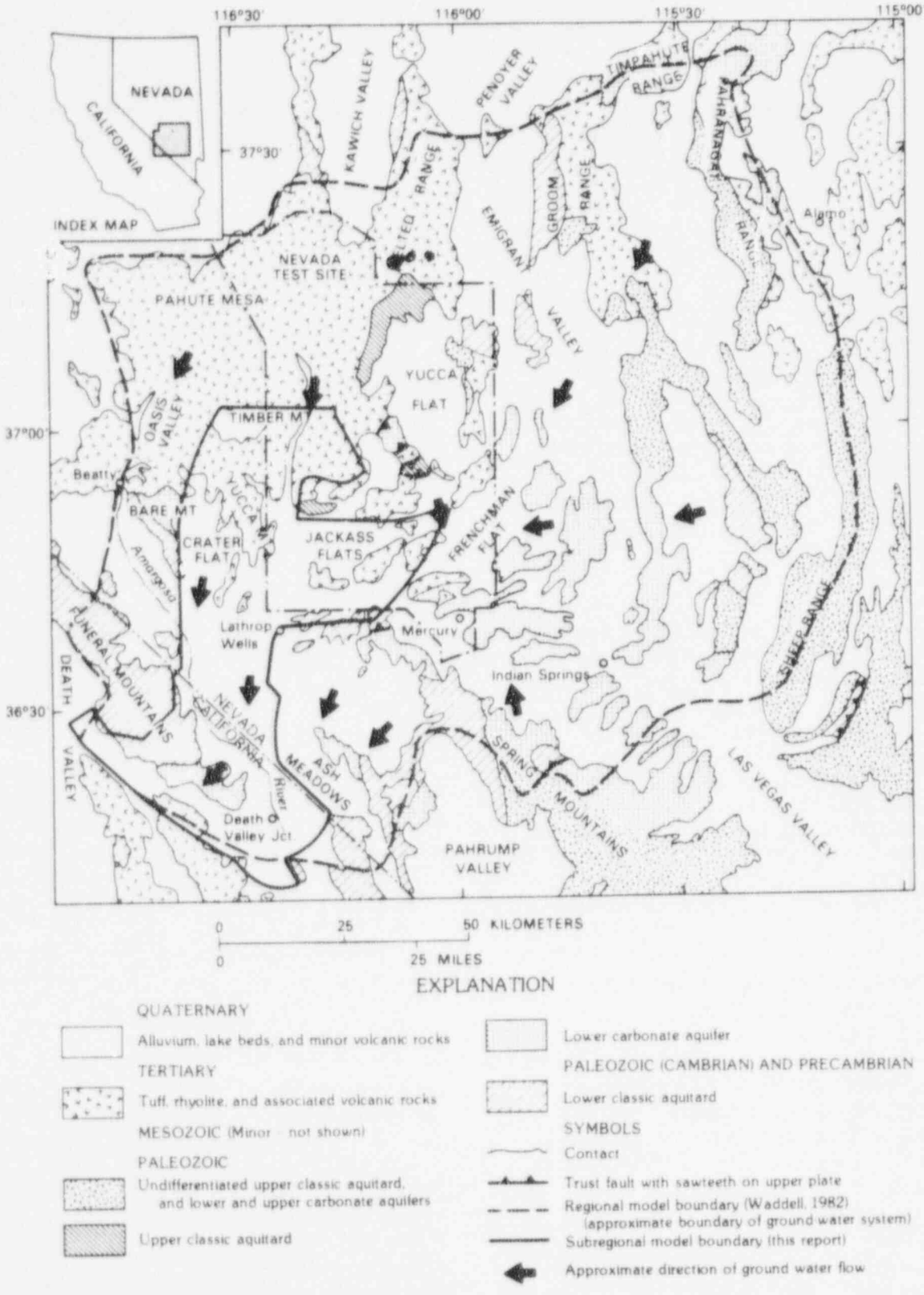

Figure I-1 Locations of regional and subregional modeled areas, with generalized ground-water flow directions, and generalized geology (Modified from Czarnecki and Waddell (1984, p. 2).)

ground-water modeling efforts. The current review will not attempt to summarize the extensive information contained in DOE's 1988 SCP. Instead, general geohydrologic conditions in the region will be described to place the regional flow modeling in perspective.

The Yucca Mountain site occurs in southern Nevada and has a climate that may be classified as mid-latitude desert. At nearby Yucca Flat the average annual precipitation for the period from 1962 to 1971 was 146 millimeters (DOE, 1988; p. 5–12). Greater amounts of precipitation occur in nearby zones of higher elevation. Annual average potential evapotranspiration greatly exceeds the average annual precipitation, ranging from about 1500 to 1700 millimeters/year (*op cit.*, p. 3–8). There are no perennial streams in or near the Yucca Mountain area. The only perennial surface water in the region is associated with springs. However, many ephemeral stream channels are present, including those associated with the drainage systems of Fortymile Wash and the Amargosa River. Runoff occurs at irregular intervals and magnitudes and is associated mainly with summer and winter storms. The estimated discharge for the 100-year flood along Fortymile Wash is 340 cubic meters/second (*op cit.*, p. 3–21). Data on rainfall, runoff, and evaporation are inadequate to determine rainfall-runoff-recharge relationships (*op cit.*, p. 3–9).

The Yucca Mountain site occurs within the Alkali Flat-Furnace Creek Ranch subbasin of the Death Valley ground-water basin. The subbasin is part of the Basin and Range physiographic province. The geology and structure of this province created the complex hydrogeologic conditions that exist within the subbasin. The regional hydrostratigraphic units within the subbasin are: (1) the valley fill aquifer; (2) volcanic rock aquifers and aquitards; (3) upper carbonate aquifer; (4) upper clastic aquitard; (5) lower carbonate aquifer; and (6) the lower clastic aquitard (DOE, 1988; p. 3–58). Yucca Mountain itself (and surrounding uplands) consists of layered volcanic rocks of Tertiary age. In the vicinity of Yucca Mountain the water table occurs within these volcanic rocks. Deeper within the volcanic rocks, flow conditions may be confined or semi-confined. A much deeper, confined system exists within the lower carbonate aquifer that underlies the volcanics.

Most of the recharge within the subbasin is thought to occur in areas of higher elevation and correspondingly higher precipitation, located north of Yucca Mountain. A major proportion of recharge occurs in the winter and spring due to lower temperatures and evaporation rates. Recharge rates in lower elevation areas of the Amargosa Desert are unknown but are estimated to be very small. Czarnecki (1985) estimated recharge to be 0.7 millimeters/year for a zone of precipitation that includes Yucca Mountain. Principal discharge areas for the subbasin occur to the south at Franklin Lake Playa (*aka* Alkali Flat), with the closed basin of Death Valley serving as the ultimate discharge area for the region. Large areas of this valley occur at elevations below sea level.

I-3 USGS REGIONAL MODEL

I-3.1 *MODFE* Computer Code

The subregional ground-water model of Czarnecki (1985) was developed using the *MODFE* computer code (formerly known as *FEMOD*). Documentation for this code has been under development for many years, and has recently been published (Torak, 1992a, 1992b). Using this code, quasi-three-dimensional (3–D) models can be simulated with an areal, 2–D grid if one assumes vertical integration of aquifer properties (over a specified depth) and recharge or discharge conditions. *MODFE* is a finite-element code, permitting external and internal boundaries with complex outlines to be represented. This is a definite advantage over finite-difference codes. Physical properties can be specified for individual nodes or for groups of nodes called "zones".

MODFE is a modular code in the tradition of previous modular codes developed by the USGS (e.g., *MODFLOW*—see McDonald and Harbaugh, 1988). The modular nature of *MODFE* allows the user to tailor the source code to the problem at hand. For example, a code version for steady-state solutions can be built that excludes all those subroutines that relate only to transient problems. This greatly reduces the size of the compiled code and allows users to run the code even in the limited RAM environments of personal computers.

To reproduce Czarnecki's (1985) baseline results, the code version known as *NSSFE3* was used.

This version incorporates steady-state, water table conditions and includes the ability to simulate non-linear vertical recharge and discharge. This latter capability was used to simulate evapotranspiration (ET), which is the principal discharge mechanism in southern Nevada.

I–3.2 Model Design

Czarnecki and Waddell (1984) constructed their numerical model based on what was known about the Alkali Flat-Furnace Creek flow system in the early 1980's. The domain of this model covers an area of 6000 square kilometers and is a subset of Waddell's (1982) model domain (Figure I–1). Geographic features in the vicinity of the model are shown in Figure I–2. The Timber Mountain Caldera is located along the northern boundary, and Death Valley occurs at the southwestern extremity of the model.

Czarnecki and Waddell (1984) prepared a horizontal 2-D mesh of 2245 nodes (comprising 4222 elements), with nodal coordinates being expressed as meters north and east of an arbitrary origin. The model mesh is more finely discretized in the vicinity of Yucca Mountain to accommodate the large hydraulic gradient that is present. The finer mesh would also have advantages if a transport model were to be developed to evaluate radionuclide migration near Yucca Mountain. Elements in the finer part of the mesh down-gradient from the site have a representative length of about 800 meters, allowing for dispersivities as small as 80 meters (*op cit.*). Model nodes were divided into 13 zones for the specification of areally distributed fluxes and transmissive properties. Transmissivity values were selected using numerical parameter estimation techniques developed by Cooley (1977, 1979). The method used is also known as the "inverse" approach, in which hydraulic head data are input to the parameter estimation model and a transmissivity "solution" is obtained. More than 90 values of hydraulic head were obtained from water levels in wells and springs. Data locations are shown in Figure I–3.

The northern boundary of the model consisted of a line of specified head nodes to represent the area near Timber Mountain. Zones of specified flux were used to represent discharge from the model at Franklin Lake Playa and Furnace Creek Ranch. Specified fluxes into the model were applied along Rock Valley, the western edge of the Amargosa Desert, the western edge of Ash Meadows, and along the northern boundary of Jackass Flat. A flux was also specified along Fortymile Wash and at the high-ET location of Franklin Lake Playa. The flux values used in the model are not well known (Czarnecki and Waddell, 1984), but were intended to make the simulations more realistic by allowing flow into and out of the model in areas where springs exist, extensive ET is occurring, or where geologic conditions favor flow.

The steady-state solution ultimately arrived at by Czarnecki and Waddell (1984) through trial and error was a set of transmissivity zones and other parameters (lateral and areally distributed flux values) which reasonably represented the observed hydraulic head values. It is emphasized that the result of the calibration procedure is not unique and that different sets of parameters may fit the model equally well. Only geohydrologic experience and judgement can determine which solution is more likely and identify where additional field data need to be collected to improve reliability of the simulations.

Czarnecki (1985) used the same mesh described above, but the steady-state model was revised and improved by providing altitude data for each node and incorporating a routine to treat ET as a head-dependent function. The zonation and input parameters were also partly changed. Specified head nodes used in the parameter estimation model were replaced with specified flux boundaries. Specified head conditions were established at Furnace Creek and Alkali Flat, in place of prescribed flow conditions in the earlier model. An aquifer thickness of 1000 meters was assumed and transmissive properties were input as hydraulic conductivities. This constitutes Czarnecki's baseline model, which was subsequently modified to evaluate future ground-water scenarios (see Section I–4, "Subsequent Work Related to the USGS Regional Model"). The following subsections provide details about the construction of Czarnecki's (1985) baseline model.

I–3.3 Model Boundaries

Czarnecki and Waddell (1984) point out that the boundaries of the Alkali Flat-Furnace Creek Ranch ground-water basin are not well known.

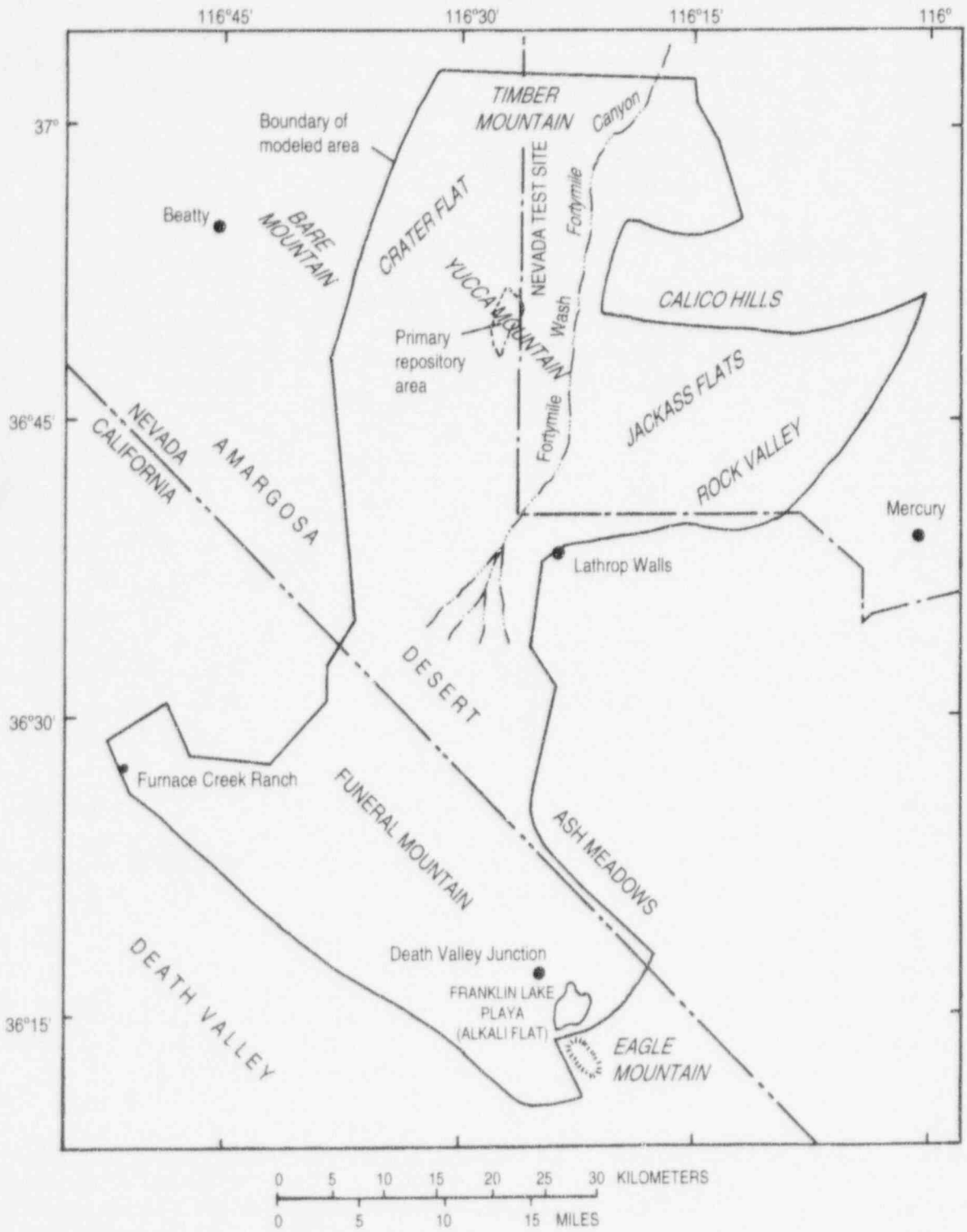

Figure I-2 Location of subregional modeled area and nearby geographic features (From Czarnecki and Waddell (1984, p. 6).)

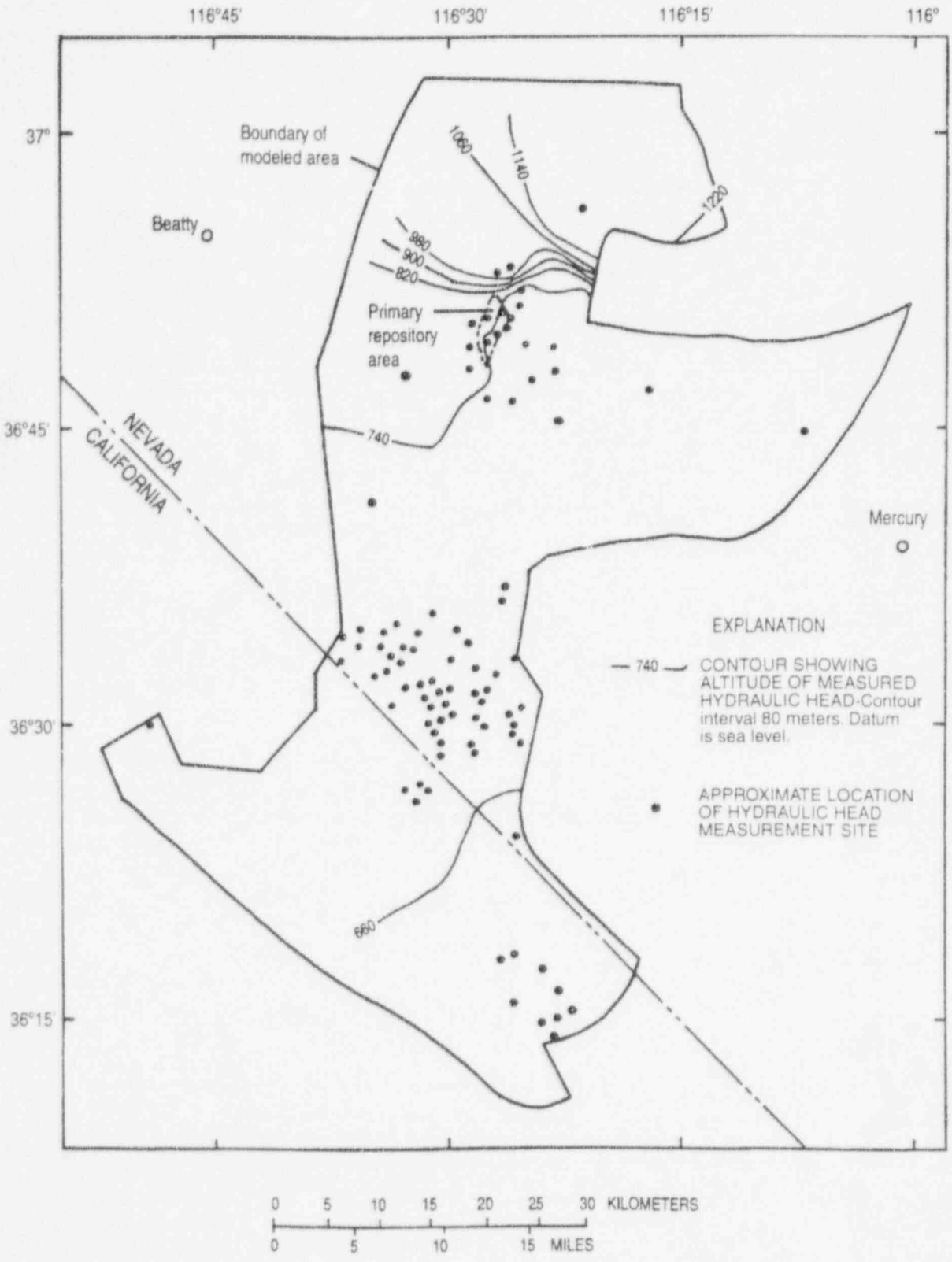

Figure I–3 Hydraulic head and location of measurement sites (After Czarnecki and Waddell (1984, p. 13).)

They were estimated from potentiometric data, geology, locations of discharge areas, and hydrochemistry. Outer boundaries in the model were derived on the basis of flow system characteristics that were assumed to exist. For example, no-flow boundaries were placed along the model edges where little or no input or output was expected to occur, or where flow was considered to be roughly parallel to the boundary itself. Head-dependent flux boundaries were defined for areas where flow was known or assumed to be occurring. Six zones of specified flux were defined to describe volumetric flow into the model domain along boundary segments. Figure I–4 represents these specified fluxes as a series of arrows. For example, based on hydraulic gradients and stratigraphy, flow must enter the subbasin along its northern boundary with the Timber Mountain area. Flow is also assumed to be entering the subbasin from the Calico Hills and Frenchman Flat, from the Ash Meadows area, and from the western Amargosa Desert. All other exterior boundaries of the model were assumed to represent no-flow (or parallel-flow) conditions.

An internal boundary was effectively created by assigning a low hydraulic conductivity value to the zone of high hydraulic gradient located north and northeast of Yucca Mountain. The resulting conductivity contrast diverts ground-water flux around the western portion of this zone and then east and southeast across the Yucca Mountain area.

I–3.4 Aquifer Properties

There is a general lack of hydraulic property data in the modeled region, although some field data exist in the vicinity of Yucca Mountain, the Nevada Test Site, and elsewhere. Much of the available transmissivity data were estimated from specific capacity data. The most transmissive unit in the region is the lower carbonate aquifer, which has transmissivity values as large as 10,000 square meters/day. All other aquifers have transmissivities that are more than an order of magnitude smaller (DOE, 1988; p. 3–68). Transmissivity for the valley-fill aquifer ranges from about 10 to 400 square meters/day.

Hydraulic properties of the volcanic tuffs that form and underlie Yucca Mountain are dominated by the degree of faulting and fracturing that is present, and on the rock properties that contribute to fracturing. Based on pumping tests at Well J–13, Thordarson (1983) concluded that the Topopah Spring Member of the Paintbrush Tuff has a transmissivity of 120 square meters/day and a hydraulic conductivity of 1.0 meter/day. This welded tuff unit, which is the proposed candidate horizon for a HLW repository, is unsaturated beneath Yucca Mountain. However, because the volcanic units dip toward the E–SE, it becomes saturated in the vicinity of Well J–13. Near Yucca Mountain this regional dip causes the top of the water table to occur in various volcanic units, including the Prow Pass and Bullfrog members of the Crater Flat Tuff, tuffaceous beds of the Calico Hills, and the Topopah Spring Member of the Paintbrush Tuff. Table I–1 gives average hydraulic conductivity data for these units in the vicinity of Yucca Mountain, as reported by DOE in its 1988 SCP.

The hydraulic property data presented above are based on analyses that assume the aquifers to be porous media rather than fractured rock aquifers. An important part of the site characterization program will be to determine under what conditions such assumptions are acceptable. It is often acceptable to make such assumptions in regional modeling. However, at the smaller site scale it may be necessary to consider discrete flow paths within the fractured volcanic rock aquifer.

Czarnecki and Waddell (1984) developed zones of uniform transmissivity based on dominant lithologies considered to be present at the water table (e.g., alluvium, tuffs, carbonate rocks). Using transmissivity values obtained during the earlier parameter estimation modeling, Czarnecki (1985) estimated hydraulic conductivities by dividing the transmissivity values by an assumed uniform saturated thickness of 1000 meters. The value of saturated thickness was estimated using borehole data from Yucca Mountain and the Amargosa Desert and using resistivity surveys conducted in the Amargosa Desert (Czarnecki, 1985).

Using the *MODFE* code, hydraulic property data are assigned to groups of finite-element nodes which comprise discrete zones. Czarnecki (1985) divided the model mesh into 12 zones of varying hydraulic conductivity and areal recharge (see Figure I–4). The general pattern of these zones

Table I-1 Hydraulic Conductivity Data (from DOE, 1988; p. 3-182)

Stratigraphic Unit	*Well Number*	*Average Hydraulic Conductivity (m/day)*
Topopah Spring Member (Paintbrush Tuff)	J-13	0.7
Tuffaceous beds of Calico Hills	UE-25b#1	0.5
Prow Pass Member (Crater Flat Tuff)	USW H-1	1.1 to 1.4
	USW H-4	0.2 to 0.8
	UE-25b#1	0.4
	UE-25p#1	0.1
Bullfrog Member (Crater Flat Tuff)	USW H-1	0.006
	USW H-4	0.6 to 2.3
	UE-25b#1	0.4
	UE-25p#1	0.05

was developed during the previous parameter estimation modeling (Czarnecki and Waddell, 1984). An important difference is that Czarnecki (1985) subdivided the Amargosa Desert into three distinct areas. Table I-2 shows that the 12 zones actually comprise 14 different combinations of hydraulic conductivity and areally distributed recharge. Values of hydraulic conductivity used in the model range from a high of 12.8 meters/day for Rock Valley to a low of 0.004 meters/day used to represent the zone of high hydraulic gradient located north and northeast of the Yucca Mountain site. A value of 3.65 meters/day was used to represent the area which includes Yucca Mountain and western Jackass Flats. This value of hydraulic conductivity is somewhat higher than the average values shown in Table I-1.

I-3.5 Recharge and Discharge

Recharge to the model (Czarnecki, 1985) occurs as a series of specified fluxes along the outer boundaries of the model. The locations of these fluxes are shown in Figure I-4. The other source of recharge to the model consists of steady-state, areally distributed recharge that is applied by zone. Values of areally distributed recharge were based on those estimated by Rush (1970, pp. 10-16). Rush estimated average annual groundwater recharge using the technique of Eakin *et al.* (1951, pp. 14-16). Table I-2 shows the amounts of recharge in millimeters/year for each zone. Four different values of recharge were applied, i.e., 0.0, 0.5, 2.0, and 410 millimeters/year. The largest recharge rate was applied along Fortymile Wash, the value being obtained through trial and error during parameter estimation modeling (Czarnecki and Waddell, 1984).

Discharge from the model occurs in the vicinity of the constant head nodes at Furnace Creek Ranch and at Franklin Lake Playa (*aka* Alkali Flat), which are located at the southeastern and southwestern extremities of the regional model. These areas are topographic lows, with the result that the assigned heads control discharge fluxes out of the model at these locations. The water table altitudes for these nodes were made to correspond to a depth of 5 meters below land surface to be consistent with the 5-meter extinction depth assigned to the routine to compute ET. A hydraulic head of -68 meters was specified for the vicinity of Furnace Creek Ranch. A head of 606 meters was specified for Franklin Lake Playa, a known discharge area with high rates of ET. In the baseline model of Czarnecki (1985), discharge from the model domain across specified head boundaries totaled 0.188 cubic meters/second.

Discharge also occurs as ET at model grid nodes where the simulated water table rises to less than 5 meters below land surface. No surface water is permitted to form in the model (i.e., springs or

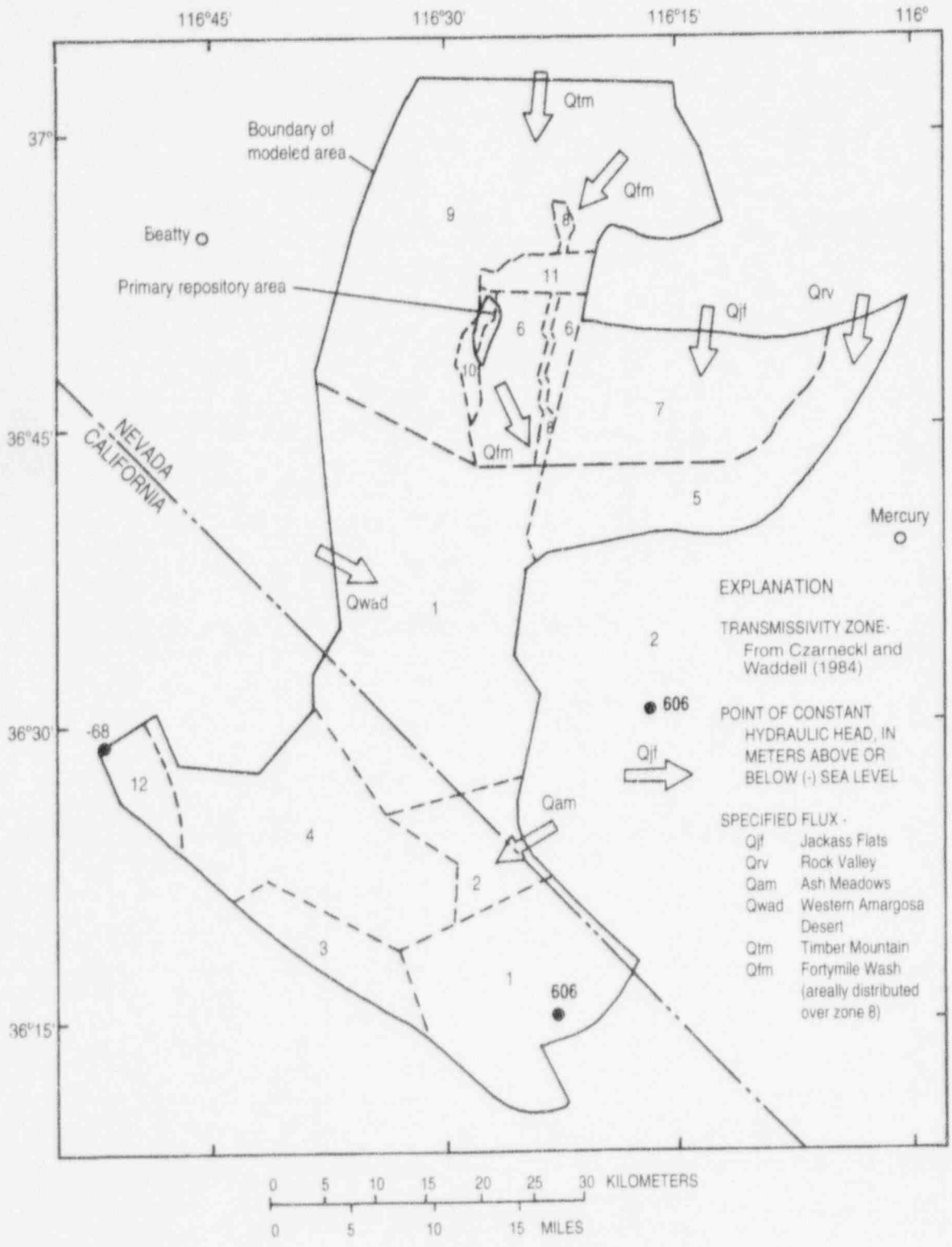

Figure I–4 Model boundary fluxes, constant-head nodes, and transmissivity zones (From Czarnecki (1985, p. 7).)

Table I-2 Hydraulic Conductivity and Recharge Data for Zones in Baseline Regional Model of Czarnecki (1985)

Zone Number	*Hydraulic Conductivity*		*Areally Distributed Recharge*		*Locale*
	(m/sec)	*(m/day)*	*(m/sec)*	*(mm/yr)*	
1	0.1691E-04	1.46	0.0	0.0	Amargosa Desert and Franklin Lake Playa
	0.1691E-04	1.46	0.1585E-10	0.5	Amargosa Desert (northern portion)
2	0.1105E-04	0.955	0.0	0.0	Area west of Ash Meadows
3	0.1484E-05	0.128	0.1585E-10	0.5	Greenwater Range (western portion)
4	0.1385E-05	0.120	0.0	0.0	Funeral Mountains
5	0.1480E-03	12.8	0.0	0.0	Rock Valley (western portion)
	0.1480E-03	12.8	0.1585E-10	0.5	Rock Valley (east) and Frenchman Flat
6	0.4229E-04	3.65	0.1585E-10	0.5	Yucca Mountain and western Jackass Flats (highly discretized)
7	0.4229E-04	3.65	0.1585E-10	0.5	Jackass Flats (eastern portion)
8	0.4229E-04	3.65	0.1300E-07	410	Fortymile Wash
9	0.1105E-05	0.095	0.6340E-10	2.0	Timber Mountain
	0.1105E-05	0.095	0.1585E-10	0.5	Crater Flat
10	0.9100E-06	0.079	0.1585E-10	0.5	Solitario Canyon and Yucca Mountain
11	0.4500E-07	0.0038	0.6340E-10	2.0	Zone NE of Yucca Mountain (with high hydraulic gradient)
12	0.2000E-05	0.173	0.0	0.0	Furnace Creek (Death Valley)

creeks). Wherever the simulated water table rises to the land surface, it is discharged entirely as ET.

To treat ET in the model, a value for land surface altitude had to be assigned to each node. This information was used by the model subroutine that simulates ET as a non-linear vertical discharge per unit area. This was an important improvement introduced by Czarnecki (1985) over the previous version of this model (Czarnecki and Waddell, 1984), providing a reference altitude for each node to compare with computed water table altitudes. An "extinction" depth of 5 meters was assigned; this was considered the maximum depth from which bare-soil evaporation could occur. During a simulation, ET would occur whenever the simulated water level at a node rose to a depth of less than 5 meters. The ET coefficient used was 0.864 meters/day per unit area at land surface. This very large ET rate was used to prevent the simulated water table from rising above the surface. It also removed water from the model area that might have left through runoff. The ET rate decreased linearly to zero at the extinction depth of 5 meters below land surface (Czarnecki, 1985). Thus, the maximum ET would occur for simulated heads at land surface, and all of the discharge would be treated as ET rather than allowing the creation of surface water bodies like springs and streams.

Discharge data are available for springs in the Furnace Creek Ranch area. Some of the springs occur several hundred meters above the floor of Death Valley. Discharges in this area were estimated at 0.2 cubic meters/second (Waddell, 1982). DOE (1988, Tables B-3—B-5) lists data for more than 20 spring outlets (plus numerous seeps and phreatophyte areas) in the Furnace Creek Ranch area. For those springs for which discharge was determined, the combined discharge totals more than 0.15 cubic meters/second. This is a minimum discharge because it does not include the many seeps and phreatophyte areas in the vicinity. Czarnecki and Waddell (1984) attribute a total discharge flux of 0.22 cubic meters/second to the Furnace Creek Ranch area.

Walker and Eakin (1963) estimated discharge by ET from Franklin Lake Playa to be ~0.4 cubic meters/second. Czarnecki (1990b) estimated an average volumetric discharge rate of ~0.26 cubic meters/second based on field studies at the playa (June 1983 to April 1984). Using Czarnecki's estimate, the ET discharge from this playa, when combined with estimated spring discharges in the region near Furnace Creek (~0.2 cubic meters/second (Waddell, 1982)), yields a total discharge at these locations of about ~0.4 to ~0.5 cubic meters/second. This can be compared with the simulated steady-state discharges for these areas obtained using Czarnecki's (1985) model. The combined discharge across specified-head boundaries at Franklin Lake Playa and Furnace Creek Ranch is ~0.19 cubic meters/second. The nonlinear routine that calculates ET yields a discharge of ~0.27 cubic meters/second. The total simulated discharge occurring in the vicinity of Franklin Lake Playa and Furnace Creek Ranch is approximately ~0.46 cubic meters/second.

There is apparent agreement between the observed and simulated discharges in the southern part of the model. However, the estimated spring and ET discharges do not include ground-water underflow which may exit the subbasin in these areas. For example, a significant amount of discharge likely occurs through the alluvial sediments that underlie the Amargosa River. This river basin hydrologically connects the Amargosa Desert to Death Valley, even when no surface water is flowing. The course of the ephemeral Amargosa River eventually descends into Death Valley, with a terminus at Badwater Basin (the lowest topographic basin in the U.S.). Some ground-water underflow may also occur beneath the Greenwater and Funeral Mountains via the Paleozoic carbonate aquifer. Further discussion about the discharges in the southern part of the model may be moot given the new conceptual model of flow that includes a possible flow divide in the Greenwater Range (see discussion later in this review).

Czarnecki and Waddell (1984) had previously determined that simulated rates of ET at Franklin Lake Playa had the largest effect (of all the model-boundary conditions) on estimated values for aquifer transmissivity at Yucca Mountain. Therefore, ET estimates for the playa had to be better defined. Czarnecki (1990b) documents an extensive program of field investigations at Franklin Lake Playa between June 1983 and April 1984. The playa shows extensive evidence of ground-water discharge. It is characterized by salt pan and porous surfaces, phreatophytes, very shallow ground water, and upward vertical

gradients that greatly exceed horizontal hydraulic gradients. In general, the ET rate depends on the types and density of phreatophytes, depth to the water table, ground-water salinity, soil-moisture properties, and climatic conditions (Czarnecki, 1990b). Czarnecki estimated rates of ET (centimeters/day) using various approaches, including energy-balance eddy correlation and analyses of temporal changes in soil moisture content, temperature profiles, vertical gradients in the saturated zone, and others. He concluded that the eddy correlation technique gave the most reliable estimates for ET because it is the most direct method. Czarnecki reported an estimated ET range of 38 to 41 centimeters/year at Franklin Lake Playa for 1983–84.

I-3.6 Model Results

Czarnecki (1985) obtained a baseline, steady-state solution of simulated hydraulic heads for the subbasin (see Figure I-5). Compared to the solution from the parameter-estimation model of Czarnecki and Waddell (1984), the model results showed a decrease in the range of head residuals (−18.9 to +21.0 meters) and a reduced estimated sum-of-squared errors for observed-versus-calculated hydraulic heads (4101 square meters). However, these comparisons may not have much meaning because the observed hydraulic head data are concentrated in areas that have small hydraulic gradients (e.g., the Amargosa Desert). Data are needed in areas where water table elevations change more rapidly (e.g., Furnace Creek area, and the region north and west of Yucca Mountain). Figure I-6 shows the vertically integrated ground-water flux vectors in the vicinity of the Yucca Mountain site for the baseline simulation.

I-3.7 Model Sensitivity and Stability

Modeling studies by Waddell (1982) and Czarnecki and Waddell (1984) showed recharge to be a highly sensitive element of their regional flow models. In particular, the recharge value applied to Fortymile Wash had a strong influence over the simulated heads at nearby Yucca Mountain. The solution was also found to be very sensitive to the rate of ET at Franklin Lake Playa.

Czarnecki (1985) reported instability problems with the model that were probably caused by the nonlinear routine in *MODFE* that handles ET. It is known that nonlinear routines can cause instability problems in numerical solutions (Roache, 1973). Significant mass-balance errors resulted when extinction depths of less than 5 meters were specified. Discretization errors may be produced by the presence of obtuse angles within the triangular elements of the finite-element mesh (Torak, 1992a). The finite-element mesh prepared by Czarnecki and Waddell (1984) contains 4222 elements. The mesh was analyzed with a *BASIC* routine and found to contain almost 600 elements that include obtuse angles. For a more accurate numerical solution, all angles within the triangular elements should be acute.

In independent simulations, the NRC staff found that Czarnecki's modeling results could be reproduced using 386 and 486 personal computers equipped with *WEITEK* math coprocessors. Serious instability problems caused by round-off errors arose when running the model on computers equipped with another type of math coprocessor. The problem was corrected by specifying floating point double precision (DECLARE ALL REAL*8) in each subroutine of the *FORTRAN* source code. Of course, the use of double precision greatly increases the memory (RAM) required to run the model.

I-4 SUBSEQUENT WORK RELATED TO THE USGS REGIONAL MODEL

I-4.1 Modeling of the Alkali Flat-Furnace Creek Ranch Subbasin

Czarnecki (1985) investigated the possible effects on the water table of a wetter future climate. He revised the baseline model to simulate the effects of increased recharge in the region. Both recharge amounts and lateral fluxes were increased, resulting in water table rises at the Yucca Mountain site. Based on this model, Czarnecki concluded that a 100 percent increase in precipitation caused the simulated position of the water table at Yucca Mountain to rise as much as 130 meters. This degree of water table rise would not be enough to flood a hypothetical repository in the Topopah

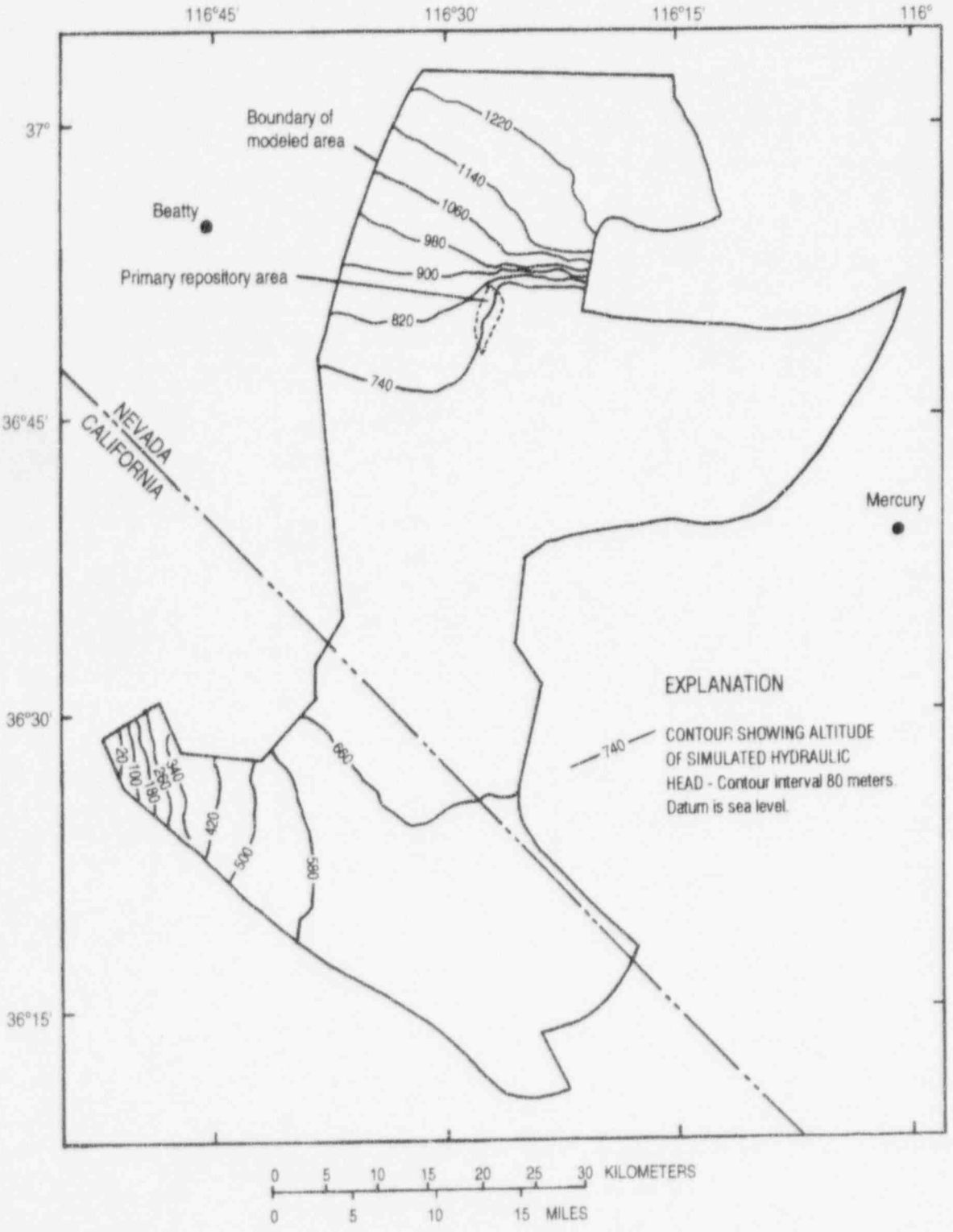

Figure I-5 Simulated hydraulic head for the baseline-condition simulation (From Czarnecki (1985, p. 10).)

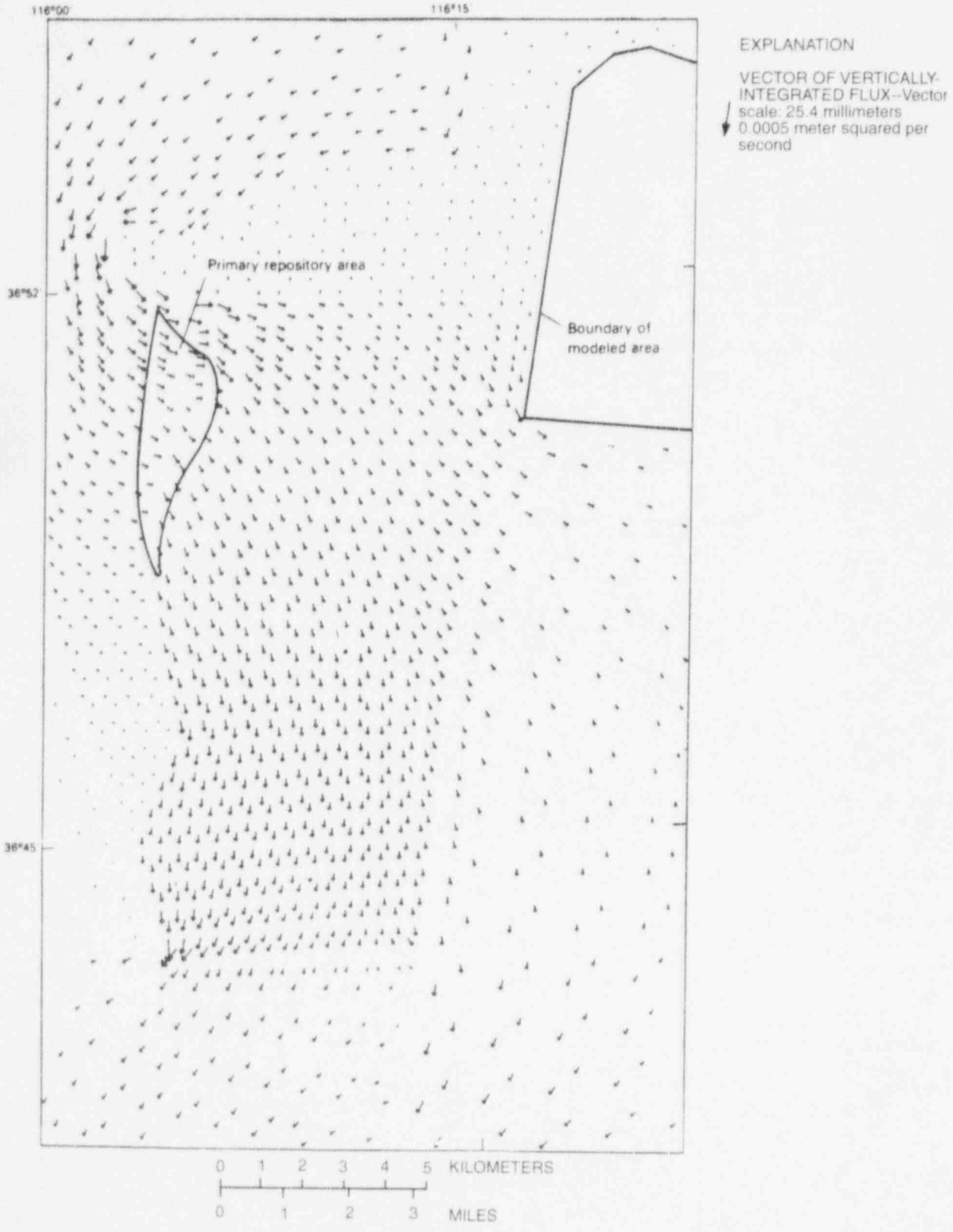

Figure I–6 Baseline, vertically integrated ground-water flux vectors at and in the vicinity of the primary repository area (From Czarnecki (1985, p. 29).)

Spring Member of the Paintbrush Tuff. However, the simulated water table rise would greatly reduce the thickness of the unsaturated zone and would be sufficient to cause springs to form south and west of Timber mountain, along Fortymile Wash, in the Amargosa Desert near Lathrop Wells and Franklin Lake Playa, and near Furnace Creek Ranch in Death Valley.

Czarnecki (1985) noted that the future water table rise due to a wetter climate (and increased recharge) may be exaggerated because surface water runoff was not permitted in the model. All discharges from the model occurred as either ET or lateral ground-water flow. However, it is noted that the future simulations were derived by revising a baseline model that had assumed zero modern-day recharge over large areas of the model domain. It is not yet known whether the recharge assumptions used in the baseline model are reasonable (see discussion under "Revised Conceptual Model, Section I-4.3").

There is evidence that the water table at Yucca Mountain was significantly higher in the past. Marshall *et al.* (1993) describe strontium isotopic evidence for a higher water table at Yucca Mountain. They conclude that the water table may have been about 85 meters higher in the past. This degree of water table rise is of the same order of magnitude as that predicted by Czarnecki (1985) under wetter climatic conditions. This is significant with respect to performance of a potential repository. Any long-term rise of the water table over the next 10,000 years would reduce the thickness of the unsaturated zone beneath the repository. This portion of the unsaturated zone is considered the key barrier within the natural system.

Other evidence of a higher water table in the Yucca Mountain region is provided by Quade *et al.* (1995). They describe a group of spring deposits, informally named the Lathrop Wells diatomites, located about 20 kilometers southwest of the Yucca Mountain site. The diatomites represent fluvial and shallow aquatic environments, and are similar to other spring deposits. Although the age of the deposits is still under study, fossils of horse, camel, mammoth, and rabbit confirm that parts of them date to the Pleistocene. The position of the Lathrop Wells diatomites, relative to the modern water table, suggests that the water table was formerly no more than 115 meters higher than it is today (*op cit.*, p. 227).

There is also evidence that a perennial water source existed in Fortymile Canyon near Yucca Mountain during the Wisconsin glacial stage. Spaulding (1994, p. 40) concluded that plant macrofossils from a packrat midden site in Fortymile Canyon provide unequivocal evidence that a perennial water source existed there approximately 47,000 years before the present (ybp) (and possibly earlier). This midden site, designated FMC-7, is located about 13 kilometers northeast of Yucca Mountain adjacent to Fortymile Canyon (in Area 29 of the Nevada Test Site). The site is north of the zone of high hydraulic gradient in an area where the water table is presently much shallower than at Yucca Mountain. FMC-7 occurs at an elevation of 1250 meters, about 75 meters above the current drainage of Fortymile Canyon. The location of midden site FMC-7, along with its macrofossil and pollen assemblages, led Spaulding (1994) to conclude that the water table was at least 75 meters higher during the Early or Early-Middle Wisconsin (ca. 73,000 to 47,000 ybp). He found it likely that the bed of Fortymile Canyon was 75 to 95 meters higher than today, with 65 meters of alluvium having been removed by stream incision approximately 18,500 ybp. Spaulding (1994, p. 50) provided recommendations for future paleoecological research, noting the ". . . contrast between the widely held belief that the last glacial maximum [ca. 18,000 ybp] was a time of maximum water-table rise and spring discharge, and the utter lack of stratigraphic evidence for spring discharge during that time...."

Czarnecki (1990a) developed a transient version of his model to investigate phenomena like the large hydraulic gradient located north of the site. In one scenario, a postulated hydrologic barrier was disrupted and large volumes of ground water were released to flow southward. Such a scenario could arise due to faulting associated with an earthquake. This scenario caused a maximum rise of about 40 meters in the simulated water level at Yucca Mountain (National Research Council, 1992 (citing personal communication with J. Czarnecki)).

Czarnecki (1992) simulated water level declines in the Yucca Mountain area in response to future ground-water withdrawals from Wells J-13 and

J-12, located about 7 kilometers southeast of the Yucca Mountain site. This work is very important because it represents a 10-year forecast of how future ground-water levels will be affected by human activities. This work supported a request from DOE to the State of Nevada for a permit to pump up to 5.7×10^{-3} cubic meters/second from Well J-13 (*op cit.*). DOE requested the water to support site characterization work at Yucca Mountain over the next 10 years. Eight different pumping scenarios were analyzed using a transient version of Czarnecki's 1985 model and various combinations of withdrawal rates. Four of the scenarios involved pumping from a single well, while both wells were pumped in the other four scenarios. For each withdrawal rate, simulations were made with aquifer specific yields set at 0.001, 0.005, and 0.01. Czarnecki (1992) considered a specific yield of 0.01 to be the value that is best supported by available data. The most extreme scenario represented the combined maximum pumping capacities from both wells (8.771×10^{-2} cubic meters/second) and assumed an aquifer specific yield of 0.001. This resulted in a drawdown of over 12.2 meters at both Wells J-12 and J-13 at the end of the 10-year period. Under the same pumping conditions, and assuming a specific yield of 0.01, simulated drawdowns at Wells J-13 and J-12 were about 3.0 meters and varied from 1.8 to 2.4 meters at the Yucca Mountain site. The simulated drawdown for the anticipated withdrawal rate of 5.7×10^{-3} cubic meters/second from Well J-13 (based on a 10-year pumping period and a specific yield of 0.01) was 0.29 meters at Well J-13. The drawdown at the Yucca Mountain site would be about 0.2 It is expected that one of the many scenarios analyzed by Czarnecki (1992) will be representative of actual ground-water withdrawals during site characterization and can be used to test how well the regional model represents the flow system.

Oatfield and Czarnecki (1989) analyzed drillers' logs and data from geophysical surveys to identify areas in the Amargosa Desert that have relatively higher or lower transmissivities. They concluded, based on drillers' logs, that the thick alluvial deposits cannot easily be subdivided into correlative stratigraphic units. However, the drillers' logs suggested a trend of increasing consolidation of sediments from north to south. Hydrogeologic interpretation of a resistivity (vertical electric sounding) survey was complicated by a lack of information about aquifer properties and ground water quality at depth. However, high resistivity values in the upper 75 meters of alluvium were interpreted to coincide with relatively fresh, shallow ground water that may enter the Amargosa Desert via the Fortmile Wash drainage system.

I-4.2 The Szymanski Hypothesis

Szymanski (1989) asserted that ground water at Yucca Mountain had risen to repository level repeatedly in the past, primarily because of tectonic processes. This assertion was based largely on Szymanski's hydrothermal interpretation of the origin of fracture-cementing carbonates and silica exposed in Trench 14. This trench was excavated across the Bow Ridge fault just east of Yucca Mountain. Contrary to Szymanski's interpretation of Trench 14, Quade *et al.* (1995, p. 228) observed that many years of scrutiny by different researchers (including themselves) have ". . . failed to identify unequivocal paleospring deposits adjacent to Yucca Mountain. . . ." Based on their study of modern and fossil spring deposits in the region, they found that the mineralogy of Trench 14 has no modern analog. Quade *et al.* concluded that morphologically, mineralogically, and isotopically, ". . . the fracture carbonates in Trench 14 closely resemble pedogenic carbonate in the region. . . ." (*op cit.*)

Before the work of Quade *et al.* (1995), a panel of the National Research Council (1992) had evaluated the potential for future rises of the water table to occur at Yucca Mountain. The panel assessed the likelihood that the water table could rise to the height of the repository horizon by any plausible geological process, or whether such a rise had occurred in the past. The panel cited the previous work of Waddell and Czarnecki, and emphasized the importance of field evidence in establishing the presence of past discharge areas.

With respect to earthquakes, the National Research Council Panel (1992, p. 124) concluded that ". . . while there are uncertainties in current interpretations because specific site data are not available, . . . there is nevertheless sufficient confidence in the aseismicity of the site and in the inability of earthquakes to generate large water table changes at the site . . . to warrant further characterization of the site to determine its suitability. . . ." The panel recommended that the

DOE conduct a literature search regarding the hydrologic effects of historic earthquakes, locally and worldwide, to determine the potential for large water table rises in response to the coupling of seismic and hydrologic systems.

The earthquake that occurred near Little Skull Mountain on June 29, 1992 (magnitude 5.6) caused only a minor, transient change in the water table at the Yucca Mountain site. The maximum fluctuation of the water table at the site was estimated at only 0.4 meters (O'Brien and Tucci, 1992). The data were obtained from two wells instrumented to continuously monitor fluctuations in the water table and fluid-pressure in a deeper, isolated interval. Water table fluctuations of similar magnitude were caused by more distant and more powerful earthquakes. Two major earthquakes occurred in southern California on June 28, 1992. Both were about 300 kilometers from Yucca Mountain and were measured as having magnitudes of 7.5 (Landers) and 6.6 (Big Bear Lake). The Landers and Big Bear Lake quakes caused estimated water table fluctuations of 0.9 meters and 0.2 meters, respectively (*op cit.*).

I–4.3 Revised Conceptual Model

New ideas about regional flow in the subbasin were presented and documented by Czarnecki (1987, 1989) and Czarnecki and Wilson (1989). The previously accepted conceptual model of the regional ground-water system assumed that flow beneath the central Amargosa Desert ultimately discharges from two major areas: Furnace Creek Ranch and Franklin Lake Playa. In the baseline model of Czarnecki (1985), zero recharge was assumed to be occurring over most of the subregion south of Yucca Mountain. New data were obtained by Czarnecki (1989) which led to an alternate conceptual model of subregional flow. Potentiometric data were obtained from mining property boreholes in the Greenwater Range (between Death Valley and the Amargosa Desert). These data show a water table altitude in that area of about 875 meters (Figure I–7), providing evidence of significant ground-water recharge and the probable presence of a ground-water flow divide beneath this range. The data suggest that flow divides beneath the Greenwater and Funeral Mountains may isolate the water table aquifer in the Amargosa Desert from the flow system in Death Valley. Geographic features of this area are illustrated in Figure I–8.

The inclusion of flow divides beneath the Greenwater and Funeral Mountains is a major revision of the conceptual model used to develop Czarnecki's regional flow model, in that the discharge area at Furnace Creek Ranch may be relatively isolated from the water table aquifer underlying the Amargosa Desert. Instead, Franklin Lake Playa may serve as the principal discharge area for the subregional water table flow system that includes Yucca Mountain, and discharge at Furnace Creek Ranch may be derived primarily from the confined carbonate aquifer. Winograd and Thordarson (1975) had previously suggested this possibility, based on the proximity of spring discharge to the lower carbonate aquifer and temperature and hydrochemical conditions (DOE, 1988; p. 3–79). A portion of the discharge at Furnace Creek Ranch may also be derived from recharge in the nearby mountains. To help confirm the new conceptual model, a number of wells would be needed to better define hydraulic heads in the ground-water divide areas north and east of Furnace Creek Ranch. DOE (1990, p. 3.2–6) describes plans to drill new wells, including one planned for the eastern edge of the Funeral Mountains. Figure I–7 shows Czarnecki's proposed revision of the flow system with inferred water-level contours based on the data from the Greenwater Range and a principal discharge area at Franklin Lake Playa.

As discussed in Czarnecki and Wilson (1989), a revised conceptual model for the subbasin would include the following:

- The presence of a regional Paleozoic carbonate aquifer which underlies the subbasin that includes Yucca Mountain;
- Upward flow originating from the carbonate aquifer occurs from great depths within the subbasin;
- Spring flow in Death Valley near Furnace Creek Ranch is from the carbonate aquifer, which forms a confined aquifer that is separate from the overlying water table system; and
- Some recharge to the ground-water system may be occurring even in arid areas such as

the Funeral Mountains and the Greenwater Range.

The revised conceptual model is significant in that it would require less volumetric flow through the region that includes Yucca Mountain. Other conditions being equal, this means that simulated ground-water velocities would generally be less than in the original model. But it also suggests that the flow system may be more susceptible to future large-scale stresses such as extensive ground-water overdrafts.

I–4.4 Site Characterization Study Plans

In support of the Yucca Mountain project, DOE has developed study plans that outline a program for characterizing and modeling the regional flow system. DOE (1990) describes plans to characterize the regional ground-water flow system. The study, "Regional Hydrologic Synthesis and Modeling" (DOE, 1991), will analyze regional ground-water data, formulate conceptual models of the regional flow system, and develop and calibrate numerical models. Other study plans, such as those involving climatology, geochemistry, and geology, are also related to the characterization and modeling of the ground-water system. Results of the regional modeling will be used to specify boundary conditions for site-scale models of the saturated zone at Yucca Mountain. Regional models will also be used to estimate changes in the regional (and local) ground-water system caused by future climatic conditions, human activities, and tectonic events. In this way the modeling results are intended to support site-scale evaluations of repository performance with respect to the NRC's criterion for ground-water travel time (10 CFR 60.113(a)(2)) and the EPA standards under 40 CFR Part 191.[1]

[1]Currently, a revised set of standards specific to the Yucca Mountain site is being developed in accordance with the provisions of the Energy Policy Act of 1992. The Energy Policy Act of 1992 (Public Law 102–486), approved October 24, 1992, directs NRC to promulgate a rule, modifying 10 CFR Part 60 of its regulations, so that these regulations are consistent with EPA's public health and safety standards for protection of the public from releases to the accessible environment from radioactive materials stored or disposed of at Yucca Mountain, Nevada, consistent with the findings and recommendations made by the National Academy of Sciences, to EPA, on issues relating to the environmental standards governing the Yucca Mountain repository. It is assumed that the revised EPA standards for the Yucca Mountain site will not be substantially different from those currently contained in 40 CFR Part 191, particularly as they pertain to the need to conduct a quantitative performance assessment as the means to estimate postclosure performance of the repository system.

I–4.5 Data Requirements to Improve Regional Model

Documentation of Well Data: Previous reports on regional modeling in the Yucca Mountain region do not provide sufficient information about wells and boreholes used to obtain hydraulic heads for model calibration. For example, Czarnecki and Waddell (1984) provide a table of hydraulic heads and a list of data sources. However, of the five data sources listed, only two are published reports, and only one of these (Walker and Eakin, 1963) lists tabular information about wells in the region. The Walker and Eakin (1963) reference is almost 30 years old and presents well locations using township and range coordinates rather than the currently-used Nevada State plane coordinate system. The other published data source cited by Czarnecki and Waddell (1984) is Waddell (1982). This reference cites Thordarson and Robinson's (1971) inventory of over 6000 wells and springs within a 161-kilometer radius of the Nevada Test Site, but that reference is more than 20 years old. Because these references are decades old, the current status of the documented wells is unknown.

It is recognized that regional modeling studies rely heavily on existing data sources such as irrigation wells, farm and ranch wells, and mining exploration boreholes. These wells and boreholes were not designed for the scientific collection of ground-water data; therefore, details of their construction are usually not well documented. Nevertheless, they are indispensable for establishing long-term water-level changes and calibrating regional models, and known details about such data sources should be documented. Such wells and boreholes are generally privately owned and may become inaccessible to future investigators; therefore, they should be documented to the extent practicable.

Regional Evapotranspiration (ET) and Recharge: DOE (1990) describes characterization of the regional ground-water flow system and includes an activity titled "Evapotranspiration Studies." The objective of the activity is to estimate ET rates in the Amargosa Desert to provide data for regional and subregional models. Although the objective refers to the Amargosa Desert, the activity mainly emphasizes work at Franklin Lake

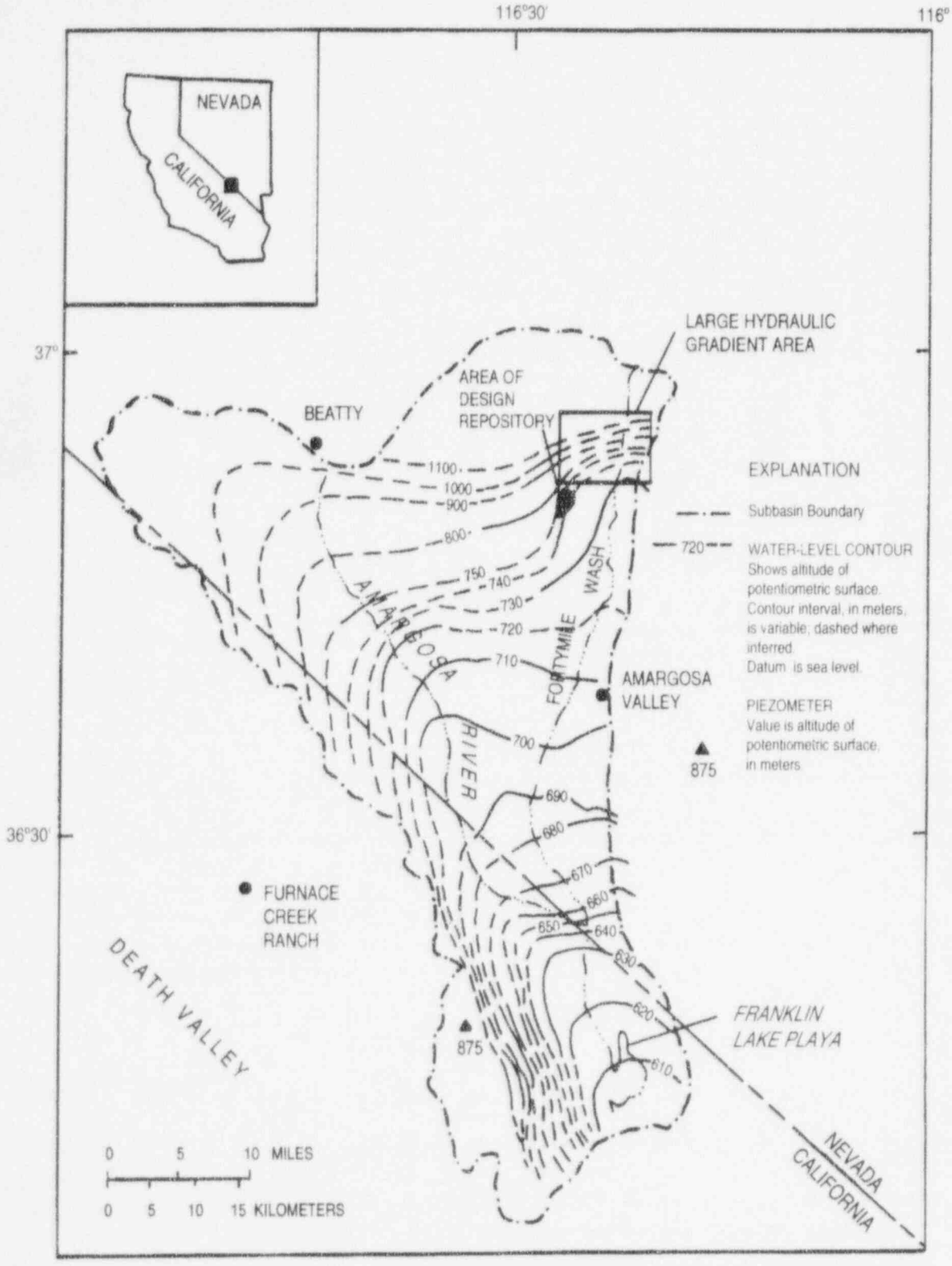

Figure I–7 Subregional potentionmetric surface (From DOE (1990b, p. 1.2-7).)

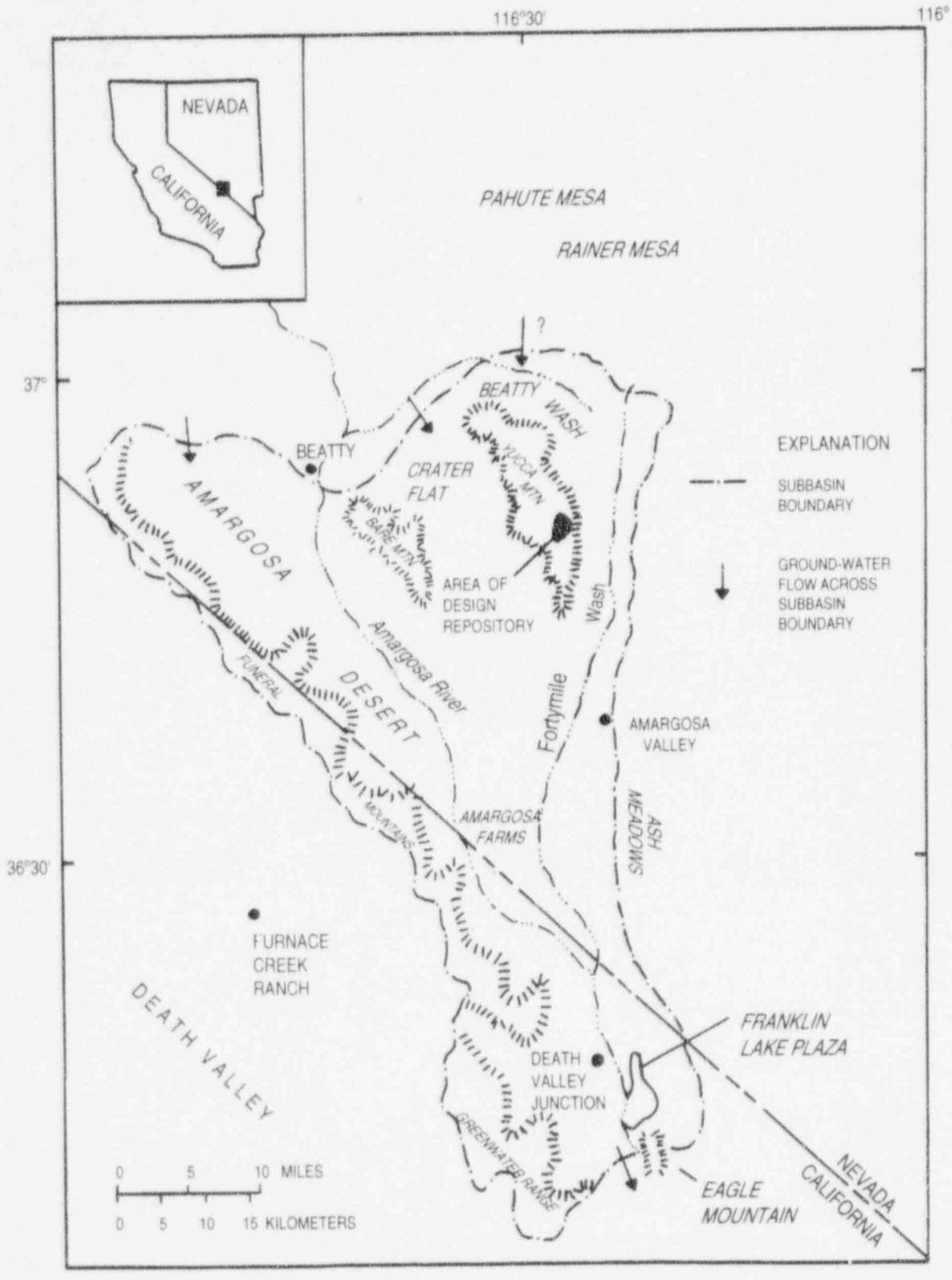

Figure I–8 Location map of ground-water subbasin (Modified from DOE (1990b, p. 1.2-3).)

Playa, a key discharge area. It is not clear how estimates of ET and recharge will be obtained for other areas in the regional model. In fact, Czarnecki (1985) assumed zero recharge for most of the area of the regional model that is south of Yucca Mountain.

Ground-water recharge rates are thought to be small over most of southern Nevada. More ground-water recharge is expected to occur in areas of higher elevation due to lower temperatures and greater annual precipitation. Some areas, such as Fortymile Wash and other alluvial valleys, are capable of producing high recharge fluxes during infrequent, surface-water runoff events of large magnitude. In his steady-state, subregional model, Czarnecki (1985) used recharge rates ranging from 0.0 millimeters/year (Amargosa Desert, western Rock Valley, Franklin Lake Playa, Funeral Mountains) to 410 millimeters/year (Fortymile Wash). Intermediate recharge rates of 0.5 and 2.0 millimeters/year were assigned to other areas, with Timber Mountain having a designated rate of 2.0 millimeters/year.

In most of Nevada, actual rates of ET are much less than the potential evapotranspiration (PET), which is the maximum amount that can occur under given meteorologic conditions. This is true because in many areas the only water available for ET is obtained from scanty precipitation. Franklin Lake Playa is an exception in that ground-water flows upward in this discharge area, producing a shallow water table and maximizing the amount of ET that can occur.

In sensitivity studies of the parameter estimation model of Czarnecki and Waddell (1984), specified flux at the Franklin Lake Playa had the largest effect of all the specified fluxes on the estimate of hydraulic properties in the vicinity of Yucca Mountain. As a result of these sensitivity studies, Czarnecki (1990b) performed extensive fieldwork at the playa to evaluate various methods to estimate ET and to measure hydraulic gradients and aquifer properties (see previous discussion). Czarnecki (1990b) considered a range of 38 to 41 centimeters/year as the most reliable ET estimate at Franklin Lake for 1983–84. Although rates of ET can be estimated at given locations, to obtain volumetric fluxes it is necessary to estimate the area over which a given ET rate is occurring. This is difficult to accomplish in practice and limits the accuracy of areal estimates of ET over various scales. For example, at Franklin Lake Playa the total area of shallow ground water and relatively high ET is not well known.

There is a need to obtain improved estimates of ET and ground-water underflow at Franklin Lake Playa, especially in light of the alternate conceptual flow model presented in Czarnecki (1989) in which the playa area may act as the principal water table discharge area for the subbasin that includes Yucca Mountain. There is also a need for improved estimates of ET for other areas within the region in order to better estimate rates of deep percolation through the unsaturated zone to the water table. Such estimates are dominated by ET rates because the percentage of precipitation that returns to the atmosphere via ET greatly exceeds the percentage of rainfall that ultimately becomes ground-water recharge.

Hydraulic Heads: Although some aquifer property data exist in the modeled region, the regional model was calibrated primarily based on hydraulic heads. As shown in Figure I-3, wells in the USGS model are concentrated in three areas: (1) the Amargosa Desert; (2) the vicinity of Yucca Mountain; and (3) near Franklin Lake Playa. For some key areas, well data are practically nonexistent. There are no wells along the northernmost boundary where a ground-water influx is assumed from the Timber Mountain caldera. Insufficient wells exist north of Yucca Mountain to define the extent and nature of a zone of high hydraulic gradient. This high gradient zone is the dominant feature in the potentiometric surface at the site. It is important to determine the source of this feature and its physical properties. This issue was raised by the NRC staff in Comment 20 of its Site Characterization Analysis (NRC, 1989; p. 4-25). DOE has specific plans to explore the high hydraulic gradient, which include the drilling of new wells. Wells WT-23 and WT-24 will be located at intermediate distances between two of the wells that currently define the high gradient, Wells H-1 and I-1 (DOE, 1991).

Wells are also lacking in the geologic transition zone that occurs between the volcanic terrane of Yucca Mountain and the Amargosa Desert. Wells are similarly lacking in the Funeral Mountains area, south of the Amargosa Desert. The head contours simulated by Czarnecki show a steepened gradient in the vicinity of Furnace Creek

Ranch. This cannot be verified due to a lack of wells, but it does correspond with a drop in elevation toward Death Valley. But most importantly, the preliminary information, which indicates that a flow divide may exist between Franklin Lake Playa and Furnace Creek Ranch, if confirmed, would require a reconfiguration of the model to properly reflect newly inferred subbasin boundaries.

Three-Dimensional Modeling: DOE (1991) describes plans to proceed with 3-D modeling of the regional ground-water system. Three-dimensional (multi-layer) numerical models can be useful tools for understanding the interactions between unconfined and confined aquifers. However, there must be sufficient potentiometric (and other hydrogeologic) data to reasonably define and calibrate a model to justify the use of 3-D techniques. In other words, to model in three spatial dimensions, supporting hydrogeologic data must be reasonably distributed in three dimensions. DOE (1991) discusses previous regional modeling and indicates that a preliminary quasi-3-D model has already been developed, citing Sinton and Downey (written communication). This model consists of two layers, the lower of which represents the Paleozoic carbonate rocks. DOE (1991, p. 3.4-1) states that ". . . with the existing data base, use of more than two layers to represent the regional ground-water-flow system is not expected to be justified because of a sparsity of data on the 3-D hydrogeologic properties of the system . . . ."

It is not clear whether 3-D modeling of even two layers can be supported given that very little hydrologic information presently exists for the deep Paleozoic aquifer system (upper and lower carbonate aquifers). In the vicinity of Yucca Mountain, only one well (UE-25p#1) penetrates Paleozoic carbonate rocks. At this location the carbonates are 1.2 kilometers deep, and have a hydraulic head that is about 19 meters higher than in the overlying zone. Although this is a significant upward gradient, it is not known whether it could significantly influence flow directions and magnitudes in the upper part of the saturated zone, more than 1000 m above the carbonates at the location of borehole UE-25p#1. Even within the tuffs that overlie the deep carbonate rocks, there are zones that are confined or semi-confined, illustrating the complexity of the saturated zone flow system. Without the necessary subsurface data, there may not be enough potentiometric or physical property data from the Paleozoic carbonates to adequately calibrate a 3-D model.

Data limitations are also discussed in the study plan to characterize the "Yucca Mountain Regional Ground-Water Flow System (DOE, 1990)." That is the key study plan under which data will be collected to support the regional ground-water modeling activities. DOE (1990, p. 3.1-6) states that ". . . little is known about the distribution of hydraulic head with depth within the flow system. Hydraulic-head data in the vertical dimension are critical for calibrating 3-D models of ground-water flow. At present, only a handful of points exist where hydraulic head has been determined at various depths. . . ."

DOE has identified additional wells to be drilled in the vicinity of Yucca Mountain that may penetrate the Paleozoic aquifer and would contribute to 3-D site models. They would not, however, significantly add to regional well coverage. Wells proposed to be drilled in Crater Flat, near Lathrop Wells, and near the Funeral Mountains (DOE, 1990) would improve the regional data base, but it is questionable whether the data would be sufficient to calibrate a 3-D model that includes the Paleozoic carbonates as a separate layer.

Downey *et al.* (1990) describe a conceptual ground-water model of the southern Nevada and Death Valley region. This conceptual model illustrates the geologic complexity of the region. Downey *et al.* criticize existing models of the Yucca Mountain region for being 2-D, and inadequate to represent long-term changes in the ground-water flow system. They state that existing models are based on limited head data, elevation and precipitation estimates, and simplified geology. Downey *et al.* advocate a 3-D approach for boundary selection and estimation to properly represent the ground-water system. Their approach to estimating unknown boundary conditions for the regional flow system includes six steps (*op cit.*, p. 725):

(1) Incorporate known boundary conditions from playas in Death Valley and Ash Meadows;

(2) Use geological, pedological, geomorphological, botanical, and hydrological observations

to develop initial boundary conditions for other boundaries;

(3) Test the initial conditions using steady-state and transient 3–D models;

(4) Back-calculate the boundary conditions for flux boundaries to the northwest, north, and east, thereby obtaining new, improved boundary-condition estimates;

(5) Compare calculated values with known data during calibration steps; and

(6) Adjust the model.

The apparent intent is to integrate all existing geologic, hydrologic, geophysical, and hydrochemical data for the Death Valley flow system using a Geographic Information System. DOE's intent is to synthesize all existing data into the best regional models that can be generated (Shelor, 1993). Notwithstanding the recommendations of Downey *et al.* (1990), it is not clear whether their approach will, in practice, be greatly superior to or substantially different from past modeling efforts. Their recommended Step "No. 2" basically says to incorporate more data from interdisciplinary sources. Obtaining more data will improve any model. The 3–D approach will require specification of hydrologic conditions within model layers and along the boundary between layers. Overall, it is not clear whether sufficient data exist or will become available to justify 3–D modeling, particularly for the Paleozoic carbonate aquifer. A commitment to perform 3–D modeling will have to be accompanied by a commitment to obtain enough data to reasonably justify the 3-D approach.

Other Information Needs: Previous reports that document regional modeling do not include adequate information about how model boundaries were selected. It is recognized that the selection of boundaries for any model includes qualitative professional judgements about subsurface flow conditions. Future reports should present the general rationale used in constructing model boundaries. There is also a need to systematically incorporate hydrochemical data in the development and verification of conceptual models of regional flow. The data may provide insight about general recharge conditions, groundwater age, flowpaths, and interformational hydraulic communication.

I–5 SUMMARY

A number of key activities should be performed in the next few years to improve the regional modeling efforts. The DOE is planning a drilling and testing program to characterize the zone of high hydraulic gradient located north of the Yucca Mountain site. The results of that program could lead to significant changes in numerical models of the site and region. Also, the search should continue for additional evidence of past discharge areas in the currently dry water courses near Yucca Mountain, particularly Fortymile Wash. This would provide further information about possible water table rises over the past several millennia.

Better estimates of present-day recharge over the site and region are needed to improve future estimates of recharge under varying climatic conditions. There is also a need for additional hydraulic conductivity data over the site and region. In particular, there are virtually no data on vertical hydraulic conductivities at the contacts of hydrostratigraphic units. Such data would be needed to support 3–D modeling. Currently available data may not be sufficient to justify the use of 3–D modeling on a regional scale. DOE needs to determine whether the data are sufficient and whether 3–D modeling will be required to adequately represent the regional flow system.

The work of Czarnecki and Waddell (1984), Czarnecki (1985, 1989, 1990a, 1990b), and Czarnecki and Wilson (1989) illustrates a methodical process for developing and improving numerical models of ground-water flow. An initial conceptual model was developed and parameter estimation techniques were applied to help construct a corresponding numerical model. Sensitivity studies were performed to determine where parameters needed to be refined. Most importantly, the search was continued for hydrologic data in areas where little information existed, leading to the discovery of new potentiometric data from the Greenwater Range. Based on this data, a new conceptual model of regional ground-water flow was developed which will guide future data collection and modeling work. Each of the above steps was documented through professional presentations and publications. In order to use the

regional flow model to predict future conditions in the regional flow system, the model may need to be modified based on the hydraulic head data from the Greenwater Range and other locations. Other changes may be needed based on results of ongoing site characterization work.

Finally, the work of Czarnecki (1992) represents an important 10-year forecast of how future ground-water levels will be affected by human activities. After 10 years of site characterization, it will be possible to see how well the regional model has predicted the perturbations caused by pumping at Wells J-13 and J-12. It is expected that one of the many scenarios analyzed by Czarnecki will approximate actual ground-water withdrawals at the well sites. This will provide a test of how well the regional model represents present-day conditions in the flow system near Yucca Mountain.

In closing, it is appropriate to consider remarks by Konikow and Bredehoeft (1992, p. 78) in their commentary on model interpretation, validation, and use. They criticize use of the expressions "model validation" and "model verification" because they tend ". . . to lend undue credibility to a process that . . . is, in the end, inherently subjective. . . ." They prefer to describe the process using expressions such as model testing, model evaluation, model calibration, sensitivity testing, benchmarking, history matching, and parameter estimation. Konikow and Bredehoeft (1992, p. 82) consider that it is ". . . naive to believe that we will somehow validate a computer model so that it will make accurate predictions of system responses far into the future. . . ." They note, however, that models ". . . provide a tool for critical analysis. They are a means to organize our thinking, test ideas for their reasonableness, and indicate which are the sensitive parameters. They point the way for further investigation. . . They serve to sharpen our professional judgement. In the end, action concerning waste disposal will be a judgement; a professional judgement by the scientific community and a judgement by society. . . ."

I-6 REFERENCES

Cooley, R.L., "A Method of Estimating Parameters and Assessing Reliability for Models of Steady State Groundwater Flow, 1—Theory and Numerical Properties," *Water Resources Research*, 13:318–324 [1977].

Cooley, R.L., "A Method of Estimating Parameters and Assessing Reliability for Models of Steady State Groundwater Flow, 2—Application of Statistical Analysis," *Water Resources Research*, 15:603–617 [1979].

Cooley, R.L., "Incorporation of Prior Information on Parameters into Nonlinear Regression Groundwater Flow Models, 1—Theory," *Water Resources Research*, 18:965–976 [1982].

Czarnecki, J.B., "Simulated Effects of Increased Recharge on the Ground-Water Flow System of Yucca Mountain and Vicinity, Nevada-California," U.S. Geological Survey, Water-Resources Investigations Report, WRI–84–4344, 1985.

Czarnecki, J.B., "Should the Furnace Creek Ranch-Franklin Lake Playa Ground-Water Subbasin Simply be the Franklin Lake Playa Ground-Water Subbasin? [Abstract]," *EOS Transactions*, American Geophysical Union, 68:1292 [1987].

Czarnecki, J.B., "Characterization of the Subregional Ground-Water Flow system at Yucca Mountain and Vicinity, Nevada-California," *Radioactive Waste Management and the Nuclear Fuel Cycle*, 13:51–61 [1989].

Czarnecki, J.B., "Preliminary Simulations Related to a Large Horizontal Hydraulic Gradient at the North End of Yucca Mountain, Nevada [Abstract]," American Institute of Hydrology, *1990 Spring Meeting: Abstracts with Program [Topic: Minimizing Risk to the Hydrologic Environment]*, March 12–16, 1990, Las Vegas, Nevada, p. 18, 1990.

Czarnecki, J.B., "Geohydrology and Evapotranspiration at Franklin Lake Playa, Inyo County, California," U.S. Geological Survey, Open-File Report 90–356, 1990b.

Czarnecki, J.B., "Simulated Water-Level Declines Caused by Withdrawals from Wells J-13 and J-12 Near Yucca Mountain, Nevada," U.S. Geological Survey, Open-File Report 91–478, 1992.

Czarnecki, J.B. and R.K. Waddell, "Finite-Element Simulation of Ground-Water Flow in the

Vicinity of Yucca Mountain, Nevada-California," U.S. Geological Survey, Water-Resources Investigations Report, WRI-84-4349, 1984.

Czarnecki, J.B. and E. E. Wilson, "Site Characterization and Conceptual Models of the Regional Ground-Water Flow System, Yucca Mountain and Vicinity, Nevada-California [Abstract]," in Post, R.G. (ed.), *Waste Management '89: Proceedings of the Symposium on Waste Management*, February 26–March 2, 1989, Tucson, Arizona, 1:473 [1989].

Downey, J.S., K.E. Kolm, and E.D. Gutentag, "Selection of Geohydrologic Boundaries for Ground-Water Flow Models, Yucca Mountain, Nevada," in Post, R.G. (ed.), *Waste Management '90: Proceedings of the Symposium on Waste Management*, February 26–March 1, 1990, Tucson, Arizona, 2:725–734 [1990].

Eakin, T.E., *et al.*, "Contributions to the Hydrology of Eastern Nevada," Nevada Department of Conservation and Natural Resources, Water Resources Bulletin 12, 1951.

Konikow, L.F. and J.D. Bredehoeft, "Ground-Water Models Cannot Be Validated," *Advances in Water Resources*, 15:75–83 [1992].

Marshall, B.D., Z.E. Peterman, and J.S. Stuckless, "Strontium Isotopic Evidence for a Higher Water Table at Yucca Mountain," American Nuclear Society/American Society of Civil Engineers, *Proceedings of the Fourth Annual International Conference: High-Level Radioactive Waste Management*, April 26–30, 1993, Las Vegas, Nevada, 2:1948–1952 [1993].

McDonald, M.G., and Harbaugh, A.W., "A Modular Three-Dimensional Finite Difference Ground-Water Flow Model: Techniques of Water Resources Investigations of the U.S. Geological Survey," U.S. Geological Survey, Book 6, Chapter A1, 1988.

National Research Council, "Ground Water at Yucca Mountain: How High Can it Rise?—Final Report of the Panel on Coupled Hydrologic Tectonic/Hydrothermal Systems at Yucca Mountain: Board on Radioactive Waste Management; Commission on Geosciences, Environment, and Resources," Washington, D.C., National Academy Press, April 1992.

Oatfield, W.J. and J.B. Czarnecki, "Hydrogeologic Inferences from Drillers' Logs and from Gravity and Resistivity Surveys in the Amargosa Desert, Southern Nevada," U.S. Geological Survey, Open-File Report 89–234, 1989.

O'Brien, G.M. and P. Tucci, "Earthquake-Induced Water-Level and Fluid-Pressure Fluctuations of Yucca Mountain, Nevada [Abstract]," *EOS Transactions*, American Geophysical Union, 73:157 [1992].

Quade, J., *et al.*, "Fossil Spring Deposits in the Southern Great Basin and Their Implications for Changes in Water-Table Levels near Yucca Mountain, Nevada, During Quaternary Time," *Geological Society of America Bulletin*, 107(2):213–230 [1995].

Rice, W.A., "Preliminary Two-Dimensional Regional Hydrologic Model of the Nevada Test Site and Vicinity," Albuquerque, New Mexico, Sandia National Laboratories, SAND83-7466, 1984. [Prepared by Pacific Northwest Laboratory, Richland, Washington.]

Roache, P.J., *Computational Fluid Dynamics*, Albuquerque, New Mexico, Hermosa Publishers, 1973.

Rush, F.E., "Regional Ground-water Systems in the Nevada Test Site Area, Nye, Lincoln, and Clark Counties, Nevada," Nevada Department of Conservation and Natural Resources Water Resources Reconnaissance Series Report 54, 1970.

Shelor, D.E., U.S. Department of Energy/Office of Civilian Radioactive Waste Management, Letter to J.J. Holonich, U.S. Nuclear Regulatory Commission/Division of High-Level Waste Management [Subject: "DOE response to NRC's Phase II Review of Study Plan 8.3.1.2.1.4 ("Regional Hydrologic System Synthesis and Modeling")], August 30, 1993.

Szymanski, J.S., "Conceptual Considerations of the Yucca Mountain Groundwater System with Special Emphasis on the Adequacy of this System to Accommodate a High-Level Nuclear Waste Repository," U.S. Department of Energy, Nevada Operations Office, Yucca Mountain Project Office, Las Vegas, Nevada, July 26, 1989.

Spaulding, W.G., "Paleohydrologic Investigations in the Vicinity of Yucca Mountain: Late Quaternary Paleobotanical and Palynological Records," State of Nevada, Agency for Nuclear Projects/Nuclear Waste Project Office, Report No. NWPO-TR-022-94, October 1994.

Thordarson, W., "Geohydrologic Data and Test Results from Well J-13, Nevada Test Site, Nye County, Nevada," U.S. Geological Survey, Water-Resources Investigations Report, WRI-83-4171, 1983.

Thordarson, W. and B.P. Robinson, "Wells and Springs in California and Nevada Within 100 Miles of the Point 37 Deg. 15 Min. N., 116 Deg. 25 Min. W., on Nevada Test Site," U.S. Geological Survey, USGS-474-85, 1971.

Torak, L.J., "A Modular Finite-Element Model (MODFE) for Areal and Axisymmetric Ground-Water Flow-Problems, Part 1: Model Description and User's Manual," U.S. Geological Survey, Open-File Report 90-194, 1992a.

Torak, L.J., "A Modular Finite-Element Model (MODFE) for Areal and Axisymmetric Ground-Water-Flow Problems, Part 3: Design Philosophy and Programming Details," U.S. Geological Survey, Open-File Report 91-471, 1992b.

U.S. Department of Energy, "Site Characterization Plan, Yucca Mountain Site, Nevada Research and Development Area, Nevada," Office of Civilian Radioactive Waste Management, Nevada, DOE/RW-0199, 9 vols., December 1988.

U.S. Department of Energy, "Characterization of the Site Saturated-Zone Ground-Water Flow System (Revision 0)" Office of Civilian Radioactive Waste Management, Study Plan 8.3.1.2.3.1.1-6, May 1990a. [Prepared by the U.S. Geological Survey.]

U.S. Department of Energy, "Characterization of the Yucca Mountain Regional Ground-Water Flow System (Revision 0)" Office of Civilian Radioactive Waste Management, Study Plan 8.3.1.2.1.3, September 1990b. [Prepared by the U.S. Geological Survey.]

U.S. Department of Energy, "Regional Hydrologic Synthesis and Modeling (Revision 0)" Office of Civilian Radioactive Waste Management, Study Plan 8.3.1.2.1.4, July 1991. [Prepared by the U.S. Geological Survey.]

U.S. Nuclear Regulatory Commission, "NRC Staff Site Characterization Analysis of the Department of Energy's Site Characterization Plan, Yucca Mountain Site, Nevada," Office of Nuclear Material Safety and Safeguards, NUREG-1347, August 1989.

Waddell, R.K., "Two-Dimensional, Steady-State Model of Ground-Water Flow, Nevada Test Site and Vicinity, Nevada-California," U.S. Geological Survey, Water Resources Investigations Report, WRI-82-4085, 1982.

Walker, G.E. and T.E. Eakin, "Geology and Ground Water of Amargosa Desert, Nevada-California," U.S. Geological Survey, Ground-Water Resources-Reconnaissance Series, Report 14, 1963.

Winograd I.J. and W. Thordarson, "Hydrogeologic and Hydrochemical Framework, SouthCentral Great Basin, Nevada-California, with Special Reference to the Nevada Test Site (Hydrology of Nuclear Test Sites)," U.S. Geological Survey Professional Paper 712-C, 1975.

APPENDIX J
MODELING SATURATED ZONE FLOW TO THE ACCESSIBLE ENVIRONMENT

J-1 INTRODUCTION

In the development of the ground-water flow and transport module, several different modeling approaches were attempted. One of the approaches used *DCM3D*, a **D**ual-**C**ontinuum, **T**hree[**3**]-**D**imensional, ground-water flow code for unsaturated, fractured, porous media (Updegraff *et al.*, 1991). Using this code, a one-dimensional saturated zone flow model was built from a Yucca Mountain site geologic cross-section. The cross-section ran in a southeast direction from Well H-4 to Well J-13 (Figures J-1 and J-2) and was built using stratigraphic data and water-level data from Wells H-4, UE25p#1, and J-13 (Thordarson, 1983; Whitfield *et al.*; 1984, Craig and Robinson, 1984; DOE, 1988; and Czarnecki *et al.*, 1984). It should be noted that Well H-4 is located at the proposed repository boundary and Well J-13 is near the presently defined "accessible environment boundary" (10 CFR 60.2). This means the cross-section passes through that portion of the saturated zone simulated by the performance assessment flow module.

J-2 DISCUSSION

Water levels and stratigraphic changes along the surface of the water table were used to construct a one-dimensional model of ground-water flow. In building the model, some changes from the cross-section were made. The cross-section covers a length of 5582.1 meters, whereas the model covers a length of 5000 meters. Furthermore, the head elevation at well H-4 is 730.1 meters mean seal level (msl) and at J-13, 728.1 meters msl. In the model, head elevations at well H-4 were set at 730 meters msl and at the other end of the model (5000 meters), head elevations were set at 728 meters msl. At the time, these changes were made for ease of input, with the result that model output could come close, but could never duplicate actual head elevations.

Saturated hydraulic conductivity and porosity values were varied, whereas, head values at both boundaries were fixed. A constant head boundary of 730 meters msl was assigned to the upgradient end and 728 meters to the down gradient end. Calico Hills nonwelded zeolitized unit properties were assigned from the up gradient end to 2310 meters and Topopah Spring welded unit properties were assigned from 2310 meters to the down gradient end at 5000 meters.

Saturated hydraulic conductivity and porosity data for the Calico Hills and Topopah Spring units were obtained from a variety of sources. Table J-1 contains saturated hydraulic conductivity and porosity inputs used in the runs. Run No. 1 used average matrix and porosity values and Run No. 2 used maximum matrix values. Run No. 3 used minimum bulk fracture properties and Run No. 4 used maximum bulk fracture properties. Properties for Run Nos. 1, 2, 3, and 4 were obtained from Peters *et al.* (1984), Ababou (1991), Barnard *et al.* (1991), and Dudley *et al.* (1988). These runs reflect the hydrologic parameters of the Calico Hills and Topopah Spring units used in the iterative performance assessment simulations.

Run No. 5 was constructed using average values from Yucca Mountain well tests (Lahoud *et al.*, 1984; Montazer *et al.*, 1988; and Thordarson, 1983). This run illustrates how saturated zone data may be used to help characterize the unsaturated zone (or vice versa). At Yucca Mountain, it may be difficult to determine bulk fracture saturated hydraulic conductivities in the unsaturated zone. However, within a few kilometers of the site, rock units in the Yucca Mountain unsaturated zone dip below the water table. If it is assumed that saturated hydraulic conductivities determined from well tests are representative of bulk fracture saturated hydraulic conductivities, well test data may be used to help determine parameters useful in unsaturated zone modeling.

At this time, well test data from the site are limited. Therefore, Run No. 5 used average saturated hydraulic conductivity values from just five wells; with two wells (J-13 and UE-25b#1), supplying much of the data. Furthermore, because porosity data were not available, the same

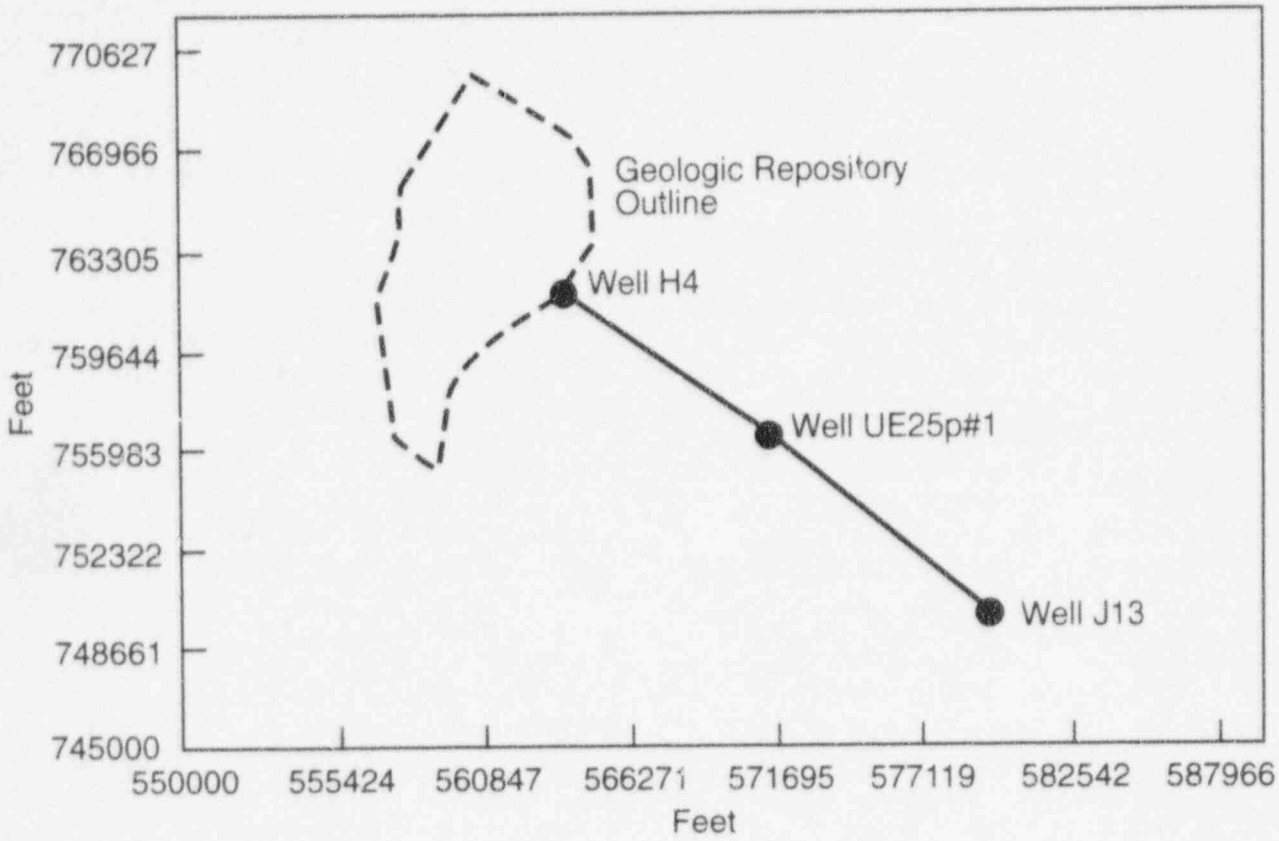

Figure J-1 Location of geologic cross-section used to construct one-dimensional *DCM3D* saturated flow simulations

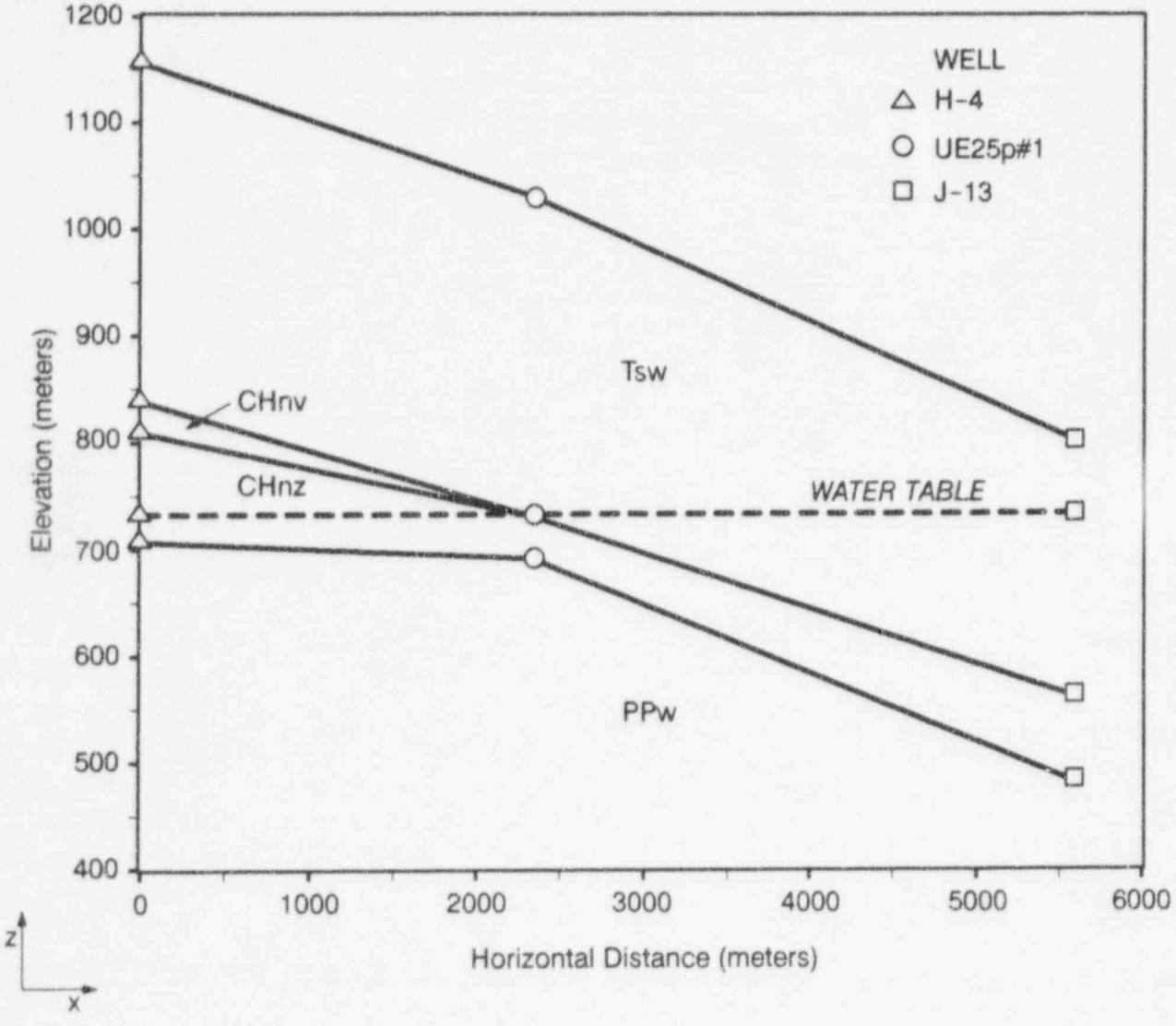

Figure J-2 Geologic cross-section based on Wells H-4, UE25p#1, and J-13

Table J-1 Input Data for *DCM3D* One-Dimensional Simulations

		Topopah Spring		*Calico Hills*	
Run No.	*Description*	*Ksat (m/yr)*	*Porosity*	*Ksat (m/yr)*	*Porosity*
1	Average matrix	6.0×10^{-4}	0.11	6.0×10^{-4}	0.28
2	Maximum matrix	6.0×10^{-2}	0.11	6.0×10^{-2}	0.28
3	Minimum fracture	3.0×10^{-4}	0.000021	3.0×10^{-3}	0.000046
4	Maximum fracture	3.0×10^{0}	0.000041	3.0×10^{0}	0.000046
5	From well tests	2.8×10^{2}	0.000041	2.0×10^{1}	0.000046

porosity values as Run Nos. 3 and 4 were used in Run No. 5.

Each simulation was run until it approached steady-state conditions. Table J-2 contains output from these runs. Output is presented in the form of average Darcy velocity, average seepage velocity, and flow time from one end of the simulation to the other (calculated from the seepage velocities).

J-3 SUMMARY OBSERVATIONS/ CONCLUSIONS FROM RUNS

A number of interesting observations can be made from these runs:

(1) The slowest velocities and longest flow times were obtained from runs that used matrix properties. Seepage velocities were 1.3×10^{-6} and 1.6×10^{-5} meters/year, resulting in extremely long calculated flow times of 3180 million years and 31.7 million years. This indicates that in this model, matrix flow cannot readily transport radionuclides from the site.

(2) The fastest velocities and shortest flow times were obtained from runs that used hydrologic properties from well tests. The average seepage velocity was 473 meters/year and the calculated flow time was 10.6 years.

(3) Run No. 3 was constructed using minimum fracture flow properties with saturated hydraulic conductivities as low as the matrix property runs (Run Nos. 1 and 2). However, Run No. 3 produced faster flow velocities and shorter flow times than the matrix property runs, because of the small porosity values used in the Run No. 3 simulation. Since porosity values used in all the fracture property runs were hypothetically determined, they illustrate the importance of porosity in flow velocity calculations and the need to determine representative bulk fracture porosities during site characterization.

A plot of hydraulic heads for each of the runs was prepared to compare the results from each simulation to the cross-section water levels (see Figure J-3). The cross-section water table illustrates the low head gradient over this distance (2 meters). A change in the head gradient occurs at 2310 meters, which is where the hydrogeologic stratigraphy in the cross-section changes from the Calico Hills unit to the Topopah Spring unit. Run No. 3, using minimum bulk fracture values, produced the best match in heads. The staff recognizes that a match between predicted and actual heads does not prove that a model is correct. However, it does provide added confidence that the range of iterative performance assessment hydraulic conductivity values may be conservative (produce fast flow rates).

J-4 REFERENCES

Ababou, A.C., "Approaches to Large Scale Unsaturated Flow in Heterogenous, Stratified, and Fractured Geologic Media," U.S. Nuclear Regulatory Commission, NUREG/CR-5743,

Table J-2 Output Data for *DCM3D* One-Dimensional Simulations

Run No.	*Description*	*Average Darcy Velocity (m/yr)*	*Average Seepage Velocity (m/yr)*	*Flow Time (yrs)*
1	Average matrix	2.4×10^{-7}	1.3×10^{-6}	3.81×10^{9}
2	Maximum matrix	4.0×10^{-5}	1.6×10^{-5}	3.17×10^{7}
3	Minimum fracture	2.1×10^{-7}	4.8×10^{-3}	1.05×10^{6}
4	Maximum fracture	2.3×10^{-3}	54	92.4
5	From well tests	2.0×10^{-2}	473	10.6

August 1991. [Prepared by the Center for Nuclear Waste Regulatory Analyses.]

Barnard, R.W., *et al*, "Technical Summary of the Performance Assessment Calculational Exercises for 1990 (PACE-90)—Volume 1: 'Nominal Configuration' Hydrogeologic Parameters and Calculational Results," Albuquerque, New Mexico, Sandia National Laboratories, SAND90-2726, June 1991. [Prepared for the U.S. Department of Energy.]

Craig, R.W. and Robison, J.H., "Geohydrology of Rocks Penetrated by Test Well UE-25p#1, Yucca Mountain Area, Nye County, Nevada," U.S. Geological Survey, Water Resources Investigations Report, WRI-34-4248, 1984.

Czarnecki, J.B., *et al.*, "Finite-Element Simulation of Ground-Water Flow in the Vicinity of Yucca Mountain, Nevada-California," U.S. Geological Survey, Water Resources Investigations Report, WRI-84-4349, 1984.

Dudley, A.L., *et al.*, "Total System Performance Assessment Code (TOSPAC)", Volume 1, "Physical and Mathematical Bases, Sandia National Laboratories," Albuquerque, New Mexico, Sandia National Laboratories, SAND85-0002, December 1988. [Prepared for the U.S. Department of Energy.]

Lahoud, D.H., *et al.*, "Geohydrology of Volcanic Tuff Penetrated by Test Well UE-25b#1, Yucca Mountain, Nye County, Nevada," U.S. Geological Survey, Water Resources Investigations Report, WRI-84-4253, 1984.

Montazer, P., *et al.*, "Monitoring the Vadose Zone in Fractured Tuff," *Ground Water Monitoring Review*, 8(2):72-78 [Spring 1988].

Peters, R.R., *et al.*, "Fracture and Matrix Hydrologic Characteristics of Tuffaceous Materials from Yucca Mountain, Nye County, Nevada," Albuquerque, New Mexico, Sandia National Laboratories, SAND84-1471, December 1984.

Thordarson, W., "Geohydrologic Data and Test Results From Well J-13, Nevada Test Site, Nye County, Nevada," U.S. Geological Survey, Water Resources Investigations Report, WRI-83-4171, 1983.

U.S. Department of Energy, "Site Characterization Plan Overview, Yucca Mountain Site, Nevada Research and Development Area, Nevada," Office of Civilian Radioactive Waste Management, DOE/RW-0198, 9 vols., December 1988.

Updegraff, C.D., *et al.*, "DCM3D, A Dual-Continuum, Three-Dimensional, Ground-Water Flow Code for Unsaturated, Fractured, Porous Media," U.S. Nuclear Regulatory Commission, NUREG/CR-5536, February 1991. [Prepared by the Sandia National Laboratories.]

Whitfield, M.S., *et al.*, "Geohydrologic and Drill-Hole Data for Test Well USW H-4, Yucca Mountain, Nye County, Nevada," U.S. Geological Survey, Open File Report 84-449, 1984.

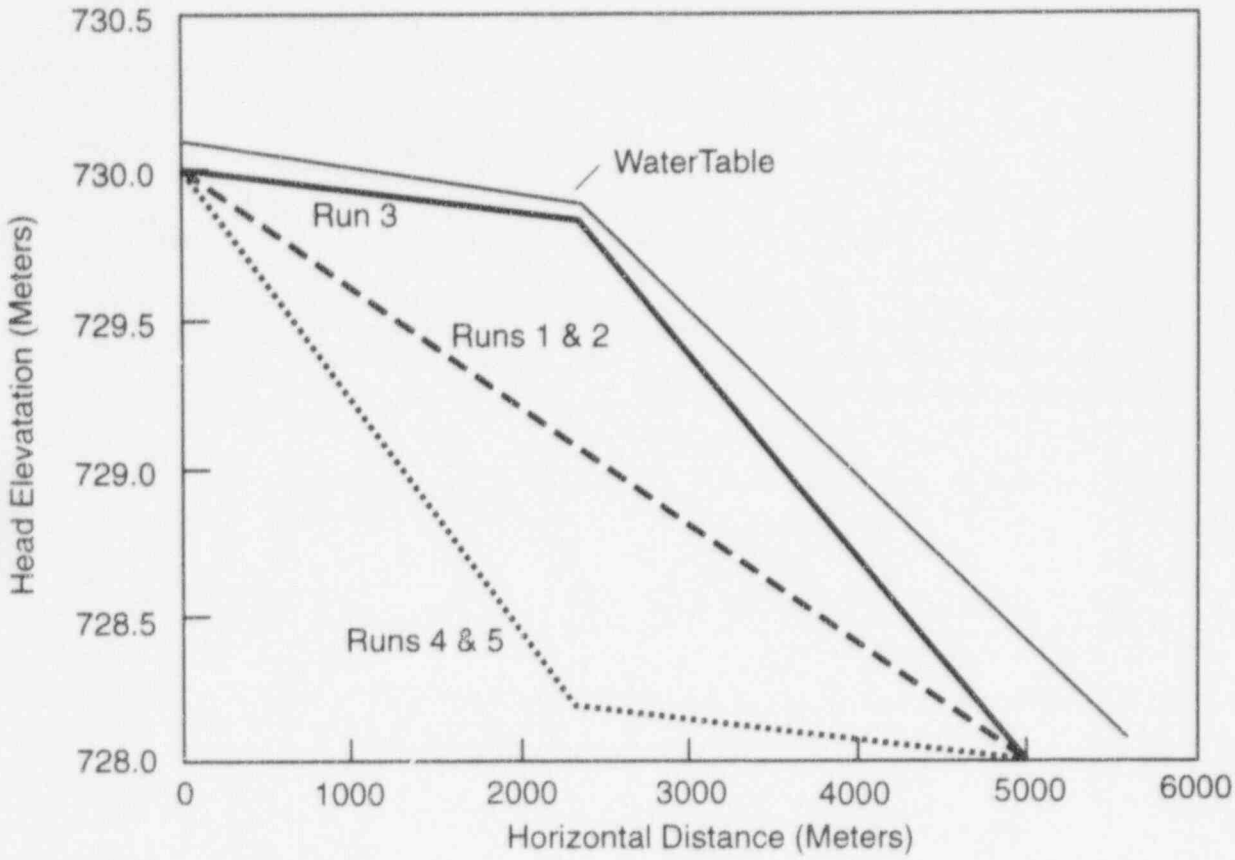

Figure J-3 Plot of water table and computer run head elevations

APPENDIX K
GEOCHEMICAL MODEL FOR ^{14}C TRANSPORT IN UNSATURATED ROCK

K-1 INTRODUCTION

Under oxidizing conditions in a geologic repository, ^{14}C in high-level radioactive waste might be released as $^{14}CO_2$ (Light *et al.*, 1990). Any such gas escaping the engineered barrier will be incorporated in the existing carbon system of the geosphere, and be transported along with gaseous and dissolved carbon. Several recent studies addressed ^{14}C gaseous transport at the Yucca Mountain repository environment using simplified models of geochemical retardation (Ampter and Ross, 1990; Light *et al.*, 1990; and Knapp, 1990). Accurate modeling of ^{14}C transport requires coupling of relations between the source, heat flow, two-phase fluid flow, and the distribution of chemical species among solid *(s)*, liquid *(l)*, and gas *(g)* phases (Codell and Murphy, 1992). Interphase exchange of carbon could result in a significant retardation of released ^{14}C, thereby delaying its arrival at the accessible environment. This auxiliary analysis reports on a mechanistic model for the geochemical interaction of ^{14}C for a geologic repository in partially saturated rock.

The ^{14}C transport model consists of three parts:

(1) A geochemical model describing the state of all carbon species in a representative volume of rock;

(2) A flow and transport model for movement of total carbon through the system which consists of a number of connected volumes or "cells"; and

(3) A model of ^{14}C migration as a trace quantity in the general movement of total carbon.

K-2 GEOCHEMICAL MODEL

A carbon system geochemical model which incorporates all reactions of primary significance to ^{14}C transport in unsaturated fractured rock can be based on local chemical equilibrium and mass and charge conservation in a representative volume. Chemical reactions in the model comprise carbonate equilibria among aqueous *(aq)* species, dissociation of water, vapor-liquid equilibria for CO_2 and H_2O, and calcite dissolution and precipitation. In addition to the aqueous species in these equilibria, the present model includes Na^+ to represent other aqueous cations. The reactions represented in the present model are given next:

$$H_2O(l) + CO_2(aq) \leftrightarrows H^+ + HCO_3^- \quad \textbf{(K-1)}$$

$$HCO_3^- \leftrightarrows H^+ + HCO_3^{2-} \quad \textbf{(K-2)}$$

$$H^+ + OH^- \leftrightarrows H_2O \quad \textbf{(K-3)}$$

$$CaCO_3(s) + H^+ \leftrightarrows Ca^{2+} + HCO_3^- \quad \textbf{(K-4)}$$

$$CO_2(g) = CO_2(aq) \quad \textbf{(K-5)}$$

Local charge balance in the model aqueous phase is represented by equating sums of aqueous cation and anion equivalents. Local mass conservations for carbon and calcium are maintained within each cell, and the mass of sodium is conserved in the aqueous phase.

Given the total masses of C, Ca and other species, mass of water, and the temperature, pore volume and pressure of each cell, the above relationships lead to a set of nonlinear algebraic equations that are solved simultaneously to characterize local equilibrium in each cell for each time step. Equilibrium constants for reactions 1 to 5 are functions of temperature only at one bar pressure. Activity coefficients are functions of ionic strength, and are generated from an extended Debye-Hückel equation. Calcite is permitted to precipitate or dissolve at equilibrium, and the model solution is undersaturated with respect to calcite in its absence. The partial pressure of CO_2 is calculated from the activity of aqueous CO_2, assuming ideal gas relations.

K–3 TOTAL CARBON TRANSPORT MODEL

The calculation of transport of total carbon through the modeled system is performed by sequential iteration in the following steps:

(1) Local chemical equilibrium is calculated in each cell at time t, using the geochemical model;

(2) Inputs and outputs to each cell are determined from an independent flow model for the next time step $t + \Delta t$. In the present model, only advective transport by gaseous flow is allowed. Therefore, the input of CO_2 to a cell is determined only by the partial pressure of CO_2 in the previous cell or upstream boundary and the flow of the transporting gas from that cell. Gaseous flow and condensation/evaporation of water are accounted for independently as part of the flow model and input to the chemical model; and

(3) Mass distributions are revised in the cells for time step $t + \Delta t$, using the geochemical model with updated temperature and liquid saturation states.

The carbon transport algorithm in the preceding steps simulates changes to the chemistry of each phase in the system, as a function of time and space. The carbon transport model determines the quantities of CO_2 gas moving through the system of cells, as well as the exchange rates of carbon between the various phases.

K–4 ^{14}C TRANSPORT MODEL

The ^{14}C transport model uses the state and evolution of total carbon speciation to simulate transport of trace amounts of ^{14}C through the system. ^{14}C is assumed to behave exactly in proportion to the total carbon, with no isotopic fractionation. However, radioactive decay removes ^{14}C from the solid, liquid, and gas inventories. The model assumes ^{14}C enters the system as an instantaneous pulse within a specified cell. ^{14}C is removed from the liquid/gas phases if calcite precipitates from solution. It re-enters the system if previously contaminated calcite dissolves. The model assumes that calcite dissolves first from the ^{14}C-contaminated calcite inventory before uncontaminated calcite redissolves. The model further assumes that the ^{14}C is distributed homogeneously within the contaminated calcite of each cell.

K–5 EXAMPLE

The present geochemical transport model has been applied to simplified examples, to demonstrate the range of possible phenomena associated with the release and transport of $^{14}CO_2$ in unsaturated fractured rock. The model system is a one-dimensional column of 145 cells, represented in Figure K–1, with constant hydraulic properties and cross section, passing through the center of a hypothetical repository plane, which is located at cell 55. Water, gas, and relevant mineral chemistries, as well as the geothermal gradient that resemble those factors observed at Yucca Mountain, are provided as initial conditions. The system chosen for the example was simple, so as not to confound the results of the geochemical transport model with other phenomena. For example, gas is assumed to flow in the upward direction only, even though thermal-hydraulic simulations indicate an initially outward gas flow in all directions from a heated repository in unsaturated tuff (Nitao, 1990). Additionally, there is no transport of ^{14}C by water flow or diffusion in gas or water.

Time-dependent temperature and gas flow used in the present example were generated from two-dimensional (2–D) codes, developed by the U.S. Nuclear Regulatory Commission staff for predicting air flow through Yucca Mountain. The NRC models are similar to those developed by Ampter and Ross (1990). Temperature, represented in Figure K–2, was calculated from a 2–D thermal conduction model that included the geothermal gradient. Gas flux, shown in Figure K–3, varied with time, but was uniform through the one-dimensional column.

Liquid saturation is shown in Figure K–4. The temperature and gas flow models did not include water saturation explicitly. Therefore, an approximate empirical model for saturation of the column was derived from the results of simulations of two-phase thermally induced circulation near repositories in tuff. The empirical model

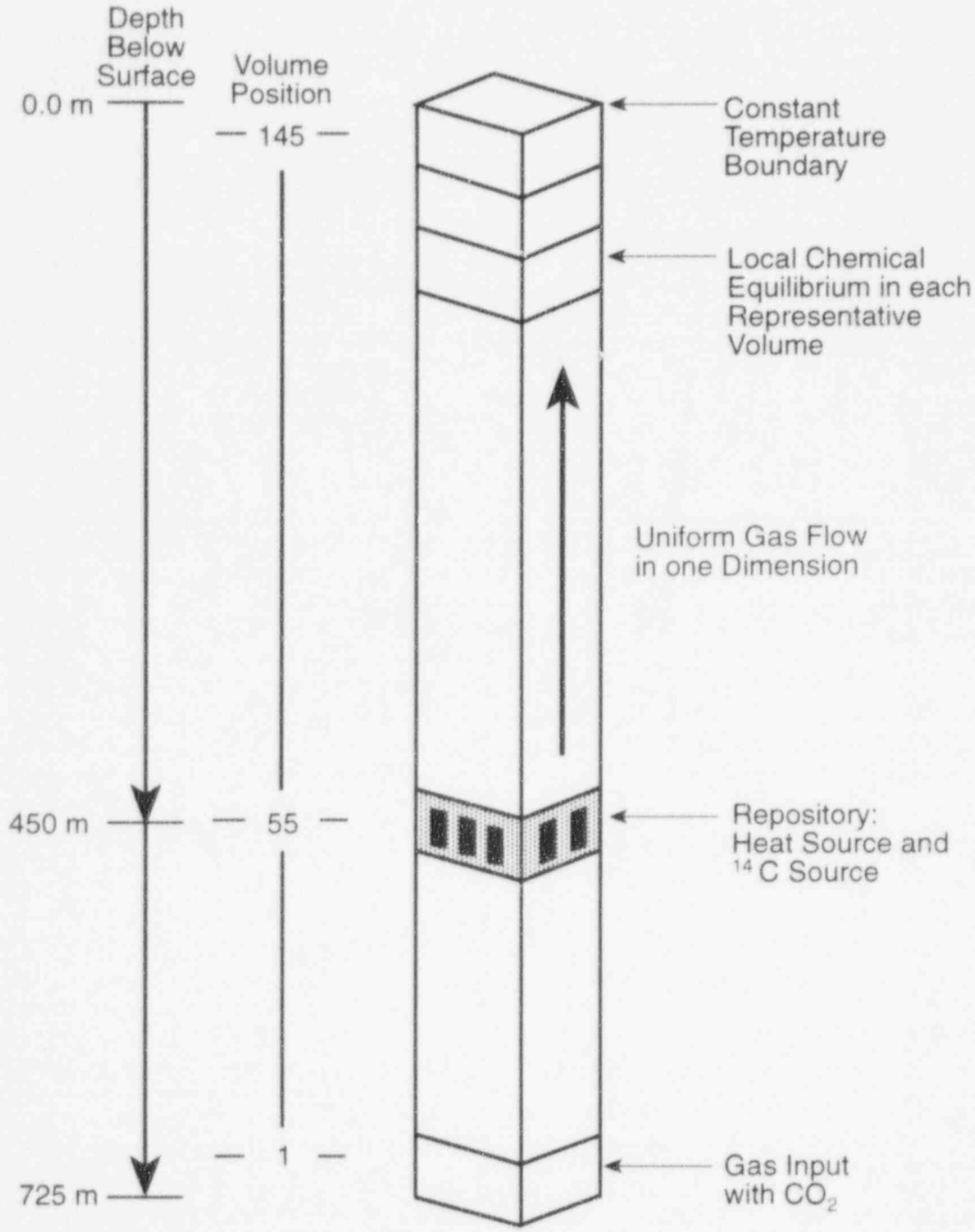

Figure K-1 One-dimensional flow and transport model

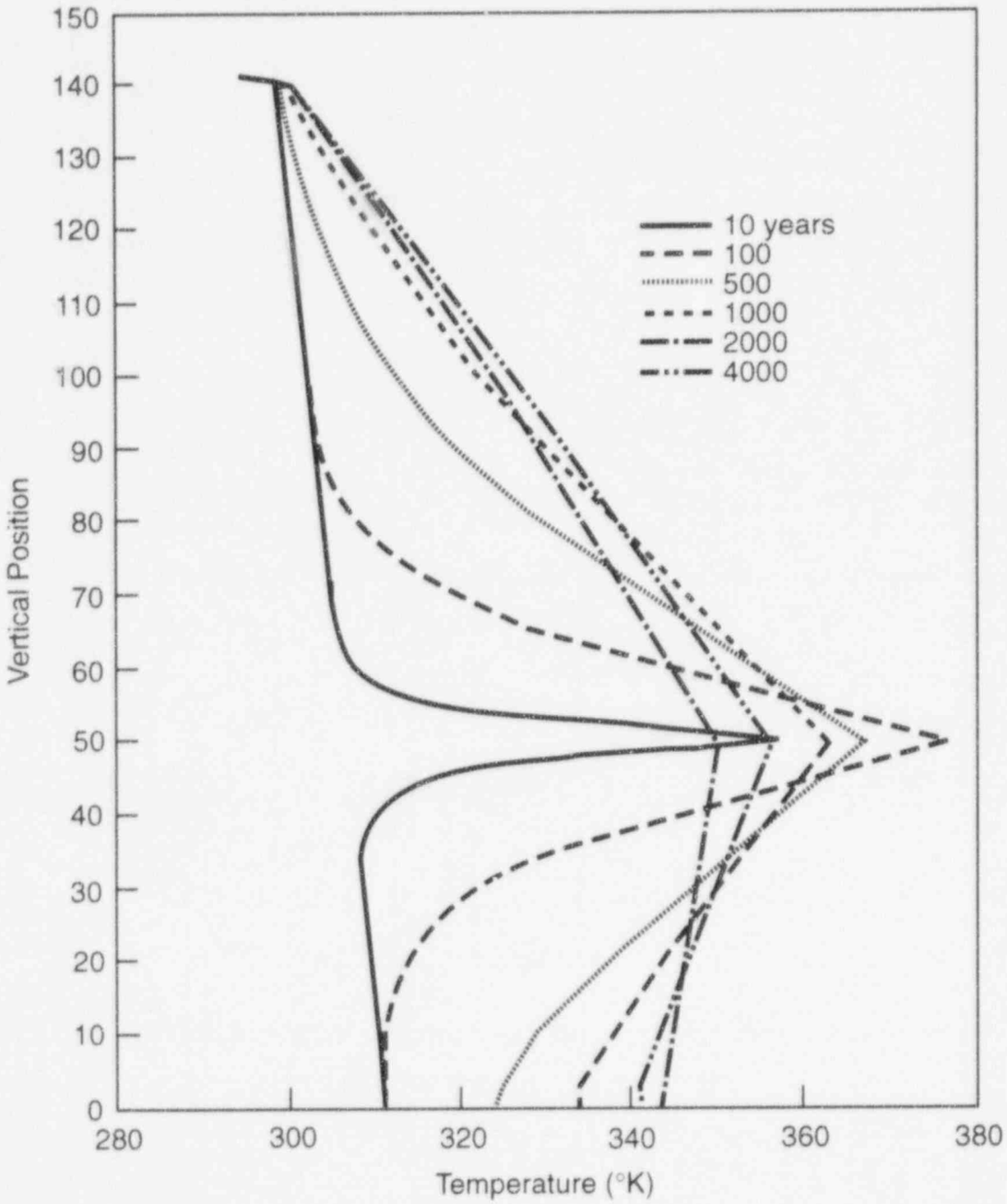

Figure K–2 Temperature in one-dimensional model as a function of time

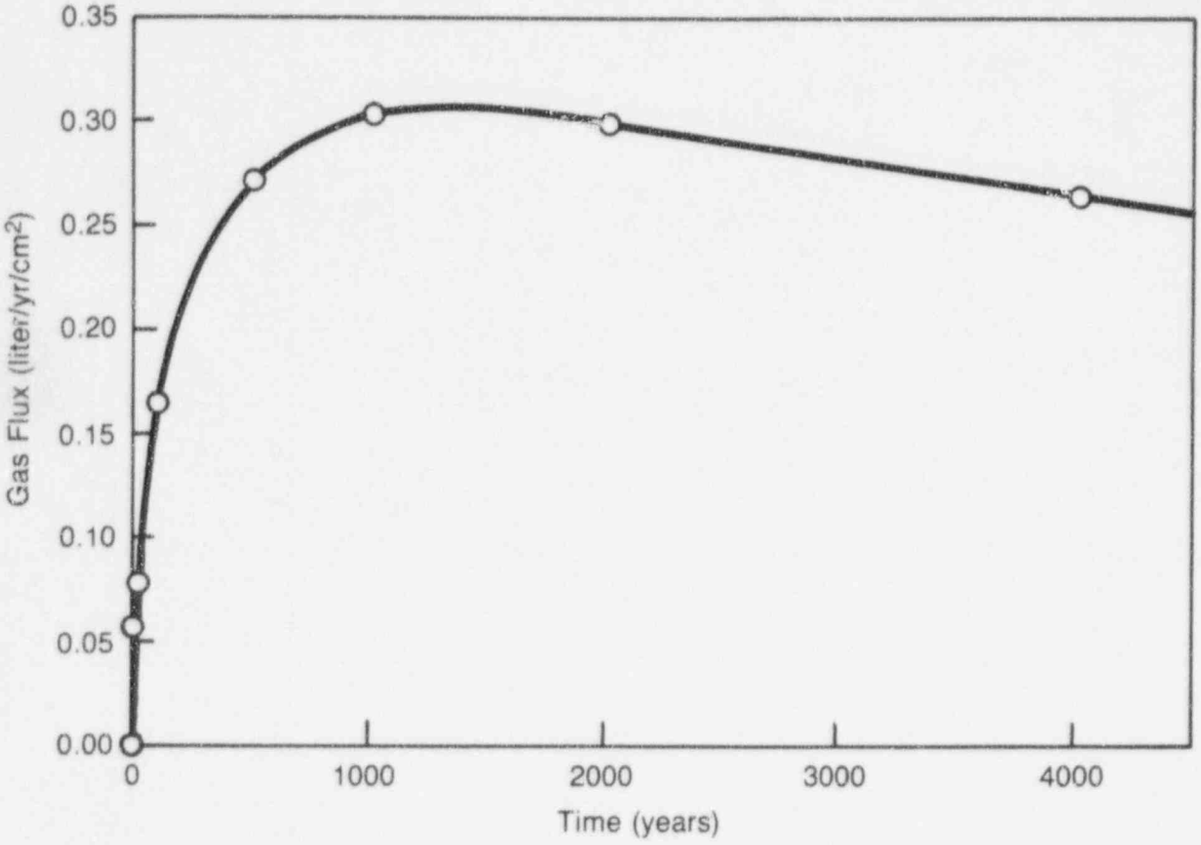

Figure K-3 Gas flux as function of time through column

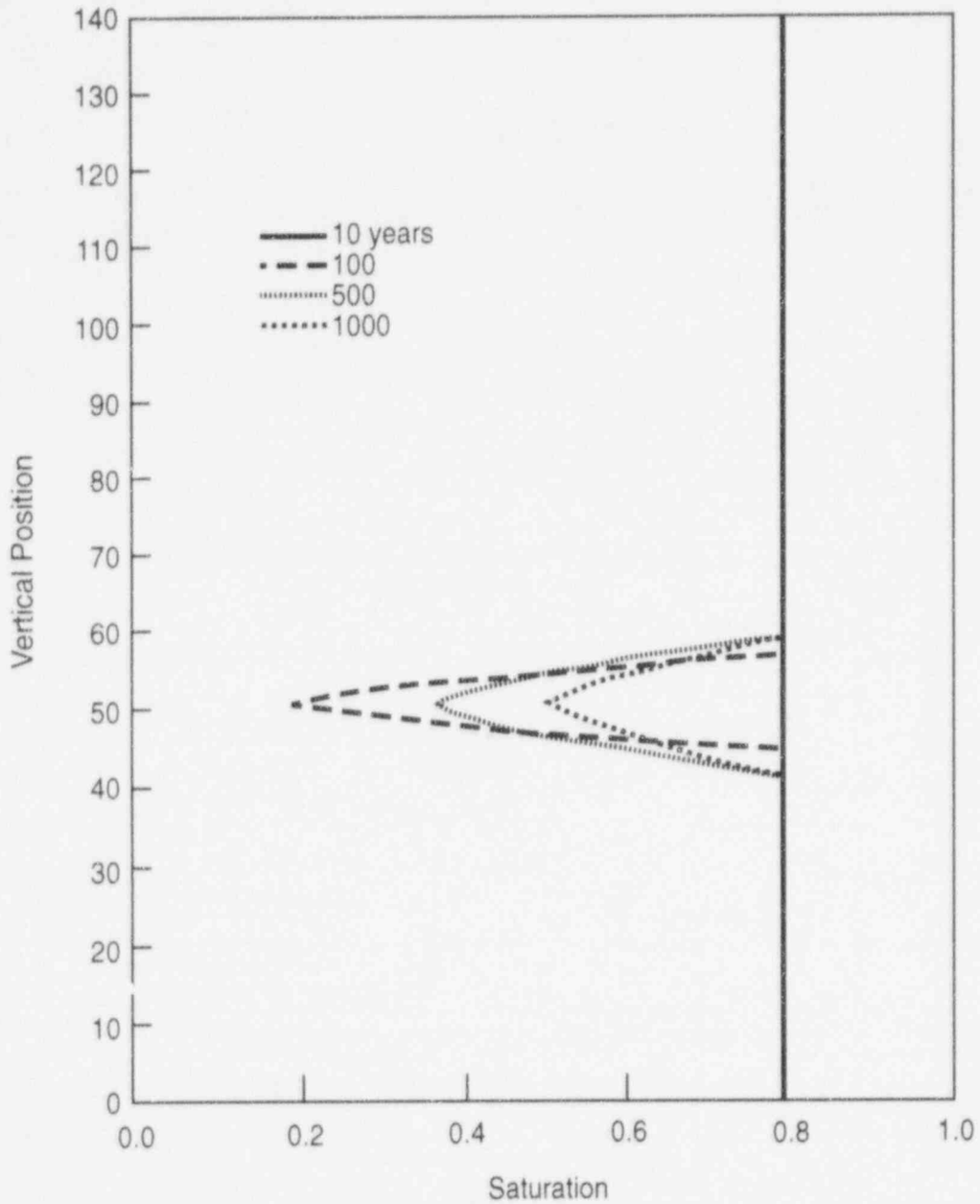

Figure K–4 Water saturation in column as function of time

used in the example predicts that water saturation is 80 percent except within a zone of about 50 meters above and below the repository for a period of less than 2000 years.

Other initial conditions and parameters of the example system are given in the Table K–1. These conditions lead to an initial solution with pH ≈ 7.2, moderately undersaturated with respect to calcite with the Q/K (saturation index/equilibrium constant) about 0.2, and partial pressures of CO_2 in the range 0.005 to 0.008 bar, depending on temperature.

Results for the Carbon Model: Results for the carbon transport model are given in Figure K–5, which shows the distribution of carbon for each cell among the gas, liquid, and solid phases for various times after repository closure. Initially, the carbon content decreases in the liquid phase and increases in the solid and gas phases near the repository level. Just above the repository, however, the carbon content of the gas and liquid phases increases, a reflection of gas transport of the pulse of CO_2 initially volatilized from the liquid near the repository and transported. Increasing temperature, decreasing solvent mass, and increasing pH because of CO_2 volatilization all promote calcite precipitation near the repository horizon.

At 500 years, the initially volatilized CO_2 pulse has been flushed out the top of the column. The calcite content continues to grow, spreading above and below the repository level, as temperature increases. At 2000 and 4000 years, the calcite progressively redissolves while the liquid content of carbon increases as the rock cools.

Results of ^{14}C Model: Figure K–6 shows the distribution of ^{14}C for each cell in the gas, liquid and solid phases, at various times for 10^{-6} curies of ^{14}C released 15 meters below the assumed repository plane at time zero. The ^{14}C was released below the repository plane to account for gas circulation expected near the repository, and allows interaction of the contaminant below as well as above the engineered barrier.

At 100 years, most of the ^{14}C has redistributed to the liquid phase. The liquid and gas inventories of ^{14}C have moved above the repository plane because of gas transport, even though the fraction of ^{14}C in the gas phase is small. The ^{14}C in the calcite remains fixed until calcite redissolves. At 500 years, the gas and liquid inventories of ^{14}C have moved further above the repository plane. Some of the calcite near the repository plane redissolves, releasing its ^{14}C inventory, which in turn is partially captured by precipitating calcite further from the repository plane, where temperature continues to increase.

Table K–1 Initial Conditions and Parameters

Parameter	*Value*
Cell Cross Section	12.5 cm^2
Cell Spacing	5 m
Cell Volume	6250 cm^3
Porosity	0.2
Initial Saturation	0.8
Initial C/cell	0.00202 moles
Na/cell	0.001 moles
Ca/cell	0.0004 moles
CO_2 Input Gas	2.53×10^{-4} moles/liter

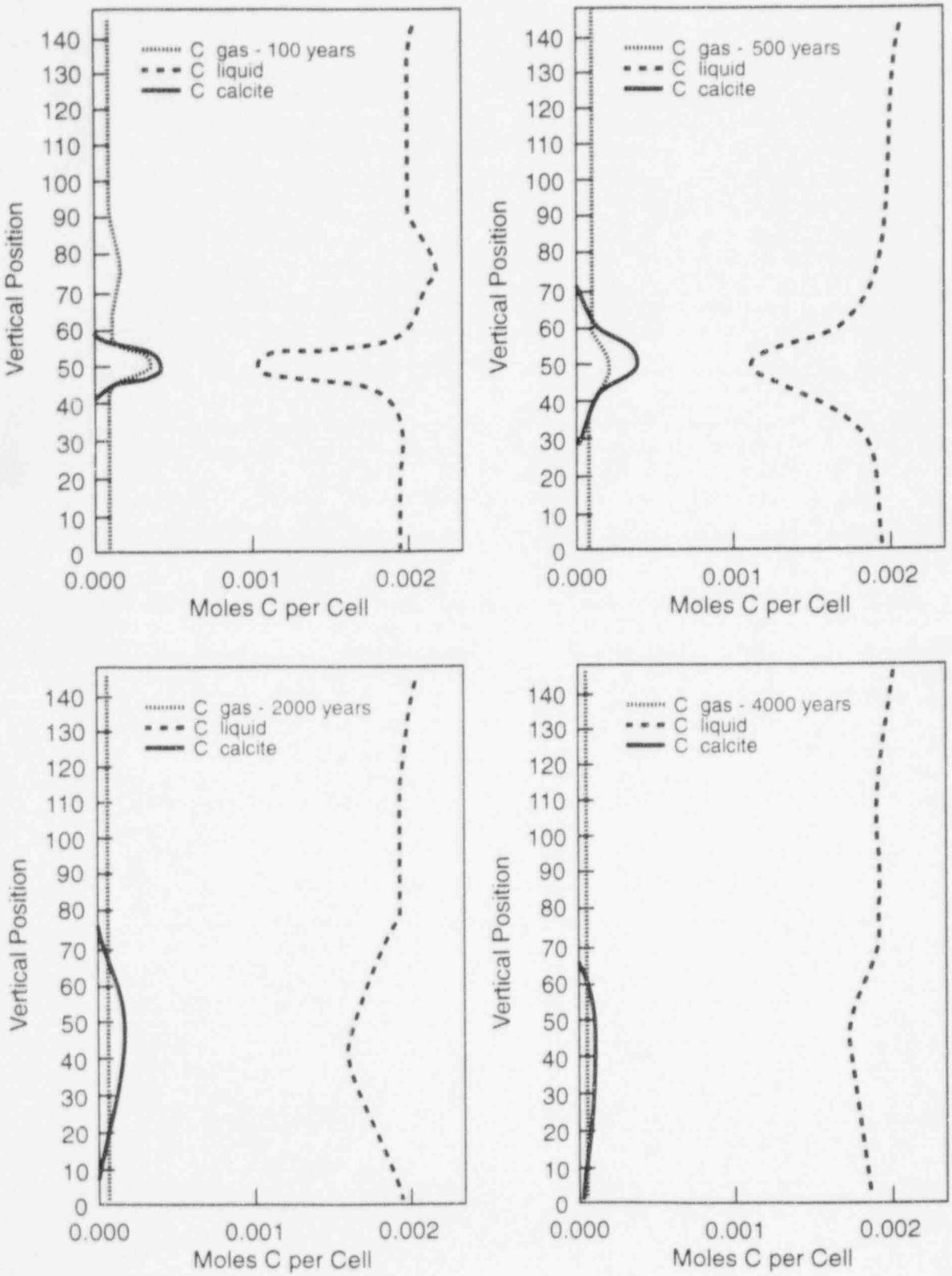

Figure K-5 Carbon content of gas, liquid and solid phases

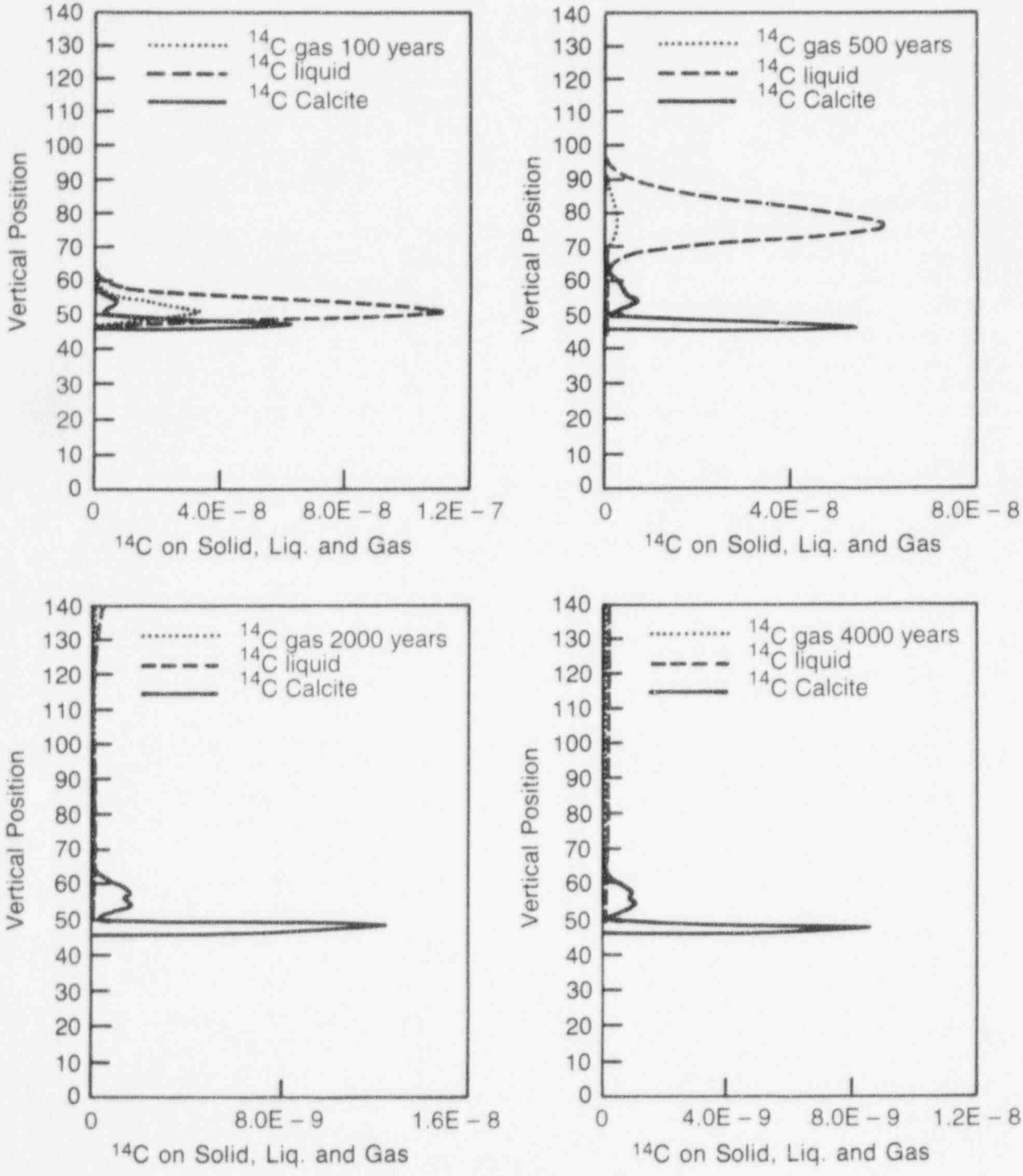

Figure K–6 ^{14}C content of gas, liquid and solid phases, with scale changes

By 2000 years, nearly all ^{14}C is swept from the column, except that which remains trapped in the calcite. At this point in time, calcite is redissolving everywhere, so the contaminated calcite acts as a long-term source of ^{14}C to the system. Some of this residual ^{14}C remains even at 4000 years.

Dependence on Time of Release: The model predicts that calcite starts to precipitate shortly after repository closure and then redissolves. Therefore, the timing of the release of ^{14}C from the waste is important to its ultimate fate. ^{14}C released after most calcite has precipitated will not be removed from the liquid and gas phases as effectively as ^{14}C released during the period of active calcite precipitation. Figure K–7 shows the cumulative release, over 1500 years after repository closure, of ^{14}C past several points in the column as a function of time of ^{14}C release. This figure demonstrates the interesting phenomenon that ^{14}C released at early times can arrive at the end of the column after ^{14}C released at later times.

K–6 CONCLUSIONS

Numerical experiments with a flow and transport model that includes coupled nonisothermal geochemistry provide insights into the behavior of ^{14}C in an unsaturated geologic repository for nuclear waste. These experiments have been applied to a system resembling the proposed repository at Yucca Mountain, Nevada. Model results show a significant redistribution of autochthonous carbon among solid, liquid, and gas phases, even in areas remote from the repository plane. Carbon remains predominantly in the aqueous solution, in spite of the fact that near-field heating results in a reduction of liquid saturation, abundant calcite precipitation, and increased equilibrium fractionation of CO_2 into the gas phase.

Transport of ^{14}C released from the repository is generally retarded by a factor of approximately 30 to 40, because of immobilization in the liquid phase. In addition, ^{14}C released early during the period of solid calcite precipitation can be fixed for a long period before repository cooling leads to redissolution of the calcite.

Although simplified, the model demonstrates the complex nature of the geochemical processes affecting ^{14}C release. Results of the simulation depend strongly on model assumptions, and retardation of ^{14}C in the liquid or solid phases could be greater or smaller under different conditions of chemistry, hydrology, temperature, or gas flow. The staff contemplate coupling geochemistry and carbon transport models with more realistic two-or-three-dimensional treatments of heat and mass transfer near a repository in unsaturated tuff, which would include transport in the gas and liquid phases and allow for molecular diffusion.

K–7 REFERENCES

Amter, S. and B. Ross, "Simulation of Gas Flow Beneath Yucca Mountain, Nevada, with a Model Based on Fresh Water Head," in Post, R.G. (ed.), *Waste Management '90: Proceedings of the Symposium on Waste Management*, February 25 – March 1, 1990, Tucson, Arizona, 2:915–925 [1990].

Codell, R.B. and W.M. Murphy, "Geochemical Model for ^{14}C Transport in Unsaturated Rock," American Nuclear Society/American Society of Civil Engineers, *Proceedings of the Third International Conference: High-Level Radioactive Waste Management*, April 12–16, 1992, Las Vegas, Nevada, 2:1959–1965 [1992].

Knapp, R.B., "An Approximate Calculation of Advective Gas-Phase Transport of ^{14}C at Yucca Mountain, Nevada", *Journal of Contaminant Hydrology*, 5:133–154 [1990].

Light, W.B., *et al.*, "Analytical Models for C–14 Transport in a Partially Saturated, Fractured, Porous Media," American Nuclear Society, *Proceedings of the Topical Meeting on Nuclear Waste Isolation in the Unsaturated Zone (FOCUS '89)*, September 17–21, 1989, Las Vegas, Nevada, pp. 271–277 [1990].

Nitao, J.J., "Numerical Modeling of the Thermal and Hydrological Environment Around a Nuclear Waste Package Using the Equivalent Continuum Approximation: Horizontal Emplacement," Livermore, California, Lawrence Livermore National Laboratory, UCID–21444, May 1990.

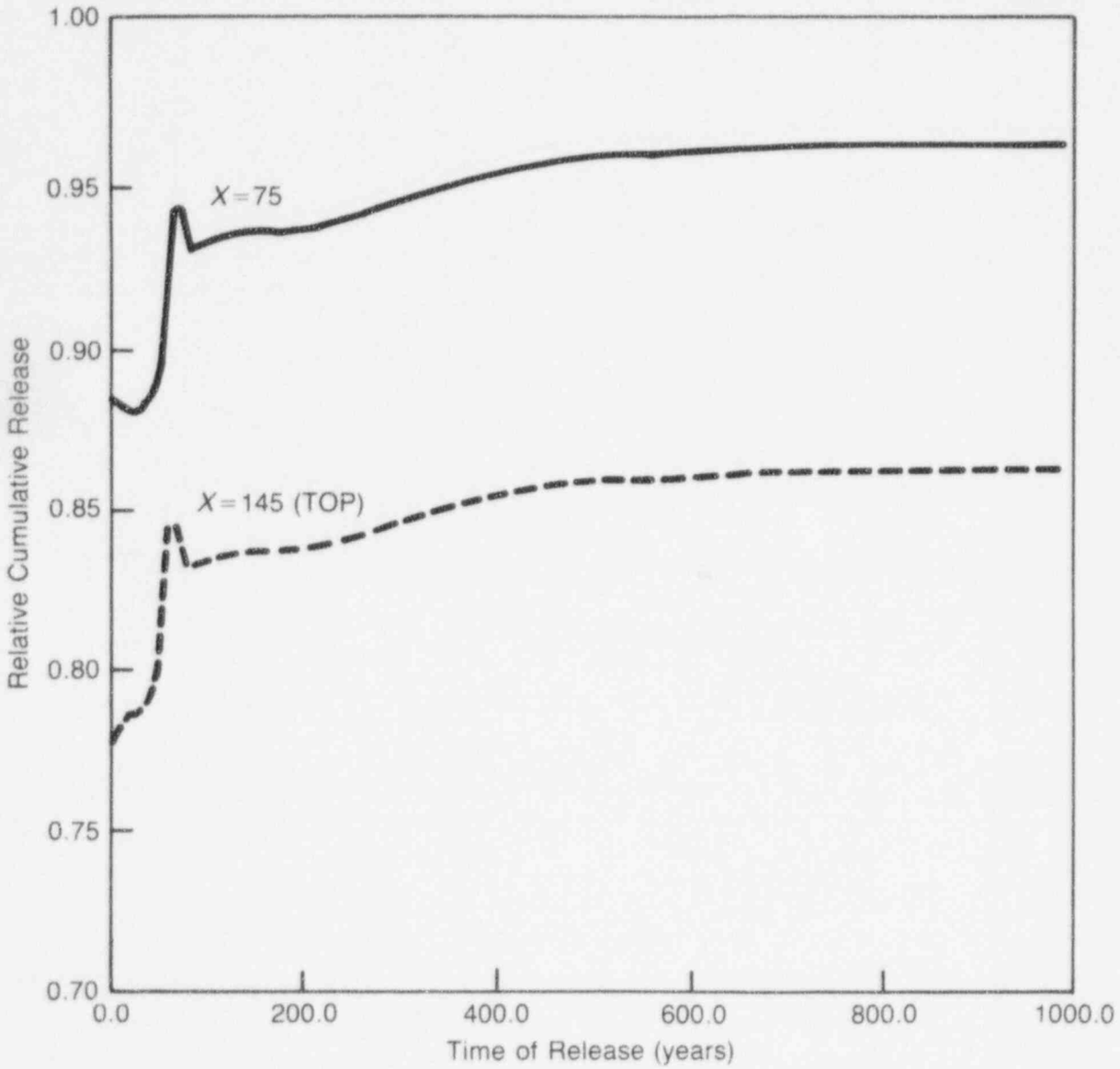

Figure K-7 Cumulative release by 1500 years as a function of when ^{14}C was released

APPENDIX L
THE EXCHANGE OF MAJOR CATIONS AT YUCCA MOUNTAIN

L–1 INTRODUCTION

An important characteristic of Yucca Mountain, the proposed geologic repository for high-level radioactive waste (HLW), is the presence of zeolitic tuffs. Zeolites are crystalline, hydrated aluminosilicates, which are characterized by an ability to readily exchange cations with aqueous solutions. The presence of zeolites is seen as an important barrier to the migration of radionuclides to the accessible environment. This auxiliary analysis was designed to answer two questions related to the exchange of cations in Yucca Mountain.

The first question concerned the stability (i.e., constancy of exchangeable cation composition) of zeolites. Using potassium/argon (K/Ar) dating techniques, WoldeGabriel *et al.* (1992) determined that the zeolites from drillholes in the Yucca Mountain vicinity range in age from 2 million years to 10 million years old. However, ion exchange involving potassium and sodium on zeolites has been shown to reach equilibrium in about 2 days (Pabalan, 1991). How, then, can a mineral that can alter within a couple of days exist for at least 2 million years? To answer that question, simulations were performed in which pore water, whose composition approximates that found at Yucca Mountain, percolates through site-specific zeolite layers for a period of approximately 150,000 years. The simulation was intended to represent the chemical reactions that would take place between the cations dissolved in the pore water and the cations sorbed onto zeolites. If, in the simulation, the K ions attached to the zeolites become mobile, there would be reason to doubt the zeolites could be accurately dated, using a K/Ar technique. If, however, the K is immobile, the K/Ar ratios would not be affected by ion-exchange reactions. This information is important to the siting of the repository, for it supports the conceptualization that the zeolites should remain stable for the lifetime of the repository and should act as a barrier for the release of radionuclides to the accessible environment (10 CFR 60.2).

The second question to be answered by this analysis involved the determination of pore water compositions from the unsaturated zone. Peters *et al.* (1992) describe methods of measuring pore water compositions from rocks of the unsaturated zone, plus the possible causes of changes in the compositions of the pore waters because of the method of extraction (compression). Given that ion-exchange reactions involving zeolites are fast (Pabalan, 1991), can we determine the chemical composition of pore water from the unsaturated zone, if the composition of the zeolite in direct contact with the pore water is known? If the answer is yes, then are there any significant spatial patterns of these compositions?

L–2 BACKGROUND

Ion exchange is a process by which ions in one phase displace ions in another phase. For example:

$$m\,A^{n+} + nBX_m = m\,AX_n + nB^{m+} \quad , \qquad \textbf{(L–1)}$$

where A and B represent cations of charge n and m, respectively, and X represents the sorption site on the solid phase. The cation exchange capacity (CEC) and the quantity of major cations present in a system can strongly influence the exchange or distribution coefficient (K_d) of radionuclides, as shown in the following equations:

$$Rn + NaX = RnX + Na \quad , \qquad \textbf{(L–2)}$$

$$K = \frac{[RnX][Na]}{[Rn][NaX]} \quad , \qquad \textbf{(L–3)}$$

$$K_d = K\frac{[NaX]}{[Na]} \quad , \qquad \textbf{(L–4)}$$

where Rn represents a radionuclide, K_d is the distribution of the radionuclide between the solid and the aqueous phase, K is the equilibrium constant, and brackets represent activities. The K_d of a specific nuclide in a specific environment is commonly used when describing sorptive properties. Since K_d is directly related to the cation content, an understanding of the major

cation chemistry (Na^+, Ca^{2+}, and K^+) is needed to fully understand the ability of Yucca Mountain to sorb radionuclides.

L–3 GEOCHEMICAL CODE

The simulations performed to address the first question in this auxiliary analysis concerning the validity of K/Ar dating relied on the geochemical modeling code *PHREEQM*, a code for use in mixing cell flowtube simulations, described by Appelo and Willemsen (1987). *PHREEQM* (**Ph**-**RE**dox-**EQ**uilibrium-**M**ixing), a modification of *PHREEQE*, has the same capabilities of *PHREEQE*, plus it can simulate one-dimensional fluid flow, diffusion, dispersion, and ion exchange. *PHREEQE* (**Ph**-**RE**dox-**EQ**uilibrium-**E**quations) is based on an ion-pairing aqueous model and can calculate pH, redox potential, and mass transfer as a function of reaction progress (Parkhurst *et al.*, 1980).

PHREEQM has the ability to simulate the flow of a solution through a multilayered heterogeneous column of porous material. Up to 10 layers, or a total of 100 cells, can be included in the simulated column. In each layer, equilibration with up to 10 minerals and reaction with up to 10 components can be simulated. Initial solid and liquid compositions in the column are input parameters of the code. Other input parameters are the length of each cell, the dispersivity associated with each cell, the porosity of any cell, the number of cell volumes of flushing solution added to the column, the composition of the flushing solution, the time allowed for diffusion/mixing of chemical constituents between adjacent cells, and the molecular diffusivity of elements in water.

Output includes composition of liquid, quantities of minerals precipitated or dissolved, and composition of solid ion exchanger in each cell for all time-steps. The output is presented in spreadsheet format, to facilitate the graphing of the results.

L–4 SIMULATIONS

L–4.1 Effect of Ion Exchange on K/Ar Dating

This analysis involved simulating the flow of site-specific ground water, through site-specific porous rock, at a site-specific rate. The simulation that was performed used mole fractions of Na, Ca + Mg, and K derived from the zeolite compositions reported by Broxton *et al.* (1986). In that study, the mole fractions of the exchangeable cations were determined for an extensive array of samples taken from boreholes in the vicinity of Yucca Mountain, in both the saturated and unsaturated zones. The zeolitic compositions vary both laterally and vertically. To simplify the simulation, a solid ion-exchanger composition was chosen that approximates the average composition of zeolites from the Topopah Spring member of the Paintbrush Tuff, where the proposed HLW repository is to be sited. The relative mole fractions for Ca + Mg, Na, and K were 33 percent, 19 percent, and 48 percent, respectively. The flushing solution composition in the simulation approximates that of the site-specific water from Peters *et al.* (1992). This site-specific water was extracted from pores, from several representative samples of tuff, by means of compression. Given that the zeolite compositions from Broxton *et al.* summed the concentrations of the exchangeable cations, Ca and Mg, the same was done for the liquid. The composition of the simulated water (flushing solution) was 3.10 moles/liter Ca + Mg, 1.83 moles/liter Na, and 8.03 moles/liter Cl. Other chemical constituents measured in the pore water from the squeezed rock but not included in this simulation, were H, HCO_3, SO_4, and SiO_2. These constituents have no effect on the reaction modeled.

The column through which water flowed in the simulation was divided into 100 cells. Each cell was 5 meters long. The whole column was then composed of 500 meters of the Paintbrush Tuff unit. The porosity of the column is assumed to be 0.3, which lies within the range of porosities found at Yucca Mountain.

The percolation flux of flushing solution through the column was set at 0.6 millimeters/year. This is comparable to moving the liquid from one cell to an adjacent cell downstream every 2500 years. This value approximates that derived from matrix potentials in Well USW UZ–1 (Montazer *et al.*, 1986). The range of estimates of percolation fluxes, however, extend from negative values (upward fluxes) to 100 millimeters/year (Montazer and Wilson, 1984; and Montazer *et al.*, 1986). The dispersivity associated with each cell was arbitrarily set at 0.02 meters. Molecular diffusivity was 3 square meters/100 years.

The CEC was set at 6667 milliequivalents/liter. This value lies approximately halfway between the extremes of CEC's of rocks from Yucca Mountain (from Thomas, 1987). The three ion-exchange reactions modeled are:

$$NaX + K^+ \leftrightarrows KX + Na^+ \quad , \qquad \text{(L–5)}$$

$$2Na^+ + CaX_2 \leftrightarrows 2NaX + Ca^{2+} \quad , \qquad \text{(L–6)}$$

$$2K^+ + CaX_2 \leftrightarrows 2KX + Ca^{2+} \quad . \qquad \text{(L–7)}$$

Equilibrium constants for Equations (L–5) and (L–6) were from Pabalan (1991). The equilibrium constant for Equation (L–7) was derived by multiplying Equation (L–5) by two and adding the result to Equation (L–6). In this simulation, ideal mixing was assumed in the solid phase. This assumption is most likely incorrect, as indicated by the experimental evidence of nonideality in the binary systems Na-K and Na-Ca clinoptilolite (Pabalan, 1991). However, experimental studies on mixing in the solid phase of the ternary system Na-K-Ca clinoptilolite have yet to be performed, so the assumption of ideality in the solid phase was required.

L–4.2 Calculated Compositions of Water from the Unsaturated Zone

By using the compositions of clinoptilolites from the unsaturated zone of Yucca Mountain (from Broxton *et al.*, 1986) and the equilibrium constants from Pabalan (1991) and this study for Equations (L–5) through (L–7), the relative concentrations of the exchangeable cations in the pore were calculated. Again, ideality of mixing in the solid was assumed. Activity coefficients for species in the liquid phase were derived from the Debye-Hückel formulation. However, the ionic strength of pore water in equilibrium with the zeolites is assumed to be constant and comparable to the extracted pore water from Peters *et al.* (1992). Consequently, the activity coefficients are likewise constant.

L–5 RESULTS

L–5.1 Effect of Ion Exchange on K/Ar Dating

Figure L–1 shows the concentration of exchangeable cations in the solid versus distance along flow path (represented as cell numbers). Cell 0 represents the top of the column; cell 100 represents the bottom of the column. The flushing solution is input into the top of the column at cell 0. The horizontal lines represent the chemical composition of the solid phase in the column after 60 shifts (cell volumes) or 150,000 years. The composition is relatively constant, except in the first few cells.

Figure L–2 represents the composition of the solution passing through the column after 60 shifts. The original water composition is shown on the *Y*-axis. This graph demonstrates that the composition of the pore water is dominated by the composition of the zeolites. Since the composition of the zeolites varies, it is reasonable to assume that the pore water chemistry will also vary, as the water percolates through the zeolites.

The results of this auxiliary analysis demonstrate that the K in the zeolites is relatively immobile. This is because of the large reservoir of K held in the zeolite versus the amount of exchangeable cations in the liquid. There simply are not enough cations in the pore water to exchange with the K on the zeolites, and therefore the K remains immobile. Consequently, the K/Ar technique for determining the age of the zeolites should not be affected by ion exchange, given the low concentrations of cations in the ground water.

L–5.2 Calculated Compositions of Water from the Unsaturated Zone

The compositions of zeolites and ground waters in equilibrium with those zeolites were plotted on ternary diagrams using the code *GRAPHER*. The ternary diagrams illustrate the relative concentrations of sodium, potassium, and calcium and not the total concentrations. This representation for the liquid compositions is consistent with ternary representations of solid compositions in Broxton *et al.* (1986). Figure L–3 is a ternary diagram showing the relationship of the zeolite compositions to the liquid compositions, in equilibrium with those solids in Well G–4. This figure contains solid and liquid compositions from the unsaturated zone. The solid compositions have an average K content of 50 percent. However, the water in equilibrium with these solids contains very little potassium. The saturated zone information was not included in the graph, so the unsaturated zone information is

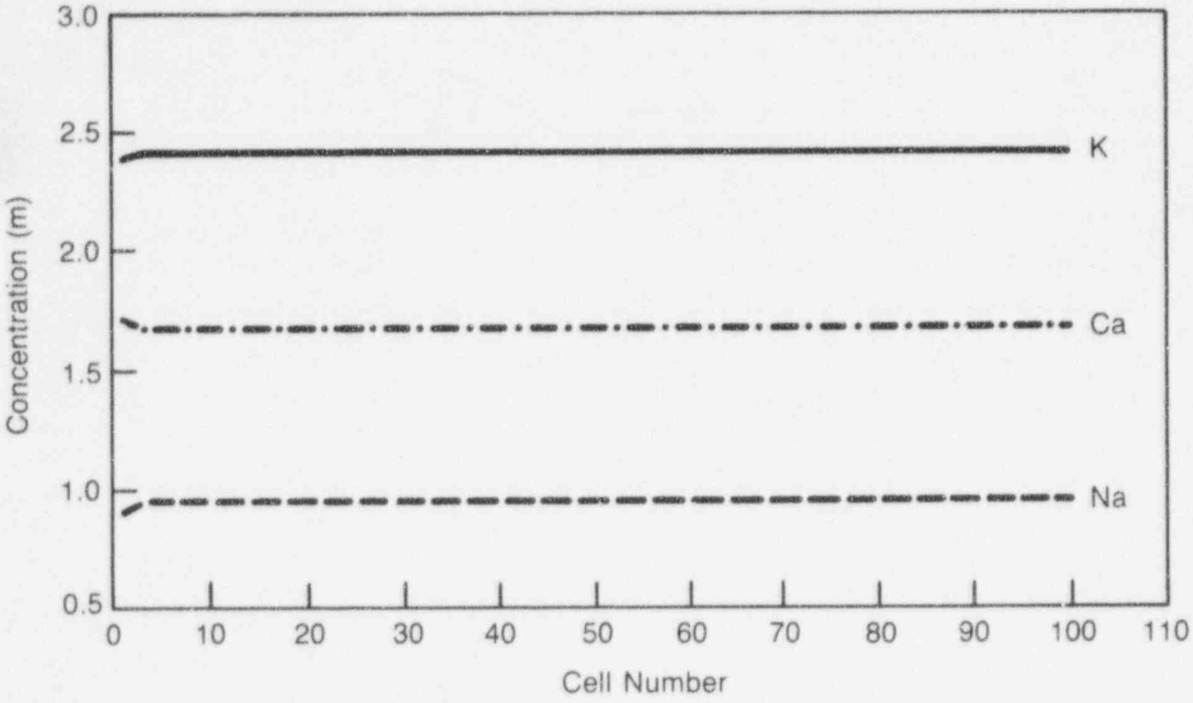

Figure L–1 Concentration of exchangeable cations in solid versus distance along flow path

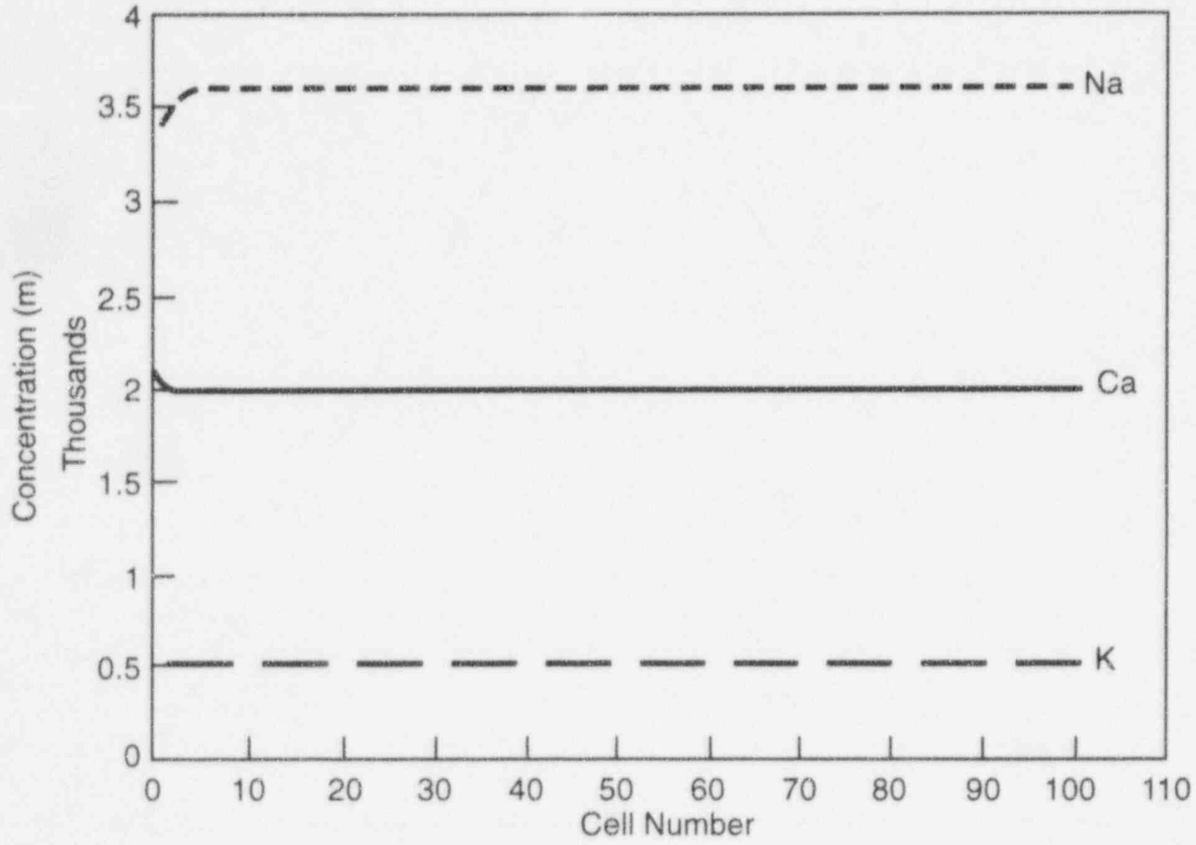

Figure L–2 Composition of solution passing through column

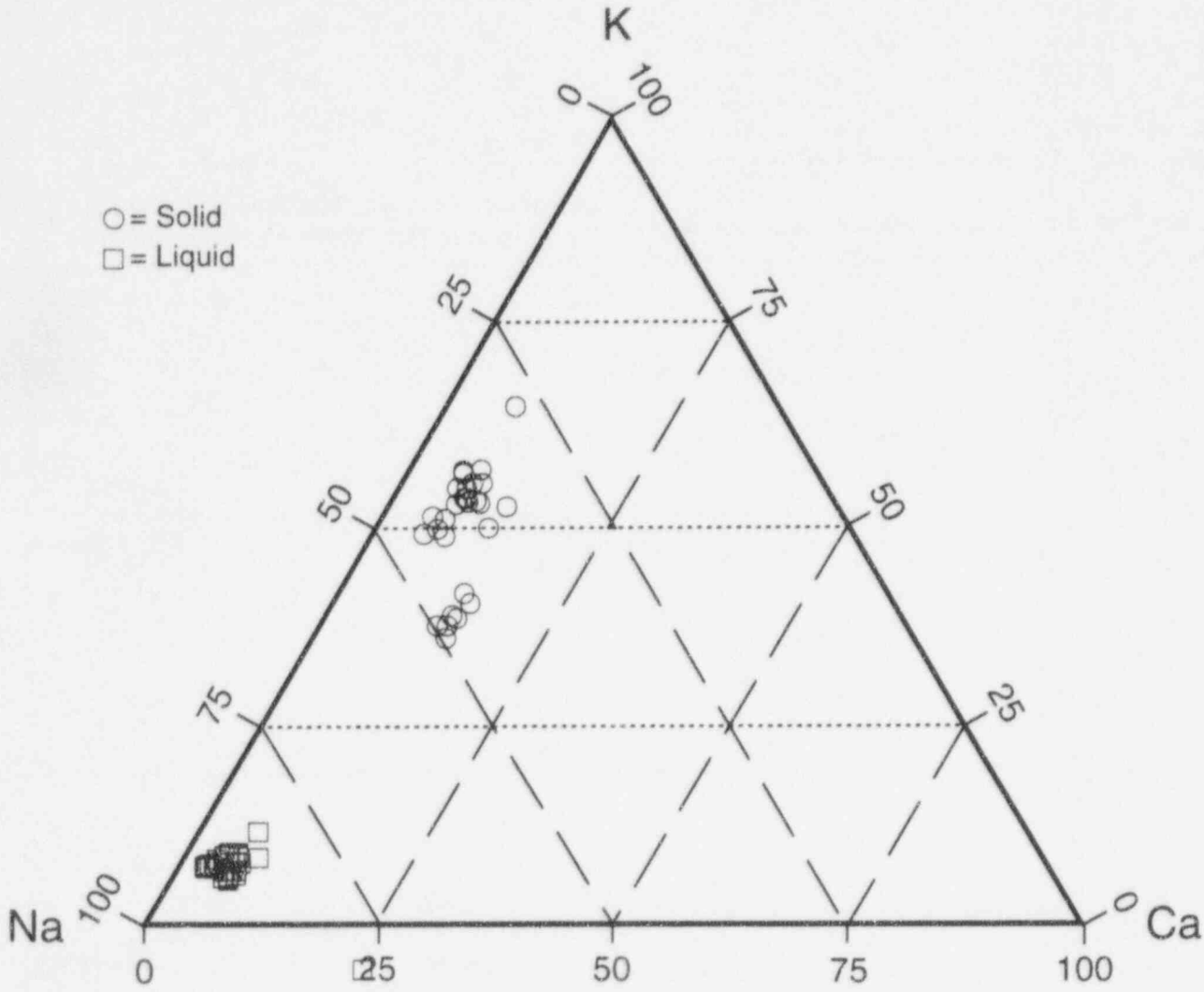

Figure L–3 Ternary diagram of zeolite compositions to liquid compositions in Well G–4 saturated and unsaturated zones using Broxton's solid compositions with liquid in equilibrium

more defined. Figure L–3 clearly demonstrates that the zeolites of the unsaturated zone are deficient in Na, where the pore water in equilibrium is Na-rich and K-deficient. The potassium concentrations of the unsaturated zone pore water measured by Peters *et al.* (1992) were suspect, and so were not reported. The potassium concentration measured in replicate samples varied, but generally was less than 10 parts per million (C.A. Peters, personal communication, 1993).

Figures L–4 through L–8 illustrate the compositions of zeolites and coexisting ground waters in Wells G–1, G–2, G–3, H–3, and H–4. On Figure L–8, the composition of J–13 well water is plotted, as well as the composition of the water removed from Well USW–H4. The Na–rich composition of the water from USW–H4 is consistent with Na-K-rich zeolites analyzed from this well in the saturated zone. Establishing a comparable match with J–13 ground water/zeolite is not apparent, possibly because of not knowing the depth from which the water comes.

L–6 CONCLUSIONS

In summary, this auxiliary analysis has produced valuable information on the exchange of the major cations in Yucca Mountain. The results indicate that the potassium associated with the zeolites is relatively immobile for the time period of these modeling runs. It also demonstrates the wide variation, in the pore water chemistry, which is possible in this environment. In addition, this analysis has shown that the chemical composition of the pore waters in contact with the solids in the unsaturated zone may be different from the composition of the water in the saturated zone. This is important for those who wish to do exchange experiments and require the solution and solids to be in equilibrium.

L–7 REFERENCES

Appelo, C.A.T. and A. Willemsen, "Geochemical Calculations and Observations on Salt Water Intrusions, I., A Combined Geochemical/Mixing Cell Model," *Journal of Hydrology*, 94:313–330 [1987].

Broxton, D.E., *et al.*, "Chemistry of Diagenetically Altered Tuffs at a Potential Nuclear Waste Repository, Yucca Mountain, Nye County, Nevada," Los Alamos, New Mexico, Los Alamos National Laboratory, LA–10802–MS, October 1986.

Montazer, P., and W.E Wilson, "Conceptual Hydrologic Model Flow in the Unsaturated Zone, Yucca Mountain, Nevada, Water Resources Investigations," U.S. Geological Survey, Water Resources Investigations Report, WRI–84–4345, 1984.

Montazer, P., *et al.*, "Monitoring the Vadose Zone in Fractured Tuff, Yucca Mountain, Nevada," *Proceedings of the National Water Well Association Conference on Characterization and Monitoring of the Vadose (Unsaturated) Zone*, Worthington, Ohio, November 19–21, 1985, pp. 439–469 [1986].

Pabalan, R.T., "Nonideality Effects on the Ion Exchange Behavior of the Zeolite Mineral Clinoptilolite," in Abrajano, T., Jr. and L.H. Johnson (eds.), *Scientific Basis for Nuclear Waste Management XIV: Materials Research Society Symposium Proceedings*, 212:559–567 [1991].

Parkhurst, D.L., D.C. Thorstenson, and L.N. Plummer, "PHREEQE—A Computer Program for Geochemical Calculations," U.S. Geological Survey, Water Resources Investigations Report, WRI–80–96, August 1980.

Peters, C.A., *et al.*, "A Preliminary Study of the Chemistry of Pore Water Extracted from Tuff by One–Dimensional Compression," in Kharaka Y.K., and A.S. Maest (eds.), *International Water-Rock Interaction Symposium Proceedings*, Park City, Utah, July 13–23, 1992, pp. 741–745 [1992]. [Published by A.A. Balkema, Rotterdam, Holland.]

Thomas, K., "Summary of Sorption Measurements Performed with Yucca Mountain, Nevada, Tuff Samples and Water from Well J–13," Los Alamos, New Mexico, Los Alamos National Laboratory, LA–10960–MS, December 1987.

WoldeGabriel, G., *et al.*, "Preliminary Assessment of Clinoptilolite K/Ar Results from Yucca Mountain, Nevada, USA: A Potential High-Level Radioactive Waste Repository Site," in Kharaka, Y.K., and A.S. Maest (eds.), *International Water-Rock Interaction Symposium Proceedings*, Park City, Utah, July 13–23, 1992, pp. 457–461 [1992].

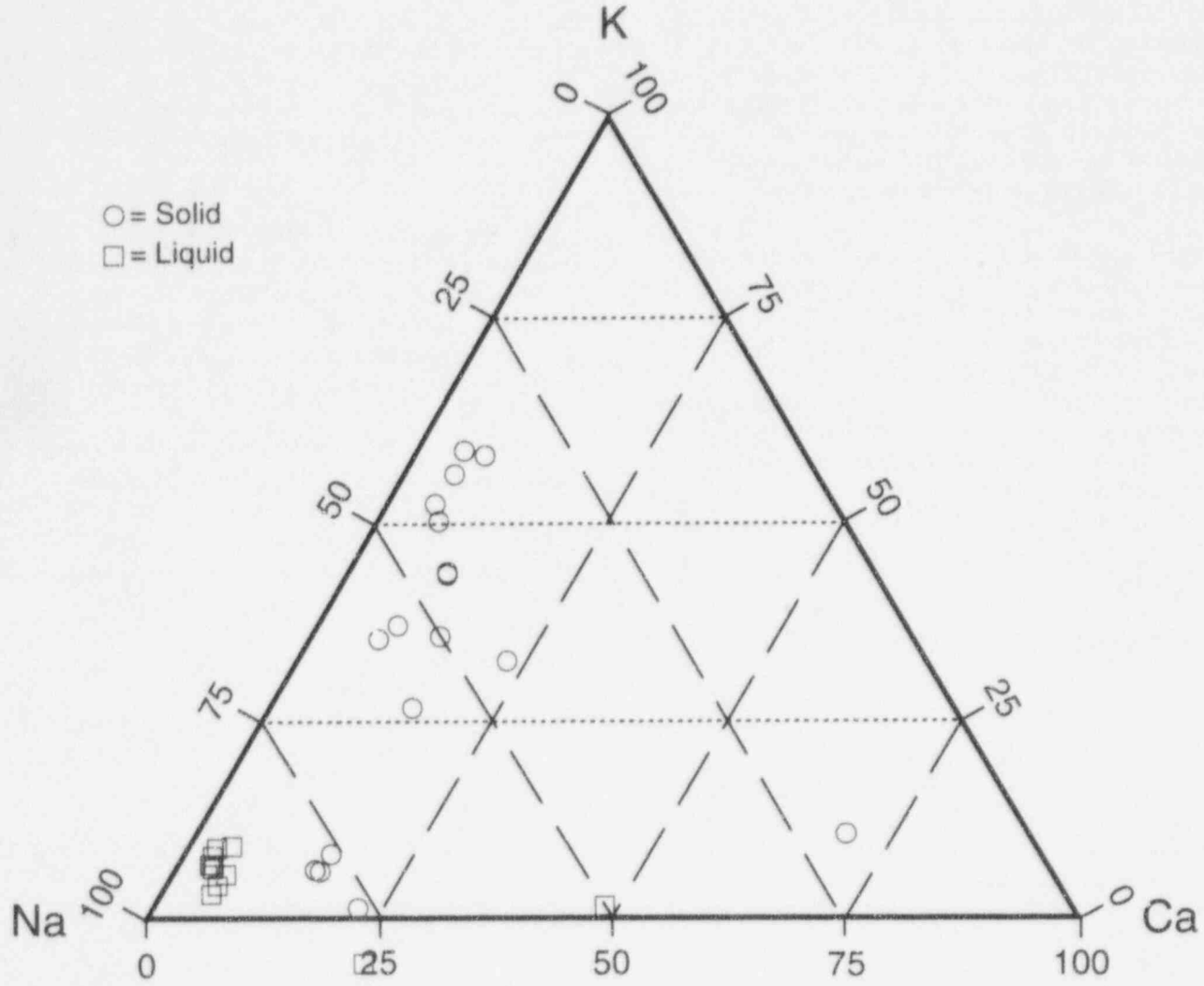

Figure L–4 Ternary diagram of zeolite compositions to liquid compositions for Well G–1 using Broxton's solid compositions with liquid in equilibrium

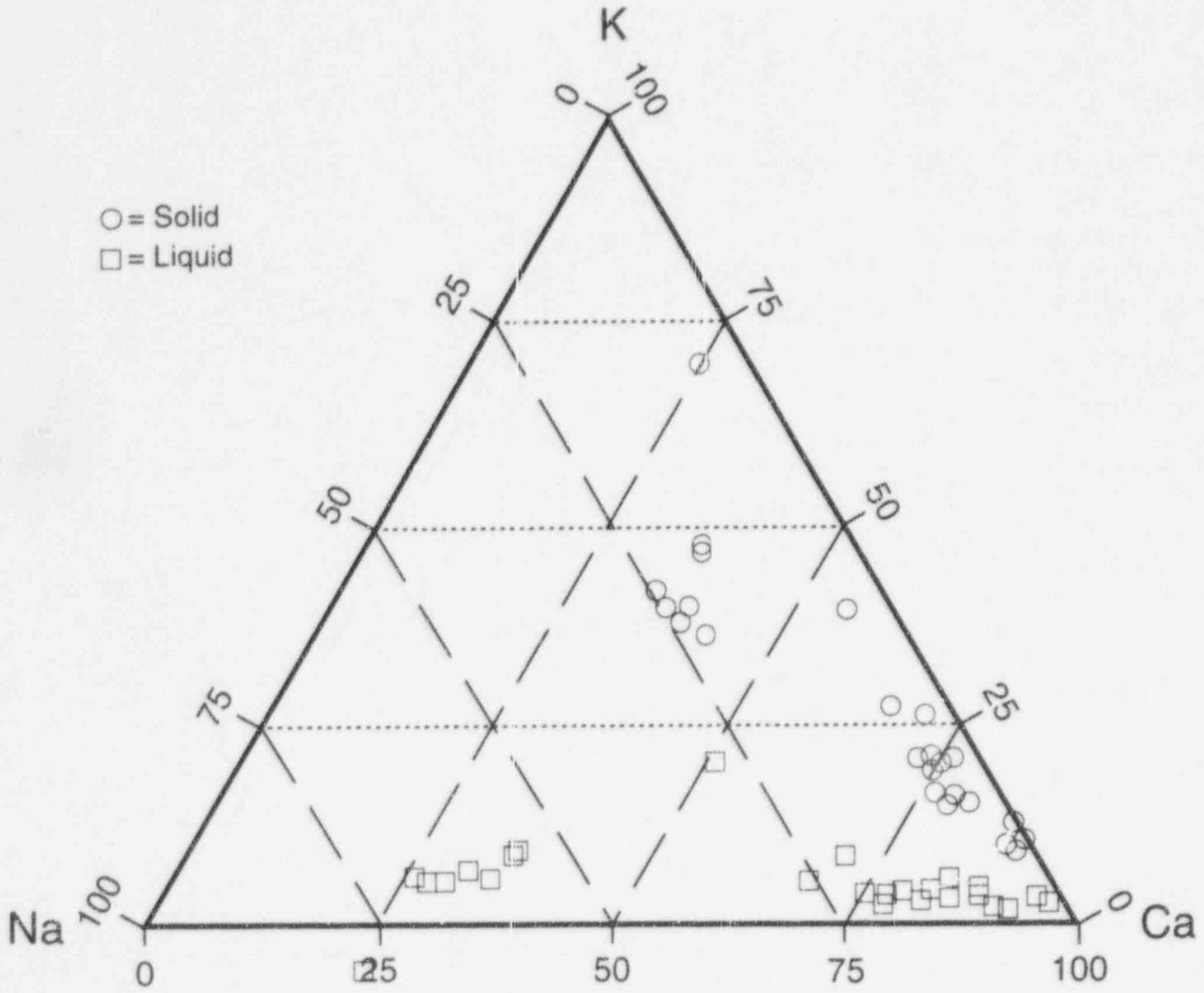

Figure L–5 Ternary diagram of zeolite compositions to liquid compositions for Well G–2 using Broxton's solid compositions with liquid in equilibrium

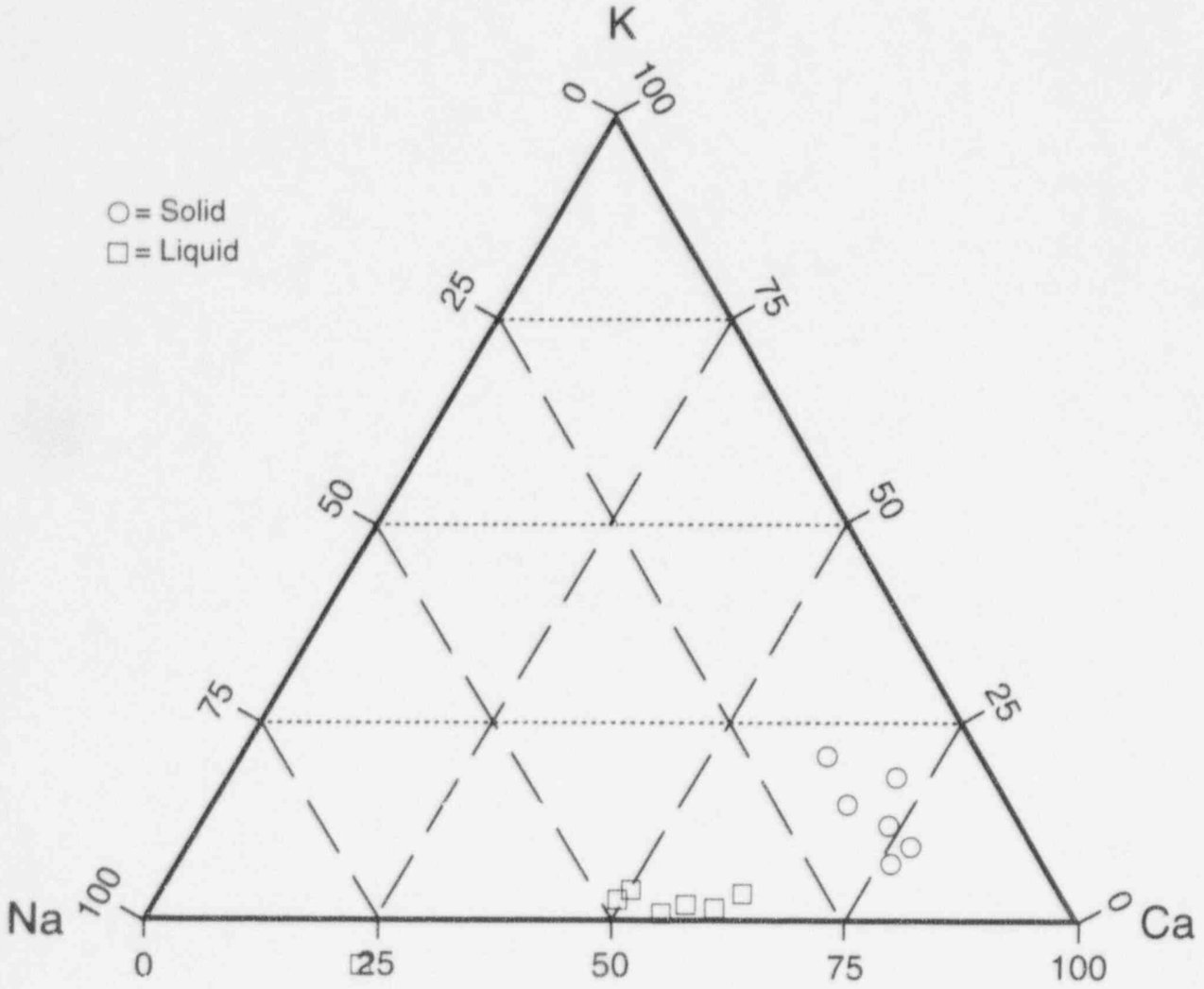

Figure L–6 Ternary diagram of zeolite compositions to liquid compositions for Well G–3 using Broxton's solid compositions with liquid in equilibrium

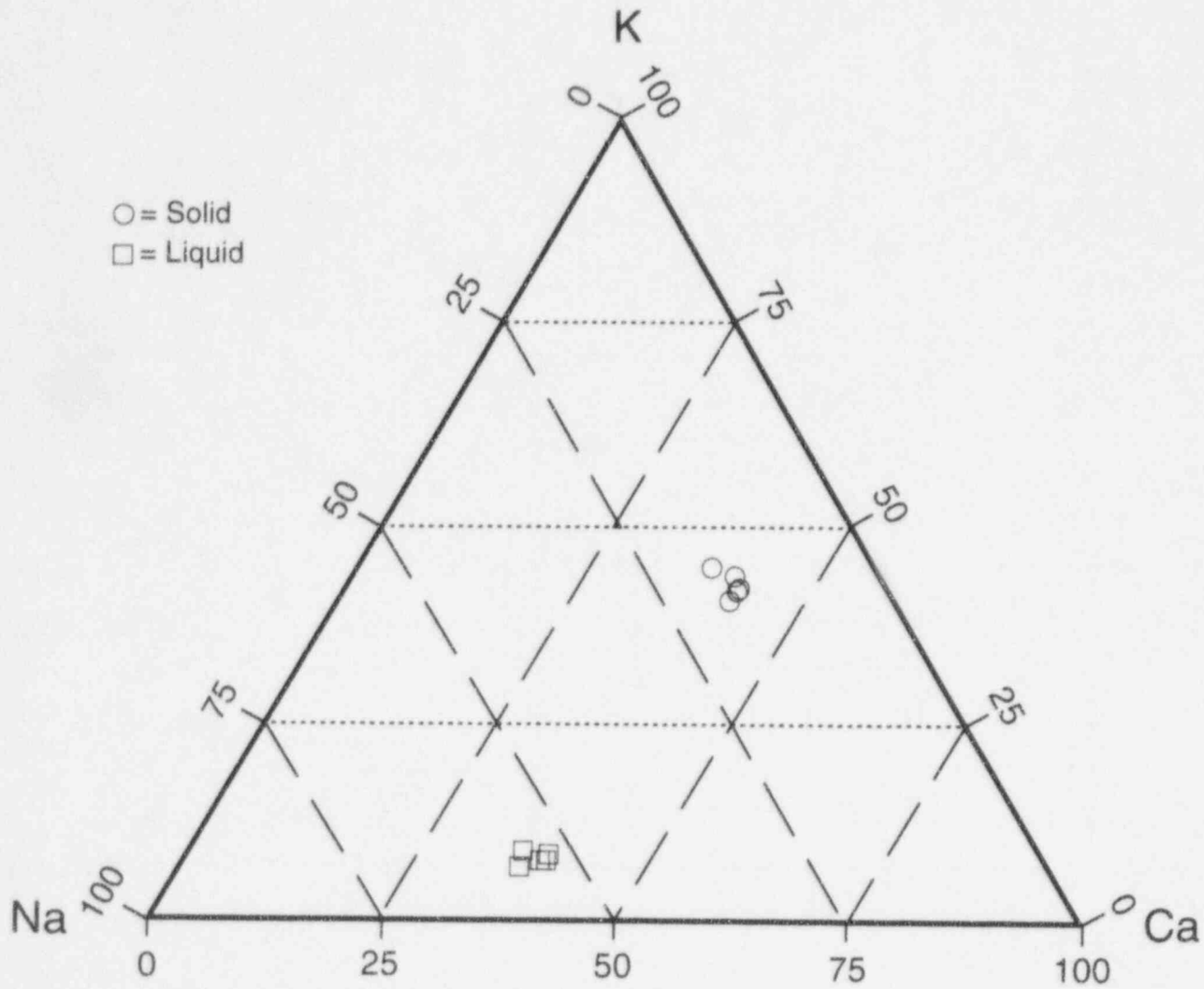

Figure L–7 Ternary diagram of zeolite compositions to liquid compositions for Well H–3 using Broxton's solid compositions with liquid in equilibrium

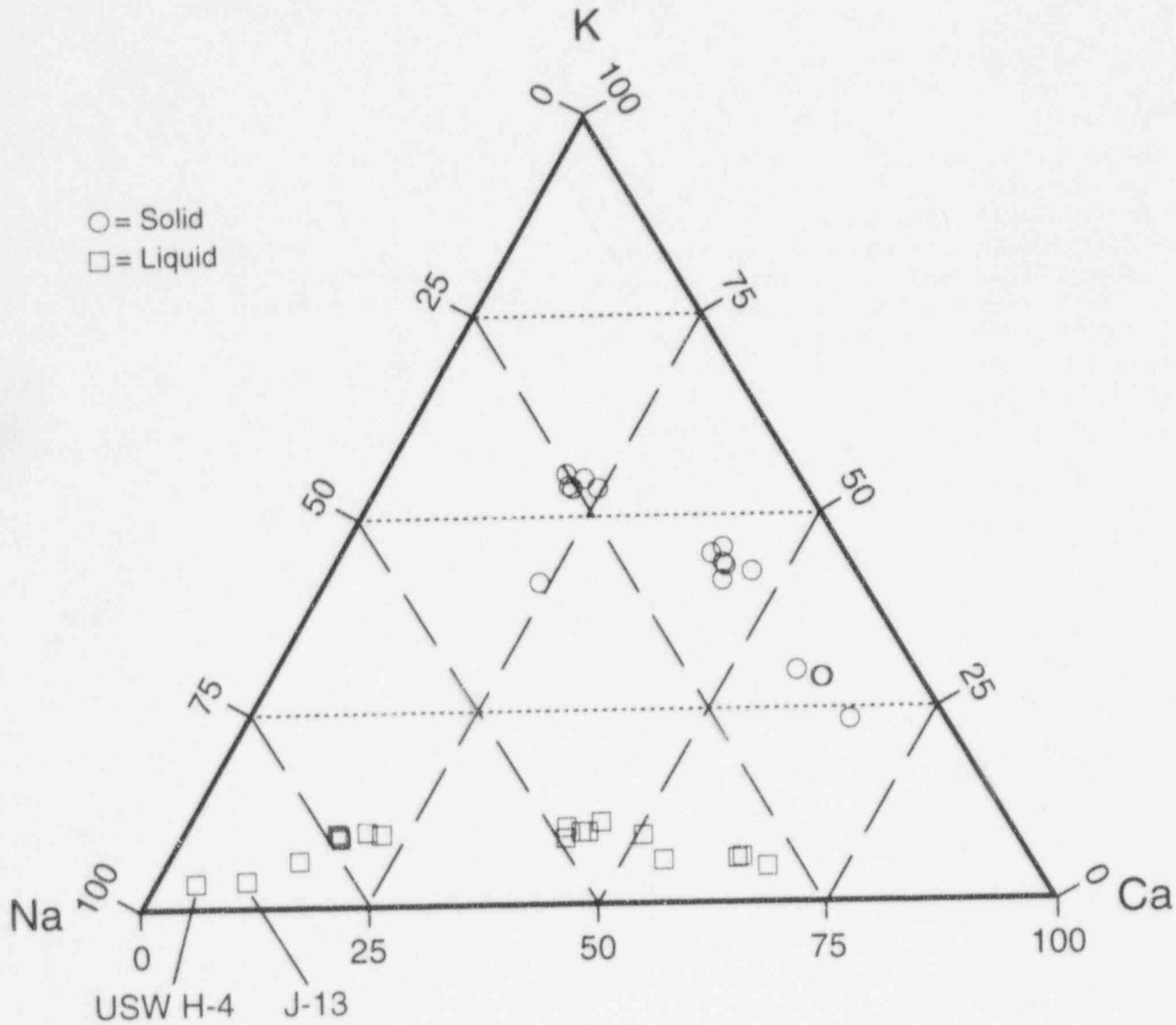

Figure L–8 Ternary diagram of zeolite compositions to liquid compositions for Well H–4 using Broxton's solid compositions with liquid in equilibrium

APPENDIX M
ENSEMBLE AVERAGING FOR SOURCE TERM PARAMETERS

M-1 INTRODUCTION

For the sake of computational speed, the Iterative Performance Assessment (IPA) Phase 2 analysis used a "lumped-parameter" approach, in which the entire geologic repository is represented by a relatively small number of representative waste packages. Since the entire repository source term, consisting of over 25,000 waste packages, is being represented by only seven zones or sub-areas, with only one waste package per repository sub-area, there must be careful consideration given to the way in which the repository sub-areas represent the ensemble of waste packages they are supposed to represent.

Presently, the arithmetic average of external environmental parameter values (e.g., temperature, infiltration) for all waste packages in the repository sub-area are chosen for a representative waste package. Additionally, there is only one set of source term parameter values (e.g., corrosion parameters, solubilities) representing the corrosion, liquid, and gaseous release submodels per repository sub-area. The present auxiliary analysis examines the relationships of several key independent parameters, in the source term models, from the standpoint of their behavior under ensemble averaging.

The flow rate q and the volume V affect the dissolved release model in two ways:

- They determine the time that the waste package fills to the point of overflowing; and
- They determine the release rate for solubility limited radionuclides.

The demonstration of the effects of ensemble averaging on the cumulative release rate was performed for only two radionuclides, one solubility limited and the other limited by congruent dissolution of the UO_2 fuel. To further simplify the calculations, both radionuclides have infinite half lives, no other isotopes are present, and daughter products are not considered.

M-2 SOLUBILITY LIMITED CASE

For the stated conditions within a given vector, the concentration C_s within the waste package will be constant (i.e., the solubility). Therefore, the cumulative release for 10,000 years per waste package m_a for a solubility limited radionuclide by advection will be proportional to the flow rate through the waste package:

$$m_a = C_s q_i [10,000 - t_f] \quad , \qquad \textbf{(M-1)}$$

where t_f = time to fill waste package, and years $= V_0/q$.

The cumulative diffusive release m_d, is proportional to the concentration:

$$m_d = kC_s [10,000 - t_{fail}] \quad , \qquad \textbf{(M-2)}$$

where k is a proportionality constant related to the diffusion coefficient and retardation coefficient in the surrounding rock, which are constants within a given vector. The waste package failure time t_{fail}, is related to a number of parameters in the waste package failure model or disruptive failure models, and varies from place to place within a vector.

The cumulative release of the radionuclide for all waste packages is equal to the sum of the releases from each waste package after their filling, that is,

$$M = \sum_{i=1}^{N} \left[C_s q_i (10,000 - \frac{V_0}{q_i}) + kC_s (10,000 - t_{fail}) \right] \quad . \qquad \textbf{(M-3)}$$

The average cumulative release per waste package is therefore the result of Equation (M-3), divided by N. After some rearrangement, Equation (M-3) can be shown to reduce to:

$$< m > = C_s [10,000 < q > - < V_0 > + 10,000k - k < t_{fail} >] \quad . \qquad \textbf{(M-4)}$$

where the angle brackets ($< >$) denote ensemble average over all N waste packages.

M-3 CONGRUENTLY RELEASE RATE

For the case where the release rate is controlled not by the solubility of the radionuclide, but by the rate of release from the fuel matrix, a different set of relationships controls the ensemble average. In this case, the concentration of the radionuclide in the waste package, C_0, is no longer a constant, but changes with time and is a function of the rate of release by advection and diffusion. Since C_0 is no longer a constant, the integration for cumulative release over 10,000 years must be done formally:

$$M = \int_{t_{fail}}^{10,000} kC_0\, dt + \int_{t_f}^{10,000} q_i C_0\, dt \quad . \qquad \textbf{(M-5)}$$

For a long half life, C_0 is related to the alteration rate of the matrix r, the inventory in the matrix M_0, and the flow rate, all of which are constant within a given vector. Therefore:

$$C_0 = \frac{rM_0}{q_i} \quad , \quad \text{and} \qquad \textbf{(M-6)}$$

$$m = \int_{t_{fail}}^{10,000} kC_0\, dt + \int_{t_f}^{10,000} rM_0\, dt \quad . \qquad \textbf{(M-7)}$$

Applying the same definitions for t_f and after evaluating the integrals, the cumulative release becomes:

$$m = rm_0\left[\frac{k}{q_i}\,(10,000 - t_{fail}) + 10,000 - \frac{V_0}{q_i}\right] \quad . \qquad \textbf{(M-8)}$$

The ensemble average for N waste packages can be found by summing, as in the case of the concentration limited release:

$$< m > = \frac{1}{N}\sum_{i=1}^{N} rm_0\left[10,000 + \frac{1}{q_i}[k(10,000 - t_{fail}) - V_0]\right] \quad . \qquad \textbf{(M-9)}$$

which reduces, after some rearrangement, to:

$$< m > = 10,000M_0\, kr < \left(\frac{1}{q}\right) > - M_0\, kr < \left(\frac{t_{fail}}{q}\right) > + 10,000rM_0 + M_0 r < \left(\frac{V_0}{q}\right) > \quad . \qquad \textbf{(M-10)}$$

M-4 CONCLUSIONS

solubility limited releases of single, long-lived radionuclides, the ensemble average cumulative release per waste package is represented exactly by the arithmetic averages of the flow rate per waste package $< q >$, the waste package failure time $< t_{fail} >$, and the waste package failure volume $< V_0 >$.

The ensemble mean parameters for the congruent release case, should be $< 1/q >$ (the harmonic mean), $< t_{fail}/q >$, and $< V_0/q >$.

Experiments with the release rate models, themselves, confirm that cumulative release of the long-lived solubility limited radionuclides is proportional to flow, which demonstrates that the arithmetic mean flow rate is the correct ensemble mean to use for these radionuclides. Release of congruently released radionuclides is not proportional to the flow rate, but for these radionuclides, the flow rate is relatively unimportant. A 35-fold increase in flow rate led to only about a 60 percent increase in releases. The effects of using the arithmetic mean of the V_0 and the parameters for the failure model have not been determined for IPA Phase 2.

NRC FORM 335 (2-89) NRCM 1102, 3201, 3202

U.S. NUCLEAR REGULATORY COMMISSION

BIBLIOGRAPHIC DATA SHEET

(See instructions on the reverse)

1. REPORT NUMBER (Assigned by NRC, Add Vol., Supp., Rev., and Addendum Numbers, if any.)

NUREG-1464

2. TITLE AND SUBTITLE

NRC Iterative Performance Assessment Phase 2: Development of Capabilities for Review of a Performance Assessment for a High-Level Waste Repository

3. DATE REPORT PUBLISHED

MONTH	YEAR
October	1995

4. FIN OR GRANT NUMBER

5. AUTHOR(S)

R. G. Wescott[1], M. P. Lee[1], T. J. McCartin[2], N. A. Eisenberg[1], and R. G. Baca[3] (editors)

6. TYPE OF REPORT

Technical

7. PERIOD COVERED (Inclusive Dates)

8. PERFORMING ORGANIZATION - NAME AND ADDRESS (If NRC, provide Division, Office or Region, U.S. Nuclear Regulatory Commission, and mailing address; if contractor, provide name and mailing address.)

[1]Office of Nuclear Material Safety and Safeguards
[2]Office of Nuclear Regulatory Research
U.S. Nuclear Regulatory Commission
Washington, DC 20555-0001

[3]Center for Nuclear Waste Regulatory Analyses
6220 Culebra Road
San Antonio, TX 78228-0510

9. SPONSORING ORGANIZATION - NAME AND ADDRESS (If NRC, type "Same as above"; if contractor, provide NRC Division, Office or Region, U.S. Nuclear Regulatory Commission, and mailing address.)

Same as 8. above

10. SUPPLEMENTARY NOTES

11. ABSTRACT (200 words or less)

In order to better review a potential license application to construct and operate a geologic repository for spent nuclear fuel and high-level radioactive waste (HLW), the Nuclear Regulatory Commission staff (and its contractor) has expanded and improved its capability to conduct performance assessments. This report documents the demonstration of the second phase of this capability. The demonstration made use of the scenario selection procedure developed by Sandia National Laboratories to provide a set of scenarios, with corresponding probabilities, for use in the consequence analysis of a potential HLW disposal site in unsaturated tuff. Models of release of radionuclides from the waste form and transport in ground water, air and by direct pathways provided preliminary estimates of releases to the accessible environment for a 10,000 year period. The input values of parameters necessary for the consequence models were sampled numerous times using Latin Hypercube Sampling from assumed probability distributions. The results from the consequence models were then used to generate Complementary Cumulative Distribution Functions (CCDFs) for either release to the accessible environment or effective dose equivalents to a target population. CCDFs were calculated for probabilistically significant combinations (scenarios) of four disruptive events; drilling, pluvial climate, seismicity and magmatism. Sensitivity and uncertainty analyses of the calculated releases and effective dose equivalents were also used to determine the importance of the parameters. Because of the preliminary nature of the analysis and the lack of an adequate data base, the results and conclusions presented in this report should be carefully interpreted. They should not be misconstrued to represent the actual performance of the proposed Yucca Mountain repository nor serve as an endorsement of the methods used.

12. KEY WORDS/DESCRIPTORS (List words or phrases that will assist researchers in locating the report.)

Computer code
Dose
Geologic repository
Performance assessment
Sensitivity and uncertainty analysis
Source term
Yucca Mountain
Disruptive consequences
EPA Standard
High-level waste
Probabilistic risk assessment
Scenario
Transport
Parameter

13. AVAILABILITY STATEMENT

Unlimited

14. SECURITY CLASSIFICATION

(This Page) Unclassified

(This Report) Unclassified

15. NUMBER OF PAGES

16. PRICE

Federal Recycling Program

UNITED STATES
NUCLEAR REGULATORY COMMISSION
WASHINGTON, DC 20555-0001

OFFICIAL BUSINESS
PENALTY FOR PRIVATE USE, $300

SPECIAL FOURTH-CLASS MAIL
POSTAGE AND FEES PAID
USNRC
PERMIT NO. G-67